

C. Pozrikidis

Fluid Dynamics

Theory, Computation,
and Numerical Simulation

Third Edition

 Springer

Fluid Dynamics

Theory, Computation, and Numerical Simulation

C. Pozrikidis

Fluid Dynamics

Theory, Computation, and Numerical Simulation

Third Edition

 Springer

C. Pozrikidis
University of Massachusetts
Amherst, Massachusetts, USA

Author retains ownership and copyright of all computer codes listed, discussed, or referred to in the book.

MATLAB® and Simulink® are registered trademarks of The MathWorks, Inc., 3 Apple Hill Drive, Natick, MA 01760-2098, USA, <http://www.mathworks.com>

ISBN 978-1-4899-7990-2 ISBN 978-1-4899-7991-9 (eBook)
DOI 10.1007/978-1-4899-7991-9

Library of Congress Control Number: 2016949478

© Springer Science + Business Media LLC 2001, 2009, 2017

This work is subject to copyright. All rights are reserved by the Publisher, whether the whole or part of the material is concerned, specifically the rights of translation, reprinting, reuse of illustrations, recitation, broadcasting, reproduction on microfilms or in any other physical way, and transmission or information storage and retrieval, electronic adaptation, computer software, or by similar or dissimilar methodology now known or hereafter developed.

The use of general descriptive names, registered names, trademarks, service marks, etc. in this publication does not imply, even in the absence of a specific statement, that such names are exempt from the relevant protective laws and regulations and therefore free for general use.

The publisher, the authors and the editors are safe to assume that the advice and information in this book are believed to be true and accurate at the date of publication. Neither the publisher nor the authors or the editors give a warranty, express or implied, with respect to the material contained herein or for any errors or omissions that may have been made.

Printed on acid-free paper

This Springer imprint is published by Springer Nature
The registered company is Springer Science + Business Media LLC
The registered company address is: 233 Spring Street, New York, NY 10013, U.S.A.

Contents

Preface	xvii
Notation	xix
1 Introduction to kinematics	1
1.1 Fluids and solids	1
1.2 Fluid parcels and flow kinematics	2
1.3 Coordinates, velocity, and acceleration	4
1.3.1 Cylindrical polar coordinates	7
1.3.2 Spherical polar coordinates	10
1.3.3 Plane polar coordinates	13
1.4 Fluid velocity	16
1.4.1 Continuum approximation	17
1.4.2 Steady flow	17
1.4.3 Two-dimensional flow	18
1.4.4 Swirling and axisymmetric flow	18
1.4.5 Velocity vector field, streamlines and stagnation points	18
1.5 Point particles and their trajectories	19
1.5.1 Path lines	20
1.5.2 Ordinary differential equations (ODEs)	21
1.5.3 Explicit Euler method	26
1.5.4 Modified Euler method	28
1.5.5 Description in polar coordinates	32
1.5.6 Streaklines	33
1.6 Material surfaces and elementary motions	34
1.6.1 Fluid parcel rotation	34
1.6.2 Fluid parcel deformation	36
1.6.3 Fluid parcel expansion	37
1.6.4 Superposition of rotation, deformation, and expansion	38
1.6.5 Rotated coordinates	38
1.6.6 Fundamental decomposition of a two-dimensional flow	41

1.7	Numerical interpolation	46
1.7.1	Interpolation in one dimension	47
1.7.2	Interpolation in two dimensions	50
1.7.3	Interpolation of the velocity in a two-dimensional flow	53
1.7.4	Streamlines by interpolation	57
2	More on kinematics	63
2.1	Fundamental modes of fluid parcel motion	63
2.1.1	Function linearization	64
2.1.2	Velocity gradient tensor	67
2.1.3	Relative motion of point particles	69
2.1.4	Fundamental motions in two-dimensional flow	69
2.1.5	Fundamental motions in three-dimensional flow	71
2.1.6	Gradient in polar coordinates	72
2.2	Fluid parcel expansion	75
2.3	Fluid parcel rotation and vorticity	76
2.3.1	Curl and vorticity	78
2.3.2	Two-dimensional flow	79
2.3.3	Axisymmetric flow	80
2.4	Fluid parcel deformation	81
2.5	Numerical differentiation	84
2.5.1	Numerical differentiation in one dimension	84
2.5.2	Numerical differentiation in two dimensions	86
2.5.3	Velocity gradient and related functions	88
2.6	Flow rates	95
2.6.1	Areal flow rate and flux	96
2.6.2	Areal flow rate across a line	97
2.6.3	Analytical integration	98
2.6.4	Numerical integration	99
2.6.5	The Gauss divergence theorem in two dimensions	101
2.6.6	Flow rate in a three-dimensional flow	102
2.6.7	Gauss divergence theorem in three dimensions	102
2.6.8	Axisymmetric flow	103
2.7	Mass conservation and the continuity equation	105
2.7.1	Mass flux and mass flow rate	105
2.7.2	Mass flow rate across a closed line	105
2.7.3	The continuity equation	106
2.7.4	Three-dimensional flow	107
2.7.5	Control volume and integral mass balance	109
2.7.6	Rigid-body translation	109
2.7.7	Evolution equation for the density	110
2.7.8	Continuity equation for axisymmetric flow	112
2.8	Properties of point particles	114
2.8.1	The material derivative	114

2.8.2	The continuity equation	116
2.8.3	Point particle acceleration	116
2.9	Incompressible fluids and stream functions	120
2.9.1	Kinematic consequence of incompressibility	121
2.9.2	Mathematical consequence of incompressibility	121
2.9.3	Stream function for two-dimensional flow	122
2.9.4	Stream function for axisymmetric flow	124
2.10	Kinematic conditions at boundaries	126
2.10.1	The no-penetration boundary condition	127
3	Flow computation based on kinematics	131
3.1	Flow classification based on kinematics	131
3.2	Irrotational flow and the velocity potential	133
3.2.1	Two-dimensional flow	134
3.2.2	Incompressible fluids and the harmonic potential	135
3.2.3	Three-dimensional flow	137
3.2.4	Boundary conditions	137
3.2.5	Cylindrical polar coordinates	138
3.2.6	Spherical polar coordinates	138
3.2.7	Plane polar coordinates	139
3.3	Finite-difference methods	140
3.3.1	Boundary conditions	140
3.3.2	Finite-difference grid	142
3.3.3	Finite-difference discretization	143
3.3.4	Compilation of a linear system	145
3.4	Linear solvers	154
3.4.1	Gauss elimination	155
3.4.2	A menagerie of other methods	156
3.5	Two-dimensional point sources and point-source dipoles	157
3.5.1	Function superposition and fundamental solutions	157
3.5.2	Two-dimensional point source	158
3.5.3	Two-dimensional point-source dipole	160
3.5.4	Flow past a circular cylinder	165
3.5.5	Sources and dipoles in the presence of boundaries	166
3.6	Three-dimensional point sources and point-source dipoles	168
3.6.1	Three-dimensional point source	168
3.6.2	Three-dimensional point-source dipole	169
3.6.3	Streaming flow past a sphere	170
3.6.4	Sources and dipoles in the presence of boundaries	171
3.7	Point vortices and line vortices	172
3.7.1	The potential of irrotational circulatory flow	173
3.7.2	Flow past a circular cylinder	174
3.7.3	Circulation	176
3.7.4	Line vortices in three-dimensional flow	177

4	Forces and stresses	181
4.1	Forces acting in a fluid	181
4.1.1	Body force	181
4.1.2	Surface force	182
4.2	Traction and the stress tensor	183
4.2.1	Traction on either side of a fluid surface	187
4.2.2	Traction on a boundary	188
4.2.3	Symmetry of the stress tensor	188
4.3	Traction jump across a fluid interface	189
4.3.1	Interfacial tension	189
4.3.2	Force balance at a two-dimensional interface	190
4.4	Force balance at a three-dimensional interface	197
4.4.1	Mean curvature	199
4.4.2	Directional curvatures	200
4.4.3	Axisymmetric interfaces	201
4.5	Stresses in a fluid at rest	204
4.5.1	Pressure from molecular motions	205
4.5.2	Jump in pressure across an interface in hydrostatics	206
4.6	Constitutive equations	207
4.6.1	Simple fluids	209
4.6.2	Incompressible Newtonian fluids	210
4.6.3	Viscosity	211
4.6.4	Viscosity of a gas	211
4.6.5	Ideal fluids	214
4.6.6	Significance of the pressure in an incompressible fluid	214
4.7	Pressure in compressible fluids	215
4.8	Simple non-Newtonian fluids	219
4.8.1	Unidirectional shear flow	219
4.8.2	Channel flow	220
4.8.3	Yield-stress fluids	221
4.9	Stresses in polar coordinates	222
4.9.1	Cylindrical polar coordinates	222
4.9.2	Spherical polar coordinates	225
4.9.3	Plane polar coordinates	226
4.10	Boundary conditions for the tangential velocity	228
4.10.1	No-slip boundary condition	228
4.10.2	Slip boundary condition	229
4.11	Wall stresses in Newtonian fluids	229
4.12	Interfacial surfactant transport	231
4.12.1	Two-dimensional interfaces	232
4.12.2	Axisymmetric interfaces	236
4.12.3	Three-dimensional interfaces	238

5	Hydrostatics	241
5.1	Equilibrium of pressure and body forces	241
5.1.1	Equilibrium of an infinitesimal parcel	243
5.1.2	Gases in hydrostatics	246
5.1.3	Liquids in hydrostatics	247
5.2	Force exerted on an immersed surface	250
5.2.1	A sphere floating on a flat interface	250
5.2.2	Newton’s method	253
5.3	Archimedes’ principle	256
5.3.1	Net force on a submerged body	258
5.3.2	Moments	258
5.4	Interfacial shapes	260
5.4.1	Curved interfaces	261
5.4.2	The Laplace-Young equation for a two-dimensional interface	262
5.4.3	Three-dimensional and axisymmetric interfaces	263
5.5	A semi-infinite interface attached to an inclined plate	264
5.5.1	Numerical method	266
5.5.2	A floating cylinder	270
5.6	A meniscus between two parallel plates	273
5.7	A two-dimensional drop on a horizontal plane	282
5.8	A two-dimensional drop on an inclined plane	292
5.8.1	First contact angle specified	295
5.8.2	Specified contact points	302
5.9	Axisymmetric meniscus inside a tube	310
5.10	Axisymmetric drop on a horizontal plane	320
5.11	A sphere straddling an interface	334
5.12	A three-dimensional meniscus	349
5.12.1	Elliptic coordinates	350
5.12.2	Finite-difference method	352
5.12.3	Capillary force and torque	357
6	Equation of motion and vorticity transport	361
6.1	Newton’s second law of motion for a fluid parcel	361
6.1.1	Rate of change of linear momentum	362
6.1.2	Equation of parcel motion	363
6.1.3	Two-dimensional flow	363
6.2	Integral momentum balance	366
6.2.1	Control volume and integral momentum balance	369
6.2.2	Flow through a sudden enlargement	371
6.2.3	Isentropic flow through a conduit	372
6.3	Cauchy’s equation of motion	374
6.3.1	Hydrodynamic volume force	374

6.3.2	Hydrodynamic force on an infinitesimal parcel	375
6.3.3	The equation of motion	376
6.3.4	Evolution equations	377
6.3.5	Cylindrical polar coordinates	377
6.3.6	Spherical polar coordinates	379
6.3.7	Plane polar coordinates	379
6.3.8	Vortex force	380
6.3.9	Summary of governing equation	380
6.3.10	Accelerating frame of reference	381
6.4	Euler and Bernoulli equations	381
6.4.1	Boundary conditions	382
6.4.2	Irrotational flow	383
6.4.3	Torricelli's law	386
6.4.4	Decay of perturbations in a wind or water tunnel	389
6.4.5	Flow of a horizontal stream over a hump	390
6.4.6	Steady rotational flow	391
6.4.7	Flow with uniform vorticity	392
6.5	The Navier–Stokes equation	394
6.5.1	Pressure and viscous forces	395
6.5.2	A radially expanding or contracting bubble	395
6.5.3	Boundary conditions	397
6.5.4	Polar coordinates	398
6.6	Vorticity transport	400
6.6.1	Two-dimensional flow	400
6.6.2	Axisymmetric flow	403
6.6.3	Three-dimensional flow	404
6.7	Dynamic similitude and the Reynolds number	407
6.7.1	Dimensional analysis	410
6.8	Structure of a flow as a function of the Reynolds number	413
6.8.1	Stokes flow	414
6.8.2	Flows at high Reynolds numbers	415
6.8.3	Laminar and turbulent flow	415
6.9	Dimensionless numbers in fluid dynamics	415
7	Channel, tube, and film flow	419
7.1	Steady flow in a two-dimensional channel	419
7.1.1	Alternative coordinates	423
7.1.2	Two-layer flow	426
7.1.3	Multi-layer flow	428
7.1.4	Power-law fluids	435
7.2	Steady film flow down an inclined plane	440
7.2.1	Multi-film flow	441
7.2.2	Power-law fluids	446
7.3	Steady flow through a circular tube	447

7.3.1	Multi-layer tube flow	453
7.3.2	Flow due to a translating sector	458
7.4	Steady flow through an annular tube	461
7.4.1	Small gaps	462
7.4.2	Multi-layer annular flow	464
7.5	Steady flow through channels and tubes	469
7.5.1	Elliptical tube	470
7.5.2	Equilateral triangular tube	472
7.5.3	Rectangular tube	475
7.5.4	Rectangular duct	478
7.5.5	Semi-infinite rectangular channel	480
7.6	Steady swirling flows	483
7.6.1	Annular flow	483
7.6.2	Multi-layer swirling flow	486
7.7	Transient channel flows	491
7.7.1	Couette flow	491
7.7.2	Impulsive motion of a plate in a semi-infinite fluid	494
7.7.3	Pressure- and gravity-driven flow	497
7.8	Oscillatory channel flows	501
7.8.1	Oscillatory Couette flow	501
7.8.2	Rayleigh's oscillating plate	504
7.8.3	Pulsating pressure-driven flow	506
7.9	Transient and oscillatory flow in a circular tube	509
7.9.1	Transient Poiseuille flow	509
7.9.2	Pulsating pressure-driven flow	514
7.9.3	Transient circular Couette flow	517
7.9.4	Orthogonality of Bessel functions	518
8	Finite-difference methods	521
8.1	Choice of governing equations	521
8.2	Unidirectional flow; velocity/pressure formulation	522
8.2.1	Governing equations	523
8.2.2	Explicit finite-difference method	523
8.2.3	Implicit finite-difference method	526
8.2.4	Thomas algorithm	530
8.2.5	Steady state	532
8.2.6	Two-layer flow	533
8.3	Unidirectional flow; velocity/vorticity formulation	540
8.3.1	Boundary conditions for the vorticity	540
8.3.2	Alternative set of equations	541
8.3.3	Comparison with the velocity/pressure formulation	543
8.4	Unidirectional flow; stream function/vorticity formulation	543
8.4.1	Boundary conditions for the vorticity	544

8.4.2	A semi-implicit method	545
8.5	Two-dimensional flow; stream function/vorticity formulation	547
8.5.1	Flow in a cavity	547
8.5.2	Finite-difference grid	549
8.5.3	Unsteady flow	549
8.5.4	Steady flow	551
8.5.5	Summary	557
8.6	Velocity/pressure formulation	559
8.6.1	Alternative system of governing equations	561
8.6.2	Pressure boundary conditions	561
8.6.3	Compatibility condition for the pressure	562
8.7	Operator splitting and solenoidal projection	563
8.7.1	Convection–diffusion step	564
8.7.2	Projection step	566
8.7.3	Boundary conditions for the intermediate velocity	567
8.7.4	Flow in a cavity	568
8.7.5	Computation of the pressure	580
8.8	Staggered grids	582
9	Low-Reynolds-number flow	591
9.1	Flow in a narrow channel	591
9.1.1	Governing equations	592
9.1.2	Scaling	593
9.1.3	Equations of lubrication flow	594
9.1.4	Lubrication flow in a slider bearing	594
9.1.5	Flow in a wavy channel	597
9.1.6	Dynamic lifting	600
9.2	Film flow on a horizontal or inclined wall	610
9.2.1	Thin-film flow	610
9.2.2	Numerical methods	613
9.3	Multi-film flow on a horizontal or inclined wall	615
9.3.1	Evolution equations	619
9.3.2	Numerical methods	620
9.4	Two-layer channel flow	627
9.5	Flow due to the motion of a sphere	639
9.5.1	Formulation in terms of the stream function	640
9.5.2	Traction, force, and the Archimedes–Stokes law	644
9.6	Point forces and point sources in Stokes flow	646
9.6.1	The Oseen tensor and the point force	647
9.6.2	Flow representation in terms of singularities	649
9.6.3	A sphere moving inside a circular tube	649
9.6.4	Boundary integral representation	652
9.7	Two-dimensional Stokes flow	654

9.7.1	Flow due to the motion of a cylinder	654
9.7.2	Rotation of a circular cylinder	657
9.7.3	Simple shear flow past a circular cylinder	658
9.7.4	The Oseen tensor and the point force	658
9.8	Local solutions	660
9.8.1	Solution by separation of variables	660
9.8.2	Stagnation-point flow on a plane wall	661
9.8.3	Flow inside a corner	663
10	High-Reynolds-number flow	669
10.1	Changes in the structure of a flow with increasing Reynolds number	669
10.1.1	Flow past a cylinder	670
10.2	Prandtl boundary-layer analysis	673
10.2.1	Simplifications	673
10.2.2	Boundary-layer equations	676
10.2.3	Surface curvilinear coordinates	677
10.2.4	Parabolization	677
10.2.5	Flow separation	677
10.3	Blasius boundary layer on a semi-infinite plate	678
10.3.1	Self-similarity and the Blasius equation	679
10.3.2	Numerical solution	681
10.3.3	Wall shear stress and drag force	684
10.3.4	Vorticity transport	685
10.4	Displacement and momentum thickness	686
10.4.1	Von Kàrmàn's approximate method	689
10.5	Boundary layers in accelerating or decelerating flow	691
10.5.1	Self-similarity	692
10.5.2	Numerical solution	693
10.6	Momentum integral method	694
10.6.1	The von Kàrmàn–Pohlhausen method	696
10.6.2	Pohlhausen polynomials	696
10.6.3	Numerical solution	699
10.6.4	Boundary layer around a curved body	701
10.7	Instability of shear flows	705
10.7.1	Stability analysis of shear flow	706
10.7.2	Normal-mode analysis	707
10.8	Finite-difference solution of the Rayleigh equation	710
10.8.1	Finite-difference equations	710
10.8.2	A generalized eigenvalue problem	712
10.8.3	Determinant of a tridiagonal matrix	713
10.8.4	Numerical implementation	714
10.9	Finite-difference solution of the Orr–Sommerfeld equation	722

10.10	Turbulent flow	731
10.10.1	Transition to turbulence	733
10.10.2	Lagrangian turbulence	734
10.10.3	Features of turbulent motion	735
10.10.4	Decomposition into mean and fluctuating components	736
10.10.5	Inviscid scales	738
10.10.6	Viscous scales	739
10.10.7	Relation between inviscid and viscous scales	740
10.11	Spectrum of a turbulent flow	741
10.12	Analysis and modeling of turbulent flow	745
10.12.1	Reynolds stresses	745
10.12.2	Prandtl's mixing length	747
10.12.3	Logarithmic law for wall-bounded shear flow	749
10.12.4	Correlations	750
11	Vortex motion	753
11.1	Vorticity and circulation in two-dimensional flow	753
11.2	Point vortices	755
11.2.1	Dirac's delta function in a plane	756
11.2.2	Evolution of the point vortex strength	758
11.2.3	Velocity of a point vortex	758
11.2.4	Motion of a collection of point vortices	758
11.2.5	Effect of boundaries	759
11.2.6	A periodic array of point vortices	761
11.2.7	A point vortex between two parallel walls	765
11.2.8	A point vortex in a semi-infinite strip	766
11.3	Two-dimensional flow with distributed vorticity	767
11.3.1	Vortex patches with uniform vorticity	769
11.3.2	Contour dynamics	772
11.3.3	Gauss integration quadrature	774
11.3.4	Representation with circular arcs	775
11.4	Vorticity and circulation in three-dimensional flow	780
11.4.1	Preservation of circulation	781
11.4.2	Flow induced by vorticity	783
11.5	Axisymmetric flow induced by vorticity	784
11.5.1	Biot–Savart integral for axisymmetric flow	786
11.5.2	Line vortex ring	789
11.5.3	Vortex ring with finite core	791
11.5.4	Motion of a collection of vortex rings	795
11.5.5	Vortex patch in axisymmetric flow	796
11.6	Three-dimensional vortex motion	798
11.6.1	Vortex particles	799
11.6.2	Line vortices and the local-induction approximation (LIA)	799

12 Aerodynamics	803
12.1 General features of flow past an aircraft	803
12.2 Airfoils and the Kutta–Joukowski condition	805
12.2.1 The Kutta–Joukowski theorem	810
12.2.2 The Kutta–Joukowski condition	811
12.3 Vortex panels	812
12.3.1 From point vortices to vortex panels	813
12.3.2 Vortex panels with uniform strength	814
12.3.3 Vortex panel with linear strength density	816
12.4 Vortex panel method	819
12.4.1 Velocity in terms of the panel strength	822
12.4.2 Point collocation	823
12.4.3 Circulation and pressure coefficient	824
12.4.4 Lift	825
12.4.5 Vortex panel code	827
12.5 Vortex sheet representation	833
12.5.1 Thin airfoil theory	834
12.6 Point-source-dipole panels	842
12.6.1 Source-dipole panel method	844
12.6.2 Source-dipole representation	845
12.6.3 Solution of the interior problem	846
12.7 Point-source panels and Green’s third identity	847
12.7.1 Source panels with constant density	848
12.7.2 Green’s third identity	849
A FDLIB Software Library	853
B References	864
C Matlab Primer	866
C.1 Launching MATLAB	866
C.2 MATLAB programming	867
C.3 MATLAB commands	869
C.4 MATLAB examples	873
C.5 MATLAB functions	876
C.6 User-defined functions	876
C.7 MATLAB graphics	881
Index	889

Preface

Ready access to computers has defined a new era in teaching and learning. The opportunity to extend the subject matter of traditional science and engineering curricula into the realm of scientific computing has become not only desirable, but also necessary. Thanks to portability and low overhead and operating cost, experimentation by numerical simulation has become a viable substitute, and occasionally the only alternative, to physical experimentation.

The new framework has necessitated the writing of texts and monographs from a modern perspective that incorporates numerical and computer programming aspects as an integral part of the discourse. Under this modern approach, methods, concepts, and ideas are presented in a unified fashion that motivates and underlines the urgency of the new elements, but neither compromises nor oversimplifies the rigor of the classical discourse.

Interfacing fundamental concepts and practical methods of scientific computing can be implemented at different levels. In one approach, theory and implementation are kept complementary and presented in a sequential fashion. In another approach, the coupling involves deriving computational methods and simulation algorithms, and translating equations into computer code instructions immediately following problem formulations. Seamlessly interjecting methods of scientific computing in the traditional discourse offers a powerful venue for developing analytical skills and obtaining physical insight.

My goal in this book is to offer an introductory course in traditional and modern fluid mechanics, covering topics in a way that unifies theory, computation, computer programming, and numerical simulation. The approach is truly introductory in that only a few prerequisites are required. The intended audience includes undergraduate and entry-level graduate students, as well as a broader class of scientists, engineers, fluid dynamics and computational science enthusiasts with a general interest in computing. This book should be especially appealing to those who are making a first excursion into the world of numerical computation and computational fluid dynamics (CFD) beyond the black-box and drop-down menu approach. This book should be an ideal text for an introductory course in fluid mechanics and CFD.

The presentation of the material is distinguished by two features. First, solution procedures and algorithms are developed immediately after problem formulations are presented, and illustrative MATLAB[®] codes are listed and discussed in the text. Second, numerical methods are introduced on a need-to-know basis and in order of ascending difficulty: function interpolation, function differentiation, function integration, solution of algebraic equations, finite-difference methods, etc. Computer problems at the end of each section require performing computation and simulation to study the effect of various parameters determining a flow.

In concert with the intended usage of this book as a stand-alone introductory text and as a tutorial on numerical fluid dynamics and scientific computing, only a few references are

provided in the discussion. Instead, a selected compilation of introductory, advanced, and specialized texts on fluid dynamics, calculus, numerical methods, and computational fluid dynamics are listed in Appendix B. The reader who wishes to focus on a particular topic is directed to these resources for further details.

FDLIB

A major feature of this book is the accompanying fluid dynamics software library **FDLIB** discussed in Appendix A. The FORTRAN 77 and MATLAB programs of **FDLIB** explicitly illustrate how computational algorithms translate into computer instructions. The codes of **FDLIB** range from introductory to advanced, and the topics span a broad range of applications discussed in this text: from laminar channel flows, to vortex flows, to flow past airfoils. The MATLAB codes of **FDLIB** combine numerical computation, graphics display, data visualization and animation.

To run the FORTRAN 77 codes of **FDLIB**, a FORTRAN 77 or FORTRAN 90 compiler is required. Free compilers are available thanks to the gnu foundation. The input data is either entered from the keyboard or read from data files. The output is recorded in output files in tabular form so that it can be read and displayed using independent graphics, visualization, and animation applications on any computer platform, including MATLAB.

Third edition

The third edition incorporates significant enhancements and improvements. Further examples, clarifications, solved problems, and new material have been added for a more comprehensive treatment of the various topics. Additional MATLAB programs integrating numerical computation and graphics visualization are listed and discussed in the text. The revised text refers to the latest version of the accompanying library **FDLIB**. The integrated approach pursued in this book overrides the Graphical User Interface or black-box approach, which is often misrepresented as an educational or learning tool. The book Internet site is located at: <http://dehesa.freeshell.org/FD3>

C. Pozrikidis

Notation

Italic symbols denote scalars. Bold symbols denote vectors, matrices, or tensors. Some symbols have multiple meanings.

a	acceleration vector	Bo	Bond number
e	unit vector	E	rate-of-deformation tensor
<i>g</i>	acceleration of gravity		
g	acceleration of gravity vector	J_p	Bessel function of order p
		L	characteristic length
<i>p</i>	pressure		
<i>t</i>	time	U	fluid velocity
u	fluid velocity	V	boundary velocity
		X	position of a point particle
x	position vector	Q	flow rate
		Re	Reynolds number
α	rate of expansion		
γ	surface (interfacial) tension or strength of a vortex sheet		
κ	curvature strength of a point vortex		
κ_m	mean curvature	Σ	hydrodynamic volume force
ρ	density		
μ	viscosity		
ν	viscosity		
σ	stress tensor		
ϕ	velocity potential	Ξ	vorticity tensor
χ	projection function	Ω	angular velocity
ψ	stream function		
ω	vorticity		
(x, y, z)	Cartesian coordinates		
(x, σ, φ)	Cylindrical polar coordinates		
(x, θ, φ)	Spherical polar coordinates		
∇	gradient operator		
∇^2	Laplacian operator		
ℓ	arc length or a typical length		

Introduction to kinematics

- 1.1 Fluids and solids**
- 1.2 Fluid parcels and flow kinematics**
- 1.3 Coordinates, velocity, and acceleration**
- 1.4 Fluid velocity**
- 1.5 Point particles and their trajectories**
- 1.6 Material surfaces and elementary motions**
- 1.7 Numerical interpolation**

We begin the study of fluid mechanics by pointing out the differences between fluids and solids and by describing a fluid flow in terms of the motion of elementary fluid parcels. As the volume of a parcel becomes infinitesimal, the parcel reduces to a point particle and the average velocity of the parcel reduces to the local fluid velocity computed just before the molecular nature of the fluid becomes apparent. The study of the motion and deformation of material lines and surfaces consisting of collections of point particles reveals the nature and illustrates the diversity of motion in fluid mechanics.

1.1 Fluids and solids

Casual observation of the world around us reveals materials that are classified as solids and fluids; the second category includes gases and liquids. What are the distinguishing features of these two groups? The answer can be given on a wide variety of levels: from the molecular level of the physicist, to the macroscopic level of the engineer or oceanographer, to the cosmic level of the astronomer.

From the perspective of mainstream fluid mechanics underlying this book, the single most important difference between fluids and solids is that a fluid must assume the shape of the container in which it is placed, whereas a solid is able to stand alone, sustaining its own shape. As a consequence, a body of fluid is not able to resist a shearing force exerted on its surface parallel to the surface, but must keep deforming in perpetuity when subjected to it. An example is the motion of water in a lake due to an overpassing wind. In contrast, a solid is able to deform and assume a new stationary shape. An example is the deformation of a squeezed sponge.

Certain materials, such as polymeric melts and solutions, exhibit properties that are intermediate between those of fluids and solids in that they exhibit viscous and elastic response. These materials are classified as viscoelastic.

Intermolecular forces

The differences between fluids and solids can be attributed to the intensity of the forces holding the molecules together to form a coherent piece of material. The inability of a fluid to assume its own shape is due to the weakness of the potential energy associated with intermolecular forces relative to the kinetic energy associated with the vibrations of the individual molecules. The molecules of a fluid are too busy vibrating to hang onto one another and thus form a long-lived crystalline material.

Fluids can be transformed into solids, and *vice versa*, by manipulating the relative magnitude of the potential energy due to intermolecular forces and the kinetic energy due to thermal motion. In practice, this is done by heating or by changing the pressure of the ambient environment.

PROBLEMS

1.1.1 Nature of a liquid/solid suspension

Fluids containing particles, called suspensions, abound in nature, physiology, and technology. Examples include (a) blood consisting of a dense suspension of red, white, and other blood cells, (b) slurry used in the petroleum industry for the hydrodynamic transport of particulates, (c) toothpaste and dough. Discuss whether a suspension should be classified as a fluid or solid with reference to the volume fraction of the suspended solid phase.

1.1.2 Water and milk

A glass is filled half way with water, and another glass is filled half way with milk. Half the water is transfer into the milk glass and the contents of the milk glass are thoroughly mixed. One third of the diluted milk is then transferred back into the water glass and the contents of the water glass are thoroughly mixed. What is the volume and constitution of the liquid in each glass at the end?

1.2 Fluid parcels and flow kinematics

The motion of a non-deformable solid body, called a rigid body, can be described in terms of the velocity of translation vector, \mathbf{V} , and the angular velocity of rotation vector, $\boldsymbol{\Omega}$, where rotation occurs around a specified center of rotation, as shown in [Figure 1.2.1](#). A rigid body moves as a whole in the direction of the velocity vector, while rotating as a whole around the angular velocity vector that is pinned at the designated center of rotation. For example, a rigid sphere translates with the velocity of its center, while rotating about the center.

In contrast, the motion of a deformable body, such as an elastic solid or a fluid, cannot generally be described in terms of two vectors alone. A more advanced framework that

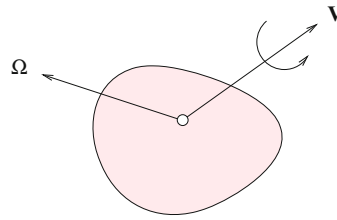


Figure 1.2.1 A rigid body translates with velocity \mathbf{V} while rotating with angular velocity Ω around a specified center of rotation. A fluid exhibits a more general type of motion that involves local or global deformation in addition to local or global translation and rotation.

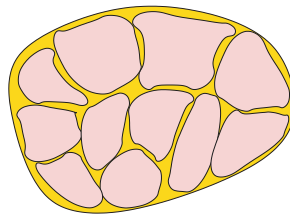


Figure 1.2.2 A body of fluid can be divided into small parcels whose relative motion determines the local fluid flow in a certain neighborhood. The parcels are drawn detached for clarity and esthetics.

allows for an extended range of motions, in addition to translation and rotation, is required.

Decomposition of a fluid into parcels

To establish the necessary generalized framework, we subdivide a body of fluid into parcels, as shown in [Figure 1.2.2](#). For simplicity, we assume that all molecules comprising the parcels are identical, which means that the fluid is homogeneous. Each molecule in a certain parcel moves with its own highly fluctuating velocity. However, if the parcel exhibits a net motion, the velocities of the individual molecules are coordinated to reflect or, more accurately, give rise to the net motion. A molecule of a gas collides frequently with other molecules after having traveled a distance comparable to the mean free path.

The macroscopic motion of a small fluid parcel can be described in terms of its velocity of translation, which can be quantified in terms of the average velocity of the individual molecules, as will be discussed in [Section 1.3](#). If the parcel is sufficiently small, rotation is neglected as a first approximation.

Relative parcel motion

A key observation is that the motion of a fluid can be described in terms of the *relative* motion of the individual fluid parcels. If all parcels move with the same velocity, the relative parcel velocity is zero and the fluid translates as a rigid body. It is possible that the velocity

of the parcels is coordinated so that the fluid rotates as a whole like a rigid body about a designated center of rotation.

As an example, we consider a fluid-filled flexible rubber tube that is closed at both ends, and assume that the tube is stretched to elongate the fluid. The fluid has undergone neither translation nor rotation, but a new type of motion that can only be described as deformation. Combinations of translation, rotation, and deformation whose relative strength varies with position in the fluid gives rise to a wide variety of fluid motions.

Kinematics as a field of fluid dynamics

Establishing in quantitative terms the relationship between the relative motion of fluid parcels and the global structure of a flow is the main objective of kinematics. The term *kinematics* derives from the Greek work *κίνησις* which means *motion*. Grammatically, *kinematics* is a singular or plural noun, whereas *kinematic* is an adjective. The complementary discipline of dynamics (*δυναμική*) addresses the forces exerted on a fluid by an ambient surface or body force field, such as the gravitational field, as well as the forces developing inside a fluid as the result of the motion.

PROBLEM

1.2.1 *Athens, Ohio*

A car with 18" diameter tires is driven from Athens, Ohio to Athens, Georgia. How many times have the wheels turned during the journey?

1.2.2 *A rolling sphere*

A sphere of radius a is rolling down a plane on a rectilinear path. How is the velocity at the center of the sphere, V , related to the angular velocity of rotation about the center of the sphere, Ω ?

1.3 Coordinates, velocity, and acceleration

To describe the motion of a molecule, we work under the auspices of classical mechanics. We begin by introducing three mutually orthogonal axes forming a Cartesian coordinate system, (x, y, z) , as illustrated in [Figure 1.3.1](#). Each point in space has an associated position vector that starts at the common origin of the Cartesian axes and ends at the point. The point is identified by the values of x , y , and z , defined as the positive or negative projections of the position vector onto the corresponding axes.

In vector notation, the Cartesian coordinates are expressed by an ordered triplet

$$\mathbf{x} = (x, y, z), \tag{1.3.1}$$

where x , y , and z take values in the range $(-\infty, \infty)$. Accordingly, the Cartesian coordinates of a point have a dual interpretation: *they represent a geometrical entity associated with the position vector, and they also form an ordered triplet of real numbers.*

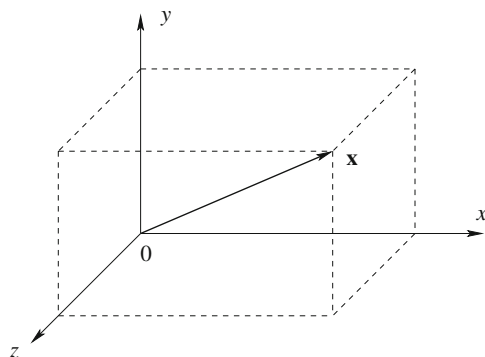


Figure 1.3.1 Three mutually orthogonal axes define a Cartesian coordinate system, (x, y, z) . The arrow indicates the position vector corresponding to a point, \mathbf{x} .

Unit vectors

The three dimensionless (unit-less) vectors,

$$\mathbf{e}_x = (1, 0, 0), \quad \mathbf{e}_y = (0, 1, 0), \quad \mathbf{e}_z = (0, 0, 1), \quad (1.3.2)$$

point in the positive directions of the x , y , or z axis. The end points of these vectors lie on the x , y , or z axis. We say that the three vectors \mathbf{e}_x , \mathbf{e}_y , and \mathbf{e}_z are mutually orthogonal Cartesian unit vectors.

Combining these definitions, we express the position vector in the form

$$\mathbf{x} = x \mathbf{e}_x + y \mathbf{e}_y + z \mathbf{e}_z. \quad (1.3.3)$$

In physical terms, this equation states that, to get to the point \mathbf{x} departing from the origin, we may move along each one of the unit vectors \mathbf{e}_x , \mathbf{e}_y , and \mathbf{e}_z , by respective distances equal to x , y , and z units of length. The order of motion along the three directions is immaterial.

Velocity

Because a molecule moves with a highly fluctuating velocity, its position changes rapidly in time. Formally, we say that the coordinates of the molecule are functions of time, t , denoted by

$$x = X(t), \quad y = Y(t), \quad z = Z(t). \quad (1.3.4)$$

To economize our notation, we introduce the vector function

$$\mathbf{X}(t) = (X(t), Y(t), Z(t)), \quad (1.3.5)$$

and consolidate expressions (1.3.4) into the form

$$\mathbf{x} = \mathbf{X}(t). \quad (1.3.6)$$

By definition, the velocity of a molecule is equal to the rate of change of its position, displacement over time elapsed. If the x coordinate of a molecule has changed by an infinitesimal increment, dX , during an infinitesimal period of time, dt , then, by definition, $v_x = dX/dt$. Writing the counterparts of this equation for the y and z coordinates, and collecting the three expressions, we obtain

$$v_x = \frac{dX}{dt}, \quad v_y = \frac{dY}{dt}, \quad v_z = \frac{dZ}{dt}, \quad (1.3.7)$$

which can be compiled into an ordered triplet,

$$(v_x, v_y, v_z) = \left(\frac{dX}{dt}, \frac{dY}{dt}, \frac{dZ}{dt} \right). \quad (1.3.8)$$

In vector notation,

$$\mathbf{v} = \frac{d\mathbf{X}}{dt}. \quad (1.3.9)$$

We have demonstrated that the velocity of a molecule is a vector described by its three Cartesian components, v_x , v_y , and v_z , representing the positive or negative distances between the projections of the last and first points of the velocity vector onto the x , y , or z axis. The distances are then multiplied by a scaling factor to acquire units of velocity, length divided by time. A negative value for v_x indicates that the x coordinate of the last point of the velocity vector is lower than the x value of the first point, and therefore the motion occurs toward the negative direction of the x axis. Similar interpretations apply to the y and z components.

In terms of the unit vectors defined in equations (1.3.2), the velocity vector is given by

$$\mathbf{v} = v_x \mathbf{e}_x + v_y \mathbf{e}_y + v_z \mathbf{e}_z. \quad (1.3.10)$$

It is evident from these definitions that the velocity vector is a free Cartesian vector, which means that it can be translated in space to any desired location. In contrast, the first point of the position vector, \mathbf{x} , is always pinned to the origin.

Acceleration

The acceleration vector, \mathbf{a} , is defined as the rate of change of the velocity vector in time,

$$\mathbf{a} = \frac{d\mathbf{v}}{dt} = \frac{d^2\mathbf{X}}{dt^2}. \quad (1.3.11)$$

By definition then,

$$\mathbf{a} = a_x \mathbf{e}_x + a_y \mathbf{e}_y + a_z \mathbf{e}_z, \quad (1.3.12)$$

where the Cartesian components of the acceleration vector are given by

$$a_x = \frac{d^2X}{dt^2}, \quad a_y = \frac{d^2Y}{dt^2}, \quad a_z = \frac{d^2Z}{dt^2}. \quad (1.3.13)$$

If the Cartesian coordinates of a molecule are constant or change linearly in time, the second time derivatives vanish and the acceleration is zero.

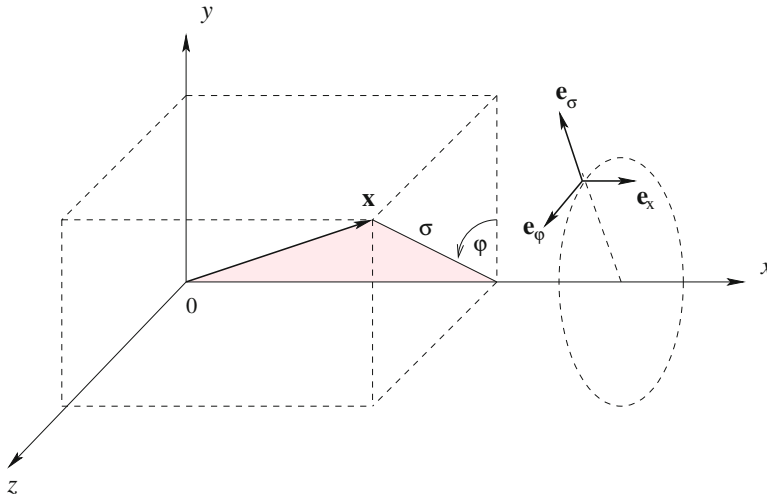


Figure 1.3.2 Illustration of cylindrical polar coordinates, (x, σ, φ) , defined with respect to Cartesian coordinates, (x, y, z) , where σ is the distance from the x axis.

1.3.1 Cylindrical polar coordinates

A point in space can be identified by the values of an ordered triplet, (x, σ, φ) , as illustrated in [Figure 1.3.2](#), where:

- x is the projection of the position vector onto the straight (rectilinear) x axis passing through a designated origin, taking values in the range $(-\infty, +\infty)$.
- σ is the distance of a point of interest from the x axis, taking values in the range $[0, \infty)$.
- φ is the azimuthal angle measured around the x axis, taking values in the range $[0, 2\pi)$. The value $\varphi = 0$ corresponds to the first and second quadrants of the xy plane, and the value $\varphi = \pi$ corresponds to the third and fourth quadrants.

Using elementary trigonometry, we derive relations between the Cartesian and associated polar cylindrical coordinates,

$$y = \sigma \cos \varphi, \quad z = \sigma \sin \varphi. \quad (1.3.14)$$

The inverse relations between the polar cylindrical and Cartesian coordinates are

$$\sigma = \sqrt{y^2 + z^2}, \quad \varphi = \arccos \frac{y}{\sigma}. \quad (1.3.15)$$

In computing the inverse cosine function, arccos, care must be taken to ensure that the azimuthal angle, φ , is a continuous function of y and σ with reference to a specified branch cut.

Unit vectors

Consider an arbitrary point in space and define three dimensionless unit vectors, denoted by \mathbf{e}_x , \mathbf{e}_σ , and \mathbf{e}_φ , pointing in the direction of the x axis, normal to the x axis, and in the azimuthal direction of varying angle φ , respectively, as depicted in [Figure 1.3.2](#). Note that the orientation of the unit vectors \mathbf{e}_σ and \mathbf{e}_φ changes with position in space, whereas the orientation of the unit vector \mathbf{e}_x is fixed and independent of position in space.

Position and velocity

In terms of the first two local unit vectors, \mathbf{e}_x and \mathbf{e}_σ , the position vector is given by

$$\mathbf{x} = x \mathbf{e}_x + \sigma \mathbf{e}_\sigma. \quad (1.3.16)$$

The dependence of the position vector on the azimuthal angle, φ , is mediated through the unit vector \mathbf{e}_σ on the right-hand side. The absence of \mathbf{e}_φ from the right-hand side of (1.3.16) can be justified by observing that the distance from the origin, expressed by the position vector \mathbf{x} , is perpendicular to the third unit vector, \mathbf{e}_φ .

Correspondingly, the velocity vector at a point can be expressed in the form

$$\mathbf{v} = v_x \mathbf{e}_x + v_\sigma \mathbf{e}_\sigma + v_\varphi \mathbf{e}_\varphi, \quad (1.3.17)$$

where the coefficients v_x , v_σ , and v_φ are the cylindrical polar components of the velocity.

Relation to Cartesian vector components

Using elementary trigonometry, we derive relations between the Cartesian and cylindrical polar unit vectors,

$$\mathbf{e}_\sigma = \cos \varphi \mathbf{e}_y + \sin \varphi \mathbf{e}_z, \quad \mathbf{e}_\varphi = -\sin \varphi \mathbf{e}_y + \cos \varphi \mathbf{e}_z. \quad (1.3.18)$$

The inverse relations are

$$\mathbf{e}_y = \cos \varphi \mathbf{e}_\sigma - \sin \varphi \mathbf{e}_\varphi, \quad \mathbf{e}_z = \sin \varphi \mathbf{e}_\sigma + \cos \varphi \mathbf{e}_\varphi. \quad (1.3.19)$$

The corresponding relations for the velocity components are

$$v_\sigma = \cos \varphi v_y + \sin \varphi v_z, \quad v_\varphi = -\sin \varphi v_y + \cos \varphi v_z \quad (1.3.20)$$

and

$$v_y = \cos \varphi v_\sigma - \sin \varphi v_\varphi, \quad v_z = \sin \varphi v_\sigma + \cos \varphi v_\varphi. \quad (1.3.21)$$

The Cartesian and cylindrical polar components of other vectors transform in similar ways.

Rates of change

The counterparts of expressions (1.3.4) for the cylindrical polar coordinates are

$$x = X(t), \quad \sigma = \Sigma(t), \quad \varphi = \Phi(t). \quad (1.3.22)$$

The rates of change of the unit vectors following the motion of a molecule are given by the relations

$$\frac{d\mathbf{e}_x}{dt} = \mathbf{0}, \quad \frac{d\mathbf{e}_\sigma}{dt} = \frac{d\Phi}{dt} \mathbf{e}_\varphi, \quad \frac{d\mathbf{e}_\varphi}{dt} = -\frac{d\Phi}{dt} \mathbf{e}_\sigma. \quad (1.3.23)$$

Consistent with our earlier observation, the first unit vector, \mathbf{e}_x , is fixed, while the second and third unit vectors, \mathbf{e}_σ and \mathbf{e}_φ , change with position in space.

Velocity components

Substituting expressions (1.3.22) into the right-hand side of (1.3.16), taking the time derivative, and using expressions (1.3.23), we find that

$$\frac{d\mathbf{X}}{dt} = \frac{d}{dt}(X \mathbf{e}_x + \Sigma \mathbf{e}_\sigma) = \frac{dX}{dt} \mathbf{e}_x + X \frac{d\mathbf{e}_x}{dt} + \frac{d\Sigma}{dt} \mathbf{e}_\sigma + \Sigma \frac{d\mathbf{e}_\sigma}{dt}, \quad (1.3.24)$$

and then

$$\frac{d\mathbf{X}}{dt} = \frac{dX}{dt} \mathbf{e}_x + \frac{d\Sigma}{dt} \mathbf{e}_\sigma + \Sigma \frac{d\Phi}{dt} \mathbf{e}_\varphi. \quad (1.3.25)$$

Comparing this expression with the decomposition (1.3.17), we extract the cylindrical polar components of the velocity,

$$v_x = \frac{dX}{dt}, \quad v_\sigma = \frac{d\Sigma}{dt}, \quad v_\varphi = \Sigma \frac{d\Phi}{dt}. \quad (1.3.26)$$

Since Φ is a dimensionless function, all three right-hand sides have units of length divided by time.

Acceleration

Differentiating expression (1.3.25) with respect to time, t , and expanding the derivatives, we find that

$$\frac{d^2\mathbf{X}}{dt^2} = \frac{d}{dt} \left(\frac{dX}{dt} \mathbf{e}_x + \frac{d\Sigma}{dt} \mathbf{e}_\sigma + \Sigma \frac{d\Phi}{dt} \mathbf{e}_\varphi \right). \quad (1.3.27)$$

Carrying out the differentiations, we obtain

$$\frac{d^2\mathbf{X}}{dt^2} = \frac{d^2X}{dt^2} \mathbf{e}_x + \frac{d^2\Sigma}{dt^2} \mathbf{e}_\sigma + \frac{d\Sigma}{dt} \frac{d\mathbf{e}_\sigma}{dt} + \frac{d\Sigma}{dt} \frac{d\Phi}{dt} \mathbf{e}_\varphi + \Sigma \frac{d^2\Phi}{dt^2} \mathbf{e}_\varphi + \Sigma \frac{d\Phi}{dt} \frac{d\mathbf{e}_\varphi}{dt}. \quad (1.3.28)$$

Now we substitute expressions (1.3.23) and find that

$$\frac{d^2\mathbf{X}}{dt^2} = \frac{d^2X}{dt^2} \mathbf{e}_x + \frac{d^2\Sigma}{dt^2} \mathbf{e}_\sigma + \frac{d\Sigma}{dt} \frac{d\Phi}{dt} \mathbf{e}_\varphi + \frac{d\Sigma}{dt} \frac{d\Phi}{dt} \mathbf{e}_\varphi + \Sigma \frac{d^2\Phi}{dt^2} \mathbf{e}_\varphi - \Sigma \frac{d\Phi}{dt} \frac{d\Phi}{dt} \mathbf{e}_\sigma. \quad (1.3.29)$$

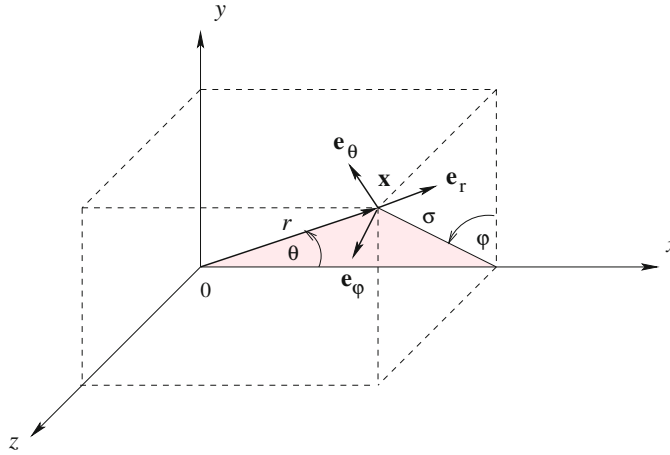


Figure 1.3.3 Illustration of spherical polar coordinates, (r, θ, φ) , defined with respect to the Cartesian coordinates, (x, y, z) , and cylindrical polar coordinates, (x, σ, φ) , where r is the distance from the origin, θ is the meridional angle, φ is the azimuthal angle, and σ is the distance from the x axis.

Finally, we consolidate the terms on the right-hand side and derive the cylindrical polar components of the acceleration vector,

$$\begin{aligned}
 a_x &= \frac{d^2 X}{dt^2}, & a_\sigma &= \frac{d^2 \Sigma}{dt^2} - \Sigma \left(\frac{d\Phi}{dt} \right)^2, \\
 a_\varphi &= \Sigma \frac{d^2 \Phi}{dt^2} + 2 \frac{d\Sigma}{dt} \frac{d\Phi}{dt} = \frac{1}{\Sigma} \frac{d}{dt} \left(\Sigma^2 \frac{d\Phi}{dt} \right).
 \end{aligned}
 \tag{1.3.30}$$

Note that a change in the azimuthal angle determined by the function Φ is accompanied by radial acceleration, a_σ .

1.3.2 Spherical polar coordinates

An arbitrary point in space can be identified by the values of an ordered triplet (r, θ, φ) , as illustrated in [Figure 1.3.3](#), where:

- r is the distance from the designated origin taking values in the range $[0, \infty)$.
- θ is the meridional angle subtended between the x axis, the origin, and the chosen point, taking values in the range $[0, \pi]$.
- φ is the azimuthal angle measured around the x axis, taking values in the range $[0, 2\pi)$. The value $\varphi = 0$ corresponds to the first and second quadrants of the xy plane, and the value $\varphi = \pi$ corresponds to the third and fourth quadrants.

Using elementary trigonometry, we derive relations between the Cartesian, cylindrical polar, and spherical polar coordinates,

$$x = r \cos \theta, \quad \sigma = r \sin \theta,
 \tag{1.3.31}$$

and

$$y = \sigma \cos \varphi = r \sin \theta \cos \varphi, \quad z = \sigma \sin \varphi = r \sin \theta \sin \varphi. \quad (1.3.32)$$

The inverse relations are

$$r = \sqrt{x^2 + y^2 + z^2} = \sqrt{x^2 + \sigma^2}, \quad \theta = \arccos \frac{x}{r}, \quad \varphi = \arccos \frac{y}{\sigma}. \quad (1.3.33)$$

In computing the inverse cosine functions, care must be taken so that θ and φ emerge as continuous functions of x , y , r , and σ .

Unit vectors

Consider a point in space and define three dimensionless unit vectors, \mathbf{e}_r , \mathbf{e}_θ , and \mathbf{e}_φ , pointing in the radial, meridional, and azimuthal directions, respectively, as illustrated in [Figure 1.3.3](#). Note that the orientations of all three unit vectors change with position in space. In contrast the orientations of the Cartesian unit vectors, \mathbf{e}_x , \mathbf{e}_y , and \mathbf{e}_z , are fixed.

Position and velocity

In terms of the local unit vectors \mathbf{e}_r , \mathbf{e}_θ , and \mathbf{e}_φ , the position vector is given by

$$\mathbf{x} = r \mathbf{e}_r. \quad (1.3.34)$$

The dependence on θ and φ is mediated through the unit vector \mathbf{e}_r on the right-hand side. The absence of \mathbf{e}_θ and \mathbf{e}_φ from the right-hand side of (1.3.34) can be explained by observing that the distance from the origin, expressed by the position vector \mathbf{x} , is perpendicular to the unit vectors \mathbf{e}_θ and \mathbf{e}_φ .

Correspondingly, the velocity vector is given by

$$\mathbf{v} = v_r \mathbf{e}_r + v_\theta \mathbf{e}_\theta + v_\varphi \mathbf{e}_\varphi, \quad (1.3.35)$$

where the coefficients v_r , v_θ , and v_φ are the spherical polar components of the velocity.

Relation to Cartesian vector components

Using elementary trigonometry, we derive relations between the spherical polar, cylindrical polar, and Cartesian unit vectors,

$$\begin{aligned} \mathbf{e}_r &= \cos \theta \mathbf{e}_x + \sin \theta \cos \varphi \mathbf{e}_y + \sin \theta \sin \varphi \mathbf{e}_z = \cos \theta \mathbf{e}_x + \sin \theta \mathbf{e}_\sigma, \\ \mathbf{e}_\theta &= -\sin \theta \mathbf{e}_x + \cos \theta \cos \varphi \mathbf{e}_y + \cos \theta \sin \varphi \mathbf{e}_z = -\sin \theta \mathbf{e}_x + \cos \theta \mathbf{e}_\sigma, \\ \mathbf{e}_\varphi &= -\sin \varphi \mathbf{e}_y + \cos \varphi \mathbf{e}_z. \end{aligned} \quad (1.3.36)$$

The corresponding relations for the velocity components are

$$\begin{aligned} v_r &= \cos \theta v_x + \sin \theta \cos \varphi v_y + \sin \theta \sin \varphi v_z = \cos \theta v_x + \sin \theta v_\sigma, \\ v_\theta &= -\sin \theta v_x + \cos \theta \cos \varphi v_y + \cos \theta \sin \varphi v_z = -\sin \theta v_x + \cos \theta v_\sigma, \\ v_\varphi &= -\sin \varphi v_y + \cos \varphi v_z. \end{aligned} \quad (1.3.37)$$

The Cartesian and polar components of other vectors transform in similar ways.

Rates of change

The counterparts of expressions (1.3.4) for the spherical polar coordinates are

$$r = R(t), \quad \theta = \Theta(t), \quad \varphi = \Phi(t). \quad (1.3.38)$$

The rate of change of the unit vectors following the motion of a molecule is given by the relations

$$\begin{aligned} \frac{d\mathbf{e}_r}{dt} &= \frac{d\Phi}{dt} \sin\theta \mathbf{e}_\varphi + \frac{d\Theta}{dt} \mathbf{e}_\theta, & \frac{d\mathbf{e}_\theta}{dt} &= \frac{d\Phi}{dt} \cos\theta \mathbf{e}_\varphi - \frac{d\Theta}{dt} \mathbf{e}_r, \\ \frac{d\mathbf{e}_\varphi}{dt} &= -\frac{d\Phi}{dt} \cos\theta \mathbf{e}_\theta - \frac{d\Theta}{dt} \sin\theta \mathbf{e}_r. \end{aligned} \quad (1.3.39)$$

All three unit vectors change with position in space.

Velocity components

Substituting the first expression in (1.3.38) into the right-hand side of (1.3.50), and using (1.3.39), we obtain

$$\frac{d\mathbf{X}}{dt} = \frac{dR}{dt} \mathbf{e}_r + R \frac{d\mathbf{e}_r}{dt} = \frac{dR}{dt} \mathbf{e}_r + R \frac{d\Phi}{dt} \sin\theta \mathbf{e}_\varphi + R \frac{d\Theta}{dt} \mathbf{e}_\theta. \quad (1.3.40)$$

Comparing this expression with the decomposition (1.3.35), we derive expressions for the spherical polar components of the velocity,

$$v_r = \frac{dR}{dt}, \quad v_\theta = R \frac{d\Theta}{dt}, \quad v_\varphi = R \sin\theta \frac{d\Phi}{dt}. \quad (1.3.41)$$

Since the functions Θ and Φ are dimensionless, all three right-hand sides have units of length divided by time.

Acceleration

Differentiating expression (1.3.40) with respect to time, t , and expanding the derivatives, we find that

$$\begin{aligned} \frac{d^2\mathbf{X}}{dt^2} &= \left(\frac{d^2R}{dt^2} \mathbf{e}_r + \frac{dR}{dt} \frac{d\mathbf{e}_r}{dt} \right) + \left(\frac{dR}{dt} \frac{d\Phi}{dt} \sin\theta \mathbf{e}_\varphi + R \frac{d^2\Phi}{dt^2} \sin\theta \mathbf{e}_\varphi \right. \\ &\quad \left. + R \frac{d\Phi}{dt} \cos\theta \frac{d\Theta}{dt} \mathbf{e}_\varphi + R \frac{d\Phi}{dt} \sin\theta \frac{d\mathbf{e}_\varphi}{dt} \right) + \left(\frac{dR}{dt} \frac{d\Theta}{dt} \mathbf{e}_\theta + R \frac{d^2\Theta}{dt^2} \mathbf{e}_\theta + R \frac{d\Theta}{dt} \frac{d\mathbf{e}_\theta}{dt} \right), \end{aligned} \quad (1.3.42)$$

where the parentheses enclose terms originating from each term on the right-hand side of (1.3.40).

Now we substitute expressions (1.3.39) and obtain

$$\frac{d^2\mathbf{X}}{dt^2} = \mathbf{A} + \mathbf{B} + \mathbf{C}, \quad (1.3.43)$$

where the first contribution to the right-hand side is

$$\mathbf{A} = \frac{d^2R}{dt^2} \mathbf{e}_r + \frac{dR}{dt} \frac{d\Phi}{dt} \sin \theta \mathbf{e}_\varphi + \frac{dR}{dt} \frac{d\Theta}{dt} \mathbf{e}_\theta, \quad (1.3.44)$$

the second contribution is

$$\begin{aligned} \mathbf{B} = \frac{dR}{dt} \frac{d\Phi}{dt} \sin \theta \mathbf{e}_\varphi + R \frac{d^2\Phi}{dt^2} \sin \theta \mathbf{e}_\varphi + R \frac{d\Phi}{dt} \frac{d\Theta}{dt} \cos \theta \mathbf{e}_\varphi, \\ - R \left(\frac{d\Phi}{dt} \right)^2 \sin \theta (\sin \theta \mathbf{e}_r + \cos \theta \mathbf{e}_\theta), \end{aligned} \quad (1.3.45)$$

and the third contribution is

$$\mathbf{C} = \frac{dR}{dt} \frac{d\Theta}{dt} \mathbf{e}_\theta + R \frac{d^2\Theta}{dt^2} \mathbf{e}_\theta + R \frac{d\Phi}{dt} \frac{d\Theta}{dt} \cos \theta \mathbf{e}_\varphi - R \left(\frac{d\Theta}{dt} \right)^2 \mathbf{e}_r. \quad (1.3.46)$$

Consolidating the various terms, we derive the cylindrical polar components of the acceleration vector,

$$\begin{aligned} a_r &= \frac{d^2R}{dt^2} - R \left(\frac{d\Phi}{dt} \right)^2 \sin^2 \theta - R \left(\frac{d\Theta}{dt} \right)^2, \\ a_\theta &= R \frac{d^2\Theta}{dt^2} + 2 \frac{dR}{dt} \frac{d\Theta}{dt} - R \left(\frac{d\Phi}{dt} \right)^2 \sin \theta \cos \theta, \\ a_\varphi &= R \frac{d^2\Phi}{dt^2} \sin \theta + 2 \frac{dR}{dt} \frac{d\Phi}{dt} \sin \theta + 2R \frac{d\Theta}{dt} \frac{d\Phi}{dt} \cos \theta = \frac{1}{R \sin \theta} \frac{d}{dt} \left(R^2 \sin^2 \theta \frac{d\Phi}{dt} \right). \end{aligned} \quad (1.3.47)$$

Note that a change in the meridional angle described by Θ , or azimuthal angle described by Φ , is accompanied by radial acceleration.

1.3.3 Plane polar coordinates

A point in the xy plane can be identified by the values of the doublet (r, θ) , where r is the distance from the origin, and θ is the angle subtended between the x axis, the origin, and the chosen point, measured in the counterclockwise direction, as illustrated in [Figure 1.3.4](#). The radial distance, r , takes values in the range $[0, \infty)$, and the polar angle, θ , takes values in the range $[0, 2\pi)$.

Using elementary trigonometry, we derive the following relations between the Cartesian and plane polar coordinates,

$$x = r \cos \theta, \quad y = r \sin \theta, \quad (1.3.48)$$

and the inverse relations

$$r = \sqrt{x^2 + y^2}, \quad \theta = \arccos \frac{y}{r}. \quad (1.3.49)$$

In computing the inverse cosine function, care must be taken so that θ emerges as a continuous function of y and r .

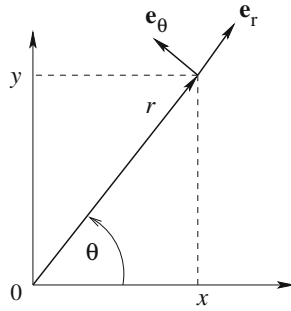


Figure 1.3.4 Illustration of a system of plane polar coordinates, (r, θ) , in the xy plane defined with respect to Cartesian coordinates, (x, y) .

Unit vectors

Consider a point in the xy plane and define two dimensionless unit vectors, \mathbf{e}_r and \mathbf{e}_θ , pointing in the radial or polar direction, as depicted in [Figure 1.3.4](#). Note that the orientations of these unit vectors change with position in the xy plane, whereas the orientations of the Cartesian unit vectors \mathbf{e}_x and \mathbf{e}_y are fixed.

Position and velocity

In terms of the local unit vectors \mathbf{e}_r and \mathbf{e}_θ , the position vector is given by

$$\mathbf{x} = r \mathbf{e}_r, \quad (1.3.50)$$

and the velocity vector is given by

$$\mathbf{v} = v_r \mathbf{e}_r + v_\theta \mathbf{e}_\theta. \quad (1.3.51)$$

The coefficients v_r and v_θ are the plane polar components of the velocity.

Relation to Cartesian vector components

Using elementary trigonometry, we derive the following relations between the Cartesian and plane polar unit vectors,

$$\mathbf{e}_r = \cos \theta \mathbf{e}_x + \sin \theta \mathbf{e}_y, \quad \mathbf{e}_\theta = -\sin \theta \mathbf{e}_x + \cos \theta \mathbf{e}_y, \quad (1.3.52)$$

and the inverse relations

$$\mathbf{e}_x = \cos \theta \mathbf{e}_r - \sin \theta \mathbf{e}_\theta, \quad \mathbf{e}_y = \sin \theta \mathbf{e}_r + \cos \theta \mathbf{e}_\theta. \quad (1.3.53)$$

The corresponding relations for the velocity components are

$$v_r = \cos \theta v_x + \sin \theta v_y, \quad v_\theta = -\sin \theta v_x + \cos \theta v_y \quad (1.3.54)$$

and

$$v_x = \cos \theta v_r - \sin \theta v_\theta, \quad v_y = \sin \theta v_r + \cos \theta v_\theta. \quad (1.3.55)$$

The Cartesian components of other vectors transform in similar ways.

Rates of change

The counterparts of expressions (1.3.4) for the plane polar coordinates are

$$r = R(t), \quad \theta = \Theta(t). \quad (1.3.56)$$

The rates of change of the unit vectors following the motion of a molecule are given by the relations

$$\frac{d\mathbf{e}_r}{dt} = \frac{d\Theta}{dt} \mathbf{e}_\theta, \quad \frac{d\mathbf{e}_\theta}{dt} = -\frac{d\Theta}{dt} \mathbf{e}_r. \quad (1.3.57)$$

Both unit vectors change as we move around the origin.

Velocity components

To derive the velocity components, we substitute the first equation in (1.3.56) into the right-hand side of (1.3.50), and take the time derivative of the resulting equation. Next, we identify the left-hand side with the velocity, expand the derivatives of the products on the right-hand side, and use the first relation in (1.3.57) to eliminate the time derivative of the radial unit vector, \mathbf{e}_r . Comparing the result with expressions (1.3.51), we obtain the plane polar components of the velocity,

$$v_r = \frac{dR}{dt}, \quad v_\theta = R \frac{d\Theta}{dt}. \quad (1.3.58)$$

Note that the right-hand sides have units of length divided by time.

Acceleration

Working as in the case of the cylindrical polar coordinates, we find that the plane polar components of the acceleration are given by

$$\begin{aligned} a_r &= \frac{d^2R}{dt^2} - R \left(\frac{d\Theta}{dt} \right)^2, \\ a_\theta &= R \frac{d^2\Theta}{dt^2} + 2 \frac{dR}{dt} \frac{d\Theta}{dt} = \frac{1}{R} \frac{d}{dt} \left(R^2 \frac{d\Theta}{dt} \right). \end{aligned} \quad (1.3.59)$$

Consider a molecule moving on a circular path of radius R centered at the origin, so that $dR/dt = 0$. The acceleration components are

$$a_r = R \left(\frac{d\Theta}{dt} \right)^2 = \frac{v_\theta^2}{R}, \quad a_\theta = R \frac{d^2\Theta}{dt^2}. \quad (1.3.60)$$

Note that radial acceleration arises even when a molecule moves at constant polar velocity, v_θ .

PROBLEMS

1.3.1 Spherical polar coordinates

Derive the inverse of the transformation rules shown in equations (1.3.37). That is, derive expressions for the Cartesian components of the velocity in terms of the spherical polar components of the velocity.

1.3.2 Acceleration

Derive the plane polar components of the acceleration given in (1.3.59).

1.4 Fluid velocity

Having prepared the ground for describing the motion of molecules of a fluid in quantitative terms, we turn to considering the motion of fluid parcels consisting of a large collection of molecules. For simplicity, we consider a homogeneous fluid parcel consisting of identical molecules and label the N constituent molecules by an integer index, i for $i = 1, \dots, N$.

Let $v_x^{(i)}$, $v_y^{(i)}$, and $v_z^{(i)}$ be the Cartesian components of the velocity of the i th molecule at a particular time instant. The corresponding components of the mean velocity are defined as

$$\bar{v}_x = \frac{1}{N} \sum_{i=1}^N v_x^{(i)}, \quad \bar{v}_y = \frac{1}{N} \sum_{i=1}^N v_y^{(i)}, \quad \bar{v}_z = \frac{1}{N} \sum_{i=1}^N v_z^{(i)}, \quad (1.4.1)$$

where a bar over v denotes the average value (arithmetic mean) over all N molecules. Equations (1.4.1) can be combined into a vector form,

$$\bar{\mathbf{v}} = \frac{1}{N} \sum_{i=1}^N \mathbf{v}^{(i)}. \quad (1.4.2)$$

Consider a fluid parcel of interest at a particular time, t , centered at a point, \mathbf{x} . As the size of the parcel becomes decreasingly small, the parcel tends to occupy an infinitesimal volume in space containing the point \mathbf{x} . In this limit, the components of the parcel velocity defined in equations (1.4.1) reduce to the corresponding components of the fluid velocity, denoted by u_x , u_y , and u_z , forming an ordered triplet,

$$\mathbf{u} = (u_x, u_y, u_z). \quad (1.4.3)$$

In terms of the Cartesian unit vectors,

$$\mathbf{u} = u_x \mathbf{e}_x + u_y \mathbf{e}_y + u_z \mathbf{e}_z. \quad (1.4.4)$$

Polar cylindrical and other curvilinear velocity components can be defined in a similar fashion, as discussed in Section 1.3.

1.4.1 Continuum approximation

A conceptual difficulty undermines the physical relevance of the fluid velocity: in the limit as the size of a fluid parcel tends to zero, the number of molecules residing inside the parcel also tends to zero, and the averages defined in equations (1.4.1) become ill-defined. To see this, we consider a spherical particle of radius ϵ . As ϵ tends to zero, a graph of the average molecular velocity, \bar{v}_x , plotted against ϵ , shows strong fluctuations that are manifestations of random molecular excursions.

To circumvent this difficulty, we adopt the continuum approximation prescribing that, as the size of a fluid parcel tends to zero, the limit of the average molecular velocity is computed before the discrete nature of the fluid becomes apparent.

Since different choices for the designated parcel center at difference times produce different fluid velocities, the components of the velocity vector, \mathbf{u} , may be regarded as functions of the components of the position vector, $\mathbf{x} = (x, y, z)$, and time, t . To signify this dependence, we append to u_x , u_y , and u_z a set of parentheses enclosing four independent variables, writing

$$u_x(x, y, z, t), \quad u_y(x, y, z, t), \quad u_z(x, y, z, t). \quad (1.4.5)$$

In compact notation, we write

$$u_x(\mathbf{x}, t), \quad u_y(\mathbf{x}, t), \quad u_z(\mathbf{x}, t). \quad (1.4.6)$$

In full vector notation, we write

$$\mathbf{u}(\mathbf{x}, t). \quad (1.4.7)$$

If a fluid translates as a rigid body in a certain direction, possibly with a time-dependent velocity, we omit the position vector \mathbf{x} in the list of arguments, and write $\mathbf{u}(t)$.

For example, the Cartesian components of a certain velocity field are given by the expressions

$$\begin{aligned} u_x(x, y, z, t) &= a(y^2 + z^2) + (b + ct)x^3yz + ce^{dxt}, \\ u_y(x, y, z, t) &= a(z^2 + x^2) + (b + ct)xy^3z + ce^{dyt}, \\ u_z(x, y, z, t) &= a(x^2 + y^2) + (b + ct)xyz^3 + ce^{dzt}, \end{aligned} \quad (1.4.8)$$

where a , b , c , and d are four constants. Velocity has units of length over time L/T , and the position vector has units of length, L . In order for both sides of equations (1.4.8) to have the same units, the constant a must have dimensions of inverse length-time, $1/(LT)$.

1.4.2 Steady flow

If a flow is steady, the components of the fluid velocity are constant in time. Consequently, t is omitted from the list of arguments in (1.4.5)–(1.4.7), so that $\mathbf{u}(\mathbf{x})$.

1.4.3 Two-dimensional flow

The z component of the fluid velocity in a two-dimensional flow in the xy plane is identically zero,

$$u_z = 0, \quad (1.4.9)$$

while the x and y components depend on x and y but not on z ,

$$u_x(x, y), \quad u_y(x, y). \quad (1.4.10)$$

The velocity vector lies in the xy plane at every point.

1.4.4 Swirling and axisymmetric flow

Consider the cylindrical polar coordinates depicted in [Figure 1.3.2](#). The cylindrical polar components of the velocity, u_σ and u_φ , are related to the Cartesian components by the counterparts of equations (1.3.20),

$$u_\sigma = \cos \varphi u_x + \sin \varphi u_y, \quad u_\varphi = -\sin \varphi u_x + \cos \varphi u_y. \quad (1.4.11)$$

In a swirling flow, the axial and radial velocity components are identically zero, $u_x = 0$ and $u_\sigma = 0$, while the azimuthal component, u_φ , is nonzero and independent of the azimuthal angle, φ , that is $u_\varphi(x, \sigma)$. Consequently, the velocity vector points in the direction of the azimuthal angle, φ , at every point.

In an axially symmetric flow, also called an axisymmetric flow, the azimuthal velocity component vanishes at every point,

$$u_\varphi = 0, \quad (1.4.12)$$

while the axial and radial components, u_x and u_σ , are nonzero but independent of φ ,

$$u_x(x, \sigma), \quad u_\sigma(x, \sigma). \quad (1.4.13)$$

The velocity vector lies in an azimuthal plane, defined as a plane that passes through the x axis, at every point in an axisymmetric flow.

Superposing a swirling flow and an axisymmetric flow, we obtain a three-dimensional flow described as axisymmetric flow with swirling motion. All three velocity components, u_x , u_σ , and u_φ , are generally nonzero but independent of the meridional angle φ in this flow.

1.4.5 Velocity vector field, streamlines and stagnation points

Consider a flow at a certain time instant, and draw velocity vectors at a large number of points distributed in the domain of flow. The collection of these vectors defines a vector field called the velocity field. Starting at a certain point in the flow, we may draw a line that is

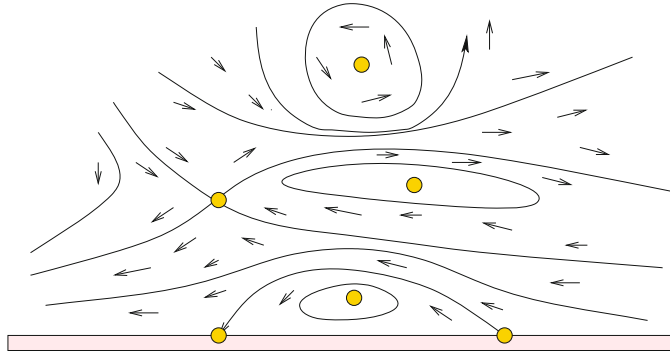


Figure 1.4.1 Illustration of a velocity vector field and associated streamline pattern in a two-dimensional flow involving stagnation points marked by circular symbols. Stagnation points may occur in the interior or at the boundaries of a flow.

tangential to the velocity vector at each point, as illustrated in [Figure 1.4.1](#). This generally curved three-dimensional line is an instantaneous streamline. A collection of streamlines composes an instantaneous streamline pattern.

Two or more streamlines may meet at a stagnation point, as illustrated in [Figure 1.4.1](#). Since the velocity is unique at each point in a flow, all velocity components must necessarily vanish at a stagnation point. A streamline must be a closed line, extend to infinity, cross a moving boundary, or terminate at a stagnation point.

PROBLEMS

1.4.1 Units of coefficients

Deduce the units of the coefficients b , c , and d on the right-hand sides of equations (1.4.8).

1.4.2 Streamline patterns

Sketch the streamline pattern of (a) a two-dimensional flow, (b) a swirling flow, (c) an axisymmetric flow, and (d) an axisymmetric flow with swirling motion.

1.5 Point particles and their trajectories

As the size of a fluid parcel tends to zero, the parcel reduces to an abstract entity called a *point particle*. In the context of continuum mechanics, a point particle is large enough to contain a large number of molecules whose average velocity is well-defined, but small enough so that its volume is infinitesimal. This means that the ratio of the volume of a point particle to the volume of the whole fluid is zero. Two consequences of this idealization are the following:

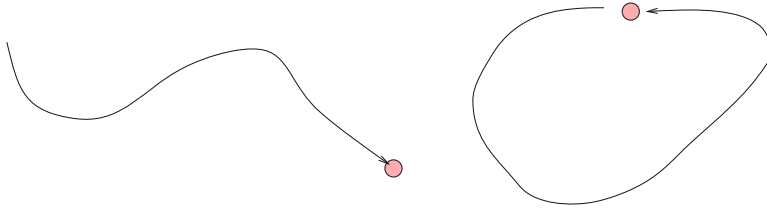


Figure 1.5.1 Illustration of path lines defined as the trajectories of point particles in a steady (time-independent) or unsteady (time-dependent) flow.

- A finite fluid parcel is comprised of an infinite number of point particles.
- The product of the infinite number of point particles to the infinitesimal volume of each point particle is finite, nonzero, and equal to the parcel volume.

By definition, the rate of change of the position of a point particle is equal to the velocity of the fluid evaluated at the instantaneous position of the point particle. If the x coordinate of a point particle located at the position $\mathbf{x} = \mathbf{X}$ has changed by the infinitesimal distance, dX , during an infinitesimal period of time, dt , then $u_x = dX/dt$, where the velocity u_x is evaluated at $\mathbf{x} = \mathbf{X}$ at the current time, t . Writing the counterparts of this equation for the y and z components, we obtain

$$\begin{aligned} \frac{dX}{dt} &= u_x(X(t), Y(t), Z(t), t), & \frac{dY}{dt} &= u_y(X(t), Y(t), Z(t), t), \\ & & \frac{dZ}{dt} &= u_z(X(t), Y(t), Z(t), t). \end{aligned} \tag{1.5.1}$$

The first set of parentheses on the right-hand side of each equation enclose the four scalar arguments of the velocity.

1.5.1 Path lines

Since a point particle moves with the local fluid velocity, its coordinates generally change in time according to equations (1.5.1), even if the flow is steady. Point particles in a fluid remain stationary only if they lie precisely at a stagnation point in a steady flow, or if the velocity field vanishes and the fluid is macroscopically quiescent. The trajectory of a point particle is called a path line. Typical path lines are illustrated in [Figure 1.5.1](#).

Instantaneous streamlines

By definition, a streamline is tangential to the instantaneous velocity vector field at every point. An instantaneous streamline is the path described by a point particle moving with the frozen instantaneous velocity field. An instantaneous streamline is physically meaningful only in the case of steady flow.

1.5.2 Ordinary differential equations (ODEs)

Equations (1.5.1) comprise a system of three first-order ordinary differential equations (ODEs). If the flow is steady, the system is *autonomous*, meaning that there is no explicit time dependence on the right-hand side. If the flow is unsteady, the system is *non-autonomous*, exhibiting an explicit time dependence on the right-hand side. The right-hand side of a non-autonomous system depends on time implicitly through the arguments of the dependent variables, $X(t)$, $Y(t)$, and $Z(t)$, and explicitly through the possible unsteadiness of the flow.

Unidirectional flow

For example, the Cartesian velocity components of a steady unidirectional flow with parabolic velocity profile are given by

$$u_x = ay^2 + by + c, \quad u_y = 0, \quad u_z = 0, \quad (1.5.2)$$

where a , b , and c are three constants with appropriate units. In this case, the fluid moves along the x axis with velocity that depends on the y coordinate alone. The trajectory of a point particle is a straight line described by an autonomous system of ODEs,

$$\frac{dX}{dt} = aY^2 + bY + c, \quad \frac{dY}{dt} = 0, \quad \frac{dZ}{dt} = 0. \quad (1.5.3)$$

The solution of these equations is readily found to be

$$X(t) = X_0 + (aY^2 + bY + c)t, \quad Y(t) = Y_0, \quad Z(t) = Z_0, \quad (1.5.4)$$

where X_0 , Y_0 , and Z_0 are the coordinates of a point particle at the initial instant, $t = 0$.

Method of integrating factors

Consider a steady three-dimensional flow with velocity components

$$u_x = \xi(x + y + 3z), \quad u_y = -\xi(2y + z), \quad u_z = \xi z, \quad (1.5.5)$$

where ξ is a constant with units of inverse time. The trajectory of a point particle is described by an autonomous system of ODEs,

$$\frac{dX}{dt} = \xi(X + Y + 3Z), \quad \frac{dY}{dt} = -\xi(2Y + Z), \quad \frac{dZ}{dt} = \xi Z. \quad (1.5.6)$$

The third equation can be integrated readily to give

$$Z(t) = Z_0 e^{\xi t}. \quad (1.5.7)$$

Substituting this expression into the second equation of (1.5.6) and rearranging, we obtain

$$\frac{dY}{dt} + 2\xi Y = -\xi Z_0 e^{\xi t}. \quad (1.5.8)$$

This equation can be solved by the method of integrating factors. Multiplying each term on both sides by the integrating factor $\exp(2\xi t)$ and rearranging, we obtain

$$\frac{d(Y e^{2\xi t})}{dt} = -\xi Z_0 e^{3\xi t}. \quad (1.5.9)$$

Integrating in time and enforcing the initial condition $Y(0) = Y_0$, we obtain

$$Y e^{2\xi t} = \frac{1}{3} Z_0 (1 - e^{3\xi t}) + Y_0, \quad (1.5.10)$$

and then

$$Y(t) = \frac{1}{3} Z_0 (e^{-2\xi t} - e^{\xi t}) + Y_0 e^{-2\xi t}. \quad (1.5.11)$$

The first equation in (1.5.6) then becomes

$$\frac{dX}{dt} - \xi X = \frac{1}{3} \xi Z_0 (e^{-2\xi t} + 8 e^{\xi t}) + \xi Y_0 e^{-2\xi t}. \quad (1.5.12)$$

Multiplying each term by the integrating factor $\exp(-\xi t)$, we obtain

$$\frac{d(X e^{-\xi t})}{dt} = \frac{1}{3} \xi Z_0 (e^{-3\xi t} + 8) + \xi Y_0 e^{-3\xi t}. \quad (1.5.13)$$

Integrating in time and enforcing the initial condition $X(0) = X_0$, we obtain

$$X e^{-\xi t} = \frac{1}{9} Z_0 (1 - e^{-3\xi t} + 24 \xi t) + \frac{1}{3} Y_0 (1 - e^{-3\xi t}) + X_0, \quad (1.5.14)$$

and then

$$X(t) = \frac{1}{9} Z_0 (1 - e^{-2\xi t} + 24 \xi t e^{\xi t}) + \frac{1}{3} Y_0 (e^{\xi t} - e^{-2\xi t}) + X_0 e^{\xi t}. \quad (1.5.15)$$

We have managed to derive explicit expressions for the particle position in time.

Steady linear flow

The velocity field of a three-dimensional steady linear flow is given by

$$\begin{aligned} u_x &= A_{11}x + A_{12}y + A_{13}z, & u_y &= A_{21}x + A_{22}y + A_{23}z, \\ u_z &= A_{31}x + A_{32}y + A_{33}z, \end{aligned} \quad (1.5.16)$$

where A_{ij} for $i, j = 1, 2, 3$ are nine constant coefficients. The trajectories of point particles are described by an autonomous system of ODEs,

$$\begin{aligned} \frac{dX}{dt} &= A_{11}X + A_{12}Y + A_{13}Z, & \frac{dY}{dt} &= A_{21}X + A_{22}Y + A_{23}Z, \\ \frac{dZ}{dt} &= A_{31}X + A_{32}Y + A_{33}Z. \end{aligned} \quad (1.5.17)$$

These equations can be conveniently collected into the matrix form

$$\frac{d}{dt} \begin{pmatrix} X(t) \\ Y(t) \\ Z(t) \end{pmatrix} = \begin{bmatrix} A_{11} & A_{12} & A_{13} \\ A_{21} & A_{22} & A_{23} \\ A_{31} & A_{32} & A_{33} \end{bmatrix} \cdot \begin{pmatrix} X(t) \\ Y(t) \\ Z(t) \end{pmatrix}. \quad (1.5.18)$$

In vector notation,

$$\frac{d\mathbf{X}}{dt} = \mathbf{A} \cdot \mathbf{X}, \quad (1.5.19)$$

where

$$\mathbf{X} = \begin{bmatrix} X \\ Y \\ Z \end{bmatrix}, \quad \mathbf{A} = \begin{bmatrix} A_{11} & A_{12} & A_{13} \\ A_{21} & A_{22} & A_{23} \\ A_{31} & A_{32} & A_{33} \end{bmatrix} \quad (1.5.20)$$

is the position vector and a constant 3×3 matrix. For the velocity field given in (1.5.6),

$$\mathbf{A} = \xi \begin{bmatrix} 1 & 1 & 3 \\ 0 & -2 & -1 \\ 0 & 0 & 1 \end{bmatrix}. \quad (1.5.21)$$

This matrix is classified as upper triangular. The trace of this matrix, defined as the sum of the three diagonal elements, is zero.

The solution of the ordinary differential equations is given by

$$\begin{bmatrix} X(t) \\ Y(t) \\ Z(t) \end{bmatrix} = \alpha_1 \begin{bmatrix} v_1^{(1)} \\ v_2^{(1)} \\ v_3^{(1)} \end{bmatrix} e^{\lambda_1 t} + \alpha_2 \begin{bmatrix} v_1^{(2)} \\ v_2^{(2)} \\ v_3^{(2)} \end{bmatrix} e^{\lambda_2 t} + \alpha_3 \begin{bmatrix} v_1^{(3)} \\ v_2^{(3)} \\ v_3^{(3)} \end{bmatrix} e^{\lambda_3 t}, \quad (1.5.22)$$

where λ_1 , λ_2 , and λ_3 are the eigenvalues of the matrix \mathbf{A} and

$$\mathbf{v}^{(1)} = \begin{bmatrix} v_1^{(1)} \\ v_2^{(1)} \\ v_3^{(1)} \end{bmatrix}, \quad \mathbf{v}^{(2)} = \begin{bmatrix} v_1^{(2)} \\ v_2^{(2)} \\ v_3^{(2)} \end{bmatrix}, \quad \mathbf{v}^{(3)} = \begin{bmatrix} v_1^{(3)} \\ v_2^{(3)} \\ v_3^{(3)} \end{bmatrix} \quad (1.5.23)$$

are the corresponding eigenvectors satisfying the equations

$$\mathbf{A} \cdot \mathbf{v}^{(1)} = \lambda_1 \mathbf{v}^{(1)}, \quad \mathbf{A} \cdot \mathbf{v}^{(2)} = \lambda_2 \mathbf{v}^{(2)}, \quad \mathbf{A} \cdot \mathbf{v}^{(3)} = \lambda_3 \mathbf{v}^{(3)}. \quad (1.5.24)$$

In vector notation,

$$\mathbf{X}(t) = \alpha_1 \mathbf{v}^{(1)} e^{\lambda_1 t} + \alpha_2 \mathbf{v}^{(2)} e^{\lambda_2 t} + \alpha_3 \mathbf{v}^{(3)} e^{\lambda_3 t}. \quad (1.5.25)$$

This solution can be confirmed by substituting it into (1.5.19) and using (1.5.24).

The coefficients α_1 , α_2 , and α_3 are determined by the initial condition,

$$X(t=0) = X_0, \quad Y(t=0) = Y_0, \quad Z(t=0) = Z_0, \quad (1.5.26)$$

requiring that

$$\alpha_1 \begin{bmatrix} v_1^{(1)} \\ v_2^{(1)} \\ v_3^{(1)} \end{bmatrix} + \alpha_2 \begin{bmatrix} v_1^{(2)} \\ v_2^{(2)} \\ v_3^{(2)} \end{bmatrix} + \alpha_3 \begin{bmatrix} v_1^{(3)} \\ v_2^{(3)} \\ v_3^{(3)} \end{bmatrix} = \begin{bmatrix} X_0 \\ Y_0 \\ Z_0 \end{bmatrix}, \quad (1.5.27)$$

which provides us with a system of linear algebraic equations for α_1 , α_2 , and α_3 ,

$$\begin{bmatrix} v_1^{(1)} & v_1^{(2)} & v_1^{(3)} \\ v_2^{(1)} & v_2^{(2)} & v_2^{(3)} \\ v_3^{(1)} & v_3^{(2)} & v_3^{(3)} \end{bmatrix} \cdot \begin{bmatrix} \alpha_1 \\ \alpha_2 \\ \alpha_3 \end{bmatrix} = \begin{bmatrix} X_0 \\ Y_0 \\ Z_0 \end{bmatrix}. \quad (1.5.28)$$

The solution can be found using, for example, Cramer's rule.

Exceptions arise in the case of multiple eigenvalues. An example is provided by the matrix (1.5.21) whose eigenvalues are 1 (twice) and -2 (once). In that case, products of powers of t with exponential terms arise.

Eigenvalues and eigenvectors

As an example, we consider a steady two-dimensional flow with velocity components

$$u_x = \xi(x + 3y), \quad u_y = \xi(2x - y), \quad (1.5.29)$$

where ξ a constant shear rate with units of inverse time. In this case, the coefficient matrix is

$$\mathbf{A} = \xi \begin{bmatrix} 1 & 3 \\ 2 & -1 \end{bmatrix}. \quad (1.5.30)$$

To compute the eigenvalues of \mathbf{A} , we formulate the linear system

$$(\mathbf{A} - \lambda \mathbf{I}) \cdot \mathbf{v} = \mathbf{0}, \quad (1.5.31)$$

where \mathbf{v} is an eigenvector of \mathbf{A} and \mathbf{I} is the 2×2 identity matrix, and compute the roots of the characteristic polynomial,

$$\det(\mathbf{A} - \lambda \mathbf{I}) = \det \begin{bmatrix} \xi - \lambda & 3\xi \\ 2\xi & -\xi - \lambda \end{bmatrix} = (\xi - \lambda)(-\xi - \lambda) - 6\xi^2 = 0, \quad (1.5.32)$$

yielding a quadratic equation,

$$\lambda^2 - 7\xi^2 = 0. \quad (1.5.33)$$

The eigenvalues are

$$\lambda_1, \lambda_2 = \pm\sqrt{7}\xi. \quad (1.5.34)$$

Next we compute the eigenvectors by solving the linear system

$$\begin{bmatrix} \xi \mp \sqrt{7}\xi & 3\xi \\ 2\xi & -\xi \mp \sqrt{7}\xi \end{bmatrix} \cdot \begin{bmatrix} v_1 \\ v_2 \end{bmatrix} = 0. \quad (1.5.35)$$

In fact, because the two equations encapsulated in this system are identical, the system can be replaced by a single equation,

$$(1 \mp \sqrt{7})v_1 + 3v_2 = 0. \quad (1.5.36)$$

Two eigenvectors are found corresponding to the plus or minus sign,

$$\mathbf{v}^{(1)} = \frac{1}{3} \begin{bmatrix} 3 \\ -1 + \sqrt{7} \end{bmatrix}, \quad \mathbf{v}^{(2)} = \frac{1}{3} \begin{bmatrix} 3 \\ -1 - \sqrt{7} \end{bmatrix}. \quad (1.5.37)$$

The solution of the linear system is

$$\mathbf{X}(t) = \alpha_1 \mathbf{v}^{(1)} e^{\lambda_1 t} + \alpha_2 \mathbf{v}^{(2)} e^{\lambda_2 t} = \begin{bmatrix} \alpha_1 v_1^{(1)} e^{\lambda_1 t} + \alpha_2 v_1^{(2)} e^{\lambda_2 t} \\ \alpha_1 v_2^{(1)} e^{\lambda_1 t} + \alpha_2 v_2^{(2)} e^{\lambda_2 t} \end{bmatrix}, \quad (1.5.38)$$

where the coefficients α_1 and α_2 are determined by the initial condition.

Setting

$$\begin{bmatrix} X(0) \\ Y(0) \end{bmatrix} = \frac{1}{3} \begin{bmatrix} 3\alpha_1 + 3\alpha_2 \\ \alpha_1(-1 + \sqrt{7}) + \alpha_2(-1 - \sqrt{7}) \end{bmatrix} = \begin{bmatrix} X_0 \\ Y_0 \end{bmatrix}, \quad (1.5.39)$$

we obtain a linear system of two equations for α_1 and α_2 ,

$$\alpha_1 + \alpha_2 = X_0, \quad \alpha_1(-1 + \sqrt{7}) + \alpha_2(-1 - \sqrt{7}) = 3Y_0. \quad (1.5.40)$$

Using Cramer's rule, we obtain

$$\alpha_1 = \frac{\det \begin{bmatrix} X_0 & 1 \\ 3Y_0 & -1 - \sqrt{7} \end{bmatrix}}{\det \begin{bmatrix} 1 & 1 \\ -1 + \sqrt{7} & -1 - \sqrt{7} \end{bmatrix}}, \quad \alpha_2 = \frac{\det \begin{bmatrix} 1 & X_0 \\ -1 + \sqrt{7} & 3Y_0 \end{bmatrix}}{\det \begin{bmatrix} 1 & 1 \\ -1 + \sqrt{7} & -1 - \sqrt{7} \end{bmatrix}}, \quad (1.5.41)$$

where \det denotes the determinant. Evaluating the determinants, we finally obtain

$$\alpha_1 = \frac{1}{2\sqrt{7}} [(1 + \sqrt{7})X_0 + 3Y_0] \quad \alpha_2 = \frac{1}{2\sqrt{7}} [(-1 + \sqrt{7})X_0 - 3Y_0]. \quad (1.5.42)$$

Families of streamlines can be drawn for different choices of the initial doublet, (X_0, Y_0) .

Steady linear flows with drift

The linear system (1.5.19) can be generalized into the system

$$\frac{d\mathbf{X}}{dt} = \mathbf{A} \cdot \mathbf{X} - \mathbf{b}, \quad (1.5.43)$$

where \mathbf{b} is a constant vector representing a drift velocity. The solution is given by

$$\begin{bmatrix} X(t) \\ Y(t) \\ Z(t) \end{bmatrix} = \alpha_1 \begin{bmatrix} v_1^{(1)} \\ v_2^{(1)} \\ v_3^{(1)} \end{bmatrix} e^{\lambda_1 t} + \alpha_2 \begin{bmatrix} v_1^{(2)} \\ v_2^{(2)} \\ v_3^{(2)} \end{bmatrix} e^{\lambda_2 t} + \alpha_3 \begin{bmatrix} v_1^{(3)} \\ v_2^{(3)} \\ v_3^{(3)} \end{bmatrix} e^{\lambda_3 t} + \begin{bmatrix} \tilde{X} \\ \tilde{Y} \\ \tilde{Z} \end{bmatrix}, \quad (1.5.44)$$

where $\tilde{\mathbf{X}} = (\tilde{X}, \tilde{Y}, \tilde{Z})$ is the *fixed point* satisfying the linear system

$$\mathbf{A} \cdot \tilde{\mathbf{X}} = \mathbf{b}. \quad (1.5.45)$$

In vector notation,

$$\mathbf{X}(t) = \alpha_1 \mathbf{v}^{(1)} e^{\lambda_1 t} + \alpha_2 \mathbf{v}^{(2)} e^{\lambda_2 t} + \alpha_3 \mathbf{v}^{(3)} e^{\lambda_3 t} + \tilde{\mathbf{X}} \quad (1.5.46)$$

where the coefficients α_1 , α_2 , and α_3 are determined by the initial condition.

As an example, we consider a steady two-dimensional flow with velocity components

$$u_x = \xi(x + 3y) + U_x, \quad u_y = \xi(2x - y) + U_y, \quad (1.5.47)$$

where ξ a constant shear rate with units of inverse time and U_x, U_y are two constant velocities. In this example,

$$\mathbf{A} = \xi \begin{bmatrix} 1 & 3 \\ 2 & -1 \end{bmatrix}, \quad \mathbf{b} = - \begin{bmatrix} U_x \\ U_y \end{bmatrix}. \quad (1.5.48)$$

The fixed point satisfies the equation

$$\begin{bmatrix} 1 & 3 \\ 2 & -1 \end{bmatrix} \cdot \tilde{\mathbf{X}} = -\frac{1}{\xi} \begin{bmatrix} U_x \\ U_y \end{bmatrix}, \quad (1.5.49)$$

whose solution is

$$\tilde{\mathbf{X}} = \frac{1}{7\xi} \begin{bmatrix} -U_x - 6U_y \\ -2U_x + U_y \end{bmatrix}. \quad (1.5.50)$$

The constants, α_1 and α_2 are determined by the initial condition.

1.5.3 Explicit Euler method

In general, the solution of system (1.5.1) cannot be found by analytical methods. A numerical method for generating the trajectory of a point particle can be developed by considering the change in the position of the point particle over a small time interval, Δt , and replacing the differential equations (1.5.1) with the algebraic equations

$$\begin{aligned} \frac{X(t + \Delta t) - X(t)}{\Delta t} &= u_x(X(t), Y(t), Z(t), t), \\ \frac{Y(t + \Delta t) - Y(t)}{\Delta t} &= u_y(X(t), Y(t), Z(t), t), \\ \frac{Z(t + \Delta t) - Z(t)}{\Delta t} &= u_z(X(t), Y(t), Z(t), t). \end{aligned} \quad (1.5.51)$$

To obtain these equations, we have approximated the time derivatives on the left-hand sides of equations (1.5.1) with forward finite-difference ratios. Since, by definition, the first derivative dX/dt is equal to the ratio $[X(t + \Delta t) - X(t)]/\Delta t$ in the limit as Δt tends to zero, we expect that, as long as Δt is sufficiently small, the error introduced by replacing the derivative with a forward-difference approximation will also be reasonably small.

In fact, performing a Taylor series expansion, we find that the magnitude of the error associated with the approximate forms (1.5.51) is comparable to the magnitude of Δt . This means that, if Δt is equal to 0.1 in some units, the error associated with the difference approximation will be on the order of 0.1 multiplied by a constant whose absolute value ranges roughly between 0.5 and 5 in corresponding units.

In vector notation, the discrete form of the differential system (1.5.1) expressed by the algebraic system (1.5.51) takes the form

$$\frac{\mathbf{X}(t + \Delta t) - \mathbf{X}(t)}{\Delta t} = \mathbf{u}(\mathbf{X}(t), t) + O(\Delta t), \quad (1.5.52)$$

where the symbol $O(\Delta t)$ on the right-hand side signifies the order of the error due to the difference approximation.

Solving the first equation in (1.5.51) for $X(t + \Delta t)$, the second equation for $Y(t + \Delta t)$, and the third equation for $Z(t + \Delta t)$, we obtain

$$\begin{aligned} X(t + \Delta t) &= X(t) + u_x(X(t), Y(t), Z(t), t) \times \Delta t, \\ Y(t + \Delta t) &= Y(t) + u_y(X(t), Y(t), Z(t), t) \times \Delta t, \\ Z(t + \Delta t) &= Z(t) + u_z(X(t), Y(t), Z(t), t) \times \Delta t. \end{aligned} \quad (1.5.53)$$

In vector notation,

$$\mathbf{X}(t + \Delta t) = \mathbf{X}(t) + \mathbf{u}(\mathbf{X}(t), t) \times \Delta t. \quad (1.5.54)$$

In physical terms, equation (1.5.54) states that the position of a point particle at next time instant, $t + \Delta t$, is equal to the position at the current time instant, t , plus a small displacement that is equal to the distance traveled over the small time interval Δt . The travel velocity has been assumed constant and equal to the local fluid velocity at the beginning of the time step, corresponding to time t , which is a sensible approximation.

Algorithm

Equations (1.5.53) provide us with a numerical scheme for computing the trajectory of a point particle according to the following algorithm implementing the explicit Euler method:

1. Specify the initial time; for example, set $t = 0$.
2. Select the size of the time step, Δt .
3. Specify the initial coordinates, X_0 , Y_0 , and Z_0 .

4. Evaluate the velocity components on the right-hand side of equations (1.5.53),

$$u_x(X(t), Y(t), Z(t), t), \quad u_y(X(t), Y(t), Z(t), t), \quad u_z(X(t), Y(t), Z(t), t), \quad (1.5.55)$$

5. Evaluate the right-hand sides of (1.5.53) to obtain the new point particle coordinates, $X(t + \Delta t)$, $Y(t + \Delta t)$, and $Z(t + \Delta t)$.
6. Reset the time to $t + \Delta t$.
7. Stop, if desired, or return to execute Steps 4-6.

The method is explicit in that the new position of a point particle is computed in terms of the old position using information available exclusively at the old position.

We have mentioned that approximating the derivative $d\mathbf{X}/dt$ with a forward difference introduces an error that is comparable to the magnitude of Δt , as shown in equations (1.5.52). Accordingly, the error in the position of the point particle after it has traveled for a time interval Δt is on the order of Δt^2 . Based on the value of the exponent of Δt , we say that the explicit Euler method carries a stepwise error of *second order* with respect to the time step.

If N_{steps} steps are executed from time $t = 0$ to time $t = t_{\text{final}}$, the stepwise error will accumulate to an amount that is comparable to the product $N_{\text{steps}} \times \Delta t^2$. Since, by definition, $N_{\text{steps}} \times \Delta t = t_{\text{final}}$, the cumulative error will be on the order of

$$t_{\text{final}} \times \Delta t. \quad (1.5.56)$$

This expression shows that the cumulative error is of first order with respect to the time step. Unless Δt is sufficiently small, this level of error is hardly acceptable.

1.5.4 Modified Euler method

To reduce the magnitude of the error, we modify the explicit Euler method according to the following steps:

1. Set the initial time; for example, set $t = 0$.
2. Select the size of the time step, Δt .
3. Specify the initial coordinates, $X(0)$, $Y(0)$, and $Z(0)$.
4. Evaluate the current velocity components,

$$\begin{aligned} u_x^{\text{current}} &= u_x(X(t), Y(t), Z(t), t), \\ u_y^{\text{current}} &= u_y(X(t), Y(t), Z(t), t), \\ u_z^{\text{current}} &= u_z(X(t), Y(t), Z(t), t), \end{aligned} \quad (1.5.57)$$

on the right-hand sides of (1.5.53), and save them for future use.

5. Evaluate the right-hand sides of (1.5.53) to obtain the predicted coordinates at time $t + \Delta t$, denoted by X^{pred} , Y^{pred} , and Z^{pred} .

6. Evaluate the velocities at the predicted position at time $t + \Delta t$,

$$\begin{aligned} u_x^{\text{pred}} &= u_x(X^{\text{pred}}, Y^{\text{pred}}, Z^{\text{pred}}, t + \Delta t), \\ u_y^{\text{pred}} &= u_y(X^{\text{pred}}, Y^{\text{pred}}, Z^{\text{pred}}, t + \Delta t), \\ u_z^{\text{pred}} &= u_z(X^{\text{pred}}, Y^{\text{pred}}, Z^{\text{pred}}, t + \Delta t), \end{aligned} \quad (1.5.58)$$

7. Compute the average of the current and predicted velocities,

$$\begin{aligned} u_x^{\text{aver}} &= \frac{1}{2} (u_x^{\text{current}} + u_x^{\text{pred}}), \\ u_y^{\text{aver}} &= \frac{1}{2} (u_y^{\text{current}} + u_y^{\text{pred}}), \\ u_z^{\text{aver}} &= \frac{1}{2} (u_z^{\text{current}} + u_z^{\text{pred}}). \end{aligned} \quad (1.5.59)$$

8. Compute the coordinates of the point particle at time $t + \Delta t$ by returning to the position at time t and traveling with the mean velocity computed in Step 7 using the formulas

$$\begin{aligned} X(t + \Delta t) &= X(t) + u_x^{\text{aver}} \Delta t, \\ Y(t + \Delta t) &= Y(t) + u_y^{\text{aver}} \Delta t, \\ Z(t + \Delta t) &= Z(t) + u_z^{\text{aver}} \Delta t. \end{aligned} \quad (1.5.60)$$

9. Advance the time to $t + \Delta t$.
10. Stop if desired, or return to execute Steps 4–9.

In fact, the modified Euler method is a special implementation of the inclusive second-order Runge–Kutta method for solving systems of ordinary differential equations. An error analysis shows that each time step introduces a numerical error in the position of the point particle that is comparable to the cubic power of time step, Δt^3 . The cumulative error is thus on the order of

$$t_{\text{final}} \times \Delta t^2, \quad (1.5.61)$$

which is much smaller than that incurred by the explicit Euler method.

To ensure a smooth particle trajectory, we may specify an approximate travel distance in each step, Δs , and adjust the time step accordingly using $\Delta t = \Delta s/u$, where u is the magnitude of the local velocity.

Program *path.lines*

The following MATLAB code entitled *path.lines*, located in directory *04_various* of **FDLIB**, computes and displays path lines originating from specified initial points. The integration terminates when a path line escapes the plotting window or returns to the initial position to form a closed loop:

```
Nsteps = 400; % number of steps
Ds = 0.01; % spatial step
```

```

xmin = -1.0; xmax = 1.0; % plotting window
ymin = -1.0; ymax = 1.0;

Xstart = [0.1, 0.2, 0.3]; % starting points of path lines
Ystart = [0.1, 0.2, 0.3];

%---
% prepare to plot
%---

figure(1)
hold on
axis equal
set(gca,'fontsize',13)
xlabel('x','fontsize',13)
ylabel('y','fontsize',13)
box on

%---
for n=1:size(Xstart') % run over starting points
%---

X0 = Xstart(n);
Y0 = Ystart(n);
Xsave = X0;
Ysave = Y0;

clear Xplot Yplot

Xplot(1) = X0;
Yplot(1) = Y0;

X = X0; Y = Y0; t = 0;

%--
for i=1:Nsteps
%--

    [ux, uy] = path_lines_vel(X,Y,t);

    um = sqrt(ux*ux + uy*uy);
    Dt = Ds/um;
    X1 = X + ux*Dt;
    Y1 = Y + uy*Dt;
    t1 = t + Dt;

    [ux1, uy1] = path_lines_vel(X1,Y1,t1);

```

```

X = X + 0.5*Dt*(ux+ux1);
Y = Y + 0.5*Dt*(uy+uy1);
t = t + Dt;
Xplot(i+1) = X;
Yplot(i+1) = Y;

%---
% stopping check for window limits and closed paths
%---

closed = sqrt((X-Xsave)^2+(Y-Ysave)^2);

if(closed < 0.9*Ds | X<xmin | X>xmax | Y<ymin | Y>ymax)
    break
end

%--
end
%--

plot(Xplot,Yplot,'k. ')

end % of path lines

```

The velocity components are evaluated by the following user-defined companion MATLAB function entitled *path_lines_vel*:

```

function [ux,uy] = path_lines_vel(x,y,t)

%----
% evaluate the velocity
%---

Omega = 1.0;
G = 0.5;
alpha = 0.0;
ux = G*x-Omega*y+0.5*alpha*x*exp(-t);
uy = Omega*x-G*y+0.5*alpha*y*exp(t);

%----
% done
%---

return

```

Running the code *path_lines* generates the patterns shown in [Figure 1.5.2](#). In this case, point particles move along closed loops.

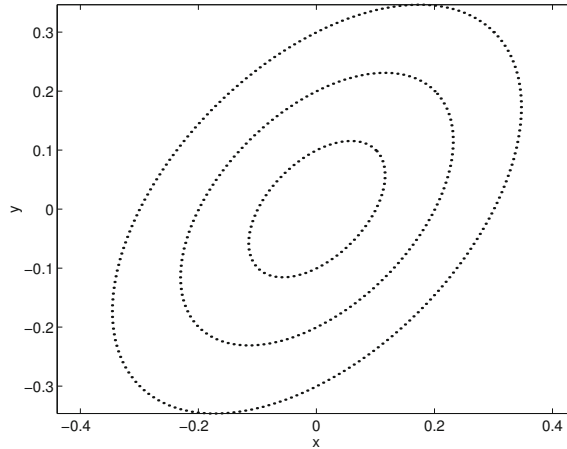


Figure 1.5.2 Path lines computed by the code `path_lines` for the velocity field defined in the code.

1.5.5 Description in polar coordinates

The position of a point particle can be described in the cylindrical polar coordinates depicted in [Figure 1.3.2](#) by three functions,

$$x = X(t), \quad \sigma = \Sigma(t), \quad \varphi = \Phi(t). \quad (1.5.62)$$

Using the transformation rules given in [Section 1.3](#), we derive the differential equations

$$\begin{aligned} \frac{dX}{dt} &= u_x(X(t), \Sigma(t), \Phi(t), t), & \frac{d\Sigma}{dt} &= u_\sigma(X(t), \Sigma(t), \Phi(t), t), \\ \frac{d\Phi}{dt} &= \frac{u_\varphi(X(t), \Sigma(t), \Phi(t), t)}{\Sigma(t)}. \end{aligned} \quad (1.5.63)$$

Note the implicit and explicit dependence on time on the right-hand sides.

In the spherical polar coordinates depicted in [Figure 1.3.3](#), the position of a point particle is described by three functions

$$r = R(t), \quad \theta = \Theta(t), \quad \varphi = \Phi(t). \quad (1.5.64)$$

Using the transformation rules given in [Section 1.3](#), we derive the differential equations

$$\begin{aligned} \frac{dR}{dt} &= u_r(X(t), \Theta(t), \Phi(t), t), & \frac{d\Theta}{dt} &= \frac{u_\theta(X(t), \Theta(t), \Phi(t), t)}{R(t)}, \\ \frac{d\Phi}{dt} &= \frac{u_\varphi(X(t), \Theta(t), \Phi(t), t)}{R(t) \sin \Theta(t)}. \end{aligned} \quad (1.5.65)$$

Note the implicit and explicit dependence on time on the right-hand sides.

In the plane polar coordinates depicted in Figure 1.3.4, the position of a point particle is described by two functions,

$$r = R(t), \quad \theta = \Theta(t) \quad (1.5.66)$$

Using the transformation rules given in Section 1.3, we derive the differential equations

$$\frac{dR}{dt} = u_r(R(t), \Theta(t), t), \quad \frac{d\Theta}{dt} = \frac{u_\theta(R(t), \Theta(t), t)}{R(t)}. \quad (1.5.67)$$

Note the implicit and explicit dependence on time on the right-hand sides.

The systems of differential equations (1.5.63), (1.5.65), or (1.5.67) can be integrated in time using the methods discussed previously in this section for Cartesian coordinates, including the Euler method and the modified Euler method. To deduce the position vector at any time, we use the transformation rules to obtain the Cartesian coordinates in terms of the chosen polar coordinates.

1.5.6 Streaklines

A streakline emerges by connecting the instantaneous positions of point particles that have been released or injected into the flow from a stationary or moving source at previous times. Alternatively, the point particles may have been residing in the fluid at all times, but they have been colored or tagged as they passed through the tip of a stationary or moving probe. If the flow is steady and the probe is stationary, a streakline is also a streamline.

To compute a streakline, we solve the differential equations describing the motion of the point particles after they have entered the flow or passed through the coloring probe using the methods described in this section for particle paths. Since the motion of point particles is independent of their relative position, the trajectory of each point particle can be computed individually and independently, as though each point particle moved in isolation.

PROBLEMS

1.5.1 Streamlines by analytical integration

Consider a steady two-dimensional flow with velocity components

$$u_x = \xi x + \eta y, \quad u_y = \eta x - \xi y. \quad (1.5.68)$$

Deduce the units of the constants ξ and η and derive analytical expressions for the position of a point particle similar to those shown in (1.5.4).

1.5.2 Streamlines by analytical integration

Derive analytical expressions for the position of a point particle in a steady three-dimensional linear flow described by the matrix

$$\mathbf{A} = \xi \begin{bmatrix} -1 & 0 & 0 \\ -3 & -2 & 0 \\ 2 & 1 & 3 \end{bmatrix}, \quad (1.5.69)$$

where ξ is a constant shear rate. For obvious reasons, this matrix is classified as lower triangular.

1.5.3 Path lines by numerical integration

Program *path.lines*, located in directory *04_various* of **FDLIB**, computes and displays path lines originating from specified initial points, as discussed in the text. Run the program for the velocity field given in (1.5.68) with $\eta = 0.5\xi$ and discuss the nature of the path lines.

1.5.4 Streamlines by numerical integration

Program *strml*, located in directory *04_various* of **FDLIB**, generates streamlines originating from a specified set of points. The streamlines are computed by the modified Euler method.

(a) Run the program for three velocity fields of your choice implemented in the code. Generate and discuss the structure of the streamlines patterns.

(b) Add to the code a new flow of your choice. Generate and discuss the corresponding streamline pattern.

1.6 Material surfaces and elementary motions

An infinite collection of point particles distributed over a surface that resides inside or at the boundary of a fluid defined a material surface. A cylindrical material surface in a two-dimensional flow can be identified by its trace in the xy plane. A material surface of revolution in an axisymmetric flow can be identified by its trace in an azimuthal plane corresponding to a certain azimuthal angle, φ .

Any patch on the surface of a cup of coffee is a material surface with distinct identity. Under most conditions, if a material patch lies at the boundary of a fluid at a certain time, it will remain at the boundary of the fluid at any time. This means that the point particles comprising the patch are not able to penetrate the fluid.

Material parcels

A closed material surface is the boundary of a material parcel consisting of a fixed amount of fluid with a permanent identity. Under most conditions, if a material surface is located at the boundary of a material parcel at a certain time, it will remain at the boundary of the parcel at any time. To analyze the evolution of a material parcel and visualize its motion, we may compute the trajectories of the point particles that lie on its boundary by analytical or numerical methods.

1.6.1 Fluid parcel rotation

Consider a two-dimensional flow in the xy plane with velocity components

$$u_x = -\Omega y, \quad u_y = \Omega x, \quad (1.6.1)$$

where Ω is a constant with units of inverse time. In vector notation, equations (1.6.1) are collected into the form

$$[u_x \quad u_y] = [x \quad y] \cdot \begin{bmatrix} 0 & \Omega \\ -\Omega & 0 \end{bmatrix}. \quad (1.6.2)$$

According to our discussion in Section 1.5, the trajectory of a point particle with Cartesian coordinates $X(t)$ and $Y(t)$ is governed by the differential equations

$$\frac{dX}{dt} = -\Omega Y, \quad \frac{dY}{dt} = \Omega X, \quad (1.6.3)$$

subject to a specified initial condition, $X_0 \equiv X(t=0)$ and $Y_0 \equiv Y(t=0)$. The solution is readily found to be

$$X(t) = \cos(\Omega t) X_0 - \sin(\Omega t) Y_0, \quad Y(t) = \sin(\Omega t) X_0 + \cos(\Omega t) Y_0. \quad (1.6.4)$$

In vector notation,

$$\begin{bmatrix} X(t) \\ Y(t) \end{bmatrix} = \begin{bmatrix} \cos(\Omega t) & -\sin(\Omega t) \\ \sin(\Omega t) & \cos(\Omega t) \end{bmatrix} \cdot \begin{bmatrix} X_0 \\ Y_0 \end{bmatrix}. \quad (1.6.5)$$

To deduce the nature of the motion, we refer to plane polar coordinates and find that the square of the distance of a point particle from the origin,

$$R^2(t) \equiv X^2(t) + Y^2(t), \quad (1.6.6)$$

remains constant in time, equal to the initial distance, $R_0 \equiv R(t=0)$. The polar angle, θ , defined by the equation $\tan \theta = Y(t)/X(t)$, increases linearly in time at the rate $d\theta/dt = \Omega$,

$$\theta = \Omega t + \theta_0, \quad (1.6.7)$$

where θ_0 is the polar angle at $t=0$. To show this, we write

$$\tan \theta = \frac{Y(t)}{X(t)} = \frac{\sin(\Omega t) X_0 + \cos(\Omega t) Y_0}{\cos(\Omega t) X_0 - \sin(\Omega t) Y_0}, \quad (1.6.8)$$

yielding

$$\tan \theta = \frac{\sin(\Omega t) \cos \theta_0 + \cos(\Omega t) \sin \theta_0}{\cos(\Omega t) \cos \theta_0 - \sin(\Omega t) \sin \theta_0} = \frac{\sin(\Omega t + \theta_0)}{\cos(\Omega t + \theta_0)} = \tan(\Omega t + \theta_0). \quad (1.6.9)$$

Using the relations developed in Section 1.3.3, we find that the radial and polar velocity components are given by $u_r = 0$ and $u_\theta = \Omega r$. Applying (1.5.67), we recover $R(t) = R_0$ and $\theta = \Omega t + \theta_0$.

The preceding analysis suggests that a circular material line centered at the origin rotates around the origin as a rigid body with angular velocity Ω while retaining its circular shape. Accordingly, the velocity field associated with (1.6.1) expresses rigid-body rotation around the origin of the xy plane.

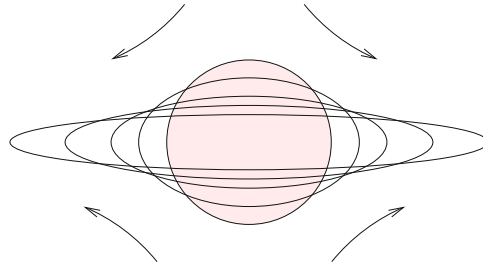


Figure 1.6.1 Deformation of a circular material line under the influence of a two-dimensional elongational flow.

1.6.2 Fluid parcel deformation

Now we consider a different type of two-dimensional flow in the xy plane with velocity components

$$u_x = Gx, \quad u_y = -Gy, \quad (1.6.10)$$

where G is a constant with units of inverse time. In vector–matrix notation,

$$\begin{bmatrix} u_x & u_y \end{bmatrix} = \begin{bmatrix} x & y \end{bmatrix} \cdot \begin{bmatrix} G & 0 \\ 0 & -G \end{bmatrix}. \quad (1.6.11)$$

In this case, the trajectory of a point particle is governed by the differential equations

$$\frac{dX}{dt} = GX, \quad \frac{dY}{dt} = -GY, \quad (1.6.12)$$

subject to a specified initial condition. Note that equations (1.6.12) are decoupled, that is, the first equation contains only X and the second equation contains only Y . The solution is readily found to be

$$X(t) = e^{Gt} X_0, \quad Y(t) = e^{-Gt} Y_0. \quad (1.6.13)$$

In vector–matrix notation,

$$\begin{bmatrix} X(t) \\ Y(t) \end{bmatrix} = \begin{bmatrix} e^{Gt} & 0 \\ 0 & e^{-Gt} \end{bmatrix} \cdot \begin{bmatrix} X_0 \\ Y_0 \end{bmatrix}. \quad (1.6.14)$$

The diagonal matrix elements increase or decrease exponentially in time and the off-diagonal elements remain zero.

The evolution of a circular material line of radius a centered at the origin is illustrated in [Figure 1.6.1](#) for a positive value of G . As soon as the motion begins, the circular contour deforms into an ellipse with major semi-axis

$$b(t) = ae^{Gt} \quad (1.6.15)$$

oriented in the x direction, and minor semi-axis

$$c(t) = a e^{-Gt} \quad (1.6.16)$$

oriented in the y direction. To show this, we confirm that the coordinates of a point particle satisfy the equation of the ellipse,

$$\frac{X^2(t)}{b^2(t)} + \frac{Y^2(t)}{c^2(t)} = 1, \quad (1.6.17)$$

where $X_0^2 + Y_0^2 = a^2$ describes the initial circle. The area enclosed by the deforming circle remains constant in time, equal to

$$A(t) = \pi b(t) c(t) = \pi a^2. \quad (1.6.18)$$

The preceding analysis suggests that the velocity field described by (1.6.11) describes pure deformation occurring at an exponential rate in the absence of expansion or contraction; the constant G is the rate of deformation. The deformation conserves the area of the parcel enclosed by the continuously deforming ellipse.

1.6.3 Fluid parcel expansion

As a third case study, we consider a two-dimensional flow in the xy plane with velocity components

$$u_x = \frac{1}{2} \alpha x, \quad u_y = \frac{1}{2} \alpha y, \quad (1.6.19)$$

where α is a constant with units of inverse time. In vector-matrix notation,

$$[u_x \quad u_y] = [x \quad y] \cdot \begin{bmatrix} \frac{1}{2}\alpha & 0 \\ 0 & \frac{1}{2}\alpha \end{bmatrix}. \quad (1.6.20)$$

The trajectory of a point particle is governed by two decoupled differential equations,

$$\frac{dX}{dt} = \frac{1}{2} \alpha X, \quad \frac{dY}{dt} = \frac{1}{2} \alpha Y, \quad (1.6.21)$$

subject to a specified initial condition. The solution is found by elementary methods to be

$$X(t) = e^{\frac{1}{2} \alpha t} X_0, \quad Y(t) = e^{\frac{1}{2} \alpha t} Y_0. \quad (1.6.22)$$

In vector-matrix notation,

$$\begin{bmatrix} X(t) \\ Y(t) \end{bmatrix} = \begin{bmatrix} e^{\frac{1}{2} \alpha t} & 0 \\ 0 & e^{\frac{1}{2} \alpha t} \end{bmatrix} \cdot \begin{bmatrix} X_0 \\ Y_0 \end{bmatrix}. \quad (1.6.23)$$

Based on these expressions, we deduce that a circular material line centered at the origin expands at an exponential rate while retaining its circular shape. Accordingly, the velocity field associated with equations (1.6.19) expresses isotropic expansion.

If $a(t)$ is the radius of the circular material line at time t , then

$$a(t) = a(t=0) e^{\frac{1}{2} \alpha t}, \quad (1.6.24)$$

where $a(t=0)$ is the radius at the origin of time. Raising both sides to the second power, multiplying the result by π , and rearranging, we find that the ratio of the enclosed areas is

$$\frac{\pi a^2(t)}{\pi a^2(t=0)} = e^{\alpha t}. \quad (1.6.25)$$

Accordingly, the constant α is the rate of areal expansion.

1.6.4 Superposition of rotation, deformation, and expansion

For future convenience, we relabel the Cartesian coordinates from (x, y) to (x', y') . Superposing the three types of motion discussed in the preceding three sections, we obtain a compound velocity field with components

$$[u_{x'} \quad u_{y'}] = [x' \quad y'] \cdot \left(\begin{bmatrix} 0 & \Omega \\ -\Omega & 0 \end{bmatrix} + \begin{bmatrix} G & 0 \\ 0 & -G \end{bmatrix} + \begin{bmatrix} \frac{1}{2} \alpha & 0 \\ 0 & \frac{1}{2} \alpha \end{bmatrix} \right). \quad (1.6.26)$$

The three matrices on the right-hand side of (1.6.26) express fluid parcel rotation, pure deformation, and isotropic expansion. Summing corresponding elements, we obtain the composite vector form

$$\mathbf{u}' = \mathbf{x}' \cdot \mathbf{A}, \quad (1.6.27)$$

where $\mathbf{u}' = (u_{x'}, u_{y'})$, $\mathbf{x}' = (x', y')$, and the matrix \mathbf{A} is defined as

$$\mathbf{A} = \begin{bmatrix} G + \frac{1}{2} \alpha & \Omega \\ -\Omega & -G + \frac{1}{2} \alpha \end{bmatrix}. \quad (1.6.28)$$

Because the velocity field shown in (1.6.27) depends linearly on the position vector, \mathbf{x}' , the associated flow is linear.

Varying the relative magnitudes of the three adjustable flow parameters, Ω , G , and α , allows us to alter the character of the flow by forming hybrid forms of the three fundamental constituents.

1.6.5 Rotated coordinates

Although fluid parcel rotation, deformation, and expansion have been deduced with reference to the $x'y'$ system of Cartesian coordinates, expressing the position and velocity vectors in a different system of coordinates should not affect the physical nature of the motion. Motivated by this observation, we set out to generalize the velocity field described by equation (1.6.27) in a way that clarifies further its physical interpretation.

Consider a two-dimensional Cartesian system, $x'y'$, that has been rotated with respect to a reference system, xy , by an angle β , as shown in [Figure 1.6.2](#). Note that the angle β is

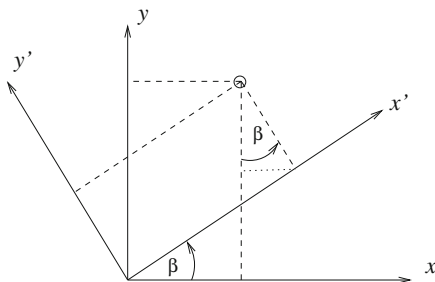


Figure 1.6.2 A system of Cartesian axes, (x', y') , arises by rotating another system, (x, y) , by an angle, β . The length of the dotted horizontal segment is $y' \sin \beta$.

positive when the system $x'y'$ arises from the counterclockwise rotation of xy , and negative otherwise. The unprimed system, xy , provides us with our working coordinates.

A point in the $x'y'$ or xy plane can be identified either by its primed coordinates, (x', y') , or unprimed coordinates, (x, y) . Using elementary trigonometry, we find that the two sets of coordinates are related by

$$x = x' \cos \beta - y' \sin \beta, \quad y = x' \sin \beta + y' \cos \beta. \quad (1.6.29)$$

In vector-matrix notation,

$$\begin{bmatrix} x & y \end{bmatrix} = \begin{bmatrix} x' & y' \end{bmatrix} \cdot \begin{bmatrix} \cos \beta & \sin \beta \\ -\sin \beta & \cos \beta \end{bmatrix}. \quad (1.6.30)$$

Note the left-to-right vector-matrix multiplication on the right-hand side.

Rotation matrix

To simplify the analysis, we introduce the rotation matrix

$$\mathbf{R} \equiv \begin{bmatrix} \cos \beta & \sin \beta \\ -\sin \beta & \cos \beta \end{bmatrix}, \quad (1.6.31)$$

and express (1.6.30) in the form

$$\mathbf{x} = \mathbf{x}' \cdot \mathbf{R}, \quad (1.6.32)$$

where $\mathbf{x}' = (x', y')$ and $\mathbf{x} = (x, y)$.

The rotation matrix has two important properties. First, its determinant is equal to unity,

$$\det(\mathbf{R}) = 1. \quad (1.6.33)$$

To explain the second property, we introduce the transpose of \mathbf{R} , which arises by interchanging the off-diagonal elements R_{12} and R_{21} , to formulate the new matrix

$$\mathbf{R}^T = \begin{bmatrix} \cos \beta & -\sin \beta \\ \sin \beta & \cos \beta \end{bmatrix}, \quad (1.6.34)$$

where the superscript T denotes the transpose. Using the rules of matrix multiplication, we find that

$$\mathbf{R} \cdot \mathbf{R}^T = \mathbf{I}, \quad \mathbf{R}^T \cdot \mathbf{R} = \mathbf{I}, \quad (1.6.35)$$

where \mathbf{I} is the unit or identity matrix defined as

$$\mathbf{I} = \begin{bmatrix} 1 & 0 \\ 0 & 1 \end{bmatrix}. \quad (1.6.36)$$

The inverse of an arbitrary square matrix, \mathbf{A} , is another matrix, denoted as \mathbf{A}^{-1} , with the properties

$$\mathbf{A} \cdot \mathbf{A}^{-1} = \mathbf{I}, \quad \mathbf{A}^{-1} \cdot \mathbf{A} = \mathbf{I}. \quad (1.6.37)$$

If the inverse matrix, \mathbf{A}^{-1} , is equal to the matrix transpose, \mathbf{A}^T , then the matrix \mathbf{A} is called orthogonal. In light of this definition, equations (1.6.35) ensure that the rotation matrix, \mathbf{R} , is orthogonal. Relation (1.6.32) can then be inverted to give

$$\mathbf{x}' = \mathbf{x} \cdot \mathbf{R}^T, \quad (1.6.38)$$

providing us with the primed coordinates in terms of the unprimed coordinates.

Velocities

Working in a similar fashion, we find that the components of the velocity vector in the xy and $x'y'$ coordinates are related by the counterparts of relations (1.6.32) and (1.6.38),

$$\mathbf{u} = \mathbf{u}' \cdot \mathbf{R}, \quad \mathbf{u}' = \mathbf{u} \cdot \mathbf{R}^T, \quad (1.6.39)$$

where $\mathbf{u}' = (u_{x'}, u_{y'})$ and $\mathbf{u} = (u_x, u_y)$.

Having made the necessary preparations, we multiply both sides of equation (1.6.27) by the rotation matrix, \mathbf{R} , and exploit the first orthogonality property in (1.6.35) to obtain

$$\mathbf{u}' \cdot \mathbf{R} = \mathbf{x}' \cdot \mathbf{A} \cdot \mathbf{R} = \mathbf{x}' \cdot \mathbf{I} \cdot \mathbf{A} \cdot \mathbf{R} = \mathbf{x}' \cdot \mathbf{R} \cdot \mathbf{R}^T \mathbf{A} \cdot \mathbf{R}. \quad (1.6.40)$$

Using equations (1.6.32) and (1.6.39), we obtain

$$\mathbf{u} = \mathbf{x} \cdot \mathbf{B}, \quad (1.6.41)$$

where

$$\mathbf{B} \equiv \mathbf{R}^T \cdot \mathbf{A} \cdot \mathbf{R} \quad (1.6.42)$$

is a new matrix. Substituting (1.6.28), (1.6.31), and (1.6.34) into the right-hand side of (1.6.42) and using the trigonometric identities

$$\cos(2\beta) = \cos^2 \beta - \sin^2 \beta, \quad \sin(2\beta) = 2 \sin \beta \cos \beta, \quad (1.6.43)$$

we derive the explicit form

$$\mathbf{B} = \begin{bmatrix} G \cos(2\beta) + \frac{1}{2} \alpha & -G \sin(2\beta) + \Omega \\ -G \sin(2\beta) - \Omega & -G \cos(2\beta) + \frac{1}{2} \alpha \end{bmatrix}. \quad (1.6.44)$$

Note that, when $\beta = 0$ or π , the matrix \mathbf{B} reduces to the matrix \mathbf{A} given in equation (1.6.28). The four elements of the matrix \mathbf{B} are defined in terms of the three flow parameters Ω , G , and α , and the rotation angle, β .

1.6.6 Fundamental decomposition of a two-dimensional flow

In practice, we are interested in the inverse problem: given the four elements of the matrix \mathbf{B} , obtained by laboratory measurements or numerical computation, we want to evaluate the four parameters Ω , G , and α , and β , and thereby extract, respectively, the rate of rotation, the rate of deformation, the rate of expansion, and the direction of deformation.

By way of an example, we consider a linear flow whose velocity components are given by

$$u_x = ax + cy, \quad u_y = bx + dy, \quad (1.6.45)$$

where a , b , c , and d are four constants with units of inverse time. In vector notation,

$$\begin{bmatrix} u_x & u_y \end{bmatrix} = \begin{bmatrix} x & y \end{bmatrix} \cdot \begin{bmatrix} a & b \\ c & d \end{bmatrix}. \quad (1.6.46)$$

Setting each component of the matrix on the right-hand side of (1.6.46) equal to the corresponding component of the matrix \mathbf{B} on the right-hand side of (1.6.44), we obtain a nonlinear system of four trigonometric equations for the four unknowns, Ω , G , α , and β ,

$$\begin{aligned} G \cos(2\beta) + \frac{1}{2} \alpha &= a, & -G \sin(2\beta) + \Omega &= b, \\ -G \sin(2\beta) - \Omega &= c, & -G \cos(2\beta) + \frac{1}{2} \alpha &= d. \end{aligned} \quad (1.6.47)$$

The solution can be found most readily according to the following steps.

First, we resolve the matrix on the right-hand side of (1.6.46) into three constituents,

$$\mathbf{B} = \begin{bmatrix} a & b \\ c & d \end{bmatrix} = \frac{1}{2} \begin{bmatrix} 0 & b - c \\ c - b & 0 \end{bmatrix} + \frac{1}{2} \begin{bmatrix} a - d & b + c \\ c + b & d - a \end{bmatrix} + \frac{1}{2} \begin{bmatrix} a + d & 0 \\ 0 & a + d \end{bmatrix}. \quad (1.6.48)$$

The first matrix on the right-hand side of (1.6.48) is antisymmetric or skew-symmetric, which means that the 12 component is equal to the negative of the 21 component. The

second matrix is symmetric with zero trace.¹ The third matrix is diagonal and isotropic, which means that the two diagonal elements are identical. The decomposition into these three components is unique by construction.

With reference to the first matrix on the right-hand side of (1.6.48), we identify the rate of rotation,

$$\Omega = \frac{1}{2} (b - c). \quad (1.6.49)$$

With reference to the third matrix on the right-hand side of (1.6.48), we identify the rate of expansion,

$$\alpha = a + d. \quad (1.6.50)$$

Eigenvalues and eigenvectors

To extract the remaining two unknowns, G and β , we consider the second matrix on the right-hand side of (1.6.48), defined as

$$\mathbf{E} = \frac{1}{2} \begin{bmatrix} a - d & b + c \\ c + b & d - a \end{bmatrix}. \quad (1.6.51)$$

An eigenvalue of \mathbf{E} , denoted by λ , and the corresponding eigenvector, denoted by

$$\mathbf{w} = \begin{bmatrix} w_x \\ w_y \end{bmatrix}, \quad (1.6.52)$$

satisfy the equation

$$\mathbf{E} \cdot \mathbf{w} = \lambda \mathbf{w}, \quad (1.6.53)$$

or

$$(\mathbf{E} - \lambda \mathbf{I}) \cdot \mathbf{f} = \mathbf{0}, \quad (1.6.54)$$

where \mathbf{I} is the 2×2 unit matrix and

$$\mathbf{E} - \lambda \mathbf{I} = \frac{1}{2} \begin{bmatrix} a - d - 2\lambda & b + c \\ c + b & d - a - 2\lambda \end{bmatrix}. \quad (1.6.55)$$

The eigenvalues of \mathbf{E} are found by setting the determinant of the matrix $\mathbf{E} - \lambda \mathbf{I}$ to zero, thereby ensuring that the system (1.6.54) admits a nontrivial solution. Formulating the determinant, we obtain the quadratic equation

$$\left(\frac{1}{2} (a - d) - \lambda \right) \left(\frac{1}{2} (d - a) - \lambda \right) - \frac{1}{4} (b + c)^2 = 0, \quad (1.6.56)$$

¹The trace of an arbitrary square matrix is defined as the sum of the diagonal elements. For example, the trace of the $N \times N$ identity matrix is equal to N . The trace of a matrix is equal to the sum of its eigenvalues.

whose roots are found to be

$$\lambda = \pm \frac{1}{2} \sqrt{(a-d)^2 + (b+c)^2}. \quad (1.6.57)$$

The corresponding eigenvectors are found by solving the homogeneous system (1.6.54). Having computed the eigenvalues and eigenvectors of the matrix \mathbf{E} , we recover the constants G and β by setting

$$G = \lambda, \quad (1.6.58)$$

with the plus or minus sign selected on the right-hand side of (1.6.57), and identifying β with the angle subtended between the corresponding eigenvector \mathbf{w} and the x axis, that is, we compute the angle β from the equation

$$\tan \beta = \frac{w_y}{w_x}. \quad (1.6.59)$$

A typical linear flow

To be more specific, we consider a two-dimensional linear velocity field with velocity components

$$u_x(x, y, t) = \xi(t)(2x - y), \quad u_y(x, y, t) = \xi(t)(-3x + 3y), \quad (1.6.60)$$

where $\xi(t)$ is an arbitrary function of time with dimensions of inverse time. The four time-dependent parameters a , b , c , and d introduced in (1.6.46) are specified as

$$a = 2\xi(t), \quad b = -3\xi(t), \quad c = -\xi(t), \quad d = 3\xi(t). \quad (1.6.61)$$

Thus,

$$\mathbf{B} = \xi(t) \begin{bmatrix} 2 & -3 \\ -1 & 3 \end{bmatrix}. \quad (1.6.62)$$

Carrying out the decomposition shown in equation (1.6.48), we find that

$$\mathbf{B} = \xi(t) \left(\frac{1}{2} \begin{bmatrix} 0 & -2 \\ 2 & 0 \end{bmatrix} + \frac{1}{2} \begin{bmatrix} -1 & -4 \\ -4 & 1 \end{bmatrix} + \frac{1}{2} \begin{bmatrix} 5 & 0 \\ 0 & 5 \end{bmatrix} \right). \quad (1.6.63)$$

Using equations (1.6.49) and (1.6.50), we find that the rate of rotation and rate of expansion are given by

$$\Omega = -\xi(t), \quad \alpha = 5\xi(t). \quad (1.6.64)$$

The symmetric matrix \mathbf{E} defined in equation (1.6.51) is given by the second term on the right-hand side of (1.6.63),

$$\mathbf{E} = \xi(t) \begin{bmatrix} -\frac{1}{2} & -2 \\ -2 & \frac{1}{2} \end{bmatrix}. \quad (1.6.65)$$

The eigenvalues of \mathbf{E} are found by setting the determinant of the following matrix to zero:

$$\mathbf{E} - \lambda \mathbf{I} = \begin{bmatrix} -\frac{1}{2}\xi(t) - \lambda & -2\xi(t) \\ -2\xi(t) & \frac{1}{2}\xi(t) - \lambda \end{bmatrix}. \quad (1.6.66)$$

The roots of the resulting quadratic equation are found to be

$$\lambda = \pm \frac{\sqrt{17}}{2} \xi(t). \quad (1.6.67)$$

Either one of these values can be identified with the rate of extension, G , as indicated by equation (1.6.58).

Substituting expressions (1.6.67) into (1.6.54) we obtain two homogeneous equations,

$$\begin{bmatrix} -\frac{1}{2}(1 \pm \sqrt{17}) & -2 \\ -2 & -\frac{1}{2}(-1 \pm \sqrt{17}) \end{bmatrix} \cdot \begin{bmatrix} w_x \\ w_y \end{bmatrix} = \begin{bmatrix} 0 \\ 0 \end{bmatrix}. \quad (1.6.68)$$

In fact, the two scalar equations comprising this system are identical; the redundancy underlines the notion of an eigensolution. Using the first equation, we obtain

$$\frac{w_y}{w_x} = -\frac{1 \pm \sqrt{17}}{4}. \quad (1.6.69)$$

Following the instructions given in the paragraph following equation (1.6.57), we finally obtain

$$\beta = -\arctan \frac{1 \pm \sqrt{17}}{4}. \quad (1.6.70)$$

In summary, we have managed to extract the rate of rotation, rate of expansion, two rates of deformation, and the corresponding eigenvectors in a linear two-dimensional flow.

Simple shear flow

The velocity components of simple shear flow in the xy plane are given by

$$u_x = \xi(t) y, \quad u_y = 0, \quad (1.6.71)$$

where $\xi(t)$ is a constant or time-dependent coefficient with units of inverse time, called the *shear rate*, as shown in [Figure 1.6.3](#). The four coefficients, a , b , c , and d , introduced in (1.6.46) are

$$a = 0, \quad b = 0, \quad c = \xi(t), \quad d = 0. \quad (1.6.72)$$

Thus,

$$\mathbf{B} = \begin{bmatrix} 0 & 0 \\ \xi(t) & 0 \end{bmatrix}. \quad (1.6.73)$$

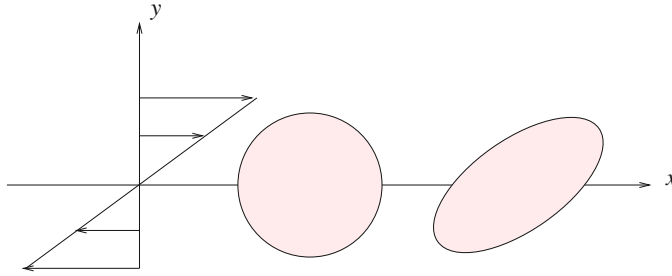


Figure 1.6.3 Illustration of simple shear flow in the xy plane. A circular fluid parcel deforms into an inclined ellipse as the upper part of the parcel moves forward and the lower part of the parcel moves backward relative to the parcel center.

Carrying out the decomposition shown in equation (1.6.48), we find that

$$\mathbf{B} = \frac{1}{2} \xi(t) \left(\begin{bmatrix} 0 & -1 \\ 1 & 0 \end{bmatrix} + \begin{bmatrix} 0 & 1 \\ 0 & 1 \end{bmatrix} + \begin{bmatrix} 0 & 0 \\ 0 & 0 \end{bmatrix} \right). \quad (1.6.74)$$

Using equations (1.6.49) and (1.6.50), we find that the rate of rotation and rate of expansion are given by

$$\Omega = -\frac{1}{2} \xi(t), \quad \alpha = 0. \quad (1.6.75)$$

When $\xi > 0$, a fluid parcel rotates in the clockwise direction, $\Omega < 0$; when $\xi < 0$, a fluid parcel rotates in the counterclockwise direction, $\Omega > 0$.

The symmetric matrix \mathbf{E} defined in equation (1.6.51) is given by the second term on the right-hand side of (1.6.74),

$$\mathbf{E} = \frac{1}{2} \xi(t) \begin{bmatrix} 0 & 1 \\ 1 & 0 \end{bmatrix}. \quad (1.6.76)$$

The eigenvalues of \mathbf{E} are found by setting the determinant of the following matrix to zero,

$$\mathbf{E} - \lambda \mathbf{I} = \begin{bmatrix} -\lambda & \frac{1}{2} \xi(t) \\ \frac{1}{2} \xi(t) & -\lambda \end{bmatrix}. \quad (1.6.77)$$

The roots of the resulting quadratic equation are found readily to be

$$\lambda = \pm \frac{1}{2} \xi(t). \quad (1.6.78)$$

Either one of these values can be identified with the rate of extension, G , as indicated by equation (1.6.58).

Substituting the eigenvalues given in (1.6.78) into (1.6.54), we obtain a linear system for the eigenvector components,

$$\begin{bmatrix} \mp 1 & 1 \\ 1 & \mp 1 \end{bmatrix} \cdot \begin{bmatrix} w_x \\ w_y \end{bmatrix} = \begin{bmatrix} 0 \\ 0 \end{bmatrix}, \quad (1.6.79)$$

yielding

$$\frac{w_y}{w_x} = \pm 1. \quad (1.6.80)$$

The first eigenvector corresponding to the + sign is inclined by 45° with respect to the x axis. The second eigenvector corresponding to the – sign is inclined at 135° with respect to the x axis. These results are consistent with the physical interpretation of the deformation of a circular patch, as illustrated in [Figure 1.6.3](#).

PROBLEMS

1.6.1 Material lines

A collection of point particles distributed along a line in a flow defines a material line. Explain why, if the flow is steady, a material line that lies at a streamline at a certain time will remain on the streamline at any time.

1.6.2 Rotation of coordinates

Use elementary trigonometry to derive two equations that relate the old coordinates, (x', y') , to the new coordinates, (x, y) , and *vice versa*.

1.6.3 Fundamental decomposition of a flow

Carry out the decomposition of a two-dimensional flow with velocity components

$$u_x(x, y, t) = \xi(t) (2x + 3y) \quad u_y(x, y, t) = \xi(t) (-x - 2y), \quad (1.6.81)$$

where $\xi(t)$ is a given function of time.

1.7 Numerical interpolation

In practice, the components of the fluid velocity are rarely available in an explicit form, as shown in equations (1.4.8) and (1.5.2). Instead, they are either measured in the laboratory with velocity probes or computed by numerical methods at data points inside the domain of a flow.

Typically, but not always, the data points are located at the nodes of a grid defined by the intersections of straight or curved lines in two dimensions, or by the intersection of planar or curved surfaces in three dimensions. The velocity at an arbitrary point is then obtained by a numerical procedure known as function interpolation.

A Cartesian grid is defined by the intersection of straight lines that are normal to the x or y axis in two dimensions, and by the intersection of planes that are normal to x , y , or z axis in three dimensions. A one-dimensional, a two-dimensional, and a three-dimensional Cartesian grid with evenly spaced grid lines are shown in [Figure 1.7.1](#).

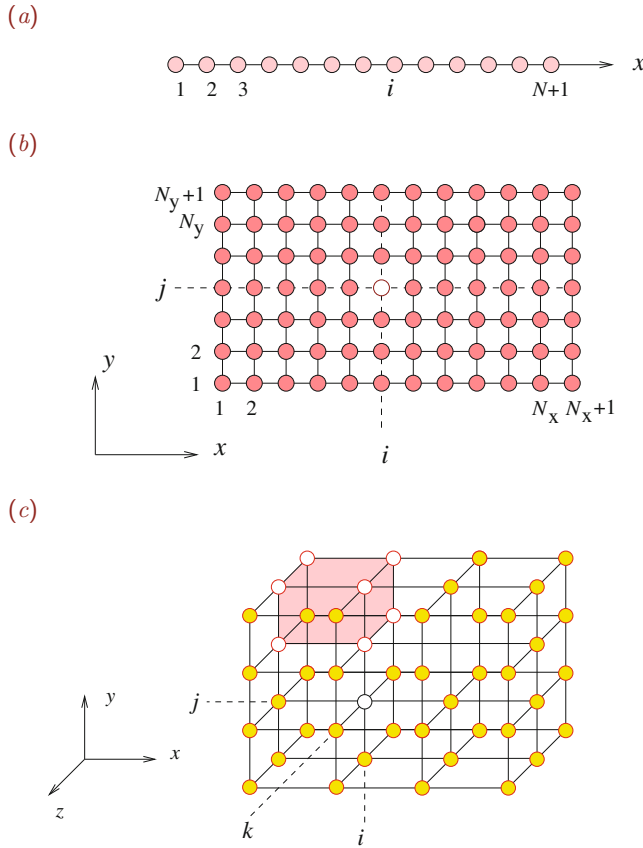


Figure 1.7.1 Illustration of (a) a one-dimensional grid with N divisions, (b) a two-dimensional $N_x \times N_y$ Cartesian grid, and (c) a three-dimensional $N_x \times N_y \times N_z$ Cartesian grid with evenly spaced grid lines.

1.7.1 Interpolation in one dimension

To prepare the ground for computing the components of the velocity at an arbitrary point in a flow from specified grid values, we develop methods of interpolating a function, $f(x)$, of one independent variable, x .

Let us assume that the values of a function, $f(x)$, are available at $N + 1$ nodes of a one-dimensional grid, located at x_i for $i = 1, \dots, N + 1$, where $x_1 < x_2 < \dots < x_{N+1}$, as shown in [Figure 1.7.1\(a\)](#). Effectively, we are provided with a three-column table of $N + 1$ entries listing i , x_i , and $f(x_i)$; for simplicity, we denote $f(x_i)$ by f_i , that is,

$$f_i \equiv f(x_i). \tag{1.7.1}$$

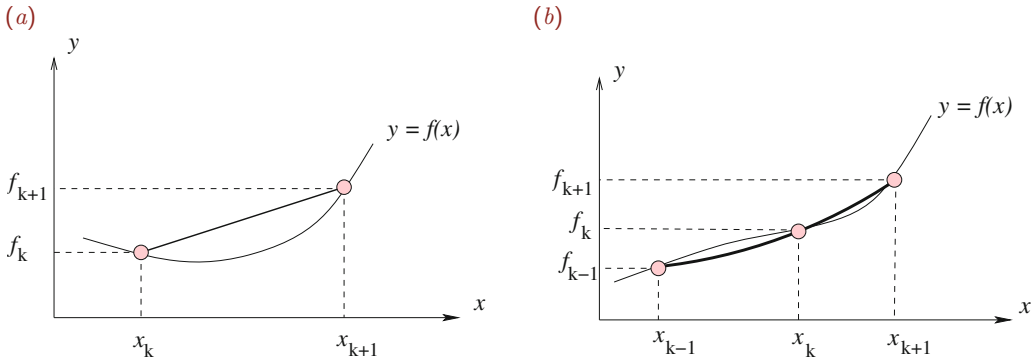


Figure 1.7.2 Local approximation of a function, $f(x)$, with (a) a linear interpolating function represented by the straight line or (b) a parabolic interpolating function represented by the bold line.

Our goal is to compute the value of the function $f(x)$ at a point, x , that does not necessarily coincide with a node.

A set of $N + 1$ nodes define N intervals, where the i th interval starts at the i th node and ends at the $i + 1$ node. Suppose that the point x lies inside the k th interval subtended between the nodes x_k and x_{k+1} . A simple way of finding the value of k is by computing the products

$$p_i = (x - x_i)(x - x_{i+1}) \quad (1.7.2)$$

for $i = 1, \dots, N$. The appropriate value of k is the unique value of i for which p_i is negative.

Better and faster methods of finding the label of the host interval, k , are available. For example, in the method of logarithmic search, we first examine whether the point x lies on the left or on the right of the mid-point of the interpolation domain (x_1, x_{N+1}) . Having found the host half-interval, we repeat the process until the host sub-interval has been reduced to the k th interval.

Linear interpolation

To compute the value $f(x)$, we may approximate the graph of the function $f(x)$ in the host interval, (x_k, x_{k+1}) , with a straight line, and require that the straight line interpolates through the data points (x_k, f_k) and (x_{k+1}, f_{k+1}) , as illustrated in [Figure 1.7.2\(a\)](#).

In mathematical terms, we approximate the function $f(x)$ inside the interval (x_k, x_{k+1}) with a linear function expressed by the first-degree polynomial

$$P_1^{(k)}(x) = a^{(k)}(x - x_k) + b^{(k)}, \quad (1.7.3)$$

where the coefficient $a^{(k)}$ is the slope and the constant $b^{(k)}$ is the intercept. To facilitate forthcoming algebraic manipulations, we have expressed the polynomial in terms of the shifted monomial $x - x_k$, rather than in terms of the unshifted monomial, x .

To compute the constants $a^{(k)}$ and $b^{(k)}$, we enforce the interpolation conditions

$$\begin{aligned} P_1^{(k)}(x_k) &= b^{(k)} = f_k, \\ P_1^{(k)}(x_{k+1}) &= a^{(k)}(x_{k+1} - x_k) + b^{(k)} = f_{k+1}, \end{aligned} \quad (1.7.4)$$

which ensure that the graph of the polynomial passes through the data labeled k and $k+1$. Solving the system of the two linear equations (1.7.4) for the two monomial coefficients, we obtain

$$a^{(k)} = \frac{f_{k+1} - f_k}{x_{k+1} - x_k}, \quad b^{(k)} = f_k. \quad (1.7.5)$$

To compute the linear polynomial $P_1^{(k)}(x)$, we first calculate the coefficients $a^{(k)}$ and $b^{(k)}$ using equations (1.7.5), and then evaluate the right-hand side of (1.7.3) for a desired value of x that lies between x_k and x_{k+1} . The result will be a reasonable approximation to the desired value, $f(x)$.

Quadratic interpolation

Interpolation based on the straight-line approximation overlooks the curvature of the graph of the function $f(x)$. For better accuracy, we may approximate the function $f(x)$ with a parabola defined in the interval (x_k, x_{k+1}) , as depicted in [Figure 1.7.2\(b\)](#). In mathematical terms, we approximate the function $f(x)$ with a quadratic function expressed by the second-degree polynomial

$$P_2^{(k)}(x) = a^{(k)}(x - x_k)^2 + b^{(k)}(x - x_k) + c^{(k)}. \quad (1.7.6)$$

To simplify the forthcoming algebraic manipulations, we have expressed the polynomial in terms of the shifted monomial $x - x_k$, rather than the unshifted monomial, x .

To compute the three constants, $a^{(k)}$, $b^{(k)}$, and $c^{(k)}$, we require three equations. First, we demand that the parabola interpolates through the two data points (x_k, f_k) and (x_{k+1}, f_{k+1}) , and obtain the interpolation conditions

$$\begin{aligned} P_2^{(k)}(x_k) &= c^{(k)} = f_k, \\ P_2^{(k)}(x_{k+1}) &= a^{(k)}(x_{k+1} - x_k)^2 + b^{(k)}(x_{k+1} - x_k) + c^{(k)} = f_{k+1}. \end{aligned} \quad (1.7.7)$$

One more datum point is required, and we may choose either the backward point, (x_{k-1}, f_{k-1}) , or the forward point, (x_{k+2}, f_{k+2}) . The backward choice provides us with the condition

$$P_2^{(k)}(x_{k-1}) = a^{(k)}(x_{k-1} - x_k)^2 + b^{(k)}(x_{k-1} - x_k) + c^{(k)} = f_{k-1}. \quad (1.7.8)$$

With the choice expressed by equations (1.7.7) and (1.7.8), the coefficients of the binomial are found to be

$$a^{(k)} = \frac{\frac{f_{k+1} - f_k}{h_k} - \frac{f_k - f_{k-1}}{h_{k-1}}}{h_k + h_{k-1}}, \quad b^{(k)} = \frac{h_{k-1} \frac{f_{k+1} - f_k}{h_k} + h_k \frac{f_k - f_{k-1}}{h_{k-1}}}{h_k + h_{k-1}}, \quad c^{(k)} = f_k, \quad (1.7.9)$$

where

$$h_{k-1} = x_k - x_{k-1}, \quad h_k = x_{k+1} - x_k \quad (1.7.10)$$

are the lengths of the backward and forward intervals.

When the data points are spaced evenly, $h_{k-1} = h_k \equiv h$, we obtain the simplified expressions

$$a^{(k)} = \frac{f_{k+1} - 2f_k + f_{k-1}}{2h^2}, \quad b^{(k)} = \frac{f_{k+1} - f_{k-1}}{2h}, \quad c^{(k)} = f_k. \quad (1.7.11)$$

To compute $P_2^{(k)}(x)$, we first calculate the coefficients $a^{(k)}$, $b^{(k)}$, and $c^{(k)}$ using the preceding equations, and then evaluate the right-hand side of (1.7.6). The result will be an approximation to $f(x)$ that is improved with respect to that computed by linear interpolation.

1.7.2 Interpolation in two dimensions

Next, we consider a function of two independent variables, x and y . For the present purposes, a function of two variables is an engine that receives a pair of numbers, x and y , and generates a new number, $f(x, y)$.

Cartesian grid

Assume that values of a function, $f(x, y)$, are given at the nodes of a two-dimensional Cartesian grid defined by the intersections of x -level lines x_i for $i = 1, \dots, N_x + 1$, and y -level lines y_j for $j = 1, \dots, N_y + 1$, as shown in [Figure 1.7.1\(b\)](#). A grid node is identified by the values of two indices, i and j , forming an ordered integer doublet, (i, j) . The value of the function $f(x, y)$ at the (i, j) node is equal to $f(x_i, y_j)$. Our goal is to compute the value of f at a point, (x, y) , that is not necessarily a node.

Grid generation

The following function entitled *grid_2d*, located in directory *rec_2d* inside directory *02_grids* of **FDLIB**, generates evenly spaced grid lines and grid points in a rectangular domain in the xy plane confined between $a_x \leq x \leq b_x$ and $a_y \leq y \leq b_y$, with N_x intervals in the x direction and N_y intervals in the y direction:

```
function [glx,gly,gx,gy] = grid_2d (ax,bx,ay,by,Nx,Ny)

%-----
% grid spacing
%-----

Dx = (bx-ax)/Nx;
Dy = (by-ay)/Ny;
```

```

%---
% generate the grid lines
%---

for i=1:Nx+1
    glx(i) = ax+(i-1.0)*Dx;
end

for j=1:Ny+1
    gly(j) = ay+(j-1.0)*Dy;
end

%---
% generate the grid points
%---

for i=1:Nx+1
    for j=1:Ny+1
        gx(i,j) = glx(i);
        gy(i,j) = gly(j);
    end
end

%-----
% done
%-----

return

```

Suppose that a value of x lies inside the k_x th x -interval confined between the x_{k_x} and x_{k_x+1} x -level lines, and a value of y lies inside the k_y th y -interval confined between the y_{k_y} and y_{k_y+1} y -level lines, as shown in [Figure 1.7.3](#). The values of k_x and k_y can be found by the methods discussed in Section 1.7.1 for one-dimensional interpolation.

Bilinear interpolation

A sensible approximation to $f(x, y)$ can be obtained by replacing $f(x, y)$, with a bilinear function,

$$\Pi^{k_x, k_y}(x, y), \quad (1.7.12)$$

defined in a rectangular domain that is confined between the x -level lines $x = x_{k_x}$ and $x = x_{k_x+1}$, and y -level lines $y = y_{k_y}$ and $y = y_{k_y+1}$. The bilinear function is distinguished by the following properties:

1. For a fixed value of x , call it x_0 , the function $\Pi^{k_x, k_y}(x_0, y)$ varies linearly with respect to y .
2. For a fixed value of y , call it y_0 , the function $\Pi^{k_x, k_y}(x, y_0)$ varies linearly with respect to x .

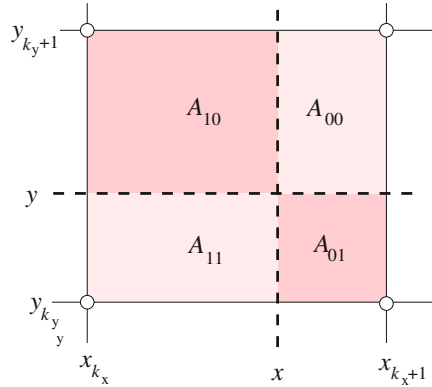


Figure 1.7.3 Bilinear interpolation of a scalar function at a point, (x, y) , through a rectangular grid. The four areas shown determine the interpolation weights.

3. The following four interpolation conditions ensure that the bilinear function reproduces the neighboring grid values:

$$\begin{aligned}
 \Pi^{k_x, k_y}(x_{k_x}, y_{k_y}) &= f(x_{k_x}, y_{k_y}), \\
 \Pi^{k_x, k_y}(x_{k_x}, y_{k_y+1}) &= f(x_{k_x}, y_{k_y+1}), \\
 \Pi^{k_x, k_y}(x_{k_x+1}, y_{k_y}) &= f(x_{k_x+1}, y_{k_y}), \\
 \Pi^{k_x, k_y}(x_{k_x+1}, y_{k_y+1}) &= f(x_{k_x+1}, y_{k_y+1}).
 \end{aligned} \tag{1.7.13}$$

The first and second properties require that the bilinear function has the functional form

$$\Pi^{k_x, k_y}(x, y) = (a_x^{k_x, k_y} x + b_x^{k_x, k_y})(a_y^{k_x, k_y} y + b_y^{k_x, k_y}). \tag{1.7.14}$$

To evaluate the four constants, $a_x^{k_x, k_y}$, $b_x^{k_x, k_y}$, $a_y^{k_x, k_y}$, and $b_y^{k_x, k_y}$, we use the four interpolation conditions (1.7.13), obtaining

$$\begin{aligned}
 \Pi^{k_x, k_y}(x, y) &= w_{00}^{k_x, k_y}(x, y) f(x_{k_x}, y_{k_y}) + w_{10}^{k_x, k_y}(x, y) f(x_{k_x+1}, y_{k_y}) \\
 &\quad + w_{01}^{k_x, k_y}(x, y) f(x_{k_x}, y_{k_y+1}) + w_{11}^{k_x, k_y}(x, y) f(x_{k_x+1}, y_{k_y+1}),
 \end{aligned} \tag{1.7.15}$$

where

$$\begin{aligned}
 w_{00}^{k_x, k_y}(x, y) &= \frac{A_{00}}{A}, & w_{10}^{k_x, k_y}(x, y) &= \frac{A_{10}}{A}, \\
 w_{01}^{k_x, k_y}(x, y) &= \frac{A_{01}}{A}, & w_{11}^{k_x, k_y}(x, y) &= \frac{A_{11}}{A}.
 \end{aligned} \tag{1.7.16}$$

are position-dependent interpolation weights. The numerators, A_{00} , A_{10} , A_{01} , and A_{11} , are the areas of the four sub-rectangles depicted in [Figure 1.7.3](#), given by

$$\begin{aligned}
 A_{00} &= (x_{k_x+1} - x)(y_{k_y+1} - y), & A_{10} &= (x - x_{k_x})(y_{k_y+1} - y), \\
 A_{01} &= (x_{k_x+1} - x)(y - y_{k_y}), & A_{11} &= (x - x_{k_x})(y - y_{k_y}).
 \end{aligned} \tag{1.7.17}$$

The common denominator, A , is the area of the interpolation rectangle, given by

$$A = A_{00} + A_{01} + A_{10} + A_{11} = (x_{k_x+1} - x_{k_x})(y_{k_y+1} - y_{k_y}). \quad (1.7.18)$$

It is reassuring to observe that the sum of the four interpolation weights given in (1.7.16) is equal to unity for any x and y ,

$$w_{00}^{k_x, k_y}(x, y) + w_{10}^{k_x, k_y}(x, y) + w_{01}^{k_x, k_y}(x, y) + w_{11}^{k_x, k_y}(x, y) = 1. \quad (1.7.19)$$

This property guarantees that, if the four participating grid values are equal,

$$f(x_{k_x}, y_{k_y}) = f(x_{k_x}, y_{k_y+1}) = f(x_{k_x+1}, y_{k_y}) = f(x_{k_x+1}, y_{k_y+1}) = \phi, \quad (1.7.20)$$

then bilinear interpolation based on (1.7.15) predicts that

$$\Pi^{k_x, k_y}(x, y) = \phi (w_{00}^{k_x, k_y} + w_{10}^{k_x, k_y} + w_{01}^{k_x, k_y} + w_{11}^{k_x, k_y}) = \phi, \quad (1.7.21)$$

as required.

1.7.3 Interpolation of the velocity in a two-dimensional flow

Returning to fluid mechanics, we consider a two-dimensional flow in the xy plane and specify the values of the x and y velocity components, u_x and u_y , at the nodes of a two-dimensional Cartesian grid. To obtain the corresponding values at an arbitrary point, (x, y) , we employ bilinear interpolation, finding that

$$\begin{aligned} u_x(x, y) = & w_{00}^{k_x, k_y}(x, y) u_x(x_{k_x}, y_{k_y}) + w_{10}^{k_x, k_y}(x, y) u_x(x_{k_x+1}, y_{k_y}) \\ & + w_{01}^{k_x, k_y}(x, y) u_x(x_{k_x}, y_{k_y+1}) + w_{11}^{k_x, k_y}(x, y) u_x(x_{k_x+1}, y_{k_y+1}) \end{aligned} \quad (1.7.22)$$

and

$$\begin{aligned} u_y(x, y) = & w_{00}^{k_x, k_y}(x, y) u_y(x_{k_x}, y_{k_y}) + w_{10}^{k_x, k_y}(x, y) u_y(x_{k_x+1}, y_{k_y}) \\ & + w_{01}^{k_x, k_y}(x, y) u_y(x_{k_x}, y_{k_y+1}) + w_{11}^{k_x, k_y}(x, y) u_y(x_{k_x+1}, y_{k_y+1}). \end{aligned} \quad (1.7.23)$$

The following MATLAB function entitled *rec_2d_int*, residing in directory *rec_2d* inside directory *02_grids* of *FDLIB*, performs the interpolation in a rectangular domain confined in $a_x \leq x \leq b_x$ and $a_y \leq y \leq b_y$:

```
function [ux,uy] = rec_2d_int ...
...
(ax,bx ...      % x end points
,ay,by ...      % y end points
,Nx,Ny ...      % grid size
,glx,gly ...    % grid lines
,gux,guy ...    % grid velocity
```

```

,x,y ...      % interpolation point
)

%=====
% Bilinear interpolation of the velocity
% at a point, (x, y)
%=====

%-----
% locate the x and y intervals
%-----

for kx=1:Nx
    prod = (x-glx(kx))*(x-glx(kx+1));
    if(prod<0) break; end
end

for ky=1:Ny
    prod = (y-gly(ky))*(y-gly(ky+1));
    if(prod<0) break; end
end

%-----
% interpolation weights
%-----

A00 = (glx(kx+1)-x)*(gly(ky+1)-y);
A01 = (glx(kx+1)-x)*(y-gly(ky));
A10 = (x-glx(kx))*(gly(ky+1)-y);
A11 = (x-glx(kx))*(y-gly(ky));
A = (glx(kx+1)-glx(kx))*(gly(ky+1)-gly(ky));

w00 = A00/A; w01 = A01/A; w10 = A10/A; w11 = A11/A;

%-----
% interpolation
%-----

ux = w00 * gux(kx ,ky) + w01 * gux(kx ,ky+1) ...
    + w10 * gux(kx+1,ky) + w11 * gux(kx+1,ky+1);
uy = w00 * guy(kx ,ky) + w01 * guy(kx ,ky+1) ...
    + w10 * guy(kx+1,ky) + w11 * guy(kx+1,ky+1);

%---
% done
%---

return

```

The following MATLAB code entitled *rec_2d*, located in directory *02_grids* of *FDLIB*, generates a grid and calls this function to display a velocity vector field:

```

%=====
% rec_2d: velocity vector field by interpolation
%=====

ax = -1.3; bx = 1.3; ay = -1.0; by = 1.0;

Nx = 16; Ny = 8; % grid size

%---
% prepare to plot
%---

figure(1)
hold on
axis([ax-0.1, bx+0.1, ay-0.1, by+0.1])
axis equal
xlabel('x','fontsize',14)
ylabel('y','fontsize',14)
set(gca,'fontsize',14)
box on
title('Velocity vector field')

plot([ax, bx, bx, ax, ax],[ay, ay, by, by, ay],'-k')

%-----
% generate the grid
%-----

[ glx,gly,gx,gy ] = grid_2d (ax,bx,ay,by,Nx,Ny);

%---
% specify the grid velocities (typical)
%---

for i=1:Nx+1
    for j=1:Ny+1
        gux(i,j) = gx(i,j);
        guy(i,j) = -gy(i,j);
    end
end

%---
% velocity vector field
% in the middle of each cell
%---

```

```

for i=1:Nx
  x = 0.5*(glx(i)+glx(i+1));
  for j=1:Ny
    y = 0.5*(gly(j)+gly(j+1));

    plot(x,y,'g.')

```

The graphics display generated by the code for the velocity field specified in the code is shown in [Figure 1.7.4](#).

The following MATLAB function *draw_arrow_2d*, located in directory *rec_2d* inside directory *02_grids* of *FDLIB*, is invoked to generate beautiful arrows:

```

function vector = draw_arrow_2d (x1,y1,dx,dy)

%-----
% Generate coordinates for plotting
% a five-point arrow starting at the point
% (x1,x2) and ending at the point (x1+dx, y1+dy)
%
% SYMBOLS:
% -----
%
% dx, dy:  arrow vector
%
% vector(i,1):  x-coordinate of the ith point
% vector(i,2):  y-coordinate of the ith point
% where i=1,2,3,4,5
%

```



```

% angle:  angle of arrow tip in radians
% tip:    length of arrow tip sides
% as a fraction of the arrow length
%-----

angle = 0.3;
tip = 0.50;

%-----
% prepare
%-----

x2 = x1+dx; y2 = y1+dy;
cs = cos(angle);
sn = sin(angle);
dxi = -dx; dyi = -dy;

%-----
% five points
%-----

vector(1,1) = x1; vector(1,2) = y1;
vector(2,1) = x2; vector(2,2) = y2;
vector(3,1) = x2+( dxi*cs+dyi*sn)*tip;
vector(3,2) = y2+(-dxi*sn+dyi*cs)*tip;
vector(4,1) = x2; vector(4,2) = y2;
vector(5,1) = x2+(dxi*cs-dyi*sn)*tip;
vector(5,2) = y2+(dxi*sn+dyi*cs)*tip;

%-----
% done
%-----

return

```

MATLAB encapsulates the graphics function *quiver* that also generates a velocity vector field over a grid.

1.7.4 Streamlines by interpolation

Our ability to interpolate the velocity components at any point in a flow from specified grid values allows us to generate particle paths and streamlines in the absence of explicit expressions for the velocity field. In computational fluid dynamics (CFD), grid values are computed by solving the equations governing the motion of a fluid using a variety of numerical methods, as discussed in Chapters 3 and 8.

The following MATLAB code entitled *rec_2d_strml*, located in directory *rec_2d* inside directory *02_grids* of **FDLIB**, generates and draws streamlines:

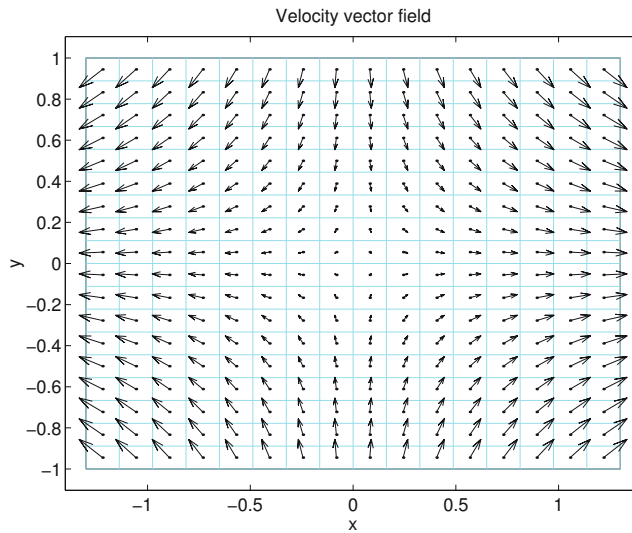


Figure 1.7.4 Bilinear interpolation of a velocity vector field through a Cartesian grid in a two-dimensional flow.

```

%=====
% streamlines in a rectangular cavity
%
% confined in ax<x<bx and ay<y<by
%=====

ax = -1.2; bx = 1.2;
ay = -1.0; by = 1.0;

Nx = 16; Ny = 20; % grid size

Nmax = 400; % maximum steps along a streamline
Ds = 0.020; % travel distance in each step

%-----
% prepare to plot
%-----

figure(1)
hold on
axis([ax-0.1, bx+0.1, ay-0.1, by+0.1])
axis equal
xlabel('x','fontsize',14)
ylabel('y','fontsize',14)
set(gca,'fontsize',14)
box on

```

```

%-----
% generate the grid
%-----

[ glx,gly,gx,gy ] = grid_2d(ax,bx,ay,by,Nx,Ny);

%---
% specify the grid velocities (typical)
%---

for i=1:Nx+1
    for j=1:Ny+1
        gux(i,j) =-gy(i,j);
        guy(i,j) = gx(i,j);
    end
end

%-----
% initial streamline points
%-----

x0 = [0.05 0.1 0.2 0.3 0.4 0.5 0.6 0.7 0.8 0.9 1.0 1.2];

Nstr = size(x0');

for i=1:Nstr
    y0(i) = 0.001;
end

%-----
% loop over streamlines
%-----

for l=1:Nstr

    xn = x0(l);
    yn = y0(l);
    xstr(1) = xn;    % new point
    ystr(1) = yn;    % new point

%----
% integrate by the modified Euler method
%----

    for i=2:Nmax    % step in time

        [ux,uy] = rec_2d_int ...
            ...

```

```

(ax,bx ... % x end points
,ay,by ... % y end points
,Nx,Ny ... % grid size
,glx,gly ... % grid lines
,gux,guy ... % grid velocity
,xn,yn ... % interpolation point
);

Umag = sqrt(ux*ux+uy*uy);
Dt = Ds/Umag;
x1 = xn + Dt*ux;
y1 = yn + Dt*uy;

[ux1,uy1] = rec_2d_int ...
...
(ax,bx ...
,ay,by ...
,Nx,Ny ...
,glx,gly ...
,gux,guy ...
,x1,y1 ...
);

Dth = 0.5*Dt;
xn = xn + Dth*(ux+ux1);
yn = yn + Dth*(uy+uy1);
xstr(i) = xn;
ystr(i) = yn;

%----
% check for a closed streamline after 5 steps (typical)
%---

if(i>5)

    Dist = sqrt((xn-xstr(1))^2+(yn-ystr(1))^2);
    if(Dist<Ds)
        xstr(i+1) = xstr(1);
        ystr(i+1) = ystr(1);
        break;
    end

end

end % over time

plot(xstr,ystr,'r-')

clear xstr ystr

```

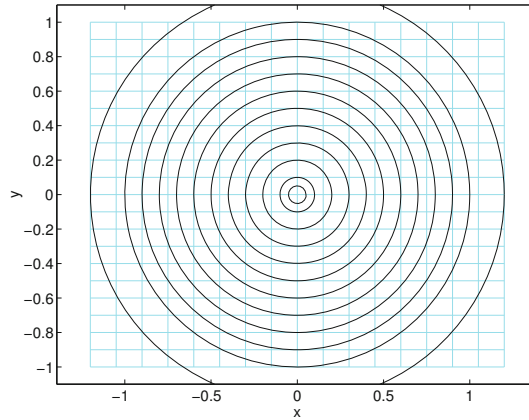


Figure 1.7.5 Streamlines of a rotary flow generated by interpolation from an underlying Cartesian grid.

```

end % of run over streamlines

%---
% done
%---

axis([ax-0.1, bx+0.1, ay-0.1, by+0.1])

```

The graphics display generated by the code for the specified velocity field expressing rigid-body rotation is shown in [Figure 1.7.5](#).

PROBLEMS

1.7.1 Quadratic interpolation

Solve the linear system of three equations (1.7.7) and (1.7.8) to derive formulas (1.7.9). *Hint:* Compute first the coefficient $c^{(k)}$ using the first of equations (1.7.7).

1.7.2 Forward-point parabolic interpolation

Consider the parabolic interpolation of a function of one variable, $f(x)$, as discussed in the text. Forward interpolation employs the interpolation condition

$$P_2^{(k)}(x_{k+2}) = a^{(k)}(x_{k+2} - x_k)^2 + b^{(k)}(x_{k+2} - x_k) + c^{(k)} = f_{k+2}, \quad (1.7.24)$$

in place of (1.7.8). Derive expressions for the coefficients $a^{(k)}$, $b^{(k)}$, and $c^{(k)}$ in terms of the grid values f_k , f_{k+1} , and f_{k+2} , and the interval sizes h_k and h_{k+1} . Then derive simplified expressions when h_k and h_{k+1} are both equal to h .

1.7.3 Trilinear interpolation

Consider a function of three variables, $f(x, y, z)$. Extend the method of bilinear interpolation of a function of two variables, discussed in the text, to the method of trilinear interpolation that generates the value of f at an arbitrary point (x, y, z) using the values of f at the nodes of a three-dimensional Cartesian grid, as shown in [Figure 1.7.1\(c\)](#). The interpolation formula should be the counterpart of (1.7.15) with properly defined interpolation weights.

1.7.4 Bilinear interpolation

Run the code `rec_2d` for a velocity field of your choice. Confirm that the interpolated values are identical to the specified grid values and prepare a plot of the velocity vector field similar to that displayed in [Figure 1.7.4](#). Discuss the structure of the flow.

1.7.5 Streamlines by interpolation

Run the code `rec_2d_strml` for a velocity field of your choice. Generate, plot, and discuss the streamline pattern.

More on kinematics

- 2.1 Fundamental modes of fluid parcel motion**
- 2.2 Fluid parcel expansion**
- 2.3 Fluid parcel rotation and vorticity**
- 2.4 Fluid parcel deformation**
- 2.5 Numerical differentiation**
- 2.6 Flow rates**
- 2.7 Mass conservation and the continuity equation**
- 2.8 Properties of point particles**
- 2.9 Incompressible fluids and stream functions**
- 2.10 Kinematic conditions at boundaries**

In this chapter, we continue the study of kinematics by considering in more detail the motion of fluid parcels, by deriving expressions for the areal, volumetric, and mass flow rates across lines and surfaces drawn in a fluid, and by developing numerical methods for evaluating kinematic variables of interest in terms of derivatives and integrals of the velocity field. Mass conservation and physical conditions imposed at boundaries introduce mathematical constraints that motivate the description of a flow in terms of ancillary functions that expedite the mathematical analysis and considerably simplify the numerical computation.

2.1 Fundamental modes of fluid parcel motion

In Chapter 1, we pointed out that the nature of the motion of a small fluid parcel is determined by the relative motion of point particles residing inside the parcel. If variations in the point particle velocity are negligible compared to the average point particle velocity, the parcel exhibits rigid-body translation. Significant variations in the point particle velocity are responsible for further general types of motion, including local rotation, deformation, and isotropic expansion.

To study the relative motion of point particles in the vicinity of a certain point, $\mathbf{x}_0 = (x_0, y_0, z_0)$, we consider differences in the corresponding velocity components evaluated at a point $\mathbf{x} = (x, y, z)$ that lies close to \mathbf{x}_0 , and at the chosen point, \mathbf{x}_0 , as shown in [Figure 2.1.1](#). If the differences are small compared to the distance between the points \mathbf{x} and \mathbf{x}_0 , both measured in proper units, then the relative motion is negligible. If the differences are substantial, the relative motion is significant and needs to be properly analyzed.

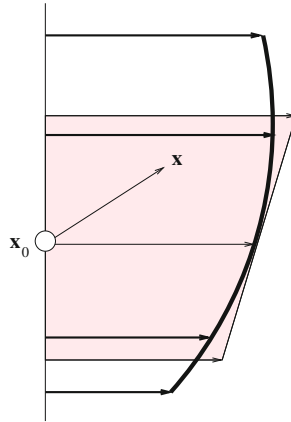


Figure 2.1.1 Illustration of relative motion of a fluid in the neighborhood of a point, \mathbf{x}_0 . The bold line represents an actual velocity profile and the straight line represents the linearized velocity profile.

2.1.1 Function linearization

To prepare the ground for our analysis, we consider a scalar function of three independent variables that receives a triplet of numbers, (x, y, z) , and generates a number, $f(x, y, z)$. If the function f is locally well behaved, and if the point \mathbf{x} lies sufficiently near the point \mathbf{x}_0 , then we expect that the value $f(x, y, z)$ will be close to the value $f(x_0, y_0, z_0)$. Stated differently, in the limit as \mathbf{x} tends to \mathbf{x}_0 , that is, all three scalar differences $x - x_0$, $y - y_0$, and $z - z_0$ tend to zero, the difference in the function values,

$$f(x, y, z) - f(x_0, y_0, z_0), \quad (2.1.1)$$

will vanish.

The variable point, \mathbf{x} , may approach the fixed point, \mathbf{x}_0 , from different directions. Selecting the direction that is parallel to the x axis, we set $\mathbf{x} = (x, y_0, z_0)$, and consider the limit of the difference $f(x, y_0, z_0) - f(x_0, y_0, z_0)$ as $x - x_0$ tends to zero. Because the function f has been assumed well behaved, the ratio of the differences,

$$\frac{f(x, y_0, z_0) - f(x_0, y_0, z_0)}{x - x_0}, \quad (2.1.2)$$

tends to a finite number, which is defined as the first partial derivative of the function f with respect to the variable x evaluated at the point \mathbf{x}_0 , and is denoted by $(\partial f / \partial x)(\mathbf{x}_0)$. Elementary calculus ensures that the partial derivative can be computed using the usual rules of differentiation of a function of one variable with respect to x , regarding all other independent variables as constant. For example, if $f = xyz$, then $\partial f / \partial x = yz$, and thus $(\partial f / \partial x)(\mathbf{x}_0) = y_0 z_0$,

Setting the fraction shown in (2.1.2) equal to $(\partial f/\partial x)(\mathbf{x}_0)$, and solving the resulting equation for $f(x, y_0, z_0)$, we obtain

$$f(x, y_0, z_0) \simeq f(x_0, y_0, z_0) + (x - x_0) \left(\frac{\partial f}{\partial x} \right)_{\mathbf{x}_0}. \quad (2.1.3)$$

It is important to bear in mind that this equation is exact only in the limit as $\Delta x \equiv x - x_0$ tends to zero. For small but non-infinitesimal values of Δx , the difference between the left- and right-hand sides is on the order of Δx^2 , which is small compared to Δx . For example, if Δx is equal to 0.01 in some units, then Δx^2 is equal to 0.0001 in corresponding units.

The point \mathbf{x} may also approach the point \mathbf{x}_0 along the y or z axis, yielding the following counterparts of equation (2.1.3),

$$f(x_0, y, z_0) \simeq f(x_0, y_0, z_0) + (y - y_0) \left(\frac{\partial f}{\partial y} \right)_{\mathbf{x}_0}, \quad (2.1.4)$$

and

$$f(x_0, y_0, z) \simeq f(x_0, y_0, z_0) + (z - z_0) \left(\frac{\partial f}{\partial z} \right)_{\mathbf{x}_0}. \quad (2.1.5)$$

Combining the arguments that led us to equations (2.1.3)–(2.1.5), we let the point \mathbf{x} approach the point \mathbf{x}_0 from an arbitrary direction and derive the approximation

$$f(x, y, z) \simeq f(x_0, y_0, z_0) + (x - x_0) \left(\frac{\partial f}{\partial x} \right)_{\mathbf{x}_0} + (y - y_0) \left(\frac{\partial f}{\partial y} \right)_{\mathbf{x}_0} + (z - z_0) \left(\frac{\partial f}{\partial z} \right)_{\mathbf{x}_0}. \quad (2.1.6)$$

We pause to emphasize that relation (2.1.6) is exact only in the limit as all three spatial differences, $\Delta x = x - x_0$, $\Delta y = y - y_0$, and $\Delta z = z - z_0$, tend to zero. For small but non-infinitesimal values of any of these differences, the left-hand side of (2.1.6) differs from the right-hand side by an amount that is generally on the order of the maximum of Δx^2 , Δy^2 , or Δz^2 .

Taylor series

Equation (2.1.6) can be rendered exact for any value of Δx , Δy , or Δz , by adding to the right-hand side a term called the remainder. As all three differences Δx , Δy , and Δz , tend to zero, the remainder vanishes faster than these differences. Elementary calculus shows that, if Δx , Δy , and Δz are sufficiently small, the remainder can be expressed as an infinite series involving products of powers of Δx , Δy , and Δz , called the Taylor series of the function f about the point \mathbf{x}_0 .

The process of deriving (2.1.6) is called *linearization* of the function $f(\mathbf{x})$ about the point \mathbf{x}_0 . The linearized form (2.1.6) states that, in the immediate vicinity of a point, \mathbf{x}_0 , any regular function resembles a linear function of the shifted monomials Δx , Δy , and Δz . If all three first partial derivatives happen to vanish at the point \mathbf{x}_0 , the function $f(\mathbf{x})$ behaves like a quadratic function; however, this is a rare exception.

Gradient of a scalar function

To economize our notation, we introduce the gradient of a function, f , denoted by ∇f , defined as the vector of the three partial derivatives,

$$\nabla f \equiv \mathbf{e}_x \frac{\partial f}{\partial x} + \mathbf{e}_y \frac{\partial f}{\partial y} + \mathbf{e}_z \frac{\partial f}{\partial z}, \quad (2.1.7)$$

where \mathbf{e}_x , \mathbf{e}_y , and \mathbf{e}_z are the unit vectors along the x , y , or z axes. The symbol ∇ is a vector operator called the del or gradient operator, defined as

$$\nabla = \mathbf{e}_x \frac{\partial}{\partial x} + \mathbf{e}_y \frac{\partial}{\partial y} + \mathbf{e}_z \frac{\partial}{\partial z}. \quad (2.1.8)$$

Unlike a regular vector, ∇ may not stand alone, but must operate on a scalar function of position from the left to acquire a meaningful interpretation.

Inner vector product

As a second preliminary, we define the inner product of a pair of three-dimensional vectors,

$$\mathbf{f} = (f_x, f_y, f_z), \quad \mathbf{g} = (g_x, g_y, g_z), \quad (2.1.9)$$

as the scalar

$$\mathbf{f} \cdot \mathbf{g} = f_x g_x + f_y g_y + f_z g_z. \quad (2.1.10)$$

In index notation,

$$\mathbf{f} \cdot \mathbf{g} \equiv f_i g_i, \quad (2.1.11)$$

where summation of the repeated index i is implied over x , y , and z , according to Einstein's repeated-index summation convention: *if an index appears twice in a product, then summation of that index is implied over its range*. In two dimensions, i is summed over x and y . An index may not appear more than twice in a product. An index that appears once is a *free index*

Interpretation of the inner vector product

It can be shown using the rule of cosines that the inner product defined in (2.1.10) is equal to the product of (a) the length of the first vector, \mathbf{f} , (b) the length of the second vector, \mathbf{g} , and (c) the cosine of the angle subtended between the two vectors, β ,

$$\mathbf{f} \cdot \mathbf{g} = |\mathbf{f}| |\mathbf{g}| \cos \beta. \quad (2.1.12)$$

If the angle β is equal to $\frac{1}{2}\pi$, which means that the two vectors are orthogonal, the cosine of the angle is zero and the inner product vanishes. If the angle is zero, which means the two vectors are parallel, the inner product is equal to the product of the two vector lengths.

If the angle is equal to π , which means the two vectors are anti-parallel, the inner product is equal to the negative of the product of the two vector lengths.

If both \mathbf{f} and \mathbf{g} are unit vectors, that is, their lengths are equal to one unit of length, then the inner product is equal to the cosine of the angle subtended between the corresponding directions.

Linearized expansion in compact form

Using the preceding definitions, we state equation (2.1.6) in a compact vector form

$$f(\mathbf{x}) \simeq f(\mathbf{x}_0) + (\mathbf{x} - \mathbf{x}_0) \cdot (\nabla f)_{\mathbf{x}_0}, \quad (2.1.13)$$

where the subscript \mathbf{x}_0 signifies that the gradient, ∇f , is evaluated at the point \mathbf{x}_0 . The second term on the right-hand side of (2.1.13) is the inner product of the distance vector, $\mathbf{x} - \mathbf{x}_0$, and the gradient vector, ∇f , evaluated at a point of interest, \mathbf{x}_0 . The magnitude of this term attains an extreme value when the two vectors are collinear.

2.1.2 Velocity gradient tensor

To derive the linearized form of the velocity field in the vicinity of a point, \mathbf{x}_0 , we identify the function $f(\mathbf{x})$ with the x , y , or z velocity component, u_x , u_y , or u_z , and obtain the approximations

$$\begin{aligned} u_x(\mathbf{x}) &\simeq u_x(\mathbf{x}_0) + (x - x_0) \left(\frac{\partial u_x}{\partial x} \right)_{\mathbf{x}_0} + (y - y_0) \left(\frac{\partial u_x}{\partial y} \right)_{\mathbf{x}_0} + (z - z_0) \left(\frac{\partial u_x}{\partial z} \right)_{\mathbf{x}_0}, \\ u_y(\mathbf{x}) &\simeq u_y(\mathbf{x}_0) + (x - x_0) \left(\frac{\partial u_y}{\partial x} \right)_{\mathbf{x}_0} + (y - y_0) \left(\frac{\partial u_y}{\partial y} \right)_{\mathbf{x}_0} + (z - z_0) \left(\frac{\partial u_y}{\partial z} \right)_{\mathbf{x}_0}, \\ u_z(\mathbf{x}) &\simeq u_z(\mathbf{x}_0) + (x - x_0) \left(\frac{\partial u_z}{\partial x} \right)_{\mathbf{x}_0} + (y - y_0) \left(\frac{\partial u_z}{\partial y} \right)_{\mathbf{x}_0} + (z - z_0) \left(\frac{\partial u_z}{\partial z} \right)_{\mathbf{x}_0}. \end{aligned} \quad (2.1.14)$$

Collecting these equations into a unified vector form, we obtain the vector equation

$$\mathbf{u}(\mathbf{x}) \simeq \mathbf{u}(\mathbf{x}_0) + (\mathbf{x} - \mathbf{x}_0) \cdot \mathbf{L}(\mathbf{x}_0), \quad (2.1.15)$$

where \mathbf{L} is a 3×3 matrix called the velocity-gradient tensor, defined as

$$\mathbf{L} \equiv \begin{bmatrix} \frac{\partial u_x}{\partial x} & \frac{\partial u_y}{\partial x} & \frac{\partial u_z}{\partial x} \\ \frac{\partial u_x}{\partial y} & \frac{\partial u_y}{\partial y} & \frac{\partial u_z}{\partial y} \\ \frac{\partial u_x}{\partial z} & \frac{\partial u_y}{\partial z} & \frac{\partial u_z}{\partial z} \end{bmatrix}. \quad (2.1.16)$$

The notation $\mathbf{L}(\mathbf{x}_0)$ in (2.1.15) emphasizes that the nine components of the velocity-gradient tensor are evaluated at the chosen point \mathbf{x}_0 around which linearization has taken place. An actual and a linearized velocity profile is shown in [Figure 2.1.1](#).

Denoting $x_1 = x$, $y_1 = y$, and $z_1 = z$, and also $u_1 = u_x$, $u_2 = u_y$, and $u_3 = u_z$, we compute the components of the velocity-gradient tensor

$$L_{ij} = \frac{\partial u_j}{\partial x_i} \quad (2.1.17)$$

for $i, j = 1, 2, 3$ or $i, j = x, y, z$.

An application

As an example, we consider the velocity field expressed by equations (1.4.8), repeated below for convenience,

$$\begin{aligned} u_x(x, y, z, t) &= a(y^2 + z^2) + x^3yz(b + ct) + ce^{dxt}, \\ u_y(x, y, z, t) &= a(z^2 + x^2) + xy^3z(b + ct) + ce^{dyt}, \\ u_z(x, y, z, t) &= a(x^2 + y^2) + xyz^3(b + ct) + ce^{dzt}, \end{aligned} \quad (2.1.18)$$

where a , b , c , and d are four constants. Applying the rules of partial differentiation, we obtain the associated velocity-gradient tensor

$$\mathbf{L} = \begin{bmatrix} 3x^2yz(b + ct) + cdt e^{dxt} & 2ax + y^3z(b + ct) & 2ax + yz^3(b + ct) \\ 2ay + x^3z(b + ct) & 3y^2xz(b + ct) + cdt e^{dyt} & 2ay + xz^3(b + ct) \\ 2az + x^3y(b + ct) & 2az + xy^3(b + ct) & 3z^2xy(b + ct) + cdt e^{dzt} \end{bmatrix}. \quad (2.1.19)$$

Placing the point \mathbf{x}_0 along the x axis, that is, setting $y_0 = 0$ and $z_0 = 0$, we find that

$$\mathbf{L}(x_0, 0, 0) = \begin{bmatrix} cdt e^{dx_0t} & 2ax_0 & 2ax_0 \\ 0 & cdt & 0 \\ 0 & 0 & cdt \end{bmatrix}. \quad (2.1.20)$$

Thus, in the vicinity of the point $\mathbf{x}_0 = (x_0, 0, 0)$, the flow expressed by equations (2.1.18) can be approximated with a linear flow described by

$$\begin{aligned} u_x(x, y, z) &\simeq u_x(\mathbf{x}_0) + cdt e^{dx_0t} (x - 1), \\ u_y(x, y, z) &\simeq u_y(\mathbf{x}_0) + 2a(x - 1) + cdt y, \\ u_z(x, y, z) &\simeq u_z(\mathbf{x}_0) + 2a(x - 1) + cdt z. \end{aligned} \quad (2.1.21)$$

The right-hand sides of equations (2.1.21) are linear functions of the spatial coordinates x , y , and z , but not necessarily linear functions of time, t .

What is a tensor?

The velocity-gradient tensor is a matrix containing the three first partial derivatives of the three components of the velocity with respect to x , y , or z , a total of nine scalar elements. Why have we called this matrix a tensor?

A tensor is a matrix whose elements are physical entities evaluated with reference to a chosen system of Cartesian coordinates. If the coordinate system is changed, for example,

by translation or rotation, the elements of the matrix will also change to reflect the new Cartesian base. This change is analogous to that undergone by the components of the position or velocity vector when a new system of coordinates is introduced, as discussed in Section 1.5.

If the elements of the matrix corresponding to the new system are related to the elements corresponding to the old system by certain rules discussed in texts of matrix calculus and continuum mechanics, then the matrix is called a tensor.¹ Establishing whether or not a matrix is a tensor is important in deriving physical laws that relate matrices with different physical interpretations.

2.1.3 Relative motion of point particles

According to equation (2.1.15), the motion of a point particle near a point, \mathbf{x}_0 , is governed by the equation

$$\frac{d\mathbf{X}}{dt} = \mathbf{u}(\mathbf{X}) \simeq \mathbf{u}(\mathbf{x}_0) + (\mathbf{X} - \mathbf{x}_0) \cdot \mathbf{L}(\mathbf{x}_0), \quad (2.1.22)$$

where \mathbf{X} is the position of the point particle and $\mathbf{u}(\mathbf{X})$ is the point-particle velocity, which is equal to the local and instantaneous fluid velocity.

The first term on the right-hand side of (2.1.22) states that a point particle located at the point \mathbf{X} translates with the velocity of the point particle located at the point \mathbf{x}_0 . The second term expresses the relative motion with respect to the point particle located at \mathbf{x}_0 . Different velocity-gradient tensors, $\mathbf{L}(\mathbf{x}_0)$, represent different types of relative motion. Our next goal is to delineate the nature of the relative motion in terms of the components of $\mathbf{L}(\mathbf{x}_0)$.

2.1.4 Fundamental motions in two-dimensional flow

We begin by considering a two-dimensional flow in the xy plane and introduce the 2×2 velocity-gradient tensor

$$\mathbf{L} = \begin{bmatrix} \frac{\partial u_x}{\partial x} & \frac{\partial u_y}{\partial x} \\ \frac{\partial u_x}{\partial y} & \frac{\partial u_y}{\partial y} \end{bmatrix}. \quad (2.1.23)$$

In Section 1.6, we studied the velocity field associated with the linear flow expressed by equation (1.6.46), repeated below for convenience,

$$[u_x \quad u_y] = [x \quad y] \cdot \begin{bmatrix} a & b \\ c & d \end{bmatrix}, \quad (2.1.24)$$

¹Pozrikidis, C. (2011) *Introduction to Theoretical and Computational Fluid Dynamics*. Second Edition, Oxford University Press.

where a , b , c , and d are four constants with units of inverse time. Comparing equations (2.1.15) and (2.1.23) with equation (2.1.24), we set

$$a = \frac{\partial u_x}{\partial x}, \quad b = \frac{\partial u_y}{\partial x}, \quad c = \frac{\partial u_x}{\partial y}, \quad d = \frac{\partial u_y}{\partial y}, \quad (2.1.25)$$

where all partial derivatives are evaluated at the point \mathbf{x}_0 .

To study the nature of the linearized flow, we carry out the decomposition shown in equation (1.6.48), setting

$$\mathbf{L} = \mathbf{\Xi} + \mathbf{E} + \frac{1}{2} \alpha \mathbf{I}, \quad (2.1.26)$$

where

$$\mathbf{\Xi} \equiv \frac{1}{2} \begin{bmatrix} 0 & \frac{\partial u_y}{\partial x} - \frac{\partial u_x}{\partial y} \\ \frac{\partial u_x}{\partial y} - \frac{\partial u_y}{\partial x} & 0 \end{bmatrix} \quad (2.1.27)$$

is a skew-symmetric matrix with zero trace called the *vorticity tensor*,

$$\mathbf{E} \equiv \frac{1}{2} \begin{bmatrix} \frac{\partial u_x}{\partial x} - \frac{\partial u_y}{\partial y} & \frac{\partial u_y}{\partial x} + \frac{\partial u_x}{\partial y} \\ \frac{\partial u_x}{\partial y} + \frac{\partial u_y}{\partial x} & \frac{\partial u_y}{\partial y} - \frac{\partial u_x}{\partial x} \end{bmatrix} \quad (2.1.28)$$

is a symmetric matrix with zero trace called the *rate-of-deformation tensor*,

$$\mathbf{I} = \begin{bmatrix} 1 & 0 \\ 0 & 1 \end{bmatrix} \quad (2.1.29)$$

is the 2×2 identity matrix, and the scalar

$$\alpha = \frac{\partial u_x}{\partial x} + \frac{\partial u_y}{\partial y} \quad (2.1.30)$$

is the *rate of areal expansion*.

Areal expansion

The results of Section 1.6 suggest that a fluid parcel centered at the point \mathbf{x}_0 expands isotropically with an areal rate of expansion that is equal to the right-hand side of (2.1.30) evaluated at \mathbf{x}_0 , as illustrated in [Figure 2.1.2](#).

Rotation

Referring to equation (1.6.49), we find that a fluid parcel centered at the point \mathbf{x}_0 rotates in the xy plane around the point \mathbf{x}_0 with angular velocity

$$\Omega = \frac{1}{2} \left(\frac{\partial u_y}{\partial x} - \frac{\partial u_x}{\partial y} \right), \quad (2.1.31)$$

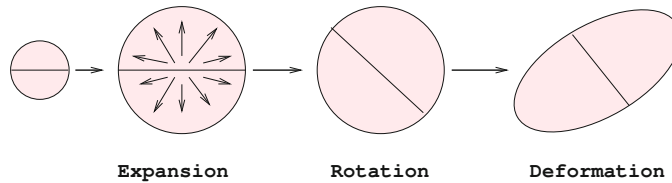


Figure 2.1.2 Expansion, rotation, and deformation of a small discoidal fluid parcel occurring during an infinitesimal period of time in a two-dimensional flow.

where the right-hand side is evaluated at \mathbf{x}_0 , as shown in Figure 2.1.2. When Ω is positive, the parcel rotates in the counterclockwise direction; whereas, when Ω is negative, the parcel rotates in the clockwise direction.

Deformation

Our discussion in Section 1.6 suggests that the flow associated with the rate-of-deformation tensor, \mathbf{E} , expresses pure deformation in the absence of rotation or expansion, as illustrated in Figure 2.1.2.

To compute the rate of deformation, G , we consider the eigenvalues of \mathbf{E} . Denoting $E_{xx} \equiv E_{11}$, introducing a similar notation for the other components, and taking into account that

$$E_{xx} + E_{yy} = 0, \quad E_{xy} = E_{yx} \quad (2.1.32)$$

by construction, we find the eigenvalues

$$G = \pm \sqrt{E_{xx}^2 + E_{xy}^2}. \quad (2.1.33)$$

The corresponding eigenvectors define the principal directions of the rate of deformation, also called the rate of strain. It can be shown that, because \mathbf{E} is symmetric, the two eigenvectors are mutually orthogonal. An eigenvalue of the rate-of-strain tensor expresses the rate of deformation of a circular fluid parcel centered at a point, \mathbf{x}_0 , in the direction of the associated eigenvector.

A theorem of matrix calculus ensures that the sum of the eigenvalues of a matrix is equal to the sum of the diagonal elements; in the case of the rate-of-deformation tensor, \mathbf{E} , this is equal to zero by construction. Because of this property, the deformation conserves the area of a fluid parcel during the motion.

2.1.5 Fundamental motions in three-dimensional flow

To generalize the analysis of Section 2.1.4 to three-dimensional flow, we resolve the three-dimensional velocity-gradient tensor into three parts, as

$$\mathbf{L} = \mathbf{\Xi} + \mathbf{E} + \frac{1}{3} \alpha \mathbf{I}, \quad (2.1.34)$$

$$\mathbf{\Xi} \equiv \frac{1}{2} \begin{bmatrix} 0 & \frac{\partial u_y}{\partial x} - \frac{\partial u_x}{\partial y} & \frac{\partial u_z}{\partial x} - \frac{\partial u_x}{\partial z} \\ \frac{\partial u_x}{\partial y} - \frac{\partial u_y}{\partial x} & 0 & \frac{\partial u_z}{\partial y} - \frac{\partial u_y}{\partial z} \\ \frac{\partial u_x}{\partial z} - \frac{\partial u_z}{\partial x} & \frac{\partial u_y}{\partial z} - \frac{\partial u_z}{\partial y} & 0 \end{bmatrix}$$

$$\mathbf{E} \equiv \begin{bmatrix} \frac{\partial u_x}{\partial x} - \frac{1}{3} \alpha & \frac{1}{2} \left(\frac{\partial u_y}{\partial x} + \frac{\partial u_x}{\partial y} \right) & \frac{1}{2} \left(\frac{\partial u_z}{\partial x} + \frac{\partial u_x}{\partial z} \right) \\ \frac{1}{2} \left(\frac{\partial u_x}{\partial y} + \frac{\partial u_y}{\partial x} \right) & \frac{\partial u_y}{\partial y} - \frac{1}{3} \alpha & \frac{1}{2} \left(\frac{\partial u_z}{\partial y} + \frac{\partial u_y}{\partial z} \right) \\ \frac{1}{2} \left(\frac{\partial u_x}{\partial z} + \frac{\partial u_z}{\partial x} \right) & \frac{1}{2} \left(\frac{\partial u_y}{\partial z} + \frac{\partial u_z}{\partial y} \right) & \frac{\partial u_z}{\partial z} - \frac{1}{3} \alpha \end{bmatrix}$$

Table 2.1.1 Definition of the vorticity tensor, $\mathbf{\Xi}$, and rate-of-deformation tensor, \mathbf{E} , in a three-dimensional flow; the scalar $\alpha \equiv \nabla \cdot \mathbf{u}$ is the volumetric rate of expansion.

where $\mathbf{\Xi}$ is the skew-symmetric vorticity tensor, \mathbf{E} is the symmetric and traceless rate-of-deformation tensor,

$$\mathbf{I} = \begin{bmatrix} 1 & 0 & 0 \\ 0 & 1 & 0 \\ 0 & 0 & 1 \end{bmatrix} \quad (2.1.35)$$

is the 3×3 identity matrix, and the scalar coefficient

$$\alpha \equiv \frac{\partial u_x}{\partial x} + \frac{\partial u_y}{\partial y} + \frac{\partial u_z}{\partial z} \quad (2.1.36)$$

is the rate of volumetric expansion. Explicit expressions for the vorticity tensor, $\mathbf{\Xi}$, and rate-of-deformation tensor, \mathbf{E} , are given in [Table 2.1.1](#).

The three terms on the right-hand side of (2.1.34) express, respectively, isotropic expansion, rotation, and pure deformation, as illustrated in [Figure 2.1.3](#). Because of the fundamental significance of these motions, these terms merit individual attention in Sections 2.2–2.4.

2.1.6 Gradient in polar coordinates

We have defined the velocity-gradient tensor as the gradient of the velocity vector field. Expressions for the gradient operator in polar coordinates can be obtained by using geometrical transformation rules combined with the chain rule of differentiation.

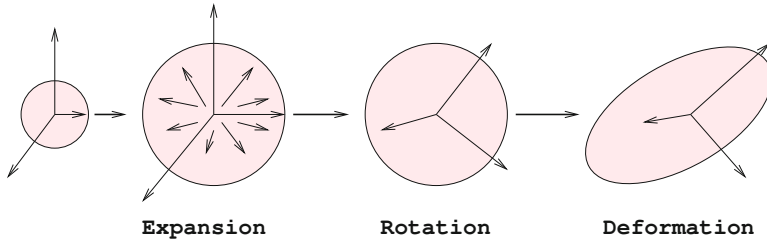


Figure 2.1.3 Expansion, rotation, and deformation of a small spherical fluid parcel occurring during an infinitesimal period of time in a three-dimensional flow.

Cylindrical polar coordinates

In the cylindrical polar coordinates depicted in Figure 1.3.2, the gradient of a scalar function, $f(\mathbf{x})$, is determined by its cylindrical polar components F_x , F_σ , and F_φ , as

$$\mathbf{F} \equiv \nabla f = F_x \mathbf{e}_x + F_\sigma \mathbf{e}_\sigma + F_\varphi \mathbf{e}_\varphi. \tag{2.1.37}$$

Using the transformation rules shown in equations (1.3.20), we find that

$$F_\sigma = \cos \varphi \frac{\partial f}{\partial y} + \sin \varphi \frac{\partial f}{\partial z}, \quad F_\varphi = -\sin \varphi \frac{\partial f}{\partial y} + \cos \varphi \frac{\partial f}{\partial z}. \tag{2.1.38}$$

To express the derivatives with respect to y and z in terms of derivatives with respect to cylindrical polar coordinates, we use the chain rule of differentiation along with the coordinate transformation rules (1.3.14) and (1.3.15), and find that

$$\left(\frac{\partial f}{\partial y}\right)_{x,z} = \left(\frac{\partial f}{\partial x}\right)_{\sigma,\varphi} \left(\frac{\partial x}{\partial y}\right)_{x,z} + \left(\frac{\partial f}{\partial \sigma}\right)_{x,\varphi} \left(\frac{\partial \sigma}{\partial y}\right)_{x,z} + \left(\frac{\partial f}{\partial \varphi}\right)_{x,\sigma} \left(\frac{\partial \varphi}{\partial y}\right)_{x,z} \tag{2.1.39}$$

or

$$\left(\frac{\partial f}{\partial y}\right)_{x,z} = \cos \varphi \left(\frac{\partial f}{\partial \sigma}\right)_{x,\varphi} - \frac{\sin \varphi}{\sigma} \left(\frac{\partial f}{\partial \varphi}\right)_{x,\sigma}, \tag{2.1.40}$$

and

$$\left(\frac{\partial f}{\partial z}\right)_{x,y} = \left(\frac{\partial f}{\partial x}\right)_{\sigma,\varphi} \left(\frac{\partial x}{\partial z}\right)_{x,y} + \left(\frac{\partial f}{\partial \sigma}\right)_{x,\varphi} \left(\frac{\partial \sigma}{\partial z}\right)_{x,y} + \left(\frac{\partial f}{\partial \varphi}\right)_{x,\sigma} \left(\frac{\partial \varphi}{\partial z}\right)_{x,y} \tag{2.1.41}$$

or

$$\left(\frac{\partial f}{\partial z}\right)_{x,y} = \sin \varphi \left(\frac{\partial f}{\partial \sigma}\right)_{x,\varphi} + \frac{\cos \varphi}{\sigma} \left(\frac{\partial f}{\partial \varphi}\right)_{x,\sigma}. \tag{2.1.42}$$

Substituting relations (2.1.40) and (2.1.42) into the right-hand sides of relations (2.1.38), we find that

$$F_x = \frac{\partial f}{\partial x}, \quad F_\sigma = \frac{\partial f}{\partial \sigma}, \quad F_\varphi = \frac{1}{\sigma} \frac{\partial f}{\partial \varphi}. \tag{2.1.43}$$

Equations (2.1.43) illustrate that the polar components of the gradient are equal to the partial derivatives with respect to the corresponding coordinates multiplied by an appropriate scaling factor.

Spherical polar coordinates

In the spherical polar coordinates depicted in [Figure 1.3.3](#), the gradient of a scalar function, f , is defined by its spherical polar components F_r , F_θ , and F_φ , as

$$\mathbf{F} \equiv \nabla f = F_r \mathbf{e}_r + F_\theta \mathbf{e}_\theta + F_\varphi \mathbf{e}_\varphi. \quad (2.1.44)$$

Working as in the case of cylindrical polar coordinates, we obtain

$$F_r = \frac{\partial f}{\partial r}, \quad F_\theta = \frac{1}{r} \frac{\partial f}{\partial \theta}, \quad F_\varphi = \frac{1}{r \sin \theta} \frac{\partial f}{\partial \varphi}. \quad (2.1.45)$$

Note that the expression for F_φ is consistent with that given in the third relation of (2.1.43), subject to the substitution $\sigma = r \sin \theta$.

Plane polar coordinates

In the plane polar coordinates depicted in [Figure 1.3.4](#), the gradient of a scalar function, f , is defined by its plane polar components, F_r and F_θ , as

$$\mathbf{F} \equiv \nabla f = F_r \mathbf{e}_r + F_\theta \mathbf{e}_\theta. \quad (2.1.46)$$

Working as in the case of cylindrical coordinates, we obtain

$$F_r = \frac{\partial f}{\partial r}, \quad F_\theta = \frac{1}{r} \frac{\partial f}{\partial \theta}. \quad (2.1.47)$$

PROBLEMS

2.1.1 Inner vector product

Prove the interpretation of the inner vector product discussed after equation (2.1.11). *Hint:* Use the law of cosines.

2.1.2 Decomposition of a linearized flow

(a) Linearize the velocity described by equations (1.5.2) around the origin of the y axis, and then decompose the velocity-gradient tensor of the linearized flow into the three constituents shown on the right-hand side of (2.1.34).

(b) Decompose the velocity gradient-tensor of the linearized flow expressed by equations (2.1.21) into the three constituents shown on the right-hand side of (2.1.34).

2.2 Fluid parcel expansion

The velocity field associated with the third term on the right-hand side of (2.1.34) is described by

$$\mathbf{u}^{\text{expansion}}(\mathbf{x}) = \frac{1}{3} \alpha(\mathbf{x}_0) (\mathbf{x} - \mathbf{x}_0) \cdot \begin{bmatrix} 1 & 0 & 0 \\ 0 & 1 & 0 \\ 0 & 0 & 1 \end{bmatrix} = \frac{1}{3} \alpha(\mathbf{x}_0) (\mathbf{x} - \mathbf{x}_0). \quad (2.2.1)$$

Under the influence of this field, a spherical fluid parcel centered at the point \mathbf{x}_0 expands when the coefficient $\alpha(\mathbf{x}_0)$ is positive, or contracts when the coefficient $\alpha(\mathbf{x}_0)$ is negative, all the while retaining the spherical shape.

To see this behavior more clearly, we consider the motion of a point particle that lies at the surface of the spherical parcel. Using (2.2.1), we find that the radius of the parcel, $a(t)$, is given by

$$\frac{a(t)}{a(t=0)} = e^{\frac{1}{3}\alpha t}. \quad (2.2.2)$$

Raising both sides to the third power and multiplying the result by the factor $\frac{4\pi}{3}$, we find that the ratio of the instantaneous parcel volume to the initial parcel volume is

$$\frac{\frac{4\pi}{3} a^3(t)}{\frac{4\pi}{3} a^3(t=0)} = e^{\alpha t}. \quad (2.2.3)$$

This result explains why the constant α is called the rate of volumetric expansion.

Divergence of the velocity field

The rate of expansion defined in equation (2.1.36) can be expressed in a compact form that simplifies the notation. Taking the inner product of the del operator defined in (2.1.8) and the velocity, we find that

$$\nabla \cdot \mathbf{u} \equiv \frac{\partial u_x}{\partial x} + \frac{\partial u_y}{\partial y} + \frac{\partial u_z}{\partial z}. \quad (2.2.4)$$

In index notation,

$$\nabla \cdot \mathbf{u} \equiv \frac{\partial u_i}{\partial x_i}, \quad (2.2.5)$$

where summation over the repeated index i is implied for x , y , and z . In the case of two-dimensional flow in the xy plane, the derivative of u_z with respect to z does not appear. Accordingly, we write

$$\alpha = \nabla \cdot \mathbf{u}. \quad (2.2.6)$$

The right-hand side of (2.2.6) is the *divergence of the velocity field*.

Solenoidal velocity fields

We have found that the rate of volumetric expansion at an arbitrary point in a three-dimensional flow and the rate of areal expansion at a point in a two-dimensional flow are equal to the divergence of the velocity evaluated at that point. If the divergence of the velocity vanishes everywhere in a flow, with the physical consequence that no parcel undergoes expansion but only exhibits translation, rotation, and deformation, then the velocity field is called solenoidal.

PROBLEM

2.2.1 Rate of expansion

Derive the rate of expansion of the flow described by equations (2.1.18), and then evaluate the rate of expansion at the point $\mathbf{x}_0 = (1, 0, 1)$.

2.3 Fluid parcel rotation and vorticity

The velocity field associated with the first term on the right-hand side of (2.1.34) is given by

$$\mathbf{u}^{\text{rotation}}(x, y, z) = (\mathbf{x} - \mathbf{x}_0) \cdot \Xi(\mathbf{x}_0), \quad (2.3.1)$$

where Ξ is the vorticity tensor defined in Table 2.1.1.

A planar fluid parcel in a two-dimensional flow in the xy plane may only rotate around the z axis. In contrast, a three-dimensional fluid parcel in a three-dimensional flow may rotate around any arbitrary axis that passes through the designated center of rotation, \mathbf{x}_0 , and points in any arbitrary direction.

The orientation, magnitude, and direction of rotation define an angular velocity vector, $\boldsymbol{\Omega}$, whose components can be deduced from the three upper triangular or three lower triangular entries of the vorticity tensor shown in Table 2.1.1, and are given by

$$\Omega_x = \frac{1}{2} \left(\frac{\partial u_z}{\partial y} - \frac{\partial u_y}{\partial z} \right), \quad \Omega_y = \frac{1}{2} \left(\frac{\partial u_x}{\partial z} - \frac{\partial u_z}{\partial x} \right), \quad \Omega_z = \frac{1}{2} \left(\frac{\partial u_y}{\partial x} - \frac{\partial u_x}{\partial y} \right), \quad (2.3.2)$$

where the right-hand sides are evaluated at the designated parcel center, \mathbf{x}_0 . As we look down into the vector $\boldsymbol{\Omega}$ from the tip of its arrow, the fluid rotates in the clockwise direction.

Equation (2.3.1) can be recast into a compact form in terms of the angular velocity vector as

$$\mathbf{u}^{\text{rotation}}(x, y, z) = (\mathbf{x} - \mathbf{x}_0) \cdot \begin{bmatrix} 0 & \Omega_z & -\Omega_y \\ -\Omega_z & 0 & \Omega_x \\ \Omega_y & -\Omega_x & 0 \end{bmatrix}, \quad (2.3.3)$$

where $\boldsymbol{\Omega}$ derives from the velocity by way of (2.3.2).

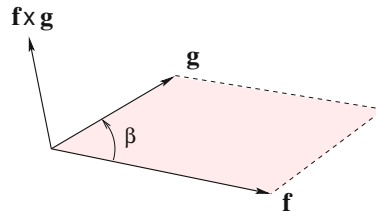


Figure 2.3.1 The outer product of two vectors, \mathbf{f} and \mathbf{g} , is a new vector that is perpendicular to the plane of \mathbf{f} and \mathbf{g} .

We note that the three components of the angular velocity vector arise by combining selected partial derivatives of the components of the velocity field in a particular fashion. Stated differently, the angular velocity vector field arises from the velocity field by operating with a differential operator, just as the rate of expansion arises from the velocity field by operating with the divergence operator ($\nabla \cdot$), as discussed in Section 2.2.

Outer vector product

To identify the differential operator that generates the point particle angular velocity field, $\boldsymbol{\Omega}$, from the velocity field, \mathbf{u} , according to equations (2.3.2), we introduce the outer vector product. Consider a pair of vectors,

$$\mathbf{f} = (f_x, f_y, f_z), \quad \mathbf{g} = (g_x, g_y, g_z). \quad (2.3.4)$$

The outer product of the first vector with the second vector, taken in this particular order, is a new vector, denoted as $\mathbf{f} \times \mathbf{g}$, defined as

$$\mathbf{f} \times \mathbf{g} = (f_y g_z - f_z g_y) \mathbf{e}_x + (f_z g_x - f_x g_z) \mathbf{e}_y + (f_x g_y - f_y g_x) \mathbf{e}_z, \quad (2.3.5)$$

where \mathbf{e}_x , \mathbf{e}_y , and \mathbf{e}_z are unit vectors along the x , y , or z axis. We find that

$$\mathbf{f} \times \mathbf{g} = -\mathbf{g} \times \mathbf{f}. \quad (2.3.6)$$

If the order of the two vectors is switched, a minus sign must be included.

Interpretation of the outer vector product

It can be shown that the outer-product vector $\mathbf{f} \times \mathbf{g}$ is normal to the plane containing the vectors \mathbf{f} and \mathbf{g} , as illustrated in Figure 2.3.1. The magnitude of $\mathbf{f} \times \mathbf{g}$ is equal to the product of (a) the length of the vector \mathbf{f} , (b) the length of the vector \mathbf{g} , and (c) the absolute value of the sine of the angle, β , subtended between the two vectors.

The orientation of the outer-product vector $\mathbf{f} \times \mathbf{g}$ is such that, as we look down at the plane defined by \mathbf{f} and \mathbf{g} toward the negative direction of $\mathbf{f} \times \mathbf{g}$, the angle β measured in the counterclockwise direction from \mathbf{f} is less than π . If β is equal to 0 or π , the two vectors are parallel or anti-parallel, the sine of the angle is zero, and the outer product vanishes.

The three directions defined by the triplet of vectors \mathbf{f} , \mathbf{g} , and $\mathbf{f} \times \mathbf{g}$, arranged in this particular order, form a right-handed system of coordinates. This is another way of saying that $\mathbf{f} \times \mathbf{g}$ arises from \mathbf{f} and \mathbf{g} according to the right-hand rule.

Now invoking the definition of the cross product, we recast equation (2.3.3) into the form

$$\mathbf{u}^{\text{rotation}}(x, y, z) = \boldsymbol{\Omega} \times (\mathbf{x} - \mathbf{x}_0), \quad (2.3.7)$$

which describes rigid-body rotation with angular velocity $\boldsymbol{\Omega}$ around the point \mathbf{x}_0 , in agreement with the previously stated physical interpretation.

2.3.1 Curl and vorticity

Taking the outer product of the del operator and the velocity field, we obtain the curl of the velocity defined as the vorticity,

$$\boldsymbol{\omega} \equiv \nabla \times \mathbf{u} = \left(\frac{\partial u_z}{\partial y} - \frac{\partial u_y}{\partial z} \right) \mathbf{e}_x + \left(\frac{\partial u_x}{\partial z} - \frac{\partial u_z}{\partial x} \right) \mathbf{e}_y + \left(\frac{\partial u_y}{\partial x} - \frac{\partial u_x}{\partial y} \right) \mathbf{e}_z. \quad (2.3.8)$$

Comparing equation (2.3.8) with equations (2.3.2), we find that

$$\boldsymbol{\Omega} = \frac{1}{2} \boldsymbol{\omega}, \quad (2.3.9)$$

which shows that the angular-velocity vector is equal to half the vorticity vector, or half the curl of the velocity.

Irrotational flow

If the curl of a velocity field vanishes at every point in a flow, with the consequence that no spherical fluid parcel undergoes rotation, then the velocity field is called irrotational. The properties and computation of irrotational flow will be discussed in Chapter 3, and then again in Chapter 12 in the context of aerodynamics.

The alternating tensor

The long expression on the right-hand side of equation (2.3.5) defining the outer vector product is cumbersome. To simplify the notation, we introduce the three-index alternating tensor, ϵ_{ijk} , defined as follows:

1. If $i = j$, or $j = k$, or $k = i$, then $\epsilon_{ijk} = 0$. For example, $\epsilon_{xxy} = \epsilon_{zyz} = \epsilon_{zyy} = 0$.
2. If i, j , and k are all different, then $\epsilon_{ijk} = \pm 1$. The plus sign applies when the triplet ijk is a cyclic permutation of xyz , and the minus sign applies otherwise. For example, $\epsilon_{xyz} = \epsilon_{zxy} = \epsilon_{yxz} = 1$, but $\epsilon_{xzy} = -1$.

Two important properties of the alternating tensor stemming from its definition are

$$\epsilon_{ijk} \epsilon_{mjk} = 2 \delta_{im}, \quad (2.3.10)$$

where double summation of the repeated indices j and k is implied on the left-hand side, and

$$\epsilon_{ijk} \epsilon_{lmk} = \delta_{il} \delta_{jm} - \delta_{im} \delta_{jl}, \quad (2.3.11)$$

where summation of the repeated index k is implied on the left-hand side. Kronecker's delta, δ_{ij} , represents the identity matrix: $\delta_{ij} = 1$ if $i = j$, or 0 if $i \neq j$. Additional properties of the alternating tensor are listed in Problem 2.3.2.

In terms of the alternating tensor, the i th component of the outer vector product $\mathbf{f} \times \mathbf{g}$ defined in equation (2.3.5) is given by

$$(\mathbf{f} \times \mathbf{g})_i = \epsilon_{ijk} f_j g_k, \quad (2.3.12)$$

where double summation of the two repeated indices j and k is implied on the right-hand side.

Using the definition (2.3.8), we find that the i th component of the vorticity is given by

$$\omega_i = \epsilon_{ijk} \frac{\partial u_k}{\partial x_j}. \quad (2.3.13)$$

Straightforward manipulation of (2.3.13) provides us with an expression for the vorticity vector in terms of the vorticity tensor,

$$\omega_i = \frac{1}{2} (\epsilon_{ijk} \frac{\partial u_k}{\partial x_j} + \epsilon_{ikj} \frac{\partial u_k}{\partial x_j}) = \frac{1}{2} (\epsilon_{ijk} \frac{\partial u_k}{\partial x_j} - \epsilon_{ikj} \frac{\partial u_k}{\partial x_j}), \quad (2.3.14)$$

and then

$$\omega_i = \frac{1}{2} (\epsilon_{ijk} \frac{\partial u_k}{\partial x_j} - \epsilon_{ikj} \frac{\partial u_j}{\partial x_k}) = \epsilon_{ijk} \frac{1}{2} (\frac{\partial u_k}{\partial x_j} - \frac{\partial u_j}{\partial x_k}) \quad (2.3.15)$$

or

$$\omega_i = \epsilon_{ijk} \Xi_{jk}. \quad (2.3.16)$$

The inverse relationship is

$$\Xi_{ij} = \frac{1}{2} \epsilon_{ijk} \omega_k \quad (2.3.17)$$

(Problem 2.3.3).

2.3.2 Two-dimensional flow

Consider a two-dimensional flow in the xy plane. Inspecting the right-hand side of (2.3.8), we find that the x and y components of the vorticity vanish. The vorticity vector is then parallel to the z axis, and thus perpendicular to the plane of the flow,

$$\boldsymbol{\omega} = \omega_z \mathbf{e}_z, \quad (2.3.18)$$

where \mathbf{e}_z is the unit vector along the z axis. The scalar ω_z is the strength of the vorticity, defined as

$$\omega_z = \frac{\partial u_y}{\partial x} - \frac{\partial u_x}{\partial y}. \quad (2.3.19)$$

For example, in the case of simple shear flow, $u_x = \xi y$, $u_y = 0$, and $\omega_z = -\xi$, where the coefficient ξ is the shear rate.

Using the transformation rules discussed in Section 1.1, we find that the strength of the vorticity in the plane polar coordinates depicted in Figure 1.1.4 is given by

$$\omega_z = \frac{1}{r} \left(\frac{\partial(ru_\theta)}{\partial r} - \frac{\partial u_r}{\partial \theta} \right). \quad (2.3.20)$$

In the case of rigid-body rotation with angular velocity Ω , $u_\theta = \Omega r$, $u_r = 0$, and $\omega_z = \frac{1}{2} \Omega$.

2.3.3 Axisymmetric flow

Consider an axisymmetric flow in the absence of swirling motion and refer to the polar cylindrical coordinates (x, σ, φ) depicted in Figure 1.1.2 and to the spherical polar coordinates (r, θ, φ) depicted in Figure 1.1.3.

A fluid patch that lies in an azimuthal plane, defined as plane of constant azimuthal angle φ , is able to rotate only around an axis that is perpendicular to this plane. Consequently, the vorticity vector points in the direction of increasing or decreasing azimuthal angle, φ . This observation suggests that the vorticity vector takes the form

$$\boldsymbol{\omega} = \omega_\varphi \mathbf{e}_\varphi, \quad (2.3.21)$$

where \mathbf{e}_φ is the unit vector in the azimuthal direction and ω_φ is the corresponding vorticity component given by

$$\omega_\varphi = \frac{\partial u_\sigma}{\partial x} - \frac{\partial u_x}{\partial \sigma} = \frac{1}{r} \left(\frac{\partial(ru_\theta)}{\partial r} - \frac{\partial u_r}{\partial \theta} \right). \quad (2.3.22)$$

Note that the expression in spherical polar coordinates, (r, θ) , given on the right-hand side of (2.3.22) is identical to that in plane polar coordinates given in (2.3.20).

PROBLEMS

2.3.1 Properties of the outer vector product

(a) Show that $\mathbf{f} \times \mathbf{g} = -\mathbf{g} \times \mathbf{f}$, where the outer vector product, denoted by \times , is defined in equation (2.3.5).

(b) The outer vector product of two vectors, \mathbf{f} and \mathbf{g} , can be identified with the determinant of a matrix,

$$\mathbf{f} \times \mathbf{g} = \det \left(\begin{bmatrix} \mathbf{e}_x & \mathbf{e}_y & \mathbf{e}_z \\ f_x & f_y & f_z \\ g_x & g_y & g_z \end{bmatrix} \right). \quad (2.3.23)$$

Confirm that this rule is consistent with the definition of the curl of the velocity in (2.3.8).

2.3.2 Properties of Kronecker's delta and alternating tensor

Prove the properties

$$\delta_{ii} = 3, \quad \epsilon_{ljk} \delta_{jk} = 0, \quad a_j \delta_{jk} = a_k, \quad A_{lj} \delta_{jk} = A_{lk}, \quad (2.3.24)$$

where δ_{ij} is Kronecker's delta representing the 3×3 identity matrix, \mathbf{a} is an arbitrary vector, \mathbf{A} is an arbitrary matrix, and summation is implied over a repeated index.

2.3.3 Relation between the vorticity tensor and vector

Prove relation (2.3.17). *Hint:* Express the vorticity in terms of the velocity as shown in (2.3.13), and then use property (2.3.11).

2.3.4 The vorticity field is solenoidal

Show that the divergence of the vorticity is identically zero, $\nabla \cdot \boldsymbol{\omega} = 0$, that is, the vorticity field is solenoidal.

2.4 Fluid parcel deformation

The velocity field associated with the second term on the right-hand side of (2.1.34) is

$$\mathbf{u}^{\text{deformation}}(x, y, z) = (\mathbf{x} - \mathbf{x}_0) \cdot \mathbf{E}(\mathbf{x}_0), \quad (2.4.1)$$

where \mathbf{E} is the symmetric and traceless rate-of-deformation tensor defined in [Table 2.1.1](#).

To develop insights into the nature of the motion described by (2.4.1), we consider a special case where $\mathbf{E}(\mathbf{x}_0)$ is a diagonal matrix,

$$\mathbf{E}(\mathbf{x}_0) = \begin{bmatrix} \frac{\partial u_x}{\partial x} - \frac{1}{3} \alpha & 0 & 0 \\ 0 & \frac{\partial u_y}{\partial y} - \frac{1}{3} \alpha & 0 \\ 0 & 0 & \frac{\partial u_z}{\partial z} - \frac{1}{3} \alpha \end{bmatrix}, \quad (2.4.2)$$

with the understanding that the derivatives on the right-hand side are evaluated at the point \mathbf{x}_0 . The trace of the matrix on the right-hand side is zero, as required. The eigenvalues of a diagonal matrix are equal to the diagonal elements. The corresponding eigenvectors point along the x , y , or z axes.

Cursory inspection reveals that, under the action of the flow described by (2.4.1), subject to (2.4.2), a spherical fluid parcel centered at a point, \mathbf{x}_0 , deforms to obtain an ellipsoidal shape while preserving its volume, as illustrated in [Figure 2.1.2](#). The three eigenvalues of the rate-of-deformation tensor express the rate of deformation in three principal directions corresponding to the eigenvectors. If an eigenvalue is negative, the parcel is compressed in the corresponding direction to obtain an oblate shape.

More generally, the rate-of-deformation tensor has three real eigenvalues, λ_1 , λ_2 , and λ_3 , that are found by setting the determinant of the following matrix to zero,

$$\mathbf{E} - \lambda \mathbf{I} = \begin{bmatrix} E_{xx} - \lambda & E_{xy} & E_{xz} \\ E_{yx} & E_{yy} - \lambda & E_{yz} \\ E_{zx} & E_{zy} & E_{zz} - \lambda \end{bmatrix}, \quad (2.4.3)$$

and then computing the roots of the emerging cubic equation for λ , where \mathbf{I} is the 3×3 identity matrix. It can be shown that, because \mathbf{E} is symmetric, all three eigenvalues are real and each eigenvalue has a distinct corresponding eigenvector. Moreover, the three eigenvectors are mutually orthogonal, pointing in the principal directions of the rate of strain.

Under the action of the flow stated in (2.4.1), a spherical fluid parcel centered at the point \mathbf{x}_0 deforms to obtain an ellipsoidal shape whose axes are generally inclined with respect to the x , y , and z axis. The three axes of the ellipsoid are parallel to the eigenvectors of \mathbf{E} , and the respective rates of deformation of the ellipsoid are equal to the corresponding eigenvalues. A theorem of matrix calculus states that the sum of the eigenvalues is equal to the sum of the diagonal elements of \mathbf{E} , which is zero. Because of this property, the deformation preserves the parcel volume.

Computation of the rates of strain

Setting the determinant of the matrix (2.4.3) to zero, we obtain a cubic algebraic equation for λ ,

$$\lambda^3 + a\lambda^2 + b\lambda + c = 0, \quad (2.4.4)$$

where

$$\begin{aligned} a &= -\text{trace}(\mathbf{E}) = -(E_{xx} + E_{yy} + E_{zz}), \\ b &= (E_{yy}E_{zz} - E_{yz}E_{zy}) + (E_{xx}E_{zz} - E_{xz}E_{zx}) + (E_{xx}E_{yy} - E_{xy}E_{yx}), \\ c &= \det(\mathbf{E}), \end{aligned} \quad (2.4.5)$$

and \det stands for the determinant. Using Cardano's formulas, we find that the three roots of (2.4.4) are given by

$$\lambda_1 = -\frac{a}{3} + d \cos \frac{\chi}{3}, \quad \lambda_{2,3} = -\frac{a}{3} - d \cos \frac{\chi \pm \pi}{3}, \quad (2.4.6)$$

where

$$d = 2 \left(\frac{1}{3} |p| \right)^{1/2}, \quad \chi = \arccos \left(-\frac{1}{2} \frac{q}{\left(\frac{1}{3} |p| \right)^{3/2}} \right) \quad (2.4.7)$$

and

$$p = b - \frac{1}{3} a^2, \quad q = c + \frac{2}{27} a^3 - \frac{1}{3} ab. \quad (2.4.8)$$

In general, we may find three real eigenvalues or one real eigenvalue accompanied by a pair of complex conjugate eigenvalues.

In the case of the rate-of-deformation tensor, because the trace is zero, $a = 0$, we obtain the simplified expressions

$$\lambda_1 = d \cos \frac{\chi}{3}, \quad \lambda_{2,3} = -d \cos \frac{\chi \pm \pi}{3}, \quad (2.4.9)$$

where

$$d = 2 \left(\frac{1}{3} |b| \right)^{1/3}, \quad \chi = \arccos \left(-\frac{1}{2} \frac{c}{\left(\frac{1}{3} |b| \right)^{3/2}} \right) \quad (2.4.10)$$

and b, c can be arbitrary.

Once the eigenvalues have been found, the eigenvectors are computed by solving a homogeneous system of three equations for three unknowns. For example, the eigenvector $\mathbf{e}^{(1)} = (e_x^{(1)}, e_y^{(1)}, e_z^{(1)})$ corresponding to the eigenvalue λ_1 is found by solving the homogeneous linear system

$$(\mathbf{E} - \lambda_1 \mathbf{I}) \cdot \mathbf{e}^{(1)} = \mathbf{0}, \quad (2.4.11)$$

which can be restated as

$$\begin{aligned} (E_{xx} - \lambda_1) e_x^{(1)} + E_{xy} e_y^{(1)} &= -E_{xz} e_z^{(1)}, \\ E_{yx} e_x^{(1)} + (E_{yy} - \lambda_1) e_y^{(1)} &= -E_{yz} e_z^{(1)}, \\ E_{zx} e_x^{(1)} + E_{zy} e_y^{(1)} &= -(E_{zz} - \lambda_1) e_z^{(1)}. \end{aligned} \quad (2.4.12)$$

To solve system (2.4.12), we may assign an arbitrary value to the first component, $e_z^{(1)}$, evaluate the first two right-hand sides, and solve the first two equations for $e_x^{(1)}$ and $e_y^{(1)}$ using, for example, Cramer's rule. The solution is guaranteed to also satisfy the third equation. A solution cannot be found if the eigenvector is perpendicular to the z axis, in which case $e_z^{(1)}$ is zero. If this occurs, we simply transfer the term involving $e_x^{(1)}$ or $e_y^{(1)}$ to the right-hand side instead, and solve for the other two components.

PROBLEMS

2.4.1 Properties of eigenvalues

- Confirm that the sum of the three eigenvalues given in (2.4.6) is equal to the trace of \mathbf{E} .
- Confirm that the product of the three eigenvalues given in (2.4.6) is equal to the determinant of the rate-of-deformation tensor, \mathbf{E} .
- Confirm that, when \mathbf{E} is diagonal, formulas (2.4.6) identify the eigenvalues with the diagonal elements.

2.4.2 Eigenvalues and eigenvectors

Directory `05_eigen`, located inside directory `01_num_meth` of `FDLIB`, contains a program entitled `eigen33` that computes the eigenvalues of a 3×3 matrix. Use the program to compute the eigenvalues and eigenvectors of the rate of deformation tensor corresponding to the linearized flow (2.1.21) for $a = 1 \text{ s}^{-1}$ and $cdt = 2 \text{ s}^{-1}$.

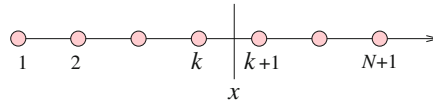
2.5 Numerical differentiation

We have mentioned that, in practice, the components of a velocity field are hardly ever given in analytical form by way of mathematical expressions. Instead, their values are either measured in the laboratory with probes, or computed by numerical methods at data points represented by grid nodes located in the domain of flow. The partial derivatives of the velocity are then recovered by a numerical procedure called numerical differentiation.

2.5.1 Numerical differentiation in one dimension

As a prelude to computing the partial derivatives of the components of the velocity from specified grid values, we consider computing the first derivative of a function, $f(x)$, of one independent variable, x , defined on a grid.

To be more specific, we assume that values of $f(x)$ are given at $N + 1$ nodes of a one-dimensional uniform grid with nodes located at x_i for $i = 1, \dots, N + 1$, as shown below:



Our goal is to compute the derivative, df/dx , at a point, x , that lies in the k th interval subtended between the nodes x_k and x_{k+1} .

First-order differentiation

In the simplest approach, the graph of the function $f(x)$ in the interval (x_k, x_{k+1}) is approximated with a straight line, as shown in [Figure 1.7.2](#), and the derivative df/dx is approximated with the slope. Using equations (1.7.3) and (1.7.5), we derive the finite-difference approximation

$$f'(x) \simeq \frac{f_{k+1} - f_k}{x_{k+1} - x_k}, \quad (2.5.1)$$

where a prime denotes a derivative with respect to x .

Now identifying the evaluation point, x , with the grid point, x_k , we obtain the forward-difference approximation

$$f'(x_k) \simeq \frac{f_{k+1} - f_k}{x_{k+1} - x_k}. \quad (2.5.2)$$

The error associated with this approximation is proportional to the interval size, $h_k = x_{k+1} - x_k$.

Using instead the straight-line approximation for the $k - 1$ interval, we obtain the backward-difference approximation

$$f'(x_k) \simeq \frac{f_k - f_{k-1}}{x_k - x_{k-1}}. \quad (2.5.3)$$

Formulas (2.5.2) and (2.5.3) carry a comparable amount of error due to the straight-line approximation.

To evaluate the derivative at the first point, $f'(x_1)$, we use a forward difference; to evaluate the derivative at the last point, $f'(x_{N+1})$, we use a backward difference; to evaluate $f'(x_i)$ at an interior grid point, where $i = 2, \dots, N$, we use either a forward or a backward difference, whichever is deemed more convenient or appropriate.

Second-order differentiation

Numerical differentiation based on linear interpolation neglects the curvature of the graph of the function $f(x)$. To improve the accuracy of the interpolation, we approximate $f(x)$ with a parabolic function defined in the interval (x_k, x_{k+1}) , as depicted in [Figure 1.7.3](#), and then approximate the slope of the function, f' , with the slope of the parabola. Differentiating (1.7.6), we derive the second-order finite-difference approximation

$$f'(x) \simeq 2a^{(k)}(x - x_k) + b^{(k)}, \quad (2.5.4)$$

where the coefficients $a^{(k)}$ and $b^{(k)}$ are given in (1.7.9).

Now identifying the evaluation point, x , with the grid point, x_k , we obtain the centered-difference approximation

$$f'(x_k) \simeq b^{(k)}. \quad (2.5.5)$$

When the grid points are spaced evenly, $x_k - x_{k-1} = x_{k+1} - x_k = h$, we obtain the simple form

$$f'(x_k) \simeq \frac{f_{k+1} - f_{k-1}}{2h}, \quad (2.5.6)$$

where h is the grid spacing. The error associated with this approximation is proportional to the square of the interval size, h^2 .

The parabolic approximation allows us to also obtain an estimate for the second derivative, d^2f/dx^2 . Differentiating (1.7.6) twice with respect to x , we derive the finite-difference approximation

$$f''(x) \simeq 2a^{(k)}, \quad (2.5.7)$$

where the coefficient $a^{(k)}$ is given in (1.7.9).

When the grid points are spaced evenly along the x axis with separation h , we obtain the simpler formula

$$f''(x) \simeq \frac{f_{k+1} - 2f_k + f_{k-1}}{h^2}. \quad (2.5.8)$$

Identifying the evaluation point, x , with the grid point, x_k , we obtain the centered-difference approximation

$$f''(x_k) \simeq \frac{f_{k+1} - 2f_k + f_{k-1}}{h^2}. \quad (2.5.9)$$

The error associated with this approximation is proportional to the square of the interval size, h^2 .

2.5.2 Numerical differentiation in two dimensions

Consider the computation of the first partial derivatives of a function of two independent variables, $f(x, y)$, $\partial f/\partial x$ and $\partial f/\partial y$, from given values of the function at the nodes of a two-dimensional grid defined by the intersection of the x -level lines, x_i for $i = 1, \dots, N_x + 1$, and y -level lines, y_j for $j = 1, \dots, N_y + 1$, as illustrated in [Figure 1.7.2\(b\)](#). The value of x lies in the k_x th x -interval confined between the x_{k_x} and x_{k_x+1} x -level lines, and the value of y lies in the k_y th y -interval confined between the y_{k_y} and y_{k_y+1} y -level lines.

First-order differentiation

Using the method of bilinear interpolation discussed in Section 1.7, we approximate the first partial derivatives of the function $f(x, y)$ with the partial derivatives of the bilinear function defined in equation (1.7.15). Considering the derivative with respect to x , we obtain the forward-difference approximation

$$\left(\frac{\partial f}{\partial x}\right)_{x,y} \simeq \left(\frac{\partial \Pi^{k_x, k_y}}{\partial x}\right)_{x,y}, \quad (2.5.10)$$

where Π^{k_x, k_y} is the bilinear function given in (1.7.15). Performing the differentiation, we obtain

$$\begin{aligned} \left(\frac{\partial f}{\partial x}\right)_{x,y} &\simeq \left(\frac{\partial w_{00}^{k_x, k_y}}{\partial x}\right)_{x,y} f(x_{k_x}, y_{k_y}) + \left(\frac{\partial w_{10}^{k_x, k_y}}{\partial x}\right)_{x,y} f(x_{k_x+1}, y_{k_y}) \\ &+ \left(\frac{\partial w_{01}^{k_x, k_y}}{\partial x}\right)_{x,y} f(x_{k_x}, y_{k_y+1}) + \left(\frac{\partial w_{11}^{k_x, k_y}}{\partial x}\right)_{x,y} f(x_{k_x+1}, y_{k_y+1}). \end{aligned} \quad (2.5.11)$$

Using expressions (1.7.16) and (1.7.17), we obtain

$$\begin{aligned} \left(\frac{\partial f}{\partial x}\right)_{x,y} &= -\frac{y_{k_y+1} - y}{A} f(x_{k_x}, y_{k_y}) + \frac{y_{k_y+1} - y}{A} f(x_{k_x+1}, y_{k_y}) \\ &- \frac{y - y_{k_y}}{A} f(x_{k_x}, y_{k_y+1}) + \frac{y - y_{k_y}}{A} f(x_{k_x+1}, y_{k_y+1}). \end{aligned} \quad (2.5.12)$$

where

$$A = (x_{k_x+1} - x_{k_x})(y_{k_y+1} - y_{k_y}), \quad (2.5.13)$$

as given in (1.7.18). Using this formula, we derive the first-order, forward-difference approximation at the southwestern grid node,

$$\left(\frac{\partial f}{\partial x}\right)_{x_{k_x}, y_{k_y}} \simeq \frac{f(x_{k_x+1}, y_{k_y}) - f(x_{k_x}, y_{k_y})}{x_{k_x+1} - x_{k_x}}. \quad (2.5.14)$$

A similar approximation for the y derivative yields

$$\left(\frac{\partial f}{\partial y}\right)_{x_{k_x}, y_{k_y}} \simeq \frac{f(x_{k_x}, y_{k_y+1}) - f(x_{k_x}, y_{k_y})}{y_{k_y+1} - y_{k_y}}. \quad (2.5.15)$$

Both formulas express forward-difference approximations with respect to the respective variable, x or y .

Second-order differentiation

Second-order centered-difference formulas for evaluating the first partial derivative of a function at a grid point can be derived based on the one-dimensional formula (2.5.5). Using the expression for the coefficient $b^{(k)}$ given in (1.7.9), we obtain

$$\left(\frac{\partial f}{\partial x}\right)_{x_{k_x}, y_{k_y}} \simeq \frac{(x_{k_x} - x_{k_x-1}) \frac{f_{k_x+1, k_y} - f_{k_x, k_y}}{x_{k_x+1} - x_{k_x}} + (x_{k_x+1} - x_{k_x}) \frac{f_{k_x, k_y} - f_{k_x-1, k_y}}{x_{k_x} - x_{k_x-1}}}{x_{k_x+1} - x_{k_x-1}}. \quad (2.5.16)$$

The corresponding expression for the derivative with respect to y is

$$\left(\frac{\partial f}{\partial y}\right)_{x_{k_x}, y_{k_y}} \simeq \frac{(y_{k_y} - y_{k_y-1}) \frac{f_{k_x, k_y+1} - f_{k_x, k_y}}{y_{k_y+1} - y_{k_y}} + (y_{k_y+1} - y_{k_y}) \frac{f_{k_x, k_y} - f_{k_x, k_y-1}}{y_{k_y} - y_{k_y-1}}}{y_{k_y+1} - y_{k_y-1}}. \quad (2.5.17)$$

When the grid lines are spaced evenly,

$$x_{k_x} - x_{k_x-1} = x_{k_x+1} - x_{k_x} \equiv h_x, \quad (2.5.18)$$

and

$$y_{k_y} - y_{k_y-1} = y_{k_y+1} - y_{k_y} \equiv h_y, \quad (2.5.19)$$

we obtain the simpler formulas

$$\left(\frac{\partial f}{\partial x}\right)_{x_{k_x}, y_{k_y}} = \frac{f_{k_x+1, k_y} - f_{k_x-1, k_y}}{2h_x} \quad (2.5.20)$$

and

$$\left(\frac{\partial f}{\partial y}\right)_{x_{k_x}, y_{k_y}} = \frac{f_{k_x, k_y+1} - f_{k_x, k_y-1}}{2h_y}, \quad (2.5.21)$$

which express centered-difference approximations in x or y .

2.5.3 Velocity gradient and related functions

The formulas derived in Section 2.5.2 can be applied to obtain approximations to the elements of the velocity-gradient tensor, rate-of-deformation tensor, vorticity vector, and rate of expansion, from specified values of the velocity at grid points. To illustrate the methodology, we consider a two-dimensional flow and employ a uniform grid with constant x and y grid spacings equal to h_x and h_y .

Using the second-order, centered-difference approximations (2.5.20) and (2.5.21), we find that the rate of expansion can be approximated with the finite-difference formula

$$(\nabla \cdot \mathbf{u})_{x_{k_x}, y_{k_y}} \simeq \frac{(u_x)_{k_x+1, k_y} - (u_x)_{k_x-1, k_y}}{2h_x} + \frac{(u_y)_{k_x, k_y+1} - (u_y)_{k_x, k_y-1}}{2h_y}. \quad (2.5.22)$$

The corresponding finite-difference approximation for the z component of the vorticity takes the form

$$\omega_z(x_{k_x}, y_{k_y}) \simeq \frac{(u_y)_{k_x+1, k_y} - (u_y)_{k_x-1, k_y}}{2h_x} - \frac{(u_x)_{k_x, k_y+1} - (u_x)_{k_x, k_y-1}}{2h_y}. \quad (2.5.23)$$

Similar finite-difference approximations can be written for the elements of the rate-of-deformation tensor, and subsequently used to obtain approximations to its eigenvalues and eigenvectors.

The following MATLAB function entitled *rec_2d_vgt*, located in directory *rec_2d* inside directory *02_grids* of *FDLIB*, computes the velocity gradient tensor at the nodes of a two-dimensional Cartesian grid:

```
function [Axx,Axy,Ayx,Ayy] = rec_2d_vgt ...
...
    (glx,gly,Nx,Ny,gux,guy)

%-----
% compute the velocity gradient
% tensor L_ij at the grid points
%-----

%-----
% interior points
% compute derivatives by central differences
%-----

for i=2:Nx
    for j=2:Ny
        Lxx(i,j) = (gux(i+1,j)-gux(i-1,j))/(glx(i+1)-glx(i-1));
        Lxy(i,j) = (guy(i+1,j)-guy(i-1,j))/(glx(i+1)-glx(i-1));
        Lyx(i,j) = (gux(i,j+1)-gux(i,j-1))/(gly(j+1)-gly(j-1));
        Lyy(i,j) = (guy(i,j+1)-guy(i,j-1))/(gly(j+1)-gly(j-1));
```



```

end
end

%-----
% left wall
% compute derivatives by central or forward differences
%-----

i=1;
for j=2:Ny
    Lxx(i,j) = (gux(i+1,j)-gux(i,j))/(glx(i+1)-glx(i));
    Lxy(i,j) = (guy(i+1,j)-guy(i,j))/(glx(i+1)-glx(i));
    Lyx(i,j) = (gux(i,j+1)-gux(i,j-1))/(gly(j+1)-gly(j-1));
    Lyy(i,j) = (guy(i,j+1)-guy(i,j-1))/(gly(j+1)-gly(j-1));
end

%-----
% bottom wall
% compute derivatives by central or forward differences
%-----

j=1;
for i=2:Nx
    Lxx(i,j) = (gux(i+1,j)-gux(i-1,j))/(glx(i+1)-glx(i-1));
    Lxy(i,j) = (guy(i+1,j)-guy(i-1,j))/(glx(i+1)-glx(i-1));
    Lyx(i,j) = (gux(i,j+1)-gux(i,j))/(gly(j+1)-gly(j));
    Lyy(i,j) = (guy(i,j+1)-guy(i,j))/(gly(j+1)-gly(j));
end

%-----
% right wall
% compute derivatives by central or backward differences
%-----

i=Nx+1;
for j=2:Ny
    Lxx(i,j) = (gux(i,j)-gux(i-1,j))/(glx(i)-glx(i-1));
    Lxy(i,j) = (guy(i,j)-guy(i-1,j))/(glx(i)-glx(i-1));
    Lyx(i,j) = (gux(i,j+1)-gux(i,j-1))/(gly(j+1)-gly(j-1));
    Lyy(i,j) = (guy(i,j+1)-guy(i,j-1))/(gly(j+1)-gly(j-1));
end

%-----
% top wall
% compute derivatives by central or backward differences
%-----

j=Ny+1;
for i=2:Nx

```

```

Lxx(i,j) = (gux(i+1,j)-gux(i-1,j))/(glx(i+1)-glx(i-1));
Lxy(i,j) = (guy(i+1,j)-guy(i-1,j))/(glx(i+1)-glx(i-1));
Lyx(i,j) = (gux(i,j)-gux(i,j-1))/(gly(j)-gly(j-1));
Lyy(i,j) = (guy(i,j)-guy(i,j-1))/(gly(j)-gly(j-1));
end

%-----
% four corner points
%-----

i=1; j=1;
Lxx(i,j) = (gux(i+1,j)-gux(i,j))/(glx(i+1)-glx(i));
Lxy(i,j) = (guy(i+1,j)-guy(i,j))/(glx(i+1)-glx(i));
Lyx(i,j) = (gux(i,j+1)-gux(i,j))/(gly(j+1)-gly(j));
Lyy(i,j) = (guy(i,j+1)-guy(i,j))/(gly(j+1)-gly(j));

i=Nx+1; j=1;
Lxx(i,j) = (gux(i,j)-gux(i-1,j))/(glx(i)-glx(i-1));
Lxy(i,j) = (guy(i,j)-guy(i-1,j))/(glx(i)-glx(i-1));
Lyx(i,j) = (gux(i,j+1)-gux(i,j))/(gly(j+1)-gly(j));
Lyy(i,j) = (guy(i,j+1)-guy(i,j))/(gly(j+1)-gly(j));

i=Nx+1; j=Ny+1;
Lxx(i,j) = (gux(i,j)-gux(i-1,j))/(glx(i)-glx(i-1));
Lxy(i,j) = (guy(i,j)-guy(i-1,j))/(glx(i)-glx(i-1));
Lyx(i,j) = (gux(i,j)-gux(i,j-1))/(gly(j)-gly(j-1));
Lyy(i,j) = (guy(i,j)-guy(i,j-1))/(gly(j)-gly(j-1));

i=1; j=Ny+1;
Lxx(i,j) = (gux(i+1,j)-gux(i,j))/(glx(i+1)-glx(i));
Lxy(i,j) = (guy(i+1,j)-guy(i,j))/(glx(i+1)-glx(i));
Lyx(i,j) = (gux(i,j)-gux(i,j-1))/(gly(j)-gly(j-1));
Lyy(i,j) = (guy(i,j)-guy(i,j-1))/(gly(j)-gly(j-1));

%-----
% done
%-----

return

```

The following MATLAB code appended to the code *rec_2d* discussed in Section 1.10, residing in directory *rec_2d* inside directory *02_grids* of FDLIB, computes various flow variables:

```

%---
% specify the grid velocities
%---

for i=1:Nx+1

```

```

for j=1:Ny+1
    px = gx(i,j); py = gy(i,j);
    wnx = 2*pi/(bx-ax); wny = 2*pi/(by-ay);
    gux(i,j) = cos(wnx*px)*cos(wny*py);
    guy(i,j) = sin(wnx*px)*sin(wny*py);
end
end

%---
% velocity gradient tensor
%----

Lxx,Lxy,Lyx,Lyy] = rec_2d_vgt (glx,gly,Nx,Ny,gux,guy);

%---
% compute the rate of expansion
%   the rate of strain tensor
%   the strains
%   the vorticity
%---

for i=1:Nx+1
    for j=1:Ny+1
        roe(i,j) = Lxx(i,j)+Lyy(i,j); % rate of expansion
        omega(i,j) = Lxy(i,j)-Lyx(i,j); % vorticity
        Exx(i,j) = Lxx(i,j)-0.5*roe(i,j); % rate of deformation
        Exy(i,j) = 0.5*(Lxy(i,j)+Lyx(i,j)); % rate of deformation
        Eyx(i,j) = Exy(i,j); % rate of deformation
        Eyy(i,j) = Lyy(i,j)-0.5*roe(i,j); % rate of deformation
        det = 4.0*(Exx(i,j)^2+Exy(i,j)^2); % eigenvalues
        srd = sqrt(det);
        strain1(i,j) = 0.5*srd;
        strain2(i,j) = -0.5*srd;

%---
% compute the eigenvectors of the rate of strain
%---

if(abs(Exy(i,j))<0.0001) % E is diagonal

if(abs(Exx(i,j)-strain1(i,j))>0.0001)
    egv1x(i,j) = 0.0; egv1y(i,j) = 1.0;
else
    egv1x(i,j) = 1.0; egv1y(i,j) = 0.0;
end
if(abs(Exx(i,j)-strain2(i,j))>0.0001)
    egv2x(i,j) = 0.0; egv2y(i,j) = 1.0;
else
    egv2x(i,j) = 1.0; egv2y(i,j) = 0.0;

```

```

end

else % E is not diagonal

egv1x(i,j) = 1.0;
egv1y(i,j) = -(Exx(i,j)-strain1(i,j))/Exy(i,j);
egv2x(i,j) = 1.0;
egv2y(i,j) = -(Exx(i,j)-strain2(i,j))/Exy(i,j);

end

%---
% normalize the eigenvectors
%---

fc1 = 1.0/sqrt(egv1x(i,j)^2+egv1y(i,j)^2);
egv1_x(i,j) = fc1*egv1x(i,j); egv1_y(i,j) = fc1*egv1y(i,j);
fc2 = 1.0/sqrt(egv2x(i,j)^2+egv2y(i,j)^2);
egv2_x(i,j) = fc2*egv2x(i,j); egv2_y(i,j) = fc2*egv2y(i,j);

end
end

%---
% plotting
%---

figure
mesh(glx,gly,omega')
xlabel('x','fontsize',15)
ylabel('y','fontsize',15)
zlabel('\omega','fontsize',15)

figure
mesh(glx,gly,roe')
xlabel('x','fontsize',15);
ylabel('y','fontsize',15)
zlabel('\alpha','fontsize',15)

figure
mesh(glx,gly,strain1')
xlabel('x','fontsize',15)
ylabel('y','fontsize',15)
zlabel('s_1','fontsize',15)

figure
mesh(glx,gly,strain2')
xlabel('x','fontsize',15);
ylabel('y','fontsize',15)

```

```

xlabel('s\_{2}','fontsize',15)

figure
hold on
[ glx,gly,gx,gy ] = grid_2d (ax,bx,ay,by,Nx,Ny);
for i=1:Nx+1
    for j=1:Ny+1
        vector = draw_arrow_2d ...
            (gx(i,j),gy(i,j),egv1x(i,j)/Ny,egv1y(i,j)/Ny);
        plot(vector(:,1),vector(:,2));
    end
end
xlabel('x','fontsize',15)
ylabel('y','fontsize',15)
box on

figure
hold on
[glx,gly,gx,gy] = grid_2d (ax,bx,ay,by,Nx,Ny);
for i=1:Nx+1
    for j=1:Ny+1
        vector = draw_arrow_2d ...
            (gx(i,j),gy(i,j),egv2x(i,j)/Ny,egv2y(i,j)/Ny);
        plot(vector(:,1),vector(:,2));
    end
end
xlabel('x','fontsize',15)
ylabel('y','fontsize',15)

```

The graphics display generated by the code for the velocity field implemented in the code is shown in [Figure 2.5.1](#).

PROBLEMS

2.5.1 Numerical differentiation

Use formula (2.5.9) to evaluate the second derivative of the exponential function $f(x) = e^x$ at $x = 0$ in terms of the values of $f(x)$ at $x = -h, 0, h$, for $h = 0.16, 0.08, 0.04, 0.02$, and 0.01 . Compute and plot the difference between the numerical value and the exact value against h on a log-log scale. Assess and discuss the slope of the graph.

2.5.2 Numerical differentiation of a two-dimensional flow

Run the code *rec_2d* for a velocity field of your choice. Prepare and discuss plots of the vorticity, eigenvalues, and eigenvectors of the rate-of-strain tensor.

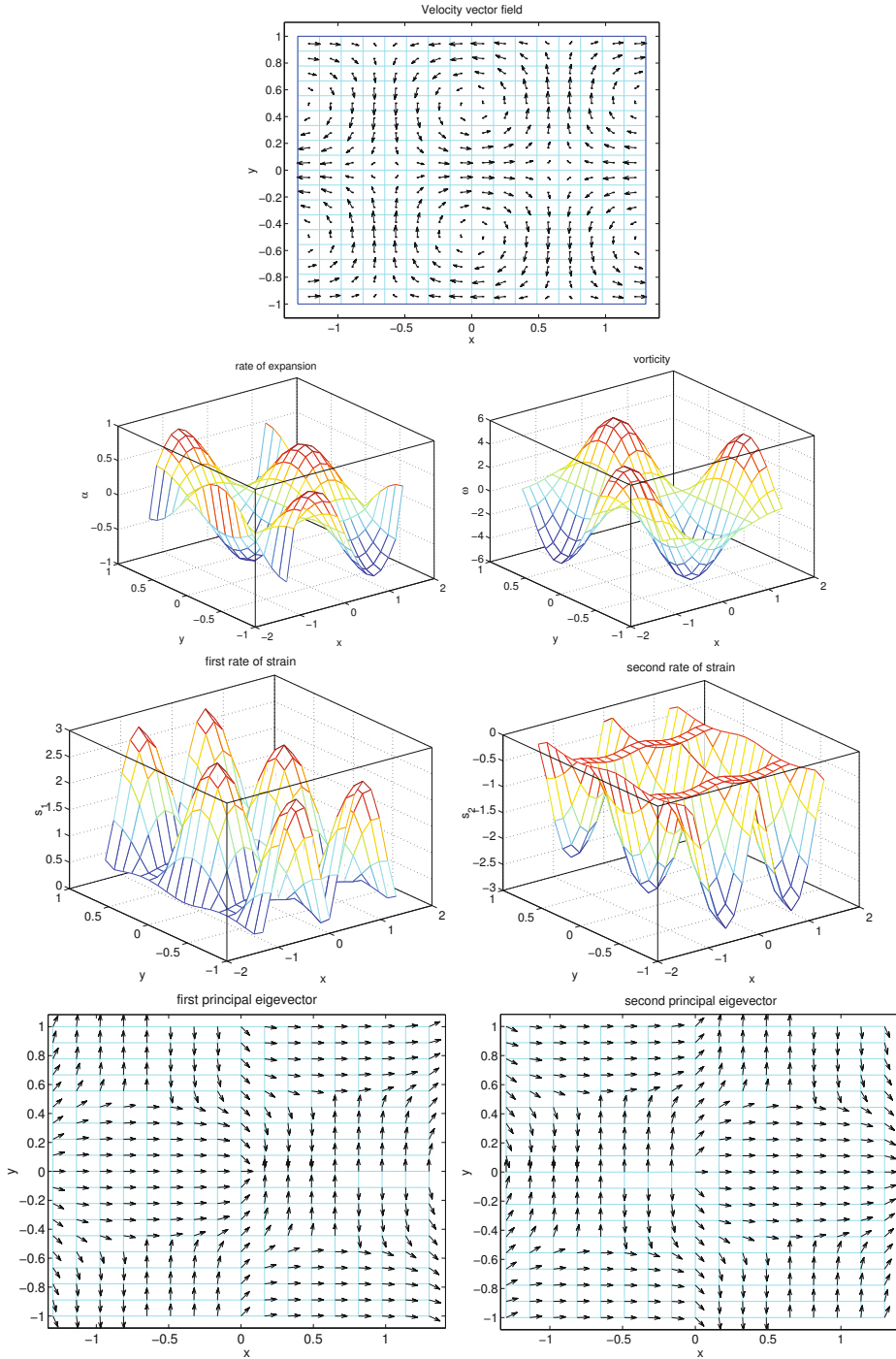


Figure 2.5.1 Velocity vector field, rate of expansion, vorticity, principal strains, and principal eigenvectors computed by numerical differentiation on a uniform Cartesian grid.

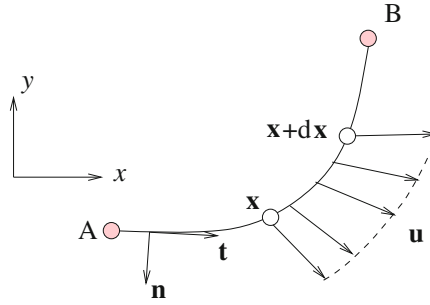


Figure 2.6.1 Illustration of a stationary open line that starts at a point, A, and ends at another point, B, used to define the areal flow rate and flux in a two-dimensional flow. When the end points A and B coincide, we obtain a closed loop.

2.6 Flow rates

Consider a two-dimensional flow in the xy plane and draw a *stationary* line that resides in its entirety inside the fluid. At any instant, point particles cross the line generating a net, positive or negative, areal flow rate in a designated direction. Our goal is to quantify this flow rate in terms of the shape of the line and the fluid velocity.

Unit tangent and unit normal vectors

First, we consider an open line that starts at a point, A, and ends at another point, B, as shown in [Figure 2.6.1](#). As a preliminary, we introduce the unit tangent vector, $\mathbf{t} = (t_x, t_y)$, defined as the vector that is tangential to the line at a point, subject to the normalization condition

$$t_x^2 + t_y^2 = 1. \quad (2.6.1)$$

The direction of \mathbf{t} is chosen such that, if we start moving along the line from point A in the direction of \mathbf{t} , we will finally end up at point B.

Next, we introduce the unit normal vector, $\mathbf{n} = (n_x, n_y)$, defined as the unit vector that is perpendicular to the line at a point. The magnitude of \mathbf{n} is equal to unity,

$$n_x^2 + n_y^2 = 1. \quad (2.6.2)$$

The orientation of \mathbf{n} is such that the tangent vector \mathbf{t} arises by rotating \mathbf{n} around the z axis in the counterclockwise direction by an angle equal to $\frac{1}{2}\pi$.

Now we consider an infinitesimal section of the line that starts at a point, \mathbf{x} , and ends at the point $\mathbf{x} + d\mathbf{x}$, where the differential distance, $d\mathbf{x} = (dx, dy)$ is parallel to, and points in the direction of the unit tangent vector, \mathbf{t} . The components of the unit tangent vector and unit normal vector are given by

$$t_x = \frac{dx}{d\ell}, \quad t_y = \frac{dy}{d\ell} \quad (2.6.3)$$

and

$$n_x = \frac{dy}{d\ell}, \quad n_y = -\frac{dx}{d\ell}, \quad (2.6.4)$$

where $d\ell$ is the differential arc length of the infinitesimal section of the line, given by

$$d\ell = \sqrt{dx^2 + dy^2} = \sqrt{1 + \left(\frac{dy}{dx}\right)^2} |dx| \quad (2.6.5)$$

Because \mathbf{t} and \mathbf{n} are mutually orthogonal, their inner product is zero,

$$\mathbf{t} \cdot \mathbf{n} = \mathbf{n} \cdot \mathbf{t} = 0. \quad (2.6.6)$$

To confirm this, we merely substitute (2.6.3) and (2.6.4) into the right-hand side of (2.1.10).

Normal and tangential velocities

Next, we consider a group of adjacent point particles distributed along the infinitesimal arc length, $d\ell$, at a particular time instant, t . During an infinitesimal period of time, dt , the point particles move to a new position, thus allowing other point particles located behind or in front of them to cross the line into the other side.

To compute the net area of fluid that has crossed the infinitesimal arc length $d\ell$, we resolve the velocity of the point particles into a normal component and a tangential component, writing

$$\mathbf{u} = u_n \mathbf{n} + u_t \mathbf{t}. \quad (2.6.7)$$

The normal and tangential velocities, u_n and u_t , can be computed readily in terms of the inner vector product defined in equation (2.1.10). Taking the inner product of the unit normal vector with both sides of (2.6.7), and using (2.6.6) and (2.6.2), we obtain

$$u_n = \mathbf{u} \cdot \mathbf{n} = u_x n_x + u_y n_y. \quad (2.6.8)$$

Taking the inner product of the unit tangent vector with both sides of (2.6.7), and using (2.6.6) and (2.6.1), we obtain

$$u_t = \mathbf{u} \cdot \mathbf{t} = u_x t_x + u_y t_y. \quad (2.6.9)$$

2.6.1 Areal flow rate and flux

By definition, the local areal flow rate across an infinitesimal section, $d\ell$, is the area of fluid, dA_f , that crosses the infinitesimal section during an infinitesimal period of time, dt , given by

$$\frac{dA_f}{dt} = u_n d\ell, \quad (2.6.10)$$

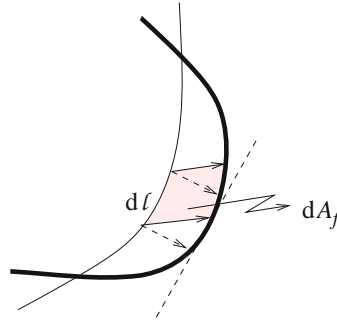


Figure 2.6.2 Two point particles move from the thin line to the bold line over small period of time, dt , thereby allowing for an areal flow rate, dA_f . The particles can be assumed to move first normal to the bold line (dashed vectors) and then tangential to the line to reach their final destination.

as shown in [Figure 2.6.2](#). To see why we selected the normal component of the velocity on the right-hand side, we observe that, if the normal component vanishes, the particles move tangentially to the line and fluid does not cross the line. In general, although point particles move both in the tangential and normal directions, only the normal motion contributes to the local areal flow rate.

The corresponding local areal flux, q , is defined as the ratio of the local areal flow rate, dA_f/dt , to the infinitesimal length of the line across which transport takes place,

$$q \equiv \frac{dA_f}{dt d\ell} = u_n. \quad (2.6.11)$$

We have found that the local areal flux is merely the normal component of the fluid velocity.

Substituting expression (2.6.8) for the normal velocity component into (2.6.10), and using (2.6.4), we obtain

$$\frac{dA_f}{dt} = u_n d\ell = q d\ell \quad (2.6.12)$$

and then

$$\frac{dA_f}{dt} = (u_x n_x + u_y n_y) d\ell = u_x dy - u_y dx. \quad (2.6.13)$$

These expressions allow us to evaluate the local areal flow rate in terms of the components of the velocity.

2.6.2 Areal flow rate across a line

To compute the areal flow rate across the stationary open line depicted in [Figure 2.6.1](#), denoted by Q_{areal} , we subdivide the line into an infinite collection of infinitesimal sections

with differential lengths, $d\ell$, and add all contributions. In mathematical terms, we integrate the local areal flux along the line with respect to arc length, finding that

$$Q^{\text{areal}} = \int_A^B q \, d\ell = \int_A^B \frac{dA_f}{dt \, d\ell} \, d\ell = \int_A^B \frac{dA_f}{dt} = \int_A^B (u_x n_x + u_y n_y) \, d\ell, \quad (2.6.14)$$

and then

$$Q^{\text{areal}} = \int_A^B u_n \, d\ell = \int_A^B (u_x \, dy - u_y \, dx). \quad (2.6.15)$$

The integral on the right-hand side of (2.6.15) allows us to evaluate Q^{areal} in terms of the geometry of the line and the two velocity components.

Note that the areal flow rate, Q^{areal} , has units of area divided by time. The associated volumetric flow rate with units of volume divided by time, is given by

$$Q = w \, Q^{\text{areal}}, \quad (2.6.16)$$

where w is a chosen width along the z axis.

Parcel expansion

The integral representation for the areal flow rate is also applicable in the case of a closed line, \mathcal{L} , described as a loop, as shown in [Figure 2.6.3](#). In that case, the last point, B, simply coincides with the first point, A, yielding a closed integral,

$$Q^{\text{areal}} = \oint_{\mathcal{L}} u_n \, d\ell = \oint_{\mathcal{L}} (u_x \, dy - u_y \, dx). \quad (2.6.17)$$

In fact, the areal flow rate across a closed loop is equal to the rate of change of the area of the fluid parcel that is enclosed by the loop at a certain instant, A_p , that is,

$$\frac{dA_p}{dt} = Q^{\text{areal}}. \quad (2.6.18)$$

The area of the parcel can change only if the fluid occupying the parcel is compressible.

2.6.3 Analytical integration

If a line has a sufficiently simple shape and the components of the velocity are known functions of position with simple forms, the integrals in (2.6.15) can be computed by standard analytical methods.

As an example, we consider a line that has the shape of a section of a circle of radius a centered at a point, \mathbf{x}_c , with end points corresponding to polar angles θ_A and θ_B . Points along the circular arc are described by the equations

$$x = x_c + a \cos \theta, \quad y = y_c + a \sin \theta. \quad (2.6.19)$$

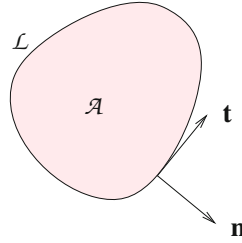


Figure 2.6.3 When the end points of a line coincide, we obtain a closed loop enclosing an area, \mathcal{A} .

Differentiating these equations with respect to θ , we obtain

$$dx = -a \sin \theta d\theta, \quad dy = a \cos \theta d\theta. \quad (2.6.20)$$

Substituting these expressions into the last integral in (2.6.15), we obtain

$$Q^{\text{areal}} = a \int_{\theta_A}^{\theta_B} (u_x \cos \theta + u_y \sin \theta) d\theta. \quad (2.6.21)$$

Substituting the expressions for the velocity components in terms of the angle θ , we obtain an integral representation in terms of θ .

As an application, we assume that

$$u_x = \frac{\alpha}{2\pi} \frac{1}{r} \cos \theta, \quad u_y = \frac{\alpha}{2\pi} \frac{1}{r} \sin \theta, \quad (2.6.22)$$

where α is a constant and r is the distance from the origin. The flow rate is given by

$$Q^{\text{areal}} = a \frac{\alpha}{2\pi} \frac{1}{a} \int_{\theta_A}^{\theta_B} d\theta = \frac{\alpha}{2\pi} (\theta_B - \theta_A). \quad (2.6.23)$$

If the circular segment forms a complete circle and the integration is performed in the counterclockwise direction from $\theta_A = \theta_0$ to $\theta_B = 2\pi - \theta_0$, then $Q^{\text{areal}} = \alpha$, independent of the radius, a , where θ_0 is an arbitrary angle.

2.6.4 Numerical integration

Under most conditions, we will not be able to compute the line integrals in (2.6.15) exactly by analytical methods and we must resort to numerical computation.

To perform numerical integration, we mark the location of a line with $N + 1$ sequential nodes denoted by \mathbf{x}_i for $i = 1, \dots, N + 1$, as depicted in [Figure 2.6.4](#). The first node coincides with the first end point, A, and the last node coincides with the second end point, B. If the line is closed, the first node labeled 1 coincides with the last node labeled $N + 1$.

Next, we approximate the shape of the line between two successive nodes labeled i and $i + 1$ with a straight segment that passes through these nodes, denoted by E_i , where E

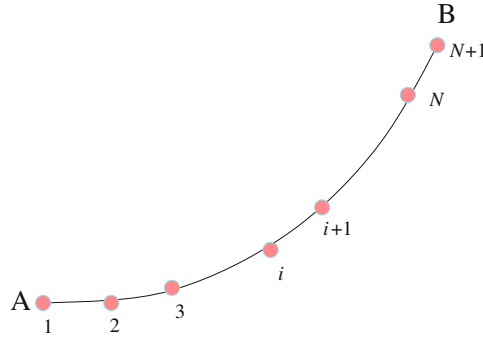


Figure 2.6.4 An array of points along a line in the xy plane is introduced to compute the areal flow rate across a line by numerical methods.

stands for *element*. The union of the N elements forms a polygonal line, called a polyline, starting at the first end point, A, and ending at the second end point, B.

Trapezoidal rule

A key step in developing a numerical approximation is the replacement of the line integrals in (2.6.15) with the sum of integrals over the elements, and the approximation of the velocity components over each element with the average of the values at the element end points. With these approximations, the last integral in (2.6.15) takes the form

$$Q^{\text{areal}} = \sum_{i=1}^N \left[\frac{u_x(\mathbf{x}_i) + u_x(\mathbf{x}_{i+1})}{2} (y_{i+1} - y_i) - \frac{u_y(\mathbf{x}_i) + u_y(\mathbf{x}_{i+1})}{2} (x_{i+1} - x_i) \right]. \quad (2.6.24)$$

Writing out the sum and rearranging, we obtain

$$\begin{aligned} Q^{\text{areal}} &= \frac{1}{2} [u_x(\mathbf{x}_1)(y_2 - y_1) - u_y(\mathbf{x}_1)(x_2 - x_1)] \\ &\quad + \frac{1}{2} \sum_{i=2}^N [u_x(\mathbf{x}_i)(y_{i+1} - y_{i-1}) - u_y(\mathbf{x}_i)(x_{i+1} - x_{i-1})] \\ &\quad + \frac{1}{2} [u_x(\mathbf{x}_{N+1})(y_{N+1} - y_N) - u_y(\mathbf{x}_{N+1})(x_{N+1} - x_N)]. \end{aligned} \quad (2.6.25)$$

If the line is closed, nodes labeled 1 and $N + 1$ coincide, and the first and last contributions on the right-hand side of (2.6.25) combine to yield the simpler form

$$Q^{\text{areal}} = \frac{1}{2} \sum_{i=1}^N [u_x(\mathbf{x}_i)(y_{i+1} - y_{i-1}) - u_y(\mathbf{x}_i)(x_{i+1} - x_{i-1})], \quad (2.6.26)$$

where the wrapped point labeled 0 coincides with the penultimate point labeled N .

The computation of the right-hand sides of (2.6.25) and (2.6.26) requires knowledge of the velocity components at the nodes. In practice, the nodal values are either given explicitly or computed by interpolation from grid values, as discussed in Section 1.7.

2.6.5 The Gauss divergence theorem in two dimensions

Consider a closed loop in the xy plane, denoted by \mathcal{L} , and a vector function of position $\mathbf{h} = (h_x, h_y)$, where $h_x(x, y)$ and $h_y(x, y)$ are two scalar functions. The normal component of \mathbf{h} along \mathcal{L} is given by the inner vector product

$$h_n \equiv \mathbf{h} \cdot \mathbf{n} = h_x n_x + h_y n_y. \quad (2.6.27)$$

The divergence of \mathbf{h} is a scalar function of position given by

$$\nabla \cdot \mathbf{h} \equiv \frac{\partial h_x}{\partial x} + \frac{\partial h_y}{\partial y}. \quad (2.6.28)$$

The Gauss divergence theorem states that the line integral of the normal component, h_n , along the loop, \mathcal{L} , is equal to the integral of the divergence of \mathbf{h} over the area \mathcal{A} enclosed by \mathcal{L} ,

$$\oint_{\mathcal{L}} \mathbf{h} \cdot \mathbf{n} \, d\ell = \iint_{\mathcal{A}} \nabla \cdot \mathbf{h} \, dA, \quad (2.6.29)$$

where \mathbf{n} is the unit vector normal to \mathcal{L} pointing outward, $d\ell$ is a differential arc length, and dA is a differential area.

Areal flow rate across a loop

Now we consider the areal flow rate across a closed loop, as shown in [Figure 2.6.3](#). Applying (2.6.29) with $\mathbf{h} = \mathbf{u}$, we find that the areal flow rate across this loop is equal to the areal integral of the divergence of the velocity over the area enclosed by the loop,

$$Q^{\text{areal}} = \oint_{\mathcal{L}} \mathbf{u} \cdot \mathbf{n} \, d\ell = \iint_{\mathcal{A}} \nabla \cdot \mathbf{u} \, dA, \quad (2.6.30)$$

where the unit normal vector points outward, as shown in [Figure 2.6.3](#). The expression on the right-hand side of (2.6.30) allows us to compute the instantaneous areal flow rate across a closed loop in terms of the integral of the rate of expansion over the enclosed area.

Incompressible fluids

It is clear from expression (2.6.30) that, if the velocity field is solenoidal, that is, the divergence of the velocity vanishes at every point,

$$\nabla \cdot \mathbf{u} = 0, \quad (2.6.31)$$

then the areal flow rate across any closed loop is zero. In physical terms, fluid parcels deform and rotate but do not expand. As a consequence, the amount of fluid entering an area that is enclosed by a stationary closed loop is equal to the amount of fluid exiting the loop during any period of time.

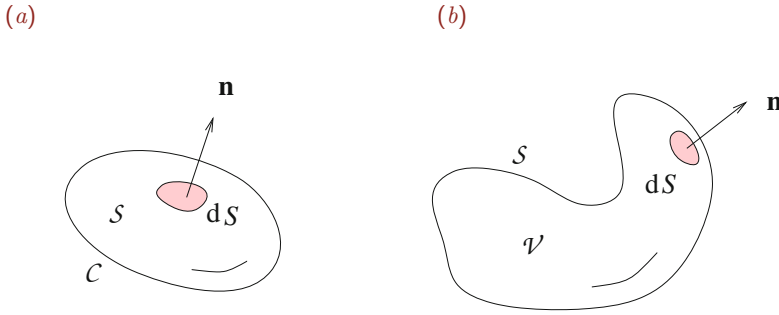


Figure 2.6.5 (a) Illustration of an open surface, S , in a three-dimensional flow, bounded by a closed line, C , (b) Illustration of a closed surface, S , enclosing a volume, \mathcal{V} .

2.6.6 Flow rate in a three-dimensional flow

The preceding discussion for two-dimensional flow can be extended in a straightforward fashion to three-dimensional flow. To carry out this extension, we replace the line integrals along open or closed loops with surface integrals over open or closed surfaces residing inside the flow. The volumetric flow rate across an open or closed surface, S , is given by the surface integral

$$Q = \iint_S \mathbf{u} \cdot \mathbf{n} \, dS. \quad (2.6.32)$$

The unit vector normal to S , denoted by \mathbf{n} , and the differential area of a surface element, dS , are defined in Figure 2.6.5. Note that Q has units of volume divided by time.

If V_p is the volume of a parcel confined by a closed surface, then the rate of change of the parcel volume is

$$\frac{dV_p}{dt} = Q. \quad (2.6.33)$$

Parcel expansion or shrinkage is possible only if the fluid is compressible.

2.6.7 Gauss divergence theorem in three dimensions

Consider a closed surface, S , and a vector function of position, $\mathbf{h} = (h_x, h_y, h_z)$. The normal component of \mathbf{h} over S is given by the inner product

$$h_n \equiv \mathbf{h} \cdot \mathbf{n} = h_x n_x + h_y n_y + h_z n_z. \quad (2.6.34)$$

The divergence of \mathbf{h} is defined as

$$\nabla \cdot \mathbf{h} \equiv \frac{\partial h_x}{\partial x} + \frac{\partial h_y}{\partial y} + \frac{\partial h_z}{\partial z}. \quad (2.6.35)$$

The Gauss divergence theorem states that the surface integral of h_n over \mathcal{S} is equal to the integral of the divergence of \mathbf{h} over the volume \mathcal{V} enclosed by \mathcal{S} ,

$$\iint_{\mathcal{S}} \mathbf{h} \cdot \mathbf{n} \, dS = \iiint_{\mathcal{V}} \nabla \cdot \mathbf{h} \, dV, \quad (2.6.36)$$

where \mathbf{n} is the unit vector normal to the surface \mathcal{S} pointing outward, dS is a differential surface area and dV is a differential volume.

Flow rate

Now we consider the flow rate across a closed surface \mathcal{V} , given in (2.6.32). Applying (2.6.36) for the fluid velocity, $\mathbf{h} = \mathbf{u}$, we obtain

$$Q = \iint_{\mathcal{S}} \mathbf{u} \cdot \mathbf{n} \, dS = \iiint_{\mathcal{V}} \nabla \cdot \mathbf{u} \, dV. \quad (2.6.37)$$

This expression shows that, if the velocity field is solenoidal, $\nabla \cdot \mathbf{u} = 0$, the volumetric flow rate across any closed surface enclosing fluid alone must vanish.

2.6.8 Axisymmetric flow

Next, we consider an axisymmetric flow and draw a line that begins at a point, A, and ends at another point, B, in a azimuthal plane, as illustrated in [Figure 2.6.6](#). The volumetric flow rate across the axisymmetric surface that arises by rotating the line around the x axis is given by

$$Q = 2\pi \int_A^B \sigma (u_x n_x + u_\sigma n_\sigma) \, d\ell, \quad (2.6.38)$$

where $d\ell$ is the differential arc length along the generating line, u_x it the velocity component along the x axis, and u_σ is the velocity component normal to the x axis.

Expression (2.6.38) arises by adding the fluxes across all elementary axisymmetric surfaces confined between two parallel planes that are perpendicular to the x axis and are separated by an infinitesimal distance, dx , corresponding to the arc length, $d\ell$, taking into consideration that the surface area of an elementary surface centered at a ring of radius σ is equal to $2\pi\sigma d\ell$.

Substituting the components of the normal vector,

$$n_x = \frac{d\sigma}{d\ell}, \quad n_\sigma = -\frac{dx}{d\ell}, \quad (2.6.39)$$

we obtain

$$Q = 2\pi \int_A^B \sigma (u_x d\sigma - u_\sigma dx). \quad (2.6.40)$$

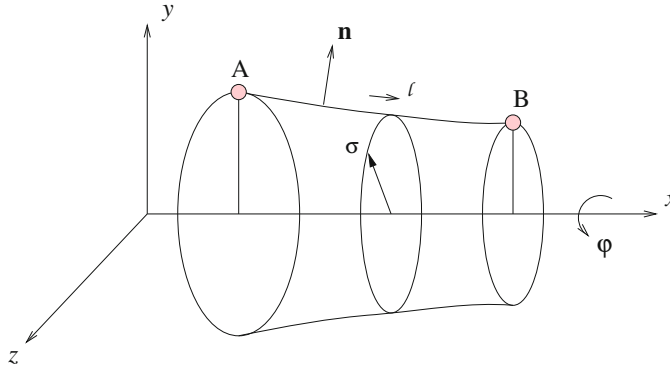


Figure 2.6.6 Illustration of an axisymmetric surface whose trace in an azimuthal plane is an open line that begins at a point, A, and ends at another point, B.

PROBLEMS

2.6.1 Flow rate across an ellipse

Consider a closed loop in the xy plane in the shape of a horizontal ellipse centered at a point, $\mathbf{x}_c = (x_c, y_c)$, with major and minor semi-axes equal to a and b . The elliptical shape is described in parametric form by the equations

$$x = x_c + a \cos \eta, \quad y = y_c + b \sin \eta, \quad (2.6.41)$$

where η is the native parameter of the ellipse ranging in the interval $(0, 2\pi]$. We will assume that, in plane polar coordinates in the xy plane with origin at the center of the ellipse, (r, θ) , the velocity components are given by

$$u_x = \frac{\alpha}{2\pi} \frac{1}{r} \cos \theta, \quad u_y = \frac{\alpha}{2\pi} \frac{1}{r} \sin \theta, \quad (2.6.42)$$

where α is a constant. Show that

$$\tan \theta = \frac{b}{a} \tan \eta \quad (2.6.43)$$

and derive an expression for the flow rate across the ellipse as an integral with respect to η .

2.6.2 Flow rate across an ellipse

With reference to Problem 2.6.1, write a code that computes the flow rate across the ellipse using a numerical method based on equation (2.6.26). Perform computations for ellipses with aspect ratios, $a/b = 1, 2, 4,$ and 8 , in each case for $N = 8, 16, 32,$ and 64 numerical divisions. Discuss the results of your computations.

2.7 Mass conservation and the continuity equation

In Section 1.5, we defined a point particle as an idealized entity arising in the limit as the size of a small fluid parcel becomes decreasingly small and eventually infinitesimal. In this limit, the ratio between the mass of the parcel and the volume of the parcel tends to a finite, nonzero, and non-infinite value, which is defined as the fluid density, ρ . To indicate that the density is a function of position and time in a fluid, we write

$$\rho(\mathbf{x}, t), \quad (2.7.1)$$

with the understanding that the density at a particular point in a flow is equal to the density of the point particle that happens to be at that position at the designated time.

2.7.1 Mass flux and mass flow rate

Consider a two-dimensional flow in the xy plane and draw a *stationary line* that begins at a point, A, and ends at another point, B, as illustrated in [Figure 2.6.1](#). At any instant, point particles cross this line, thereby generating a net *mass flow rate* in a specified direction. Our goal is to quantify this mass flow rate in terms of the shape of the line and the velocity and density distributions in the fluid.

Repeating the analysis of Section 2.6, we find that the mass flux across an infinitesimal section of the line is given by the following counterpart of equation (2.6.11),

$$q_{\text{mass}} = \rho u_n, \quad (2.7.2)$$

where $u_n = \mathbf{u} \cdot \mathbf{n}$ is the component of the fluid velocity normal to the line. The mass flow rate across a line that begins at a point, A, and ends at another point, B, is given by the following counterpart of equation (2.6.15),

$$Q_{\text{mass}}^{\text{areal}} = \int_A^B q_{\text{mass}} \, dl = \int_A^B \rho \mathbf{u} \cdot \mathbf{n} \, dl = \int_A^B \rho (u_x \, dy - u_y \, dx). \quad (2.7.3)$$

Note that $Q_{\text{mass}}^{\text{areal}}$ has units of mass divided by length and time. The integrals in (2.7.3) can be computed by analytical or numerical methods, as discussed in Section 2.6.

2.7.2 Mass flow rate across a closed line

The net mass flow rate outward from a closed line in a two-dimensional flow can be expressed in terms of a closed line integral in the form

$$Q_{\text{mass}}^{\text{areal}} = \oint q_{\text{mass}} \, dl = \oint \rho \mathbf{u} \cdot \mathbf{n} \, dl = \oint \rho (u_x \, dy - u_y \, dx), \quad (2.7.4)$$

where the unit normal vector, \mathbf{n} , points into the exterior of the area enclosed by the closed line, as depicted in [Figure 2.6.3](#).

The Gauss divergence theorem expressed by equation (2.6.29) states that the line integral in (2.7.4) is equal to the integral of the divergence of the velocity multiplied by the fluid density over the area enclosed by the line, \mathcal{A} ,

$$Q_{\text{mass}}^{\text{areal}} = \iint_{\mathcal{A}} \nabla \cdot (\rho \mathbf{u}) \, dx \, dy, \quad (2.7.5)$$

where

$$\nabla \cdot (\rho \mathbf{u}) = \frac{\partial(\rho u_x)}{\partial x} + \frac{\partial(\rho u_y)}{\partial y} \quad (2.7.6)$$

is the divergence of the mass velocity, $\rho \mathbf{u}$.

For future reference, we expand the derivatives of the products on the left-hand side of (2.7.6) using the rules of product differentiation, finding that

$$\nabla \cdot (\rho \mathbf{u}) = \frac{\partial \rho}{\partial x} u_x + \frac{\partial u_x}{\partial x} \rho + \frac{\partial \rho}{\partial y} u_y + \frac{\partial u_y}{\partial y} \rho \quad (2.7.7)$$

or

$$\nabla \cdot (\rho \mathbf{u}) = \mathbf{u} \cdot \nabla \rho + \rho \nabla \cdot \mathbf{u}. \quad (2.7.8)$$

We have introduced the vector of the first partial derivatives of the density,

$$\nabla \rho = \left(\frac{\partial \rho}{\partial x}, \frac{\partial \rho}{\partial y} \right), \quad (2.7.9)$$

defined as the gradient of the density.

2.7.3 The continuity equation

The first principle of thermodynamics mandates that the rate of change of the mass residing inside an area, \mathcal{A} , that is enclosed by a stationary closed line, \mathcal{L} , given by

$$\iint_{\mathcal{A}} \rho \, dA, \quad (2.7.10)$$

is equal to the mass flow rate inward across the line, which is equal to the negative of the mass flow rate outward across the line. If the outward mass flow rate is positive, the rate of the change of mass enclosed by the line is negative, reflecting a reduction in time.

In terms of the mass flow rate defined in equation (2.7.4) and expressed as an areal integral in equation (2.7.5), mass conservation requires that

$$\frac{d}{dt} \iint_{\mathcal{A}} \rho \, dA = -Q_{\text{mass}}^{\text{areal}} = - \oint_{\mathcal{L}} \rho \mathbf{u} \cdot \mathbf{n} \, d\ell = - \iint_{\mathcal{A}} \nabla \cdot (\rho \mathbf{u}) \, dA. \quad (2.7.11)$$

Since the area \mathcal{A} is fixed in space, we can interchange the order of the time differentiation and space integration on the left-hand side of (2.7.11), and then combine the two integrals to obtain

$$\iint_{\mathcal{A}} \left(\frac{\partial \rho}{\partial t} + \nabla \cdot (\rho \mathbf{u}) \right) dA = 0. \quad (2.7.12)$$

Since the shape of the area \mathcal{A} is arbitrary, the integrand on the right-hand side of (2.7.12) must be identically zero, yielding a partial differential equation in time-space expressing mass conservation,

$$\frac{\partial \rho}{\partial t} + \nabla \cdot (\rho \mathbf{u}) = 0, \quad (2.7.13)$$

called the *continuity equation*. This terminology emphasizes that, in the absence of singularities in the form of point sources and sinks, mass neither appears nor disappears in the flow and the fluid must move in a continuous fashion in the available domain of flow.

Combining equations (2.7.8) and (2.7.13), we derive an alternative form of the continuity equation,

$$\frac{\partial \rho}{\partial t} + \mathbf{u} \cdot \nabla \rho + \rho \nabla \cdot \mathbf{u} = 0, \quad (2.7.14)$$

involving the vectorial density gradient, $\nabla \rho$, and the scalar rate of expansion, $\nabla \cdot \mathbf{u}$.

Differential mass balance

It is instructive to derive the continuity equation based on a mass balance over a small stationary rectangular control area in the xy plane, as shown in [Figure 2.7.1](#). Balancing the rate of mass accumulation inside the control area with the rates of mass crossing the four edges, we obtain

$$\frac{d}{dt} (\rho dx dy) = (\rho u_x dy)_x - (\rho u_x dy)_{x+dx} + (\rho u_y dx)_y - (\rho u_y dx)_{y+dy}. \quad (2.7.15)$$

Dividing both sides by $dx dy$ and noting that the variables, x , y , and t are independent, we obtain

$$\frac{d\rho}{dt} = \frac{(\rho u_x)_x - (\rho u_x)_{x+dx}}{dx} + \frac{(\rho u_y dx)_y - (\rho u_y dx)_{y+dy}}{dy}. \quad (2.7.16)$$

To derive the continuity equation (2.7.13), we merely invoke the definition of the partial derivative.

2.7.4 Three-dimensional flow

Our discussion earlier in this section for two-dimensional flow can be generalized in a straightforward fashion to three-dimensional flow. To carry out this extension, we replace the line integrals with surface integrals over a closed or open surface. The mass flow rate

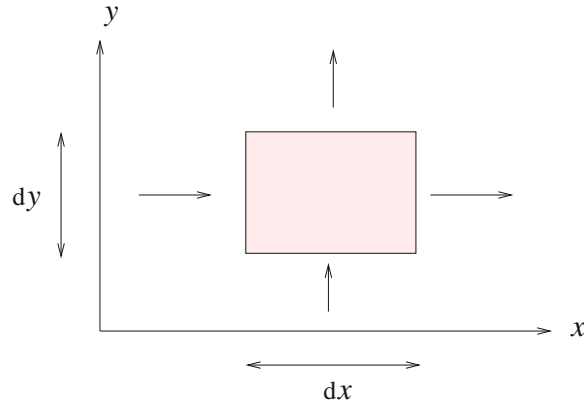


Figure 2.7.1 To derive the continuity equation for two-dimensional flow, we write a mass balance over an infinitesimal rectangular control area.

across a stationary, open or closed surface \mathcal{S} depicted in [Figure 2.6.5](#) is given by the surface integral

$$Q_{\text{mass}} = \iint_{\mathcal{S}} \rho \mathbf{u} \cdot \mathbf{n} \, dS, \quad (2.7.17)$$

involving the normal velocity component, $u_n = \mathbf{u} \cdot \mathbf{n}$.

If the surface is closed and the unit normal vector points outward, as shown in [Figure 2.6.5\(b\)](#), we may use the divergence theorem to convert the surface integral on the right-hand side of (2.7.17) into an integral of the rate of expansion over the volume \mathcal{V} enclosed by the surface, obtaining

$$Q_{\text{mass}} = \iiint_{\mathcal{V}} \nabla \cdot (\rho \mathbf{u}) \, dV. \quad (2.7.18)$$

The counterpart of the mass balance equation (2.7.11) is

$$\iiint_{\mathcal{V}} \frac{\partial \rho}{\partial t} \, dV = -Q_{\text{mass}} = - \iint_{\mathcal{S}} \rho \mathbf{u} \cdot \mathbf{n} \, dS = - \iiint_{\mathcal{V}} \nabla \cdot (\rho \mathbf{u}) \, dV. \quad (2.7.19)$$

Since the area D is fixed in space, we can interchange the order of

The continuity equation expressed by (2.7.13) or (2.7.14) stands true, with the understanding that $\nabla \rho$ is the three-dimensional density gradient with components

$$\nabla \rho = \left(\frac{\partial \rho}{\partial x}, \frac{\partial \rho}{\partial y}, \frac{\partial \rho}{\partial z} \right) \quad (2.7.20)$$

defined over the domain of flow.

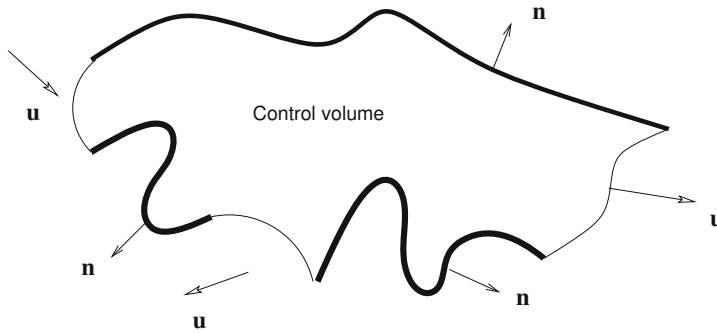


Figure 2.7.2 Illustration of a stationary control volume in a flow (cv) bounded by solid or fluid surfaces.

2.7.5 Control volume and integral mass balance

In the context of transport phenomena, a volume, \mathcal{V} , bounded by a closed surface, \mathcal{S} , is regarded as a control volume (cv), as shown in Figure 2.7.2. Equation (2.7.11) requires that

$$\iiint_{\text{cv}} \frac{\partial \rho}{\partial t} dV + \iint_{\text{cv}} \rho \mathbf{u} \cdot \mathbf{n} dS = 0, \quad (2.7.21)$$

physically stating that mass accumulation in a stationary control volume is due to convective motion through the boundaries of the control volume. Equation (2.7.21) expresses an integral or macroscopic mass balance.

2.7.6 Rigid-body translation

When a fluid translates as a rigid body, the fluid velocity, \mathbf{u} , has a constant and possibly time-dependent value, $\mathbf{U}(t)$. In this case, the continuity equation (2.7.13) simplifies to a linear convection equation,

$$\frac{\partial \rho}{\partial t} + \mathbf{U} \cdot \nabla \rho = 0. \quad (2.7.22)$$

Consider a steady flow where \mathbf{U} is independent of time. Using equation (2.7.22), we find that, if $\rho_0(\mathbf{x})$ is the density field at $t = 0$, then

$$\rho(\mathbf{x}, t) = \rho_0(\mathbf{x} - \mathbf{U}t) \quad (2.7.23)$$

will be the density field at any other time, t . Physically, the density at the point $\mathbf{x} = \mathbf{x}_0 - \mathbf{U}t$ at time t is equal to the density at the point \mathbf{x}_0 at $t = 0$. We may say that the density field is *convected* by the uniform flow.

To confirm (2.7.23), we introduce an auxiliary vector variable, $\mathbf{w} = \mathbf{x} - \mathbf{U}t$, with components

$$w_x \equiv x - U_x t, \quad w_y \equiv y - U_y t, \quad w_z \equiv z - U_z t. \quad (2.7.24)$$

Using the chain rule of differentiation, we write

$$\frac{\partial \rho}{\partial t} = \frac{\partial \rho_0}{\partial w_x} \frac{\partial w_x}{\partial t} + \frac{\partial \rho_0}{\partial w_y} \frac{\partial w_y}{\partial t} + \frac{\partial \rho_0}{\partial w_z} \frac{\partial w_z}{\partial t}, \quad (2.7.25)$$

and then

$$\frac{\partial \rho}{\partial t} = \frac{\partial \rho_0}{\partial w_x} (-U_x) + \frac{\partial \rho_0}{\partial w_y} (-U_y) + \frac{\partial \rho_0}{\partial w_z} (-U_z). \quad (2.7.26)$$

The proof follows by observing that

$$\frac{\partial \rho_0}{\partial w_x} = \frac{\partial \rho_0}{\partial x}, \quad \frac{\partial \rho_0}{\partial w_y} = \frac{\partial \rho_0}{\partial y}, \quad \frac{\partial \rho_0}{\partial w_z} = \frac{\partial \rho_0}{\partial z}. \quad (2.7.27)$$

2.7.7 Evolution equation for the density

The continuity equation can be regarded as an evolution equation for the density, determined by the fluid velocity. To see this, we recast equation (2.7.13) into the form

$$\frac{\partial \rho}{\partial t} = -\nabla \cdot (\rho \mathbf{u}). \quad (2.7.28)$$

Evaluating the right-hand side of (2.7.28) at a certain point, \mathbf{x} , in terms of the local and instantaneous velocity and density, we obtain an expression for the local and current rate of change of the density in time.

Temporal discretization

Consider the change in density occurring during a small time interval, Δt , following the current time t . Evaluating both sides of equation (2.7.28) at a point, \mathbf{x} , and approximating the right-hand side with a first-order forward difference, we obtain

$$\frac{\rho(\mathbf{x}, t + \Delta t) - \rho(\mathbf{x}, t)}{\Delta t} = -\nabla \cdot (\rho \mathbf{u}), \quad (2.7.29)$$

where the right-hand side is evaluated at (\mathbf{x}, t) . Solving for $\rho(\mathbf{x}, t + \Delta t)$, we obtain

$$\rho(\mathbf{x}, t + \Delta t) = \rho(\mathbf{x}, t) - \Delta t \nabla \cdot (\rho \mathbf{u}), \quad (2.7.30)$$

which provides us with an explicit expression for $\rho(\mathbf{x}, t + \Delta t)$ in terms of the density and velocity at the current time, t .

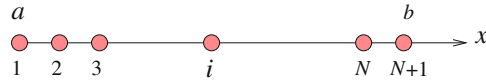
Finite-difference method

In practice, equation (2.7.28) is solved by numerical methods. Consider an idealized one-dimensional flow along the x axis representing, for example, the flow along a conduit with a known axial velocity, $u(x, t)$. The one-dimensional version of the continuity equation (2.7.28) is

$$\frac{\partial \rho}{\partial t} = -\frac{\partial(\rho u)}{\partial x}. \quad (2.7.31)$$

The solution must be found inside a specified interval, $a \leq x \leq b$, subject to an initial condition that specifies the density distribution at the designated origin of time, $\rho(x, t = 0)$, and a boundary condition that specifies the density at the left end of the solution domain, $x = a$.

To develop the numerical method, we divide the solution domain into N intervals defined by $N + 1$ nodes, x_i for $i = 1, \dots, N + 1$, as shown below:



The first node coincides with the left end point, $x = a$, and the last node coincides with the right end point, $x = b$. Our goal is to generate the values of ρ at the nodes at a sequence of time instants separated by the time interval Δt . To simplify the notation, we denote the density at the i th node at the k th time level, corresponding to time $t_k = k \Delta t$, by ρ_i^k .

Evaluating both sides of (2.7.31) at the i th node at the k th time level, and approximating the time derivative on the left-hand side with a first-order forward difference and the spatial derivative on the right-hand side with a first-order backward difference, we derive the finite-difference approximation

$$\frac{\rho_i^{k+1} - \rho_i^k}{\Delta t} = - \frac{(\rho u)_i^k - (\rho u)_{i-1}^k}{x_i - x_{i-1}}. \quad (2.7.32)$$

Solving for ρ_i^{k+1} , we obtain the updating formula

$$\rho_i^{k+1} = \rho_i^k - \frac{\Delta t}{x_i - x_{i-1}} [(\rho u)_i^k - (\rho u)_{i-1}^k]. \quad (2.7.33)$$

Algorithm

The numerical method involves the following steps:

1. Specify the initial values ρ_i^0 for $i = 1, \dots, N + 1$.
2. Use equation (2.7.33) to compute ρ_i^1 for $i = 2, \dots, N + 1$.
3. Use the left end boundary value to set the value of ρ_1^1 .
4. Use equation (2.7.33) to compute ρ_i^2 for $i = 2, \dots, N + 1$.
5. Use the left end boundary value to set the value of ρ_1^2 .
6. Stop, or continue for further steps.

Note that a boundary condition at the right end of the solution domain is not required. Numerical analysis shows that the success of this method depends on the size of the time step, Δt , and sign of the convection velocity, u .

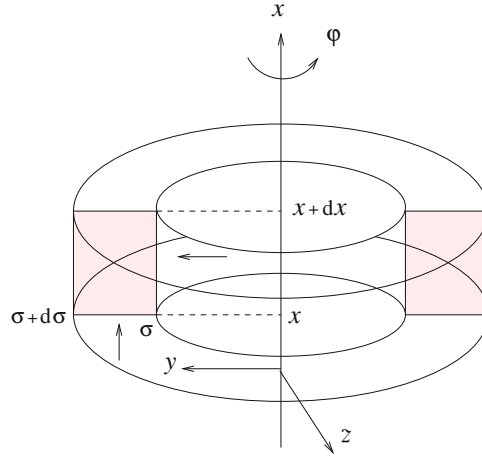


Figure 2.7.2 To derive the continuity equation for axisymmetric flow, we write a mass balance over an infinitesimal toroidal control volume in cylindrical polar coordinates.

2.7.8 Continuity equation for axisymmetric flow

Consider an axisymmetric flow and introduce cylindrical polar coordinates, (x, σ, φ) , as shown in [Figure 2.7.2](#). We will demonstrate that the continuity equation takes the form

$$\frac{\partial \rho}{\partial t} + \frac{\partial(\rho u_x)}{\partial x} + \frac{1}{\sigma} \frac{\partial(\sigma \rho u_\sigma)}{\partial \sigma} = 0. \quad (2.7.34)$$

To derive this equation, we perform a differential mass balance over a toroidal control volume with two sides parallel sides at x and $x+dx$ and the other two coaxial sides at σ and $\sigma+d\sigma$, as shown in [Figure 2.7.2](#). The volume of the differential control volume is

$$dV_{cv} = 2\pi\sigma dx d\sigma \quad (2.7.35)$$

and the mass of the fluid residing inside the control volume at any instant is $dm_{cv} = \rho dV_{cv}$.

Balancing the rate of accumulation of fluid inside the control volume with the rates of convection of mass across the four sides, we obtain

$$\begin{aligned} \frac{d}{dt} (\rho 2\pi\sigma dx d\sigma) &= (\rho u_x 2\pi\sigma d\sigma)_x - (\rho u_x 2\pi\sigma d\sigma)_{x+dx} \\ &\quad + (\rho u_\sigma 2\pi\sigma dx)_\sigma - (\rho u_\sigma 2\pi\sigma dx)_{\sigma+d\sigma}. \end{aligned} \quad (2.7.36)$$

Simplifying, we obtain

$$\sigma \frac{d}{dt} (\rho dx d\sigma) = \sigma (\rho u_x d\sigma)_x - \sigma (\rho u_x d\sigma)_{x+dx} + (\rho u_\sigma \sigma dx)_\sigma - (\rho u_\sigma \sigma dx)_{\sigma+d\sigma}. \quad (2.7.37)$$

Now dividing both sides by $\sigma dx d\sigma$ and noting that x, σ , and t are independent variables, we obtain

$$\frac{d\rho}{dt} = \frac{(\rho u_x)_x - (\rho u_x)_{x+dx}}{dx} + \frac{1}{\sigma} \frac{(\sigma \rho u_\sigma dx)_\sigma - (\sigma \rho u_\sigma dx)_{\sigma+d\sigma}}{d\sigma}. \quad (2.7.38)$$

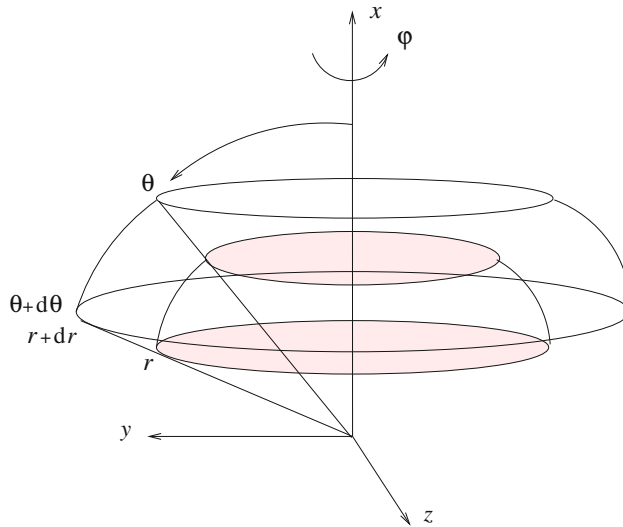


Figure 2.7.3 To derive the continuity equation for axisymmetric flow, we write a mass balance over an infinitesimal control volume in spherical polar coordinates.

To derive (2.7.34), we invoke the definition of the partial derivative and transfer all terms to the left-hand side. Note that the density, ρ , remains inside the derivatives.

In spherical polar coordinates, (r, θ, φ) , equation (2.7.34) takes the form

$$\frac{\partial \rho}{\partial t} + \frac{1}{r^2} \frac{\partial (r^2 \rho u_r)}{\partial r} + \frac{1}{r \sin \theta} \frac{\partial (\sin \theta \rho u_\theta)}{\partial \theta} = 0. \quad (2.7.39)$$

To derive this equation, we perform a differential mass balance over a toroidal control volume with two faces at r and $r + dr$ and the other two faces at θ and $\theta + d\theta$, as shown in [Figure 2.7.3](#).

PROBLEMS

2.7.1 Convection under constant velocity

Consider the one-dimensional flow discussed in the text where the density field is governed by (2.7.31) with the velocity u being a constant. Sketch a profile of the density distribution along the x axis at the initial time, $t = 0$, and at a subsequent time.

2.7.2 Steady state

Consider a steady one-dimensional flow with a specified velocity distribution, $u(x)$. Derive an expression for the density distribution at steady state based on (2.7.31). Discuss the behavior of the density at a point where the velocity is zero.

2.7.3 Finite-difference method

Consider a steady, one-dimensional, periodic flow along the x axis with sinusoidal velocity distribution,

$$u(x) = U [1 + \epsilon \cos(2\pi x/L)], \quad (2.7.40)$$

where U is a constant velocity, ϵ is a specified dimensionless constant, and L is the period. Write a computer program that uses the numerical method discussed in the text to compute the evolution of the density over one spatial period, L , subject to a uniform initial distribution. Run the program for $\epsilon = 0, 0.2, 0.4,$ and 0.8 , prepare graphs of the density distribution at different times, and discuss the behavior of the solution at long times.

2.8 Properties of point particles

The physical properties of a homogeneous fluid parcel consisting of a single chemical species are determined by the number of molecules, the kinetic energy, the potential energy, and the thermal energy of the molecules that comprise the parcel. Each one of these physical properties is *extensive*, in that, the larger the parcel volume, the higher the magnitude of the physical property.

As the size of a parcel tends to zero, the ratio between the value of an extensive property and the parcel volume tends to a limit that is regarded as an *intensive* physical property of the point particle that emerges from the parcel immediately before the molecular nature of the fluid becomes apparent.

For example, we have already seen that, as the volume of a parcel tends to zero, the ratio between the mass of the parcel and the volume of the parcel tends to a finite limit that is defined as the fluid density, ρ . Similarly, the ratio of the number of molecules residing within the parcel and the volume of the parcel tends to the molecular number density, and the ratio of the potential energy of the molecules and the volume of the parcel tends to the specific potential energy.

2.8.1 The material derivative

To prepare the ground for establishing evolution laws governing the motion and physical state of a fluid, we seek corresponding laws determining the rate of change of physical and kinematic properties of point particles moving with the local fluid velocity. Kinematic properties include the point particle velocity and its first time derivative defined as the point particle acceleration, the vorticity, and the rate of strain.

A key concept is the material derivative, defined as the *rate of change of a physical or kinematic property following a point particle*. Our first objective is to derive an expression for the material derivative in terms of Eulerian derivatives; that is, partial derivatives with respect to spatial coordinates and time.

Taylor series expansion

Consider the material derivative of the density of a point particle which, at a certain time t_0 , is located at the point \mathbf{x}_0 . In three-dimensional flow, the density is a function of four independent variables, including the three Cartesian coordinates, (x, y, z) , determining position in space, and time, t .

We begin by linearizing the density field, $\rho(x, y, z, t)$, around (x_0, y_0, z_0, t_0) , as discussed in Section 2.1. Adding time dependence to equation (2.1.6) and identifying the generic function $f(\mathbf{x}, t)$ with the density, we obtain the linearized form

$$\begin{aligned} \rho(\mathbf{x}, t) \simeq & \rho(\mathbf{x}_0, t_0) + (t - t_0) \left(\frac{\partial \rho}{\partial t} \right)_{\mathbf{x}_0, t_0} \\ & + (x - x_0) \left(\frac{\partial \rho}{\partial x} \right)_{\mathbf{x}_0, t_0} + (y - y_0) \left(\frac{\partial \rho}{\partial y} \right)_{\mathbf{x}_0, t_0} + (z - z_0) \left(\frac{\partial \rho}{\partial z} \right)_{\mathbf{x}_0, t_0}, \end{aligned} \quad (2.8.1)$$

where $\mathbf{x}_0 = (x_0, y_0, z_0)$. Next, we bring the first term on the right-hand side, $\rho(\mathbf{x}_0)$, to the left-hand side, and divide both sides of the resulting equation by the time elapsed, $t - t_0$, to derive the expression

$$\frac{\rho(\mathbf{x}, t) - \rho(\mathbf{x}_0, t_0)}{t - t_0} = \left(\frac{\partial \rho}{\partial t} \right)_{\mathbf{x}_0, t_0} + \frac{x - x_0}{t - t_0} \left(\frac{\partial \rho}{\partial x} \right)_{\mathbf{x}_0, t_0} + \frac{y - y_0}{t - t_0} \left(\frac{\partial \rho}{\partial y} \right)_{\mathbf{x}_0, t_0} + \frac{z - z_0}{t - t_0} \left(\frac{\partial \rho}{\partial z} \right)_{\mathbf{x}_0, t_0}, \quad (2.8.2)$$

which is applicable at any point, \mathbf{x} , in the neighborhood of a chosen point of interest, \mathbf{x}_0 , and for time t near t_0 .

Moving with the fluid

The second key step involves the judicious choice of the field point, \mathbf{x} . This point is selected so that, if a point particle is located at the position \mathbf{x}_0 at time t_0 , then the same point particle is located at the position \mathbf{x} at a later time, t . By definition then, the left-hand side of (2.8.2) reduces to the material derivative.

Since the point particle moves with the fluid velocity, the three fractions on the right-hand side of (2.8.2) are equal the three components of the fluid velocity, u_x , u_y , and u_z . Denoting the material derivative by D/Dt , we find that

$$\left(\frac{D\rho}{Dt} \right)_{\mathbf{x}_0, t_0} = \left(\frac{\partial \rho}{\partial t} + u_x \frac{\partial \rho}{\partial x} + u_y \frac{\partial \rho}{\partial y} + u_z \frac{\partial \rho}{\partial z} \right)_{\mathbf{x}_0, t_0}. \quad (2.8.3)$$

In terms of the density gradient defined in (2.7.20), equation (2.8.3) takes the simpler form

$$\frac{D\rho}{Dt} = \frac{\partial \rho}{\partial t} + \mathbf{u} \cdot \nabla \rho, \quad (2.8.4)$$

where both sides are evaluated at the arbitrary point, \mathbf{x}_0 , at an arbitrary time instant, t_0 .

Lagrangian and Eulerian derivatives

Equation (2.8.3) allows us to compute the material derivative of the density, sometimes also called the Lagrangian derivative, in terms of Eulerian derivatives, that is, in terms of partial derivatives of the density with respect to time and spatial coordinates, x , y , and z . In numerical practice, the partial derivatives are computed by finite-difference approximations, as discussed in Section 2.5.

2.8.2 The continuity equation

Comparing equations (2.8.4) and (2.7.14), we find that, in terms of the material derivative of the density, the continuity equation takes the form

$$\frac{D\rho}{Dt} + \rho \nabla \cdot \mathbf{u} = 0, \quad (2.8.5)$$

which reveals that the rate of change of the density of a point particle is determined exclusively by the local rate of expansion, $\nabla \cdot \mathbf{u}$. However, the inverse interpretation is physically more appropriate: *the structure of the velocity field is determined, in part, by the rate of change of the density of all point particles.*

Consider a small fluid parcel with volume δV_p , density ρ , and mass $\delta m_p = \rho \delta V_p$. Mass conservation requires that δm_p remains constant in time, $D\delta m_p/Dt = 0$. Expanding the material derivative, we obtain

$$\frac{D(\rho \delta V_p)}{Dt} = \delta V_p \frac{D\rho}{Dt} + \rho \frac{D\delta V_p}{Dt} = 0 \quad (2.8.6)$$

(Problem 2.8.1). Using the continuity equation (2.8.5) and rearranging, we find that

$$\frac{1}{\delta V_p} \frac{D\delta V_p}{Dt} = \nabla \cdot \mathbf{u}, \quad (2.8.7)$$

which reinforces our interpretation of the divergence of the velocity as the rate of volumetric expansion.

2.8.3 Point particle acceleration

The acceleration of a point particle, \mathbf{a} , is defined as the rate of change of the point particle velocity. Invoking the definition of the material derivative, we find that the x component of the acceleration is equal to the material derivative of the x component of the point particle velocity, which is equal to the local fluid velocity, $a_x = Du_x/Dt$. Similar arguments reveal that

$$a_x = \frac{Du_x}{Dt}, \quad a_y = \frac{Du_y}{Dt}, \quad a_z = \frac{Du_z}{Dt}. \quad (2.8.8)$$

In vector form,

$$\mathbf{a} = \frac{D\mathbf{u}}{Dt}. \quad (2.8.9)$$

Not surprisingly, the acceleration vector is the material derivative of the velocity vector.

Replacing ρ in equation (2.8.4) with u_x , u_y , or u_z , we find that the three Cartesian components of the point particle acceleration are given by

$$\begin{aligned} a_x &\equiv \frac{Du_x}{Dt} = \frac{\partial u_x}{\partial t} + \mathbf{u} \cdot \nabla u_x = \frac{\partial u_x}{\partial t} + u_x \frac{\partial u_x}{\partial x} + u_y \frac{\partial u_x}{\partial y} + u_z \frac{\partial u_x}{\partial z}, \\ a_y &\equiv \frac{Du_y}{Dt} = \frac{\partial u_y}{\partial t} + \mathbf{u} \cdot \nabla u_y = \frac{\partial u_y}{\partial t} + u_x \frac{\partial u_y}{\partial x} + u_y \frac{\partial u_y}{\partial y} + u_z \frac{\partial u_y}{\partial z}, \\ a_z &\equiv \frac{Du_z}{Dt} = \frac{\partial u_z}{\partial t} + \mathbf{u} \cdot \nabla u_z = \frac{\partial u_z}{\partial t} + u_x \frac{\partial u_z}{\partial x} + u_y \frac{\partial u_z}{\partial y} + u_z \frac{\partial u_z}{\partial z}. \end{aligned} \quad (2.8.10)$$

The three scalar equations (2.8.10) can be collected conveniently into a vector form,

$$\mathbf{a} \equiv \frac{D\mathbf{u}}{Dt} = \frac{\partial \mathbf{u}}{\partial t} + \mathbf{u} \cdot \mathbf{L} = \frac{\partial \mathbf{u}}{\partial t} + \mathbf{u} \cdot \nabla \mathbf{u}, \quad (2.8.11)$$

where $\mathbf{L} = \nabla \mathbf{u}$ is the velocity-gradient tensor defined in equation (2.1.16), with components $L_{ij} = \partial u_j / \partial x_i$. In index notation, the j th component of (2.8.11) takes the form

$$\frac{Du_j}{Dt} = \frac{\partial u_j}{\partial t} + u_i \frac{\partial u_j}{\partial x_i}, \quad (2.8.12)$$

where summation is implied over the repeated index i .

Linear momentum

The linear momentum of a small fluid parcel is the product of the mass of the parcel, $\delta m_p = \rho \delta V_p$, and the parcel velocity, \mathbf{u} . Requiring mass conservation, that is, demanding that δm_p remains constant in time, we find that the rate of change of the linear momentum can be expressed in terms of the point particle acceleration in the form

$$\frac{D(\delta m_p \mathbf{u})}{Dt} = \frac{D\mathbf{u}}{Dt} \rho \delta V_p = \frac{D\mathbf{u}}{Dt} \delta m_p. \quad (2.8.13)$$

Thus, the mass of an infinitesimal parcel can be extracted from the material derivative, just like a constant can be extracted from an ordinary derivative.

Cylindrical polar coordinates

In the cylindrical polar coordinates defined in [Figure 1.3.2](#), the point particle acceleration is expressed in terms of its cylindrical polar components, a_x , a_σ , and a_φ , as

$$\mathbf{a} = a_x \mathbf{e}_x + a_\sigma \mathbf{e}_\sigma + a_\varphi \mathbf{e}_\varphi. \quad (2.8.14)$$

Using the transformation rules shown in (1.3.20), we find that

$$a_\sigma = \cos \varphi a_y + \sin \varphi a_z, \quad a_\varphi = -\sin \varphi a_y + \cos \varphi a_z. \quad (2.8.15)$$

Substituting the right-hand sides of the second and third relations in (2.8.10) into the right-hand sides of the equations in (2.8.15), and then using the chain rule of differentiation to

convert derivatives with respect to x, y , and z to derivatives with respect to x, σ , and φ in the resulting equations as well as in the first equation in (2.8.10), we obtain

$$\begin{aligned} a_x &= \frac{\partial u_x}{\partial t} + u_x \frac{\partial u_x}{\partial x} + u_\sigma \frac{\partial u_x}{\partial \sigma} + \frac{u_\varphi}{\sigma} \frac{\partial u_x}{\partial \varphi}, \\ a_\sigma &= \frac{\partial u_\sigma}{\partial t} + u_x \frac{\partial u_\sigma}{\partial x} + u_\sigma \frac{\partial u_\sigma}{\partial \sigma} + \frac{u_\varphi}{\sigma} \frac{\partial u_\sigma}{\partial \varphi} - \frac{u_\varphi^2}{\sigma}, \\ a_\varphi &= \frac{\partial u_\varphi}{\partial t} + u_x \frac{\partial u_\varphi}{\partial x} + u_\sigma \frac{\partial u_\varphi}{\partial \sigma} + \frac{u_\varphi}{\sigma} \frac{\partial u_\varphi}{\partial \varphi} + \frac{u_\sigma u_\varphi}{\sigma}. \end{aligned} \quad (2.8.16)$$

Using the expression for the gradient of a function in cylindrical polar coordinates defined in equations (2.1.37) and (2.1.43), we recast expressions (2.8.16) into compact form involving the material derivative,

$$\begin{aligned} a_x &= \frac{\partial u_x}{\partial t} + \mathbf{u} \cdot \nabla u_x = \frac{Du_x}{Dt}, \\ a_\sigma &= \frac{\partial u_\sigma}{\partial t} + \mathbf{u} \cdot \nabla u_\sigma - \frac{u_\varphi^2}{\sigma} = \frac{Du_\sigma}{Dt} - \frac{u_\varphi^2}{\sigma}, \\ a_\varphi &= \frac{\partial u_\varphi}{\partial t} + \mathbf{u} \cdot \nabla u_\varphi + \frac{u_\sigma u_\varphi}{\sigma} = \frac{Du_\varphi}{Dt} + \frac{u_\sigma u_\varphi}{\sigma}. \end{aligned} \quad (2.8.17)$$

These expressions illustrate that the cylindrical polar components of the acceleration are *not* simply equal to the material derivative of the corresponding polar components of the velocity.

Spherical polar coordinates

In the spherical polar coordinates depicted in [Figure 1.3.3](#), the point particle acceleration is expressed in terms of its spherical polar components, a_r, a_θ , and a_φ , as

$$\mathbf{a} = a_r \mathbf{e}_r + a_\theta \mathbf{e}_\theta + a_\varphi \mathbf{e}_\varphi. \quad (2.8.18)$$

Working as previously for the cylindrical polar coordinates, we find the somewhat more involved expressions

$$\begin{aligned} a_r &= \frac{\partial u_r}{\partial t} + u_r \frac{\partial u_r}{\partial r} + \frac{u_\theta}{r} \frac{\partial u_r}{\partial \theta} + \frac{u_\varphi}{r \sin \theta} \frac{\partial u_r}{\partial \varphi} - \frac{u_\theta^2 + u_\varphi^2}{r}, \\ a_\theta &= \frac{\partial u_\theta}{\partial t} + u_r \frac{\partial u_\theta}{\partial r} + \frac{u_\theta}{r} \frac{\partial u_\theta}{\partial \theta} + \frac{u_\varphi}{r \sin \theta} \frac{\partial u_\theta}{\partial \varphi} + \frac{u_r u_\theta}{r} - \frac{u_\varphi^2 \cot \theta}{r}, \\ a_\varphi &= \frac{\partial u_\varphi}{\partial t} + u_r \frac{\partial u_\varphi}{\partial r} + \frac{u_\theta}{r} \frac{\partial u_\varphi}{\partial \theta} + \frac{u_\varphi}{r \sin \theta} \frac{\partial u_\varphi}{\partial \varphi} + \frac{u_r u_\varphi}{r} + \frac{u_\theta u_\varphi}{r} \cot \theta, \end{aligned} \quad (2.8.19)$$

which can be expressed in a more compact form involving the material derivative,

$$\begin{aligned} a_r &= \frac{Du_r}{Dt} - \frac{u_\theta^2 + u_\varphi^2}{r}, & a_\theta &= \frac{Du_\theta}{Dt} + \frac{u_r u_\theta}{r} - \frac{u_\varphi^2 \cot \theta}{r}, \\ a_\varphi &= \frac{Du_\varphi}{Dt} + \frac{u_r u_\varphi}{r} + \frac{u_\theta u_\varphi}{r} \cot \theta. \end{aligned} \quad (2.8.20)$$

These expressions illustrate that the spherical polar components of the acceleration are *not* simply equal to the material derivative of the corresponding polar components of the velocity.

Plane polar coordinates

In the system of plane polar coordinates depicted in [Figure 1.3.4](#), the point particle acceleration is expressed in terms of its plane polar components, a_r and a_θ , as

$$\mathbf{a} = a_r \mathbf{e}_r + a_\theta \mathbf{e}_\theta. \quad (2.8.21)$$

Working in the familiar way, we obtain

$$a_r = \frac{\partial u_r}{\partial t} + u_r \frac{\partial u_r}{\partial \theta} + \frac{u_\theta}{r} \frac{\partial u_r}{\partial \theta} - \frac{u_\theta^2}{r} = \frac{Du_r}{Dt} - \frac{u_\theta^2}{r}, \quad (2.8.22)$$

$$a_\theta = \frac{\partial u_\theta}{\partial t} + u_r \frac{\partial u_\theta}{\partial r} + \frac{u_\theta}{r} \frac{\partial u_\theta}{\partial \theta} + \frac{u_r u_\theta}{r} = \frac{Du_\theta}{Dt} + \frac{u_r u_\theta}{r}.$$

Note that these components are related to the σ and φ components in polar cylindrical coordinates.

Acceleration at a point with zero vorticity

If all components of the vorticity vector are zero at a certain point in a flow, the velocity gradient tensor is symmetric at that point. Consequently, selected partial derivatives of the velocity must be such that the three terms enclosed by the parentheses on the right-hand side of (2.3.8) are zero,

$$\frac{\partial u_z}{\partial y} = \frac{\partial u_y}{\partial z}, \quad \frac{\partial u_x}{\partial z} = \frac{\partial u_z}{\partial x}, \quad \frac{\partial u_y}{\partial x} = \frac{\partial u_x}{\partial y}. \quad (2.8.23)$$

The sum of the last three terms on the right-hand side of the first equation in (2.8.10) may then be written as

$$u_x \frac{\partial u_x}{\partial x} + u_y \frac{\partial u_y}{\partial x} + u_z \frac{\partial u_z}{\partial x} = \frac{1}{2} \frac{\partial u_x^2}{\partial x} + \frac{1}{2} \frac{\partial u_y^2}{\partial x} + \frac{1}{2} \frac{\partial u_z^2}{\partial x} = \frac{1}{2} \frac{\partial (u_x^2 + u_y^2 + u_z^2)}{\partial x}. \quad (2.8.24)$$

Working in a similar fashion with the y and z components, and collecting the derived expressions into a vector form, we obtain

$$\mathbf{u} \cdot \nabla \mathbf{u} = \frac{1}{2} \nabla u^2 = \left(\frac{\partial u^2}{\partial x}, \frac{\partial u^2}{\partial y}, \frac{\partial u^2}{\partial z} \right), \quad (2.8.25)$$

where

$$u^2 \equiv u_x^2 + u_y^2 + u_z^2 \quad (2.8.26)$$

is the square of the magnitude of the velocity, and ∇u^2 is its gradient. The point particle acceleration may thus be expressed in the alternative form

$$\mathbf{a} \equiv \frac{D\mathbf{u}}{Dt} = \frac{\partial \mathbf{u}}{\partial t} + \frac{1}{2} \nabla u^2. \quad (2.8.27)$$

The first term on the right-hand side of (2.8.27) is zero in a steady flow. The point particle acceleration is then equal to half the gradient of the square of the magnitude of the local velocity, which is a measure of the local kinetic energy of the fluid. We conclude that the acceleration is oriented in the direction of maximum change of kinetic energy indicated by the gradient.

In Chapter 6, we will see that the simplified expression (2.8.27) serves as a point of departure for the theoretical analysis and numerical computation of irrotational flows.

PROBLEMS

2.8.1 Properties of the material derivative

Consider two scalar physical or kinematic fluid properties, such as the density or a component of the velocity, denoted, respectively, by f and g . Prove that the following usual rule of product differentiation applies,

$$\frac{D(fg)}{Dt} = g \frac{Df}{Dt} + f \frac{Dg}{Dt}, \quad (2.8.28)$$

where D/Dt is the material derivative.

2.8.2 Point particle acceleration in rotational flow

Show that the counterpart of equation (2.8.25) at a point where the vorticity $\boldsymbol{\omega}$ is not necessarily zero is the inclusive equation

$$\mathbf{u} \cdot \nabla \mathbf{u} = \frac{1}{2} \nabla u^2 - \mathbf{u} \times \boldsymbol{\omega}, \quad (2.8.29)$$

where u the magnitude of the velocity. How does this expression simplify at a point where the velocity vector is parallel to the vorticity vector?

2.8.3 Point particle motion in one-dimensional flow

Consider an idealized one-dimensional flow along the x axis with velocity $u(x, t)$ satisfying the inviscid Burgers equation

$$\frac{\partial u}{\partial t} + u \frac{\partial u}{\partial x} = 0. \quad (2.8.30)$$

Explain why point particles in this flow travel with a time-independent velocity that is equal to the velocity assigned to them at the initial instant; different point particles may travel with different velocities.

2.9 Incompressible fluids and stream functions

If the volume of a fluid parcel is preserved as the parcel is convected in a flow, the fluid residing inside the parcel is incompressible. In contrast, if the volume of the parcel is allowed to change in time, the fluid residing inside the parcel is compressible.

Mass conservation requires that the mass of any fluid parcel is conserved irrespective of whether the fluid is compressible or incompressible.

Since both the mass and the volume of an arbitrary incompressible fluid parcel are conserved during the motion, the density of the point particles that comprise the parcel remain constant in time. Using the physical interpretation of the material derivative, D/Dt , we derive the mathematical statement of incompressibility,

$$\frac{D\rho}{Dt} = 0. \quad (2.9.1)$$

It is important to bear in mind that the density of an incompressible fluid is not necessarily uniform throughout the domain of flow. Different point particles may have different densities, but the density of each individual point particle is conserved during the motion.

2.9.1 Kinematic consequence of incompressibility

Using the incompressibility condition expressed by equation (2.9.1), we find that the continuity equation (2.8.5) for an incompressible fluid simplifies to

$$\nabla \cdot \mathbf{u} = 0, \quad (2.9.2)$$

which states that the velocity field should be *solenoidal*. By definition, the divergence of any solenoidal vector field is identically zero. Consequently, the rate of expansion α defined in equation (2.2.6) is identically zero. An incompressible fluid parcel may undergo translation, rotation, and isochoric (volume-preserving) deformation, but not expansion. The word *isochoric* is composed from the Greek words $\iota\sigma\omicron\varsigma$ which means equal, and the word $\chi\omega\rho\omicron\varsigma$ which means volume or space.

It is important to bear in mind that the stipulation (2.9.1) is the defining property of an incompressible fluid, while the simplified form of the continuity equation (2.9.2) is a consequence of mass conservation.

2.9.2 Mathematical consequence of incompressibility

Equation (2.9.2) states that the x , y , and z components of the velocity of an incompressible fluid may not be prescribed arbitrarily, but must be such that the differential constraint imposed on them by the requirement that the velocity field be solenoidal is satisfied throughout the domain of flow at any time. In contrast, the three components of the velocity of a compressible fluid may be arbitrary; the density of the point particles will then adjust to ensure mass conservation, as dictated by the continuity equation.

A second important consequence of incompressibility is that, because the evolution of the density is governed by the kinematic constraint (2.9.1), an equation of state relating the pressure to the density to the temperature is not needed. The important significance of this consequence will be discussed further in Chapters 4 and 8 in the context of hydrodynamics.

2.9.3 Stream function for two-dimensional flow

The continuity equation for a two-dimensional flow in the xy plane stated in (2.9.2) takes the form

$$\frac{\partial u_x}{\partial x} + \frac{\partial u_y}{\partial y} = 0. \quad (2.9.3)$$

In computing the velocity field of an incompressible fluid by analytical or numerical methods, it is convenient to satisfy this constraint at the outset and concentrate on satisfying boundary conditions and other constraints that arise by balancing forces and torques, as will be discussed in later chapters.

To achieve this, we may express the two velocity components in terms of a scalar function, ψ , called the stream function, as

$$u_x = \frac{\partial \psi}{\partial y}, \quad u_y = -\frac{\partial \psi}{\partial x}. \quad (2.9.4)$$

If the two velocity components, u_x and u_y derive from ψ by equations (2.9.4), then the satisfaction of the incompressibility constraint (2.9.3) is guaranteed. To confirm this, we substitute (2.9.4) into (2.9.3) and find that

$$\frac{\partial^2 \psi}{\partial x \partial y} - \frac{\partial^2 \psi}{\partial y \partial x} = 0. \quad (2.9.5)$$

Since the order of partial differentiation with respect to the two independent spatial variables x and y is immaterial, the equality is satisfied.

Extensional flow

As an example, we consider a two-dimensional flow with velocity components

$$u_x = \xi x, \quad u_y = -\xi y \quad (2.9.6)$$

describing an extensional flow, where ξ is a constant with units of inverse time. It can be verified readily that the continuity equation is fulfilled, $\nabla \cdot \mathbf{u} = 0$. Substituting these expressions into (2.9.3), we confirm that the fluid is incompressible. The stream function corresponding to this flow is given by

$$\psi = \xi xy + c, \quad (2.9.7)$$

where c is an unspecified and inconsequential constant.

Non-uniqueness of the stream function

The example discussed in the last section illustrates that the stream function of a specified two-dimensional flow is not unique. cursory inspection of equation (2.9.4) shows that an arbitrary constant may be added to a particular stream function to yield another perfectly acceptable stream function describing the same flow. However, this ambiguity is neither

essential nor alarming. In performing analytical or numerical computation, the arbitrary constant simply provides us with one degree of freedom that can be used to simplify numerical and algebraic manipulations.

Physical interpretation

Consider the areal flow rate, Q^{areal} , across a line that begins at a point, A, and ends at another point, B, as illustrated in [Figure 2.6.1](#). Substituting expressions (2.9.4) into the right-hand side of the last integral in (2.6.15) for the areal flow rate, we obtain

$$Q^{\text{areal}} = \int_A^B \left(\frac{\partial \psi}{\partial y} dy + \frac{\partial \psi}{\partial x} dx \right). \quad (2.9.8)$$

We may then write

$$Q^{\text{areal}} = \int_A^B d\psi = \psi_B - \psi_A, \quad (2.9.9)$$

where ψ_A and ψ_B are the values of the stream function at the end points, A and B.

Equation (2.9.9) shows that the difference in the values of the stream function between two points is equal to the areal flow rate across any arbitrary line that begins at the first point and ends at the second point. Because the fluid is incompressible, the flow rate is independent of the actual shape of the line, provided that the line begins and ends at two specified points.

Vorticity

The z component of the vorticity of a two-dimensional flow in the xy plane was given in equation (2.3.19) in terms of selected derivatives of the velocity,

$$\omega_z = \frac{\partial u_y}{\partial x} - \frac{\partial u_x}{\partial y}. \quad (2.9.10)$$

Substituting expressions (2.9.4), we find that

$$\omega_z = -\left(\frac{\partial^2 \psi}{\partial x^2} + \frac{\partial^2 \psi}{\partial y^2} \right) \equiv -\nabla^2 \psi, \quad (2.9.11)$$

where

$$\nabla^2 \equiv \frac{\partial^2}{\partial x^2} + \frac{\partial^2}{\partial y^2} \quad (2.9.12)$$

is the Laplacian operator in the xy plane, as discussed in Section 3.2. Thus, the z component of the vorticity is equal to the negative of the Laplacian of the stream function.

If the stream function satisfies Laplace's equation, $\nabla^2 \psi = 0$, the velocity field is solenoidal and the flow is irrotational. A function that satisfies Laplace's equation is called harmonic.

Plane polar coordinates

Departing from equations (2.9.4) and (2.3.19), and using the rules of coordinate transformation, we derive the velocity components of a two-dimensional flow in plane polar coordinates, (r, θ) , in terms of the stream function,

$$u_r = \frac{1}{r} \frac{\partial \psi}{\partial \theta}, \quad u_\theta = -\frac{\partial \psi}{\partial r}. \quad (2.9.13)$$

The vorticity is

$$\omega_z = -\frac{1}{r} \frac{\partial}{\partial r} \left(r \frac{\partial \psi}{\partial r} \right) - \frac{1}{r^2} \frac{\partial^2 \psi}{\partial \theta^2} \equiv -\nabla^2 \psi, \quad (2.9.14)$$

where

$$\nabla^2 \equiv \frac{\partial^2}{\partial x^2} + \frac{\partial^2}{\partial y^2} = \frac{1}{r} \frac{\partial}{\partial r} \left(r \frac{\partial}{\partial r} \right) + \frac{1}{r^2} \frac{\partial^2}{\partial \theta^2} \quad (2.9.15)$$

is the Laplacian operator in plane polar coordinates.

Expressions (2.9.13) satisfy the continuity equation in plane polar coordinates,

$$\frac{1}{r} \frac{\partial (r u_r)}{\partial r} + \frac{1}{r} \frac{\partial u_\theta}{\partial \theta} = 0 \quad (2.9.16)$$

for any differentiable and single valued stream function, ψ .

2.9.4 Stream function for axisymmetric flow

In the case of axisymmetric flow without swirling motion, we express all dependent and independent variables in the continuity equation, $\nabla \cdot \mathbf{u} = 0$, in cylindrical polar coordinates, (x, σ, φ) . After carrying out a fair amount of algebra using the chain rule, we find that the continuity equation takes the form of a constraint on the axial and radial velocity components, u_x and u_σ ,

$$\nabla \cdot \mathbf{u} = \frac{\partial u_x}{\partial x} + \frac{1}{\sigma} \frac{\partial (\sigma u_\sigma)}{\partial \sigma} = 0. \quad (2.9.17)$$

To ensure the satisfaction of this equation, we express the axial and radial components of the velocity in terms of an axisymmetric stream function, ψ , also called the Stokes stream function, defined by the equations

$$u_x = \frac{1}{\sigma} \frac{\partial \psi}{\partial \sigma}, \quad u_\sigma = -\frac{1}{\sigma} \frac{\partial \psi}{\partial x}. \quad (2.9.18)$$

Notice the minus sign in the second expression. Straightforward substitutions confirm that the velocity components given in (2.9.18) satisfy the continuity equation (2.9.17) for any regular stream function, ψ .

Extensional flow

As an example, we consider an axisymmetric flow with velocity components

$$u_x = \xi x, \quad u_\sigma = -\frac{1}{2} \xi \sigma, \quad (2.9.19)$$

representing an extensional flow, where ξ is a constant with units of inverse time. Substituting these expressions into (2.9.17), we confirm that the left-hand side vanishes and the fluid is incompressible. The corresponding stream function is given by

$$\psi = \frac{1}{2} \xi x \sigma^2 + c, \quad (2.9.20)$$

where c is an unspecified constant.

Physical interpretation

Working as in Section 2.9.3 for two-dimensional flow, we find that the volumetric flow rate across an axisymmetric surface whose trace in an azimuthal plane of constant angle φ starts at a point, A, and ends at another point, B, as illustrated in [Figure 2.6.6](#), is

$$Q = \psi_B - \psi_A \quad (2.9.21)$$

(Problem 2.9.2). This result is consistent with the units of the axisymmetric stream function, velocity multiplied by length squared, evident from equations (2.9.18). In contrast, the stream function for two-dimensional has units of velocity multiplied by length.

Vorticity

The azimuthal component of the vorticity in an axisymmetric flow was given in equation (2.3.22) in terms of derivatives of the cylindrical polar components of the velocity,

$$\omega_\varphi = \frac{\partial u_\sigma}{\partial x} - \frac{\partial u_x}{\partial \sigma}. \quad (2.9.22)$$

Substituting expressions (2.9.18), we obtain

$$\omega_\varphi = -\frac{1}{\sigma} \mathcal{E}^2 \psi = -\frac{1}{\sigma} \left(\frac{\partial^2 \psi}{\partial x^2} + \frac{\partial^2 \psi}{\partial \sigma^2} - \frac{1}{\sigma} \frac{\partial \psi}{\partial \sigma} \right), \quad (2.9.23)$$

where \mathcal{E}^2 is a second-order linear differential operator defined as

$$\mathcal{E}^2 \equiv \frac{\partial^2}{\partial x^2} + \frac{\partial^2}{\partial \sigma^2} - \frac{1}{\sigma} \frac{\partial}{\partial \sigma}. \quad (2.9.24)$$

If the stream function is such that the right-hand side of (2.9.23) is zero throughout the domain of flow, the flow is irrotational.

Spherical polar coordinates

Departing from equations (2.9.18) and (2.3.22), and using the rules of coordinate transformation, we derive the velocity components in spherical polar coordinates, (r, θ, φ) ,

$$u_r = \frac{1}{r^2 \sin \theta} \frac{\partial \psi}{\partial \theta}, \quad u_\theta = -\frac{1}{r \sin \theta} \frac{\partial \psi}{\partial r}. \quad (2.9.25)$$

The azimuthal component of the vorticity is given by

$$\omega_\varphi = -\frac{1}{r \sin \theta} \mathcal{E}^2 \psi, \quad (2.9.26)$$

where \mathcal{E}^2 is the second-order differential operator defined in (2.9.24). In spherical polar coordinates,

$$\mathcal{E}^2 \equiv \frac{\partial^2}{\partial r^2} + \frac{\sin \theta}{r^2} \frac{\partial}{\partial \theta} \left(\frac{1}{\sin \theta} \frac{\partial}{\partial \theta} \right) = \frac{\partial^2}{\partial r^2} + \frac{1}{r^2} \frac{\partial^2}{\partial \theta^2} - \frac{\cot \theta}{r^2} \frac{\partial}{\partial \theta}. \quad (2.9.27)$$

If the stream function is such that the right-hand side of (2.9.26) is zero throughout the domain of flow, the flow is irrotational.

PROBLEMS

2.9.1 Stream function for two-dimensional flow

Derive the Cartesian components of the velocity and the z vorticity component of a two-dimensional flow whose stream function is (a) $\psi = \frac{1}{2} \xi y^2$ or (b) $\psi = \frac{1}{2} \xi (x^2 - y^2)$, where ξ is a constant. Deduce the units of ξ and discuss the nature of each flow.

2.9.2 Stream function of axisymmetric flow

Substitute expressions (2.9.18) into the right-hand side of (2.6.38) and perform the integration to confirm (2.9.21).

2.10 Kinematic conditions at boundaries

In real life, a flow occurs in a domain that is bounded by stationary or moving surfaces with different constitutions and physical properties. Examples include the flow in an internal combustion engine generated by the motion of an engine piston, the flow induced by the motion of an aircraft or ground vehicle, the flow induced by the sedimentation of an aerosol particle in the atmosphere, the flow induced by a small bubble rising in a carbonated beverage, and the flow induced by the motion of an elephant running through the Savannah to escape a mouse.

Types of boundary conditions

In the context of kinematics, boundaries are classified into the following four main categories:

1. *Impermeable solid boundaries*: examples include the surface of a rigid or flexible solid body, such as a vibrating radio antenna or a swimming microorganism.
2. *Permeable solid boundaries*: examples include the surface of a porous medium, such as a rock bed or a biological tissue composed of cells separated by gaps in the intervening spaces.
3. *Sharp interfaces between immiscible fluids*: examples include the free surface of the ocean and the interface between oil and vinegar in an Italian salad dressing.
4. *Diffuse interfaces between miscible fluids*: examples include the fuzzy edge of a river discharging into the ocean and the ambiguous edge of a smoke ring rising in still air.

Different boundary conditions are imposed on each of these surfaces according to the prevailing physical context.

2.10.1 The no-penetration boundary condition

By definition, a point particle moving with the fluid velocity may not cross an impermeable solid boundary or a sharp interface between two immiscible fluids, but is required to lie on one side of the boundary or interface at all times. As a consequence, the velocity of a point particle that lies at a stationary or moving impermeable boundary or sharp interface must be consistent with, but not necessarily equal to, the velocity of the boundary or interface. To ensure compatibility, the no-penetration boundary condition is required.

Impermeable solid boundaries

Consider a flow that is bounded by an impermeable solid, but not necessarily rigid, boundary (rubber is a non-rigid, elastic yet solid boundary.) The no-penetration boundary condition requires that the component of the fluid velocity normal to the boundary is equal to the component of the boundary velocity normal to its instantaneous shape. The tangential component of the velocity is left unspecified. If the boundary is stationary, the normal component of the fluid velocity must vanish.

To derive the mathematical statement of the no-penetration condition, we introduce the unit vector normal to the boundary at a point, \mathbf{n} , and the velocity of the boundary, \mathbf{v}^B , where the orientation of \mathbf{n} is left unspecified. If the boundary is stationary, the boundary velocity is zero, $\mathbf{v}^B = \mathbf{0}$; if the boundary translates as a rigid body, \mathbf{v}^B is constant; if the boundary rotates as a rigid body or exhibits some type of deformation, \mathbf{v}^B is a function of position, as will be discussed later in this section.

In all cases, the no-penetration boundary condition requires that

$$\mathbf{u} \cdot \mathbf{n} = \mathbf{v}^B \cdot \mathbf{n}, \quad (2.10.1)$$

where both sides are evaluated at a point on the boundary.

Rigid-body motion

Consider an impermeable rigid boundary that translates with velocity \mathbf{U}^B while rotating with angular velocity $\boldsymbol{\Omega}^B$ around a specified center of rotation, \mathbf{x}_R . The angular velocity vector, $\boldsymbol{\Omega}^B$, passes through the center of rotation, \mathbf{x}_R . The magnitude and orientation of $\boldsymbol{\Omega}^B$ express the rate of direction and direction of rotation. As we look down at the angular velocity vector from above, the body rotates in the counterclockwise direction.

In terms of the velocity of translation and angular velocity of rotation, the velocity at a point \mathbf{x} that lies at the boundary is given by the expression

$$\mathbf{v}^B = \mathbf{U}^B + \boldsymbol{\Omega}^B \times (\mathbf{x} - \mathbf{x}_R), \quad (2.10.2)$$

where \times denotes the outer vector product defined in equation (2.3.5). In component form,

$$\begin{aligned} \mathbf{v}^B = & [U_x^B + \Omega_y^B (z - z_R) - \Omega_z^B (y - y_R)] \mathbf{e}_x \\ & + [U_y^B + \Omega_z^B (x - x_R) - \Omega_x^B (z - z_R)] \mathbf{e}_y \\ & + [U_z^B + \Omega_x^B (y - y_R) - \Omega_y^B (x - x_R)] \mathbf{e}_z, \end{aligned} \quad (2.10.3)$$

where \mathbf{e}_x , \mathbf{e}_y , and \mathbf{e}_z are unit vectors along the x , y , or z axes.

In the case of two-dimensional flow in the xy plane, the z velocity component is zero, $U_z^B = 0$, and the angular velocity vector is parallel to the z axis, $\Omega_x^B = 0$ and $\Omega_y^B = 0$, yielding the simplified form

$$\mathbf{v}^B = [U_x^B - \Omega_z^B (y - y_R)] \mathbf{e}_x + [U_y^B + \Omega_z^B (x - x_R)] \mathbf{e}_y, \quad (2.10.4)$$

which is linear in x and y .

The no-penetration boundary condition arises by substituting expression (2.10.3) or (2.10.4) into the right-hand side of (2.10.1), respectively, for three-dimensional or two-dimensional flow. If the boundary is stationary, $\mathbf{v}^B = \mathbf{0}$, we obtain the simple form

$$\mathbf{u} \cdot \mathbf{n} = 0, \quad (2.10.5)$$

where the direction of the unit normal vector, \mathbf{n} , is unspecified.

The no-penetration condition in terms of the stream function

Next, we consider an incompressible fluid in a two-dimensional flow and express the velocity in terms of the stream function, ψ , defined in equations (2.9.4). The no-penetration boundary condition (2.10.1) requires that

$$\mathbf{u} \cdot \mathbf{n} = u_x n_x + u_y n_y = \frac{\partial \psi}{\partial y} n_x - \frac{\partial \psi}{\partial x} n_y = \mathbf{v}^B \cdot \mathbf{n}. \quad (2.10.6)$$

Substituting expressions (2.6.4) for the components of the normal vector in terms of differential displacements along the boundary, we obtain

$$\frac{\partial \psi}{\partial y} \frac{dy}{d\ell} + \frac{\partial \psi}{\partial x} \frac{dx}{d\ell} = \frac{d\psi}{d\ell} = \mathbf{v}^B \cdot \mathbf{n}, \quad (2.10.7)$$

where $d\ell$ is an infinitesimal arc length measured along the boundary from an arbitrary origin.

If the boundary is stationary, the right-hand side of (2.1.8) is zero, $d\psi/d\ell = 0$, and the stream function is constant over the boundary. The no-penetration boundary condition takes the simple form

$$\psi = \psi_0, \quad (2.10.8)$$

where the constant ψ_0 is either assigned arbitrarily or computed as part of the solution.

Similar arguments can be made to show that the stream function is constant over an impermeable stationary boundary in axisymmetric flow (Problem 2.10.2(b)).

Sharp interfaces

Next, we consider the no-penetration condition over a stationary or moving sharp interface separating two immiscible fluids. Physical arguments suggest that the normal component of the fluid velocity on one side of the interface must be equal to the normal component of the velocity on the other side of the interface. However, the tangential velocities may be different.

To derive the mathematical statement of the no-slip condition, we introduce the velocity on one side of the interface, denoted by $\mathbf{u}^{(1)}$, and the velocity on the other side of the interface, denoted by $\mathbf{u}^{(2)}$, and require that

$$\mathbf{u}^{(1)} \cdot \mathbf{n} = \mathbf{u}^{(2)} \cdot \mathbf{n}, \quad (2.10.9)$$

where \mathbf{n} is the unit vector normal to the interface. Both sides are evaluated at a point at the interface with an unspecified direction of the unit normal vector, \mathbf{n} .

PROBLEMS

2.10.1 Changing the center of rotation

The center of rotation of a rigid body can be placed at any arbitrary position. Suppose that we choose a point, \mathbf{x}'_R , instead of the point \mathbf{x}_R discussed in the text. The counterpart of equation (2.10.2) is

$$\mathbf{v}^B = \mathbf{U}^{B'} + \boldsymbol{\Omega}^{B'} \times (\mathbf{x} - \mathbf{x}'_R). \quad (2.10.10)$$

Set the right-hand side of (2.10.10) equal to the right-hand side of (2.10.2) to derive expressions for $\mathbf{U}^{B'}$ and $\boldsymbol{\Omega}^{B'}$ in terms of \mathbf{U}^B and $\boldsymbol{\Omega}^B$, and *vice versa*.

2.10.2 Stream functions

(a) Use the no-penetration boundary condition to derive an expression for the stream function over a translating but non-rotating impermeable boundary in two-dimensional flow.

(b) Show that the no-penetration condition over a stationary boundary in axisymmetric flow takes the form expressed by (2.10.8).

Flow computation based on kinematics

- 3.1 Flow classification based on kinematics**
- 3.2 Irrotational flow and the velocity potential**
- 3.3 Finite-difference methods**
- 3.4 Linear solvers**
- 3.5 Two-dimensional point sources and point-source dipoles**
- 3.6 Three-dimensional point sources and point-source dipoles**
- 3.7 Point vortices and line vortices**

Flows can be classified according to the vorticity distribution as *irrotational flows* if the vorticity vanishes or is nearly zero throughout the domain of flow, *vortex flows* dominated by the presence of compact regions of concentrated vorticity embedded in an otherwise irrotational fluid, and *rotational flows* if the vorticity is significant throughout the domain of flow. In this chapter, we discuss the kinematic structure and mathematical description of the simplest and most tractable class of irrotational flows.

Following the mathematical analysis, we will develop finite-difference methods for computing the velocity field from knowledge of the velocity distribution at the boundaries, and then present a class of elementary irrotational flows that serve as fundamental building blocks for generating desired solutions. Complementary building blocks associated with elementary vortex flows provide us with additional elementary units that allow us to address a broader class of irrotational flows where the fluid exhibits circulatory motion.

3.1 Flow classification based on kinematics

In Chapters 1 and 2, we discussed the general kinematic properties of a flow with reference to the motion of fluid parcels and infinitesimal point particles. To make further progress, we establish a taxonomy by classifying flows according to sensible criteria. Examples of possible classifications include internal and external flows, inviscid and viscous flows, subsonic and supersonic flows.

On the basis of kinematics alone, flows can be classified into three main categories, including irrotational flows, flows containing compact regions of intense vorticity embedded in an otherwise perfectly or nearly irrotational fluid, and rotational flows with distributed vorticity.

Irrotational flows

The first category includes flows where the vorticity vector vanishes, and the magnitude of the vorticity is zero throughout the domain of flow. According to our discussion in Chapter 2, small spherical fluid parcels in a three-dimensional irrotational flow and discoidal fluid parcels in a two-dimensional irrotational flow translate, deform, and expand or contract, but do not rotate.

A perfectly irrotational flow is a mathematical idealization. In practice, because a small amount of vorticity is always present, a nominally irrotational flow is nearly but not perfectly irrotational. An example is high-speed flow past a slender airfoil under conditions of no-stall, as will be discussed in Chapter 12 in the context of aerodynamics.

Vortex flows

The second category includes flows that contain well-defined compact regions where the magnitude of the vorticity is significant, embedded in an otherwise irrotational fluid. The vortical flow regions cannot be neglected without introducing serious discrepancies and compromising the physics of the flow under consideration. In practice, regions of intense vorticity appear in the form of narrow layers, thin filaments, wakes behind bluff bodies, tornadoes and swirls. A vortex flow familiar to the aircraft traveler is the flow associated with a high-speed jet emerging from a turbine engine.

Rotational flows

The third category includes flows where the vorticity is significant throughout the domain of flow. The distinction between vortex flows and rotational flows is somewhat vague, as some flows can be classified into both categories. However, we will see that vortex flows can be analyzed and computed using a special class of numerical methods, called vortex methods. The availability of these methods provides us with a practical criterion for the distinction between vortex and rotational flows.

Flows in nature and technology

The vast majority of flows in nature and technology are rotational. Examples include the flow due to a small particle settling in the atmosphere, the flow through the engine of a turbine, and blood flow in the heart and through large blood vessels and small capillaries. High-speed flows develop regions of concentrated vorticity and are typically classified as vortex flows. High-speed turbulent flows contain random collections of rapidly evolving vortices, called eddies or coherent structures, embedded in a low- or moderate-vorticity background fluid.

Irrotational flows are simplified models of vortex flows that emerge by neglecting the regions of concentrated vorticity, or else by shifting the actual boundaries of the flow to the edges of the vortex regions, thereby placing them outside the domain of flow.

Considerable physical insight and practical experience are necessary to accurately predict whether a flow will develop to become irrotational, rotational, or vortex flow. Insights can be gained by studying model flows that are amenable to analytical and simple numerical methods. Additional insights can be gained by analyzing the laws governing the generation and evolution of the vorticity field from a given initial state.

Flow computation

The difficulty of computing the structure or evolution of a flow increases sharply as we transition from irrotational flows, to vortex flows, to rotational flows. Exceptions to this general rule arise in special cases. Our discussion of analytical and computational methods for flow computation begins in this chapter by considering the most amenable class of irrotational flows. In the context of kinematics alone, the problem can be stated as follows: given the boundary geometry and the velocity distribution over the boundaries, compute the structure of a steady irrotational flow or the evolution of an unsteady irrotational flow from a specified initial state.

PROBLEM

3.1.1 Flow classification

Suggest a possible way of classifying flows according to sensible criteria apart from the those discussed in the text.

3.2 Irrotational flow and the velocity potential

The vorticity of a three-dimensional flow was defined in equation (2.3.8) as the curl of the velocity,

$$\boldsymbol{\omega} \equiv \nabla \times \mathbf{u}. \quad (3.2.1)$$

The z component of the vorticity of a two-dimensional flow in the xy plane was given in equation (2.3.19) as

$$\omega_z = \frac{\partial u_y}{\partial x} - \frac{\partial u_x}{\partial y}, \quad (3.2.2)$$

and the azimuthal component of the vorticity of an axisymmetric flow was given in equation (2.3.22) as

$$\omega_\varphi = \frac{\partial u_\sigma}{\partial x} - \frac{\partial u_x}{\partial \sigma} = \frac{1}{r} \left(\frac{\partial(ru_\theta)}{\partial r} - \frac{\partial u_r}{\partial \theta} \right). \quad (3.2.3)$$

If a flow is irrotational, the structure of the velocity field must be such that the right-hand sides of these equations are zero.

3.2.1 Two-dimensional flow

Consider a two-dimensional irrotational flow in the xy plane. Setting the left-hand side of equation (3.2.2) to zero, we obtain a constraint on selected partial derivatives of the velocity,

$$\frac{\partial u_y}{\partial x} = \frac{\partial u_x}{\partial y}. \quad (3.2.4)$$

To describe a two-dimensional irrotational flow, we may attempt to compute the two velocity components individually, subject to constraints imposed by the continuity equation and boundary conditions, while ensuring that condition (3.2.4) is fulfilled at every point in the flow. Alternatively, we may choose to satisfy condition (3.2.4) at the outset and then concentrate on fulfilling the rest of the requirements.

It should not be surprising that the second approach is more expedient in both theoretical analysis and numerical computation.

The velocity potential

The key idea is to introduce a new scalar function, ϕ , called the velocity potential, such that the two velocity components of a two-dimensional flow derive from the relations

$$u_x = \frac{\partial \phi}{\partial x}, \quad u_y = \frac{\partial \phi}{\partial y}. \quad (3.2.5)$$

In vector notation, equations (3.2.5) are collected into the compact form

$$\mathbf{u} = \nabla \phi, \quad (3.2.6)$$

where

$$\nabla \phi = \left(\frac{\partial \phi}{\partial x}, \quad \frac{\partial \phi}{\partial y} \right), \quad (3.2.7)$$

is the two-dimensional gradient of the potential. The velocity, and thus the velocity potential, ϕ , is a function of position, $\mathbf{x} = (x, y, z)$, and, in the case of unsteady flow, time, t . Inspection of (3.2.5) reveals that the velocity potential has units of velocity multiplied by length, which amounts to length squared divided by time.

It is a straightforward exercise to confirm that, if the velocity components derive from ϕ in terms of equations (3.2.5), then the irrotationality constraint (3.2.4) is automatically satisfied. Substituting expressions (3.2.5) into (3.2.4), we obtain

$$\frac{\partial^2 \phi}{\partial x \partial y} = \frac{\partial^2 \phi}{\partial y \partial x}. \quad (3.2.8)$$

Since the order of partial differentiation with respect to the two independent spatial variables, x and y , can be interchanged, relation (3.2.4) is satisfied. Accordingly, an irrotational flow is also a potential flow, and *vice versa*.

The velocity potential of a certain irrotational flow is not unique. An arbitrary constant can be added to a particular potential to produce another perfectly acceptable potential. However, this ambiguity is neither essential nor alarming. In performing analytical or numerical computation, the arbitrary constant is determined by introducing a proper constraint.

Deriving the potential

Given the velocity field of an irrotational flow, we can derive the corresponding potential by integrating the system of differential equations (3.2.5), where the left-hand sides are treated as a known.

As an example, we consider two-dimensional unidirectional streaming (uniform) flow with velocity components

$$u_x = U_x, \quad u_y = U_y, \quad (3.2.9)$$

where U_x and U_y are two constant velocities. Integrating the first equation in (3.2.5), we find that the potential must take the form

$$\phi = U_x x + f(y), \quad (3.2.10)$$

where $f(y)$ is an unknown function of y . Differentiating both sides of this equation with respect to y and using the second equation in (3.2.5), we find that $df/dy = U_y$, which can be integrated to give $f(y) = U_y y + c$, where c is an arbitrary constant. Combining these expressions, we find that the velocity potential corresponding to (3.2.9) is

$$\phi = U_x x + U_y y + c = \mathbf{U} \cdot \mathbf{x} + c. \quad (3.2.11)$$

In agreement with our previous observation, the velocity potential is defined uniquely up to an arbitrary constant, c .

Computation of the potential based on kinematics

The automatic satisfaction of the irrotationality constraint (3.2.4) by way of the velocity potential is helpful, but we still require one equation, or a system of equations, that will allow us to compute the potential. Normally, these equations would have to be derived by considering forces and torques exerted on the surfaces and over the volume of small fluid parcels, as will be discussed in subsequent chapters with reference to the more general class of rotational flows. Fortunately, this is not necessary in the case of irrotational flow. Given the boundary distribution of the velocity, an irrotational flow can be computed in the framework of kinematics alone pivoted on the continuity equation.

3.2.2 Incompressible fluids and the harmonic potential

Mass conservation requires that the velocity field of an incompressible fluid is solenoidal, which means that the velocity components must satisfy the constraint expressed by the continuity equation (2.9.2),

$$\nabla \cdot \mathbf{u} = 0. \quad (3.2.12)$$

In the case of two-dimensional flow, we obtain

$$\frac{\partial u_x}{\partial x} + \frac{\partial u_y}{\partial y} = 0. \quad (3.2.13)$$

Substituting expressions (3.2.5) into (3.2.12), we obtain Laplace's equation in two dimensions,

$$\frac{\partial^2 \phi}{\partial x^2} + \frac{\partial^2 \phi}{\partial y^2} = 0. \quad (3.2.14)$$

It is convenient to define the two-dimensional Laplacian operator,

$$\nabla^2 \equiv \frac{\partial^2}{\partial x^2} + \frac{\partial^2}{\partial y^2}, \quad (3.2.15)$$

and recast (3.2.14) into the more compact form

$$\nabla^2 \phi = 0. \quad (3.2.16)$$

A function that satisfies Laplace's equation (3.2.16) is called harmonic.

It is instructive to derive Laplace's equation working in vector notation. Substituting (3.2.6) into (3.2.12), we find that

$$\nabla \cdot \mathbf{u} = \nabla \cdot (\nabla \phi) \equiv \nabla^2 \phi = 0, \quad (3.2.17)$$

which identifies the Laplacian operator with the divergence of the gradient,

$$\nabla^2 = \nabla \cdot \nabla, \quad (3.2.18)$$

regarded as a differential operator.

Laplace's equation arises in a broad range of contexts under and beyond the auspices of fluid mechanics. For example, Laplace's equation governs the distribution of temperature at steady state in a conductive material, such as a fin or a cooling plate.

Quasi-steady state

Laplace's equation (3.2.16) conveys a statement of mass conservation for an incompressible fluid. Although time does not appear explicitly in this equation, the velocity field, and thus the velocity potential, may change in time, so that $\phi(\mathbf{x}, t)$. The absence of explicit time dependence classifies an the irrotational flow of an incompressible fluid as a quasi-steady flow. This terminology implies that the instantaneous structure of the flow depends on the instantaneous boundary geometry and boundary conditions, but is independent of the motion at previous times. Thus, if all boundaries are stationary at a particular time instant, the fluid will also be stationary at that instant, independent of the history of the fluid and boundary motion.

3.2.3 Three-dimensional flow

The foregoing analysis can be extended in a straightforward fashion to three-dimensional flow. The velocity components of a three-dimensional flow derive from the velocity potential by the equations

$$u_x = \frac{\partial \phi}{\partial x}, \quad u_y = \frac{\partial \phi}{\partial y}, \quad u_z = \frac{\partial \phi}{\partial z}. \quad (3.2.19)$$

The velocity components, and thus the potential, ϕ , are functions of position $\mathbf{x} = (x, y, z)$ and time, t , in the case of unsteady flow.

If the fluid is incompressible, the velocity potential satisfies the counterpart of Laplace's equation (3.2.17) for three-dimensional flow,

$$\nabla \cdot \mathbf{u} = \nabla \cdot (\nabla \phi) \equiv \nabla^2 \phi \equiv \frac{\partial^2 \phi}{\partial x^2} + \frac{\partial^2 \phi}{\partial y^2} + \frac{\partial^2 \phi}{\partial z^2} = 0, \quad (3.2.20)$$

where

$$\nabla^2 \equiv \frac{\partial^2}{\partial x^2} + \frac{\partial^2}{\partial y^2} + \frac{\partial^2}{\partial z^2} \quad (3.2.21)$$

is the Laplacian operator in three dimensions.

3.2.4 Boundary conditions

Laplace's equation for the velocity potential, ϕ , in two or three dimensions is a second-order, elliptic partial differential equation. One consequence of this classification is that, in order to compute the solution, we must specify one scalar boundary condition for ϕ , one of its first partial derivatives, or a combination thereof, along each boundary.

Impermeable boundaries

Over an impermeable boundary, we require the no-penetration condition discussed in Section 2.10. If the boundary is stationary, $\mathbf{u} \cdot \mathbf{n} = 0$, where \mathbf{n} is the unit vector normal to the boundary pointing either into or outward from the domain of flow. Using equations (3.2.5), we find that

$$n_x \frac{\partial \phi}{\partial x} + n_y \frac{\partial \phi}{\partial y} = 0. \quad (3.2.22)$$

in the case of two-dimensional flow. This is truly a boundary condition for the normal component of the gradient of the potential, which is equal to the derivative with respect to distance normal to the boundary, called a *Neumann boundary condition*. Because the right-hand side of (3.2.22) is zero, this boundary condition is classified as homogeneous.

Permeable boundaries

Over a permeable boundary, we may specify the tangential component of the velocity and allow the normal component to arise as part of the solution. To implement this condition in

the case of two-dimensional flow, we introduce the unit vector tangential to the boundary, \mathbf{t} , defined in equations (2.6.3). The tangential component of the velocity in the direction of \mathbf{t} is given by the inner product

$$u_t \equiv \mathbf{u} \cdot \mathbf{t} = t_x \frac{\partial \phi}{\partial x} + t_y \frac{\partial \phi}{\partial y} = \frac{dx}{d\ell} \frac{\partial \phi}{\partial x} + \frac{dy}{d\ell} \frac{\partial \phi}{\partial y} = \frac{d\phi}{d\ell}, \quad (3.2.23)$$

where ℓ is the arc length measured in the direction of \mathbf{t} . If the distribution of ϕ over the boundary is known, the right-hand side of (3.2.23) can be computed by differentiating the potential with respect to arc length using analytical or numerical methods.

The last observation suggests that, instead of specifying the tangential component of the velocity, we may specify the boundary distribution of the potential. A boundary condition for the distribution of the potential is a *Dirichlet boundary condition*.

A word of caution is in order. If a flow is bounded by a number of disconnected boundaries, replacing the boundary condition for the tangential velocity with a boundary condition for the distribution of the potential is permissible only over one boundary; otherwise, inconsistencies may arise.

3.2.5 Cylindrical polar coordinates

Consider a three-dimensional irrotational flow and introduce cylindrical polar coordinates, (x, σ, φ) , as shown in Figure 1.3.2. Using expressions (2.1.43), we find that the cylindrical polar components of the velocity are given by

$$u_x = \frac{\partial \phi}{\partial x}, \quad u_\sigma = \frac{\partial \phi}{\partial \sigma}, \quad u_\varphi = \frac{1}{\sigma} \frac{\partial \phi}{\partial \varphi}. \quad (3.2.24)$$

Laplace's equation for the harmonic potential takes the form

$$\nabla^2 \phi \equiv \frac{\partial^2 \phi}{\partial x^2} + \frac{1}{\sigma} \frac{\partial}{\partial \sigma} \left(\sigma \frac{\partial \phi}{\partial \sigma} \right) + \frac{1}{\sigma^2} \frac{\partial^2 \phi}{\partial \varphi^2} = 0. \quad (3.2.25)$$

If a flow is axisymmetric, the velocity potential is a function of x and σ but not φ , as required for u_φ to vanish.

3.2.6 Spherical polar coordinates

Consider a three-dimensional irrotational flow and introduce spherical polar coordinates, (r, θ, φ) , as shown in Figure 1.3.3. Using relations (2.1.45), we find that the spherical polar components of the velocity are given by

$$u_r = \frac{\partial \phi}{\partial r}, \quad u_\theta = \frac{1}{r} \frac{\partial \phi}{\partial \theta}, \quad u_\varphi = \frac{1}{r \sin \theta} \frac{\partial \phi}{\partial \varphi}. \quad (3.2.26)$$

Laplace's equation for the harmonic potential takes the form

$$\nabla^2 \phi \equiv \frac{1}{r^2} \frac{\partial}{\partial r} \left(r^2 \frac{\partial \phi}{\partial r} \right) + \frac{1}{r^2 \sin \theta} \frac{\partial}{\partial \theta} \left(\sin \theta \frac{\partial \phi}{\partial \theta} \right) + \frac{1}{r^2 \sin^2 \theta} \frac{\partial^2 \phi}{\partial \varphi^2} = 0. \quad (3.2.27)$$

If a flow is axisymmetric, the velocity potential is a function of r and θ but not φ , as required for u_φ to vanish.

3.2.7 Plane polar coordinates

Consider a two-dimensional irrotational flow and introduce plane polar coordinates, (r, θ) , as shown in [Figure 1.3.4](#). Using relations (2.1.47), we find that the plane polar components of the velocity are

$$u_r = \frac{\partial \phi}{\partial r}, \quad u_\theta = \frac{1}{r} \frac{\partial \phi}{\partial \theta}. \quad (3.2.28)$$

Laplace's equation for the harmonic potential takes the form

$$\nabla^2 \phi \equiv \frac{1}{r} \frac{\partial}{\partial r} \left(r \frac{\partial \phi}{\partial r} \right) + \frac{1}{r^2} \frac{\partial^2 \phi}{\partial \theta^2} = 0. \quad (3.2.29)$$

Note that this equation derives from (3.2.25) by replacing σ with r and φ with θ , and then discarding the x dependence.

PROBLEMS

3.2.1 Deriving the velocity potential

(a) Consider a two-dimensional flow with velocity components

$$u_x = U \cos(kx) e^{-ky}, \quad u_y = -U \sin(kx) e^{-ky}, \quad (3.2.30)$$

where U and k are two constants. Confirm that this flow is irrotational, derive the corresponding velocity potential, investigate whether or not the potential is harmonic, and explain why. Sketch the streamline pattern and discuss the structure of the flow and the physical interpretation of the constant k .

(b) Consider a three-dimensional flow with velocity components

$$\begin{aligned} u_x &= U \frac{k_x}{k} \cos(k_x x) \sin(k_y y) e^{-kz}, & u_y &= U \frac{k_y}{k} \sin(k_x x) \cos(k_y y) e^{-kz}, \\ u_z &= -U \sin(k_x x) \sin(k_y y) e^{-kz}, \end{aligned} \quad (3.2.31)$$

where U , k_x , and k_y , are three constants and $k = (k_x^2 + k_y^2)^{1/2}$. This is the three-dimensional counterpart of the two-dimensional flow discussed in (a). Confirm that this flow is irrotational, derive the corresponding velocity potential, investigate whether or not the potential is harmonic, and explain why. Discuss the structure of the flow and the physical interpretation of the constants k_x and k_y .

(c) Explain why it is not possible to find a velocity potential for simple shear flow along the x axis varying along the y axis whose velocity components are given by $u_x = \xi y$, $u_y = 0$, and $u_z = 0$, where ξ is a constant with units of inverse time called the shear rate.

3.2.2 Irrotational flow in cylindrical polar coordinates

Verify by direct substitution that the potential

$$\phi = Ux \left(1 + \frac{1}{2} \frac{a^3}{(x^2 + \sigma^2)^{3/2}} \right) \quad (3.2.32)$$

satisfies Laplace's equation (3.2.25), where U and a are two constants. Discuss the structure of the axisymmetric flow described by this potential.

3.2.3 Irrotational flow in spherical polar coordinates

Verify by direct substitution that the potential

$$\phi = Ur \cos \theta \left(1 + \frac{1}{2} \frac{a^3}{r^3} \right) \quad (3.2.33)$$

satisfies Laplace's equation (3.2.27), where U and a are two constants. Discuss the structure of the axisymmetric flow described by this potential.

3.2.4 Irrotational flow in plane polar coordinates

Verify by direct substitution that the potential

$$\phi = Ur \cos \theta \left(1 + \frac{a^2}{r^2} \right) + \frac{\kappa}{2\pi} \theta, \quad (3.2.34)$$

satisfies Laplace's equation (3.2.29), where κ , U , and a are three constants. Discuss the structure of the two-dimensional flow described by this potential.

3.3 Finite-difference methods

In practice, Laplace's equation for a harmonic potential, ϕ , is solved by a variety of numerical methods. To illustrate the implementation of the finite-difference method, we consider a two-dimensional potential flow in the xy plane in a rectangular domain confined between two pairs of parallel straight lines,

$$a_x \leq x \leq b_x, \quad a_y \leq y \leq b_y, \quad (3.3.1)$$

as illustrated in [Figure 3.3.1](#). The left, bottom, and right walls are impermeable, whereas the top wall is exposed to an external flow.

3.3.1 Boundary conditions

Before attempting to compute the solution, we must specify boundary conditions for the scalar potential, ϕ .

Over the left wall, the unit vector normal to the wall pointing into the fluid is $\mathbf{n} = (1, 0)$. Accordingly, the no-penetration condition (3.2.22) provides us with the Neumann boundary condition

$$\frac{\partial \phi}{\partial x} = 0 \quad \text{at} \quad x = a_x. \quad (3.3.2)$$

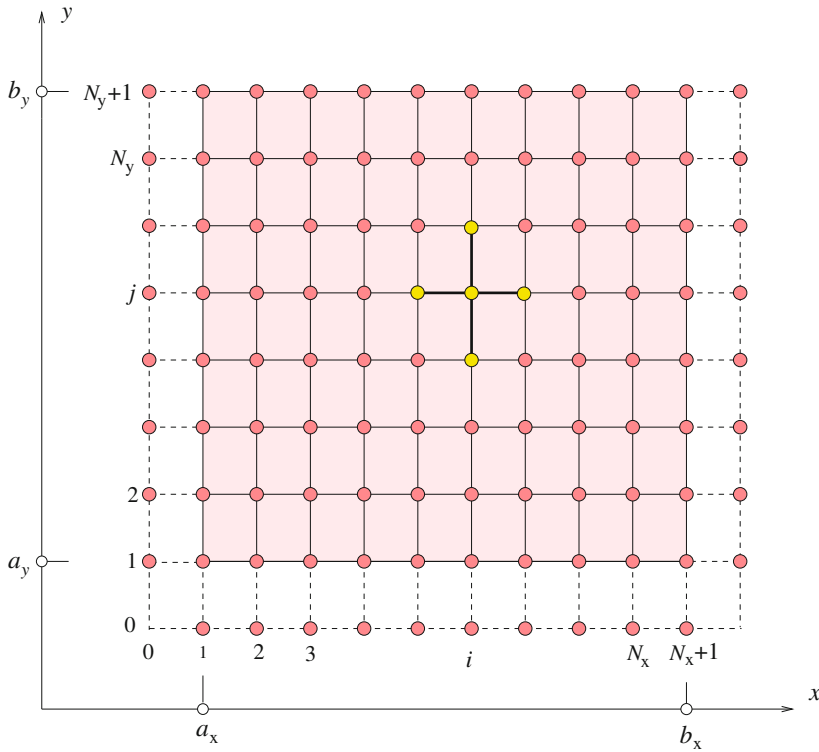


Figure 3.3.1 Illustration of a Cartesian grid used to compute the harmonic potential of a two-dimensional irrotational flow in a rectangular domain. The grid nodes are parametrized by two indices, i and j , where $i = 1, \dots, N_x + 1$ and $j = 1, \dots, N_y + 1$. Phantom grid lines are introduced at $i = 0$, $i = N_x + 2$, and $j = 0$, to implement the Neumann boundary conditions. The solution is found by solving Laplace's equation using a finite-difference method. The five-point stencil indicates the nodal pattern used to approximate the Laplacian at an interior node.

Over the bottom wall, the unit vector normal to the wall pointing into the flow is $\mathbf{n} = (0, 1)$. Accordingly, the no-penetration condition (3.2.22) provides us with the Neumann boundary condition

$$\frac{\partial \phi}{\partial y} = 0 \quad \text{at} \quad y = a_y. \tag{3.3.3}$$

Over the right wall, the unit vector normal to the wall pointing into the flow is $\mathbf{n} = (-1, 0)$. Accordingly, the no-penetration condition (3.2.22) provides us with the Neumann boundary condition

$$\frac{\partial \phi}{\partial x} = 0 \quad \text{at} \quad x = b_x. \tag{3.3.4}$$

Over the top wall, we stipulate for the purpose of illustration that the tangential component of the velocity is constant and equal to V . Other boundary conditions can be imposed to reflect different flow conditions. Since the top wall is parallel to the x axis, the unit tangent vector is $\mathbf{t} = (1, 0)$. Accordingly, expression (3.2.23) provides us with the boundary condition

$$u_t \equiv \mathbf{u} \cdot \mathbf{t} = \frac{\partial \phi}{\partial x} = V \quad \text{at} \quad y = b_y. \quad (3.3.5)$$

Straightforward integration of (3.3.5) with respect to x shows that this condition is equivalent to a Dirichlet boundary condition,

$$\phi = Vx + c \quad \text{at} \quad y = b_y. \quad (3.3.6)$$

The constant c can be assigned an arbitrary value that is inconsequential to the structure of the flow.

The problem formulation is now complete, and we may proceed to compute the solution. Our task is to solve Laplace's equation

$$\frac{\partial^2 \phi}{\partial x^2} + \frac{\partial^2 \phi}{\partial y^2} = 0, \quad (3.3.7)$$

subject to the four boundary conditions expressed by equations (3.3.2), (3.3.3), (3.3.4), and (3.3.6).

3.3.2 Finite-difference grid

We begin implementing the finite-difference method by dividing the x interval, $[a_x, b_x]$, into N_x evenly spaced sub-intervals separated by the spacing $\Delta x = (b_x - a_x)/N_x$, and draw vertical grid lines at

$$x_i = a_x + (i - 1) \Delta x \quad (3.3.8)$$

for $i = 1, \dots, N_x + 1$, as shown in [Figure 3.3.1](#).

Similarly, we divide the y interval, $[a_y, b_y]$, into N_y evenly spaced sub-intervals separated by the spacing $\Delta y = (b_y - a_y)/N_y$, and draw horizontal grid lines at

$$y_j = a_y + (j - 1) \Delta y \quad (3.3.9)$$

for $j = 1, \dots, N_y + 1$, as shown in [Figure 3.3.1](#).

The intersections of vertical and horizontal grid lines define grid points or nodes. For convenience, we denote the value of the harmonic potential ϕ at the (i, j) node as

$$\phi_{i,j} \equiv \phi(x_i, y_j) \quad (3.3.10)$$

for $i = 1, \dots, N_x + 1$ and $j = 1, \dots, N_y + 1$.

Dirichlet boundary condition

The Dirichlet boundary condition (3.3.6) provides us with the values

$$\phi_{i,N_y+1} = V x_i. \quad (3.3.11)$$

Without loss of generality, we have made the arbitrary choice $c = 0$. Our objective is to compute the remaining unknown values, $\phi_{i,j}$, at the grid points $i = 1, \dots, N_x + 1$ and $j = 1, \dots, N_y$, comprising a set of

$$N_u = (N_x + 1) N_y \quad (3.3.12)$$

unknowns.

3.3.3 Finite-difference discretization

To build a system of equations for the unknown grid values, we require the satisfaction of Laplace's equation (3.2.14) at the (i, j) node, and approximate the second partial derivatives with finite differences. Introducing the approximations implemented in formula (2.5.9), we write

$$\left(\frac{\partial^2 \phi}{\partial x^2}\right)_{i,j} \simeq \frac{\phi_{i-1,j} - 2\phi_{i,j} + \phi_{i+1,j}}{\Delta x^2} \quad (3.3.13)$$

and

$$\left(\frac{\partial^2 \phi}{\partial y^2}\right)_{i,j} \simeq \frac{\phi_{i,j-1} - 2\phi_{i,j} + \phi_{i,j+1}}{\Delta y^2}. \quad (3.3.14)$$

These approximations transform the differential equation (3.3.7) to an algebraic equation,

$$\frac{\phi_{i-1,j} - 2\phi_{i,j} + \phi_{i+1,j}}{\Delta x^2} + \frac{\phi_{i,j-1} - 2\phi_{i,j} + \phi_{i,j+1}}{\Delta y^2} = 0 \quad (3.3.15)$$

at the (i, j) node. Rearranging the left-hand side, we obtain

$$\phi_{i+1,j} - 2(1 + \beta)\phi_{i,j} + \phi_{i-1,j} + \beta\phi_{i,j+1} + \beta\phi_{i,j-1} = 0, \quad (3.3.16)$$

where

$$\beta \equiv (\Delta x / \Delta y)^2 \quad (3.3.17)$$

is the square of the grid spacing ratio. In the case of a square grid, $\beta = 1$.

Equation (3.3.15) and its equivalent equation (3.3.16) can be applied at the interior nodes, $i = 2, \dots, N_x$ and $j = 2, \dots, N_y$, to obtain a system of

$$N_{\text{fde interior}} = (N_x - 1)(N_y - 1) \quad (3.3.18)$$

difference equations. However, equation (3.3.15) cannot be applied at a boundary node, since one grid point involved in the finite-difference approximation will lie outside the domain of flow. We must somehow generate

$$N_u - N_{\text{fde interior}} = (N_x + 1)N_y - (N_x - 1)(N_y - 1) = N_x + 2N_y - 1 \quad (3.3.19)$$

additional equations.

Neumann boundary condition

The missing equations originate from the Neumann boundary condition at the left, bottom, and right walls where the no-penetration condition is prescribed. One way of implementing these boundary conditions with an error that is comparable to that of the finite-difference approximations (3.3.13) and (3.3.14), is to extend the domain of solution beyond the physical boundaries of the flow and introduce fictitious or phantom nodes located at

$$x = x_0 = a_x - \Delta x, \quad y = y_0 = a_y - \Delta y \quad (3.3.20)$$

at the left and bottom walls, and

$$x = x_{N_x+2} = b_x + \Delta x \quad (3.3.21)$$

at the right wall. Having introduced these extensions, we apply the second-order finite-difference approximation (2.5.6) to recast the Neumann boundary condition into the discrete form

$$\frac{\phi_{2,j} - \phi_{0,j}}{2\Delta x} = 0 \quad (3.3.22)$$

for $j = 1, \dots, N_y$, corresponding to the left wall,

$$\frac{\phi_{i,2} - \phi_{i,0}}{2\Delta y} = 0 \quad (3.3.23)$$

for $i = 1, \dots, N_x + 1$, corresponding to the bottom wall, and

$$\frac{\phi_{N_x+2,j} - \phi_{N_x,j}}{2\Delta x} = 0 \quad (3.3.24)$$

for $j = 1, \dots, N_y$, corresponding to the right wall.

Algebraic balance

To this end, we pause to confirm that the number of unknowns matches the number of available equations. First, we note that the difference equation (3.3.15) or (3.3.16) may now be applied at the interior and boundary nodes for $i = 1, \dots, N_x + 1$ and $j = 1, \dots, N_y$, to yield

$$N_{\text{fde}} = (N_x + 1)N_y \quad (3.3.25)$$

equations. Adding to these equations the

$$N_{bc} = N_x + 2N_y + 1 \quad (3.3.26)$$

boundary conditions expressed by (3.3.22), (3.3.23), and (3.3.24), we obtain

$$N_{eq} = (N_x + 1)(N_y + 1) + 2N_y \quad (3.3.27)$$

equations. The total number of equations matches the number of unknowns, including the values of ϕ at the $(N_x + 1)N_y$ interior and boundary nodes and the values of ϕ at the $2N_y + N_x + 1$ phantom nodes marked with circular symbols in [Figure 3.3.1](#).

3.3.4 Compilation of a linear system

To formalize the method, we collect the interior and boundary unknowns into a long vector, \mathbf{w} , consisting of row-blocks, beginning from the bottom,

$$\begin{aligned} \mathbf{w} = [& \phi_{1,1}, \phi_{2,1}, \dots, \phi_{N_x+1,1}, \\ & \phi_{1,2}, \phi_{2,2}, \dots, \phi_{N_x+1,2}, \\ & \dots, \\ & \phi_{1,N_y-1}, \phi_{2,N_y-1}, \dots, \phi_{N_x+1,N_y-1}, \\ & \phi_{1,N_y}, \phi_{2,N_y}, \dots, \phi_{N_x+1,N_y}] \end{aligned} \quad (3.3.28)$$

Next, we apply the finite-difference equation (3.3.16) successively at boundary and interior nodes. Without loss of generality, we scan the grid points row-by-row starting from the bottom; a column-by-column compilation would also be acceptable.

Southwestern corner node

For the southwestern corner node $(1, 1)$, we obtain the finite-difference equation

$$\phi_{2,1} - 2(1 + \beta)\phi_{1,1} + \phi_{0,1} + \beta\phi_{1,2} + \beta\phi_{1,0} = 0. \quad (3.3.29)$$

Boundary condition (3.3.22) for $j = 1$ requires that $\phi_{2,1} = \phi_{0,1}$, and boundary condition (3.3.21) for $j = 1$ requires that $\phi_{1,2} = \phi_{1,0}$. Using these equations to eliminate $\phi_{0,1}$ and $\phi_{1,0}$ in favor of $\phi_{2,1}$ and $\phi_{1,2}$ on the right-hand side of (3.3.29), we obtain

$$2\phi_{2,1} - 2(1 + \beta)\phi_{1,1} + 2\beta\phi_{1,2} = 0. \quad (3.3.30)$$

For future reference, we express this equation in the form of the inner product of a vector, $\mathbf{a}^{(1,1)}$, and the vector of unknowns \mathbf{w} defined in (3.3.28), as

$$\mathbf{a}^{(1,1)} \cdot \mathbf{w} = 0, \quad (3.3.31)$$

where

$$\mathbf{a}^{(1,1)} = [-2(1 + \beta), 2, 0, \dots, 0 \mid 2\beta, 0, \dots, 0 \mid 0, \dots, 0 \mid \dots \mid 0, \dots, 0] \quad (3.3.32)$$

is a sparse block vector. Each one of the N_y blocks on the right-hand side of (3.3.32) has $N_x + 1$ entries.

Southwestern bordering node

Next, we consider the boundary node (2, 1) and obtain

$$\phi_{3,1} - 2(1 + \beta)\phi_{2,1} + \phi_{1,1} + \beta\phi_{2,2} + \beta\phi_{2,0} = 0. \quad (3.3.33)$$

Boundary condition (3.3.23) applied for $i = 2$ requires that $\phi_{2,2} = \phi_{2,0}$. Using this equation to eliminate $\phi_{2,0}$ in favor of $\phi_{2,2}$ on the right-hand side of (3.3.33), we obtain

$$\phi_{3,1} - 2(1 + \beta)\phi_{2,1} + \phi_{1,1} + 2\beta\phi_{2,2} = 0. \quad (3.3.34)$$

For future reference, we express this equation in the form of an inner vector product,

$$\mathbf{a}^{(2,1)} \cdot \mathbf{w} = 0. \quad (3.3.35)$$

where

$$\mathbf{a}^{(2,1)} = [1, -2(1 + \beta), 1, 0, \dots, 0 \mid 0, 2\beta, 0, \dots, 0 \mid 0, \dots, 0 \mid \dots \mid 0, \dots, 0] \quad (3.3.36)$$

is a sparse block vector. Each one of the N_y blocks on the right-hand side of (3.3.36) has $N_x + 1$ entries.

Other nodes

Continuing in this fashion, we build the rest of the vectors $\mathbf{a}^{(i,j)}$ for $i = 1, \dots, N_x + 1$ and $j = 1, \dots, N_y - 1$, until we have reached the penultimate row corresponding to $j = N_y$. In simplifying the finite-difference equations for this row, we take into consideration not only the Neumann boundary conditions (3.3.22) and (3.3.24) for the side walls, but also the Dirichlet condition (3.3.11) for the top wall.

For example, considering the northwestern node (1, N_y), we obtain the difference equation

$$-2(1 + \beta)\phi_{1,N_y} + 2\phi_{2,N_y} + \beta\phi_{1,N_y-1} = -\beta V x_1, \quad (3.3.37)$$

which can be expressed in the form of the inner product

$$\mathbf{a}^{(1,N_y)} \cdot \mathbf{w} = -\beta V x_1, \quad (3.3.38)$$

where

$$\mathbf{a}^{(1,N_y)} = [0, \dots, 0 \mid \dots \mid 0, \dots, 0 \mid \beta, 0, \dots, 0 \mid -2(1 + \beta), 2, 0, \dots, 0] \quad (3.3.39)$$

is a sparse block vector. Each one of the N_y blocks on the right-hand side of (3.3.39) has $N_x + 1$ entries.

Assembly

Finally, we collect equations (3.3.31), (3.3.35), (3.3.38) and their counterparts for the rest of the interior and boundary nodes into a large system of equations,

$$\mathbf{A} \cdot \mathbf{w} = \mathbf{b}. \tag{3.3.40}$$

The first row of the matrix \mathbf{A} is the vector $\mathbf{a}^{(1,1)}$ defined in (3.3.32); the second row is the vector $\mathbf{a}^{(2,1)}$ defined in (3.3.36); subsequent rows have similar identities. The block vector \mathbf{b} on the right-hand side of (3.3.40) is given by

$$\mathbf{b} = [0, \dots, 0 \mid \dots \mid 0, \dots, 0 \mid -\beta Vx_1, -\beta Vx_2, \dots, -\beta Vx_{N_x+1}]. \tag{3.3.41}$$

The coefficient matrix \mathbf{A} consists of N_y vertical and N_y horizontal partitions in the block tridiagonal form

$$\mathbf{A} = \begin{bmatrix} \mathbf{T} & 2\mathbf{D} & \mathbf{0} & \cdots & \mathbf{0} & \mathbf{0} & \mathbf{0} \\ \mathbf{D} & \mathbf{T} & \mathbf{D} & \mathbf{0} & \cdots & \mathbf{0} & \mathbf{0} \\ \mathbf{0} & \mathbf{D} & \mathbf{T} & \mathbf{D} & \mathbf{0} & \cdots & \mathbf{0} \\ \vdots & \vdots & \vdots & \ddots & \vdots & \vdots & \vdots \\ \mathbf{0} & \cdots & \mathbf{0} & \mathbf{D} & \mathbf{T} & \mathbf{D} & \mathbf{0} \\ \mathbf{0} & \mathbf{0} & \cdots & \mathbf{0} & \mathbf{D} & \mathbf{T} & \mathbf{D} \\ \mathbf{0} & \mathbf{0} & \mathbf{0} & \cdots & \mathbf{0} & \mathbf{D} & \mathbf{T} \end{bmatrix}. \tag{3.3.42}$$

The factor *two* in front of the \mathbf{D} block in the first row is due to the Neumann boundary condition. We have introduced the $(N_x + 1) \times (N_x + 1)$ tridiagonal matrix

$$\mathbf{T} = \begin{bmatrix} -2(1+\beta) & 2 & 0 & 0 & \cdots & 0 & 0 \\ 1 & -2(1+\beta) & 1 & 0 & \cdots & 0 & 0 \\ 0 & 1 & -2(1+\beta) & 1 & \cdots & 0 & 0 \\ \vdots & \vdots & \vdots & \ddots & \vdots & \vdots & \vdots \\ \vdots & \vdots & \vdots & \vdots & \ddots & \vdots & \vdots \\ 0 & 0 & \cdots & \cdots & 1 & -2(1+\beta) & 1 \\ 0 & 0 & \cdots & \cdots & 0 & 2 & -2(1+\beta) \end{bmatrix}, \tag{3.3.43}$$

and the $(N_x + 1) \times (N_x + 1)$ diagonal matrix

$$\mathbf{D} = \begin{bmatrix} \beta & 0 & \cdots & 0 & 0 \\ 0 & \beta & \cdots & 0 & 0 \\ \vdots & \vdots & \ddots & \vdots & \vdots \\ 0 & 0 & \cdots & \beta & 0 \\ 0 & 0 & \cdots & 0 & \beta \end{bmatrix}. \tag{3.3.44}$$

Note that the super- and sub-diagonal elements of \mathbf{T} are equal to unity, except for the elements in the first the last rows that are equal to two. The origin of these irregular elements can be traced back to the Neumann boundary condition. Cursory inspection reveals that all

elements of the matrix \mathbf{A} are zero, except for the elements along five diagonal lines. Because of the dominant presence of zeros, the matrix \mathbf{A} is classified as sparse.

The following MATLAB function entitled *cvt_2d_fdm*, located in directory *cvt_2d* inside directory *07_ptf* of *FDLIB*, generates the coefficient matrix \mathbf{A} for a specified grid size:

```
function A = cvt_2d_fdm (Nx,Ny,beta)

%-----
% Generate the coefficient matrix
% of a linear system for the potential
%-----

N = Ny*(Nx+1); % matrix size
A = zeros(N,N);
cf = -2.0*(1.0+beta);

%-----
% set the five diagonals
%-----

A(1,1) = cf; % first row
A(1,2) = 2.0; A(1,Nx+2) = 2.0*beta;

for i=2:Nx+1 % first block
    A(i,i) = cf;
    A(i,i+1) = 1.0;
    A(i,i-1) = 1.0;
    A(i,i+Nx+1) = 2.0*beta;
end

for i=Nx+2:N-Nx-1 % intermediate blocks
    A(i,i) = cf;
    A(i,i+1) = 1.0;
    A(i,i-1) = 1.0;
    A(i,i+Nx+1) = beta;
    A(i,i-Nx-1) = beta;
end

for i=N-Nx:N-1 % last block
    A(i,i) = cf;
    A(i,i+1) = 1.0;
    A(i,i-1) = 1.0;
    A(i,i-Nx-1) = beta;
end

A(N,N) = cf; % last row
A(N,N-1) = 2.0;
A(N,N-Nx-1) = beta;
```

```

%-----
% reset the ones to twos and
% the faulty betas to zeros
%-----

for i=2:Ny % run over horizontal partitions
    loc = (i-1)*(Nx+1)+1;
    A(loc,loc-1) = 0.0;
    A(loc,loc+1) = 2.0;
end

for i=1:Ny-1 % run over horizontal partitions
    loc = i*(Nx+1);
    A(loc,loc-1) = 2.0;
    A(loc,loc+1) = 0.0;
end

%----
% done
%----

return

```

For $N_x = 2$, $N_y = 3$, and $\beta = 1$, the code generates the matrix:

```

|-4  2  0 | 2  0  0 | 0  0  0 |
| 1 -4  1 | 0  2  0 | 0  0  0 |
| 0  2 -4 | 0  0  2 | 0  0  0 |
|-----|
| 1  0  0 | -4  2  0 | 1  0  0 |
| 0  1  0 | 1 -4  1 | 0  1  0 |
| 0  0  1 | 0  2 -4 | 0  0  1 |
|-----|
| 0  0  0 | 1  0  0 | -4  2  0 |
| 0  0  0 | 0  1  0 | 1 -4  1 |
| 0  0  0 | 0  0  1 | 0  2 -4 |

```

which is consistent with the general form displayed in (3.3.42).

Solving the linear system

We have formulated the problem in terms of the linear system of equations (3.3.40) for the vector \mathbf{w} defined in (3.3.28). Our next task is to solve this system by numerical methods. Once this has been accomplished, the velocity components at the grid nodes arise as partial derivatives of the potential computed by finite-difference methods.

The following MATLAB code entitled *cvt_2d*, located in directory *07_ptf* of *FDLIB*, assembles and solves the linear system using a numerical method implemented in an internal MATLAB function invoked by a vector-by-matrix division:

```

ax = 0.0; bx = 1.0;
ay = 0.0; by = 0.4;
veltop = 1.0;
Nx = 16; Ny = 32;

%-----
% prepare
%-----

Dx = (bx-ax)/Nx; % grid spacing
Dy = (by-ay)/Ny; % grid spacing
beta = (Dx/Dy)^2;
N = Ny*(Nx+1); % system size

%-----
% generate the grid
%-----

[glx,gly,gx,gy] = grid_2d (ax,bx,ay,by,Nx,Ny);

%-----
% specify the potential at the top row
%-----

for i=1:Nx+1
    phitop(i) = veltop*glx(i);
end

%-----
% coefficient matrix
%-----

A = cvt_2d_fdm (Nx,Ny,beta);

%-----
% right-hand side
%-----

for i=1:N-Nx-1
    rhs(i) = 0.0;
end

for i=1:Nx+1
    rhs(N-Nx-1+i) = -beta*phitop(i);
end

%-----
% solve the linear system
%-----

```

```

sln = rhs/A';

%-----
% assign solution to nodes
%-----

Ic = 1;   % counter

for j=1:Ny
    for i=1:Nx+1
        ptl(i,j) = sln(Ic);
        Ic = Ic+1;
    end
end

for i=1:Nx+1
    ptl(i,Ny+1) = phitop(i);
end

%-----
% surface plot
%-----

surf(glx,gly,ptl')
xlabel('x','fontsize',15)
ylabel('y','fontsize',15)
zlabel('\phi','fontsize',15)

%-----
% compute the velocity at the internal nodes
% by numerical differentiation
% using central differences
%-----

for i=2:Nx
    for j=2:Ny
        gux(i,j) = (ptl(i+1,j) -ptl(i-1,j)) ...
            /(gx(i+1,j)-gx(i-1,j));
        guy(i,j) = (ptl(i,j+1) -ptl(i,j-1)) ...
            /(gy(i,j+1)-gy(i,j-1));
    end
end

%-----
% compute the velocity on the walls
% by numerical differentiation
%-----

```

```

%---
% left wall:  i=1
%---

for j=2:Ny
    gux(1,j) = 0.0;
    guy(1,j) = ( ptl(1,j+1)- ptl(1,j-1)) ...
                /(gy(1,j+1)-gy(1,j-1));
end

%---
% bottom wall:  j=1
%---

for i=2:Nx
    gux(i,1) = ( ptl(i+1,1)- ptl(i-1,1)) ...
                /(gx(i+1,1)-gx(i-1,1));
    guy(i,1) = 0.0;
end

%---
% right wall:  i=Nx+1
%---

for j=2:Ny
    gux(Nx+1,j) = 0.0;
    guy(Nx+1,j) = ( ptl(Nx+1,j+1) -ptl(Nx+1,j-1)) ...
                /(gy(Nx+1,j+1)-gy(Nx+1,j-1));
end

%---
% top wall:  j=Ny+1
%---

for i=2:Nx
    gux(i,Ny+1) = veltop;
    guy(i,Ny+1) = ( ptl(i,Ny+1)- ptl(i,Ny)) ...
                /(gy(i,Ny+1)-gy(i,Ny));
end

%---
% four corners
% velocity is zero or singular;
% set it to zero
%---

gux(1 ,1) = 0.0; gux(Nx+1,1) = 0.0;
gux(1 ,Ny+1) = 0.0; gux(Nx+1,Ny+1) = 0.0;
guy(1 ,1) = 0.0; guy(Nx+1,1) = 0.0;

```

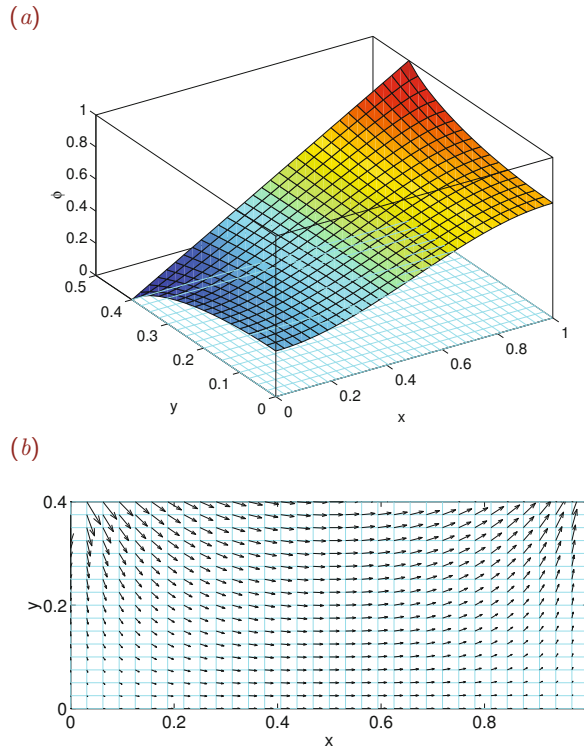


Figure 3.3.2 (a) Surface plot of the potential and (b) velocity vector field of a two-dimensional potential flow in a rectangular cavity computed by a finite-difference method.

```

guy(1 ,Ny+1) = 0.0; guy(Nx+1,Ny+1) = 0.0;

%---
% graphics
%---

figure
hold on
quiver(gx,gy,gux,guy)
axis equal
xlabel('x','fontsize',15)
ylabel('y','fontsize',15)
box

```


The graphics display generated by the code is shown in [Figure 3.3.2](#). The velocity vector field shown in [Figure 3.3.2\(b\)](#) was visualized by the internal MATLAB graphics function *quiver*.

PROBLEMS**3.3.1** *Explicit form of a linear system*

Present the explicit form of the linear system (3.3.40) for discretization levels $N_x = 3$ and $N_y = 3$.

3.3.2 *Neumann boundary conditions all around*

Derive the counterpart of the linear system (3.3.40) when the no-penetration boundary condition is applied along all four walls. Specifically, present the components of the unknown vector \mathbf{w} , constant vector \mathbf{b} , and coefficient matrix \mathbf{A} , in a form that is analogous to that displayed in (3.3.42). Then confirm that the sum of the elements in each row of the matrix \mathbf{A} is zero. Based on this observation, explain why the matrix \mathbf{A} is singular; that is, its determinant is equal to zero.

3.3.3  *Irrotational flow in a cavity*

(a) Run the code `cvt_2d` for a cavity with length to depth ratio equal to unity and discretization level as high as you can afford. Plot the velocity vector field and discuss the structure of the flow.

(b) Repeat (a) for a cavity with length to depth ratio equal to 4.0. Discuss the effect of the cavity aspect ratio on the structure of the flow.

3.4 Linear solvers

In Section 3.3, we reduced the problem of solving Laplace's equation for the harmonic potential in the rectangular domain of a two-dimensional flow to the problem of solving the linear system of equations (3.3.40) for the values of the potential at the nodes of a finite-difference grid deployed over the domain of flow. The reduction was carried out by implementing finite-difference approximations. The solution of the linear system was found using an internal MATLAB function. Since such systems of linear equations arise in broad range of applications within and beyond fluid mechanics, in this section, we review pertinent numerical methods in a generalized framework.

Consider a system of N linear algebraic equations for N unknown scalar variables, x_1, x_2, \dots, x_N ,

$$\begin{aligned} A_{1,1} x_1 + A_{1,2} x_2 + \cdots + A_{1,N-1} x_{N-1} + A_{1,N} x_N &= b_1, \\ A_{2,1} x_1 + A_{2,2} x_2 + \cdots + A_{2,N-1} x_{N-1} + A_{2,N} x_N &= b_2, \\ \cdots, \\ A_{N,1} x_1 + A_{N,2} x_2 + \cdots + A_{N,N-1} x_{N-1} + A_{N,N} x_N &= b_N, \end{aligned} \tag{3.4.1}$$

where $A_{i,j}$ for $i, j = 1, \dots, N$ are given coefficients and b_i are given constants. In matrix notation, the system takes the compact form

$$\mathbf{A} \cdot \mathbf{x} = \mathbf{b}, \tag{3.4.2}$$

where \mathbf{A} is an $N \times N$ coefficient matrix,

$$\mathbf{A} = \begin{bmatrix} A_{1,1} & A_{1,2} & \cdots & A_{1,N-1} & A_{1,N} \\ A_{2,1} & A_{2,2} & \cdots & A_{2,N-1} & A_{2,N} \\ \vdots & \vdots & \ddots & \vdots & \vdots \\ A_{N-1,1} & A_{N-1,2} & \cdots & A_{N-1,N-1} & A_{N-1,N} \\ A_{N,1} & A_{N,2} & \cdots & A_{N,N-1} & A_{N,N} \end{bmatrix}, \quad (3.4.3)$$

and \mathbf{b} is an N -dimensional vector,

$$\mathbf{b} = \begin{bmatrix} b_1 \\ b_2 \\ \vdots \\ b_{N-1} \\ b_N \end{bmatrix}. \quad (3.4.4)$$

A variety of direct and iterative solution procedures are available.

3.4.1 Gauss elimination

A general procedure for solving system (3.4.2) employs the method of Gauss elimination. The basic idea is to solve the first equation in (3.4.2) for the first unknown, x_1 , and use the expression thus obtained to eliminate x_1 from all subsequent equations. We then retain the first equation as is, and replace all subsequent equations with their descendants that do not contain x_1 .

At the second stage, we solve the second equation for the second unknown, x_2 , and use the expression thus obtained to eliminate x_2 from all subsequent equations. We then retain the first and second equations, and replace all subsequent equations with their descendants that do not contain x_1 or x_2 . Continuing in this fashion, we arrive at the last equation, which contains only the last unknown, x_N .

Having completed the elimination, we compute the unknowns by the method of backward substitution. First, we solve the last equation for x_N , which thus becomes a known. Second, we solve the penultimate equation for x_{N-1} , which also becomes a known. Continuing in the backward direction, we scan the reduced system until we have computed all unknowns.

Pivoting

Immediately before the m th equation has been solved for the m th unknown, where $m = 1, \dots, N-1$, the linear system takes the form shown in Table 3.4.1, where $A_{i,j}^{(m)}$ are intermediate coefficients and $b_i^{(m)}$ are intermediate right-hand sides.

A difficulty arises when the diagonal element, $A_{m,m}^{(m)}$, is nearly or precisely zero, for then we may no longer solve the m th equation for x_m , as required. However, the failure

$$\begin{bmatrix} A_{1,1}^{(m)} & A_{1,2}^{(m)} & \cdots & \cdots & \cdots & A_{1,N}^{(m)} \\ 0 & A_{2,2}^{(m)} & \cdots & \cdots & \cdots & A_{2,N}^{(m)} \\ 0 & 0 & \cdots & \cdots & \cdots & \cdots \\ 0 & 0 & A_{m-1,m-1}^{(m)} & A_{m-1,m}^{(m)} & \cdots & A_{m-1,N}^{(m)} \\ 0 & \cdots & 0 & A_{m,m}^{(m)} & \cdots & A_{m,N}^{(m)} \\ 0 & \cdots & 0 & \cdots & \cdots & \cdots \\ 0 & \cdots & 0 & A_{N,m}^{(m)} & \cdots & A_{N,N}^{(m)} \end{bmatrix} \begin{bmatrix} x_1 \\ x_2 \\ x_3 \\ \vdots \\ x_{N-1} \\ x_N \end{bmatrix} = \begin{bmatrix} b_1^{(m)} \\ b_2^{(m)} \\ b_3^{(m)} \\ \vdots \\ b_{N-1}^{(m)} \\ b_N^{(m)} \end{bmatrix},$$

Table 3.4.1 Transient structure of a linear system of equations at the m th stage of Gauss elimination. The first equation of the transient system is the same as the first equation in the original system (3.4.2) for any m . Subsequent equations are different, except at the first stage corresponding to $m = 1$.

of the method does not imply that the linear system does not have a unique solution. To circumvent this difficulty, we simply rearrange the equations or relabel the unknowns so as to bring the m th unknown to the m th equation using the method of pivoting. If there is no way we can make this happen, the matrix \mathbf{A} is singular and the linear system has either no solution or an infinite number of solutions.

In the method of row pivoting, potential difficulties are bypassed by switching the m th equation of the transient system displayed in Table 3.4.1 with the subsequent k th equation, where $k > m$. The value of k is chosen such that $|A_{k,m}^{(m)}|$ is the maximum value of the elements in the m th column below the diagonal, $A_{i,m}^{(m)}$ for $i \geq m$. If $A_{i,m}^{(m)} = 0$ for all $i \geq m$, the matrix \mathbf{A} is singular and the system under consideration does not have a unique solution.

3.4.2 A menagerie of other methods

In practice, the size of system (3.3.40) can be on the order of $10^4 \times 10^4$ or even higher, corresponding to discretization levels N_x and N_y on the order of 10^2 . For such large systems, the method of Gauss elimination requires a prohibitive computational time. The practical need for solving systems of large size has motivated the development of a host of powerful methods for general or specific applications.¹

Iterative methods

Iterative methods are appropriate for sparse systems with large dimensions. The main idea is to split the coefficient matrix, \mathbf{A} , into two matrices, \mathbf{A}' and \mathbf{A}'' , writing

$$\mathbf{A} = \mathbf{A}' - \mathbf{A}'', \tag{3.4.5}$$

and then recast the system (3.4.2) into the form

$$\mathbf{A}' \cdot \mathbf{x} = \mathbf{A}'' \cdot \mathbf{x} + \mathbf{b}. \tag{3.4.6}$$

¹Pozrikidis, C. (2008) *Numerical Computation in Science and Engineering*, Second Edition, Oxford University Press.

The procedure involves guessing the solution, \mathbf{x} , computing the right-hand side of (3.4.6), and solving for \mathbf{x} on the left-hand side. The advantage of this approach is that, if the splitting (3.4.5) is done craftily, it is much easier to solve (3.4.6) than (3.4.2) for \mathbf{x} on the left-hand side. The computation is repeated until the value of \mathbf{x} used to compute the right-hand side of (3.4.6) is virtually identical to that arising by solving the linear system (3.4.6). Examples of iterative methods are the Jacobi, the Gauss–Seidel, and the successive over-relaxation (SOR) method.

A different class of iterative methods search for the solution vector, \mathbf{x} , by making steps in the N -dimensional space toward craftily designed or optimal directions. The multi-grid method is another powerful technique for solving systems of linear equations arising from finite-difference and related discretization.

Directory *03_lin_eq* inside directory *01_num_meth* of **FDLIB** contains programs that implement the conjugate and biconjugate gradients methods.

PROBLEM

3.4.1 Gauss elimination

Program *gel*, located in directory *03_lin_eq* inside directory *01_num_meth* of **FDLIB**, solves a system of linear equations using the method of Gauss elimination with row pivoting. Use the program to solve a system of your choice and verify the accuracy of the solution.

3.5 Two-dimensional point sources and point-source dipoles

Laplace’s equation for the harmonic velocity potential–equation (3.2.16) for two-dimensional flow or equation (3.2.20) for three-dimensional flow—is linear. This means that if ϕ_1 and ϕ_2 are two harmonic potentials representing two elementary flows, any linear combination of these potentials,

$$\phi = c_1 \phi_1 + c_2 \phi_2, \quad (3.5.1)$$

will also be a harmonic potential representing a hybrid flow, where c_1 and c_2 are two arbitrary coefficients.

3.5.1 Function superposition and fundamental solutions

The linearity of Laplace’s equation allows us to generate exact and approximate solutions by the method of superposition. The key idea is to introduce a family of harmonic potentials playing the role of basis functions, also called fundamental solutions, and then use them as building blocks to generate further solutions.

For example, if ϕ_1 and ϕ_2 are two such fundamental solutions, a desired solution can be expressed by the right-hand side of (3.5.1), and the two coefficients c_1 and c_2 can be adjusted to satisfy the boundary conditions.

Various families of fundamental solutions are available for flows in infinite or semi-infinite domains, and for singly, doubly, or triply periodic flows. The most general class of fundamental solutions consists of the fundamental singularities of potential flow.

3.5.2 Two-dimensional point source

Imagine that an incompressible fluid is discharged into an infinite pool through the walls of an infinite perforated cylinder, thereby generating a radial flow in the xy plane outward from the inlet point. In plane polar coordinates centered at the point of discharge, $\mathbf{x}_0 = (x_0, y_0)$, the radial and polar components of the velocity at an arbitrary field point, $\mathbf{x} = (x, y)$, are given by

$$u_r(r) = \frac{m}{2\pi} \frac{1}{r}, \quad u_\theta = 0, \quad (3.5.2)$$

where

$$r = \sqrt{(x - x_0)^2 + (y - y_0)^2} \quad (3.5.3)$$

is the distance of the field point, \mathbf{x} , from the discharge point, \mathbf{x}_0 , and m is a constant expressing the rate of areal discharge. The units of m are velocity multiplied by length.

The flow described by equations (3.5.2) is attributed to a two-dimensional point source, and the rate of areal discharge m is the strength of the point source. If m is negative, we obtain a point source with negative strength described as a point sink.

The radial velocity of the flow due to a point source decays as the inverse of the distance from the point of discharge, r , for the following physical reason. Since the fluid is incompressible, the flow rate Q across any circular loop of arbitrary radius a centered at the point of discharge must be independent of the loop radius. To verify that the velocity field (3.5.2) satisfies this constraint, we use expression (2.6.21) and find that

$$Q = a \int_0^{2\pi} u_r \, d\theta = \frac{m}{2\pi} a \int_0^{2\pi} \frac{1}{r} \, d\theta = \frac{m}{2\pi} a \frac{1}{a} \int_0^{2\pi} d\theta = m, \quad (3.5.4)$$

as required. If we had set, for example, $u_r = m/(2\pi r^k)$, where the exponent k is not equal to unity, the restriction of constant areal flow rate associated with an incompressible fluid would not be satisfied.

Singular behavior of the point source

As the distance from the point source r tends to zero, the right-hand side of the radial velocity in (3.5.2) tends to infinity. This singular behavior is a manifestation of the idealized nature of the flow due to a point source, and explains why the point source is classified as a singularity.

In practice, the flow expressed by (3.5.2) is valid only for $r > b$, where b is the radius of the perforated cylinder discharging the fluid. Extending the domain of flow inward all the way up to the center of the cylinder, located at \mathbf{x}_0 , we allow for a mathematical singularity.

Velocity potential

The velocity potential of a two-dimensional point source, denoted by $\phi^{2\text{DPS}}$, is related to the velocity components according to equations (3.2.28),

$$u_r = \frac{\partial \phi^{2\text{DPS}}}{\partial r} = \frac{m}{2\pi} \frac{1}{r}, \quad u_\theta = \frac{\partial \phi^{2\text{DPS}}}{\partial \theta} = 0. \quad (3.5.5)$$

Integrating the first equation and using the second equation to evaluate the integration constant, we find that

$$\phi^{2\text{DPS}} = \frac{m}{2\pi} \ln \frac{r}{\mathcal{L}} = \frac{m}{4\pi} \ln \frac{(x-x_0)^2 + (y-y_0)^2}{\mathcal{L}^2}, \quad (3.5.6)$$

where \mathcal{L} is a specified length introduced to ensure that the argument of the logarithm is dimensionless, as required. Straightforward differentiation confirms that $\phi^{2\text{DPS}}$ satisfies Laplace's equation in two dimensions at every point,

$$\nabla^2 \phi^{2\text{DPS}} = 0, \quad (3.5.7)$$

except at the singular point, \mathbf{x}_0 , where the potential and its derivatives are not defined.

Cartesian velocity components and stream function

To derive the Cartesian components of the velocity due to a point source, we take the partial derivatives of $\phi^{2\text{DPS}}$ with respect to x or y , and obtain

$$u_x^{2\text{DPS}} = \frac{\partial \phi^{2\text{DPS}}}{\partial x} = \frac{m}{2\pi} \frac{x-x_0}{(x-x_0)^2 + (y-y_0)^2} \quad (3.5.8)$$

and

$$u_y^{2\text{DPS}} = \frac{\partial \phi^{2\text{DPS}}}{\partial y} = \frac{m}{2\pi} \frac{y-y_0}{(x-x_0)^2 + (y-y_0)^2}. \quad (3.5.9)$$

The streamlines of the flow due to a point source are radial straight lines emanating from the singular point, \mathbf{x}_0 . The associated stream function is

$$\psi^{2\text{DPS}} = \frac{m}{2\pi} \arctan \frac{y-y_0}{x-x_0} + \psi_0, \quad (3.5.10)$$

where ψ_0 is an inconsequential constant. Note that the stream function is a multi-valued function of position.

A point source embedded in uniform flow

As an application, consider the superposition of uniform (streaming) flow along the x axis with velocity U_x , and the flow due to a point source with strength m situated at the origin, $x_0 = 0$ and $y_0 = 0$. Using the potential $\phi = U_x x$ for the streaming flow and the potential

given in (3.5.6) for the point source, we find that the potential of the composite irrotational flow is

$$\phi(\mathbf{x}) = U_x x + \frac{m}{4\pi} \ln \frac{x^2 + y^2}{\mathcal{L}^2}, \quad (3.5.11)$$

where \mathcal{L} is an arbitrary length. The associated Cartesian components of the velocity are given by

$$u_x = U_x + \frac{m}{2\pi} \frac{x}{x^2 + y^2}, \quad u_y = \frac{m}{2\pi} \frac{y}{x^2 + y^2}. \quad (3.5.12)$$

Note the absence of the inconsequential reference length, \mathcal{L} .

To study the structure of the flow, we introduce dimensionless variables denoted by a caret (hat),

$$\hat{x} = \frac{x}{\mathcal{L}}, \quad \hat{y} = \frac{y}{\mathcal{L}}, \quad \hat{u}_x = \frac{u_x}{U_x}, \quad \hat{u}_y = \frac{u_y}{U_x}, \quad (3.5.13)$$

and recast equations (3.5.12) into the dimensionless form

$$\hat{u}_x = 1 + \beta \frac{\hat{x}}{\hat{x}^2 + \hat{y}^2}, \quad \hat{u}_y = \beta \frac{\hat{y}}{\hat{x}^2 + \hat{y}^2}, \quad (3.5.14)$$

where

$$\beta = \frac{1}{2\pi} \frac{m}{\mathcal{L}U_x} \quad (3.5.15)$$

is a dimensionless parameter expressing the strength of the point source relative to the magnitude of the incident flow. Equations (3.5.14) demonstrate that the structure of the flow is determined by the value of the parameter β .

The streamline pattern shown in [Figure 3.5.1](#) for $\beta = 0.25$ reveals that the velocity potential (3.5.11) describes uniform flow along the x axis past a semi-infinite two-dimensional body whose surface can be identified with two streamlines emanating from a stagnation point lying on the negative part of the x axis. Using the first equation in (3.5.14), we find that the x component of the velocity at the x axis is zero when $\hat{x} = -\beta$. Thus, the larger the value of β , expressing the relative strength of the point source, the farther the stagnation point is located from the origin.

3.5.3 Two-dimensional point-source dipole

Next, we consider the flow due to the superposition of a point source with strength m located at a point, $(x_0 + b, y_0)$, and a point sink with strength $-m$ located at the nearby point $(x_0 - b, y_0)$, where b is a specified half distance, as shown in [Figure 3.5.2\(a\)](#).

Using expression (3.5.6), we find that the combined harmonic potential induced by these singularities is given by

$$\phi(\mathbf{x}) = \frac{m}{4\pi} \ln \frac{(x - (x_0 + b))^2 + (y - y_0)^2}{b^2} - \frac{m}{4\pi} \ln \frac{(x - (x_0 - b))^2 + (y - y_0)^2}{b^2}. \quad (3.5.16)$$

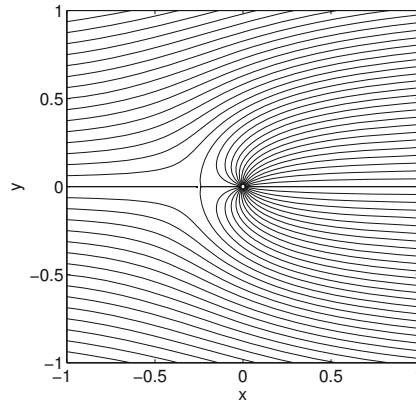


Figure 3.5.1 Streamline pattern of the flow due to the superposition of streaming (uniform) flow along the x axis and the flow due to a two-dimensional point source located at the origin.

Consolidating the logarithms, we obtain

$$\phi(\mathbf{x}) = \frac{m}{4\pi} \ln \frac{(x - (x_0 + b))^2 + (y - y_0)^2}{(x - (x_0 - b))^2 + (y - y_0)^2}. \quad (3.5.17)$$

The Cartesian components of the fluid velocity are found by differentiation,

$$u_x = \frac{\partial \phi}{\partial x} = \frac{m}{2\pi} \left(\frac{x - (x_0 + b)}{(x - (x_0 + b))^2 + (y - y_0)^2} - \frac{x - (x_0 - b)}{(x - (x_0 - b))^2 + (y - y_0)^2} \right) \quad (3.5.18)$$

and

$$u_y = \frac{\partial \phi}{\partial y} = \frac{m}{2\pi} \left(\frac{y - y_0}{(x - (x_0 + b))^2 + (y - y_0)^2} - \frac{y - y_0}{(x - (x_0 - b))^2 + (y - y_0)^2} \right). \quad (3.5.19)$$

Now we hold the position of the field point (x, y) fixed and decrease the distance between the two singularities, that is, we let b tend to zero. In this limit, the flow due to the point sink tends to cancel the flow due to the point source. However, if the strengths of the point source and the point sink, $\pm m$, also increase in inverse proportion with the distance between the two singularities, $2b$, then a nontrivial flow due to a point source dipole arises in the limit.

To derive the flow due to a point-source dipole, we recast the expression for the potential on the right-hand side of (3.5.17) into the form

$$\phi(\mathbf{x}) = \frac{m}{4\pi} \left(\ln \left(1 - b \frac{2(x - x_0) - b}{(x - x_0)^2 + (y - y_0)^2} \right) - \ln \left(1 + b \frac{2(x - x_0) + b}{(x - x_0)^2 + (y - y_0)^2} \right) \right), \quad (3.5.20)$$

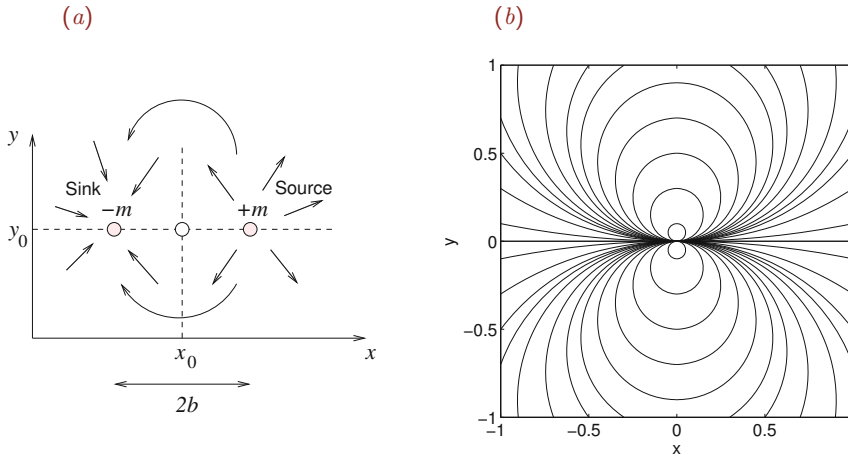


Figure 3.5.2 (a) A point source and a point sink merge to yield a point-source dipole. The depicted dipole is oriented along the x axis. (b) Streamline pattern due to a two-dimensional dipole pointing along the x axis.

and then

$$\phi = \frac{m}{4\pi} \left(\ln(1 - \epsilon_1) - \ln(1 + \epsilon_2) \right), \tag{3.5.21}$$

where

$$\epsilon_1 \equiv b \frac{2(x - x_0) - b}{(x - x_0)^2 + (y - y_0)^2}, \quad \epsilon_2 \equiv b \frac{2(x - x_0) + b}{(x - x_0)^2 + (y - y_0)^2} \tag{3.5.22}$$

are dimensionless variables. As the distance, b , becomes decreasingly smaller than the distance between the field point, \mathbf{x} , and the point \mathbf{x}_0 , both ϵ_1 and ϵ_2 tend to zero.

The Taylor series expansion of the logarithmic function $\ln w$ about the point $w = 1$ provides us with the approximations

$$\ln(1 - \epsilon_1) = -\epsilon_1 + \dots, \quad \ln(1 + \epsilon_2) = \epsilon_2 + \dots. \tag{3.5.23}$$

Substituting these expressions into the right-hand side of (3.5.21) and neglecting quadratic and higher-order terms represented by the dots, we obtain the velocity potential due to a point-source dipole located at the point (x_0, y_0) and oriented along the x axis,

$$\phi^{2\text{DPSD}\mathbf{x}} = -\frac{m}{4\pi}(\epsilon_1 + \epsilon_2) \tag{3.5.24}$$

or

$$\phi^{2\text{DPSD}\mathbf{x}} = -\frac{d_x}{2\pi} \frac{x - x_0}{(x - x_0)^2 + (y - y_0)^2}, \tag{3.5.25}$$

where

$$d_x \equiv 2mb \tag{3.5.26}$$

is the strength of the dipole.

Now comparing (3.5.6), (3.5.25), and (3.5.26), we obtain

$$\phi^{2\text{DPSDx}} = 2b \frac{\partial \phi^{2\text{DPS}}}{\partial x_0}, \tag{3.5.27}$$

which shows that the potential due to a point-source dipole oriented along the x axis arises by differentiating the potential due to a point source with respect to the x coordinate of the singular point, x_0 . This property classifies the dipole as a derivative singularity descending from the point source.

Velocity components and stream function

The velocity components associated with a two-dimensional (2D) point-source dipole (PSD) oriented along the x axis are given by

$$u_x^{2\text{DPSDx}} = \frac{\partial \phi^{2\text{DPSDx}}}{\partial x} = 2b \frac{\partial^2 \phi^{2\text{DPS}}}{\partial x \partial x_0} = -2b \frac{\partial^2 \phi^{2\text{DPS}}}{\partial x^2} \tag{3.5.28}$$

and

$$u_y^{2\text{DPSDx}} = \frac{\partial \phi^{2\text{DPSDx}}}{\partial y} = 2b \frac{\partial^2 \phi^{2\text{DPS}}}{\partial y \partial x_0} = -2b \frac{\partial^2 \phi^{2\text{DPS}}}{\partial x \partial y}. \tag{3.5.29}$$

Carrying out the differentiations, we obtain

$$u_x^{2\text{DPSDx}} = \frac{d_x}{2\pi} \left(-\frac{1}{(x-x_0)^2 + (y-y_0)^2} + 2 \frac{(x-x_0)^2}{((x-x_0)^2 + (y-y_0)^2)^2} \right) \tag{3.5.30}$$

and

$$u_y^{2\text{DPSDx}} = \frac{d_x}{2\pi} 2 \frac{(x-x_0)(y-y_0)}{((x-x_0)^2 + (y-y_0)^2)^2}. \tag{3.5.31}$$

The associated streamline pattern is shown in [Figure 3.5.2\(b\)](#). The stream function is given by

$$\psi^{2\text{DPSDx}} = \frac{d_x}{2\pi} \frac{y-y_0}{(x-x_0)^2 + (y-y_0)^2} + \psi_0, \tag{3.5.32}$$

where ψ_0 is an inconsequential constant.

Dipole along the y axis

Working in a similar fashion, we derive the flow due to a point-source dipole with strength d_y oriented along the y axis. The associated harmonic potential is

$$\phi^{2\text{DPSD}_y} = 2b \frac{\partial \phi^{2\text{DPS}}}{\partial y_0} = -\frac{d_y}{2\pi} \frac{y - y_0}{(x - x_0)^2 + (y - y_0)^2}, \quad (3.5.33)$$

where $d_y = 2mb$ is the strength of the dipole. The corresponding Cartesian components of the velocity are given by

$$u_x^{2\text{DPSD}_y} = \frac{\partial \phi^{2\text{DPSD}_y}}{\partial x} = 2b \frac{\partial^2 \phi^{2\text{DPS}}}{\partial x \partial y_0} = -2b \frac{\partial^2 \phi^{2\text{DPS}}}{\partial x \partial y} \quad (3.5.34)$$

and

$$u_y^{2\text{DPSD}_y} = \frac{\partial \phi^{2\text{DPSD}_y}}{\partial y} = 2b \frac{\partial^2 \phi^{2\text{DPS}}}{\partial y \partial y_0} = -2b \frac{\partial^2 \phi^{2\text{DPS}}}{\partial y^2}. \quad (3.5.35)$$

Carrying out the differentiations, we obtain the explicit expressions

$$u_x^{2\text{DPSD}_y} = \frac{d_y}{2\pi} 2 \frac{(x - x_0)(y - y_0)}{((x - x_0)^2 + (y - y_0)^2)^2} \quad (3.5.36)$$

and

$$u_y^{2\text{DPSD}_y} = \frac{d_y}{2\pi} \left(-\frac{1}{(x - x_0)^2 + (y - y_0)^2} + 2 \frac{(y - y_0)^2}{((x - x_0)^2 + (y - y_0)^2)^2} \right). \quad (3.5.37)$$

The streamline pattern is found by rotating the pattern shown in [Figure 3.5.2\(b\)](#) by 90° around the location of the dipole. The stream function is given by

$$\psi^{2\text{DPSD}_y} = -\frac{d_y}{2\pi} \frac{x - x_0}{(x - x_0)^2 + (y - y_0)^2} + \psi_0, \quad (3.5.38)$$

where ψ_0 is an inconsequential constant.

General dipole orientation

Combining the expressions given in (3.5.25) and (3.5.33), we find that the harmonic potential due to a potential dipole with vectorial strength $\mathbf{d} \equiv (d_x, d_y)$ located at the point \mathbf{x}_0 is given by

$$\phi^{2\text{DPSD}} = \mathbf{d} \cdot \mathbf{\Phi}^{2\text{DPSD}}, \quad (3.5.39)$$

where the vector function $\mathbf{\Phi}^{2\text{DPSD}}$ is defined as

$$\mathbf{\Phi}^{2\text{DPSD}} \equiv -\frac{1}{2\pi} \frac{1}{(x - x_0)^2 + (y - y_0)^2} \begin{bmatrix} x - x_0 \\ y - y_0 \end{bmatrix}. \quad (3.5.40)$$

The velocity field can be expressed in the corresponding form

$$\mathbf{u} = -\mathbf{d} \cdot \mathbf{U}^{2\text{DPSD}}, \quad (3.5.41)$$

where $\mathbf{U}^{2\text{DPSD}}$ is a 2×2 matrix function of position (Problem 3.5.2).

3.5.4 Flow past a circular cylinder

As an application, we consider the superposition of uniform (streaming) flow along the x axis with velocity U_x , and the flow due to a point-source dipole oriented along the x axis located at the origin. Using the potential $\phi = U_x x$ for the streaming flow and the potential given in (3.5.25) with $x_0 = 0$ and $y_0 = 0$ for the dipole, we derive the potential of the composite flow,

$$\phi(x, y) = U_x x - \frac{d_x}{2\pi} \frac{x}{x^2 + y^2} = U_x x \left(1 - \frac{1}{2\pi} \frac{d_x}{U_x} \frac{1}{r^2} \right), \quad (3.5.42)$$

where

$$r = \sqrt{x^2 + y^2} \quad (3.5.43)$$

is the distance of the field point, $\mathbf{x} = (x, y)$, from the center of the cylinder. In plane polar coordinates, (r, θ) ,

$$\phi(r, \theta) = U_x \left(r - \frac{1}{2\pi} \frac{d_x}{U_x} \frac{1}{r} \right) \cos \theta, \quad (3.5.44)$$

where the polar angle θ is measured in the counterclockwise direction around the center of the cylinder, defined such that $x = r \cos \theta$.

Now using the expression for the radial component of the velocity in terms of the potential given in the first of equations (3.2.28), we find that

$$u_r = \frac{\partial \phi}{\partial r} = U_x \left(1 + \frac{1}{2\pi} \frac{d_x}{U_x} \frac{1}{r^2} \right) \cos \theta. \quad (3.5.45)$$

The expression inside the parentheses on the right-hand side is zero at the radial distance

$$r = \left(-\frac{1}{2\pi} \frac{d_x}{U_x} \right)^{1/2}, \quad (3.5.46)$$

where the quantity under the square root is assumed positive. Conversely, if the strength of the dipole has the value

$$d_x = -2\pi U_x a^2, \quad (3.5.47)$$

then the radial velocity will be zero at the radial distance $r = a$. The negative sign underlines that the dipole is oriented against the incident streaming flow.

It is evident that the potential (3.5.44) with d_x evaluated from expression (3.5.47) describes uniform flow with velocity U_x past a circular cylinder of radius a centered at the origin, where the no-penetration condition is satisfied over the surface of the cylinder. Substituting the value for d_x given in (3.5.47) into (3.5.44), we derive the explicit solution

$$\phi = U_x \left(r + \frac{a^2}{r} \right) \cos \theta. \quad (3.5.48)$$

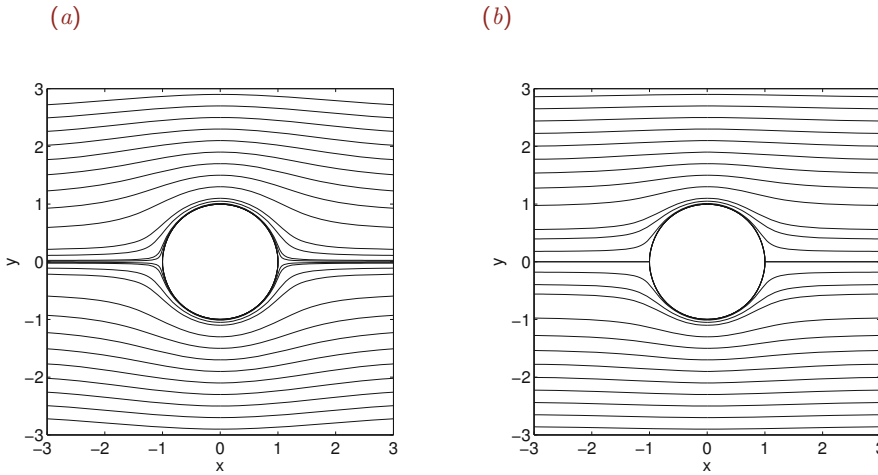


Figure 3.5.3 Streamline pattern of (a) uniform (streaming) flow past a circular cylinder with vanishing circulation around the cylinder, and (b) uniform (streaming) flow past a sphere.

The corresponding Cartesian velocity components are

$$u_x = U_x \left(1 + \frac{a^2}{r^4} - 2 \frac{a^2}{r^2} x^2 \right), \quad u_y = -2 U_x \frac{a^2}{r^4} xy. \quad (3.5.49)$$

The associated streamline pattern is shown in [Figure 3.5.3\(a\)](#). We recall that the origin has been set at the center of the cylinder and the solution applies in the exterior of the cylinder, $r \geq a$.

3.5.5 Sources and dipoles in the presence of boundaries

When the domain of flow is bounded by an impermeable surface, the flow due to a point source or point source dipole must be accompanied with a complementary flow whose purpose is to satisfy the no-penetration boundary condition. For simple boundary geometries, the complementary flow can be identified with the flow generated by singularities located at image positions.

Directory *lgf_2d*, located inside directory *07_ptf* of **FDLIB**, contains a collection of sub-routines that evaluate the harmonic potential and associated velocity field for several boundary geometries. Two examples are discussed in the remainder of this section.

Point source above a wall

In the case of a point source placed above a plane wall located at $y = y_w$, the complementary flow is generated by reflecting the point source with respect to the wall. If a primary point source with strength m is located at a point, (x_0, y_0) , then an image point source with equal strength is located at the point $(x_0, 2y_w - y_0)$. The streamline pattern is shown in [Figure 3.5.4\(a\)](#).

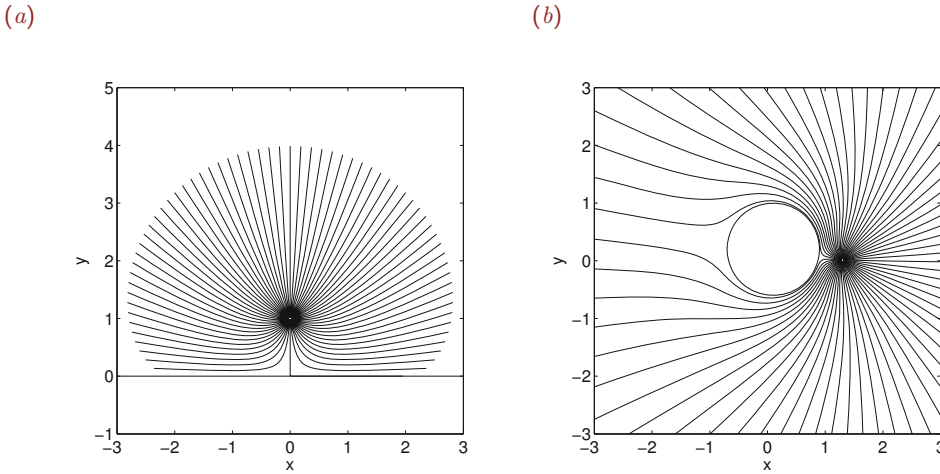


Figure 3.5.4 Streamline pattern of the flow due to a two-dimensional point source (a) above a plane wall and (b) in front of a circular cylinder.

Point source outside a circular cylinder

In the case of a point source located outside a circular cylinder of radius a centered at a point $\mathbf{x}_c = (x_c, y_c)$, the complementary flow is generated by two image point sources. The first image point source is located at the inverse point of the primary point source with respect to the cylinder. If a primary point source with strength m is located at (x_0, y_0) , then an image point source with the same strength is located at the point

$$x_0^{\text{image}} = x_c + (x_0 - x_c) \frac{a^2}{|\mathbf{x}_0 - \mathbf{x}_c|^2}, \quad y_0^{\text{image}} = y_c + (y_0 - y_c) \frac{a^2}{|\mathbf{x}_0 - \mathbf{x}_c|^2}, \quad (3.5.50)$$

where

$$|\mathbf{x}_0 - \mathbf{x}_c|^2 = (x_0 - x_c)^2 + (y_0 - y_c)^2 \quad (3.5.51)$$

is the square of the distance of the primary point source from the center of the cylinder. A second image point source with strength $-m$ is located at the center of the cylinder. Note that the sum of the strengths of the image singularities is zero to ensure that a net flow rate across the surface of the cylinder does not arise. The streamline pattern of the induced flow is shown in [Figure 3.5.4\(b\)](#).

PROBLEMS

3.5.1 *Oblique streaming flow past a circular cylinder*

Derive an expression for the harmonic potential and Cartesian components of the velocity of oblique streaming flow with uniform velocity, $u_x = U_x$, $u_y = U_y$, past a circular cylinder of radius a centered at the origin.

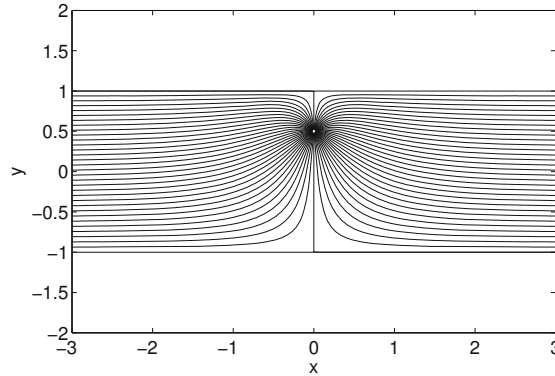


Figure 3.5.5 Streamline pattern of the flow due to a two-dimensional point source between two parallel plates.

3.5.2 Flow due to a point-source dipole

Use expressions (3.5.30) and (3.5.36) to derive the explicit form of the matrix $\mathbf{U}^{2\text{DPSD}}$ introduced in (3.5.41).

3.5.3 Stream functions

Confirm the stream functions associated with (a) a two-dimensional point source given in (3.5.10) and (b) a two-dimensional point-source dipole pointing along the x or y axis, given in (3.5.32) and (3.5.38).

3.5.4 Point source in a semi-infinite rectangular strip

Directory *strml*, located inside directory *04_various* of **FDLIB**, contains a program that generates the streamline pattern of the flow induced by a point source for several boundary geometries. Examples are shown in [Figures 3.5.4](#) and [3.5.5](#). Run the program to generate the streamline pattern of the flow due to a point source in a semi-infinite rectangular strip and discuss the structure of the flow.

3.6 Three-dimensional point sources and point-source dipoles

The fundamental solutions derived in Section 3.5 for two-dimensional potential flow can be extended in a straightforward fashion to three-dimensional flow.

3.6.1 Three-dimensional point source

The harmonic potential due to a three-dimensional point source with strength m located at the point $\mathbf{x}_0 = (x_0, y_0, z_0)$ is

$$\phi^{3\text{DPS}} = -\frac{m}{4\pi} \frac{1}{r}, \quad (3.6.1)$$

where

$$r = \sqrt{(x - x_0)^2 + (y - y_0)^2 + (z - z_0)^2} \quad (3.6.2)$$

is the distance of the field point, \mathbf{x} , from the location of the point source, \mathbf{x}_0 . The corresponding Cartesian velocity components are

$$u_x^{3DPS} = \frac{m}{4\pi} \frac{x - x_0}{r^3}, \quad u_y^{3DPS} = \frac{m}{4\pi} \frac{y - y_0}{r^3}, \quad u_z^{3DPS} = \frac{m}{4\pi} \frac{z - z_0}{r^3}. \quad (3.6.3)$$

The streamlines are radial straight lines emanating from the singular point, \mathbf{x}_0 . The fluid moves outward from a point source ($m > 0$) and inward into a point sink ($m < 0$).

3.6.2 Three-dimensional point-source dipole

The harmonic potential due to a three-dimensional point-source dipole oriented along the x , y , or z axis is given, respectively, by

$$\phi^{3DPSDx} = -\frac{d_x}{4\pi} \frac{x - x_0}{r^3}, \quad \phi^{3DPSDy} = -\frac{d_y}{4\pi} \frac{y - y_0}{r^3}, \quad \phi^{3DPSDz} = -\frac{d_z}{4\pi} \frac{z - z_0}{r^3}, \quad (3.6.4)$$

where d_x , d_y , and d_z are the directional strengths of the dipole. The corresponding velocity components are found by straightforward differentiation with respect to x , y , or z .

For a dipole oriented along the x axis, we find that

$$\begin{aligned} u_x^{3DPSDx} &= \frac{\partial \phi^{3DPSDx}}{\partial x} = \frac{d_x}{4\pi} \left(-\frac{1}{r^3} + 3 \frac{(x - x_0)^2}{r^5} \right), \\ u_y^{3DPSDx} &= \frac{\partial \phi^{3DPSDx}}{\partial y} = \frac{d_x}{4\pi} 3 \frac{(x - x_0)(y - y_0)}{r^5}, \\ u_z^{3DPSDx} &= \frac{\partial \phi^{3DPSDx}}{\partial z} = \frac{d_x}{4\pi} 3 \frac{(x - x_0)(z - z_0)}{r^5}. \end{aligned} \quad (3.6.5)$$

The streamline pattern in the xy plane is qualitatively similar, but not identical, to that shown in [Figure 3.5.2\(b\)](#) for two-dimensional flow.

For a dipole oriented along the y axis, we find that

$$\begin{aligned} u_x^{3DPSDy} &= \frac{\partial \phi^{3DPSDy}}{\partial x} = \frac{d_y}{4\pi} 3 \frac{(y - y_0)(x - x_0)}{r^5}, \\ u_y^{3DPSDy} &= \frac{\partial \phi^{3DPSDy}}{\partial y} = \frac{d_y}{4\pi} \left(-\frac{1}{r^3} + 3 \frac{(y - y_0)^2}{r^5} \right), \\ u_z^{3DPSDy} &= \frac{\partial \phi^{3DPSDy}}{\partial z} = \frac{d_y}{4\pi} 3 \frac{(y - y_0)(z - z_0)}{r^5}. \end{aligned} \quad (3.6.6)$$

For a dipole oriented along the z axis, we find that

$$\begin{aligned} u_x^{3D-PSD-z} &= \frac{\partial \phi^{3DPSDz}}{\partial x} = \frac{d_z}{4\pi} 3 \frac{(z-z_0)(x-x_0)}{r^5}, \\ u_y^{3D-PSD-z} &= \frac{\partial \phi^{3DPSDz}}{\partial y} = \frac{d_z}{4\pi} 3 \frac{(z-z_0)(y-y_0)}{r^5}, \\ u_z^{3D-PSD-z} &= \frac{\partial \phi^{3DPSDz}}{\partial z} = \frac{d_z}{4\pi} \left(-\frac{1}{r^3} + 3 \frac{(z-z_0)^2}{r^5} \right). \end{aligned} \quad (3.6.7)$$

Expressions (3.6.5)–(3.6.7) can be conveniently placed into a compact vector-matrix form, as discussed in Problem 3.6.1.

3.6.3 Streaming flow past a sphere

As an application, we consider the superposition of streaming (uniform) flow along the x axis with velocity U_x , and the flow due to a three-dimensional point-source dipole positioned at the origin, $x_0 = 0$, $y_0 = 0$, $z_0 = 0$, and pointing along the x axis.

Using the potential $\phi = U_x x$ for the streaming flow and the first expression in (3.6.4) for the point-source dipole, we find that the potential of the composite axisymmetric flow is given by

$$\phi = U_x x - \frac{d_x}{4\pi} \frac{x}{r^3} = U_x x \left(1 - \frac{d_x}{4\pi U_x} \frac{1}{r^3} \right), \quad (3.6.8)$$

where $r = (x^2 + y^2 + z^2)^{1/2}$ is the distance from the origin. Rearranging, we obtain

$$\phi(r, \theta) = U_x \left(1 - \frac{d_x}{4\pi U_x} \frac{1}{r^3} \right) r \cos \theta, \quad (3.6.9)$$

where θ is the meridional angle defined such that $x = r \cos \theta$.

Using the first expression in (3.2.26), we find that the radial velocity component is given by

$$u_r = \frac{\partial \phi}{\partial r} = U_x \left(1 + \frac{d_x}{2\pi U_x} \frac{1}{r^3} \right) \cos \theta. \quad (3.6.10)$$

The sum inside the parentheses on the right-hand side of (3.6.10) is zero at the radial distance

$$r = \left(-\frac{d_x}{2\pi U_x} \right)^{1/3}. \quad (3.6.11)$$

Conversely, if the strength of the dipole has the value

$$d_x = -2\pi U_x a^3, \quad (3.6.12)$$

then the radial velocity vanishes at the radial distance $r = a$.

These observations suggest that the potential (3.6.9) with d_x evaluated from expression (3.6.12) describes uniform flow along the x axis with velocity U_x past a stationary sphere of radius a centered at the origin. Substituting (3.6.12) into (3.6.9), we obtain an explicit expression for the potential,

$$\phi = U_x \left(r + \frac{1}{2} \frac{a^3}{r^2} \right) \cos \theta. \quad (3.6.13)$$

The corresponding Cartesian velocity components are given by

$$\begin{aligned} u_x &= U_x \left(1 + \frac{1}{2} a^3 \left(\frac{1}{r^3} - 3 \frac{x^2}{r^5} \right) \right), \\ u_y &= -\frac{3}{2} U_x a^3 \frac{xy}{r^5}, \quad u_z = -\frac{3}{2} U_x a^3 \frac{xz}{r^5}. \end{aligned} \quad (3.6.14)$$

The streamline pattern in an azimuthal plane is shown in [Figure 3.5.3\(b\)](#). The structure of the flow is similar to that of flow past a cylinder with zero circulation shown in [Figure 3.5.3\(a\)](#).

3.6.4 Sources and dipoles in the presence of boundaries

To account for the presence of boundaries, we introduce a complementary flow whose purpose is to ensure the satisfaction of the no-penetration boundary condition, as discussed in Section 3.5.5 for two-dimensional flow. For simple boundary geometries, the complementary flow can be identified with the flow generated by singularities located at image positions outside the domain of flow.

Directory *lgf-3d*, residing inside directory *07-ptf* of **FDLIB**, contains a collection of sub-routines that evaluate the velocity field for several boundary geometries. The streamline pattern of the flow due to a point source located above a plane wall is shown in [Figure 3.6.1\(a\)](#). In this case, the complementary flow is due to a reflected point source. The streamline pattern of the flow due to a point source outside a sphere is shown in [Figure 3.6.1\(b\)](#).

PROBLEMS

3.6.1 Flow due to a three-dimensional point-source dipole

Express the potential and velocity field of a three-dimensional point source dipole in terms of (a) the vectorial strength of the dipole, (b) a three-component vector function, $\Phi^{3\text{DPSD}}$, and (c) a 3×3 matrix function, $\mathbf{U}^{3\text{DPSD}}$.

3.6.2 Stream functions

Introduce cylindrical polar coordinates with origin at the location of a three-dimensional point source or point-source dipole, and derive expressions for the axisymmetric (Stokes) stream function.

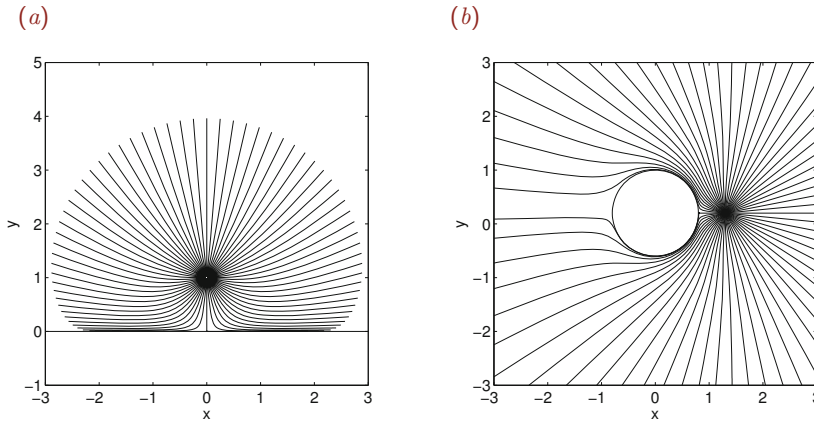


Figure 3.6.1 Streamline pattern in a azimuthal plane of the flow due to a three-dimensional point source (a) above a plane wall or (b) outside a sphere.

3.7 Point vortices and line vortices

Consider a long circular cylinder immersed in an infinite ambient fluid and rotating around its axis with a constant angular velocity, thereby generating a two-dimensional swirling flow in the xy plane.

In plane polar coordinates with origin at the center of the cylinder, $\mathbf{x}_0 = (x_0, y_0)$, the radial and angular velocity components are

$$u_r(\mathbf{x}) = 0, \quad u_\theta(\mathbf{x}) = \frac{\kappa}{2\pi} \frac{1}{r}, \quad (3.7.1)$$

where

$$r = \sqrt{(x - x_0)^2 + (y - y_0)^2} \quad (3.7.2)$$

is the distance of the point where the velocity is evaluated, $\mathbf{x} = (x, y)$, from the center of the cylinder, and κ is a constant with units of velocity multiplied by length.

The magnitude κ expresses the strength of the flow due to the rotation of the cylinder, and the sign of κ expresses the direction of rotation. If κ is positive, point particles in the flow rotate around the cylinder in the counterclockwise direction. If κ is negative, point particles in the flow rotate around the cylinder in the clockwise direction.

We note that the magnitude of the polar velocity component, u_θ , decays like $1/r$. If the fluid rotated as a rigid body with angular velocity Ω around the point \mathbf{x}_0 , the polar velocity u_θ would increase linearly with respect to radial distance, as $u_\theta = \Omega r$. It is clear that the velocity field expressed by (3.7.1) represents a flow that is different than rigid-body rotation.

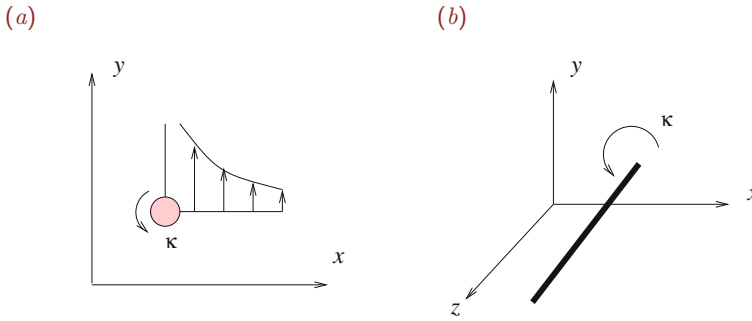


Figure 3.7.1 (a) Two-dimensional and (b) three-dimensional perspectives of a point vortex with positive strength representing a rectilinear line vortex parallel to the z axis.

Point vortex singularity

The flow described by equations (3.7.1) is physically meaningful only in the exterior of the cylinder. Neglecting the surface of the cylinder and extending the domain of flow all the way up to the center of the cylinder, we obtain a singular flow described as the flow due to a point vortex with strength κ , as illustrated in Figure 3.7.1(a). The singularity occurs because, as the distance of an observation point from the point vortex, r , tends to zero, the magnitude of the velocity diverges to infinity.

To confirm that the flow due to a point vortex is irrotational, we substitute expressions (3.7.1) into (2.3.20), and find that the z component of the vorticity vanishes everywhere in the flow, except at the location of the point vortex, \mathbf{x}_0 , where a singularity appears. These properties classify the point vortex as a singularity of two-dimensional irrotational flow.

A seemingly paradoxical behavior should be noted. Because the flow is irrotational at every point except at the location of the point vortex, small circular fluid parcels not containing the point vortex translate and deform but do not rotate around their center, and yet the fluid exhibits net circulatory motion. The apparent but not essential contradiction serves to underscore that global circulatory motion does not necessarily imply the occurrence of rotational flow.

3.7.1 The potential of irrotational circulatory flow

The presence of circulation has important implications on our ability to describe a flow in terms of a velocity potential. To see this, we use equations (3.2.28) and find that the potential due to a point vortex, denoted by ϕ^{PV} , satisfies the equations

$$\frac{\partial \phi^{\text{PV}}}{\partial r} = 0, \quad \frac{1}{r} \frac{\partial \phi^{\text{PV}}}{\partial \theta} = \frac{\kappa}{2\pi} \frac{1}{r}. \quad (3.7.3)$$

Integrating these equations, we obtain

$$\phi^{\text{PV}} = \frac{\kappa}{2\pi} \theta, \quad (3.7.4)$$

where θ is the polar angle measured around the point vortex in the counterclockwise direction. An arbitrary but irrelevant constant can be added to the right-hand side of (3.7.4). The corresponding stream function is

$$\psi^{\text{pv}} = -\frac{\kappa}{2\pi} \ln \frac{r}{\mathcal{L}}, \quad (3.7.5)$$

where \mathcal{L} is a specified length.

According to expression (3.7.4), as we move around the point vortex on a circular path in the counterclockwise direction, the potential increases in proportion to the angle θ . But then, as we return to the point of departure, because θ has increased by 2π , the potential has undergone a jump with respect to the initial value, equal to κ . We can continue traveling around the point vortex for one more turn, only to find that, each time we perform a complete rotation, the potential undergoes a jump equal to κ . This observation illustrates that the potential associated with a point vortex is multi-valued. Moreover, since the point of departure is arbitrary, the potential is multi-valued at every point in the flow.

We have discovered by example that circulatory motion is associated with a multi-valued potential and *vice versa*. In practice, a multi-valued potential is too much to handle by analytical and numerical methods. To circumvent this difficulty, we decompose the potential into an easy multi-valued part and a harder complementary single-valued part; we specify the former, and extract the latter by analytical or numerical methods. The implementation of this method will be discussed in Chapter 12 in the context of aerodynamics.

In an alternative approach, we introduce an artificial boundary residing inside the fluid called a branch cut, and work under the assumption that the potential has two different values on either side of the brunch cut. If the flow does not exhibit net circulatory motion, the two values are identical.

3.7.2 Flow past a circular cylinder

To illustrate the usefulness of the point vortex singularity, we consider streaming (uniform) flow past a circular cylinder, as discussed in Section 3.5. Equation (3.5.48) provides us with the single-value harmonic potential in the absence of circulatory motion around the cylinder.

To allow for circulatory motion, we add to the right-hand side of (3.5.48) the potential due to a point vortex situated at the center of cylinder, given in equation (3.7.4), obtaining

$$\phi = U_x \left(r + \frac{a^2}{r} \right) \cos \theta + \frac{\kappa}{2\pi} \theta. \quad (3.7.6)$$

The corresponding Cartesian velocity components are

$$u_x = U_x \left(1 + \frac{a^2}{r^2} - 2 \frac{x^2}{r^4} a^2 \right) - \frac{\kappa}{2\pi} \frac{y}{r^2}, \quad u_y = -U_x 2 \frac{xy}{r^4} a^2 + \frac{\kappa}{2\pi} \frac{x}{r^2}. \quad (3.7.7)$$

Since the radial velocity component, $u_r = \partial\phi/\partial r$, is zero over the surface of the cylinder located at $r = a$, the no-penetration condition is satisfied.

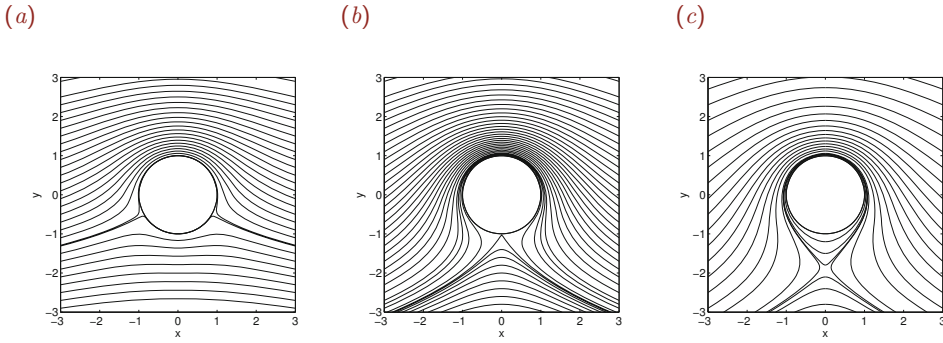


Figure 3.7.2 Streamline pattern of uniform (streaming) flow past a circular cylinder with different degrees of circulation around the cylinder determined by the dimensionless parameter β defined in equation (3.7.9); (a) $\beta = 0.5$, (b) 1.0 , and (c) 1.2 . The streamline pattern in the absence of circulation, $\beta = 0$, is shown in Figure 3.5.3(a).

Rearranging (3.7.6), we obtain the dimensionless form

$$\phi = U_x a \left(\cos \theta \left(\hat{r} + \frac{1}{\hat{r}} \right) - 2\beta \theta \right), \tag{3.7.8}$$

where $\hat{r} = r/a$ is the scaled radial distance defined such that $\hat{r} = 1$ corresponds to the cylinder surface, and

$$\beta \equiv -\frac{\kappa}{4\pi V_x a} \tag{3.7.9}$$

is a dimensionless circulation parameter. When $\beta = 0$, the circulation around the cylinder vanishes. Expression (3.7.8) reveals that the structure of the flow is determined by the dimensionless parameter β .

The tangential component of the velocity at the surface of the cylinder is given by

$$u_\theta(r = a) = -2 V_x \sin \theta + \frac{\kappa}{2\pi a} = -2 V_x (\sin \theta + \beta). \tag{3.7.10}$$

We note that the magnitude of the velocity is zero when $\theta = \arcsin(-\beta)$, and conclude that stagnation points develop on the surface on the cylinder when $-1 \leq \beta \leq 1$.

When $\beta = 0$, two stagnation points occur in the horizontal mid-plane of the cylinder located at $\theta = 0$ and π . As β increases from zero to unity, the stagnation points move downward and finally merge at lowest point of the cylinder, $\theta = -\frac{1}{2}\pi$. When β exceeds the value of unity, the merged stagnation points move off the surface of the cylinder into the flow. Streamline patterns for $\beta = 0.5$, 1.0 , and 1.2 illustrating this transition are shown in Figure 3.7.2.

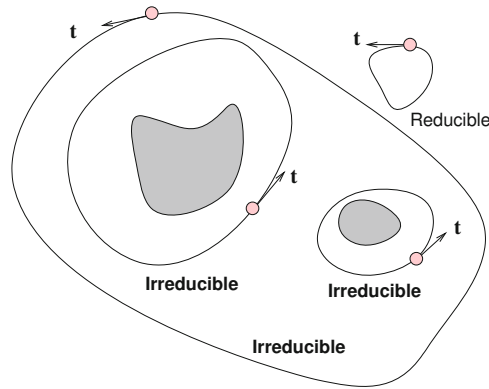


Figure 3.7.3 Illustration of reducible and irreducible loops in a two-dimensional flow. The shaded areas represent flow boundaries.

3.7.3 Circulation

Having discussed the effect of the circulation around a cylinder placed in a uniform flow, we proceed to extend the concept of circulation to a more general framework.

Consider a two-dimensional flow in the xy plane, and draw a simple closed loop inside the flow. If the loop encloses fluid alone and no boundaries, the loop is called reducible. If the loop encloses fluid and one or more boundaries, the loop is called irreducible. The distinguishing feature of a reducible loop is that it can be shrunk to a point without crossing flow boundaries. One reducible and three irreducible loops are depicted in [Figure 3.7.3](#).

Next, we select a point on a reducible or irreducible loop and introduce the unit tangent vector pointing in the counterclockwise direction, $\mathbf{t} = (t_x, t_y)$, as shown in [Figure 3.7.3](#). The inner product of the velocity and the unit tangent vector is given by

$$u_t = \mathbf{u} \cdot \mathbf{t} = u_x t_x + u_y t_y. \quad (3.7.11)$$

The circulation around the loop is defined as the line integral of the tangential component of the velocity with respect to arc length around the loop, ℓ ,

$$C \equiv \oint_{\mathcal{L}} u_t \, d\ell = \oint_{\mathcal{L}} \mathbf{u} \cdot \mathbf{t} \, d\ell, \quad (3.7.12)$$

where \mathcal{L} denotes the loop and $d\ell = \sqrt{dx^2 + dy^2}$ is an infinitesimal arc length around the loop.

Reducible loops

Stokes's circulation theorem discussed in Section 11.1 states that, in the absence of point vortices inside the area enclosed by a reducible loop, the circulation around the loop is equal

to the strength of the vorticity integrated over the area of fluid enclosed by the loop, \mathcal{D} ,

$$C = \iint_{\mathcal{D}} \omega_z \, dA. \quad (3.7.13)$$

In this case, the right-hand sides of (3.7.12) and (3.7.13) are equal.

An important consequence of Stokes's circulation theorem is that, because the vorticity of an irrotational flow vanishes at every point, the circulation around any reducible loop drawn in an irrotational flow is precisely zero. Important implications of this property will be discussed in Chapter 11 in the context of vortex dynamics.

Reducible loops enclosing point vortices

The circulation around a reducible loop that encloses a collection of N point vortices with strengths $\kappa_1, \kappa_2, \dots, \kappa_N$ is equal to the sum of the strengths of the point vortices,

$$C = \sum_{i=1}^N \kappa_i. \quad (3.7.14)$$

If some point vortices have positive strength and other point vortices have negative strength, so that the sum of the strengths is zero, the circulation around the loop is also zero.

As an example, we consider uniform flow past a circular cylinder described by the potential shown in (3.7.6). To confirm that the circulation around any loop that encloses the cylinder is equal to κ , we compute the circulation around a loop of radius b centered at the cylinder, and find the expected result

$$C \equiv \oint u_t \, d\ell = \oint u_\theta b \, d\theta = b \oint \frac{1}{r} \frac{\partial \phi}{\partial \theta} \, d\theta = b \frac{1}{b} \oint \frac{\kappa}{2\pi} \, d\theta = \kappa, \quad (3.7.15)$$

where $d\ell = b \, d\theta$ is the arc length around the loop.

Irreducible loops

The circulation around a loop that encloses one boundary or multiple boundaries in a two-dimensional irrotational flow can be arbitrary. In practice, the amount of circulation is set up internally during a start up period when the flow develops from the state of rest. The circulation established spontaneously around a moving body is of central interest in aerodynamics, as discussed in Chapter 12.

3.7.4 Line vortices in three-dimensional flow

Viewed from a three-dimensional perspective, a point vortex in the xy plane appears like a rectilinear line vortex parallel to the z axis, as shown in [Figure 3.7.1\(b\)](#). Deforming this rectilinear line vortex or merging its two ends to form a loop, we obtain a curved three-dimensional line vortex in a three-dimensional flow. One example familiar to cigar smokers is a closed line vortex with a circular or wobbly shape, called a line vortex ring.

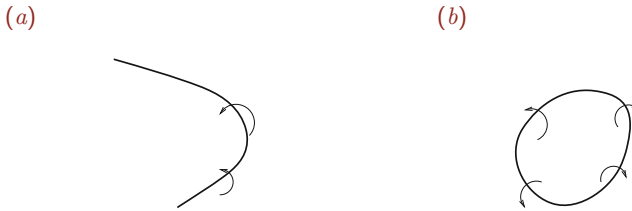


Figure 3.7.4 Illustration of (a) an open and (b) a closed line vortex in a three-dimensional flow.

A line vortex can be infinite, as illustrated in Figure 3.7.4(a), or closed, as illustrated in Figure 3.7.4(b). However, a line vortex may not end suddenly in the interior of a fluid. In real life, a fluid is always bounded by a rigid or deformable surface and an otherwise infinite line vortex inevitably ends at the boundaries.

The analysis and computation of the flow associated with, or induced by a three-dimensional line vortex constitutes an important field of fluid mechanics with important applications in turbulent fluid motion and aerodynamics, as discussed in Chapters 11 and 12.

PROBLEMS

3.7.1 Circulation around a loop in the xy plane

Consider a closed loop in the xy plane performing m turns around a point vortex with strength κ , where m is an arbitrary integer. Explain why the circulation around this loop is equal to $m\kappa$.

3.7.2 Point vortex dipole

Just as the point-source dipole arises from a point source/sink dipole, as discussed in Section 3.5, a point-vortex dipole arises from a point vortex with positive strength and a point vortex with negative strength of equal magnitude, in the limit as the distance between the two point vortices tends to zero while their strength increases by inverse proportion. The harmonic potential associated with a point vortex dipole oriented along the x or y axis is given, respectively, by

$$\phi^{\text{PVD}_x}(x, y) = \lambda_x \frac{\partial \phi^{\text{PV}}}{\partial x_0}, \quad \phi^{\text{PVD}_y}(x, y) = \lambda_y \frac{\partial \phi^{\text{PV}}}{\partial y_0}, \quad (3.7.16)$$

where λ_x and λ_y are the components of the vectorial strength of the point-vortex dipole in the x and y direction.

Carry out the differentiations on the right-hand sides of (3.7.16) and compare the resulting expressions with those shown in equations (3.5.25) and (3.5.33) for the two-dimensional point-source dipole. Based on this comparison, establish a relationship between the flow due to a point-vortex dipole and the flow due to a point-source dipole.

3.7.3 Irreducible loops in three-dimensional flow

- (a) Consider a three-dimensional domain of flow extending to infinity and bounded internally by a toroidal boundary having the shape of a donut. Show that this flow contains irreducible loops that may not be shrunk to a point without crossing flow boundaries.
- (b) Invent another three-dimensional domain of flow containing irreducible loops.

Forces and stresses

- 4.1 Body forces and surface forces**
- 4.2 Traction and the stress tensor**
- 4.3 Traction jump across a fluid interface**
- 4.4 Force balance at a three-dimensional interface**
- 4.5 Stresses in a fluid at rest**
- 4.6 Constitutive equations**
- 4.7 Pressure in compressible fluids**
- 4.8 Simple non-Newtonian fluids**
- 4.9 Stresses in polar coordinates**
- 4.10 Boundary conditions for the tangential velocity**
- 4.11 Wall stresses in Newtonian fluids**
- 4.12 Interfacial surfactant transport**

Previously in this book, we discussed the kinematic structure of a flow but made no reference to the external action that is necessary to establish a flow or to the physical mechanism that is necessary to sustain the motion of the fluid. To address these issues, in this chapter we turn our attention to the hydrodynamic forces developing in a fluid as a result of the motion and introduce constitutive equations relating the stresses developing at the surface of infinitesimal fluid parcels to the parcel motion and deformation. The constitutive equations will then be incorporated into an integrated theoretical framework based on Newton's law of motion that will allow us to compute the structure of a steady flow and the evolution of an unsteady flow from a specified initial configuration.

4.1 Forces acting in a fluid

Two types of forces are exerted on any coherent piece of a material: a homogeneous force acting on its volume, and a surface force acting on its boundaries.

4.1.1 Body force

A fluid parcel, like any other piece of material, is subject to a force mediated by an ambient gravitational, electrical, electromagnetic, or any other external force field acting on its volume. Electrical and electromagnetic forces arise when the fluid is electrically charged or contains molecules or small particles of a polarized material.

Under the influence of such fields, the molecules residing inside a fluid parcel are acted upon individually and independently by a force that may be constant or vary with position inside the parcel. The sum of the forces exerted on the individual molecules amounts to a net body force that is proportional to the number of molecules residing inside the parcel, and thus to the parcel volume.

Gravitational body force

Let $\delta\mathbf{F}_p$ be the gravitational force exerted on a small fluid parcel with volume δV_p , density ρ , and mass $\delta m_p = \rho \delta V_p$. By definition,

$$\delta\mathbf{F}_p = \mathbf{g} \rho \delta V_p, \quad (4.1.1)$$

where \mathbf{g} is the acceleration of gravity. The right-hand side of (4.1.1) has units of acceleration multiplied by mass, which amounts to force.

One distinguishing feature of the body force due to gravity is that it is considered to be independent of molecular motions. This means that a certain mass of fluid weighs the same, independent of whether the fluid is stationary or flows.

4.1.2 Surface force

A different type of force arises at the surface of a fluid parcel and at the boundaries of a flow, such as the surface of a bubble rising through an ambient liquid or the windshield of a moving vehicle. More generally, a surface force can be defined on any fictitious surface that is drawn inside the bulk of a fluid or over its boundary.

Understanding the physical origin of the surface force requires consideration of molecular motions and necessitates a distinction between gases and liquids. A key idea is the equivalence between local hydrodynamic force and rate of exchange of momentum between adjacent fluid layers due to molecular excursions.

Gases

To understand the origin of surface forces developing in a gas, we draw a surface in the interior of the gas and consider the momentum of the molecules that cross the surface from either side. A key realization is that the momentum normal to the surface is responsible for a normal force.

If the molecules move with different average tangential velocities on either side of the surface, the net transport of tangential momentum is responsible for a tangential surface force necessary to accelerate or decelerate the molecules. In the present context, the average velocity of a molecule can be identified with the velocity of the fluid at the location where a molecule last underwent a collision with one of its peers. The effective force field due to the tangential surface force slows down fast-moving molecules as they approach regions of slower-moving fluid.

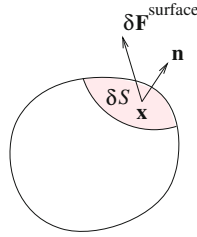


Figure 4.2.1 Illustration of a small section on the surface of a fluid parcel, δS , introduced to define the hydrodynamic traction exerted on the parcel.

Liquids

The physical origin of surface forces developing in a liquid is somewhat different. The molecules of a liquid perform oscillatory motion around a mean position with an amplitude that is determined by their distance from closely spaced neighbors. Occasional excursions into vacant spots are responsible for momentum transport attributed to the action of a surface force.

PROBLEM

4.1.1 Friction

The friction on a body sliding over a horizontal surface imparts to the body a tangential surface force that depends on the body weight. Does this frictional force also depend on the contact area?

4.2 Traction and the stress tensor

Consider a small surface with area δS centered at a point, $\mathbf{x} = (x, y, z)$, in a stationary or moving fluid, as illustrated in [Figure 4.2.1](#). The designated outer side of the surface is indicated by the direction of the unit vector normal to the surface at the point \mathbf{x} , denoted by $\mathbf{n} = (n_x, n_y, n_z)$. According to our discussion in Section 4.1, a body of fluid whose instantaneous boundary includes the small surface under consideration experiences a surface force, $\delta \mathbf{F}^{\text{surface}}$, that may point in any direction; that is, it may have a component normal to the surface and a component tangential to the surface.

Traction

The ratio between the surface force, $\delta \mathbf{F}^{\text{surface}}$, and the area of the surface, δS , is the average stress exerted on the small surface. As the surface area δS becomes infinitesimal, the average stress tends to a limit defined as the traction exerted on an infinitesimal surface and is denoted by \mathbf{f} . Thus, by definition,

$$\mathbf{f} \equiv \frac{\delta \mathbf{F}^{\text{surface}}}{\delta S} \quad (4.2.1)$$

in the limit as δS becomes infinitesimal. The three scalar components of the traction have units of force per area, which amounts to stress.

Force in terms of traction

Rearranging equation (4.2.1), we obtain an expression for the surface force exerted on an infinitesimal surface in terms of the traction,

$$\delta \mathbf{F}^{\text{surface}} = \mathbf{f} \delta S. \quad (4.2.2)$$

Integrating the traction over a specified surface area, such as the boundary of a fluid parcel, we obtain a resultant surface force.

Dependence on position and orientation

It is clear from relation (4.2.1) that the traction is defined only when the location and orientation of an infinitesimal surface upon which the traction is exerted are specified, respectively, in terms of the coordinates of the center-point, \mathbf{x} , and orientation of the unit normal vector, \mathbf{n} . This requirement is signified by writing

$$\mathbf{f}(\mathbf{x}, \mathbf{n}), \quad (4.2.3)$$

where the parentheses enclose the arguments of the three scalar components of the traction. If a flow is unsteady, or the position or orientation of the surface change in time, time, t , should be added to the arguments on the right-hand side of (4.2.3).

The stress tensor

The traction exerted on a small surface that is perpendicular to the x , y , or z axis, is denoted by

$$\begin{aligned} \mathbf{f}^{(x)} &= [f_x^{(x)}, f_y^{(x)}, f_z^{(x)}], \\ \mathbf{f}^{(y)} &= [f_x^{(y)}, f_y^{(y)}, f_z^{(y)}], \\ \mathbf{f}^{(z)} &= [f_x^{(z)}, f_y^{(z)}, f_z^{(z)}], \end{aligned} \quad (4.2.4)$$

respectively, where the unit normal vector, \mathbf{n} points in the positive directions of these axes, as depicted in [Figure 4.2.2](#). Stacking these vectors on top of one another in a particular order, we obtain the 3×3 stress tensor

$$\boldsymbol{\sigma} \equiv \begin{bmatrix} f_x^{(x)} & f_y^{(x)} & f_z^{(x)} \\ f_x^{(y)} & f_y^{(y)} & f_z^{(y)} \\ f_x^{(z)} & f_y^{(z)} & f_z^{(z)} \end{bmatrix} \quad (4.2.5)$$

in a three-dimensional flow, and a corresponding 2×2 tensor in a two-dimensional flow.

Next, we introduce the standard two-index notation for the components of the stress tensor,

$$\boldsymbol{\sigma} = \begin{bmatrix} \sigma_{xx} & \sigma_{xy} & \sigma_{xz} \\ \sigma_{yx} & \sigma_{yy} & \sigma_{yz} \\ \sigma_{zx} & \sigma_{zy} & \sigma_{zz} \end{bmatrix}, \quad (4.2.6)$$

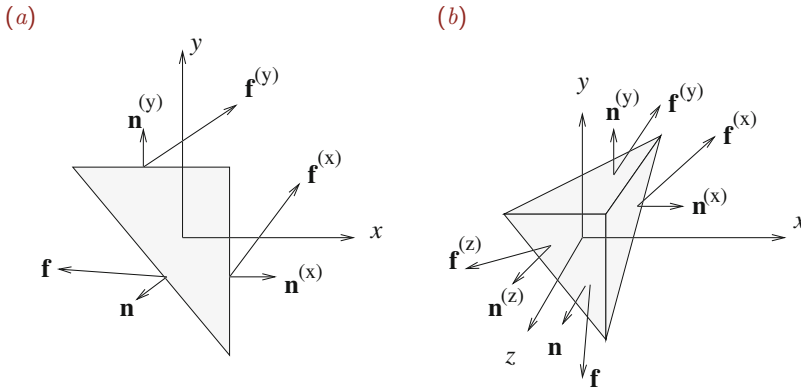


Figure 4.2.2 Illustration of (a) a triangular fluid parcel in a two-dimensional flow and (b) a tetrahedral fluid parcel in a three-dimensional fluid. These parcels are used as devices for computing the traction exerted on an arbitrary surface in terms of (a) the unit vector normal to the surface, and (b) the stress tensor.

and find that, by definition,

$$\sigma_{ij} \equiv f_j^{(i)} \tag{4.2.7}$$

for $i, j = x, y, z$. The first index of σ_{ij} indicates the component of the normal vector on the infinitesimal surface upon which the traction is exerted. The second index indicates the component of the corresponding traction.

We will see that, in the absence of an externally induced torque, the stress tensor is symmetric,

$$\sigma_{ij} = \sigma_{ji}. \tag{4.2.8}$$

For example, $\sigma_{xy} = \sigma_{yx}$.

In the case of two-dimensional flow in the xy plane, the stresses are encapsulated in a 2×2 stress tensor,

$$\boldsymbol{\sigma} = \begin{bmatrix} \sigma_{xx} & \sigma_{xy} \\ \sigma_{yx} & \sigma_{yy} \end{bmatrix}. \tag{4.2.9}$$

The five omitted components involving the subscript z are either constant or zero.

Traction in terms of the stress tensor

We will demonstrate that the dependence of the traction on the position vector, \mathbf{x} , and normal vector, \mathbf{n} , displayed symbolically in (4.2.3), can be decoupled in a simple fashion, yielding

$$\mathbf{f}(\mathbf{x}, \mathbf{n}) = \mathbf{n} \cdot \boldsymbol{\sigma}(\mathbf{x}). \tag{4.2.10}$$

Specifically,

$$[f_x, f_y, f_z] = [n_x, n_y, n_z] \cdot \begin{bmatrix} \sigma_{xx} & \sigma_{xy} & \sigma_{xz} \\ \sigma_{yx} & \sigma_{yy} & \sigma_{yz} \\ \sigma_{zx} & \sigma_{zy} & \sigma_{zz} \end{bmatrix}. \quad (4.2.11)$$

In index notation,

$$f_j(\mathbf{x}, \mathbf{n}) = n_i \sigma_{ij} = n_x \sigma_{xj} + n_y \sigma_{yj} + n_z \sigma_{zj}, \quad (4.2.12)$$

where summation is implied over the repeated index, i , in the middle expression of (4.2.12), while the index j is free to vary over x , y , or z .

An important consequence of (4.2.10) is that, if the nine components of the stress tensor are known at a point, then the traction exerted on any infinitesimal surface centered at that point can be evaluated in terms of the unit normal vector, \mathbf{n} , merely by carrying out a vector-matrix multiplication.

To confirm that expression (4.2.10) is consistent with the foregoing definitions, we choose $\mathbf{n} = (1, 0, 0)$ and carry out the vector-matrix multiplication on the right-hand side of (4.2.12) to find that $\mathbf{f} = \mathbf{f}^{(x)}$, as required. Working in a similar fashion with $\mathbf{n} = (0, 1, 0)$ and $\mathbf{n} = (0, 0, 1)$, we obtain $\mathbf{f} = \mathbf{f}^{(y)}$ and $\mathbf{f} = \mathbf{f}^{(z)}$, as required.

It remains to show that (4.2.10) holds true for general orientations of the unit normal vector, \mathbf{n} . For simplicity, we present the proof for two-dimensional flow in the xy plane with reference to the 2×2 stress tensor defined in (4.2.9).

Force balance on a small triangular parcel

Consider a small area of fluid enclosed by an infinitesimal triangle with two sides perpendicular to the x and y axes, as shown in [Figure 4.2.2\(a\)](#). Newton's second law of motion requires that the rate of change of the momentum of the fluid enclosed by the triangle is balanced by the forces exerted on the triangle. The forces include the body force and the surface force associated with the traction exerted on the three sides.

The momentum of the parcel and the body force exerted on the parcel are both proportional to the area of the triangle, $\frac{1}{2} \Delta x \Delta y$. The surface force exerted on the vertical side is equal to $\mathbf{f}^{(x)} \Delta y$, the surface force exerted on the horizontal side is equal to $\mathbf{f}^{(y)} \Delta x$, and the surface force exerted on the slanted side is equal to $\mathbf{f} \Delta \ell$, where $\Delta \ell$ is the length of the slanted side, $\Delta \ell = (\Delta x^2 + \Delta y^2)^{1/2}$.

In the limit as Δx and Δy tend to zero, the fluid momentum and the body force become negligible compared to the surface force exerted on the sides, and the sum of the three surface forces must balance to zero. Setting the x and y components of the sum to zero, we obtain

$$f_x \Delta \ell + \sigma_{xx} \Delta y + \sigma_{yx} \Delta x = 0, \quad f_y \Delta \ell + \sigma_{xy} \Delta y + \sigma_{yy} \Delta x = 0. \quad (4.2.13)$$

Using elementary trigonometry, we find that the x and y components of the outward unit

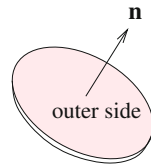


Figure 4.2.3 Illustration of a thin fluid layer with a designated inner and outer side. The outer side is indicated by the direction of the unit normal vector, \mathbf{n} .

vector normal to the slanted side of the triangle are given by

$$n_x = -\frac{\Delta y}{\Delta \ell}, \quad n_y = -\frac{\Delta x}{\Delta \ell}. \quad (4.2.14)$$

Combining equations (4.2.13) and (4.2.14), we find that

$$f_x = n_x \sigma_{xx} + n_y \sigma_{yx}, \quad f_y = n_x \sigma_{xy} + n_y \sigma_{yy}, \quad (4.2.15)$$

which are precisely the x and y components of (4.2.10).

To carry out an analogous proof for three-dimensional flow, we consider the forces exerted on the sides and over the volume of a tetrahedral fluid parcel, as illustrated in Figure 4.2.2(b), and work in similar ways (Problem 4.2.1).

4.2.1 Traction on either side of a fluid surface

Next, we consider a thin fluid layer with a designated outer side indicated by the direction of the unit normal vector, \mathbf{n} , and a designated inner side indicated by the direction of the opposite normal vector, $\mathbf{n}^{\text{inner}} = -\mathbf{n}$, as illustrated in Figure 4.2.3. Balancing the rate of change of momentum of the fluid residing inside the thin layer with the forces exerted on the layer, and repeating the preceding arguments on the insignificance of the fluid momentum and body force compared to the surface force, we derive the force balance equation

$$\mathbf{f}^{\text{outer}} + \mathbf{f}^{\text{inner}} = \mathbf{0}, \quad (4.2.16)$$

which is a statement of Newton's third law of action and reaction, stating that the force exerted on one body by a second body is equal in magnitude and opposite in direction to the force exerted by the second body on the first body.

It is reassuring to confirm that expression (4.2.10) is consistent with the physical law expressed by (4.2.16). Substituting the former into the latter, we obtain

$$\mathbf{n} \cdot \boldsymbol{\sigma} + \mathbf{n}^{\text{inner}} \cdot \boldsymbol{\sigma} = \mathbf{0}, \quad (4.2.17)$$

which is true in light of the definition $\mathbf{n}^{\text{inner}} = -\mathbf{n}$. More generally, for (4.2.16) to be true, it must be that

$$\mathbf{f}(\mathbf{x}, -\mathbf{n}) = -\mathbf{f}(\mathbf{x}, \mathbf{n}), \quad (4.2.18)$$

which is clearly satisfied by the right-hand side of (4.2.10).

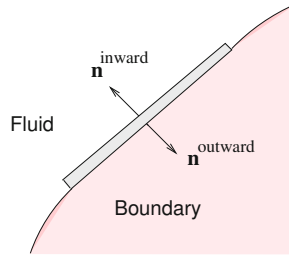


Figure 4.2.4 Illustration of a thin fluid layer adjacent to a boundary used to define the hydrodynamic force exerted on the boundary.

4.2.2 Traction on a boundary

Now we consider a small fluid surface residing at the boundary of a flow. The outer side of the fluid surface is indicated by the unit normal vector $\mathbf{n}^{\text{outward}}$ pointing into the boundary, as illustrated in Figure 4.2.4. Newton's third law of action and reaction requires that the traction exerted on the surface should balance the traction exerted by the fluid on the boundary, $\mathbf{f}^{\text{boundary}}$, so that

$$\mathbf{f}^{\text{boundary}} + \mathbf{n}^{\text{outward}} \cdot \boldsymbol{\sigma} = \mathbf{0}. \quad (4.2.19)$$

In terms of the inward unit normal vector pointing into the fluid, $\mathbf{n}^{\text{inward}} = -\mathbf{n}^{\text{outward}}$, we obtain

$$\mathbf{f}^{\text{boundary}} = \mathbf{n}^{\text{inward}} \cdot \boldsymbol{\sigma}. \quad (4.2.20)$$

Expression (4.2.20) allows us to compute the traction exerted on a boundary in terms of the stress tensor evaluated at the boundary.

4.2.3 Symmetry of the stress tensor

The torque with respect to a specified point, \mathbf{x}_0 , due to a force, \mathbf{F} , applied at a point, \mathbf{x} , is defined by the outer vector product

$$\mathbf{T}(\mathbf{x}_0) \equiv (\mathbf{x} - \mathbf{x}_0) \times \mathbf{F}. \quad (4.2.21)$$

A fundamental law of mechanics originating from Newton's second law of motion requires that the rate of change of angular momentum of a fluid parcel should be balanced by the torque exerted on the fluid parcel, including the torque due to the body force and the torque due to the surface force.

Applying this law for a rectangular fluid parcel whose sides are parallel to the x , y , and z , axes, we find, that, in the absence of a body force inducing a torque, the tangential component of the traction in the j th direction exerted on the side that is perpendicular to the i th axis must be equal to the tangential component of the traction in the i th direction

exerted on the side that is perpendicular to the j th axis, otherwise an imbalance will arise (Problem 4.2.2). Thus,

$$f_j^{(i)} = f_i^{(j)}, \quad (4.2.22)$$

stating that the stress tensor is symmetric,

$$\sigma_{ij} = \sigma_{ji}. \quad (4.2.23)$$

The diagonal components of the stress tensor can be arbitrary.

It is important to emphasize that the stress tensor is symmetric only in the absence of an externally induced torque, that is, in the absence of an external force field causing point particles to spin. This condition is tacitly assumed in the remainder of this book.

PROBLEMS

4.2.1 Traction in three-dimensional flow

Prove expression (4.2.10) for three-dimensional flow. *Hint:* Perform a force balance over the polyhedral volume depicted in Figure 4.2.2(b).

4.2.2 Symmetry of the stress tensor

Demonstrate the symmetry of the stress tensor for two-dimensional flow in the absence of an externally induced torque.

4.3 Traction jump across a fluid interface

Equation (4.2.16) states that the traction exerted on one side of a surface drawn inside a fluid is equal in magnitude and opposite in direction to that exerted on the other side. To derive this relation, we performed a force balance over a thin fluid layer centered at the surface, considering the force exerted along the edges infinitesimal. If the fluid residing inside this layer is homogeneous, the edge force scales with the layer thickness and is negligible indeed compared to the surface force exerted on the two sides.

However, if a thin layer straddles the interface between two different fluids instead of a regular surface residing inside a homogeneous fluid, differences in the magnitude of intermolecular forces on either side of the layer generate an effective edge force that does not scale with the layer thickness.

4.3.1 Interfacial tension

The interfacial edge force can be expressed in terms of the interfacial tension, also called the surface tension, γ , defined as the *tangential force per differential arc length* exerted around the edge of a section of an interface. In fact, the surface tension is the integrated normal stress exerted in a plane that is normal to the interface over a thin interfacial layer where the

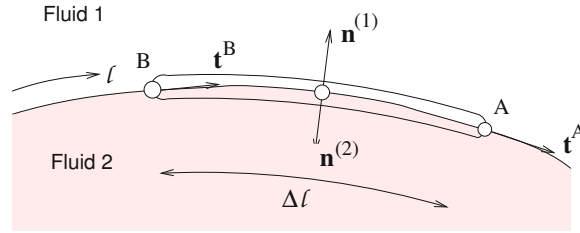


Figure 4.3.1 Illustration of forces exerted on a thin fluid layer centered at a two-dimensional interface, including the hydrodynamic force due to the fluid stresses and the force due to the surface tension.

physical properties of the medium undergo a rapid transition. Interfaces with membrane-like constitution exhibit tangential as well as normal interfacial tensions and possibly bending moments. In the most general case, an interface behaves like a thin shell, such as a dome or an egg shell.

Simple interfaces and surfactants

Consider a simple interface separating two immiscible liquids or a gas from a liquid. The surface tension pulls the interfacial layer in a direction that is tangential to the interface and normal to the edges. The magnitude of the surface tension depends on the local temperature and on the molecular constitution of the interface determined by the concentration of surface active substances residing over the interface, called surfactants, as will be discussed in Section 4.10. The higher the temperature or the concentration of a surfactant, the lower the surface tension.

Surfactants are often added to liquids to lower the surface tension and achieve a desired effect. A dish or laundry detergent is a common household surfactant used to lower the strength of the forces anchoring particles to a soiled surface. In engineering applications, surfactants are used to disperse oil spills.

4.3.2 Force balance at a two-dimensional interface

To illustrate the action of the surface tension, we consider a small section of a two-dimensional interface with length $\Delta\ell$, as shown in Figure 4.3.1. Surface tension pulls the layer forward and backward at the two edges in directions that are tangential to the interface at the two end points, A and B.

Balancing the surface force exerted on the upper and lower sides due to the stresses in each fluid and the edge forces, we obtain the vectorial equilibrium condition

$$[\mathbf{n}^{(1)} \cdot \boldsymbol{\sigma}^{(1)}] \Delta\ell + [\mathbf{n}^{(2)} \cdot \boldsymbol{\sigma}^{(2)}] \Delta\ell + \gamma^A \mathbf{t}^A - \gamma^B \mathbf{t}^B = \mathbf{0}, \quad (4.3.1)$$

where the unit normal vector $\mathbf{n}^{(1)}$ points into the fluid labeled 1 by convention, while the unit normal vector $\mathbf{n}^{(2)} = -\mathbf{n}^{(1)}$ points into the fluid labeled 2.

Now we express the second normal vector in terms of the first normal vector and rearrange the resulting expression to obtain

$$\mathbf{n}^{(1)} \cdot (\boldsymbol{\sigma}^{(1)} - \boldsymbol{\sigma}^{(2)}) = -\frac{\gamma^A \mathbf{t}^A - \gamma^B \mathbf{t}^B}{\Delta\ell}. \quad (4.3.2)$$

If the surface tension is uniform across the length of the interfacial element under consideration, then $\gamma^B = \gamma^A$. If, in addition, the interface is flat, $\mathbf{t}^B = \mathbf{t}^A$, the vectorial difference $\mathbf{t}^B - \mathbf{t}^A$ is zero and the right-hand side of (4.3.2) vanishes. Equation (4.3.2) then requires that the traction is continuous across the interface in the absence of a net contribution due to the surface tension.

As the length of the interfacial segment, $\Delta\ell$, tends to zero, the fraction on the right-hand side of (4.3.2) tends to the derivative of the product $\gamma\mathbf{t}$ with respect to arc length, ℓ , measured in the direction of the tangent vector \mathbf{t} from an arbitrary origin, yielding

$$\mathbf{n}^{(1)} \cdot (\boldsymbol{\sigma}^{(1)} - \boldsymbol{\sigma}^{(2)}) = -\frac{d(\gamma\mathbf{t})}{d\ell}. \quad (4.3.3)$$

Expanding the derivative of the product on the right-hand side, we find that

$$\mathbf{n}^{(1)} \cdot (\boldsymbol{\sigma}^{(1)} - \boldsymbol{\sigma}^{(2)}) = -\gamma \frac{d\mathbf{t}}{d\ell} - \frac{d\gamma}{d\ell} \mathbf{t}. \quad (4.3.4)$$

The second term on the right-hand side contributes a traction discontinuity tangential to the interface, known as the *Marangoni traction*. If the surface tension is uniform over the interface, the Marangoni traction does not appear.

Curvature

To interpret the first term on the right-hand side of (4.3.4), we consider the difference between the two nearly equal tangential vectors \mathbf{t}^A and \mathbf{t}^B . As the arc length, $\Delta\ell$, tends to zero, the difference between these vectors tends to a new vector that is directed normal to the interface. More precisely, in this limit, the ratio $(\mathbf{t}^A - \mathbf{t}^B)/\Delta\ell$ tends to the derivative

$$\frac{d\mathbf{t}}{d\ell} = -\kappa \mathbf{n}^{(1)}, \quad (4.3.5)$$

where κ is the positive or negative curvature of the interface; for the shape shown in [Figure 4.3.1](#), the curvature is positive, $\kappa > 0$.

To understand why the derivative $d\mathbf{t}/d\ell$ is normal to the interface, we approximate the derivative with the ratio $(\mathbf{t}^A - \mathbf{t}^B)/\Delta\ell$, and rearrange to obtain

$$\mathbf{t}^A \simeq \mathbf{t}^B - \kappa \mathbf{n}^{(1)}. \quad (4.3.6)$$

The second term on the right-hand side inclines \mathbf{t}^B against $\mathbf{n}^{(1)}$ to generate \mathbf{t}^A , as shown in [Figure 4.3.1](#).

Taking the inner product of both sides of equation (4.3.5) with the unit normal vector $\mathbf{n}^{(1)}$, we derive an expression for the curvature,

$$\kappa = -\mathbf{n}^{(1)} \cdot \frac{d\mathbf{t}}{d\ell}, \quad (4.3.7)$$

which can be restated as

$$\kappa = -\frac{dx}{d\ell} \mathbf{n}^{(1)} \cdot \frac{d\mathbf{t}}{dx} = -\frac{dy}{d\ell} \mathbf{n}^{(1)} \cdot \frac{d\mathbf{t}}{dy}. \quad (4.3.8)$$

By definition, $\kappa = 1/R$, where R is the positive or negative radius of curvature of the interface. For the shape shown in [Figure 4.3.1](#), the radius of curvature is positive, $R > 0$.

Conversely, the derivative of the unit normal vector is parallel to the unit tangential vector,

$$\frac{d\mathbf{n}^{(1)}}{d\ell} = \kappa \mathbf{t}, \quad (4.3.9)$$

yielding

$$\kappa = \mathbf{t} \cdot \frac{d\mathbf{n}^{(1)}}{d\ell}. \quad (4.3.10)$$

Equations (4.3.5) and (4.3.9) comprise the *Frenet–Serret relations* in differential geometry.

Laplace pressure

Substituting (4.3.5) into (4.3.4) and rearranging, we derive the final expression for the jump in the interfacial traction across a two-dimensional interface,

$$\Delta \mathbf{f} \equiv \mathbf{n}^{(1)} \cdot (\boldsymbol{\sigma}^{(1)} - \boldsymbol{\sigma}^{(2)}) = \gamma \kappa \mathbf{n}^{(1)} - \frac{d\gamma}{d\ell} \mathbf{t}. \quad (4.3.11)$$

The first term on the right-hand side of (4.3.11) contributes a traction discontinuity normal to the interface, known as the *Laplace pressure*; however, bear in mind that the term *pressure* is appropriate only in the absence of fluid motion on either side of the interface. If either the curvature of the interface or the surface tension vanishes, the Laplace pressure is zero and the normal stress is continuous across the interface.

It is important to bear in mind that the interfacial tension is independent of the radius of curvature of the interface, except when the radius of curvature is so small that it becomes comparable to the molecular size. In mainstream engineering applications, the surface tension is regarded as a genuine physical constant.

Local coordinates

Consider the jump in traction across the curved interface depicted in [Figure 4.3.2\(a\)](#). The origin of the Cartesian axes lies at a point on the interface, the x axis is tangential to the

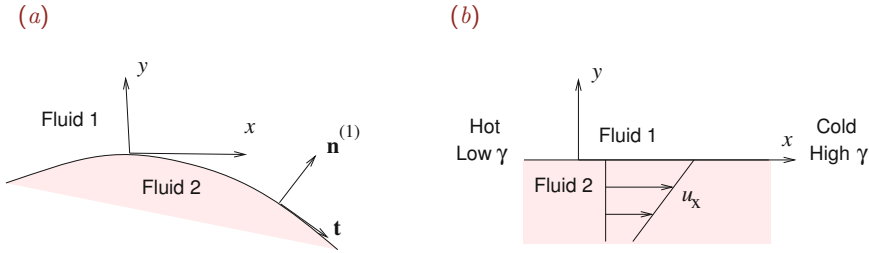


Figure 4.3.2 (a) A local coordinate system with the x axis tangential to a two-dimensional interface at a point is used to evaluate the jump in the traction across the interface. (b) A differentially heated interface drives a thermocapillary flow.

interface, and the y axis is normal to the interface pointing into the fluid labeled 1. At the origin of the Cartesian axes, the components of the unit normal vector, $\mathbf{n}^{(1)}$, are

$$n_x^{(1)} = 0, \quad n_y^{(1)} = 1, \quad (4.3.12)$$

and the jump in the interfacial traction is given by

$$\Delta \mathbf{f} \equiv \mathbf{n}^{(1)} \cdot (\boldsymbol{\sigma}^{(1)} - \boldsymbol{\sigma}^{(2)}) = (\sigma_{yx}^{(1)} - \sigma_{yx}^{(2)}) \mathbf{e}_x + (\sigma_{yy}^{(1)} - \sigma_{yy}^{(2)}) \mathbf{e}_y, \quad (4.3.13)$$

where \mathbf{e}_x and \mathbf{e}_y are unit vectors parallel to the x or y axis.

Applying equation (4.3.11) at the origin and setting $\mathbf{t} = \mathbf{e}_x$ and $\mathbf{n}^{(1)} = \mathbf{e}_y$, we obtain

$$\Delta \mathbf{f} = \gamma \kappa \mathbf{e}_y - \frac{d\gamma}{d\ell} \mathbf{e}_x. \quad (4.3.14)$$

Comparing this equation with (4.3.13), we derive an expression for the jump in the shear stress,

$$\sigma_{yx}^{(1)} - \sigma_{yx}^{(2)} = -\frac{d\gamma}{d\ell}, \quad (4.3.15)$$

and another expression for the jump in the normal stress,

$$\sigma_{yy}^{(1)} - \sigma_{yy}^{(2)} = \gamma \kappa. \quad (4.3.16)$$

For the configuration shown in [Figure 4.3.2\(a\)](#), the curvature κ is positive

A heated liquid layer

As an application, we consider a liquid layer that is hot at the left end and cold at the right end, as illustrated in [Figure 4.3.2\(b\)](#). In this case, $dT/dx < 0$ and therefore $d\gamma/dx > 0$, where T is the temperature. Equation (4.3.15) yields

$$\sigma_{yx}^{(1)} - \sigma_{yx}^{(2)} = -\frac{d\gamma}{dx} < 0. \quad (4.3.17)$$

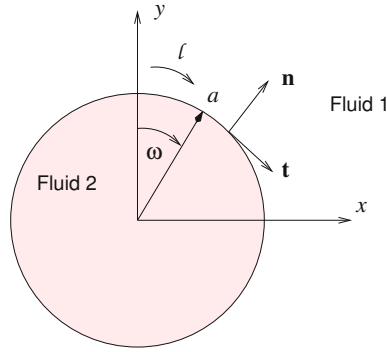


Figure 4.3.3 Illustration of a circular interface of radius a enclosing a fluid labeled 2, showing the unit tangent vector, \mathbf{t} , and the outward unit normal vector, \mathbf{n} .

Because the shear stress is insignificant in the gas above the layer, we can approximate

$$\sigma_{yx}^{(1)} \simeq 0. \quad (4.3.18)$$

For a Newtonian fluid,

$$\sigma_{yx}^{(2)} = \mu_2 \frac{du_x}{dy} > 0, \quad (4.3.19)$$

where μ_2 is the viscosity of the lower fluid, as discussed in Section 4.5. The positive sign of the slope du_x/dy is consistent with the velocity profile drawn in [Figure 4.3.2\(b\)](#). Physically, the high surface tension at the cold end pulls the fluid against the low surface tension at the hot end to drive a surface-tension induced flow.

A flow induced by temperature differences causing variations in surface tension is called a *thermocapillary flow*.

Curvature of a circle

We have seen that the curvature of an interface determines the jump in the normal component of the traction due to surface tension. To gain experience on the computation of the curvature, we consider a circle of radius a centered at the origin, described in parametric form by the equations

$$x = a \sin \omega, \quad y = a \cos \omega, \quad (4.3.20)$$

where ω is the polar angle measured around the center of the circle in the clockwise direction, varying from 0 to 2π , as shown in [Figure 4.3.3](#). The components of the unit tangent vector pointing in the clockwise direction are

$$t_x = \frac{dx}{d\ell}, \quad t_y = \frac{dy}{d\ell}, \quad (4.3.21)$$

where $d\ell = (dx^2 + dy^2)^{1/2}$ is the differential arc length measured in the clockwise direction. Using the parametric representation, we find that

$$dx = a \cos \omega \, d\omega, \quad dy = -a \sin \theta \, d\omega, \quad d\ell = a \, d\omega, \quad (4.3.22)$$

and thus

$$t_x = \cos \omega, \quad t_y = -\sin \omega. \quad (4.3.23)$$

Based on these formulas, we compute

$$\frac{dt_x}{d\ell} = \frac{d(\cos \omega)}{d(a\omega)} = -\frac{1}{a} \sin \omega, \quad \frac{dt_y}{d\ell} = \frac{d(-\sin \theta)}{d(a\theta)} = -\frac{1}{a} \cos \omega. \quad (4.3.24)$$

In unified vector form,

$$\frac{d\mathbf{t}}{d\ell} = -\frac{1}{a} \mathbf{n}, \quad (4.3.25)$$

where $\mathbf{n} = (\sin \omega, \cos \omega)$ is the unit vector normal to the circle pointing outward, as shown in Figure 4.3.3. Comparing (4.3.25) with (4.3.5), we confirm that the curvature of the circle is equal to the inverse of its radius, $\kappa = 1/a$.

Formulas for the curvature

The shape of a two-dimensional interface that does not turn upon itself but has a monotonic shape can be described by a single-valued function,

$$y = f(x). \quad (4.3.26)$$

Using elementary geometry, we find that

$$\mathbf{n}^{(1)} = \frac{1}{(1 + f'^2)^{1/2}} (-f' \mathbf{e}_x + \mathbf{e}_y), \quad \mathbf{t} = \frac{1}{(1 + f'^2)^{1/2}} (\mathbf{e}_x + f' \mathbf{e}_y), \quad (4.3.27)$$

$$\frac{d\ell}{dx} = \sqrt{1 + f'^2},$$

where a prime denotes a derivative with respect to x . Substituting these expressions into the formula (4.3.7) for the curvature, and simplifying, we derive the expressions

$$\kappa = -\frac{f''}{(1 + f'^2)^{3/2}} = \frac{1}{f'} \left(\frac{1}{\sqrt{1 + f'^2}} \right)' = -\left(\frac{f'}{\sqrt{1 + f'^2}} \right)'. \quad (4.3.28)$$

The slope angle of the interface, θ , is defined by the equation

$$\tan \theta = f'. \quad (4.3.29)$$

We note that the fraction in the second expression of (4.3.28) is equal to $|\cos \theta|$ and derive the alternative expression

$$\kappa = \frac{1}{f'} \frac{d|\cos \theta|}{dx}. \quad (4.3.30)$$

The curvature of an interface that is described parametrically by the functions

$$x = X(\xi), \quad y = Y(\xi) \quad (4.3.31)$$

is given by

$$\kappa = \frac{X_{\xi\xi} Y_{\xi} - Y_{\xi\xi} X_{\xi}}{(X_{\xi}^2 + Y_{\xi}^2)^{3/2}}, \quad (4.3.32)$$

where a subscript denotes a derivative with respect to the parametric variable, ξ . Formula (4.3.28) arises by setting $\xi = x$.

PROBLEMS

4.3.1 Curvature of an ellipse

Consider a horizontal ellipse centered at the origin of the xy plane, described in parametric form by the equations $x = a \cos \eta$ and $y = b \sin \eta$, where η is the natural parameter of the ellipse varying between 0 and 2π , and a, b are the ellipse semi-axes. Derive an expression for the curvature of the ellipse in terms of a, b , and η . Confirm that, as b tends to a , the curvature of the ellipse reduces to that of a circle.

4.3.2 Computation of the curvature

A line in the xy plane can be described by a set of $N + 1$ marker points with coordinates (x_i, y_i) for $i = 1, \dots, N + 1$. An approximation to the components of the tangent vector at the i th point is provided by the central-difference formulas

$$t_x^{(i)} = \frac{x_{i+1} - x_{i-1}}{\Delta \ell_i}, \quad t_y^{(i)} = \frac{y_{i+1} - y_{i-1}}{\Delta \ell_i}, \quad (4.3.33)$$

where

$$\Delta \ell_i = [(x_{i+1} - x_{i-1})^2 + (y_{i+1} - y_{i-1})^2]^{1/2}. \quad (4.3.34)$$

The derivatives of the components of the tangent vector with respect to arc length can be approximated with the corresponding formulas

$$\frac{dt_x^{(i)}}{d\ell} = \frac{t_x^{(i+1)} - t_x^{(i-1)}}{\Delta \ell_i}, \quad \frac{dt_y^{(i)}}{d\ell} = \frac{t_y^{(i+1)} - t_y^{(i-1)}}{\Delta \ell_i}. \quad (4.3.35)$$

The components of the outward normal vector at the marker points are given by

$$n_x^{(i)} = t_y^{(i)}, \quad n_y^{(i)} = -t_x^{(i)}. \quad (4.3.36)$$

Write a computer program that reads or generates the coordinates of a set of marker points, computes the right-hand sides of (4.3.33)–(4.3.36), and then evaluates the curvature

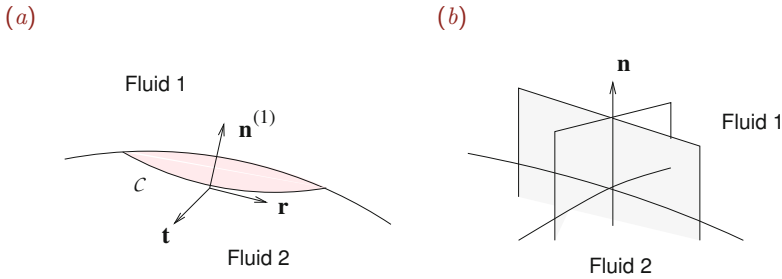


Figure 4.4.1 (a) Illustration of a thin fluid layer straddling a three-dimensional interface. The surface tension pulls the interfacial patch in the direction of the unit tangent vector, \mathbf{t} . (b) The mean curvature of a three-dimensional surface is equal to the average of two directional curvatures in two perpendicular planes containing the normal vector.

at the marker points from the expression $\kappa = -\mathbf{n} \cdot d\mathbf{t}/d\ell$. Perform a series of computations with marker points distributed evenly along a circle, and compare the numerically computed with the exact curvature.

4.3.3 Motion induced by curvature

Interfaces exhibit a variety of motions under the influence of surface tension. In a simplified model, point particles distributed along a two-dimensional interface move normal to the interface with velocity that is proportional to the local curvature. If $\mathbf{X}^{(i)}$ is the position of the i th marker point, then the motion of the marker point is described by the vectorial differential equation

$$\frac{d\mathbf{X}^{(i)}}{dt} = \kappa [\mathbf{n}^{(1)}]_i, \quad (4.3.37)$$

where t stands for time, $\mathbf{n}^{(1)}$ is the outward normal vector, and κ is the curvature.

Write a computer program that computes the motion of marker points distributed along an interface using the finite-difference approximations discussed in Problem 4.3.2 and the modified Euler method for integrating in time the differential equations (4.3.37). Run the program to compute the evolution of marker points distributed along a circle or an ellipse with axes ratio equal to two. Discuss the nature of the motion in each case.

4.4 Force balance at a three-dimensional interface

In Section 4.3, we derived a force balance at a two-dimensional interface and discussed the computation of the curvature. To derive the counterpart of the force balance equation (4.3.11) for a three-dimensional interface, we consider a thin material patch straddling the interface, as illustrated in Figure 4.4.1(a).

Let $\mathbf{n}^{(1)}$ be the unit vector normal to the interface pointing into fluid labeled 1, and \mathbf{r} be the unit vector tangential to the edge of the patch, C . Surface tension pulls the layer

in the direction of the unit vector \mathbf{t} that is tangential to the interface and normal to both $\mathbf{n}^{(1)}$ and \mathbf{r} . Recalling the geometrical interpretation of the outer vector product, discussed in Section 2.3, we write

$$\mathbf{t} = \mathbf{r} \times \mathbf{n}^{(1)}. \quad (4.4.1)$$

All vectors involved in this equation are unit vectors, that is, they have unit length.

Next, we balance the surface force due to the fluid stresses on either side of the interface and the edge force due to the surface tension, writing

$$(\mathbf{n}^{(1)} \cdot \boldsymbol{\sigma}^{(1)}) \Delta S + (\mathbf{n}^{(2)} \cdot \boldsymbol{\sigma}^{(2)}) \Delta S + \oint_{\mathcal{C}} \gamma \mathbf{t} \, d\ell = \mathbf{0}, \quad (4.4.2)$$

where ΔS is the surface area of the patch, ℓ is the arc length around the edge of the patch, \mathcal{C} , and $\mathbf{n}^{(2)}$ is the unit vector normal to the interface pointing into the fluid labeled 2. Equation (4.4.2) is the three-dimensional counterpart of equation (4.3.1). Setting $\mathbf{n}^{(2)} = -\mathbf{n}^{(1)}$ and rearranging, we obtain

$$\Delta \mathbf{f} \equiv \mathbf{n}^{(1)} \cdot (\boldsymbol{\sigma}^{(1)} - \boldsymbol{\sigma}^{(2)}) = -\frac{1}{\Delta S} \oint_{\mathcal{C}} \gamma \mathbf{t} \, d\ell. \quad (4.4.3)$$

In the limit as the loop \mathcal{C} shrinks to a point and ΔS tends to zero, equation (4.4.3) provides us with the expression

$$\Delta \mathbf{f} = \gamma 2 \kappa_m \mathbf{n}^{(1)} - \frac{\partial \gamma}{\partial \ell} \boldsymbol{\tau}, \quad (4.4.4)$$

subject to the following definitions:

- κ_m is the mean curvature of the interface defined in terms of the surface divergence of the unit normal vector, as discussed in Section 4.4.1.
- $\boldsymbol{\tau}$ is the unit vector tangent to the interface pointing in the direction where the surface tension changes most rapidly.
- ℓ is the arc length measured in the direction of the tangential vector $\boldsymbol{\tau}$, and $\partial \gamma / \partial \ell$ is the corresponding maximum rate of change of the surface tension with respect to arc length.

The first term on the right-hand side of (4.4.4) expresses a discontinuity in the normal direction identified as the *Laplace pressure*, whereas the second term expresses a discontinuity in the tangential direction identified as the *Marangoni traction*.

Tangential coordinates

If the x axis is chosen to be normal to the interface at a point, and correspondingly the yz plane is tangential to the interface at that point, then

$$\Delta \mathbf{f} = \gamma 2 \kappa_m \mathbf{e}_x - \frac{\partial \gamma}{\partial y} \mathbf{e}_y - \frac{\partial \gamma}{\partial z} \mathbf{e}_z, \quad (4.4.5)$$

where \mathbf{e}_y and \mathbf{e}_z are tangential unit vectors along the y and z axes.

4.4.1 Mean curvature

If the yz plane is tangential to an interface at a point, then the mean curvature at that point is given by the surface divergence of the normal vector,

$$2\kappa_m \equiv \nabla_s \cdot \mathbf{n} = \frac{\partial n_y}{\partial y} + \frac{\partial n_z}{\partial z}. \quad (4.4.6)$$

Requiring that

$$n_x^2 + n_y^2 + n_z^2 = 1, \quad (4.4.7)$$

and then

$$n_x \frac{\partial n_x}{\partial x} + n_y \frac{\partial n_x}{\partial y} + n_z \frac{\partial n_x}{\partial z} = 0, \quad (4.4.8)$$

and setting $n_x = 0$, $n_y = 0$, and $n_z = 0$, we find that $\partial n_x / \partial x = 0$, which shows that the normal derivative of the normal component of the normal vector is zero. This property allows us to write the more general expression

$$2\kappa_m \equiv \nabla \cdot \mathbf{n} = \frac{\partial n_x}{\partial x} + \frac{\partial n_y}{\partial y} + \frac{\partial n_z}{\partial z}, \quad (4.4.9)$$

with reference to an arbitrary system of Cartesian coordinates whose axes are not necessarily tangential or normal to the interface.

Mean curvature of a surface described as $F(x, y, z) = 0$

A three-dimensional interface can be described implicitly by an equation of the form

$$F(x, y, z) = 0. \quad (4.4.10)$$

Given two of the three coordinates, x , y , or z , this equation can be used to compute the third coordinate by analytical or numerical methods. The unit vector normal to the interface is given by

$$\mathbf{n} = \frac{1}{|\nabla F|} \nabla F \quad (4.4.11)$$

and the mean curvature is given by

$$2\kappa_m = \nabla \cdot \left(\frac{1}{|\nabla F|} \nabla F \right) = \frac{1}{|\nabla F|} \nabla^2 F - \frac{1}{|\nabla F|^3} \nabla F \cdot (\nabla \nabla F) \cdot \nabla F, \quad (4.4.12)$$

where $\nabla \nabla F \equiv \Phi$ is a symmetric matrix encapsulating the second partial derivatives,

$$\Phi_{ij} = \frac{\partial^2 F}{\partial x_i \partial x_j}. \quad (4.4.13)$$

Mean curvature of a surface described as $z = f(x, y)$

For an interface that is described explicitly by a function

$$z = f(x, y), \quad (4.4.14)$$

we set $F(x, y, z) = z - f(x, y)$ and derive the formula

$$2\kappa_m = -\frac{(1 + f_y^2) f_{xx} - 2f_x f_y f_{xy} + (1 + f_x^2) f_{yy}}{(1 + f_x^2 + f_y^2)^{3/2}}, \quad (4.4.15)$$

where the subscript x denotes a derivative with respect to x and the subscript y denotes a derivative with respect to y .

For a nearly flat interface, the partial derivatives are small compared to unity, yielding

$$2\kappa_m \simeq -(f_{xx} + f_{yy}). \quad (4.4.16)$$

The term inside the parentheses is the Laplacian of $f(x, y)$.

Spherical polar coordinates

The unit normal vector for an interface that is described in spherical polar coordinates, (r, θ, φ) , as

$$r = f(\theta, \varphi), \quad (4.4.17)$$

is computed from (4.4.11) with

$$\nabla F = \mathbf{e}_r - \frac{f_\theta}{r} \mathbf{e}_\theta - \frac{f_\varphi}{r \sin \theta} \mathbf{e}_\varphi, \quad (4.4.18)$$

where a subscript after f indicates a corresponding partial derivative.

For a nearly spherical interface of radius r , the mean curvature can be approximated with the linearized expression

$$2\kappa_m \simeq \frac{2}{r} - \frac{\cot \theta}{r^2} f_\theta - \frac{1}{r^2} f_{\theta\theta} - \frac{1}{r^2 \sin^2 \theta} f_{\varphi\varphi} \quad (4.4.19)$$

involving first and second partial derivatives.

4.4.2 Directional curvatures

To compute the mean curvature of a three-dimensional interface, we consider the traces of the interface in two conjugate orthogonal planes that are normal to the interface at a point, and thus contain the normal vector, as depicted in [Figure 4.4.1\(b\)](#).

If κ_1 and κ_2 are the curvatures of the two traces at that point, computed using formula (4.3.5) with the x and y axes residing in each of the two planes, then the mean curvature of the interface is given by

$$\kappa_m = \frac{1}{2} (\kappa_1 + \kappa_2). \quad (4.4.20)$$

A theorem due to Euler reassures us that the mean value of the conjugate directional curvatures is independent of the orientation of the two planes, provided that the planes remain mutually orthogonal.

Principal curvatures

There is a particular orientation of the normal plane corresponding to maximum directional curvature, κ_{\max} , and a conjugate orthogonal orientation corresponding to minimum directional curvature, κ_{\min} . These are the principal curvatures of the interface at the chosen point. The mean curvature is

$$\kappa_m = \frac{1}{2} (\kappa_{\max} + \kappa_{\min}). \quad (4.4.21)$$

In the case of a sphere, the principal curvatures and the mean curvature are equal.

Euler's theorem states that the curvature in an arbitrary direction is related to the principal curvatures by

$$\kappa = \kappa_{\max} \cos^2 \alpha + \kappa_{\min} \sin^2 \alpha, \quad (4.4.22)$$

where α is the angle subtended between (a) the tangential vector pointing in a chosen direction, and (b) the tangential vector pointing in the direction of maximum curvature.

4.4.3 Axisymmetric interfaces

Next, we consider the geometrical properties of an axisymmetric interface, as shown in [Figure 4.4.2](#). The mean curvature is the average of the two principal curvatures: one is the curvature of the trace of the interface in the σx (azimuthal) plane, corresponding to a certain value of the azimuthal angle, φ , denoted by κ_1 , and the second is the curvature of the trace of the interface in the conjugate orthogonal plane, denoted by κ_2 .

Description as $\sigma = w(x)$

The shape of an interface in an azimuthal plane can be described by a function,

$$\sigma = w(x), \quad (4.4.23)$$

as shown in [Figure 4.4.2\(a\)](#). The unit normal vector is

$$\mathbf{n} = \frac{1}{\sqrt{1+w'^2}} (\mathbf{e}_\sigma - w' \mathbf{e}_x), \quad (4.4.24)$$

where a prime denotes a derivative with respect to x . The mean curvature is given by the divergence of the normal vector,

$$2\kappa_m = \frac{\partial n_x}{\partial x} + \frac{1}{\sigma} \frac{\partial(\sigma n_\sigma)}{\partial \sigma}. \quad (4.4.25)$$

Making substitutions, we obtain

$$2\kappa_m = -\left(\frac{w'}{\sqrt{1+w'^2}}\right)' + \frac{1}{\sigma} \frac{\partial}{\partial \sigma} \left(\frac{\sigma}{\sqrt{1+w'^2}}\right). \quad (4.4.26)$$

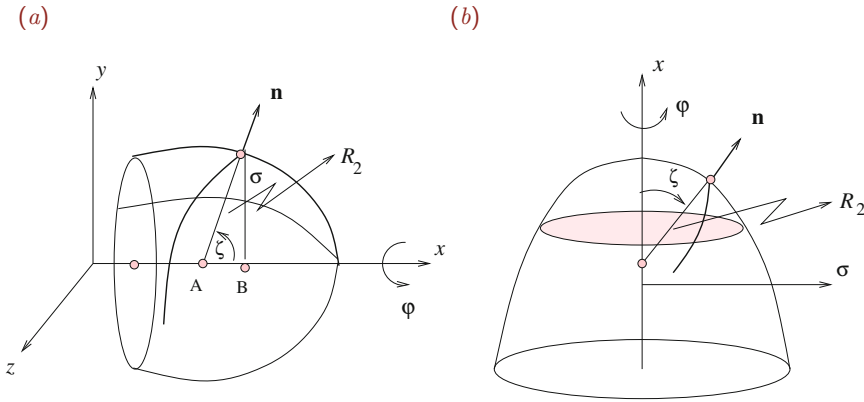


Figure 4.4.2 Illustration of an axisymmetric interface. (a) The second principal curvature at a point in the xy plane is the curvature of the line representing the trace of the interface in a plane that is normal to the interface and normal to the xy plane, drawn as a heavy line. (b) An axisymmetric interface can be described by a function $x = f(\sigma)$. The second principal curvature is the curvature of the line drawn with a heavy line.

Carrying out the differentiations, we find that

$$2 \kappa_m = -\frac{w''}{(1 + w'^2)^{3/2}} + \frac{1}{w} \frac{1}{\sqrt{1 + w'^2}} \tag{4.4.27}$$

or

$$2 \kappa_m = \frac{1}{ww'} \left(\frac{w}{\sqrt{1 + w'^2}} \right)' \tag{4.4.28}$$

The first term on the right-hand side of (4.4.27) is the principal curvature in an azimuthal plane. The second term is the second principal curvature,

$$\kappa_2 = \frac{1}{R_2}, \quad R_2 = \sigma \sqrt{1 + w'^2} = \frac{\sigma}{\sin \zeta} = \frac{\sigma}{n_\sigma}, \tag{4.4.29}$$

where R_2 is the second principal radius of curvature and the angle ζ is defined in Figure 4.4.2(a). We have found that R_2 is the signed distance between (a) the point where the curvature is evaluated and (b) the intersection of the extension of the normal vector with the x axis. If n_σ is negative, R_2 is also negative.

In the case of a sphere, points A and B in Figure 4.4.2(a) coincide with the center of the sphere, and both principal curvatures are equal to the radius of the sphere.

Description as $x = f(\sigma)$

Alternatively, the shape of an interface can be described by a function

$$x = f(\sigma), \tag{4.4.30}$$

as shown in [Figure 4.4.2\(b\)](#). The unit normal vector is given by

$$\mathbf{n} = \frac{1}{\sqrt{1+f'^2}} (\mathbf{e}_x - f' \mathbf{e}_\sigma), \quad (4.4.31)$$

where a prime denotes a derivative with respect to σ . The mean curvature is given by the divergence of the normal vector,

$$2\kappa_m = \frac{\partial n_x}{\partial x} + \frac{1}{\sigma} \frac{\partial(\sigma n_\sigma)}{\partial \sigma}. \quad (4.4.32)$$

Making substitutions, we obtain

$$2\kappa_m = -\frac{1}{\sigma} \left(\frac{\sigma f'}{\sqrt{1+f'^2}} \right)'. \quad (4.4.33)$$

Carrying out the differentiations, we find that

$$2\kappa_m = -\frac{f''}{(1+f'^2)^{3/2}} - \frac{1}{\sigma} \frac{f'}{\sqrt{1+f'^2}}. \quad (4.4.34)$$

The first term on the right-hand side is the principal curvature in a meridional plane,

$$\kappa_1 = -\frac{f''}{(1+f'^2)^{3/2}} = \frac{1}{f'} \left(\frac{1}{\sqrt{1+f'^2}} \right)'. \quad (4.4.35)$$

The second term is the second principal curvature,

$$\kappa_2 = \frac{1}{R_2}, \quad R_2 = -\frac{\sigma}{f'} \sqrt{1+f'^2} = \frac{\sigma}{\sin \zeta} = \frac{\sigma}{n_\sigma}, \quad (4.4.36)$$

where R_2 is the second principal radius of curvature and the angle ζ is defined in [Figure 4.4.2\(b\)](#).

PROBLEMS

4.4.1 Mean curvature

(a) Compute the mean curvature of a periodic surface described by the equation

$$z = a \sin(kx) + b \sin(ly), \quad (4.4.37)$$

where a , b , k , and l are given constants. State the units of each constant.

(b) Based on formula (4.4.20) and its accompanying interpretation discussed in the text, show that the mean curvature of a sphere of radius a is equal to $\kappa_m = 1/a$, whereas the mean curvature of a circular cylinder of radius a is equal to $\kappa_m = 1/(2a)$.

(c) The sphere and the circular cylinder are two shapes with constant mean curvature. Describe and discuss one additional shape.

4.4.2 Jump in traction in local coordinates

Derive the counterparts of equations (4.3.15) and (4.3.16) for a three-dimensional interface.

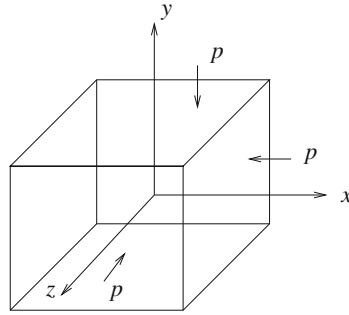


Figure 4.5.1 The traction exerted at the three sides of a cubical parcel of a stationary fluid has only a normal component defined in terms of the thermodynamic pressure, p .

4.5 Stresses in a fluid at rest

If a fluid does not exhibit macroscopic motion as seen by a stationary observer, that is, the observable fluid velocity vanishes, the molecules are in a state of dynamic equilibrium determined by the physical conditions prevailing in their immediate environment.

Consider a small cubic fluid parcel with all six faces perpendicular to the x , y , or z axis, as illustrated in [Figure 4.5.1](#). In the absence of macroscopic fluid motion, the traction exerted on the sides that are perpendicular to the x axis must be directed normal to these side. To demonstrate this by *reduction ad absurdum*, we note that, if this were not true, a tangential component pointing in a physically indeterminate direction would arise. In the notation of Section 4.2,

$$f_x^{(x)} \neq 0, \quad f_y^{(x)} = 0, \quad f_z^{(x)} = 0, \quad (4.5.1)$$

where $\mathbf{f}^{(x)}$ is the traction exerted on the right side of a face that is perpendicular to the x axis.

Similar arguments can be made to show that the traction exerted on the sides that are perpendicular to the y or z axis are directed normal to these sides,

$$f_x^{(y)} = 0, \quad f_y^{(y)} \neq 0, \quad f_z^{(y)} = 0, \quad (4.5.2)$$

and

$$f_x^{(z)} = 0, \quad f_y^{(z)} = 0, \quad f_z^{(z)} \neq 0. \quad (4.5.3)$$

If the size of the cubic parcel is infinitesimal, the fluid residing inside the parcel is perfectly or nearly homogeneous and the non-vanishing components of the three tractions, $f_x^{(x)}$, $f_y^{(y)}$, and $f_z^{(z)}$, must be identical. By definition, the common value of these normal components is the negative of the pressure, p ,

$$f_x^{(x)} = f_y^{(y)} = f_z^{(z)} \equiv -p. \quad (4.5.4)$$

We conclude that, in hydrostatics, the stress tensor introduced in equation (4.2.6) in terms of three tractions is defined exclusively in terms of the pressure, and is given by

$$\boldsymbol{\sigma} = \begin{bmatrix} -p & 0 & 0 \\ 0 & -p & 0 \\ 0 & 0 & -p \end{bmatrix} = -p \begin{bmatrix} 1 & 0 & 0 \\ 0 & 1 & 0 \\ 0 & 0 & 1 \end{bmatrix}. \quad (4.5.5)$$

In compact notation,

$$\boldsymbol{\sigma} = -p \mathbf{I}, \quad (4.5.6)$$

where \mathbf{I} is the unit or identity matrix shown on the right-hand side of (4.5.5).

Traction on a surface

As an application, we use expression (4.5.6) to evaluate the traction exerted on a surface that resides inside or at the boundary a stationary fluid. Substituting (4.5.6) into formula (4.2.10), we find that

$$\mathbf{f}(\mathbf{x}, \mathbf{n}) = \mathbf{n} \cdot (-p \mathbf{I}) = -p \mathbf{n} \cdot \mathbf{I}, \quad (4.5.7)$$

and then

$$\mathbf{f}(\mathbf{x}, \mathbf{n}) = -p \mathbf{n}. \quad (4.5.8)$$

The last equation results from the identity $\mathbf{n} \cdot \mathbf{I} = \mathbf{I} \cdot \mathbf{n} = \mathbf{n}$. Equation (4.6.1) shows that the traction exerted on a surface in hydrostatics is directed normal to the surface and points against the surface, while the tangential component is identically zero.

Traction on a boundary

Substituting (4.2.20) into expression (4.5.6) to evaluate the traction on a boundary that is immersed in, or confines a stationary fluid, we obtain

$$\mathbf{f}^{\text{boundary}} = \mathbf{n}^{\text{inward}} \cdot (-p \mathbf{I}) = -p \mathbf{n}^{\text{inward}} \cdot \mathbf{I}, \quad (4.5.9)$$

and then

$$\mathbf{f}^{\text{boundary}} = -p \mathbf{n}^{\text{inward}}. \quad (4.5.10)$$

The last equality results from the identity $\mathbf{n}^{\text{inward}} \cdot \mathbf{I} = \mathbf{n}^{\text{inward}}$. Thus, the traction exerted on a fluid boundary in hydrostatics is directed normal to the boundary and points against the boundary, while the tangential component of the traction is identically zero.

4.5.1 Pressure from molecular motions

The hydrostatic pressure distribution established in a fluid at rest cannot be computed working exclusively in the context of fluid mechanics. Additional information concerning the

relationship between the density and the pressure for a particular fluid under consideration is required.

Gases

Molecular thermodynamics states that the pressure of a small gas parcel is determined by (a) the number of molecules residing inside the parcel expressed by the local fluid density, ρ , (b) the kinetic energy of the molecules determined by the absolute temperature, T , and (c) the nature and intensity of the intermolecular forces due to an intermolecular potential.

For an ideal gas, intermolecular forces are negligible and the pressure derives from the density and temperature in terms of the ideal gas law,

$$p = \frac{RT}{M} \rho, \quad (4.5.11)$$

where M is the molecular mass, defined as the mass of one mole comprised of a collection of N_A molecules;

$$N_A = 6.022 \times 10^{26} \quad (4.5.12)$$

is the Avogadro number;

$$R = 8.314 \times 10^3 \text{ kg m}^2 / (\text{sec}^2 \cdot \text{kmole} \cdot \text{K}) \quad (4.5.13)$$

is the ideal gas constant; T is Kelvin's absolute temperature, which is equal to the Celsius centigrade temperature reduced by 273 units. The gram-molecular mass of an element is equal to the atomic weight of the element listed in the periodic table, expressed in grams.

Liquids

Because liquids are nearly incompressible, the pressure can be regarded a function of the density alone, independent of pressure. The computation of the hydrostatic pressure distribution in gases and liquids will be discussed in detail in Chapter 5.

4.5.2 Jump in pressure across an interface in hydrostatics

Equations (4.3.11) and (4.4.4) provide us with expressions for the jump in the traction across a two- or three-dimensional interface. If the fluids on either side of the interface are stationary, the corresponding stress tensors are given by (4.5.6) in term of the pressure and the jump in the traction is given by

$$\Delta \mathbf{f} \equiv \mathbf{n}^{(1)} \cdot (\boldsymbol{\sigma}^{(1)} - \boldsymbol{\sigma}^{(2)}) = \mathbf{n}^{(1)} \cdot [-p^{(1)} \mathbf{I} - (-p^{(2)} \mathbf{I})], \quad (4.5.14)$$

where the superscript 1 or 2 denotes the choice of fluid. Simplifying, we obtain

$$\Delta \mathbf{f} = (p^{(2)} - p^{(1)}) \mathbf{n}^{(1)}. \quad (4.5.15)$$

Because the jump in traction is normal to the interface, surface tension variations are not accepted in hydrostatics.

Comparing the right-hand side of (4.5.15) with the right-hand side of the force equilibrium equation (4.3.11) for a two-dimensional interface with uniform surface tension, γ , we find that

$$p^{(2)} - p^{(1)} = \gamma \kappa, \quad (4.5.16)$$

where κ is the curvature of the interface. We have shown that the jump in the pressure across a two-dimensional interface in hydrostatics is equal to the product of the surface tension and the curvature of the interface.

Working in a similar fashion for a three-dimensional interface, we refer to (4.4.4) and find that

$$p^{(2)} - p^{(1)} = \gamma 2 \kappa_m, \quad (4.5.17)$$

where κ_m is the mean curvature of the interface. We have found that the jump in the pressure across a three-dimensional interface in hydrostatics is equal to the product of the surface tension and twice the mean curvature of the interface.

Laplace's law

As an application, we compute the jump in pressure across a spherical interface of radius a representing the surface of a liquid drop or bubble. Designating the outer fluid as fluid 1 and the inner fluid as fluid 2, we find that the mean curvature is $\kappa_m = 1/a$. Consequently, the pressure jump across the spherical interface is given by Laplace's law,

$$p^{(2)} - p^{(1)} = 2 \frac{\gamma}{a}. \quad (4.5.18)$$

The pressure inside a drop or bubble is higher than the ambient pressure due to the interfacial tension by $2\gamma/a$.

PROBLEMS

4.5.1 *Jump in pressure across a circular interface*

Derive an expression for the jump in pressure across a circular interface of radius a representing the trace of a cylindrical thread in the xy plane.

4.5.2 *Curvature of a soap film*

Explain why the mean curvature of a thin soap film attached to a wire frame must be zero.

4.6 Constitutive equations

In the absence of macroscopically observable fluid motion, the traction exerted on a specified side of a small fluid surface indicated by the unit normal vector, \mathbf{n} , is given by equation (4.6.1),

$$\mathbf{f}(\mathbf{x}, \mathbf{n}) = -p \mathbf{n}, \quad (4.6.1)$$

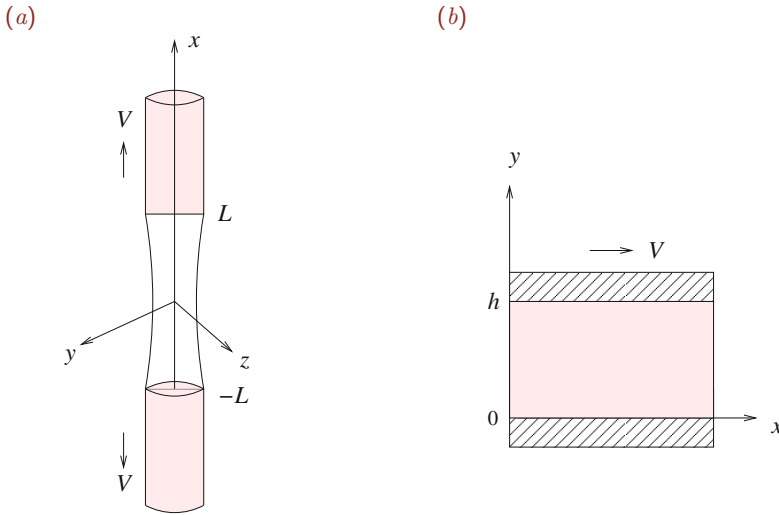


Figure 4.6.1 (a) Stretching of a liquid bridge between two coaxial cylinders that are pulled apart along their axes with velocity V . (b) Shear flow in a two-dimensional channel confined between two parallel plates located at $y = 0$ and h ; the motion is due to the parallel translation of the upper plate with velocity V .

in terms of the pressure, p . In the presence of macroscopic fluid motion, this equation is modified in two ways. First, the normal component of the traction is accompanied by a new contribution that depends on the physical properties of the fluid and the nature of the fluid motion. Second, a tangential component of the traction is established.

To understand how these new contributions arise from a physical point of view, it is helpful to consider the tractions developing in two complementary flows: (a) an extensional flow where the fluid stretches and elongates, and (b) a channel flow where the fluid is sheared due to boundary motion, as shown in Figure 4.6.1.

Stretching of a thread

In one experiment, a thread of liquid is suspended between two rods forming an axisymmetric bridge, and the rods are pulled apart with velocity V extending the thread, as illustrated in Figure 4.6.1(a). A force is required to pull the rods apart and thus overcome the normal component of the hydrodynamic traction imparted by the fluid to the tips of the rods, so that

$$f_x^{(x)} \neq -p, \quad (4.6.2)$$

where p is the pressure discussed in Section 4.5 in the context of hydrostatics. Our intuition suggests that the faster the rods are pulled apart, the higher the magnitude of the normal component of the traction. The greater the distance between the rods, the lower the magnitude of the normal component of the traction.

For most common fluids, a linear relationship exists between the traction, the velocity of the rods, and the inverse of their distance, so that

$$f_x^{(x)} = -p + 2\mu_{\text{ext}} \frac{V}{L}, \quad (4.6.3)$$

where L is half the instantaneous distance between the rods and μ_{ext} is a physical constant associated with the fluid called the extensional viscosity of the fluid.

Shearing of a layer

In another experiment, a fluid is placed in a channel confined between two parallel plates. The upper plate translates in the direction of the x axis parallel to itself with constant velocity V , while the lower plate is held stationary, as depicted in [Figure 4.6.1\(b\)](#). A force in the x direction must be exerted on the upper plate to balance the tangential component of the traction developing due to the fluid motion, so that

$$f_x^{(y)} \neq 0. \quad (4.6.4)$$

The faster the velocity of the translating plate, the higher the magnitude of the traction; the greater the distance between the two plates, the lower the magnitude of the traction.

For most common fluids, a linear relationship exists between the traction, the velocity of the moving plate, and the inverse of the distance between the plates, h ,

$$f_x^{(y)} = \mu_{\text{shear}} \frac{V}{h}, \quad (4.6.5)$$

where μ_{shear} is a physical constant associated with the fluid called the shear viscosity of the fluid.

4.6.1 Simple fluids

We have demonstrated by example that stresses develop in a fluid as a result of the motion. To proceed further, we consider the tractions developing at the surface of a small fluid parcel in motion and argue the following properties characterizing a simple fluid:

- If a fluid parcel translates, rotates, or translates and rotates as a rigid body, tractions do not develop at the parcel surface.
- Tractions develop only when a parcel deforms.
- The distribution of traction over the parcel surface at any particular time instant depends only on the type and rate of deformation of the parcel at that particular time instant.

Our analysis of kinematics in Chapter 2 has revealed that a small spherical fluid parcel in motion deforms to obtain an ellipsoidal shape whose axes are parallel to the three eigenvectors of the rate-of-deformation tensor given in [Table 2.1.1](#). The directional rates of deformation are equal to the corresponding eigenvalues.

$$\begin{bmatrix} \sigma_{xx} & \sigma_{xy} & \sigma_{xz} \\ \sigma_{yx} & \sigma_{yy} & \sigma_{yz} \\ \sigma_{zx} & \sigma_{zy} & \sigma_{zz} \end{bmatrix} = \begin{bmatrix} -p + 2\mu \frac{\partial u_x}{\partial x} & \mu \left(\frac{\partial u_y}{\partial x} + \frac{\partial u_x}{\partial y} \right) & \mu \left(\frac{\partial u_z}{\partial x} + \frac{\partial u_x}{\partial z} \right) \\ \mu \left(\frac{\partial u_x}{\partial y} + \frac{\partial u_y}{\partial x} \right) & -p + 2\mu \frac{\partial u_y}{\partial y} & \mu \left(\frac{\partial u_z}{\partial y} + \frac{\partial u_y}{\partial z} \right) \\ \mu \left(\frac{\partial u_x}{\partial z} + \frac{\partial u_z}{\partial x} \right) & \mu \left(\frac{\partial u_y}{\partial z} + \frac{\partial u_z}{\partial y} \right) & -p + 2\mu \frac{\partial u_z}{\partial z} \end{bmatrix}$$

Table 4.6.1 Components of the stress tensor for an incompressible Newtonian fluid in Cartesian coordinates.

Temperature ($^{\circ}\text{C}$)	Water (cp)	Air (cp)
20	1.002	0.0181
40	0.653	0.0191
80	0.355	0.0209

Table 4.6.2 The viscosity of water and air at three temperatures; cp stands for centipoise, which is one hundredth of the viscosity unit poise defined as $1 \text{ g}/(\text{cm sec})$. Thus, $\text{cp} \equiv 10^{-2} \text{ g}/(\text{cm sec})$.

With these observations as a point of departure, we proceed to relate the stress tensor to the physical properties of the fluid and to the structure of the velocity field by a constitutive equation.

4.6.2 Incompressible Newtonian fluids

The constitutive equation for an incompressible Newtonian fluid reads

$$\boldsymbol{\sigma} = -p\mathbf{I} + \mu 2\mathbf{E}, \quad (4.6.6)$$

where p is the pressure, the coefficient μ is the fluid viscosity, sometimes also called the dynamic viscosity, and \mathbf{E} is the rate-of-deformation tensor given in [Table 2.1.1](#). Note that the Newtonian constitutive relation respects the symmetry of the stress tensor discussed at the end of Section 4.2. Explicitly, the components of the stress tensor are given by the matrix equation shown in [Table 4.6.1](#). The viscosity of water and air at three temperatures is given in [Table 4.6.2](#).

In the absence of flow, we recover the hydrostatic stress tensor defined in equation (4.5.6), involving the hydrostatic pressure alone.

Unidirectional shear flow

As an example, we consider flow in a two-dimensional channel confined between two parallel plane walls. The motion of the fluid is generated by the translation of the upper wall, as shown in [Figure 4.6.1\(b\)](#). Physical intuition suggests that, at low and moderate velocities,

the fluid will translate along the x axis with a position-dependent velocity u_x varying along the y axis; to signify this dependence, we write $u_x(y)$. Using equation (2.1.28), we find that the rate-of-deformation tensor is given by

$$\mathbf{E} = \frac{1}{2} \begin{bmatrix} 0 & \frac{du_x}{dy} \\ \frac{du_x}{dy} & 0 \end{bmatrix}. \quad (4.6.7)$$

Substituting this expression into the right-hand side of (4.6.6), we obtain the stress tensor

$$\boldsymbol{\sigma} = \begin{bmatrix} -p & \mu \frac{du_x}{dy} \\ \mu \frac{du_x}{dy} & -p \end{bmatrix}. \quad (4.6.8)$$

The off-diagonal components involving the local slope of the velocity profile, du_x/dy arise as a result of the fluid motion.

The x component of the traction exerted on a fluid surface that is perpendicular to the y axis, identified as the shear stress, is

$$f_x^{(y)} = \sigma_{yx} = \mu \frac{du_x}{dy}. \quad (4.6.9)$$

Physically, this traction can be attributed to the friction experienced by adjacent fluid layers as they slide over one another with gradually varying velocities.

4.6.3 Viscosity

Strictly speaking, the viscosity of a Newtonian fluid is a proportionality coefficient relating the stress tensor to the rate-of-deformation tensor, as shown in equation (4.6.6). However, it is reassuring to know that this mathematical definition, established by phenomenological observation, has a firm physical foundation. In fact, the viscosity is a genuine physical property dependent on the local physical conditions, including the temperature.

As the temperature increases, the viscosity of liquids decreases whereas the viscosity of gases increases, as shown in [Table 4.6.2](#). This dichotomy is a reflection of the different physical mechanisms that are responsible for the development of stresses in these two complementary classes of fluids.

In the case of liquids, the viscosity is due to occasional molecular excursions from a mean position to neighboring empty sites. In the cases of gases, the viscosity is due to the relentless molecular excursions from regions of high velocity to regions of low velocity in the course of random motion due to thermal fluctuations.

4.6.4 Viscosity of a gas

To demonstrate the relation between molecular and macroscopic fluid motion, we consider a gas in unidirectional shear flow and derive an expression for the viscosity in terms of

molecular properties. In the simplest kinetic theory, the molecules are modeled as rigid spheres moving with the local fluid velocity defined in Section 1.4, and with a randomly fluctuating velocity. The square of the average magnitude of the fluctuating component is

$$\overline{v^2} = \frac{8}{\pi} \frac{k_B T}{M}, \quad (4.6.10)$$

where k_B is the Boltzmann's constant, T is the absolute temperature, and M is the molecular mass. In the course of the random motion, two molecules occasionally collide after having traveled an average distance equal to the mean free path, λ .

Consider a macroscopically stationary gas with vanishing fluid velocity. The number of molecules crossing an infinitesimal surface area during an infinitesimal time interval as a result of the fluctuating motion is denoted by n_{crossing} . Using principles of statistical mechanics, we find that n_{crossing} is proportional to (a) the number of molecules per infinitesimal volume, defined as the number density n , and (b) the average magnitude of the fluctuating velocity, \overline{v} . It can be shown that

$$n_{\text{crossing}} = \frac{1}{4} n \overline{v}. \quad (4.6.11)$$

The units of n_{crossing} are number of particles over time and length squared.

A molecule crossing a surface at a particular instant has collided with another molecule above or below the surface at an average distance a . Using principles of statistical mechanics, we find that

$$a = \frac{2}{3} \lambda, \quad (4.6.12)$$

where λ is the mean free path. Relations (4.6.11) and (4.6.12) have been derived taking into consideration that, since the molecules move randomly in all directions, only one component of the velocity brings them toward the crossing surface under consideration.

Relations (4.6.10)–(4.6.12) also hold true when the fluid exhibits macroscopic motion, provided that the molecular velocity is computed relative to the average velocity at the position where a molecule last underwent a collision.

Momentum transport

Shown in [Figure 4.6.2](#) is a schematic illustration of the instantaneous distribution of molecules in a gas undergoing unidirectional shear flow along the x axis. Without loss of generality, we have assumed that the fluid velocity increases in the positive direction of the y axis. In the course of the motion, gas molecules cross a horizontal plane corresponding to a certain value of y , drawn with the heavy horizontal line, from either side. Because the x velocity of molecules crossing from above is higher than the x velocity of molecules crossing from below, x momentum is transferred in the negative direction of the y axis. The rate of transport of x momentum across a surface that is perpendicular to the y axis amounts to a hydrodynamic traction, $f_x^{(y)}$.

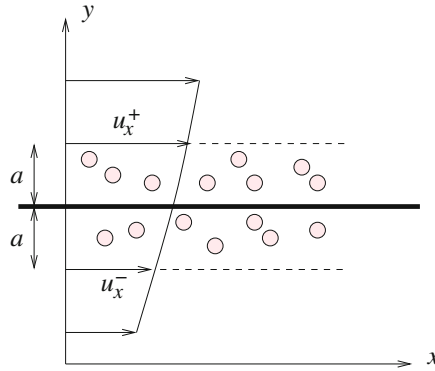


Figure 4.6.2 A molecular model of a gas in shear flow is used to derive an expression for the viscosity in terms of molecular properties, as shown in equation (4.6.17).

The rate of momentum transport defined in the last paragraph can be quantified by setting

$$f_x^{(y)} = -M (n_{\text{crossing}}^- u_x^- - n_{\text{crossing}}^+ u_x^+), \tag{4.6.13}$$

where u_x is the fluid velocity and the superscripts + and - indicate that the superscripted variable is evaluated at a distance equal to a above or below the transport surface. Effectively, the collection of molecules crossing the y plane during an infinitesimal period of time are represented by model molecules distinguished by the following two important properties:

- The model molecules last underwent a collision at a distance a above or below the y plane.
- The model molecules move with an average velocity that is equal to the local fluid velocity evaluated at the position of the last collision.

Because the flow is unidirectional, the mean fluid velocity normal to a horizontal plane is zero and the number of molecules crossing the y plane from either side during an infinitesimal time period are equal,

$$n_{\text{crossing}}^- = n_{\text{crossing}}^+. \tag{4.6.14}$$

Combining equations (4.6.11)–(4.6.13), we obtain

$$f_x^{(y)} = M \frac{1}{4} n \bar{v} \frac{u_x^+ - u_x^-}{2a} \frac{4}{3} \lambda. \tag{4.6.15}$$

Since a is small compared to the macroscopic length scale of the shear flow, the fraction on the right-hand side can be approximated with a derivative, yielding the final result

$$f_x^{(y)} = \frac{1}{3} n M \bar{v} \lambda \frac{du_x}{dy}. \tag{4.6.16}$$

Now comparing equations (4.6.16) and (4.6.9), we derive an expression for the viscosity of a gas in terms of the number density, n , the molecular mass, M , the magnitude of the fluctuating velocity component, \bar{v} , and the mean free path, λ ,

$$\mu = \frac{1}{3} n M \bar{v} \lambda. \quad (4.6.17)$$

The units of the four terms on the right-hand side following the numerical fraction $\frac{1}{3}$ are as follows:

$$\frac{\text{Particle}}{\text{Volume}} \times \frac{\text{Mass}}{\text{Particle}} \times \frac{\text{Length}}{\text{Time}} \times \text{Length} = \frac{\text{Mass}}{\text{Length Time}}, \quad (4.6.18)$$

as required.

We have derived the Newtonian constitutive equation from molecular considerations and obtained a prediction for the viscosity of a gas in terms of molecular properties.

4.6.5 Ideal fluids

If the viscosity of a fluid vanishes, the fluid is frictionless and is called ideal. The stress tensor in an ideal fluid is given by a simplified version of (4.6.6),

$$\boldsymbol{\sigma} = -p \mathbf{I}. \quad (4.6.19)$$

However, in practice, no fluid is ideal and the absence of viscosity should be interpreted strictly as insignificance of hydrodynamic forces or stresses associated with the fluid viscosity. Viscous stresses are always important near solid boundaries, as discussed in Chapter 10. The formal requirement for viscous stresses to be negligible will be discussed in Chapter 6 with reference to the Reynolds number.

4.6.6 Significance of the pressure in an incompressible fluid

The physical interpretation of the pressure in the Newtonian constitutive equation (4.6.6), or any other constitutive equation, is not entirely clear. Strictly speaking, the pressure is a mathematical entity defined in terms of the trace of the stress tensor,

$$p = -\frac{1}{3} \text{trace}(\boldsymbol{\sigma}) = -\frac{1}{3} (\sigma_{xx} + \sigma_{yy} + \sigma_{zz}). \quad (4.6.20)$$

All we can say with confidence is that, as a fluid becomes quiescent, the dynamic pressure reduces to the hydrostatic pressure computed from consideration of random molecular motions.

In the case of compressible gases, an equation relating the pressure to the density to the temperature can be derived working in the framework of equilibrium thermodynamics, as discussed in Section 4.7

PROBLEMS**4.6.1 Flow in a channel.**

Consider steady unidirectional flow in a channel due to the translation of the upper wall, as depicted in Figure 4.6.1(b).

(a) Perform a force balance over a rectangular fluid layer confined between two y levels to show that, if the pressure is uniform, the shear stress $f_x^{(y)}$ must be independent of y .

(b) Having established that $f_x^{(y)}$ is constant, solve the first-order differential equation (4.6.9) for u_x in terms of y subject to the no-slip boundary conditions $u_x(y=0) = 0$ and $u_x(y=h) = V$, and evaluate $f_x^{(y)}$ in terms of μ , V , and the channel width, h .

4.6.2 Extensional flow

(a) Consider a two-dimensional extensional flow in the xy plane with velocity components

$$u_x = \xi x, \quad u_y = -\xi y, \quad (4.6.21)$$

where ξ is the rate of extension with units of inverse time. The corresponding pressure field is uniform throughout the domain of flow. Confirm that the fluid is incompressible, sketch the streamline pattern, and evaluate the stress tensor.

(b) Repeat (a) for axisymmetric extensional flow with Cartesian velocity components

$$u_x = \xi x, \quad u_y = -\frac{1}{2} \xi y, \quad u_z = -\frac{1}{2} \xi z. \quad (4.6.22)$$

(c) The axisymmetric extensional flow discussed in (b) describes the motion inside the thread illustrated in Figure 4.6.1(a). Assuming that the fluid is Newtonian, compute the force necessary to pull the rods apart with velocity V in terms of the half-length of the thread, L , the fluid viscosity, μ , and the cross-sectional area of the rods, A .

4.7 Pressure in compressible fluids

Consider a small fluid parcel of a compressible gas with volume V . To decrease the volume of the parcel by a differential amount, dV , we may apply an external pressure, p , by way of an ideal *frictionless* piston. The differential work required to carry out this reduction is

$$\delta W = -p dV = -p n dv, \quad (4.7.1)$$

where n is the number of moles contained in the parcel and v is the specific volume defined as the volume occupied by one mole of gas; by definition,

$$V = nv. \quad (4.7.2)$$

In our experiment, dV and dv are both negative due to compression, while δW is positive. In the case of expansion, dV and dv would be both positive, while δW would be negative, indicating that energy would be released instead of supplied.

The notation δW emphasizes that the differential work can be computed only after the frictional properties of the piston have been specified. In formal thermodynamics, we say that δW is an *inexact differential*.

Part of the work in compression or expansion is spent to increase the temperature of the parcel, T , by a differential amount, dT , and therefore the internal (thermal) energy of the parcel, U , by a differential amount, dU . The remainder of the work escapes as a (negative) process-dependent heat loss, δQ .

Energy conservation for a closed system in the absence of significant kinetic or potential energy requires that

$$dU = \delta W + \delta Q, \quad (4.7.3)$$

which can be rearranged as

$$\delta W = dU - \delta Q. \quad (4.7.4)$$

A certain change in internal energy, dU , can be achieved by different combinations of δW and δQ satisfying this equation.

Reversible process

To quantify the heat loss in the case of a *reversible process*, we write

$$\delta Q_{\text{rev}} = T dS, \quad (4.7.5)$$

and obtain

$$\delta W_{\text{rev}} = dU - T dS, \quad (4.7.6)$$

where S is the entropy. Dividing this equation by the number of moles of the gas, n , we obtain

$$\delta w_{\text{rev}} = du - T ds, \quad (4.7.7)$$

where

$$w = \frac{W}{n}, \quad u = \frac{U}{n}, \quad s = \frac{S}{n} \quad (4.7.8)$$

are the specific work, specific internal energy, and specific entropy.

Now substituting into (4.7.7) the expression $\delta w_{\text{rev}} = -p dv$ and rearranging, we derive a process-independent differential relation in the absence of inexact differentials,

$$du = T ds - p dv. \quad (4.7.9)$$

If the specific volume of a gas is made to change by the same small amount, dv , according to two different processes, the corresponding changes in the specific internal energy, du , and specific entropy, ds , will be such that equation (4.7.9) is satisfied in both cases.

Ideal gas

The specific internal energy of an arbitrary gas depends on the temperature, T , and specific volume, v . Due to the absence of intermolecular forces, the specific internal energy of an ideal gas depends on the temperature alone. The change in the specific internal energy is given by

$$du = c_v dT, \quad (4.7.10)$$

where c_v is the specific heat capacity under constant volume. Substituting this equation into the balance equation (4.7.9) and rearranging, we find that

$$ds = \frac{c_v}{T} dT + \frac{p}{T} dv, \quad (4.7.11)$$

which shows that

$$\frac{c_v}{T} = \left(\frac{\partial s}{\partial T} \right)_v, \quad (4.7.12)$$

that is, the ratio c_v/T is the partial derivative of the specific entropy with respect to the temperature under constant volume. For a mono-atomic ideal gas, $c_v = \frac{3}{2} R$. For a diatomic ideal gas, $c_v = \frac{5}{2} R$.

Change of entropy

Now solving the equation of state for an ideal gas, $pv = RT$, for the pressure, and substituting the result into (4.7.1), we find that

$$\delta w = -p dv = -RT \frac{dv}{v}. \quad (4.7.13)$$

Substituting this expression into the balance equation (4.7.11), we obtain

$$-R \frac{dv}{v} = c_v \frac{dT}{T} - ds. \quad (4.7.14)$$

Rearranging, we derive an expression for the change in the specific entropy,

$$ds = c_v \frac{dT}{T} + R \frac{dv}{v}, \quad (4.7.15)$$

applicable for an ideal gas.

Next, we treat c_v as a constant and integrate (4.7.15) between two states labeled A and B to derive an expression for the difference in entropy,

$$\Delta s \equiv s_B - s_A = c_v \ln \frac{T_B}{T_A} + R \ln \frac{v_B}{v_A}, \quad (4.7.16)$$

which can be rearranged into

$$\Delta s \equiv s_B - s_A = \ln \left[\left(\frac{T_B}{T_A} \right)^{c_v} \left(\frac{v_B}{v_A} \right)^R \right]. \quad (4.7.17)$$

For example, in the case of constant pressure, $p_B = p_A$, we use the equation of state to write $v_B/v_A = T_B/T_A$ and

$$\Delta s = c_p \ln \frac{T_B}{T_A}, \quad (4.7.18)$$

where $c_p = c_v + R$ is the specific heat capacity under constant pressure.

Isentropic compression or expansion

In the case of a constant entropy (isentropic) reversible process, $s_B = s_A$, the general equation (4.7.17) for an ideal gas yields

$$\left(\frac{T_B}{T_A}\right)^{c_v} \left(\frac{v_B}{v_A}\right)^R = 1, \quad (4.7.19)$$

and thus

$$T^{c_v} v^R = A, \quad (4.7.20)$$

where A is a constant. This equation provides us with a relation between the specific volume, v , and the temperature, T . Introducing the density, $\rho = M/v$, we write

$$T^{c_v} = B\rho^R, \quad (4.7.21)$$

where M is the molecular weight and $B \equiv A/M^R$ is a new constant. Using the ideal gas law expressed in the form

$$T = \frac{Mp}{R\rho}, \quad (4.7.22)$$

we eliminate the temperature and thus obtain a relation between the density and the pressure in an ideal compressible gas in isentropic transition,

$$p = D\rho^k, \quad (4.7.23)$$

where D is a new constant and

$$k \equiv \frac{c_v + R}{c_v} = \frac{c_p}{c_v} \quad (4.7.24)$$

is the heat capacity ratio.

Speed of sound

The square of the speed of sound, c , is given by the formula

$$c^2 = \left(\frac{\partial p}{\partial \rho}\right)_s. \quad (4.7.25)$$

The right-hand side is the derivative of the pressure with respect to the density at constant entropy. Using (4.7.23), we find that

$$c^2 = D k \rho^{k-1} = k \frac{p}{\rho}, \quad (4.7.26)$$

and then

$$c^2 = k \frac{RT}{M}. \quad (4.7.27)$$

The higher the temperature, the faster the speed of sound, in agreement with physical intuition.

PROBLEM

4.7.1 Speed of sound in the atmosphere

Use equation (4.7.27) to predict the speed of sound in the atmosphere regarded as an ideal gas with $k = 1.4$ and molecular mass $M = 28.97$ kg/kmole at 25° C.

4.8 Simple non-Newtonian fluids

The Newtonian constitutive law for an incompressible fluid, expressed by equation (4.6.6), describes the stresses developing in a fluid consisting of small molecules. Fluids containing or consisting of macromolecules, such as polymeric solutions and melts, and fluids containing suspended rigid or deformable particles, exhibit a more complicated behavior described by more involved constitutive equations. Examples include pastes, bubbly liquids, and biological fluids, such as blood.

To derive a constitutive equation for a non-Newtonian fluid, we consider the motion of a small fluid parcel and seek to establish a relation between the instantaneous traction exerted on the parcel surface, expressed in terms of the stress tensor, $\boldsymbol{\sigma}$, and the entire history of the parcel deformation. In the simplest class of materials, the traction depends only on the instantaneous rate of parcel deformation expressed by the rate-of-deformation tensor, \mathbf{E} .

A distinguishing feature of a non-Newtonian fluid is that the relation between the stress tensor, $\boldsymbol{\sigma}$, and the rate-of-deformation tensor, \mathbf{E} , is nonlinear. In contrast, the corresponding relation for a Newtonian fluid is linear.

4.8.1 Unidirectional shear flow

In the case of two-dimensional unidirectional shear flow along the x axis, the Newtonian shear stress, given by

$$\sigma_{yx} = \mu \frac{du_x}{dy}, \quad (4.8.1)$$

can be generalized by allowing the viscosity to depend on the magnitude of the shear rate, $|du_x/dy|$, where the vertical bars indicate the absolute value. If the viscosity decreases as the shear rate increases, the fluid is shear-thinning or pseudo-plastic. If the viscosity increases as the shear rate increases, the fluid is shear-thickening or dilatant.

Physically, the dependence of the viscosity on the shear rate is attributed to changes in the configuration of molecules, changes in the shape and relative position of particles suspended in a fluid, and to the spontaneous formation of internal microstructure due to intermolecular force fields and other particle interactions.

Power-law fluids

The shear stress developing in a certain class of non-Newtonian fluids in unidirectional shear flow can be described by the *Ostwald-de Waele model*. In this model, the viscosity is proportional to the magnitude of the shear rate raised to a certain power,

$$\mu = \mu_0 \left| \frac{du_x}{dy} \right|^{n-1}, \quad (4.8.2)$$

where μ_0 is a reference viscosity and n is the power-law exponent. When $n = 1$, we obtain a Newtonian fluid with viscosity μ_0 ; when $n < 1$, we obtain a shear-thinning fluid; when $n > 1$, we obtain a shear-thickening fluid.

Substituting (4.8.2) into expression (4.6.9), we derive an expression for the shear stress,

$$f_x^{(y)} = \sigma_{yx} = \mu_0 \left| \frac{du_x}{dy} \right|^{n-1} \frac{du_x}{dy}. \quad (4.8.3)$$

When $n = 1$, we recover the Newtonian shear stress.

4.8.2 Channel flow

As an application, we consider flow in a channel due to the translation of the upper wall with velocity V , as illustrated in [Figure 4.6.1\(b\)](#). Performing a force balance over a rectangular fluid layer, we find that, if the pressure is uniform, the shear stress, σ_{yx} , is independent of y and the right-hand side of (4.8.3) is constant (Problem 4.5.1).

The fluid velocity at the upper wall located at $y = h$ is equal to the wall velocity, V , while the fluid velocity at the stationary lower wall located at $y = 0$ is zero. Integrating equation $du_x/dy = c$, where c is the constant shear rate, and using the aforementioned boundary conditions, we derive a linear velocity profile with shear rate

$$\frac{du_x}{dy} = \frac{V}{h}, \quad (4.8.4)$$

independent of the value of the power-law exponent, n .

Although the velocity profile is linear for any value of n , the magnitude of the shear stress depends on n , as shown in equation (4.8.3). This distinction emphasizes that the

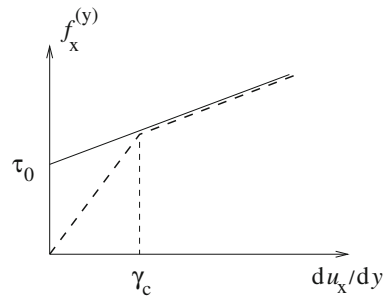


Figure 4.8.1 Rheological response of a Bingham plastic showing a yield-stress behavior in unidirectional flow.

kinematic appearance of a flow does not necessarily reflect the magnitude of the stresses developing in the fluid. Two flows that are kinematically identical may support different stress fields.

4.8.3 Yield-stress fluids

A class of heterogeneous fluids, called Bingham plastics, flow only when the shear stress established due to the motion exceeds a certain threshold. Examples include pastes and concentrated suspensions of fine particles. An idealized constitutive equation between stress and shear rate for this class of materials is

$$\frac{du_x}{dy} = 0 \quad \text{if} \quad |\sigma_{yx}| < \tau_0 \quad (4.8.5)$$

and

$$f_x^{(y)} = \sigma_{yx} = \tau_0 + \mu \frac{du_x}{dy} \quad \text{if} \quad |\sigma_{yx}| > \tau_0, \quad (4.8.6)$$

where μ is the viscosity and τ_0 is the yield stress. The relation between the shear stress and the shear rate is represented by the solid line in [Figure 4.8.1](#).

As an application, we consider the familiar unidirectional flow in a channel confined between two parallel walls, generated by exerting on the upper wall a force, F , parallel to the x axis. If the fluid is a Bingham plastic whose rheological behavior is described by equations (4.8.5) and (4.8.6), a shear flow across the entire cross-section of the channel will be established only if the externally imposed force F over a certain length of the channel, L , counteracting the shear stress, $\sigma_{yx} = F/L$, is greater than the yield-stress threshold, τ_0 .

Assuming that this occurs, we treat σ_{yx} as a constant, solve equation (4.8.6) for du_x/dy , and then integrate with respect to y subject to the boundary condition $u_x(y = 0) = 0$ to obtain a linear velocity profile,

$$u_x = \frac{y}{\mu} \left(\frac{F}{L} - \tau_0 \right). \quad (4.8.7)$$

The velocity at the upper wall is

$$u_x(y = h) = \frac{h}{\mu} \left(\frac{F}{L} - \tau_0 \right) = V. \quad (4.8.8)$$

In practice, equation (4.8.8) allows us to estimate the values of the physical constants μ and τ_0 from laboratory observations.

PROBLEM

4.8.1 Yield-stress fluid

The relation between the shear stress and shear rate for a class of yield-stress fluids in unidirectional flow is described by the broken line in [Figure 4.8.1](#), where γ_c is the critical shear rate.

(a) State the equations describing this rheological behavior.

(b) Compute the shear stress established in a channel with parallel walls, where the upper wall translates with velocity V while the lower wall is held stationary.

4.9 Stresses in polar coordinates

We have discussed tractions and stresses in Cartesian coordinates. In practice, it is often convenient to work in cylindrical, spherical, or plane polar coordinates, with the benefit of reduced algebraic manipulations and ease in the implementation of boundary conditions. In this section, we define the components of the stress tensor in polar coordinates and relate them to the pressure and to the corresponding components of the rate-of-deformation tensor using the constitutive equation for an incompressible Newtonian fluid.

4.9.1 Cylindrical polar coordinates

Consider the cylindrical polar coordinates, (x, σ, φ) , depicted in [Figure 4.9.1\(a\)](#). The traction exerted on a small surface that is perpendicular to the x axis, $\mathbf{f}^{(x)}$, acting on the side that faces the positive direction of the x axis, can be resolved into its cylindrical polar components as

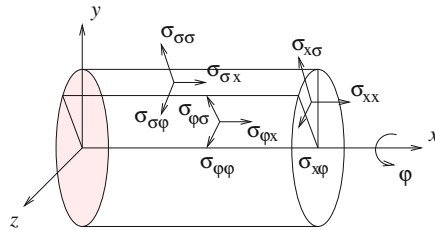
$$\mathbf{f}^{(x)} = f_x^{(x)} \mathbf{e}_x + f_\sigma^{(x)} \mathbf{e}_\sigma + f_\varphi^{(x)} \mathbf{e}_\varphi, \quad (4.9.1)$$

where \mathbf{e}_x , \mathbf{e}_σ , and \mathbf{e}_φ are unit vectors pointing, respectively, in the axial, radial, and azimuthal direction. Note that the orientation of \mathbf{e}_x is constant, whereas the orientations of \mathbf{e}_σ and \mathbf{e}_φ change with position in the flow.

The traction exerted on a small surface that is perpendicular to the distance from the x axis, $\mathbf{f}^{(\sigma)}$, and is thus parallel to the axial and azimuthal directions at a designated center of the surface, can be resolved into corresponding components as

$$\mathbf{f}^{(\sigma)} = f_x^{(\sigma)} \mathbf{e}_x + f_\sigma^{(\sigma)} \mathbf{e}_\sigma + f_\varphi^{(\sigma)} \mathbf{e}_\varphi. \quad (4.9.2)$$

(a)



(b)

$$\begin{aligned} \sigma_{xx} &= -p + 2\mu \frac{\partial u_x}{\partial x}, & \sigma_{x\sigma} &= \sigma_{\sigma x} = \mu \left(\frac{\partial u_x}{\partial \sigma} + \frac{\partial u_\sigma}{\partial x} \right) \\ \sigma_{x\varphi} &= \sigma_{\varphi x} = \mu \left(\frac{\partial u_\varphi}{\partial x} + \frac{1}{\sigma} \frac{\partial u_x}{\partial \varphi} \right), & \sigma_{\sigma\sigma} &= -p + 2\mu \frac{\partial u_\sigma}{\partial \sigma} \\ \sigma_{\sigma\varphi} &= \sigma_{\varphi\sigma} = \mu \left(\sigma \frac{\partial}{\partial \sigma} \left(\frac{u_\varphi}{\sigma} \right) + \frac{1}{\sigma} \frac{\partial u_\sigma}{\partial \varphi} \right), & \sigma_{\varphi\varphi} &= -p + 2\mu \left(\frac{1}{\sigma} \frac{\partial u_\varphi}{\partial \varphi} + \frac{u_\sigma}{\sigma} \right) \end{aligned}$$

Table 4.9.1 (a) Physical depiction of the components of the stress tensor in cylindrical polar coordinates and (b) expressions for the components of the stress tensor in a Newtonian fluid. Note that the stress tensor remains symmetric in these coordinates.

The traction exerted on a small surface that is normal to the azimuthal direction, $\mathbf{f}^{(\varphi)}$, can be resolved as

$$\mathbf{f}^{(\varphi)} = f_x^{(\varphi)} \mathbf{e}_x + f_\sigma^{(\varphi)} \mathbf{e}_\sigma + f_\varphi^{(\varphi)} \mathbf{e}_\varphi. \tag{4.9.3}$$

Stacking the coefficients of the unit vectors on the right-hand sides of (4.9.1)–(4.9.3) on top of one another in a particular order, we obtain the cylindrical polar components of the stress tensor,

$$(\sigma_{\alpha\beta}) = \begin{pmatrix} f_x^{(x)} & f_\sigma^{(x)} & f_\varphi^{(x)} \\ f_x^{(\sigma)} & f_\sigma^{(\sigma)} & f_\varphi^{(\sigma)} \\ f_x^{(\varphi)} & f_\sigma^{(\varphi)} & f_\varphi^{(\varphi)} \end{pmatrix}, \tag{4.9.4}$$

where Greek indices stand for x , σ , or φ . We have used large parentheses instead of the square brackets to indicate that the matrix shown in (4.9.4) should not be misinterpreted as a Cartesian tensor.

Now we define

$$\sigma_{\alpha\beta} \equiv f_\beta^{(\alpha)}, \tag{4.9.5}$$

where Greek indices stand for x , σ , or φ . With the convention expressed by (4.9.5), the cylindrical polar components of the stress tensor are collected in the matrix

$$(\sigma_{\alpha\beta}) = \begin{pmatrix} \sigma_{xx} & \sigma_{x\sigma} & \sigma_{x\varphi} \\ \sigma_{\sigma x} & \sigma_{\sigma\sigma} & \sigma_{\sigma\varphi} \\ \sigma_{\varphi x} & \sigma_{\varphi\sigma} & \sigma_{\varphi\varphi} \end{pmatrix}. \quad (4.9.6)$$

This matrix should not be misinterpreted as a Cartesian tensor.

Newtonian fluids

The stress components in an incompressible Newtonian fluid derive from the constitutive equation (4.6.6) as shown in [Table 4.9.1\(a\)](#). To derive these relations, we may write

$$\mathbf{f}^{(x)} = \sigma_{xx} \mathbf{e}_x + \sigma_{xy} \mathbf{e}_y + \sigma_{xz} \mathbf{e}_z, \quad (4.9.7)$$

for the axial component,

$$\begin{aligned} \mathbf{f}^{(\sigma)} &= \mathbf{f}^{(y)} \cos \varphi + \mathbf{f}^{(z)} \sin \varphi \\ &= (\sigma_{yx} \mathbf{e}_x + \sigma_{yy} \mathbf{e}_y + \sigma_{yz} \mathbf{e}_z) \cos \varphi + (\sigma_{zx} \mathbf{e}_x + \sigma_{zy} \mathbf{e}_y + \sigma_{zz} \mathbf{e}_z) \sin \varphi, \end{aligned} \quad (4.9.8)$$

for the radial component, and

$$\begin{aligned} \mathbf{f}^{(\varphi)} &= -\mathbf{f}^{(y)} \sin \varphi + \mathbf{f}^{(z)} \cos \varphi \\ &= -(\sigma_{yx} \mathbf{e}_x + \sigma_{yy} \mathbf{e}_y + \sigma_{yz} \mathbf{e}_z) \sin \varphi + (\sigma_{zx} \mathbf{e}_x + \sigma_{zy} \mathbf{e}_y + \sigma_{zz} \mathbf{e}_z) \cos \varphi, \end{aligned} \quad (4.9.9)$$

for the azimuthal component. Substituting

$$\mathbf{e}_y = \mathbf{e}_\sigma \cos \varphi - \mathbf{e}_\varphi \sin \varphi, \quad \mathbf{e}_z = \mathbf{e}_\sigma \sin \varphi + \mathbf{e}_\varphi \cos \varphi, \quad (4.9.10)$$

and consolidating terms multiplying the unit cylindrical polar vectors in (4.9.7), we obtain

$$\sigma_{x\sigma} = \sigma_{xy} \cos \varphi + \sigma_{xz} \sin \varphi = \mu \left(\cos \varphi \frac{\partial u_x}{\partial y} + \sin \varphi \frac{\partial u_x}{\partial z} \right) + \mu \frac{\partial (u_y \cos \varphi + u_z \sin \varphi)}{\partial x} \quad (4.9.11)$$

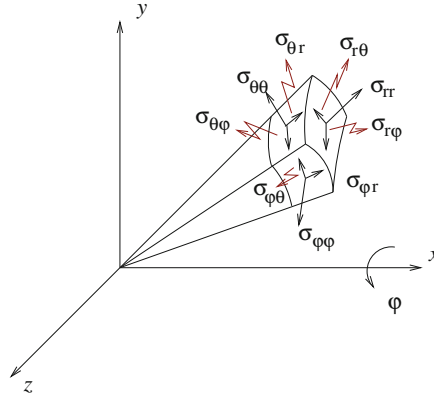
and

$$\sigma_{x\varphi} = -\sigma_{xy} \sin \varphi + \sigma_{xz} \cos \varphi = \mu \left(-\sin \varphi \frac{\partial u_x}{\partial y} + \cos \varphi \frac{\partial u_x}{\partial z} \right) + \mu \frac{\partial (-u_y \sin \varphi + u_z \cos \varphi)}{\partial x}, \quad (4.9.12)$$

which reproduce the second and third relations in [Table 4.9.1\(b\)](#). The rest of the relations can be derived working in a similar fashion. More expedient methods of deriving these relations are available.¹

¹Pozrikidis, C. (2011) *Introduction to Theoretical and Computational Fluid Dynamics*. Second Edition, Oxford University Press.

(a)



(b)

$$\begin{aligned} \sigma_{rr} &= -p + 2\mu \frac{\partial u_r}{\partial r}, & \sigma_{r\theta} = \sigma_{\theta r} &= \mu \left(r \frac{\partial}{\partial r} \left(\frac{u_\theta}{r} \right) + \frac{1}{r} \frac{\partial u_r}{\partial \theta} \right) \\ \sigma_{r\varphi} = \sigma_{\varphi r} &= \mu \left(\frac{1}{r \sin \theta} \frac{\partial u_r}{\partial \varphi} + r \frac{\partial}{\partial r} \left(\frac{u_\varphi}{r} \right) \right), & \sigma_{\theta\theta} &= -p + 2\mu \left(\frac{1}{r} \frac{\partial u_\theta}{\partial \theta} + \frac{u_r}{r} \right) \\ \sigma_{\theta\varphi} = \sigma_{\varphi\theta} &= \mu \left(\frac{\sin \theta}{r} \frac{\partial}{\partial \theta} \left(\frac{u_\varphi}{\sin \theta} \right) + \frac{1}{r \sin \theta} \frac{\partial u_\theta}{\partial \varphi} \right) \\ \sigma_{\varphi\varphi} &= -p + \mu \frac{2}{r \sin \theta} \left(\frac{\partial u_\varphi}{\partial \varphi} + u_r \sin \theta + u_\theta \cos \theta \right) \end{aligned}$$

Table 4.9.2 (a) Physical depiction of the components of the stress tensor in spherical polar coordinates and (b) components of the stress tensor in a Newtonian fluid. Note that the stress tensor remains symmetric in these coordinates.

4.9.2 Spherical polar coordinates

Consider a system of spherical polar coordinates, (r, θ, φ) , defined in Table 4.9.2(a). The traction exerted on a small surface that is normal to the distance from the origin, acting on the side of the surface that faces away from the origin, $\mathbf{f}^{(r)}$, can be resolved into its spherical polar components as

$$\mathbf{f}^{(r)} = f_r^{(r)} \mathbf{e}_r + f_\theta^{(r)} \mathbf{e}_\theta + f_\varphi^{(r)} \mathbf{e}_\varphi, \tag{4.9.13}$$

where \mathbf{e}_r , \mathbf{e}_θ , and \mathbf{e}_φ are unit vectors pointing in the radial, meridional, and azimuthal directions.

The traction exerted on a small surface that is normal to the meridional direction corresponding to the angle θ , and is thus parallel to the radial and azimuthal directions,

$\mathbf{f}^{(\theta)}$, can be resolved as

$$\mathbf{f}^{(\theta)} = f_r^{(\theta)} \mathbf{e}_r + f_\theta^{(\theta)} \mathbf{e}_\theta + f_\varphi^{(\theta)} \mathbf{e}_\varphi. \quad (4.9.14)$$

The traction exerted on a small surface that is normal to the azimuthal direction, and is thus parallel to the radial and meridional directions, $\mathbf{f}^{(\varphi)}$, can be resolved as

$$\mathbf{f}^{(\varphi)} = f_r^{(\varphi)} \mathbf{e}_r + f_\theta^{(\varphi)} \mathbf{e}_\theta + f_\varphi^{(\varphi)} \mathbf{e}_\varphi. \quad (4.9.15)$$

Stacking the coefficients of the unit vectors on the right-hand sides of (4.9.13)–(4.9.15) on top of one another in a particular order, we obtain a matrix containing the spherical polar components of the stress tensor,

$$(\sigma_{\alpha\beta}) = \begin{pmatrix} f_r^{(r)} & f_\theta^{(r)} & f_\varphi^{(r)} \\ f_r^{(\theta)} & f_\theta^{(\theta)} & f_\varphi^{(\theta)} \\ f_r^{(\varphi)} & f_\theta^{(\varphi)} & f_\varphi^{(\varphi)} \end{pmatrix}, \quad (4.9.16)$$

where Greek indices stand for x , σ , or φ .

Now we introduce the standard two-index notation for the stress tensor, writing

$$\sigma_{\alpha\beta} \equiv f_\beta^{(\alpha)}, \quad (4.9.17)$$

where Greek indices stand for r , θ , or φ . With the convention expressed by (4.9.17), the matrix containing the spherical polar components of the stress tensor is given by

$$(\sigma_{\alpha\beta}) = \begin{pmatrix} \sigma_{rr} & \sigma_{r\theta} & \sigma_{r\varphi} \\ \sigma_{\theta r} & \sigma_{\theta\theta} & \sigma_{\theta\varphi} \\ \sigma_{\varphi r} & \sigma_{\varphi\theta} & \sigma_{\varphi\varphi} \end{pmatrix}. \quad (4.9.18)$$

This matrix should not be misinterpreted as a Cartesian tensor.

Newtonian fluids

The stress components for an incompressible Newtonian fluid derive from the constitutive equation (4.6.6) as shown in [Table 4.9.2\(b\)](#).

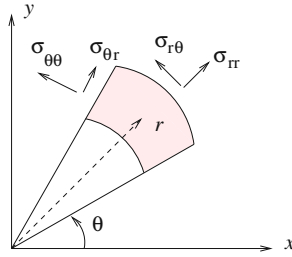
4.9.3 Plane polar coordinates

Consider a two-dimensional flow in the xy plane and refer to the plane polar coordinates, (r, θ) , depicted in [Table 4.9.3\(a\)](#). The traction exerted on a small segment that is normal to the distance from the origin, acting on the side facing away from the origin, $\mathbf{f}^{(r)}$, can be resolved into its plane polar components as

$$\mathbf{f}^{(r)} = f_r^{(r)} \mathbf{e}_r + f_\theta^{(r)} \mathbf{e}_\theta, \quad (4.9.19)$$

where \mathbf{e}_r and \mathbf{e}_θ are unit vectors pointing in the radial and polar direction.

(a)



(b)

$$\begin{aligned} \sigma_{rr} &= -p + 2\mu \frac{\partial u_r}{\partial r}, & \sigma_{r\theta} = \sigma_{\theta r} &= \mu \left(r \frac{\partial}{\partial r} \left(\frac{u_\theta}{r} \right) + \frac{1}{r} \frac{\partial u_r}{\partial \theta} \right) \\ \sigma_{\theta\theta} &= -p + 2\mu \left(\frac{1}{r} \frac{\partial u_\theta}{\partial \theta} + \frac{u_r}{r} \right) \end{aligned}$$

Table 4.9.3 (a) Components of the stress tensor in plane polar coordinates (r, θ) and (b) components of the stress tensor in a Newtonian fluid. Note that the stress tensor remains symmetric in these coordinates.

The traction exerted on a small surface that is normal to the direction of the polar angle θ , and is thus parallel to the distance from the origin, $\mathbf{f}^{(\theta)}$, can be resolved as

$$\mathbf{f}^{(\theta)} = f_r^{(\theta)} \mathbf{e}_r + f_\theta^{(\theta)} \mathbf{e}_\theta. \tag{4.9.20}$$

Stacking the coefficients of the unit vectors on the right-hand sides of (4.9.19) and (4.9.20) on top of one another in a particular order, we obtain the plane polar components of the stress tensor,

$$\begin{pmatrix} f_r^{(r)} & f_\theta^{(r)} \\ f_r^{(\theta)} & f_\theta^{(\theta)} \end{pmatrix}. \tag{4.9.21}$$

Next, we introduce the familiar two-index notation,

$$\sigma_{\alpha\beta} \equiv f_\beta^{(\alpha)}, \tag{4.9.22}$$

where Greek indices stand for r or θ . With the convention expressed by (4.9.22), the matrix containing the plane polar components of the stress tensor is given by

$$(\sigma_{\alpha\beta}) = \begin{pmatrix} \sigma_{rr} & \sigma_{r\theta} \\ \sigma_{\theta r} & \sigma_{\theta\theta} \end{pmatrix}. \tag{4.9.23}$$

This matrix should not be confused with a Cartesian tensor.

Newtonian fluids

The stress components for an incompressible Newtonian fluid derive from the constitutive equation (4.6.6) as shown in [Table 4.9.3\(b\)](#).

PROBLEM

4.9.1 Plane polar coordinates

Work as discussed in the text for the cylindrical polar coordinates to derive the Newtonian constitutive equations in plane polar coordinates shown in [Table 4.9.3](#).

4.10 Boundary conditions for the tangential velocity

In Section 2.10.1, we discussed the no-penetration boundary condition over impermeable boundaries and interfaces between immiscible fluids, involving the normal component of the fluid velocity. Viscous fluids obey an additional boundary condition concerning the tangential component of the fluid velocity.

4.10.1 No-slip boundary condition

Under most conditions, the vast majority of fluids satisfy the no-slip boundary condition requiring that:

- The tangential component of the fluid velocity over a solid boundary is equal to the tangential component of the boundary velocity.
- The tangential component of the fluid velocity is continuous across an interface between two immiscible fluids.

The no-slip boundary condition has been confirmed in the overwhelming majority of applications and is the standard choice in mainstream fluid dynamics. Combined with the no-slip condition, the no-penetration condition requires that the fluid velocity is equal to the local velocity of an impermeable solid boundary and continuous across an interface.

Physical origin

The physical origin of the no-slip boundary condition over a solid surface has not been established with absolute certainty. One theory argues that the molecules of a fluid next to a solid surface are adsorbed onto the surface for a short period of time, only to be desorbed and ejected into the fluid. This relentless process slows down the fluid and effectively renders the tangential component of the fluid velocity equal to the corresponding component of the boundary velocity. Another theory argues that the true boundary condition is the condition of vanishing shear stress, and the no-slip boundary condition arises due to microscopic boundary roughness. Thus, a perfectly smooth boundary would allow the fluid to slip.

4.10.2 Slip boundary condition

Exceptions to the no-slip boundary condition arise in the case of rarefied gas flow, high-pressure flow of polymer melts, flow near a three-phase contact line where a solid meets two liquids or a gas and a liquid, and flow past interfaces consisting of dual or multiple molecular layers that may exhibit relative motion, yielding a discontinuous macroscopic velocity. The no-slip boundary condition is sometimes relaxed in numerical simulations to prevent singularities stemming from excessive idealization. One example is the development of an infinite force on a sharp plate scraping fluid off a flat surface.

Consider steady unidirectional flow in a channel with parallel walls driven by the parallel translation of the upper wall along the x axis with velocity V , as illustrated in [Figure 4.6.1\(b\)](#). In this case, we may specify that the fluid slips over the lower wall such that the slip velocity, $u_x(y = 0)$, is related to the wall shear stress by

$$u_x(y = 0) = \frac{L}{\mu\beta} \sigma_{yx}(y = 0) = \frac{L}{\beta} \left(\frac{\partial u_x}{\partial y} \right)_{y=0}, \quad (4.10.1)$$

where the constant β is the slip coefficient and L is a reference length identified, for example, with the channel width. As β tends infinity, the slip velocity tends to zero and the no-slip boundary condition prevails. The slip length is defined as $\ell = L/\beta$.

Rarefied gases

In the case of a rarefied gas, the slip coefficient, β , and slip length, ℓ , can be rigorously related to the molecular mean free path, λ , by the Maxwell relation

$$\frac{\lambda}{\ell} = \beta K_n = \frac{\sigma}{2 - \sigma}, \quad (4.10.2)$$

where $K_n \equiv \lambda/L$ is the Knudsen number and σ is the tangential momentum accommodation coefficient (TMAC) expressing the fraction of molecules that undergo diffusive instead of specular reflection. In the limit $\sigma \rightarrow 2$ we recover the no-slip boundary condition, $\beta \rightarrow \infty$. In the limit $\sigma \rightarrow 0$ we recover the perfect-slip boundary condition, $\beta \rightarrow 0$.

PROBLEM

4.10.1 Flow in a channel with slip

In the case of shear-driven channel flow illustrated in [Figure 4.6.1\(b\)](#), the pressure is uniform and the shear stress σ_{yx} is constant, independent of y . Assuming that the slip condition applies at the upper and lower walls, derive expressions for the shear stress and velocity profile of a Newtonian fluid in terms of V , h , μ , and the slip length, ℓ .

4.11 Wall stresses in Newtonian fluids

Combining the no-slip boundary condition discussed in Section 4.10.1 with the no-penetration boundary condition discussed in Section 2.10.1, we derive remarkably simple expressions for

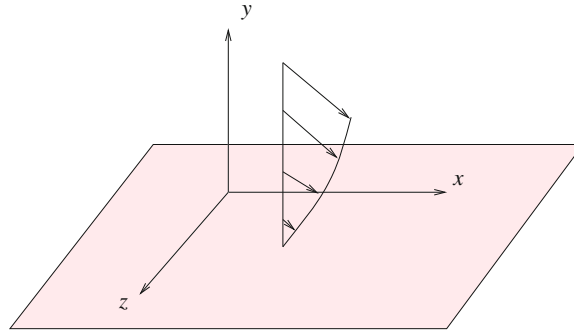


Figure 4.11.1 Flow over a plane wall subject to the no-slip boundary condition. The wall shear stress is proportional to the slope of the velocity profile with respect to distance normal to the wall, in this case y . The normal stress is equal to the negative of the pressure.

the Newtonian traction exerted on a solid surface, called the *wall stress*, amenable to a simple physical interpretation.

Consider a viscous flow above a stationary flat solid surface located at $y = 0$, as illustrated in Figure 4.11.1. The no-slip boundary condition requires that the tangential components of the velocity, and thus their derivatives with respect to z and x , are identically zero over the surface,

$$\frac{\partial u_x}{\partial x} = 0, \quad \frac{\partial u_z}{\partial x} = 0, \quad \frac{\partial u_x}{\partial z} = 0, \quad \frac{\partial u_z}{\partial z} = 0, \quad (4.11.1)$$

where all partial derivatives are evaluated at $y = 0$. The no-penetration boundary condition requires that the normal component of the velocity, and thus its derivatives with respect to z and x , also vanish over the surface,

$$\frac{\partial u_y}{\partial x} = 0, \quad \frac{\partial u_y}{\partial z} = 0, \quad (4.11.2)$$

where all partial derivatives are evaluated at $y = 0$. Thus, six of the nine components of the velocity-gradient tensor vanish over the surface.

Shear stress

The two components of the Newtonian shear stress exerted on the surface are given by

$$\sigma_{yx} = \mu \left(\frac{\partial u_x}{\partial y} + \frac{\partial u_y}{\partial x} \right), \quad \sigma_{yz} = \mu \left(\frac{\partial u_z}{\partial y} + \frac{\partial u_y}{\partial z} \right) \quad (4.11.3)$$

evaluated at $y = 0$. Using (4.11.2) to simplify (4.11.3), we find that

$$\sigma_{yx} = \mu \frac{\partial u_x}{\partial y}, \quad \sigma_{yz} = \mu \frac{\partial u_z}{\partial y} \quad (4.11.4)$$

evaluated at $y = 0$. Equations (4.11.4) reveal that the wall shear stress is equal to the slope of the tangential velocity with respect to distance normal to the wall multiplied by the fluid viscosity in any flow, not just in a unidirectional flow.

Normal stress

The Newtonian normal stress exerted on a solid surface is given by

$$\sigma_{yy} = -p + 2\mu \frac{\partial u_y}{\partial y} \quad (4.11.5)$$

evaluated at $y = 0$, where p is the pressure. Since the fluid has been assumed incompressible, we may use the continuity equation (2.9.2) to write

$$\frac{\partial u_y}{\partial y} = -\frac{\partial u_x}{\partial x} - \frac{\partial u_z}{\partial z} \quad (4.11.6)$$

evaluated at $y = 0$, and then invoke the first and fourth equations in (4.11.1) to find that $\partial u_y / \partial y = 0$. Expression (4.11.5) thus simplifies to

$$\sigma_{yy} = -p, \quad (4.11.7)$$

which shows that the normal stress exerted on a solid surface is equal to the negative of the pressure.

Generalization

The results displayed in equations (4.11.4) and (4.11.7) apply even when a surface translates with a constant or time-dependent velocity. Moreover, these results apply when a surface is curved, provided that the zx plane is tangential to the surface and the y axis is normal to the surface at the position when the shear and normal stress are evaluated.

PROBLEM

4.11.1 Vorticity at a no-slip surface

Show that the component of the vorticity vector normal to an impermeable wall vanishes, and thus the vortex lines are tangential to the surface. *Hint:* Use the second and third of equations (4.11.1).

4.12 Interfacial surfactant transport

An impure interface between two immiscible fluids is sometimes occupied by a molecular layer of surfactants affecting the local surface tension, γ . Dividing the number of surfactant molecules residing inside an infinitesimal surface patch centered at a point by the surface area of the patch, we obtain the surface concentration of the surfactant, Γ . The higher the surfactant concentration of the surfactant, the lower the surface tension.

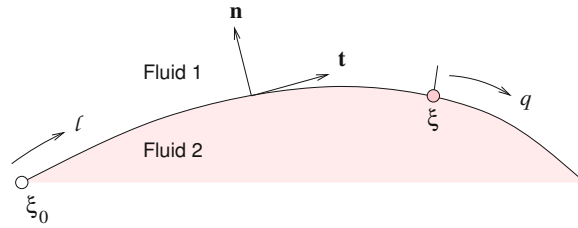


Figure 4.12.1 Point particles along a two-dimensional interface are identified by a parameter ξ that increases monotonically but in an otherwise arbitrary fashion along the interface.

Surface equation of state

For small surfactant concentrations, a linear surface equation of state can be assumed relating γ to Γ according to Gibbs' law,

$$\gamma = \frac{\gamma_0}{1 - \beta} \left(1 - \beta \frac{\Gamma}{\Gamma_0}\right), \quad (4.12.1)$$

where Γ_0 is a reference surfactant concentration and γ_0 is the corresponding surface tension. The dimensionless physical constant

$$\beta = RT \frac{\Gamma_0}{\gamma_c} \quad (4.12.2)$$

expresses the sensitivity of the surface tension to the surfactant concentration, where R is the ideal gas constant, T is the absolute temperature, and γ_c is the surface tension of a clean interface that is devoid of surfactants. More involved surface equations of state for moderate and large surfactant concentrations near saturation are available.

Interfacial convection-diffusion

The molecules of an insoluble surfactant are convected and diffuse over the interface, but do not enter the bulk of the fluid. Our objective in this section is to derive an evolution equation for the surface surfactant concentration determining the local surface tension and thus the jump in the traction across an interface.

4.12.1 Two-dimensional interfaces

Consider a chain of material point particles distributed along the inner or outer side of a two-dimensional interface. We begin by labeling the point particles using a parameter, ξ , so that their position can be described in parametric form as $\mathbf{X}(\xi)$ at any time, as shown in [Figure 4.12.1](#).

Let ℓ be the arc length measured along the interface from an arbitrary point particle labeled ξ_0 . The number of surfactant molecules residing inside a material test section of the

interface confined between ξ_0 and ξ is

$$n(\xi, t) = \int_{\ell(\xi_0, t)}^{\ell(\xi, t)} \Gamma(\xi', t) d\ell(\xi') = \int_{\xi_0}^{\xi} \Gamma(\xi', t) \frac{\partial \ell}{\partial \xi'} d\xi', \quad (4.12.3)$$

where ξ' is an integration variable. Conservation of the total number of surfactant molecules inside the test section requires that

$$\frac{\partial n}{\partial t} = q(\xi_0) - q(\xi), \quad (4.12.4)$$

where $q(\xi)$ is the flux of surfactant molecules along the interface due to diffusion, and the time derivative is taken keeping ξ fixed. Substituting the expression for n from the last integral in (4.12.3), and transferring the derivative inside the integral as a material derivative, we obtain

$$\int_{\xi_0}^{\xi} \frac{D}{Dt} \left(\Gamma(\xi', t) \frac{\partial \ell}{\partial \xi'} \right) d\xi' = q(\xi_0) - q(\xi), \quad (4.12.5)$$

where D/Dt is the material derivative. Now taking the limit as ξ tends to ξ_0 , we derive a differential equation,

$$\frac{D}{Dt} \left(\Gamma \frac{\partial \ell}{\partial \xi} \right) = -\frac{\partial q}{\partial \xi}. \quad (4.12.6)$$

Expanding the material derivative of the product on the left-hand side, we obtain

$$\frac{D\Gamma}{Dt} \frac{\partial \ell}{\partial \xi} + \Gamma \frac{D}{Dt} \left(\frac{\partial \ell}{\partial \xi} \right) = -\frac{\partial q}{\partial \xi}. \quad (4.12.7)$$

Interfacial stretching

Next, we use the Pythagorean theorem to write

$$\frac{\partial \ell}{\partial \xi} = \left[\left(\frac{\partial X}{\partial \xi} \right)^2 + \left(\frac{\partial Y}{\partial \xi} \right)^2 \right]^{1/2}, \quad (4.12.8)$$

and compute the material derivative

$$\frac{D}{Dt} \left(\frac{\partial \ell}{\partial \xi} \right) = \frac{1}{2} \frac{1}{\partial \ell / \partial \xi} \left[2 \frac{\partial X}{\partial \xi} \frac{D}{Dt} \left(\frac{\partial X}{\partial \xi} \right) + 2 \frac{\partial Y}{\partial \xi} \frac{D}{Dt} \left(\frac{\partial Y}{\partial \xi} \right) \right]. \quad (4.12.9)$$

Interchanging the material derivative with the ξ derivative, and setting

$$\frac{DX}{Dt} = u_x \quad \frac{DY}{Dt} = u_y, \quad (4.12.10)$$

we find that

$$\frac{D}{Dt} \left(\frac{\partial \ell}{\partial \xi} \right) = \frac{1}{\partial \ell / \partial \xi} \left(\frac{\partial X}{\partial \xi} \frac{\partial u_x}{\partial \xi} + \frac{\partial Y}{\partial \xi} \frac{\partial u_y}{\partial \xi} \right), \quad (4.12.11)$$

where $\mathbf{u} = (u_x, u_y)$ is the fluid velocity. Rearranging, we obtain

$$\frac{D}{Dt} \left(\frac{\partial \ell}{\partial \xi} \right) = \frac{1}{\partial \ell / \partial \xi} \frac{\partial \mathbf{X}}{\partial \xi} \cdot \frac{\partial \mathbf{u}}{\partial \xi} = \frac{\partial \ell}{\partial \xi} \frac{\partial \mathbf{X}}{\partial \ell} \cdot \frac{\partial \mathbf{u}}{\partial \ell} = \frac{\partial \ell}{\partial \xi} \mathbf{t} \cdot \frac{\partial \mathbf{u}}{\partial \ell}, \quad (4.12.12)$$

where $\mathbf{t} = \partial \mathbf{X} / \partial \ell$ is the unit tangent vector shown in [Figure 4.12.1](#).

Evolution equation

Substituting the last expression into (4.12.7), we obtain

$$\frac{D\Gamma}{Dt} + \Gamma \mathbf{t} \cdot \frac{\partial \mathbf{u}}{\partial \ell} = -\frac{\partial q}{\partial \ell}, \quad (4.12.13)$$

which is the targeted evolution equation for the surfactant concentration.

Fick's law

The diffusive flux can be described by Fick's law,

$$q = -D_s \frac{\partial \Gamma}{\partial \ell}, \quad (4.12.14)$$

where D_s is the surfactant surface diffusivity. Substituting this expression into (4.12.13), we derive a convection–diffusion equation,

$$\frac{D\Gamma}{Dt} + \Gamma \mathbf{t} \cdot \frac{\partial \mathbf{u}}{\partial \ell} = \frac{\partial}{\partial \ell} \left(D_s \frac{\partial \Gamma}{\partial \ell} \right). \quad (4.12.15)$$

In practice, the surfactant diffusivity is typically small.

Stretching and expansion

It is illuminating to resolve the velocity into a tangential and a normal component,

$$\mathbf{u} = u_t \mathbf{t} + u_n \mathbf{n}. \quad (4.12.16)$$

Noting that $\mathbf{t} \cdot \mathbf{n} = 0$, $\mathbf{t} \cdot \mathbf{t} = 1$, and $\mathbf{n} \cdot \mathbf{n} = 1$, and using the Frenet relations (4.3.5) and (4.3.9),

$$\frac{d\mathbf{t}}{d\ell} = -\kappa \mathbf{n}, \quad \frac{d\mathbf{n}}{d\ell} = \kappa \mathbf{t}, \quad (4.12.17)$$

we compute

$$\mathbf{t} \cdot \frac{\partial \mathbf{u}}{\partial \ell} = \frac{\partial u_t}{\partial \ell} + u_n \mathbf{t} \cdot \frac{\partial \mathbf{n}}{\partial \ell} = \frac{\partial u_t}{\partial \ell} + \kappa u_n, \quad (4.12.18)$$

where κ is the interfacial curvature. Substituting this expression into (4.12.15), we obtain the evolution equation

$$\frac{D\Gamma}{Dt} + \Gamma \left(\frac{\partial u_t}{\partial \ell} + \kappa u_n \right) = \frac{\partial}{\partial \ell} \left(D_s \frac{\partial \Gamma}{\partial \ell} \right). \quad (4.12.19)$$

The first and second terms inside the parentheses on the left-hand side express, respectively, the rate of change of the surfactant concentration due to interfacial stretching, and the rate of change of the surfactant concentration due to interfacial expansion.

Stretching of a flat interface

Consider a flat interface situated along the x axis, stretched uniformly under the influence of a tangential velocity field, $u_x(x)$. Identifying ℓ with x and setting $\kappa = 0$, we find that the transport equation (4.12.19) reduces to

$$\frac{D\Gamma}{Dt} + \Gamma \frac{\partial u_x}{\partial x} = \frac{\partial}{\partial x} \left(D_s \frac{\partial \Gamma}{\partial x} \right). \quad (4.12.20)$$

The material derivative can be resolved into Eulerian derivatives with respect to x and t , yielding

$$\frac{\partial \Gamma}{\partial t} + u_x \frac{\partial \Gamma}{\partial x} + \Gamma \frac{\partial u_x}{\partial x} = \frac{\partial}{\partial x} \left(D_s \frac{\partial \Gamma}{\partial x} \right) \quad (4.12.21)$$

or

$$\frac{\partial \Gamma}{\partial t} + \frac{\partial (u_x \Gamma)}{\partial x} = \frac{\partial}{\partial x} \left(D_s \frac{\partial \Gamma}{\partial x} \right). \quad (4.12.22)$$

In fact, this equation could have been derived directly by performing a surfactant molecular balance over a differential control volume along the x axis, taking into consideration the convective and diffusive flux.

In the case of a uniformly stretched interface, $u_x = kx$, where k is a constant identified as the rate of extension. If the surfactant concentration is uniform at the initial instant, it will remain uniform at any time, governed by the linear equation

$$\frac{d\Gamma}{dt} + k\Gamma = 0. \quad (4.12.23)$$

The solution reveals that the surfactant concentration decreases exponentially due to dilution,

$$\Gamma(t) = \Gamma(t=0) \exp(-kt). \quad (4.12.24)$$

Expansion of a circular interface

Now consider a cylindrical interface with circular cross-section of radius a centered at the origin, expanding under the influence of a uniform radial velocity, $u_r(t)$, in the absence of circumferential motion. In plane polar coordinates, (r, θ) , the transport equation (4.12.19) with constant diffusivity becomes

$$\frac{D\Gamma}{Dt} + \Gamma \frac{u_r}{a} = \frac{D_s}{a^2} \frac{\partial^2 \Gamma}{\partial \theta^2}. \quad (4.12.25)$$

In this case, the material derivative is the partial derivative with respect to time, yielding

$$\frac{\partial \Gamma}{\partial t} + \Gamma \frac{u_r}{a} = \frac{D_s}{a^2} \frac{\partial^2 \Gamma}{\partial \theta^2}. \quad (4.12.26)$$

If the surfactant concentration is uniform at the initial instant, it will remain uniform at any time, governed by the linear equation

$$\frac{d\Gamma}{dt} + \Gamma \frac{u_r}{a} = 0. \quad (4.12.27)$$

In the case of expansion, $u_r > 0$, the surfactant concentration decreases exponentially due to dilution.

Interfacial markers

The material derivative expresses the rate of change of the surfactant concentration following the motion of *material point particles* residing on a selected side of an interface. In numerical practice, it may be expedient to follow the motion of interfacial marker points that move with the normal component of the fluid velocity and with an arbitrary tangential velocity, v_t . If $v_t = 0$, the marker points move normal to the interface at any instant. The velocity of a marker point is

$$\mathbf{v} = u_n \mathbf{n} + v_t \mathbf{t}. \quad (4.12.28)$$

By definition,

$$\frac{D\Gamma}{Dt} = \frac{d\Gamma}{dt} + (u_t - v_t) \frac{\partial \Gamma}{\partial \ell}, \quad (4.12.29)$$

where d/dt is the rate of change of the surfactant concentration following the marker points. Substituting this expression into (4.12.19), we find that

$$\frac{d\Gamma}{dt} + (u_t - v_t) \frac{\partial \Gamma}{\partial \ell} + \Gamma \left(\frac{\partial u_t}{\partial \ell} + \kappa u_n \right) = \frac{\partial}{\partial \ell} \left(D_s \frac{\partial \Gamma}{\partial \ell} \right), \quad (4.12.30)$$

which can be restated as

$$\frac{d\Gamma}{dt} + \frac{\partial(u_t \Gamma)}{\partial \ell} - v_t \frac{\partial \Gamma}{\partial \ell} + \Gamma \kappa u_n = \frac{\partial}{\partial \ell} \left(D_s \frac{\partial \Gamma}{\partial \ell} \right). \quad (4.12.31)$$

The second term on the left-hand side is the derivative of the interfacial convective flux.

4.12.2 Axisymmetric interfaces

Next, we consider a chain of material point particles distributed along the inner or outer side of the trace of an axisymmetric interface in an azimuthal plane, and label the point particles using a parameter, ξ , so that their position in the chosen azimuthal plane is described in parametric form at any instant as $\mathbf{X}(\xi)$, as shown in [Figure 4.12.2](#).

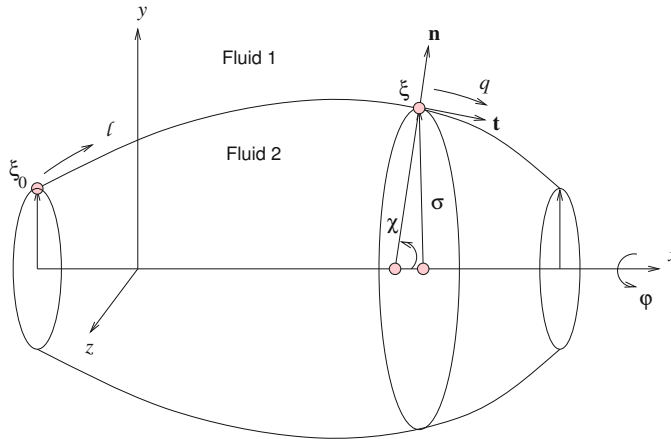


Figure 4.12.2 Point particles along the trace of an axisymmetric interface in an azimuthal plane are identified by a parameter ξ . The angle χ is subtended between the x axis and the straight line defined by the extension of the normal vector.

Let ℓ be the arc length measured along the trace of the interface from an arbitrary point particle labeled ξ_0 . To derive an evolution equation for the surface surfactant concentration, we introduce cylindrical polar coordinates, (x, σ, φ) , and express the number of surfactant molecules inside a ring-shaped material section of the interface confined between ξ_0 and ξ as

$$n(\xi, t) = 2\pi \int_{\ell(\xi_0, t)}^{\ell(\xi, t)} \Gamma(\xi', t) \sigma(\xi') d\ell(\xi') = 2\pi \int_{\xi_0}^{\xi} \Gamma(\xi', t) \frac{\partial \ell}{\partial \xi'} \sigma(\xi') d\xi'. \quad (4.12.32)$$

Conservation of the total number of surfactant molecules inside the test section requires that

$$\frac{\partial n}{\partial t} = 2\pi (\sigma_0 q(\xi_0) - \sigma q(\xi)), \quad (4.12.33)$$

where q is the flux of surfactant molecules along the interface by diffusion, and the time derivative is taken keeping ξ fixed.

The counterpart of the balance equation (4.12.6) is

$$\frac{D}{Dt} \left(\Gamma(\xi, t) \sigma(\xi, t) \frac{\partial \ell}{\partial \xi} \right) = - \frac{\partial(\sigma q)}{\partial \xi}, \quad (4.12.34)$$

and the counterpart of equation (4.12.13) is

$$\frac{D\Gamma}{Dt} + \Gamma \left(\mathbf{t} \cdot \frac{\partial \mathbf{u}}{\partial \ell} + \frac{u_\sigma}{\sigma} \right) = - \frac{1}{\sigma} \frac{\partial(\sigma q)}{\partial \ell}. \quad (4.12.35)$$

In deriving this equation, we have set $D\sigma/Dt = u_\sigma$.

In terms of the normal and tangential velocities, u_n and u_t ,

$$\frac{D\Gamma}{Dt} + \Gamma \left(\frac{\partial u_t}{\partial \ell} + \kappa u_n + \frac{u_\sigma}{\sigma} \right) = -\frac{1}{\sigma} \frac{\partial(\sigma q)}{\partial \ell}, \quad (4.12.36)$$

where κ is the curvature of the interface in a meridional plane. Substituting

$$u_\sigma = u_n \sin \chi - u_t \cos \chi, \quad (4.12.37)$$

we find that

$$\frac{D\Gamma}{Dt} + \Gamma \left(\frac{\partial u_t}{\partial \ell} - \frac{\cos \chi}{\sigma} u_t + \left(\kappa + \frac{\sin \chi}{\sigma} \right) u_n \right) = -\frac{1}{\sigma} \frac{\partial(\sigma q)}{\partial \ell}, \quad (4.12.38)$$

where the angle χ is defined in Figure 4.12.2. The sum of the terms inside the inner parentheses on the left-hand side is twice the mean curvature of the interface, $2\kappa_m$. The first two terms inside the outer parentheses can be consolidated to yield the final form

$$\frac{D\Gamma}{Dt} + \Gamma \left(\frac{1}{\sigma} \frac{\partial(\sigma u_t)}{\partial \ell} + 2\kappa_m u_n \right) = -\frac{1}{\sigma} \frac{\partial(\sigma q)}{\partial \ell}. \quad (4.12.39)$$

The first term inside the parentheses on the left-hand side expresses the rate of change of the surface area of an axisymmetric material ring.

Marker points

An evolution equation for interfacial marker points can be derived working as in Section 4.12.1 for a two-dimensional interface. The result is

$$\frac{d\Gamma}{dt} + (u_t - v_t) \frac{\partial \Gamma}{\partial \ell} + \Gamma \left(\frac{1}{\sigma} \frac{\partial(\sigma u_t)}{\partial \ell} + 2\kappa_m u_n \right) = -\frac{1}{\sigma} \frac{\partial(\sigma q)}{\partial \ell}, \quad (4.12.40)$$

which can be restated as

$$\frac{d\Gamma}{dt} + \frac{1}{\sigma} \frac{\partial(\sigma u_t \Gamma)}{\partial \ell} - v_t \frac{\partial \Gamma}{\partial \ell} + \Gamma 2\kappa_m u_n = -\frac{1}{\sigma} \frac{\partial(\sigma q)}{\partial \ell}. \quad (4.12.41)$$

When the marker points move normal to the interface, $v_t = 0$, the third term on the right-hand side of (4.12.41) does not appear.

4.12.3 Three-dimensional interfaces

The equations derived previously in this section for two-dimensional and axisymmetric interfaces can be generalized to three-dimensional interfaces.² The normal component of the marker-point velocity over a three-dimensional interface must be equal to the normal component of the fluid velocity, but the tangential component can be arbitrary. The general form of marker point velocity is

$$\mathbf{v} = u_n \mathbf{n} + \mathbf{v}^{\text{tangential}}, \quad (4.12.42)$$

²Yon, S. & Pozrikidis, C. (1998) A finite-volume/boundary-element method for interfacial flow in the presence of surfactants, with applications to shear flow past a viscous drop, *Computers & Fluids* **27**, 879–902.

where $\mathbf{v}^{\text{tangential}}$ is an arbitrary tangential component. When $\mathbf{v}^{\text{tangential}} = \mathbf{0}$, the marker points move with the fluid velocity normal to the interface alone. When $\mathbf{v}^{\text{tangential}} = \mathbf{u} - u_n \mathbf{n}$, the marker points are point particles moving with the fluid velocity.

Adopting Fick's law for the surface diffusion, we find that the evolution of the concentration of an immiscible surfactant following the motion of interfacial marker points takes the form

$$\frac{d\Gamma}{dt} + \nabla_s \cdot (\mathbf{u}_s \Gamma) - \mathbf{v}^{\text{tangential}} \cdot \nabla_s \Gamma + \Gamma 2 \kappa_m \mathbf{u} \cdot \mathbf{n} = \nabla_s \cdot (D_s \nabla_s \Gamma). \quad (4.12.43)$$

To define the various terms, we introduce the tangential projection matrix, $\mathbf{P} = \mathbf{I} - \mathbf{n} \otimes \mathbf{n}$, with elements

$$P_{ij} = \delta_{ij} - n_i n_j, \quad (4.12.44)$$

where δ_{ij} is Kronecker's delta representing the identity matrix and the symbol \otimes denotes the tensor product. Subject to this definition,

$$\mathbf{u}_s = \mathbf{P} \cdot \mathbf{u} \quad (4.12.45)$$

is the component of the fluid velocity tangential to the interface and

$$\nabla_s \equiv \mathbf{P} \cdot \nabla \quad (4.12.46)$$

is the surface gradient.

In the case of two-dimensional flow, depicted in [Figure 4.12.1](#), or axisymmetric flow, depicted in [Figure 4.12.2](#), equation (4.12.43) reduces to (4.12.41) or (4.12.31) by setting $\mathbf{v}^{\text{tangential}} = v_t \mathbf{t}$.

PROBLEMS

4.12.1 Expanding spherical interface

Derive an evolution equation for the surface concentration of a surfactant over a uniformly expanding spherical interface.

4.12.2 Transport on a flat interface

Simplify equation (4.12.43) for a flat interface in the xy plane.

Hydrostatics

- 5.1 Equilibrium of pressure and body forces
- 5.2 Force exerted on immersed surfaces
- 5.3 Archimedes' principle
- 5.4 Interfacial shapes
- 5.5 A semi-infinite interface attached to a horizontal plane
- 5.6 A semi-infinite interface attached to an inclined plane
- 5.7 A meniscus between two parallel plates
- 5.8 A two-dimensional drop on a horizontal or inclined plane
- 5.9 Axisymmetric meniscus inside a tube
- 5.10 Axisymmetric drop on a horizontal plane
- 5.11 A sphere straddling an interface
- 5.12 A three-dimensional meniscus

The simplest state of a fluid is the state of rest. The macroscopically observable velocity vanishes and the forces developing in the fluid are described in terms of the pressure field established in response to a body force. The subject of hydrostatics encompasses two main topics: the computation of forces exerted on immersed surfaces and submerged bodies, and the study of the shapes of interfaces separating stationary, translating, or rotating fluids. Although the problem statement and mathematical formulation is straightforward in both cases, deriving solutions for all but the simplest configurations requires the use of numerical methods for solving algebraic, ordinary, and partial differential equations.

5.1 Equilibrium of pressure and body forces

Consider a parcel of a stationary fluid, as illustrated in [Figure 5.1.1\(a\)](#). Newton's second law of motion requires that, in the absence of macroscopically observable flow, the forces exerted on the parcel should balance to zero. In Chapter 4, we saw that two kinds of forces are exerted on a parcel: a body force due to the gravitational or another force field mediated by long-range molecular interactions, and a surface force associated with the hydrodynamic traction.

Body force

The body force due to gravity can be expressed as an integral over the volume of the parcel

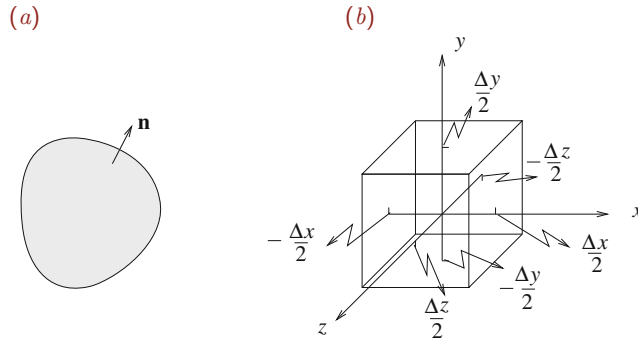


Figure 5.1.1 (a) Illustration of a parcel of a stationary fluid showing the outward unit normal vector, \mathbf{n} . (b) A parcel with a rectangular parallelepiped shape serves as a control volume for deriving the differential equations governing the pressure distribution in hydrostatics.

involving the possibly position-dependent fluid density, ρ , in the form

$$\mathbf{F}^{\text{body}} = \iiint_{\text{parcel}} \rho \mathbf{g} \, dV, \quad (5.1.1)$$

where $\mathbf{g} = (g_x, g_y, g_z)$ is the acceleration of gravity vector. On the surface of the earth, the magnitude of \mathbf{g} takes the approximate value $|\mathbf{g}| \equiv g = 9.80665 \text{ m/sec}^2$.

Surface force

The surface force can be expressed in terms of the traction exerted on the parcel surface, \mathbf{f} , in the corresponding form

$$\mathbf{F}^{\text{surface}} = \iint_{\text{parcel}} \mathbf{f} \, dS. \quad (5.1.2)$$

In the absence of fluid motion, the traction is due to the pressure, p , alone pushing the parcel surface toward the interior. If \mathbf{n} is the unit vector normal to the parcel surface pointing outward, as illustrated in Figure 5.1.1(a), then

$$\mathbf{f} = -p \mathbf{n}. \quad (5.1.3)$$

The minus sign on the right-hand side accounts for the opposite orientations of the normal vector and traction due to the pressure.

Substituting (5.1.3) into (5.1.2), we derive an expression for the surface force in terms of the pressure,

$$\mathbf{F}^{\text{surface}} = - \iint_{\text{parcel}} p \mathbf{n} \, dS. \quad (5.1.4)$$

The integral on the right-hand side can be evaluated by analytical or numerical methods.

Force equilibrium

Setting the sum of the body force given in (5.1.1) and the surface force given in (5.1.4) to zero, we obtain a vectorial equilibrium condition,

$$\iiint_{\text{parcel}} \rho \mathbf{g} \, dV - \iint_{\text{parcel}} p \mathbf{n} \, dS = \mathbf{0}. \quad (5.1.5)$$

The three scalar components of this equation are

$$\begin{aligned} \iiint_{\text{parcel}} \rho g_x \, dV &= \iint_{\text{parcel}} p n_x \, dS, & \iiint_{\text{parcel}} \rho g_y \, dV &= \iint_{\text{parcel}} p n_y \, dS, \\ \iiint_{\text{parcel}} \rho g_z \, dV &= \iint_{\text{parcel}} p n_z \, dS, \end{aligned} \quad (5.1.6)$$

where the unit normal vector, $\mathbf{n} = (n_x, n_y, n_z)$, points outward from the parcel, as shown in Figure 5.1.1(a).

5.1.1 Equilibrium of an infinitesimal parcel

Next, we consider a small fluid parcel in the shape of a rectangular parallelepiped centered at the origin with six flat sides perpendicular to the x , y , or z axis and edges with length Δx , Δy , and Δz , as illustrated in Figure 5.1.1(b). Because the size of the parcel is small, density variations over the parcel volume can be neglected and the volume integrals on the left-hand side of equations (5.1.6) can be approximated with the products

$$\rho_0 g_x \Delta V, \quad \rho_0 g_y \Delta V, \quad \rho_0 g_z \Delta V, \quad (5.1.7)$$

where ρ_0 is the density of the fluid at the center of the parcel located at the origin, and $\Delta V = \Delta x \Delta y \Delta z$ is the parcel volume.

Now we consider the surface integral on the left-hand side of the first equation in (5.1.6). The x component of the normal vector vanishes on all sides, except on the two sides that are perpendicular to the x axis, located at $x = \frac{1}{2}\Delta x$, and $x = -\frac{1}{2}\Delta x$, designated as the first and second side. On the first side $n_x = 1$, and on the second side $n_x = -1$. Because the parcel size is small, variations in pressure over each side can be neglected and the pressure over a side can be approximated with the value at the side center.

Subject to this approximation, the surface integral on the right-hand side of the first equation in (5.1.6) over the first or second side is, respectively,

$$p\left(x = \frac{1}{2}\Delta x, y = 0, z = 0\right) \Delta y \Delta z, \quad -p\left(x = -\frac{1}{2}\Delta x, y = 0, z = 0\right) \Delta y \Delta z, \quad (5.1.8)$$

where the parentheses enclose the arguments of the pressure. Adding these two contributions, we obtain the net pressure force

$$F_x \equiv \Delta p_x \Delta y \Delta z, \quad (5.1.9)$$

where

$$\Delta p_x \equiv p(x = \frac{1}{2}\Delta x, y = 0, z = 0) - p(x = -\frac{1}{2}\Delta x, y = 0, z = 0). \quad (5.1.10)$$

In the limit as Δx tends to zero, the ratio of the differences in the pressure and corresponding x positions,

$$\frac{\Delta p_x}{\frac{1}{2}\Delta x - (-\frac{1}{2}\Delta x)} = \frac{\Delta p_x}{\Delta x}, \quad (5.1.11)$$

tends to the partial derivative $\partial p/\partial x$ evaluated at the origin. The expression for the net pressure force then becomes

$$F_x = \left(\frac{\partial p}{\partial x}\right)_0 \Delta x \Delta y \Delta z = \left(\frac{\partial p}{\partial x}\right)_0 \Delta V, \quad (5.1.12)$$

where the partial derivative is evaluated at the origin.

Equations of hydrostatics

Substituting (5.1.12) along with the first approximate form in (5.1.7) into the x component of the force balance (5.1.6), and simplifying by eliminating ΔV on both sides, we obtain the differential equation

$$\rho g_x = \frac{\partial p}{\partial x}, \quad (5.1.13)$$

where the density, ρ , and the partial derivative of the pressure are evaluated at the origin. However, since the location of the origin is arbitrary, equation (5.1.13) can be applied at every point in the fluid.

Working in a similar fashion with the second and third hydrostatic equilibrium equations in (5.1.6), we obtain the corresponding differential equations

$$\rho g_y = \frac{\partial p}{\partial y}, \quad \rho g_z = \frac{\partial p}{\partial z}. \quad (5.1.14)$$

The three scalar equations (5.1.13) and (5.1.14) can be collected into a compact vector form,

$$\rho \mathbf{g} = \nabla p, \quad (5.1.15)$$

where

$$\nabla p = \left(\frac{\partial p}{\partial x}, \quad \frac{\partial p}{\partial y}, \quad \frac{\partial p}{\partial z} \right) \quad (5.1.16)$$

is the pressure gradient. In physical terms, the differential equation (5.1.15) expresses a balance between the gravitational and the pressure force in hydrostatics, that is, in the absence of fluid motion.

Derivation by the Gauss divergence theorem

The differential equilibrium equation (5.1.4) can be derived directly from the force balance (5.1.5) by applying the Gauss divergence theorem stated in equation (2.6.36),

$$\iint_S \mathbf{h} \cdot \mathbf{n} \, dS = \iiint_V \nabla \cdot \mathbf{h} \, dV. \quad (5.1.17)$$

Selecting

$$h_x = \phi, \quad h_y = 0, \quad h_z = 0 \quad (5.1.18)$$

to formulate the vector function $\mathbf{h} = (\phi, 0, 0)$, we obtain

$$\iint_S \phi n_x \, dS = \iiint_V \frac{\partial \phi}{\partial x} \, dV, \quad (5.1.19)$$

where ϕ is an arbitrary scalar function of position. The complementary choices $\mathbf{h} = (0, \phi, 0)$ and $\mathbf{h} = (0, 0, \phi)$ yield the corresponding identities

$$\iint_S \phi n_y \, dS = \iiint_V \frac{\partial \phi}{\partial y} \, dV, \quad \iint_S \phi n_z \, dS = \iiint_V \frac{\partial \phi}{\partial z} \, dV. \quad (5.1.20)$$

Relations (5.1.19) and (5.1.20) can be collected into a vector identity,

$$\iint_S \phi \mathbf{n} \, dS = \iiint_V \nabla \phi \, dV, \quad (5.1.21)$$

where

$$\nabla \phi = \left(\frac{\partial \phi}{\partial x}, \frac{\partial \phi}{\partial y}, \frac{\partial \phi}{\partial z} \right) \quad (5.1.22)$$

is the gradient of ϕ .

Applying (5.1.21) to the second integral on the left-hand side of (5.1.5) expressing the surface force due to the pressure, we obtain

$$\iiint_{\text{parcel}} \rho \mathbf{g} \, dV - \iiint_{\text{parcel}} \nabla p \, dV = \mathbf{0}. \quad (5.1.23)$$

The differential equation (5.1.15) follows from the realization that the volume is arbitrary.

Gases and liquids

Equation (5.1.15) provides us with a basis for computing the distributions of pressure and density in a fluid, subject an additional stipulation concerning the physical properties of the fluid required by thermodynamics. Specifically, given the density field, or a relation between the density and the pressure, equation (5.1.15) allows us to compute the associated pressure and *vice versa*. To this end, we make a distinction between compressible gases and incompressible liquids.

5.1.2 Gases in hydrostatics

The density of a gas, ρ , is related to the pressure, p , and temperature, T , by an equation of state provided by thermodynamics. For an ideal gas,

$$\rho = \frac{M}{RT} p, \quad (5.1.24)$$

where M is the molecular mass and R is the ideal-gas constant, as discussed in Section 4.4. Substituting (5.1.24) into (5.1.15) and rearranging, we obtain a vectorial equation involving the pressure and temperature,

$$\frac{M}{RT} \mathbf{g} = \frac{1}{p} \nabla p. \quad (5.1.25)$$

The x component of this equation reads

$$\frac{M}{RT} g_x = \frac{1}{p} \frac{\partial p}{\partial x} = \frac{\partial}{\partial x} \left(\ln \frac{p}{\pi_0} \right), \quad (5.1.26)$$

where π_0 is an unspecified reference pressure.

When the temperature of the fluid is uniform, we may integrate (5.1.26) with respect to x to obtain

$$\ln \frac{p}{\pi_0} = \frac{M}{RT} g_x x + f_x(y, z), \quad (5.1.27)$$

where $f_x(y, z)$ is an unknown function. Working in a similar fashion with the y and z components of (5.1.25) under the assumption of uniform temperature, we obtain

$$\ln \frac{p}{\pi_0} = \frac{M}{RT} g_y y + f_y(x, z), \quad \ln \frac{p}{\pi_0} = \frac{M}{RT} g_z z + f_z(x, y), \quad (5.1.28)$$

where $f_y(z, x)$ and $f_z(x, y)$ are two unknown functions. Combining the last three equations, we obtain the pressure distribution

$$\ln \frac{p}{\pi_0} = \frac{M}{RT} (g_x x + g_y y + g_z z). \quad (5.1.29)$$

The reference pressure π_0 is determined by requiring an appropriate boundary condition.

Expressing the term in the parentheses on the right-hand side of (5.1.29) in terms of the inner product of the gravity vector, \mathbf{g} , and the position vector, \mathbf{x} , and transferring the last term to the left-hand side, we obtain the compact form

$$\ln \frac{p}{\pi_0} = \frac{M}{RT} \mathbf{g} \cdot \mathbf{x}, \quad (5.1.30)$$

which describes the pressure distribution in an ideal gas with uniform temperature.

Pressure distribution in the atmosphere

As an application, we consider the pressure distribution in the atmosphere regarded as an ideal gas with molar mass $M = 28.97$ kg/kmole, at temperature 25°C corresponding to absolute temperature $T = 298$ K. In Cartesian coordinates with origin at sea level, where the y axis points upward and the x and z axes are horizontal, the components of the acceleration of gravity vector are

$$g_x = 0, \quad g_y = -g, \quad g_z = 0, \quad (5.1.31)$$

where $g = 9.80665$ m/s². Equation (5.1.30) simplifies to

$$\ln \frac{p}{p_{\text{sea}}} = -\frac{Mg}{RT} y, \quad (5.1.32)$$

where p_{sea} is the pressure at sea level. Solving for p , we derive an exponentially decaying field,

$$p = p_{\text{sea}} \exp\left(-\frac{Mg}{RT} y\right). \quad (5.1.33)$$

Taking

$$p_{\text{sea}} = 1.0 \text{ atm} = 1.0133 \times 10^5 \text{ Pascal} = 1.0133 \times 10^5 \text{ kg m}^{-1} \text{ sec}^{-2}, \quad (5.1.34)$$

we find that the pressure at the elevation of $y = 1 \text{ km} = 1,000 \text{ m}$ is

$$p = 1.0 \exp\left(-\frac{28.97 \times 9.80665}{8.314 \times 10^3 \times 298} 1000\right) \text{ atm} = 0.892 \text{ atm}. \quad (5.1.35)$$

The corresponding density distribution is found by substituting the pressure distribution (5.1.33) into the right-hand side of the equation of state (5.1.24).

5.1.3 Liquids in hydrostatics

Because liquids at low and moderate pressures are nearly incompressible, their density is a physical property determined primarily by the prevailing temperature. Working as in the case of gases but treating the density as a constant, we find that the pressure distribution is given by the counterpart of equation (5.1.30),

$$p = \rho (g_x x + g_y y + g_z z) + \pi_0 \quad (5.1.36)$$

or, more concisely,

$$p = \rho \mathbf{g} \cdot \mathbf{x} + \pi_0, \quad (5.1.37)$$

where π_0 is a constant with units of pressure determined by an appropriate boundary condition.

Pressure distribution in a pool

As an application, we consider the pressure distribution in a liquid pool with a horizontal surface. In Cartesian coordinates where the y axis is perpendicular to the pool surface pointing in the vertical direction upward and the x and z axes are horizontal, the components of the acceleration of gravity vector are

$$g_x = 0, \quad g_y = -g, \quad g_z = 0, \quad (5.1.38)$$

where g is the magnitude of the acceleration of gravity. The general equation (5.1.37) then simplifies to

$$p = -\rho g y + \pi_0. \quad (5.1.39)$$

Setting the origin of the y axis at the pool surface where the liquid pressure is equal to the atmospheric pressure, p_{atm} , we find that $\pi_0 = p_{\text{atm}}$.

Manometer

The pressure distribution given in (5.1.37) also applies when a contiguous liquid occupies a convoluted domain. In practice, this property is exploited for computing the pressure difference across the two ends of a tube in terms of the difference in the levels of a liquid column placed inside the tube. A simple device serving this purpose is the U-tube manometer illustrated in [Figure 5.1.2](#).

The pressure distribution in the liquid inside the U-tube manometer is given by equation (5.1.39). Applying this equation at the two ends of the liquid, located at $y = y_1$ and y_2 , and subtracting the resulting expressions, we find that

$$\Delta p \equiv p(y_1) - p(y_2) = \rho g (y_2 - y_1). \quad (5.1.40)$$

If the tube is exposed to the atmosphere at the first end, $p(y_1) = p_{\text{atm}}$, and thus

$$p(y_2) = p_{\text{atm}} + \rho g h, \quad (5.1.41)$$

where $h \equiv y_1 - y_2$ is the readily measurable rise of the liquid column in the manometer.

PROBLEMS**5.1.1 Hydrostatic pressure distribution**

- (a) Derive the pressure distribution in an incompressible liquid given in equation (5.1.37).
 (b) Derive the pressure distribution in an ideal gas occupying the semi-infinite region $y > 0$ when the temperature decreases exponentially with distance as

$$T = T_0 - \Delta T (1 - e^{-\alpha y}), \quad (5.1.42)$$

where T_0 , ΔT , and α are three specified constants. The gravity vector points in the negative direction of the y axis.

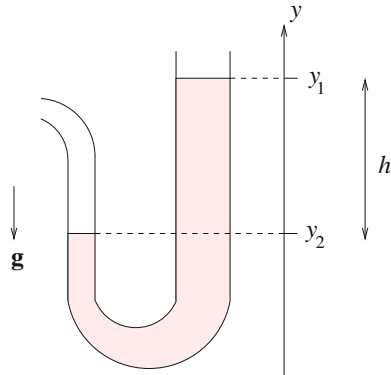


Figure 5.1.2 Illustration of a U-tube manometer. The pressure distribution in the fluid is described by the equations of hydrostatics even if the fluid has a convoluted shape, as long as it remains contiguous and uninterrupted.

5.1.2 Function of an aircraft altimeter

The temperature in the lower part of the troposphere extending 10 km above the surface of the earth decreases at a nearly linear rate as $T = T_0 - \alpha y$, where T_0 is the temperature at the surface of the earth positioned at $y = 0$, and α is the lapse rate. In North America, $\alpha = 6.5$ K/km.

(a) Assuming that the atmosphere behaves like an ideal gas, derive the atmospheric pressure distribution

$$p = \pi_0 \left(1 - \frac{\alpha}{T_0} y\right)^\beta, \quad (5.1.43)$$

and evaluate the dimensionless exponent $\beta \equiv Mg/(R\alpha)$, where π_0 is the pressure at sea level.

Solving (5.1.43) for the elevation y , we find that

$$y = \frac{T_0}{\alpha} \left(1 - \left(\frac{p}{\pi_0}\right)^{1/\beta}\right). \quad (5.1.44)$$

This equation is used for calibrating an aircraft altimeter, that is, for converting pressure measured with a barometer into altitude.

(b) Show that, as α tends to zero, in which case the temperature distribution tends to become constant, the pressure distribution (5.1.43) reduces to that shown in (5.1.33).

5.1.3 How many molecules inside a certain volume of gas?

How many molecules are there inside one cubic centimeter (1 milliliter) of a gas under atmospheric pressure and temperature 25°C?

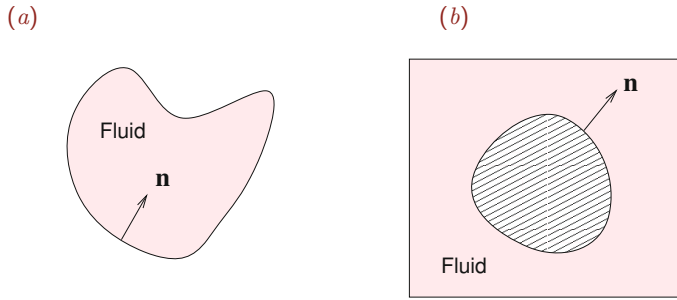


Figure 5.2.1 Illustration of a surface that (a) contains or (b) is immersed in a stationary fluid.

5.2 Force exerted on an immersed surface

To compute the hydrostatic surface force exerted on a surface that contains or is immersed in a stationary fluid, as illustrated in Figure 5.2.1, we repeat the arguments that led us to equation (5.1.4) and obtain

$$\mathbf{F}^{\text{surface}} = - \iint p \mathbf{n} \, dS, \quad (5.2.1)$$

where \mathbf{n} is the unit vector normal to the surface pointing into the fluid and the integration is performed over the surface.

To evaluate the integral on the right-hand side of (5.2.1), we must first determine the pressure distribution in the fluid, as discussed in Section 5.1, and then evaluate the integral by analytical or numerical methods.

5.2.1 A sphere floating on a flat interface

As an application, we consider the force exerted on a sphere floating on the flat surface of a liquid pool underneath a zero-density gas, as depicted in Figure 5.2.2. In spherical polar coordinates with origin at the center of the sphere and the x axis pointing upward, the circular contact line where the surface of the liquid meets the sphere is located at the meridional angle $\theta = \beta$.

Symmetry requires that the horizontal component of the surface force exerted on the sphere must vanish. The vertical component of the surface force is given by

$$F_x^{\text{surface}} = - \iint p n_x \, dS, \quad (5.2.2)$$

where $n_x = \cos \theta$ is the x component of the unit normal vector. The pressure distribution is described by equation (5.1.37) with gravitational acceleration components

$$g_x = -g, \quad g_y = 0, \quad g_z = 0, \quad (5.2.3)$$

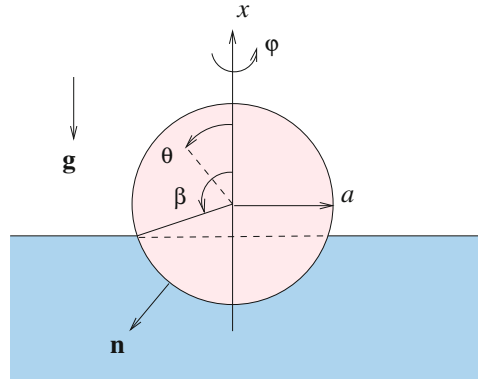


Figure 5.2.2 Illustration of a sphere floating in the flat surface of a liquid at floating angle β . The dashed line represents the horizontal circular contact line.

yielding

$$p = -\rho g x + \pi_0. \quad (5.2.4)$$

To compute the reference pressure π_0 , we require that the pressure at the contact line is equal to the atmospheric pressure, $p = p_{\text{atm}}$ at $x = a \cos \beta$, and find that $p_{\text{atm}} = -\rho g a \cos \beta + \pi_0$, which can be rearranged to give

$$\pi_0 = \rho g a \cos \beta + p_{\text{atm}}, \quad (5.2.5)$$

where a is the sphere radius. Writing $x = a \cos \theta$, we find that the pressure distribution over the sphere is given by

$$p = -\rho g a (\cos \theta - \cos \beta) + p_{\text{atm}}. \quad (5.2.6)$$

Now substituting the pressure distribution (5.2.6) into the integral on the right-hand side of (5.2.2), we find that the force exerted on the sphere by the liquid is given by

$$F_x^{\text{surface}} = \iint (\rho g a (\cos \theta - \cos \beta) - p_{\text{atm}}) \cos \theta \, dS. \quad (5.2.7)$$

The differential surface area of the sphere can be expressed in the form

$$dS = (\sigma d\varphi)(a d\theta), \quad (5.2.8)$$

where $\sigma = a \sin \theta$ is the distance of a point on the surface of the sphere from the x axis and φ is the azimuthal angle. Substituting this expression into the right-hand side of (5.2.7) and integrating with respect to φ , we obtain

$$F_x^{\text{surface}} = 2\pi a^2 \int_{\beta}^{\pi} (\rho g a (\cos \theta - \cos \beta) - p_{\text{atm}}) \cos \theta \sin \theta \, d\theta. \quad (5.2.9)$$

Next, we set $\sin \theta \, d\theta = -d \cos \theta$ and carry out the integration on the right-hand side with respect to $\cos \theta$ to find that

$$F_x^{\text{surface}} = \pi a^2 \left[\rho g a \frac{1}{3} (2 + 3 \cos \beta - \cos^3 \beta) + p_{\text{atm}} (1 - \cos^2 \beta) \right]. \quad (5.2.10)$$

Working in a similar fashion, we find that the x component of the force due to the atmospheric pressure exerted on the non-immersed portion of the sphere subtended between the meridional angles $\theta = 0$ and β is given by

$$F_x^{\text{atm}} = -2\pi a^2 \int_0^\beta p_{\text{atm}} \cos \theta \sin \theta \, d\theta = -\pi a^2 p_{\text{atm}} (1 - \cos^2 \beta). \quad (5.2.11)$$

Adding the two contributions expressed by (5.2.10) and (5.2.11), we obtain the buoyancy force exerted on the sphere,

$$F_x^{\text{buoyancy}} \equiv F_x^{\text{surface}} + F_x^{\text{atm}} = \rho g \left(\pi \frac{1}{3} (2 + 3 \cos \beta - \cos^3 \beta) a^3 \right). \quad (5.2.12)$$

It can be shown using elementary trigonometry that the term enclosed by the large parentheses on the right-hand side of (5.2.12) is equal to the immersed volume of the sphere underneath the flat surface of the liquid, which is equal to the volume of fluid displaced by the sphere, $V_{\text{displaced}}$. For example, if the sphere is completely immersed, $\beta = 0$, the term enclosed by the short parentheses on the right-hand side of (5.2.12) is equal to 4, and the term enclosed by the large parentheses is equal to the volume of the sphere, $V_{\text{sphere}} = \frac{4\pi}{3} a^3$.

Equation (5.2.12) states that the hydrostatic force exerted on a floating sphere is equal in magnitude and opposite in direction to the weight of the fluid displaced by the sphere. In Section 5.3, we will see that this is a more general result applicable to an arbitrarily shaped floating or immersed object.

Computation of the floating angle

The floating angle, β , is determined by the weight of the sphere: the heavier the sphere, the smaller the angle; the lighter the sphere, the larger the angle. There is a critical weight where β becomes equal to zero and the sphere is completely submerged.

To compute the floating angle corresponding to a certain weight, W , we set W equal to the buoyancy force given in (5.2.12) and rearrange to obtain a cubic equation for $\cos \beta$,

$$\cos^3 \beta - 3 \cos \beta + 2(2s - 1) = 0, \quad (5.2.13)$$

where

$$s \equiv \frac{W}{\rho g V_{\text{sphere}}} \quad (5.2.14)$$

is a dimensionless parameter and $V_{\text{sphere}} = \frac{4\pi}{3} a^3$ is the volume of the sphere. If the sphere is made of a homogeneous material with density ρ_s , then $s = \rho_s / \rho$ is the density ratio. A neutrally buoyant sphere corresponds to $s = 1$, in which case $\cos \beta = 1$ and $\beta = 0$ satisfy equation (5.2.13), as expected. When $s = \frac{1}{2}$, the floating angle is $\frac{1}{2}\pi$.

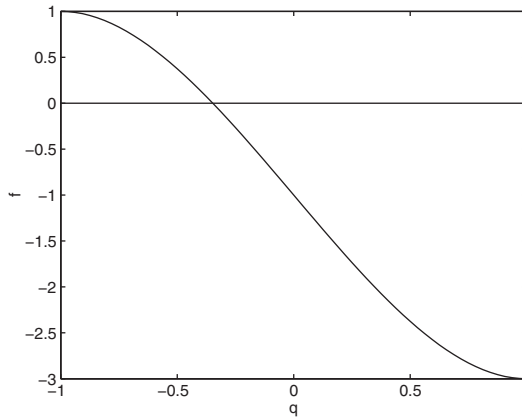


Figure 5.2.3 Graph of the function $f(q)$ defined in equation (5.2.16) whose root, Q , is desired, for $s = \frac{1}{4}$. To compute the root using Newton's method, we make an initial guess, $q^{(0)}$, and then improve the guess by moving along the tangential vector to the graph toward the q axis.

5.2.2 Newton's method

A variety of numerical methods are available for solving the nonlinear algebraic equation (5.2.13) for β , given s . Newton's method, also known as the Newton–Raphson method, strikes an optimal balance between conceptual simplicity and numerical efficiency. To formalize the method, we introduce the variable $q \equiv \cos \beta$, and express equation (5.2.13) in the generic form

$$f(q) = 0, \quad (5.2.15)$$

where

$$f(q) \equiv q^3 - 3q + 2(2s - 1) \quad (5.2.16)$$

is the function of interest. A graph of the function $f(q)$ for $s = 0.25$ is shown in [Figure 5.2.3](#). The requisite value of q , denoted by Q , is located at the intersection of the graph of $f(q)$ and the q axis, satisfying $f(Q) = 0$.

To implement Newton's method, we make an initial guess for the desired root Q , denoted by $q^{(0)}$, and then generate a sequence of improvements working as follows. Near the point $q^{(0)}$, the function $f(q)$ can be approximated with a linear function that arises by expanding $f(q)$ in a Taylor series about $q^{(0)}$. Discarding all nonlinear terms, we obtain the approximate form

$$f(q) \simeq f(q^{(0)}) + \left(\frac{df}{dq} \right)_{q=q^{(0)}} (q - q^{(0)}). \quad (5.2.17)$$

Setting $f(q) = 0$, solving for the q inside the parentheses on the right-hand side of (5.2.17), and denoting the solution as $q^{(1)}$, we obtain the improved value

$$q^{(1)} = q^{(0)} - \left(\frac{f}{f'} \right)_{q=q^{(0)}}, \quad (5.2.18)$$

where a prime denotes a derivative with respect to q . The process is then repeated to yield a sequence of successive approximations based on the recursive formula

$$q^{(k+1)} = q^{(k)} - \left(\frac{f}{f'} \right)_{q=q^{(k)}} \quad (5.2.19)$$

for $k = 0, 1, \dots$. Erroneously omitting the minus sign on the right-hand side of (5.2.19) is a common source of frustration. The iterations terminate when the correction falls below a specified tolerance.

In the case of a floating sphere presently considered,

$$f' = 3q^2 - 3 \quad (5.2.20)$$

and Newton's formula takes the form

$$q \leftarrow q - \frac{q^3 - 3q + 2(2s - 1)}{3q^2 - 3} = \frac{2}{3} \frac{q^3 - (2s - 1)}{q^2 - 1}, \quad (5.2.21)$$

where the arrow stands for *replace*. The method is implemented in the following MATLAB function

```
function q = floating_sphere(s,q)

tolerance = 0.000001;
itermax = 10;
cf = 2.0*s-1.0;

error = tolerance + 1.0;
iter = 0;  % iteration counter

while (error>tolerance & iter<itermax)
    iter = iter+1;
    qsave = q;
    q2 = q*q; q3 = q2*q;
    q = 2/3 * (q3-cf)/(q2-1);
    error = abs(q-qsave)
end

return
```

The input field includes the parameter s and the initial guess. For a given s , the solution satisfying $|q| \leq 1$ is accepted; we recall that $q = \cos \beta$.

Convergence

Analysis shows that the sequence defined by (5.2.19) converges to Q as long as the initial guess $q^{(0)}$ is sufficiently close to the root, Q . The rate of convergence depends on the multiplicity of the root.

If the graph of the function $f(q)$ is not horizontal at the root, $f'(q = Q) \neq 0$, the rate of convergence is quadratic, which means that

$$q^{(k+1)} - Q \simeq \delta (q^{(k)} - Q)^2, \quad (5.2.22)$$

where $\delta = f''(Q)/[2f'(Q)]$ is an *a priori* unknown coefficient. Equation (5.2.22) states that the magnitude of the error in the current iteration, expressed by the left-hand side, is roughly equal to the square of the magnitude of the error in the previous iteration multiplied by a constant. Consequently, if the initial error, $q^{(0)} - Q$, is sufficiently small, the magnitude of the error, $q^{(k)} - Q$, will keep decreasing during the iterations, no matter how large the value of the coefficient δ . A prerequisite is that the initial guess is close enough to the root so that (5.2.22) applies.

If the graph of the function $f(q)$ is horizontal at the root, $(df/dq)_{q=Q} = 0$, the rate of convergence is linear, which means that

$$q^{(k+1)} - Q \simeq \frac{m-1}{m} (q^{(k)} - Q), \quad (5.2.23)$$

where m is the multiplicity of the root; for a double root, $m = 2$. Equation (5.2.23) states that the magnitude of the error at the current iteration, $q^{(k+1)} - Q$, is roughly equal to that in the previous iteration, $q^{(k)} - Q$, multiplied by the positive coefficient $(m-1)/m$, which is less than unity for any $m > 1$. Consequently, the error $|q^{(k)} - Q|$ will keep decreasing during the iterations as long as the initial guess is close enough to the root for (5.2.23) to apply.

PROBLEMS

5.2.1 Pycnometer

A pycnometer is an antiquated device used to measure the specific gravity of a liquid, defined as the ratio of the density of the liquid to the density of water. In practice, this is done by reading the level of the free surface on a scale printed on a vertical tube attached to a spherical flask floating on the liquid, as illustrated in [Figure 5.2.4](#). Pycnometer derives from the Greek word $\pi\upsilon\kappa\nu\omicron\sigma\tau\eta\tau\alpha$, which means density. Derive an equation that allows us to calibrate a pycnometer based on the known density of water.

5.2.2 A sphere straddling the interface between two fluids

Derive the counterpart of expression (5.2.12) for a sphere straddling the interface between a lower fluid with density ρ_2 and an upper fluid with density ρ_1 .

5.2.3 A floating cylinder

(a) Show that the buoyancy force exerted on a floating cylinder of radius a is given by

$$F_x^{\text{buoyancy}} = \rho g a^2 \left(\pi - \beta + \frac{1}{2} \sin 2\beta \right), \quad (5.2.24)$$

where β is the floating angle defined in [Figure 5.2.2](#).

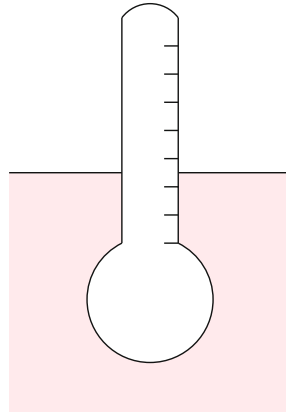


Figure 5.2.4 A pycnometer is used to measure the specific gravity of a liquid defined as the ratio between the density of the liquid to the density of water.

(b) Show that the floating angle of a solid cylinder satisfies the equation

$$\sin(2\beta) - 2\beta + 2\pi(1 - s) = 0, \quad (5.2.25)$$

where $s \equiv \rho_B/\rho$ is the ratio of the density of the cylinder, ρ_B , to the density of the liquid, ρ .

5.2.4 Floating sphere

(a) Directory *04_nl_eq*, located inside directory *01_num_meth* of **FDLIB**, includes a program entitled *newton1_2* that implements Newton's method for solving one nonlinear equation. Use the program to solve equation (5.2.13) and prepare a plot the floating angle, β , against the dimensionless parameter s defined in equation (5.2.14). Discuss the convergence of the iterations in light of equations (5.2.22) and (5.2.23).

(b) Directory *04_nl_eq*, located inside directory *01_num_meth* of **FDLIB**, includes a program entitled *cubic* that computes the three roots of a cubic equation using Cardano's formula. Use the program to solve equation (5.2.13). Prepare a plot of the floating angle, β , against the dimensionless parameter, s .

5.3 Archimedes' principle

Consider the force exerted on a body with arbitrary shape immersed in a stationary fluid. Using equation (5.2.1), we find that the surface force exerted on the body is given by

$$\mathbf{F}^{\text{surface}} = - \iint_{\text{body}} p \mathbf{n} \, dS, \quad (5.3.1)$$

where \mathbf{n} is the unit vector normal to the body pointing into the fluid. It would appear that the computation of the integral on the right-hand side of (5.3.1) requires detailed knowledge of the shape of the body. In fact, if the fluid is incompressible, the integral can be evaluated

in a generic fashion, yielding a remarkably simple expression for the force in terms of the body volume alone.

Substituting the pressure distribution for an incompressible fluid given in (5.1.37) into the right-hand side of (5.3.1), we find that

$$\mathbf{F}^{\text{surface}} = - \iint_{\text{body}} (\rho (g_x x + g_y y + g_z z) + \pi_0) \mathbf{n} \, dS. \quad (5.3.2)$$

A key observation in evaluating the surface integral is that the integrand is the product of the unit normal vector, \mathbf{n} , and a scalar function that is *linear* with respect to the components of the position vector, $\mathbf{x} = (x, y, z)$.

Rectangular body

To see how the evaluation of the integral can be simplified, we consider a body having the shape of a rectangular parallelepiped. The six flat sides of the body are perpendicular to the x, y , or z axis, the lengths of the edges are equal to Δx , Δy , and Δz , and the volume of the body is equal to $V_B = \Delta x \Delta y \Delta z$. The unit normal vector is constant over each of the six sides. For example, over the side that is perpendicular to the x axis and faces the positive direction of the x axis, $\mathbf{n} = (1, 0, 0)$. Taking into consideration this and similar simplifications, we evaluate the integral on the right-hand side of (5.3.2) without approximation, finding that

$$\mathbf{F}^{\text{surface}} = -\rho V_B \mathbf{g}, \quad (5.3.3)$$

which expresses Archimedes' principle, stating that *the force exerted on an immersed body by the ambient fluid is equal in magnitude and opposite in direction to the weight of the fluid displaced by the body.*

Arbitrary body

To compute the integral on the right-hand side of (5.3.2) over an arbitrarily shaped body, we may subdivide the volume of the body into small rectangular parallelepipeds and approximate the surface of the body with the collection of the faces of the parallelepipeds that are in contact with the fluid. Because of cancellations, the sum of the integrals over the faces of all elementary parallelepipeds is equal to the sum of the integrals of the faces that are wetted by the fluid. Summing all contributions, we find that the force exerted on the body is given by (5.3.3) independent of the body shape. We have found that Archimedes' principles stands true for arbitrarily shaped bodies. To confirm this intuitive result, we employ the Gauss divergence theorem.

Gauss divergence theorem

An identity stemming from the Gauss divergence theorem in three dimensions was stated in equation (5.1.21),

$$\iint_S \phi \mathbf{n} \, dS = \iiint_V \nabla \phi \, dV. \quad (5.3.4)$$

Comparing (5.1.21) with (5.3.2), we set

$$\phi = \rho (g_x x + g_y y + g_z z) + \pi_0, \quad (5.3.5)$$

compute the gradient

$$\nabla \phi = \rho (g_x, g_y, g_z) = \rho \mathbf{g}, \quad (5.3.6)$$

and find that the surface force is given by

$$\mathbf{F}^{\text{surface}} = - \iint_{\text{body}} [\rho (g_x x + g_y y + g_z z) + \pi_0] \mathbf{n} dS = -\rho \mathbf{g} \iiint_{\text{body}} dV = -\rho V_B \mathbf{g}, \quad (5.3.7)$$

which reproduces precisely equation (5.3.3).

5.3.1 Net force on a submerged body

The mass of a body with volume V_B made of a homogeneous material with density ρ_B is $m_B = \rho_B V_B$, and the weight of the body is

$$\mathbf{W} = \rho_B V_B \mathbf{g}, \quad (5.3.8)$$

where \mathbf{g} is the gravitational acceleration. Adding to the weight the buoyancy force given in (5.3.3), we find that the net force exerted on an immersed body is

$$\mathbf{F} = \mathbf{F}^{\text{surface}} + \mathbf{W} = (\rho_B - \rho) V_B \mathbf{g}. \quad (5.3.9)$$

Since the density of a neutrally buoyant body is equal to the density of the ambient fluid, the right-hand side of (5.3.9) vanishes, yielding a zero net force.

5.3.2 Moments

The moment of the surface force about a chosen point, \mathbf{x}_0 , is found by integrating the moment of the traction expressed in terms of the pressure,

$$\mathbf{M}^{\text{surface}} = \iint_{\text{body}} (\mathbf{x} - \mathbf{x}_0) \times (-p \mathbf{n}) dS, \quad (5.3.10)$$

where \times denotes the outer vector product. Substituting the linear hydrostatic pressure distribution for an incompressible fluid, we obtain

$$\mathbf{M}^{\text{surface}} = -\rho \iint_{\text{body}} (\mathbf{g} \cdot \mathbf{x} + \pi_0) (\mathbf{x} - \mathbf{x}_0) \times \mathbf{n} dS. \quad (5.3.11)$$

Unlike the force, the moment depends on the particular geometry of the body.

To evaluate the integral on the right-hand side of (5.3.11), we resort once again to the Gauss divergence theorem in three dimensions stated in equation (2.6.36) for an arbitrary vector field, \mathbf{h} ,

$$\iint_S \mathbf{h} \cdot \mathbf{n} dS = \iiint_V \nabla \cdot \mathbf{h} dV. \quad (5.3.12)$$

Setting $\mathbf{h} = \mathbf{a} \times \mathbf{w}$, where \mathbf{a} is a constant vector and \mathbf{w} is a differentiable function, and then discarding the arbitrary constant \mathbf{a} , we obtain the identity

$$\iint_S \mathbf{n} \times \mathbf{w} \, dS = \iiint_V \nabla \times \mathbf{w} \, dV, \quad (5.3.13)$$

where $\nabla \times \mathbf{w}$ is the curl of \mathbf{w} . Now setting

$$\mathbf{w} = (\mathbf{g} \cdot \mathbf{x} + \pi_0)(\mathbf{x} - \mathbf{x}_0), \quad (5.3.14)$$

we find that

$$\mathbf{M}^{\text{surface}} = \rho \iiint_{\text{body}} \nabla \times ((\mathbf{g} \cdot \mathbf{x} + \pi_0)(\mathbf{x} - \mathbf{x}_0)) \, dV. \quad (5.3.15)$$

Using a vector identity, we obtain

$$\mathbf{M}^{\text{surface}} = \rho \iiint_{\text{body}} (\nabla(\mathbf{g} \cdot \mathbf{x}) \times (\mathbf{x} - \mathbf{x}_0) + (\mathbf{g} \cdot \mathbf{x} + \pi_0) \nabla \times \mathbf{x}) \, dV. \quad (5.3.16)$$

Noting that $\nabla(\mathbf{g} \cdot \mathbf{x}) = \mathbf{g}$ and $\nabla \times \mathbf{x} = \mathbf{0}$, we obtain the final expression

$$\mathbf{M}^{\text{surface}} = \rho \mathbf{g} \times \iiint_{\text{body}} (\mathbf{x} - \mathbf{x}_0) \, dV. \quad (5.3.17)$$

We observe that, if the point \mathbf{x}_0 is identified with the center of mass of a homogeneous fluid displaced by a body with volume V_B , given by

$$\mathbf{x}_c = \frac{1}{V_B} \iiint_{\text{body}} \mathbf{x} \, dV, \quad (5.3.18)$$

then the surface moment is zero.

The moment exerted on a homogeneous body due to gravity is given by

$$\mathbf{M}^{\text{gravity}} = -\mathbf{g} \times \iiint_{\text{body}} \rho_B (\mathbf{x} - \mathbf{x}_0) \, dV, \quad (5.3.19)$$

and the total moment exerted on the body is

$$\mathbf{M} = \mathbf{M}^{\text{surface}} + \mathbf{M}^{\text{gravity}} = \mathbf{g} \iiint_{\text{body}} (\rho - \rho_B) (\mathbf{x} - \mathbf{x}_0) \, dV, \quad (5.3.20)$$

which is zero if the point \mathbf{x}_0 is identified with the center of mass of a homogeneous fluid displaced by the body, or else if the density of the fluid matches the density of the body.

Equilibrium of an immersed body

The buoyancy force vector passes through the *center of mass of the fluid* displaced by the body, whereas the body weight vector passes through the *center of mass of the body*. If the

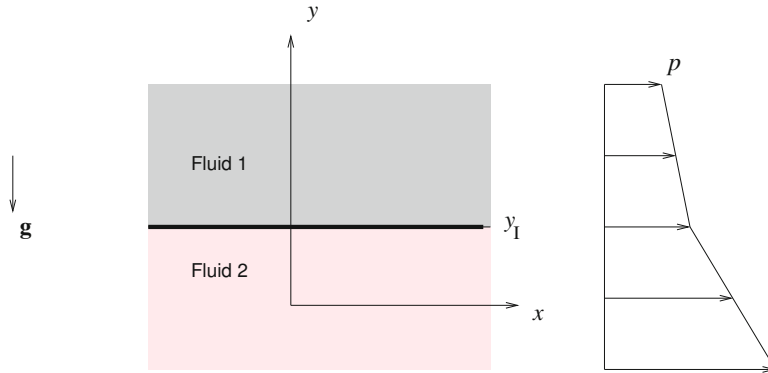


Figure 5.4.1 Illustration of an infinite horizontal interface located at $y = y_I$, separating two stationary fluids. The pressure distribution is shown on the right.

former lies above the latter, the body is in a state of stable equilibrium and will remain stationary. In the opposite case, the body will rotate spontaneously to reach a stable configuration.

PROBLEM

5.3.1 Applications of the Gauss divergence theorem

(a) Apply (5.1.21) for a constant function f and discuss the results.

(b) Show that the center of gravity of a homogeneous body can be computed in terms of a surface integral as

$$\mathbf{x}_c = \frac{1}{2V_B} \iint_{\text{body}} (x^2 + y^2 + z^2) \mathbf{n} \, dS. \quad (5.3.21)$$

5.4 Interfacial shapes

Consider two superposed stationary incompressible fluids separated by an infinite horizontal interface located at $y = y_I$, as illustrated in Figure 5.4.1. The acceleration of gravity points against the y axis. The upper fluid is labeled 1 and the lower fluid is labeled 2.

Using the general expression for the pressure distribution in an incompressible liquid, given in equation (5.1.37), and setting $g_x = 0$, $g_y = -g$, and $g_z = 0$, we find that the pressure distributions in the two fluids are given by

$$p^{(1)}(y) = -\rho_1 g y + \pi_1, \quad p^{(2)}(y) = -\rho_2 g y + \pi_2. \quad (5.4.1)$$

The constants π_1 and π_2 are related by the condition for the jump in the traction across an interface with uniform surface tension stated in equation (4.5.16).

Since in this case the curvature of the interface vanishes, $\kappa = 0$, condition (4.5.16) requires that the pressure is continuous across the interface,

$$p^{(1)}(y = y_I) = p^{(2)}(y = y_I). \quad (5.4.2)$$

Substituting the pressure distributions given in (5.4.1) into (5.4.2), we obtain

$$-\rho_1 g y_I + \pi_1 = -\rho_2 g y_I + \pi_2, \quad (5.4.3)$$

which can be rearranged to give

$$\pi_2 = \pi_1 + (\rho_2 - \rho_1) g y_I. \quad (5.4.4)$$

One of the two reference pressures, π_1 and π_2 , is determined by requiring an appropriate boundary condition far from the interface, and the other follows from (5.4.4). For example, if the pressure on the upper side of the interface is equal to the atmospheric pressure p_{atm} , then

$$\pi_1 = p_{\text{atm}} + \rho_1 g y_I, \quad \pi_2 = p_{\text{atm}} + \rho_2 g y_I. \quad (5.4.5)$$

5.4.1 Curved interfaces

In practice, the flat interface depicted in Figure 5.4.1 terminates at a side wall, as illustrated in Figure 5.4.2. Additional examples of terminated interfaces are depicted in Figure 5.5.1, illustrating a semi-infinite interface ending at an inclined plate, in Figure 5.6.1, illustrating an interface confined between two parallel plates, and in Figure 5.7.1, illustrating the interface of a drop attached to a horizontal plane.

Contact line

The line where two fluids meet on a solid surface is called the contact line. In the case of a two-dimensional or axisymmetric interface, the contact line is represented by a contact point, which is the trace of the contact line in the xy or an azimuthal plane, marked by a circular symbol in Figures 5.5.1, 5.6.1, and 5.7.1.

Contact angle

The angle subtended between (a) the line that is normal to the contact line and tangential to the solid surface, and (b) the line that is normal to the contact line and tangential to the interface, measured by convention on the side of fluid labeled 2, as illustrated in Figure 5.4.2, is called the contact angle.

The static contact angle is a physical constant determined by the prevailing physical conditions and physical properties of the solid and fluids. If fluid 1 wets the solid better than fluid 2, then the contact angle is less than $\frac{1}{2}\pi$ but higher than the minimum possible value of 0. If fluid 2 wets the solid better than fluid 1, the contact angle is higher than $\frac{1}{2}\pi$ but less than the maximum possible value of π .

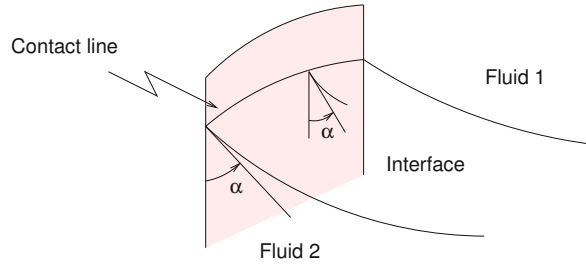


Figure 5.4.2 Illustration of an interface terminating at a contact line on a surface. By convention, the contact angle, α , is measured on the side of the fluid labeled 2.

If the side-wall illustrated in Figure 5.4.2 is vertical and the static contact angle is equal to $\frac{1}{2}\pi$, the interface remains flat all the way up to the contact line. Under more general conditions, the interface assumes a curved shape established spontaneously to satisfy a physical requirement on the contact angle.

5.4.2 The Laplace-Young equation for a two-dimensional interface

To derive an equation governing the shape of a two-dimensional curved interface separating two immiscible fluids, we substitute the pressure distributions (5.4.1) into the interfacial condition (4.5.16),

$$p^{(2)} - p^{(1)} = \gamma \kappa, \quad (5.4.6)$$

finding

$$-\rho_2 g y + \pi_2 + \rho_1 g y - \pi_1 = \gamma \kappa, \quad (5.4.7)$$

where κ is the interfacial curvature and y is the elevation of the interface. Rearranging, we obtain the Laplace-Young equation governing the shape of a two-dimensional interface in hydrostatics,

$$\kappa = -\frac{\Delta \rho g}{\gamma} y + B, \quad (5.4.8)$$

where $\Delta \rho \equiv \rho_2 - \rho_1$ is the density difference and

$$B \equiv \frac{\pi_2 - \pi_1}{\gamma} \quad (5.4.9)$$

is a constant with units of inverse length. In applications, the constant B is determined by enforcing an appropriate boundary condition or global constraint.

The Laplace-Young equation (5.4.8) essentially requires that the curvature of an interface is a linear function of the elevation from a reference state, y . An obvious solution is found by assuming that the elevation y is constant along the interface, $y = b$, and then setting $B = \Delta \rho g b / \gamma$, finding that $\kappa = 0$. However, the flat shape of the interface computed in

this fashion will not necessarily satisfy the boundary condition on the static contact angle; consequently, the obvious solution will not be admissible. The shape of the interface must be found so that equation (5.4.8) and a prescribed boundary condition on the contact angle are both satisfied.

Capillary length

Assuming that the fluids separated by an interface are stably stratified, that is, $\rho_2 > \rho_1$ or $\Delta\rho \equiv \rho_2 - \rho_1 > 0$, we introduce the capillary length defined as

$$\lambda \equiv \left(\frac{\gamma}{\Delta\rho g} \right)^{1/2}. \quad (5.4.10)$$

For an air-water interface at 20° Celsius, $\gamma = 73$ dynes/cm = 73×10^{-3} kg/sec², $\rho_1 = 0.0$ kg/m³, $\rho_2 = 1000.0$ kg/m³, yielding a capillary length of 2.72 mm. Equation (5.4.8) may now be recast into the compact form

$$\kappa = -\frac{y}{\lambda^2} + B. \quad (5.4.11)$$

All three terms in this equation have units of inverse length.

Arbitrary orientation

Implicit in (5.4.8) is the assumption that the acceleration of gravity vector, \mathbf{g} , points against the y axis. The general expression for an arbitrary orientation of the gravitational acceleration with respect to the working coordinates is

$$\kappa = \frac{\Delta\rho}{\gamma} \mathbf{g} \cdot \mathbf{x} + B, \quad (5.4.12)$$

where the point \mathbf{x} lies at the interface, the pressure distributions in the two fluids are given by

$$p^{(1)}(\mathbf{x}) = \rho_1 \mathbf{g} \cdot \mathbf{x} + \pi_1, \quad p^{(2)}(\mathbf{x}) = \rho_2 \mathbf{g} \cdot \mathbf{x} + \pi_2, \quad (5.4.13)$$

and the constant B is given in (5.4.9).

5.4.3 Three-dimensional and axisymmetric interfaces

The equations derived in Section 5.4.2 for a two-dimensional interface also apply for an axisymmetric or a genuinely three-dimensional interface, provided that the curvature in the xy plane is replaced by twice the mean curvature, $2\kappa_m$. The counterpart of the Laplace–Young equation (5.4.10) is

$$2\kappa_m = -\frac{y}{\lambda^2} + B, \quad (5.4.14)$$

where the constant B is given in (5.4.9). We recall that the mean curvature is the average of two conjugate curvatures at any point on the interface.

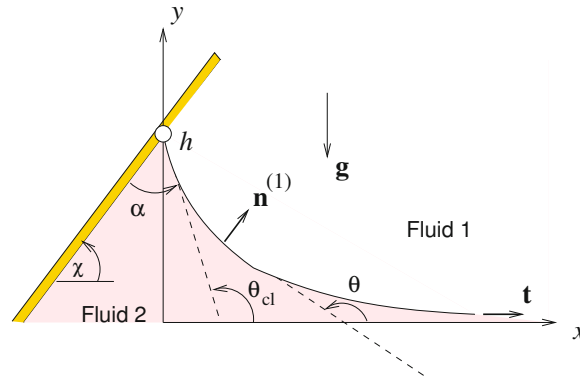


Figure 5.5.1 Illustration of a semi-infinite interface attached to an inclined plate. Far from the plate, the interface becomes horizontal.

When gravitational effects are not important, the first term on the right-hand side of (5.4.14) is insignificant. Consequently, the interface adjusts to obtain a uniform mean-curvature shape, such as that assumed by a thin soap film attached to a wire frame.

Numerical solutions of the unsimplified Laplace–Young equation for a variety of interfacial configurations are discussed in the remainder of this chapter.

PROBLEM

5.4.1 Pressure in a layer

Derive expressions for the pressure distribution across a horizontal liquid layer of thickness h sandwiched between two semi-infinite fluids.

5.4.2 Constant mean curvature

Compile a list of five geometrical shapes with constant mean curvature.

5.5 A semi-infinite interface attached to an inclined plate

We begin the study of two-dimensional interfacial shapes by considering a semi-infinite interface attached to a flat plate that is inclined by an angle χ with respect to the horizontal plane, as illustrated in Figure 5.5.1. Far from the plate, as x tends to infinity, the interface tends to become horizontal. The contact angle subtended between the inclined plate and the tangent to the interface at the contact point is required to have a prescribed value, α .

It is convenient to set the origin of the y axis at the position of the flat interface far from the plate, and describe the interface by a function

$$y = f(x). \quad (5.5.1)$$

As x tends to infinity, the function $f(x)$ decays to zero to yield a flat interface. Since the interfacial curvature tends to zero far from the plate, the constant B on the right-hand side of the governing Laplace–Young equation (5.4.10) must be zero, yielding the simpler form

$$\kappa = -\frac{f}{\lambda^2}. \tag{5.5.2}$$

The curvature is given by expressions (4.3.28) and (4.3.30) as

$$\kappa = -\frac{f''}{(1+f'^2)^{3/2}} = \frac{1}{f'} \left(\frac{1}{\sqrt{1+f'^2}} \right)' = \frac{1}{f'} \frac{d|\cos\theta|}{dx} = -\left(\frac{f'}{\sqrt{1+f'^2}} \right)', \tag{5.5.3}$$

where $f' = \tan\theta$, as shown in Figure 5.5.1, and a prime denotes a derivative with respect to x . Substituting the last expression into (5.5.2) and integrating with respect to x , we find that

$$\left(\frac{f'}{\sqrt{1+f'^2}} \right)_{\text{cl}} = \sin\theta_{\text{cl}} = \frac{1}{\lambda^2} \int_0^\infty f(x) dx, \tag{5.5.4}$$

where the subscript cl denotes evaluation at the contact line,

$$\theta_{\text{cl}} = \alpha + \chi. \tag{5.5.5}$$

The integral on the right-hand side of (5.5.4) is the area of fluid 2 confined between the meniscus above the flat interface and the vertical line passing through the contact line. The weight of the corresponding fluid, reduced by the buoyancy force, is balance by the vertical component of the capillary force.

Substituting the second and third expressions in (5.5.3) into (5.5.2), and rearranging, we derive a nonlinear differential equation governing the interfacial shape,

$$\frac{d}{dx} \left(\frac{1}{\sqrt{1+f'^2}} \right) = \frac{d|\cos\theta|}{dx} = -\frac{ff'}{\lambda^2} = -\frac{1}{2} \frac{(f^2)'}{\lambda^2}. \tag{5.5.6}$$

Integrating once with respect to x , we obtain

$$\frac{1}{\sqrt{1+f'^2}} = |\cos\theta| = -\frac{1}{2} \frac{f^2}{\lambda^2} + C, \tag{5.5.7}$$

where C is a dimensionless integration constant. Requiring that f decays to zero as x tends to infinity, and correspondingly θ tends to π , we obtain $C = 1$.

Capillary rise

At the contact line located at $x = 0$, the slope angle θ takes the value given in (5.5.5). Evaluating equation (5.5.7) at $x = 0$ with $C = 1$ and rearranging, we obtain an expression for the positive or negative capillary rise, $h \equiv f(0)$,

$$\frac{1}{2} \frac{h^2}{\lambda^2} = 1 - |\cos(\alpha + \chi)|, \tag{5.5.8}$$

which shows that the maximum possible value of $|h|$ occurs when $\alpha + \chi$ is a multiple of $\frac{1}{2}\pi$, and is equal to $\sqrt{2}\lambda$.

Numerical formulation

To compute the shape of the interface, we apply (5.5.7) with $C = 1$ and rearrange to obtain a first-order ordinary differential equation,

$$\frac{df}{dx} = \pm \left(\frac{4}{(2 - \phi^2)^2} - 1 \right)^{1/2} = \pm \frac{\phi}{2 - \phi^2} \sqrt{4 - \phi^2}, \quad (5.5.9)$$

where $\phi \equiv f/\lambda$ is a dimensionless function. The plus or minus sign on the right-hand side must be selected according to the expected interface shape.

The preceding analysis assumes that the interface has a monotonic shape, which is true if the angle θ_{cl} lies in the range $(\frac{1}{2}\pi, \frac{3}{2}\pi)$. Outside this range, the capillary rise is given by equation (5.5.8) with the minus sign replaced by a plus sign on the right-hand side.

When the shape of the interface is non-monotonic, the interface becomes vertical at a point, the function $f(x)$ is multi valued, and the integration of (5.5.9) requires careful consideration. To bypass this subtlety, we regard the x coordinate along the interface as a function of the independent variable f , and recast (5.5.9) into the form

$$\frac{dx}{df} = \pm \frac{2 - \phi^2}{\phi} \frac{1}{\sqrt{4 - \phi^2}}. \quad (5.5.10)$$

The solution of (5.5.10) must be found for $|f| < |h|$, where $|h|$ is the capillary rise computed from equation (5.5.8).

5.5.1 Numerical method

A numerical solution of (5.5.10) can be computed according to the following steps:

1. Compute the angle θ_{cl} from equation (5.5.5).
2. Compute the capillary rise h using the formulas

$$\frac{h}{\sqrt{2}\lambda} = \begin{cases} (1 + |\cos \theta_{cl}|)^{1/2} & \text{if } 0 < \theta_{cl} < \frac{1}{2}\pi, \\ (1 - |\cos \theta_{cl}|)^{1/2} & \text{if } \frac{1}{2}\pi < \theta_{cl} < \pi, \\ -(1 - |\cos \theta_{cl}|)^{1/2} & \text{if } \pi < \theta_{cl} < \frac{3}{2}\pi, \\ -(1 + |\cos \theta_{cl}|)^{1/2} & \text{if } \frac{3}{2}\pi < \theta_{cl} < 2\pi. \end{cases} \quad (5.5.11)$$

3. Integrate the differential equation (5.5.10) from $f = h$ to 0 subject to the initial condition $x(f = h) = 0$ using, for example, the explicit Euler method or the modified Euler method discussed in Section 1.5. If h is negative, use a negative spatial step.

To implement the explicit Euler method, we select a small positive or negative integration step, $\Delta f = h/N$, where N defines the level of numerical discretization, evaluate equation

(5.5.10) at the point f , and approximate the derivative on the left-hand side with the finite difference, setting

$$\frac{dx}{df} \simeq \frac{x(f + \Delta f) - x(f)}{\Delta f}. \quad (5.5.12)$$

Rearranging, we obtain

$$x(f + \Delta f) = x(f) + \Delta f \frac{2 - \phi^2}{\phi} \frac{1}{\sqrt{4 - \phi^2}}. \quad (5.5.13)$$

The repetitive application of this formula starting from $f = h$ where $x = 0$ generates a sequence of points distributed over the interface.

Modified Euler method (RK2)

To implement the modified Euler method, we replace formula (5.5.13) with a slightly more involved formula,

$$x(f + \Delta f) = x(f) + \Delta f \frac{1}{2} \left(\frac{2 - \phi^2}{\phi} \frac{1}{\sqrt{4 - \phi^2}} + \frac{2 - \phi_{\text{tmp}}^2}{\phi_{\text{tmp}}} \frac{1}{\sqrt{4 - \phi_{\text{tmp}}^2}} \right), \quad (5.5.14)$$

where $\phi_{\text{tmp}} = \phi + \Delta\phi$ and $\Delta\phi = \Delta f/\lambda$.

The modified Euler method is implemented in the following MATLAB code entitled *men_2d_plate* residing in directory *03_hydrostat* of **FDLIB**. The program scans tilting angles, while holding the contact angle α constant, and displays the interfacial profile in animation, as follows:

```
%---
% data
%---

gac = 1.0;   % acceleration of gravity
rhop = 1.0;  % pool density
rhoa = 0.0;  % ambient fluid density
gamma = 1.0; % surface tension
chi = 0.01*pi; % plate inclination
alpha = 0.01*pi; % contact angle
ndiv = 2*64; % interface divisions

%---
% prepare
%---

drho = rhop-rhoa;

if(drho<0)
    disp 'The density of the pool must be higher than'
```



```

disp 'the density of the ambient fluid'
return
end

capls = gamma/(gac*abs(drho));
capl = sqrt(capls);
dchi = 0.05;

Irepeat = 1;

%=====
while (Irepeat==1)
%=====

%-----
% angle theta at the contact line
%-----

thcl = alpha+chi;
cst = cos(thcl);

%-----
% compute the magnitude of meniscus rise h
%-----

if((thcl>0.5*pi)&(thcl<1.5*pi))
    h = sqrt(2.0*capls*(1.0-abs(cst)));
else
    h = sqrt(2.0*capls*(1.0+abs(cst)));
end

%---
% sign of meniscus rise
%---

if(thcl<pi)
    h = abs(h);    % meniscus goes up
else
    h =-abs(h);   % meniscus goes down
end

%---
% plate position at y=0
%---

xpl = -h/tan(chi);

%-----
% integrate meniscus equation dx/df = G(f)

```

```

% from f=h to f=0 using the modified Euler
% method with constant step
%-----

df = h/ndiv; % note that df can be positive or negative
dfh = 0.5*df;

y(1) = h;
x(1) = 0.0; % starting point

for i=1:ndiv-1
    fred = y(i)/capl;
    freds = fred*fred;
    xp = (2.0-freds)/sqrt(4.0-freds)/fred;
    xsv = x(i); % save
    xpsv = xp; % save
    y(i+1) = y(i)-df;
    x(i+1) = x(i)+xp*df;
    fred = y(i+1)/capl;
    freds = fred*fred;
    xp = (2.0-freds)/(fred*sqrt(4.0-freds));
    x(i+1) = xsv+(xpsv*xp)*dfh;
end

%---
% plotting
%---

plot(x,y)
hold on
patch([xpl, 0, x, x(ndiv), (-2-h)/tan(chi)] ...
      ,[0, h, y,-2, -2],'y');
plot([-1 3 3 -1 -1],[-2 -2 2 2 -2])
plot([-10 10],[-10*tan(chi)+h, 10*tan(chi)+h] ...
      ,'r','LineWidth',3);
plot([xpl, 10],[0, 0],'c--','LineWidth',1);
hold off
axis equal
xlabel('x','fontsize',15); ylabel('y','fontsize',15);
axis([-1 3 -2 2])
pause(0.1)

%---
% tilt the plate
%---

chi = chi + dchi;

if(chi > 0.99*pi | chi<0.01*pi)

```

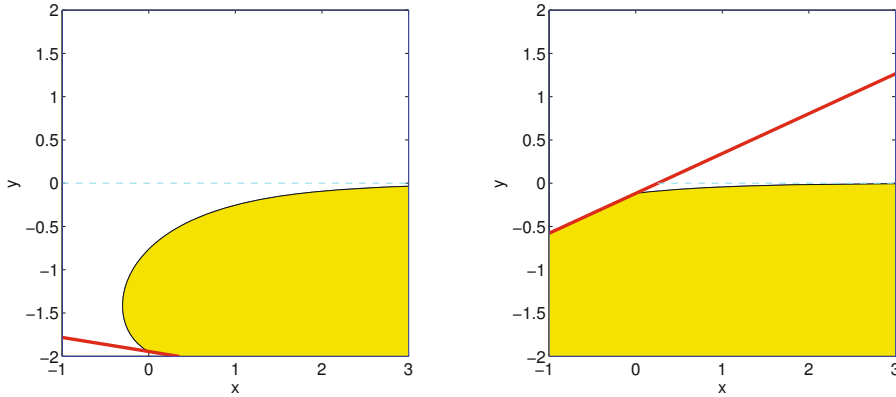


Figure 5.5.2 A semi-infinite meniscus attached to an inclined plate generated by the FDLIB code *men_2d_plate*. The plate inclination angles χ are different, but the contact angle α is the same in both cases.

```
dchi = -dchi;
end

%====
end
%====
```

The graphics display generated by the code for two plate inclination angles and a fixed contact angle is shown in [Figure 5.5.2](#).

5.5.2 A floating cylinder

The flat-plate solution derived in this section can be used to derive a trigonometric equation governing the floating angle, β , and position of the center of a floating circular cylinder of radius a , as shown in [Figure 5.5.3](#). In the case of a flat interface, the cylinder center is located at $y_c = -a \cos \beta$.

In the chosen system of Cartesian coordinates, the undisturbed interface far from the floating cylinder is located at $y = 0$. The contact point on the right side of the cylinder is located at

$$x_{cl} = a \sin \beta, \quad y_{cl} = y_c + a \cos \beta, \quad (5.5.15)$$

and the local inclination angle is $\chi = \pi - \beta$. Setting $h = y_{cl}$ and substituting the expression for y_{cl} into (5.5.8), we obtain

$$\frac{1}{2} \left(\frac{y_{cl}}{\lambda} \right)^2 = 1 - |\cos(\alpha - \beta + \pi)| = 2 \sin^2 \frac{\alpha - \beta}{2}, \quad (5.5.16)$$

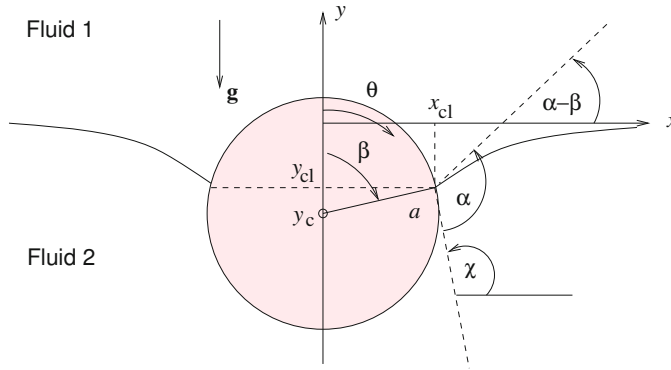


Figure 5.5.3 Illustration of a cylinder floating at the interface between two immiscible fluids. A curved meniscus is established on either side of the cylinder.

yielding

$$y_{cl} = -2 \lambda \sin \frac{\alpha - \beta}{2}. \tag{5.5.17}$$

The hydrostatic pressure distributions in the upper and lower fluid are given by

$$p^{(1)}(y) = -\rho_1 g y + \pi_0, \quad p^{(2)}(y) = -\rho_2 g y + \pi_0, \tag{5.5.18}$$

where ρ_1 is the density of the upper fluid, ρ_2 is the density of the lower fluid, g is the gravitational acceleration, and π_0 is an inconsequential constant. The buoyancy force exerted by the fluids on the cylinder is given by

$$F_y^{\text{buoyancy}} = -2 \int_0^\beta p^{(1)} n_y a \, d\theta - 2 \int_\beta^\pi p^{(2)} n_y a \, d\theta, \tag{5.5.19}$$

where θ is the polar angle defined in [Figure 5.5.3](#), $n_y = \cos \theta$ is the y component of the outward unit vector, and the factor of 2 accounts for both sides of the cylinder. Substituting the pressure distributions (5.5.18) and setting $y = y_c + a \cos \theta$, we obtain

$$F_y^{\text{buoyancy}} = 2ga \left(\rho_1 \int_0^\beta (y_c + a \cos \theta) \cos \theta \, d\theta + \rho_2 \int_\beta^\pi (y_c + a \cos \theta) \cos \theta \, d\theta \right). \tag{5.5.20}$$

Performing the integration, we find that

$$F_y^{\text{buoyancy}} = ag \left(-2 y_c \Delta\rho \sin \beta + a \Delta\rho \frac{1}{2} (\pi - 2\beta - \sin(2\beta)) + \pi a \bar{\rho} \right), \tag{5.5.21}$$

where $\Delta\rho = \rho_2 - \rho_1$ and

$$\bar{\rho} = \frac{1}{2} (\rho_1 + \rho_2) \tag{5.5.22}$$

is the mean density of the fluids.

The y component of the capillary force per unit length of the cylinder, acting on both sides of the cylinder, is given by

$$F_y^{\text{capillary}} = 2\gamma \sin(\alpha - \beta). \quad (5.5.23)$$

Balancing the weight of the cylinder, the buoyancy force, and the capillary force, we obtain the equilibrium equation

$$\pi a^2 \rho_b - F_y^{\text{buoyancy}} = F_y^{\text{capillary}}, \quad (5.5.24)$$

where ρ_b is the cylinder (body) density.

Making substitutions, setting $y_c = y_{cl} - a \cos \beta$, using (5.5.17), and simplifying, we obtain a trigonometric equation for β ,

$$8\lambda \sin \frac{\alpha - \beta}{2} \sin \beta + \pi(1 + \tau) - 2\beta + \sin(2\beta) + 4\lambda^2 \sin(\alpha - \beta) = 0, \quad (5.5.25)$$

which is also a quadratic equation for the dimensionless variable

$$\lambda \equiv \frac{\lambda}{a} \equiv \frac{1}{\sqrt{\text{Bo}}}, \quad (5.5.26)$$

where $\text{Bo} \equiv (a/\lambda)^2$ is a Bond number, and

$$\tau = 2 \frac{\bar{\rho} - \rho_b}{\Delta \rho} \quad (5.5.27)$$

is a dimensionless density parameter. Given α and τ , equation (5.5.25) can be solved readily for β using Newton's method.

PROBLEMS

5.5.1 Floating cylinder

Show that the buoyancy force exerted on the floating cylinder is given by the alternative expression

$$F_y^{\text{buoyancy}} = -2a(x_c + a \cos \beta) \Delta \rho g \sin \beta + \frac{1}{2} \Delta \rho g (A_2 - A_1) + \bar{\rho} g A, \quad (5.5.28)$$

where A_1 and A_2 are the cylinder areas above and below the horizontal plane passing through the rectilinear contact lines on either side of the cylinder, and $A = \pi a^2$ is the cylinder cross-sectional area. Derive the expressions

$$A_1 = a^2 \left(\beta - \frac{1}{2} \sin(2\beta) \right), \quad A_2 = a^2 \left(\pi - \beta + \frac{1}{2} \sin(2\beta) \right). \quad (5.5.29)$$

5.5.2 Semi-infinite meniscus

Run the code `men_2d_plate` to generate a family of shapes corresponding to a fixed plate inclination angle, β , and various contact angles, α . Generate another family of shapes corresponding to a fixed contact angle and various plate inclination angles. Discuss the behavior of the capillary rise in each case.

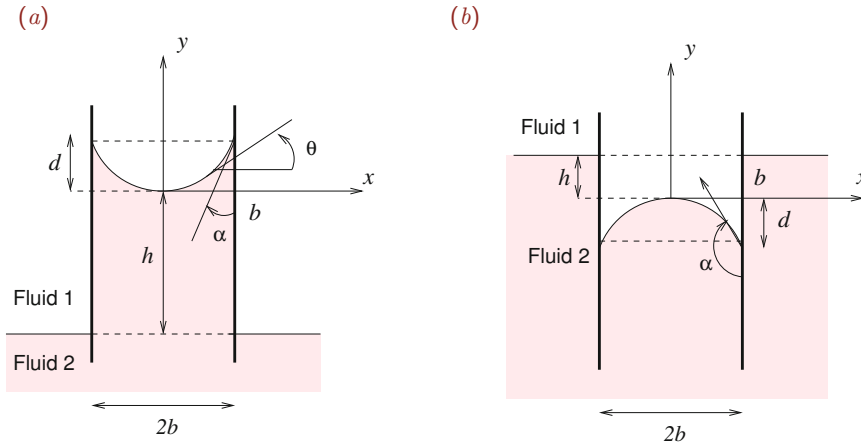


Figure 5.6.1 Illustration of a meniscus between two parallel vertical plates for contact angle (a) $\alpha < \frac{1}{2}\pi$ and (b) $\alpha > \frac{1}{2}\pi$. In the second case, the meniscus submerges and the capillary rise h is negative.

5.6 A meniscus between two parallel plates

Consider a two-dimensional interface between two fluids subtended between two parallel vertical plates, as illustrated in Figure 5.6.1(a). It is reasonable to assume that the two contact points are at the same elevation and the interface is symmetric with respect to the mid-plane located at $x = 0$.

It is convenient to set the origin of the Cartesian axes at the interface midway between the plates and describe the position of the interface by a function

$$y = f(x). \tag{5.6.1}$$

Outside and far from the plates, the interface assumes a horizontal shape located at $y = -h$, where h is the positive or negative capillary rise of the meniscus midway between the plates.

The lower fluid is labeled as fluid 2 and the upper fluid is labeled as fluid 1. The pressure distributions in the two fluids are given by

$$p^{(1)}(y) = -\rho_1 g y + \pi_1, \quad p^{(2)}(y) = -\rho_2 g y + \pi_2, \tag{5.6.2}$$

where π_1 and π_2 are two reference pressures. Our objective is to compute the capillary rise, h , along with the unknown shape of the meniscus by solving the Laplace–Young equation (5.4.10),

$$\kappa = -\frac{f}{\lambda^2} + B, \tag{5.6.3}$$

where $B \equiv (\pi_2 - \pi_1)/\gamma$ and $\lambda^2 \equiv \gamma/(\Delta\rho g)$ is the square of the capillary length. We have assumed that $\Delta\rho \equiv \rho_2 - \rho_1 > 0$, so that the fluids are stably stratified.

Evaluating equation (5.6.3) at a point outside and far from the plates where the curvature of the interface tends to vanish and the interfacial elevation tends to $-h$, we obtain

$$B = -\frac{h}{\lambda^2}. \quad (5.6.4)$$

The Laplace–Young equation (5.6.3) then becomes

$$\kappa = -\frac{f+h}{\lambda^2}, \quad (5.6.5)$$

where $f+h$ is the unknown elevation of the curved interface between the plates measured with respect to the flat interface outside the plates.

The curvature is given by equations (4.3.28) and (4.3.30), repeated below for convenience,

$$\kappa = -\frac{f''}{(1+f'^2)^{3/2}} = \frac{1}{f'} \left(\frac{1}{\sqrt{1+f'^2}} \right)' = -\left(\frac{f'}{\sqrt{1+f'^2}} \right)' \quad (5.6.6)$$

and

$$\kappa = \frac{1}{\tan \theta} \frac{d \cos \theta}{dx} = -\frac{d \sin \theta}{dx}, \quad (5.6.7)$$

where $f' = \tan \theta$, the slope angle θ is defined in [Figure 5.6.1](#), and a prime denotes a derivative with respect to x .

Mid-plane curvature and capillary rise

Our choice of Cartesian axes requires that $f = 0$ at the mid-plane, $x = 0$. Equation (5.6.3) then gives

$$\kappa(0) = B. \quad (5.6.8)$$

Because the interface is symmetric with respect to $x = 0$, $f' = 0$ at $x = 0$, the first expression in (5.6.6) yields

$$\kappa(0) = -f''(0). \quad (5.6.9)$$

Combining equations (5.6.8) and (5.6.9), we find that

$$B = -f''(0), \quad (5.6.10)$$

and thus

$$\frac{h}{\lambda^2} = -\kappa(0) = f''(0), \quad (5.6.11)$$

which shows that the capillary rise is determined by the curvature of the interface at the mid-plane, and *vice versa*. If the capillary rise is zero, the curvature of the interface at the mid-plane is also zero, and *vice versa*.

Meniscus height

Substituting the first expression for the curvature in terms of the slope angle θ given in (5.6.7) into (5.6.5), and recalling that $\tan \theta = f'$, we obtain

$$\frac{d \cos \theta}{dx} = -\frac{f+h}{\lambda^2} f' = -\frac{1}{\lambda^2} \left(\frac{1}{2} (f^2)' + h f' \right). \quad (5.6.12)$$

Integrating with respect to x from 0 to b , and noting that

$$\theta_b = \frac{1}{2} \pi - \alpha, \quad \cos \theta_b = \sin \alpha, \quad (5.6.13)$$

we obtain a quadratic equation for the meniscus height, $d \equiv f(b)$,

$$1 - \sin \alpha = \frac{1}{\lambda^2} \left(\frac{1}{2} d + h \right) d, \quad (5.6.14)$$

where $\theta_b = \theta(x=0)$.

Vertical force balance

Substituting into (5.6.5) the second expression for the curvature in terms of the slope angle θ given in (5.6.7), and integrating with respect to x from 0 to b , we obtain

$$\cos \alpha = \frac{1}{\lambda^2} \int_0^b (f+h) dx. \quad (5.6.15)$$

In fact, this equation expresses a balance of the weight of fluid between the plates above or below the flat interface, the buoyancy force, and the capillary force at the rectilinear contact lines.

Differential equations

To compute the shape of the interface, we substitute the first expression for the curvature given in (5.6.6) into the Laplace–Young equation (5.6.5), and rearrange to derive a second-order ordinary differential equation involving the capillary rise h as an unknown,

$$f'' = \frac{1}{\lambda^2} (f+h) (1+f'^2)^{3/2}. \quad (5.6.16)$$

The solution must be found in the interval $0 < x < b$ subject to the boundary conditions

$$f(0) = 0, \quad f'(0) = 0, \quad f'(b) = \tan\left(\frac{1}{2}\pi - \alpha\right) = \cot \alpha. \quad (5.6.17)$$

The third condition specifies the prescribed value of the contact angle. It is important to bear in mind that h is an implicit function of the shape function f by way of equation (5.6.11).

When $\alpha = \frac{1}{2} \pi$, all three boundary (5.6.17) are homogeneous and the obvious solution describes a flat, non-elevated and non-submerged interface, $h = 0$ and $f = 0$.

Canonical form

To compute the meniscus shape under general conditions, we recast the second-order differential equation (5.6.16) involving the unspecified parameter h into the canonical form of a system of three first-order differential equations. The word *canonical* derives from the Greek work $\kappa\alpha\nu\omicron\nu\iota\kappa\omicron\varsigma$, which means *normal*. This is done by introducing three new variables,

$$y_1 \equiv f, \quad y_2 \equiv f', \quad y_3 \equiv h. \quad (5.6.18)$$

Given these definitions, and noting that $y_2' = f''$, we resolve equation (5.6.16) into three first-order component equations,

$$\frac{dy_1}{dx} = y_2, \quad \frac{dy_2}{dx} = \frac{1}{\lambda^2} (y_1 + y_3) (1 + y_2^2)^{3/2}, \quad \frac{dy_3}{dx} = 0. \quad (5.6.19)$$

The third equation simply states that $y_3 \equiv h$ is a constant. In terms of the new variables, the boundary conditions (5.6.17) become

$$y_1(0) = 0, \quad y_2(0) = 0, \quad y_2(b) = \cot \alpha. \quad (5.6.20)$$

If the value of $y_3(0) = h$ were known, we would be able to integrate the system (5.6.19) from $x = 0$ to b using, for example, the explicit Euler or the modified Euler method discussed in Sections 1.5 and 5.5.

Explicit Euler method

To implement the explicit Euler method, we recast the system (5.6.19) into the general symbolic form

$$\frac{dy_1}{dx} = f_1(y_1, y_2, y_3, x), \quad \frac{dy_2}{dx} = f_2(y_1, y_2, y_3, x), \quad \frac{dy_3}{dx} = f_3(y_1, y_2, y_3, x), \quad (5.6.21)$$

where

$$f_1 \equiv y_2, \quad f_2 = \frac{1}{\lambda^2} (y_1 + y_3) (1 + y_2^2)^{3/2}, \quad f_3 \equiv 0 \quad (5.6.22)$$

are the phase-space velocities.

Next, we evaluate equations (5.6.21) at a point, x , choose a small spatial step, Δx , and approximate the derivatives on the left-hand sides with finite differences writing, for example,

$$\frac{dy_1}{dx} = \frac{y_1(x + \Delta x) - y_1(x)}{\Delta x}. \quad (5.6.23)$$

Solving for $y_1(x + \Delta x)$ and repeating for the second and third equation, we obtain

$$\begin{bmatrix} y_1(x + \Delta x) \\ y_2(x + \Delta x) \\ y_3(x + \Delta x) \end{bmatrix} = \begin{bmatrix} y_1(x) \\ y_2(x) \\ y_3(x) \end{bmatrix} + \begin{bmatrix} f_1(y_1(x), y_2(x), y_3(x), x) \\ f_2(y_1(x), y_2(x), y_3(x), x) \\ f_3(y_1(x), y_2(x), y_3(x), x) \end{bmatrix} \Delta x. \quad (5.6.24)$$

In vector notation,

$$\mathbf{y}(x + \Delta x) = \mathbf{y}(x) + \mathbf{f}(\mathbf{y}(x), x) \Delta x, \quad (5.6.25)$$

where $\mathbf{y} \equiv (y_1, y_2, y_3)$ is the solution vector and $\mathbf{f} \equiv (f_1, f_2, f_3)$ is the corresponding phase-space velocity vector. The repetitive application of formula (5.6.25) starting from $x = 0$ allows us to generate a sequence of points along the meniscus.

Modified Euler method

To implement the modified Euler method, we replace formula (5.6.25) with a predictor formula,

$$\mathbf{y}^{\text{tmp}} = \mathbf{y}(x) + \mathbf{f}(\mathbf{y}(x), x) \Delta x, \quad (5.6.26)$$

followed by a corrector formula,

$$\mathbf{y}(x + \Delta x) = \mathbf{y}(x) + \frac{1}{2} [\mathbf{f}(\mathbf{y}(x), x) + \mathbf{f}(\mathbf{y}^{\text{tmp}}, x + \Delta x)] \Delta x,$$

where the superscript “tmp” denotes a preliminary value computed by the explicit Euler method. The first equation generates a provisional (temporary) value, and the second equation advances the solution using the initial and provisional values.

The modified Euler method is implemented in the following MATLAB code entitled *men_2d_ode*, located in directory *men_2d* inside directory *03_hydrostat* of FDLIB:

```
function [x,y1,y2] = men_2d_ode (npts,capls,b,h)

%-----
% Integrate ODEs by the modified Euler method
% Integration interval: (0, b)
% Initial condition y1(0) = 0, y2(0) = 0
%-----

%-----
% prepare and initialize
%-----

dx = b/npts; % uniform x step
x(1) = 0.0; y1(1) = 0.0; y2(1) = 0.0;

%-----
% integrate by the modified Euler method
%-----

for i=1:npts

    if(i==1)
        y1p = 0.0 % value at mid-plane
```

```

    y2p = h/capls % value at mid-plane
else
    y1p = y2(i);
    y2p = (y1(i)+h)*sqrt( (1.0+y2(i)*y2(i))^3 )/capls;
end

y1sv = y1(i); y2sv = y2(i); % save
y1psv = y1p; y2psv = y2p;
x(i+1) = x(i) + dx;
y1(i+1) = y1(i) + y1p*dx;
y2(i+1) = y2(i) + y2p*dx;

y1p = y2(i+1); % second velocity evaluation
y2p = (y1(i+1)+h)*sqrt((1.0+y2(i+1)^2)^3 )/capls;
y1(i+1) = y1sv + 0.5*(y1psv+y1p)*dx;
y2(i+1) = y2sv + 0.5*(y2psv+y2p)*dx;

end

%-----
% done
%-----

return

```

Note that the capillary rise, h , is specified in the input field.

The shooting method

Because the value of h is *a priori* unknown, the starting vector $\mathbf{y}(0)$ is not available and the solution of (5.6.19) must be found by iteration. The shooting method prescribes the obvious:

1. Guess a value for $y_3(0) = h$.
2. Compute the solution of (5.6.19).
3. Check whether the third condition in (5.6.20) is fulfilled within a specified tolerance; if not, repeat the computation with an improved guess.

To improve the guess in a systematic fashion that guarantees rapid convergence, we note that the value of $x_2(b)$ computed by solving equations (5.6.19) depends on the guessed value, $y_3(0) = h$. To signify this dependence, we extend the list of arguments of y_2 , writing $y_2(b; h)$. The third boundary condition in (5.6.20) requires that

$$q_2(b; h) - \cot \alpha = 0, \quad (5.6.27)$$

which means that h is a root of an objective function defined as

$$Q(h) \equiv y_2(b; h) - \cot \alpha. \quad (5.6.28)$$

The problem has been reduced to computing the solution of the algebraic equation $Q(h) = 0$, where the left-hand side is evaluated by integrating equations (5.6.19) with a specified value of h .

Secant updates

The secant method provides us with a simple algorithm for solving the targeted nonlinear algebraic equation, $Q(h) = 0$, according to the following steps:

1. Select a value for h that approximates the root, $h^{(1)}$, and compute $Q(h^{(1)})$ by integrating system (5.6.19).
2. Select another value for h that approximates the root, $h^{(2)}$, and compute $Q(h^{(2)})$ by integrating (5.6.19).
3. Approximate the graph of the function $Q(h)$ with a straight line passing through the points computed in Steps 1 and 2. The slope of the approximating straight line is

$$s^{(2)} = \frac{Q(h^{(2)}) - Q(h^{(1)})}{h^{(2)} - h^{(1)}}. \quad (5.6.29)$$

4. Identify the improved value $h^{(3)}$ with the root of the linear function that describes the approximating straight line. Elementary algebra shows that the root is given by

$$h^{(3)} = h^{(2)} - \frac{Q(h^{(2)})}{s^{(2)}}. \quad (5.6.30)$$

5. Repeat the computation with the pairs $h^{(2)}$ and $h^{(3)}$ until convergence.

A reasonable guess for h can be obtained by assuming that the meniscus has a circular shape of radius R , which is positive when the interface is concave upward and negative when the interface is concave downward. Using elementary trigonometry, we find that the prescribed boundary condition on the contact angle will be satisfied when $\cos \alpha = b/R$. Rearranging, we derive the approximation

$$\kappa \simeq -\frac{1}{R} = -\frac{1}{b} \cos \alpha. \quad (5.6.31)$$

Using equation (5.6.11) we obtain the desired educated guess,

$$h \simeq \frac{\lambda^2}{b} \cos \alpha. \quad (5.6.32)$$

Equation (5.6.32) reveals that the maximum possible value of $|h|$ for a circular interface is λ^2/b .

The shooting method is implemented in the following MATLAB function entitled *men_2d*, located in directory *03_hydrostat* of **FDLIB**:

```

function [Iflag,x,y1,hmen] = men_2d ...
...
    (b,gac,gamma,rhop,rhoa ...
    ,alpha,npts,epsilon,maxiter,tol)

%-----
% Hydrostatic shape of a 2D meniscus between
% two vertical parallel plates computed
% by the shooting method
%-----

Iflag = 0;    % flag for success

%-----
% prepare
%-----

drho = rhop-rhoa;    % density difference

% square of the capillary length:
    capls = gamma/(gac*abs(drho));

%-----
% initial guess for h
% computed by assuming a circular interface
%-----

h(1) = capls*cos(alpha)/b;

if(abs(alpha-0.5*pi)<0.000001)
    cota = 0.0;
else
    cota = 1.0/tan(alpha);
end

%---
% compute the first solution of the odes
% to start-up the secant method
%---

Ic = 1;    % counter
[x,y1,y2] = men_2d_ode(npts,capls,b,h(Ic));

error(Ic) = y2(npts+1)-cota;

%-----
% second start-up solution
%-----

```

```

Ic = 2;
h(2) = h(1)+epsilon;
[x,y1,y2] = men_2d_ode(npts,capls,b,h(Ic));

error(Ic) = y2(npts+1)-cota;

%-----
% iterate using the secant method
% until convergence
%-----

for iter=1:maxiter

    Ic = Ic+1;

    %---
    % secant updating
    %---

    Icb = Ic-2; Ica = Ic-1;
    dedh = (error(Ica)-error(Icb))/(h(Ica)-h(Icb));
    h(Ic) = h(Ica)-error(Ica)/dedh;

    [x,y1,y2] = men_2d_ode(npts,capls,b,h(Ic));

    error(Ic) = y2(npts+1)-cota;

    if(abs(error(Ic))<tol)
        break
    end

    %---
end
%---

if(iter==maxiter)
    disp('men_2d: ODE solver failed')
    Iflag=1;
    return
end

hmen = h(Ic);

%---
% done
%---

return

```

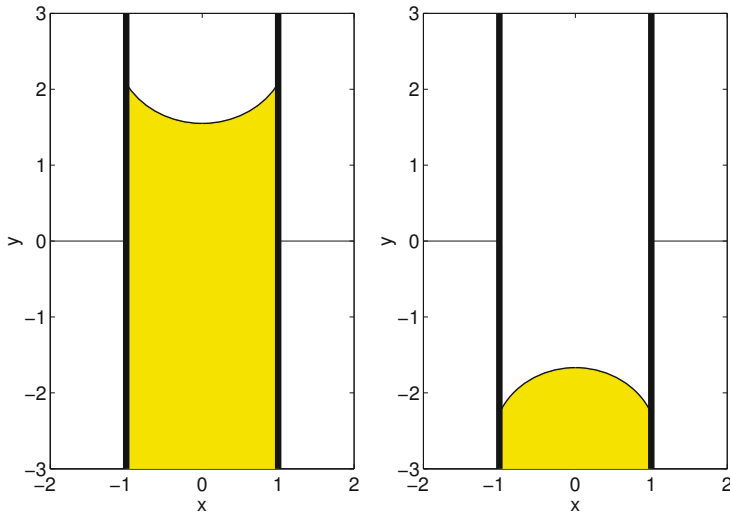


Figure 5.6.2 Shape of a meniscus inside a circular capillary tube generated by the FDLIB code *men_2d*.

Results of computations for a contact angle that is lower than $\frac{1}{2}\pi$ and a contact angle that is higher than $\frac{1}{2}\pi$ are shown in Figure 5.6.2. In the second case, the meniscus submerges below the level of the liquid outside the plates. Scaling all lengths by the plate half-separation, b , we find that the shape of the meniscus depends on the contact angle, α , and on the ratio λ/b . As λ/b increases, the meniscus tends to obtain a circular shape.

PROBLEM

5.6.1 Meniscus between plates

- Run the code *men_2d* to generate a family of shapes corresponding to fixed plate separation and various contact angles. Discuss the behavior of the capillary rise.
- Generate another family of shapes corresponding to fixed contact angle and various plate separations. Discuss the behavior of the capillary rise.

5.7 A two-dimensional drop on a horizontal plane

In the next application, we study the shape of a two-dimensional liquid drop or gas bubble surrounded by a stationary ambient fluid, resting above or hanging below a horizontal plane, as shown in Figure 5.7.1. The drop or bubble fluid is labeled 2 and the surrounding fluid is labeled 1.

The resting drop shown in Figure 5.7.1(a) is called a *sessile* drop, while the hanging drop shown in Figure 5.7.1(b) is called a *pendant* drop.

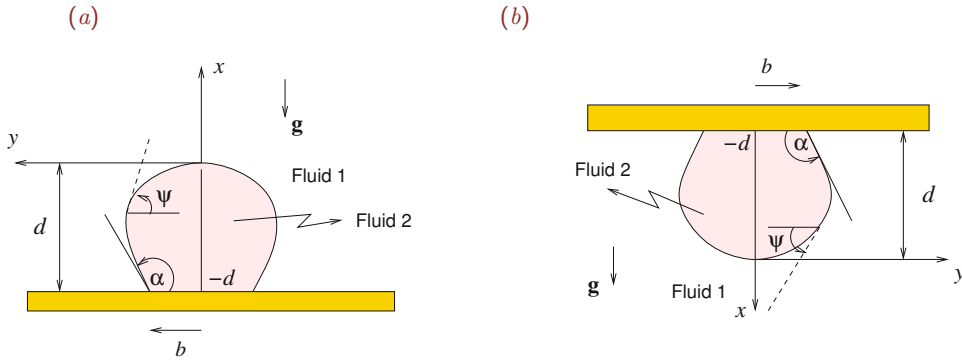


Figure 5.7.1 Illustration of a two-dimensional (a) sessile liquid drop or gas bubble resting on a horizontal plane and (b) pendant liquid drop or gas bubble hanging below a horizontal plane.

Our objective is to compute the shape of the interface for specified surface tension, γ , contact angle, α , and drop area, A_D . The forthcoming analysis also applies for a gas bubble regarded as a zero-density drop, $\rho_2 = 0$.

Working coordinates

It is convenient to work in Cartesian coordinates with origin located at the extreme point of the interface, as shown in Figure 5.7.1 for a sessile or pendant drop. The x axis points normal to the interface into the ambient fluid. The pressure distribution in the two fluids is given by

$$p^{(1)}(x) = -s_1 \rho_1 g x + \pi_1, \quad p^{(2)}(x) = -s_1 \rho_2 g x + \pi_2, \quad (5.7.1)$$

where π_1 and π_2 are two reference pressures. The coefficient s_1 is equal to 1 for a sessile drop or -1 for a pendant drop, reflecting the orientation of the gravity with respect to the positive direction of the x axis.

The shape of the interface is governed by the Laplace–Young equation determining the jump in pressure across the interface due to surface tension in terms of the curvature,

$$\kappa = -s_1 \frac{\Delta \rho g}{\gamma} x + B, \quad (5.7.2)$$

where $\Delta \rho = \rho_2 - \rho_1$ and $B \equiv (\pi_2 - \pi_1)/\gamma$ is an *a priori* unknown constant with dimensions of inverse length. In terms of the square of the capillary length, $\lambda^2 \equiv \gamma/(|\Delta \rho|g)$, equation (5.7.2) takes the compact form

$$\kappa = -s_1 s_2 \frac{x}{\lambda^2} + B, \quad (5.7.3)$$

where the coefficient s_2 is equal to 1 if $\rho_2 > \rho_1$ or -1 if $\rho_2 < \rho_1$.

Evaluating equation (5.7.2) at the origin, $x = 0$, we find that the constant B is equal to the unknown curvature of the interface at the plane of symmetry located at $y = 0$,

$$B = \kappa_0, \quad (5.7.4)$$

where $\kappa_0 \equiv \kappa(x = 0)$.

Describing the interface by a function,

$$y = f(x), \quad (5.7.5)$$

we obtain the following expressions for the curvature given in (4.3.28),

$$\kappa = -\frac{f''}{(1 + f'^2)^{3/2}} = \frac{1}{f'} \left(\frac{1}{\sqrt{1 + f'^2}} \right)' = -\left(\frac{f'}{\sqrt{1 + f'^2}} \right)', \quad (5.7.6)$$

where a prime denotes a derivative with respect to x .

Drop height

Substituting the last expression for the curvature given in (5.7.6) into the Young–Laplace equation (5.7.3), we obtain

$$-\left(\frac{f'}{\sqrt{1 + f'^2}} \right)' = -s_1 s_2 \frac{x}{\lambda^2} + B. \quad (5.7.7)$$

Integrating with respect to x across the height of the drop, from $x = -d$ to 0, as shown in Figure 5.7.1, we obtain

$$1 - \cos \alpha = 2 \sin^2 \frac{\alpha}{2} = s_1 s_2 \frac{1}{2} \frac{d^2}{\lambda^2} + Bd. \quad (5.7.8)$$

When $s_1 s_2 = 1$ and the top of the drop is nearly flat due to strong gravitational effects, $Bd \simeq 0$, we find that

$$d \simeq 2 \lambda \sin \frac{\alpha}{2}, \quad (5.7.9)$$

which is consistent with the capillary height of a semi-infinite meniscus attached to a flat plate.

Vertical force balance

Substituting into (5.7.3) the second expression for the curvature given in (5.7.6), and multiplying both sides by f' , we obtain

$$\left(\frac{1}{\sqrt{1 + f'^2}} \right)' = -s_1 s_2 \frac{1}{\lambda^2} [(xf)' - f] + Bf'. \quad (5.7.10)$$

Integrating with respect to x across the height of the drop from $x = -d$ to 0, we obtain

$$\sin \alpha = s_1 s_2 \frac{1}{\lambda^2} \left(db - \frac{1}{2} A_D \right) + Bb, \quad (5.7.11)$$

where

$$A_D = 2 \int_{-d}^0 f(x) dx \quad (5.7.12)$$

is the drop area, b is half the length of the drop base, and d is the drop height, as shown in Figure 5.7.1. Equation (5.7.11) can be used to compute one of b , d , and $B = \kappa_0$ from two of the others.

In fact, equation (5.7.11) expresses a force balance. To demonstrate this directly, we observe that the additional force exerted on a longitudinal strip of the substrate covering the base of the drop is

$$\Delta F_x = -(2bw) (p^{(2)} - p^{(1)})_{x=-d} = -(2bw) (s_1 \Delta \rho g d + B\gamma), \quad (5.7.13)$$

where w is the width the strip. Adding to this force the capillary force exerted on the substrate at the contact line due to surface tension, we obtain the total force,

$$F_x = \Delta F_x + 2w\gamma \sin \alpha = -s_1 \Delta \rho g 2bwd - \gamma 2w (Bb - \sin \alpha). \quad (5.7.14)$$

The first term on the right-hand side is the weight of of a cylindrical slab of fluid with length $2b$, width w , and height d , reduced by the buoyancy force. The net force is precisely equal to the weight of the drop reduced by the buoyancy force,

$$F_x = -s_1 \Delta \rho g A_D w, \quad (5.7.15)$$

yielding the relation

$$s_1 s_2 (A_D - 2bd) = 2 \lambda^2 (Bb - \sin \alpha), \quad (5.7.16)$$

as given in (5.7.11).

Parametric representation

One important difference between the problem presently considered and those discussed previously in this chapter, is that, neither the range of x nor the range of y is known over the span of the drop interface at the outset.

To circumvent this difficulty, we describe the shape of the interface in parametric form in terms of the slope angle ψ defined in Figure 5.7.1, increasing from zero at the origin to α at the contact point. Our objective is to compute two scalar functions of ψ such that the x and y coordinates of a point at the interface are described by the functions

$$x = X(\psi), \quad y = Y(\psi) \quad (5.7.17)$$

for $0 \leq \psi \leq \alpha$. One important advantage of the adopted parametrization is that the boundary condition for the contact angle at the contact point is satisfied automatically and can be removed from further discussion. To compute the functions $X(\psi)$ and $Y(\psi)$, we

require two ordinary differential equations and a suitable number of boundary conditions or global constraints.

Ordinary differential equations

The first differential equation is the definition of the chosen parameter ψ in terms of the interface slope,

$$\cot \psi = -\frac{dY}{dX}. \quad (5.7.18)$$

The second differential equation must originate from the Young–Laplace equation. Referring to expressions (5.7.6) for the curvature, we set $f' = dY/dX$ and find that

$$\kappa = -\frac{1}{\cot \psi} \frac{d}{dX} \left(\frac{1}{\sqrt{1 + \cot^2 \psi}} \right) = -\frac{1}{\cot \psi} \frac{d \sin \psi}{dX} = -\sin \psi \frac{d\psi}{dX} = \frac{d \cos \psi}{dX}. \quad (5.7.19)$$

Substituting the penultimate expression into the left-hand side of (5.7.3), we obtain

$$\sin \psi \frac{d\psi}{dX} = -\frac{d \cos \psi}{dX} = s_1 s_2 \frac{X}{\lambda^2} - B, \quad (5.7.20)$$

which can be rearranged to give the desired parametric dependence

$$\frac{dX}{d\psi} = \frac{\sin \psi}{Q}, \quad (5.7.21)$$

where

$$Q \equiv s_1 s_2 \frac{X}{\lambda^2} - B. \quad (5.7.22)$$

To derive a corresponding parametric dependence for Y , we recast (5.7.18) into the form

$$\frac{dY}{d\psi} = -\cot \psi \frac{dX}{d\psi}. \quad (5.7.23)$$

Substituting (5.7.21) into (5.7.23), we obtain

$$\frac{dY}{d\psi} = -\frac{\cos \psi}{Q}. \quad (5.7.24)$$

Equations (5.7.21) and (5.7.24) provide us with the desired system of two first-order differential equations involving an unspecified parameter, B . The boundary conditions require that $X(0) = 0$ and $Y(0) = 0$. The constraint on the drop area requires that

$$2 \int_{-d}^0 Y dx = A_D, \quad (5.7.25)$$

where $x = -d$ describes the position of the plane.

Shooting method

Because the value of the constant B is *a priori* unknown, the solution must be found by iteration. The shooting method combined with the secant method for improving the guess provides us with an efficient algorithm. The numerical procedure involves the following steps:

1. Guess a value for B .
2. Integrate the system of equations (5.7.21) and (5.7.24).
3. Compute the integral on the right-hand side of (5.7.25) using the trapezoidal rule and then evaluate the objective function

$$Q \equiv 2 \int_{-d}^0 y \, dx - A_D. \quad (5.7.26)$$

4. Improve the guess for B with the goal of driving the objective function Q to zero using, for example, the secant method discussed in Section 5.6.

Since the constant B is equal to the unknown curvature of the interface at the mid-plane located at $y = 0$, a reasonable guess can be obtained by assuming that the interface is a section of a circle, and then computing the radius of the circle, ρ , according to specified values of the contact angle and drop area. Using elementary trigonometry, we find that

$$\rho = \left(\frac{2A_D}{2\alpha - \sin 2\alpha} \right)^{1/2} \quad (5.7.27)$$

and set $B = 1/\rho$.

Fourth-order Runge–Kutta method

The fourth-order Runge–Kutta method (RK4) is an improvement of the modified Euler method discussed earlier in this section, involving three exploratory steps and one final step.

The following MATLAB function entitled *drop_2d_ode*, located in directory *drop_2d* inside subdirectory *03_hydrostat* of *FDLIB*, implements the method for solving the system of equations (5.7.21) and (5.7.24) and simultaneously computing the drop area:

```
function [x,y,area] = drop_2d_ode ...
...
(npts ...
, capls ...
, lisp ...
, dpsi ...
, B ...
)
```

```

%-----
% Integrate two ODEs by RK4 with uniform
% step size for the angle psi
%-----

%-----
% prepare
%-----

dpsih = 0.5*dpsi;

%-----
% top of the drop
%-----

psi = 0.0; x(1) = 0.0; y(1) = 0.0;

%-----
% integrate
%-----

for i=1:npts

    if(i==1)
        xp = 0.0; yp = 1.0/B;
    else
        Q = Isp*x(i)/capls-B;
        xp = sin(psi)/Q;
        yp = -cos(psi)/Q;
    end
    xp1 = xp; yp1 = yp;

    psi = psi +dpsih;
    x(i+1) = x(i)+xp*dpsih;
    y(i+1) = y(i)+yp*dpsih;

    Q = Isp*x(i+1)/capls-B;
    xp = sin(psi)/Q;
    yp = -cos(psi)/Q;
    xp2 = xp; yp2 = yp;

    x(i+1) = x(i)+xp*dpsih;
    y(i+1) = y(i)+yp*dpsih;

    Q = Isp*x(i+1)/capls-B;
    xp = sin(psi)/Q;
    yp = -cos(psi)/Q;
    xp3 = xp; yp3 = yp;

```

```

psi = psi +dpsih;
x(i+1) = x(i)+xp*dpsi;
y(i+1) = y(i)+yp*dpsi;

Q = Isp*x(i+1)/capls-B;
xp = sin(psi)/Q;
yp = -cos(psi)/Q;
xp4 = xp; yp4 = yp;

x(i+1) = x(i) + (xp1+2*xp2+2*xp3+xp4)*dpsi/6.0;
y(i+1) = y(i) + (yp1+2*yp2+2*yp3+yp4)*dpsi/6.0;

end

%-----
% compute the area of the integrated shape
% by the trapezoidal rule
%-----

area = 0.0;
for i=1:npts
    area= area+(y(i+1)+y(i))*abs(x(i+1)-x(i));
end

area = 0.5*area;    % to account for trapezoidal weights

%---
% double the area to get the full shape
%---

area = 2.0*area

%-----
% done
%-----

return

```

The following MATLAB function entitled *drop_2d*, located in directory *03_hydrostat* of *FDLIB*, implements the secant method:

```

function [a,Bfinal,x,y] = drop_2d ...
...
(Jsp,gac,gamma,rhod,rhoa,area...
,alpha,npts,epsilon,maxiter,tol)

%-----
% Hydrostatic shape of a two-dimensional
% sessile drop resting on a horizontal plane,

```

```

% or pendant drop hanging underneath
% a horizontal plane, for a specified
% specified area and contact angle
%
% Jsp = 1 for a sessile drop
% Jsp = -1 for a pendant drop
%-----

%-----
% prepare
%-----

Iflag=0; % signals failure

drho = rhod-rhoa; % density difference
% square of the capillary length:
capls = gamma/(gac*abs(drho));

Isp = 1; % Isp is an orientation index

if(drho<0)
    Isp = -Isp;
end

if(Jsp== -1)
    Isp = -Isp;
end

%-----
% to start, assume that the drop shape
% is a truncated circle
% and compute the circle radius "a"
% in terms of the drop area and contact angle
%-----

a = sqrt(area/(alpha-0.5*sin(2.0*alpha)));
B(1) = 1.0/a;

%---
% compute the initial solution of the odes
% to start-up the secant method
%---

dpsi = alpha/npts;
Ic = 1; % counter

[x,y,area_sh] = drop_2d_ode ...
...
(npts ...

```

```

,capls ...
,Isp ...
,dpsi ...
,B(Ic) ...
);

error(Ic) = area_sh - area;
err = abs(error(Ic));

%-----
% second start-up solution
%-----

Ic=2;
B(2) = B(1)+epsilon;

[x,y,area_sh] = drop_2d_ode ...
...
(npts ...
,capls ...
,Isp ...
,dpsi ...
,B(Ic) ...
);

error(Ic) = area_sh - area;
err = abs(error(Ic));

%-----
% iterate on B using the secant method
% until convergence
%-----

for iter=1:maxiter

    Ic = Ic+1;

%---
% secant updating
%---

    Icb = Ic-2;
    Ica = Ic-1;
    dedc = (error(Ica)-error(Icb))/(B(Ica)-B(Icb));
    B(Ic) = B(Ica)-error(Ica)/dedc;

[x,y,area_sh] = drop_2d_ode ...
...
(npts ...

```



```

    ,capls ...
    ,Isp ...
    ,dpsi ...
    ,B(Ic) ...
  );

  error(Ic) = area_sh - area;
  err = abs(error(Ic));
  if(err<tol) break; end

%---
end
%---

if(iter==maxiter)
  disp('drop_2d: ODE solver failed')
  Iflag=1; return
end

Bfinal = B(Ic);

%---
% done
%---

return

```

Families of drop shapes computed using the code are shown in [Figure 5.7.2](#). Gravity squeezes the sessile drop toward the wall and pulls the pendant drop away from the wall.

PROBLEMS

5.7.1 Radius of a circular drop

Derive formula (5.7.27) for the radius of a circular drop.

5.7.2 Two-dimensional drop on a horizontal plane

Run the code *drop_2d* to generate a family of interfacial shapes corresponding to a fixed value of the drop area and various contact angles. Discuss the computed interfacial shapes.

5.8 A two-dimensional drop on an inclined plane

We proceed to consider the more challenging problem of a two-dimensional drop resting above or hanging underneath an inclined plane, as shown in [Figure 5.8.1](#). In the working Cartesian coordinates defined in this figure, the origin of the x axis is set at the inclined plane at the location of the front or rear contact point.

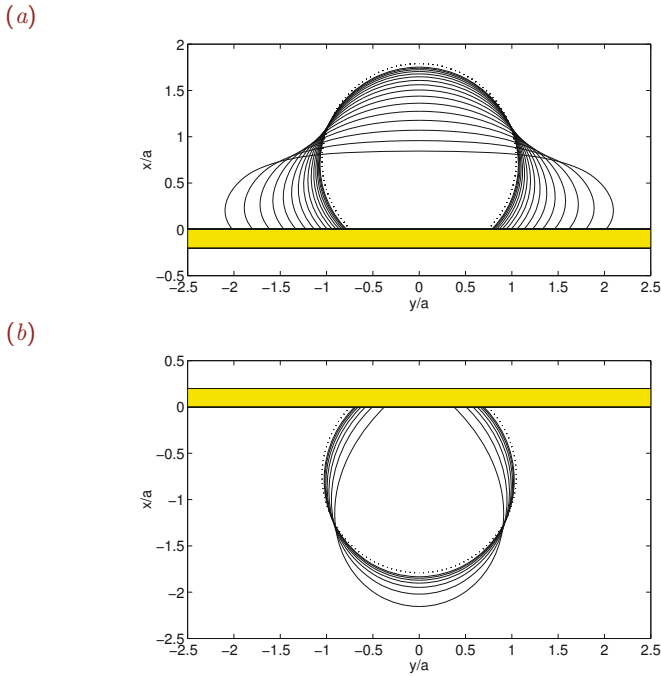


Figure 5.7.2 Shapes of (a) sessile and (b) pendant two-dimensional drops for contact angle $\alpha = \frac{3\pi}{4}$ and different surface tensions computed using the FDLIB code `drop_2d`. The dotted lines trace the approximate circular shape established for small drops or high surface tension. The x and y coordinates have been scaled by the equivalent drop radius, a , defined in terms of the drop area as $A_D = \pi a^2$.

In the case of the sessile drop, depicted in Figure 5.8.1(a), the contact angle at the first contact point, α_1 , is larger than the contact angle at the second contact point, α_2 . In the case of the pendant drop, shown in Figure 5.8.1(b), the first contact angle, α_1 , is smaller than the second contact angle, α_2 .

In the inclined system of coordinates depicted in Figure 5.8.1(a, b), the Cartesian components of the acceleration of gravity vector are given by

$$g_x = -g \cos \beta, \quad g_y = -g \sin \beta, \tag{5.8.1}$$

where β is the plane inclination angle ranging from 0 to 2π .

The pressure distributions in the ambient fluid and inside the drop are given by

$$p^{(1)}(x, y) = -\rho_1 g (x \cos \beta + y \sin \beta) + \pi_1 \tag{5.8.2}$$

and

$$p^{(2)}(x, y) = -\rho_2 g (x \cos \beta + y \sin \beta) + \pi_2, \tag{5.8.3}$$

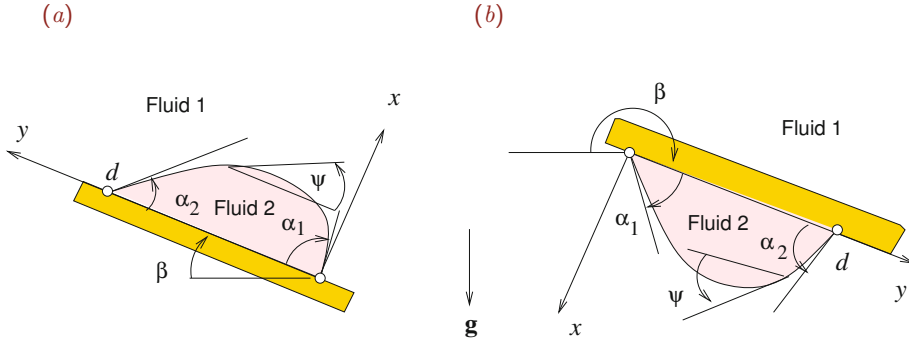


Figure 5.8.1 Illustration of a two-dimensional liquid drop (a) resting above and (b) hanging underneath an inclined plane.

where π_1 and π_2 are two reference pressures. Substituting these expressions into the interfacial balance (4.5.16), we obtain

$$-\rho_2 g (X \cos \beta + Y \sin \beta) + \pi_2 + \rho_1 g (X \cos \beta + Y \sin \beta) + \pi_1 = \gamma \kappa, \quad (5.8.4)$$

where (X, Y) are interfacial coordinates. Rearranging, we obtain the Laplace–Young equation

$$\kappa = -s_1 \frac{\Delta \rho g}{\gamma} (X \cos \beta + Y \sin \beta) + C, \quad (5.8.5)$$

where $\Delta \rho \equiv \rho_2 - \rho_1$ and $C \equiv (\pi_2 - \pi_1)/\gamma$. Physically, the constant C represents the curvature of the interface at the first contact point where $X = 0$ and $Y = 0$.

Parametric representation

The interface will be described parametrically in terms of the slope angle, ψ , varying from $-\alpha_1$ at the first contact point, to α_2 at the second contact point, as shown in Figure 5.8.1. Regarding X and Y as functions of ψ and working as in Section 5.7 for a drop attached to a horizontal plane, we derive the differential equations

$$\frac{dX}{d\psi} = \frac{\sin \psi}{Q}, \quad \frac{dY}{d\psi} = -\frac{\cos \psi}{Q}, \quad (5.8.6)$$

where

$$Q \equiv s \frac{X \cos \beta + Y \sin \beta}{\lambda^2} - C, \quad (5.8.7)$$

and the coefficient s is equal to 1 if $\rho_2 > \rho_1$ or -1 if $\rho_2 < \rho_1$.

The first contact line boundary condition sets the origin of the Cartesian axes at the inclined plane,

$$X(-\alpha_1) = 0, \quad Y(-\alpha_1) = 0. \quad (5.8.8)$$

The second contact line boundary condition requires that

$$X(\alpha_2) = 0. \quad (5.8.9)$$

The constraint on the drop area, A_D , requires that

$$\int_0^d X \, dy = A_D, \quad (5.8.10)$$

where $y = d$ marks the position of the second contact line.

5.8.1 First contact angle specified

Given the drop area, A_D , we may specify the first contact angle, α_1 , and compute the second contact angle, α_2 , and the constant C to satisfy conditions (5.8.9) and (5.8.10). A shooting method can be implemented for this purpose according to the following steps:

1. Guess values for C and α_2 .
2. Integrate the system of equations (5.8.6) with the initial conditions given in (5.8.8).
3. Compute the integral on the right-hand side of (5.8.10) using the trapezoidal rule.
4. Evaluate the two components of an objective function,

$$F(1) \equiv X(\alpha_2), \quad F(2) \equiv \int_0^d X \, dy - A_D. \quad (5.8.11)$$

5. Improve the values of C and α_2 to drive the two components of the objective function, $F(1)$ and $F(2)$ to zero,

$$F(1) = 0, \quad F(2) = 0, \quad (5.8.12)$$

and return to Step 2.

The following MATLAB function entitled *drop_2di1_ode*, located in directory *drop_2di1* inside directory *03_hydrostat* of **FDLIB**, solves the system of equations (5.8.6) and computes the first and second components of the objective function, **F**:

```
function F = drop_2di1_ode(solution)

%-----
% Two-dimensional drop on an inclined plane.
% Integrate ODEs by RK4 with uniform
% step size for the slope angle psi
%
% SYMBOLS:
% -----
%
% dpsi: increments in psi
% C: shooting parameter
```

```

% solution(1) = C
% solution(2) = alpha_2
%-----

global area capls Isp npts beta alpha1 alpha2 x y

%-----
% dispense variables
%-----

C = solution(1);
alpha2 = solution(2);

%-----
% prepare
%-----

csb = cos(beta);
snb = sin(beta);
dpsi = (alpha1+alpha2)/npts;
dpsih = 0.5*dpsi;

%-----
% first contact point
%-----

psi = -alpha1; x(1) = 0.0; y(1) = 0.0;

%-----
% integrate
%-----

for i=1:npts

    Q = Isp*(csb*x(i)+snb*y(i))/capls-C;
    xp = sin(psi)/Q; yp =-cos(psi)/Q;
    xp1 = xp; yp1 = yp;

    psi = psi +dpsih;
    x(i+1) = x(i)+xp*dpsih;
    y(i+1) = y(i)+yp*dpsih;

    Q = Isp*(csb*x(i+1)+snb*y(i+1))/capls-C;
    xp = sin(psi)/Q; yp =-cos(psi)/Q;
    xp2 = xp; yp2 = yp;

    x(i+1) = x(i)+xp*dpsih;
    y(i+1) = y(i)+yp*dpsih;

```

```

Q = Isp*(csb*x(i+1)+snb*y(i+1))/capls-C;
xp = sin(psi)/Q; yp =-cos(psi)/Q;
xp3 = xp; yp3 = yp;

psi = psi +dpsih;
x(i+1) = x(i)+xp*dpsi;
y(i+1) = y(i)+yp*dpsi;

Q = Isp*(csb*x(i+1)+snb*y(i+1))/capls-C;
xp = sin(psi)/Q; yp =-cos(psi)/Q;
xp4 = xp; yp4 = yp;

x(i+1) = x(i) + (xp1+2*xp2+2*xp3+xp4)*dpsi/6.0;
y(i+1) = y(i) + (yp1+2*yp2+2*yp3+yp4)*dpsi/6.0;

end

F(1) = x(npts+1);

%-----
% compute the area of the integrated shape
% by the trapezoidal rule
%-----

ar = 0.0;

for i=1:npts
    ar = ar+(x(i+1)+x(i))*(y(i+1)-y(i));
end
ar = 0.5*ar;    % to account for trapezoidal weights

F(2) = ar-area;

%-----
% done
%-----

return

```

The improvement in the values of C and α_2 in Step 5 of the algorithm can be done using Newton's method for solving a system of two nonlinear equations (5.8.12).¹ The method is implemented in the following **FDLIB** function entitled *drop_2di1_newton2*, located in directory *drop_2di1* inside directory *03_hydrostat* of **FDLIB**:

```

function [x,f,Iflag] = drop_2di1_newton2 ...
...

```

¹Pozrikidis, C. (2008) *Numerical Computation in Science and Engineering*. Second Edition, Oxford University Press.

```

(Niter ...
,eps ...
,x ...
)

%=====
% Solve two nonlinear equations by Newton's method
%
% SYMBOLS:
% -----
%
% x:  solution vector
% eps: small number for computing the Jacobian
%      by numerical differentiation
% Dx:  correction vector
% tol: accuracy
% Iflag: will set equal to 1 if something is wrong
%=====

tol = 0.0000001; % tolerance
relax = 1.0;

%-----
% initialize
%-----

Iflag = 1;

%-----
% start the iterations
%-----

for Iter=1:Niter

    f = drop_2di1_ode(x);

    %-----
    % compute the Jacobian
    % by numerical differentiation
    %-----

    for j=1:2
        x(j) = x(j)+eps; % perturb
        f1 = drop_2di1_ode(x);
        x(j) = x(j)-eps; % reset
        for i=1:2
            Jac(i,j) = (f1(i)-f(i))/eps;
        end
    end
end

```

```

%---
% solve the equation: Jac . Dx = - f
% for the correction vector Dx by Cramer's rule
%---

b1 = -f(1);
b2 = -f(2);
Det = Jac(1,1)*Jac(2,2)-Jac(1,2)*Jac(2,1);
dx(1) = (b1*Jac(2,2)-Jac(1,2)*b2)/Det;
dx(2) = (b2*Jac(1,1)-Jac(2,1)*b1)/Det;

%-----
% correct
%-----

x(1) = x(1) + relax*dx(1);
x(2) = x(2) + relax*dx(2);

%-----
% escape
%-----

Iescape = 1;
if(abs(dx(1)) > tol) Iescape = 0; end
if(abs(dx(2)) > tol) Iescape = 0; end

if(Iescape==1)
    Iflag = 0;
    f = drop_2di_ode(x);
    return
end

%----
end % of iterations
%----

%----
% done
%----

return

```

The overall procedure is implemented in the following MATLAB code entitled *drop_2di1*, located in directory *drop_2di1* inside directory *03_hydrostat* of *FDLIB*:

```

%-----
% Hydrostatic shape of a two-dimensional
% sessile drop resting on an inclined plane

```



```

% or a pendant drop hanging underneath a inclined plane,
% for a specified area and first contact angle
%-----

global area capls Isp npts beta alpha1 alpha2 x y

gac = 1.0;   % acceleration of gravity
rhod = 1.0;  % density of the drop
rhoa = 0.0;  % density of the ambient fluid

area = pi;   % drop area
beta = 0.125*pi; % inclination angle
alpha1 = 0.35*pi; % first contact angle
npts = 64;   % number of interfacial markers

%---
% prepare
%---

drho = rhod-rhoa; % density difference

Isp = 1.0; % orientation index

if(drho<0)
    Isp = -Isp;
end

csb = cos(beta);
snb = sin(beta);

ROT = [csb, snb; -snb, csb]; % rotation matrix for graphics

%---
% initial guess for a circular interface
%---

a = sqrt(area/(alpha1-0.5*sin(2.0*alpha1)));
Crc = 1.0/a;
solution = [Crc alpha1];

%---
% loop over surface tension and animate
%---

for repeat=1:100

    gamma = 10.0-repeat*0.10;
    capls = gamma/(gac*abs(drho)); % square of the cap length

```

```

%---
% newton's method for two equations
%---

Niter = 10; % maximum number of iterations
eps = 0.001; % step for numerical differentiation

[solution,F,Iflag] = drop_2di1_newton2 ...
...
(Niter ...
,eps ...
,solution ...
);

if(Iflag==1) break; end

%---
% dispense the solution
%---

C = solution(1)
alpha2 = solution(2)

xplot = -y;
yplot = x;

for i=1:npts+1
    xx = [xplot(i), yplot(i)];
    xx = ROT*xx';
    xplot(i) = xx(1);
    yplot(i) = xx(2);
end

plot(xplot,yplot,'-')

hold on
plot(csb*[0.2,-2.5],snb*[-0.2,2.5],'r','LineWidth',3)
axis equal
hold off
pause(0.1)

if(alpha2<0.05*pi) break; end
if(alpha2>0.95*pi) break; end

end

```

The shapes of a sessile and a pendant drop for $\alpha_1 = 0.45\pi$ computed using the code are shown in [Figure 5.8.2](#).

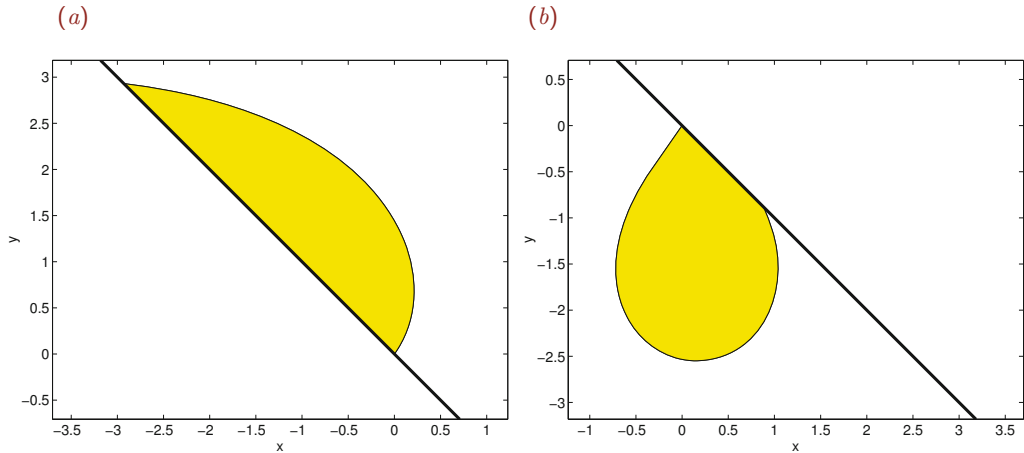


Figure 5.8.2 Interfacial shapes of (a) a sessile two-dimensional drop for inclination angle $\beta = 0.25\pi$, and (b) pendant two-dimensional drop for inclination angle $\beta = 1.25\pi$, generated by the FDLIB code `drop_2di1`.

Those who can afford access to MATLAB toolboxes may use the internal MATLAB function `fsolve` for solving the two nonlinear equations instead of the custom-made function `drop_2di1_newton2`. Bear in mind that some programmers consider the usage of a *global* statement an anathema.

5.8.2 Specified contact points

Consider a physical experiment where a droplet is placed on a horizontal plane and adjusts to a symmetric equilibrium shape corresponding to a specified static contact angle at both contact points, α . The distance between the two contact points is denoted by d , as shown in Figure 5.8.1.

The plane is now rotated and the drop deforms while both contact points remain pinned at the plane. Instead, the first and second contact angles, α_1 and α_2 , deviate from the reference value α in response to the changing orientation of the acceleration of gravity vector with respect to the inclination of the plane. In the physical world, the contact points will remain stationary only if the two contact angles are confined inside a contact angle hysteresis window bounded by the advancing and receding contact lines.

For each plane inclination angle, the three unknowns, C , α_1 , and α_2 , must be found as part of the solution to satisfy (a) the requirement on the drop area expressed by (5.8.10), and (b) the two second contact point conditions

$$X(\alpha_2) = 0, \quad Y(\alpha_2) = d. \quad (5.8.13)$$

A shooting method can be implemented according to the following steps:

1. Guess values for C , α_1 , and α_2 .
2. Integrate the system of equations (5.8.6) with initial conditions provided in (5.8.8).
3. Compute the integral on the right-hand side of (5.8.10) using the trapezoidal rule.
4. Evaluate the three components of the objective function

$$F(1) = X(\alpha_2), \quad F(2) = Y(\alpha_2) - d, \quad F(3) \equiv \int_0^d X \, dy - A_D. \quad (5.8.14)$$

5. Improve the values of C , α_1 , and α_2 , to drive the three components of the objective function, $F(1)$, $F(2)$, and $F(3)$, to zero

$$F(1) = 0, \quad F(2) = 0, \quad F(3) = 0, \quad (5.8.15)$$

and return to Step 2.

The following MATLAB function entitled *drop_2di2_ode*, located in directory *drop_2di* inside directory *03-hydrostat* of **FDLIB**, solves the system of equations (5.8.6) and computes the three components of the objective function, **F**:

```
function F = drop_2di2_ode (solution)

%-----
% Two-dimensional drop on an inclined plane.
%
% Integrate ODEs by the RK4 method with uniform
% step size for the slope angle psi
%
% SYMBOLS:
% -----
%
% dpsi: increments in psi
% C: shooting parameter
%-----

global area capls Isp npts beta alpha1 alpha2 d x y

%-----
% dispense variables
%-----

C = solution(1);
alpha1 = solution(2);
alpha2 = solution(3);

%-----
% prepare
%-----
```

```

csb = cos(beta);
snb = sin(beta);
dpsi = (alpha1+alpha2)/npts;
dpsih = 0.5*dpsi;

%-----
% first contact point
%-----

psi = -alpha1; x(1) = 0.0; y(1) = 0.0;

%-----
% integrate
%-----

for i=1:npts

    Q = Isp*(csb*x(i)+snb*y(i))/capls-C;
    xp = sin(psi)/Q; yp =-cos(psi)/Q;
    xp1 = xp; yp1 = yp;

    psi = psi +dpsih;
    x(i+1) = x(i)+xp*dpsih;
    y(i+1) = y(i)+yp*dpsih;

    Q = Isp*(csb*x(i+1)+snb*y(i+1))/capls-C;
    xp = sin(psi)/Q; yp =-cos(psi)/Q;
    xp2 = xp; yp2 = yp;

    x(i+1) = x(i)+xp*dpsih;
    y(i+1) = y(i)+yp*dpsih;

    Q = Isp*(csb*x(i+1)+snb*y(i+1))/capls-C;
    xp = sin(psi)/Q; yp =-cos(psi)/Q;
    xp3 = xp; yp3 = yp;

    psi = psi +dpsih;
    x(i+1) = x(i)+xp*dpsi;
    y(i+1) = y(i)+yp*dpsi;

    Q = Isp*(csb*x(i+1)+snb*y(i+1))/capls-C;
    xp = sin(psi)/Q; yp = -cos(psi)/Q;
    xp4 = xp; yp4 = yp;

    x(i+1) = x(i) + (xp1+2*xp2+2*xp3+xp4)*dpsi/6.0;
    y(i+1) = y(i) + (yp1+2*yp2+2*yp3+yp4)*dpsi/6.0;

end

```

```

F(1) = x(npts+1);
F(2) = y(npts+1)-d;

%-----
% compute the are of the integrated shape
% by the trapezoidal rule
%-----

ar = 0.0;
for i=1:npts
    ar = ar+(x(i+1)+x(i))*(y(i+1)-y(i));
end
ar = 0.5*ar; % to account for trapezoidal weights

F(3) = ar-area;

%-----
% done
%-----

return

```

The improvement in the values of C , α_1 , and α_2 in Step 5 of the algorithm can be done using Newton's method for solving a system of three nonlinear equations (5.8.12).² The method is implemented in the following `FDLIB` function entitled `drop_2di2_newton3`, located in directory `drop_2di1` inside directory `03_hydrostat` of `FDLIB`:

```

function [x,f,Iflag] = drop_2di2_newton3 ...
...
    (Niter ...
    ,eps ...
    ,x ...
    )

%-----
% Newton's method for three nonlinear equations
%
% SYMBOLS:
% -----
%
% eps: small interval for computing the Jacobian
% by numerical differentiation
% Dx: correction vector
% tol: accuracy
% Iflag: will set equal to 1 if something is wrong
%-----

```

²Pozrikidis, C. (2008) *Numerical Computation in Science and Engineering*. Second Edition, Oxford University Press.

```

tol = 0.0000001;

%-----
% initialize
%-----

Iflag = 1;

%-----
% start the iterations
%-----

for Iter=1:Niter

f = drop_2di2_ode(x);

%-----
% compute the Jacobian
% by numerical differentiation
%-----

for j=1:3
    x(j) = x(j)+eps;    % perturb
    f1 = drop_2di2_ode(x);
    x(j) = x(j)-eps;    % reset
    for i=1:3
        Jac(i,j) = (f1(i)-f(i))/eps;
    end
end

%---
% solve the equation: Jac . Dx = - f
% for the correction vector Dx
% by Cramer's rule
%---

A11 = Jac(1,1); A12 = Jac(1,2); A13 = Jac(1,3);
A21 = Jac(2,1); A22 = Jac(2,2); A23 = Jac(2,3);
A31 = Jac(3,1); A32 = Jac(3,2); A33 = Jac(3,3);

B1 = -f(1);
B2 = -f(2);
B3 = -f(3);

Det = A11*( A22*A33-A23*A32 ) ...
- A12*( A21*A33-A23*A31 ) ...
+ A13*( A21*A32-A22*A31 );

```

```

Det1 = B1*( A22*A33-A23*A32 ) ...
- A12*( B2*A33-A23*B3 ) ...
+ A13*( B2*A32-A22*B3 );

Det2 = A11*( B2 *A33-A23*B3 ) ...
- B1*( A21*A33-A23*A31 ) ...
+ A13*( A21* B3-B2 *A31 );

Det3 = A11*( A22* B3-A32* B2 ) ...
- A12*( A21* B3-A31* B2 ) ...
+ B1*( A21*A32-A22*A31 );

dx(1) = Det1/Det;
dx(2) = Det2/Det;
dx(3) = Det3/Det;

%-----
% correct
%-----

x(1) = x(1)+dx(1);
x(2) = x(2)+dx(2);
x(3) = x(3)+dx(3);

%-----
% escape
%-----

Iescape = 1;
if(abs(dx(1)) > tol) Iescape = 0; end
if(abs(dx(2)) > tol) Iescape = 0; end
if(abs(dx(3)) > tol) Iescape = 0; end

if(Iescape==1)
    Iflag = 0;
    f = drop_2di2.ode(x);
    return
end

%----
end % of iterations
%----

%----
% done
%----

return

```


The overall method is implemented in the following MATLAB code entitled *drop_2di2*, located in directory *drop_2di* inside directory *03_hydrostat* of FDLIB:

```

%-----
% Hydrostatic shape of a two-dimensional
% sessile drop resting on an inclined plane
% or a pendant drop hanging underneath a inclined plane,
% for a specified area and first contact points
%
% This code animates interfacial profiles on a
% continuously rotated plane.
%-----

global area capls Isp npts beta alpha1 alpha2 d x y

Jsp = -1; % pendant
Jsp = 1; % sessile

gac = 1.0; % acceleration of gravity
gamma = 2.0; % surface tension
rhod = 1.0; % density of the drop
rhoa = 0.0; % density of the ambient fluid
area = pi; % drop area

alpha = 0.75*pi; % contact angle on a plane
npts = 32; % number of interfacial markers

epsilon = 0.01; % for the shooting method
maxiter = 16; % on a horizontal plane
tol = 0.000000001; % for the shooting method

%---
% compute the drop shape on a horizontal plane
% rcrc: radius of the circular drop
%---

rcrc = sqrt(area/(alpha-0.5*sin(2.0*alpha)));
B = 1.0/rcrc;

[B,x,y] = drop_2d ...
...
(Jsp,gac,gamma,rhod,rhoa,area ...
,alpha,npts,epsilon,maxiter,tol ...
,B);

%---
% shift to reset the origin at the wall
%---

```

```

shiftx = x(npts+1);
x = x-shiftx;

%---
% position of the contact line
%---

d = 2*y(npts+1);

%---
% prepare to rotate
%---

drho = rhod-rhoa; % density difference
Isp = 1.0; % Isp is an orientation index
if(drho<0) Isp = -1.0; end
capls = gamma/(gac*abs(drho)); % square of the capillary length
npts = 2*npts;
C = B-shiftx/capls;
alpha1 = alpha;
alpha2 = alpha;

%-----
% start rotating
%-----

for repeat=1:1024

    beta = 0.002*(repeat-1.0)*pi;
    csb = cos(beta); snb = sin(beta);
    ROT = [csb, snb; -snb, csb]; % rotation matrix for graphics

    solution = [C alpha1 alpha2];

    Niter = 10; % number of iterations
    eps = 0.001; % step for numerical differentiation

    [solution,F,Iflag] = drop_2di2_newton3 ...
        ...
        (Niter ...
        ,eps ...
        ,solution ...
        );

%---
% distribute the solution
%---

C = solution(1)

```

```

alpha1 = solution(2)
alpha2 = solution(3)

% ---
% plot
% ---

xplot = -y; yplot = y;

for i=1:npts+1
    xx = [xplot(i), yplot(i)];
    xx = ROT*xx';
    xplot(i) = xx(1);
    yplot(i) = xx(2);
end

plot(xplot,yplot,'-')
hold on
plot(csb*[0.5,-2.0],snb*[-0.5,2.0],'r','LineWidth',3)
axis equal
xlabel('x','fontsize',15)
ylabel('y','fontsize',15)
hold off
pause(0.1)

end

```

PROBLEMS

5.8.1 *Two-dimensional drop on a horizontal or inclined plane*

Derive a relation between the constant B introduced in (5.7.2) and the constant C introduced in (5.8.5) for a horizontal plane, $\beta = 0$.

5.8.2 *Two-dimensional drop on an inclined plane*

Write a code that computes interfacial shapes for a fixed drop area and contact points, and unspecified contact lines.

5.9 Axisymmetric meniscus inside a tube

To compute the shape of an axisymmetric interface, we work as in the case of a two-dimensional interface discussed previously in this chapter, with some minor differences. Added considerations include possible subtleties in the computation of the mean curvature and a more pronounced sensitivity to numerical parameters. The new features will be illustrated with reference to the axisymmetric versions of the two-dimensional configurations studied in Sections 5.6 and 5.7.

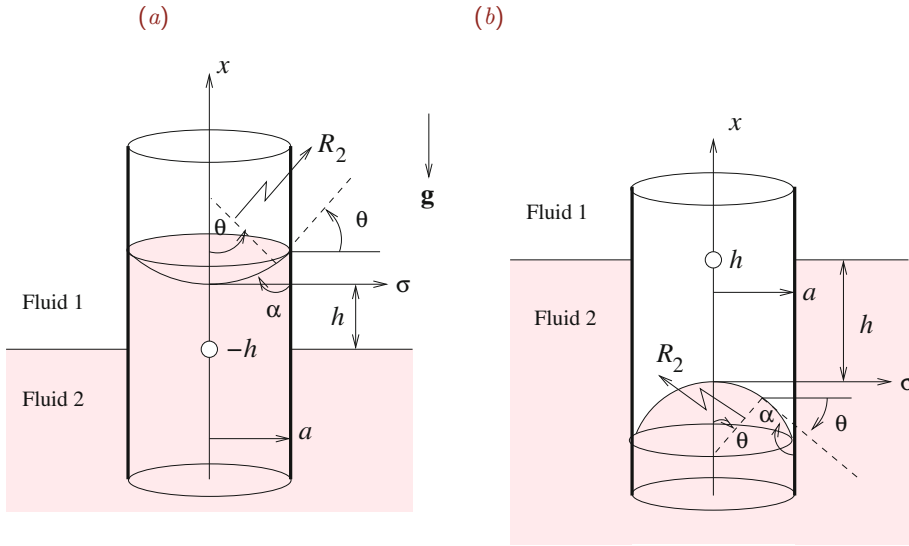


Figure 5.9.1 Illustration of an axisymmetric meniscus inside a vertical circular tube for (a) contact angle α less than $\frac{1}{2}\pi$, and (b) α greater than $\frac{1}{2}\pi/2$.

In this section, we consider the shape of an axisymmetric meniscus inside a vertical cylindrical tube of radius a , as illustrated in Figure 5.9.1. The axisymmetric meniscus is the counterpart of the two-dimensional meniscus between two vertical plates shown in Figure 5.6.1.

In cylindrical polar coordinates, (x, σ) , the axisymmetric meniscus can be described by a function,

$$x = f(\sigma), \tag{5.9.1}$$

where the ordered pair (σ, x) comprise Cartesian coordinates in an azimuthal plane with origin positioned such that $f(0) = 0$, as shown in Figure 5.9.1. Regularity requires that $f'(0) = 0$, and the condition on the contact angle requires that

$$f'(a) = \cot \alpha. \tag{5.9.2}$$

Outside the tube, the interface assumes a flat horizontal shape with vanishing curvature located at $x = -h$, where h is positive in Figure 5.9.1(a) and negative in Figure 5.9.1(b).

The pressure distributions in the two fluids are given by

$$p^{(1)}(y) = -\rho_1 g y + \pi_1, \quad p^{(2)}(y) = -\rho_2 g y + \pi_2, \tag{5.9.3}$$

where π_1 and π_2 are two reference pressures.

Laplace–Young equation

Our main objective is to compute the capillary rise, h , along with the unknown meniscus shape by solving the Laplace–Young equation (5.4.14). In the present problem, this equation takes the specific form

$$2\kappa_m = -\frac{\Delta\rho g}{\gamma}x + B, \quad (5.9.4)$$

where κ_m is the mean curvature, $B \equiv (\pi_2 - \pi_1)/\gamma$ is a constant, and $\Delta\rho \equiv \rho_2 - \rho_1$.

Evaluating equation (5.9.4) at a point outside and far from the tube where the mean curvature of the interface tends to vanish and the interfacial elevation tends to $-h$, we obtain the relation

$$B = -\frac{h}{\lambda^2}, \quad (5.9.5)$$

where h is the capillary rise and $\lambda^2 \equiv \gamma/(\Delta\rho g)$ is the square of the capillary length, under the assumption that $\Delta\rho \equiv \rho_2 - \rho_1 > 0$.

Combining the last two equations, we obtain the governing equation

$$2\kappa_m = -\frac{f+h}{\lambda^2}, \quad (5.9.6)$$

involving the *a priori* unknown capillary rise, h . The numerator of the fraction on the right-hand side, $f+h$, is the elevation of the meniscus with respect to the flat interface outside the tube.

Mean curvature

The mean curvature is given by formulas (4.4.33) and (4.4.34), repeated below for convenience,

$$2\kappa_m = -\frac{1}{\sigma} \left(\sigma \frac{f'}{\sqrt{1+f'^2}} \right)' = -\frac{f''}{(1+f'^2)^{3/2}} - \frac{1}{\sigma} \frac{f'}{\sqrt{1+f'^2}} \quad (5.9.7)$$

and

$$2\kappa_m = \frac{1}{f'} \left(\frac{1}{\sqrt{1+f'^2}} \right)' - \frac{1}{\sigma} \frac{f'}{\sqrt{1+f'^2}}, \quad (5.9.8)$$

where a prime denotes a derivative with respect to σ .

Applying equation (5.9.6) at the origin, $x=0$, where $f'=0$, we find that

$$\frac{h}{\lambda^2} = -2\kappa_m^0 = 2f''(0) \quad (5.9.9)$$

where $\kappa_m^0 = \kappa_m(0)$ is the centerline mean curvature.

Meniscus height

Substituting the expression for the mean curvature given in (5.9.8) into the left-hand side of the Laplace–Young equation (5.9.6), multiplying by f' , and rearranging, we obtain

$$\left(\frac{1}{\sqrt{1+f'^2}}\right)' - \frac{1}{\sigma} \frac{f'^2}{\sqrt{1+f'^2}} = -\frac{1}{\lambda^2} \left[\frac{1}{2}(f^2)' + hf'\right]. \quad (5.9.10)$$

Integrating with respect to σ across the tube radius from $\sigma = 0$ to a , we obtain

$$1 - \sin \alpha = \frac{1}{\lambda^2} \left(\frac{1}{2}d + h\right)d - \mathcal{J}, \quad (5.9.11)$$

where

$$\mathcal{J} \equiv \int_0^a \frac{1}{\sigma} \frac{f'^2}{\sqrt{1+f'^2}} d\sigma. \quad (5.9.12)$$

The appearance of the integral \mathcal{J} , associated with the second principal curvature, distinguishes the axisymmetric from the two-dimensional meniscus discussed in Section 5.6.

Vertical force balance

Substituting the first expression for the mean curvature given in (5.9.7) into the left-hand side of the Laplace–Young equation (5.9.6), and multiplying both sides by σ , we obtain

$$\left(\sigma \frac{f'}{\sqrt{1+f'^2}}\right)' = \frac{f+h}{\lambda^2} \sigma. \quad (5.9.13)$$

Integrating with respect to σ from 0 to a and noting that $f'(a) = \cot \alpha$, we obtain

$$a \cos \alpha = \frac{1}{\lambda^2} \int_0^b (f+h) \sigma dx. \quad (5.9.14)$$

This equation expresses a balance between the weight of the fluid inside the tube above or below the flat interface, the buoyancy force, and the capillary force at the circular contact line.

Differential equations

Substituting the second expression for the mean curvature given in (5.9.7) into the left-hand side of the Laplace–Young equation (5.9.6), and rearranging, we derive a second-order differential equation,

$$f'' = (1+f'^2) \left(-\frac{f'}{\sigma} + \sqrt{1+f'^2} \frac{f+h}{\lambda^2}\right). \quad (5.9.15)$$

An equivalent first-order system is

$$\frac{df}{d\sigma} = q, \quad \frac{dq}{d\sigma} = (1+q^2) \left(-\frac{q}{\sigma} + \sqrt{1+q^2} \frac{f+h}{\lambda^2}\right). \quad (5.9.16)$$

The first equation defines the slope function q , and the second equation enforces the Laplace–Young equation.

Parametric representation

It is expedient to describe the shape of the interface in parametric form in terms of the slope angle θ , varying from 0 at the centerline of the tube to the value $\frac{1}{2}\pi - \alpha$ at the inner wall of the tube, defined by

$$f' = \tan \theta, \quad (5.9.17)$$

where α is the contact angle, as shown in [Figure 5.9.1](#). The axial and radial positions of a point at the interface are described by the functions

$$x = X(\theta), \quad \sigma = \Sigma(\theta). \quad (5.9.18)$$

In terms of the slope angle, the mean curvature is given by the expressions

$$2\kappa_m = \frac{1}{\tan \theta} \frac{d}{d\sigma} \left(\frac{1}{\sqrt{1 + \tan^2 \theta}} \right) - \frac{\sin \theta}{\sigma} = \frac{1}{\tan \theta} \frac{d \cos \theta}{d\sigma} - \frac{\sin \theta}{\sigma} \quad (5.9.19)$$

and

$$2\kappa_m = -\cos \theta \frac{d\theta}{d\sigma} - \frac{\sin \theta}{\sigma}. \quad (5.9.20)$$

In the case of a raised meniscus depicted in [Figure 5.9.1\(a\)](#), the angle θ is positive and the second principal radius of curvature is negative, $R_2 < 0$. In the case of a submerged meniscus depicted in [Figure 5.9.1\(b\)](#), θ is negative and $R_2 > 0$.

Substituting expression (5.9.20) into the left-hand side of the Laplace–Young equation (5.9.6) and rearranging, we obtain the differential equation

$$\frac{d\Sigma}{d\theta} = \frac{\cos \theta}{Q}, \quad (5.9.21)$$

where

$$Q \equiv \frac{X + h}{\lambda^2} - \frac{\sin \theta}{\Sigma}. \quad (5.9.22)$$

Equation (5.9.21) governs the parametric representation of the radial position, $\sigma = \Sigma(\theta)$, in terms of the slope angle, θ . To derive a corresponding equation for the axial position X , we combine the definition

$$f' = \tan \theta = \frac{dX}{d\Sigma} \quad (5.9.23)$$

with equation (5.9.21), and obtain

$$\frac{dX}{d\theta} = \frac{\sin \theta}{Q}. \quad (5.9.24)$$

The boundary conditions require that $\Sigma = 0$ and $X = 0$ at $\theta = 0$, and $\Sigma = a$ at $\theta = \frac{1}{2}\pi - \alpha$.

Evaluation at the origin

An apparent difficulty is encountered when we attempt to evaluate the function Q defined in (5.9.22) at $\theta = 0$, corresponding to the centerline, $\Sigma = 0$, as the second fraction on the right-hand side becomes undefined.

However, using the l'Hôpital rule, we find that, as θ tends to zero, this ratio reduces to the derivative $d\theta/d\Sigma$. Substituting this asymptotic limit into (5.9.22) and the result into (5.9.21) and (5.9.24), we derive the regularized initial conditions

$$\left(\frac{d\Sigma}{d\theta}\right)_{\theta=0} = 2 \frac{\lambda^2}{h}, \quad \left(\frac{dX}{d\theta}\right)_{\theta=0} = 0, \quad (5.9.25)$$

which are used to start up the integration.

Computer code

The following MATLAB function entitled *men_ax_ode*, located in directory *men_ax* inside subdirectory *03_hydrostat* of *FDLIB*, integrates the differential equations using the modified Euler method subject to a given value for h provided in the input:

```
function [x,s] = men_ax_ode (npts,capls,a,dthet,h)

%-----
% Integrate the ODEs for an axisymmetric meniscus
% by the modified Euler method
%
% npts:  number of integration intervals
% cpls:  square of the capillary length
%-----

%-----
% prepare
%-----

dthet = 0.5*dthet;

%-----
% centerline
%-----

thet = 0.0; s(1) = 0.0; x(1) = 0.0;

%---
for i=1:npts
%---
```



```

if(i==1)
    sp = 2.0*capls/h;
    xp = 0.0D0;
else
    cs = cos(thet);
    sn = sin(thet);
    Q = (x(i)+h)/capls-sn/s(i);
    xp = sn/Q;
    sp = cs/Q;
end

xsv = x(i); % save
ssv = s(i); % save
xpsv = xp;
spsv = sp;

thet = thet+dthet;
x(i+1) = x(i)+xp*dthet;
s(i+1) = s(i)+sp*dthet;

cs = cos(thet);
sn = sin(thet);
Q = (x(i+1)+h)/capls-sn/s(i+1);
xp = sn/Q;
sp = cs/Q;

x(i+1) = xsv + (xpsv+xp)*dthet;
s(i+1) = ssv + (spsv+sp)*dthet;

%---
end
%---

%-----
% done
%-----

return

```

Solution by iteration

Since the value of the capillary rise, h , is *a priori* unknown, the solution must be found by iteration. A shooting method for computing h can be implemented according to the following steps:

1. Guess a value for h .
2. Solve equations (5.9.21) and (5.9.24) subject to the initial conditions $\Sigma = 0$ and $X = 0$ at $\theta = 0$.

3. Check whether the condition $\Sigma = a$ at $\theta = \frac{1}{2}\pi - \alpha$ is satisfied. If not, improve the guess using, for example, the secant method discussed in Section 5.7.

A reasonable guess for h at Step 1 can be obtained by assuming that the meniscus has a spherical shape consistent with the prescribed contact angle, α . Using elementary trigonometry, we find that

$$h \simeq 2 \frac{\lambda^2}{a} \cos \alpha. \quad (5.9.26)$$

Note that, when $\alpha > \frac{1}{2}\pi$, the predicted rise is negative, in agreement with physical intuition.

The improvement in Step 3 can be made using the secant method discussed in Section 5.6.1 for the corresponding problem in two dimensions.

The algorithm is implemented in the following MATLAB function entitled *men_ax* located in directory *03_hydrostat* of *FDLIB*:

```
function [Iflag,x,s,hout] = men_ax ...
...
(a,gac,gamma,rhop,rhoa ...
,alpha,npts ...
,epsilon,maxiter,tol ...
,hin ...
)

%-----
% shape of an axisymmetric meniscus
% inside a tube of radius computed
% by a shooting method for h
%
% hin:  initial guess for h
%-----

Iflag = 0;  % flag for success

%----
% prepare
%----

drho = rhop-rhoa ;  % density difference
%          square of the capillary length:
capls = gamma/(gac*abs(drho));

npts1 = npts+1;

dthet = (0.5*pi-alpha)/npts;

%-----
```

```

% initial guess for h
%-----

h(1) = hin;

%---
% compute the first solution of the odes
% to start-up the secant method
%---

Ic = 1; % counter
[x,s] = men_ax_ode(npts,capls,a,dthet,h(Ic));

error(Ic) = s(npts1)-a;

%-----
% second start-up solution
%-----

Ic = 2;
h(2) = h(1)+epsilon;
[x,s] = men_ax_ode(npts,capls,a,dthet,h(Ic));

error(Ic) = s(npts1)-a;

%-----
% iterate using the secant method
% until convergence
%-----

for iter=1:maxiter

    Ic = Ic+1;

%---
% secant updating
%---

    Icb = Ic-2;
    Ica = Ic-1;

    dedh = (error(Ica)-error(Icb))/(h(Ica)-h(Icb));
    h(Ic) = h(Ica) - error(Ica)/dedh;

    [x,s] = men_ax_ode(npts,capls,a,dthet,h(Ic));

    error(Ic) = s(npts1)-a;

    if(abs(error(Ic))<tol)

```

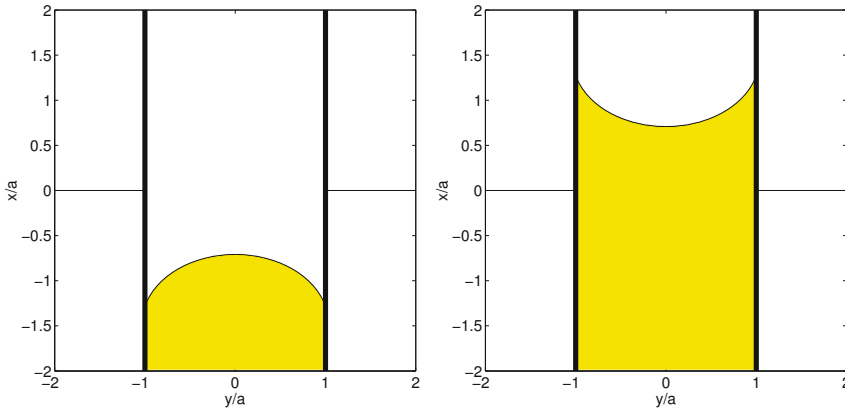


Figure 5.9.2 Shape of a meniscus inside a vertical tube generated by the FDLIB code `men_ax` for two contact angles.

```

    break
end

%---
end
%---

if(iter==maxiter)
    disp('men_ax: ODE solver failed')
    Iflag=1;
    return
end

hout = h(Ic);

%---
% done
%---

return

```

Results of computations for a contact angle that is lower than $\frac{1}{2}\pi$ and a contact angle that is higher than $\frac{1}{2}\pi$ are shown in [Figure 5.9.2](#). In the second case, the meniscus submerges below the level of the liquid outside the tube.

Scaling all lengths by the tube radius, a , we find that the shape of the meniscus depends on the contact angle, α , and ratio λ/a . As λ/a increases, the meniscus tends to obtain a spherical shape.

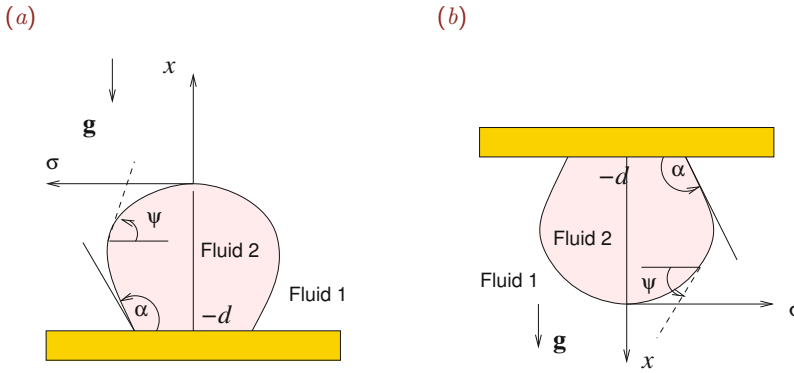


Figure 5.10.1 Illustration of (a) an axisymmetric sessile liquid drop resting on a horizontal plane and (b) an axisymmetric pendant liquid drop hanging under a horizontal plate.

PROBLEM

5.9.1 Axisymmetric meniscus

Run the code `men_ax` to generate a family of shapes corresponding to a fixed tube radius and various contact angles. Generate another family of shapes corresponding to a contact angle and various tube radii. Discuss the behavior of the capillary rise in each case.

5.10 Axisymmetric drop on a horizontal plane

Consider an axisymmetric drop of a fluid labeled 2 resting above or hanging underneath a horizontal plane, as shown in Figure 5.10.1. The drop is surrounded by an ambient fluid labeled 1. The resting drop shown in Figure 5.10.1(a) is a *sessile* drop, while the hanging drop shown in Figure 5.10.1(b) is a *pendant* drop.

Our objective is to compute the shape of the interface for specified surface tension, γ , contact angle, α , and drop volume, V_D . The forthcoming analysis also applies for a gas bubble regarded as a zero-density drop, $\rho_2 = 0$.

The pressure distribution in the two fluids is given by the familiar expressions

$$p^{(1)}(x) = -s_1 \rho_1 g x + \pi_1, \quad p^{(2)}(x) = -s_1 \rho_2 g x + \pi_2, \quad (5.10.1)$$

where π_1 and π_2 are two reference pressures. The coefficient s_1 is equal to 1 for a sessile drop or -1 for a pendant drop, reflecting the orientation of gravity with respect to the positive direction of the x axis. The shape of the interface is governed by the Laplace–Young equation stated in (5.4.14),

$$2 \kappa_m = -s_1 \frac{\Delta \rho g}{\gamma} x + B, \quad (5.10.2)$$

where κ_m is the mean curvature of the interface, $\Delta\rho = \rho_2 - \rho_1$, and $B \equiv (\pi_2 - \pi_1)/\gamma$ is an *a priori* constant with units of inverse length. In terms of the square of the capillary length, $\lambda^2 \equiv \gamma/(|\Delta\rho|g)$, equation (5.10.2) takes the compact form

$$2\kappa_m = -s_1s_2 \frac{x}{\lambda^2} + B, \quad (5.10.3)$$

where the coefficient s_2 is equal to 1 if $\rho_2 > \rho_1$ or -1 if $\rho_2 < \rho_1$.

Applying equation (5.10.2) at the origin, we find that the constant B is equal to twice the mean curvature of the interface at the centerline,

$$B = 2\kappa_m^0, \quad (5.10.4)$$

where we have denoted $\kappa_m^0 = \kappa_m(0)$.

Mean curvature

In Section 4.3, we saw that, if the position of the drop surface is described by a function

$$\sigma = w(x), \quad (5.10.5)$$

then the mean curvature is given by the expressions

$$2\kappa_m = -\frac{w''}{(1+w'^2)^{3/2}} + \frac{1}{w} \frac{1}{\sqrt{1+w'^2}} = -\left(\frac{w'}{\sqrt{1+w'^2}}\right)' + \frac{1}{w} \frac{1}{\sqrt{1+w'^2}} \quad (5.10.6)$$

and

$$2\kappa_m = \frac{1}{ww'} \left(\frac{w}{\sqrt{1+w'^2}}\right)', \quad (5.10.7)$$

where a prime denotes a derivative with respect to x .

Drop height

Substituting the second expression for the mean curvature given in (5.10.6) into the Young-Laplace equation (5.10.3), we obtain

$$-\left(\frac{w'}{\sqrt{1+w'^2}}\right)' + \frac{1}{w} \frac{1}{\sqrt{1+w'^2}} = -s_1s_2 \frac{x}{\lambda^2} + B. \quad (5.10.8)$$

Integrating with respect to x across the height of the drop from $x = -d$ to 0, we obtain

$$1 - \cos \alpha = 2 \sin^2 \frac{\alpha}{2} = s_1s_2 \frac{1}{2} \frac{d^2}{\lambda^2} + B d - \mathcal{J}, \quad (5.10.9)$$

where

$$\mathcal{J} \equiv \int_{-d}^0 \frac{1}{w} \frac{dx}{\sqrt{1+w'^2}} = \int_{-d}^0 \frac{\sin \psi}{\sigma} dx, \quad (5.10.10)$$

and the slope angle, ψ , is defined by the equation

$$w' = -\cot \psi, \quad (5.10.11)$$

as shown in [Figure 5.10.1](#). The appearance of the integral \mathcal{J} associated with the second principal curvature distinguishes the axisymmetric from the two-dimensional drop discussed in [Section 5.7](#).

When $s_1 s_2 = 1$, the top of the drop is nearly flat due to dominant gravitational effects, $Bd \simeq 0$. Under these conditions, the integral \mathcal{J} can be approximated by integrating around the sides of the drop where $w \simeq b$. Using the two-dimensional meniscus equation (5.5.10), we obtain

$$w' \simeq \frac{1}{\phi} \frac{2 - \phi^2}{\sqrt{4 - \phi^2}} \quad (5.10.12)$$

and approximate

$$\mathcal{J} \simeq \frac{\lambda}{2b} \int_0^{d/\lambda} \phi \sqrt{4 - \phi^2} \, d\phi = \frac{1}{6} \frac{\lambda}{b} \left(8 - \left(4 - \frac{d^2}{\lambda^2} \right)^{3/2} \right), \quad (5.10.13)$$

where $\xi \equiv x + d$ is the distance of the interface from the support and $\phi = \xi/\lambda$. For a nearly flat drop, equation (5.10.9) then gives

$$2 \sin^2 \frac{\alpha}{2} \simeq \frac{1}{2} \frac{d^2}{\lambda^2} + \frac{1}{6} \frac{\lambda}{b} \left[8 - \left(4 - \frac{d^2}{\lambda^2} \right)^{3/2} \right], \quad (5.10.14)$$

which provides us with a relation between the drop height, b , and the radius of the base, b . When the ratio d/λ is small, we obtain

$$d \simeq 2 \lambda \sin \frac{\alpha}{2}, \quad (5.10.15)$$

consistent with the elevation of a semi-infinite meniscus attached to a vertical plate.

Vertical force balance

Substituting the expression for the curvature given in (5.10.7) into the Young–Laplace equation (5.10.3), and rearranging, we obtain

$$\left(\frac{w}{\sqrt{1 + w'^2}} \right)' = -s_1 s_2 \frac{1}{2} \frac{1}{\lambda^2} [(xw^2)' - w^2] + B \frac{1}{2} (w^2)'. \quad (5.10.16)$$

Integrating with respect to x across the height of the drop from $x = -d$ to 0, we obtain

$$b \sin \alpha = s_1 s_2 \frac{1}{2} \frac{1}{\lambda^2} \left(db^2 - \frac{1}{\pi} V_D \right) + \frac{1}{2} B b^2, \quad (5.10.17)$$

where

$$V_D = \pi \int_{-d}^0 w^2(x) \, dx \quad (5.10.18)$$

is the drop volume and d is the drop height, as shown in [Figure 5.10.1](#). Given α and V_D , equation (5.10.17) can be used to compute b , d , or $B = 2\kappa_m^0$, from knowledge of two others.

In fact, equation (5.10.17) expresses a force balance. To demonstrate this, we note that the additional force exerted on the plane due to the drop is

$$\Delta F_x = -(\pi b^2) (p^{(2)} - p^{(1)})_{x=-d} = -(\pi b^2) (s_1 \Delta \rho g d + B \gamma). \quad (5.10.19)$$

Adding to this force the capillary force around the circular contact line, we obtain the total vertical force

$$F_x = \Delta F_x + 2\pi b \gamma \sin \alpha = -s_1 \Delta \rho g \pi b^2 d - \gamma \pi b (B b - 2 \sin \alpha). \quad (5.10.20)$$

The first term on the right-hand side is the weight of a cylindrical column of fluid with radius b and height d reduced by the buoyancy force. This force is precisely equal to the weight of the drop reduced by the buoyancy force,

$$F_x = -s_1 \Delta \rho g V_D, \quad (5.10.21)$$

yielding the relation

$$s_1 s_2 (V_D - \pi d b^2) = \pi b \lambda^2 (B b - 2 \sin \alpha), \quad (5.10.22)$$

which is precisely equation (5.10.17).

Parametric representation

Working as in Section 5.7 for a two-dimensional drop, we describe the interface parametrically in terms of the slope angle ψ defined in [Figure 5.10.1](#) as

$$x = X(\psi), \quad \sigma = \Sigma(\psi), \quad (5.10.23)$$

where

$$\cot \psi = -\frac{d\Sigma}{dX}. \quad (5.10.24)$$

Substituting these expressions into (5.10.7), we obtain

$$2\kappa_m = -\frac{1}{\cot \psi} \frac{d}{dX} \left(\frac{1}{(1 + \cot^2 \psi)^{1/2}} \right) + \frac{\sin \psi}{\Sigma} = -\frac{1}{\cot \psi} \frac{d \sin \psi}{dX} + \frac{\sin \psi}{\Sigma} \quad (5.10.25)$$

and

$$2\kappa_m = -\sin \psi \frac{d\psi}{dX} + \frac{\sin \psi}{\Sigma} = \frac{d \cos \psi}{dX} + \frac{\sin \psi}{\Sigma}. \quad (5.10.26)$$

Substituting these expressions into the Young–Laplace equation (5.10.2), we obtain

$$\sin \psi \frac{d\psi}{dX} - \frac{\sin \psi}{\Sigma} = -\frac{d \cos \psi}{dX} - \frac{\sin \psi}{\Sigma} = s_1 \frac{\Delta \rho g}{\gamma} X - B. \quad (5.10.27)$$

Rearranging, we obtain

$$\sin \psi \frac{d\psi}{dX} = s_1 \frac{\Delta \rho g}{\gamma} X - B + \frac{\sin \psi}{\Sigma}, \quad (5.10.28)$$

which provides us with the differential equations

$$\frac{dX}{d\psi} = \frac{\sin \psi}{Q}, \quad \frac{d\Sigma}{d\psi} = -\frac{\cos \psi}{Q}, \quad (5.10.29)$$

where

$$Q \equiv \frac{\sin \psi}{\Sigma} + s_1 s_2 \frac{X}{\lambda^2} - B. \quad (5.10.30)$$

We observe that the shape of a bubble on a flat plate, $s_1 = 1$ and $s_2 = -1$, is similar to that of a drop underneath a flat plate, $s_1 = -1$ and $s_2 = 1$.

Since the origin of the x axis is set at the *a priori* unknown highest elevation of the interface where $\psi = 0$,

$$X(0) = 0, \quad \Sigma(0) = 0. \quad (5.10.31)$$

The constraint on the drop volume, V_D , takes the form

$$\pi \int_{-d}^0 \Sigma^2 dx = V_D, \quad (5.10.32)$$

where $x = -d$ describes the position of the plane, as shown in [Figure 5.10.1](#). At the axis of symmetry located at $\sigma = 0$, equations (5.10.29) are replaced by the regularized equations

$$\left(\frac{d\Sigma}{d\psi} \right)_{\psi=0} = \frac{2}{B}, \quad \left(\frac{dX}{d\psi} \right)_{\psi=0} = 0, \quad (5.10.33)$$

arising from Taylor series expansions.

Equations (5.10.29) can be solved by the shooting method discussed in Section 5.7 for the corresponding problem in two dimensions. A reasonable guess for the constant B can be obtained by assuming that the interface is a section of a sphere, and then computing the radius of the sphere, ϱ , to satisfy the constraints on the contact angle and drop volume. Using elementary trigonometry, we find that

$$\varrho = \left(\frac{3 V_D / \pi}{2 + \cos^3 \alpha - 3 \cos \alpha} \right)^{1/3}, \quad (5.10.34)$$

and set $B = 2/\varrho$.

A numerical method for solving the boundary-value problem is implemented in a code entitled *drop_ax*, located in directory *03_hydrostat* of **FDLIB**, not listed in the text. The algorithm incorporates minor modifications of the code *drop_2d* listed in Section 5.7.

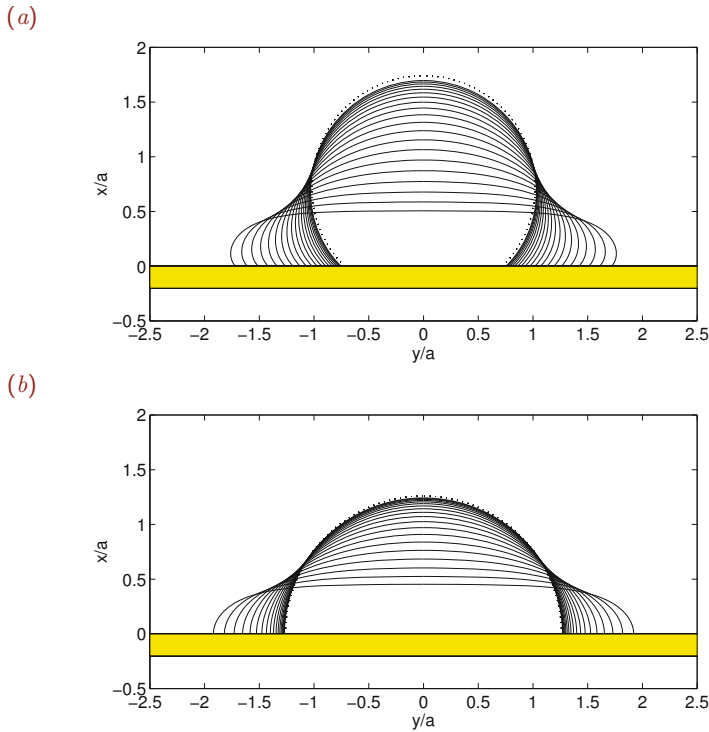


Figure 5.10.2 Shapes of (a) a sessile and (b) a pendant drops for contact angle $\alpha = \frac{3}{4}\pi$ and $\alpha = \frac{1}{4}\pi$ computed by code `drop_ax` of `FDLIB`. The dotted lines show the approximate spherical shape arising for small drops or large surface tension.

Drop shapes computed using this code are shown in [Figure 5.10.2](#) where the x and y coordinates are scaled by the equivalent drop radius, a , defined by the equation $V_D = 4\pi a^3/3$. Gravity squeezes the sessile drop toward the wall and pulls the pendant drop away from the wall.

Solution space

The numerical method described earlier in this section fails when the drop develops a re-entrant shape near the base. The reason is that, when this occurs, the functions $X(\psi)$ and $\Sigma(\psi)$ cease to be single valued.

To address this difficulty, we integrate the parametric differential equations from $\psi = 0$ up to a specified maximum value $\psi_{\max} < \alpha$, and then continue the integration regarding the radial distance as a function of the axial position, $\sigma = w(x)$. To perform the integration with respect to x , we substitute the expression for the mean curvature given in (5.10.6) into

the Laplace–Young equation and obtain

$$-\frac{w''}{(1+w'^2)^{3/2}} + \frac{1}{\sigma} \frac{1}{\sqrt{1+w'^2}} = -\frac{\Delta\rho g}{\gamma} x + B, \quad (5.10.35)$$

where a prime denotes a derivative with respect to x . Rearranging, we derive the second-order differential equation,

$$w'' = (1+w'^2) \left(\frac{1}{w} + \sqrt{1+w'^2} \left(s_1 s_2 \frac{x}{\lambda^2} - B \right) \right), \quad (5.10.36)$$

which can be resolved into a system of two first-order equations,

$$\frac{dw}{dx} = q, \quad \frac{dq}{dx} = (1+q^2) \left(\frac{1}{w} + \sqrt{1+q^2} \left(s_1 s_2 \frac{x}{\lambda^2} - B \right) \right). \quad (5.10.37)$$

Initial conditions are provided by the values computed at the end of the integration domain with respect to ψ .

The following MATLAB function entitled *drop_ax1_ode*, located in directory *drop_ax* inside directory *03_hydrostat* of *FDLIB*, integrates successively the two sets of differential equations:

```
function [x,s,Ntot,vlm,slope] = drop_ax1_ode ...
...
(npts1 ...    % number of steps using the psi parametrization
 ,capls ...   % square of the capillary length
 ,Isp ...
 ,psi_max ...
 ,B ...
 ,ratio ...   % grading of psi integration intervals
 ,Next ...    % determines the x position of the drop base
 ,npts2 ...   % number of steps using the x parametrization
 )

%-----
% Integrate ODEs using RK4
% Return the interfacial profile (x, s)
% total number of divisions (Ntot)
% volume of the drop (vlm)
% slope at the base (slope)
%-----

%=====
% first section
%=====

%-----
% set the step size vector dpsl
% so that it increases geometrically
```

```

% by the factor "ratio"
%-----

if(ratio==1)
    alp = 1.0;
    factor = 1.0/npts1;
else
    texp = 1/(npts1-1);
    alp = ratio^texp1;
    factor = (1.0-alp)/(1.0-alp^npts1);
end

dpsi(1) = psi_max*factor;

for i=2:npts1
    dpsi(i) = dpsi(i-1)*alp;
end

%-----
% top of the drop
%-----

psi = 0.0;
x(1) = 0.0;
s(1) = 0.0;

%-----
% integrate
%-----

for i=1:npts1

    dpsih(i) = 0.5*dpsi(i);

    if(i==1)
        xp = 0.0;
        sp = 2.0/B;
    else
        Q = sin(psi)/s(i)+Isp*x(i)/capls-B;
        xp = sin(psi)/Q;
        sp = -cos(psi)/Q;
    end

    xp1 = xp;
    sp1 = sp;

    psi = psi +dpsih(i);
    x(i+1) = x(i)+xp*dpsih(i);
    s(i+1) = s(i)+sp*dpsih(i);

```

```

Q = sin(psi)/s(i+1)+Isp*x(i+1)/capls-B;
xp = sin(psi)/Q;
sp = -cos(psi)/Q;
xp2 = xp;
sp2 = sp;

x(i+1) = x(i)+xp*dpsih(i);
s(i+1) = s(i)+sp*dpsih(i);

Q = sin(psi)/s(i+1)+Isp*x(i+1)/capls-B;
xp = sin(psi)/Q;
sp = -cos(psi)/Q;
xp3 = xp;
sp3 = sp;

psi = psi +dpsih(i);
x(i+1) = x(i)+xp*dpsi(i);
s(i+1) = s(i)+sp*dpsi(i);

Q = sin(psi)/s(i+1)+Isp*x(i+1)/capls-B;
xp = sin(psi)/Q;
sp = -cos(psi)/Q;
xp4 = xp;
sp4 = sp;

x(i+1) = x(i) + (xp1+2*xp2+2*xp3+xp4)*dpsi(i)/6.0;
s(i+1) = s(i) + (sp1+2*sp2+2*sp3+sp4)*dpsi(i)/6.0;

end

Ntot = npts1;

%=====
% continue the integration with a uniform step "dx"
% using the x parametrization up to x = Next*x(npts1+1)
%=====

dx = Next*x(npts1+1)/npts2;

%---
% initial slope
%---

Q = sin(psi)/s(npts1+1)+Isp*x(npts1+1)/capls-B;
xp = sin(psi)/Q;
sp = -cos(psi)/Q;
q(npts1+1) = xp/sp; % dx/dsigma

```

```

%---
% integrate
%---

for i=npts1+1:npts1+npts2+2

    dsdx = q(i);
    tmp = 1+q(i)*q(i);
    dqdx = tmp*( 1/s(i)+sqrt(tmp)*(Isp*x(i)/capls-B) );
    dsdx1 = dsdx;
    dqdx1 = dqdx;

    x(i+1) = x(i)+0.5*dx;
    s(i+1) = s(i)+0.5*dx*dsdx;
    q(i+1) = q(i)+0.5*dx*dqdx;

    dsdx = q(i+1);
    tmp = 1+q(i+1)*q(i+1);
    dqdx = tmp*( 1/s(i+1)+sqrt(tmp)*(Isp*x(i+1)/capls-B) );
    dsdx2 = dsdx;
    dqdx2 = dqdx;

    x(i+1) = x(i)+0.5*dx;
    s(i+1) = s(i)+0.5*dx*dsdx;
    q(i+1) = q(i)+0.5*dx*dqdx;

    dsdx = q(i+1);
    tmp = 1+q(i+1)*q(i+1);
    dqdx = tmp*( 1/s(i+1)+sqrt(tmp)*(Isp*x(i+1)/capls-B) );
    dsdx3 = dsdx;
    dqdx3 = dqdx;

    x(i+1) = x(i)+dx;
    s(i+1) = s(i)+dx*dsdx;
    q(i+1) = q(i)+dx*dqdx;

    dsdx = q(i+1);
    tmp = 1+q(i+1)*q(i+1);
    dqdx = tmp*( 1/s(i+1)+sqrt(tmp)*(Isp*x(i+1)/capls-B) );
    dsdx4 = dsdx;
    dqdx4 = dqdx;

    s(i+1) = s(i)+dx*(dsdx1+2.0*dsdx2+2.0*dsdx3+dsdx4)/6.0;
    q(i+1) = q(i)+dx*(dqdx1+2.0*dqdx2+2.0*dqdx3+dqdx4)/6.0;

    Ntot = Ntot+1;
    if(s(i+1)<0) break; end

end

```

```

slope = q(i+1);

%-----
% compute the volume of the integrated shape
% by the trapezoidal rule
%-----

vlm = 0.0;
for i=1:Ntot
    vlm = vlm+(s(i+1)*s(i+1)+s(i)*s(i))*abs(x(i+1)-x(i));
end
vlm = 0.5*vlm;    % to account for trapezoidal weights
vlm = pi*vlm;

%-----
% done
%-----

return

```

Families of shapes parametrized by the constant B can be generated by specifying the capillary length, λ , and then computing the numerical parameter N_{ext} to ensure a specified drop volume. The constant B determines the contact angle implicitly, while the parameter N_{ext} determines the location of the drop base explicitly. Finding the proper value of N_{ext} can be done using the secant method.

The numerical procedure is implemented in the following MATLAB function entitled *drop_ax1*, located in directory *drop_ax* inside directory *03_hydrostat* of **FDLIB**:

```

%----
% Solution branches of a sessile or pendant drop
%----

a = 1.0;    % drop radius
Isp = -1;   % pendant drop
psi_max = 0.25*pi;
npts1 = 24;
npts2 = 48;
ratio = 0.9;
maxiter = 10;    % for secant iterations
tol = 0.0000001; % for secant iterations

%---
% prepare
%---

volume = 1.0*4*pi*a^3/3;

```

```

%---
% family parameters
%---

capls = 2.0;
Nloop = 2*2*2*2*2*2*128;
Bmin = 1.00;
Bmax = 4.0;
DB = 0.0020;
Nplot = 32; % will plot after Nplot shapes

%---
% prepare to plot
%---

figure(1)
hold on
xlabel('y/a','fontsize',15)
ylabel('x/a','fontsize',15)
set(gca,'fontsize',15)
axis equal
box on

xwall(1) = -1.8; ywall(1) = 0;
xwall(2) = 1.8; ywall(2) = 0;

if(Isp==1)
    patch([xwall xwall(2) xwall(1)], ...
          [ywall ywall(2)-0.2 ywall(1)-0.2],'g')
else
    patch([xwall xwall(2) xwall(1)], ...
          [ywall ywall(2)+0.2 ywall(1)+0.2],'g')
end

plot(xwall,ywall,'k')

%---
% prepare to loop
%---

B = Bmin;
Next(1) = 2.0;
Iplot = Nplot;

%=====
for Iloop=1:Nloop % loop over B
%=====

    B = B+DB;

```



```

Ic = 1;      % counter

[ x,s,Ntot,vlm,slope ] = drop_ax1_ode ...
...
(npts1 ...
, capls ...
, Isp ...
, psi_max ...
, B ...
, ratio ...
, Next(1) ...
, npts2 ...
);

error(Ic) = vlm-volume;

Ic = 2;
Next(Ic) = Next(Ic-1)+0.10;

[x,s,Ntot,vlm,slope] = drop_ax1_ode ...
...
(npts1 ...
, capls ...
, Isp ...
, psi_max ...
, B ...
, ratio ...
, Next(2) ...
, npts2 ...
);

error(Ic) = vlm-volume;

%-----
% iterate on Next using the secant method
% until convergence
%-----

Icconverged = 0;

for iter=1:maxiter

    Ic = Ic+1;

%---
% secant updating
%---

    Icb = Ic-2;

```

```

Ica = Ic-1;
dedc = (error(Ica)-error(Icb))/(Next(Ica)-Next(Icb));
Next(Ic) = Next(Ica)-error(Ica)/dedc;

[x,s,Ntot,vlm,slope] = drop_ax1_ode ...
...
(npts1 ...
, capls ...
, Isp ...
, psi_max ...
, B ...
, ratio ...
, Next(Ic) ...
, npts2 ...
);

error(Ic) = vlm-volume;
err = abs(error(Ic));

if(err<tol)
    Iconverged = 1;
    break;
end

%----
end
%----

Next(1) = Next(Ic);

if(Iplot==Nplot)
    figure(1)
    x = x-x(Ntot+1); % shift the profile
    plot( s,Isp*x,'k-')
    plot(-s,Isp*x,'k-')
    Iplot = 0;
end

Iplot = Iplot+1;

if(B>Bmax) break; end

%=====
end
%=====

```

A family of shapes generated by the code is shown in [Figure 5.10.2](#). We observe interesting compact, light-bulb, and hourglass interfacial contours. However, not all of these shapes are stable and therefore expected to occur in practice.

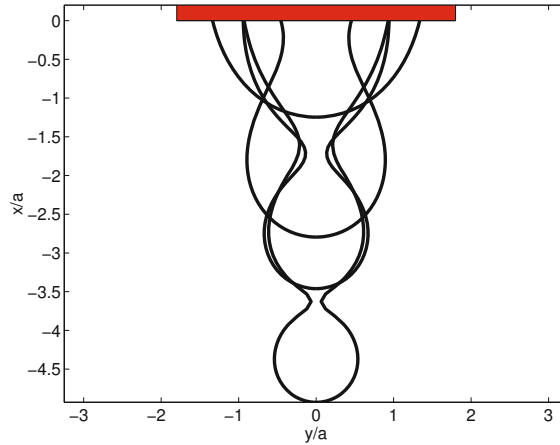


Figure 5.10.2 A family of axisymmetric drop shapes corresponding to a fixed capillary length and varying contact angle.

PROBLEMS

5.10.1 Drop on a plane

(a) Derive the regularized expressions (5.10.33) departing from equations (5.10.29) and (5.10.30). (b) Derive formula (5.10.34).

5.10.2 Axisymmetric drops

Run the code `drop_ax` to generate a family of shapes corresponding to a fixed value drop volume and various contact angles. Generate another family of shapes corresponding to a fixed contact angle and various drop volumes.

5.11 A sphere straddling an interface

In Section 5.2.1, we discussed the equilibrium position of a spherical particle floating on a flat interface. The flat interfacial shape is established under specific conditions, or else when the capillary length, λ , is much smaller than the particle size. A more sophisticated analysis is required under more general circumstances.

Shown in Figure 5.11.1 is a floating sphere of radius a straddling an axisymmetrically deformed and otherwise flat interface. The origin of the x axis is set at the position of the flat interface far from the sphere. The center of the sphere is located at $x = x_c$ and the circular contact line is located at the axial and radial positions

$$x_{cl} = x_c + a \cos \beta, \quad \sigma_{cl} = a \sin \beta, \quad (5.11.1)$$

where the floating angle, β , varies in the range $[0, \pi]$. In the case of a flat interface, $x_{cl} = 0$ and $x_c = -a \cos \beta$.

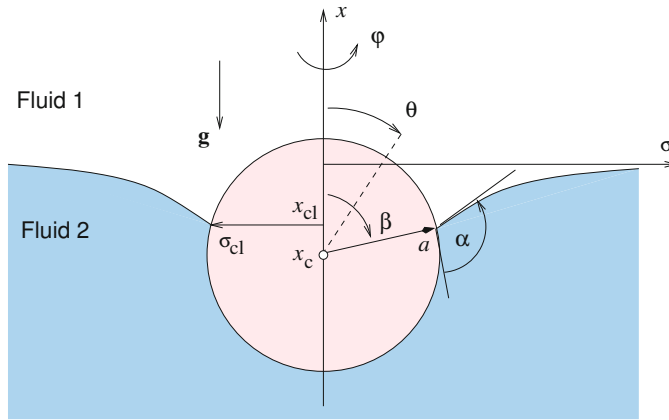


Figure 5.11.1 Illustration of a sphere straddling a curved axisymmetric interface between two fluids.

The shape of the axisymmetric meniscus can be described by a function,

$$x = f(\sigma). \tag{5.11.2}$$

Working as in Section 5.9 for an axisymmetric meniscus, and requiring that the mean curvature of the interface decays to zero far from the particle, as σ tends to infinity, we derive a system of two first-order differential equations,

$$\frac{df}{d\sigma} = q, \quad \frac{dq}{d\sigma} = (1 + q^2) \left(-\frac{q}{\sigma} + \sqrt{1 + q^2} \frac{f}{\lambda^2} \right), \tag{5.11.3}$$

where $\lambda^2 = \gamma/(\Delta\rho g)$ is the square of the capillary length and $\Delta\rho = \rho_2 - \rho_1$ is the density difference between the lower and upper fluids. A Bond number can be defined in the terms of the capillary length as

$$\text{Bo} = \frac{\Delta\rho g a^2}{\gamma} = \left(\frac{a}{\lambda} \right)^2. \tag{5.11.4}$$

Physically, the Bond number is a measure of the extent of the interfacial deformation around the contact line.

The contact line condition requires that

$$f(\sigma_{cl}) = x_{cl}, \quad q(\sigma_{cl}) = \tan(\alpha - \beta), \tag{5.11.5}$$

and the far-field condition requires that

$$f(\infty) = 0, \tag{5.11.6}$$

where α is the contact angle, as shown in Figure 5.11.1.

The following MATLAB function entitled *flsphere_ode*, located in directory *flsphere* inside directory *03_hydrostat* of *FDLIB*, integrates the differential equations (5.11.3) using the fourth-order Runge–Kutta method:

```

function [f,s,q] = flsphere_ode (ndiv,smax,capls,xcl,scl,slope);

%=====
% solve ODEs for a semi-infinite axisymmetric meniscus
% by the RK4 method
%
% scl:  sigma of contact line
%
% will integrate from scl to smax
%=====

dsg = (smax-scl)/ndiv;
dsgh = 0.5*dsg;

s(1) = scl;  % starting point
f(1) = xcl;
q(1) = slope;

%---
% integrate
%---

for i=1:ndiv

    fp = q(i);
    tmp = 1+q(i)*q(i);
    tmg = sqrt(tmp)/capls;
    qp = tmp*(-fp/s(i) + f(i)*tmg);
    fp1 = fp;
    qp1 = qp;

    s(i+1) = s(i)+ dsgh;
    f(i+1) = f(i)+fp*dsgh;
    q(i+1) = q(i)+qp*dsgh;
    fp2 = fp;
    qp2 = qp;

    fp = q(i+1);
    tmp = 1+q(i+1)*q(i+1);
    tmg = sqrt(tmp)/capls;
    qp = tmp*(-fp/s(i+1) + f(i+1)*tmg);
    fp3 = fp;
    qp3 = qp;

    f(i+1) = f(i)+fp*dsgh;
    q(i+1) = q(i)+qp*dsgh;

    fp = q(i+1);
    tmp = 1+q(i+1)*q(i+1);

```

```

tmg = sqrt(tmp)/capls;
qp = tmp*(-fp/s(i+1) + f(i+1)*tmg);

s(i+1) = s(i)+ dsg;
f(i+1) = f(i)+fp*dsg;
q(i+1) = q(i)+qp*dsg;

fp = q(i+1);
tmp = 1+q(i+1)*q(i+1);
tmg = sqrt(tmp)/capls;
qp = tmp*(-fp/s(i+1) + f(i+1)*tmg);
fp4 = fp;
qp4 = qp;

f(i+1) = f(i) + (fp1+2*fp2+2*fp3+fp4)*dsg/6.0;
q(i+1) = q(i) + (qp1+2*qp2+2*qp3+qp4)*dsg/6.0;

end

%---
% done
%---

return

```

Note that the interfacial slope, $q(\sigma_{c1})$, is provided in the last argument of the input.

Force exerted on the sphere

To compute the force exerted on the sphere, we note that the pressure distribution in the upper or lower fluid is given by

$$p^{(1)}(x) = -\rho_1 g x + \pi_0, \quad p^{(2)}(x) = -\rho_2 g x + \pi_0, \quad (5.11.7)$$

where π_0 is the interfacial pressure far from the sphere. By symmetry, the y and z components of the buoyancy force exerted on the sphere are identically zero. The x component of the buoyancy force is given by

$$F_x^{\text{buoyancy}} = - \iint p n_x dS, \quad (5.11.8)$$

where $n_x = \cos \theta$ is the x component of the unit vector normal to the sphere and θ is the meridional angle defined in [Figure 5.11.1](#). Writing

$$dS = (\sigma d\varphi)(a d\theta), \quad \sigma = a \sin \theta, \quad (5.11.9)$$

and thus

$$dS = a^2 \sin \theta d\theta d\varphi, \quad (5.11.10)$$

and integrating with respect to the azimuthal angle, φ , we find that

$$F_x^{\text{buoyancy}} = 2\pi a^2 \left(\int_0^\beta p^{(1)}(\theta) \cos \theta \, d \cos \theta + \int_\beta^\pi p^{(2)}(\theta) \cos \theta \, d \cos \theta \right). \quad (5.11.11)$$

Next, we substitute the expressions for the pressure, set $x = x_c + a \cos \theta$, and simplify to obtain

$$F_x^{\text{buoyancy}} = -2\pi a^2 g \left(\rho_1 \int_0^\beta (x_c + a \cos \theta) \cos \theta \, d \cos \theta + \rho_2 \int_\beta^\pi (x_c + a \cos \theta) \cos \theta \, d \cos \theta \right). \quad (5.11.12)$$

As expected on physical grounds, the constant π_0 does not make a net contribution to the force. Carrying out the integration, we find that

$$F_x^{\text{buoyancy}} = -2\pi g a^2 \left(\rho_1 x_c \frac{\cos^2 \beta - 1}{2} + \rho_1 a \frac{\cos^3 \beta - 1}{3} + \rho_2 x_c \frac{1 - \cos^2 \beta}{2} - \rho_2 a \frac{1 + \cos^3 \beta}{3} \right). \quad (5.11.13)$$

Rearranging, we obtain

$$F_x^{\text{buoyancy}} = \pi g a^2 \left(x_c \Delta \rho (\cos^2 \beta - 1) + \frac{2}{3} a \Delta \rho \cos^3 \beta + \frac{4}{3} a \bar{\rho} \right), \quad (5.11.14)$$

where

$$\bar{\rho} = \frac{1}{2} (\rho_1 + \rho_2) \quad (5.11.15)$$

is the mean fluid density. When $\rho_1 = \rho_2 = \bar{\rho}$, only the last term survives, yielding the buoyancy force on a submerged sphere.

Surface tension pulls the sphere tangentially to the interface at the contact line. Integrating the tension along the circular contact line, we derive the resultant x component of the capillary force,

$$F_x^{\text{capillary}} = \gamma (2\pi \sigma_{\text{cl}}) \sin(\alpha - \beta) = 2\pi a \gamma \sin \beta \sin(\alpha - \beta), \quad (5.11.16)$$

where $\sigma_{\text{cl}} = a \sin \beta$ is the radius of the circular contact line.

Force equilibrium requires that

$$F_x^{\text{buoyancy}} + F_x^{\text{capillary}} = W, \quad (5.11.17)$$

where W is the weight of the sphere. We may set $W = \frac{4\pi}{3} a^3 \rho_s g$, where ρ_s is the actual or effective density of the sphere. Simplifying, we derive a force equilibrium equation,

$$\frac{x_c}{a} \sin^2 \beta = \frac{2}{3} \cos^3 \beta + \frac{2}{3} \kappa + 2 \frac{\lambda^2}{a^2} \sin \beta \sin(\alpha - \beta), \quad (5.11.18)$$

where

$$\kappa = 2 \frac{\bar{\rho} - \rho_s}{\Delta\rho} \quad (5.11.19)$$

is a dimensionless parameter. The limits $\kappa \rightarrow -1$ or 1 correspond to $\rho_s = \rho_2$ or ρ_1 , where the sphere is neutrally buoyant in the lower or upper fluid.

Far-field meniscus

Far from the sphere, the interfacial slope is small. Linearizing the Laplace–Young equation, we obtain the zeroth-order Bessel equation,

$$f'' = -\frac{f'}{\sigma} + \frac{f}{\lambda^2}. \quad (5.11.20)$$

An acceptable solution that decays at infinity is proportional to the modified Bessel function of zeroth order, K_0 ,

$$f(\sigma) \simeq \xi a K_0(\sigma/\lambda), \quad (5.11.21)$$

where ξ is a dimensionless constant. It is beneficial to eliminate the constant ξ by formulating the ratio between the shape function f and its derivative, finding

$$f(\sigma) + \lambda \frac{K_0(\sigma/\lambda)}{K_1(\sigma/\lambda)} f'(\sigma) \simeq 0, \quad (5.11.22)$$

where K_1 is the first-order modified Bessel function. This condition can be applied at a sufficiently large value of σ in place of the far-field condition (5.11.6) to improve the performance of the numerical methods.

Flat interface solution

In the case of a flat interface, $x_c = -a \cos \beta$, the expression for the buoyancy force simplifies to

$$F_x^{\text{buoyancy, flat}} = \pi g a^3 \Delta\rho \cos \beta \left(1 - \frac{1}{3} \cos^2 \beta\right) + \frac{2}{3} \pi g a^3 (\rho_2 + \rho_1). \quad (5.11.23)$$

The contact angle is equal to the contact line aperture, $\alpha = \beta$, the capillary force vanishes, and the trigonometric equation (5.11.18) simplifies to a cubic equation for $\cos \beta$,

$$\cos^3 \beta - 3 \cos \beta - 2\kappa = 0. \quad (5.11.24)$$

A solution for $\cos \beta$ in the admissible range $[-1, 1]$ exists only when $|\kappa| < 1$.

Solution algorithm

When $|\kappa| < 1$, equation (5.11.18) and the accompanying Laplace–Young equation admit a solution in a limited range of sufficiently high capillary lengths. A numerical method for computing hydrostatic shapes can be implemented according to the following steps:

1. Begin by considering a flat interface, solve the cubic equation (5.11.24) for $\cos \beta$, and recover an approximation to β .
2. Choose a value for the contact angle, $\alpha \simeq \beta$.
3. Solve equation (5.11.18) for x_c to satisfy the vertical force balance.
4. Integrate the system of differential equations (5.11.3) from $\sigma = \sigma_{cl}$ up to a specified distance, $\sigma = \sigma_{max}$, and check whether $f(\sigma_{max}) = 0$. If not, we adjust β to make it so. The adjustment can be done using the secant or Newton's method.
5. Change the contact angle, α , and return to Step 3 to obtain a new configuration.

The procedure ensures that a good initial guess is available for the shooting method, obtained by parameter continuation.

The numerical method is implemented in a MATLAB function entitled *flsphere*, located in directory *03_hydrostat* of FDLIB:

```
function [s,x,q,beta,alpha,xc,xcl,scl ...
        ,beta_flat,xc_flat ...
        ,al_scan,bt_scan,xc_scan] ...
    ...
    = flsphere(a,cap1,rho1,rho2,kappa,alpha_in ...
    ,smax,ndiv ...
    ,mincut,maxcut ...
    ,iplot_shape)

%=====
% Compute families of floating sphere configurations
%
% alpha_in:  targeted value of alpha
%           (will stop when alpha = alpha_in)
%=====

%-----
% parameters
%-----

eps = 0.0000001; % for Newton's method
tol = 0.0000001; % for Newton's method

%---
% will scan the contact angle space with step dal
% that depends on the capillary length
%---

dal = -0.005;

if(cap1<1.5) dal = -0.002; end
```

```

if(cap1<0.9) dal = -0.001; end
if(cap1<0.8) dal = -0.0005; end

Nmax = 2*abs(floor(pi/dal)) % to prevent run off

%----
% prepare
%---

Drho = rho2-rho1;
Brho = 0.5*(rho1+rho2); % mean fluid density
rhos = Brho-0.5*kappa*Drho; % density of the sphere
capls = cap1^2; % square of the capillary number

%----
% flat interface solution
%
% computed by solving a cubic equation using
% the "roots" matlab function (internal)
%---

C(1) = 1.0;
C(2) = 0.0;
C(3) = -3.0;
C(4) = -2*kappa;

cosbeta = roots(C); % roots() is an internal matlab function

if(abs(cosbeta(1))<1)
    beta = acos(cosbeta(1));
elseif(abs(cosbeta(2))<1)
    beta = acos(cosbeta(2));
elseif(abs(cosbeta(3))<1)
    beta = acos(cosbeta(3));
end

xc = -a*cos(beta);
beta_flat = beta; xc_flat = xc;

%---
% prepare to scan the contact angle (alpha)
%---

Ido = 1;
Iflag = 0;
Icount = 0; % counter
Jcount = 0; % counter
Irecord = 1; % recording flag
alpha = beta; % flat plate contact angle

```

```

%---
while(Ido==1)      % loop over contact angles
%---

Icount = Icount+1;

itermax = 20;

for iter=1:itermax

%---
% solve for beta using Newton's method
%---

cs = cos(beta);
sn = sin(beta);
amb = alpha-beta;
xc = (2/3*cs^3 + 2/3*kappa + 2*capls/a^2*sn*sin(amb))/sn^2;
xcl = xc+a*cs;
scl = a*sn;
slope = tan(amb);

[x,s,q] = flsphere_ode(ndiv,smax,capls,xcl,scl,slope);

% obj = x(ndiv+1); % primary far-field
arg = s(ndiv+1)/capl; % far-field from asymptotics
obj = x(ndiv+1) + capl*besselk(0,arg) ...
/besselk(1,arg)*q(ndiv+1);

if(abs(obj)<tol) break; end
beta = beta+eps;
cs = cos(beta);

sn = sin(beta);
amb = alpha-beta;
xc = (2/3*cs^3 + 2/3*kappa + 2*capls/a^2*sn*sin(amb))/sn^2;
xcl = xc+a*cs;
scl = a*sn;

slope = tan(amb);

[x1,s1,q1] = flsphere_ode(ndiv,smax,capls,xcl,scl,slope);

% obj1 = x1(ndiv+1); % primary far-field
arg1 = s1(ndiv+1)/capl; % far-field from asymptotics
obj1 = x1(ndiv+1) + capl*besselk(0,arg) ...
/besselk(1,arg)*q1(ndiv+1);

```

```

beta = beta-eps; % reset
der = (obj1-obj)/eps;
correction = -obj/der;
beta = beta+correction;

if(abs(correction)<0.0000001) break; end

end % of Newton iterations

if(iter==itermax)
    disp("flsphere: Newton iterations did not converge")
    return
end

cs = cos(beta);
sn = sin(beta);
amb = alpha-beta;
xc = (2/3*cs^3 + 2/3*kappa + 2*capls/a^2*sn*sin(amb))/sn^2;

%=====
% plotting session
%=====

%---
if(iplot_shape==1)
%---

    figure(10)
    hold on
    xlabel('y/a','fontsize',15)
    ylabel('x/a','fontsize',15)

%---
% plot the interface profile
%---

    plot(s,x,'k');
    plot(-s,x,'k');
    axis equal

%---
% plot the particle contour
%---

    ncrc=64;

    for i=1:ncrc+1
        tht = (i-1)*2*pi/ncrc;
        xcrc(i) = xc+a*cos(tht);
    end

```

```

    scrc(i) = a*sin(tht);
end

plot(scrc,xcrc,'k');
patch(scrc,xcrc,'y');
pause(0.001)

%=====
end % of plotting
%=====

if(Irecord==1)
    Jcount = Jcount +1;
    al_scan(Jcount) = alpha/pi;
    bt_scan(Jcount) = beta/pi;
    xc_scan(Jcount) = xc/a;
end

if(Iflag==1)
    break;
end

alpha = alpha+dal;

%-----
% change alpha scanning direction or lock
%-----

if(alpha<0.01*pi)
    dal = abs(dal);
    alpha = alpha + dal;
elseif(alpha>0.99*pi)
    dal = -abs(dal);
    alpha = alpha+dal;
elseif(abs(alpha-alphain)<1.0*abs(dal)) % lock on alphain
    alpha = alphain + 0.00;
    Iflag = 1;
end

if(Icount>Nmax) break; end

%---
end
%---

return

```

Nondimensionalizing lengths by the sphere radius, a , we find that the interfacial profile depends on the ratio of the capillary length to the sphere radius, λ/a , the density difference

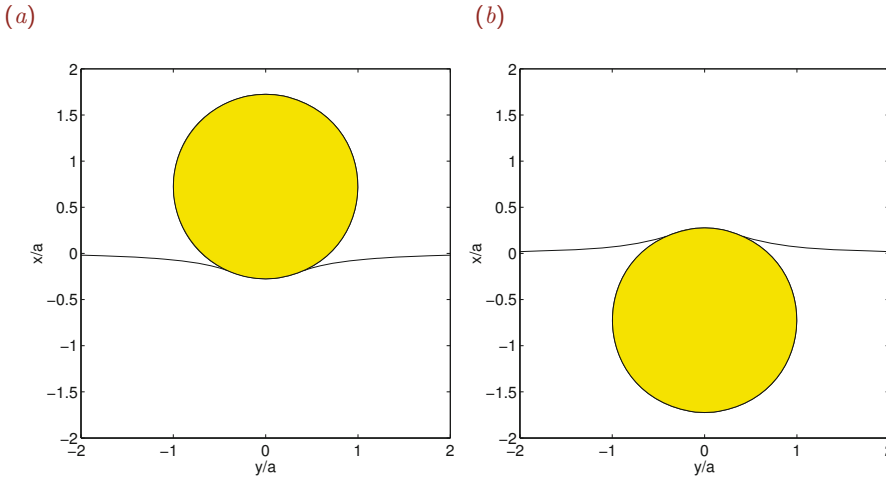


Figure 5.11.2 Axisymmetric interfacial profiles attached to a floating sphere for $\lambda/a = 1$ and (a) $\kappa = 0.5$, $\alpha = 0.98\pi$, or (b) $\kappa = -0.5$, $\alpha = 0.0242\pi$.

ratio, κ , and the contact angle, α . Two interfacial shapes are shown in Figure 5.11.2(a, b). In Figure 5.11.2(a), a heavy hydrophobic particle is kept afloat. In Figure 5.11.2(b), a light hydrophilic particle is held captive.

Graphs of the particle center position against the contact angle, α , are shown in Figure 5.11.3 for $\kappa = 0$ and $\frac{1}{2}$. When $\kappa = 0$ and the contact angle is $\alpha = \frac{1}{2}\pi$, the interface is flat and the particle is divided equally between the upper and lower fluids, independent of the capillary length. When $\kappa = \frac{1}{2}$, the interface is flat at a certain contact angle that is insensitive to the capillary length. The particle center position for $\kappa = -\frac{1}{2}$ is the mirror image of that for $\kappa = \frac{1}{2}$, subject to a reflection in the contact angle. As λ/a increases, the particle center becomes independent of κ and is given by $x_c = -a \cos \alpha$.

Spheroidal particle

As a straightforward generalization, we consider the equilibrium position of a floating spheroidal particle whose axis revolution is parallel to the acceleration of gravity, as shown in Figure 5.11.4. The origin of the x axis is set at the position of the infinite flat interface far from the particle.

The elliptical particle contour in an azimuthal plane is described by the equations

$$x = x_c + a \cos \zeta, \quad \sigma = b \sin \zeta, \quad (5.11.25)$$

where x_c describes the location of the particle center, a and b are the particle semi-axes, and the parameter ζ varies from 0 at the top of the particle to π at the bottom of the particle, as shown in Figure 5.11.4. The parameter ζ should not be confused with the meridional angle, θ . They are equal only in the case of a spherical particle.

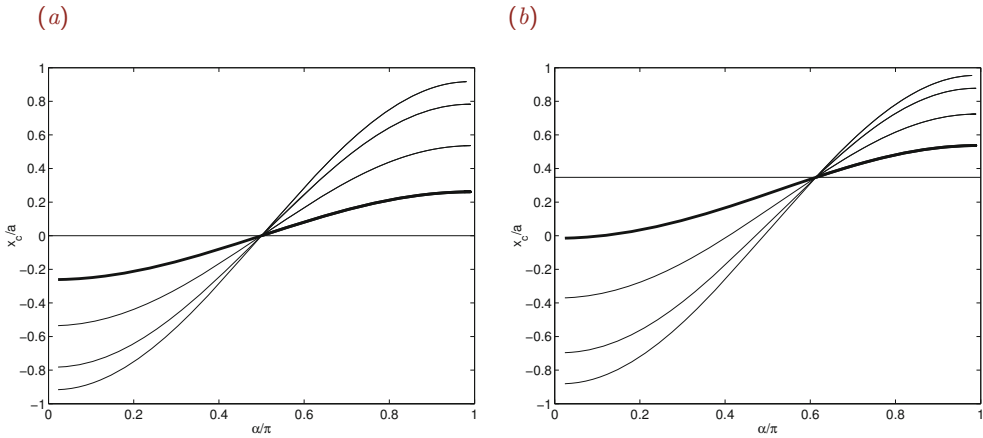


Figure 5.11.3 Floating spherical particle center position for $\lambda/a = 0.5$ (bold lines), 1.0, 2.0, and 4.0, and (a) $\kappa = 0$ or (b) 0.5.

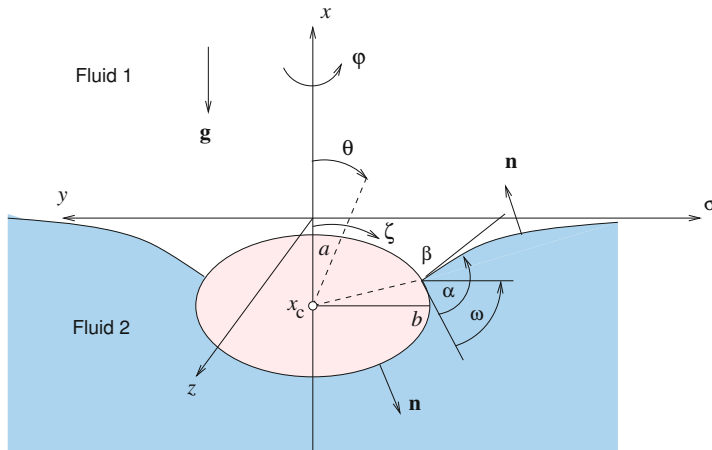


Figure 5.11.4 Illustration of a spheroidal particle floating at the interface between two immiscible fluids. The axis of revolution is normal to the plane of the undisturbed interface.

The circular contact line is located at the axial position

$$x_{cl} = x_c + a \cos \beta \tag{5.11.26}$$

and at the radial position

$$\sigma_{cl} = b \sin \beta, \tag{5.11.27}$$

where the parameter β varies in the range $[0, \pi]$. In the case of a flat interface, $x_{cl} = 0$ and

$x_c = -a \cos \beta$. The shape of the meniscus is governed by the equations described previously in this section for a spherical particle.

Buoyancy force

The vertical component of the force exerted on the spheroidal particle is given in equation (5.11.8),

$$F_x^{\text{buoyancy}} = - \iint p n_x \, dS, \quad (5.11.28)$$

where n_x is the x component of the unit vector normal to the spheroid. Introducing the arc length around the particle contour, ℓ , measured in the direction of increasing parameter ζ , setting

$$dS = 2\pi\sigma d\ell, \quad n_x = \frac{d\sigma}{d\ell}, \quad n_x \, dS = 2\pi \, d\sigma, \quad (5.11.29)$$

and performing the integration around the axis of revolution, we derive an expression for the x component of the buoyancy force,

$$F_x^{\text{buoyancy}} = -\pi b^2 \int_0^\pi p \sin 2\zeta \, d\zeta. \quad (5.11.30)$$

Now we recall that $\zeta = \beta$ marks the location of the contact line in the two fluids and write

$$F_x^{\text{buoyancy}} = -\pi b^2 \left(\int_0^\beta p^{(1)} \sin 2\zeta \, d\zeta + \int_\beta^\pi p^{(2)} \sin 2\zeta \, d\zeta \right). \quad (5.11.31)$$

Substituting the expressions for the pressure, and setting $x = x_c + a \cos \zeta$, we obtain

$$F_x^{\text{buoyancy}} = -2\pi b^2 g \left(\rho_1 \int_0^\beta (x_c + a \cos \zeta) \cos \zeta \, d \cos \zeta + \rho_2 \int_\beta^\pi (x_c + a \cos \zeta) \cos \zeta \, d \cos \zeta \right). \quad (5.11.32)$$

Carrying out the integration, we find that

$$F_x^{\text{buoyancy}} = 2\pi g b^2 \left(\rho_1 x_c \frac{\sin^2 \beta}{2} - \rho_1 a \frac{\cos^3 \beta - 1}{3} - \rho_2 x_c \frac{\sin^2 \beta}{2} + \rho_2 a \frac{1 + \cos^3 \beta}{3} \right). \quad (5.11.33)$$

Rearranging, we obtain

$$F_x^{\text{buoyancy}} = \pi g b^2 \left(-x_c \Delta \rho \sin^2 \beta + \frac{2}{3} a \Delta \rho \cos^3 \beta + \frac{4}{3} a \bar{\rho} \right) \quad (5.11.34)$$

involving the *a priori* unknown particle center position, x_c .

Capillary force

The x component of the capillary force is given by

$$F_x^{\text{capillary}} = \gamma (2\pi\sigma_{\text{cl}}) \sin(\alpha - \omega), \quad (5.11.35)$$

where ω is the angle subtended between the tangent vector and the σ axis at the contact line, as shown in [Figure 5.11.4](#), given by

$$\omega = \arctan\left(\frac{b}{a} \tan \beta\right). \quad (5.11.36)$$

Substituting $\sigma_{\text{cl}} = b \sin \beta$, we obtain

$$F_x^{\text{capillary}} = 2\pi b \gamma \sin \beta \sin(\alpha - \lambda). \quad (5.11.37)$$

Vertical force balance

Now substituting into the force equilibrium equation

$$F_x^{\text{buoyancy}} + F_x^{\text{capillary}} = W \quad (5.11.38)$$

the expression

$$W = \frac{4\pi}{3} b^2 a \rho_s g \quad (5.11.39)$$

for the particle weight, and simplifying, we obtain the governing equation

$$\frac{x_c}{a} \sin^2 \beta = \frac{2}{3} \cos^3 \beta + \frac{2}{3} \kappa + 2 \frac{\lambda^2}{ab} \sin \beta \sin(\alpha - \lambda). \quad (5.11.40)$$

In the case of a flat interface, $x_c = -a \cos \beta$, the expression for the buoyancy force simplifies to

$$F_x^{\text{buoyancy}} = \pi g b^2 a \Delta \rho \cos \beta \left(1 - \frac{1}{3} \cos^2 \beta\right) + \frac{4}{3} \pi g b^2 a \bar{\rho}, \quad (5.11.41)$$

the contact angle is equal to the contact line aperture angle, $\alpha = \omega$, the capillary force vanishes, and the trigonometric equation (5.11.40) simplifies to (5.11.24).

The particle position and meniscus shape can be found by a modification of the method discussed previously in this section for a spherical particle (Problem 5.11.3).

PROBLEMS**5.11.1 Flat interface**

Prove that a solution of (5.11.24) for $\cos \beta$ in the admissible range $[-1, 1]$ exists only when $|\kappa| < 1$.

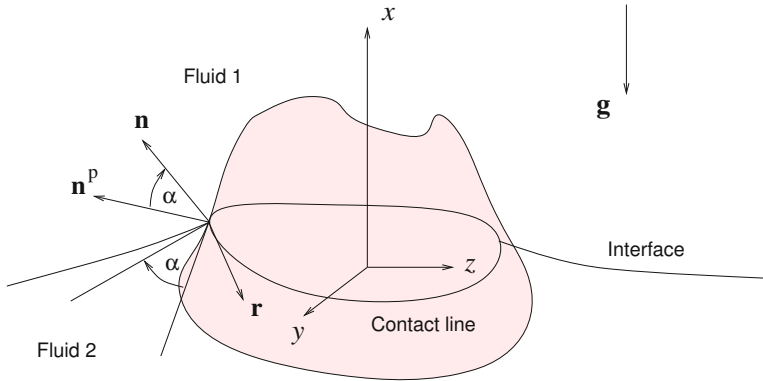


Figure 5.12.1 Illustration of a three-dimensional particle straddling the interface between two immiscible fluids.

5.11.2 *Floating position of a spherical particle*

Prepare the counterparts of the graphs shown in Figure 5.11.3 for $\kappa = 0.1$ and 0.9 . Discuss the physical interpretation of the results.

5.11.3 *Spheroidal particle*

Modify the code given in the text for a spherical particle to compute the floating position of a spheroidal particle. Prepare the counterparts of the graphs shown in Figure 5.11.3 for particle aspect ratio $a/b = 0.5$ and 0.1 .

5.12 A three-dimensional meniscus

Having discussed two-dimensional and axisymmetric interfacial configurations, now we consider a genuinely three-dimensional configuration with reference to the shape of a meniscus developing around a small particle with an arbitrary shape straddling the interface between two stationary immiscible fluids, as shown in Figure 5.12.1. The upper fluid is labeled 1 and the lower fluid is labeled 2. The fluids are assumed to be stably stratified, that is, $\rho_2 > \rho_1$ or $\Delta\rho \equiv \rho_2 - \rho_1 > 0$.

The interface meets the particle around a closed contact line and becomes horizontal far from the contact line. The contact angle, α , is given by

$$\alpha = \arccos(\mathbf{n}^p \cdot \mathbf{n}), \tag{5.12.1}$$

where $0 < \alpha < \pi$, \mathbf{n}^p is the unit vector normal to the particle, \mathbf{n} is the unit vector normal to the interface, and the left-hand side is evaluated at a point \mathbf{x} around the contact line.

Laplace–Young equation

The working Cartesian system is defined such that the x axis points against the acceleration of gravity and passes through a designated particle center. The shape of the interface can

be described by a function of two variables, y and z , as

$$x = \zeta(y, z). \quad (5.12.2)$$

Far from the particle, as y and z tend to infinity, the function ζ decays to zero, yielding a planar shape. The Laplace–Young equation requires that

$$2\kappa_m = -\frac{\zeta}{\lambda^2}, \quad (5.12.3)$$

where $\lambda^2 = \gamma/(\Delta\rho g)$ is the square of the capillary length, γ is the surface tension, g is the magnitude of the acceleration of gravity, and κ_m is the mean curvature reckoned to be positive when the interface is downward concave. The absence of a constant on the right-hand side of (5.12.3) guarantees that the mean curvature vanishes far from the contact line where ζ decays to zero.

Substituting into the Laplace–Young equation the expression for the mean curvature given in (4.4.15) with appropriate changes in the notation,

$$2\kappa_m = -\frac{(1 + \zeta_z^2)\zeta_{yy} - 2\zeta_y\zeta_z\zeta_{yz} + (1 + \zeta_y^2)\zeta_{zz}}{(1 + \zeta_y^2 + \zeta_z^2)^{3/2}}, \quad (5.12.4)$$

we derive a nonlinear partial differential equation,

$$\nabla^2\zeta + \zeta_z^2\zeta_{yy} - 2\zeta_y\zeta_z\zeta_{yz} + \zeta_y^2\zeta_{zz} - (1 + |\nabla\zeta|^2)^{3/2}\frac{\zeta}{\lambda^2} = 0, \quad (5.12.5)$$

where ∇ is the gradient and ∇^2 is the Laplacian operator in the yz plane, a subscript y denotes a partial derivative with respect to y , and a subscript z denotes a partial derivative with respect to z . We will assume that the elevation of the contact line around the contact line is specified in lieu of a Dirichlet boundary condition.

5.12.1 Elliptic coordinates

Consider a configuration where the projection of the contact line in the yz plane is an ellipse arising by rotating a circle, as shown in [Figure 5.12.2\(a\)](#). To solve equation (5.12.5) in the exterior of the ellipse, we introduce elliptic coordinates, (u, φ) , defined by the conformal mapping function

$$y + iz = A \sinh(u + i\varphi), \quad (5.12.6)$$

where i is the imaginary unit, $i^2 = -1$, and A is a real constant. Resolving the mapping function into its real and imaginary parts, we obtain

$$y = A \sinh u \cos \varphi, \quad z = A \cosh u \sin \varphi. \quad (5.12.7)$$

The variable u ranges from a certain value u_0 around the ellipse to infinity far from the ellipse. The variable φ varies in the range $[0, 2\pi]$ around the contact line. Note that φ is *not* the meridional angle measured around the vertical x axis. As u tends to infinity,

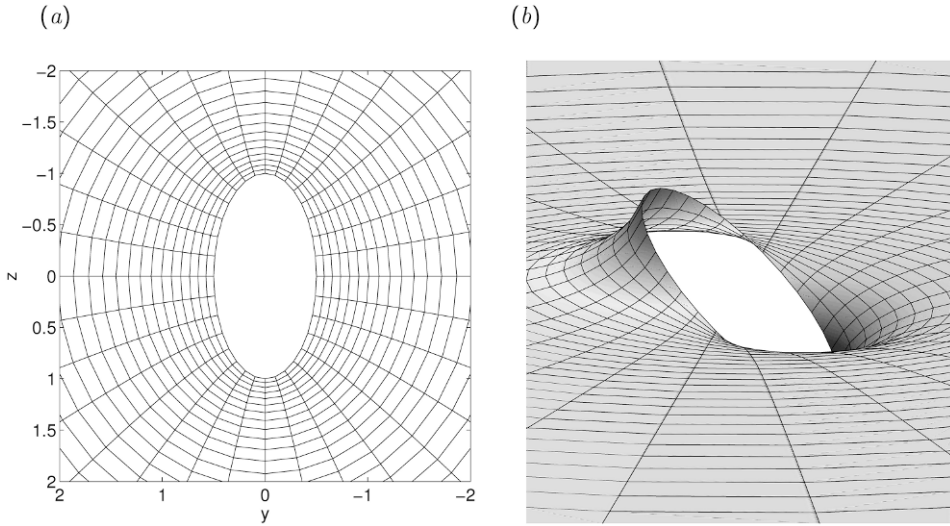


Figure 5.12.2 (a) Illustration of grid lines based on orthogonal elliptic coordinates. (b) Hydrostatic shape of a meniscus attached to a rotated circle computed in the elliptic coordinates.

the contour lines of constant u tend to become circles, as shown in Figure 5.12.2(a). The elliptic coordinates (u, φ) are orthogonal in the yz plane but not over the three-dimensional interface.

To accommodate the elliptical shape of the projection of the contact line onto the yz plane, we set

$$b = A \sinh u_0, \quad c = A \cosh u_0, \tag{5.12.8}$$

where b and c are the ellipse semi-axes along the y and z axes. Solving for A and u_0 , we find that

$$A = \frac{b}{\sinh u_0}, \quad \tanh u_0 = \frac{b}{c}. \tag{5.12.9}$$

The magnitude of the gradient in the yz plane is given by

$$|\nabla\zeta| = \frac{1}{h} |\widehat{\nabla}\zeta| \tag{5.12.10}$$

and the Laplacian is given by

$$\nabla^2\zeta = \frac{1}{h^2} \widehat{\nabla}^2\zeta, \tag{5.12.11}$$

where a caret (hat) indicates differentiation with respect to the elliptic coordinates (u, φ) , and h is the metric coefficient of the transformation given by

$$h = A |\cosh(u + i\varphi)| = A \sqrt{\cosh^2 u - \sin^2 \varphi}. \tag{5.12.12}$$

The Laplace–Young equation (5.12.5) takes the form

$$\frac{1}{h^2} \widehat{\nabla}^2 \zeta + \zeta_z^2 \zeta_{yy} - 2 \zeta_y \zeta_z \zeta_{yz} + \zeta_y^2 \zeta_{zz} - (1 + |\nabla \zeta|^2)^{3/2} \frac{\zeta}{\lambda^2} = 0, \quad (5.12.13)$$

which can be regarded as a nonlinear Poisson-like equation, forced by an *a priori* unknown source term involving the interfacial elevation.

5.12.2 Finite-difference method

The solution of (5.12.13) can be found numerically using a finite-difference method in elliptic coordinates with evenly spaced grid lines. The second-order finite-difference representation of (5.12.13) at the (i, j) interior grid point in the $u\varphi$ plane is

$$\begin{aligned} \frac{1}{h_{i,j}^2} \left(\frac{\zeta_{i-1,j} - 2\zeta_{i,j} + \zeta_{i+1,j}}{\Delta u^2} + \frac{\zeta_{i,j-1} - 2\zeta_{i,j} + \zeta_{i,j+1}}{\Delta \varphi^2} \right) \\ + (\zeta_z^2 \zeta_{yy} - 2\zeta_y \zeta_z \zeta_{yz} + \zeta_y^2 \zeta_{zz})_{i,j} - (1 + |\nabla \zeta|^2)_{i,j}^{3/2} \frac{\zeta_{i,j}}{\lambda^2} = 0. \end{aligned} \quad (5.12.14)$$

To implement Gauss–Seidel iterations, we rearrange to obtain

$$\begin{aligned} \zeta_{i,j} = \frac{1}{G} \left[\frac{1}{h_{i,j}^2} \left(\frac{\zeta_{i-1,j} + \zeta_{i+1,j}}{\Delta u^2} + \frac{\zeta_{i,j-1} + \zeta_{i,j+1}}{\Delta \varphi^2} \right) \right. \\ \left. + (\zeta_z^2 \zeta_{yy} - 2\zeta_y \zeta_z \zeta_{yz} + \zeta_y^2 \zeta_{zz})_{i,j} \right], \end{aligned} \quad (5.12.15)$$

where

$$G = \frac{2}{h_{i,j}^2} \left(\frac{1}{\Delta u^2} + \frac{1}{\Delta \varphi^2} \right) + \frac{1}{\lambda^2} (1 + |\nabla \zeta|^2)_{i,j}^{3/2}. \quad (5.12.16)$$

The iterations proceed by guessing grid values, and then replacing the guesses with the right-hand side of (5.12.15) at each grid point.

The first derivatives of ζ with respect to y and z can be computed from derivatives with respect to u and φ by solving a system of 2×2 equations arising from the chain rule,

$$\begin{bmatrix} \partial y / \partial u & \partial z / \partial u \\ \partial y / \partial \varphi & \partial z / \partial \varphi \end{bmatrix} \begin{bmatrix} \partial \zeta / \partial y \\ \partial \zeta / \partial z \end{bmatrix} = \begin{bmatrix} \partial \zeta / \partial u \\ \partial \zeta / \partial \varphi \end{bmatrix}. \quad (5.12.17)$$

The derivatives with respect to u and φ on the right-hand side can be computed by numerical differentiation. The second derivatives can be computed by a similar method.

The numerical method is implemented in the following MATLAB code entitled *men_3d*, residing inside directory *03_hydrostat* of **FDLIB**:

```
%=====
% meniscus in the exterior of an ellipse
```

```

% in the yz plane
%=====

b = 0.5;
c = 1.0;
capl = 0.75;    % capillary length
xcline = 0.5;   % height of the contact line

tol = 0.000001; % iteration tolerance
Niter = 1000;

%-----
% divisions
%-----

Nu = 32; Nphi = 32;

%---
% prepare
%---

Dphi = 2*pi/Nphi;
capls = capl*capl;
Dphi2 = 2.0*Dphi;
u0 = atanh(b/c);
snhu0 = sinh(u0);
cshu0 = cosh(u0);
A = b/snhu0;
umax = log(32.0*b/A);
Du = (umax-u0)/Nu;
Du2 = 2.0*Du;

%---
% grid
%---

for i=1:Nu+1
    u(i) = u0+(i-1)*Du;
    snhu(i) = sinh(u(i));
    cshu(i) = cosh(u(i));
    for j=1:Nphi+1
        phi(j) = (j-1)*Dphi;
        csphi(j) = cos(phi(j));
        snphi(j) = sin(phi(j));
        y(i,j) = A*snhu(i)*csphi(j);
        z(i,j) = A*cshu(i)*snphi(j);
        h(i,j) = A*sqrt(cshu(i)^2-snphi(j)^2);
    end
end
end

```

```

%---
% plot the grid
%---

figure(1)
hold on
axis square
axis([-2 2 -2 2 -2 2])
view(140,30)
xlabel('y','fontsize',15);
ylabel('z','fontsize',15);
zlabel('x','fontsize',15);
set(gca,'fontsize',15)

for i=1:Nu+1
    plot(y(i,:),z(i,:), 'k')
end
for j=1:Nphi
    plot(y(:,j),z(:,j), 'k')
end

%---
% initialize the interfacial elevation
%---

for i=1:Nu+1
    for j=1:Nphi+2
        x(i,j) = 0.0;
    end
end

%---
% boundary conditions
%---

for j=1:Nphi+1
    x(1,j) = xcline*y(1,j);
    x(Nu+1,j) = 0.0;
end

x(1,Nphi+2) = x(1,2);
x(Nu+1,Nphi+2) = 0.0;

%---
% iterations
%---

```

```

for iterations=1:Niter

%---
% compute the first derivatives: dx/dy and dx/dz
%---

% interior nodes:

for i=2:Nu
  for j=2:Nphi+1
    MAT(1,1) = A*cshu(i)*csphi(j);
    MAT(1,2) = A*snhu(i)*snphi(j);
    MAT(2,1) = -A*snhu(i)*snphi(j);
    MAT(2,2) = A*cshu(i)*csphi(j);
    RHS(1) = (x(i+1,j)-x(i-1,j))/Du2;
    RHS(2) = (x(i,j+1)-x(i,j-1))/Dphi2;
    SOL = RHS/MAT';
    dxdy(i,j) = SOL(1);
    dxdz(i,j) = SOL(2);
  end
  dxdy(i,1) = dxdy(i,Nphi+1);
  dxdz(i,1) = dxdz(i,Nphi+1);
  dxdy(i,Nphi+2) = dxdy(i,2);
  dxdz(i,Nphi+2) = dxdz(i,2);
end

% boundary nodes by one-sided differences:

for j=1:Nphi+2
  dxdy(1,j) = 2.0*dxdy(2,j)-dxdy(3,j);
  dxdy(Nu+1,j) = 2.0*dxdy(Nu,j)-dxdy(Nu-1,j);
  dxdz(1,j) = 2.0*dxdz(2,j)-dxdz(3,j);
  dxdz(Nu+1,j) = 2.0*dxdz(Nu,j)-dxdz(Nu-1,j);
end

%---
% compute the second derivatives
%---

for i=2:Nu
  for j=2:Nphi+1
    MAT(1,1) = A*cshu(i)*csphi(j);
    MAT(1,2) = A*snhu(i)*snphi(j);
    MAT(2,1) = -A*snhu(i)*snphi(j);
    MAT(2,2) = A*cshu(i)*csphi(j);
    RHS(1) = (dxdy(i+1,j)-dxdy(i-1,j))/Du2;
    RHS(2) = (dxdy(i,j+1)-dxdy(i,j-1))/Dphi2;
    SOL = RHS/MAT';
    dxdyy(i,j) = SOL(1);
  end
end

```



```

dxdyz(i,j) = SOL(2);
RHS(1) = (dxdz(i+1,j)-dxdz(i-1,j))/Du2;
RHS(2) = (dxdy(i,j+1)-dxdy(i,j-1))/Dphi2;
    SOL = RHS/MAT';
dxddy(i,j) = SOL(1);
dxdyz(i,j) = SOL(2);
RHS(1) = (dxdz(i+1,j)-dxdz(i-1,j))/Du2;
RHS(2) = (dxdz(i,j+1)-dxdz(i,j-1))/Dphi2;
    SOL = RHS/MAT';
dxdzy(i,j) = SOL(1);
dxdzz(i,j) = SOL(2);
    end
end

%-----
% scan the grid points
%-----

errr = 0.0;

for i=2:Nu
    for j=2:Nphi+1
        H = h(i,j); HS = H*H;
        tmp = 1.0+dxdy(i,j)^2+dxdz(i,j)^2;
        G = 2.0*(1.0/Du^2+1.0/Dphi^2)/HS + tmp^(3/2)/capls;
        xnew = (x(i+1,j)+x(i-1,j))/(HS*Du^2) ...
            +(x(i,j+1)+x(i,j-1))/(HS*Dphi^2);
        xnew = xnew + dxdz(i,j)^2 * dxddy(i,j);
        xnew = xnew - 2.0*dxdy(i,j)*dxdz(i,j)*dxdyz(i,j);
        xnew = xnew + dxdy(i,j)^2 * dxdzz(i,j);
        xnew=xnew/G;
        corr = abs(xnew-x(i,j));
        x(i,j) = xnew;
        if(corr>errr) errr = corr; end
    end
end

for i=2:Nu+1
    x(i,1) = x(i,Nphi+1);
    x(i,Nphi+2) = x(i,2);
end

if(errr<tol) break; end

%--
end    % of iterations
%--

if(errr>tol)

```

```

disp('the iterations did not converge')
errr
return
end

%---
% plotting
%---

figure(2)
hold on
xlabel('y','fontsize',15);
ylabel('z','fontsize',15);
zlabel('x','fontsize',15);
axis square
axis([-1 1 -1 1 -1 1])
view(162, 12)

for i=1:Nu
    for j=1:Nphi
        patch([y(i,j), y(i,j+1), y(i+1,j+1), y(i+1,j)], ...
            [z(i,j), z(i,j+1), z(i+1,j+1), z(i+1,j)], ...
            [x(i,j), x(i,j+1), x(i+1,j+1), x(i+1,j)], ...
            [x(i,j), x(i,j+1), x(i+1,j+1), x(i+1,j)]]);
    end
end
end

```

A solution subject to the boundary condition for the contact angle elevation implemented in the code, reflecting a rotating circle, is shown in [Figure 5.12.2\(b\)](#).

5.12.3 Capillary force and torque

Surface tension pulls the particle around the contact line in a direction that is tangential to the interface and lies in a plane that is normal to the contact line at each point. The resultant capillary force is given by

$$\mathbf{F}^{\text{capillary}} = \gamma \oint \mathbf{r} \times \mathbf{n} \, d\ell, \quad (5.12.18)$$

where \mathbf{n} is the unit vector normal to the interface given by

$$\mathbf{n} = \frac{1}{\left| \frac{\partial \mathbf{x}}{\partial u} \times \frac{\partial \mathbf{x}}{\partial \varphi} \right|} \frac{\partial \mathbf{x}}{\partial u} \times \frac{\partial \mathbf{x}}{\partial \varphi}, \quad (5.12.19)$$

\mathbf{r} is the unit vector tangential to the contact line, as shown in [Figure 5.12.1](#), ℓ is the arc length around the contact line, and the integration is performed around the contact line.

The resultant capillary torque with respect to an arbitrary point, \mathbf{x}_0 , is given by

$$\mathbf{T}^{\text{capillary}} = \gamma \oint (\mathbf{x} - \mathbf{x}_0) \times (\mathbf{r} \times \mathbf{n}) \, d\ell. \quad (5.12.20)$$

Using a vector identity, we may express the capillary torque in the form

$$\mathbf{T}^{\text{capillary}} = \gamma \oint \left([(\mathbf{x} - \mathbf{x}_0) \cdot \mathbf{n}] \mathbf{r} - [(\mathbf{x} - \mathbf{x}_0) \cdot \mathbf{r}] \mathbf{n} \right) d\ell. \quad (5.12.21)$$

Once the computation of the meniscus shape has been concluded, the capillary force and torque can be obtained using the following module:

```
%---
% compute dxdu, dxdphi,
% the surface normal and tension vector
% around the contact line
%---

x0 = 0.0; y0 = 0.0; z0 = 0.0;

for j=1:Nphi+1

    dxdu(j) = (-x(3,j)+4.0*x(2,j)-3.0*x(1,j))/Du2;
    dydu(j) = A*cshu0*cspphi(j);
    dzdu(j) = A*snhu0*snphi(j);
    dmdu(j) = sqrt(dxdu(j)^2+dydu(j)^2+dzdu(j)^2);

    if(j==1)
        dxdphi(j) = (x(1,2)-x(1,Nphi))/Dphi2;
    else
        dxdphi(j) = (x(1,j+1)-x(1,j-1))/Dphi2;
    end

    dydphi(j) = -A*snhu0*snphi(j);
    dzdphi(j) = A*cshu0*cspphi(j);
    dmdphi(j) = sqrt(dxdphi(j)^2+dydphi(j)^2+dzdphi(j)^2);
    vnx(j) = dydu(j)*dzdphi(j)-dzdu(j)*dydphi(j);
    vny(j) = dzdu(j)*dxdphi(j)-dxdu(j)*dzdphi(j);
    vnz(j) = dxdu(j)*dydphi(j)-dydu(j)*dxdphi(j);
    vnm(j) = sqrt(vnx(j)^2+ vny(j)^2+vnz(j)^2);
    vnx(j) = vnx(j)/vnm(j); vny(j) = vny(j)/vnm(j);
    vnz(j) = vnz(j)/vnm(j);
    tngx(j) = dydphi(j)*vnz(j)-dzdphi(j)*vny(j);
    tngy(j) = dzdphi(j)*vnx(j)-dxdphi(j)*vnz(j);
    tngz(j) = dxdphi(j)*vny(j)-dydphi(j)*vnx(j);
    crsx(j) = (y(1,j)-y0)*tngz(j)-(z(1,j)-z0)*tngy(j);
    crsy(j) = (z(1,j)-z0)*tngx(j)-(x(1,j)-x0)*tngz(j);
    crsz(j) = (x(1,j)-x0)*tngy(j)-(y(1,j)-y0)*tngx(j);
```

```
end

%---
% force and torque
%---

forcex = 0.0; forcey = 0.0; forcez = 0.0;
torqux = 0.0; torquy = 0.0; torquz = 0.0;

for j=1:Nphi
    forcex = forcex+tngx(j);
    forcey = forcey+tngy(j);
    forcez = forcez+tngz(j);
    torqux = torqux+crsx(j);
    torquy = torquy+crsy(j);
    torquz = torquz+crsz(j);
end

forcex = forcex*Dphi;
forcey = forcey*Dphi;
forcez = forcez*Dphi;
torqux = torqux*Dphi;
torquy = torquy*Dphi;
torquz = torquz*Dphi;
```

PROBLEM

5.12.1 Convergence of iterations

Consider a meniscus originating from a horizontal elliptical contact line. Study the shape of the meniscus for several contact line elevations and capillary lengths. Investigate the convergence of the Gauss–Seidel iterations.

Equation of motion and vorticity transport

- 6.1 Newton's second law of motion for a fluid parcel**
- 6.2 Integral momentum balance**
- 6.3 Cauchy's equation of motion**
- 6.4 Euler and Bernoulli equations**
- 6.5 The Navier–Stokes equation**
- 6.6 Vorticity transport**
- 6.7 Dynamic similitude and the Reynolds number**
- 6.8 Structure of a flow as a function of the Reynolds number**
- 6.9 Dimensionless numbers in fluid dynamics**

Fluid flow is established in response to an external action mediated by boundary motion, by the application of a surface force, or by the presence of a body force. The evolution of a transient flow and the structure of a steady flow established after an initial start-up period of time are governed by two fundamental principles of thermodynamics and classical mechanics: mass conservation, and Newton's second law for the motion of a fluid parcel. The implementation of Newton's law of motion in continuum mechanics leads us to Cauchy's equation of motion, which provides us with an expression for the point particle acceleration in terms of stresses, and to the vorticity transport equation governing the point particle rotation. The derivation and interpretation of these governing equations in general and specific terms, and their solution for simple flow configurations are discussed in this chapter.

6.1 Newton's second law of motion for a fluid parcel

Consider a fluid parcel in motion, as illustrated in [Figure 6.1.1](#). Newton's second law of motion requires that the rate of change of the parcel's linear momentum, $\mathbf{M}_{\text{parcel}}$, must be equal to the sum of the forces exerted on the parcel at any instant. The forces include the surface force given in equation (5.1.2) and the body force due to gravity given in equation (5.1.1),

$$\frac{d\mathbf{M}_{\text{parcel}}}{dt} = \mathbf{F}^{\text{surface}} + \mathbf{F}^{\text{body}}. \quad (6.1.1)$$

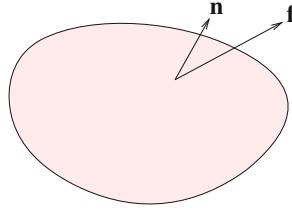


Figure 6.1.1 Illustration of a fluid parcel in motion, showing the unit normal vector, \mathbf{n} , and the traction vector, \mathbf{f} . The motion of the parcel is governed by Newton's second law of motion.

Expressing the surface force in terms of the traction exerted on the parcel surface, \mathbf{f} , and the body force in terms of the fluid density, ρ , and the acceleration of gravity, \mathbf{g} , we obtain

$$\frac{d\mathbf{M}_{\text{parcel}}}{dt} = \iiint_{\text{parcel}} \mathbf{f} dS + \iiint_{\text{parcel}} \rho \mathbf{g} dV. \quad (6.1.2)$$

Expressing the traction in terms of the stress tensor, as shown in (4.2.10), we obtain

$$\frac{d\mathbf{M}_{\text{parcel}}}{dt} = \iiint_{\text{parcel}} \mathbf{n} \cdot \boldsymbol{\sigma} dS + \iiint_{\text{parcel}} \rho \mathbf{g} dV, \quad (6.1.3)$$

where the unit normal vector, \mathbf{n} , points into the parcel exterior. Our next task is to relate the rate of change of the parcel momentum to the fluid density and velocity.

6.1.1 Rate of change of linear momentum

An expression for the linear momentum arises by subdividing a parcel into elementary subparcels with volume dV_{parcel} and corresponding mass $dm_{\text{parcel}} = \rho dV_{\text{parcel}}$, and summing the contributions by integration to obtain

$$\mathbf{M}_{\text{parcel}} = \iiint_{\text{parcel}} \mathbf{u} dm = \iiint_{\text{parcel}} \mathbf{u} \rho dV, \quad (6.1.4)$$

where \mathbf{u} is the fluid velocity. The rate of change of the parcel's linear momentum is given by

$$\frac{d\mathbf{M}_{\text{parcel}}}{dt} = \frac{d}{dt} \iiint_{\text{parcel}} \mathbf{u} dm = \frac{d}{dt} \iiint_{\text{parcel}} \mathbf{u} \rho dV, \quad (6.1.5)$$

where the time derivative is taken for a fixed parcel identity.

Because the integral is computed over the volume of the parcel, which is not stationary but changes in time, switching the order of time differentiation and volume integration on the right-hand side of (6.1.5) is permissible only if the time derivative is replaced by the material derivative, D/Dt , under the integral sign, yielding

$$\frac{d\mathbf{M}_{\text{parcel}}}{dt} = \iiint_{\text{parcel}} \frac{D(\mathbf{u} dm)}{Dt} = \iiint_{\text{parcel}} \left(\frac{D\mathbf{u}}{Dt} dm + \frac{D dm}{Dt} \mathbf{u} \right). \quad (6.1.6)$$

Mass conservation requires that the material derivative of the elementary mass, dm should be zero, yielding the simplified expression

$$\frac{dM_{\text{parcel}}}{dt} = \iiint_{\text{parcel}} \frac{D\mathbf{u}}{Dt} dm = \iiint_{\text{parcel}} \frac{D\mathbf{u}}{Dt} \rho dV, \quad (6.1.7)$$

where $D\mathbf{u}/Dt$ is the point particle acceleration. The density may vary over the parcel volume.

6.1.2 Equation of parcel motion

Substituting the right-hand side of (6.1.7) into the left-hand side of (6.1.3), we obtain the desired equation of parcel motion,

$$\iiint_{\text{parcel}} \frac{D\mathbf{u}}{Dt} \rho dV = \iint_{\text{parcel}} \mathbf{n} \cdot \boldsymbol{\sigma} dS + \iiint_{\text{parcel}} \rho \mathbf{g} dV, \quad (6.1.8)$$

involving the point particle acceleration, the stress tensor, and the body force. Explicitly, the x , y , and z components of (6.1.8) are

$$\begin{aligned} \iiint_{\text{parcel}} \frac{Du_x}{Dt} \rho dV &= \iint_{\text{parcel}} (n_x \sigma_{xx} + n_y \sigma_{yx} + n_z \sigma_{zx}) dS + \iiint_{\text{parcel}} \rho g_x dV, \\ \iiint_{\text{parcel}} \frac{Du_y}{Dt} \rho dV &= \iint_{\text{parcel}} (n_x \sigma_{xy} + n_y \sigma_{yy} + n_z \sigma_{zy}) dS + \iiint_{\text{parcel}} \rho g_y dV, \\ \iiint_{\text{parcel}} \frac{Du_z}{Dt} \rho dV &= \iint_{\text{parcel}} (n_x \sigma_{xz} + n_y \sigma_{yz} + n_z \sigma_{zz}) dS + \iiint_{\text{parcel}} \rho g_z dV. \end{aligned} \quad (6.1.9)$$

Equations (6.1.10) are valid irrespective of whether the fluid is compressible or incompressible.

6.1.3 Two-dimensional flow

The counterpart of the parcel equation of motion (6.1.8) for two-dimensional flow in the xy plane is

$$\iint_{\text{parcel}} \frac{D\mathbf{u}}{Dt} \rho dA = \oint_{\text{parcel}} \mathbf{n} \cdot \boldsymbol{\sigma} d\ell + \iint_{\text{parcel}} \rho \mathbf{g} dA, \quad (6.1.10)$$

where dA is a differential area and $d\ell$ is the differential arc length along the boundary of a parcel in the xy plane. Explicitly, the x and y components of (6.1.10) are

$$\begin{aligned} \iint_{\text{parcel}} \frac{Du_x}{Dt} \rho dA &= \oint_{\text{parcel}} (n_x \sigma_{xx} + n_y \sigma_{yx}) d\ell + \iint_{\text{parcel}} \rho g_x dA, \\ \iint_{\text{parcel}} \frac{Du_y}{Dt} \rho dA &= \oint_{\text{parcel}} (n_x \sigma_{xy} + n_y \sigma_{yy}) d\ell + \iint_{\text{parcel}} \rho g_y dA. \end{aligned} \quad (6.1.11)$$

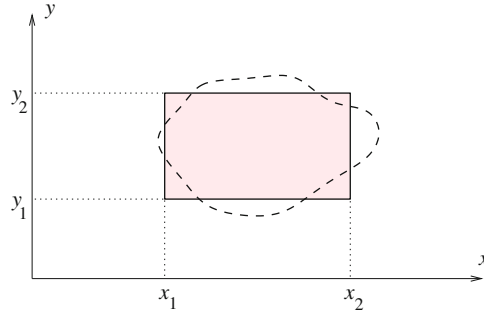


Figure 6.1.2 Illustration of a fluid parcel with a rectangular instantaneous shape, drawn with the solid line, in a two-dimensional flow. Even though the parcel generally deforms to obtain a warped shape, drawn with the dashed line, Newton's second law of motion in its integral form can be applied over the instantaneous parcel shape.

These equations are valid irrespective of whether the fluid is compressible or incompressible.

A rectangular parcel

As an application, we consider the motion of a fluid parcel with an instantaneous rectangular shape whose sides are parallel to the x or y axis, as depicted in Figure 6.1.2. The parcel will remain rectangular only if the fluid exhibits rigid-body motion. Under more general conditions, the parcel will deform to obtain the warped shape, drawn with the dashed line in Figure 6.1.1. However, parcel deformation does not prevent us from evaluating the integrals in (6.1.11) over the instantaneous rectangular shape.

For simplicity, we assume that the density of the fluid is uniform and the acceleration of gravity is constant over the parcel volume. We note that the unit normal vector is parallel to the x or y axis over each side, and find that equations (6.1.11) take the simpler forms

$$\begin{aligned} \int_{x_1}^{x_2} \int_{y_1}^{y_2} \left(\frac{Du_x}{Dt} - g_x \right) \rho \, dy \, dx & \quad (6.1.12) \\ & = \int_{y_1}^{y_2} [(\sigma_{xx})_{x=x_2} - (\sigma_{xx})_{x=x_1}] \, dy + \int_{x_1}^{x_2} [(\sigma_{yx})_{y=y_2} - (\sigma_{yx})_{y=y_1}] \, dx \end{aligned}$$

and

$$\begin{aligned} \int_{x_1}^{x_2} \int_{y_1}^{y_2} \left(\frac{Du_y}{Dt} - g_y \right) \rho \, dy \, dx & \quad (6.1.13) \\ & = \int_{y_1}^{y_2} [(\sigma_{xy})_{x=x_2} - (\sigma_{xy})_{x=x_1}] \, dy + \int_{x_1}^{x_2} [(\sigma_{yy})_{y=y_2} - (\sigma_{yy})_{y=y_1}] \, dx. \end{aligned}$$

The first integral on the right-hand side of (6.1.12) involves normal stresses exerted on the vertical sides; the second integral involves shear stresses exerted on the horizontal sides; the converse is true for (6.1.13).

Steady unidirectional flow

In the case of steady unidirectional flow along the x axis, point particles move along the x axis with constant velocity and vanishing acceleration, $D\mathbf{u}/Dt = 0$. Setting the left-hand side of the equation of parcel motion (6.1.10) to zero, we obtain a balance between the hydrodynamic and the body force,

$$\oint_{\text{parcel}} \mathbf{n} \cdot \boldsymbol{\sigma} \, d\ell + \iint_{\text{parcel}} \rho \mathbf{g} \, dA = \mathbf{0}. \quad (6.1.14)$$

Now restricting our attention to Newtonian fluids, we use the constitutive equation shown in Table 4.5.1 and make two key observations:

- In the absence of axial and transverse stretching, $\partial u_x/\partial x = 0$ and $\partial u_y/\partial y = 0$, the normal stresses σ_{xx} and σ_{yy} are equal to the negative of the pressure, $\sigma_{xx} = \sigma_{yy} = -p$.
- The shear stresses $\sigma_{xy} = \sigma_{yx}$ are independent of streamwise position, x , but may depend on the lateral position, y .

Subject to these simplifications, the balance equations (6.1.12) and (6.1.13) reduce to

$$\int_{y_1}^{y_2} (p_{x=x_2} - p_{x=x_1}) \, dy - [(\sigma_{yx})_{y=y_2} - (\sigma_{yx})_{y=y_1}] \Delta x = \rho g_x \Delta x \Delta y \quad (6.1.15)$$

and

$$\int_{x_1}^{x_2} (p_{y=y_2} - p_{y=y_1}) \, dx = \rho g_y \Delta x \Delta y, \quad (6.1.16)$$

where $\Delta x \equiv x_2 - x_1$ and $\Delta y = y_2 - y_1$.

Equation (6.1.16) is satisfied when

$$\frac{p_{x,y=y_2} - p_{x,y=y_1}}{\Delta y} = \rho g_y \quad (6.1.17)$$

for any x , reflecting the hydrostatic pressure variation. Equation (6.1.15) is satisfied when

$$\frac{p_{x=x_2,y} - p_{x=x_1,y}}{\Delta x} = \rho g_x - \chi \quad (6.1.18)$$

and

$$\frac{(\sigma_{yx})_{x,y=y_2} - (\sigma_{yx})_{x,y=y_1}}{\Delta y} = -\chi, \quad (6.1.19)$$

where χ is a free parameter. Physically, the constant χ is determined by the mechanism driving the flow. Three modular flow configurations can be identified, as discussed next.

Shear-driven flow

When $\chi = 0$, equation (6.1.18) shows that the pressure variation in the direction of the x axis is hydrostatic. Equation (6.1.19) shows that the shear stress σ_{yx} is constant, independent of y ,

$$(\sigma_{yx})_{x,y=y_2} - (\sigma_{yx})_{x,y=y_1} = 0. \quad (6.1.20)$$

This is the case of shear-driven flow.

Gravity-driven flow

When the streamwise pressure drop is zero, $p_{x=x_2,y} = p_{x=x_1,y}$, equation (6.1.18) requires that $\chi = \rho g_x$. Equation (6.1.19) shows that the difference in the shear stress is given by

$$(\sigma_{yx})_{x,y=y_2} - (\sigma_{yx})_{x,y=y_1} = -\rho g_x \Delta y. \quad (6.1.21)$$

This is the case of gravity-driven flow.

Pressure-driven flow

When the flow is horizontal, $g_x = 0$, equation (6.1.18) shows that χ is the negative of the streamwise pressure gradient. Equation (6.1.19) shows that the difference in the shear stress is given by

$$(\sigma_{yx})_{x,y=y_2} - (\sigma_{yx})_{x,y=y_1} = -\chi \Delta y. \quad (6.1.22)$$

This is the case of pressure-driven flow.

PROBLEM**6.1.1** *Body force in terms of a surface integral*

Show that the body force expressed by the second integral on the right-hand side of (6.1.8) can be expressed as a surface integral in the form

$$\iint_{\text{parcel}} \rho (\mathbf{g} \cdot \mathbf{x}) \mathbf{n} \, dS. \quad (6.1.23)$$

Hint: Use the Gauss divergence theorem (2.6.36).

6.2 Integral momentum balance

Consider the integrand of the rate of change of momentum on the left-hand side of equation (6.1.8). Using the rules of product differentiation and the continuity equation (2.8.5), we write

$$\rho \frac{D\mathbf{u}}{Dt} = \frac{D(\rho\mathbf{u})}{Dt} - \mathbf{u} \frac{D\rho}{Dt} = \frac{D(\rho\mathbf{u})}{Dt} + (\rho\mathbf{u})(\nabla \cdot \mathbf{u}), \quad (6.2.1)$$

where

$$\nabla \cdot \mathbf{u} \equiv \frac{\partial u_x}{\partial x} + \frac{\partial u_y}{\partial y} + \frac{\partial u_z}{\partial z} \quad (6.2.2)$$

is the divergence of the velocity expressing the rate of the expansion of the fluid. If the fluid is incompressible, the second term on the right-hand side of (6.2.1) does not appear.

The x component of the vectorial expression (6.2.1) can be manipulated to give

$$\rho \frac{Du_x}{Dt} = \frac{D(\rho u_x)}{Dt} + (\rho u_x) (\nabla \cdot \mathbf{u}) \quad (6.2.3)$$

or

$$\rho \frac{Du_x}{Dt} = \frac{\partial(\rho u_x)}{\partial t} + \mathbf{u} \cdot \nabla(\rho u_x) + (\rho u_x) (\nabla \cdot \mathbf{u}), \quad (6.2.4)$$

where the time derivative $\partial/\partial t$ is taken keeping the spatial position fixed. More explicitly,

$$\rho \frac{Du_x}{Dt} = \frac{\partial(\rho u_x)}{\partial t} + u_x \frac{\partial(\rho u_x)}{\partial x} + u_y \frac{\partial(\rho u_x)}{\partial y} + u_z \frac{\partial(\rho u_x)}{\partial z} + (\rho u_x) (\nabla \cdot \mathbf{u}). \quad (6.2.5)$$

Combining the last four terms in the last expression, we find that

$$\rho \frac{Du_x}{Dt} = \frac{\partial(\rho u_x)}{\partial t} + \frac{\partial(\rho u_x u_x)}{\partial x} + \frac{\partial(\rho u_y u_x)}{\partial y} + \frac{\partial(\rho u_z u_x)}{\partial z}. \quad (6.2.6)$$

This expression applies to incompressible as well as compressible fluids.

Working in a similar fashion with the y and z components of (6.2.1), we derive the corresponding expressions

$$\rho \frac{Du_y}{Dt} = \frac{\partial(\rho u_y)}{\partial t} + \frac{\partial(\rho u_x u_y)}{\partial x} + \frac{\partial(\rho u_y u_y)}{\partial y} + \frac{\partial(\rho u_z u_y)}{\partial z} \quad (6.2.7)$$

and

$$\rho \frac{Du_z}{Dt} = \frac{\partial(\rho u_z)}{\partial t} + \frac{\partial(\rho u_x u_z)}{\partial x} + \frac{\partial(\rho u_y u_z)}{\partial y} + \frac{\partial(\rho u_z u_z)}{\partial z}. \quad (6.2.8)$$

These expressions hold true for incompressible as well as compressible fluids.

Momentum tensor

To recast equations (6.2.6)–(6.2.8) into a unified form, we introduce the momentum tensor, M_{ij} , defined as

$$M_{ij} \equiv \rho u_i u_j, \quad (6.2.9)$$

where the indices i and j range over x , y , and z or, correspondingly, 1, 2, and 3. In vector notation, we write

$$\mathbf{M} = \rho \mathbf{u} \otimes \mathbf{u}, \quad (6.2.10)$$

where the symbol \otimes denotes the tensor product. It is evident from the definition (6.2.9) that the tensor \mathbf{M} is symmetric,

$$M_{ij} = M_{ji}. \quad (6.2.11)$$

Explicitly, the momentum tensor is given by

$$\mathbf{M} = \rho \begin{bmatrix} u_x^2 & u_x u_y & u_x u_z \\ u_y u_x & u_y^2 & u_y u_z \\ u_z u_x & u_z u_y & u_z^2 \end{bmatrix}. \quad (6.2.12)$$

Next, we introduce the divergence of the momentum tensor defined as a vector whose i th component is given by

$$(\nabla \cdot \mathbf{M})_i = \frac{\partial M_{ji}}{\partial x_j} = \frac{\partial M_{ij}}{\partial x_j}, \quad (6.2.13)$$

where summation is implied over the repeated index j . For example, the x component of the divergence of \mathbf{M} is

$$(\nabla \cdot \mathbf{M})_x = \frac{\partial M_{jx}}{\partial x_j} = \frac{\partial M_{xx}}{\partial x} + \frac{\partial M_{yx}}{\partial y} + \frac{\partial M_{zx}}{\partial z}. \quad (6.2.14)$$

Subject to these definitions, equations (6.2.6)–(6.2.8) can be compiled into the form

$$\rho \frac{D u_i}{D t} = \frac{\partial(\rho u_i)}{\partial t} + \frac{\partial M_{ji}}{\partial x_j} \quad (6.2.15)$$

for $i = x, y, z$. The corresponding vector form is

$$\rho \frac{D \mathbf{u}}{D t} = \frac{\partial(\rho \mathbf{u})}{\partial t} + \nabla \cdot \mathbf{M}. \quad (6.2.16)$$

The right-hand sides of equations (6.2.15) and (6.2.16) involve Eulerian derivatives; that is, derivatives with respect to time and spatial coordinates.

Equation of parcel motion

Substituting (6.2.16) into the left-hand side of the equation of parcel motion (6.1.8), we derive the alternative form

$$\iiint_{\text{parcel}} \left(\frac{\partial(\rho \mathbf{u})}{\partial t} + \nabla \cdot \mathbf{M} \right) dV = \iint_{\text{parcel}} \mathbf{n} \cdot \boldsymbol{\sigma} dS + \iiint_{\text{parcel}} \rho \mathbf{g} dV. \quad (6.2.17)$$

We can use the Gauss divergence theorem stated in equation (2.6.36) to convert the volume integral of the divergence of the momentum tensor into a surface integral over the parcel volume, obtaining

$$\iiint_{\text{parcel}} \frac{\partial(\rho \mathbf{u})}{\partial t} dV + \iint_{\text{parcel}} \mathbf{n} \cdot \mathbf{M} dS = \iint_{\text{parcel}} \mathbf{n} \cdot \boldsymbol{\sigma} dS + \iiint_{\text{parcel}} \rho \mathbf{g} dV, \quad (6.2.18)$$

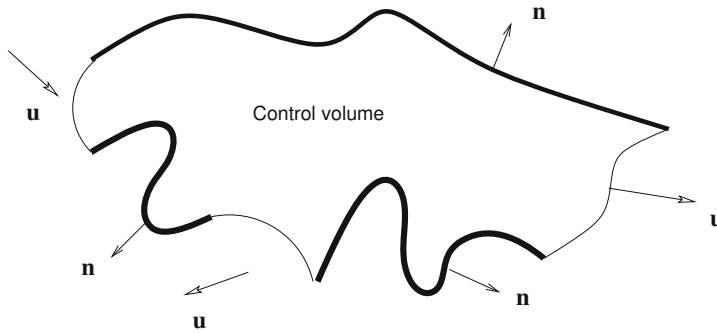


Figure 6.2.1 Illustration of a stationary control volume (cv) in a flow bounded by solid or fluid surfaces.

where the unit normal vector, \mathbf{n} , points outward from the parcel. In index notation,

$$\iiint_{\text{parcel}} \frac{\partial(\rho u_i)}{\partial t} dV + \iint_{\text{parcel}} n_j M_{ji} dS = \iint_{\text{parcel}} n_j \sigma_{ji} dS + \iiint_{\text{parcel}} \rho g_i dV \quad (6.2.19)$$

for $i = x, y, z$, where summation is implied over the repeated index j .

6.2.1 Control volume and integral momentum balance

It is important to bear in mind that equation (6.2.19) originates from Newton's second law of motion applied to a fluid parcel. In the process of expressing the material derivative in terms of Eulerian derivatives taken with respect to time and position in space, the parcel has lost its significance as a material body and became relevant only insofar as to define the volume it occupies in space at any instant.

To emphasize the new interpretation, we rewrite the integral momentum balance (6.2.19) in identical form, except that the volume of integration is now regarded as a control volume (cv), as shown in [Figure 6.2.1](#).

Using the definition of the momentum tensor shown in (6.2.9), we express the integral momentum balance in the form

$$\iiint_{\text{cv}} \frac{\partial(\rho u_i)}{\partial t} dV + \iint_{\text{cv}} \rho u_i u_n dS = \iint_{\text{cv}} n_j \sigma_{ji} dS + \iiint_{\text{cv}} \rho g_i dV, \quad (6.2.20)$$

where $i = x, y, z$ is a free index, summation is implied over the repeated index, j , and

$$u_n \equiv \mathbf{u} \cdot \mathbf{n} = u_j n_j \quad (6.2.21)$$

is the normal component of the fluid velocity. Equation (6.2.20) expresses an *integral momentum balance*, well known to chemical engineers and others in the framework of transport phenomena.

Accumulation, convection, boundary and homogeneous forcing

The four integrals on the left- and right-hand sides of (6.2.20) admit the following interpretation with regard to the underlying control volume:

1. The first integral is the rate of change of the i th component of momentum of the fluid residing inside the control volume. At steady state, this term vanishes.
2. The scalar $n_j u_j = \mathbf{n} \cdot \mathbf{u}$ in the second integrand on the left-hand side is the component of the fluid velocity normal to the boundary of the control volume. The corresponding integral expresses the rate of convective transport of the i th component of the fluid momentum across the boundary of the control volume.
3. The first integral on the right-hand side is the i th component of the surface force exerted on the boundary of the control volume.
4. The second integral on the right-hand side is the i th component of the body force exerted on the control volume.

It is important to bear in mind that the integral momentum balance has been derived in Cartesian coordinates. Every term must be rederived when working in polar or other curvilinear coordinates.

Vector form of the integral momentum balance

In vector notation, the integral momentum balance takes the form

$$\iiint_{cv} \frac{\partial(\rho \mathbf{u})}{\partial t} dV + \iint_{cv} \rho \mathbf{n} \cdot (\mathbf{u} \otimes \mathbf{u}) dS = \iint_{cv} \mathbf{n} \cdot \boldsymbol{\sigma} dS + \iiint_{cv} \rho \mathbf{g} dV. \quad (6.2.22)$$

The second integral on the left-hand side is given by

$$\iint_{cv} \rho \mathbf{n} \cdot (\mathbf{u} \otimes \mathbf{u}) dS = \iint_{cv} (\rho \mathbf{u}) u_n dS, \quad (6.2.23)$$

where $u_n = \mathbf{n} \cdot \mathbf{u}$ is the normal velocity and the symbol \otimes denotes the tensor product.

Stress-momentum tensor

Combining the second integral on the left-hand side with the first integral on the right-hand side of (6.2.22), we obtain the more compact form

$$\iiint_{cv} \frac{\partial(\rho \mathbf{u})}{\partial t} dV = \iint_{cv} \mathbf{n} \cdot \boldsymbol{\tau} dS + \iiint_{cv} \rho \mathbf{g} dV, \quad (6.2.24)$$

where

$$\boldsymbol{\tau} \equiv \boldsymbol{\sigma} - \rho \mathbf{u} \otimes \mathbf{u} \quad (6.2.25)$$

is the stress-momentum tensor with components $\tau_{ij} = \sigma_{ij} - \rho u_i u_j$.

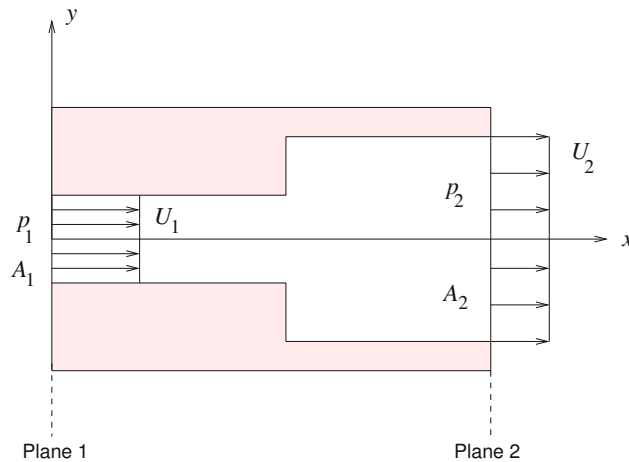


Figure 6.2.1 Simplified model of flow through a duct with a sudden enlargement. An integral momentum balance allows us to compute the rise in pressure, $p_2 - p_1$, in terms of the inlet and outlet cross-sectional areas, A_1 and A_2 .

Applications in engineering analysis

Equation (6.2.24) expresses an integral momentum balance that can be interpreted as an integral evolution equation or conservation law applied to a chosen control volume. The solution of practical engineering problems by the use of integral mass, momentum, and energy balances is discussed in a classical text by Bird, Stewart and Lightfoot.¹ Illustrative examples are presented in the remainder of this section.

6.2.2 Flow through a sudden enlargement

To demonstrate the usefulness of the integral momentum balance in engineering analysis, we consider steady flow through a duct with a sudden enlargement, as illustrated in [Figure 6.2.1](#).

We begin by introducing a control volume identified with the section of the duct confined between the vertical planes labeled 1 and 2, and assume that the density of the fluid is uniform and the velocity profile is flat at the inlet and outlet. The cross-sectional areas at the inlet and outlet are denoted as A_1 and A_2 .

Neglecting the shear stress at the walls, approximating the normal stress at the inlet and outlet with the negative of the pressure, assuming that the pressure at the washer-shaped area is equal to the inlet pressure, and considering the effects of gravity insignificant, we find that the x component of the integral momentum balance (6.2.20) at steady state simplifies

¹Bird, R. B., Stewart, W. E. & Lightfoot, E. N. (2006) *Transport Phenomena*, Second Edition, Wiley.

into

$$\rho U_2^2 A_2 - \rho U_1^2 A_1 = -p_2 A_2 + p_1 A_1 + p_1 (A_2 - A_1). \quad (6.2.26)$$

The three terms on the right-hand side of (6.2.26) are approximations to the first integral on the right-hand side of (6.2.20) for the outlet, washer-shaped area, and inlet. Mass conservation requires that

$$U_1 A_1 = U_2 A_2. \quad (6.2.27)$$

Solving for U_1 and substituting the result into (6.2.26), we derive the desired expression for the pressure difference,

$$p_2 - p_1 = (\beta - 1) \rho U_2^2, \quad (6.2.28)$$

where $\beta = A_2/A_1$ is the area ratio, which predicts a rise in pressure for $\beta > 1$, in agreement with laboratory observations.

6.2.3 Isentropic flow through a conduit

In a second application, we consider the flow of a compressible fluid through a conduit with variable cross-sectional area, A . A mass balance over a control volume confined between two cross-sections labeled 1 and 2 requires that

$$\rho_1 U_1 A_1 = \rho_2 U_2 A_2. \quad (6.2.29)$$

The counterpart of equation (6.2.26) is

$$\rho_2 U_2^2 A_2 - \rho_1 U_1^2 A_1 = -p_2 A_2 + p_1 A_1 - D_x, \quad (6.2.30)$$

where D_x is the drag force due to wall friction. In the case of isentropic flow, we use equation (4.7.23) and find that

$$\frac{p_1}{\rho_1^k} = \frac{p_2}{\rho_2^k} \quad (6.2.31)$$

where $k \equiv c_p/c_v$ is the ratio of two heat capacities. The last three equations can be used to compute p_2 , U_2 , and D_x , from knowledge of p_1 , ρ_1 , and U_1 .

Energetics

Energy conservation under adiabatic conditions requires that

$$h_1 + \frac{1}{2} U_1^2 + g y_1 = h_2 + \frac{1}{2} U_2^2 + g y_2, \quad (6.2.32)$$

where h is the specific enthalpy and y is the vertical position of the conduit centerline. In terms of the heat capacity under constant pressure, $h = c_p T$, yielding

$$c_p T_1 + \frac{1}{2} U_1^2 + g y_1 = c_p T_2 + \frac{1}{2} U_2^2 + g y_2, \quad (6.2.33)$$

where T is the absolute temperature. This equation relates the velocity to the temperature to the elevation of the conduit centerline at two stations.

Stagnation-point temperature

At a stagnation point, $U_2 = 0$. Equation (6.2.33) with $y_1 = y_2$ and $U \equiv U_1$, $T \equiv T_1$, $T_2 \equiv T_{\text{sp}}$ yields

$$T_{\text{sp}} - T = \frac{1}{2} \frac{U_1^2}{c_p} = \frac{1}{2} \frac{k-1}{k} \frac{U^2}{R} \quad (6.2.34)$$

or

$$T_{\text{sp}} - T = \frac{1}{2} (k-1) \frac{U^2}{c^2} T, \quad (6.2.35)$$

where c is the speed of sound given in (4.7.27). Rearranging, we derive an expression for the stagnation-point temperature,

$$\frac{T_{\text{sp}} - T}{T} = \frac{1}{2} (k-1) M^2, \quad (6.2.36)$$

where

$$M \equiv \frac{U}{c} \quad (6.2.37)$$

is the Mach number. Using the equation of state for isentropic conditions, we obtain

$$\frac{p_2}{p_1} = \left(\frac{1}{2} (k-1) M^2 + 1 \right)^{k/(k-1)}. \quad (6.2.38)$$

For sufficiently small Mach numbers,

$$\frac{p_2}{p_1} \simeq 1 + \frac{1}{2} k M^2, \quad (6.2.39)$$

providing us with a convenient expression for the pressure ratio.

PROBLEM

6.2.1 Pressure rise in an ejector pump

A schematic illustration of an ejector pump is shown in [Figure 6.2.2](#). At plane 1, two fluid streams merge: the first stream with uniform velocity U_1 over a cross-sectional area A_1 , and the second stream with uniform velocity U_0 over a cross sectional area A_0 . At plane 2, the velocity profile is uniform over the cross-sectional area $A_2 = A_0 + A_1$. The pressure is assumed to be uniform over the cross-section of the inlet and outlet, respectively, equal to p_1 and p_2 . The fluid density is assumed to be uniform throughout the flow. Derive an expression for the rise in pressure, $p_2 - p_1$, in terms of ρ , U_0 , U_1 , A_0 , and A_1 , similar to that shown in equation (6.2.28).

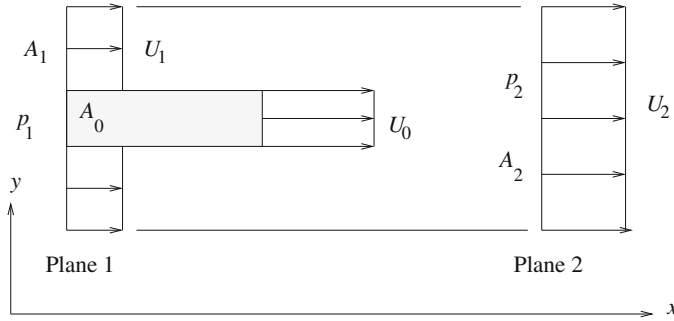


Figure 6.2.2 Schematic illustration of an ejector pump. The pressure rise between the inlet and outlet, $p_2 - p_1$, can be estimated by performing an integral momentum balance.

6.3 Cauchy's equation of motion

Equation (6.1.8), repeated below for convenience,

$$\iiint_{\text{parcel}} \frac{D\mathbf{u}}{Dt} \rho \, dV = \iint_{\text{parcel}} \mathbf{n} \cdot \boldsymbol{\sigma} \, dS + \iiint_{\text{parcel}} \rho \mathbf{g} \, dV, \tag{6.3.1}$$

contains one surface integral involving the traction over the boundary of a fluid parcel, and two volume integrals involving the point particle acceleration and the body force.

If we could manage to convert the surface integral into a volume integral, we would be able to collect all integrands into a unified integrand. Since the shape and volume of the parcel is arbitrary, the unified integrand would have to be identically zero, providing us with a differential equation.

6.3.1 Hydrodynamic volume force

Transforming the surface integral of the traction into a volume integral can be done using once again the Gauss divergence theorem stated in equation (2.6.36). Identifying the vector \mathbf{h} with each one of the three columns of the stress tensor, we obtain

$$\iint_{\text{parcel}} \mathbf{n} \cdot \boldsymbol{\sigma} \, dS = \iiint_{\text{parcel}} \nabla \cdot \boldsymbol{\sigma} \, dV. \tag{6.3.2}$$

In index notation, the i th component of this equation is

$$\iint_{\text{parcel}} n_j \sigma_{ji} \, dS = \iiint_{\text{parcel}} \frac{\partial \sigma_{ji}}{\partial x_j} \, dV, \tag{6.3.3}$$

where summation of the repeated index j is implied.

The divergence of the stress tensor under the integral sign on the right-hand side of (6.3.2) is a vector denoted by

$$\boldsymbol{\Sigma} \equiv \nabla \cdot \boldsymbol{\sigma}, \tag{6.3.4}$$

with Cartesian components

$$\begin{aligned}\Sigma_x &= \frac{\partial\sigma_{xx}}{\partial x} + \frac{\partial\sigma_{yx}}{\partial y} + \frac{\partial\sigma_{zx}}{\partial z}, & \Sigma_y &= \frac{\partial\sigma_{xy}}{\partial x} + \frac{\partial\sigma_{yy}}{\partial y} + \frac{\partial\sigma_{zy}}{\partial z}, \\ \Sigma_z &= \frac{\partial\sigma_{xz}}{\partial x} + \frac{\partial\sigma_{yz}}{\partial y} + \frac{\partial\sigma_{zz}}{\partial z}.\end{aligned}\tag{6.3.5}$$

Physically, the vector Σ is the hydrodynamic force per differential volume of fluid; in contrast, the traction \mathbf{f} is the hydrodynamic force per differential surface area of fluid.

6.3.2 Hydrodynamic force on an infinitesimal parcel

To confirm identity (6.3.3), we consider a small fluid parcel in the shape of a rectangular parallelepiped centered at the origin, as illustrated in [Figure 5.1.1\(b\)](#). The six flat sides of the parcel are perpendicular to the x , y , or z axis, the lengths of the three edges are equal to Δx , Δy , and Δz , and the volume of the parcel is equal to $\Delta V = \Delta x \Delta y \Delta z$.

Consider the surface integral on the left-hand side of equation (6.3.3). Over the sides that are perpendicular to the x axis, located at $x = \pm \frac{\Delta x}{2}$, designated as the *first* or *second* side, the unit normal vector is parallel to the x axis; over the first side $n_x = 1$, and over the second side $n_x = -1$. Because the size of the parcel is small, the stresses over each side can be approximated with corresponding values at the center-point.

Subject to this approximation, the surface integral on the left-hand side over the first side takes the form

$$\mathcal{F}_1 \equiv \sigma_{xi}(x = \frac{1}{2} \Delta x, y = 0, z = 0) \Delta y \Delta z,\tag{6.3.6}$$

while the surface integral over the second side takes the form

$$\mathcal{F}_2 \equiv -\sigma_{xi}(x = -\frac{1}{2} \Delta x, y = 0, z = 0) \Delta y \Delta z\tag{6.3.7}$$

for $i = x, y, z$, where the parentheses enclose the coordinates of the evaluation point.

Adding these two contributions and factoring out the common product $\Delta y \Delta z$ expressing the surface area, we obtain

$$\mathcal{F}_1 + \mathcal{F}_2 = \left(\sigma_{xi}(x = \frac{1}{2} \Delta x, y = 0, z = 0) - \sigma_{xi}(x = -\frac{1}{2} \Delta x, y = 0, z = 0) \right) \Delta y \Delta z.\tag{6.3.8}$$

Next, we observe that, in the limit as Δx tends to zero, the ratio of the differences

$$\begin{aligned}& \frac{\sigma_{xi}(x = \frac{\Delta x}{2}, y = 0, z = 0) - \sigma_{xi}(x = -\frac{\Delta x}{2}, y = 0, z = 0)}{\frac{\Delta x}{2} - (-\frac{\Delta x}{2})} \\ &= \frac{\sigma_{xi}(x = \frac{\Delta x}{2}, y = 0, z = 0) - \sigma_{xi}(x = -\frac{\Delta x}{2}, y = 0, z = 0)}{\Delta x}\end{aligned}\tag{6.3.9}$$

tends to the partial derivative $\partial\sigma_{xi}/\partial x$ evaluated at the origin. Correspondingly, the difference (6.3.8) reduces to

$$\frac{\partial\sigma_{xi}}{\partial x} \Delta x \Delta y \Delta z = \frac{\partial\sigma_{xi}}{\partial x} \Delta V, \quad (6.3.10)$$

where the derivatives are evaluated at the origin.

Working in a similar fashion with pairs of sides that are perpendicular to the y or z axis, and summing the three contributions, we find that the left-hand side of (6.3.3) takes the approximate form

$$\left(\frac{\partial\sigma_{xi}}{\partial x} + \frac{\partial\sigma_{yi}}{\partial y} + \frac{\partial\sigma_{zi}}{\partial z} \right) \Delta V, \quad (6.3.11)$$

where the quantity enclosed by the parentheses is evaluated at the origin. Expression (6.3.11) is an approximation to the volume integral on the right-hand side of (6.3.3).

6.3.3 The equation of motion

Substituting (6.3.2) into (6.1.8), consolidating various terms, and noting that, since the volume of integration is arbitrary, the combined integrand must vanish, we obtain Cauchy's differential equation governing the motion of an incompressible or compressible fluid,

$$\rho \frac{D\mathbf{u}}{Dt} = \nabla \cdot \boldsymbol{\sigma} + \rho \mathbf{g}. \quad (6.3.12)$$

In index notation,

$$\rho \frac{Du_i}{Dt} = \frac{\partial\sigma_{ji}}{\partial x_j} + \rho g_i, \quad (6.3.13)$$

where summation over the repeated index j is implied on the right-hand side, while the index i is free to vary over x , y , or z .

In terms of the point particle acceleration, \mathbf{a} , and the hydrodynamic volume force $\boldsymbol{\Sigma} \equiv \nabla \cdot \boldsymbol{\sigma}$ defined in (6.3.4), Cauchy's equation of motion takes the simple form

$$\rho \mathbf{a} = \boldsymbol{\Sigma} + \rho \mathbf{g} \quad (6.3.14)$$

for an incompressible or compressible fluid.

Eulerian form

Using equations (2.8.11) and (6.2.16), we derive two alternative forms of (6.3.12) involving derivatives with respect to time and position in space,

$$\rho \left(\frac{\partial \mathbf{u}}{\partial t} + \mathbf{u} \cdot \nabla \mathbf{u} \right) = \nabla \cdot \boldsymbol{\sigma} + \rho \mathbf{g} \quad (6.3.15)$$

$$\begin{aligned} \rho \left(\frac{\partial u_x}{\partial t} + u_x \frac{\partial u_x}{\partial x} + u_y \frac{\partial u_x}{\partial y} + u_z \frac{\partial u_x}{\partial z} \right) &= \frac{\partial \sigma_{xx}}{\partial x} + \frac{\partial \sigma_{yx}}{\partial y} + \frac{\partial \sigma_{zx}}{\partial z} + \rho g_x \\ \rho \left(\frac{\partial u_y}{\partial t} + u_x \frac{\partial u_y}{\partial x} + u_y \frac{\partial u_y}{\partial y} + u_z \frac{\partial u_y}{\partial z} \right) &= \frac{\partial \sigma_{xy}}{\partial x} + \frac{\partial \sigma_{yy}}{\partial y} + \frac{\partial \sigma_{zy}}{\partial z} + \rho g_y \\ \rho \left(\frac{\partial u_z}{\partial t} + u_x \frac{\partial u_z}{\partial x} + u_y \frac{\partial u_z}{\partial y} + u_z \frac{\partial u_z}{\partial z} \right) &= \frac{\partial \sigma_{xz}}{\partial x} + \frac{\partial \sigma_{yz}}{\partial y} + \frac{\partial \sigma_{zz}}{\partial z} + \rho g_z \end{aligned}$$

Table 6.3.1 The Cartesian components of the equation of motion involving the point particle momentum, the hydrodynamic volume force, and the body force.

and

$$\frac{\partial(\rho \mathbf{u})}{\partial t} + \nabla \cdot (\rho \mathbf{u} \otimes \mathbf{u}) = \nabla \cdot \boldsymbol{\sigma} + \rho \mathbf{g}. \quad (6.3.16)$$

Both equations apply for incompressible as well as compressible fluids.

Explicitly, the three scalar components of (6.3.15) are given in [Table 6.3.1](#). The terms enclosed by the parentheses on the left-hand sides are the Cartesian components of the point particle acceleration. The right-hand sides include the Cartesian components of the volume force due to the hydrodynamic stresses and the components of the body force.

6.3.4 Evolution equations

Given the instantaneous velocity and stress fields, \mathbf{u} and $\boldsymbol{\sigma}$, we can evaluate the right-hand sides of (6.3.12) and (6.3.15), as well as the second term on the left-hand side of (6.3.15), and thereby compute the rates of change $D\mathbf{u}/Dt$ and $\partial\mathbf{u}/\partial t$. This observation suggests that the equation of motion (6.3.12) is, in fact, an evolution equation for the point particle velocity, whereas equation (6.3.15) is an evolution equation for the velocity at a fixed point in the flow.

A similar evolution equation for the density was derived in Chapter 2 on the basis of the continuity equation, as shown in (2.7.28). The evolution equations for the density and velocity originate from two fundamental physical laws: mass conservation, and Newton's second law of motion for a deformable medium.

6.3.5 Cylindrical polar coordinates

In the cylindrical polar coordinates defined in [Figure 1.3.2](#), the hydrodynamic volume force defined in equation (6.3.4) is resolved into corresponding components,

$$\boldsymbol{\Sigma} = \Sigma_x \mathbf{e}_x + \Sigma_\sigma \mathbf{e}_\sigma + \Sigma_\varphi \mathbf{e}_\varphi. \quad (6.3.17)$$

(a)

$$\Sigma_x = \frac{\partial \sigma_{xx}}{\partial x} + \frac{1}{\sigma} \frac{\partial(\sigma \sigma_{\sigma x})}{\partial \sigma} + \frac{1}{\sigma} \frac{\partial \sigma_{\varphi x}}{\partial \varphi}, \quad \Sigma_\sigma = \frac{\partial \sigma_{x\sigma}}{\partial x} + \frac{1}{\sigma} \frac{\partial(\sigma \sigma_{\sigma\sigma})}{\partial \sigma} + \frac{1}{\sigma} \frac{\partial \sigma_{\varphi\sigma}}{\partial \varphi} - \frac{1}{\sigma} \sigma_{\varphi\varphi}$$

$$\Sigma_\varphi = \frac{\partial \sigma_{x\varphi}}{\partial x} + \frac{1}{\sigma^2} \frac{\partial(\sigma^2 \sigma_{\varphi\sigma})}{\partial \sigma} + \frac{1}{\sigma} \frac{\partial \sigma_{\varphi\varphi}}{\partial \varphi}$$

(b)

$$\Sigma_r = \frac{1}{r^2} \frac{\partial(r^2 \sigma_{rr})}{\partial r} + \frac{1}{r \sin \theta} \frac{\partial(\sigma_{r\theta} \sin \theta)}{\partial \theta} + \frac{1}{r \sin \theta} \frac{\partial \sigma_{\varphi r}}{\partial \varphi} - \frac{\sigma_{\theta\theta} + \sigma_{\varphi\varphi}}{r}$$

$$\Sigma_\theta = \frac{1}{r^2} \frac{\partial(r^2 \sigma_{r\theta})}{\partial r} + \frac{1}{r \sin \theta} \frac{\partial(\sigma_{\theta\theta} \sin \theta)}{\partial \theta} + \frac{1}{r \sin \theta} \frac{\partial \sigma_{\varphi\theta}}{\partial \varphi} + \frac{\sigma_{r\theta} - \sigma_{\varphi\varphi} \cot \theta}{r}$$

$$\Sigma_\varphi = \frac{1}{r^2} \frac{\partial(r^2 \sigma_{r\varphi})}{\partial r} + \frac{1}{r} \frac{\partial \sigma_{\theta\varphi}}{\partial \theta} + \frac{1}{r \sin \theta} \frac{\partial \sigma_{\varphi\varphi}}{\partial \varphi} + \frac{\sigma_{r\varphi} + 2 \sigma_{\theta\varphi} \cot \theta}{r}$$

(c)

$$\Sigma_r = \frac{1}{r} \frac{\partial(r \sigma_{rr})}{\partial r} + \frac{1}{r} \frac{\partial \sigma_{\theta r}}{\partial \theta} - \frac{1}{r} \sigma_{\theta\theta}, \quad \Sigma_\theta = \frac{1}{r^2} \frac{\partial(r^2 \sigma_{r\theta})}{\partial r} + \frac{1}{r} \frac{\partial \sigma_{\theta\theta}}{\partial \theta}$$

Table 6.3.2 Components of the hydrodynamic volume force in terms of corresponding stress components in (a) cylindrical, (b) spherical, and (c) plane polar coordinates.

Using the rules of coordinate transformation and the chain rule of differentiation, we derive the expressions shown in [Table 6.3.2\(a\)](#).

Equation of motion

The cylindrical polar components of the equation of motion are

$$\rho a_x = \Sigma_x + \rho g_x, \quad \rho a_\sigma = \Sigma_\sigma + \rho g_\sigma, \quad \rho a_\varphi = \Sigma_\varphi + \rho g_\varphi, \quad (6.3.18)$$

where a_x , a_σ , and a_φ are the cylindrical polar components of the point particle acceleration given in equations (2.8.16). Using the alternative expressions (2.8.17), we obtain

$$\rho \frac{Du_x}{Dt} = \Sigma_x + \rho g_x, \quad \rho \frac{Du_\sigma}{Dt} = \rho \frac{u_\varphi^2}{\sigma} + \Sigma_\sigma + \rho g_\sigma,$$

$$\rho \frac{Du_\varphi}{Dt} = -\rho \frac{u_\sigma u_\varphi}{\sigma} + \Sigma_\varphi + \rho g_\varphi. \quad (6.3.19)$$

These equations apply for incompressible as well as compressible fluids.

Centrifugal force

The first term on the right-hand side of the second equation in (6.3.19), $\rho u_\varphi^2/\sigma$, expresses an effective volume force in the radial (σ) direction due to fluid motion in the azimuthal (φ) direction, known as the centrifugal force. A centrifugal force arises in the flow generated by the rotation of a solid circular cylinder about its axis in a viscous liquid, as will be discussed in Section 7.5.

Coriolis force

The negative of the first term on the right-hand side of third equation in (6.3.19), $\rho u_\sigma u_\varphi/\sigma$, expresses an effective force in the azimuthal (φ) direction, known as the Coriolis force, arising when flow occurs in both the σ and φ directions. A Coriolis force is established in the flow due to a spinning circular disk immersed in a liquid.

6.3.6 Spherical polar coordinates

In the spherical polar coordinates defined in Figure 1.3.3, the hydrodynamic volume force defined in equation (6.3.4) is described as

$$\Sigma = \Sigma_r \mathbf{e}_r + \Sigma_\theta \mathbf{e}_\theta + \Sigma_\varphi \mathbf{e}_\varphi. \quad (6.3.20)$$

Using the rules of coordinate transformation and the chain rule of differentiation, we derive the expressions shown in Table 6.3.2(b).

The spherical polar components of the equation of motion are

$$\rho a_r = \Sigma_r + \rho g_r, \quad \rho a_\theta = \Sigma_\theta + \rho g_\theta, \quad \rho a_\varphi = \Sigma_\varphi + \rho g_\varphi, \quad (6.3.21)$$

where a_r , a_θ , and a_φ are the spherical polar components of the point particle acceleration given in (2.8.19).

6.3.7 Plane polar coordinates

In the plane polar coordinates defined in Figure 1.3.4, the hydrodynamic volume force defined in equation (6.3.4) is described as

$$\Sigma = \Sigma_r \mathbf{e}_r + \Sigma_\theta \mathbf{e}_\theta. \quad (6.3.22)$$

Using the coordinate transformation rules and the chain rule of differentiation, we derive the expressions shown in table 6.3.2(c).

The plane polar components of the equation of motion are

$$\rho a_r = \Sigma_r + \rho g_r, \quad \rho a_\theta = \Sigma_\theta + \rho g_\theta, \quad (6.3.23)$$

where a_r and a_θ are the plane polar components of the point particle acceleration given by the expressions in (2.8.22). Alternative expressions are

$$\rho \frac{Du_r}{Dt} = \rho \frac{u_\theta^2}{r} + \Sigma_r + \rho g_r, \quad \rho \frac{Du_\theta}{Dt} = -\rho \frac{u_r u_\theta}{r} + \Sigma_\theta + \rho g_\theta, \quad (6.3.24)$$

involving, respectively, the centrifugal force and the negative of the Coriolis force on the right-hand sides, where D/Dt is the material derivative.

6.3.8 Vortex force

Returning to equation (6.3.15), we use identity (2.8.29),

$$\mathbf{u} \cdot \nabla \mathbf{u} = \frac{1}{2} \nabla u^2 - \mathbf{u} \times \boldsymbol{\omega}, \quad (6.3.25)$$

and obtain an alternative form of the equation of motion,

$$\rho \left(\frac{\partial \mathbf{u}}{\partial t} + \frac{1}{2} \nabla u^2 + \boldsymbol{\omega} \times \mathbf{u} \right) = \nabla \cdot \boldsymbol{\sigma} + \rho \mathbf{g}, \quad (6.3.26)$$

where

$$u^2 \equiv u_x^2 + u_y^2 + u_z^2 \quad (6.3.27)$$

is the square of the magnitude of the velocity. The third term on the left-hand side of (6.3.26),

$$\rho \boldsymbol{\omega} \times \mathbf{u}, \quad (6.3.28)$$

represents a vortex force established when the vorticity vector is not parallel to the velocity vector; otherwise, their cross product is identically zero. In a Beltrami flow, the vorticity vector is parallel to the velocity vector at every point and the vortex force is identically zero.

6.3.9 Summary of governing equation

In summary, the flow of an incompressible or compressible fluid is governed by the continuity equation (2.7.13),

$$\frac{\partial \rho}{\partial t} + \nabla \cdot (\rho \mathbf{u}) = 0, \quad (6.3.29)$$

and Cauchy's equation of motion expressed by (6.3.15) or (6.3.16). The Cauchy stress tensor is defined in terms of the velocity and the pressure by means of a constitutive equation, as discussed in Chapter 4. The five unknowns include the three velocity components, u_x , u_y , u_z , the density, ρ , and the pressure, p .

The continuity equation and the three components of the equation of motion provide us with four equations. In the case of incompressible fluids, a fifth equation is provided by the idealized incompressibility condition, $D\rho/Dt = 0$. In the case of compressible fluids, a fifth equation relating the density to the pressure is provided by thermodynamics, as shown in (4.7.23) for isentropic flow.

6.3.10 Accelerating frame of reference

The equation of motion is valid for a stationary frame of reference where Newton's second law of motion applies. Suppose that the Cartesian axes translate with velocity $\mathbf{V}(t)$ in the absence of rotation. The point particle acceleration in the stationary frame is

$$\mathbf{a}^{\text{stationary}} = \mathbf{a} + \frac{d\mathbf{V}}{dt}. \quad (6.3.30)$$

Substituting this expression in the equation of motion (6.3.14) and rearranging, we derive the equation

$$\rho \mathbf{a} = \boldsymbol{\Sigma} + \rho \mathbf{g} - \rho \frac{d\mathbf{V}}{dt}. \quad (6.3.31)$$

The last term on the right-hand side represents a fictitious inertial acceleration force. A more general equation can be written to describe fluid motion in a frame of reference that undergoes simultaneous steady or unsteady translation and rotation.²

PROBLEMS

6.3.1 Beltrami flow

Explain why a two-dimensional or axisymmetric flow cannot be a Beltrami flow.

6.3.2 Free fall

A bucket of fluid is moving in free gravitational fall. Write the equation of motion in a frame of reference attached to the bucket.

6.4 Euler and Bernoulli equations

Euler's equation arises from the equation of motion (6.3.12) by substituting the simplest possible constitutive equation for the stress tensor describing an ideal fluid, expressed by equation (4.6.19). Considering the individual components of the volume force $\boldsymbol{\Sigma}$ given in (6.3.5), we obtain

$$\boldsymbol{\Sigma} \equiv \nabla \cdot \boldsymbol{\sigma} = -\nabla p, \quad (6.4.1)$$

that is,

$$\boldsymbol{\Sigma} = -\frac{\partial p}{\partial x} \mathbf{e}_x - \frac{\partial p}{\partial y} \mathbf{e}_y - \frac{\partial p}{\partial z} \mathbf{e}_z, \quad (6.4.2)$$

where p is the pressure. Cauchy's equation of motion (6.3.12) then reduces to Euler's equation of motion,

$$\rho \frac{D\mathbf{u}}{Dt} = -\nabla p + \rho \mathbf{g}. \quad (6.4.3)$$

²Pozrikidis, C. (2011) *Introduction to Theoretical and Computational Fluid Dynamics*, Second Edition, Oxford University Press.

$$\begin{aligned}\rho \left(\frac{\partial u_x}{\partial t} + u_x \frac{\partial u_x}{\partial x} + u_y \frac{\partial u_x}{\partial y} + u_z \frac{\partial u_x}{\partial z} \right) &= -\frac{\partial p}{\partial x} + \rho g_x \\ \rho \left(\frac{\partial u_y}{\partial t} + u_x \frac{\partial u_y}{\partial x} + u_y \frac{\partial u_y}{\partial y} + u_z \frac{\partial u_y}{\partial z} \right) &= -\frac{\partial p}{\partial y} + \rho g_y \\ \rho \left(\frac{\partial u_z}{\partial t} + u_x \frac{\partial u_z}{\partial x} + u_y \frac{\partial u_z}{\partial y} + u_z \frac{\partial u_z}{\partial z} \right) &= -\frac{\partial p}{\partial z} + \rho g_z\end{aligned}$$

Table 6.4.1 The three Cartesian components of Euler's equation describing the motion of a fluid in the absence of viscous forces.

The associated Eulerian form is

$$\rho \left(\frac{\partial \mathbf{u}}{\partial t} + \mathbf{u} \cdot \nabla \mathbf{u} \right) = -\nabla p + \rho \mathbf{g}. \quad (6.4.4)$$

The three Cartesian components of (6.4.4) are shown in Table 6.4.1. Euler's equation applies for incompressible as well as compressible fluids.

Polar coordinates

The cylindrical, spherical, and plane polar components of Euler's equation follow readily from equations (6.3.18), (6.3.21), and (6.3.23), using the constitutive equations given in Tables 4.7.1–Table 4.7.3 for vanishing fluid viscosity.

Vortex force

Using identity (2.8.29), repeated below for convenience,

$$\mathbf{u} \cdot \nabla \mathbf{u} = \frac{1}{2} \nabla u^2 - \mathbf{u} \times \boldsymbol{\omega}, \quad (6.4.5)$$

we derive an alternative form of Euler's equation involving the vortex force,

$$\rho \left(\frac{\partial \mathbf{u}}{\partial t} + \frac{1}{2} \nabla u^2 - \mathbf{u} \times \boldsymbol{\omega} \right) = -\nabla p + \rho \mathbf{g}, \quad (6.4.6)$$

where

$$u^2 \equiv u_x^2 + u_y^2 + u_z^2 \quad (6.4.7)$$

is the square of the magnitude of the velocity.

6.4.1 Boundary conditions

Euler's equation is a first-order differential equation for the velocity and pressure in the domain of flow. To compute a solution, we require one scalar boundary condition or two

scalar continuity or jump conditions for the velocity or pressure over each boundary of the flow.

Impermeable surfaces

Over an impermeable surface, we require the no-penetration condition requiring that the normal component of the fluid velocity matches the normal component of the boundary velocity.

Free surfaces

Over a free surface, we require that the pressure is equal to the ambient pressure increased or decreased by an amount that is equal to the product of the surface tension and twice the local mean curvature.

Fluid interfaces

Over a fluid interface, we require a kinematic and a dynamic continuity or jump condition. The kinematic condition requires that the normal component of the fluid velocity is continuous across the interface. The dynamic condition requires that the pressure undergoes a discontinuity by an amount that is equal to the product of the surface tension and twice the local mean curvature.

6.4.2 Irrotational flow

The third term on the left-hand side of Euler's equation (6.4.6) disappears in the case of irrotational flow, since $\boldsymbol{\omega} = \mathbf{0}$ throughout the domain of flow. Expressing the velocity as the gradient of a velocity potential, ϕ , as shown in equation (3.2.6) and more explicitly in equations (3.2.19),

$$\mathbf{u} = \nabla\phi, \quad (6.4.8)$$

we find that Euler's equation (6.4.6) takes the form

$$\rho \left(\frac{\partial \nabla\phi}{\partial t} + \frac{1}{2} \nabla u^2 \right) = -\nabla p + \rho \mathbf{g}. \quad (6.4.9)$$

The order of time and space differentiation in the gradient of the potential can be switched in the first term on the left-hand side.

The acceleration of gravity can be expressed as the gradient of the scalar $v \equiv \mathbf{g} \cdot \mathbf{x}$,

$$\mathbf{g} = \nabla v = \nabla(\mathbf{g} \cdot \mathbf{x}) = \nabla(g_x x + g_y y + g_z z). \quad (6.4.10)$$

Substituting this expression into (6.4.9), assuming that the density is uniform throughout the domain of flow, and collecting all terms under the gradient, we find that

$$\nabla \left(\frac{\partial \phi}{\partial t} + \frac{1}{2} u^2 + \frac{p}{\rho} - \mathbf{g} \cdot \mathbf{x} \right) = \mathbf{0}. \quad (6.4.11)$$

The curl of the left-hand side is identically zero at every point in the flow.

Bernoulli's equation for irrotational flow

Since all spatial derivatives of the scalar quantity enclosed by the parentheses on the left-hand side of (6.4.11) are zero, the quantity must be independent of position, although it may change in time. Euler's equation for irrotational flow then provides us with Bernoulli's equation describing the irrotational flow of a uniform-density fluid,

$$\frac{\partial \phi}{\partial t} + \frac{1}{2} u^2 + \frac{p}{\rho} - \mathbf{g} \cdot \mathbf{x} = c(t), \quad (6.4.12)$$

where $c(t)$ is an unspecified and typically inconsequential function of time.

Evolution of the velocity potential

Bernoulli's equation (6.4.12) can be regarded as an evolution equation for the harmonic potential. Given the instantaneous velocity and pressure fields, we can evaluate the second, third, and fourth terms on the left-hand side, compute the time derivative $\partial\phi/\partial t$, and advance the potential over a small period of time elapsed.

The last term, $c(t)$, causes the potential to increase or decrease uniformly by the same rate throughout the domain of flow. However, because the velocity is computed by taking derivatives of the potential with respect to the spatial coordinates, this uniform change is inconsequential to the velocity.

Lagrangian form

When a flow is bounded by a free surface where the pressure is prescribed on one side, it is beneficial to convert the Eulerian time derivative $\partial\phi/\partial t$ on the left-hand side of (6.4.12) to the material derivative, $D\phi/Dt$. Expressing the velocity as the gradient of the potential, $\mathbf{u} = \nabla\phi$, we obtain

$$\frac{D\phi}{Dt} \equiv \frac{\partial\phi}{\partial t} + \mathbf{u} \cdot \nabla\phi = \frac{\partial\phi}{\partial t} + \mathbf{u} \cdot \mathbf{u} = \frac{\partial\phi}{\partial t} + u^2, \quad (6.4.13)$$

where

$$u^2 \equiv u_x^2 + u_y^2 + u_z^2 \quad (6.4.14)$$

is the square of the magnitude of the velocity. Combining equations (6.4.12) and (6.4.13), we obtain

$$\frac{D\phi}{Dt} = \frac{1}{2} u^2 - \frac{p}{\rho} + \mathbf{g} \cdot \mathbf{x} - c(t), \quad (6.4.15)$$

which provides us with the rate of change of the potential following a point particle according to Bernoulli's equation for irrotational flow.

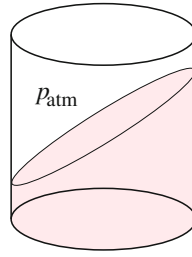


Figure 6.4.1 Irrotational flow due to the sloshing of a fluid in a container. Bernoulli's equation provides us with an evolution equation for the potential following the motion of point particles distributed over the free surface.

Fluid sloshing in a container

As an application, we consider the sloshing of a fluid inside a container, as illustrated in Figure 6.4.1. The pressure at the free surface on the side of the liquid, p_{fs} , is related to the ambient pressure, p_{atm} , by the dynamic boundary condition

$$p_{fs} = p_{atm} + \gamma 2 \kappa_m, \quad (6.4.16)$$

where γ is the surface tension and κ_m is the mean curvature of the free surface.

Applying equation (6.4.15) at a point in the free surface and using equation (6.4.16), we derive an expression for the rate of change of the potential following a point particle at the free surface,

$$\frac{D\phi}{Dt} = \frac{1}{2} u^2 - \frac{p_{atm} + \gamma 2 \kappa_m}{\rho} + \mathbf{g} \cdot \mathbf{x} - c(t). \quad (6.4.17)$$

Integrating this equation in time by following the motion of interfacial point particles provides us with a boundary condition for the potential over the free surface.

Steady irrotational flow

The time derivative of the potential on the left-hand side of (6.4.12) disappears at steady state, yielding the best known version of Bernoulli's equation,

$$\frac{1}{2} u^2 + \frac{p}{\rho} - \mathbf{g} \cdot \mathbf{x} = c(t). \quad (6.4.18)$$

The time-dependent function $c(t)$ on the right-hand side accounts for a possible uniform change in the pressure throughout the domain of flow.

The three terms on the left-hand side of (6.4.18) express, respectively, the kinetic energy, the potential energy due to the pressure, and the potential energy due to the body force, all three per unit mass of the fluid. Bernoulli's equation requires that the sum of the three energies is the same at every point in the flow.

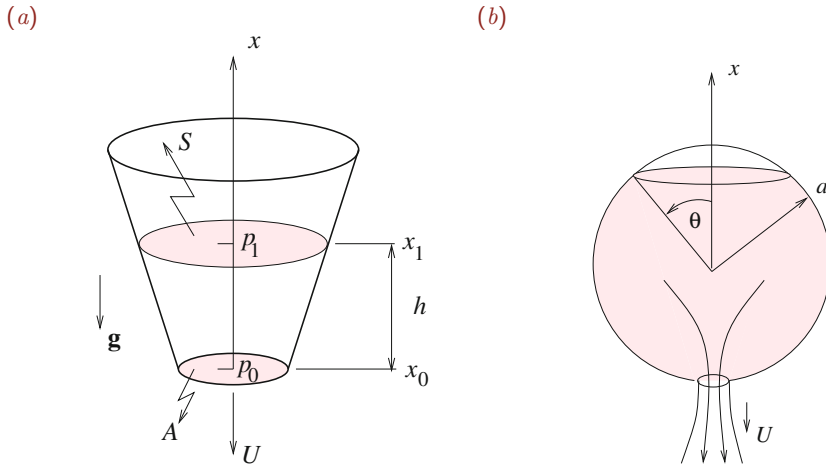


Figure 6.4.2 Illustration of the gravitational drainage of a fluid from a (a) conical or (b) spherical tank. The exit velocity can be computed from Bernoulli's equation for irrotational flow, resulting in Torricelli's law.

Bernoulli's equation allows us to perform approximate engineering analysis of a broad class of internal and external irrotational flows, subject to the underlying assumptions. Examples are discussed in the remainder of this section.

6.4.3 Torricelli's law

Consider the gravitational drainage of a fluid from a tank, as illustrated in Figure 6.4.2. If the rate of drainage is sufficiently slow, the flow can be assumed to be in a quasi-steady state. This means that the magnitude of the time derivative of the scalar potential is small compared to the rest of the terms in the unsteady Bernoulli equation (6.4.12), and the steady version of Bernoulli's equation (6.4.18) can be employed.

To compute the velocity at the point of drainage, U , we evaluate the left-hand side of (6.4.18) first at the free surface and then at the point of drainage, and equate the two expressions. Since the velocity at the free surface is small compared to the drainage velocity, it can be set to zero to leading-order approximation, yielding

$$\frac{1}{2} U^2 + \frac{p_0}{\rho} + g x_0 = \frac{p_1}{\rho} + g x_1, \quad (6.4.19)$$

where the pressures p_0 and p_1 and the elevations x_0 and x_1 , are defined in Figure 6.4.2(a). Rearranging, we find that

$$U = \left(2 \frac{\Delta p}{\rho} + 2gh \right)^{1/2}, \quad (6.4.20)$$

where $h = x_1 - x_0$ is the liquid height inside the container and $\Delta p = p_1 - p_0$.

In the case of an open tank, the pressure at the free surface and the pressure at the point of drainage are equal to the ambient atmospheric pressure. Setting $\Delta p = 0$, and derive Torricelli's law expressed by

$$U = \sqrt{2gh}, \quad (6.4.21)$$

which also describes the velocity of a rigid body in free gravitational fall.

Drainage time

The expression for the velocity in terms of the liquid height, h , can be used to compute the time it takes for a fluid to drain from a tank with a specified geometry, t_{drain} . During a small period of time, dt , the volume of liquid in the tank decreases by

$$dV = S(x) dh, \quad (6.4.22)$$

where $S(h)$ is the tank cross-sectional area. Setting this change in volume equal to $-UA dt$, where A is the cross-sectional area of the drainage hole, and substituting Torricelli's law, we obtain

$$S(h) dh = -\sqrt{2gh} A dt, \quad (6.4.23)$$

which can be rearranged into

$$\frac{dt}{dh} = -\frac{1}{A} \frac{S(h)}{\sqrt{2gh}}. \quad (6.4.24)$$

Integrating, we obtain an expression for the drainage time,

$$t_{\text{drain}} = \frac{1}{A} \int_0^{h_0} \frac{S(h)}{\sqrt{2gh}} dh, \quad (6.4.25)$$

where h_0 is the initial height of the liquid in the container.

Cylindrical tank

In the case of a cylindrical tank with arbitrary cross-section, the cross-sectional area is constant, $S(h) \equiv B$, yielding

$$t_{\text{drain}} = \frac{B}{A} \frac{1}{\sqrt{2g}} \int_0^{h_0} \frac{1}{\sqrt{h}} dh = \frac{B}{A} \left(2 \frac{h_0}{g}\right)^{1/2}. \quad (6.4.26)$$

This functional form could have been predicted at the outset on the basis of dimensional analysis. In the case of a vertical barrel, $B = \pi b^2$, where b is the barrel radius.

Conical container

In the case of a conical container illustrated in [Figure 6.4.2\(a\)](#), the radius of the cross-section at height h is approximately $r \simeq r_0 h/h_0$, where r_0 is the radius of the cross-section at the initial height, h_0 . Setting $S(h) = \pi r^2$, we obtain

$$t_{\text{drain}} = \frac{B_0}{Ah_0^2} \frac{1}{\sqrt{2g}} \int_0^{h_0} h^{3/2} dh, \quad (6.4.27)$$

where $B_0 = \pi r_0^2$ is the cross-sectional area at height h_0 , and the origin of the x axis has been set at the hole. Performing the integration, we obtain

$$t_{\text{drain}} = \frac{1}{5} \frac{B_0}{A} \left(2 \frac{h_0}{g} \right)^{1/2}, \quad (6.4.28)$$

$B_0/A = (r_0/a)^2$, and r_0 is the hole radius. The drainage time is one fifth of that for the cylindrical container with cross-sectional area $B = B_0$.

Spherical container

In the case of a spherical container of radius a , the height of the liquid can be parametrized by the meridional angle, θ ,

$$h = (1 + \cos \theta) a, \quad (6.4.29)$$

as illustrated in [Figure 6.4.2\(b\)](#). The radius of the cross-section at height h is $r = a \sin \theta$ and the corresponding cross-sectional area is $S = \pi a^2 \sin^2 \theta$. Substituting these expressions into the master equation (6.4.25), we obtain

$$t_{\text{drain}} = \frac{\pi a^2}{A} \left(\frac{b}{2g} \right)^{1/2} \int_{\pi}^{\alpha} \frac{\sin^2 \theta}{\sqrt{1 + \cos \theta}} (-\sin \theta) d\theta, \quad (6.4.30)$$

where α is the initial meridional angle. In the case of a full spherical container, $\alpha = 0$; in the case of a full hemispherical container, $\alpha = \pi/2$.

Substituting for convenience $w = \cos \theta$, we obtain

$$t_{\text{drain}} = \frac{\pi a^2}{A} \left(\frac{a}{2g} \right)^{1/2} \int_{-1}^{\cos \alpha} (1 - w) \sqrt{1 + \cos w} dw. \quad (6.4.31)$$

Recalling the indefinite integrals

$$\int \sqrt{1 + w} dw = \frac{2}{3} (1 + w)^{3/2} \quad (6.4.32)$$

and

$$\int w \sqrt{1 + w} dw = \frac{2}{15} (3w - 2) (1 + w)^{3/2}, \quad (6.4.33)$$

we obtain

$$t_{\text{drain}} = \frac{2}{15} \frac{\pi a^2}{A} \left(\frac{a}{2g} \right)^{1/2} (1 + \cos \alpha)^{3/2} (7 - 3 \cos \alpha). \quad (6.4.34)$$

In the case of a full spherical container, $\cos \alpha = 1$; in the case of a full hemispherical container, $\cos \alpha = 0$.

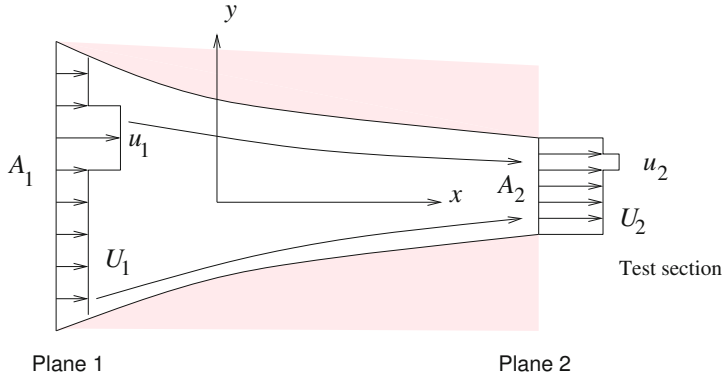


Figure 6.4.3 Illustration of flow in a wind or water tunnel with a contraction that dampens small perturbations.

6.4.4 Decay of perturbations in a wind or water tunnel

Wind and water tunnels are used extensively in laboratory studies of high-speed flow. To obtain a desirable uniform velocity profile, the tunnel is designed with a smooth contraction upstream from a test section where measurement or observation takes place, as illustrated in Figure 6.4.3. Consider a small perturbation of the otherwise flat upstream velocity profile at plane 1, as illustrated in Figure 6.4.3. The pressure is nearly uniform over any cross-section along the contraction.

Applying Bernoulli’s equation (6.4.18) for the fluid outside or inside the perturbed region, and neglecting the effect of gravity, we find that

$$\frac{1}{2} U_1^2 + \frac{p_1}{\rho} = \frac{1}{2} U_2^2 + \frac{p_2}{\rho}, \quad \frac{1}{2} u_1^2 + \frac{p_1}{\rho} = \frac{1}{2} u_2^2 + \frac{p_2}{\rho}. \quad (6.4.35)$$

Combining these equations to eliminate the pressure and rearranging, we obtain

$$\frac{U_2 - u_2}{U_1 - u_1} = \frac{U_1 + u_1}{U_2 + u_2}. \quad (6.4.36)$$

Because the perturbation has been assumed small, the actual velocities, u_1 and u_2 , can be replaced with the unperturbed velocities U_1 and U_2 in the numerator and denominator of the fraction on the right-hand side of (6.4.36), yielding

$$\frac{U_2 - u_2}{U_1 - u_1} = \frac{U_1}{U_2}. \quad (6.4.37)$$

Now combining the approximate mass balance $U_1 A_1 = U_2 A_2$ with equation (6.4.37) and rearranging, we obtain

$$\frac{1 - u_2/U_2}{1 - u_1/U_1} = \left(\frac{A_2}{A_1} \right)^2, \quad (6.4.38)$$

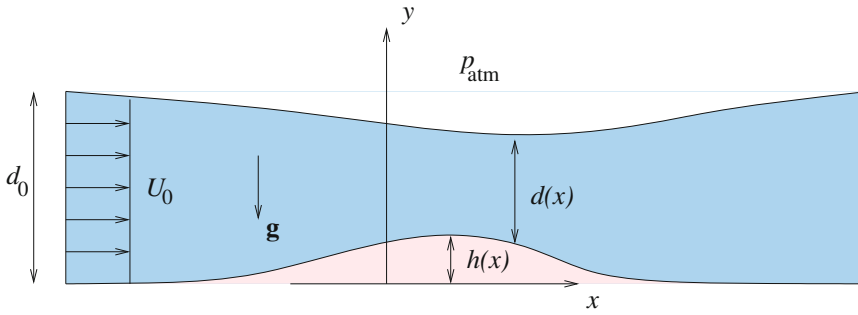


Figure 6.4.4 Irrotational free-surface flow of a horizontal stream over a hump.

which shows that the relative magnitude of the perturbation decays like the square of the contraction ratio, A_2/A_1 , thereby confirming that the contraction promotes a uniform velocity profile.

6.4.5 Flow of a horizontal stream over a hump

In the third application, we consider steady two-dimensional irrotational flow of a horizontal stream over a gently sloped hump, called the Venturi flume, as illustrated in Figure 6.4.4. The free surface is located at

$$y = h(x) + d(x), \quad (6.4.39)$$

where $h(x)$ is the height of the hump and $d(x)$ is the depth of the stream. As x tends to infinity on either side, $h(x)$ tends to zero. The profile of the streamwise velocity is assumed to be uniform across the stream, that is, $u_x = u(x)$.

Applying Bernoulli's equation (6.4.18) first at a point at the free surface located far upstream and then at an arbitrary point at the free surface, neglecting the y component of the free-surface velocity and the pressure drop across the free surface due to surface tension, and noting that the gravitational acceleration vector is given by $\mathbf{g} = (0, -g)$, we obtain

$$\frac{1}{2} U_0^2 + \frac{p_{\text{atm}}}{\rho} + g d_0 = \frac{1}{2} u^2(x) + \frac{p_{\text{atm}}}{\rho} + g (h(x) + d(x)), \quad (6.4.40)$$

where U_0 is the upstream velocity and $d_0 \equiv d(x = -\infty)$ is the upstream depth. Combining the mass conservation equation

$$U_0 d_0 = u(x) d(x) \quad (6.4.41)$$

with equation (6.4.40) to eliminate $u(x)$, and rearranging the resulting expression, we derive a cubic equation for the scaled layer depth $\hat{d}(x) \equiv d(x)/d_0$,

$$\hat{d}^3(x) + \hat{d}^2(x) (\hat{h}(x) - 1 - \frac{1}{2} \text{Fr}^2) + \frac{1}{2} \text{Fr}^2 = 0, \quad (6.4.42)$$

where $\widehat{h}(x) \equiv h(x)/d_0$ is the scaled height of the hump. We have introduced the dimensionless ratio

$$\text{Fr} \equiv \frac{U_0}{\sqrt{g d_0}}, \quad (6.4.43)$$

expressing the relative magnitude of inertial and gravitational forces, called the Froude number.

In practice, the Venturi flume is used to deduce the flow rate from measurements of the deflection of the free surface from the horizontal position. As the Froude number tends to zero, gravitational forces dominate and equation (6.4.42) has the obvious solution $\widehat{d}(x) = 1 - \widehat{h}(x)$, which shows that the free surface tends to become flat. As the Froude number tends to infinity, inertial forces dominate and equation (6.4.42) has an obvious solution, $\widehat{d}(x) = 1$, which shows that the depth of the stream remains constant and the free surface follows the topography of the hump. Intermediate values of the Froude number yield free surface profiles with a downward deflection (Problem 6.4.6).

6.4.6 Steady rotational flow

We return to Euler's equation (6.4.6) and consider a rotational flow at steady state. The time derivative on the left-hand side vanishes, yielding

$$\frac{1}{2} \nabla u^2 - \mathbf{u} \times \boldsymbol{\omega} = -\frac{1}{\rho} \nabla p + \mathbf{g}, \quad (6.4.44)$$

where

$$u^2 \equiv u_x^2 + u_y^2 + u_z^2 \quad (6.4.45)$$

is the square of the magnitude of the velocity. The x component of equation (6.4.44) reads

$$\frac{1}{2} \frac{\partial u^2}{\partial x} - u_y \omega_z + u_z \omega_y = -\frac{1}{\rho} \frac{\partial p}{\partial x} + g_x. \quad (6.4.46)$$

Similar equations can be written for the y and z components.

Next, we place the origin of the Cartesian axes at a point in the fluid, identify the streamline that passes through that point, and orient the x axis tangentially to the streamline and thus parallel to the local velocity, as shown in [Figure 6.4.5](#). By design, the y and z velocity components are zero at the origin; consequently, the second and third terms on the left-hand side of equation (6.4.46) vanish. Taking advantage of these simplifications, we derive the reduced form

$$\frac{\partial}{\partial x} \left(\frac{1}{2} u^2 + \frac{p}{\rho} - g_x x \right) = 0, \quad (6.4.47)$$

where the left-hand side is evaluated at the origin.

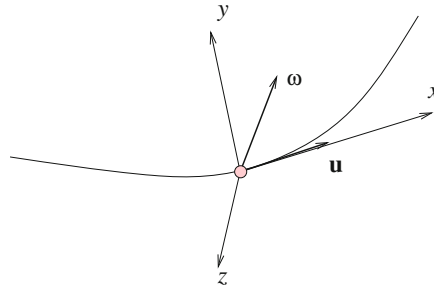


Figure 6.4.5 A system of Cartesian coordinates with the x axis tangential to a streamline is used to derive Bernoulli's equation for steady rotational flow, given in equation (6.4.48).

Equation (6.4.47) states that the rate of change of the quantity enclosed by the parentheses on the left-hand side with respect to distance along the streamline is zero. Consequently, the quantity enclosed by the parentheses must remain constant along the streamline,

$$\frac{1}{2} u^2 + \frac{p}{\rho} - \mathbf{g} \cdot \mathbf{x} = f(x, y, z), \quad (6.4.48)$$

where the function $f(x, y, z)$ remains constant along a streamline. In a two-dimensional or axisymmetric flow, $f(x, y, z)$ is a function of the stream function, ψ , which, by definition, is constant along a streamline.

6.4.7 Flow with uniform vorticity

The velocity field, \mathbf{u} , of a two-dimensional flow with uniform vorticity in the xy plane, $\omega_z = \Omega$, can be resolved into (a) the velocity field, \mathbf{v} , of a simple two-dimensional flow with uniform vorticity Ω , and (b) the velocity field of a potential flow expressed by a harmonic potential ϕ , such that

$$\mathbf{u} = \mathbf{v} + \nabla\phi. \quad (6.4.49)$$

One example of a simple flow is simple shear flow with velocity

$$v_x = -\Omega y, \quad v_y = 0. \quad (6.4.50)$$

A second example is flow expressing rigid-body rotation with velocity

$$v_x = -\frac{1}{2} \Omega y, \quad v_y = \frac{1}{2} \Omega x. \quad (6.4.51)$$

Using this decomposition, we derive Bernoulli's equation

$$\frac{\partial\phi}{\partial t} + \frac{1}{2} u^2 + \frac{p}{\rho} - \mathbf{g} \cdot \mathbf{x} + \Omega\psi = c(t), \quad (6.4.52)$$

where ψ is the stream function and $u = |\mathbf{u}|$ is the magnitude of the velocity (Problem 6.4.2).

PROBLEMS**6.4.1** *Flow through a sudden enlargement*

Consider the flow through a sudden enlargement depicted in [Figure 6.2.1](#). Use Bernoulli's equation to compute the rise in pressure, $p_2 - p_1$. Compare your answer to that shown in equation (6.2.28) obtained by an approximate integral momentum balance.

6.4.2 *Flow with uniform vorticity*

(a) Derive Bernoulli's equation (6.4.52) for two-dimensional flow. (b) Derive a similar equation for axisymmetric flow where the azimuthal component of the vorticity, ω_φ , is proportional to the distance from the axis of symmetry, σ .

6.4.3 *Flow due to an unsteady point source or point vortex*

(a) Discuss whether the flow due to a two- or three-dimensional point source with time-dependent strength satisfies the Euler equation for inviscid flow. (b) Repeat (a) for a two-dimensional point vortex.

6.4.4 *Force on a sphere in accelerating potential flow*

Consider an unsteady irrotational flow past a sphere that is held stationary in an accelerating stream along the x axis with velocity $U_x(t)$. The velocity potential and Cartesian components of the velocity are given in equations (3.6.13) and (3.6.14). Use Bernoulli's equation (6.4.12) to evaluate the pressure and then compute the force exerted on the sphere by evaluating the surface integral


$$\mathbf{F} = - \iint_{\text{sphere}} p \mathbf{n} \, dS, \quad (6.4.53)$$

where $\mathbf{n} = \frac{1}{a}(x, y, z)$ is the unit vector normal to the sphere pointing into the fluid. Based on this result, compute the force exerted on a sphere that is held stationary in a non-accelerating steady flow. Discuss the physical relevance of the assumption of irrotational flow.

6.4.5 *Drainage from a spheroidal tank*

(a) Derive a formula for the time it takes a liquid to drain completely from a vertical spheroidal tank with axes a and b through a small hole at the bottom, based on Torricelli's law. You may assume that the gas pressure is equal to the atmospheric pressure above the liquid in the tank.

(b) Repeat (a) for a horizontal spheroidal tank.

6.4.6  *Flow over a hump*

Consider the flow of a horizontal stream over a hump, as illustrated in [Figure 6.4.4](#). The height of the hump is described by the parabolic shape function

$$h(x) = h_0 (1 - \hat{x}^2) \quad (6.4.54)$$

for $-1 \leq \hat{x} \leq 1$, where h_0 is the maximum height, $\hat{x} \equiv x/a$ is the scaled distance from the midpoint, and a is the half-length of the hump. Substituting this profile into (6.4.42), we derive the equation

$$\hat{d}^3(x) + \hat{d}^2(x) \left(\frac{h_0}{d_0} (1 - \hat{x}^2) - 1 - \frac{1}{2} \text{Fr}^2 \right) + \frac{1}{2} \text{Fr}^2 = 0 \quad (6.4.55)$$

for $-1 \leq \hat{x} \leq 1$. Compute and plot the scaled layer depth \hat{d} against \hat{x} for $h_0/d_0 = 0.01, 0.05, \text{ and } 0.10$, and $\text{Fr} = 0.01, 0.1, 10, \text{ and } 100$. Discuss the free surface shapes.

6.5 The Navier–Stokes equation

The Navier–Stokes equation arises from the equation of motion (6.3.12) by substituting the constitutive equation for the stress tensor for an incompressible Newtonian fluid, given in (4.6.6). The hydrodynamic volume force for a fluid with uniform viscosity is given by

$$\Sigma \equiv \nabla \cdot \boldsymbol{\sigma} = \nabla \cdot (-p \mathbf{I} + \mu 2 \mathbf{E}) = -\nabla p + \mu 2 \nabla \cdot \mathbf{E}, \quad (6.5.1)$$

where \mathbf{I} is the identity matrix and \mathbf{E} is the rate-of-deformation tensor.

Working in index notation, we find that the i th component of twice the divergence of the rate-of-deformation tensor on the right-hand side is

$$2 \frac{\partial E_{ji}}{\partial x_j} = 2 \frac{\partial}{\partial x_j} \left[\frac{1}{2} \left(\frac{\partial u_i}{\partial x_j} + \frac{\partial u_j}{\partial x_i} \right) \right], \quad (6.5.2)$$

where summation is implied over the repeated index j . Carrying out the differentiations, we obtain

$$2 \frac{\partial E_{ji}}{\partial x_j} = \frac{\partial^2 u_i}{\partial x_j \partial x_j} + \frac{\partial^2 u_j}{\partial x_j \partial x_i} = \frac{\partial^2 u_i}{\partial x_j \partial x_j} + \frac{\partial}{\partial x_i} \left(\frac{\partial u_j}{\partial x_j} \right). \quad (6.5.3)$$

Because the fluid has been assumed incompressible, the divergence of the velocity in the last term enclosed by the parentheses is zero. The penultimate term is the Laplacian of the i th component of the velocity,

$$\frac{\partial^2 u_i}{\partial x_j \partial x_j} = \frac{\partial^2 u_i}{\partial x^2} + \frac{\partial^2 u_i}{\partial y^2} + \frac{\partial^2 u_i}{\partial z^2} \equiv \nabla^2 u_i. \quad (6.5.4)$$

Using these results to simplify expression (6.5.1), we find that the hydrodynamic volume force is given by

$$\Sigma \equiv \nabla \cdot \boldsymbol{\sigma} = -\nabla p + \mu \nabla^2 \mathbf{u}. \quad (6.5.5)$$

Correspondingly, Cauchy's equation of motion (6.3.12) reduces to the Navier–Stokes equation,

$$\rho \frac{D\mathbf{u}}{Dt} = -\nabla p + \mu \nabla^2 \mathbf{u} + \rho \mathbf{g}, \quad (6.5.6)$$

$$\begin{aligned}\rho \left(\frac{\partial u_x}{\partial t} + u_x \frac{\partial u_x}{\partial x} + u_y \frac{\partial u_x}{\partial y} + u_z \frac{\partial u_x}{\partial z} \right) &= -\frac{\partial p}{\partial x} + \mu \left(\frac{\partial^2 u_x}{\partial x^2} + \frac{\partial^2 u_x}{\partial y^2} + \frac{\partial^2 u_x}{\partial z^2} \right) + \rho g_x \\ \rho \left(\frac{\partial u_y}{\partial t} + u_x \frac{\partial u_y}{\partial x} + u_y \frac{\partial u_y}{\partial y} + u_z \frac{\partial u_y}{\partial z} \right) &= -\frac{\partial p}{\partial y} + \mu \left(\frac{\partial^2 u_y}{\partial x^2} + \frac{\partial^2 u_y}{\partial y^2} + \frac{\partial^2 u_y}{\partial z^2} \right) + \rho g_y \\ \rho \left(\frac{\partial u_z}{\partial t} + u_x \frac{\partial u_z}{\partial x} + u_y \frac{\partial u_z}{\partial y} + u_z \frac{\partial u_z}{\partial z} \right) &= -\frac{\partial p}{\partial z} + \mu \left(\frac{\partial^2 u_z}{\partial x^2} + \frac{\partial^2 u_z}{\partial y^2} + \frac{\partial^2 u_z}{\partial z^2} \right) + \rho g_z\end{aligned}$$

Table 6.5.1 Eulerian form of the three Cartesian components of the Navier–Stokes equation applicable to incompressible Newtonian fluids.

which is distinguished from Euler’s equation (6.4.3) by the presence of the viscous force represented by the product of the viscosity and the Laplacian of the velocity on the right-hand side.

The Eulerian form of the Navier–Stokes equation involving time and space derivatives is

$$\rho \left(\frac{\partial \mathbf{u}}{\partial t} + \mathbf{u} \cdot \nabla \mathbf{u} \right) = -\nabla p + \mu \nabla^2 \mathbf{u} + \rho \mathbf{g}. \quad (6.5.7)$$

The three Cartesian scalar components of the Navier–Stokes equation are shown in [Table 6.5.1](#).

6.5.1 Pressure and viscous forces

The negative of the pressure gradient on the right-hand side of (6.5.7) represents the pressure force, $-\nabla p$. The Laplacian of the velocity multiplied by the viscosity on the right-hand side of (6.5.7) represents the viscous force, $\mu \nabla^2 \mathbf{u}$.

Working in index notation under the assumption that the fluid is incompressible and therefore the velocity field is solenoidal, $\nabla \cdot \mathbf{u} = 0$, we find that the Laplacian of the velocity is equal to the negative of the curl of the vorticity

$$\nabla^2 \mathbf{u} = -\nabla \times \boldsymbol{\omega} \quad (6.5.8)$$

(Problem 6.5.1). An important consequence of this identity is that, if the flow is irrotational, or the vorticity is uniform, or the vorticity field is irrotational, the viscous force vanishes identically even though the fluid is not inviscid. In that case, the Navier–Stokes equation reduces to Euler’s equation, which can be integrated to yield Bernoulli’s equation (6.4.12) for irrotational flow or equation (6.4.48) for steady rotational flow.

6.5.2 A radially expanding or contracting bubble

An example of an irrotational flow with nonzero viscous stresses but vanishing viscous forces is provided by the flow generated by the radial expansion or contraction of a spherical bubble

with time-dependent radius, $a(t)$. The induced velocity field can be represented by a three-dimensional point source with time dependent strength, $m(t)$, placed at the center of the bubble. In spherical polar coordinates with the origin at the bubble center, the velocity potential is given by

$$\phi(r, t) = -m(t) \frac{1}{4\pi} \frac{1}{r}, \quad (6.5.9)$$

and the radial component of the velocity is given by

$$u_r(r, t) = \frac{\partial \phi}{\partial r} = m(t) \frac{1}{4\pi} \frac{1}{r^2}, \quad (6.5.10)$$

where r is the distance from the bubble center.

The no-penetration condition at the surface of the bubble requires that

$$\frac{da}{dt} = u_r(r = a), \quad (6.5.11)$$

which can be rearranged into an expression for the strength of the point source in terms of the bubble radius,

$$m(t) = 4\pi a^2(t) \frac{da}{dt}. \quad (6.5.12)$$

Substituting expression (6.5.12) into equations (6.5.9) and (6.5.10), we obtain

$$\phi(r) = -a^2(t) \frac{da}{dt} \frac{1}{r} = -\frac{1}{3} \frac{da^3}{dt} \frac{1}{r} \quad (6.5.13)$$

and

$$u_r(r) = \frac{\partial \phi}{\partial r} = \frac{1}{3} \frac{da^3}{dt} \frac{1}{r^2}. \quad (6.5.14)$$

Now referring to Bernoulli's equation (6.4.12) for unsteady irrotational flow,

$$\frac{\partial \phi}{\partial t} + \frac{1}{2} u^2 + \frac{p}{\rho} - \mathbf{g} \cdot \mathbf{x} = c(t), \quad (6.5.15)$$

we compute the first and second terms on the left-hand side,

$$\frac{\partial \phi}{\partial t} = -\frac{1}{3} \frac{d^2 a^3}{dt^2} \frac{1}{r}, \quad u^2 = u_r^2(r) = \frac{1}{9} \left(\frac{da^3}{dt} \right)^2 \frac{1}{r^4}. \quad (6.5.16)$$

Substituting these expressions into Bernoulli's equation and solving for the pressure, we derive the expression

$$\frac{p(r)}{\rho} = \frac{1}{3} \frac{d^2 a^3}{dt^2} \frac{1}{r} - \frac{1}{18} \left(\frac{da^3}{dt} \right)^2 \frac{1}{r^4} + c(t) + \mathbf{g} \cdot \mathbf{x}. \quad (6.5.17)$$

Far from the bubble, the first and second terms on the right-hand side vanish and the pressure assumes a linear and possibly time-dependent distribution,

$$p_\infty(\mathbf{x}, t) = \rho (c(t) + \mathbf{g} \cdot \mathbf{x}). \quad (6.5.18)$$

The normal stress, σ_{rr} , undergoes a jump across the bubble surface, determined by the mean curvature and the surface tension, γ . Using the simplified version of the interfacial condition (4.4.4) for an interface with uniform surface tension, we obtain

$$\sigma_{rr}(r = a) + p_B(t) = \gamma 2\kappa_m = \gamma \frac{2}{a}, \quad (6.5.19)$$

where $p_B(t)$ is the pressure in the bubble interior and $\kappa_m = 1/a$ is the mean curvature of the spherical interface. Substituting the second equation in (6.5.14) into the Newtonian constitutive equation

$$\sigma_{rr} = -p + 2\mu \frac{\partial u_r}{\partial r}, \quad (6.5.20)$$

and the resulting expression into (6.5.19), we find that

$$p(r = a) = p_B(t) - 4\mu \frac{da}{dt} \frac{1}{a} - \gamma \frac{2}{a}. \quad (6.5.21)$$

In the last step, we apply expression (6.5.17) at the bubble surface, evaluate the surface pressure from (6.5.21), neglect hydrostatic variations over the diameter of the bubble, and rearrange the resulting expression to obtain the generalized Rayleigh equation

$$\rho a \frac{d^2 a}{dt^2} + \frac{3}{2} \rho \left(\frac{da}{dt} \right)^2 + 4\mu \frac{da}{dt} \frac{1}{a} + \gamma \frac{2}{a} = p_B(t) - p_\infty(\mathbf{x}_B, t), \quad (6.5.22)$$

where \mathbf{x}_B is the location of the bubble center.

The evolution of the bubble radius from a given initial state is governed by the second-order nonlinear ordinary differential equation (6.5.22). To compute the solution, we require the initial bubble radius, a , the initial rate of expansion, da/dt , the bubble pressure, p_B , and the ambient liquid pressure at infinity, p_∞ . The bubble pressure may be further related to the bubble volume by an appropriate equation of state provided by thermodynamics.

6.5.3 Boundary conditions

The Navier–Stokes equation is a second-order differential equation for the velocity with respect to spatial coordinates. To compute a solution, we require one scalar boundary condition for each component of the velocity or traction over each boundary of the flow.

Impermeable solid surface

Over an impermeable solid surface, we require the no-penetration boundary condition and the no-slip or slip boundary condition, as discussed in Sections 2.10 and 4.8.

Free surface

Over a free surface with uniform surface tension, we require that the tangential component of the traction vanishes, while the normal component is equal to the negative of the ambient pressure increased or decreased by the capillary pressure defined as the product of the surface tension and twice the local mean curvature, as discussed in Section 4.3.

Fluid interface

Over a fluid interface, we require kinematic and dynamic continuity or jump conditions. The kinematic condition requires that all velocity components are continuous across the interface. The dynamic condition requires that the normal component of the traction undergoes a discontinuity by an amount that is equal to the capillary pressure, while the tangential component of the traction undergoes a discontinuity that is determined by the Marangoni traction due to variations in surface tension, as discussed in Section 4.3.

6.5.4 Polar coordinates

The cylindrical polar components of the hydrodynamic volume force for a Newtonian fluid arise by substituting the constitutive relations shown in Table 4.7.1 into the expressions shown in Table 4.3.1(a). After a fair amount of algebra, we derive the expressions shown in Table 6.5.2(a). The cylindrical polar components of the Navier–Stokes equation arise by substituting these relations into the right-hand sides of (6.3.18).

The spherical polar components of the hydrodynamic volume force arise by substituting the constitutive relations given in Table 4.7.2 into the expressions shown in Table 4.3.1(b). After a fair amount of algebra, we derive the expressions shown in Table 6.5.2(b). The Laplacian operator ∇^2 in spherical polar coordinates is defined as

$$\nabla^2\phi \equiv \frac{1}{r^2} \frac{\partial}{\partial r} \left(r^2 \frac{\partial\phi}{\partial r} \right) + \frac{1}{r^2 \sin\theta} \frac{\partial}{\partial\theta} \left(\sin\theta \frac{\partial\phi}{\partial\theta} \right) + \frac{1}{r^2 \sin^2\theta} \frac{\partial^2\phi}{\partial\varphi^2} = 0. \quad (6.5.23)$$

The spherical polar components of the Navier–Stokes equation arise by substituting these expressions into the right-hand sides of (6.3.21).

The plane polar components of the hydrodynamic volume force arise by substituting the constitutive relations shown in Table 4.7.3 into the expressions shown in Table 4.3.1(c). After a fair amount of algebra, we derive the expressions shown in Table 6.5.2(c). The plane polar components of the Navier–Stokes equation arise by substituting these expressions into the right-hand sides of (6.3.24).

PROBLEMS

6.5.1 Viscous force

Prove identity (6.5.8) for an incompressible fluid. *Hint:* Set the vorticity equal to the curl of the velocity, express the curl of the vorticity in index notation, and then use identity (2.3.11).

(a)

$$\begin{aligned}\Sigma_x &= -\frac{\partial p}{\partial x} + \mu \left(\frac{\partial^2 u_x}{\partial x^2} + \frac{1}{\sigma} \frac{\partial}{\partial \sigma} \left(\sigma \frac{\partial u_x}{\partial \sigma} \right) + \frac{1}{\sigma^2} \frac{\partial^2 u_x}{\partial \varphi^2} \right) \\ \Sigma_\sigma &= -\frac{\partial p}{\partial \sigma} + \mu \left(\frac{\partial^2 u_\sigma}{\partial x^2} + \frac{\partial}{\partial \sigma} \left(\frac{1}{\sigma} \frac{\partial(\sigma u_\sigma)}{\partial \sigma} \right) + \frac{1}{\sigma^2} \frac{\partial^2 u_\sigma}{\partial \varphi^2} - \frac{2}{\sigma^2} \frac{\partial u_\varphi}{\partial \varphi} \right) \\ \Sigma_\varphi &= -\frac{1}{\sigma} \frac{\partial p}{\partial \varphi} + \mu \left(\frac{\partial^2 u_\varphi}{\partial x^2} + \frac{\partial}{\partial \sigma} \left(\frac{1}{\sigma} \frac{\partial(\sigma u_\varphi)}{\partial \sigma} \right) + \frac{1}{\sigma^2} \frac{\partial^2 u_\varphi}{\partial \varphi^2} + \frac{2}{\sigma^2} \frac{\partial u_\sigma}{\partial \varphi} \right)\end{aligned}$$

(b)

$$\begin{aligned}\Sigma_r &= -\frac{\partial p}{\partial r} + \mu \left(\nabla^2 u_r - \frac{2}{r^2} u_r - \frac{2}{r^2} \frac{\partial u_\theta}{\partial \theta} - \frac{2}{r^2} u_\theta \cot \theta - \frac{2}{r^2 \sin \theta} \frac{\partial u_\varphi}{\partial \varphi} \right) \\ \Sigma_\theta &= -\frac{1}{r} \frac{\partial p}{\partial \theta} + \mu \left(\nabla^2 u_\theta + \frac{2}{r^2} \frac{\partial u_r}{\partial \theta} - \frac{u_\theta}{r^2 \sin^2 \theta} - \frac{2 \cos \theta}{r^2 \sin^2 \theta} \frac{\partial u_\varphi}{\partial \varphi} \right) \\ \Sigma_\varphi &= -\frac{1}{r \sin \theta} \frac{\partial p}{\partial \varphi} + \mu \left(\nabla^2 u_\varphi - \frac{u_\varphi}{r^2 \sin^2 \theta} + \frac{2}{r^2 \sin \theta} \frac{\partial u_r}{\partial \varphi} + \frac{2 \cos \theta}{r^2 \sin^2 \theta} \frac{\partial u_\theta}{\partial \varphi} \right)\end{aligned}$$

(c)

$$\begin{aligned}\Sigma_r &= -\frac{\partial p}{\partial r} + \mu \left(\frac{\partial}{\partial r} \left(\frac{1}{r} \frac{\partial(r u_r)}{\partial r} \right) + \frac{1}{r^2} \frac{\partial^2 u_r}{\partial \theta^2} - \frac{2}{r^2} \frac{\partial u_\theta}{\partial \varphi} \right) \\ \Sigma_\theta &= -\frac{1}{r} \frac{\partial p}{\partial \theta} + \mu \left(\frac{\partial}{\partial r} \left(\frac{1}{r} \frac{\partial(r u_\theta)}{\partial r} \right) + \frac{1}{r^2} \frac{\partial^2 u_\theta}{\partial \theta^2} + \frac{2}{r^2} \frac{\partial u_r}{\partial \theta} \right)\end{aligned}$$

Table 6.5.2 Components of the hydrodynamic volume force for a Newtonian fluid in (a) cylindrical, (b) spherical, and (c) plane polar coordinates. The Laplacian operator ∇^2 in spherical polar coordinates is defined in equation (6.5.23).

6.5.2 Steady flow

Consider a flow at steady state. Explain why it is not generally possible to specify an arbitrary solenoidal velocity field that satisfies the boundary conditions, and then compute the pressure by solving the Navier–Stokes equation (6.5.7).

Hint: Consider the conditions for the equation $\nabla p = \mathbf{F}$ to have a solution for p , where \mathbf{F} is a given vector field. Recall that the curl of the gradient of a scalar function vanishes, as shown in equation (6.6.20).

6.5.3 Expansion of a bubble

Show that, when the right-hand side of (6.5.22) vanishes and viscous stresses and surface

tension are both insignificant, an exact solution of equation (6.5.22) is

$$\frac{a(t)}{a(t=0)} = \left(1 + \frac{5}{2} \frac{t}{a(t=0)} \left(\frac{da}{dt} \right)_{t=0} \right)^{2/5}. \quad (6.5.24)$$

Note that both the initial bubble radius and the initial rate of expansion or contraction must be specified.

6.6 Vorticity transport

In Section 6.3, we interpreted the equation of motion as an evolution equation determining the rate of change of the velocity (acceleration) of a point particle or the rate of change of the fluid velocity at a given point in a flow. Descendant evolution equations governing the rate of change of the spatial derivatives of the velocity comprising the velocity-gradient tensor and its symmetric and skew-symmetric components comprising the rate-of-deformation and vorticity tensors can be derived by straightforward differentiation.

Of particular interest is the evolution of the skew-symmetric part of the velocity-gradient tensor, Ξ , which is related to the vorticity, ω , as shown in (2.3.17),

$$\Xi_{ij} = \frac{1}{2} \epsilon_{ijk} \omega_k, \quad (6.6.1)$$

where ϵ_{ijk} is the alternating tensor. The availability of an evolution equation for the vorticity allows us to study the rate of change of the angular velocity of small fluid parcels as they translate and deform while they are convected in a flow.

6.6.1 Two-dimensional flow

We begin by considering the evolution of the z vorticity component in a two-dimensional flow in the xy plane, defined in terms of the velocity as

$$\omega_z = \frac{\partial u_y}{\partial x} - \frac{\partial u_x}{\partial y}. \quad (6.6.2)$$

To derive an evolution equation for ω_z , we divide both sides of the equation of motion (6.3.15) by the density, ρ , so as to remove it from the left-hand side, obtaining

$$\frac{\partial \mathbf{u}}{\partial t} + \mathbf{u} \cdot \nabla \mathbf{u} = \frac{1}{\rho} \Sigma + \mathbf{g}, \quad (6.6.3)$$

where $\Sigma \equiv \nabla \cdot \sigma$ is the hydrodynamic volume force. Taking the y derivative of the x component of this equation, and then subtracting the result from the x derivative of the corresponding y component, we derive the vorticity transport equation

$$\frac{\partial \omega_z}{\partial t} + \frac{\partial}{\partial x} \left(u_x \frac{\partial u_y}{\partial x} + u_y \frac{\partial u_y}{\partial y} \right) - \frac{\partial}{\partial y} \left(u_x \frac{\partial u_x}{\partial x} + u_y \frac{\partial u_x}{\partial y} \right) = \frac{\partial}{\partial x} \left(\frac{1}{\rho} \Sigma_y \right) - \frac{\partial}{\partial y} \left(\frac{1}{\rho} \Sigma_x \right). \quad (6.6.4)$$

Expanding the derivatives on the left-hand side and using the continuity equation for an incompressible fluid,

$$\frac{\partial u_x}{\partial x} + \frac{\partial u_y}{\partial y} = 0, \quad (6.6.5)$$

we obtain the simpler form

$$\frac{D\omega_z}{Dt} \equiv \frac{\partial\omega_z}{\partial t} + u_x \frac{\partial\omega_z}{\partial x} + u_y \frac{\partial\omega_z}{\partial y} = \frac{\partial}{\partial x} \left(\frac{1}{\rho} \Sigma_y \right) - \frac{\partial}{\partial y} \left(\frac{1}{\rho} \Sigma_x \right), \quad (6.6.6)$$

where D/Dt is the material derivative. The left-hand side of (6.6.6) expresses the material derivative of the vorticity, which is equal to twice the rate of change of the angular velocity of a small fluid parcel according to equation (2.3.9).

Next, we expand the derivatives on the right-hand side of (6.6.6) setting, for example,

$$\frac{\partial}{\partial x} \left(\frac{1}{\rho} \Sigma_y \right) = \frac{1}{\rho} \frac{\partial \Sigma_y}{\partial x} - \Sigma_y \frac{1}{\rho^2} \frac{\partial \rho}{\partial x}, \quad (6.6.7)$$

and express the hydrodynamic volume force in terms of the stresses using the definitions

$$\Sigma_x \equiv \frac{\partial \sigma_{xx}}{\partial x} + \frac{\partial \sigma_{yx}}{\partial y}, \quad \Sigma_y \equiv \frac{\partial \sigma_{xy}}{\partial x} + \frac{\partial \sigma_{yy}}{\partial y}. \quad (6.6.8)$$

The result is a general form of the vorticity transport equation for an incompressible fluid,

$$\frac{D\omega_z}{Dt} = \frac{1}{\rho^2} \left(-\Sigma_y \frac{\partial \rho}{\partial x} + \Sigma_x \frac{\partial \rho}{\partial y} \right) + \frac{1}{\rho} \left(\frac{\partial^2 \sigma_{xy}}{\partial x^2} - \frac{\partial^2 \sigma_{xy}}{\partial y^2} + \frac{\partial^2 (\sigma_{yy} - \sigma_{xx})}{\partial x \partial y} \right). \quad (6.6.9)$$

We recall that the density is allowed to vary with position inside an incompressible fluid.

Baroclinic production of vorticity

The first term on the right-hand side of (6.6.9),

$$\frac{1}{\rho^2} \left(-\Sigma_y \frac{\partial \rho}{\partial x} + \Sigma_x \frac{\partial \rho}{\partial y} \right), \quad (6.6.10)$$

expresses production of vorticity due to density inhomogeneity, known as *baroclinic production*.

To illustrate the physical mechanism underlying this term, we consider a vertical column of fluid whose density increases upward in the direction of the y axis, so that $\partial\rho/\partial y > 0$, as shown in [Figure 6.6.1](#). The x component of the hydrodynamic volume force, Σ_x , causes the column to accelerate forward in the positive direction of the x axis. Because the density and thus the inertia of the fluid increases with elevation, the top portion accelerates less than the bottom portion. As a result, the column buckles backward, exhibiting counterclockwise rotation expressed by the second term inside the parentheses on the right-hand side of (6.6.10).

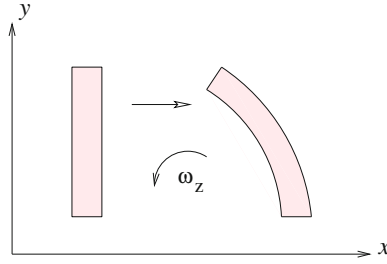


Figure 6.6.1 Vorticity is generated when a column of fluid that is heavy at the top buckles in acceleration under the influence of a horizontal volume force.

A similar interpretation is possible in the case of a horizontal layer whose density increases in the direction of the x axis, so that $\partial\rho/\partial x > 0$. The preceding arguments suggest that the layer rotates under the influence of a vertical volume force, Σ_y . The associated baroclinic production of vorticity is expressed the first term inside the parentheses on the right-hand side of (6.6.10).

Flow with negligible viscous forces

When viscous forces are insignificant, the shear stresses virtually vanish while the normal stresses, σ_{xx} and σ_{yy} , are equal to the negative of the pressure, $-p$. Consequently, the term enclosed by the tall parentheses on the right-hand side of (6.6.9) makes a negligible contribution to the vorticity transport equation.

In the absence of viscous stresses, the hydrodynamic volume force is equal to the negative of the pressure gradient, $\Sigma = -\nabla p$. Substituting $\Sigma_x = -\partial p/\partial x$ and $\Sigma_y = -\partial p/\partial y$, we find that the term expressing baroclinic production of vorticity takes a simple form, yielding the vorticity transport equation

$$\rho^2 \frac{D\omega_z}{Dt} = \frac{\partial p}{\partial y} \frac{\partial \rho}{\partial x} - \frac{\partial p}{\partial x} \frac{\partial \rho}{\partial y}. \quad (6.6.11)$$

The right-hand side can be expressed in terms of a triple mixed vector product, yielding

$$\rho^2 \frac{D\omega_z}{Dt} = (\nabla \rho \times \nabla p) \cdot \mathbf{e}_z, \quad (6.6.12)$$

where \mathbf{e}_z is the unit vector along the z axis that is perpendicular to the xy plane of the flow.

In the case of a fluid with uniform density, $\nabla \rho = \mathbf{0}$, equation (6.6.11) predicts that

$$\frac{D\omega_z}{Dt} = 0, \quad (6.6.13)$$

which shows that a small fluid parcel rotates with constant angular velocity as it moves about the domain of flow. The physical origin of this remarkably simple result can be traced back to conservation of angular momentum in the absence of a shearing stress imparting a torque.

Temperature °C	Water cm ² /sec	Air cm ² sec
20	1.004×10^{-2}	15.05×10^{-2}
40	0.658×10^{-2}	18.86×10^{-2}
80	0.365×10^{-2}	20.88×10^{-2}

Table 6.6.1 The kinematic viscosity of water and air at three temperatures. Note that the kinematic viscosity of air is higher than that of water due to its much lower density.

Incompressible Newtonian fluids

Next, we consider the evolution of vorticity in an incompressible Newtonian fluid with uniform density and viscosity. Substituting the constitutive equation for the stress tensor shown in Table 4.5.1 into the right-hand side of (6.6.9), and simplifying the resulting expression using the continuity equation, we derive the vorticity transport equation

$$\frac{\partial \omega_z}{\partial t} + u_x \frac{\partial \omega_z}{\partial x} + u_y \frac{\partial \omega_z}{\partial y} = \nu \left(\frac{\partial^2 \omega_z}{\partial x^2} + \frac{\partial^2 \omega_z}{\partial y^2} \right), \quad (6.6.14)$$

where $\nu \equiv \mu/\rho$ is a physical constant with dimensions of length squared divided by time, called the *kinematic viscosity* of the fluid. In compact notation, the vorticity transport equation reads

$$\frac{D\omega_z}{Dt} \equiv \nu \nabla^2 \omega_z, \quad (6.6.15)$$

where D/Dt is the material derivative and ∇^2 is the Laplacian operator in the xy plane.

The kinematic viscosity of water and air is shown in Table 6.6.1 at three temperatures. Note that the kinematic viscosity of air is higher than that of water by two or three orders of magnitude. In contrast, the viscosity of water is higher than that of air by one or two orders of magnitude. Curiously, air is kinematically more viscous than water due to its lower density.

The right-hand side of (6.6.14) expresses diffusion of vorticity in the xy plane. Like temperature or concentration of a species, vorticity spreads from regions of highly rotational flow to regions of irrotational flow; that is, from regions where small spherical parcels exhibit intense rotation to regions of weakly rotational or irrotational motion. The actual mechanism by which this occurs will be exemplified in Chapters 7 and 10 with reference to unsteady and boundary-layer flow.

6.6.2 Axisymmetric flow

Consider an axisymmetric flow in the absence swirling motion and refer to cylindrical polar coordinates, (x, σ, φ) , as shown in Figure 6.6.2. Working as previously for two-dimensional

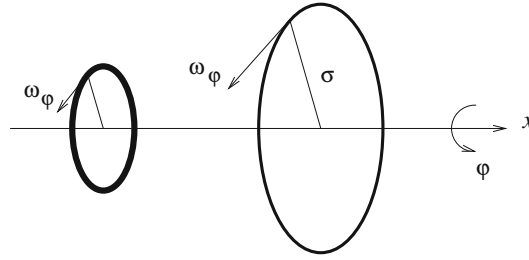


Figure 6.6.2 The vorticity of a point particle in an axisymmetric flow increases as the particle moves farther away from the axis of symmetry due to vortex stretching.

flow, we derive the vorticity transport equation for an incompressible Newtonian fluid with uniform density and viscosity,

$$\frac{D}{Dt} \left(\frac{\omega_\varphi}{\sigma} \right) = \nu \frac{1}{\sigma^2} \mathcal{E}^2(\sigma \omega_\varphi), \quad (6.6.16)$$

where σ is the distance from the x axis, The second-order linear differential operator \mathcal{E}^2 on the right-hand side, defined in equations (2.9.24) and (2.9.27), is the counterpart of the Laplacian operator for two-dimensional flow shown in (6.6.14).

Vortex stretching

When viscous forces are negligible, the right-hand side of (6.6.16) is zero and the resulting vorticity transport equation takes the simple form

$$\frac{D}{Dt} \left(\frac{\omega_\varphi}{\sigma} \right) = 0. \quad (6.6.17)$$

This equation requires that the azimuthal component of the vorticity of a point particle, ω_φ , is proportional to the distance of the point particle from the axis of symmetry, σ , so that the ratio between the two is constant in time and equal to the initial value, as illustrated schematically in Figure 6.6.2. This fundamental evolution law expresses a physical process known as *vortex stretching*. The significance of vortex stretching will be discussed in Chapter 11 in the context of vortex flow.

6.6.3 Three-dimensional flow

Generalizing the preceding discussion, we proceed to derive an evolution equation for the vorticity vector field in a three-dimensional incompressible Newtonian flow. The density and viscosity are assumed to be uniform throughout the domain of flow.

Our point of departure is the Navier–Stokes equation (6.4.3). Using the expression for the point particle acceleration shown on the left-hand side of equation (6.3.26), we derive the following alternative form of the Navier–Stokes equation in terms of the vortex force,

$$\rho \left(\frac{\partial \mathbf{u}}{\partial t} + \frac{1}{2} \nabla u^2 + \boldsymbol{\omega} \times \mathbf{u} \right) = -\nabla p + \mu \nabla^2 \mathbf{u} + \rho \mathbf{g}, \quad (6.6.18)$$

where

$$u^2 \equiv u_x^2 + u_y^2 + u_z^2 \quad (6.6.19)$$

is the square of the magnitude of the velocity.

To derive an evolution equation for the vorticity, we take the curl of both sides of equation (6.6.18). A vector identity states that the curl of the gradient of a smooth scalar function of position, $f(\mathbf{x})$, is identically zero,

$$\nabla \times \nabla f = \mathbf{0}. \quad (6.6.20)$$

To prove this identity, we work in index notation and express the i th component of the left-hand side as

$$\epsilon_{ijk} \frac{\partial}{\partial x_j} \left(\frac{\partial f}{\partial x_k} \right) = \epsilon_{ijk} \frac{\partial^2 f}{\partial x_j \partial x_k} = -\epsilon_{ikj} \frac{\partial^2 f}{\partial x_k \partial x_j}. \quad (6.6.21)$$

The symmetry of the second derivative on the right-hand side, combined with the inherent antisymmetry of the alternating tensor, ensures that the right-hand side is identically zero.

Using identity (6.6.20), we find that the curl of the second term on the left-hand side of (6.6.18), involving the square of the velocity, and the curl of the first term on the right-hand side of (6.6.18), involving the pressure gradient, are both zero. Invoking the definition of the vorticity, $\boldsymbol{\omega} = \nabla \times \mathbf{u}$, we obtain the vorticity transport equation for three-dimensional flow,

$$\frac{\partial \boldsymbol{\omega}}{\partial t} + \nabla \times (\boldsymbol{\omega} \times \mathbf{u}) = \nu \nabla^2 \boldsymbol{\omega}, \quad (6.6.22)$$

where $\nu \equiv \mu/\rho$ is the kinematic viscosity of the fluid.

Evolution of the point particle vorticity

The second term on the left-hand side of (6.6.22), denoted by

$$\mathcal{A} \equiv \nabla \times (\boldsymbol{\omega} \times \mathbf{u}), \quad (6.6.23)$$

can be manipulated to acquire a precise physical interpretation. In index notation,

$$\mathcal{A}_i = \epsilon_{ijk} \frac{\partial}{\partial x_j} (\epsilon_{klm} \omega_l u_m) = \epsilon_{ijk} \epsilon_{klm} \frac{\partial (\omega_l u_m)}{\partial x_j}. \quad (6.6.24)$$

Rearranging the indices, we obtain

$$\mathcal{A}_i = \epsilon_{ijk} \epsilon_{lmk} \frac{\partial (\omega_l u_m)}{\partial x_j}. \quad (6.6.25)$$

Using the property of the alternating tensor

$$\epsilon_{ijk} \epsilon_{lmk} = \delta_{il} \delta_{jm} - \delta_{im} \delta_{jl}, \quad (6.6.26)$$

we find that

$$\mathcal{A}_i = (\delta_{il} \delta_{jlm} - \delta_{im} \delta_{jl}) \frac{\partial(\omega_l u_m)}{\partial x_j} = \frac{\partial(\omega_i u_j)}{\partial x_j} - \frac{\partial(\omega_j u_i)}{\partial x_j}. \quad (6.6.27)$$

Expanding the product of the derivative on the right-hand side, we obtain

$$\mathcal{A}_i = u_j \frac{\partial \omega_i}{\partial x_j} + \omega_i \frac{\partial u_j}{\partial x_j} - u_i \frac{\partial \omega_j}{\partial x_j} - \omega_j \frac{\partial u_i}{\partial x_j}. \quad (6.6.28)$$

An identity states that the divergence of the curl of a smooth vector field is zero. A consequence of this identity is that the vorticity field is solenoidal,

$$\nabla \cdot \boldsymbol{\omega} = \nabla \cdot (\nabla \times \mathbf{u}) = 0. \quad (6.6.29)$$

Because the fluid has been assumed incompressible, the velocity field is also solenoidal, $\nabla \cdot \mathbf{u} = 0$. Consequently, the second and third terms on the right-hand side of (6.6.28) are zero, yielding

$$\mathcal{A}_i = u_j \frac{\partial \omega_i}{\partial x_j} - \omega_j \frac{\partial u_i}{\partial x_j}. \quad (6.6.30)$$

Substituting the result back into equation (6.6.22), we derive the targeted vorticity transport equation

$$\frac{D \omega_i}{Dt} = \frac{\partial \omega_i}{\partial t} + u_j \frac{\partial \omega_i}{\partial x_j} = \omega_j \frac{\partial u_i}{\partial x_j} + \nu \nabla^2 \omega_i. \quad (6.6.31)$$

In vector notation,

$$\frac{D \boldsymbol{\omega}}{Dt} = \frac{\partial \boldsymbol{\omega}}{\partial t} + \mathbf{u} \cdot \nabla \boldsymbol{\omega} = \boldsymbol{\omega} \cdot \nabla \mathbf{u} + \nu \nabla^2 \boldsymbol{\omega}, \quad (6.6.32)$$

where $D\boldsymbol{\omega}/Dt$ is the material derivative of the vorticity expressing the rate of change of the vorticity vector following the motion of a point particle.

Vorticity rotation and vortex stretching

To understand the nature of the first term on the right-hand side of (6.6.32), $\boldsymbol{\omega} \cdot \nabla \mathbf{u}$, we consider a small material vector, $d\mathbf{X}$, and label the first point A and the last point B. Using a Taylor series expansion, we find that the difference in the velocity across the end points is

$$\mathbf{u}^B - \mathbf{u}^A \simeq d\mathbf{X} \cdot \nabla \mathbf{u}. \quad (6.6.33)$$

Comparing this expression with the expression of interest $\boldsymbol{\omega} \cdot \nabla \mathbf{u}$, we find that the vorticity vector behaves like a material vector convected by the flow. This means that the vorticity vector rotates and stretches or compresses under the influence of the local flow.

In the case of two-dimensional flow, because the vorticity vector is normal to the plane of the flow, neither rotation, nor stretching, nor compression can take place. In the case of axisymmetric flow, because the vorticity vector points in direction of the azimuthal angle, φ , rotation is prohibited but stretching or compression can take place, as discussed in Section 6.6.2.

Persistence of irrotational motion in an inviscid flow

One important consequence of the vorticity transport equation (6.6.32) is that, if the vorticity of a point particle is zero at the initial instant, it will remain zero at any time. Thus, volumes of rotational fluid remain rotational, volumes of irrotational fluid remain irrotational, and the interface between rotational and irrotational fluid remains sharp and well-defined at any time.

Source of vorticity in viscous flow

In practice, because a fluid flow is always established from the state of rest, the initial vorticity distribution is zero. Since the right-hand side of the vorticity transport equation (6.6.32) vanishes throughout the fluid, the initial rate of production of vorticity is also zero, and this may suggest deceptively that the flow will remain irrotational at any time. In fact, vorticity, like heat, enters the fluid by diffusion across the boundaries. The precise mechanism by which this occurs is discussed in Chapters 7 and 10.

PROBLEMS

6.6.1 *Reduction to two-dimensional flow*

Show that the vorticity transport equation (6.6.32) reproduces the transport equation (6.6.14) for the strength of the vorticity, ω_z , in a two-dimensional flow in the xy plane.

6.6.2 *Convection of vorticity*

Prove the identity

$$\omega_j \frac{\partial u_i}{\partial x_j} = \omega_j \frac{\partial u_j}{\partial x_i}. \quad (6.6.34)$$

This identity allows us to express the first term on the left-hand side of (6.6.32) in the alternative form

$$\boldsymbol{\omega} \cdot \nabla \mathbf{u} = \nabla \mathbf{u} \cdot \boldsymbol{\omega}. \quad (6.6.35)$$

Hint: Begin with the identity $\boldsymbol{\omega} \times \boldsymbol{\omega} = \boldsymbol{\omega} \times \nabla \times \mathbf{u} = \mathbf{0}$, and then work in index notation using identity (2.3.11).

6.7 Dynamic similitude and the Reynolds number

Consider a uniform (streaming) flow along the x axis with velocity U_1 past a stationary body with designated size L_1 , as illustrated in Figure 6.7.1(a). Also consider another streaming

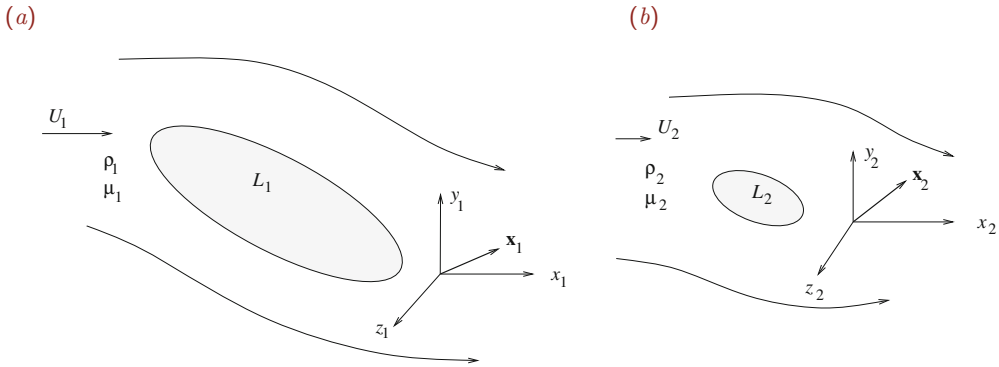


Figure 6.7.1 Illustration of flow in two similar domains. If the Reynolds numbers of the two flows are equal, as shown in equation (6.7.10), the velocity and pressure field of the second flow may be deduced those in the first flow, and *vice versa*, by rescaling.

flow along the x axis with velocity U_2 past a second body that arises by shrinking or expanding the first body by a certain factor, α , as illustrated in [Figure 6.7.1\(b\)](#). If the second body is smaller than the first body, $\alpha < 1$; if the second body is larger than the first body, $\alpha > 1$.

If the surface of the first body is described by an equation of the general form

$$f_1(x_1, y_1, z_1) = 0, \quad (6.7.1)$$

then the surface of the second body is described by the equation

$$f_2(x_2, y_2, z_2) = f_1\left(\frac{x_2}{\alpha}, \frac{y_2}{\alpha}, \frac{z_2}{\alpha}\right) = 0, \quad (6.7.2)$$

where

$$\alpha \equiv \frac{L_2}{L_1} \quad (6.7.3)$$

is a scaling factor. Corresponding points on the first and second body are related by $\mathbf{x}_2 = \alpha \mathbf{x}_1$.

A sphere

For example, if the first body is a sphere of radius L_1 centered at a point, $\mathbf{x}_{c_1} = (x_{c_1}, y_{c_1}, z_{c_1})$, then the equation describing the surface of this body is

$$f_1(x_1, y_1, z_1) = (x_1 - x_{c_1})^2 + (y_1 - y_{c_1})^2 + (z_1 - z_{c_1})^2 - L_1^2 = 0 \quad (6.7.4)$$

and the equation describing the surface of the second body is

$$f_2(x_2, y_2, z_2) = f_1\left(\frac{x_2}{\alpha}, \frac{y_2}{\alpha}, \frac{z_2}{\alpha}\right) \quad (6.7.5)$$

or

$$f_2(x_2, y_2, z_2) = \left(\frac{x_2}{\alpha} - x_{c_1}\right)^2 + \left(\frac{y_2}{\alpha} - y_{c_1}\right)^2 + \left(\frac{z_2}{\alpha} - z_{c_1}\right)^2 - L_1^2 = 0. \quad (6.7.6)$$

Simplifying, we obtain

$$f_2(x_2, y_2, z_2) = \frac{1}{\alpha^2} \left((x_2 - \alpha x_{c_1})^2 + (y_2 - \alpha y_{c_1})^2 + (z_2 - \alpha z_{c_1})^2 - L_2^2 \right) = 0, \quad (6.7.7)$$

which the equation of a sphere of radius $L_2 = \alpha L_1$ centered at the point $\mathbf{x}_{c_2} = \alpha \mathbf{x}_{c_1}$. We may set without loss of generality $\mathbf{x}_{c_1} = \mathbf{0}$, in which case both spheres are centered at the origin.

Reynolds number

Let ρ_1 and μ_1 be the density and viscosity of the first fluid, and ρ_2 and μ_2 be the density and viscosity of the second fluid. Both fluids are assumed to be incompressible and Newtonian. We will show that, when the values of the four control and physical parameters defining the first flow,

$$L_1, \quad U_1, \quad \rho_1, \quad \mu_1, \quad (6.7.8)$$

and the corresponding values of the four control and physical parameters defining the second flow,

$$L_2, \quad U_2, \quad \rho_2, \quad \mu_2, \quad (6.7.9)$$

are related by the equation

$$\frac{\rho_1 U_1 L_1}{\mu_1} = \frac{\rho_2 U_2 L_2}{\mu_2}, \quad (6.7.10)$$

then the structure of the second flow can be inferred from the structure of the first flow, and *vice versa*, by a simple computation described as rescaling. The left-hand side of (6.7.10) is the Reynolds number of the first flow, and the right-hand side of (6.7.10) is the Reynolds number of the second flow.

Rescaling

To deduce the structure of the second flow from the structure of the first flow, we introduce the dynamic pressure established due to the flow, defined as the pressure deviation from the hydrostatic distribution,

$$\varsigma_1 \equiv p_1 - \rho_1 \mathbf{g} \cdot \mathbf{x}_1, \quad \varsigma_2 \equiv p_2 - \rho_2 \mathbf{g} \cdot \mathbf{x}_2. \quad (6.7.11)$$

In the absence of flow, the pressure assumes the hydrostatic distribution and the dynamic pressure vanishes throughout both domains of flow.

Now we consider an arbitrary point in the first flow, \mathbf{x}_1 , and a corresponding point in the second flow whose coordinates are given by

$$\mathbf{x}_2 = \alpha \mathbf{x}_1. \quad (6.7.12)$$

Equations (6.7.1) and (6.7.2) ensure that, if the point \mathbf{x}_1 lies at the surface of the body in the first flow, then the point \mathbf{x}_2 will lie at the surface of the body in the second flow.

We will demonstrate that, when relation (6.7.10) is fulfilled, the velocity and dynamic pressure at the point \mathbf{x}_2 in the second flow are related to those at the point \mathbf{x}_1 in the first flow by the equations

$$\mathbf{u}_2(\mathbf{x}_2) = \delta \mathbf{u}_1(\mathbf{x}_1), \quad \varsigma_2(\mathbf{x}_2) = \beta \delta^2 \varsigma_1(\mathbf{x}_1), \quad (6.7.13)$$

where δ is the ratio of the velocities of the incident flow and β is the density ratio,

$$\delta \equiv \frac{U_2}{U_1}, \quad \beta \equiv \frac{\rho_2}{\rho_1}. \quad (6.7.14)$$

The equality of the Reynolds numbers expressed by (6.7.10) requires that

$$\beta \delta = \alpha \lambda, \quad (6.7.15)$$

where

$$\lambda \equiv \frac{\mu_2}{\mu_1} \quad (6.7.16)$$

is the viscosity ratio.

Unsteady flow

Relations (6.7.13) are also valid for unsteady flow, provided that the velocity field of the first flow at the designated origin of time is related to the velocity of the second flow at the designated origin of time by the first of equations (6.7.13), and the comparison is made at times t_1 and t_2 related by

$$t_2 = \frac{\delta}{\alpha} t_1. \quad (6.7.17)$$

A implicit assumption is that both flows have been started at the same time.

6.7.1 Dimensional analysis

To prove relations (6.7.13), we consider the Navier–Stokes equation (6.5.7),

$$\rho \left(\frac{\partial \mathbf{u}}{\partial t} + \mathbf{u} \cdot \nabla \mathbf{u} \right) = -\nabla p + \mu \nabla^2 \mathbf{u} + \rho \mathbf{g}, \quad (6.7.18)$$

and the continuity equation for an incompressible fluid,

$$\nabla \cdot \mathbf{u} = 0, \quad (6.7.19)$$

governing the structure and dynamics of each flow with appropriate physical constants corresponding to the two fluids, subject to appropriate far-field and boundary conditions, and work in three stages.

First flow

In the first stage, we consider the first flow and introduce the dimensionless independent variables

$$\hat{x}_1 = \frac{x_1}{L_1}, \quad \hat{y}_1 = \frac{y_1}{L_1}, \quad \hat{z}_1 = \frac{z_1}{L_1}, \quad \hat{t}_1 = \frac{t_1 U_1}{L_1}, \quad (6.7.20)$$

and the dimensionless dependent variables

$$\hat{u}_{x_1} = \frac{u_{x_1}}{U_1}, \quad \hat{u}_{y_1} = \frac{u_{y_1}}{U_1}, \quad \hat{u}_{z_1} = \frac{u_{z_1}}{U_1}, \quad \hat{s}_1 = \frac{s_1}{\rho_1 U_1^2}, \quad (6.7.21)$$

all indicated by a caret (hat). Solving for the dimensional variables in terms of their dimensionless counterparts, and substituting the result into the Navier–Stokes equation and the continuity equation, we obtain

$$\frac{\partial \hat{\mathbf{u}}_1}{\partial \hat{t}_1} + \hat{\mathbf{u}}_1 \cdot \hat{\nabla}_1 \hat{\mathbf{u}}_1 = -\hat{\nabla}_1 \hat{s}_1 + \frac{1}{\text{Re}_1} \hat{\nabla}_1^2 \hat{\mathbf{u}}_1 \quad (6.7.22)$$

and

$$\hat{\nabla}_1 \cdot \hat{\mathbf{u}}_1 = 0, \quad (6.7.23)$$

where

$$\text{Re}_1 \equiv \frac{\rho_1 U_1 L_1}{\mu_1} \quad (6.7.24)$$

is the Reynolds number of the first flow, as shown on the left-hand side of (6.7.10). We have introduced the dimensionless gradient and associated Laplacian operator

$$\hat{\nabla}_1 \equiv \left(\frac{\partial}{\partial \hat{x}_1}, \quad \frac{\partial}{\partial \hat{y}_1}, \quad \frac{\partial}{\partial \hat{z}_1} \right), \quad \hat{\nabla}_1^2 \equiv \frac{\partial^2}{\partial \hat{x}_1^2} + \frac{\partial^2}{\partial \hat{y}_1^2} + \frac{\partial^2}{\partial \hat{z}_1^2}. \quad (6.7.25)$$

The far-field condition requires that, far from the body, the dimensionless velocity components \hat{u}_{x_1} tends to unity, whereas \hat{u}_{y_1} and \hat{u}_{z_1} decay to zero. The no-slip and no-penetration boundary conditions require that the velocity vanishes at points (x_1, y_1, z_1) that satisfy equation (6.7.1) or, equivalently, points $(\hat{x}_1, \hat{y}_1, \hat{z}_1)$ that satisfy the equation

$$f_1(L_1 \hat{x}_1, L_1 \hat{y}_1, L_1 \hat{z}_1) = 0 \quad (6.7.26)$$

in dimensionless space.

Second flow

In the second stage, we consider the second flow and introduce the dimensionless independent variables

$$\hat{x}_2 = \frac{x_2}{L_2}, \quad \hat{y}_2 = \frac{y_2}{L_2}, \quad \hat{z}_2 = \frac{z_2}{L_2}, \quad \hat{t}_2 = \frac{t_2 U_2}{L_2}, \quad (6.7.27)$$

and the dimensionless dependent variables

$$\hat{u}_{x_2} = \frac{u_{x_2}}{U_2}, \quad \hat{u}_{y_2} = \frac{u_{y_2}}{U_2}, \quad \hat{u}_{z_2} = \frac{u_{z_2}}{U_2}, \quad \hat{s}_2 = \frac{s_2}{\rho_2 U_2^2}. \quad (6.7.28)$$

Solving for the dimensional variables in terms of their dimensionless counterparts, and substituting the result into the Navier–Stokes and continuity equation, we find that

$$\frac{\partial \hat{\mathbf{u}}_2}{\partial \hat{t}_2} + \hat{\mathbf{u}}_2 \cdot \hat{\nabla}_2 \hat{\mathbf{u}}_2 = -\hat{\nabla}_2 \hat{s}_2 + \frac{1}{\text{Re}_2} \hat{\nabla}_2^2 \hat{\mathbf{u}}_2 \quad (6.7.29)$$

and

$$\hat{\nabla}_2 \cdot \hat{\mathbf{u}}_2 = 0, \quad (6.7.30)$$

where

$$\text{Re}_2 \equiv \frac{\rho_2 U_2 L_2}{\mu_2} \quad (6.7.31)$$

is the Reynolds number of the second flow, as shown on the right-hand side of (6.7.10). We have introduced the dimensionless gradient and associated Laplacian operator

$$\hat{\nabla}_2 \equiv \left(\frac{\partial}{\partial \hat{x}_2}, \quad \frac{\partial}{\partial \hat{y}_2}, \quad \frac{\partial}{\partial \hat{z}_2} \right), \quad \hat{\nabla}_2^2 \equiv \frac{\partial^2}{\partial \hat{x}_2^2} + \frac{\partial^2}{\partial \hat{y}_2^2} + \frac{\partial^2}{\partial \hat{z}_2^2}. \quad (6.7.32)$$

The far-field condition requires that the dimensionless velocity component \hat{u}_{x_2} tends to unity, whereas \hat{u}_{y_2} and \hat{u}_{z_2} decay to zero far from the body. The no-slip and no-penetration boundary conditions require that the velocity vanishes at points (x_2, y_2, z_2) that satisfy equation (6.7.2) or, equivalently, points $(\hat{x}_2, \hat{y}_2, \hat{z}_2)$ that satisfy the equation

$$f_1(L_1 \hat{x}_2, L_1 \hat{y}_2, L_1 \hat{z}_2) = 0 \quad (6.7.33)$$

in dimensionless space.

Comparison

In the third stage, we compare one by one corresponding equations and boundary conditions governing the two flows in the dimensionless variables indicated by a hat, and draw four important conclusions:

1. The Navier–Stokes equation (6.7.22) is identical to the Navier–Stokes equation (6.7.29), provided that the two Reynolds numbers are equal, $\text{Re}_1 = \text{Re}_2$, as stated in (6.7.10).
2. The continuity equation (6.7.23) is identical to the continuity equation (6.7.30) independent of the Reynolds numbers.
3. The far-field conditions are identical: both dimensionless velocities designated by a caret tend to $[1, 0, 0]$ far from the body.

4. The boundary conditions on the first body described by (6.7.26) are identical to the boundary conditions on the second body described by (6.7.33).

These results demonstrate that, when the Reynolds numbers of the two flows are equal, values of the dimensionless dependent variables in the two flows at corresponding dimensionless times and dimensionless positions are the same. For example, setting

$$\widehat{\varsigma}_1(\widehat{\mathbf{x}}_1) = \widehat{\varsigma}_2(\widehat{\mathbf{x}}_2) \quad (6.7.34)$$

and using the definitions (6.7.21) and (6.7.28), we derive the second relation in (6.7.13), subject to the definitions given in (6.7.14).

An important implication of the scaling analysis is that a flow of interest in a large domain, such as the flow past an aircraft, can be studied conveniently in a miniaturized geometry. Conversely, a flow of interest in a small domain, such as the flow over a small pit due to surface corrosion, can be studied conveniently in an enlarged domain.

PROBLEM

6.7.1 Reynolds number

Compute the Reynolds number of (a) an ant crawling, (b) a person running, (c) a car moving at 100 km per hour, and (d) an elephant running across a plain at maximum speed.

6.8 Structure of a flow as a function of the Reynolds number

Consider the flow of an incompressible fluid in a domain with characteristic length L , identify an appropriate characteristic velocity, U , and compute the Reynolds number

$$\text{Re} \equiv \frac{\rho LU}{\mu} = \frac{LU}{\nu}, \quad (6.8.1)$$

where $\nu \equiv \mu/\rho$ is the kinematic viscosity of the fluid. Next, introduce the dimensionless independent variables

$$\widehat{x} = \frac{x}{L}, \quad \widehat{y} = \frac{y}{L}, \quad \widehat{z} = \frac{z}{L}, \quad \widehat{t} = \frac{tU}{L}, \quad (6.8.2)$$

and the dimensionless dependent variables

$$\widehat{u}_x = \frac{u_x}{U}, \quad \widehat{u}_y = \frac{u_y}{U}, \quad \widehat{u}_z = \frac{u_z}{U}, \quad \widehat{\varsigma} = \frac{\varsigma}{\rho U^2}, \quad (6.8.3)$$

where ς is the dynamic pressure excluding variations in hydrostatics. Solving for the dimensional variables in terms of their dimensionless counterparts and substituting the result into the Navier–Stokes equation and the continuity equation, we obtain the dimensionless forms

$$\frac{\partial \widehat{\mathbf{u}}}{\partial \widehat{t}} + \widehat{\mathbf{u}} \cdot \widehat{\nabla} \widehat{\mathbf{u}} = -\widehat{\nabla} \widehat{\varsigma} + \frac{1}{\text{Re}} \widehat{\nabla}^2 \widehat{\mathbf{u}} \quad (6.8.4)$$

and

$$\widehat{\nabla} \cdot \widehat{\mathbf{u}} = 0. \quad (6.8.5)$$

These dimensionless forms reveal that, given the boundary shape, the structure of a flow is determined by L , U , ρ , and μ collectively through the dimensionless Reynolds number rather than individually, in the sense of the dynamic similitude expressed by equations (6.7.13) and (6.7.14).

Velocity and length scales

The choice of characteristic velocity, U , and length scale, L , is not always apparent. Subtleties arise when the domain of flow contains an intrinsic length scale or a multitude of length scales. Examples include the flow of a suspension of small particles and the flow established spontaneously due to a hydrodynamic instability, in the absence of external forcing.

For the successful choices of L and U , all terms in the dimensionless Navier–Stokes equation (6.8.4), with the possible exception of the pressure gradient term, are of order unity. The Reynolds number then expresses the relative importance of inertial forces, assumed to scale with $\rho U^2/L$, and viscous forces, assumed to scale with $\mu U/L^2$. Their ratio is precisely the Reynolds number defined in (6.8.1).

6.8.1 Stokes flow

If the Reynolds number is small, viscous forces dominate in that the left-hand side of the dimensionless Navier–Stokes equation (6.8.4) makes a negligible contribution to the underlying balance. Although the dimensionless pressure gradient also appears to make a negligible contribution, this is only a mathematical illusion.

To see this, we observe that the dimensionless pressure arose from the arbitrary scaling shown in the equation in (6.8.3), which can be contrasted with the physical scaling of the position vector and velocity in terms of the unambiguous length and velocity scales, L and U . As a consequence, the dimensionless pressure gradient may become singular as the Reynolds number tends to zero, requiring an alternative scaling. To prevent this failure, we retain the pressure gradient in the dimensionless form of the Navier–Stokes equation irrespective of the Reynolds number.

Reverting to dimensional variables, we find that the Navier–Stokes equation reduces to the Stokes equation,

$$\mathbf{0} = -\nabla p + \mu \nabla^2 \mathbf{u} + \rho \mathbf{g}, \quad (6.8.6)$$

which describes steady or unsteady creeping flow with negligible inertial forces. cursory inspection reveals that the pressure scales with $\mu U/L$ rather than ρU^2 . The analysis and computation of creeping flow will be the exclusive topic of Chapter 9.

6.8.2 Flows at high Reynolds numbers

Inspecting (6.8.4), we find that, when the Reynolds number is high, viscous forces can be neglected, provided that the velocity does not change rapidly over a small distance across a fluid layer that is thin compared to the global size of the boundaries. Otherwise, the standard scaling with respect to U and L may cease to be valid.

Thin layers supporting large velocity differences typically occur along flow boundaries or interfaces between two adjacent streams of the same fluid or different fluids. In Chapter 10, we will see that viscous forces are significant inside these layers, even though the bulk of the flow may occur at high Reynolds numbers.

6.8.3 Laminar and turbulent flow

When the Reynolds number exceeds a certain threshold, an unsteady small-scale motion characterized by rapid fluctuations in the velocity and vorticity fields is spontaneously established. In practice, turbulent motion is often superposed on a steady or unsteady macroscopic or large-scale flow that evolves at a slower rate. A flow below the critical Reynolds number is called *laminar* to indicate that the streamlines are smooth, whereas a flow above the critical Reynolds number is called *turbulent* to indicate that the streamlines are highly convoluted.

Transition to turbulence

The transition from laminar to turbulent flow may occur by several venues, including the amplification of spontaneous internal waves. The critical Reynolds number where transition occurs can be estimated theoretically by carrying out a stability analysis, as discussed in Chapter 10. The dynamics of turbulent motion can be studied by several methods, including statistical analysis, nonlinear dynamical systems theory, and vortex dynamics.

PROBLEMS

6.8.1 Characteristic scales

Identify the characteristic velocity scale, U , length scale, L , and Reynolds number of (a) simple shear flow past a stationary body, (b) flow due to the settling of a small particle in the atmosphere, and (c) flow due to a breaking wave in the ocean.

6.9 Dimensionless numbers in fluid dynamics

We have demonstrated that two geometrically related flows occurring at the same Reynolds number are similar, in that one flow can be deduced from the other by rescaling. Arguments have been made for a flow that is bounded by a solid surface over which the no-slip and no-penetration boundary conditions apply. A time-independent velocity field was imposed in the far field as a driving mechanism.

If the driving mechanism is time dependent or the flow is bounded by fluid interfaces and free surfaces, additional conditions for dynamic similitude requiring the equality of further dimensionless numbers are necessary. These dimensionless numbers enter the problem formulation either through the governing equations or through boundary and interfacial conditions.

Frequency number for a time-dependent flow

Let us consider an externally forced time-dependent flow and identify a velocity scale, U , a length scale, L , and a time scale, T . In the case of periodic flow with angular frequency ω due, for example, to an oscillating pressure gradient, T can be identified with the period, $T = 2\pi/\omega$. The relative importance of inertial and viscous forces in the equation of motion is expressed by the dimensionless frequency parameter

$$\beta \equiv \frac{L^2}{\nu T}, \quad (6.9.1)$$

where ν is the kinematic viscosity of the fluid. In the case of an intrinsically time-dependent flow, $T = L/U$, the frequency parameter reduces to the Reynolds number $\beta = \text{Re} = LU/\nu$.

Froude number

Consider flow in the ocean due to the propagation of water waves. The relative importance of inertial and gravitational forces is determined by the Froude number,

$$\text{Fr} \equiv \frac{U}{\sqrt{gL}}, \quad (6.9.2)$$

where g is the magnitude of the acceleration of gravity. In the case of flow over a hump discussed in Section 6.4, the Froude number takes the specific form shown in equation (6.4.43).

Bond number

The relative importance of gravitational forces and surface tension in a fluid that is confined by a free surface or fluid interface is determined by the Bond number,

$$\text{Bo} \equiv \frac{\rho g L^2}{\gamma}, \quad (6.9.3)$$

where γ is the surface tension (Problem 6.9.1).

Weber number

The relative importance of inertial forces and surface tension in a flow that is confined by a free surface or fluid interface is determined by the Weber number,

$$\text{We} \equiv \frac{\rho U^2 L}{\gamma}. \quad (6.9.4)$$

For example, the Weber number determines the deformation and structure of the flow around a gas bubble rising or convected at high speed through an ambient liquid.

Capillary number

The relative importance of viscous forces and surface tension in a fluid bounded by a free surface or fluid interface is determined by the capillary number,

$$\text{Ca} \equiv \frac{\mu U}{\gamma}. \quad (6.9.5)$$

For example, the capillary number determines the deformation and thus the structure of the flow around a liquid droplet immersed in a shear flow.

PROBLEMS

6.9.1 *Bond number in hydrostatics*

Explain how the Bond number arises from the scaling of the Laplace-Young equation (5.4.8) in hydrostatics.

6.9.2 *Ratio of two numbers*

What is the ratio between the Weber number and the capillary number?

Channel, tube, and film flow

- 7.1 Steady flow in a two-dimensional channel
- 7.2 Steady film flow down an inclined plane
- 7.3 Steady flow through a circular tube
- 7.4 Steady flow through an annular tube
- 7.5 Steady flow in channels and tubes
- 7.6 Steady swirling flows
- 7.7 Transient channel flows
- 7.8 Oscillatory channel flows
- 7.9 Transient and oscillatory flow in a circular tube

In previous chapters, we derived the differential equations governing the motion of an incompressible Newtonian fluid by requiring mass conservation and enforcing Newton's second law of motion for infinitesimal fluid parcels. The governing equations are accompanied by initial, boundary, and interfacial conditions, as required. In this chapter, we proceed to derive analytical and semi-analytical solutions for an important class of steady and unsteady flows with rectilinear or circular streamlines. The engineering significance of these flows, combined with their ability to demonstrate the salient mechanisms of momentum and vorticity transport at steady or unsteady state, justify an extensive consideration.

7.1 Steady flow in a two-dimensional channel

We begin by considering flow in a two-dimensional channel confined between two parallel plane walls that are separated by distance $2a$ and are inclined by an angle β with respect to the horizontal plane, as illustrated in [Figure 7.1.1](#).

In the inclined system of Cartesian coordinates defined in [Figure 7.1.1](#), the x axis is parallel to the walls and the y axis is perpendicular to the walls. The corresponding Cartesian components of the acceleration of gravity vector are

$$g_x = g \sin \beta, \quad g_y = -g \cos \beta, \quad (7.1.1)$$

where g is the magnitude of the acceleration of gravity. The lower wall translates parallel to itself with constant velocity V_1 , and the upper wall translates parallel to itself with constant velocity V_2 .

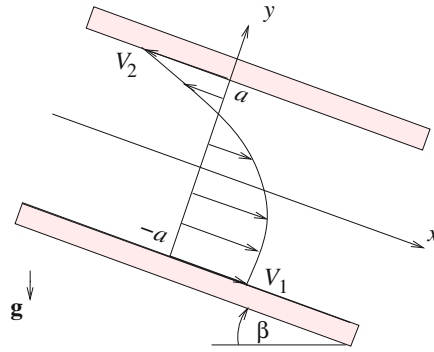


Figure 7.1.1 Illustration of steady unidirectional flow through a two-dimensional inclined channel confined between two parallel walls located at $y = \pm a$.

The motion of the fluid is governed by the Navier–Stokes equation (6.5.6) whose Cartesian components are displayed in [Table 6.5.1](#).

Unidirectional and fully developed flow

Our analysis will be based on the assumption of steady unidirectional flow, requiring that the y and z velocity components vanish, $u_y = 0$ and $u_z = 0$, while the x component remains constant in time, $\partial u_x / \partial t = 0$. This assumption precludes the occurrence of turbulent motion where small-scale three-dimensional fluctuations are observed, as discussed in Chapter 10. The continuity equation for two-dimensional flow,

$$\frac{\partial u_x}{\partial x} + \frac{\partial u_y}{\partial y} = 0, \quad (7.1.2)$$

requires that $\partial u_x / \partial x = 0$, which states that the flow is fully developed. Thus, the axial velocity, u_x , is a function of position across the channel, y , alone, that is, $u_x(y)$.

Governing equations and pressure field

Simplifying the x and y components of the equation of motion shown in [Table 6.5.1](#) by discarding terms that are identically zero, we obtain

$$0 = -\frac{\partial p}{\partial x} + \mu \frac{d^2 u_x}{dy^2} + \rho g_x \quad (7.1.3)$$

and

$$0 = -\frac{\partial p}{\partial y} + \rho g_y. \quad (7.1.4)$$

In fact, equation (7.1.4) determines the pressure distribution in hydrostatics.

It is convenient to screen out the hydrostatic variations in the direction normal to the flow by expressing the pressure in the form

$$p(x, y) = -\chi x + \rho g_y y + \pi_0, \quad (7.1.5)$$

where π_0 is a reference pressure and

$$\chi \equiv -\frac{\partial p}{\partial x} \quad (7.1.6)$$

is the negative of the pressure gradient (derivative) along the x axis.

Velocity profile

The simplified equation of motion (7.1.3) takes the form of a second-order linear ordinary differential equation,

$$\frac{d^2 u_x}{dy^2} = -\frac{\chi + \rho g_x}{\mu}. \quad (7.1.7)$$

Integrating twice with respect to y , we derive the parabolic velocity profile

$$u_x(y) = -\frac{1}{2} \frac{\chi + \rho g_x}{\mu} y^2 + By + A, \quad (7.1.8)$$

where A and B are two constants.

To evaluate the constants A and B , we enforce the no-slip boundary condition at the two walls by requiring that the fluid velocity is equal to the wall velocity. Referring to the Cartesian coordinates defined in [Figure 7.1.1](#), we require that

$$u_x = V_1 \quad \text{at} \quad y = -a \quad (7.1.9)$$

and

$$u_x = V_2 \quad \text{at} \quad y = a, \quad (7.1.10)$$

yielding

$$-\frac{1}{2} \frac{\chi + \rho g_x}{\mu} a^2 \pm Ba + A = 0. \quad (7.1.11)$$

Equations (7.1.11) provide us with two linear equations for two unknowns. Solving for A and B by adding or subtracting the equations for \pm , and substituting the result back into (7.1.8), we derive the velocity profile

$$u_x(y) = V_1 + \frac{V_2 - V_1}{2} \frac{y + a}{a} + \frac{1}{2} \frac{\chi + \rho g_x}{\mu} (a^2 - y^2) \quad (7.1.12)$$

for $-a \leq y \leq a$.

Function *chan_2d*, located in directory *04_various* of **FDLIB**, not listed in the text, evaluates the velocity profile given in (7.1.12).

Boundary- pressure- and gravity-driven flow

It is instructive to identify three special cases of the general flow expressed by equation (7.1.12), corresponding to different physical flow configurations:

1. When $\chi + \rho g_x = 0$, the last term on the right-hand side of (7.1.12) disappears and the flow is driven by boundary motion in a shear or boundary-driven mode; this is the case of *plane Couette flow*.
2. When $V_1 = 0$, $V_2 = 0$, and the channel is horizontal, $g_x = 0$, the flow is driven by an imposed pressure gradient along the x axis, which is equal to the negative of the constant χ , in a pressure-driven mode; this is the case of *Hagen* or *plane Poiseuille flow*, also called the *Hagen–Poiseuille flow*.
3. When $V_1 = 0$, $V_2 = 0$, and in the absence of pressure variation along the x axis at any y position, $\chi = 0$, we obtain *gravity-driven flow*. This flow occurs when both ends of a channel are open to the atmosphere.

Mixed cases of boundary-, pressure-, and gravity-driven flow can be obtained by linear superposition.

Shear stress

The shear stress, σ_{xy} , arises by differentiating the velocity profile (7.1.12) with respect to y , finding

$$\sigma_{xy} = \mu \frac{du_x}{dy} = \mu \frac{V_2 - V_1}{2a} - (\chi + \rho g_x) y. \quad (7.1.13)$$

In Couette flow, the shear stress is a constant determined by the difference between the velocities of the two walls and the distance between the walls, $2a$. In gravity- and pressure-driven flow, the shear stress varies linearly with position across the channel walls.

Flow rate

The flow rate along the x axis per unit width of the channel is found by integrating the velocity profile across the channel cross-section,

$$Q = \int_{-a}^a u_x(y) dy. \quad (7.1.14)$$

Substituting the velocity profile and performing the integration, we obtain

$$Q = (V_1 + V_2) a + \frac{2}{3} \frac{\chi + \rho g_x}{\mu} a^3. \quad (7.1.15)$$

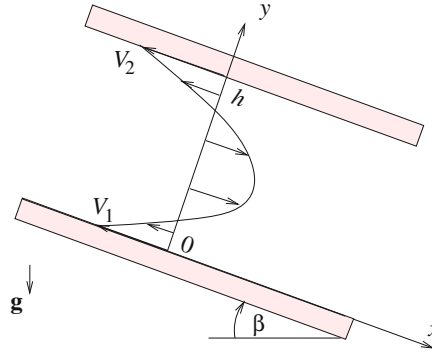


Figure 7.1.2 Illustration of steady unidirectional flow through a two-dimensional channel confined between two inclined parallel walls located at $y = 0$ and h . The x axis is attached to the lower wall.

Note the dependence on a or a^3 in the two terms on the right-hand side. The mean velocity is defined as

$$u_{\text{mean}} \equiv \frac{Q}{2a} = \frac{V_1 + V_2}{2} + \frac{1}{3} \frac{\chi + \rho g_x}{\mu} a^2. \quad (7.1.16)$$

In Couette flow, the mean velocity is the mean of the wall velocities.

7.1.1 Alternative coordinates

Expressions for the velocity profile, shear stress, flow rate, and mean velocity can be derived in the alternative coordinates defined in [Figure 7.1.2](#) where the walls are located at $y = 0$ and h . Substituting in the preceding expressions

$$a \rightarrow \frac{1}{2} h, \quad y \rightarrow y - \frac{1}{2} h, \quad (7.1.17)$$

where $h = 2a$ is the wall separation, we obtain the velocity profile

$$u_x(y) = V_1 + (V_2 - V_1) \frac{y}{h} + \frac{1}{2} \frac{\chi + \rho g_x}{\mu} y(h - y) \quad (7.1.18)$$

for $0 \leq y \leq h$. The shear stress is given by

$$\sigma_{xy} = \mu \frac{du_x}{dy} = \mu \frac{V_2 - V_1}{h} - (\chi + \rho g_x) \left(y - \frac{1}{2} h\right). \quad (7.1.19)$$

for $0 \leq y \leq h$. The flow rate is given by

$$Q \equiv \int_0^h u_x dy = \frac{V_1 + V_2}{2} h + \frac{1}{12} \frac{\chi + \rho g_x}{\mu} h^3 \quad (7.1.20)$$

and the mean velocity is given by

$$u_{\text{mean}} \equiv \frac{Q}{h} = \frac{V_1 + V_2}{2} + \frac{1}{12} \frac{\chi + \rho g_x}{\mu} h. \quad (7.1.21)$$

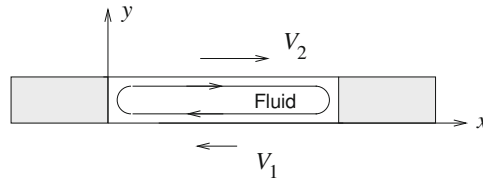


Figure 7.1.3 Flow inside a long horizontal channel that is closed at both ends. A pressure gradient is established spontaneously to satisfy the condition of vanishing flow rate.

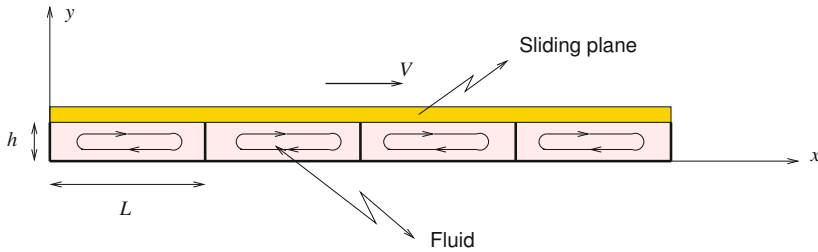


Figure 7.1.4 Illustration of a plate sliding over a stationary surface fitted with vertical plates. The space between the plates is filled with a viscous fluid.

Flow in a slender cavity

As an application, we consider flow in a slender rectangular cavity that is closed at the left and right ends so that the flow rate is zero, $Q = 0$, as shown in [Figure 7.1.3](#). Physically, the flow is driven by the translation of two moving belts identified with the lower and upper walls.

Equation (7.1.20) shows that a pressure gradient is established for the right-hand side to vanish. Setting $Q = 0$, we obtain

$$-\chi \equiv \frac{\partial p}{\partial x} = 6\mu \frac{V_1 + V_2}{h^2} + \rho g_x. \quad (7.1.22)$$

This pressure gradient generates a back-flow that ensures the condition of vanishing flow rate. In the case of a horizontal cavity, as shown in [Figure 7.1.3](#), $g_x = 0$.

Motion of a plane sliding over surface fitted with plates

In a related application, we consider a plane sliding with velocity V over a horizontal surface that is fitted with vertical plates, as shown in [Figure 7.1.4](#). The space between the plates is filled with a viscous fluid. We are interested in calculating the force necessary to sustain the translation of the plane, F , terms of the height of the vertical plates, h , the sliding velocity, V , and the fluid viscosity, μ .

We may assume as an approximation that the flow inside the slender space between two consecutive plates is unidirectional flow between two horizontal plates. The velocity profile sufficiently far from the vertical plates is found by setting $V_1 = 0$, $V_2 = V$, and $g_x = 0$ in (7.1.18), yielding

$$u_x(y) = V \frac{y}{h} + \frac{1}{2} \frac{\chi + \rho g_x}{2\mu} y (h - y). \quad (7.1.23)$$

The corresponding flow rate calculated from (7.1.20) is

$$Q = \frac{1}{2} V h + \frac{1}{12} \frac{\chi + \rho g_x}{\mu} h^3. \quad (7.1.24)$$

Since fluid cannot escape each cell, $Q = 0$ and

$$-\chi \equiv \frac{\partial p}{\partial x} = 6 \frac{\mu V}{h^2} + \rho g_x. \quad (7.1.25)$$

Substituting this expression into (7.1.23), we obtain the velocity profile

$$u_x(y) = V \frac{y}{h} \left(3 \frac{y}{h} - 2 \right). \quad (7.1.26)$$

The shear stress distribution is

$$\sigma_{xy} = \mu \frac{\partial u_x}{\partial y} = 2 \frac{\mu V}{h} \left(3 \frac{y}{h} - 1 \right). \quad (7.1.27)$$

The shear stress at the sliding plate is

$$\sigma_{xy}(y = h) = 4 \frac{\mu V}{h}, \quad (7.1.28)$$

and the corresponding resistive force for each plate spacing is

$$F_{\text{channel}} = 4 \frac{\mu V L}{h}, \quad (7.1.29)$$

where L is the separation between the plates. If the vertical plates are in contact with the sliding plane, an additional frictional force will be exerted on the sliding plane by each vertical plate, F_{fric} .

More important, an additional hydrodynamic force is exerted on the plane due to the local fluid flow deep inside each corner formed between the sliding plane and each vertical plate. A local analysis shows that, if the translating plane is in perfect contact with the plates and the corners are perfectly sharp, the magnitude of this force is infinite. To overcome this singularity, the plane will float over a thin fluid layer extending a small distance above the vertical plates.

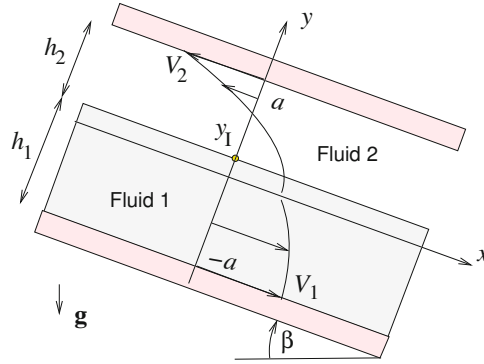


Figure 7.1.5 Illustration of steady two-layer flow through an inclined channel confined between two parallel walls located at $y = \pm a$.

7.1.2 Two-layer flow

Next, we consider the flow of two superimposed layers with generally different viscosities and densities, as illustrated in Figure 7.1.5. The lower layer is labeled 1 and the upper layer is labeled 2. In the inclined system of coordinates depicted in Figure 7.1.5, the interface is located at $y = y_I$.

Working as in the case of single-fluid flow, we derive the pressure field inside each layer corresponding to (7.1.5),

$$p^{(1)}(x, y) = -\chi x + \rho_1 g_y (y - y_I) + \pi_0 \quad (7.1.30)$$

and

$$p^{(2)}(x, y) = -\chi x + \rho_2 g_y (y - y_I) + \pi_0, \quad (7.1.31)$$

where π_0 is an unspecified reference pressure. Note that the negative of the pressure gradient, $\chi \equiv -\partial p / \partial x$, must be the same in both fluids. Otherwise, the interfacial condition requiring continuity of normal stress, which amounts to continuity of pressure, cannot be satisfied at every downstream position, x .

The velocity profile across each layer is governed by the counterparts of equation (7.1.7) for each fluid,

$$\frac{d^2 u_x^{(1)}}{dy^2} = -\frac{\chi + \rho_1 g_x}{\mu_1}, \quad \frac{d^2 u_x^{(2)}}{dy^2} = -\frac{\chi + \rho_2 g_x}{\mu_2}. \quad (7.1.32)$$

To facilitate the forthcoming algebraic manipulations, we integrate equations (7.1.32) twice with respect to y and express the solution in the form

$$u_x^{(1)}(y) = -\frac{1}{2} \frac{\chi + \rho_1 g_x}{\mu_1} (y - y_I)^2 + \xi_1 (y - y_I) + u_I \quad (7.1.33)$$

and

$$u_x^{(2)}(y) = -\frac{1}{2} \frac{\chi + \rho_2 g_x}{\mu_2} (y - y_I)^2 + \xi_2 (y - y_I) + u_I, \quad (7.1.34)$$

where u_I is the common interfacial velocity and

$$\xi_1 \equiv \left(\frac{du_x^{(1)}}{dy} \right)_{y=y_I}, \quad \xi_2 \equiv \left(\frac{du_x^{(2)}}{dy} \right)_{y=y_I} \quad (7.1.35)$$

are the interfacial shear rates expressing the slope of the velocity profile on either side of the interface.

To compute the three unknowns, u_I , ξ_1 , and ξ_2 , we enforce the no-slip boundary condition at the lower and upper walls,

$$u_x^{(1)}(y = -a) = V_1, \quad u_x^{(2)}(y = a) = V_2, \quad (7.1.36)$$

and also require that the shear stress is continuous across the interface,

$$\mu_1 \xi_1 = \mu_2 \xi_2. \quad (7.1.37)$$

After a fair amount of algebra, we derive the expressions

$$u_I = \frac{1}{2\mu_1} \frac{h_1 h_2}{\lambda + r} \left[(1 + r) \chi + \rho_1 g_x (1 + \alpha r) \right] + \frac{r V_1 + \lambda V_2}{r + \lambda} \quad (7.1.38)$$

and

$$\xi_1 = -\frac{1}{2} \frac{\chi + \rho_1 g_x}{\mu_1} h_1 + \frac{u_I - V_1}{h_1}, \quad \xi_2 = \frac{1}{2} \frac{\chi + \rho_2 g_x}{\mu_2} h_2 - \frac{u_I - V_2}{h_2}, \quad (7.1.39)$$

where

$$h_1 = a + y_I, \quad h_2 = a - y_I \quad (7.1.40)$$

are the lower and upper layer thicknesses satisfying $h_1 + h_2 = 2a$. We have introduced the viscosity ratio, the density ratio, and the layer thickness ratio,

$$\lambda \equiv \frac{\mu_2}{\mu_1}, \quad \alpha \equiv \frac{\rho_2}{\rho_1}, \quad r \equiv \frac{h_2}{h_1}. \quad (7.1.41)$$

Function *chan_2d_2l*, located in directory *04_various* of **FDLIB**, not listed in the text, evaluates the interfacial velocity, shear rates, velocity profile across the two layers, and the corresponding flow rates.

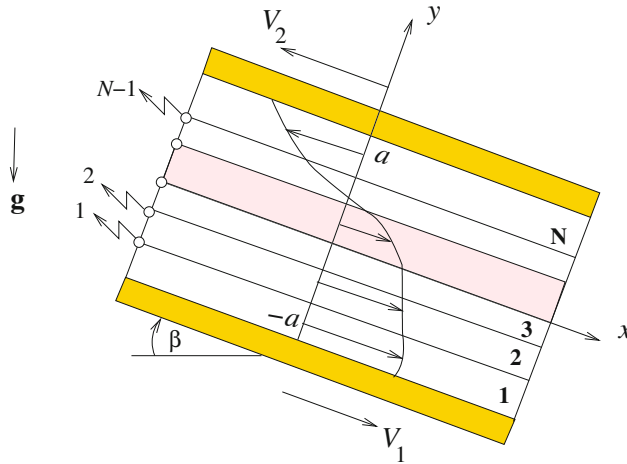


Figure 7.1.6 Illustration of steady flow of N layers through an inclined channel confined between two parallel walls located at $y = \pm a$. The interfacial labels are printed on the left and the layer labels are printed on the right.

7.1.3 Multi-layer flow

Generalizing the two-layer flow discussed in Section 7.1.2, now we consider the flow of an arbitrary number of N superimposed layers, as illustrated in Figure 7.1.6. The bottom layer is labeled 1 and the top layer is labeled N . The $N - 1$ interfaces separating the layers are located at positions

$$y = y_1^{(i)} \tag{7.1.42}$$

for $i = 1, \dots, N - 1$. In the case of two layers, $N = 2$, we obtain a single interface, as discussed in Section 7.1.2.

Governing equations

The velocity profile across the i th layer is governed by equation (7.1.7) with corresponding fluid viscosity, ρ_i , and density, μ_i ,

$$\frac{d^2 u_x^{(i)}}{dy^2} = -\frac{\chi + \rho_i g_x}{\mu_i} \tag{7.1.43}$$

for $i = 1, \dots, N$. Integrating this second-order ordinary differential equation twice with respect to y , we derive a parabolic profile,

$$u_x^{(i)}(y) = -\frac{1}{2} \frac{\chi + \rho_i g_x}{\mu_i} y^2 + B^{(i)} y + A^{(i)}, \tag{7.1.44}$$

where $A^{(i)}$ and $B^{(i)}$ are unknown constants to be determined by enforcing three conditions:

1. The no-slip boundary condition at the lower and upper walls.
2. Continuity of velocity at the interfaces expressed by the matching condition

$$\left(u_x^{(i)}\right)_{y=y_1^{(i)}} = \left(u_x^{(i+1)}\right)_{y=y_1^{(i)}} \quad (7.1.45)$$

for $i = 1, \dots, N - 1$.

3. Continuity of shear stress at the interfaces expressed by the matching condition

$$\mu_i \left(\frac{du_x^{(i)}}{dy}\right)_{y=y_1^{(i)}} = \mu_{i+1} \left(\frac{du_x^{(i+1)}}{dy}\right)_{y=y_1^{(i)}} \quad (7.1.46)$$

for $i = 1, \dots, N - 1$.

Substituting the velocity profiles (7.1.44) into (7.1.46), and solving for the coefficient $B^{(i)}$, we derive the recursive relation

$$B^{(i)} = \frac{\chi + \rho_i g_x}{\mu_i} y_1^{(i)} + \frac{\mu_{i+1}}{\mu_i} \left(B^{(i+1)} - \frac{\chi + \rho_{i+1} g_x}{\mu_{i+1}} y_1^{(i)} \right) \quad (7.1.47)$$

for $i = 1, \dots, N - 1$.

It is convenient to introduce the shear rate in the top layer at the upper wall,

$$\alpha \equiv \left(\frac{du_x^{(N)}}{dy}\right)_{y=a}. \quad (7.1.48)$$

Differentiating the profile (7.1.44) with respect to y for $i = N$, and evaluating the derivative at the upper wall, $y = a$, we obtain

$$B^{(N)} = \alpha + \frac{\chi + \rho_N g_x}{\mu_N} a. \quad (7.1.49)$$

If we knew the value of α , we would be able to compute the coefficient $B^{(N)}$ from (7.1.49), and then evaluate the rest of the coefficients, $B^{(i)}$ for $i = N - 1, \dots, 1$, using the recursion relation (7.1.47). Once this has been accomplished, we would be able to compute the coefficient $A^{(1)}$ to satisfy the no-slip condition at the bottom wall using the equation

$$u_x^{(1)}(y = -a) = -\frac{1}{2} \frac{\chi + \rho_1 g_x}{\mu_1} a^2 - B^{(1)} a + A^{(1)} = V_1, \quad (7.1.50)$$

yielding

$$A^{(1)} = V_1 + \frac{1}{2} \frac{\chi + \rho_1 g_x}{\mu_1} a^2 + B^{(1)} a, \quad (7.1.51)$$

and then compute the rest of the coefficients, $A^{(i)}$, by requiring continuity of velocity across each interface expressed by (7.1.45). At the end, the no-slip boundary condition at the

upper wall would surely be satisfied. Unfortunately, the value of α is *a priori* unknown and must be found as part of the solution.

Numerical method

An expedient method of evaluating the constant α and simultaneously computing the unknown coefficients of the velocity profiles can be devised based on the no-slip boundary condition at the upper wall. We begin by expressing this condition in the form

$$f(\alpha) \equiv u_x^{(N)}(y = a) - V_2 = 0, \quad (7.1.52)$$

where $f(\alpha)$ is an objective function. Substituting the expression for the velocity in the top layer, we obtain

$$f(\alpha) = -\frac{1}{2} \frac{\chi + \rho_N g x}{\mu_N} a^2 + B^{(N)} a + A^{(N)} - V_2 = 0. \quad (7.1.53)$$

A key observation is that, because $f(\alpha)$ is a linear function of α , it can be expressed in the form

$$f(\alpha) = C\alpha + D, \quad (7.1.54)$$

where

$$C = f(1) - f(0), \quad D = f(0). \quad (7.1.55)$$

The linear dependence becomes evident by observing that, if a certain value of α is assumed, then the procedure described in the paragraph following equation (7.1.49) can be used to evaluate the coefficients of the velocity profile across each layer, and the left-hand side of (7.1.53) can be computed by linear algebraic manipulations.

Combining equations (7.1.54) and (7.1.55), we find that the desired value of α , satisfying $f(\alpha) = 0$, is given by

$$\alpha = -\frac{D}{C} = \frac{f(0)}{f(0) - f(1)}. \quad (7.1.56)$$

The algorithm involves evaluating $f(0)$ and $f(1)$, and then using (7.1.56) to extract α .

The numerical method is coded in a function entitled *chan_2d_ml*, located in directory *04_various* of **FDLIB**. The MATLAB implementation is listed below:

```
function [Q,u,xi1,xi2,yI,uI] = chan_2d_ml ...
    (NLR,a,thick ...
    ,visc,den,gac ...
    ,V1,V2,chi,beta ...
    ,y)
```

```

%=====
% Multi-layer flow through a channel confined
% between two parallel plane walls located at y = +-a
%
% Layer numbered 1 is adjacent to the lower wall
% Layer numbered NLR is adjacent to the upper wall
%
% The velocity profile in the ith layer is given by:
%
%  $u(i) = af(i) + bf(i)*y - gf(i)*y^2$ 
%
% SYMBOLS:
% -----
%
% NLR: Number of layers
% thick: layer thicknesses
% yI(i): y position of the ith interface
% uI(i): velocity of the ith interface
% xi1(i): shear rate on lower side of the ith interface
% xi2(i): shear rate on upper side of the ith interface
% Q(i): flow rate of the ith layer
% th0: plane inclination angle
% gac: magnitude of the acceleration of gravity
% chi: negative of the pressure gradient
%=====

%-----
% set the interface positions
%-----

yI(1) = -a + thick(1);

for i=2:NLR
    yI(i) = yI(i-1) + thick(i);
end

%-----
% the velocity in the ith layer is given by:
%  $u(i) = af(i) + bf(i)*y - gf(i)*y^2$ 
% compute gf(i)
%-----

fc = gac*sin(beta);

for i=1:NLR
    gf(i) = 0.5*(chi+fc*den(i))/visc(i);
end

```

```

%-----
% In the first pass,
% we set the shear rate at upper wall "alpha" to zero
% and compute the residual of the upper wall boundary
% condition:  error0
%
% In the second pass,
% we set the shear rate at upper wall "alpha" to one
% and compute the residual of the upper wall boundary
% condition:  error1
%
% In the third pass,
% we set the proper shear rate:
% alpha = error0/(error0-error1)
%-----

alpha = 0.0;

for Ipass=1:3

%---
% specified upper wall shear stress
%---

bf(NLR) = alpha + 2.0*gf(NLR)*a;

%---
% compute bf(i) by recursion starting from the top
% and requiring continuity of shear stress
% across the interfaces
%---

for i=NLR-1:-1:1
    bf(i) = 2.0*gf(i)*yI(i) ...
        + visc(i+1)/visc(i)*(bf(i+1)-2.0*gf(i+1)*yI(i));
end

%---
% compute af(1) to satisfy the non-slip condition
% at the lower wall
%---

af(1) = V1+(bf(1)+gf(1)*a)*a;

%---
% compute af(i), i=2,...,NLR by recursion
% starting from the bottom
% and requiring continuity of velocity
%---

```

```

for i=1:NLR-1
    af(i+1) = af(i)+((bf(i)-bf(i+1)) ...
        -(gf(i)-gf(i+1))*yI(i))*yI(i);
end

%---
% error in the no-slip condition on the upper wall
% error = u(y=a)-V2
%---

if(Ipass==1)
    error0 = af(NLR)+(bf(NLR)-gf(NLR)*a)*a-V2;
    alpha = 1.0;
elseif(Ipass==2)
    error1 = af(NLR)+(bf(NLR)-gf(NLR)*a)*a-V2;
    alpha = error0/(error0-error1);
end

%---
end % of Ipass
%---

%---
% compute interfacial velocities and shear rates
%---

for i=1:NLR-1
    uI(i) = af(i)+( bf(i)-gf(i)*yI(i) ) * yI(i);
    xi1(i) = bf(i) - 2.0*gf(i)*yI(i);
    xi2(i) = bf(i+1)-2.0*gf(i+1)*yI(i);
end

%----
% compute the flow rates
% the ith layer is confined between
% the i-1 and i interfaces
%----

yI0 = -a;
Q(1) = af(1)*(yI(1)-yI0) ...
    +bf(1)*(yI(1)^2-yI0^2)/2.0 ...
    -gf(1)*(yI(1)^3-yI0^3)/3.0;

for i=2:NLR
    Q(i) = af(i)*(yI(i)-yI(i-1)) ...
        +bf(i)*(yI(i)^2-yI(i-1)^2)/2.0 ...
        -gf(i)*(yI(i)^3-yI(i-1)^3)/3.0;
end

```



Figure 7.1.7 Velocity profile across six layers in channel flow between two inclined walls generated by code *chan_2d.ml*.

```

%-----
% compute the velocity at y
%-----

% identify the host layer:

for i=1:NLR
    if(y<yI(i)) break; end
end

if(i>NLR) i=NLR; end

%---
% evaluate the velocity
%---

u = af(i) + (bf(i)-gf(i)*y)*y;

%-----
% done
%-----

return

```

The velocity profile for a configuration with six layers in an inclined channel is shown in [Figure 7.1.7](#).

7.1.4 Power-law fluids

Next, we derive the counterpart of the single-layer velocity profile (7.1.12) for a power-law fluid whose viscosity is a function of the shear rate according to the constitutive equation (4.8.2),

$$\mu = \mu_0 \left| \frac{du_x}{dy} \right|^{n-1}, \quad (7.1.57)$$

where μ_0 is a constant, n is the power-law exponent, and the vertical bars enclose the absolute value. When $n < 1$, we obtain a shear-thinning fluid; whereas, when $n > 1$, we obtain a shear-thickening fluid.

Governing equations

The x component of the equation of motion for steady unidirectional flow requires that

$$0 = \chi + \frac{d\sigma_{xy}}{dy} + \rho g_x, \quad (7.1.58)$$

where $\chi = -\partial p/\partial x$ is the negative of the streamwise pressure gradient. Integrating with respect to y , we find that the shear stress is a linear function of position,

$$\sigma_{xy} = A - (\chi + \rho g_x) y, \quad (7.1.59)$$

where A is a constant. Substituting the expression for the shear stress from the constitutive equation, we obtain a nonlinear equation,

$$\mu_0 \left| \frac{du_x}{dy} \right|^{n-1} \frac{du_x}{dy} = A - (\chi + \rho g_x) y. \quad (7.1.60)$$

The evaluation of the absolute value requires careful consideration.

Velocity profile

When $du_x/dy > 0$, we obtain the governing equation

$$\mu_0 \left(\frac{du_x}{dy} \right)^n = A - (\chi + \rho g_x) y, \quad (7.1.61)$$

yielding

$$\frac{du_x}{dy} = \frac{1}{\mu_0^{1/n}} \left(A - (\chi + \rho g_x) y \right)^{1/n}, \quad (7.1.62)$$

where the positive n th root is implied. Assuming that $\chi + \rho g_x \neq 0$, we integrate the shear rate with respect to y and derive the velocity profile

$$u_x(y) = -\frac{n}{n+1} \frac{1}{\chi + \rho g_x} \frac{1}{\mu_0^{1/n}} \left(A - (\chi + \rho g_x) y \right)^{(n+1)/n} + B, \quad (7.1.63)$$

where B is a new constant.

When $du_x/dy < 0$, we find that

$$\frac{du_x}{dy} = -\frac{1}{\mu_0^{1/n}} \left((\chi + \rho g_x) y - A \right)^{1/n}, \quad (7.1.64)$$

where the positive n th root is implied. Assuming that $\chi + \rho g_x \neq 0$, we integrate the shear rate with respect to y and derive the velocity profile

$$u_x(y) = -\frac{n}{n+1} \frac{1}{\chi + \rho g_x} \frac{1}{\mu_0^{1/n}} \left((\chi + \rho g_x) y - A \right)^{(n+1)/n} + B. \quad (7.1.65)$$

Combining the two cases, we obtain the unified form

$$u_x(y) = -\frac{n}{n+1} \frac{1}{\chi + \rho g_x} \frac{1}{\mu_0^{1/n}} \left| A - (\chi + \rho g_x) y \right|^{(n+1)/n} + B. \quad (7.1.66)$$

The constants A and B are determined by the no-slip boundary condition at the two walls. For a channel confined between two walls located at $y = \pm a$, as shown in [Figure 7.1.1](#), we require that

$$u_x(-a) = V_1, \quad u_x(a) = V_2. \quad (7.1.67)$$

Subtracting these equations to eliminate the constant B , and rearranging, we obtain

$$\begin{aligned} \left| (\chi + \rho g_x) a + A \right|^{(n+1)/n} - \left| (\chi + \rho g_x) a - A \right|^{(n+1)/n} \\ = \frac{n+1}{n} (\chi + \rho g_x) \mu_0^{1/n} (V_2 - V_1), \end{aligned} \quad (7.1.68)$$

which is a nonlinear algebraic equation for A for any power-law exponent $n \neq 1$. For $n = 1$, corresponding to a Newtonian fluid, the solution is $A = (V_2 - V_1)/(2a)$.

Pressure- and gravity-driven flow

In the case of pressure- and gravity-driven flow,

$$V_1 = 0, \quad V_2 = 0, \quad \chi + \rho g_x > 0, \quad (7.1.69)$$

the velocity profile is symmetric with respect to the centerline, $y = 0$. Requiring that $du_x/dy = 0$ at $y = 0$, we find that $A = 0$.

Equation (7.1.63) applies at the lower half of the channel, $y < 0$, whereas equation (7.1.65) applies at the upper half of the channel $y > 0$. Requiring that $u_x = 0$ at $y = \pm a$ to satisfy the no-slip boundary condition at the two walls, we obtain

$$B = \frac{n}{n+1} \frac{1}{\chi + \rho g_x} \frac{1}{\mu_0^{1/n}} \left((\chi + \rho g_x) a \right)^{(n+1)/n}. \quad (7.1.70)$$

The velocity profile is given by

$$u_x(y) = \frac{n}{n+1} \left(\frac{\chi + \rho g_x}{\mu_0} \right)^{1/n} \left(a^{(n+1)/n} - |y|^{(n+1)/n} \right). \quad (7.1.71)$$

When $n = 1$, we recover the expressions derived previously in Section 7.1.1 for Newtonian flow.

Couette flow

In the case of Couette (shear-driven) flow, $\chi + \rho g_x = 0$, we find that

$$\sigma_{xy} = A = \pm \mu_0 \left| \frac{V_2 - V_1}{2a} \right|^n. \quad (7.1.72)$$

Even though the shear stress depends on the power-law exponent, n , the velocity profile is identical to the linear profile of a Newtonian fluid.

Newton's method

Equation (7.1.68) can be solved for A under general conditions using Newton's method discussed in Section 5.2.2. As a preliminary, we restate equation (7.1.68) as

$$f(A) = 0, \quad (7.1.73)$$

where

$$f(A) = \left| (\chi + \rho g_x) a + A \right|^{(n+1)/n} - \left| (\chi + \rho g_x) a - A \right|^{(n+1)/n} - \frac{n+1}{n} (\chi + \rho g_x) \mu_0^{1/n} (V_2 - V_1) \quad (7.1.74)$$

is the function whose root is desired. The derivative, $f'(A)$, can be computed conveniently by numerical differentiation, setting $f'(A) \simeq (f(A + \epsilon) - f(A))/\epsilon$, where ϵ is a sufficiently small increment. The initial guess for A can be set equal to that for a Newtonian fluid, $A = (V_2 - V_1)/(2a)$.

Newton's method is implemented in the following function entitled *chan_pl*, located in directory *04_various* of **FDLIB**:

```
function [A,f,Iflag] = chan_pl ...
...
(chi ...
,rho ...
,gx ...
,a ...
,mu0 ...
,n ...
,V1 ...
,V2 ...
```



```

,Niter ...
,eps ...
,A ...
,tol ... % tolerance
,italk ...
)

%-----
% Solve one nonlinear equation by the
% for the channel flow of a power-law fluid
% by the second-order Newton method
%-----

Iflag = 1;
for i=1:Niter

    f = chan_pl_fun(chi,rho,gx,a,mu0,n,V1,V2,A);
    A1 = A + eps; % derivative by finite differences
    f1 = chan_pl_fun(chi,rho,gx,a,mu0,n,V1,V2,A1);
    Df = (f1-f)/eps;
    DA = -f/Df; % correction
    A = A+DA;

    if(italk==1)
        format long
        disp([A,f])
    end

    iescape = 1;
    if(abs(DA) > tol) iescape = 0; end

    if(iescape==1)
        Iflag = 0;
        f = chan_pl_fun(chi,rho,gx,a,mu0,n,V1,V2,A);
        return
    end
end

%---
% done
%---

return

```

The main function calls the following auxiliary function entitled *chan_pl_fun* to evaluate $f(A)$:

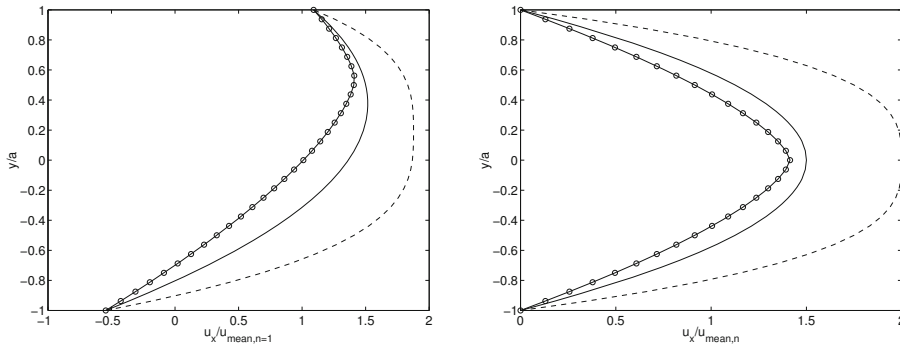


Figure 7.1.8 Velocity profiles for a typical configurations with power-law exponent $n = 0.5$ (broken line), 1 (solid line), and 2 (connected circular symbols). The velocity has been scaled with the mean velocity of a Newtonian fluid.

```
function f = chan_pl_fun(chi,rho,gx,a,mu0,n,V1,V2,A)

tmp = chi+rho*gx;

f = abs(tmp*a+A)^(1+1/n) - abs(tmp*a-A)^(1+1/n) ...
    -(n+1)/n * tmp * mu0^(1/n) *(V2-V1);

return
```

Once the constant A is available, the constant B can be evaluated by applying the boundary condition at the upper or lower wall.

The effect of the power-law exponent, n , on the velocity profile is illustrated in [Figure 7.1.8](#) for two typical sets of conditions. As n decreases from unity, the velocity profile becomes increasingly flat around the maximum. As n increases from unity, the velocity profile becomes increasingly blunt around the maximum.

PROBLEMS

7.1.1 *Integral momentum balance*

Verify that the shear stress given in (7.1.13) satisfies the integral momentum balance over the rectangular fluid parcel drawn with the solid line in [Figure 6.1.1](#).

7.1.2 *Reduction of multi-layer to single-layer flow*

(a) Verify that, when $\lambda = 1$ and $\beta = 1$, expressions (7.1.38) and (7.1.39) are consistent with the velocity profile (7.1.12) for single-fluid flow.

(b) Confirm that, when the densities and viscosities of all layers are the same, the coefficients $A^{(i)}$ and $B^{(i)}$ introduced in (7.1.44) are equal to those for single-fluid flow.

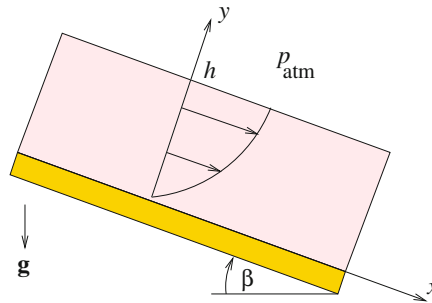


Figure 7.2.1 Illustration of gravity-driven flow of a liquid film down an inclined plane. The shear stress is zero at the free surface and the velocity profile is half-parabolic.

7.1.3 Multi-layer flow

Use program *chan_2d.ml* to compute and plot the velocity profile of a three-layer pressure-driven flow of your choice. Investigate and discuss the effect of the viscosity of each layer.

7.1.4 Non-Newtonian flow

Prepare graphs of the velocity profile expressed by (7.1.71) for $n = 0.5, 1,$ and 2 . Discuss the effect of the power-law exponent, n .

7.2 Steady film flow down an inclined plane

Gravity-driven flow of a liquid film down an inclined surface is encountered in a broad range of technological applications. Examples include the coating of paper, photographic film, electronics, magnetic recording media components, and other materials. In the simplest configuration, a liquid film of thickness h flows down a plane that is inclined by an angle β with respect to the horizontal plane, as illustrated in [Figure 7.2.1](#).

Governing equations

The motion of the fluid in steady unidirectional flow is governed by a simplified equation of motion whose x and y components are given in (7.1.3) and (7.1.4). The no-slip boundary condition requires that the velocity is zero at the plane located at $y = 0$,

$$u_x = 0 \quad \text{at } y = 0. \quad (7.2.1)$$

The free-surface condition requires that the shear stress is zero at the film surface located at $y = h$,

$$\frac{du_x}{dy} = 0 \quad \text{at } y = h. \quad (7.2.2)$$

Pressure field

The pressure distribution is given by (7.1.5) with $\chi = 0$, yielding

$$p(y) = \rho g_y y + \pi_0, \quad (7.2.3)$$

where $g_y = -g \cos \beta$ is the y component of the gravitational acceleration. Setting the pressure at the free surface equal to the ambient atmospheric pressure, we obtain $p_{\text{atm}} = \rho g_y h + \pi_0$, which can be rearranged to give $\pi_0 = p_{\text{atm}} - \rho g_y h$. The final expression for the pressure is

$$p(y) = \rho g \cos \beta (h - y) + p_{\text{atm}}. \quad (7.2.4)$$

Velocity profile

Working as in Section 7.1 for channel flow, we obtain the Nusselt parabolic streamwise velocity profile,

$$u_x(y) = \frac{1}{2} \frac{\rho g}{\mu} \sin \beta (2h - y) y. \quad (7.2.5)$$

This semi-parabolic profile is half the complete parabolic profile in pressure- or gravity-driven flow through a two-dimensional channel with width $2h$, where the free surface is located at the channel centerline.

The shear stress varies linearly from a certain value at the wall to the required value of zero at the free surface.

Flow rate

The flow rate per unit width arises by integrating the velocity profile across the film, obtaining

$$Q \equiv \int_0^h u_x(y) \, dy = \frac{1}{3} \frac{g}{\nu} h^3 \sin \beta = \frac{2}{3} h u_x(h), \quad (7.2.6)$$

where $\nu = \mu/\rho$ is the kinematic viscosity of the fluid and $u_x(h)$ is the maximum velocity occurring at the free surface. The mean velocity, $u_{\text{mean}} \equiv Q/h$, is equal to two thirds the free surface velocity.

Function *film*, located in directory *04_various* of **FDLIB**, not listed in the text, evaluates the velocity profile and flow rate given in (7.2.5) and (7.2.6).

7.2.1 Multi-film flow

Consider the gravity-driven flow of an arbitrary number of N superposed films down an inclined plane, as illustrated in [Figure 7.2.2](#). The bottom film is labeled 1 and the top film is labeled N . The $N - 1$ interfaces separating the films are located at

$$y = y_{\Gamma}^{(i)} \quad (7.2.7)$$

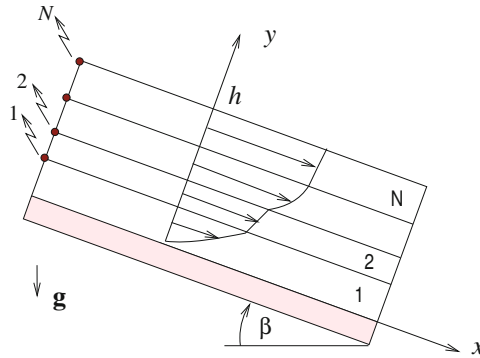


Figure 7.2.2 Illustration of gravity-driven multi-film flow down a plane that is inclined by an angle β with respect to the horizontal. The interfacial labels are printed on the left and the film labels are printed on the right.

for $i = 1, \dots, N - 1$, and the free surface is located at

$$y = y_1^{(N)} = h, \quad (7.2.8)$$

where h is the total film thickness. In photographic film manufacturing, as many as thirteen films may flow down an inclined plane to be deposited onto a moving support.

Velocity profile

The velocity profile across the i th film is governed by the simplified equations of motion (7.1.3) with $\partial p / \partial x = 0$. Integrating the first equation twice with respect to y , we derive the parabolic profile

$$u_x^{(i)}(y) = -\frac{1}{2} \frac{\rho_i g_x}{\mu_i} y^2 + B^{(i)} y + A^{(i)}, \quad (7.2.9)$$

where $A^{(i)}$ and $B^{(i)}$ are unknown constants determined by enforcing the following conditions:

1. The no-slip boundary condition at the plane.
2. Continuity of velocity at the interfaces expressed by the equation

$$\left(u_x^{(i)} \right)_{y=y_1^{(i)}} = \left(u_x^{(i+1)} \right)_{y=y_1^{(i)}} \quad (7.2.10)$$

for $i = 1, \dots, N - 1$.

3. Continuity of shear stress at the interfaces expressed by the equation

$$\mu_i \left(\frac{du_x^{(i)}}{dy} \right)_{y=y_1^{(i)}} = \mu_{i+1} \left(\frac{du_x^{(i+1)}}{dy} \right)_{y=y_1^{(i)}} \quad (7.2.11)$$

for $i = 1, \dots, N - 1$.

4. The condition of zero shear stress at the free surface requiring that

$$\alpha \equiv \left(\frac{du_x^{(N)}}{dy} \right)_{y=h} = 0. \quad (7.2.12)$$

Knowledge of the shear stress at the free surface allows us to evaluate the coefficients $B^{(i)}$ and $A^{(i)}$, working as described in the paragraph following equation (7.1.48) for multi-layer channel flow.

The numerical method is implemented in function *films*, located in directory *04_various* of **FDLIB**. The MATLAB implementation is listed below:

```
function [Q,u,yI,uI] = films ...
...
    (NLR,thick ...
    ,visc,den,gac ...
    ,beta ...
    ,y)

%=====
% Multi-film flow down an inclined plane
% located at y=0
%
% Film numbered 1 is adjacent to the plane
% The velocity in the ith film is given by:
%
% u(i) = af(i) + bf(i)*y - gf(i)*y^2
%
% SYMBOLS:
% -----
%
% NLR: Number of films
% yI(i): y-position of the ith interface
% uI(i): velocity at the ith interface
% Q(i); flow rate of ith film
% beta: plane inclination angle
% gac: magnitude of the acceleration of gravity
%=====

%-----
% set the interface positions
%-----

yI(1) = thick(1);

for i=2:NLR
    yI(i) = yI(i-1)+thick(i);
end
```

```

%-----
% The velocity in the ith film is given by:
%  $u(i) = af(i) + bf(i)*y - gf(i)*y^2$ 
% compute gf(i)
%-----

fc = 0.5*gac*sin(beta);

for i=1:NLR
    gf(i) = fc*den(i)/visc(i);
end

%---
% compute bf(i) by recursion starting from
% the top and requiring continuity of shear stress
%---

bf(NLR) = 2.0*gf(NLR)*yI(NLR);

for i=NLR-1:-1:1
    bf(i) = 2.0*gf(i)*yI(i) ...
        + visc(i+1)/visc(i)*(bf(i+1)-2.0*gf(i+1)*yI(i));
end

%---
% compute af(i) by recursion
% starting from the bottom
% and requiring continuity of velocity
%---

af(1) = 0.0;

for i=1:NLR-1
    af(i+1) = af(i)+( bf(i)-bf(i+1)) ...
        -(gf(i)-gf(i+1))*yI(i) * yI(i);
end

%---
% compute the interfacial velocities
%---

for i=1:NLR
    uI(i) = af(i) + (bf(i)-gf(i)*yI(i)) * yI(i);
end

%----
% compute the flow rates in the ith film
% is confined between interfaces labeled i-1 and i
%----

```

```

yI0 = 0.0;

Q(1) = af(1)*(yI(1)-yI0) ...
      +bf(1)*(yI(1)^2-yI0^2)/2.0 ...
      -gf(1)*(yI(1)^3-yI0^3)/3.0;

for i=2:NLR
    Q(i) = af(i)*(yI(i)-yI(i-1)) ...
          +bf(i)*(yI(i)^2-yI(i-1)^2)/2.0 ...
          -gf(i)*(yI(i)^3-yI(i-1)^3)/3.0;
end

%-----
% compute the velocity at y
%-----

% identify the host film:

for i=1:NLR
    if(y<yI(i)) break; end
end

if(i>NLR) i = NLR; end

%---
% evaluate the velocity
%---

u = af(i) + (bf(i)-gf(i)*y)*y

%----
% Done
%----

return

```

The velocity profile across a configuration with four films with different physical properties is shown in [Figure 7.2.3](#).

Wall shear stress

One interesting feature of the multi-film flow is that the wall shear stress and the velocity profile across the first film that is adjacent to the wall are independent of the viscosities of the rest of the films. To see this, we write the velocity profile (7.2.9) for $i = 1$ and require the no-slip boundary condition to find $A^{(1)} = 0$. To compute the coefficient $B^{(1)}$, we perform a force balance over a section of the multi-layered film confined between two planes at $x = x_1$ and x_2 . The balance requires that the x component of the force exerted by the shear stress

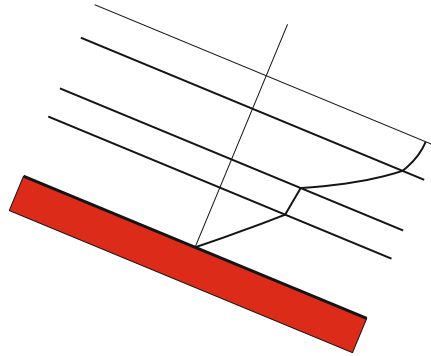


Figure 7.2.3 Velocity profile across four films with different physical properties down an inclined plane, generated by code *films*.

at the wall and at the free surface counterbalance the x component of the weight of the fluid residing inside the control volume. We note that the shear stress is zero at the free surface and obtain

$$\sigma_{xy}^{(1)}(y=0) = \sum_{i=1}^N \rho_i g_x (y_{\Gamma}^{(i)} - y_{\Gamma}^{(i-1)}), \quad (7.2.13)$$

with the understanding that $y_{\Gamma}^{(0)} = 0$. Using the profile (7.2.9) for $i = 1$, we find that

$$\sigma_{xy}^{(1)}(y=0) = \mu_1 \left(\frac{\partial u_x^{(1)}}{\partial y} \right)_{y=0} = \mu_1 B^{(1)}. \quad (7.2.14)$$

Setting the right-hand sides of the last two equations equal, solving for $B^{(1)}$, and substituting the result into the profile (7.2.9) for $i = 1$ proves the alleged independence of the first velocity profile and wall shear stress on the viscosity of the overlying fluids.

7.2.2 Power-law fluids

Next, we derive the counterpart of the velocity profile (7.2.5) for a power-law fluid whose viscosity depends on the shear rate, as shown in equation (4.8.2). We note that the x velocity component increases from zero at the wall, because of the no-slip boundary condition, to a maximum at the free surface, and conclude that $du_x/dy > 0$.

Working as in Section 7.1.4 for channel flow, we obtain the shear rate

$$\frac{du_x}{dy} = \left(\frac{A - \rho g_x y}{\mu_0} \right)^{1/n}, \quad (7.2.15)$$

where A is a constant. Integrating with respect to y , we obtain

$$u_x(y) = -\frac{n}{n+1} \frac{1}{\rho g_x} \frac{1}{\mu_0^{1/n}} (A - \rho g_x y)^{(n+1)/n} + B, \quad (7.2.16)$$

where B is a new constant.

The constants A and B are found by enforcing the boundary conditions (7.2.1) and (7.2.2). Applying (7.2.2) and using expression (7.2.15) for the shear rate, we obtain

$$A = \rho g_x h. \quad (7.2.17)$$

Applying (7.2.1), we obtain

$$B = \frac{n}{n+1} \frac{1}{\rho g_x} \frac{1}{\mu_0^{1/n}} (\rho g_x h)^{(n+1)/n}. \quad (7.2.18)$$

Substituting these expressions into (7.2.16), we derive the velocity profile

$$u_x(y) = -\frac{n}{n+1} \left(\frac{\rho g_x}{\mu_0} \right)^{1/n} \left(h^{(n+1)/n} - (h-y)^{(n+1)/n} \right). \quad (7.2.19)$$

When $n = 1$, we recover the familiar parabolic profile for Newtonian flow.

PROBLEMS

7.2.1 Multi-film flow

Confirm that the wall shear stress is independent of the viscosity of the films that are not adjacent to the wall on the basis of (a) the recursion relation (7.1.47) for gravity-driven flow, and (b) the free-surface condition expressed by (7.1.49) with $\alpha = 0$.

7.2.2 Computation of multi-film flow

Use the code `filmsin` directory `04_various` of `FDLIB` to compute and plot the velocity profile of a three-film configuration of your choice. Investigate and discuss the effect of the film densities.

7.2.3 Non-Newtonian film flow

Prepare a graph of the velocity profile expressed by (7.2.19) for $n = 0.5$, 1, and 2. Discuss the effect of the power-law exponent, n .

7.3 Steady flow through a circular tube

Having discussed steady two-dimensional channel and film flow, we proceed to consider unidirectional flow through a horizontal or inclined cylindrical tube with circular cross-section of radius a , as shown in [Figure 7.3.1](#).

To derive the velocity profile, we introduce cylindrical polar coordinates, (x, σ, φ) , where the x axis coincides with the tube centerline. The radial and meridional velocity components are identically zero in steady unidirectional flow, $u_\sigma = 0$ and $u_\varphi = 0$, while the x velocity component depends on the distance from the tube centerline alone, $u_x(\sigma)$.

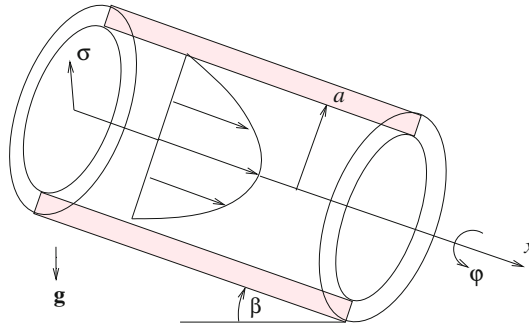


Figure 7.3.1 Illustration of steady unidirectional flow through a horizontal or inclined circular tube.

Pressure field

It is convenient to screen out the hydrostatic pressure variations normal to the x axis by expressing the pressure in the form

$$p = -\chi x + \rho(g_y y + g_z z) + \pi_0, \quad (7.3.1)$$

where $\chi = -\partial p/\partial x$ is a constant identified with the negative of the streamwise pressure gradient and π_0 is an inconsequential constant.

Governing equations

Inspecting the individual terms on the left-hand side of the x component of the equation of motion shown in the first equation in (6.3.18),

$$\rho a_x = \Sigma_x + \rho g_x, \quad (7.3.2)$$

where a_x is the streamwise component of the point particle acceleration, we find that the left-hand side is identically zero. Substituting the expression for the x component of the hydrodynamic volume force given in the first entry of Table 6.5.2(a) for axisymmetric flow,

$$\Sigma_x = -\frac{\partial p}{\partial x} + \mu \frac{1}{\sigma} \frac{\partial}{\partial \sigma} \left(\sigma \frac{\partial u_x}{\partial \sigma} \right), \quad (7.3.3)$$

and rearranging, we derive the simplified equation of motion

$$\frac{1}{\sigma} \frac{d}{d\sigma} \left(\sigma \frac{du_x}{d\sigma} \right) = -\frac{\chi + \rho g_x}{\mu}, \quad (7.3.4)$$

where

$$g_x = g \cos \beta, \quad (7.3.5)$$

β is the inclination angle of the tube generators with respect to a horizontal plane, and g is the magnitude of the acceleration of gravity. Equation (7.3.4) is the counterpart of equation (7.1.7) for two-dimensional channel flow.

The solution must satisfy the no-slip boundary condition at the tube surface, $u_x = 0$ at $\sigma = a$, and a regularity condition ensuring that u_x is finite at the centerline, $\sigma = 0$.

Velocity profile

Integrating equation (7.3.4) once with respect to σ , we obtain

$$\sigma \frac{du_x}{d\sigma} = -\frac{1}{2} \frac{\chi + \rho g_x}{\mu} \sigma^2 + B, \quad (7.3.6)$$

where B is a constant. Integrating once more, we obtain the velocity profile involving a quadratic and a logarithmic term,

$$u_x(\sigma) = -\frac{1}{4} \frac{\chi + \rho g_x}{\mu} \sigma^2 + B \ln \frac{\sigma}{a} + A, \quad (7.3.7)$$

where A is another constant. For the velocity to be finite at the centerline, $\sigma = 0$, where the logarithmic term diverges, the constant B must be zero.

To evaluate the constant A , we enforce the no-slip boundary condition at the tube surface, $u_x(a) = 0$, and derive the parabolic Poiseuille flow profile

$$u_x(\sigma) = \frac{1}{4} \frac{\chi + \rho g_x}{\mu} (a^2 - \sigma^2). \quad (7.3.8)$$

The maximum velocity occurs at the tube centerline, $\sigma = 0$, and is given by

$$u_{\max} = u_x(0) = \frac{1}{4} \frac{\chi + \rho g_x}{\mu} a^2. \quad (7.3.9)$$

We observe that doubling the tube radius, while holding the pressure gradient constant, quadruples the maximum velocity.

Function `tube_crc`, located in directory `04_various` of `FDLIB`, not listed in the text, evaluates the velocity profile described by (7.3.8).

Shear stress

The shear stress, $\sigma_{\sigma x}$, arises from (7.3.6) as

$$\sigma_{\sigma x} = \mu \frac{du_x}{d\sigma} = -\frac{1}{2} (\chi + \rho g_x) \sigma. \quad (7.3.10)$$

We see that the shear stress is proportional to the distance from the centerline, σ , and therefore reaches a maximum at the tube wall where $\sigma = a$.

Integral momentum balance

It is instructive to verify that the derived expression for the shear stress satisfies an integral momentum balance over an annular control volume confined between two arbitrary parallel planes located at $x = x_1$ and x_2 , and two arbitrary cylindrical surfaces located at $\sigma = \sigma_1$

and σ_2 . Because the flow is steady, the rate of change of the x momentum of the fluid inside the control volume is zero.

Balancing the normal force exerted on the planar sides, the shear force exerted at the cylindrical sides, and the body force, and observing that the normal viscous stress is zero while the normal stress is equal to the negative of the pressure over the planar sides, we find that

$$2\pi \int_{\sigma_1}^{\sigma_2} (-(p)_{x=x_2} + (p)_{x=x_1}) \sigma \, d\sigma + F_1 + F_2 + F_g = 0, \quad (7.3.11)$$

where

$$F_1 = -(\sigma_{\sigma x})_{\sigma=\sigma_1} 2\pi\sigma_1 (x_2 - x_1), \quad F_2 = (\sigma_{\sigma x})_{\sigma=\sigma_2} 2\pi\sigma_2 (x_2 - x_1) \quad (7.3.12)$$

are the forces due to the shear stress and

$$F_g = \rho g_x \pi (\sigma_2^2 - \sigma_1^2) (x_2 - x_1). \quad (7.3.13)$$

is the force due to gravity. Now using (7.3.1) to express the pressure difference in terms of the negative of the pressure gradient, χ , we obtain

$$\pi\chi (\sigma_2^2 - \sigma_1^2) (x_2 - x_1) + F_1 + F_2 + F_g = 0. \quad (7.3.14)$$

Setting $\sigma_1 = 0$ and solving for $(\sigma_{\sigma x})_{\sigma=\sigma_2}$, we recover precisely expression (7.3.10) evaluated at $\sigma = \sigma_2$.

Flow rate and Poiseuille's law

The flow rate through the tube is computed by integrating the velocity profile over the tube cross-section, finding

$$Q \equiv \int_0^{2\pi} \int_0^a u_x(\sigma) \sigma \, d\sigma \, d\varphi = 2\pi \int_0^a u_x(\sigma) \sigma \, d\sigma. \quad (7.3.15)$$

Substituting the velocity profile and performing the integration, we derive the expression

$$Q = \frac{1}{8} \frac{\chi + \rho g_x}{\mu} \pi a^4. \quad (7.3.16)$$

Equation (7.3.16) expresses Poiseuille's law, first established by laboratory observation of blood flow at a time when the equations governing fluid flow had not been established. The data suggested that the flow rate through a circular tube subject to a constant pressure drop is proportional to the fourth power of the tube diameter.

In terms of the maximum velocity occurring at the tube centerline, $u_{\max} = u_x(0)$, the flow rate is given by

$$Q = \frac{1}{2} u_{\max} (\pi a^2). \quad (7.3.17)$$

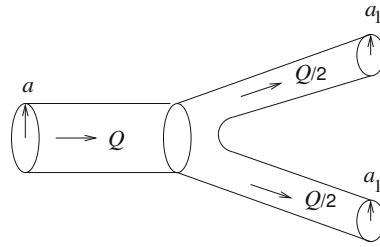


Figure 7.3.2 Bifurcation of a tube of radius a into two descendant tubes with equal radii, a_1 . The flow rate is assumed to be split into two equal parts.

The mean velocity is defined as the ratio of the flow rate to the tube cross-sectional area,

$$u_{\text{mean}} \equiv \frac{Q}{\pi a^2} = \frac{1}{2} u_{\text{max}}. \quad (7.3.18)$$

We observe that the mean velocity is equal to half the maximum velocity occurring at the centerline.

Tube bifurcation

As an application, we consider flow through a circular blood vessel with radius a , bifurcating into two vessels with equal radii, a_1 , as shown in [Figure 7.3.2](#). The flow through each vessel satisfies the equations of Poiseuille tube flow.

It has been theorized that blood vessels in the human circulation bifurcate such that the wall shear stress is constant and the endothelial cells lining the capillary walls experience the same hydrodynamic stimulus. Using expression (7.3.10) for the shear stress, we obtain

$$(\chi + \rho g_x) a = (\chi_1 + \rho g_x) a_1. \quad (7.3.19)$$

The flow rate is assumed to be split into two equal parts. Mass conservation requires that $Q = 2Q_1$. Substituting Poiseuille's law and simplifying, we find that

$$(\chi + \rho g_x) a^4 = 2(\chi_1 + \rho g_x) a_1^4. \quad (7.3.20)$$

Combining the last two equations, we obtain

$$\frac{a_1}{a} = \frac{1}{2^{1/3}} \simeq 0.794, \quad (7.3.21)$$

which suggests that the diameter of a daughter tube is approximately 80% that of a parent tube.

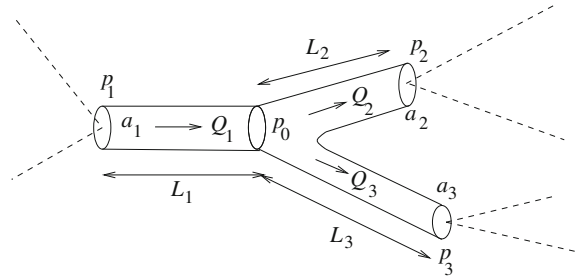


Figure 7.3.3 Illustration of a bifurcating tube in a network. The dashed lines represent other tube segments.

Tube network

Poiseuille's flow can be used to derive a system of linear algebraic equations relating the nodal pressures of a tube network at bifurcation points, such as that occurring in the microcirculation of blood flow.

Consider flow through a particular bifurcation, as illustrated in [Figure 7.3.3](#). Our objective is to derive expressions for the flow rates, Q_1 , Q_2 , and Q_3 , in terms of the tube radii, a_1 , a_2 , and a_3 , tube lengths, L_1 , L_2 , and L_3 , and inlet and outlet pressures, p_1 , p_2 , and p_3 .

Neglecting gravitational effects, substituting Poiseuille's law for the individual segments in the mass balance equation

$$Q_1 = Q_2 + Q_3, \quad (7.3.22)$$

and approximating the pressure gradient with the ratio of the pressure difference over the tube lengths, we obtain

$$\frac{p_1 - p_0}{L_1} \frac{1}{8} \frac{\pi}{\mu} a_1^4 = \frac{p_0 - p_2}{L_2} \frac{1}{8} \frac{\pi}{\mu} a_2^4 + \frac{p_0 - p_3}{L_3} \frac{1}{8} \frac{\pi}{\mu} a_3^4. \quad (7.3.23)$$

Solving for the central pressure, p_0 , and substituting the result back into each fraction provides us with the requisite flow rates.

Wall slip

The fluid may slip over the tube wall so that the wall velocity is proportional to the wall shear stress or wall shear rate,

$$u_x = -\ell \left(\frac{du_x}{d\sigma} \right)_{\sigma=a}, \quad (7.3.24)$$

where ℓ is a specified slip length. The minus sign is motivated by the expected negative slope of the velocity profile at the wall.

Substituting expressions (7.3.6) and (7.3.7) with $A = 0$ into (7.3.24), we obtain an equation involving the integration constant B ,

$$-\frac{1}{4} \frac{\chi + \rho g_x}{\mu} a^2 + B = \ell \frac{1}{2} \frac{\chi + \rho g_x}{\mu} a. \quad (7.3.25)$$

Solving for B , we find that

$$B = \frac{1}{4} \frac{\chi + \rho g_x}{\mu} a (a + 2\ell). \quad (7.3.26)$$

The velocity profile is given by

$$u_x(\sigma) = \frac{1}{4} \frac{\chi + \rho g_x}{\mu} (a(a + 2\ell) - \sigma^2). \quad (7.3.27)$$

We note that the wall shear stress is independent of the slip length, ℓ , so that the shear force balances the force exerted on the fluid due to gravity or an imposed pressure gradient.

The flow rate through the tube arises by integrating the velocity distribution over the tube cross-section. Since the velocity is constant over a small annular area of radius σ , we obtain

$$Q = 2\pi \int_0^a u_x \sigma \, d\sigma = \frac{1}{8} \frac{\chi + \rho g_x}{\mu} \pi a^3 (a + 2\ell). \quad (7.3.28)$$

When $\ell = 0$, we recover the no-slip boundary condition and obtain Poiseuille's law. Not surprising, slip increases the flow rate.

7.3.1 Multi-layer tube flow

As a generalization, we consider axisymmetric multi-layer pressure- and gravity-driven flow through a circular tube, as illustrated in [Figure 7.3.4](#). For the interfaces between the annular layers to remain concentric, the tube must be vertical or else the fluid densities must be matched. If these conditions are not met, hydrostatic pressure variations cause the onset of a non-axisymmetric configuration.

The interior of the tube is occupied by a core fluid labeled 1 and $N - 1$ annular layers, where the outermost layer, labeled N , is coated on the interior tube surface. The $N - 1$ interfaces separating the layers are located at radial positions

$$\sigma = \sigma_1^{(i)} \quad (7.3.29)$$

for $i = 1, \dots, N - 1$. When $N = 2$, we obtain a core-annular flow.

The velocity profile across the i th layer is given by equation (7.3.7) with corresponding fluid density ρ_i and viscosity μ_i ,

$$u_x^{(i)}(\sigma) = -\frac{1}{4} \frac{\chi + \rho g_x}{\mu_i} \sigma^2 + B^{(i)} \ln \frac{\sigma}{a} + A^{(i)} \quad (7.3.30)$$

for $i = 1, \dots, N$, where the coefficients $A^{(i)}$ and $B^{(i)}$ are determined by enforcing the following conditions:

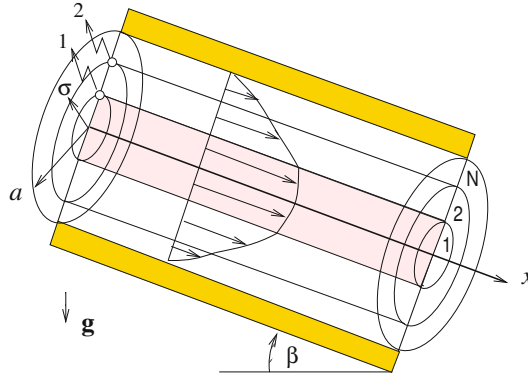


Figure 7.3.4 Illustration of multi-layer flow through a circular tube. The interface labels are shown on the left and the layer labels are shown on the right.

1. Regularity at the tube axis requiring that $u_x^{(1)}(0)$ is finite and thus $B^{(1)} = 0$.
2. Continuity of velocity at the interfaces expressed by the matching condition

$$\left(u_x^{(i)}\right)_{\sigma=\sigma_1^{(i)}} = \left(u_x^{(i+1)}\right)_{\sigma=\sigma_1^{(i)}} \quad (7.3.31)$$

for $i = 1, \dots, N - 1$.

3. Continuity of shear stress at the interfaces expressed by the matching condition

$$\mu_i \left(\frac{du_x^{(i)}}{d\sigma}\right)_{\sigma=\sigma_1^{(i-1)}} = \mu_{i-1} \left(\frac{du_x^{(i-1)}}{d\sigma}\right)_{\sigma=\sigma_1^{(i-1)}} \quad (7.3.32)$$

for $i = 2, \dots, N$.

4. The no-slip boundary condition at the tube wall requiring that

$$u_x^{(N)}(\sigma = a) = -\frac{1}{4} \frac{\chi + \rho g_x}{\mu_N} a^2 + A^{(N)} = 0. \quad (7.3.33)$$

Substituting the velocity profiles (7.3.30) into (7.3.32) and solving for the coefficient $B^{(i)}$, we derive the recursive relation

$$B^{(i)} = \frac{1}{2} \frac{\chi + \rho_i g_x}{\mu_i} \sigma_1^{(i-1)2} + \frac{\mu_{i-1}}{\mu_i} \left(B^{(i-1)} - \frac{1}{2} \frac{\chi + \rho_{i-1} g_x}{\mu_{i-1}} \sigma_1^{(i-1)2} \right) \quad (7.3.34)$$

for $i = 2, \dots, N$, where $B^{(1)} = 0$. At the second stage, the coefficients $A^{(i)} = 0$ are computed by backward recursion based on equation (7.3.31), starting with

$$A^{(N)} = \frac{1}{4} \frac{\chi + \rho g_x}{\mu_N} a^2. \quad (7.3.35)$$

The algorithm is implemented in a function entitled *tube_crc_ml*, located in directory *04_various* of **FDLIB**. The MATLAB implementation is listed next:

```

function [sI,uI,xi1,xi2,Q,u] = tube_crc_ml ...
...
(NLR,a,thick,visc,den ...
,gac,chi,beta ...
,s)

%=====
% Multi-layer core-annular flow through a circular tube
%
% Film numbered 1 is at the centerline
% Film numbered NLR is adjacent to the tube surface

% The velocity in the ith film is given by:
%
%  $u(i) = af(i) + bf(i)*\ln(\sigma/a) - gf(i)*\sigma^2$ 
%
% SYMBOLS
% -----
%
% NLR: Number of layers
% a: tube radius
% thick(i): thickness of the ith layer
% sI(i): position of the ith interface
% uI(i): velocity of the ith interface
% xi1(i): shear rate on lower side of the ith interface
% xi2(i): shear rate on upper side of the ith interface
% Q(i): flow rate of ith layer
% beta: tube inclination angle
% gac: magnitude of the acceleration of gravity
% chi: negative of the pressure gradient
%=====

%---
% set the interface positions
%---

sI(1) = thick(1);

for i=2:NLR
    sI(i) = sI(i-1)+thick(i);
end

%-----
% The velocity in the ith layer is given by:
%
%  $u(i) = af(i) + bf(i)*\ln(\sigma/a) - gf(i)*\sigma^2$ 
%
% compute gf(i)
%-----

```

```

fc = gac*sin(beta);

for i=1:NLR
    gf(i) = 0.25*(chi+fc*den(i))/visc(i);
end

%---
% compute bf(i) by recursion
% starting from the centerline and
% by requiring continuity of shear stress
% across the interfaces

bf(1) = 0.0;

for i=2:NLR
    bf(i) = 2.0*gf(i)*sI(i-1)^2 ...
        + visc(i-1)/visc(i) * (bf(i-1)-2.0*gf(i-1)*sI(i-1)^2);
end

%---
% compute af(i) by recursion
% starting from the tube wall and
% and requiring continuity of velocity
%---

af(NLR) = gf(NLR)*a^2;

for i=NLR-1:-1:1
    af(i) = af(i+1)+(bf(i+1)-bf(i))*log(sI(i)/a) ...
        -(gf(i+1)-gf(i))*sI(i)^2;
end

%---
% compute interfacial velocities
% and shear rates
%---

for i=1:NLR-1
    uI(i) = af(i) + bf(i)*log(sI(i)/a) - gf(i)*sI(i)^2;
    xi1(i) = bf(i) /sI(i) - 2.0*gf(i) *sI(i);
    xi2(i) = bf(i+1)/sI(i) - 2.0*gf(i+1)*sI(i);
end

%----
% compute the flow rates
% the ith film is confined between i-1 and i interfaces
%----

```

```

sI1s = sI(1)^2;
Q(1) = af(1)*sI1s/2.0 ...
      + bf(1)*0.5*sI1s*(log(sI(1)/a)-0.5)-gf(1)*sI1s^2/4.0;
Q(1) = 2.0*pi*Q(1);

for i=2:NLR
    sIis = sI(i)^2;
    sIias = sI(i-1)^2;
    Q(i) = af(i)*(sIis-sIias)/2.0 ...
          +bf(i)*0.5*(sIis *(log(sI(i)/a)-0.5D0) ...
          -sIias*(log(sI(i-1)/a)-0.5D0)) ...
          -gf(i)*(sIis^2-sIias^2)/4.0;
    Q(i) = 2.0*pi*Q(i);
end

%-----
% compute the velocity at s
%-----

% identify the host layer

for i=1:NLR

    if(s<sI(i)) break; end
end

if(i>NLR) i = NLR; end

%---
% evaluate the velocity at s
%---

if(s>0.000001)

    u = af(i) + bf(i)*log(s/a) - gf(i)*s^2;
else
    u = af(i)-gf(i)*s^2;
end

%-----
% Done
%-----

return

```

The velocity profile across a core fluid and four annular layers with different viscosities and densities is shown in [Figure 7.3.5](#).

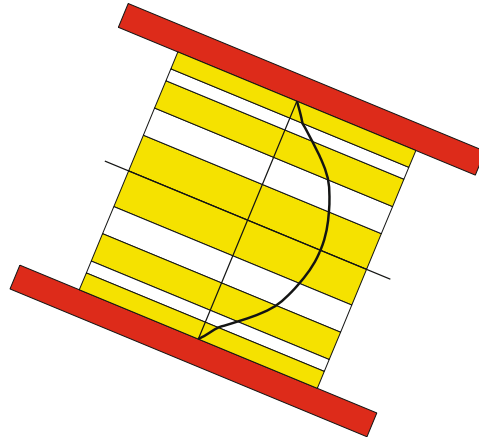


Figure 7.3.5 Velocity profile across a five-fluid configuration in axisymmetric multi-layer tube flow involving a core fluid and four annular layers.

7.3.2 Flow due to a translating sector

We have discussed pressure- and gravity-driven flow through a circular tube. Now we consider a case where the axial pressure gradient is zero, the tube is horizontal, and the flow is driven exclusively by boundary motion.

If the entire surface of the tube translates parallel to itself with constant velocity, the fluid inside the tube will also translate with the same uniform velocity in a plug-flow mode. However, if only a sector of the tube confined inside a window, $-\alpha \leq \varphi \leq \alpha$, translates with velocity V , and the remainder of the tube surface is stationary, a distributed velocity field will be established, as illustrated in [Figure 7.3.6\(a\)](#).

Governing equations and boundary conditions

Assuming that the flow is unidirectional and fully-developed, we set the radial and azimuthal velocity components to zero, $u_\sigma = 0$ and $u_\varphi = 0$, and regard the axial component, u_x , as a function of distance from the tube centerline, σ , and azimuthal angle, φ , $u_x(\sigma, \varphi)$. The no-slip boundary condition at the surface of the tube requires that

$$u_x(\sigma = a, \varphi) = V \quad (7.3.36)$$

for $-\alpha < \varphi < \alpha$, and $u_x(\sigma = a, \varphi) = 0$ otherwise.

Consideration of the individual terms on the left-hand side of the x component of the equation of motion (6.3.18) reveals that the entire left-hand side is identically zero. Using the expression for the x component of the hydrodynamic volume force shown in [Table 6.5.2\(a\)](#) with constant pressure and zero pressure gradient, we derive Laplace's equation for u_x ,

$$\nabla^2 u_x = \frac{1}{\sigma} \frac{\partial}{\partial \sigma} \left(\sigma \frac{\partial u_x}{\partial \sigma} \right) + \frac{1}{\sigma^2} \frac{\partial^2 u_x}{\partial \varphi^2} = 0, \quad (7.3.37)$$

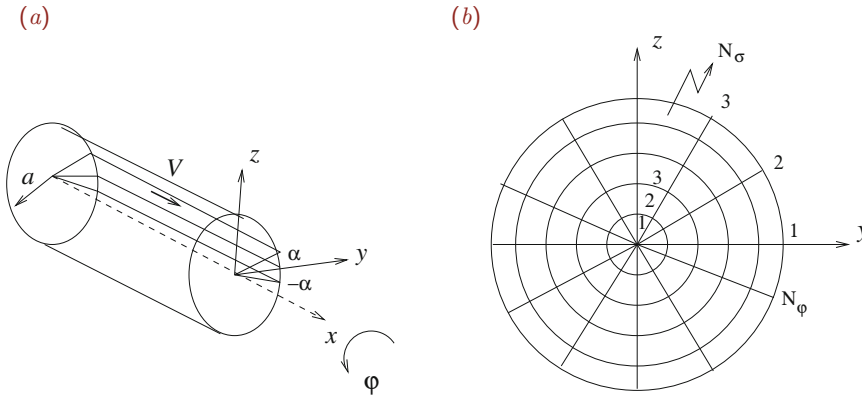


Figure 7.3.6 (a) Illustration of unidirectional flow through a circular tube due to the translation of a sector with semi-angle α . (b) Discretization of the tube cross-section for the purpose of computing the flow rate using the mid-point rule.

where ∇^2 is the Laplacian operator in the yz plane, which is normal to the tube axis, expressed in cylindrical polar coordinates.

Solution by the Poisson integral formula Poisson integral formula.

The solution can be found using a powerful method for solving Laplace's equation in two dimensions in the interior or exterior of a circle, subject to specified boundary conditions for the unknown function, expressed by the Poisson integral formula. For the problem under consideration, we find the velocity distribution

$$u_x(\sigma, \varphi) = \frac{V}{\pi} \left(\arctan \left(\frac{a + \sigma}{a - \sigma} \tan \frac{\alpha - \varphi}{2} \right) + \arctan \left(\frac{a + \sigma}{a - \sigma} \tan \frac{\alpha + \varphi}{2} \right) \right). \quad (7.3.38)$$

Examining the right-hand side, we confirm that, as the semi-angle of the translating sector, α , tends to π , the fluid tends to translate with uniform velocity in a plug-flow mode (Problem 7.3.2).

Program *tube_crc_sec*, located in directory *04_various* of FDLIB, not listed in the text, evaluates the velocity profile given in (7.3.38).

Flow rate

The flow rate through the tube arises by integrating the velocity distribution over the tube cross-section,

$$Q \equiv \int_0^{2\pi} \int_0^a u_x(\sigma, \varphi) \sigma \, d\sigma \, d\varphi. \quad (7.3.39)$$

The double integral on the right-hand side cannot be found by analytical methods.

To obtain a numerical approximation, we divide the integration domain with respect to φ and σ into N_φ or N_σ evenly spaced intervals with equal size,

$$\Delta\varphi = \frac{2\pi}{N_\varphi}, \quad \Delta\sigma = \frac{a}{N_\sigma}. \quad (7.3.40)$$

The divisions define elemental cross-sectional areas, as shown in [Figure 7.3.6\(b\)](#). The velocity over each elemental area can be approximated with the value at the center-point. Replacing the double integral in (7.3.39) with a double sum, we find that

$$Q \simeq \Delta\varphi \Delta\sigma \sum_{i=1}^{N_\varphi} \sum_{j=1}^{N_\sigma} u_x(\sigma_j, \varphi_i) \sigma_j, \quad (7.3.41)$$

where

$$\varphi_i = (i - \frac{1}{2}) \Delta\varphi, \quad \sigma_j = (j - \frac{1}{2}) \Delta\sigma. \quad (7.3.42)$$

Equation (7.3.41) implements the mid-point rule for two-dimensional integration in a plane.

PROBLEMS

7.3.1 Flow in a tube due to a translating sector

Demonstrate that, as the translating sector semi-angle α tends to π , the right-hand side of (7.3.38) tends to the wall velocity, V , everywhere inside the tube.

7.3.2 Axisymmetric film flow

A liquid film drains due to gravity downward over the exterior surface of a vertical circular rod of radius a . Show that, in cylindrical polar coordinates where the x axis is coaxial with the rod pointing upward, the velocity profile across the film is given by

$$u_x = \frac{g}{4\nu} (\sigma^2 - a^2 - 2(a+h)^2 \ln \frac{\sigma}{a}), \quad (7.3.43)$$

where h is the film thickness.

7.3.3 Flow in a circular tube due to a translating sector

Prepare a graph of the dimensionless mean velocity, $\hat{u}_{\text{mean}} \equiv Q/(\pi a^2 V)$, against the scaled semi-angle, α/π , using the numerical approximation implemented in (7.3.41). The numerical results should be accurate to the third significant figure. Deduce the slope of the graph at the origin, $\alpha = 0$.

7.3.4 Multi-layer flow through a tube

- Outline and explain the numerical procedure implemented in the code `tube_crc_ml`.
- Plot the velocity profile for a three-layer configuration of your choice. Investigate and discuss the effect of the layer viscosities.

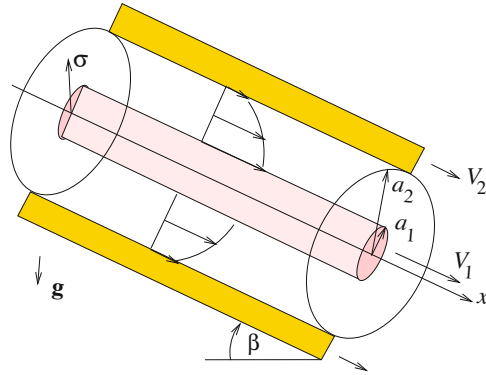


Figure 7.4.1 Illustration of unidirectional pressure- or gravity-driven flow through an annular tube with translating walls.

7.4 Steady flow through an annular tube

The velocity profile of unidirectional flow through an annular tube confined between two coaxial cylinders with radii a_1 and a_2 can be derived by a straightforward generalization of the analysis presented in Section 7.3 for a circular tube. A new feature is that the two cylinders are allowed to translate parallel to themselves along the x axis with respective velocities V_1 and V_2 , as illustrated in Figure 7.4.1.

Velocity profile and flow rate

Integrating the governing equation (7.3.4) with respect to σ , we find that the axial component of the velocity is given by

$$u_x(\sigma) = -\frac{1}{4} \frac{\chi + \rho g_x}{\mu} \sigma^2 + B \ln \frac{\sigma}{a_1} + A, \quad (7.4.1)$$

where A and B are two constants. To evaluate these constants, we enforce the no-slip condition at the two walls,

$$u_x(\sigma = a_1) = V_1, \quad u_x(\sigma = a_2) = V_2, \quad (7.4.2)$$

and derive the velocity profile

$$u_x(\sigma) = V_2 + (V_1 - V_2) \frac{\ln(a_2/\sigma)}{\ln(a_2/a_1)} + \frac{\chi + \rho g_x}{4\mu} \left(a_2^2 - \sigma^2 - (a_2^2 - a_1^2) \frac{\ln(a_2/\sigma)}{\ln(a_2/a_1)} \right). \quad (7.4.3)$$

The flow rate along the tube arises by integrating the velocity profile over the annular cross-section confined between the two concentric cylinders,

$$Q \equiv 2\pi \int_{a_1}^{a_2} u_x(\sigma) \sigma \, d\sigma. \quad (7.4.4)$$

Performing the integration, we obtain

$$Q = \pi (V_2 a_2^2 - V_1 a_1^2) - \frac{\pi}{2} (V_2 - V_1) \frac{a_2^2 - a_1^2}{\ln(a_2/a_1)} + \pi \frac{\chi + \rho g x}{8\mu} (a_2^2 - a_1^2) \left(a_2^2 + a_1^2 - \frac{a_2^2 - a_1^2}{\ln(a_2/a_1)} \right). \quad (7.4.5)$$

Program *tube_ann*, located in directory *04_various* of FDLIB, not listed in the text, evaluates the velocity profile given in (7.4.3) and the flow rate given in (7.4.5).

7.4.1 Small gaps

When the clearance of the annular channel is small compared to the inner cylinder radius, $a_2 - a_1 < a_1$, the curvature of the cylindrical surfaces is insignificant. Equations (7.4.3) and (7.4.5) then are expected to reduce to equations (7.1.12) and (7.1.15) for unidirectional flow in a channel with parallel-sided walls separated by distance $2a = a_2 - a_1$, where

$$y = \sigma - \frac{1}{2} (a_1 + a_2) = \sigma - (a_1 + a) = \sigma - (a_2 - a) \quad (7.4.6)$$

is the radial distance from the midway position.

To demonstrate this reduction, we introduce a small dimensionless number,

$$\epsilon = \frac{a_2 - a_1}{a_1} = 2 \frac{a}{a_1} \ll 1, \quad (7.4.7)$$

and write

$$\frac{a_2}{a_1} = 1 + \epsilon, \quad \ln \frac{a_2}{a_1} = \ln(1 + \epsilon) \simeq \epsilon - \frac{1}{2} \epsilon^2. \quad (7.4.8)$$

Next, we write

$$\ln \frac{a_2}{\sigma} = -\ln \frac{\sigma}{a_2} = -\ln \left(\frac{\sigma}{a_1} \frac{a_1}{a_2} \right) = -\ln \frac{\sigma}{a_1} - \ln \frac{a_1}{a_2} = -\ln \frac{\sigma}{a_1} + \ln \frac{a_2}{a_1} \quad (7.4.9)$$

and

$$\ln \frac{\sigma}{a_1} = \ln \frac{y + a_1 + a}{a_1} = \ln(1 + \eta) \simeq \eta - \frac{1}{2} \eta^2, \quad (7.4.10)$$

where

$$\eta \equiv \frac{y + a}{a_1} \quad (7.4.11)$$

is a scaled dimensionless distance from the inner cylinder. Combining these asymptotic expressions, we find that

$$\frac{\ln(a_2/\sigma)}{\ln(a_2/a_1)} = -\frac{\ln(\sigma/a_1)}{\ln(a_2/a_1)} + 1 \simeq -\frac{\eta(1 - \frac{1}{2}\eta)}{\epsilon(1 - \frac{1}{2}\epsilon)} + 1, \quad (7.4.12)$$

and then

$$\frac{\ln(a_2/\sigma)}{\ln(a_2/a_1)} \simeq -\frac{\eta}{\epsilon} \left(1 - \frac{1}{2}\eta\right) \left(1 + \frac{1}{2}\epsilon\right) + 1 \simeq 1 - \frac{\eta}{\epsilon} \left(1 - \frac{1}{2}\eta + \frac{1}{2}\epsilon\right). \quad (7.4.13)$$

We have omitted cubic terms in ϵ and η . Note that the ratio η/ϵ is of order unity.

Continuing with the analysis, we obtain the approximations

$$a_2^2 - a_1^2 = (a_2 + a_1)(a_2 - a_1) = 4(a_1 + a)a = a_1^2(2 + \epsilon)\epsilon \quad (7.4.14)$$

and

$$a_2^2 - \sigma^2 = (a_2 + \sigma)(a_2 - \sigma) = a_1^2(2 + \epsilon + \eta)(\epsilon - \eta). \quad (7.4.15)$$

Substituting expressions (7.4.13), (7.4.14), and (7.4.15) into (7.4.3), we find that

$$u_x(\sigma) \simeq V_2 + (V_1 - V_2) \left(1 - \frac{\eta}{\epsilon}\right) + \frac{\chi + \rho g_x}{4\mu} a_1^2 \left((2 + \epsilon + \eta)(\epsilon - \eta) - (2 + \epsilon) \left[\epsilon - \eta \left(1 - \frac{1}{2}\eta + \frac{1}{2}\epsilon\right)\right] \right), \quad (7.4.16)$$

which can be rearranged into

$$u_x(\sigma) \simeq V_2 + (V_1 - V_2) \frac{\epsilon - \eta}{\epsilon} + \frac{\chi + \rho g_x}{4\mu} a_1^2 \left(2(\epsilon - \eta) + \epsilon^2 - \eta^2 - (2 + \epsilon) \left[\epsilon - \eta + \frac{\eta}{2}(\eta - \epsilon)\right] \right). \quad (7.4.17)$$

Neglecting cubic terms in ϵ and η , we obtain

$$u_x(\sigma) \simeq V_2 + (V_1 - V_2) \frac{a - y}{2a} + \frac{\chi + \rho g_x}{4\mu} a_1^2 \left(2(\epsilon - \eta) + \epsilon^2 - \eta^2 - 2(\epsilon - \eta) - \eta(\eta - \epsilon) - \epsilon(\epsilon - \eta) \right), \quad (7.4.18)$$

and then

$$u_x(\sigma) \simeq V_2 + (V_1 - V_2) \frac{a - y}{2a} + \frac{\chi + \rho g_x}{2\mu} a_1^2 \eta(\epsilon - \eta). \quad (7.4.19)$$

After further simplifications, we obtain

$$u_x(y) \simeq V_2 + (V_1 - V_2) \frac{a - y}{2a} + \frac{\chi + \rho g_x}{2\mu} (a + y)(a - y), \quad (7.4.20)$$

which is precisely the profile for channel flow given in (7.1.12).

Flow rate

To recover the expression for the flow rate in channel flow, we substitute into (7.4.5) the expressions

$$a_2^2 = a_1^2(1 + \epsilon)^2, \quad \ln \frac{a_2}{a_1} = \ln(1 + \epsilon) \simeq \epsilon - \frac{1}{2}\epsilon^2 + \frac{1}{3}\epsilon^3, \quad (7.4.21)$$

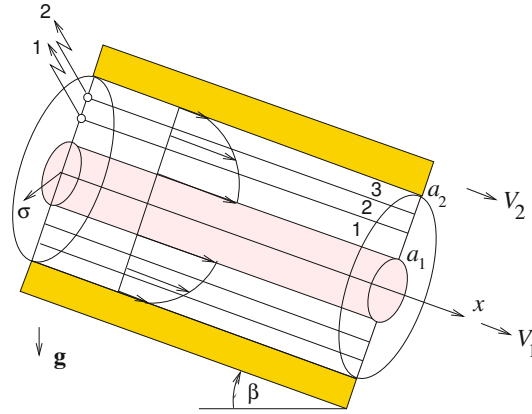


Figure 7.4.2 Illustration of unidirectional annular flow through an annular tube with translating walls for $N = 3$ layers. The interface labels are shown on the left and the layer labels are shown on the right.

and find that

$$\begin{aligned}
 Q \simeq & \pi a_1^2 (V_2 (1 + \epsilon)^2 - V_1) - \pi \frac{1}{2} (V_2 - V_1) a_1^2 \frac{\epsilon (2 + \epsilon)}{\epsilon (1 - \frac{1}{2} \epsilon)} \\
 & + \pi \frac{\chi + \rho g_x}{8\mu} a_1^4 \epsilon (2 + \epsilon) \left((1 + \epsilon)^2 + 1 - \frac{\epsilon (2 + \epsilon)}{\epsilon (1 - \frac{1}{2} \epsilon + \frac{1}{3} \epsilon^2)} \right). \tag{7.4.22}
 \end{aligned}$$

Rearranging, we obtain

$$\begin{aligned}
 Q \simeq & \pi a_1^2 (V_2 (1 + \epsilon)^2 - V_1) - \pi \frac{1}{2} (V_2 - V_1) a_1^2 (2 + \epsilon) (1 + \frac{1}{2} \epsilon) \\
 & + \pi \frac{\chi + \rho g_x}{8\mu} a_1^4 \epsilon (2 + \epsilon) \left[(1 + \epsilon)^2 + 1 - (2 + \epsilon) (1 + \frac{1}{2} \epsilon - \frac{1}{12} \epsilon^2) \right], \tag{7.4.23}
 \end{aligned}$$

which simplifies to

$$Q \simeq \pi a_1^2 (V_2 + V_1) \epsilon + \pi \frac{\chi + \rho g_x}{8\mu} a_1^4 \frac{4}{3} \epsilon^3 \tag{7.4.24}$$

or

$$Q = 2\pi a_1 \left((V_2 + V_1) a + \frac{2}{3} \frac{\chi + \rho g_x}{\mu} a^3 \right). \tag{7.4.25}$$

The product $2\pi a_1$ is the circumference of the inner cylinder, and the expression inside the tall parentheses is the flow rate of channel flow.

7.4.2 Multi-layer annular flow

As a generalization, we consider axisymmetric pressure-, gravity-, or boundary-driven annular flow of N concentric fluids through an annular tube, as illustrated in [Figure 7.4.2](#)

for three fluids. For the interfaces to remain concentric, the tube must be vertical or else the fluid densities must be the same. If these conditions are not met, hydrostatic pressure variations will cause a non-axisymmetric displacement.

A numerical method similar to that discussed in Section 7.1 for multi-layer channel flow can be developed for computing the velocity profile. The algorithm is implemented in the function *tube_ann_ml*, located in directory *04_various* of *FDLIB*. The MATLAB implementation is listed below:

```
function [sI,uI,xi1,xi2,Q,u] = tube_ann_ml ...
...
    (NLR,a1,a2,thick ...
    ,visc,den,gac ...
    ,V1,V2,chi,beta ...
    ,s ...
    )

%=====
% Multi-layer core-annular flow through an annular tube
%
% Layer numbered 1 is adjacent to the inner cylinder
% Layer numbered NLR is adjacent to the outer cylinder
%
% The velocity in the ith layer is given by:
%
%  $u(i) = af(i) + bf(i)*\ln(\sigma/a1) - gf(i)*\sigma^2$ 
%
% SYMBOLS:
% -----
%
% NLR: Number of layers
% thick(i): thickness of the ith layer
% sI(i): sigma position of the ith interface
% uI(i): velocity of the ith interface
% xi1(i): shear rate on lower side of the ith interface
% xi2(i): shear rate on upper side of the ith interface
% Q(i): flow rate of ith layer
% beta: tube inclination angle
% gac: magnitude of the acceleration of gravity
% chi: negative of the pressure gradient
% s: velocity evaluation radial position (sigma)
%=====

%---
% interface radial positions
%---

sI(1) = a1+thick(1);
```

```

for i=2:NLR
    sI(i) = sI(i-1)+thick(i);
end

%-----
% the velocity in the ith layer is given by:
%  $u(i) = af(i) + bf(i)*\ln(\sigma/a1) - gf(i)*\sigma^2$ 
% compute gf(i)
%-----

fc = gac*sin(beta);

for i=1:NLR
    gf(i) = 0.25D0*(chi+fc*den(i))/visc(i);
end

%=====
% In the first pass, set bf(1) equal to 0
% and compute the residual of the inner cylinder
% boundary condition: error0
%
% In the second pass, set bf(1) equal to 1
% and compute the residual of the inner cylinder
% boundary condition: error1
%
% In the third pass, set the proper value:
%
%  $bf(1) = error0/(error0-error1)$ 
%=====

bf(1) = 0.0;

for Ipass=1:3

%---
% compute bf(i) by recursion
% starting from the inner tube and
% requiring continuity of shear stress
% across the interfaces
%---

for i=2:NLR
    bf(i) = 2.0*gf(i) *sI(i-1)^2 ...
    + visc(i-1)/visc(i)*(bf(i-1)-2.0*gf(i-1)*sI(i-1)^2);
end

%---
% compute af(NLR) to satisfy the non-slip condition
% at the outer cylinder

```

```

%---
af(NLR) = V2 - bf(NLR)*log(a2/a1) + gf(NLR)*a2^2;

%---
% compute af(i) by recursion
% starting from the outer tube and
% requiring continuity of velocity
% across the interfaces
%---

for i=NLR-1:-1:1
    af(i) = af(i+1)+(bf(i+1)-bf(i))*log(sI(i)/a1) ...
        -(gf(i+1)-gf(i))*sI(i)^2;
end

%---
% error in the no-slip condition on the inner wall
% error = u(s=a1)-V1
%---

if(Ipass==1)
    error0 = af(1) - gf(1)*a1^2 - V1;
    bf(1) = 1.0;
elseif(Ipass==2)
    error1 = af(1) - gf(1)*a1^2 - V1;
    bf(1) = error0/(error0-error1);
end

%---
end % of Ipass
%---

%---
% compute the interfacial velocities
% and shear rates
%---

for i=1:NLR-1
    uI(i) = af(i) + bf(i)*log(sI(i)/a1) - gf(i)*sI(i)^2;
    xi1(i) = bf(i)/sI(i)-2.0*gf(i) *sI(i);
    xi2(i) = bf(i+1)/sI(i)-2.0*gf(i+1)*sI(i);
end

%----
% compute the flow rates
% the ith layer is confined between i-1 and i interfaces
%----

```

```

sI1s = sI(1)^2;
sI1as = a1^2;
Q(1) = af(1)*(sI1s-sI1as)/2.0 ...
      +bf(1)*0.5*(sI1s *(log(sI(1)/a1)-0.5)+0.5*sI1as) ...
      -gf(1)*(sI1s^2-sI1as^2)/4.0;
Q(1) = 2.0*pi*Q(1);

for i=2:NLR
    ia = i-1;
    sIis = sI(i)^2;
    sIias = sI(ia)^2;
    Q(i) = af(i)*(sIis-sIias)/2.0 ...
          +bf(i)*0.5*( sIis *(log(sI(i )/a1)-0.5)...
            -sIias*(log(sI(ia)/a1)-0.5))...
          -gf(i)*(sIis^2-sIias^2)/4.0;
    Q(i) = 2.0*pi*Q(i);
end

%-----
% compute the velocity at s
%-----

%---
% identify the host layer
%---

for i=1:NLR
    if(s<sI(i))
        break
    end
end

if(i>NLR) i=NLR; end

%---
% evaluate the velocity at s
%---

u = af(i) + bf(i)*log(s/a1) - gf(i)*s^2;

%---
% Done
%---

return

```

The velocity profile across three annular layers with different viscosities and densities is shown in [Figure 7.4.3](#).

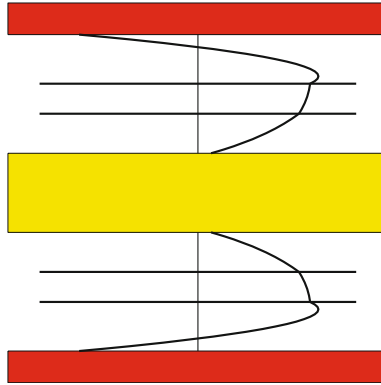


Figure 7.4.3 Velocity profile across three annular layers with different physical properties between two concentric cylinders in axial flow.

PROBLEM

7.4.1 Multi-layer annular flow

- (a) Outline and explain the numerical procedure implemented in code `tube_ann.ml`.
 (b) Plot and discuss the velocity profile of a three-layer configuration of your choice. Investigate and discuss the effect of the layer viscosities.

7.5 Steady flow through channels and tubes

Previously in this chapter, we considered flow through channels confined between parallel plates and tubes confined by concentric circular cylinders. Now we proceed to consider flow through channels or tubes with more general cross-sectional shapes where the streamwise velocity is a function of two spatial coordinates determining the position over a cross-sectional plane, $u_x(y, z)$.

Without loss of generality, we may assume that the acceleration of gravity lies in the xy plane, so that $g_z = 0$. The assumption of unidirectional flow allows us to simplify the x , y , and z components of the equation of motion displayed in Table 6.5.1, obtaining

$$0 = -\frac{\partial p}{\partial x} + \mu \left(\frac{\partial^2 u_x}{\partial y^2} + \frac{\partial^2 u_x}{\partial z^2} \right) + \rho g_x \quad (7.5.1)$$

for the streamwise component, and

$$0 = -\frac{\partial p}{\partial y} + \rho g_y, \quad 0 = -\frac{\partial p}{\partial z} \quad (7.5.2)$$

for the lateral components.

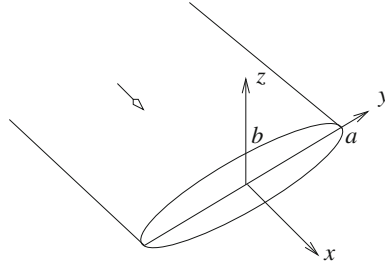


Figure 7.5.1 Illustration of steady unidirectional flow through a tube with elliptical cross-section.

The y and z components of the equation of motion stated in (7.5.2) are satisfied by the pressure distribution given in (7.1.5),

$$p = -\chi x + \rho g_y y + \pi_0, \quad (7.5.3)$$

where $\chi = -\partial p/\partial x$ is the negative of the streamwise pressure gradient and π_0 is a reference pressure.

To satisfy the x component of the equation of motion, we require that the streamwise velocity component satisfies the second-order partial differential equation

$$\nabla^2 u_x \equiv \frac{\partial^2 u_x}{\partial y^2} + \frac{\partial^2 u_x}{\partial z^2} = -\frac{\chi + \rho g_x}{\mu}, \quad (7.5.4)$$

where

$$\nabla^2 \equiv \frac{\partial^2}{\partial y^2} + \frac{\partial^2}{\partial z^2} \quad (7.5.5)$$

is the Laplacian operator in the yz plane. Equation (7.5.4) is a Poisson equation with a constant right-hand side. In fact, this partial differential equation is a generalization of the ordinary differential equation (7.1.7) for two-dimensional flow and of equation (7.3.4) for axisymmetric flow.

In the remainder of this section, we derive exact solutions of (7.5.4) for selected cross-sectional tube shapes.

7.5.1 Elliptical tube

First, we consider flow through a cylindrical tube with elliptical cross-sectional shape whose contour in the yz plane is described by the equation of the ellipse,

$$f(y, z) \equiv \frac{y^2}{a^2} + \frac{z^2}{b^2} - 1 = 0, \quad (7.5.6)$$

where a and b are the ellipse semi-axes, as illustrated in [Figure 7.5.1](#). The Cartesian coordinates of a point at the elliptical contour can be identified by a parameter, η , taking values in the range $[0, 2\pi)$, defined such that

$$y = a \cos \eta, \quad z = b \sin \eta. \quad (7.5.7)$$

The no-slip boundary condition requires that $u_x(y, z) = 0$ for coordinate pairs, (y, z) , generated by (7.5.7) and thus satisfying the equation $f(y, z) = 0$ according to (7.5.6) for any η .

Because $f(y, z)$ is a quadratic function of y and z , its Laplacian defined in (7.5.5) is constant. Motivated by this observation, we express the velocity in the form

$$u_x(y, z) = c f(y, z) \quad (7.5.8)$$

to guarantee the satisfaction of the no-slip boundary condition, and adjust the coefficient c to satisfy the Poisson equation (7.5.4). The result is a quadratic velocity distribution,

$$u_x(y, z) = \frac{1}{2} \frac{\chi + \rho g_x}{\mu} \frac{a^2 b^2}{a^2 + b^2} \left(1 - \frac{y^2}{a^2} - \frac{z^2}{b^2} \right). \quad (7.5.9)$$

The maximum velocity occurs at the tube centerline located at $y = 0$ and $z = 0$.

Flow rate

To compute the flow rate, we take advantage of the symmetry of the velocity profile with respect to the xy and xz planes, we express the axial flow rate as an integral of the velocity over the first quadrant,

$$Q = \iint_{\text{ellipse}} u_x(y, z) \, dy \, dz = 4 \int_0^a \int_0^{z_{\max}} u_x(y, z) \, dz \, dy, \quad (7.5.10)$$

where z_{\max} is computed by solving equation (7.5.6) for z , yielding

$$z_{\max} = b \sqrt{1 - y^2/a^2}. \quad (7.5.11)$$

Substituting the velocity profile (7.5.9) into the integrand, and performing the integration with respect to z , we obtain

$$Q = 2 \frac{\chi + \rho g_x}{\mu} \frac{a^2 b^2}{a^2 + b^2} \int_0^a \left(1 - \frac{y^2}{a^2} - \frac{1}{3} \frac{z_{\max}^2}{b^2} \right) z_{\max} \, dy. \quad (7.5.12)$$

Substituting the expression for z_{\max} , we obtain

$$Q = \frac{4}{3} \frac{\chi + \rho g_x}{\mu} \frac{a^2 b^3}{a^2 + b^2} \int_0^a \left(1 - \frac{y^2}{a^2} \right)^{3/2} \, dy. \quad (7.5.13)$$

Now setting $y/a = \cos \eta$, we obtain

$$Q = \frac{4}{3} \frac{\chi + \rho g_x}{\mu} \frac{a^3 b^3}{a^2 + b^2} \int_0^{\pi/2} \cos^4 \eta \, d\xi. \quad (7.5.14)$$

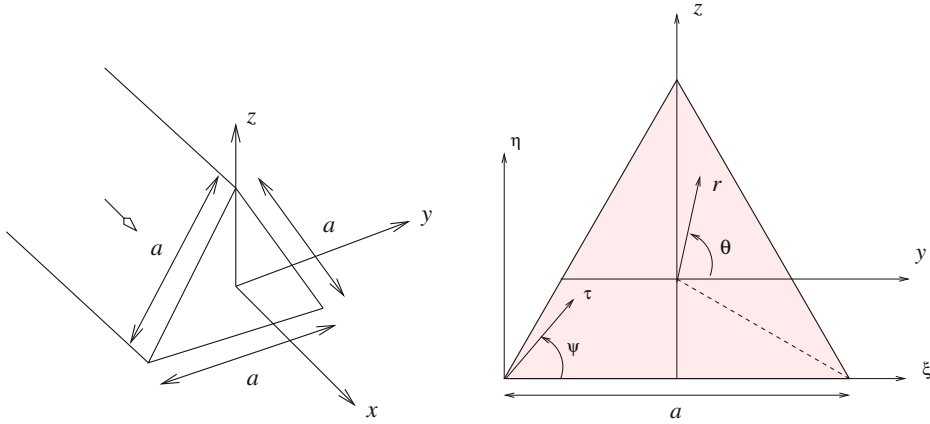


Figure 7.5.2 Illustration of steady unidirectional flow through a tube with equilateral triangular cross-sectional shape. Cross-section of a triangular tube carrying fluid in pressure- or gravity-driven flow.

Performing the integration by elementary analytical methods, or else referring to standard tables of integrals, we find that the last integral in (7.5.14) is equal to $\frac{3}{16}\pi$. The final expression for the flow rate is

$$Q = \pi \frac{1}{4} \frac{\chi + \rho g x}{\mu} \frac{a^3 b^3}{a^2 + b^2}. \tag{7.5.15}$$

Program *tube_ell*, located in directory *04_various* of **FDLIB**, not listed in the text, evaluates the velocity profile and flow rate given by (7.5.9) and (7.5.15).

As the second semi-axis, b , tends to become equal to the first semi-axis, a , the cross-section of the tube tends to become circular and the expressions for the velocity distribution and flow rate reduce to those shown in equations (7.3.8) and (7.3.16) for Poiseuille flow.

7.5.2 Equilateral triangular tube

In the second case study, we consider pressure- or gravity-driven flow through a tube whose cross-section is an equilateral triangle with side-length a , as illustrated in **Figures 7.5.2**. In the yz Cartesian coordinates defined in **Figure 7.5.2** over the tube cross-section, the origin is located at the centroid of the triangle and the y axis is parallel to the lower (horizontal) side of the triangle. The horizontal side of the triangle is described by the equation

$$2\sqrt{3}z + a = 0, \tag{7.5.16}$$

the left side is described by the equation

$$\sqrt{3}z - 3y - a = 0, \tag{7.5.17}$$

and the right side is described by the equation

$$\sqrt{3}z + 3y - a = 0. \quad (7.5.18)$$

The following velocity distribution satisfies the Poisson equation (7.5.4) and is consistent with the no-slip boundary condition along the three sides of the tube,

$$u_x(y, z) = \frac{1}{36} \frac{\chi + \rho g_x}{\mu a} (2\sqrt{3}z + a)(\sqrt{3}z + 3y - a)(\sqrt{3}z - 3y - a). \quad (7.5.19)$$

Since each factor on the right-hand side describes one side, the velocity is zero along all three sides.

Flow rate

To compute the flow rate, we introduce plane polar coordinates, (r, θ) , defined such that

$$y = r \cos \theta, \quad z = r \sin \theta, \quad (7.5.20)$$

and describe the right side of the triangle by the equation $r = a\phi(\theta)$ for $-\pi/6 \leq \theta \leq \pi/2$, as shown in [Figure 7.5.2](#). Substituting expressions (7.5.20) into (7.5.18), we find that the right side is described by the equation

$$\sqrt{3}r \sin \theta + 3r \cos \theta - a = 0. \quad (7.5.21)$$

Solving for r , we obtain

$$\phi(\theta) \equiv \frac{1}{\sqrt{3} \sin \theta + 3 \cos \theta} = \frac{1}{2\sqrt{3}} \frac{1}{\cos(\theta - \frac{\pi}{6})} \quad (7.5.22)$$

Now integrating the velocity over the tube cross-section, we derive an expression for the flow rate. In plane polar coordinates,

$$Q = 3 \int_{-\pi/6}^{\pi/2} \left(\int_0^{a\phi(\theta)} u_x r dr \right) d\theta, \quad (7.5.23)$$

where the factor of *three* accounts for the three-fold symmetry of the cross-sectional shape. Using expressions (7.5.20), we obtain

$$Q = \frac{1}{12} \frac{\chi + \rho g_x}{\mu} a^4 \int_{-\pi/6}^{\pi/2} \left(\int_0^{\phi(\theta)} \Phi(w, \theta) dw \right) d\theta. \quad (7.5.24)$$

where

$$\Phi(w, \theta) \equiv (2\sqrt{3}w \sin \theta + 1) (w(\sqrt{3} \sin \theta + 3 \cos \theta) - 1) (w(\sqrt{3} \sin \theta - 3 \cos \theta) - 1) w \quad (7.5.25)$$

is a quartic polynomial in $w \equiv r/a$. Performing the integration, we find that

$$Q = \frac{\sqrt{3}}{320} \frac{\chi + \rho g x}{\mu} a^4. \quad (7.5.26)$$

The dependence of the flow rate on the fourth power of a linear tube dimension, in this case the side length, a is typical of pressure-driven tube flow.

Alternative coordinates

The alternative $\xi\eta$ Cartesian coordinates defined in [Figure 7.5.2\(b\)](#) are related to the xy coordinates by

$$\xi = y + \frac{1}{2} a, \quad \eta = z + \frac{1}{2\sqrt{3}} a. \quad (7.5.27)$$

The three sides of the triangle are described by the equations

$$\eta = 0, \quad \eta - \sqrt{3} a + \sqrt{3} \xi = 0, \quad \eta - \sqrt{3} \xi = 0. \quad (7.5.28)$$

The velocity distribution is given by

$$u_x(\xi, \eta) = \frac{\sqrt{3}}{6} \frac{\chi + \rho g x}{\mu a} \eta (\eta - \sqrt{3} a + \sqrt{3} \xi) (\eta - \sqrt{3} \xi). \quad (7.5.29)$$

To compute the flow rate, we introduce plane polar coordinates, (τ, ψ) , defined such that

$$\xi = \tau \cos \psi, \quad \eta = \tau \sin \psi. \quad (7.5.30)$$

Substituting these expressions into the expression given in [\(7.5.28\)](#), we find that the inclined side opposite the origin is described by the equation

$$\tau \sin \psi - \sqrt{3} (a - \tau \cos \psi) = 0 \quad (7.5.31)$$

for $0 \leq \psi \leq \pi/3$. Solving for τ , we obtain $\tau = a f(\psi)$, where

$$f(\psi) \equiv \frac{\sqrt{3}}{\sin \psi + \sqrt{3} \cos \psi}. \quad (7.5.32)$$

The flow rate is given by

$$Q = \int_0^{\pi/3} \left(\int_0^{af(\psi)} u_x \tau \, d\tau \right) d\psi. \quad (7.5.33)$$

Using expressions [\(7.5.30\)](#), we obtain

$$Q = \frac{\sqrt{3}}{6} \frac{\chi + \rho g x}{\mu} a^4 \int_0^{\pi/3} \Psi(\psi) (\sin \psi - \sqrt{3} \cos \psi) \sin \psi \, d\psi, \quad (7.5.34)$$

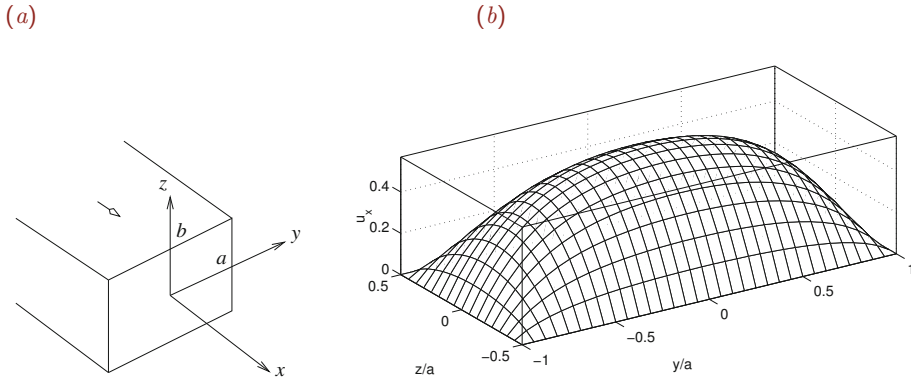


Figure 7.5.3 (a) Illustration of steady unidirectional flow through a rectangular tube or duct. (b) Velocity distribution over a tube with aspect ratio $b/a = 2$.

where

$$\Psi(\psi) \equiv \int_0^{f(\psi)} (w \sin \psi - \sqrt{3} + \sqrt{3} w \cos \psi) w^3 dw \tag{7.5.35}$$

and $w = \tau/a$. Performing the inner integration, we obtain

$$\Psi(\psi) = \left(\frac{1}{5} f(\psi) (\sin \psi + \sqrt{3} \cos \psi) - \frac{\sqrt{3}}{4} \right) f^4(\psi). \tag{7.5.36}$$

The definite integral on the right-hand of (7.5.34) is equal to $3/160$, yielding expression (7.5.26) for the flow rate.

7.5.3 Rectangular tube

Next, we consider flow through a tube whose cross-section is a rectangle with side-lengths equal to $2a$ and $2b$, as illustrated in Figure 7.5.3(a).

A standard method of solving the Poisson equation (7.5.4) involves resolving the solution for the velocity into two constituents:

1. A particular solution that satisfies the Poisson equation (7.5.4) but not all boundary conditions, denoted as $u_x^p(y, z)$.
2. A homogeneous solution, $u_x^h(y, z)$, that satisfies Laplace's equation,

$$\nabla^2 u_x^h = 0, \tag{7.5.37}$$

subject to boundary conditions that arise by requiring that the physical velocity,

$$u_x = u_x^p + u_x^h, \tag{7.5.38}$$

satisfies the no-slip boundary condition along the four walls.

A convenient particular solution is

$$u_x^p(y, z) = \frac{1}{2} \frac{\chi + \rho g x}{\mu} (b^2 - z^2). \quad (7.5.39)$$

Requiring that $u_x^p = -u_x^h$ along the four channel walls, we derive boundary conditions for the homogeneous solution,

$$u_x^h(y = \pm a, z) = -u_x^p(y = \pm a, z) = -\frac{1}{2} \frac{\chi + \rho g x}{\mu} (b^2 - z^2) \quad (7.5.40)$$

and

$$u_x^h(y, z = \pm b) = -u_x^p(y, z = \pm b) = 0. \quad (7.5.41)$$

Since a solution cannot be found in closed form, we resort to a Fourier series representation.

Fourier expansion

The homogeneous solution can be expanded in a cosine Fourier series with respect to z ,

$$u_x^h(y, z) = \sum_{n=1}^{\infty} f_n(y) \cos(\alpha_n \frac{z}{b}), \quad (7.5.42)$$

where $f_n(y)$ are position-dependent Fourier coefficients. To satisfy the boundary conditions (7.5.41), we set

$$\alpha_n = (n - \frac{1}{2}) \pi. \quad (7.5.43)$$

The functions $f_n(y)$ will be computed so that the right-hand side of (7.5.42) satisfies Laplace's equation and conforms with the boundary conditions (7.5.40).

Taking the Laplacian of (7.5.42), we obtain

$$\nabla^2 u_x^h(y, z) = \sum_{n=1}^{\infty} \left(\frac{d^2 f_n(y)}{dy^2} - \frac{\alpha_n^2}{b^2} f_n(y) \right) \cos(\alpha_n \frac{z}{b}). \quad (7.5.44)$$

For the infinite sum on the right-hand side to be zero for any y or z , each term enclosed by the parentheses must be zero, yielding the ordinary differential equation

$$\frac{d^2 f_n(y)}{dy^2} - \frac{\alpha_n^2}{b^2} f_n(y) = 0. \quad (7.5.45)$$

The general solution is

$$f_n(y) = A_n \cosh(\alpha_n \frac{y}{b}) + B_n \sinh(\alpha_n \frac{y}{b}), \quad (7.5.46)$$

where A_n and B_n are constant coefficients. Discarding the hyperbolic sines by setting $B_n = 0$ to ensure that the functions $f_n(y)$ are even, and therefore the velocity profile is

symmetric with respect to the mid-plane $y = 0$, and substituting the result into (7.5.42), we obtain

$$u_x^h(y, z) = \sum_{n=1}^{\infty} A_n \cosh\left(\alpha_n \frac{y}{b}\right) \cos\left(\alpha_n \frac{z}{b}\right). \quad (7.5.47)$$

This expression satisfies Laplace's equation for any coefficients, A_n .

To satisfy the remaining boundary conditions (7.5.40), we require that

$$\sum_{n=1}^{\infty} A_n \cosh\left(\alpha_n \frac{a}{b}\right) \cos\left(\alpha_n \frac{z}{b}\right) = -\frac{1}{2} \frac{\chi + \rho g_x}{\mu} (b^2 - z^2). \quad (7.5.48)$$

The left-hand side of (7.5.48) is the Fourier series with respect to z of the quadratic function on the right-hand side.

Fourier orthogonality

The solution follows readily using the trigonometric identity

$$\int_{-b}^b \cos\left(\alpha_n \frac{z}{b}\right) \cos\left(\alpha_m \frac{z}{b}\right) dz = \begin{cases} b & \text{if } n = m, \\ 0 & \text{if } n \neq m. \end{cases} \quad (7.5.49)$$

Multiplying both sides of (7.5.48) by $\cos(\alpha_m z/b)$, integrating with respect to z from $-b$ to b , using (7.5.49) to compute the integrals on the left-hand side, and then renaming m to n , we obtain

$$A_n = -\frac{1}{2} \frac{1}{\cosh(\alpha_n a/b)} \frac{\chi + \rho g_x}{\mu} \frac{1}{b} \int_{-b}^b (b^2 - z^2) \cos\left(\alpha_n \frac{z}{b}\right) dz. \quad (7.5.50)$$

Defining $\eta \equiv \alpha_n z/b$, we obtain

$$A_n = -\frac{1}{2} \frac{1}{\cosh(\alpha_n a/b)} \frac{\chi + \rho g_x}{\mu} b^2 \frac{1}{\alpha_n} \int_{-\alpha_n}^{\alpha_n} \left(1 - \frac{\eta^2}{\alpha_n^2}\right) \cos \eta d\eta. \quad (7.5.51)$$

The definite integral on the right-hand side is given by

$$\int_{-\alpha_n}^{\alpha_n} \left(1 - \frac{\eta^2}{\alpha_n^2}\right) \cos \eta d\eta = \left[\sin \eta + \frac{(2 - \eta^2) \sin \eta - 2\eta \cos \eta}{\alpha_n^2} \right]_{-\alpha_n}^{\alpha_n}. \quad (7.5.52)$$

Noting that $\cos \alpha_n = 0$ and $\sin \alpha_n = -(-1)^n$, we obtain

$$A_n = (-1)^n \frac{2}{\cosh(\alpha_n a/b)} \frac{\chi + \rho g_x}{\mu} b^2 \frac{1}{\alpha_n^3} \quad (7.5.53)$$

for $n \geq 1$.

Finally, we substitute expression (7.5.53) into (7.5.47) and add the homogeneous to the particular solution expressed by (7.5.39) to obtain the velocity distribution in the form of a Fourier series,

$$u_x(y, z) = \frac{1}{2} \frac{\chi + \rho g_x}{\mu} b^2 \left(1 - \frac{z^2}{b^2} + 4 \sum_{n=1}^{\infty} (-1)^n \frac{1}{\alpha_n^3} \frac{\cosh(\alpha_n y/b)}{\cosh(\alpha_n a/b)} \cos(\alpha_n \frac{z}{b}) \right). \quad (7.5.54)$$

The velocity distribution over a tube with aspect ratio $b/a = 2$ is shown in [Figure 7.5.3\(b\)](#).

Flow rate

The flow rate arises by integrating the velocity distribution over the tube cross-section in the yz plane,

$$Q \equiv \int_{-a}^a \int_{-b}^b u_x(y, z) dy dz. \quad (7.5.55)$$

Substituting expression (7.5.54) and carrying out the integration, we obtain

$$Q = \frac{4}{3} \frac{\chi + \rho g_x}{\mu} a b^3 \left(1 - 6 \frac{b}{a} \sum_{n=1}^{\infty} \frac{1}{\alpha_n^5} \tanh(\alpha_n \frac{a}{b}) \right). \quad (7.5.56)$$

By symmetry, we also have that

$$Q = \frac{4}{3} \frac{\chi + \rho g_x}{\mu} a^3 b \left(1 - 6 \frac{a}{b} \sum_{n=1}^{\infty} \frac{1}{\alpha_n^5} \tanh(\alpha_n \frac{b}{a}) \right). \quad (7.5.57)$$

Comparing the last two expressions, we derive the identity

$$1 - 6 \frac{1}{\gamma} \sum_{n=1}^{\infty} \frac{1}{\alpha_n^5} \tanh(\gamma \alpha_n) = \gamma^2 \left(1 - 6 \gamma \sum_{n=1}^{\infty} \frac{1}{\alpha_n^5} \tanh(\frac{1}{\gamma} \alpha_n) \right). \quad (7.5.58)$$

where $\gamma = a/b$ is the aspect ratio.

Program *tube_rec*, located inside directory *04_various* of **FDLIB**, not listed in the text, evaluates the velocity profile, the flow rate, and the maximum velocity occurring at the tube centerline.

7.5.4 Rectangular duct

Consider unidirectional gravity-driven flow through a tilted rectangular duct with side-lengths equal to $2a$ and $2b$, as illustrated in [Figure 7.5.3\(a\)](#). The top of the duct is open to the atmosphere and the free surface is assumed to be flat. The fluid velocity at the bottom, left, and right walls, and the shear stress at the top free surface are required to be zero.

Working as in Section 7.5.3 for a rectangular tube in the absence of a streamwise pressure gradient, we express the solution in the deliberate form

$$u_x(y, z) = \frac{1}{2} \frac{\mu g_x}{\rho} (a^2 - y^2) + \sum_{n=1}^{\infty} A_n \cosh\left(\alpha_n \frac{b-z}{a}\right) \cos\left(\alpha_n \frac{y}{a}\right), \quad (7.5.59)$$

where

$$\alpha_n = \left(n - \frac{1}{2}\right) \pi \quad (7.5.60)$$

and A_n are Fourier coefficients. This representation satisfies the governing equation and three boundary conditions,

$$u_x(y = \pm a, z) = 0, \quad u'_x(y, z = b) = 0, \quad (7.5.61)$$

where a prime denotes a partial derivative with respect to z . To satisfy the fourth boundary condition, $u_x(y, z = -b) = 0$, we require that

$$\sum_{n=1}^{\infty} A_n \cosh\left(2 \frac{b}{a} \alpha_n\right) \cos\left(\alpha_n \frac{y}{a}\right) = \frac{1}{2} \frac{\mu g_x}{\rho} (y^2 - a^2). \quad (7.5.62)$$

Working as in Section 7.5.3 and using the orthogonality property

$$\int_{-a}^a \cos\left(\alpha_n \frac{y}{a}\right) \cos\left(\alpha_m \frac{y}{a}\right) dy = \begin{cases} a & \text{if } n = m, \\ 0 & \text{if } n \neq m, \end{cases} \quad (7.5.63)$$

we find that

$$A_n = (-1)^n \frac{2}{\cosh\left(2 \frac{b}{a} \alpha_n\right)} \frac{\rho g_x}{\mu} a^2 \frac{1}{\alpha_n^3} \quad (7.5.64)$$

for $n \geq 1$. The velocity profile is thus given by

$$u_x(y, z) = \frac{1}{2} \frac{\rho g_x}{\mu} a^2 \left(1 - \frac{y^2}{a^2} + 4 \sum_{n=1}^{\infty} (-1)^n \frac{1}{\alpha_n^3} \frac{\cosh[\alpha_n(b-z)/a]}{\cosh\left(2 \frac{b}{a} \alpha_n\right)} \cos\left(\alpha_n \frac{y}{a}\right)\right). \quad (7.5.65)$$

If the duct is inclined at an angle β with respect to the horizontal, $g_x = g \sin \beta$.

The flow rate is found by straightforward integration over the duct cross-section as in the case of tube flow,

$$Q(a, b) = \frac{4}{3} \frac{\rho g_x}{\mu} a^3 b \left(1 - 3 \frac{a}{b} \sum_{n=1}^{\infty} \frac{\tanh\left(2 \frac{b}{a} \alpha_n\right)}{\alpha_n^5}\right). \quad (7.5.66)$$

Since the velocity profile for duct flow is the same as half the profile for tube flow with twice as large b , the flow rate for tube flow given in (7.5.57) arises from that for duct flow as $Q_{\text{tube}} = 2 Q_{\text{duct}}\left(a, \frac{b}{2}\right)$.

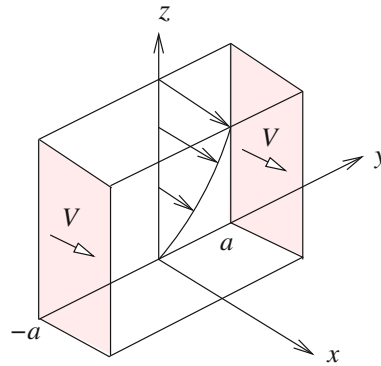


Figure 7.5.4 Illustration of steady unidirectional flow between two parallel plates sliding over a plane wall regarded as a painted surface.

7.5.5 Semi-infinite rectangular channel

Next, we consider flow between two semi-infinite parallel plates that slide with velocity V against a stationary flat surface, as illustrated in [Figure 7.5.4](#). The motion of the plates generates a unidirectional flow along the x axis, which can be regarded as a model of the flow occurring between two hairs of an idealized two-dimensional paint brush moving over a flat surface.

In the absence of a pressure gradient and significant gravitational forces, the x component of the velocity satisfies Laplace's equation,

$$\nabla^2 u_x = 0, \quad (7.5.67)$$

which arises from (7.5.4) by setting the right-hand side to zero. The no-slip boundary condition requires that the velocity is zero over the flat surface located at $z = 0$, and takes a constant value, V , over the sliding plates located at $y = \pm a$. Far from the painted surface, the fluid moves with the plate velocity V in a plug-flow mode.

Fourier expansion

To compute the solution, we expand the streamwise velocity in a Fourier series, as discussed in [Section 7.5.3](#) for flow through a tube with rectangular cross-section. Requiring that u_x tends to V as z tends to infinity, we obtain the counterpart of (7.5.47),

$$u_x(y, z) = V + \sum_{n=1}^{\infty} A_n \exp(-\alpha_n \frac{z}{a}) \cos(\alpha_n \frac{y}{a}), \quad (7.5.68)$$

where

$$\alpha_n = (n - \frac{1}{2}) \pi. \quad (7.5.69)$$

The expansion given in (7.5.68) satisfies the no-slip boundary condition at the side walls for any Fourier coefficients, A_n .

To also satisfy the no-slip condition at the painted surface, we require that

$$u_x(y, z = 0) = V + \sum_{n=1}^{\infty} A_n \cos(\alpha_n \frac{y}{a}) = 0. \quad (7.5.70)$$

Working as previously for flow in a rectangular duct and using the trigonometric identity (7.5.63), we find that

$$A_n = -\frac{V}{a} \int_{-a}^a \cos(\alpha_n \frac{y}{a}) dy = -2 \frac{V}{\alpha_n} \sin \alpha_n = 2(-1)^n \frac{V}{\alpha_n}. \quad (7.5.71)$$

Substituting this expression into (7.5.68), we obtain the desired velocity distribution

$$u_x(y, z) = V \left(1 + 2 \sum_{n=1}^{\infty} (-1)^n \frac{1}{\alpha_n} \exp(-\alpha_n \frac{z}{a}) \cos(\alpha_n \frac{y}{a}) \right). \quad (7.5.72)$$

Flow rate

As the two plates travel over the stationary surface, they dispense an amount of fluid with flow rate

$$Q = \int_0^{\infty} \int_{-a}^a (V - u_x(y, z)) dy dz. \quad (7.5.73)$$

Substituting the velocity profile, we find that

$$Q = -2V \sum_{n=1}^{\infty} (-1)^n \frac{1}{\alpha_n} \int_0^{\infty} \int_{-a}^a \exp(-\alpha_n \frac{z}{a}) \cos(\alpha_n \frac{y}{a}) dy dz. \quad (7.5.74)$$

Performing the integration, we obtain

$$Q = 4Va^2 \sum_{n=1}^{\infty} \frac{1}{\alpha_n^3} \simeq 1.085 Va^2. \quad (7.5.75)$$

The dependence of the flow rate on the second power of a linear boundary dimension, in this case, a , is typical of boundary-driven flow.

Program *chan_brush*, located inside directory *04_various* of **FDLIB**, not listed in the text, evaluates the velocity field and flow rate given by equations (7.5.72) and (7.5.75).

PROBLEMS

7.5.1 Area and perimeter of an ellipse


Show that the area of an ellipse with semi-axes a and b is equal to πab .

7.5.2 *Wall shear stress around an elliptical tube*

Derive an expression for the wall shear stress around an elliptical tube in terms of the parameter η .

7.5.3 *Flow through a triangular tube*

Compute the ratio of the flow rate through a circular tube to that through a triangular equilateral tube with the same cross-sectional area, subject to the same pressure gradient.

7.5.4  *An elliptical hose*

Using the parametrization (7.5.7), we find that the differential arc length along the contour of an ellipse is given by

$$d\ell \equiv \sqrt{dx^2 + dy^2} = \sqrt{a^2 \sin^2 \eta + b^2 \cos^2 \eta} d\eta, \quad (7.5.76)$$

which can be restated as

$$d\ell = \sqrt{a^2 - (a^2 - b^2) \cos^2 \eta} d\eta = a \sqrt{1 - k^2 \cos^2 \eta} d\eta, \quad (7.5.77)$$

where $k^2 \equiv 1 - b^2/a^2$. For convenience and without loss of generality, we have assumed that $b \leq a$.

The arc length of the perimeter of the ellipse is given by

$$L = \oint d\ell = 4a \int_0^{\pi/2} \sqrt{1 - k^2 \cos^2 \eta} d\eta = 4a \int_0^{\pi/2} \sqrt{1 - k^2 \sin^2 \eta} d\eta. \quad (7.5.78)$$

The last integral in (7.5.78) is known as the *complete elliptic integral of the second kind*. When $a = b$, we find that $k^2 = 0$ and recover the well-known result for the perimeter of a circle, $L = 2\pi a$.

In Section 11.5.1, we will see that the complete elliptic integral of the first or second kind can be evaluated using an efficient iterative method. As an alternative, we may use the mid-point rule to approximate the integral with a sum,

$$L \simeq 4a \frac{\pi}{2} \sum_{i=1}^N \sqrt{1 - k^2 \sin^2 \eta_i}, \quad (7.5.79)$$

where N is a specified discretization level and $\eta_i = (i - \frac{1}{2})\frac{\pi}{2N}$ are interval mid-points.

(a) Prepare a graph of the dimensionless scaled perimeter arc length, L/a , against the axes ratio, b/a , where $0 < b/a \leq 1$. The value of N in (7.5.79) should be large enough for the perimeter arc length to be accurate at the third decimal place.

(b) A gardener delivers water through a circular hose made of a flexible but inextensible material. By pinching the end of the hose, she is able to generate elliptical shapes with variable cross-section, while the cross-sectional perimeter of the hose remains constant. Prepare and discuss a plot of the delivered flow rate against the aspect ratio of the cross-section for a certain pressure gradient.

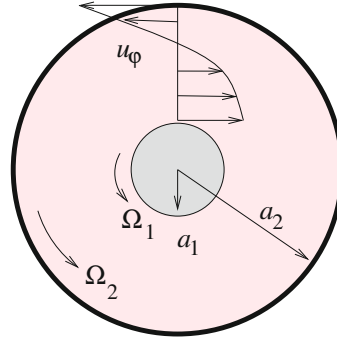


Figure 7.6.1 Illustration of swirling flow between two rotating concentric cylinders. When the gap between the cylinders is small, we obtain Couette flow between two translating parallel plates in the absence of a pressure gradient.

7.6 Steady swirling flows

We have discussed steady unidirectional flows with rectilinear streamlines. Because point particles travel with constant velocity along straight paths, inertial forces are identically zero and the flow is governed by a linear equation of motion expressing a balance between the pressure gradient, the viscous force, and the body force. In this section, we turn our attention to swirling flows with circular streamlines where centrifugal forces arise.

7.6.1 Annular flow

We begin by considering steady swirling flow between two infinite concentric cylinders with radii a_1 and a_2 rotating around their common axis with angular velocities Ω_1 and Ω_2 , as illustrated in Figure 7.6.1. The induced circular Couette flow is the counterpart of the plane Couette flow with rectilinear streamlines discussed in Section 7.1.

It is natural to introduce cylindrical polar coordinates where the x axis is coaxial with the cylinders. Our analysis will be based on two key assumptions:

- The axial and radial velocity components vanish, $u_x = 0$ and $u_\sigma = 0$.
- The azimuthal velocity component, u_φ , does not vary in the direction of the azimuthal angle φ , that is, $\partial u_\varphi / \partial \varphi = 0$.

As a consequence of these assumptions, $Du_\varphi/Dt = 0$, and u_φ depends only on the distance from the x axis, σ , where D/Dt is the material derivative.

The no-slip boundary condition at the cylinder surfaces requires that

$$u_\varphi = \Omega_1 a_1 \quad \text{at } \sigma = a_1 \quad (7.6.1)$$

and

$$u_\varphi = \Omega_2 a_2 \quad \text{at } \sigma = a_2. \quad (7.6.2)$$

Governing equations

In the case of flow with circular streamlines, the cylindrical polar components of the equation of motion displayed in equations (6.3.19) assume the simplified forms

$$0 = -\frac{\partial p}{\partial x} + \rho g_x, \quad 0 = \rho \frac{u_\varphi^2}{\sigma} - \frac{\partial p}{\partial \sigma} + \rho g_\sigma, \quad (7.6.3)$$

and

$$0 = -\frac{1}{\sigma} \frac{\partial p}{\partial \varphi} + \mu \frac{d}{d\sigma} \left(\frac{1}{\sigma} \frac{d(\sigma u_\varphi)}{d\sigma} \right) + \rho g_\varphi. \quad (7.6.4)$$

To remove the inconsequential hydrostatic pressure variation, we introduce the dynamic pressure defined as

$$\tilde{p} \equiv p - \rho (g_x x + g_y y + g_z z), \quad (7.6.5)$$

and reduce the three differential equations (7.6.3) and (7.6.4) to two ordinary differential equations,

$$\frac{d\tilde{p}}{d\sigma} = \rho \frac{u_\varphi^2}{\sigma}, \quad \frac{d}{d\sigma} \left(\frac{1}{\sigma} \frac{d(\sigma u_\varphi)}{d\sigma} \right) = 0. \quad (7.6.6)$$

Velocity and pressure profiles

Straightforward integration of the second equation in (7.6.6) with respect to σ , subject to the boundary conditions (7.6.1) and (7.6.2), provides us with the velocity profile

$$u_\varphi(\sigma) = \frac{\Omega_2 - \alpha \Omega_1}{1 - \alpha} \sigma - \frac{\Omega_2 - \Omega_1}{1 - \alpha} \frac{a_1^2}{\sigma}, \quad (7.6.7)$$

where

$$\alpha \equiv \left(\frac{a_1}{a_2} \right)^2 < 1. \quad (7.6.8)$$

The first term on the right-hand side of (7.6.7) expresses rigid-body rotation. The second term expresses swirling motion due to a point vortex situated at the cylinder axis.

The pressure distribution follows by substituting (7.6.7) into the first of equations (7.6.6) and carrying out the integration with respect to σ .

Shear stress and torque

The shear stress exerted on a cylindrical surface of radius σ is given by

$$\sigma_{\sigma\varphi}(\sigma) = \mu \left(\frac{du_\varphi}{d\sigma} \right)_\sigma. \quad (7.6.9)$$

The torque exerted on either cylinder is given by

$$T \equiv 2\pi\sigma \sigma_{\sigma\varphi}(\sigma) \quad (7.6.10)$$

for any σ . Performing the differentiation, we obtain

$$T = -4\pi\mu \frac{a_1^2}{1-\alpha} (\Omega_2 - \Omega_1). \quad (7.6.11)$$

When the cylinders rotate with the same angular velocity, the fluid rotates as a rigid body and the torque is zero.

Program *tube_ann_sw*, residing in directory *04_various* of **FDLIB**, evaluates the velocity profile given in (7.6.7).

Rigid-body rotation

Equation (7.6.7) confirms that when, $\Omega_1 = \Omega_2 = \Omega$, or when the inner cylinder is absent, $a_1 = 0$, the fluid rotates as a rigid body with angular velocity Ω . In this case, the modified pressure distribution is readily found to be

$$\tilde{p}_{\text{RBR}} = \frac{1}{2} \rho \Omega^2 \sigma^2 + \pi_0, \quad (7.6.12)$$

where π_0 is a reference pressure and the subscript RBR denotes rigid-body rotation. Thus, rigid-body rotation is associated with a quadratic pressure distribution with respect to the radial position, σ , established to counteract the inertial centrifugal force.

Small gaps

When the clearance of the channel is small compared to the inner cylinder radius, $a_2 - a_1 < a_1$, the circular Couette flow reduces to plane Couette in a channel with parallel-sided walls, as discussed in Section 7.6.1.

To demonstrate this reduction, we substitute $\Omega_1 = V_1/a_1$ and $\Omega_2 = V_2/a_2$ into (7.6.7), and thus obtain

$$u_{\varphi}(\sigma) = \frac{V_2/a_2 - \alpha V_1/a_1}{1-\alpha} \sigma - \frac{V_2/a_2 - V_1/a_1}{1-\alpha} \frac{a_1^2}{\sigma}. \quad (7.6.13)$$

Next, we define the gap, $2a = a_2 - a_1$, introduce the scaled distance from the inner cylinder

$$\eta \equiv \frac{y+a}{a_1}, \quad (7.6.14)$$

and write

$$a_2 = a_1 + 2a, \quad \epsilon = \frac{2a}{a_1}, \quad \frac{a_2}{a_1} = 1 + \epsilon, \quad \frac{\sigma}{a_1} = \eta + 1, \quad (7.6.15)$$

where ϵ is a small parameter and y is the distance from the midway position. The velocity profile becomes

$$u_\varphi(\sigma) = \frac{1}{a_2} \frac{V_2 - \alpha(1 + \epsilon)V_1}{1 - \alpha} \sigma - \frac{1}{a_2} \frac{V_2 - (1 + \epsilon)V_1}{1 - \alpha} \frac{a_1^2}{\sigma}, \quad (7.6.16)$$

which can be rearranged into

$$u_\varphi(\sigma) = \left([V_2 - \alpha(1 + \epsilon)V_1] \frac{\sigma}{a_1} - [V_2 - (1 + \epsilon)V_1] \frac{a_1}{\sigma} \right) \frac{a_1}{a_2} \frac{1}{1 - \alpha}. \quad (7.6.17)$$

By definition,

$$\alpha = \frac{1}{(1 + \epsilon)^2} \simeq \frac{1}{1 + 2\epsilon} \simeq 1 - 2\epsilon \quad (7.6.18)$$

and

$$1 - \alpha = 1 - \frac{1}{(1 + \epsilon)^2} = \frac{(1 + \epsilon)^2 - 1}{(1 + \epsilon)^2} \simeq \frac{2\epsilon}{(1 + \epsilon)^2}, \quad (7.6.19)$$

and thus

$$u_\varphi(\sigma) \simeq \left([V_2 - (1 - 2\epsilon)(1 + \epsilon)V_1] (1 + \eta) - [V_2 - (1 + \epsilon)V_1] (1 - \eta) \right) \frac{1 + \epsilon}{2\epsilon}. \quad (7.6.20)$$

Linearizing the product $(1 - 2\epsilon)(1 + \epsilon)$, we obtain

$$u_\varphi(\sigma) \simeq \left([V_2 - (1 - \epsilon)V_1] (1 + \eta) - [V_2 - (1 + \epsilon)V_1] (1 - \eta) \right) \frac{1 + \epsilon}{2\epsilon}. \quad (7.6.21)$$

Linearizing the expression inside the large parentheses, we obtain

$$u_\varphi(\sigma) \simeq \left((V_2 - V_1) 2\eta + 2\epsilon V_1 \right) \frac{1}{2\epsilon} = (V_2 - V_1) \frac{\eta}{\epsilon} + V_1, \quad (7.6.22)$$

which is precisely the linear velocity profile of plane Couette flow.

7.6.2 Multi-layer swirling flow

Next, we consider the multi-layer swirling flow of N annular layers between two concentric cylinders, as illustrated in [Figure 7.6.2\(a\)](#). For the interfaces to remain concentric, either the tube must be vertical or all fluid densities must be the same. If these conditions are not met, hydrostatic pressure variations will cause an interfacial misalignment from the axisymmetric configuration.

A numerical method similar to that discussed in Section 7.1 for multi-layer channel flow can be developed for computing the velocity profile of multi-layer rotating flow. The algorithm is implemented in the function `tube_ann_sw.ml` located in directory `04_various` of **FDLIB**. The MATLAB implementation is listed below:

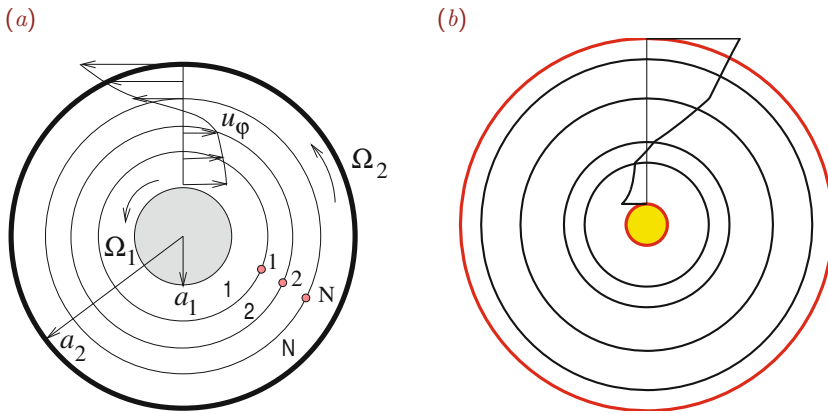


Figure 7.6.2 (a) Illustration of multi-layer annular swirling flow between two rotating concentric cylinders. (b) Velocity profile across five annular layers.

```
function [sI,uI,xi1,xi2,Q,u] = tube_ann_sw_ml ...
...
(NLR ...
,a1,a2 ...
,thick ...
,visc ...
,Omega1, Omega2 ...
,s)

%=====
% Multi-layer swirling flow inside an annular tube
%
% Layer numbered 1 is adjacent to the inner cylinder
% Layer numbered NLR is adjacent to outer cylinder
%
% The velocity in the ith film is given by:
%
% u(i) = bf(i)/sigma + cf(i)*sigma
%
% SYMBOLS
% -----
%
% a1: inner tube radius
% a2: outer tube radius
% Omega1: inner tube angular velocity
% Omega2: outer tube angular velocity
% NLR: Number of layers
% thick(i): thickness of the ith layer
% sI(i): radial position of the ith interface
```

```

% uI(i): velocity of the ith interface
% xi1(i): shear rate on lower side of the ith interface
% xi2(i): shear rate on upper side of the ith interface
% Q(i): flow rate of ith layer
%=====

%---
% set the radial interface positions
%---

sI(1) = a1+thick(1);

for i=2:NLR
    sI(i) = sI(i-1)+thick(i);
end

%-----
% The velocity in the ith layer is given by:
%
% u(i) = bf(i)/sigma + cf(i)*sigma
%
% In the first pass, set bf(1)=0
% and compute the residual of the inner cylinder
% boundary condition: error0
%
% In the second pass, set bf(1)=1
% and compute the residual of the inner cylinder
% boundary condition: error1
%
% In the third pass, set the proper value:
%
% bf(1) = error0/(error0-error1)
%-----

bf(1) = 0.0;

%---
for Ipass=1:3
%---

%---
% compute bf(i) by recursion
% starting from the inner cylinder by requiring
% continuity of shear stress across the interfaces
%
% The sigma-phi shear stress is given by:
%
% shear_stress = sigma d(u/sigma)/d(sigma)
%---

```

```

for i=1:NLR-1
    bf(i+1) = visc(i)/visc(i+1)*bf(i);
end

%---
% compute cf(i) by recursion
% to satisfy continuity of velocity across the interfaces
%---

cf(1) = (Omega1*a1-bf(1)/a1)/a1;

for i=1:NLR-1
    cf(i+1) = cf(i) + (bf(i)-bf(i+1))/sI(i)^2;
end

%---
% error in the no-slip condition on the inner wall
% error = u(s=a1)-V1
%---

if(Ipass==1)
    error0 = bf(NLR)/a2 + cf(NLR)*a2 - Omega2*a2;
    bf(1) = 1.0;
elseif(Ipass==2)
    error1 = bf(NLR)/a2 + cf(NLR)*a2 - Omega2*a2;
    bf(1) = error0/(error0-error1);
end

%---
end % of Ipass
%---

%---
% compute interfacial velocities
% and shear rates
%---

for i=1:NLR-1
    uI(i) = bf(i)/sI(i) + cf(i)*sI(i);
    xi1(i) = -2.0*bf(i) /sI(i)^3;
    xi2(i) = -2.0*bf(i+1)/sI(i)^3;
end

%-----
% compute the flow rates
% ith film is confined between i-1 and i interfaces
%-----

```

```

Q(1) = bf(1)*(log(sI(1)/a1)) ...
      + cf(1)*0.5D0*(sI(1)^2-a1^2);

for i=2:NLR
    Q(i) = bf(i)*log(sI(i)/sI(i-1)) ...
          + cf(i)*0.5*(sI(i)^2-sI(i-1)^2);
end

%-----
% compute the velocity at s
%-----

%---
% identify the host layer
%---

for i=1:NLR
    if(s<sI(i))
        break
    end
end

if(i>NLR) i=NLR; end

%---
% evaluate the velocity at s
%---

u = bf(i)/s+cf(i)*s;

%-----
% Done
%-----

return

```

The velocity profile across five annular layers with different viscosities and densities is shown in [Figure 7.6.2\(b\)](#).

PROBLEMS

7.6.1 *Free surface of a rotating liquid.*

A certain volume of a liquid is placed inside a vertical cylindrical container that is closed at the bottom and rotates with angular velocity Ω about the x axis, which points against the direction of gravity. Using equation (7.6.12), we find that the pressure distribution in the

liquid is given by

$$p = \frac{1}{2} \rho \Omega^2 + \rho g_x x + \pi_0, \quad (7.6.23)$$

where π_0 is a reference pressure.

(a) Show that, when surface tension is insignificant, the shape of the free surface is described by the equation

$$x = \frac{1}{2} \frac{\Omega^2}{g} \sigma^2 + c, \quad (7.6.24)$$

where c is a constant and g is the magnitude of the acceleration of gravity. This equation reveals that the shape of the free surface is parabolic.

(b) Derive a differential equation governing the shape of the free surface in the presence of surface tension.

7.6.2 Multi-layer swirling flow

(a) Outline and explain the numerical procedure implemented in the code *tube_ann_sw_ml*.

(b) Plot and discuss the velocity profile of a three-layer configuration of your choice.

7.7 Transient channel flows

Having investigated the structure of steady unidirectional flows with rectilinear or circular streamlines, now we turn our attention to corresponding unsteady flows generated by sudden or oscillatory boundary motion, tilting, or by the application of a time-dependent pressure gradient. Our analysis will continue to be based on the assumption of unidirectional flow with rectilinear or circular streamlines.

7.7.1 Couette flow

We begin by considering flow in a two-dimensional channel with parallel walls separated by distance h , as illustrated in [Figure 7.7.1](#). The upper wall is held stationary, while the lower wall is set in motion suddenly parallel to itself along the x axis with constant velocity, V .

Working as in Section 7.1, we find that, in the absence of a pressure gradient along the x axis other than that due to gravity,

$$\frac{\partial p}{\partial x} = \rho g_x, \quad (7.7.1)$$

which shows that the pressure distribution assumes the hydrostatic profile. The x component of the equation of motion provides us with a partial differential equation in time, t , and transverse position, y , for the x velocity component,

$$\rho \frac{\partial u_x}{\partial t} = \mu \frac{\partial^2 u_x}{\partial y^2}, \quad (7.7.2)$$

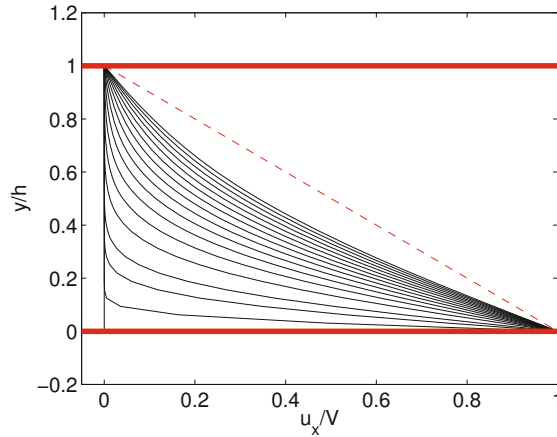


Figure 7.7.1 Transient Couette flow in a channel with parallel walls due to the impulsive translation of the lower wall. Profiles are shown at dimensionless times $\nu t/h^2 = 0.001, 0.005, 0.010, 0.020, 0.030, \dots, 0.14, \text{ and } 0.15$. The straight line is the linear profile established at long times.

subject to the initial condition

$$u_x = 0 \quad \text{for } 0 < y \leq h \quad (7.7.3)$$

at $t = 0$, and the no-slip boundary conditions

$$u_x(y = 0) = V, \quad u_x(y = h) = 0, \quad (7.7.4)$$

at any $t \geq 0$. At steady state, the solution is given by the linear Couette velocity profile

$$u_x^{\text{steady}}(y) = V \left(1 - \frac{y}{h} \right), \quad (7.7.5)$$

as discussed in Section 7.1.

Fourier expansion

To compute the solution of (7.7.2), we consider the deviation of the transient velocity profile from the linear profile established at steady state. Expanding the difference in a Fourier series with respect to y , we obtain

$$u_x(y, t) = u_x^{\text{steady}}(y) + \sum_{n=1}^{\infty} A_n(t) \sin \frac{n\pi y}{h}. \quad (7.7.6)$$

The argument of the trigonometric functions on the right-hand side was designed to satisfy the boundary conditions (7.7.4) at any time.

To compute the functions $A_n(t)$, we substitute expansion (7.7.6) into the governing equation (7.7.2), and carry out the differentiation with respect to t and y to obtain

$$\sum_{n=1}^{\infty} \left(\rho \frac{dA_n(t)}{dt} + \mu \left(\frac{n\pi}{h} \right)^2 A_n(t) \right) \sin \frac{n\pi y}{h} = 0. \quad (7.7.7)$$

To ensure the satisfaction of this equation for any y , we set the expression enclosed by the outer tall parentheses to zero and obtain a first-order linear differential equation for $A_n(t)$ whose solution is

$$A_n(t) = b_n \exp\left(-\frac{n^2\pi^2\nu}{h^2} t\right), \quad (7.7.8)$$

where $\nu = \mu/\rho$ is the kinematic viscosity of the fluid and b_n is a constant.

Now substituting expression (7.7.8) into (7.7.6), we obtain

$$u_x(y, t) = u_x^{\text{steady}}(y) + \sum_{n=1}^{\infty} b_n \exp\left(-\frac{n^2\pi^2\nu}{h^2} t\right) \sin \frac{n\pi y}{h}. \quad (7.7.9)$$

To compute the constants b_n , we require that the velocity profile (7.7.9) is consistent with the initial condition (7.7.3), and obtain

$$u_x(y, t=0) = V\left(1 - \frac{y}{h}\right) + \sum_{n=1}^{\infty} b_n \sin \frac{n\pi y}{h} = 0 \quad (7.7.10)$$

for $0 \leq y \leq h$. The solution follows readily using the trigonometric identity

$$\int_0^h \sin \frac{n\pi y}{h} \sin \frac{m\pi y}{h} dy = \begin{cases} 0 & \text{if } n = 0 \text{ or } m = 0, \\ \frac{1}{2}h & \text{if } n = m \neq 0, \\ 0 & \text{if } n \neq m. \end{cases} \quad (7.7.11)$$

Multiplying (7.7.10) by $\sin(m\pi y/h)$ for an arbitrary integer, m , integrating with respect to y from 0 to h , using identity (7.7.11), and then switching m to n , we obtain

$$b_n = -2 \frac{V}{h} \int_0^h \left(1 - \frac{y}{h}\right) \sin \frac{n\pi y}{h} dy. \quad (7.7.12)$$

Performing the integration, we obtain

$$b_n = -\frac{2}{n\pi} V. \quad (7.7.13)$$

The velocity profile (7.7.9) takes the final form

$$u_x(y, t) = V \left(1 - \frac{y}{h} - \frac{2}{\pi} \sum_{n=1}^{\infty} \frac{1}{n} \exp\left(-\frac{n^2\pi^2\nu}{h^2} t\right) \sin \frac{n\pi y}{h} \right). \quad (7.7.14)$$

Program *chan_2d_imp*, located in directory *04_various* of **FDLIB**, evaluates the velocity profile given in (7.7.14). A sequence of developing profiles of the scaled velocity u_x/V illustrating the approach to steady state is shown in [Figure 7.7.1](#).

Approach to steady state

At long times, the summed terms on the right-hand side of (7.7.14) decay at an exponential rate and the linear profile of the steady Couette flow expressed by the first two terms inside the angular brackets on the right-hand side dominates. The elapsed time where steady flow has virtually been established, t_s , can be estimated by setting the magnitude of the argument of the exponential term on the right-hand side of (7.7.14) equal to unity for the lowest possible value $n = 1$, obtaining

$$t_s \simeq \frac{1}{\pi^2} \frac{h^2}{\nu}. \quad (7.7.15)$$

Apart from the numerical factor $1/\pi^2$ in the denominator, this estimate could have been deduced on the basis of dimensional analysis at the outset.

Diffusion of vorticity

The only non-vanishing vorticity component in unidirectional flow is the component that is perpendicular to the plane of the flow,

$$\omega_z = -\frac{\partial u_x}{\partial y}. \quad (7.7.16)$$

Differentiating (7.7.2) with respect to y , we find that the evolution of the vorticity is governed by equation (7.7.2), provided that u_x is replaced by ω_z on both sides.

$$\rho \frac{\partial \omega_z}{\partial t} = \mu \frac{\partial^2 \omega_z}{\partial y^2}. \quad (7.7.17)$$

The profiles shown in [Figure 7.7.1](#) illustrate that, as soon as the lower wall starts translating, a thin layer of highly rotational flow is established. The vorticity then diffuses away from the wall to occupy the clearance of the channel. At steady state, the vorticity takes the uniform value V/h . This process exemplifies how vorticity enters a fluid across a boundary during a period of transient flow.

7.7.2 Impulsive motion of a plate in a semi-infinite fluid

A detailed analysis of the transient Couette flow at short times can be carried out by neglecting the presence of the upper stationary wall and concentrating on the behavior of the flow near the lower moving wall. In principle, this can be done by setting $h = \infty$ in the initial condition (7.7.3) and boundary conditions (7.7.4) to obtain a semi-infinite flow. However, cursory inspection reveals that the Fourier series solution (7.7.14) is no longer useful in this limit.

Similarity solution

The absence of a length scale in a semi-infinite flow suggests that the time and space dependencies must combine into a unified variable, which can be nondimensionalized by the kinematic viscosity of the fluid, ν . Recalling that the kinematic viscosity has units of length squared over time, we introduce the dimensionless variable

$$\eta \equiv \frac{y}{\sqrt{\nu t}}, \quad (7.7.18)$$

which ranges from zero to infinity, and express the velocity in the form

$$u_x(y, t) = Vf(\eta), \quad (7.7.19)$$

where $f(\eta)$ is a function of a single variable. This functional form implies that the fluid velocity as seen by an observer who finds herself at the position $y = \sqrt{\nu t}$, and is thus traveling upward with velocity $dy/dt = \sqrt{\nu/(4t)}$, remains constant in time.

The initial and boundary conditions are satisfied, provided that the function $f(\eta)$ obeys the boundary condition $f(\eta = 0) = 1$ and the far-field condition $f(\eta = \infty) = 0$.

Substituting the similarity solution (7.7.19) into the governing equation (7.7.2), we obtain

$$\rho \frac{\partial u_x}{\partial t} = \rho V \frac{df}{d\eta} \frac{\partial \eta}{\partial t} = \mu V \frac{\partial^2 u_x}{\partial y^2} = \mu V \frac{\partial}{\partial y} \left(\frac{\partial \eta}{\partial y} \frac{df}{d\eta} \right). \quad (7.7.20)$$

Rearranging, we obtain

$$\frac{1}{\nu} \frac{df}{d\eta} \frac{\partial \eta}{\partial t} = \frac{\partial}{\partial y} \left(\frac{1}{\sqrt{\nu t}} \frac{df}{d\eta} \right) = \frac{1}{\sqrt{\nu t}} \frac{d^2 f}{d\eta^2} \frac{\partial \eta}{\partial y} = \frac{1}{\nu t} \frac{d^2 f}{d\eta^2}. \quad (7.7.21)$$

We note that

$$\frac{\partial \eta}{\partial t} = -\frac{1}{2} \frac{1}{\nu^{1/2}} \frac{y}{t^{3/2}}, \quad (7.7.22)$$

and derive a second-order *nonlinear* ordinary differential equation,

$$\frac{d^2 f}{d\eta^2} = -\frac{1}{2} \eta \frac{df}{d\eta}. \quad (7.7.23)$$

To compute the solution, we recast (7.7.23) into the form

$$\frac{d}{d\eta} \left(\ln \frac{df}{d\eta} \right) = -\frac{1}{2} \eta. \quad (7.7.24)$$

Integrating, we obtain

$$\frac{df}{d\eta} = A \exp\left(-\frac{1}{4} \eta^2\right), \quad (7.7.25)$$

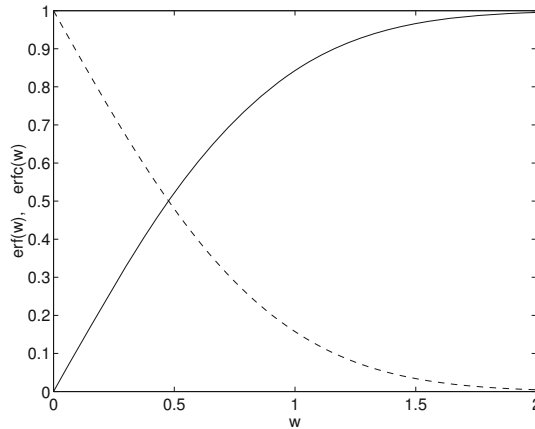


Figure 7.7.2 Graphs of the error function (solid line) and complementary error function (broken line) defined in equations (7.7.26) and (7.7.27).

where A is an integration constant. Carrying out a second integration, we find that

$$f(\eta) = A \int_0^\eta \exp\left(-\frac{1}{4} q^2\right) dq + B = 2A \int_0^{\eta/2} \exp(-v^2) dv + B, \quad (7.7.26)$$

where B is a new integration constant, q is an auxiliary integration variable, and $v \equiv \frac{1}{2}q$.

Error function

The integral on the right-hand side of (7.7.26) is not available in analytical form. To formalize the solution, we introduce the error function, defined as

$$\operatorname{erf}(w) \equiv \frac{2}{\sqrt{\pi}} \int_0^w \exp(-v^2) dv, \quad (7.7.27)$$

and the complementary error function, defined as

$$\operatorname{erfc}(w) = 1 - \operatorname{erf}(w). \quad (7.7.28)$$

Graphs of these functions are shown in [Figure 7.7.2](#). As w tends to infinity, the error function tends to the asymptotic value of unity; correspondingly, the complementary error function tends to zero.

The frequent occurrence of the error function in various branches of mathematical physics has motivated its tabulation and representation by various algebraic approximations. Program *error_f*, residing in directory *99_spec_fnc* inside directory *01_num_meth* of **FDLIB**, evaluates the error function and the complementary error function using an accurate algebraic approximation.

Velocity and vorticity profiles

Now returning to (7.7.26), we express the right-hand side in terms of the error function and require that $f(\eta = 0) = 1$ and $f(\eta = \infty) = 0$ to obtain

$$A = -\frac{1}{\sqrt{\pi}} \quad B = 1, \quad (7.7.29)$$

yielding the velocity profile

$$u_x(y, t) = Vf(\eta) = V \operatorname{erfc}\left(\frac{1}{2}\eta\right). \quad (7.7.30)$$

The accompanying vorticity profile is

$$\omega_z(y, t) = -\frac{\partial u_x}{\partial y} = -V \frac{df}{d\eta} \frac{\partial \eta}{\partial y}. \quad (7.7.31)$$

Performing the differentiations, we obtain the Gaussian distribution

$$\omega_z(y, t) = \frac{V}{\sqrt{\pi\nu t}} \exp\left(-\frac{1}{4}\frac{y^2}{\nu t}\right). \quad (7.7.32)$$

This expression illustrates explicitly the singular nature of the vorticity at the initial instant, $t = 0$, and the spreading of the vorticity away from the moving wall due to viscous diffusion at later times.

Wall shear stress

The wall shear stress is given by

$$\sigma_{xy}(y = 0, t) = \mu \left(\frac{\partial u_x}{\partial y}\right)_{y=0} = -\mu \frac{V}{\sqrt{\pi\nu t}}. \quad (7.7.33)$$

This expression illustrates that an unphysical singularity occurs at the initial instant, $t = 0$, as soon as the plate is set in motion.

In real life, a plate cannot start moving with constant velocity in an impulsive fashion. Instead, the plate velocity must increase gradually from zero to the final value over a non-infinitesimal period of time.

7.7.3 Pressure- and gravity-driven flow

As a second case study, we consider flow in a channel with stationary walls separated by distance h , located at $y = 0$ and h . The motion of the fluid is due to the sudden application of a constant pressure gradient or sudden tilting.

The x component of the equation of motion provides us with a partial differential equation for the x velocity component,

$$\rho \frac{\partial u_x}{\partial t} = \chi + \mu \frac{\partial^2 u_x}{\partial y^2} + \rho g_x, \quad (7.7.34)$$

where $\chi = -\partial p/\partial x$ is a constant. The pressure field is given in equation (7.1.5).

The velocity profile satisfies the initial condition

$$u_x(y, t = 0) = 0 \quad \text{for } 0 \leq y \leq h, \quad (7.7.35)$$

and the no-slip boundary conditions

$$u_x(y = 0, t) = 0, \quad u_x(y = h, t) = 0 \quad (7.7.36)$$

for $t \geq 0$. At steady state, we obtain the parabolic Hagen velocity profile,

$$u_x^{\text{steady}}(y) = \frac{1}{2} \frac{\chi + \rho g_x}{\mu} y (h - y), \quad (7.7.37)$$

as discussed in Section 7.1.

Fourier series solution

To compute the evolution of the flow, we consider the deviation of the transient velocity profile from the parabolic profile established at steady state. Expanding the difference in a Fourier series with respect to y , we obtain

$$u_x(y, t) = u_x^{\text{steady}}(y) + \sum_{n=1}^{\infty} A_n(t) \sin \frac{n\pi y}{h}. \quad (7.7.38)$$

The arguments of the trigonometric functions on the right-hand side have been designed to satisfy the wall boundary conditions at any time.

To compute the functions $A_n(t)$, we substitute the Fourier expansion into the governing equation (7.7.34) and carry out the differentiation with respect to t and x to find that

$$\sum_{n=1}^{\infty} \left(\rho \frac{dA_n(t)}{dt} + \mu \left(\frac{n\pi}{h} \right)^2 A_n(t) \right) \sin \frac{n\pi y}{h} = 0. \quad (7.7.39)$$

To ensure that this equation is satisfied for any y , we set the expression enclosed by the outer tall parentheses to zero, and thus obtain a first-order linear differential equation for $A_n(t)$ whose solution is

$$A_n(t) = b_n \exp\left(-\frac{n^2\pi^2\nu}{h^2} t\right), \quad (7.7.40)$$

where $\nu = \mu/\rho$ is the kinematic viscosity of the fluid and b_n is a constant. Substituting this expression into (7.7.38), we obtain

$$u_x(y, t) = u_x^{\text{steady}}(y) + \sum_{n=1}^{\infty} b_n \exp\left(-\frac{n^2\pi^2\nu}{h^2} t\right) \sin \frac{n\pi y}{h}. \quad (7.7.41)$$

This expression satisfies the governing equations for any set of Fourier coefficients, b_n .

To compute the coefficients b_n , we require that the solution given in (7.7.41) satisfies the initial condition (7.7.35), so that

$$u_x(y, t = 0) = \frac{\chi + \rho g_x}{\mu} \frac{1}{2} y (h - y) + \sum_{n=1}^{\infty} b_n \sin \frac{n\pi y}{h} = 0 \quad (7.7.42)$$

for $0 \leq y \leq h$. The solution follows readily from the trigonometric identity

$$\int_0^h \sin \frac{n\pi y}{h} \sin \frac{m\pi y}{h} dy = \begin{cases} 0 & \text{if } n = 0 \text{ or } m = 0, \\ \frac{1}{2}h & \text{if } n = m \neq 0, \\ 0 & \text{if } n \neq m. \end{cases} \quad (7.7.43)$$

Multiplying the middle and right-hand sides of (7.7.42) by $\sin(m\pi y/h)$, where m is an arbitrary integer, integrating with respect to y from 0 to h , and using identity (7.7.43), we find that

$$\frac{\chi + \rho g_x}{\mu} \frac{1}{2} \int_0^h y (h - y) \sin \frac{m\pi y}{h} dy + b_m \frac{1}{2} h = 0, \quad (7.7.44)$$

yielding

$$b_m = -\frac{\chi + \rho g_x}{\mu} \frac{1}{h} \int_0^h y (h - y) \sin \frac{m\pi y}{h} dy. \quad (7.7.45)$$

Manipulating the integral, we obtain

$$b_m = \frac{\chi + \rho g_x}{\mu} \frac{1}{m\pi} \int_0^h y (h - y) d \cos \frac{m\pi y}{h}, \quad (7.7.46)$$

and then

$$b_m = \frac{\chi + \rho g_x}{\mu} \frac{1}{m\pi} \left(\left[y(h - y) \cos \frac{m\pi y}{h} \right]_0^h - \int_0^h \cos \frac{m\pi y}{h} (h - 2y) dy \right). \quad (7.7.47)$$

Finally, we compute

$$b_m = \frac{\chi + \rho g_x}{\mu} \frac{2}{m\pi} \int_0^h \cos \frac{m\pi y}{h} y dy = h \frac{\chi + \rho g_x}{\mu} \frac{2}{\pi^2 m^2} \int_0^h y d \sin \frac{m\pi y}{h}, \quad (7.7.48)$$

yielding

$$b_m = -h \frac{\chi + \rho g_x}{\mu} \frac{2}{\pi^2 m^2} \int_0^h \sin \frac{m\pi y}{h} dy = h^2 \frac{\chi + \rho g_x}{\mu} \frac{2}{\pi^3 m^3} \left[\cos \frac{m\pi y}{h} \right]_0^h. \quad (7.7.49)$$

The term

$$\left[\cos \frac{m\pi y}{h} \right]_0^h = \cos \frac{m\pi h}{h} - 1 \quad (7.7.50)$$

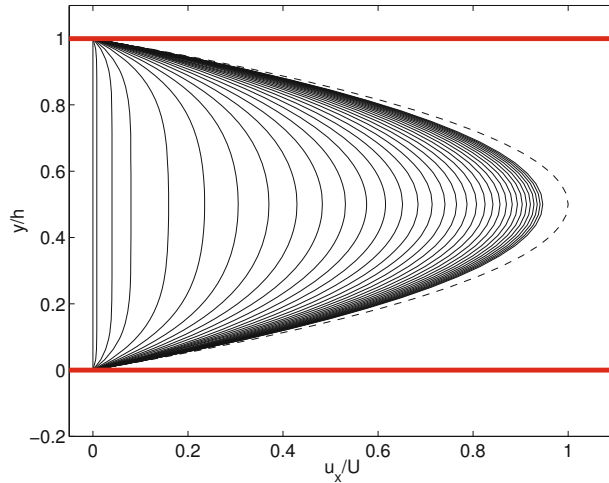


Figure 7.7.3 Transient velocity profiles in a channel with parallel walls separated by distance h , due to the sudden application of a constant pressure gradient or sudden tilting. Profiles are shown at dimensionless times $\nu t/h^2 = 0.001, 0.005, 0.01, 0.02, 0.03, \dots$. The dashed line describes the parabolic profile of the Hagen flow with centerline velocity U established at long times.

is equal to 2 when m is odd, or 0 if m is even. Substituting the expression for b_m into (7.7.42) provides us with the transient velocity profile

$$u_x(y, t) = \frac{1}{2} \frac{\chi + \rho g x}{\mu} \left(y(h - y) - \frac{8}{\pi^3} h^2 \sum_{n=1,3,\dots}^{\infty} \frac{1}{n^3} \exp\left(-\frac{n^2 \pi^2 \nu}{h^2} t\right) \sin \frac{n\pi y}{h} \right). \quad (7.7.51)$$

Program *chan_2d_trans*, located in directory *04_various* of **FDLIB**, evaluates the velocity profile at a specified time. A sequence of developing profiles of the scaled velocity u_x/U is shown in **Figure 7.7.3**, where U is the maximum velocity of the steady Hagen flow established at long times.

PROBLEM

7.7.1 Flow due to a constant shear stress

Show that the velocity profile due to the application of a constant shear stress with magnitude τ at the planar boundary of a semi-infinite fluid occupying the upper half-space, $y \geq 0$, is given by

$$u(y, t) = \frac{\tau}{\mu} \sqrt{\nu t} \left(\frac{2}{\sqrt{\pi}} \exp\left(-\frac{1}{4} \eta^2\right) - \eta \operatorname{erfc}\left(\frac{1}{2} \eta\right) \right), \quad (7.7.52)$$

where $\eta \equiv y/\sqrt{\nu t}$ is a dimensionless similarity variable. Discuss the asymptotic behavior of the flow at long times.

7.8 Oscillatory channel flows

In Section 7.7, we discussed transient Couette flow and transient pressure- or gravity-driven channel flow. We found that, in all cases, vorticity enters the flow through the boundaries and then diffuses to occupy the entire domain of flow. In this section, we consider corresponding configurations for oscillatory flow. An important new feature is that, because vorticity of alternating sign enters the fluid across the boundaries of the flow, cancellation of vorticity by diffusion prevents the establishment of significant motion sufficiently far from the boundaries of the flow.

7.8.1 Oscillatory Couette flow

Suppose that the lower wall of a two-dimensional channel oscillates parallel to itself with velocity

$$v = V \cos(\Omega t), \quad (7.8.1)$$

while the upper wall is stationary, thereby generating the unsteady unidirectional flow illustrated in Figure 7.8.1, where V is the amplitude and Ω is the angular frequency of the oscillations. The lower wall is located at $y = 0$ and the upper wall is located at $y = h$, where h is the channel width.

The induced velocity field is governed by the unsteady diffusion equation (7.7.2), subject to the no-slip boundary condition requiring that

$$u_x(y = 0) = V \cos(\Omega t), \quad u_x(y = h) = 0 \quad (7.8.2)$$

for $t \geq 0$.

Thanks to the linearity of the governing equations, the flow will be periodic in time. The velocity can be expressed in the form

$$u_x(y, t) = V [f_R(y) \cos(\Omega t) + f_I(y) \sin(\Omega t)], \quad (7.8.3)$$

where $f_R(y)$ and $f_I(y)$ are two *a priori* unknown functions, the subscript R stands for real, and the subscript I stands for imaginary.

Governing equations

To compute the functions $f_R(y)$ and $f_I(y)$, we substitute expression (7.8.3) into (7.7.2), carry out the time differentiation, collect the coefficients of the sines and cosines, and then set the compiled expressions to zero to obtain two coupled linear ordinary differential equations,

$$\frac{d^2 f_R}{dy^2} = \frac{\Omega}{\nu} f_I, \quad \frac{d^2 f_I}{dy^2} = -\frac{\Omega}{\nu} f_R, \quad (7.8.4)$$

where $\nu \equiv \mu/\rho$ is the kinematic viscosity of the fluid.

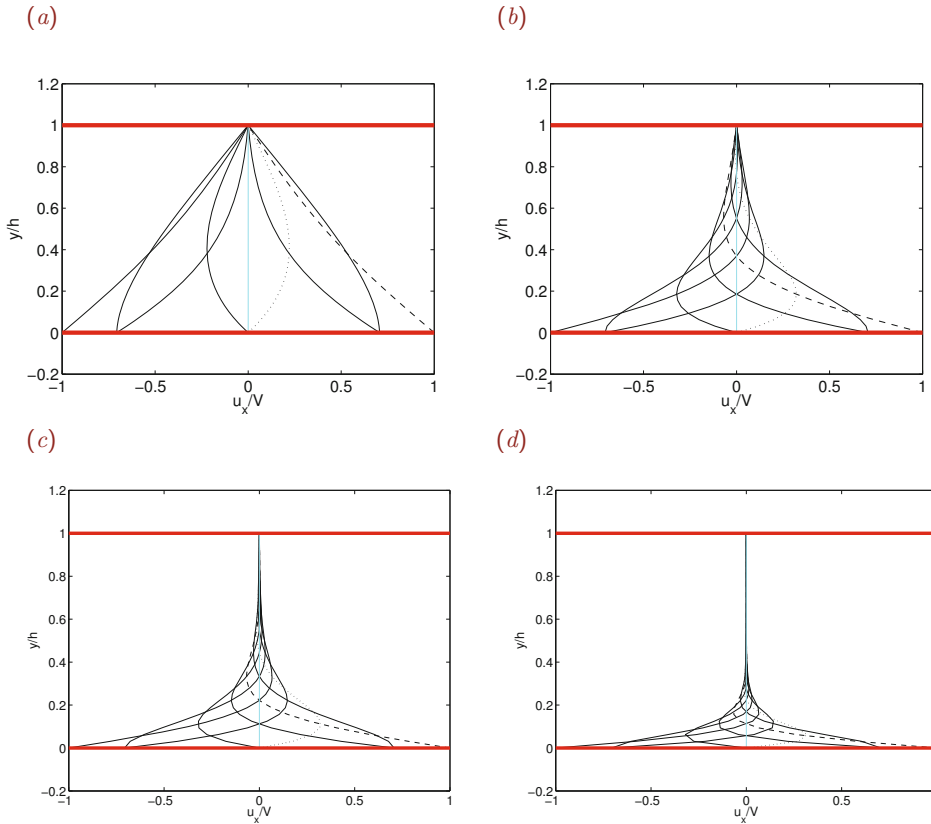


Figure 7.8.1 Periodic velocity profiles of oscillatory Couette flow in a two-dimensional channel confined between two parallel walls at phase angles $\Omega t/\pi = 0$ (dashed lines), 0.25, 0.50 (dotted lines), 0.75, 1.0, 1.25, 1.50, 1.75, and 2.0, and Womersley number (a) $Wo = 1$, (b) 3, (c) 10, and (d) 20. In the first case, $Wo = 1$, the flow is nearly quasi-steady. As Wo increases, a Stokes boundary layer is established over the oscillating lower plate.

Formulation in complex variables

To expedite the solution, we introduce the imaginary unit, i , defined such that $i^2 = -1$, and define the complex function

$$f(y) \equiv f_R(y) + i f_I(y). \quad (7.8.5)$$

The two equations in (7.8.4) can be collected into a single complex form,

$$\frac{d^2 f}{dy^2} = -i \frac{\Omega}{\nu} f. \quad (7.8.6)$$

The real and imaginary parts of the complex equation (7.8.6) are equal, respectively, to the first and second equation in (7.8.4).

Now using the Euler decomposition

$$\exp(-i\Omega t) = \cos(\Omega t) - i \sin(\Omega t), \quad (7.8.7)$$

we find that u_x is given by the real part of the complex function

$$w(y, t) \equiv V f(y) \exp(-i\Omega t). \quad (7.8.8)$$

The imaginary part of $w(y, t)$ also satisfies the governing equation (7.7.2).

The solution of (7.8.6) is readily found to be

$$f(y) = A \exp\left(y \sqrt{-i\Omega/\nu}\right) + B \exp\left(-y \sqrt{-i\Omega/\nu}\right), \quad (7.8.9)$$

where A and B are two complex constants, with the understanding that

$$\exp(\sqrt{-i}) = \exp(e^{3\pi i/4}) = \exp\left(\frac{-1+i}{\sqrt{2}}\right). \quad (7.8.10)$$

Using the Euler decomposition, we obtain

$$\exp(\sqrt{-i}) = \exp\left(-\frac{1}{\sqrt{2}}\right) \left[\cos\left(\frac{1}{\sqrt{2}}\right) + i \sin\left(\frac{1}{\sqrt{2}}\right) \right]. \quad (7.8.11)$$

The no-slip boundary conditions (7.8.2) require that $f(0) = 1$ and $f(h) = 0$. Using these equations to evaluate the constants A and B , we find that

$$A = \frac{\exp(-h \sqrt{-i\Omega/\nu})}{\exp(-h \sqrt{-i\Omega/\nu}) - \exp(h \sqrt{-i\Omega/\nu})} = \frac{1}{1 - \exp(2h \sqrt{-i\Omega/\nu})} \quad (7.8.12)$$

and $B = 1 - A$. Substituting these expressions into (7.8.8) and rearranging, we derive the targeted complex function

$$f(y) = \frac{\exp(y \sqrt{-i\Omega/\nu}) - \exp[(2h - y) \sqrt{-i\Omega/\nu}]}{1 - \exp(2h \sqrt{-i\Omega/\nu})}. \quad (7.8.13)$$

The real and imaginary parts of this function provide us with the velocity according to (7.8.3).

Stokes boundary layer

It is useful to introduce the Stokes boundary-layer thickness,

$$\delta \equiv \sqrt{\frac{2\nu}{\Omega}}, \quad (7.8.14)$$

and write

$$f(y) = \frac{\exp(y \sqrt{-2i}/\delta) - \exp[(2h - y) \sqrt{-2i}/\delta]}{1 - \exp(2h \sqrt{-2i}/\delta)}. \quad (7.8.15)$$

In terms of the scaled position and channel width,

$$\hat{y} \equiv y/\delta, \quad \hat{h} \equiv h/\delta, \quad (7.8.16)$$

we obtain

$$f(y) = \frac{\exp[-(1-i)\hat{y}] - \exp[-(1-i)(2\hat{h}-\hat{y})]}{1 - \exp[-(1-i)2\hat{h}]}. \quad (7.8.17)$$

The physical significance of the Stokes boundary-layer thickness will be discussed in Section 7.8.2.

Program *chan_2d_osc*, residing in directory *04_various* of **FDLIB**, not listed in the text, evaluates the velocity profile for a specified angular frequency and scaled temporal phase angle, Ωt .

Womersley number

The argument of the exponential term on the right-hand side of (7.8.13) suggests that the structure of the flow is determined by the dimensionless Womersley number

$$\text{Wo} \equiv \frac{1}{2} h \sqrt{\frac{\Omega}{\nu}} = \frac{1}{\sqrt{2}} \frac{h}{\delta}, \quad (7.8.18)$$

which expresses a properly scaled angular frequency. Profiles of the scaled velocity, u_x/V , are shown in Figure 7.8.1 at a sequence of dimensionless phase angles, $\Omega t/\pi$, for $\text{Wo} = 1, 3, 10$, and 20.

When the Womersley number is small, the flow evolves in quasi-steady fashion and the velocity profile is almost linear with respect to y at any time, as shown in Figure 7.8.1(a). As the Womersley number increases, the motion tends to be confined inside a boundary layer that is attached to the oscillating wall, while the rest of the fluid is virtually stationary, as shown in Figure 7.8.1(d).

7.8.2 Rayleigh's oscillating plate

To investigate the behavior at high frequencies, Ω , or large channel widths, h , we consider the structure of the flow at large values of the Womersley number. In this limit, the second term in the numerator and the second term in the denominator on the right-hand side of (7.8.13) become exponentially small, yielding the simplified form

$$f(y) \simeq \exp(y \sqrt{-i\Omega/\nu}). \quad (7.8.19)$$

Resolving the right-hand side into its real and imaginary parts, we obtain

$$f(y) \simeq [\cos(y \sqrt{\Omega/(2\nu)}) + i \sin(y \sqrt{\Omega/(2\nu)})] \exp(-y \sqrt{\Omega/(2\nu)}). \quad (7.8.20)$$

The associated velocity profile is

$$u_x(y, t) = V \left(\cos(\Omega t) \cos(y \sqrt{\Omega/(2\nu)}) + \sin(\Omega t) \sin(y \sqrt{\Omega/(2\nu)}) \right) \times \exp(-y \sqrt{\Omega/(2\nu)}). \quad (7.8.21)$$

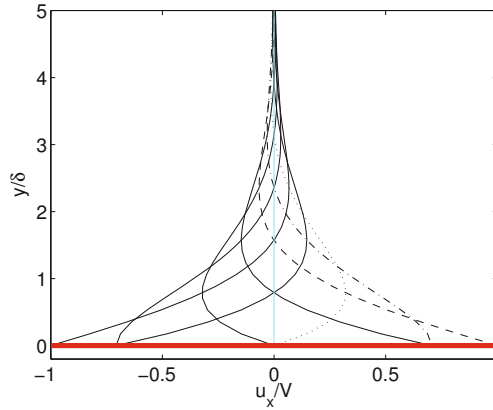


Figure 7.8.2 Velocity profiles due to the in-plane oscillation of a plate in a semi-infinite viscous fluid at phase angles $\Omega t/\pi = 0$ (dashed line), 0.25 (dashed-dotted line), 0.50 (dotted line), 0.75, 1.0, 1.25, 1.50, 1.75, and 2.0. The y coordinate is scaled by the Stokes boundary layer thickness, δ , defined in (7.8.14).

Combining the two terms in the tall parentheses, we obtain

$$u_x(y, t) = V \cos\left(\Omega t - y \sqrt{\Omega/(2\nu)}\right) \exp\left(-y \sqrt{\Omega/(2\nu)}\right). \quad (7.8.22)$$

In terms of the dimensionless position, $\hat{y} \equiv y/\delta$, the velocity profile is given by

$$u_x(y, t) = V \cos(\Omega t - \hat{y}) e^{-\hat{y}}, \quad (7.8.23)$$

where δ is the Stokes boundary-layer thickness defined in (7.8.14).

Program *plate_osc*, residing in directory *04_various* of **FDLIB**, not listed in the text, evaluates the velocity profile at a specified time. A sequence of profiles corresponding to those shown in Figure 7.8.1 is shown in Figure 7.8.2.

Stokes boundary layer

Expression (7.8.22) shows that the magnitude of the velocity decays exponentially with respect to distance normal to the oscillating plate. The region where substantial fluid motion occurs is identified as the Stokes boundary layer.

A rough measure of the thickness of the boundary layer is the distance where the magnitude of the argument of the exponential term on the right-hand side of (7.8.22) is equal to unity, which is given by the Stokes boundary-layer thickness δ defined in (7.8.14). Apart from the factor of *two* in the numerator, the expression for δ could have been deduced on the basis of dimensional analysis at the outset.

Wall shear stress

The shear stress exerted on an oscillating plate is given by

$$\sigma_{xy}(y = 0, t) = \mu \left(\frac{\partial u}{\partial y} \right)_{y=0} = V \sqrt{\mu \rho \Omega} \cos(\Omega t - \frac{3\pi}{4}). \quad (7.8.24)$$

In terms of the Stokes boundary-layer thickness,

$$\sigma_{xy}(y = 0, t) = \frac{\mu V}{\delta} \sqrt{2} \cos(\Omega t - \frac{3\pi}{4}). \quad (7.8.25)$$

This expression reveals that the wall shear stress lags behind the wall velocity by the phase angle $3\pi/4$, independent of the angular frequency.

7.8.3 Pulsating pressure-driven flow

In the last case study, we consider pulsating flow in a channel due to an oscillatory pressure gradient given by

$$\frac{\partial p}{\partial x} = \rho g_x - \zeta \sin(\Omega t), \quad (7.8.26)$$

where ζ is a specified amplitude and Ω is the angular frequency of the oscillations. The streamwise velocity component satisfies the differential equation

$$\rho \frac{\partial u_x}{\partial t} = \zeta \sin(\Omega t) + \mu \frac{\partial^2 u_x}{\partial y^2}. \quad (7.8.27)$$

The no-slip boundary condition requires that the velocity is zero at the two walls located at $y = 0$ and h , $u_x(0) = 0$ and $u_x(h) = 0$

Working as in the case of oscillatory Couette flow, we express the velocity in the form

$$u_x(y, t) = \frac{\zeta}{\rho \Omega} (f_R(y) \cos(\Omega t) + f_I(y) \sin(\Omega t)), \quad (7.8.28)$$

and introduce the complex function

$$f(y) = f_R(y) + i f_I(y), \quad (7.8.29)$$

where i is the imaginary unit. The velocity u_x is given by the real part of the complex function

$$w(y, t) = \frac{\zeta}{\rho \Omega} f(y) e^{-i\Omega t}, \quad (7.8.30)$$

satisfying the governing equation

$$\rho \frac{\partial w}{\partial t} = i \zeta e^{-i\Omega t} + \mu \frac{\partial^2 w}{\partial y^2}. \quad (7.8.31)$$

In fact, the real part of this complex equation is the governing equation (7.8.27). Substituting expression (7.8.30) into (7.8.31) and simplifying, we obtain an ordinary differential equation,

$$\frac{d^2 f}{dy^2} = -\frac{i\Omega}{\nu} (f + 1). \quad (7.8.32)$$

The no-slip boundary condition at the two channel walls requires that $f(0) = 0$ and $f(h) = 0$. The solution is

$$f(y) = \frac{\cosh \left[\left(y - \frac{1}{2}h \right) \sqrt{-i\Omega/\nu} \right]}{\cosh \left(\frac{1}{2}h \sqrt{-i\Omega/\nu} \right)} - 1. \quad (7.8.33)$$

The hyperbolic cosine of a complex argument on the right-hand side can be resolved into exponential functions by invoking the definition

$$\cosh z \equiv \frac{1}{2} (e^z + e^{-z}). \quad (7.8.34)$$

Using (7.8.11), we obtain

$$f(y) = \frac{\cosh \left[(-1 + i) \left(\hat{y} - \frac{1}{2} \hat{h} \right) \right]}{\cosh \left[(-1 + i) \frac{1}{2} \hat{h} \right]} - 1, \quad (7.8.35)$$

where $\hat{y} \equiv y/\delta$, $\hat{h} \equiv h/\delta$, and $\delta \equiv (2\nu/\Omega)^{1/2}$ is the Stokes boundary-layer thickness.

Program *chan_2d_wom*, located in directory *04_various* of **FDLIB**, not listed in the text, evaluates the velocity profile from the preceding expressions. A time sequence of profiles of the scaled velocity u_x/U is shown in [Figure 7.8.3](#), where U is the centerline velocity of the steady Hagen flow.

Low frequencies

At low frequencies, the motion is quasi-steady, which means that the velocity profile is nearly parabolic throughout each cycle. To demonstrate this behavior, we approximate the hyperbolic cosines in (7.8.33) with quadratic functions using the Maclaurin series expansion

$$f(y) = \frac{1 - i \frac{1}{2} \left(y - \frac{1}{2}h \right)^2 \frac{\Omega}{\nu} + \dots}{1 - i \frac{1}{8} h^2 \frac{\Omega}{\nu} + \dots} - 1, \quad (7.8.36)$$

yielding

$$f(y) = \left[1 - i \frac{1}{2} \left(y - \frac{1}{2}h \right)^2 \frac{\Omega}{\nu} + \dots \right] \left[1 + i \frac{1}{8} h^2 \frac{\Omega}{\nu} + \dots \right] - 1. \quad (7.8.37)$$

Carrying out the multiplication on the right-hand side and keeping only linear terms in Ω , we obtain the approximation

$$f(y) = -i \frac{1}{2} \left(y - \frac{1}{2}h \right)^2 \frac{\Omega}{\nu} + i \frac{1}{8} h^2 \frac{\Omega}{\nu} + \dots = i \frac{1}{2} y (h - y) \frac{\Omega}{\nu} + \dots \quad (7.8.38)$$

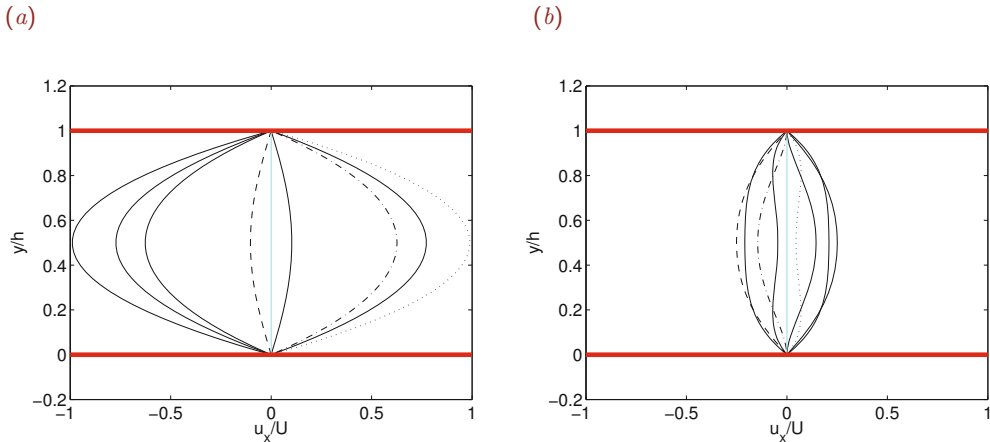


Figure 7.8.3 Velocity profiles of pulsating pressure-driven flow in a two-dimensional channel confined between two parallel walls at phase angles $\Omega t/\pi = 0$ (dashed lines), 0.25 (dashed-dotted lines), 0.50 (dotted lines), 0.75, 1.0, 1.25, 1.50, 1.75, and 2.0, for Womersley number (a) $Wo = 1/2$ and (b) 3.0.

Now substituting into (7.8.28) the approximations

$$f_R = 0, \quad f_I = \frac{1}{2} y(h-y) \frac{\Omega}{\nu}, \quad (7.8.39)$$

we obtain the expression

$$u_x(y, t) = \frac{1}{2} \frac{\zeta}{\mu} \sin(\Omega t) y(h-y) + \dots, \quad (7.8.40)$$

which describes the quasi-steady parabolic profile of the Hagen flow.

High frequencies

At high frequencies, the flow consists of a core that oscillates in a plug-flow mode, and two Stokes boundary layers, one attached to each wall (Problem 7.8.2). One interesting feature of the motion is that, under certain conditions, the amplitude of the velocity at the edges of the boundary layers may exceed that in the central core.

PROBLEMS

7.8.1 Shear stress on an oscillating plate

(a) Derive expression (7.8.24).

(b) We have noted that the wall shear stress lags behind the wall velocity by the phase angle $3\pi/4$, independent of the angular frequency, Ω . Does a similar independence arise in the case of channel flow where the velocity profile is given by (7.8.3), (7.8.5), and (7.8.13)?

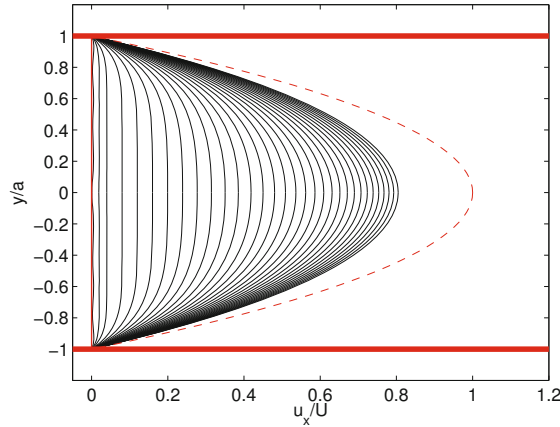


Figure 7.9.1 Transient unidirectional flow in a circular tube of radius a due to the sudden application of a constant pressure gradient or sudden tilting. Velocity profiles are shown at dimensionless times $\nu t/a^2 = 0.001, 0.005, 0.010, 0.020, 0.030, \dots$. The dashed parabolic line corresponds to the Poiseuille flow established at long times; U is the corresponding centerline velocity.

7.8.2 Oscillatory channel flow at high frequencies

Show that, at high values of the Womersley number, the function $f(y)$ defined in (7.8.33) takes the approximate form

$$f(y) \simeq 1 - \exp(y \sqrt{-i\Omega/\nu}) - \exp[(h - y) \sqrt{-i\Omega/\nu}]. \quad (7.8.41)$$

This expression confirms the development of a plug-flow core and two Stokes boundary layers, one attached to each wall.

7.9 Transient and oscillatory flow in a circular tube

Our study of transient and oscillatory channel flow in Sections 7.7 and 7.8 has revealed the physical mechanisms by which momentum is transmitted and vorticity diffuses away from planar boundaries in an unsteady flow. In this section, we consider corresponding mechanisms for curved boundaries by studying the structure of unsteady unidirectional and swirling tube flows.

7.9.1 Transient Poiseuille flow

Consider transient unidirectional flow through a cylindrical tube of radius a due to the sudden application of a pressure gradient or tilting, as illustrated in Figure 7.9.1. The motion of the fluid will be described in cylindrical polar coordinates, (x, σ, φ) , where the x axis coincides with the tube centerline.

The radial and azimuthal velocity components are identically zero, $u_\sigma = 0$ and $u_\varphi = 0$, while the axial component is a function of distance from the x axis and time, $u_x(\sigma, t)$. The no-slip boundary condition requires that the velocity vanishes at the tube surface at any time, $u_x(\sigma = a, t) = 0$. At the initial instant, the fluid is assumed to be quiescent, $u_x(\sigma, t = 0) = 0$.

Governing equations

The pressure field is given by equation (7.3.1),

$$p = -\chi x + \rho(g_y y + g_z z) + \pi_0, \quad (7.9.1)$$

with a constant axial pressure gradient, $\partial p/\partial x = -\chi$. Simplifying the x component of the equation of motion written in cylindrical polar coordinates, we obtain a partial differential equation for the axial velocity,

$$\rho \frac{\partial u_x}{\partial t} = \chi + \mu \left(\frac{\partial^2 u_x}{\partial \sigma^2} + \frac{1}{\sigma} \frac{\partial u_x}{\partial \sigma} \right) + \rho g_x. \quad (7.9.2)$$

When the flow reaches a steady state, the velocity profile assumes the parabolic distribution described by the Poiseuille solution given in (7.3.8),

$$u_x^{\text{steady}}(\sigma) = \frac{1}{4} \frac{\chi + \rho g_x}{\mu} (a^2 - \sigma^2). \quad (7.9.3)$$

To compute the solution of (7.9.2), we resolve the velocity profile into the steady Poiseuille profile and a transient profile that decays at long times, $v_x(\sigma, t)$,

$$u_x(\sigma, t) = u_x^{\text{steady}}(\sigma) + v_x(\sigma, t). \quad (7.9.4)$$

Substituting (7.9.4) into (7.9.2), we find that the transient profile satisfies a homogeneous partial differential equation,

$$\frac{\partial v_x}{\partial t} = \nu \left(\frac{\partial^2 v_x}{\partial \sigma^2} + \frac{1}{\sigma} \frac{\partial v_x}{\partial \sigma} \right), \quad (7.9.5)$$

where $\nu \equiv \mu/\rho$ is the kinematic viscosity of the fluid.

Separation of variables

Equation (7.9.5) can be solved by separation of variables implemented by the expansion

$$v_x(\sigma, t) = \sum_{n=1}^{\infty} c_n \phi_n(\sigma) \psi_n(t), \quad (7.9.6)$$

where $\phi_n(\sigma)$ and $\psi_n(t)$ are *a priori* unknown functions of their respective arguments, and c_n are constant coefficients. Substituting this expansion into (7.9.5), carrying out the differentiations, and rearranging, we obtain

$$\sum_{n=1}^{\infty} c_n \phi_n(\sigma) \psi_n(t) \left(\frac{1}{\psi_n} \frac{d\psi_n}{dt} - \frac{\nu}{\phi_n} \left(\frac{d^2 \phi_n}{d\sigma^2} + \frac{1}{\sigma} \frac{d\phi_n}{d\sigma} \right) \right) = 0. \quad (7.9.7)$$

For this equality to hold true at any position, σ , and time, t , the expression enclosed by the tall parentheses on the right-hand side must be identically zero, yielding

$$\frac{1}{\psi_n} \frac{d\psi_n}{dt} = \frac{\nu}{\phi_n} \left(\frac{d^2\phi_n}{d\sigma^2} + \frac{1}{\sigma} \frac{d\phi_n}{d\sigma} \right) = -\nu b_n^2, \quad (7.9.8)$$

where b_n^2 is a positive constant to be determined as part of the solution. The right-hand side of (7.9.8) was designed to facilitate forthcoming algebraic manipulations.

Rearranging the two equalities in (7.9.8), we derive two ordinary differential equations,

$$\frac{d\psi_n}{dt} = -\nu b_n^2 \psi_n \quad (7.9.9)$$

and

$$\frac{d^2\phi_n}{d\sigma^2} + \frac{1}{\sigma} \frac{d\phi_n}{d\sigma} + b_n^2 \phi_n = 0. \quad (7.9.10)$$

The solution of (7.9.9) is readily found to be

$$\psi_n(t) = \exp(-b_n^2 \nu t), \quad (7.9.11)$$

which reveals that the transient flow decays exponentially in time.

Bessel functions

To derive the solution of (7.9.10), we introduce the Bessel function of the first kind, $J_0(z)$, satisfying the zeroth-order Bessel equation

$$z \frac{d}{dz} \left(z \frac{dJ_0(z)}{dz} \right) + z^2 J_0(z) = z^2 \frac{d^2 J_0(z)}{dz^2} + z \frac{dJ_0(z)}{dz} + z^2 J_0(z) = 0. \quad (7.9.12)$$

A graph of $J_0(z)$ is shown with the solid line in [Figure 7.9.2](#). The frequent occurrence of the Bessel functions in various branches of mathematical physics has motivated their tabulation and representation in terms of infinite series and algebraic approximations.

Program *bess_J0*, located in directory *99_spec_fnc* inside directory *01_num_meth* of **FDLIB**, not listed in the text, evaluates the Bessel function J_0 using an accurate algebraic approximation.

Now replacing z in Bessel's equation (7.9.12) with $b_n \sigma$ and simplifying, we find that the function

$$\phi_n(\sigma) = J_0(b_n \sigma) \quad (7.9.13)$$

satisfies equation (7.9.10), and is thus the desired solution. To satisfy the no-slip boundary condition, we require that

$$\phi_n(a) = J_0(b_n a) = 0, \quad (7.9.14)$$

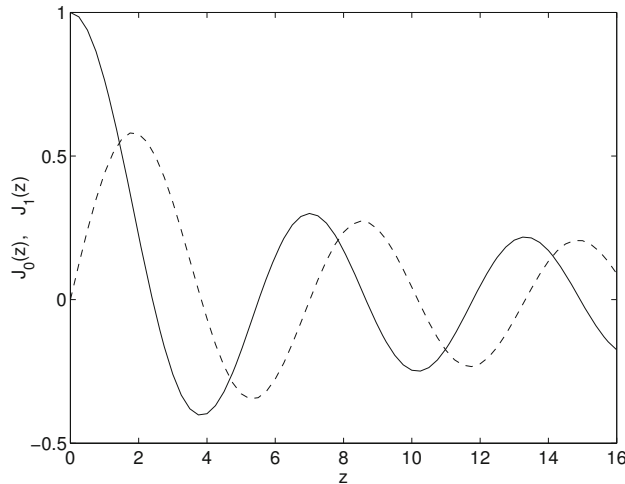


Figure 7.9.2 Graphs of the Bessel functions $J_0(z)$ and $J_1(z)$ drawn with the solid or broken line, respectively, necessary for the computation of transient tube flow.

which shows that $b_n a$ is a zero of $J_0(z)$, denoted by α_n . The first seven zeros are

$$\begin{aligned} \alpha_1 = 2.4048, \quad \alpha_2 = 5.5201, \quad \alpha_3 = 8.6537, \quad \alpha_4 = 11.7915, \\ \alpha_5 = 14.9309, \quad \alpha_6 = 18.0711, \quad \alpha_7 = 21.2116, \end{aligned} \quad (7.9.15)$$

to shown accuracy. Accordingly, we set

$$b_n = \frac{\alpha_n}{a}. \quad (7.9.16)$$

Substituting (7.9.16) into (7.9.13) and (7.9.11), and the result into (7.9.6), we derive the expansion

$$v_x(\sigma, t) = \sum_{n=1}^{\infty} c_n J_0\left(\alpha_n \frac{\sigma}{a}\right) \exp\left(-\alpha_n^2 \frac{\nu t}{a^2}\right). \quad (7.9.17)$$

This representation clearly satisfies the requirement that the transient flow decays to zero at long times.

To also satisfy the initial condition, $u_x(\sigma, t = 0) = 0$, we evaluate the decomposition (7.9.4) at $t = 0$ and use (7.9.3) and (7.9.17) to obtain

$$\sum_{n=1}^{\infty} c_n J_0\left(\frac{\alpha_n \sigma}{a}\right) = -\frac{1}{4} \frac{\chi + \rho g_x}{\mu} (a^2 - \sigma^2). \quad (7.9.18)$$

The coefficients c_n must be such that this representation holds true for any value of σ . In fact, the left-hand side is the Bessel series representation of the quadratic function on the right-hand side.

Orthogonality of the zeroth-order Bessel functions

To extract the coefficients c_n from (7.9.18), we use the following orthogonality property of the Bessel functions,

$$\int_0^1 z J_0(\alpha_n z) J_0(\alpha_m z) dz = \begin{cases} \frac{1}{2} J_1^2(\alpha_n) & \text{if } n = m, \\ 0 & \text{if } n \neq m, \end{cases} \quad (7.9.19)$$

where $J_1(z)$ is the Bessel function of the first kind. By definition, $J_1(z)$ satisfies the differential equation

$$z^2 \frac{d^2 J_1(z)}{dz^2} + z \frac{dJ_1(z)}{dz} + (z^2 - 1) J_1(z) = 0, \quad (7.9.20)$$

and is required to be finite for any value of z between, and including, zero and infinity. A graph of $J_1(z)$ is shown with the dashed line in [Figure 7.9.2](#).

Replacing z in identity (7.9.19) with σ/a , and rearranging, we obtain

$$\int_0^a \sigma J_0(\alpha_n \frac{\sigma}{a}) J_0(\alpha_m \frac{\sigma}{a}) d\sigma = \begin{cases} \frac{1}{2} a^2 J_1^2(\alpha_n) & \text{if } n = m, \\ 0 & \text{if } n \neq m. \end{cases} \quad (7.9.21)$$

Inspired by this identity, we multiply both sides of (7.9.18) by $\sigma J_0(\alpha_m \sigma/a)$, integrate with respect to σ from 0 to a , use the orthogonality property (7.9.21), and then switch m to n to obtain

$$c_n = -\frac{1}{2} \frac{\chi + \rho g x}{\mu a^2} \frac{1}{J_1^2(\alpha_n)} \int_0^a J_0(\frac{\alpha_n \sigma}{a}) (a^2 - \sigma^2) \sigma d\sigma, \quad (7.9.22)$$

which can be rearranged into

$$c_n = -\frac{1}{2} \frac{\chi + \rho g x}{\mu a^2} \frac{1}{J_1^2(\alpha_n)} \int_0^1 J_0(\alpha_n v) (1 - v^2) v dv, \quad (7.9.23)$$

where $v \equiv \sigma/a$. To compute the last integral, we replace z in Bessel's equation (7.9.12) with $\alpha_n v$, and simplify to obtain

$$\alpha_n^2 v J_0(\alpha_n v) = -\frac{d}{dv} \left(v \frac{dJ_0(\alpha_n v)}{dv} \right). \quad (7.9.24)$$

Note that the left- and thus the right-hand side of (7.9.24) vanishes when $v = 0$ or 1 . Integrating (7.9.24) with respect to v from 0 to 1, we obtain

$$\alpha_n^2 \int_0^1 J_0(\alpha_n v) v dv = - \left[v \frac{dJ_0(\alpha_n v)}{dv} \right]_{v=1} + \left[v \frac{dJ_0(\alpha_n v)}{dv} \right]_{v=0}. \quad (7.9.25)$$

Now using the identity $dJ_0(z)/dz = -J_1(z)$, we obtain

$$\int_0^1 J_0(\alpha_n v) v dv = \frac{1}{\alpha_n} J_1(\alpha_n). \quad (7.9.26)$$

A similar computation yields

$$\begin{aligned}
 \alpha_n^2 \int_0^1 J_0(\alpha_n v) v^3 dv &= - \int_0^1 v^2 \frac{d}{dv} \left(v \frac{dJ_0(\alpha_n v)}{dv} \right) dv \\
 &= - \left(v^3 \frac{dJ_0(\alpha_n v)}{dv} \right)_{v=1} + \left(v^3 \frac{dJ_0(\alpha_n v)}{dv} \right)_{v=0} + 2 \int_0^1 v^2 \frac{dJ_0(\alpha_n v)}{dv} dv \\
 &= \alpha_n J_1(\alpha_n) + 2 \left[v^2 J_0(\alpha_n v) \right]_{v=1} - 2 \left[v^2 J_0(\alpha_n v) \right]_{v=0} - 4 \int_0^1 v J_0(\alpha_n v) dv \\
 &= \left(\alpha_n - \frac{4}{\alpha_n} \right) J_1(\alpha_n).
 \end{aligned} \tag{7.9.27}$$

Substituting (7.9.26) and (7.9.27) into (7.9.23), we obtain the desired result,

$$c_n = - \frac{1}{J_1(\alpha_n)} \frac{2}{\alpha_n^3} \frac{\chi + \rho g_x}{\mu} a^2. \tag{7.9.28}$$

Finally, we substitute (7.9.28) into (7.9.17) and then into (7.9.4), and thereby derive the velocity profile

$$u_x(\sigma, t) = \frac{1}{4} \frac{\chi + \rho g_x}{\mu} \left(a^2 - \sigma^2 - 8 a^2 \sum_{n=1}^{\infty} \frac{1}{\alpha_n^3} \frac{J_0(\alpha_n \sigma/a)}{J_1(\alpha_n)} \exp\left(-\alpha_n^2 \frac{\nu t}{a^2}\right) \right). \tag{7.9.29}$$

Program *tube_crc_trans*, located in directory *04_various* of **FDLIB**, not listed in the text, evaluates the velocity described by (7.9.29). A sequence of profiles evolving toward the parabolic profile established at steady state is illustrated in [Figure 7.9.1](#).

7.9.2 Pulsating pressure-driven flow

Next, we consider pulsating flow inside a circular tube of radius a due to an oscillatory pressure gradient, as illustrated in [Figure 7.9.3](#). The axial pressure gradient is given by

$$\frac{\partial p}{\partial x} = \rho g_x - \zeta \sin(\Omega t), \tag{7.9.30}$$

where ζ is the amplitude of the pressure gradient and Ω is the angular frequency of the oscillations. The streamwise velocity component satisfies the differential equation

$$\rho \frac{\partial u_x}{\partial t} = \zeta \sin(\Omega t) + \mu \left(\frac{\partial^2 u_x}{\partial \sigma^2} + \frac{1}{\sigma} \frac{\partial u_x}{\partial \sigma} \right). \tag{7.9.31}$$

The no-slip boundary condition requires that the velocity is zero at the tube surface, that is, $u_x(\sigma = a) = 0$.

Working as in Section 7.8.3 for pulsating channel flow, we express the velocity in the form

$$u_x(\sigma, t) = \frac{\zeta}{\rho \Omega} \left[f_R(\sigma) \cos(\Omega t) + f_I(\sigma) \sin(\Omega t) \right] \tag{7.9.32}$$

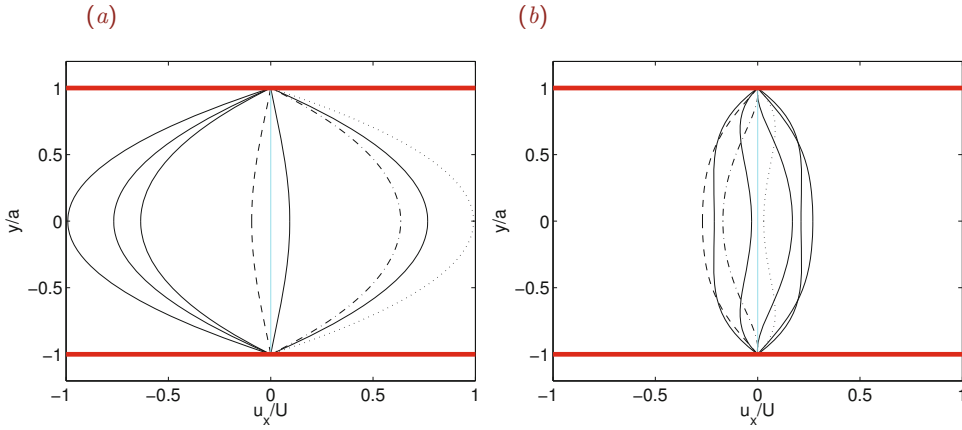


Figure 7.9.3 Velocity profiles of oscillatory pressure-driven flow in a circular tube at phase angles $\Omega t/\pi = 0$ (dashed lines), 0.25 (dash-dotted lines), 0.50 (dotted lines), 0.75, 1.0, 1.25, 1.50, 1.75, and 2.0, for Womersley number (a) $Wo = 1$ and (b) 6.

and introduce the complex function

$$f(\sigma) \equiv f_R(\sigma) + i f_I(\sigma), \tag{7.9.33}$$

where i is the imaginary unit, $i^2 = -1$. The velocity u_x is given by the real part of the complex function

$$w(\sigma, t) = \frac{\zeta}{\rho\Omega} f(y) e^{-i\Omega t}, \tag{7.9.34}$$

satisfying the governing equation

$$\rho \frac{\partial w}{\partial t} = i\zeta e^{-i\Omega t} + \mu \left(\frac{\partial^2 w}{\partial \sigma^2} + \frac{1}{\sigma} \frac{\partial w}{\partial \sigma} \right). \tag{7.9.35}$$

The real part of this complex equation is the real equation (7.9.31).

Substituting expression (7.9.34) into (7.9.35), and simplifying, we obtain an ordinary differential equation,

$$\frac{d^2 f}{d\sigma^2} + \frac{1}{\sigma} \frac{df}{d\sigma} = -\frac{i\Omega}{\nu} (f + 1). \tag{7.9.36}$$

The no-slip boundary condition at the wall requires that $f(a) = 0$. The solution is

$$f(\sigma) = \frac{J_0^*(\sigma\sqrt{-i\Omega/\nu})}{J_0^*(a\sqrt{-i\Omega/\nu})} - 1, \tag{7.9.37}$$

where $J_0(z)$ a Bessel function of the first kind and an asterisk denotes the complex conjugate. If β is a real positive number, then

$$J_0(\beta\sqrt{-i}) = J_0(\beta e^{3\pi i/4}) = \text{ber}_0(\beta) + i \text{bei}_0(\beta), \tag{7.9.38}$$

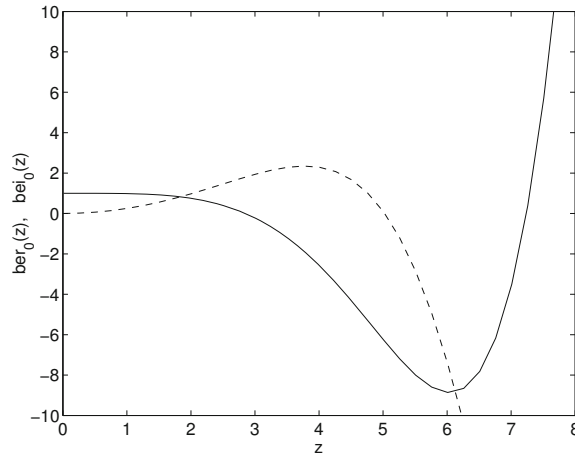


Figure 7.9.4 Graphs of the Kelvin functions $\text{ber}_0(z)$ and $\text{bei}_0(z)$ plotted, respectively, with the solid and broken line, arising in the computation of pulsating tube flow.

where ber_0 , bei_i are the zeroth-order Kelvin functions displayed in Figure 7.9.4. In terms of these functions,

$$f(\sigma) = \frac{\text{ber}_0(\sigma\sqrt{\Omega/\nu}) - i\text{bei}_0(\sigma\sqrt{\Omega/\nu})}{\text{ber}_0(a\sqrt{\Omega/\nu}) - i\text{bei}_0(a\sqrt{\Omega/\nu})} - 1. \quad (7.9.39)$$

Program *ber-bei_0*, located in directory *99_spec_fnc* inside directory *01_num_meth* of **FDLIB**, not listed in the text, evaluates the Kelvin functions using algebraic approximations.

In terms of the Stokes boundary-layer thickness, $\delta = (2\nu/\Omega)^{1/2}$, the velocity profile can be expressed in the compact form

$$u_x(\sigma, t) = \frac{\zeta}{\rho\Omega} \text{Real}\left\{ \left(\frac{J_0^*[-(1-i)\hat{\sigma}]}{J_0^*[-(1-i)\hat{a}]} - 1 \right) \exp(-i\Omega t) \right\}, \quad (7.9.40)$$

where $\hat{\sigma} = \sigma/\delta$ is the scaled radial position and $\hat{a} = a/\delta$.

Small frequencies

For small values of their arguments, the Kelvin functions behave as

$$\text{ber}_0(\beta) = 1 - \frac{1}{64}\beta^4 + \dots, \quad \text{bei}_0(\beta) = \frac{1}{4}\beta^2 - \frac{1}{2304}\beta^6 + \dots, \quad (7.9.41)$$

yielding

$$f(\sigma) \simeq \frac{1 - \frac{1}{4}i\sigma^2\Omega/\nu}{1 - \frac{1}{4}ia^2\Omega/\nu} - 1 \simeq \left(1 - i\frac{1}{4}\sigma^2\frac{\Omega}{\nu}\right) \left(1 + i\frac{1}{4}a^2\frac{\Omega}{\nu}\right) - 1 \quad (7.9.42)$$

and then

$$f(\sigma) \simeq i \frac{1}{4} (a^2 - \sigma^2) \frac{\Omega}{\nu}. \quad (7.9.43)$$

Substituting $f_R = 0$ and $f_I = \frac{1}{4} (a^2 - \sigma^2) \frac{\Omega}{\nu}$ into (7.9.32), we recover the quasi-steady parabolic profile of Hagen–Poiseuille flow,

$$u_x(\sigma, t) = \frac{\zeta}{4\mu} \sin(\Omega t) (a^2 - \sigma^2) + \dots. \quad (7.9.44)$$

Womersley number

The functional form of the arguments of the Bessel functions on the right-hand side of (7.9.37) suggests that the structure of the flow is determined by a scaled angular frequency expressed by the Womersley number

$$\text{Wo} \equiv a \sqrt{\frac{\Omega}{\nu}}, \quad (7.9.45)$$

which is the counterpart of the Womersley number for channel flow defined in (7.8.18).

Program `tube_crc_wom`, located in directory `04_various` of `FDLIB`, not listed in the text, evaluates the velocity profile using the expressions derived in this section. Profiles at two frequencies are shown in [Figure 7.9.3](#).

At low frequencies, the flow is nearly quasi-steady, which means that velocity profile is nearly parabolic. At high frequencies, the flow consists of a central core that oscillates in a plug-flow mode and a Stokes boundary layer attached to the cylindrical wall. As in the case of channel flow, the amplitude of the velocity at the edge of the boundary layer may exceed that in the central core.

7.9.3 Transient circular Couette flow

The azimuthal velocity component of an unsteady swirling flow with circular streamlines, u_φ , satisfies a linear partial differential equation,

$$\frac{\partial u_\varphi}{\partial t} = \nu \left(\frac{\partial^2 u_\varphi}{\partial \sigma^2} + \frac{1}{\sigma} \frac{\partial u_\varphi}{\partial \sigma} - \frac{u_\varphi}{\sigma^2} \right), \quad (7.9.46)$$

where $\nu \equiv \mu/\rho$ is the kinematic viscosity of the fluid.

Consider transient flow inside a hollow circular cylinder with inner radius a that is filled with a fluid. At the origin of time, the cylinder starts rotating suddenly around its axis with constant angular velocity, Ω . Working as in the case of axial flow, we derive the transient velocity profile

$$u_\varphi(\sigma, t) = \Omega \left(\sigma + 2a \sum_{n=1}^{\infty} \frac{1}{\alpha_n} \frac{J_1(\alpha_n \sigma/a)}{J_0(\alpha_n)} \exp(-\alpha_n^2 \frac{\nu t}{a^2}) \right), \quad (7.9.47)$$

where α_n are the positive zeros of the first-order Bessel function, J_1 . At long times, the summed terms on the right-hand side of (7.9.47) vanish, leaving behind a velocity profile that expresses rigid-body rotation.

Program *tube_crc_sw_trans*, located in directory *04_various* of **FDLIB**, not listed in the text, evaluates the velocity profile described by equation (7.9.47).

7.9.4 Orthogonality of Bessel functions

We have seen that Bessel functions are encountered in the computation of flow in an axisymmetric domain. In concluding this section, we state an orthogonality property that is useful in evaluating the coefficients of Bessel expansions; an example is shown in (7.9.16).

By definition, the p th-order Bessel function of the first kind, $J_p(z)$, satisfies the Bessel equation

$$z \frac{d}{dz} \left(z \frac{dJ_p(z)}{dz} \right) + (z^2 - p^2) J_p(z) = 0, \quad (7.9.48)$$

and is required to be finite at every value of z between, and including, zero and infinity. Expanding the derivative, we find that the Bessel equation can be restated as

$$z^2 \frac{d^2 J_p(z)}{dz^2} + z \frac{dJ_p(z)}{dz} + (z^2 - p^2) J_p(z) = 0. \quad (7.9.49)$$

The particular cases $p = 0$ and 1 are shown in equations (7.9.12) and (7.9.20).

The orthogonality property of the Bessel functions states that, if α_n and α_m are two zeros of $J_p(z)$, then

$$2 \int_0^1 z J_p(\alpha_n z) J_p(\alpha_m z) dz = \begin{cases} J_{p+1}^2(\alpha_n) = J_{p-1}^2(\alpha_n) = J_p'^2(\alpha_n) & \text{if } n = m, \\ 0 & \text{if } n \neq m. \end{cases} \quad (7.9.50)$$

The orthogonality property of the Bessel functions is analogous to the Fourier orthogonality property of trigonometric functions, as shown, for example, in equations (7.5.49).

PROBLEMS

7.9.1 Pulsating pressure-driven flow


Derive the velocity profile described by equations (7.9.32)–(7.9.37).

7.9.2 Transient circular Couette flow

Derive the velocity profile given in equation (7.9.47).

7.9.3 *Transient swirling flow*

Consider transient flow outside a circular cylinder of radius a immersed in an infinite liquid. At the origin of time, the cylinder starts rotating suddenly around its axis with constant angular velocity, Ω . Derive the transient velocity profile.

7.9.4  *Transient circular Couette flow*

Compute and plot profiles of the transient circular Couette flow at a sequence of times. Discuss the effect of truncation of the infinite sum on the right-hand side of (7.9.47).

Finite-difference methods

- 8.1 Choice of governing equations**
- 8.2 Unidirectional flow; velocity/pressure formulation**
- 8.3 Unidirectional flow; velocity/vorticity formulation**
- 8.4 Unidirectional flow; stream function/vorticity formulation**
- 8.5 Two-dimensional flow; stream function/vorticity formulation**
- 8.6 Velocity/pressure formulation**
- 8.7 Operator splitting and solenoidal projection**
- 8.8 Staggered grids**

In previous chapters, we have discussed the equations governing the structure of a steady flow and the evolution of an unsteady flow, and derived selected solutions for elementary flow configurations by analytical and simple numerical methods. To generate solutions for arbitrary flow conditions and boundary geometries, it is necessary to develop general-purpose numerical methods. In this chapter, we discuss the choice of governing equations whose solution is to be found, and the implementation of finite-difference methods for incompressible Newtonian flow. The discourse will reveal a set of conceptual and practical challenges encountered in the broader context of computational fluid dynamics (CFD).

8.1 Choice of governing equations

General-purpose methods for computing the flow of an incompressible Newtonian fluid can be classified into two categories distinguished by the choice of governing equations.

In the first class of methods, the flow is described in terms of primary variables, including the velocity and the pressure. The structure of the velocity and pressure fields in a steady flow, and the evolution of the velocity and pressure fields in an unsteady flow are computed by solving the Navier–Stokes equation and the continuity equation, subject to appropriate boundary conditions, initial conditions, and possibly supplemental constraints.

In the second class of methods, the flow is computed based on the vorticity transport equation. The numerical procedure involves two stages: first, the structure or evolution of the vorticity field is computed based on the vorticity transport equation discussed in Section 6.6; second, the simultaneous structure or evolution of the velocity field is obtained

by inverting the equation defining the vorticity as the curl of the velocity,

$$\boldsymbol{\omega} = \nabla \times \mathbf{u}, \quad (8.1.1)$$

subject to constraints imposed by the continuity equation and boundary conditions. Inverting (8.1.1) involves solving for \mathbf{u} in terms of $\boldsymbol{\omega}$. Descendant methods are distinguished by the particular procedure used to recover the velocity field from a specified vorticity distribution.

The strengths and weaknesses of the aforementioned two classes of methods will become apparent as we describe their implementation. One appealing feature of the second class of methods based on the vorticity transport equation is the lack of need to solve for the pressure. Bypassing the computation of the pressure is desirable when boundary conditions for the pressure are not directly available but must be derived from the governing equations. Disadvantages include the need to derive boundary conditions for the vorticity.

PROBLEM

8.1.1 Inversion of the vorticity

Show that, if \mathbf{u} is a solenoidal velocity field corresponding to a certain vorticity field $\boldsymbol{\omega}$, that is, $\nabla \cdot \mathbf{u} = 0$, then the velocity field

$$\mathbf{v} = \mathbf{u} + \nabla f \quad (8.1.2)$$

corresponds to the same vorticity field, where f is an arbitrary smooth scalar function. Explain why, for the velocity field \mathbf{v} to remain solenoidal, $\nabla \cdot \mathbf{v} = 0$, the function f must be harmonic, that is, it must satisfy Laplace's equation, $\nabla^2 f = 0$.

8.2 Unidirectional flow; velocity/pressure formulation

We begin developing finite-difference methods by discussing the velocity/pressure formulation for unidirectional flow in a channel confined between two parallel walls located at $y = 0$ and $y = h$, as illustrated in [Figure 8.2.1](#). The lower and upper walls translate parallel to themselves along the x axis with generally time-dependent velocities, $V_1(t)$ and $V_2(t)$.

In practice, channel flow occurs under two complementary conditions reflecting the physical mechanism driving the flow, as follows:

- In the first case, the flow rate along the channel $Q(t)$ is prescribed and the streamwise pressure gradient $\partial p(t)/\partial x$ is computed as part of the solution.
- In the second case, the pressure gradient is specified, and the flow rate is computed as part of the solution.

In this section and in [Section 8.3](#) we consider the case of flow driven to a specified and possibly time-dependent pressure gradient. In [Section 8.4](#), we consider the complementary case of flow subject to a specified flow rate.

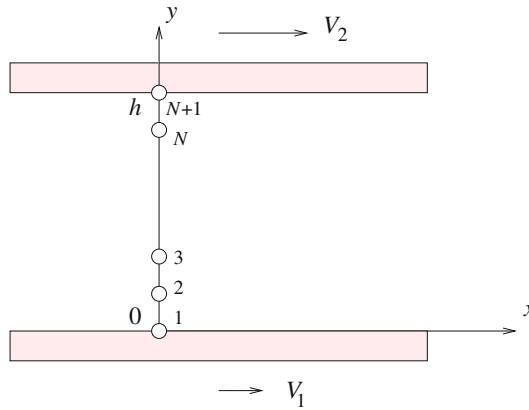


Figure 8.2.1 A one-dimensional finite-difference grid is used to compute the velocity profile in unidirectional channel flow.

8.2.1 Governing equations

To set up the mathematical formulation, we consider the x component of the equation of motion. In the case of unidirectional flow, we obtain the simplified form

$$\frac{\partial u_x}{\partial t} = -\frac{1}{\rho} \frac{\partial p}{\partial x} + \nu \frac{\partial^2 u_x}{\partial y^2} + g_x, \quad (8.2.1)$$

where ρ is the fluid density, ν is the kinematic viscosity, and g_x is the x component of the acceleration of gravity. The partial differential equation (8.2.1) is to be solved subject to a specified initial condition and to the possibly time-dependent velocity boundary conditions

$$u_x(y=0) = V_1(t), \quad u_x(y=h) = V_2(t), \quad (8.2.2)$$

enforcing no-slip at the walls.

8.2.2 Explicit finite-difference method

To implement the finite-difference method, we divide the cross-section of the channel extending over $0 \leq y \leq h$ into N intervals defined by $N+1$ grid points, as shown in [Figure 8.2.1](#). For convenience, the x component of the velocity at the i grid point is denoted as

$$u_i(t) \equiv u_x(y_i, t). \quad (8.2.3)$$

Next, we evaluate both sides of (8.2.1) at the i th interior grid point at time t for $i = 2, \dots, N$, and approximate the time derivative on the left-hand side with a first-order forward finite difference and the second derivative on the right-hand side with a second-order centered finite difference. The result is a finite-difference equation (FDE),

$$\frac{u_i(t + \Delta t) - u_i(t)}{\Delta t} = -\frac{1}{\rho} \frac{\partial p}{\partial x}(t) + \nu \frac{u_{i-1}(t) - 2u_i(t) + u_{i+1}(t)}{\Delta y^2} + g_x. \quad (8.2.4)$$

Solving for $u_i(t + \Delta t)$ on the left-hand side, we obtain

$$u_i(t + \Delta t) = \alpha u_{i-1}(t) + (1 - 2\alpha) u_i(t) + \alpha u_{i+1}(t) + \Delta t \left(-\frac{1}{\rho} \frac{\partial p}{\partial x}(t) + g_x \right) \quad (8.2.5)$$

for $i = 2, \dots, N$. We have introduced the dimensionless ratio

$$\alpha \equiv \frac{\nu \Delta t}{\Delta y^2}, \quad (8.2.6)$$

called the *numerical diffusion number*.

Equation (8.2.5) allows us to update the velocity at the interior grid points explicitly, starting from the specified initial condition, subject to the prescribed boundary conditions

$$u_1(t) = V_1(t), \quad u_{N+1}(t) = V_2(t). \quad (8.2.7)$$

The following MATLAB code entitled *channel_ftcs*, located in directory *channel* inside directory *11_fdm* of **FDLIB**, performs the animation of the evolving velocity profile:

```
%----
% parameters
%----

h = 1.0;
mu = 0.6; rho = 0.5;
N = 32;
dpx = -2.0; gx = 0.4;
V1 = 0.0; V2 = 0.0;
al = 0.51;      % alpha
nstep = 20000;  % number of steps

%---
% prepare
%---

nu = mu/rho;    % kinematic viscosity
Dy = h/N;
Dt = al*Dy*Dy/nu;

%---
% grid and initial condition
%---

for i=1:N+1
    y(i) = (i-1)*Dy;
    u(i) = 0;
end
u(1) = V1;
u(N+1) = V2;
```

```

t = 0.0;

%---
% time stepping
%---

for step=1:nstep

    t = t + Dt;

    unew(1) = V1;
    for i=2:N
        unew(i) = al*u(i-1) + (1-2*al)*u(i) + al*u(i+1) ...
            + Dt*(-dpdx/rho+gx);
    end
    unew(N+1) = V2;
    u = unew;

    if(step==1)
        Handle1 = plot(u,y,'o-');
        set(Handle1, 'erasemode', 'xor');
        set(gca,'fontsize',15)
        axis([0 0.5 0 h])
        xlabel('u','fontsize',15)
        ylabel('y','fontsize',15)
    else
        set(Handle1,'XData',u,'YData',y);
        pause(0.02)
        drawnow
    end

end      % of time stepping

```

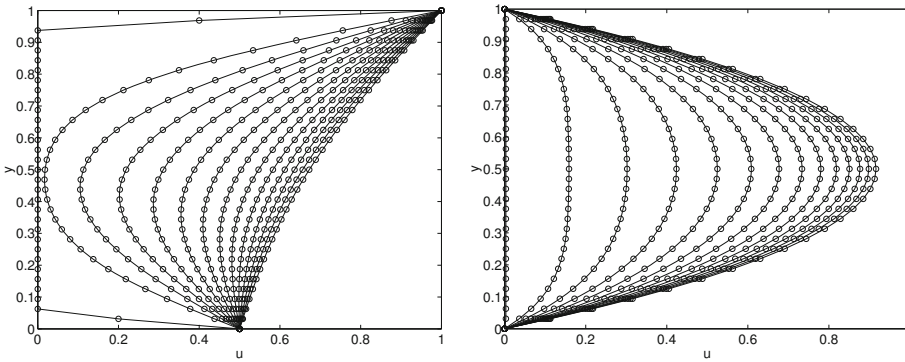
Evolving profiles are shown in [Figure 8.2.2](#) for two values of the dimensionless numerical parameter α .

Numerical stability

Numerical experimentation reveals, and theoretical analysis confirms, that the explicit method of updating the velocity based on equation (8.2.5) is free of oscillations only when the time step, Δt , is small enough so that the dimensionless numerical diffusion number α defined in (8.2.6) is less than $\frac{1}{2}$.¹ For larger time steps, the velocity profile develops unphysical growing numerical oscillations unrelated to the physics of the motion, as illustrated in [Figure 8.2.2\(b\)](#) for $\alpha = 0.51$. We say that the explicit finite-difference method is *conditionally stable*.

¹Pozrikidis, C. (2008) *Numerical Computation in Science and Engineering*. Second Edition, Oxford University Press.

(a)



(b)

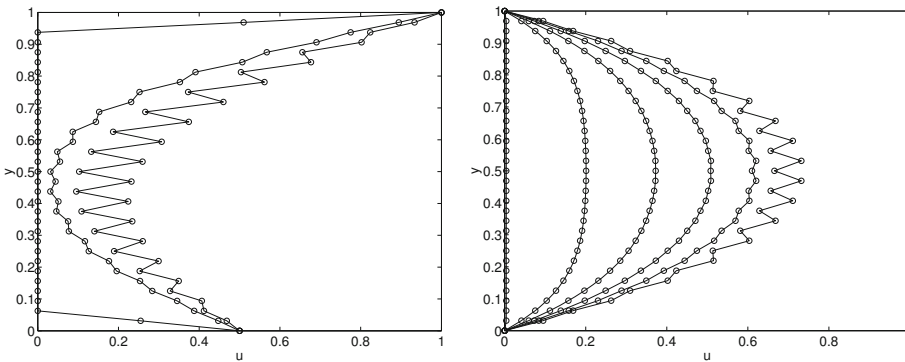


Figure 8.2.2 Evolving profiles of unidirectional flow in a channel computed by an explicit finite-difference method for numerical diffusion number (a) $\alpha = 0.40$ and (b) 0.51 . The scary oscillations in the second case are a manifestation of numerical instability.

8.2.3 Implicit finite-difference method

To avoid the restriction on the time step for numerical stability, we implement an *implicit* finite-difference method. Evaluating equation (8.2.1) at the i th interior grid point at time $t + \Delta t$ for $i = 2, \dots, N$, and then approximating the time derivative on the left-hand side with a first-order backward finite difference and the second derivative on the right-hand side with a second-order centered finite difference, we obtain the difference equation

$$\frac{u_i(t + \Delta t) - u_i(t)}{\Delta t} = -\frac{1}{\rho} \frac{\partial p}{\partial x}(t + \Delta t) + \nu \frac{u_{i+1}(t + \Delta t) - 2u_i(t + \Delta t) + u_{i-1}(t + \Delta t)}{\Delta y^2} + g_x. \quad (8.2.8)$$

Rearranging, we obtain

$$\begin{aligned} -\alpha u_{i-1}(t + \Delta t) + (1 + 2\alpha) u_i(t + \Delta t) - \alpha u_{i+1}(t + \Delta t) \\ = u_i(t) - \frac{\Delta t}{\rho} \frac{\partial p}{\partial x}(t + \Delta t) + \Delta t g_x, \end{aligned} \quad (8.2.9)$$

where α is the numerical diffusion number defined in (8.2.6), $\alpha \equiv \nu \Delta t / \Delta y^2$.

Equation (8.2.9) allows us to compute the velocity at the interior grid points at the time level $t + \Delta t$ in an implicit fashion, which means that we solve simultaneously for all unknown grid values, subject to the prescribed boundary conditions ,

$$u_1(t + \Delta t) = V_1(t + \Delta t), \quad u_{N+1}(t + \Delta t) = V_2(t + \Delta t). \quad (8.2.10)$$

To formalize the implicit solution algorithm, we write equation (8.2.9) for $i = 2, \dots, N$ and enforce the boundary conditions to obtain a system of $N - 1$ linear equations for the velocity at the $N - 1$ interior grid points at time $t + \Delta t$,

$$\mathbf{A} \cdot \mathbf{u}(t + \Delta t) = \mathbf{u}(t) + \mathbf{b}. \quad (8.2.11)$$

We have introduced the tridiagonal coefficient matrix

$$\mathbf{A} = \begin{bmatrix} 1 + 2\alpha & -\alpha & 0 & \cdots & 0 & 0 & 0 \\ -\alpha & 1 + 2\alpha & -\alpha & \cdots & 0 & 0 & 0 \\ 0 & -\alpha & 1 + 2\alpha & \cdots & 0 & 0 & 0 \\ \vdots & \vdots & \vdots & \ddots & \vdots & \vdots & \vdots \\ 0 & 0 & 0 & \cdots & 1 + 2\alpha & -\alpha & 0 \\ 0 & 0 & 0 & \cdots & -\alpha & 1 + 2\alpha & -\alpha \\ 0 & 0 & 0 & \cdots & 0 & -\alpha & 1 + 2\alpha \end{bmatrix}, \quad (8.2.12)$$

the vector of unknown velocities

$$\mathbf{u}(t + \Delta t) = \begin{bmatrix} u_2(t + \Delta t) \\ u_3(t + \Delta t) \\ \vdots \\ u_{N-1}(t + \Delta t) \\ u_N(t + \Delta t) \end{bmatrix}, \quad (8.2.13)$$

and the known vectors

$$\mathbf{u}(t) = \begin{bmatrix} u_2(t) \\ u_3(t) \\ \vdots \\ u_{N-1}(t) \\ u_N(t) \end{bmatrix}, \quad \mathbf{b} = \begin{bmatrix} -\frac{\Delta t}{\rho} \frac{\partial p}{\partial x}(t + \Delta t) + \Delta t g_x + \alpha V_1(t + \Delta t) \\ -\frac{\Delta t}{\rho} \frac{\partial p}{\partial x}(t + \Delta t) + \Delta t g_x \\ \vdots \\ -\frac{\Delta t}{\rho} \frac{\partial p}{\partial x}(t + \Delta t) + \Delta t g_x \\ -\frac{\Delta t}{\rho} \frac{\partial p}{\partial x}(t + \Delta t) + \Delta t g_x + \alpha V_2(t + \Delta t) \end{bmatrix}. \quad (8.2.14)$$

The numerical method involves solving the linear system (8.2.11) at the current time instant, t , to obtain the velocity profile at the next time instant, $t + \Delta t$, beginning from a specified initial state. The tridiagonal structure of the matrix \mathbf{A} displayed in (8.2.12) allows us to compute the solution efficiently using the legendary Thomas algorithm discussed in Section 8.2.4.

Finite-difference code

The following MATLAB code entitled *channel_btcs*, located in directory *channel* inside directory *11_fdm* of **FDLIB**, performs the time integration using the implicit method starting from a specified initial velocity profile:

```
%-----
% parameters
%-----

h = 1.0; mu = 0.6; rho = 0.5; N = 32; dpdx = -2.0;
gx = 0.4;
V1 = 0.1; V2 = -0.5;
alpha = 0.40;      % alpha
nstep = 20000;    % number of steps
nu = mu/rho;
Dy = h/N
Dt = alpha*Dy*Dy/nu;

%---
% grid and initial condition
%---

for i=1:N+1
    y(i) = (i-1)*Dy;
    u(i) = 0.0;
end
u(1) = V1;
u(N+1) = V2;

%---
% formulate the tridiagonal projection matrix
% atr is the diagonal line of the coefficient matrix
% btr is the superdiagonal line of the coefficient matrix
% ctr is the subdiagonal line of the coefficient matrix
%---

for i=1:N-1
    atr(i) = 1.0 + 2*alpha;
    btr(i) = -alpha;
    ctr(i) = -alpha;
end
```

```

%---
% time stepping
%---

t=0.0;

for step=1:nstep

    for i=1:N-1    % right-hand side
        s(i) = u(i+1) + Dt*(-dpdx/rho+gx);
    end

    t = t + Dt;
    u(1) = V1;
    u(N+1) = V2;
    s(1) = s(1) + alpha*u(1);
    s(N-1) = s(N-1) + alpha*u(N+1);

    sol = thomas(N-1,atr,btr,ctr,s);

    for i=2:N
        u(i) = sol(i-1);
    end

    if(step==1)
        Handle1 = plot(u,y,'o-');
        set(Handle1, 'erasemode', 'xor');
        set(gca,'fontsize',15)
        axis([min(V1,V2) max(V1,V2)+2.0 0 h])
        xlabel('u','fontsize',15)
        ylabel('y','fontsize',15)
    else
        set(Handle1,'XData',u,'YData',y);
        pause(0.2)
        drawnow
    end

end    % of time stepping

```

The code calls the function *thomas* discussed in Section 8.2.4 to solve a tridiagonal system of equations.

Numerical stability

Numerical experimentation reveals, and theoretical analysis confirms, that the implicit method of updating the velocity based on equation (8.2.11) is free of numerical oscillations irrespective of the size of the time step, Δt . Accordingly, the implicit finite-difference method is an unconditionally stable and thus highly desirable method.

8.2.4 Thomas algorithm

To formalize Thomas' algorithm in general terms, we consider a linear system of K equations in K unknowns,

$$\mathbf{D} \cdot \mathbf{x} = \mathbf{s}, \quad (8.2.15)$$

for an unknown vector, \mathbf{x} , where \mathbf{s} is a given vector. The $K \times K$ coefficient matrix, \mathbf{D} , is assumed to have the tridiagonal form

$$\mathbf{D} = \begin{bmatrix} a_1 & b_1 & 0 & \cdots & 0 & 0 & 0 \\ c_2 & a_2 & b_2 & \cdots & 0 & 0 & 0 \\ 0 & c_3 & a_3 & \cdots & 0 & 0 & 0 \\ \vdots & \vdots & \vdots & \ddots & \vdots & \vdots & \vdots \\ 0 & 0 & 0 & \cdots & a_{K-2} & b_{K-2} & 0 \\ 0 & 0 & 0 & \cdots & c_{K-1} & a_{K-1} & b_{K-1} \\ 0 & 0 & 0 & \cdots & 0 & c_K & a_K \end{bmatrix}. \quad (8.2.16)$$

Note that only the diagonal, superdiagonal, and subdiagonal elements of \mathbf{D} are nonzero. Thomas's algorithm proceeds in two stages.

In the first stage, the tridiagonal system (8.2.15) is transformed into an upper bidiagonal system,

$$\mathbf{D}' \cdot \mathbf{x} = \mathbf{y}, \quad (8.2.17)$$

involving an upper bidiagonal coefficient matrix with *ones* along the diagonal,

$$\mathbf{D}' = \begin{bmatrix} 1 & d_1 & 0 & \cdots & 0 & 0 & 0 \\ 0 & 1 & d_2 & \cdots & 0 & 0 & 0 \\ 0 & 0 & 1 & \cdots & 0 & 0 & 0 \\ \vdots & \vdots & \vdots & \ddots & \vdots & \vdots & \vdots \\ 0 & 0 & 0 & \cdots & 1 & d_{K-2} & 0 \\ 0 & 0 & 0 & \cdots & 0 & 1 & d_{K-1} \\ 0 & 0 & 0 & \cdots & 0 & 0 & 1 \end{bmatrix}, \quad (8.2.18)$$

where \mathbf{y} is an intermediate solution vector.

In the second stage, the upper bidiagonal system (8.2.17) is solved by backward substitution, which involves solving the last equation for the last unknown, $x_K = y_K$, and then moving upward to compute the rest of the unknowns in a sequential fashion.

The combined algorithm, shown in [Table 8.2.1](#), is implemented in the following MATLAB function:

Reduction to bidiagonal :

$$\begin{bmatrix} d_1 \\ y_1 \end{bmatrix} = \frac{1}{a_1} \begin{bmatrix} b_1 \\ s_1 \end{bmatrix}$$

Do $i = 1, K - 1$

$$\begin{bmatrix} d_{i+1} \\ y_{i+1} \end{bmatrix} = \frac{1}{a_{i+1} - c_{i+1}d_i} \begin{bmatrix} b_{i+1} \\ s_{i+1} - c_{i+1}y_i \end{bmatrix}$$

End Do

Backward substitution :

$$x_K = y_K$$

Do $i = K - 1, 1$ (step = -1)

$$x_i = y_i - d_i x_{i+1}$$

End Do

Table 8.2.1 Thomas algorithm for solving a system of K linear equations with a tridiagonal coefficient matrix.

```
function x = thomas (n,a,b,c,s)

%=====
% Thomas algorithm for a tridiagonal system
%
% n: system size
% a,b,c: diagonal, superdiagonal,
%       and subdiagonal elements
% s: right-hand side
%=====

%-----
% reduction to upper bidiagonal
%-----

d(1) = b(1)/a(1);
y(1) = s(1)/a(1);

for i=1:n-2
    i1 = i+1;
    den = a(i1)-c(i1)*d(i);
    d(i1) = b(i1)/den;
    y(i1) = (s(i1)-c(i1)*y(i))/den;
```

```

end

den = a(n)-c(n)*d(n-1);
y(n) = (rhs(n)-c(n)*y(n-1))/den;

%-----
% back substitution
%-----

x(n) = y(n);

for i=n-1:-1:1
    x(i) = y(i)-d(i)*x(i+1);
end

%-----
% done
%-----

return;

```

In fact, the Thomas algorithm is a special implementation of the inclusive method of Gauss elimination discussed in Section 3.4.1 for a general system of linear equations. The key idea is to bypass idle multiplications by zeros.

8.2.5 Steady state

To obtain the velocity profile of channel flow at steady state, we return to equation (8.2.11) and set

$$\mathbf{u}(t + \Delta t) = \mathbf{u}(t) = \mathbf{u} \quad (8.2.19)$$

to obtain

$$(\mathbf{A} - \mathbf{I}) \cdot \mathbf{u} = \mathbf{b}, \quad (8.2.20)$$

where \mathbf{I} is the unit matrix. Dividing the individual equations encapsulated in (8.2.20) by α , we obtain the simpler form

$$\mathbf{C} \cdot \mathbf{u} = \mathbf{d}, \quad (8.2.21)$$

involving the tridiagonal coefficient matrix

$$\mathbf{C} = \begin{bmatrix} 2 & -1 & 0 & \cdots & 0 & 0 & 0 \\ -1 & 2 & -1 & \cdots & 0 & 0 & 0 \\ 0 & -1 & 2 & \cdots & 0 & 0 & 0 \\ \vdots & \vdots & \vdots & \ddots & \vdots & \vdots & \vdots \\ 0 & 0 & 0 & \cdots & 2 & -1 & 0 \\ 0 & 0 & 0 & \cdots & -1 & 2 & -1 \\ 0 & 0 & 0 & \cdots & 0 & -1 & 2 \end{bmatrix}, \quad (8.2.22)$$

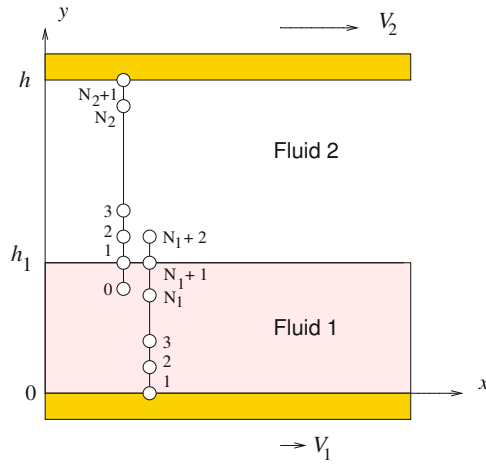


Figure 8.2.2 Illustration of a composite finite-difference grid with phantom nodes on either side an interface used to compute the velocity profile of unidirectional two-fluid channel flow. The interface is located at $y = h_1$.

the vector of unknown velocities at steady state

$$\mathbf{u} = \begin{bmatrix} u_2 \\ u_3 \\ \vdots \\ u_{N-1} \\ u_N \end{bmatrix}, \tag{8.2.23}$$

and the known vector

$$\mathbf{d} = \begin{bmatrix} -\frac{1}{\mu} \frac{\partial p}{\partial x} + \frac{\Delta y^2}{\nu} g_x + V_1 \\ -\frac{1}{\mu} \frac{\partial p}{\partial x} + \frac{\Delta x^2}{\nu} g_x \\ \vdots \\ -\frac{1}{\mu} \frac{\partial p}{\partial x} + \frac{\Delta y^2}{\nu} g_x \\ -\frac{1}{\mu} \frac{\partial p}{\partial x} + \frac{\Delta y^2}{\nu} g_x + V_2 \end{bmatrix}. \tag{8.2.24}$$

To compute the velocity profile at steady state, we simply solve the system of linear algebraic equations (8.2.21) using a numerical method.

8.2.6 Two-layer flow

Next, we consider the flow of two superimposed layers in a channel, as illustrated in [Figure 8.2.2](#). The lower layer is labeled 1 and the upper layer is labeled 2. The fluids are separated

by a flat interface located at $y = h_1$, where $h_1 < h$ is the lower-layer thickness and h is the channel width. The upper-layer thickness is $h_2 = h - h_1$.

Interfacial conditions

At the interface, we require three conditions: continuity of velocity, continuity of shear stress, and continuity of normal stress. To satisfy the third condition, we require that the streamwise pressure gradient, $\partial p / \partial x$, is the same inside both layers. Continuity of velocity at the interface requires that

$$u_x^{(1)}(y = h_1) = u_x^{(2)}(y = h_1) \quad (8.2.25)$$

and continuity of shear stress requires that

$$\mu_1 \left(\frac{\partial u_x^{(1)}}{\partial y} \right)_{y=h_1} = \mu_2 \left(\frac{\partial u_x^{(2)}}{\partial y} \right)_{y=h_1}. \quad (8.2.26)$$

where $u_x^{(1)}$ is the lower-layer velocity and $u_x^{(2)}$ is the upper-layer velocity. Using the equation of motion (8.2.1), we find that, if (8.2.25) is true at the initial instant, it will also be true at any time provided that

$$-\frac{1}{\rho_1} \frac{\partial p}{\partial x} + \nu_1 \left(\frac{\partial^2 u_x^{(1)}}{\partial y^2} \right)_{y=h_1} = -\frac{1}{\rho_2} \frac{\partial p}{\partial x} + \nu_2 \left(\frac{\partial^2 u_x^{(2)}}{\partial y^2} \right)_{y=h_1}, \quad (8.2.27)$$

where the second partial derivative are evaluated at the interface.

Finite-difference implementation

We begin developing the finite-difference method by dividing the lower layer into N_1 evenly spaced intervals defined by $N_1 + 1$ grid points, $y_i^{(1)}$ for $i = 1, \dots, N_1 + 1$, and the upper layer into N_2 evenly spaced intervals defined by $N_2 + 1$ grid points, $y_i^{(2)}$ for $i = 1, \dots, N_2 + 1$, as shown in [Figure 8.2.2](#).

For reasons that will become apparent, we also extend the domain of definition of each layer into the adjacent layer by one artificial grid point labeled $N_1 + 2$ for the lower layer or 0 for the upper layer.

To simplify the notation, we denote

$$u_i^{(1)} \equiv u_x^{(1)}(y_i^{(1)}), \quad u_i^{(2)} \equiv u_x^{(2)}(y_i^{(2)}). \quad (8.2.28)$$

Approximating the derivatives in (8.2.26) and (8.2.27) with centered finite differences, we derive two equations relating the values of the velocity at the extended nodes, $u_{N_1+2}^{(1)}$ and $u_0^{(2)}$,

$$\mu_1 \frac{u_{N_1+2}^{(1)} - u_{N_1}^{(1)}}{2\Delta y_1} = \mu_2 \frac{u_2^{(2)} - u_0^{(2)}}{2\Delta y_2} \quad (8.2.29)$$

and

$$-\frac{1}{\rho_1} \frac{\partial p}{\partial x} + \nu_1 \frac{u_{N_1+2}^{(1)} - 2u_{N_1+1}^{(1)} + u_{N_1}^{(1)}}{\Delta y_1^2} = -\frac{1}{\rho_2} \frac{\partial p}{\partial x} + \nu_2 \frac{u_2^{(2)} - 2u_1^{(2)} + u_0^{(2)}}{\Delta y_2^2}, \quad (8.2.30)$$

where $\Delta y_1 \equiv h_1/N_1$ and $\Delta y_2 \equiv h_2/N_2$ are the grid spacings. Setting $u_{N_1+1}^{(1)} = u_1^{(2)}$ and introducing the ratios

$$\lambda \equiv \frac{\mu_2}{\mu_1}, \quad \delta \equiv \frac{\rho_2}{\rho_1}, \quad \gamma \equiv \frac{\nu_2}{\nu_1} = \frac{\lambda}{\delta}, \quad \beta \equiv \frac{\Delta y_2}{\Delta y_1}, \quad (8.2.31)$$

we recast equations (8.2.29) and (8.2.30) into a system of two linear equations for the velocity at the extended nodes,

$$\beta u_{N_1+2}^{(1)} + \lambda u_0^{(2)} = \beta u_{N_1}^{(1)} + \lambda u_2^{(2)} \quad (8.2.32)$$

and

$$\beta^2 u_{N_1+2}^{(1)} - \gamma u_0^{(2)} = 2(\beta^2 - \gamma) u_{N_1+1}^{(1)} - \beta^2 u_{N_1}^{(1)} + \gamma u_2^{(2)} + \frac{\Delta y_2^2}{\mu_1} \left(1 - \frac{1}{\delta}\right) \frac{\partial p}{\partial x}. \quad (8.2.33)$$

In matrix notation,

$$\begin{bmatrix} \beta & \lambda \\ -\beta^2 & \gamma \end{bmatrix} \cdot \begin{bmatrix} u_{N_1+2}^{(1)} \\ u_0^{(2)} \end{bmatrix} = \begin{bmatrix} \beta u_{N_1}^{(1)} + \lambda u_2^{(2)}, \\ -2(\beta^2 - \gamma) u_{N_1+1}^{(1)} + \beta^2 u_{N_1}^{(1)} - \gamma u_2^{(2)} - \frac{\Delta y_2^2}{\mu_1} \left(1 - \frac{1}{\delta}\right) \frac{\partial p}{\partial x} \end{bmatrix}. \quad (8.2.34)$$

Solving for the velocity at the lower extended node, we find that

$$u_{N_1+2}^{(1)} = a_1 u_{N_1}^{(1)} + a_2 u_{N_1+1}^{(1)} + a_3 u_2^{(2)} + a_4 \frac{\partial p}{\partial x}, \quad (8.2.35)$$

where

$$\begin{aligned} a_1 &= \frac{\gamma - \beta\lambda}{\gamma + \beta\lambda}, & a_2 &= 2\lambda \frac{\beta^2 - \gamma}{\beta(\gamma + \beta\lambda)}, \\ a_3 &= \frac{2\gamma\lambda}{\beta(\gamma + \beta\lambda)}, & a_4 &= \frac{\lambda}{\beta(\gamma + \beta\lambda)} \frac{\Delta y_2^2}{\mu_1} \left(1 - \frac{1}{\delta}\right) \end{aligned} \quad (8.2.36)$$

are four constants.

When the physical properties of the layers are matched, $\lambda = \gamma = \delta = 1$, and the lower and upper grid sizes are equal, $\beta = 1$, then $u_{N_1+2}^{(1)} = u_2^{(2)}$ by equation (8.2.35), and $u_0^{(2)} = u_{N_1}^{(1)}$ by equation (8.2.32), as required.

Explicit time integration

Working as in the case of single-fluid flow, we derive the explicit finite-difference equation

$$u_i^{(1)}(t + \Delta t) = \alpha_1 u_{i+1}^{(1)}(t) + (1 - 2\alpha_1) u_i^{(1)}(t) + \alpha_1 u_{i-1}^{(1)}(t) - \Delta t \left(-\frac{1}{\rho_1} \frac{\partial p}{\partial x}(t) + g_x \right) \quad (8.2.37)$$

for the lower layer, and a corresponding equation for the upper layer,

$$u_i^{(2)}(t + \Delta t) = \alpha_2 u_{i+1}^{(2)}(t) + (1 - 2\alpha_2) u_i^{(2)}(t) + \alpha_2 u_{i-1}^{(2)}(t) - \Delta t \left(-\frac{1}{\rho_2} \frac{\partial p}{\partial x}(t) + g_x \right), \quad (8.2.38)$$

where

$$\alpha_1 \equiv \frac{\nu_1 \Delta t}{\Delta y_1^2}, \quad \alpha_2 \equiv \frac{\nu_2 \Delta t}{\Delta y_2^2} \quad (8.2.39)$$

are the numerical diffusion numbers for the lower and upper layer. The numerical procedure involves the following steps:

1. Initialize the nodal velocities.
2. Compute the velocity at the lower extended node, $u_{N_1+2}^{(1)}$, from equation (8.2.35).
3. Use equation (8.2.38) to update the velocity at the grid points in the lower layer for $i = 2, \dots, N_1 + 1$.
4. Set $u_1^{(2)} = u_{N_1+1}^{(1)}$.
5. Use equation (8.2.39) to update the velocity at the internal grid nodes in the upper layer for $i = 2, \dots, N_2$.
6. Use the boundary conditions to update the velocity at the lower and upper walls.
7. Return to Step 2 and repeat the computation for another step.

The method is implemented in the following MATLAB code entitled *two_layers*, located in directory *channel* inside directory *11_fdm* of **FDLIB**, performing the animation of the developing velocity profile:

```
%---
% parameters
%---

h = 1.0; h1 = 0.25;
N1 = 4; N2 = 32;
mu1 = 1.0; mu2 = 2.0;
rho1 = 1.5; rho2 = 1.0;
dpx = -1.0; gx = 0.2;
```

```

alpha = 0.4;

%---
% prepare
%---

h2 = h-h1;
Dy1 = h1/N1;
Dy2 = h2/N2;

lambda = mu2/mu1;
delta = rho2/rho1;
gamma = lambda/delta;
beta = Dy2/Dy1;

tmp = gamma+beta*lambda;
a1 = (gamma-beta*lambda)/tmp;
a2 = 2*lambda*(beta*beta-gamma)/(beta*tmp);
a3 = 2*gamma*lambda/(beta*tmp);
a4 = lambda*Dy2*Dy2*(1-1/delta)/(beta*mu1*tmp);

Dt1 = rho1*alpha*Dy1*Dy1/mu1;
Dt2 = rho2*alpha*Dy2*Dy2/mu2;

Dt = min(Dt1,Dt2)

a11 = Dt*mu1/(Dy1*Dy1*rho1);
a12 = Dt*mu2/(Dy2*Dy2*rho2);

%---
% initialize and define the grid
%---

for i=1:N1+1
    u1(i) = 0.0;
    y1(i) = (i-1)*Dy1;
end

for i=1:N2+1
    u2(i) = 0.0;
    y2(i) = (i-1)*Dy2+h1;
end

%---
% time stepping
%---

for step=1:1000

```

```

u1(N1+2) = a1*u1(N1)+a2*u1(N1+1)+a3*u2(2)+a4*dpx;

unew1(1) = V1;

for i=2:N1+1
    unew1(i) = a11*u1(i+1)+(1-2*a11)*u1(i)+a11*u1(i-1)...
        +Dt*(-dpx/rho1+gx);
end

unew2(1) = unew1(N1+1);

for i=2:N2
    unew2(i) = a12*u2(i+1)+(1-2*a12)*u2(i)+a12*u2(i-1)...
        +Dt*(-dpx/rho2+gx);
end

unew2(N2+1) = V2;

u1 = unew1; u2 = unew2;

%---
% animation
%---

if(step==1)
    handle1 = plot(u1,y1,'o-',u2,y2,'o-');
    set(gca,'fontsize',15)
    axis([0 0.1 0 h])
    xlabel('u','fontsize',15)
    ylabel('y','fontsize',15)
else
    set(handle1,'XData',[u1, u2],'YData',[y1, y2],'Marker','o')
    drawnow
    pause(0.01)
end

%---
end      % of time stepping
%---

```

Snapshots of an evolving profile are shown in [Figure 8.2.3](#) for two values of α defined as the minimum of α_1 and α_2 .

PROBLEMS

8.2.1 Steady state

Derive the system (8.2.20) departing from the explicit finite-difference formula (8.2.4).

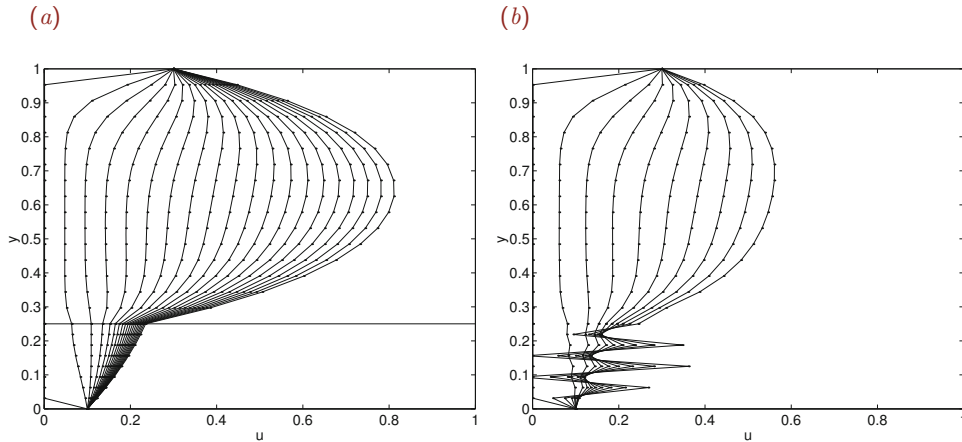


Figure 8.2.3 Evolving profiles of two-layer flow in a channel, computed by an explicit finite difference method for (a) $\alpha = 0.4$ and (b) 0.52 , where α is the minimum of α_1 and α_2 . A numerical instability arises in the second case.

8.2.2 Two-layer channel flow

Derive a system of finite-difference equations governing the velocity profile of a two-layer channel flow at steady state.

8.2.3 Flow in a circular tube

Develop an explicit finite-difference method based on the velocity/pressure formulation for computing the velocity profile developing inside a tube with circular cross-section due to a suddenly imposed constant pressure gradient.

8.2.4 Thomas algorithm

Use the MATLAB function *thomas* listed in the text to solve a system of equations of your choice. Verify the accuracy of the solution by confirming that it satisfies the tested system of equations.

8.2.5 Single-fluid channel flow

(a) Write a code that computes the evolution of the velocity profile in a channel with stationary walls due to a sinusoidal pressure gradient based on the explicit finite-difference method discussed in the text. Run the program for fluid properties and flow conditions of your choice, and for several time step sizes, Δt , corresponding to numerical diffusion number α that is larger and lower than 0.5 . Discuss the performance of the numerical method.

(b) Repeat (a) for the implicit finite-difference method discussed in the text.

8.2.6 Two-layer channel flow

Develop an implicit finite-difference method for computing the evolution of a two-layer flow. Implement the method in a program that computes the evolution of the velocity profile in a

channel with stationary walls due to the sudden application of a constant pressure gradient. Run the program for fluid properties and flow conditions of your choice and for several time step sizes. Discuss the performance of the numerical method.

8.3 Unidirectional flow; velocity/vorticity formulation

The vorticity transport equation for unsteady unidirectional flow along the x axis reduces to the unsteady diffusion equation for the z component of the vorticity, ω_z ,

$$\frac{\partial \omega_z}{\partial t} = \nu \frac{\partial^2 \omega_z}{\partial y^2}, \quad (8.3.1)$$

where ν is the kinematic viscosity of the fluid. Invoking the definition of the vorticity, $\boldsymbol{\omega} = \nabla \times \mathbf{u}$, we find that

$$\omega_z = -\frac{\partial u_x}{\partial y}. \quad (8.3.2)$$

Integrating equation (8.3.2) with respect to y from the lower wall up to an arbitrary point, we obtain an integral representation for the velocity in terms of the vorticity,

$$u_x(y) = V_1 - \int_0^y \omega_z(y') \, dy'. \quad (8.3.3)$$

Without loss of generality, we have chosen to satisfy the boundary condition at the lower wall located at $y = 0$, requiring that $u_x(0) = V_1$. It remains to ensure that the no-slip boundary condition is also satisfied at the upper wall.

The numerical method involves computing the evolution of the vorticity profile from a specified initial state using (8.3.1), while simultaneously recovering the evolution of the velocity field based on equation (8.3.2) or its integrated version shown in (8.3.3). Since the velocity does not appear in equation (8.3.1), the two steps are decoupled.

8.3.1 Boundary conditions for the vorticity

Because the unsteady diffusion equation (8.3.1) is a second-order differential equation with respect to y , two boundary conditions for the vorticity are required, one at each end of the solution domain located at $y = 0$ and h . The boundary conditions must be such that the integral constraint

$$\int_0^h \omega_z(\eta) \, d\eta = V_1 - V_2 \quad (8.3.4)$$

is satisfied so that the right-hand side of (8.3.3) is consistent with the upper-wall no-slip boundary condition $u_x(y = h) = V_2$, and either the flow rate through the channel has a prescribed value, $Q(t)$, or the streamwise pressure gradient has a prescribed value $\partial p(t)/\partial x$.

Concentrating on flow subject to a specified pressure gradient, we recast the x component of the equation of motion for unidirectional flow,

$$\frac{\partial u_x}{\partial t} = -\frac{1}{\rho} \frac{\partial p}{\partial x} + \nu \frac{\partial^2 u_x}{\partial y^2} + g_x, \quad (8.3.5)$$

into the form

$$\frac{\partial u_x}{\partial t} = -\frac{1}{\rho} \frac{\partial p}{\partial x} - \nu \frac{\partial \omega_z}{\partial y} + g_x. \quad (8.3.6)$$

Evaluating (8.3.6) at the lower and upper walls and rearranging, we obtain boundary conditions for the slope of the vorticity,

$$\left(\frac{\partial \omega_z}{\partial y} \right)_{y=0} = -\frac{1}{\nu} \frac{dV_1}{dt} - \frac{1}{\mu} \frac{\partial p}{\partial x} + \frac{1}{\nu} g_x \quad (8.3.7)$$

and

$$\left(\frac{\partial \omega_z}{\partial y} \right)_{y=h} = -\frac{1}{\nu} \frac{dV_2}{dt} - \frac{1}{\mu} \frac{\partial p}{\partial x} + \frac{1}{\nu} g_x. \quad (8.3.8)$$

These equations provide us with Neumann boundary conditions at either end of the solution domain.

Special attention must be paid to the case of impulsive motion. If a wall is set in motion suddenly in an impulsive fashion with the velocity changing from one value to another over an infinitesimal period of time, the corresponding time derivative on the right-hand side of one or both of equations (8.3.7) and (8.3.8) develops an infinite spike described by the Dirac delta function discussed in Chapter 11. This singular behavior is too demanding to be handled by the numerical method.

Next, we investigate whether the vorticity boundary conditions (8.3.7) and (8.3.8) ensure the satisfaction of the integral constraint (8.3.4), which is necessary for the satisfaction of the no-slip boundary condition at the upper wall. Integrating (8.3.1) with respect to y across the channel height, from 0 to h , interchanging the order of the integration and time differentiation on the left-hand side, and using (8.3.7) to simplify the right-hand side, we obtain

$$\frac{d}{dt} \int_0^h \omega_z(y') dy' = \frac{d}{dt} (V_1 - V_2). \quad (8.3.9)$$

Time-integration of (8.3.9) reproduces (8.3.4) up to a time-independent constant determined by the initial state. Thus, if (8.3.4) is satisfied at the initial instant, it will also be satisfied at any subsequent time.

8.3.2 Alternative set of equations

In an alternative approach, we take the derivative of (8.3.2) with respect to y to derive the second-order equation,

$$\frac{\partial^2 u_x}{\partial y^2} = -\frac{\partial \omega_z}{\partial y} \equiv -q, \quad (8.3.10)$$

where $q \equiv \partial\omega_z/\partial y$ is the slope of the vorticity. To compute the velocity, we integrate the second-order equation (8.3.10) with respect to y using the velocity boundary conditions $u_x(y=0) = V_1$ and $u_x(y=h) = V_2$.

The important benefit stemming from using (8.3.10) instead of (8.3.2), is that, in order to compute the velocity, the slope of the vorticity q , instead of the vorticity itself, is required. An evolution equation for q arises by differentiating both sides of (8.3.1) with respect to y , finding that

$$\frac{\partial q}{\partial t} = \nu \frac{\partial^2 q}{\partial y^2}. \quad (8.3.11)$$

Boundary conditions are provided by equations (8.3.7) and (8.3.8).

In summary, the numerical procedure involves integrating in time equation (8.3.11) from an initial state subject to the derived boundary conditions (8.3.7) and (8.3.8), while simultaneously computing the velocity profile by solving the second-order equation (8.3.10) subject to the velocity boundary conditions, $u_x(y=0) = V_1$ and $u_x(y=h) = V_2$.

Explicit finite-difference method

To implement a finite-difference method, we divide the flow domain $0 \leq y \leq h$ into N intervals separated by $N + 1$ grid points, as shown in [Figure 8.2.1](#), and evaluate equation (8.3.11) at time t at the interior nodes for $i = 2, \dots, N$.

Approximating the time derivative on the left-hand side with a first-order finite difference and the y derivative on the left-hand side with a second-order finite difference, we obtain

$$\frac{q_i(t + \Delta t) - q_i(t)}{\Delta t} = \nu \frac{q_{i-1}(t) - 2q_i(t) + q_{i+1}(t)}{\Delta y^2}, \quad (8.3.12)$$

where we have defined

$$q_i \equiv q(y_i). \quad (8.3.13)$$

Solving for $q_i(t + \Delta t)$ on the left-hand side, we obtain

$$q_i(t + \Delta t) = \alpha q_{i-1}(t) + (1 - 2\alpha) q_i(t) + \alpha q_{i+1}(t), \quad (8.3.14)$$

where $\alpha \equiv \nu \Delta t / \Delta y^2$ is the numerical diffusion number. Equation (8.3.14) allows us to update explicitly the values of q at the grid points subject to boundary conditions for q_1 and q_{N+1} given by the right-hand sides of equations (8.3.7) and (8.3.8).

The centered-difference discretization of equation (8.3.10) leads us to the linear system (8.2.21), where the coefficient matrix \mathbf{C} is given in (8.2.22) and the constant vector on the

right-hand side is given by

$$\mathbf{d} = \begin{bmatrix} \Delta y^2 q_2 + V_1 \\ \Delta y^2 q_3 \\ \vdots \\ \Delta y^2 q_{N-1} \\ \Delta y^2 q_N + V_2 \end{bmatrix}. \quad (8.3.15)$$

The linear system can be solved efficiently using the Thomas algorithm.

8.3.3 Comparison with the velocity/pressure formulation

Comparing the velocity/vorticity formulation with the velocity/pressure formulation discussed in Section 8.2, we find that the latter is significantly simpler in conception and implementation. While this is undoubtedly true in the case of unidirectional flow presently considered, the vorticity-velocity formulation is more competitive in the more general case of two- and three-dimensional flow.

PROBLEMS

8.3.1 Steady flow

Discuss the implementation of the velocity/vorticity formulation for steady channel flow due to a specified pressure gradient.

8.3.2 Two-layer flow

Develop a velocity/vorticity formulation for two-layer channel flow discussed in Section 8.2.

8.3.3 Flow in a circular tube

Develop an explicit method based on the velocity/vorticity formulation for computing the velocity profile developing inside a circular tube due to a suddenly imposed constant pressure gradient.

8.3.4 Explicit finite-difference method

Write a code that computes the evolution of the velocity profile in a channel with stationary walls due to the sudden application of a constant pressure gradient based on the explicit finite-difference method discussed in the text. Run the program for fluid properties and flow conditions of your choice and several time step sizes corresponding to numerical diffusion number α that is higher or lower than the critical threshold, 0.5. Discuss the performance of the numerical method.

8.4 Unidirectional flow; stream function/vorticity formulation

In Sections 8.2 and 8.3, we discussed methods of computing the evolution of the velocity profile in channel flow subject to a specified pressure gradient. In this section, we consider

the complementary case of flow subject to a specified flow rate and develop a numerical method based on the velocity/vorticity formulation.

For reasons that will become apparent, we introduce the stream function, ψ , satisfying the equation

$$u_x = \frac{\partial \psi}{\partial y}. \quad (8.4.1)$$

In the case of unidirectional flow, u_x , and thus ψ , is a function of position, y , and time, t . The flow rate across a line that begins and ends at two parallel planes located at $y = y_1$ and y_2 is equal to the difference in the corresponding values of the stream function, $Q_{12} = \psi(y_2) - \psi(y_1)$. The flow rate through the entire channel height is $Q = \psi(y = h) - \psi(y = 0)$.

Using equation (8.3.2), we find that the nonzero vorticity component is related to the stream function by the equation

$$\omega_z = -\frac{\partial^2 \psi}{\partial y^2}. \quad (8.4.2)$$

The numerical method involves computing the evolution of the vorticity profile from a specified initial state using the vorticity transport equation (8.3.1), while simultaneously recovering the evolution of the stream function using the one-dimensional Poisson equation (8.4.2). Since the differential equations (8.3.1) and (8.4.2) are of second order with respect to y , two boundary conditions for the vorticity and two boundary conditions for the stream function are required, one at each end of the solution domain, $y = 0$ and h .

Since adding an arbitrary constant to the stream function does not affect the velocity, the base level of the stream function can be specified at will. Accordingly, we may stipulate that $\psi(y = 0) = 0$, finding

$$\psi(y = h) = Q(t). \quad (8.4.3)$$

It is now evident that, by introducing the stream function, we have facilitated the implementation of the condition on the flow rate.

8.4.1 Boundary conditions for the vorticity

The boundary conditions for the vorticity must involve the specified wall velocities, V_1 and V_2 , by way of the no-slip boundary condition. To illustrate the implementation of this condition, we divide the flow domain, $0 \leq y \leq h$, into N intervals defined by $N + 1$ grid points, as shown in [Figure 8.2.1](#), and evaluate (8.4.2) at time t at the boundary nodes corresponding to $i = 1$ and $N + 1$. To simplify the notation, we denote

$$\omega_i \equiv \omega_z(y_i), \quad \psi_i \equiv \psi(y_i). \quad (8.4.4)$$

Approximating the y derivative on the right-hand side with a combination of finite differences, we obtain

$$\omega_1 = -\frac{\left(\frac{\partial \psi}{\partial y}\right)_{\frac{1}{2}(y_1+y_2)} - \left(\frac{\partial \psi}{\partial y}\right)_{y_1}}{\frac{1}{2} \Delta y} = -2 \frac{\frac{\psi_2 - \psi_1}{\Delta y} - V_1}{\Delta y} \quad (8.4.5)$$

or

$$\omega_1 = 2 \frac{\psi_1 - \psi_2}{\Delta y^2} + 2 \frac{V_1}{\Delta y}, \quad (8.4.6)$$

and

$$\omega_{N+1} = -\frac{\left(\frac{\partial\psi}{\partial y}\right)_{y_{N+1}} - \left(\frac{\partial\psi}{\partial y}\right)_{\frac{1}{2}(y_N+y_{N+1})}}{\frac{1}{2}\Delta y} = -2 \frac{V_2 - \frac{\psi_{N+1} - \psi_N}{\Delta y}}{\Delta y} \quad (8.4.7)$$

or

$$\omega_{N+1} = 2 \frac{\psi_{N+1} - \psi_N}{\Delta y^2} - 2 \frac{V_2}{\Delta y}. \quad (8.4.8)$$

It is somewhat distressing to realize that the no-slip condition is implemented indirectly in terms of the vorticity. Specifically, it is not clear that solving (8.4.2) for the stream function and subsequently differentiating it to recover the velocity generates a velocity profile that is consistent with the prescribed boundary velocity. However, a thorough analysis of the numerical method reveals that this is the case indeed, except under unusual circumstances associated with singular boundary conditions involving discontinuous functions.

8.4.2 A semi-implicit method

Proceeding with the finite-difference implementation, we apply equation (8.3.1) at the interior nodes corresponding to $i = 2, \dots, N$ at time t . Approximating the time derivative on the left-hand side with a first-order finite difference and the y derivative on the right-hand side with a second-order second finite difference, we obtain

$$\frac{\omega_i(t + \Delta t) - \omega_i(t)}{\Delta t} = \nu \frac{\omega_{i-1}(t) - 2\omega_i(t) + \omega_{i+1}(t)}{\Delta y^2}. \quad (8.4.9)$$

Solving for $\omega_i(t + \Delta t)$, we obtain

$$\omega_i(t + \Delta t) = \alpha \omega_{i+1}(t) + (1 - 2\alpha) \omega_i(t) + \alpha \omega_{i-1}(t), \quad (8.4.10)$$

where $\alpha \equiv \nu \Delta t / \Delta y^2$ is the numerical diffusion number. Equation (8.4.10) allows us to explicitly update the values of the vorticity at the interior grid points, subject to boundary conditions for ω_1 and ω_{N+1} given by the right-hand sides of (8.4.6) and (8.4.8); the stream function at time t is assumed to be known.

The implicit discretization of equation (8.4.2) leads us to a linear system,

$$\mathbf{C} \cdot \boldsymbol{\psi}(t + \Delta t) = \mathbf{d}(t + \Delta t), \quad (8.4.11)$$

where the coefficient matrix \mathbf{C} is given in (8.2.22), the vector $\boldsymbol{\psi}$ is defined as

$$\boldsymbol{\psi} = \begin{bmatrix} \psi_2 \\ \psi_3 \\ \vdots \\ \psi_{N-1} \\ \psi_N \end{bmatrix}, \quad (8.4.12)$$

and the vector on the right-hand side of (8.4.11) is given by

$$\mathbf{d} = \begin{bmatrix} \Delta y^2 \omega_2 \\ \Delta y^2 \omega_3 \\ \vdots \\ \Delta y^2 \omega_{N-1} \\ \Delta y^2 \omega_N + Q \end{bmatrix}. \quad (8.4.13)$$

The system (8.4.11) can be solved efficiently using the Thomas algorithm.

The numerical method involves the following steps:

1. Assign initial values to the stream function and vorticity at all nodes.
2. Compute the vorticity at the boundary nodes using equations (8.4.6) and (8.4.8).
3. Update the vorticity at the internal nodes using equation (8.4.10).
4. Update the stream function at the interior nodes by solving the linear system (8.4.11) for a known right-hand side.
5. Return to Step 2 and repeat the calculation for another step.

The velocity profile arises by numerically differentiating the stream function with respect to y .

PROBLEMS

8.4.1 Steady flow

Develop a finite-difference method based on the stream function/vorticity formulation for computing the velocity profile of steady channel flow subject to a specified flow rate.

8.4.2 Two-layer flow

Develop a finite-difference method based on the stream function/vorticity formulation for unsteady two-layer channel flow discussed in Section 8.2.

8.4.3 Flow inside a circular tube

Develop a finite-difference method based on the stream function/vorticity formulation for computing the velocity profile developing inside a circular tube, subject to a specified flow rate.

8.4.4 Explicit finite-difference method

Write a code that computes the evolution of the velocity profile in a channel with stationary walls using an explicit finite-difference method. The flow rate increases gradually toward a steady value according to the equation

$$Q(t) = Q_0 \left(1 - \exp\left(-\beta \frac{\nu t}{h^2}\right) \right), \quad (8.4.14)$$

where Q_0 is the constant flow rate prevailing of long times, α and β is a dimensionless constant. Run the program for fluid properties and flow conditions of your choice and for several sizes of the time step corresponding to α higher or lower than 0.5. Discuss the performance of the numerical method.

8.5 Two-dimensional flow; stream function/vorticity formulation

Having discussed finite-difference methods for unidirectional flow, now we turn our attention to the more general case of two-dimensional flow where further issues concerning the satisfaction of the continuity equation and choice of boundary conditions are encountered. In this section we discuss the stream function/vorticity formulation as an extension of the corresponding formulation for unidirectional flow discussed in Section 8.4.

Hello world

Texts on computer language programming introduce elementary programming procedures traditionally by explaining the structure of a program entitled *world*, which prints the important message *Hello World*. Texts on computational fluid dynamics (CFD) explain numerical methods by discussing the prototypical example of flow in a two-dimensional cavity driven by a moving lid, known as the *driven-cavity flow*. We will follow this time-honored tradition.

8.5.1 Flow in a cavity

Consider flow in a cavity driven by a lid that translates parallel to itself with a generally time-dependent velocity, $V(t)$, as illustrated in [Figure 8.5.1](#).

We begin developing the stream function/vorticity formulation by introducing the stream function, ψ , defined from the differential relations

$$u_x = \frac{\partial \psi}{\partial y}, \quad u_y = -\frac{\partial \psi}{\partial x}, \quad (8.5.1)$$

where u_x and u_y are the x and y velocity components. The no-penetration boundary condition requires that the component of the velocity normal to each of the four walls is zero. In terms of the stream function,

$$\psi = 0 \quad \text{over all walls}, \quad (8.5.2)$$

so that the tangential derivative of the stream function, which is equal to the normal component of the velocity, is also zero. The zero on the right-hand side of (8.5.2) could have been replaced by an arbitrary constant without consequences on the numerical solution or physical structure of the flow.

The no-slip boundary condition requires that the tangential component of the velocity is zero at the bottom, left, and right walls, and equal to $V(t)$ at the upper wall. In terms of

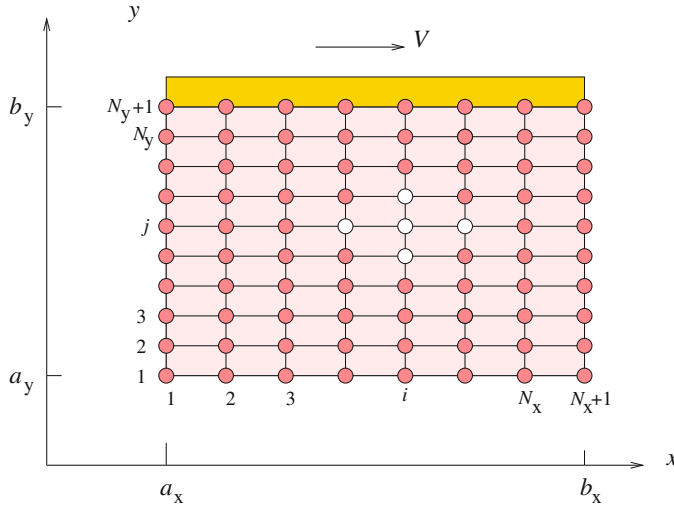


Figure 8.5.1 Illustration of a finite-difference grid used to compute flow in a cavity driven by a sliding lid.

the stream function,

$$\begin{aligned} \frac{\partial \psi}{\partial y} = 0 \quad \text{at the bottom,} \qquad \frac{\partial \psi}{\partial x} = 0 \quad \text{at the sides,} \\ \frac{\partial \psi}{\partial y} = V(t) \quad \text{at the top.} \end{aligned} \tag{8.5.3}$$

Enforcing the boundary conditions for the velocity, we derive simplified expressions for the boundary values of the only non-vanishing vorticity component in terms of the stream function,

$$\omega_z \equiv -\frac{\partial u_x}{\partial y} + \frac{\partial u_y}{\partial x}. \tag{8.5.4}$$

For example, recalling that $u_y = 0$, and thus $\partial u_y / \partial x = 0$, over the bottom wall, we find that

$$\omega_z = -\frac{\partial u_x}{\partial y} = -\frac{\partial^2 \psi}{\partial y^2}. \tag{8.5.5}$$

Working in this fashion, we find that

$$\omega_z = -\frac{\partial^2 \psi}{\partial y^2} \quad \text{at the top and bottom} \tag{8.5.6}$$

and

$$\omega_z = -\frac{\partial^2 \psi}{\partial x^2} \quad \text{at the sides,} \tag{8.5.7}$$

which are simplified versions of the more general expression for the vorticity in terms of the stream function,

$$\omega_z = -\frac{\partial^2 \psi}{\partial x^2} - \frac{\partial^2 \psi}{\partial y^2}. \quad (8.5.8)$$

8.5.2 Finite-difference grid

To prepare the ground for the implementation of the finite-difference method, we cover the rectangular solution domain with a uniform two-dimensional Cartesian grid consisting of $N_x + 1$ uniformly spaced vertical lines and $N_y + 1$ uniformly spaced horizontal lines, as shown in [Figure 8.5.1](#). Parallel grid lines are separated by intervals Δx or Δy , defining the grid size.

The intersections of grid lines define grid points or nodes labeled by a pair of integers, (i, j) for $i = 1, \dots, N_x + 1$ and $j = 1, \dots, N_y + 1$. The vertical side walls correspond to $i = 1$ and $N_x + 1$, and the bottom and top walls correspond to $j = 1$ and $N_y + 1$.

The goal of the finite-difference method is to generate values of flow variables of interest at the grid points. To simplify the notation, we denote

$$\omega_{i,j} \equiv \omega_z(x_i, y_j), \quad \psi_{i,j} \equiv \psi(x_i, y_j). \quad (8.5.9)$$

Similar notation is used for other variables.

8.5.3 Unsteady flow

Following the general protocol of methods based on the vorticity transport equation, we compute the evolution of the flow by advancing the vorticity field using the vorticity transport equation for two-dimensional flow written in the form of an evolution equation for the vorticity,

$$\frac{\partial \omega_z}{\partial t} = -u_x \frac{\partial \omega_z}{\partial x} - u_y \frac{\partial \omega_z}{\partial y} + \nu \left(\frac{\partial^2 \omega_z}{\partial x^2} + \frac{\partial^2 \omega_z}{\partial y^2} \right), \quad (8.5.10)$$

subject to appropriate derived boundary conditions for the vorticity, while simultaneously following the evolution of the stream function by solving the Poisson equation

$$\nabla^2 \psi \equiv \frac{\partial^2 \psi}{\partial x^2} + \frac{\partial^2 \psi}{\partial y^2} = -\omega_z, \quad (8.5.11)$$

subject to specified boundary conditions for the stream function.

A simple method for computing the evolution of the flow when the lid starts translating suddenly involves the following steps:

1. At the initial instant, we set the stream function and velocity at all interior and boundary grid nodes to zero. Then we set the x component of the velocity at the grid nodes along the lid equal to $V(t = 0)$.

2. At the second step, we differentiate the velocity to obtain the vorticity using the definition $\omega_z \equiv -\partial u_x/\partial y + \partial u_y/\partial x$.

For the interior grid points, we use centered differences to obtain

$$\omega_{i,j} = -\frac{(u_x)_{i,j+1} - (u_x)_{i,j-1}}{2\Delta y} + \frac{(u_y)_{i+1,j} - (u_y)_{i-1,j}}{2\Delta x}. \quad (8.5.12)$$

For the top wall, we use backward differences to obtain

$$\omega_{i,N_y+1} \simeq -\left(\frac{\partial u_x}{\partial y}\right)_{i,N_y+1} \simeq \frac{-3V + 4(u_x)_{i,N_y} - (u_x)_{i,N_y-1}}{2\Delta y}, \quad (8.5.13)$$

involving values at interior grid points.

For the rest of the walls, we use forward or backward differences to obtain

$$\omega_{i,1} \simeq -\left(\frac{\partial u_x}{\partial y}\right)_{i,1} \simeq \frac{-4(u_x)_{i,2} + (u_x)_{i,3}}{2\Delta y} \quad (8.5.14)$$

for the bottom wall,

$$\omega_{1,j} \simeq \left(\frac{\partial u_y}{\partial x}\right)_{1,j} \simeq \frac{4(u_y)_{2,j} - (u_y)_{3,j}}{2\Delta x} \quad (8.5.15)$$

for the left wall, and

$$\omega_{N_x+1,j} \simeq \left(\frac{\partial u_y}{\partial x}\right)_{N_x+1,j} \simeq \frac{-4(u_y)_{N_x,j} + (u_y)_{N_x-1,j}}{2\Delta x} \quad (8.5.16)$$

for the right wall.

3. Now we integrate in time equation (8.5.10) to obtain the vorticity at the interior grid points at time $t + \Delta t$. Using a fully explicit method, we set

$$\omega_{i,j}(t + \Delta t) = \omega_{i,j}(t) + G_{(i,j)}(t), \quad (8.5.17)$$

where $G_{(i,j)}(t)$ is the right-hand side of (8.5.10) evaluated at the (i, j) grid point at time t .

To evaluate $G_{(i,j)}(t)$, we approximate the first spatial derivatives and the Laplacian of the vorticity using centered differences. For example, the Laplacian of the vorticity can be approximated with the finite-difference formula shown in equation (3.3.15), written for ω_z .

4. Next, we solve the Poisson equation (8.5.11) for the stream function, subject to the boundary condition $\psi = 0$, using a slightly generalized version of the finite-difference method for Laplace's equation discussed in Section 3.3.

Approximating the second derivatives with centered differences, we obtain the counterpart of equation (3.3.16),

$$\psi_{i+1,j} - 2(1 + \beta)\psi_{i,j} + \psi_{i-1,j} + \beta\psi_{i,j+1} + \beta\psi_{i,j-1} = -\Delta x^2 \omega_{i,j}, \quad (8.5.18)$$

where $\beta \equiv (\Delta x/\Delta y)^2$.

5. Finally, we differentiate the stream function to compute the velocity components at time $t + \Delta t$ at the interior grid points.

Having completed one time step, we return to Step 2 and repeat the computation for another time step.

8.5.4 Steady flow

To compute the steady flow, we follow a somewhat different approach. In this case, the left-hand side of (8.5.10) vanishes, yielding a differential relation between the velocity and the vorticity. Solving for the Laplacian of the vorticity, we obtain a Poisson equation for the vorticity forced by the *a priori* unknown source function on the right-hand side,

$$\frac{\partial^2 \omega_z}{\partial x^2} + \frac{\partial^2 \omega_z}{\partial y^2} = \frac{1}{\nu} \left(u_x \frac{\partial \omega_z}{\partial x} + u_y \frac{\partial \omega_z}{\partial y} \right). \quad (8.5.19)$$

Computing the flow in terms of the stream function and vorticity involves simultaneously solving equations (8.5.11) and (8.5.19) according to the following steps:

1. Guess the distribution of the stream function and associated vorticity distribution.
2. Solve the Poisson equation (8.5.11) for the stream function, ψ

$$\nabla^2 \psi \equiv \frac{\partial^2 \psi}{\partial x^2} + \frac{\partial^2 \psi}{\partial y^2} = -\omega_z, \quad (8.5.20)$$

subject to the no-penetration boundary condition, $\psi = 0$.

3. Compute the right-hand side of (8.5.19).
4. Derive boundary conditions for the vorticity using the stream function obtained in Step 2.
5. Solve the Poisson equation (8.5.19) for the vorticity.
6. Check whether the vorticity computed in Step 5 agrees with that assigned in Step 1 within a specified tolerance. If not, we replace the latter by the former, return to Step 2, and repeat the calculations for another cycle.

Implementation

The method is implemented according to the following steps:

Step 1

Assign values to the stream function at all $(N_x + 1) \times (N_y + 1)$ interior and boundary grid nodes and to the vorticity at all $N_x \times N_y$ interior grid nodes. A simple choice is to set them all equal to zero.

Step 2

Solve the Poisson equation (8.5.11), subject to the boundary condition $\psi = 0$, using an iterative method. To perform the iterations, we approximate the second derivatives with centered differences and obtain equation (8.5.18), which we express in the form

$$\mathcal{R}_{i,j} \equiv \psi_{i+1,j} - 2(1 + \beta)\psi_{i,j} + \psi_{i-1,j} + \beta\psi_{i,j+1} + \beta\psi_{i,j-1} + \Delta x^2 \omega_{i,j} = 0, \quad (8.5.21)$$

where $\mathcal{R}_{i,j}$ is a residual. The iterative method involves computing a time-like sequence of grid values parametrized by an index, ℓ , using the formula

$$\psi_{i,j}^{(\ell+1)} = \psi_{i,j}^{(\ell)} + \frac{\varrho}{2(1 + \beta)} \mathcal{R}_{i,j}^{(\ell)} \quad (8.5.22)$$

for $l = 1, 2, \dots$, where ϱ is a specified relaxation factor used to control the iterations.

Step 3

Compute the vorticity at the boundary grid nodes taking into consideration the velocity boundary conditions.

Considering grid nodes at the lid, we expand the stream function in a Taylor series with respect to y about a top grid node. Evaluating the expansion at the grid node immediately below, we obtain

$$\psi_{i,N_y} \simeq \psi_{i,N_y+1} - \Delta y \left(\frac{\partial \psi}{\partial y} \right)_{i,N_y+1} + \frac{1}{2} \Delta y^2 \left(\frac{\partial^2 \psi}{\partial y^2} \right)_{i,N_y+1}. \quad (8.5.23)$$

Setting

$$\left(\frac{\partial \psi}{\partial y} \right)_{i,N_y+1} = V, \quad \omega_{i,N_y+1} = - \left(\frac{\partial^2 \psi}{\partial y^2} \right)_{i,N_y+1}, \quad (8.5.24)$$

as discussed in the paragraph following equation (8.5.3), and solving for ω_{i,N_y+1} , we obtain

$$\omega_{i,N_y+1} = 2 \frac{\psi_{i,N_y+1} - \psi_{i,N_y}}{\Delta y^2} - 2 \frac{V}{\Delta y}. \quad (8.5.25)$$

Working in a similar fashion, we derive corresponding expressions for the bottom, left, and right walls,

$$\omega_{i,1} = 2 \frac{\psi_{i,1} - \psi_{i,2}}{\Delta y^2}, \quad \omega_{1,j} = 2 \frac{\psi_{1,j} - \psi_{2,j}}{\Delta y^2}, \quad (8.5.26)$$

and

$$\omega_{N_x+1,j} = 2 \frac{\psi_{N_x+1,j} - \psi_{N_x,j}}{\Delta y^2}. \quad (8.5.27)$$

More accurate expressions can be derived using higher-order expansions.

Step 4

Differentiate the stream function to generate the velocity at the interior grid nodes, subject to the no-penetration condition, $\psi = 0$.

Step 5

Differentiate the vorticity to obtain the x and y derivatives at the interior grid points, subject to boundary values computed in Step 3.

Step 6

Compute the right-hand side of (8.5.19) at the interior grid nodes.

Step 7

Solve equation (8.5.19) by iteration, as discussed in Step 2. The counterparts of equations (8.5.21) and (8.5.22) are

$$\mathcal{R}_{i,j} \equiv \omega_{i+1,j} - 2(1 + \beta)\omega_{i,j} + \omega_{i-1,j} + \beta\omega_{i,j+1} + \beta\omega_{i,j-1} - \Delta x^2 N_{i,j} = 0 \quad (8.5.28)$$

and

$$\omega_{i,j}^{(\ell+1)} = \omega_{i,j}^{(\ell)} + \frac{\rho}{2(1 + \beta)} \mathcal{R}_{i,j}^{(\ell)}, \quad (8.5.29)$$

where $N_{i,j}$ is the right-hand side of (8.5.19) evaluated at the (i,j) grid point, and ρ is a relaxation factor.

The method is implemented in the following MATLAB code entitled *cvt_sv*, located in directory *11_fdm* of *FDLIB*:

```
%=====
% code cvt_sv
%=====

%-----
% parameters
%-----

Vlid = 1.0;    % lid velocity
Lx = 2.0; Ly = 1.0;    % cavity dimensions
```

```

Nx = 32; Ny = 16;      % grid size
visc = 0.01;         % viscosity
rho = 1.0;           % density
relax = 0.5;         % relaxation parameter
Niteri = 5;          % number of inner iterations
Niterg = 100;        % number of global iterations
vort_init = 0.0;     % initial vorticity

%-----
% prepare
%-----

Dx = Lx/Nx; Dy = Ly/Ny;
Dx2 = 2.0*Dx; Dy2 = 2.0*Dy;
Dxs = Dx*Dx;
Dys = Dy*Dy;
beta = Dxs/Dys; beta1 = 2.0*(1.0+beta);
nu = visc/rho;      % kinematic viscosity

%-----
% generate the grid
% initialize stream function and vorticity
%-----

for i=1:Nx+1
  for j=1:Ny+1
    x(i,j) = (i-1.0)*Dx;
    y(i,j) = (j-1.0)*Dy;
    psi(i,j) = 0.0;    % stream function
    vort(i,j) = -vort_init;
  end
end

%-----
% global iterations
%-----

for iter=1:Niterg

  save = vort;

  %-----
  % Jacobi updating of the stream function
  % at the interior nodes
  %-----

  for iteri=1:Niteri
    for j=2:Ny
      for i=2:Nx

```

```

        res = (psi(i+1,j)+psi(i-1,j)+ beta*psi(i,j+1) ...
              +beta*psi(i,j-1)+Dxs*vort(i,j))/beta1-psi(i,j);
        psi(i,j) = psi(i,j) + relax*res;
    end
end
end

%-----
% Compute the vorticity at boundary grid points
% using the velocity boundary conditions
% (lower-order boundary conditions are commented out)
%-----

%---
% top and bottom walls
%---

for i=2:Nx
% vort(i,1) = 2.0*(psi(i,1)-psi(i,2))/Dys;
% vort(i,Ny+1) = 2.0*(psi(i,Ny+1)-psi(i,Ny))/Dys-2.0*Vlid/Dys;
    vort(i,1) = (7.0*psi(i,1)-8.0*psi(i,2)+psi(i,3))/(2.0*Dys);
    vort(i,Ny+1) = (7.0*psi(i,Ny+1)-8.0*psi(i,Ny) ...
                  +psi(i,Ny-1))/(2.0*Dys)-3.0*Vlid/Dy;
end

%---
% left and right walls
%---

for j=2:Ny
% vort(1,j) = 2.0*(psi(1,j)-psi(2,j) )/Dxs;
% vort(Nx+1,j) = 2.0*(psi(Nx+1,j)-psi(Nx,j))/Dxs;
    vort(1,j) = (7.0*psi(1,j)-8.0*psi(2,j)+psi(3,j))/(2.0*Dxs);
    vort(Nx+1,j) = (7.0*psi(Nx+1,j)-8.0*psi(Nx,j) ...
                  +psi(Nx-1,j))/(2.0*Dxs);
end

%-----
% compute the velocity at the interior
% grid points by central differences
%-----

for j=2:Ny
    for i=2:Nx
        ux(i,j) = (psi(i,j+1)-psi(i,j-1))/Dy2;
        uy(i,j) = - (psi(i+1,j)-psi(i-1,j))/Dx2;
    end
end
end

```

```

%-----
% iterate on Poisson's equation for the vorticity
%-----

for iteri=1:Niteri
    for j=2:Ny
        for i=2:Nx
            source(i,j) = ux(i,j)*(vort(i+1,j)-vort(i-1,j))/Dx2...
                + uy(i,j)*(vort(i,j+1)-vort(i,j-1))/Dy2;
            source(i,j) = -source(i,j)/nu;
            res = (vort(i+1,j)+vort(i-1,j) + beta*vort(i,j+1) ...
                +beta*vort(i,j-1)+Dxs*source(i,j))/beta1-vort(i,j);
            vort(i,j) = vort(i,j) + relax*res;
        end
    end
end % of iteri

%-----
% monitor the error
%-----

cormax = 0.0;

for i=1:Nx+1
    for j=1:Ny+1
        res = abs(vort(i,j)-save(i,j));
        if(res>cormax)
            cormax = res;
        end
    end
end

if(cormax<tol)
    break
end

end % of iter
%--

%=====
% graphics
%=====

for i=1:Nx+1 % set up plotting vectors
    xgr(i) = Dx*(i-1);
end

for j=1:Ny+1
    ygr(j) = Dy*(j-1);

```

```

end

figure(1)
surf(20*xgr,20*ygr,vort')
xlabel('x','fontsize',15)
ylabel('y','fontsize',15)
zlabel('\verb1'\omega'1','fontsize',15)
set(gca,'fontsize',15)
axis([0 Lx 0 Ly -10 10])
axis equal

figure(2)
contour(xgr,ygr,psi',32)
xlabel('x','fontsize',15)
ylabel('y','fontsize',15)
zlabel('\psi','fontsize',15)
axis([0 Lx 0 Ly])
axis equal

```

The graphics module at the end of the code invokes the internal MATLAB functions *surf* and *contour*.

Vorticity and stream function contour plots for a cavity with aspect ratio $L_x/L_y = 2$ at Reynolds number $Re = VL_x/\nu = 1$ and 100 are shown in [Figure 8.5.2](#). Stream function contours are streamlines and particle paths in a two-dimensional flow. As the Reynolds number increases, the center of the eddy developing inside the cavity is shifted toward the right wall due to the fluid inertia. Regions of recirculating flow develop at the bottom two corners, requiring increased spatial resolution.

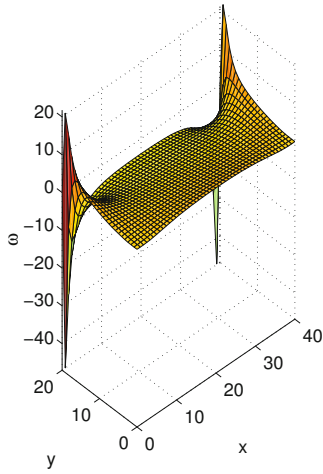
A local analysis in the context of Stokes flow shows that the shear stress diverges at the upper two cavity corners and an infinite force is required to slide the lid as a result of the sharp-corner idealization. It is remarkable that the singular behavior of the vorticity at these corners due to the discontinuous boundary velocity does not deter the overall performance of the numerical method.

8.5.5 Summary

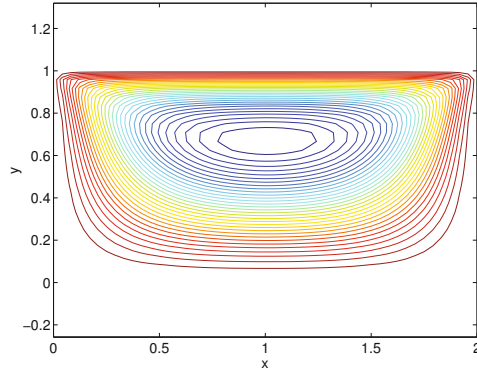
In summary, the stream function/vorticity formulation is distinguished by the following features:

1. Expressing the velocity in terms of the stream function ensures the automatic satisfaction of the continuity equation.
2. The formulation bypasses the computation of the pressure. If we had to solve for the pressure, we would have to derive appropriate boundary conditions, as discussed in [Section 8.6](#).
3. Enforcing the no-penetration and the no-slip boundary condition is done sequentially rather than simultaneously. The no-penetration condition is enforced when solving for

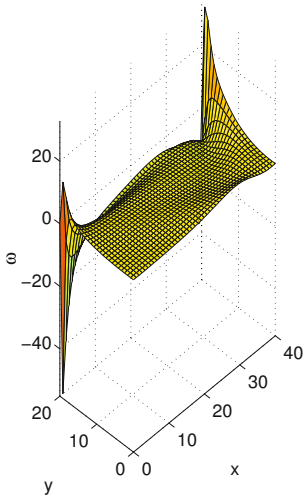
(a)



(b)



(c)



(d)

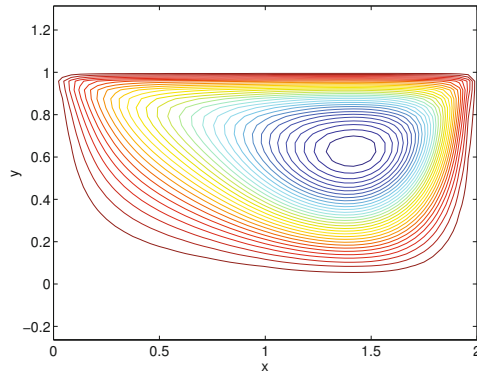


Figure 8.5.2 Vorticity and stream function contour plots for flow in a rectangular cavity with aspect ratio $L_x/L_y = 2$, at Reynolds number (a, b) $Re = VL_x/\nu = 1$ and (c, d) 100.

the stream function, while the no-slip condition is enforced when deriving boundary conditions for the vorticity.

Similar simplifications occur when solving for the Stokes stream function describing axisymmetric flow in the absence of swirling motion.

PROBLEMS**8.5.1** *Computation of the pressure*

Show that the pressure distribution in an incompressible fluid satisfies Poisson's equation

$$\frac{1}{2\rho} \nabla^2 p = \frac{\partial^2 \psi}{\partial x^2} \frac{\partial^2 \psi}{\partial y^2} - \left(\frac{\partial^2 \psi}{\partial x \partial y} \right)^2. \quad (8.5.30)$$

Hint: Take the divergence of the Navier–Stokes equation and use the continuity equation.

8.5.2 *Axisymmetric flow*

Develop a finite-difference method based on the stream function/vorticity formulation for steady axisymmetric flow in an annular cavity depressed on a circular cylinder. The flow is driven by a sleeve sliding along the cylinder surface.

8.5.3  *Steady flow in a cavity*

(a) Run the code `cvt_sv` and prepare velocity vector plots for the two flows illustrated in Figure 8.5.2. Discuss the structure of the streamline pattern.

(b) Investigate the performance of the numerical method for a square cavity at high Reynolds numbers.

(c) Duplicate the results shown in Figure 8.5.2 for a slender cavity with aspect ratio $L_x/L_y = 8$. Discuss the structure of the flow.

(d) Implement a stopping check so that the computations terminate when the vorticity field has been computed within a specified accuracy.

(e) Resolve and discuss the structure of the eddies developing near the lower two corners.

8.6 Velocity/pressure formulation

Although the stream function/vorticity formulation discussed in Section 8.5 is simple and efficient, its extension to three dimensions and its generalization to flow in the presence of interfaces are cumbersome. To handle arbitrary flow configurations, we develop a direct formulation in primary variables, including the velocity and the pressure.

Evolution equations

To compute the evolution of an unsteady flow, we require an evolution equation for the velocity and another evolution equation for the pressure. The former is provided by the Navier–Stokes equation stated as

$$\frac{\partial \mathbf{u}}{\partial t} = \mathbf{N}(\mathbf{u}) - \frac{1}{\rho} \nabla p + \nu \mathbf{L}(\mathbf{u}), \quad (8.6.1)$$

where $\mathbf{N}(\mathbf{u})$ is a nonlinear convection operator and $\mathbf{L}(\mathbf{u})$ is a linear diffusion operator defined as

$$\mathbf{N}(\mathbf{u}) \equiv -\mathbf{u} \cdot \nabla \mathbf{u}, \quad \mathbf{L}(\mathbf{u}) \equiv \nabla^2 \mathbf{u}. \quad (8.6.2)$$

If the fluid were compressible, the continuity equation would provide us with an evolution equation for the density, as shown in equations (2.7.13) and (2.7.14). An evolution equation for the pressure could then be obtained by introducing an equation of state relating the density to the local pressure and temperature.

An explicit evolution equation for the pressure developing in a incompressible fluid is not available. Instead, the continuity equation takes the form a kinematic constraint,

$$\nabla \cdot \mathbf{u} = 0, \quad (8.6.3)$$

which requires that the pressure field evolves so that the rate of expansion, $\nabla \cdot \mathbf{u}$, is zero throughout the domain of flow at any time.

To convert this requirement into a mathematical restriction, we take the divergence of the Navier–Stokes equation (8.6.1), interchange the divergence with the time derivative on the left-hand side, and thus derive an evolution equation for the rate of expansion,

$$\frac{\partial \nabla \cdot \mathbf{u}}{\partial t} = \nabla \cdot \mathbf{N}(\mathbf{u}) - \frac{1}{\rho} \nabla^2 p + \nu \nabla \cdot \mathbf{L}(\mathbf{u}). \quad (8.6.4)$$

Note that the divergence operator and the nonlinear operator \mathbf{N} on the right-hand side do not commute, that is,

$$\nabla \cdot \mathbf{N}(\mathbf{u}) \neq \mathbf{N}(\nabla \cdot \mathbf{u}). \quad (8.6.5)$$

For simplicity, we have assumed that the density and viscosity are uniform throughout the domain of flow.

Pressure Poisson equation

Equation (8.6.3) requires that the left-hand side of (8.6.4) vanishes at any time, which will be true if the pressure satisfies the pressure Poisson equation (PPE),

$$\nabla^2 p = \rho \nabla \cdot \mathbf{N}(\mathbf{u}) + \mu \nabla \cdot \mathbf{L}(\mathbf{u}). \quad (8.6.6)$$

It could be argued that, since the divergence operator and the linear operator \mathbf{L} commute,

$$\nabla \cdot \mathbf{L}(\mathbf{u}) = \mathbf{L}(\nabla \cdot \mathbf{u}), \quad (8.6.7)$$

the last term on the right-hand side of (8.6.6) could be set to zero, yielding the simplified pressure Poisson equation (SPPE),

$$\nabla^2 p = \rho \nabla \cdot \mathbf{N}(\mathbf{u}). \quad (8.6.8)$$

However, in practice, the magnitude of the last term on the right-hand side of (8.6.6) is nonzero due to numerical error associated with the approximation of partial derivatives with finite differences. It turns out that the complete absence of this term may be detrimental to the performance of the numerical method by fostering the growth of small oscillations. To prevent the onset of these oscillations, the PPE is preferred over its simplified counterpart.

8.6.1 Alternative system of governing equations

The preceding discussion suggests a numerical procedure for computing the evolution of an unsteady flow based on equations (8.6.1) and (8.6.6) or (8.6.8): compute the evolution of the velocity using (8.6.1), and simultaneously obtain the evolution of the pressure by solving the Poisson equation (8.6.6) or (8.6.8).

The method is analogous to that employed in the stream function/vorticity formulation discussed in Section 8.5. One important difference is that, by employing the stream function, the satisfaction of the continuity equation (8.6.3) is guaranteed, independent of the magnitude of the numerical error.

To examine whether the velocity/pressure formulation ensures the satisfaction of the continuity equation (8.6.3), we substitute (8.6.6) into the right-hand side of the pressure Poisson equation (8.6.4) and obtain the expected result

$$\frac{\partial \nabla \cdot \mathbf{u}}{\partial t} = 0, \quad (8.6.9)$$

which ensures that, if the rate of expansion vanishes at the initial instant by a sensible choice of the initial condition, it will also vanish at any time.

Substituting (8.6.8) into the right-hand side of the simplified pressure Poisson equation (8.6.4), we obtain an unsteady diffusion equation for the rate of expansion,

$$\frac{\partial \nabla \cdot \mathbf{u}}{\partial t} = \nu \nabla \cdot \mathbf{L}(\mathbf{u}), \quad (8.6.10)$$

which ensures that, if the rate of expansion vanishes at the initial instant by an appropriate choice of an initial condition, it will also vanish at any time provided that the boundary values of the rate of expansion also vanish at any time. The additional condition underlines the importance of accurately satisfying mass conservation at the boundaries and explains why (8.6.6) is preferred over its simplified counterpart (8.6.8).

8.6.2 Pressure boundary conditions

To solve the pressure Poisson equation, we require a pressure boundary condition derived from specified boundary conditions for the velocity. The pressure boundary condition emerges by evaluating the Navier–Stokes equation (8.6.1) at the boundaries of the flow, and then taking the inner product of both sides with the unit vector normal to the boundaries pointing outward, \mathbf{n} . The result is the Neumann boundary condition

$$\mathbf{n} \cdot \nabla p = \rho \mathbf{n} \cdot \left(-\frac{\partial \mathbf{u}}{\partial t} + \mathbf{N}(\mathbf{u}) + \nu \mathbf{L}(\mathbf{u}) \right). \quad (8.6.11)$$

The left-hand side is the derivative of the pressure normal to the boundaries, expressing the rate of change of the pressure with respect to distance normal to the boundaries. The right-hand side is then simplified by implementing the no-slip and no-penetration boundary conditions.

For example, in the case of two-dimensional flow over a horizontal stationary wall located at $y = 0$, we require that $u_x = 0$ and $u_y = 0$ at $y = 0$, and obtain

$$\mathbf{n} \cdot \nabla p = \frac{\partial p}{\partial y} = \mu \frac{\partial^2 u_y}{\partial y^2} \quad (8.6.12)$$

in a steady or unsteady flow. The left-hand side is the normal derivative of the pressure, while the right-hand side is the negative of the normal derivative of the vorticity multiplied by the fluid viscosity.

8.6.3 Compatibility condition for the pressure

The Poisson equation governing the pressure distribution in an incompressible fluid is analogous to the Poisson equation governing the steady-state temperature distribution in a conductive medium identified with the domain of flow, subject to a homogeneous heat production term expressed by the right-hand side.

The boundary condition (8.6.11) specifies the boundary distribution of the flux in terms of the instantaneous velocity. Physical reasoning suggests that a steady distribution will exist only if the total rate of heat production is balanced by the total rate of heat removal across the boundaries, so that heat neither accumulates to elevate the temperature nor is depleted to lower the temperature.

In the case of two-dimensional flow, the mathematical expression of this requirement takes the form of a compatibility condition, stating that the areal integral of the right-hand side of (8.6.6) or (8.6.8) over the domain of flow should be equal to the line integral of the right-hand side of (8.6.11) or (8.6.12) over the boundaries. If the compatibility condition is not fulfilled, a solution for the pressure cannot be found.

In the case of three-dimensional flow, the compatibility condition requires that the volume integral of the right-hand side of (8.6.6) or (8.6.8) over the domain of flow should be equal to the surface integral of the right-hand side of (8.6.11) or (8.6.12) over the boundaries. If the compatibility condition is not fulfilled, a solution for the pressure cannot be found.

In numerical practice, this compatibility condition is enforced implicitly or explicitly depending on the particulars of the implementation of the numerical method. In some oversimplified approaches, the compatibility condition is altogether ignored and an approximate solution is found.

PROBLEM

8.6.1 Pressure boundary condition

Derive the pressure boundary condition (8.6.12).

8.7 Operator splitting and solenoidal projection

In practice, the velocity/pressure formulation is implemented in a way that expedites the numerical solution and reduces the computational cost. For the purpose of illustration, we discuss the computation of an evolving two-dimensional flow. Extending the methodology to three-dimensional flow is straightforward in principle and implementation.

Operator splitting

In the most popular implementation of the velocity/pressure formulation, the Navier–Stokes equation (8.6.1) is resolved into two constituent equations,

$$\frac{\partial \mathbf{u}}{\partial t} = \mathbf{N}(\mathbf{u}) + \nu \mathbf{L}(\mathbf{u}) \quad (8.7.1)$$

and

$$\frac{\partial \mathbf{u}}{\partial t} = -\frac{1}{\rho} \nabla p, \quad (8.7.2)$$

where the operators $\mathbf{N}(\mathbf{u})$ and $\mathbf{L}(\mathbf{u})$ are defined in equations (8.6.2),

$$\mathbf{N}(\mathbf{u}) \equiv -\mathbf{u} \cdot \nabla \mathbf{u}, \quad \mathbf{L}(\mathbf{u}) \equiv \nabla^2 \mathbf{u}. \quad (8.7.3)$$

The right-hand sides of equations (8.7.1) and (8.7.2) arise by splitting the full Navier–Stokes operator on the right-hand side of (8.6.1) into two parts, subject to the following interpretation.

Consider the change in the velocity field over a small time interval, Δt , following the current time, t . The decomposition into (8.7.1) and (8.7.2) is inspired by the idea of updating the velocity in two sequential stages, where the first update is due to inertia and viscosity, while the second update is due to the pressure gradient alone. Time is to $t + \Delta t$ after the completion of the second stage. We will see that this decomposition significantly simplifies the implementation of the numerical method by allowing the convection–diffusion and pressure gradient steps to be handled independently using appropriate numerical methods.

Two main issues arise. First, the boundary condition for the velocity to be used for integrating (8.7.1) cannot be the same as the specified physical boundary condition, otherwise the second step mediated by (8.7.2) will cause a departure. Second, the boundary condition for the pressure may no longer be computed from (8.6.11), but should be derived instead using equation (8.7.2).

Projection function

The second observation suggests that p in equation (8.7.2) may no longer be regarded as the hydrodynamic pressure, p , and should be interpreted instead as a fictitious pressure whose role is to ensure that the velocity field is solenoidal at the end of the second step. To make this distinction clear, we replace equation (8.7.2) with the equation

$$\frac{\partial \mathbf{u}}{\partial t} = -\frac{1}{\rho} \nabla \chi, \quad (8.7.4)$$

where χ is a projection function. Equation (8.7.4) receives the velocity field delivered by the convection–diffusion equation (8.7.1), which is not necessarily solenoidal, and removes the non-solenoidal component in a process that can be described as projection into the space of solenoidal functions.

The choice of boundary conditions for the projection function, χ , has been the subject of extensive discussion. It can be shown that the homogeneous Neumann boundary condition, requiring that the derivative of the projection function χ with respect to distance normal to a boundary vanishes, is appropriate. The associated boundary conditions for the velocity will be discussed in Section 8.7.3.

Next, we discuss the implementation of numerical methods for performing the convection–diffusion and projection steps expressed by equations (8.7.1) and (8.7.4).

8.7.1 Convection–diffusion step

To prevent numerical instability, we perform the convection–diffusion step expressed by equation (8.7.1) by an implicit finite-difference method. This means that updating the velocity requires solving linear systems of algebraic equations for the velocity at all nodes.

Evaluating the x and y components of equation (8.7.1) at the (i, j) grid point at time $t + \Delta t$, and approximating the time derivatives with backward differences and the spatial derivatives with differences of our choice, we derive a system of equations for the unknown velocity vector comprised of the x and y velocity components at the grid points at time $t + \Delta t$. The size of the velocity vector is twice the number of grid points. For a 32×32 grid, we obtain a velocity vector with nearly 2,000 unknowns and an equal number of equations whose solution requires a significant computational cost.

Directional splitting

As an alternative, we split the operator on the right-hand side of (8.7.1) into two spatial constituents expressing convection–diffusion in the x or y direction, given by

$$\frac{\partial \mathbf{u}}{\partial t} = -u_x \frac{\partial \mathbf{u}}{\partial x} + \nu \frac{\partial^2 \mathbf{u}}{\partial x^2} \quad (8.7.5)$$

and

$$\frac{\partial \mathbf{u}}{\partial t} = -u_y \frac{\partial \mathbf{u}}{\partial y} + \nu \frac{\partial^2 \mathbf{u}}{\partial y^2}, \quad (8.7.6)$$

and advance the velocity over the time interval Δt in a sequential fashion based on this decomposition.

Crank–Nicolson integration

To achieve second-order accuracy, we discretize equation (8.7.5) using the Crank–Nicolson method. The implementation involves evaluating (8.7.5) at the (i, j) grid point at time

$t + \frac{1}{2} \Delta t$, approximating the time and space derivatives with central differences, and averaging the space derivatives over the time levels t and $t + \Delta t$,

$$\begin{aligned} \frac{\mathbf{u}_{i,j}^* - \mathbf{u}_{i,j}(t)}{\Delta t} &= -\frac{1}{2} (u_x)_{i,j}(t) \left[\left(\frac{\mathbf{u}_{i+1,j} - \mathbf{u}_{i-1,j}}{2\Delta x} \right)(t) + \frac{\mathbf{u}_{i+1,j}^* - \mathbf{u}_{i-1,j}^*}{2\Delta x} \right] \\ &+ \frac{1}{2} \nu \left[\left(\frac{\mathbf{u}_{i+1,j} - 2\mathbf{u}_{i,j} + \mathbf{u}_{i-1,j}}{\Delta x^2} \right)(t) + \frac{\mathbf{u}_{i+1,j}^* - 2\mathbf{u}_{i,j}^* + \mathbf{u}_{i-1,j}^*}{\Delta x^2} \right]. \end{aligned} \quad (8.7.7)$$

An asterisk designates the first intermediate velocity field.

To simplify the notation, we define

$$\mathbf{u}_{i,j}^n \equiv \mathbf{u}_{i,j}(t), \quad (8.7.8)$$

where the superscript n denotes the n th time level corresponding to time t . Rearranging equation (8.7.7), we derive the finite-difference equation

$$\begin{aligned} &-(c_x + 2\alpha_x) \mathbf{u}_{i-1,j}^* + 4(1 + \alpha_x) \mathbf{u}_{i,j}^* + (c_x - 2\alpha_x) \mathbf{u}_{i+1,j}^* \\ &= (c_x + 2\alpha_x) \mathbf{u}_{i-1,j}^n + 4(1 - \alpha_x) \mathbf{u}_{i,j}^n - (c_x - 2\alpha_x) \mathbf{u}_{i+1,j}^n, \end{aligned} \quad (8.7.9)$$

involving the local x convection number,

$$c_x \equiv \frac{(u_x)_{i,j}^n \Delta t}{\Delta x}, \quad (8.7.10)$$

and the x diffusion number,

$$\alpha_x \equiv \frac{\nu \Delta t}{\Delta x^2}. \quad (8.7.11)$$

The right-hand side of (8.7.9) can be computed in terms of the velocity at the grid points at the n th time level, which is available.

Evaluating (8.7.9) at grid points that lie along y grid lines corresponding to fixed values of j , we obtain tridiagonal systems of equations for the x and y components of the first intermediate velocity. The salient advantage of the method of directional splitting is that these tridiagonal systems can be solved efficiently using the Thomas algorithm discussed in Section 8.2.4, subject to boundary conditions discussed in Section 8.7.3.

An analogous discretization of (8.7.6) yields

$$\begin{aligned} &-(c_y + 2\alpha_y) \mathbf{u}_{i,j-1}^{**} + 4(1 + \alpha_y) \mathbf{u}_{i,j}^{**} + (c_y - 2\alpha_y) \mathbf{u}_{i,j+1}^{**} \\ &= (c_y + 2\alpha_y) \mathbf{u}_{i,j-1}^* + 4(1 - \alpha_y) \mathbf{u}_{i,j}^* - (c_y - 2\alpha_y) \mathbf{u}_{i,j+1}^*, \end{aligned} \quad (8.7.12)$$

where

$$c_y \equiv \frac{(u_y)_{i,j}^n \Delta t}{\Delta y} \quad (8.7.13)$$

is the local y convection number and

$$\alpha_y \equiv \frac{\nu \Delta t}{\Delta y^2} \quad (8.7.14)$$

is the y diffusion number. A double asterisk in (8.7.12) designates the second intermediate velocity field.

The right-hand side of (8.7.12) can be computed in terms of the first intermediate velocity delivered by equation (8.7.9). Evaluating (8.7.12) at grid points that lie along x grid lines corresponding to fixed values of i , we obtain tridiagonal systems of equations for the x and y components of the second intermediate velocity. The solution can be found using the Thomas algorithm discussed in Section 8.2.4, subject to boundary conditions discussed in Section 8.7.3.

8.7.2 Projection step

Next, we advance the velocity field using the projection step (8.7.4), where the projection function is computed to satisfy the continuity equation at the end of this step. Evaluating (8.7.5) at the (i, j) grid point and approximating the time derivative with a finite difference, we obtain

$$\frac{\mathbf{u}_{i,j}(t + \Delta t) - \mathbf{u}_{i,j}^{**}}{\Delta t} = -\frac{1}{\rho} (\nabla \chi)_{i,j}^n, \quad (8.7.15)$$

which can be rearranged to give

$$\mathbf{u}_{i,j}(t + \Delta t) = \mathbf{u}_{i,j}^{**} - \frac{\Delta t}{\rho} (\nabla \chi)_{i,j}^n. \quad (8.7.16)$$

The gradient on the right-hand side of (8.7.16) can be approximated by centered, forward, or backward differences.

Now we consider the numerical discretization of the continuity equation, $\nabla \cdot \mathbf{u} = 0$. Using centered differences, we approximate the rate of expansion at the (i, j) grid point with the discrete form

$$D_{i,j} \equiv (\nabla \cdot \mathbf{u})_{i,j} \simeq \frac{(u_x)_{i+1,j} - (u_x)_{i-1,j}}{2\Delta x} + \frac{(u_y)_{i,j+1} - (u_y)_{i,j-1}}{2\Delta y}. \quad (8.7.17)$$

Evaluating (8.7.17) at the $n + 1$ time level corresponding to time $t + \Delta t$, requiring that the left-hand side is zero, and using (8.7.16) to express $\mathbf{u}(t + \Delta t)$ on the right-hand side in terms of the second intermediate velocity denoted by the double asterisk and the projection function, we obtain the expression

$$\frac{\rho}{\Delta t} (\nabla \cdot \mathbf{u}^{**})_{i,j} = \frac{(\frac{\partial \chi}{\partial x})_{i+1,j} - (\frac{\partial \chi}{\partial x})_{i-1,j}}{2\Delta x} + \frac{(\frac{\partial \chi}{\partial y})_{i,j+1} - (\frac{\partial \chi}{\partial y})_{i,j-1}}{2\Delta y}. \quad (8.7.18)$$

The right-hand side of (8.7.18) is recognized as the discrete divergence of the gradient of the projection function χ .

For grid points that are not adjacent to a wall, we approximate the partial derivatives of the right-hand side of (8.7.18) with centered differences and simplify to obtain

$$\frac{\rho}{\Delta t} (\nabla \cdot \mathbf{u}^{**})_{i,j} = \frac{\chi_{i-2,j} - 2\chi_{i,j} + \chi_{i+2,j}}{4\Delta x^2} + \frac{\chi_{i,j-2} - 2\chi_{i,j} + \chi_{i,j+2}}{4\Delta y^2}. \quad (8.7.19)$$

The right-hand side of (8.7.19) is recognized as the finite-difference approximation of the Laplacian of χ , computed with spatial intervals equal to $2\Delta x$ and $2\Delta y$.

For points that are adjacent to a wall, we derive corresponding formulas incorporating the homogeneous Neumann boundary condition. For example, applying equation (8.7.18) at the near-corner point $i = 2$ and $j = 2$, and setting $(\partial\chi/\partial y)_{2,1} = 0$ and $(\partial\chi/\partial x)_{1,2} = 0$, we obtain

$$\frac{\rho}{\Delta t} (\nabla \cdot \mathbf{u}^{**})_{2,2} = \frac{\chi_{4,2} - \chi_{2,2}}{4\Delta x^2} + \frac{\chi_{2,4} - \chi_{2,2}}{4\Delta y^2}. \quad (8.7.20)$$

Returning to (8.7.19), we reduce the intervals of the centered spatial differences to Δx and Δy , and derive the alternative expression

$$\frac{\rho}{\Delta t} (\nabla \cdot \mathbf{u}^{**})_{i,j} = \frac{\chi_{i+1,j} - 2\chi_{i,j} + \chi_{i-1,j}}{\Delta x^2} + \frac{\chi_{i,j+1} - 2\chi_{i,j} + \chi_{i,j-1}}{\Delta y^2}, \quad (8.7.21)$$

which is applicable at all interior grid points. This finite-difference equation could have been derived directly from (8.7.15) by taking the divergence of both sides and then approximating the emerging Laplacian of χ on the right-hand side with the five-point formula, as shown in (8.7.21).

Evaluating (8.7.19) or (8.7.21) at the interior grid points and their counterparts for the wall-adjacent points, and introducing boundary conditions for χ , we derive a system of linear equations for the grid values of χ , which is the counterpart of the linear system descending from the pressure Poisson equation discussed in Section 8.6. Having computed the grid values of the projection function, we return to equation (8.7.16) and perform the final step, advancing the velocity to the $n + 1$ time level corresponding to time $t + \Delta t$.

Because the coefficient matrix of the linear system associated with (8.7.19) or (8.7.21) is independent of time, we may either compute the matrix inverse at the outset and then solve the system at each step by simple matrix-vector multiplication, or employ efficient custom-made iterative solution algorithms.

8.7.3 Boundary conditions for the intermediate velocity

Next, we address the issue of boundary conditions for the intermediate velocities denoted by a single or double asterisk. The choice of these boundary conditions is pivoted on a key observation: because of the homogeneous Neumann condition chosen for the projection function, the projection step introduces a tangential but not a normal component of

the boundary velocity. Accordingly, the boundary conditions for the intermediate velocity should be such that the tangential velocity introduced in the projection step brings the total velocity to the specified physical value at the end of a complete step. In practice, this is done by estimating the magnitude of the intermediate slip velocity and then improving the guess by iteration, as explained in Section 8.7.4.

8.7.4 Flow in a cavity

The implementation of the numerical method involves further considerations that are best illustrated with reference to the familiar problem of two-dimensional flow in a cavity driven by a sliding lid.

Homogeneous Neumann boundary condition for the projection function

Consider the numerical implementation of the condition of zero normal derivative of the projection function at the boundaries of the cavity illustrated in [Figure 8.5.1](#). Requiring that $\partial\chi/\partial y = 0$ at the bottom and top walls, and approximating the first derivative with a second-order forward or backward finite difference, we obtain

$$\left(\frac{\partial\chi}{\partial y}\right)_{i,1} \simeq \frac{-3\chi_{i,1} + 4\chi_{i,2} - \chi_{i,3}}{2\Delta y} = 0 \quad (8.7.22)$$

and

$$\left(\frac{\partial\chi}{\partial y}\right)_{i,N_y+1} \simeq \frac{\chi_{i,N_y-1} - 4\chi_{i,N_y} + 3\chi_{i,N_y+1}}{2\Delta y} = 0. \quad (8.7.23)$$

Requiring that $\partial\chi/\partial x = 0$ at the left and right walls, and approximating the first derivative with a second-order forward or backward finite-difference, we obtain

$$\left(\frac{\partial\chi}{\partial x}\right)_{1,j} \simeq \frac{-3\chi_{1,j} + 4\chi_{2,j} - \chi_{3,j}}{2\Delta x} = 0 \quad (8.7.24)$$

and

$$\left(\frac{\partial\chi}{\partial x}\right)_{N_x+1,j} \simeq \frac{\chi_{N_x-1,j} - 4\chi_{N_x,j} + 3\chi_{N_x+1,j}}{2\Delta x} = 0. \quad (8.7.25)$$

These difference equations complement those arising from the discretization of the Poisson equation.

Compatibility condition for system (8.7.19)

The linear system descending from the discrete Poisson equation (8.7.19) accompanied by the homogeneous Neumann boundary conditions is singular, which means that it has either no solution or an infinite number of solutions, depending on the right-hand side. If multiple solutions exist, any particular solution can be offset by an arbitrary constant vector with equal elements. Correspondingly, the value of the projection function at the grid points can be offset by a physically irrelevant constant. Reference to (8.7.16) ensures that this constant has no effect on the structure of the flow.

When the discrete divergence of the second intermediate velocity is computed using (8.7.17), the discrete form of the compatibility condition discussed at the end of Section 8.6 is fulfilled and the linear system has a multiplicity of solutions. A solution can be found by assigning an arbitrary value to one of the unknowns, discarding one equation, and solving the rest of the equations for the remaining unknowns. Unfortunately, the numerical solution computed in this fashion can be contaminated by artificial oscillations described as *odd-even coupling*.

Compatibility condition for system (8.7.21)

The linear system descending from the discrete Poisson equation (8.7.21) accompanied by the homogeneous Neumann boundary conditions is also singular, reflecting the arbitrary level of the projection function. Unfortunately, when the discrete divergence of the second intermediate velocity field is computed using (8.7.17), the discrete form of the compatibility condition is not satisfied. Consequently, one equation of the linear system cannot be satisfied to machine precision.

Resisting the temptation to fudge the computation by discarding one arbitrary equation, we add a small term to the right-hand side of (8.7.21) and then adjust the magnitude of this term to satisfy the compatibility condition of a modified system of equations. If

$$\mathbf{A} \cdot \mathbf{x} = \mathbf{b} \quad (8.7.26)$$

is the linear system corresponding to (8.7.21), then the modified system is

$$\mathbf{A} \cdot \mathbf{x} = \mathbf{b} + \epsilon \mathbf{c}, \quad (8.7.27)$$

where ϵ is an *a priori* unknown constant and \mathbf{c} is a constant vector that emerges by replacing the left-hand side of (8.7.18) with an arbitrary value, while retaining the linear equations implementing the homogeneous Neumann boundary conditions.

Our objective is to adjust the value of the constant ϵ so that the system (8.7.27) has an infinite number of solutions. In one approach, we work as follows:

1. First, we set the last component of \mathbf{x} to zero, discard the last equation of $\mathbf{A} \cdot \mathbf{x} = \mathbf{b}$, solve the remaining equations, and call the solution $\mathbf{x}^{(1)}$. Then we evaluate the difference between the left-hand side and the right-hand of the last equation, $r^{(1)}$.
2. Second, we set the last component of \mathbf{x} to zero, discard the last equation of $\mathbf{A} \cdot \mathbf{x} = \mathbf{c}$, solve the remaining equations, and call the solution \mathbf{x}^{ref} . Then evaluate the difference between the left-hand side and the right-hand of the last equation, denoted by r^{ref} .
3. The desired solution is

$$\mathbf{x} = \mathbf{x}^{(1)} + \epsilon \mathbf{x}^{\text{ref}}, \quad (8.7.28)$$

where

$$\epsilon = -\frac{r^{(1)}}{r^{\text{ref}}}. \quad (8.7.29)$$

A more rigorous approach involves removing from the right-hand side, \mathbf{b} , its projection on the eigenvector corresponding to the null eigenvalue of the transpose of the coefficient matrix, \mathbf{A}^T .

Boundary conditions for the intermediate velocity

The boundary conditions for the intermediate velocity must be such that the right-hand side of (8.7.16) is consistent with the specified physical boundary conditions at time $t + \Delta t$. Requiring that the left-hand side of (8.7.16) is zero over a stationary boundary, we obtain the boundary condition

$$\mathbf{u}_{i,j}^{**} = \frac{\Delta t}{\rho} (\nabla \chi)_{i,j}^n. \quad (8.7.30)$$

Because the projection function was required to satisfy the homogeneous Neumann boundary condition, the right-hand side of (8.7.30) has only a tangential component expressing *numerical wall slip*.

An apparent difficulty in computing the tangential component of the intermediate velocity is that the right-hand side of (8.7.30) is not available during the convection–diffusion step. To circumvent this difficulty, we may approximate the projection function with that at the previous step, proceed with the projection step, and then improve the approximation by repeating the convection–diffusion step until the slip velocity has fallen below a sufficiently small threshold.

Code *cvp_pm*

The following MATLAB code entitled *cvt_pm*, located inside directory *11_fdm* of **FDLIB**, performs the time integration using the projection method discussed in this section and animates the evolving velocity vector field. The code should be read in two columns on each page:

```

close all                                % chi:      projection function
clear all                                % uxi, uyi: intermediate velocity
                                           %          (generic)
%=====                                %=====
% Computation of evolving flow
% in a rectangular cavity                %-----
% in primary variables using the         % settings and parameters
% velocity/pressure formulation         %-----
%
% The flow is computed using a           Lx = 1.0; % cavity length
% projection method                      Ly = 0.5; % cavity depth
%
% SYMBOLS:                               Nx = 4*8; % grid size
%                                         Ny = 4*4;
% x,y:      grid nodes
% ux, uy:   velocity components          Dt = 0.1; % time step

```

```

visc = 0.01; % viscosity
dens = 1.0; % density

Vlidamp = 1.0; % lid velocity amplitude

Nstep = 2000; % number of steps

%-----
% parameters for solving the Poisson
% equation for the projection function
%-----

itermax = 50000;
tol = 0.000001;
relax = 0.2;

qleft = 0.0; % Neumann bound cond
qright = 0.0;
qbot = 0.0;
qtop = 0.0;

Ishift = 1;

%-----
% parameters for slip vel iterations
%-----

slipN = 50; % max iteration no
sliptol = 0.00001; % tolerance
sliprel = 1.0; % relaxation

%-----
% prepare
%-----

nu = visc/dens; % kinematic viscosity

Dx = Lx/Nx;
Dy = Ly/Ny;

Dx2 = 2.0*Dx;
Dy2 = 2.0*Dy;

Dxs = Dx*Dx;
Dys = Dy*Dy;

Dtor = Dt/dens;

%-----
% lid velocity
%-----

for i=1:Nx+1
    Vlid(i) = Vlidamp;
end

%-----
% define grid lines
% initialize velocity (ux, uy)
% and the projection function (chi)
%-----

time = 0.0;

for j=1:Ny+1
    for i=1:Nx+1
        x(i,j) = (i-1.0)*Dx;
        y(i,j) = (j-1.0)*Dy;
        ux(i,j) = 0.0; % x velocity
        uy(i,j) = 0.0; % y velocity
        chi(i,j) = 0.0; % projection function
        chroma(i,j) = 0.0; % for plotting
    end
end

for i=1:Nx+1
    ux(i,Ny+1) = Vlid(i);
end

%-----
% naive velocity boundary conditions
%-----

for i=1:Nx+1
    BCxt(i) = Vlid(i); % top wall
    BCxb(i) = 0.0; % bottom wall
end

for j=1:Ny+1
    BCyl(j) = 0.0; % left wall
    BCyr(j) = 0.0; % right wall
end

%-----
% time stepping
%-----

```

```

%=====
for step=1:Nstep
%=====

%---
% animation
%---

if(step==1)
    Handle1 = quiver(x,y,ux,uy,'k');
    set(Handle1, 'erasemode', 'xor');
    axis ([-0.10,Lx+0.10,-0.10,Ly+0.10])
    axis equal
    set(gca,'fontsize',15)
    xlabel('x','fontsize',15)
    ylabel('y','fontsize',15)
    hold on
    plot([0, Lx, Lx, 0, 0] ...
         , [0, 0, Ly, Ly, 0], 'k');
else
    set(Handle1,'UData',ux,'VData',uy);
    pause(0.01)
    drawnow
end

%-----
% initialize the intermediate velocity
%-----

for j=1:Ny+1
    for i=1:Nx+1
        uxi(i,j) = ux(i,j);
        uyi(i,j) = uy(i,j);
    end
end

%=====
% perform inner iterations
% for the projection function
% to satisfy the no-slip
% boundary condition
%=====

    for inner=1:slipN

%---
% zero the tridiagonal matrix
%---

        for i=1:Nx-1
            atr(i) = 0.0;
            btr(i) = 0.0;
            ctr(i) = 0.0;
        end

%-----
% Integrate conv-diff equation in x
% using the Crank-Nicolson method
% Advance the velocity from u^n to u*
%-----

        Iskip = 0;
        if(Iskip==0)

            al = nu*Dt/Dxs;

%-----
            for j=2:Ny           % run over rows
%----

                for i=2:Nx
                    Rc = ux(i,j)*Dt/Dx;
                    C1 = Rc + 2.0*al;
                    C2 = 4.0*(1.0-al);
                    C3 = -Rc + 2.0*al;
                    ctr(i-1) = -Rc - 2.0*al;
                    atr(i-1) = 4.0*(1.0+al);
                    btr(i-1) = Rc - 2.0*al;
                    rhsx(i-1) = C1*ux(i-1,j) ...
                                + C2*ux(i,j) ...
                                + C3*ux(i+1,j);
                    rhsy(i-1) = C1*uy(i-1,j) ...
                                + C2*uy(i,j) ...
                                + C3*uy(i+1,j);
                end

                rhsy(1) = rhsy(1) ...
                        - ctr(1) *BCyl(j);
                rhsy(Nx-1) = rhsy(Nx-1) ...
                        - btr(Nx-1)*BCyr(j);

                % x component:
                solx = thomas(Nx-1,atr,btr,ctr,rhsx);
                % y component:
                soly = thomas(Nx-1,atr,btr,ctr,rhsy);
            end

            for k=1:Nx-1

```

```

    uxi(k+1,j) = solx(k);
    uyi(k+1,j) = soly(k);
end
%---
end % End of running over rows
%-----

for i=1:Nx-1 % reset
    atr(i) = 0.0;
    btr(i) = 0.0;
    ctr(i) = 0.0;
end

end % of skip

%-----
% Integrate Conv-Diff equation in y
% using the Crank-Nicolson method
% Advance the velocity from u* to u**
%-----

Iskip = 0;
if(Iskip==0)

    al = nu*Dt/Dys;

%---
for i=2:Nx % run over columns
%---
    for j=2:Ny % from bottom to top
        Rc = uy(i,j)*Dt/Dy;
        C1 = Rc +2.0*al;
        C2 = 4.0*(1.0-al);
        C3 = -Rc +2.0*al;
        ctr(j-1) = -Rc -2.0*al;
        atr(j-1) = 4.0*(1.0+al);
        btr(j-1) = Rc -2.0*al;
        rhsx(j-1) = C1*uxi(i,j-1) ...
            + C2*uxi(i,j) ...
            + C3*uxi(i,j+1);
        rhsy(j-1) = C1*uyi(i,j-1) ...
            + C2*uyi(i,j) ...
            + C3*uyi(i,j+1);
    end

    rhsx(1) = rhsx(1) ...
        - ctr(1) *BCxb(i);
    rhsx(Ny-1) = rhsx(Ny-1) ...

    - btr(Ny-1)*BCxt(i);

    solx = thomas (Ny-1,atr,btr,ctr,rhsx);
    soly = thomas (Ny-1,atr,btr,ctr,rhsy);

    for k=1:Ny-1
        uxi(i,k+1) = solx(k);
        uyi(i,k+1) = soly(k);
    end
%---
end % of run over columns
%---

end % of skip

%-----
% Compute intermediate compressibility
% by centered differences
%
% Divus = Div u**
%-----

% initialize

for j=1:Ny+1
    for i=1:Nx+1
        Divus(i,j) = 0.0;
    end
end

% interior nodes

for i=2:Nx
    for j=2:Ny
        DuDx = (uxi(i+1,j)-uxi(i-1,j))/Dx2;
        DvDy = (uyi(i,j+1)-uyi(i,j-1))/Dy2;
        Divus(i,j) = DuDx+DvDy;
    end
end

% left wall

for j=1:Ny+1
    DuDx = (-3.0*uxi(1,j) ...
        +4.0*uxi(2,j)-uxi(3,j))/Dx2;
    DvDy = 0.0;
    Divus(1,j) = DuDx+DvDy;
end

% save for corners:

```

```

save111 = Divus(1,j);
save121 = Divus(1,Ny+1);

% bottom wall

for i=1:Nx+1
    DuDx = 0.0;
    DvDy = (-3.0*uyi(i,1) ...
            +4.0*uyi(i,2)-uyi(i,3))/Dy2;
    Divus(i,1) = DuDx+DvDy;
end

% save for corners:
save11b = Divus(1,1);
save21b = Divus(Nx+1,1);

% right wall

for j=1:Ny+1
    DuDx = (3.0*uxi(Nx+1,j) ...
            -4.0*uxi(Nx,j) ...
            +uxi(Nx-1,j))/Dx2;
    DvDy = 0.0;
    Divus(Nx+1,j) = DuDx+DvDy;
end

% save for corners:
save21r = Divus(Nx+1,1);
save22r = Divus(Nx+1,Ny+1);

% top wall

for i=1:Nx+1
    DuDx = 0.0;
    DvDy = (3.0*uyi(i,Ny+1) ...
            -4.0*uyi(i,Ny) ...
            +uyi(i,Ny-1))/Dy2;
    Divus(i,Ny+1) = DuDx+DvDy;
end

% save for corners:
save12t = Divus(1, Ny+1);
save22t = Divus(Nx+1,Ny+1);

% corners by averaging

Divus(1, 1) ...
    = 0.5*(save111+save11b);
Divus(1, Ny+1) ...
    = 0.5*(save121+save12t);
Divus(Nx+1, 1) ...
    = 0.5*(save21b+save21r);
Divus(Nx+1,Ny+1) ...
    = 0.5*(save22r+save22t);

%-----
% Solve for the projection function
% by Gauss-Seidel (GS) iterations
%-----

Iskip = 0;
if(Iskip==0)

%---
% source term
%-----

for i=1:Nx+1
    for j=1:Ny+1
        source(i,j) = -Divus(i,j)/Dtor;
    end
end

[chi,iter,Iflag] = pois_gs_nnnn ...
...
(Nx,Ny,Dx,Dy,source ...
,itermax,tol,relax ...
,qleft,qright,qbot,qtop,chi,Ishift);

if(Iflag==0)
    disp "cvt_pm: Poisson solver ...
        did not converge"
    break
end

%-----
% project the velocity at all nodes
% except at the corner nodes
%-----

%---
% interior nodes
%-----

for i=2:Nx
    for j=2:Ny
        DchiDx = (chi(i+1,j)-chi(i-1,j))/Dx2;
        DchiDy = (chi(i,j+1)-chi(i,j-1))/Dy2;
    end
end

```



```

    uxi(i,j) = uxi(i,j) - Dtor*DchiDx;
    uyi(i,j) = uyi(i,j) - Dtor*DchiDy;
end
end

%-----
% lower boundary
%
% Use forward differences with special
% treatment of the near-corner nodes
%-----

for i=2:Nx
    DchiDy = 0.0;
    if(i==2)
        DchiDx = (-3.0*chi(2,1) ...
            +4.0*chi(3,1)-chi(4,1))/Dx2;
    elseif(i==Nx)
        DchiDx = -(-3.0*chi(Nx,1) ...
            +4.0*chi(Nx-1,1) ...
            -chi(Nx-2,1))/Dx2;
    else
        DchiDx ...
            = (chi(i+1,1)-chi(i-1,1))/Dx2;
    end
    uxi(i,1) = BCxb(i) - Dtor*DchiDx;
    uyi(i,1) =          - Dtor*DchiDy;
end

%-----
% upper boundary
%
% Use backward difference with special
% treatment of the near-corner nodes
%-----

for i=2:Nx
    DchiDy = 0.0;
    if(i==2)
        DchiDx = (-3.0*chi(2,Ny+1) ...
            +4.0*chi(3,Ny+1) ...
            -chi(4,Ny+1))/Dx2;
    elseif(i==Nx)
        DchiDx = -(-3.0*chi(Nx,Ny+1) ...
            +4.0*chi(Nx-1,Ny+1) ...
            -chi(Nx-2,Ny+1))/Dx2;
    else
        DchiDx = (chi(i+1,Ny+1) ...
            -chi(i-1,Ny+1))/Dx2;
    end

    end
    uxi(i,Ny+1) = BCxt(i) - Dtor*DchiDx;
    uyi(i,Ny+1) =          - Dtor*DchiDy;
end

%-----
% left boundary
%
% Use forward differences with special
% treatment of the near-corner nodes
%-----

for j=2:Ny
    DchiDx = 0.0;
    if(j==2)
        DchiDy = (-3.0*chi(1,2) ...
            +4.0*chi(1,3) ...
            -chi(1,4))/Dy2;
    elseif(j==Ny)
        DchiDy = -(-3.0*chi(1,Ny) ...
            +4.0*chi(1,Ny-1) ...
            -chi(1,Ny-2))/Dy2;
    else
        DchiDy ...
            = (chi(1,j+1)-chi(1,j-1))/Dy2;
    end
    uxi(1,j) =          - Dtor*DchiDx;
    uyi(1,j) = BCyl(j) - Dtor*DchiDy;
end

%-----
% right boundary
%
% Use backward difference with special
% treatment of the near-corner nodes
%-----

for j=2:Ny
    DchiDx = 0.0;
    if(j==2)
        DchiDy = (-3.0*chi(Nx+1,2) ...
            +4.0*chi(Nx+1,3) ...
            -chi(Nx+1,4))/Dy2;
    elseif(j==Ny)
        DchiDy = -(-3.0*chi(Nx+1,Ny) ...
            +4.0*chi(Nx+1,Ny-1) ...
            -chi(Nx+1,Ny-2))/Dy2;
    else
        DchiDy = (chi(Nx+1,j+1) ...
            -chi(Nx+1,j-1))/Dy2;
    end
end

```

```

                                -chi(Nx+1,j-1))/Dy2;          end % of inner iterations
end                               %=====
uxi(Nx+1,j) =                    - Dtor*DchiDx;
uyi(Nx+1,j) = BCyr(j) - Dtor*DchiDy; %-----
end                               % update velocity to the final value
                                %-----

end % of Iskip

%-----
% Compute the wall slip velocity
% and modify the boundary conditions
% for the intermediate (star) velocities
%-----

                                for j=1:Ny+1
                                for i=1:Nx+1
                                ux(i,j) = uxi(i,j);
                                uy(i,j) = uyi(i,j);
                                end
                                end

                                %-----
                                % update time
                                %-----

slipmax = 0.0;

% top and bottom:

                                time = time + Dt

                                %=====
                                end % of time stepping
                                %=====

                                figure(2)
                                mesh(x,y,ux);
                                set(gca,'fontsize',15)
                                xlabel('x','fontsize',15)
                                ylabel('y','fontsize',15)
                                zlabel('u_x','fontsize',15)
                                set(gca,'fontsize',15)
                                box

                                figure(3)
                                mesh(x,y,uy);
                                xlabel('x','fontsize',15)
                                ylabel('y','fontsize',15)
                                zlabel('u_y','fontsize',15)
                                set(gca,'fontsize',15)
                                box

                                figure(4)
                                mesh(x,y,chi,chroma);
                                xlabel('x','fontsize',15)
                                ylabel('y','fontsize',15)
                                zlabel('\chi','fontsize',15)
                                set(gca,'fontsize',15)
                                box

                                %-----

```

The code calls the function *thomas* listed in Section 8.2.4 to solve tridiagonal systems of equations using the Thomas algorithm.

The code also calls the following MATLAB function entitled *pois-gs-nnnn* to solve the Poisson equation for the projection function, subject to the Neumann boundary condition along the four sides:

```
function [f,iter,Iflag] = pois_gs_nnnn ...
...
    (Nx,Ny,Dx,Dy,g ...
    ,itermax,tol,relax,qleft ...
    ,qright,qbot,qtop,f,Ishift)

%-----
% Solution of Poisson's equation
% in a rectangular domain
% with the uniform Neumann boundary condition
% along the four sides:
%
% bottom: df/dy = qbot
% top: df/dy = -qtop
% left: df/dx = qlleft
% right: df/dx = -qright
%
% The solution is found by
% point Gauss--Seidel iterations
%-----

%-----
% prepare
%-----

Dx2 = 2.0*Dx;
Dy2 = 2.0*Dy;
Dxs = Dx*Dx;
Dys = Dy*Dy;
beta = Dxs/Dys;
beta1 = 2.0*(beta+1.0);
Iflag = 0;    % convergence flag, 1 indicates convergence

%-----
% Gauss-Seidel iterations
%-----

for iter=1:itermax

%-----
% update nodes row-by-row
%-----
```

```

fsv = f;
cormax = 0.0;

%---
% interior nodes
%---

for j=2:Ny
    for i=2:Nx
        res = (f(i+1,j)+f(i-1,j)+beta*(f(i,j+1)+f(i,j-1)) ...
            + Dxs*g(i,j))/beta1-f(i,j);
        f(i,j) = f(i,j) + relax*res;
    end
end

%-----
% left boundary
%-----

i=1;
for j=2:Ny
    res = (2*f(i+1,j)-Dx2*qleft+beta*(f(i,j+1)+f(i,j-1)) ...
        +Dxs*g(i,j))/beta1 - f(i,j);
    f(i,j) = f(i,j) + relax*res;
end
end

% corner points:

j=1;
res = (2*f(i+1,j)-Dx2*qleft ...
    +beta*(f(i,j+1)+f(i,j+1)-Dy2*qbot) ...
    +Dxs*g(i,j))/beta1 - f(i,j);
f(i,j) = fsave(i,j) + relax*res;

j=Ny+1;
res = (2*f(i+1,j)-Dx2*qleft ...
    +beta*(f(i,j-1)+f(i,j-1)-Dy2*qtop) ...
    +Dxs*g(i,j))/beta1 - f(i,j);
f(i,j) = fsave(i,j) + relax*res;

%-----
% right boundary
%-----

i=Nx+1;
for j=2:Ny
    res = (2*f(i-1,j)+-Dx2*qright+beta*(f(i,j+1)+f(i,j-1)) ...

```

```

    +Dxs*g(i,j))/beta1 -f(i,j);
    f(i,j) = fsave(i,j) + relax*res;
end

% corner points:

j=1;
res = (2*f(i-1,j)-Dx2*qright ...
    +beta*(f(i,j+1)+f(i,j+1)-Dy2*qbot) ...
    +Dxs*g(i,j))/beta1 - f(i,j);
f(i,j) = fsave(i,j) + relax*res;

j=Ny+1;
res = (2*f(i-1,j)-Dx2*qright)+beta*(2*f(i,j-1)-Dy2*qtop) ...
    +Dxs*g(i,j))/beta1 - f(i,j);
f(i,j) = fsave(i,j) + relax*res;

%-----
% bottom boundary
%-----

j=1;
for i=2:Nx
    res = (f(i+1,j)+f(i-1,j)+beta*(2*f(i,j+1)-Dy2*qbot) ...
        +Dxs*g(i,j))/beta1 - f(i,j);
    f(i,j) = fsave(i,j) + relax*res;
end

%-----
% top boundary
%-----

j=Ny+1;
for i=2:Nx
    res = (f(i+1,j)+f(i-1,j)+beta*(2*f(i,j-1)-Dy2*qtop) ...
        +Dxs*g(i,j))/beta1 - f(i,j);
    f(i,j) = fsave(i,j) + relax*res;
end

%-----
% shift
%-----

if(Ishift==1)
    shift = f(Nx/2,Ny/2);
    for i=1:Nx+1
        for j=1:Ny+1
            f(i,j) = f(i,j)-shift;
        end
    end
end

```

```

    end
end

%-----
% maximum correction
%-----

cormax = 0;

for i=1:Nx+1
    for j=1:Ny+1
        cor = abs(f(i,j)-fsv(i,j));
        if(abs(cor)>cormax) cormax = cor; end
    end
end

%-----
% stopping check
%-----

if(cormax<tol)
    Iflag = 1;
    break
end

%---
end    % of iterations
%---

%-----
% done
%-----

return

```

The graphics display generated by the code for the parameter values implemented in the code is shown in [Figure 8.7.1](#). In the early stages of the motion, the flow is similar to that generated by the impulsive translation of a plate in a semi-infinite fluid. At later times, a fully developed recirculating flow is established.

8.7.5 Computation of the pressure

Two methods are available for extracting the pressure field, if desired. The first method involves combining equations (8.7.9), (8.7.12), and (8.7.16)—or any other appropriate set of equations—to derive a relationship between $\mathbf{u}(t)$ and $\mathbf{u}(t + \Delta t)$. Requiring that this relationship reduces to a spatially discretized version of the Navier–Stokes equation in the limit as Δt tends to zero, we derive an expression for an effective pressure. If the boundary conditions satisfied by the effective pressure are consistent with the Neumann boundary

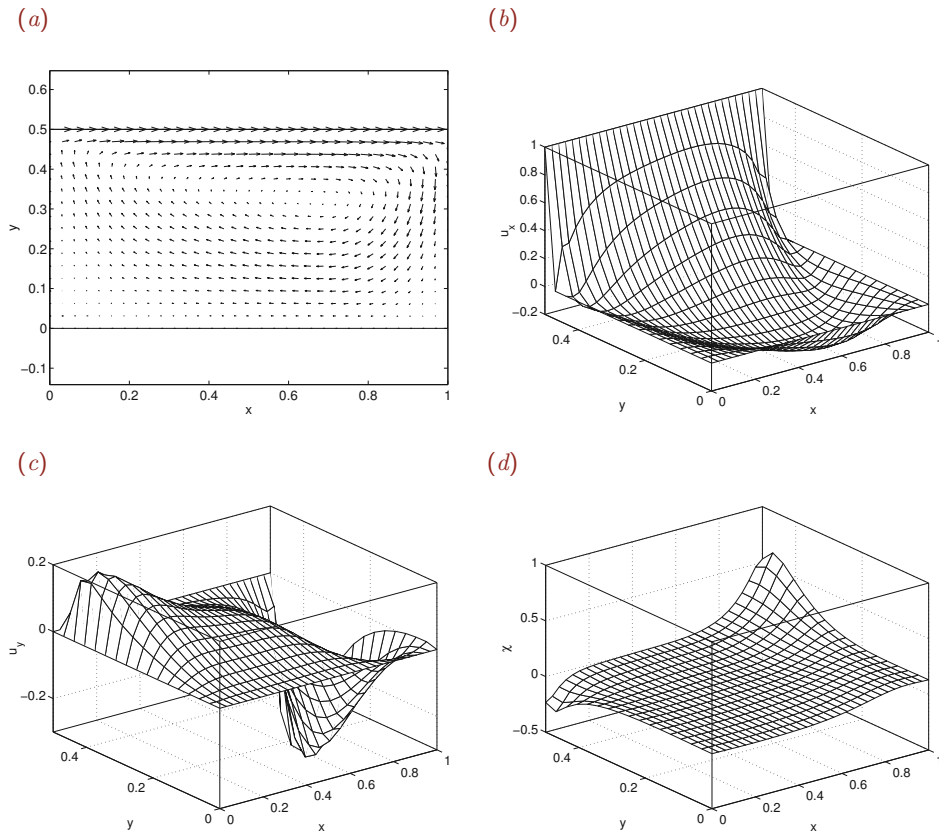


Figure 8.7.1 Flow in a rectangular cavity computed by a projection method. The graphs show (a) the velocity vector field, (b) the x velocity component, (c) the y velocity component, and (d) the projection function at steady state.

condition satisfied by the physical pressure, then the effective pressure can be accepted as an approximation to the physical pressure.

The second method involves substituting the computed velocity field into the Navier–Stokes equation and solving the resulting equation for the pressure subject to the Neumann boundary condition, as discussed in Section 8.6.2.

PROBLEMS

8.7.1 *Singular system for the projection function*

Show that equation (8.7.28) provides us with a solution of (8.7.27), subject to the homogeneous Neumann boundary condition.

8.7.2 Developing flow in a cavity

Run the code `cut_pm` located in directory `11_fdm` of `FDLIB` for a cavity with aspect ratio $L_x/L_y = 8$ and other parameter values of your choice. Prepare velocity vector fields and discuss the structure of the flow and the performance of the numerical method.

8.8 Staggered grids

The derivation of explicit boundary conditions for the pressure can be bypassed by using a staggered grid consisting of two superposed displaced grids whose intersections define nodes where the velocity components or pressure is defined. The methodology is illustrated in this section with reference to steady two-dimensional Stokes flow in a rectangular cavity driven by a moving lid.

At sufficiently low Reynolds numbers, the motion of the fluid is governed by the equations of Stokes flow, including the continuity equation and the Stokes equation,

$$\nabla \cdot \mathbf{u} = 0, \quad -\nabla p + \mu \nabla^2 \mathbf{u} + \rho \mathbf{g} = \mathbf{0}, \quad (8.8.1)$$

where \mathbf{g} is the acceleration of gravity imparting a body force.

Pressure and velocity nodes

The staggered grid consists of two interwoven grids parametrized by two pairs of indices, (i, j) and (i', j') , as illustrated in Figure 8.8.1 where the primed indices are printed in bold. The grid lines of the primary grid are represented by the solid lines and the grid lines of the secondary grid are represented by the broken lines. Note that the secondary grid conforms with the physical boundaries of the flow.

Discrete values of the pressure are assigned to the primary nodes, (i, j) , defined by the intersection of the solid lines, shown as circles.

Discrete values of the x component of the velocity are defined at the intersection of horizontal primary grid lines and vertical secondary grid lines, (i', j) , shown as horizontal arrows. The x -velocity node labeled $(2, 2)$ is shown with a circled horizontal arrow in Figure 8.8.1.

Discrete values of the y component of the velocity are defined at the intersection of vertical primary grid lines and horizontal secondary grid lines, (i, j') , shown as vertical arrows. The y -velocity node labeled $(2, 2)$ is shown with a circled vertical arrow in Figure 8.8.1.

Finite-difference equations

A distinguishing feature of the staggered grid method is that the governing equations are enforced at different nodes. For convenience, we denote u_x by u and u_y by v .

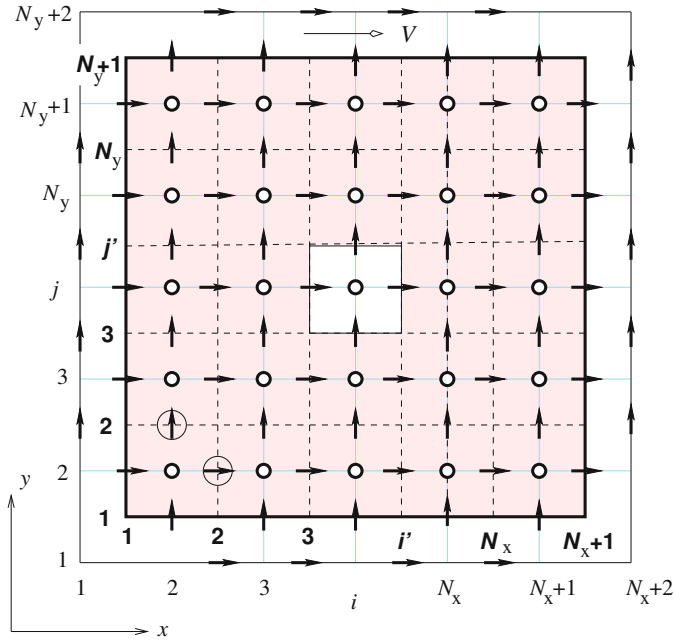


Figure 8.8.1 Illustration of a staggered grid for computing two-dimensional flow in a rectangular cavity. The pressure is defined at nodes indicated by the circles, the x velocity component is defined at nodes indicated by the horizontal arrows, and the y velocity component is defined at nodes indicated by the vertical arrows.

Applying the x component of the Stokes equation at the (i, j) interior x -velocity node and introducing similar difference approximations, we obtain

$$\frac{p_{i+1,j} - p_{i,j}}{\Delta x} = \mu \left(\frac{u_{i-1,j} - 2u_{i,j} + u_{i+1,j}}{\Delta x^2} + \frac{u_{i,j-1} - 2u_{i,j} + u_{i,j+1}}{\Delta y^2} \right) \quad (8.8.2)$$

for $i = 2, \dots, N_x$ and $j = 2, \dots, N_y + 1$, providing us with $(N_x - 1) \times N_y$ equations.

Applying the y component of the Stokes equation at the (i, j) interior y -velocity nodes and working in a similar fashion, we obtain

$$\frac{p_{i,j+1} - p_{i,j}}{\Delta y} = \mu \left(\frac{v_{i-1,j} - 2v_{i,j} + v_{i+1,j}}{\Delta x^2} + \frac{v_{i,j-1} - 2v_{i,j} + v_{i,j+1}}{\Delta y^2} \right) \quad (8.8.3)$$

for $i = 2, \dots, N + 1$ and $j = 2, \dots, N$, providing us with $N_x \times (N_y - 1)$ equations.

Enforcing the continuity equation at the (i, j) pressure node and approximating the partial derivative with central differences, we obtain

$$\frac{u_{i,j} - u_{i-1,j}}{\Delta x} + \frac{v_{i,j} - v_{i,j-1}}{\Delta y} = 0 \quad (8.8.4)$$

for $i = 2, \dots, N_x + 1$ and $j = 2, \dots, N_y + 1$, providing us with $N_x \times N_y$ equations.

We have derived a total of

$$N = (N_x - 1)N_y + N_x(N_y - 1) + N_x N_y \quad (8.8.5)$$

difference equations involving interior and phantom exterior velocity nodes, as shown with arrows in [Figure 8.8.1](#).

Boundary conditions

Unphysical x velocity components are required at the horizontal lines $j = 1$ and $j = N_y + 2$ for computing the second y derivative of u near the top and bottom boundaries. Corresponding unphysical y velocity components are required at the vertical levels $i = 1$ and $N_x + 2$ for computing the second x derivative of v near the left and right boundaries. These exterior velocities are computed by extrapolation to satisfy the boundary conditions at the physical levels $i' = 1$, $i' = N_x + 1$, $j' = 1$, and $j' = N_y + 1$.

For example, approximating u with a parabola near the lid located at $y = b_y$, and enforcing the no-slip boundary condition $u = V$, we obtain

$$u = V + A(y - b_y)^2 + B(y - b_y), \quad (8.8.6)$$

where V is the lid velocity and A, B are unknown coefficients. Applying this expression at three neighboring grid levels, we obtain,

$$\begin{aligned} u_{i,N_y} &= V + A \frac{9}{4} h^2 - B \frac{3}{2} h, & u_{i,N_y+1} &= V + A \frac{1}{4} h^2 - B \frac{1}{2} h, \\ u_{i,N_y+2} &= V + A \frac{1}{4} h^2 + B \frac{1}{2} h, \end{aligned} \quad (8.8.7)$$

where $h = \Delta y$. Eliminating A and B , we obtain the velocity at the exterior node,

$$u_{i,N_y+2} = \frac{1}{3} (8V - 6u_{i,N_y+1} + u_{i,N_y}). \quad (8.8.8)$$

Similar expressions can be derived for the other x and y external velocities.

Code

The preceding difference equations provide us with a complete system of linear algebraic equations for the nodal velocities and pressures. The system can be compiled and solved at once, as illustrated in the following MATLAB code entitled *cvt_stag*, located in directory *11_fdm* of **FDLIB**:

```
%=====
% steady Stokes flow in a rectangular cavity
% occupying 0<x<Lx, 0<y<Ly
% computed on a staggered Cartesian grid
%=====
```

```

Lx = 1.0;
Ly = 0.75;

Nx = 24; % x divisions
Ny = 16; % y divisions
visc = 1.0; % viscosity
Vlid = 1; % lid velocity

%---
% prepare
%---

Dx = ax/Nx; Dy = ay/Ny;
Dxs = Dx*Dx; Dys = Dy*Dy;

%---
% initialize
%---

% matrix size (no of eqs):
mats = (Nx-1)*Ny + Nx*(Ny-1) + Nx*Ny;

u = zeros(Nx+1,Ny+1); % impulse matrix for ux
v = zeros(Nx+1,Ny+1); % impulse matrix for uy
p = zeros(Nx+1,Ny+1); % impulse matrix for p

%=====
% compile the coefficient matrix (MAT)
%=====

Jc = 0; % counter of impulses

%---
for ipass=1:3 % impulse for u,v,p
%---

if(ipass==1)
    klim = Nx; llim = Ny+1; % u vel
elseif(ipass==2)
    klim = Nx+1; llim = Ny; % v vel
elseif(ipass==3)
    klim = Nx+1; llim = Ny+1; % pressure
end

%---
for l=2:llim % scan
    for k=2:klim
        Jc=Jc+1;
    end
%---

```

```

if(ipass==1); % impulse
    u(k,1) = 1.0;
elseif(ipass==2);
    v(k,1) = 1.0;
elseif(ipass==3);
    p(k,1) = 1.0;
end

%---
% boundary conditions
%---

for ii=2:Nx
    u(ii,1) = (-6*u(ii,2)+u(ii,3))/3.0;
    u(ii,Ny+2) = (-6*u(ii,Ny+1)+u(ii,Ny))/3.0;
end
for jj=2:Ny
    v(1,jj) = (-6*v(2,jj)+v(3,jj))/3.0;
    v(Nx+2,jj) = (-6*v(Nx+1,jj)+v(Nx,jj))/3.0;
end
%---

Ic=0; % counter of equations

for j=2:Ny+1
    for i=2:Nx % x Stokes
        Ic = Ic+1;
        MAT(Ic,Jc) = -(p(i+1,j)-p(i,j))/Dx ...
            +visc*(u(i-1,j)-2*u(i,j)+u(i+1,j))/Dxs ...
            +visc*(u(i,j-1)-2*u(i,j)+u(i,j+1))/Dys;
        MAT(Ic,Jc) = MAT(Ic,Jc)*Dxs;
    end
end

for j=2:Ny
    for i=2:Nx+1 % y Stokes
        Ic = Ic+1;
        MAT(Ic,Jc) = -(p(i,j+1)-p(i,j))/Dy ...
            +visc*(v(i-1,j)-2*v(i,j)+v(i+1,j))/Dxs ...
            +visc*(v(i,j-1)-2*v(i,j)+v(i,j+1))/Dys;
        MAT(Ic,Jc) = MAT(Ic,Jc)*Dxs;
    end
end

for j=2:Ny+1
    for i=2:Nx+1 % continuity
        Ic = Ic+1;
        MAT(Ic,Jc) = (u(i,j)-u(i-1,j))/Dx ...
            +(v(i,j)-v(i,j-1))/Dy;
    end
end

```

```

        MAT(Ic,Jc) = MAT(Ic,Jc)*Dx;
    end
end

u = zeros(Nx+1,Ny+1); % reset
v = zeros(Nx+1,Ny+1);
p = zeros(Nx+1,Ny+1);

end % of for k
end % of for l

end % of ipass

%====
% set the right-hand side
%===

for i=1:mats
    rhs(i) = 0.0;
end

Ic = (Ny-1)*(Nx-1);
for i=2:Nx % x Stokes
    Ic = Ic+1;
    rhs(Ic) = rhs(Ic)-8.0*visc*Vlid*Dxs/3/Dys;
end

%====
% set p=0 at the last node
% and find the solution
%====

SOL = rhs(1:mats-1)/MAT(1:mats-1,1:mats-1)';
SOL(mats) = 0.0;

%====
% distribute the solution
%====

Ic = 0;
for j=2:Ny+1
    for i=2:Nx
        Ic = Ic+1;
        uvel(i,j) = SOL(Ic);
    end
end

for j=2:Ny
    for i=2:Nx+1

```

```

        Ic=Ic+1;
        vvel(i,j) = SOL(Ic);
    end
end

for j=2:Ny+1
    for i=2:Nx+1
        Ic = Ic+1;
        pressure(i,j) = SOL(Ic);
    end
end

%=====
% interpolate the velocity field at the pressure nodes
% for plotting purposes
%=====

for j=2:Ny+1
    uvel(1,j) = 0;
    uvel(Nx+1,j) = 0;
    for i=2:Nx+1
        uint(i,j) = 0.5*(uvel(i,j)+uvel(i-1,j));
    end
end

for i=2:Nx+1
    vvel(i,1) = 0;
    vvel(i,Ny+1) = 0;
    for j=2:Ny+1
        vint(i,j) = 0.5*(vvel(i,j)+vvel(i,j-1));
    end
end

%====
% prepare a velocity vector plot
%====

figure(1)
hold on
plot([0 Lx Lx 0 0],[0 0 Ly Ly 0])
axis([-0.1*Lx 1.1*Lx, -0.1*Lx 1.1*Lx])
axis equal
xlabel('x'); ylabel('y')

for j=2:Ny+1
    ylevel = 0.5*Dy+(j-2)*Dy;
    for i=2:Nx+1
        xlevel = 0.5*Dx+(i-2)*Dx;
        xarrow = 0.75*Dx*uint(i,j)/Vlid;
    end
end

```

```

        yarrow = 0.75*Dx*vint(i,j)/Vlid;
        arrow = arrow_cp(xlevel,ylevel,xarrow,yarrow);
        plot(arrow(:,1),arrow(:,2));
    end
end

```

Velocity vector fields generated by the code for cavities with different aspect ratios are shown in [Figure 8.8.2](#).

Particulars of the implementation

The implementation of the numerical procedure features the following particulars:

- The linear system is compiled so that the first block of equations encapsulates the x component of the Stokes equation, the second block encapsulates the y component of the Stokes equation, and the third block encapsulates the continuity equation.
- The first block of unknowns encapsulates the x velocity components, the second block encapsulates the y velocity components, and the third block encapsulates the pressure.
- To generate the coefficient matrix of the linear system, we sequentially set one nodal value of the x velocity component, y velocity component, or pressure to unity, while holding all other values to zero. The corresponding column of the coefficient matrix is given by the residual of the governing equations scanned in the aforementioned order.
- Since the pressure field is defined up to an arbitrary constant, the pressure is set arbitrarily to zero at the last pressure node. One equation expressing the discrete implementation of the continuity equation is then discarded to balance the number of equations to the number of unknowns.

After the computation has been completed, the code calls the custom-made function *arrow_cp* near the end to draw nice-looking arrows.

Summary

By using a staggered grid, we have been able to circumvent the explicit derivation of boundary conditions for the pressure. A careful analysis shows that implicit in the numerical formulation is the Neumann boundary condition that arises by projecting the equation of motion normal to the boundaries.

Unfortunately, the staggered-grid method becomes considerably more involved and prohibitively expensive when applied to grids defined in general curvilinear coordinates.

PROBLEMS

8.8.1 *Coefficient matrix*

(a) Present a pictorial depiction of the coefficient matrix arising from the difference equations and identify large non-zero blocks.

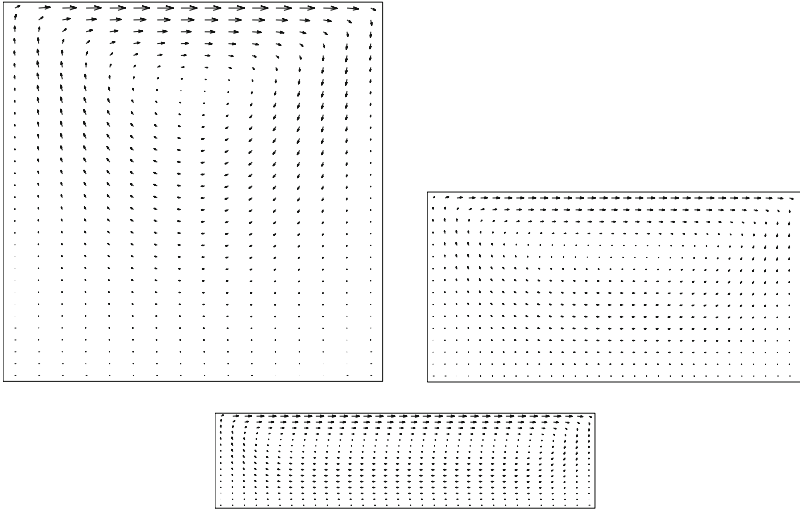


Figure 8.8.2 Velocity vector fields of two-dimensional Stokes flow in cavities with different aspect ratios driven by a sliding lid computed on a staggered grid using the FDLIB code *cvt_stag*.

(b) Verify that the coefficient matrix of the linear system is singular.

8.8.2 Pressure distribution

Modify the graphics portion of code *cvt_stag* to visualize the pressure field. Present and discuss contour plots of the pressure field for flow in a square cavity.

Low-Reynolds-number flow

- 9.1 Flow in narrow channels**
- 9.2 Film flow on a horizontal or inclined wall**
- 9.3 Multi-film flow on a horizontal or inclined wall**
- 9.4 Two-layer channel flow**
- 9.5 Flow due to the motion of a sphere**
- 9.6 Point forces and point sources in Stokes flow**
- 9.7 Two-dimensional Stokes flow**
- 9.8 Local solutions**

Newton's second law of motion stipulates that the rate of change of momentum of a fluid parcel must be balanced by the body force exerted over the parcel volume and by the surface force exerted on the parcel boundary. Under certain conditions, the rate of change of momentum of the parcel is small compared to the body and surface force, and can be neglected without introducing serious error. The flow is then governed by a balance between the body force and the surface force.

Physically, the fluid momentum is insignificant when the fluid viscosity is high, when the fluid density is small, when the velocity changes rapidly over a small distance yielding a sharp spatial gradient, or when the convection velocity of a fluid parcel is sufficiently small. The formal requirement for fluid inertia to be negligible is that a properly defined Reynolds number is sufficiently small. How small it should be depends on the particular problem under consideration.

In this chapter, we consider a family of flows occurring at low Reynolds numbers and discuss the solution of simplified systems of governing equations that arise by dropping the inertial terms in the Navier–Stokes equation. The simplification allows us to tackle successfully a multitude of physical and engineering problems and derive solutions by a host of analytical and numerical methods.

9.1 Flow in a narrow channel

We begin by considering steady, nearly unidirectional flow in a two-dimensional channel confined between a gently sloped upper wall and a perfectly flat lower wall, as illustrated in [Figure 9.1.1](#). The flow is driven by the translation of the upper wall parallel to itself

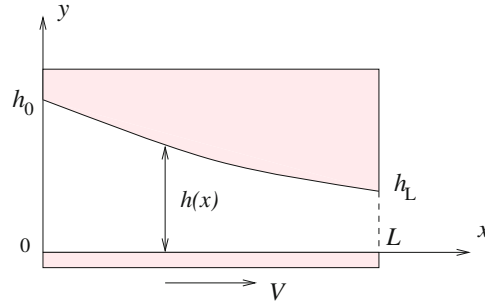


Figure 9.1.1 Lubrication flow in a slider bearing with a flat lower wall and a curved upper wall.

with velocity V , and possibly by a pressure drop imposed across the length of the channel extending between $x = 0$ and L . In the Cartesian system of coordinates depicted in [Figure 9.1.1](#), the lower wall is located at $y = 0$ and the upper wall is located at $y = h(x)$. If the channel height were constant, we would obtain steady unidirectional flow in a channel with parallel walls discussed in [Section 7.1](#).

Our objective is to compute the velocity and pressure fields, and then evaluate the force exerted on the lower wall for an arbitrary upper wall profile.

9.1.1 Governing equations

The motion of the fluid is governed by the continuity equation,

$$\frac{\partial u_x}{\partial x} + \frac{\partial u_y}{\partial y} = 0, \quad (9.1.1)$$

and by the steady version of the Navier–Stokes equation for an incompressible fluid whose x and y components are

$$\rho \left(u_x \frac{\partial u_x}{\partial x} + u_y \frac{\partial u_x}{\partial y} \right) = -\frac{\partial p}{\partial x} + \mu \left(\frac{\partial^2 u_x}{\partial x^2} + \frac{\partial^2 u_x}{\partial y^2} \right) + \rho g_x, \quad (9.1.2)$$

and

$$\rho \left(u_x \frac{\partial u_y}{\partial x} + u_y \frac{\partial u_y}{\partial y} \right) = -\frac{\partial p}{\partial y} + \mu \left(\frac{\partial^2 u_y}{\partial x^2} + \frac{\partial^2 u_y}{\partial y^2} \right) + \rho g_y. \quad (9.1.3)$$

Our first task is to show that, under certain conditions, several terms in equations (9.1.2) and (9.1.3) are negligible compared to other terms and can be discarded, yielding a simplified system of governing equations, which are known as the equations of *lubrication flow*.

9.1.2 Scaling

We begin the analysis by considering the term $\partial u_x/\partial x$ on the left-hand side of (9.1.2). If the upper wall were perfectly flat and parallel to the lower wall, the flow would be unidirectional and this term would be identically zero.

More generally, suppose that $U_x(x_1)$ is the maximum of the magnitude of the x velocity component at a particular location, $x = x_1$, and $U_x(x_2)$ is the corresponding maximum at another location, $x = x_2$, where the maximum is defined with respect to y . Common sense suggests that the magnitude of the term $\partial u_x/\partial x$ will be comparable to the ratio $[U_x(x_2) - U_x(x_1)]/(x_2 - x_1)$.

Now we identify the distance $x_2 - x_1$ with the length necessary for the difference $U_x(x_2) - U_x(x_1)$ to become comparable to $U_x(x_1)$, and scale the partial derivative $\partial u_x/\partial x$ with the ratio $U_x(x_1)/(x_2 - x_1)$. If the upper wall were perfectly flat and parallel to the lower wall, the distance $x_2 - x_1$ would be infinite and this ratio would vanish.

Similar arguments can be made to show that the term $\partial u_x/\partial y$ evaluated at $x = x_1$ scales with $U_x(x_1)/h(x_1)$, the term $\partial^2 u_x/\partial x^2$ evaluated at $x = x_1$ scales with $U_x(x_1)/(x_2 - x_1)^2$, and the term $\partial^2 u_x/\partial y^2$ evaluated at $x = x_1$ scales with $U_x(x_1)/h^2(x_1)$.

Continuity equation

Next, we consider the continuity equation (9.1.1) and scale the partial derivative $\partial u_y/\partial y$ evaluated at $x = x_1$ with $U_y(x_1)/h(x_1)$, where $U_y(x_1)$ is the maximum of the magnitude of the y velocity component at $x = x_1$. The continuity equation requires that the magnitude of $\partial u_y/\partial y$ is comparable to the magnitude of $\partial u_x/\partial x$, which was found to be of order $U_x(x_1)/(x_2 - x_1)$. This can be true only if $U_y(x_1)$ scales with $U_x(x_1) h(x_1)/(x_2 - x_1)$.

Relative magnitudes

Using the preceding arguments, we find the following:

- The ratio of the magnitude of the first term on the left-hand side of (9.1.2) to the magnitude of the penultimate term on the right-hand side is

$$\frac{\rho U_x(x_1) \frac{U_x(x_1)}{x_2 - x_1}}{\mu \frac{U_x(x_1)}{h^2(x_1)}} = \frac{\rho h(x_1) U_x(x_1)}{\mu} \frac{h(x_1)}{x_2 - x_1}. \tag{9.1.4}$$

- The ratio of the magnitude of the second term on the left-hand side of (9.1.2) to the magnitude of the penultimate term on the right-hand side is

$$\frac{\rho h(x_1) \frac{U_x(x_1)}{x_2 - x_1} \frac{U_x(x_1)}{h(x_1)}}{\mu \frac{U_x(x_1)}{h^2(x_1)}} = \frac{\rho h(x_1) U_x(x_1)}{\mu} \frac{h(x_1)}{x_2 - x_1}. \tag{9.1.5}$$

- The ratio of the magnitude of the second term on the right-hand side of (9.1.2) to the magnitude of the penultimate term on the right-hand side is

$$\frac{\mu \frac{U_x(x_1)}{(x_2 - x_1)^2}}{\mu \frac{U_x(x_1)}{h^2(x_1)}} = \left(\frac{h(x_1)}{x_2 - x_1} \right)^2. \quad (9.1.6)$$

9.1.3 Equations of lubrication flow

The first fraction on the right-hand sides of equations (9.1.4) and (9.1.5) is the local Reynolds number of the flow, defined with respect to the local channel height. If the magnitude of the local Reynolds number and the magnitude of the ratio $h(x_1)/(x_2 - x_1)$ are such that the right-hand sides of equations (9.1.4), (9.1.5), and (9.1.6) are much smaller than unity, the first and penultimate terms on the right-hand side of (9.1.2) dominate the x component of the equation of motion, leading us to the simplified equation of motion

$$0 = -\frac{\partial p}{\partial x} + \mu \frac{\partial^2 u_x}{\partial y^2} + \rho g_x, \quad (9.1.7)$$

which describes locally unidirectional flow.

Pressure field

Equation (9.1.7) requires that the magnitude of the term $-\partial p/\partial x + \rho g_x$ is comparable to the magnitude of the term $\mu \partial^2 u_x/\partial y^2$, which scales with $\mu U_x(x_1)/h^2(x_1)$.

Consideration of the individual terms on both sides of the y component of the equation of motion (9.1.3) shows that the term $-\partial p/\partial y + \rho g_y$ scales with $\mu U_x(x_1)/[(x_2 - x_1)h(x_1)]$. It is evident then that, when the ratio $h(x_1)/(x_2 - x_1)$ is small, non-hydrostatic pressure variations are negligible along the y axis. Accordingly, the y component of the equation of motion (9.1.3) reduces to

$$0 = -\frac{\partial p}{\partial y} + \rho g_y. \quad (9.1.8)$$

Differentiating this equation once with respect to x , we find that the axial pressure gradient, $\partial p/\partial x$, is independent of the lateral position, y , and depends only on the streamwise position, x .

Physically, the flow can be assumed to be locally unidirectional and parallel to the x axis. At every x station, the upper and lower walls appear to be parallel, separated by a distance that is equal to the local channel height, $h(x)$.

9.1.4 Lubrication flow in a slider bearing

As an application, we consider flow in the lubrication zone of a slider bearing, as illustrated in [Figure 9.1.2](#). The lower wall is horizontal while the the upper planar wall is sloped gently

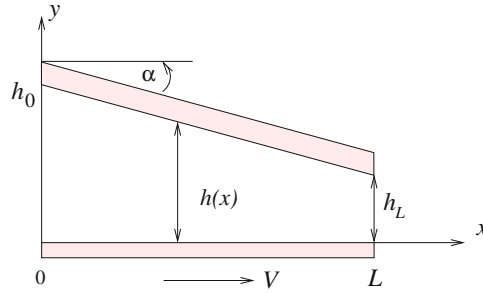


Figure 9.1.2 Lubrication flow in a slider bearing with a a flat lower wall and a planar inclined upper surface.

by an angle, α . The pressure is specified at both ends of the lubrication zone extending from $x = 0$ to L . If the fluid at an end of the lubrication zone is exposed to the atmosphere, then the pressure at that end is equal to the pressure of the atmosphere. Hydrostatic pressure variations in the y direction are assumed negligibly small.

Reviewing the scaling arguments discussed in Sections 9.1.2 and 9.1.3, we identify the distance $x_2 - x_1$ with the length of the lubrication zone, L . A special case arises when the two walls are parallel, as the distance $x_2 - x_1$ becomes infinite and no error is introduced by dropping the inertial terms in the equation of motion.

Velocity and flow rate

To simplify the analysis, we introduce the approximation $\tan \alpha \simeq \alpha$ and express the local clearance of the channel as

$$h(x) = h_0 - \alpha x, \tag{9.1.9}$$

where $h_0 \equiv h(x = 0)$ is the clearance of the channel at the beginning of the lubrication zone.

Next, we use the velocity profile derived in Section 7.1 for flow in a two-dimensional channel with parallel-sided walls, and find that the solution of the lubrication equation (9.1.7) is given by

$$u_x(x, y) = V \left(1 - \frac{y}{h(x)} \right) - \frac{1}{2\mu} y (h(x) - y) \frac{dp}{dx}. \tag{9.1.10}$$

The position-dependent streamwise pressure gradient, $(dp/dx)(x)$, is an unknown that must be computed as part of the solution. The local flow rate along the channel corresponding to the velocity profile (9.1.10) is

$$Q \equiv \int_0^{h(x)} u_x(x, y) dy = \frac{1}{2} V h(x) - \frac{1}{12} \frac{h^3(x)}{\mu} \frac{dp}{dx}. \tag{9.1.11}$$

Note the linear or cubic dependence on the local film thickness, $h(x)$, on the right-hand side.

A key observation is that, because in a stationary frame of reference the flow is steady, the flow rate, $Q(x)$, is not only constant in time, but also independent of the streamwise position, x . To confirm this assertion, we perform a mass balance over a control area confined between two cross-sections of the channel separated by an infinitesimal distance, and note that fluid neither enters nor escapes from the control volume through the bottom or top.

Computation of the pressure

Solving equation (9.1.11) for the axial pressure gradient and substituting $h(x) = h_0 - \alpha x$ for the channel height, we obtain

$$\frac{dp}{dx} = 6\mu \frac{V}{(h_0 - \alpha x)^2} - 12\mu \frac{Q}{(h_0 - \alpha x)^3}. \quad (9.1.12)$$

Integrating the pressure gradient with respect to x should produce a specified pressure drop across the lubrication zone. This mathematical condition reflects the physical environment under which the lubrication flow takes place. Performing the integration, we find that

$$\Delta p \equiv p_0 - p_L = - \int_0^L \frac{dp}{dx} dx = 6\mu \int_0^L \left(- \frac{V}{(h_0 - \alpha x)^2} + 2 \frac{Q}{(h_0 - \alpha x)^3} \right) dx, \quad (9.1.13)$$

where $p_0 = p(x = 0)$ and $p_L = p(x = L)$. Expression (9.1.13) relates the flow rate, Q , to the pressure at the two ends of the lubrication zone.

Vanishing pressure drop

If the two end pressures are equal, $\Delta p = 0$. Carrying out the integration on the right-hand side of (9.1.13), solving for Q and simplifying, we derive the expression

$$Q = V \frac{h_0 h_L}{h_0 + h_L}, \quad (9.1.14)$$

where $h_L = h_0 - \alpha L$ is the clearance of the channel at the end of the lubrication zone. If either h_0 or h_L is zero, in which case the channel is closed at one end, the flow rate is also zero.

Substituting the expression given in (9.1.14) for the flow rate into the right-hand side of (9.1.12), and carrying out the integration, we derive the desired pressure distribution,

$$p(x) = p_0 + \int_0^x \frac{dp}{d\xi} d\xi = p_0 + 6\mu V \frac{\alpha}{h_0 + h_L} \frac{1}{(h_0 - \alpha x)^2} x(L - x). \quad (9.1.15)$$

It is reassuring to confirm that the second term on the right-hand side of (9.1.15) vanishes at $x = L$, yielding the zero specified pressure drop.

It is convenient to introduce the dimensionless geometrical factor

$$\kappa \equiv \frac{h_0}{\alpha L}, \quad (9.1.16)$$

taking values in the range $(-\infty, 0)$ or $(1, \infty)$. A negative value corresponds to an upper wall that slopes upward, whereas a positive value corresponds to an upper wall that slopes downward, as shown in [Figure 9.1.2](#). Values of κ in the range $[0, 1]$ are prohibited by the requirement that the upper wall does not slope downward so much as to touch the lower wall before the end of the lubrication zone. When $\kappa = 1$, the two walls meet at $x = L$ and the channel is closed at the right end.

The y component of the hydrodynamic force exerted on the upper sloped surface can be approximated with the integral

$$F_y = \int_0^L p(x) \, dx. \tag{9.1.17}$$

Substituting the pressure distribution (9.1.15) and carrying out the integration, we obtain

$$F_y = p_0 L + 6\mu V \frac{L^2}{h_0^2} \kappa^2 \left(\ln \frac{h_0}{h_L} - 2 \frac{h_0 - h_L}{h_0 + h_L} \right). \tag{9.1.18}$$

We note the divergence of the logarithmic term for zero end-point channel height.

We have derived expressions for the flow rate, pressure distribution, and normal force given, respectively, by equations (9.1.14), (9.1.15), and (9.1.18). The derivations of these expressions concludes the main goal of our analysis.

Lift coefficient

To interpret the results in physical terms, we restate expression (9.1.18) as

$$F_y = p_0 L + 6\mu V \left(\frac{L}{h_0} \right)^2 G(\kappa), \tag{9.1.19}$$

where the function $G(\kappa)$, expressing the hydrodynamic lift or load force, is given by

$$G(\kappa) \equiv \kappa^2 \ln \frac{\kappa}{\kappa - 1} - 2 \frac{\kappa^2}{2\kappa - 1}. \tag{9.1.20}$$

A graph of $G(\kappa)$ in its domain of definition is shown in [Figure 9.1.3](#).

The results show that the lubrication force is positive when the lower wall moves toward the minimum gap, and negative when the lower wall moves towards the maximum gap. In the first case, the lift force will be able to balance the weight of an overlying object whose lower surface is represented by the inclined plane, provided that κ is sufficiently close to unity. In the second case, the lubrication force pulls the object toward the plane wall, closing the gap and choking the flow.

9.1.5 Flow in a wavy channel

The preceding analysis can be extended in a straightforward fashion to arbitrary channel geometries. A fundamental assumption is that the conditions for the right-hand sides of

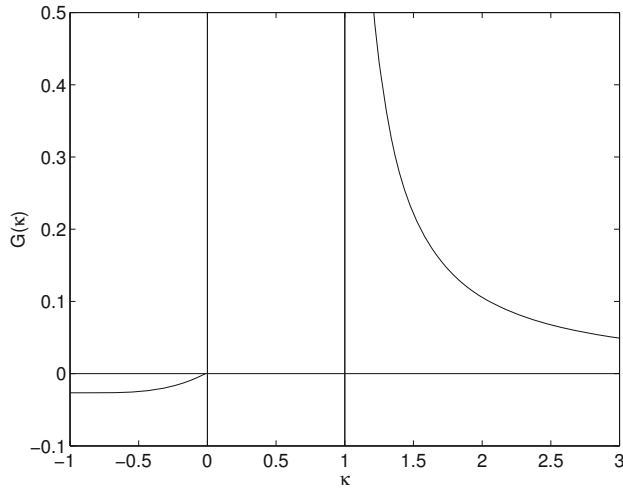


Figure 9.1.3 Graph of the function $G(\kappa)$ expressing the hydrodynamic lift force exerted on the inclined plane shown in Figure 9.1.2.

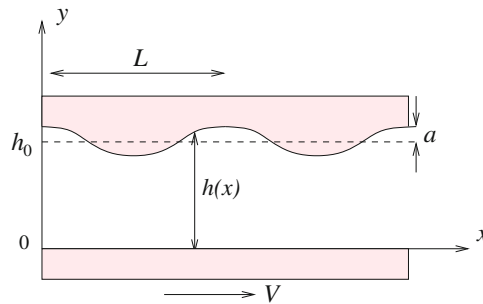


Figure 9.1.4 Lubrication flow in a furrowed channel confined between a translating plane wall and a stationary wavy wall.

(9.1.4)–(9.1.6) to be small are satisfied. This means that the local Reynolds number and the ratio $h(x_1)/(x_2 - x_1)$ must both be small.

As an example, we consider flow in a periodic channel confined between a plane and a wavy wall, as illustrated in Figure 9.1.4. The local channel height is described by the equation

$$h(x) = h_0 + a \cos kx, \tag{9.1.21}$$

where h_0 is the average channel height, L is the period, $k = 2\pi/L$ is the wave number, and a is the amplitude of the corrugations. The streamwise velocity and flow rate are described by equations (9.1.10) and (9.1.11), where $h(x)$ given in (9.1.21).

The counterpart of equation (9.1.12) is

$$\frac{dp}{dx} = 6\mu \frac{V}{(h_0 + a \cos kx)^2} - 12\mu \frac{Q}{(h_0 + a \cos kx)^3}. \quad (9.1.22)$$

The pressure drop over one period is

$$\Delta p \equiv p_0 - p_L = - \int_0^L \frac{dp}{dx} dx, \quad (9.1.23)$$

yielding

$$\Delta p = 6\mu \int_0^L \left(- \frac{V}{(h_0 + a \cos kx)^2} + 2 \frac{Q}{(h_0 + a \cos kx)^3} \right) dx. \quad (9.1.24)$$

Solving for Q , we obtain

$$Q = \frac{1}{2\mathcal{J}_3} \left(\frac{\Delta p}{6\mu} + V\mathcal{J}_2 \right), \quad (9.1.25)$$

where

$$\mathcal{J}_m = \int_0^L \frac{dx}{(h_0 + a \cos kx)^m}. \quad (9.1.26)$$

We have derived an expression for the flow rate in terms of the specified wall velocity and pressure drop.

Numerical integration

The definite integral in (9.1.26) is best computed by numerical methods. Interestingly, because the integrand is periodic in x , the best results are obtained by using the simplest algorithm of numerical integration expressed by the trapezoidal rule. The method involves dividing the integration domain, $(0, L)$, into N intervals of equal length, $\Delta x = L/N$, and introducing the approximation

$$\mathcal{J}_m \simeq \Delta x \sum_{i=1}^N \frac{1}{(h_0 + a \cos kx_i)^m}, \quad (9.1.27)$$

where $x_i = (i - 1)\Delta x$ are the interval end points. The Euler–Maclaurin theorem ensures that, as the number of divisions increases, the difference between the left- and right-hand side of (9.1.27), defined as the numerical error, decreases faster than any power of $1/N$, which allows for rapid convergence.

Once the flow rate has been found, the result can be substituted into the right-hand side of (9.1.24), and the expression thus obtained can be integrated by analytical or numerical methods to yield the pressure distribution along the channel. The velocity then follows from (9.1.10).

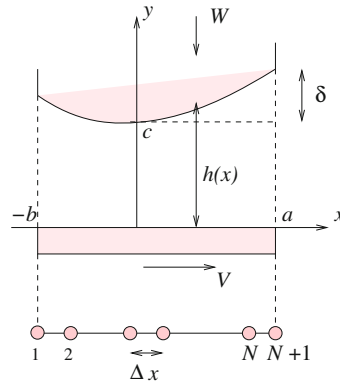


Figure 9.1.5 A two-dimensional body presses against a sliding wall under the influence of its weight or another normal force. The lubrication force developing between the body and the wall lifts the body away from the wall.

9.1.6 Dynamic lifting

A generalization of the lubrication analysis allows us to develop a method of simulating the lateral motion of a two-dimensional body pressing against a horizontal wall that translates along the x axis with velocity V , as illustrated in Figure 9.1.5. The clearance between the body and the translating wall is filled with a lubricating fluid. This configuration is a two-dimensional model of the flow between a piston ring pressing against the cylinder of a combustion chamber in an internal combustion engine of a vehicle, such as the last American sedan.

In the configuration shown in Figure 9.1.5, the origin of the x axis is set at the point of minimum clearance. Flow in the lubrication zone, extending from $x = -b$ to a , generates a pressure field. The associated lift force causes the body to move along the y axis with velocity

$$V_B = \frac{dc}{dt}, \quad (9.1.28)$$

where c is the minimum film thickness defined as the minimum clearance between the body and the translating wall. Our objective is to compute the evolution of the function $c(t)$ from a specified initial state. Hydrostatic pressure variations in the y direction are assumed to be negligibly small.

Governing equations

A mass balance for the lubricating fluid requires that

$$\frac{dc}{dt} = -\frac{\partial Q}{\partial x}. \quad (9.1.29)$$

Evaluating the flow rate, $Q(x, t)$, from the right-hand side of (9.1.11), and rearranging, we

derive a partial-differential equation for the pressure,

$$\frac{\partial}{\partial x} \left(\frac{h^3}{\mu} \frac{\partial p}{\partial x} \right) = 6V \frac{\partial h}{\partial x} + 12 \frac{dc}{dt}, \quad (9.1.30)$$

subject to an *a priori* unknown velocity dc/dt , which is to be solved subject to the specified, possibly time-dependent, boundary condition

$$p(x = -b) = p_{\text{left}}(t), \quad p(x = a) = p_{\text{right}}(t), \quad (9.1.31)$$

where $p_{\text{left}}(t)$ and $p_{\text{right}}(t)$ are two specified functions.

The vertical velocity of the body, V_B , is determined by a balance between the weight of the body, W , and the lubrication lift force due to the pressure,

$$\int_{-b}^a p(x, t) dx = W \quad (9.1.32)$$

at any instant.

Numerical method

The solution can be computed using the following algorithm:

1. Solve the following redacted version of equation (9.1.30) for a first modular pressure function, $\pi_1(x)$,

$$\frac{\partial}{\partial x} \left(\frac{h^3}{\mu} \frac{\partial \pi_1}{\partial x} \right) = 6V \frac{\partial h}{\partial x}, \quad (9.1.33)$$

subject to the required boundary conditions (9.1.31).

2. Solve the following redacted version of equation (9.1.30) for a second modular pressure function, $\pi_2(x)$,

$$\frac{\partial}{\partial x} \left(\frac{h^3}{\mu} \frac{\partial \pi_2}{\partial x} \right) = 12, \quad (9.1.34)$$

subject to the homogeneous boundary conditions $p(x = -b) = 0$ and $p(x = a) = 0$.

3. Set

$$p(x) = \pi_1(x) + \frac{dc}{dt} \pi_2(x). \quad (9.1.35)$$

Straightforward substitution shows that the pressure distribution (9.1.35) satisfies the governing equation (9.1.30) and conforms with the pressure boundary conditions at both ends.

4. Substitute the pressure distribution (9.1.35) into (9.1.32) to obtain

$$\int_{-b}^a \pi_1(x) dx + \frac{dc}{dt} \int_{-b}^a \pi_2(x) dx = W, \quad (9.1.36)$$

and carry out the integration to extract dc/dt .

5. Having evaluated dc/dt , update the minimum clearance, c , over a small time step, Δt .
6. Return to Step 1 and repeat the calculations for another time step.

Finite-difference solution for the pressure

A finite-difference method can be implemented for computing the modular pressure distributions, π_1 and π_2 , in the lubrication zone. In the numerical implementation, the lubrication zone is divided into N intervals separated by $N + 1$ nodes, x_i , as shown in Figure 9.1.5. The derivatives with respect to x in equations (9.1.33) and (9.1.34) are approximated with finite differences, yielding tridiagonal systems of algebraic equations for the nodal pressures with the same coefficient matrix.

For example, with reference to equation (9.1.33), we define for convenience

$$\mathcal{F}(x) \equiv \frac{\partial}{\partial x} \left(\frac{h^3}{\mu} \frac{\partial \pi_1}{\partial x} \right) = \frac{\partial}{\partial x} \left(\frac{h^3}{\mu} \right) \frac{\partial \pi_1}{\partial x} + \frac{h^3}{\mu} \frac{\partial^2 \pi_1}{\partial x^2}, \quad (9.1.37)$$

and use central differences to approximate

$$\mathcal{F}(x_i) \simeq \frac{\partial}{\partial x} \left(\frac{h^3}{\mu} \right)_i \frac{(\pi_1)_{i+1} - (\pi_1)_{i-1}}{2\Delta x} + \frac{h_i^3}{\mu} \frac{(\pi_1)_{i+1} - 2(\pi_1)_i - (\pi_1)_{i-1}}{\Delta x^2} \quad (9.1.38)$$

at the i th interior node for $i = 2, \dots, N$, where $(\pi_1)_1 = p_{\text{left}}$, $(\pi_1)_{N+1} = p_{\text{right}}$, and $\Delta x = (a + b)/N$. Enforcing equation (9.1.33) at the i th node provides us with the difference equation

$$c_i (\pi_1)_{i-1} + a_i (\pi_1)_i + b_i (\pi_1)_{i+1} = 6V \Delta x^2 \left(\frac{\partial h}{\partial x} \right)_i, \quad (9.1.39)$$

where

$$c_i = \frac{h_i^3}{\mu} - \frac{\Delta x}{2} \frac{\partial}{\partial x} \left(\frac{h^3}{\mu} \right)_i, \quad a_i = -2 \frac{h_i^3}{\mu}, \quad b_i = \frac{h_i^3}{\mu} + \frac{\Delta x}{2} \frac{\partial}{\partial x} \left(\frac{h^3}{\mu} \right)_i, \quad (9.1.40)$$

subject to the definition $h_i \equiv h(x_i)$. The solution can be found using the Thomas algorithm discussed in Section 8.2.4.

The following function entitled *bear_2d_press*, located in directory *bear_2d* inside directory *05_lub* of **FDLIB**, generates the tridiagonal systems of equations and computes the modular pressure distributions π_1 and π_2 :

```

function [pi1,pi2] = bear_2d_pressure ...
...
    (visc ...
    ,x ...
    ,h ...
    ,dhdX ...
    ,Dx ...
    ,V ...
    ,N ...
    ,pleft,prite ...
    )

%=====
% Solve the lubrication equation for the pressure
% using a finite-difference method
%
% Solutions are generated for
% longitudinal motion (press1)
% and normal motion (press2)
%
% x(i): grid nodes
% h(i): gap
% visc: viscosity
% pi1: left-end pressure
% pi2: right-end pressure
% act, btr, ctr: tridiagonal entries
% rhs: right-hand side
% sln: solution for the pressure
%=====

%---
% prepare
%---

Dxh = 0.5*Dx;
Dx2 = 2.0*Dx;
Dxs = Dx^2;

%---
% auxiliary
%---

for i=1:N+1
    q(i) = h(i)^3/visc;
end

dqdx(1) = (q(2)-q(1))/Dx; % forward difference

for i=2:N

```

```

    dqdx(i) = (q(i+1)-q(i-1))/Dx2; % central difference
end

dqdx(N+1) = (q(N+1)-q(N))/Dx; % backward difference

%---
% compute a particular solution
% with exact boundary conditions (pleft and prite)
%
% act, btr, ctr are the tridiagonal entries
% of the coefficient matrix
%---

factor = 6.0*V*Dxs;

atr(1) = -2.0*q(2);
tmp = dqdx(2)*Dxh;
btr(1) = q(2)+tmp;
rhs(1) = factor*dhdx(2) - pleft*(q(2)-tmp);

for i=3:N-1
    atr(i-1) = -2.0*q(i);
    tmp = dqdx(i)*Dxh;
    btr(i-1) = q(i)+tmp;
    ctr(i-1) = q(i)-tmp;
    rhs(i-1) = factor*dhdx(i);
end

atr(N-1) = -2.0*q(N);
ctr(N-1) = q(N)-tmp;
rhs(N-1) = factor*dhdx(N)-prite*(q(N)+tmp);

%---
% solve N-1 equations by the Thomas algorithm
%---

sln = thomas ...
...
    (N-1 ...
    ,atr,btr,ctr ...
    ,rhs ...
    );

pi(1) = pleft; % end node
pi(N+1) = prite; % end node

for i=1:N-1
    pi(i+1) = sln(i);
end

```

```

%---
% compute a homogeneous solution with dcdt=1.0
% and homogeneous boundary conditions
%---

cns = 12.0*Dxs;

for i=1:N-1
    rhs(i) = cns;
end

%---
% solve N-1 equations with the new rhs
%---

sln = thomas ...
...
(N-1 ...
,atr,btr,ctr ...
,rhs ...
);

pi2(1) = 0.0; % end node
pi2(N+1) = 0.0; % end node

for i=1:N-1
    pi2(i+1) = sln(i);
end

%---
% Done
%---

return

```

The following code entitled *bear_2d*, located in directory *05_lub* of *FDLIB*, performs the simulation

```

%---
% parameters
%---

a = 0.25; % lubrication zone
b = 0.75; % lubrication zone
delta = 0.05; % parabolicity delta
c = 0.01; % initial minimum film thickness c
pleft = 0.0; % pressure at left end

```

```

prite = -50.0; % pressure at right end
visc = 1.0; % viscosity
Wload = 20.0; % normal load
V = 5.0; % velocity of translation V
Dt = 0.020; % time step
N = 2*2*32; % discretization level
Nstep = 100; % number of time steps

%---
% prepare
%---

Dx = (a+b)/N;
Dx2 = 2.0*Dx;

%---
% prepare to plot
%---

figure(1)
hold on
xlabel('x','fontsize',15)
ylabel('pressure','fontsize',15)
set(gca,'fontsize',15)
box on
axis([-b a -4000 4000])

%-----
% Define nodes
% extending from x = -b to a
%-----

for i=1:N+1
    x(i) = -b+(i-1.0)*Dx;
    h(i) = c+delta*(x(i)/a)^2;
end

%-----
% Compute dh/dx at interior nodes
% using central differences
%-----

for i=2:N
    dhdx(i) = (h(i+1)-h(i-1))/Dx2;
end

%=====
for Istep=1:Nstep % time stepping
%=====

```



```

time(Istep) = (Istep-1)*Dt;
gap(Istep) = c; % c for plotting

%---
% solve for the pressures
%----

[pi1,pi2] = bear_2d_pressure ...
...
    (visc ...
    ,x ...
    ,h ...
    ,dhdx ...
    ,Dx ...
    ,V ...
    ,N ...
    ,pleft,prite ...
    );

%-----
% Integrate the pressure by the trapezoidal
% rule to obtain the normal force exerted on the body
%-----

F1 = 0.5*(pi1(1)+pi1(N+1));
F2 = 0.5*(pi2(1)+pi1(N+1));

for i=2:N
    F1 = F1 + pi1(i);
    F2 = F2 + pi2(i);
end

F1 = F1*Dx;
F2 = F2*Dx;

%---
% Compute dc/dt to balance the load
% using the equation:
%
% F1 + F2 * dcdt = Wload
%---

dcdt = (Wload-F1)/F2;

%---
% recover the physical pressure;
%---

```

```

for i=1:N+1
    press(i) = pi1(i) + dcdt*pi2(i);
end

figure(1)

if(Istep==1)
    plot(x,press,'r.-')
else
    plot(x,press,'k-')
end

%---
% advance c and update the profile h(i)
%---

dc = dcdt*Dt
c = c + dc;

for i=1:N+1
    h(i) = h(i)+dc;
end

%===
end      % of time stepping
%===

figure(2)
hold on
plot(time,gap,'k')
xlabel('time','fontsize',15)
ylabel('c','fontsize',15)
set(gca,'fontsize',15)
box on

```

Results of numerical simulations for the conditions implemented in the code are presented in [Figure 9.1.6](#).

PROBLEMS

9.1.1 Lubrication in a slider bearing

Confirm that the function $G(\kappa)$ defined in (9.1.20) satisfies the symmetry property

$$G\left(\kappa - \frac{1}{2}\right) = -G\left(\frac{1}{2} - \kappa\right). \quad (9.1.41)$$

Explain the underlying physical reason.

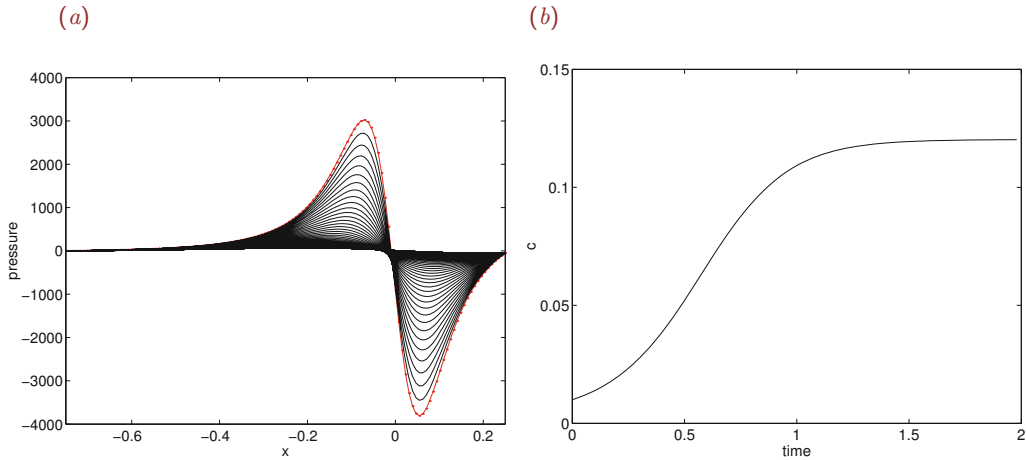


Figure 9.1.6 Evolution of (a) the pressure distribution and (b) the lubrication gap, computed by the numerical method implemented in the code *bear_2d*. The initial distribution is plotted by connected dots in (a).

9.1.2 Flow in a symmetric channel

Consider pressure-drive flow in a symmetric channel with stationary wavy walls located at

$$y = h(x) = \pm(h_0 + a \cos kx). \tag{9.1.42}$$

Derive an expression for the flow rate in terms of the pressure drop over one period.

9.1.3 Flow in a wavy channel

(a) Consider flow in a channel confined between a plane wall and a wavy wall, as discussed in the text, driven by an imposed pressure drop with $V = 0$. Prepare a graph of the dimensionless flow rate

$$\hat{Q} \equiv 12\mu LQ / (h_0^3 \Delta p) \tag{9.1.43}$$

against the scaled amplitude a/h_0 , and discuss its functional form. The integral on the right-hand side of (9.1.25) should be computed using the trapezoidal rule, as shown in equation (9.1.27).

(b) Repeat (a) for flow driven by boundary motion, $\Delta p = 0$. Prepare a graph of the dimensionless flow rate

$$\hat{Q} \equiv 2Q / (Vh_0) \tag{9.1.44}$$

against the scaled amplitude a/h_0 , and discuss its functional form.

9.1.4 Dynamical simulation of the lifting of a body due to lubrication

Run the code *bear_2d* for a set of conditions of your choice. Prepare a graph of the minimum film thickness, c , against time and discuss the results.

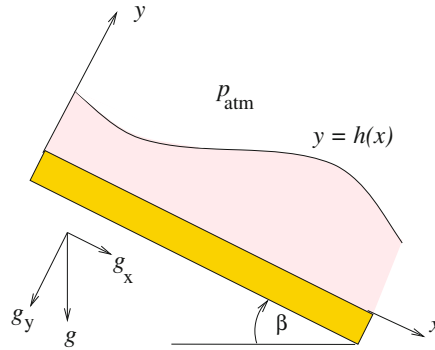


Figure 9.2.1 Illustration of a viscous film flowing down an inclined plane. The motion of the fluid is governed by the simplified equations of lubrication flow.

9.2 Film flow on a horizontal or inclined wall

One distinguishing feature of the flow in narrow channels discussed in Section 9.1 is that the velocity profile can be approximated locally with the parabolic profile of unidirectional flow in a channel confined between two parallel plane walls. An analogous simplification is possible in the case of a liquid film bounded by a free surface where the shear stress is required to vanish, discussed in this section, as well as in the case of a liquid layer bounded by a fluid interface where the shear stress is required to be continuous on either side, discussed in Section 9.3.

9.2.1 Thin-film flow

Consider a liquid film evolving on a horizontal wall or inclined plane, as illustrated in [Figure 9.2.1](#). In the inclined system of coordinates depicted in this figure, the wall is located at $y = 0$ and the free surface is located at $y = h(x, t)$. The components of the acceleration of gravity vector are given by

$$g_x = g \sin \theta_0, \quad g_y = -g \cos \theta_0, \quad (9.2.1)$$

where g is the magnitude of the acceleration of gravity and β is the inclination angle of the wall. If the wall is horizontal, $\beta = 0$; if the wall is vertical, $\beta = \pi/2$. The pressure above the film is assumed to be uniform and equal to the atmospheric pressure, p_{atm} . Our objective is to derive a differential equation governing the evolution of the film thickness, $h(x, t)$, from a specified initial profile.

Governing equations

Repeating the scaling arguments of Section 9.1 for lubrication flow, we find that, if the free surface is sloped gently, the magnitude of the streamwise derivative $\partial h / \partial x$ is uniformly small and the x and y components of the equation of motion reduce to the equations of lubrication flow stated in (9.1.7) and (9.1.8).

Integrating equation (9.1.8) with respect to y from an arbitrary location up to the location of the free surface, we obtain

$$p(x, y, t) = p_{\text{fs}} - \rho g_y (h - y), \quad (9.2.2)$$

where $p_{\text{fs}} \equiv p(x, y = h(t), t)$ is the pressure on the side of the liquid at the free surface.

The simple form of the lubrication equation (9.1.7) allows us to pretend that the flow is locally unidirectional, parallel to the x axis. Approximating the velocity profile across the uneven film with the Nusselt parabolic profile across a flat film bounded by a planar free surface, given in equation (7.2.5), we obtain

$$u_x(x, y, t) = \left(-\frac{\partial p}{\partial x} + \rho g_x \right) \frac{1}{2\mu} y(2h - y). \quad (9.2.3)$$

Note that the x dependence enters the problem formulation parametrically by way of the pressure gradient along the free surface, $\partial p/\partial x(x)$. The term enclosed by the first set of parentheses on the right-hand side of (9.2.3) incorporates the combined effects of gravity and streamwise pressure gradient due to surface tension, as will be discussed shortly.

The flow rate across a plane that is normal to the x axis is given by

$$Q(x, t) \equiv \int_0^{h(x,t)} u_x(x, y, t) dy. \quad (9.2.4)$$

Performing the integration, we obtain

$$Q(x, t) = \left(-\frac{\partial p}{\partial x} + \rho g_x \right) \frac{1}{3\mu} h^3(x, t). \quad (9.2.5)$$

Further analysis involves two key steps.

Evaluation of the pressure gradient

The normal stress undergoes a jump across the interface due to the surface tension, γ , according to the interfacial condition (4.3.4). In the case of locally unidirectional flow, the normal stress can be approximated with the negative of the pressure, yielding the pressure jump condition

$$p_{\text{fs}} = p_{\text{atm}} + \gamma \kappa, \quad (9.2.6)$$

where κ is the interfacial curvature. The curvature of a nearly planar free surface can be approximated with the linear form

$$\kappa(x) \simeq -\frac{\partial^2 h}{\partial x^2}. \quad (9.2.7)$$

Substituting (9.2.7) into (9.2.6) and the result into (9.2.2), we obtain an expression for the pressure distribution inside the film in terms of the film thickness,

$$p(x, y, t) \simeq p_{\text{atm}} - \rho g_y (h - y) - \gamma \frac{\partial^2 h}{\partial x^2}. \quad (9.2.8)$$

Substituting further (9.2.8) into the right-hand side of (9.2.5), we derive an expression for the flow rate in terms of the film thickness,

$$Q(x, t) = \frac{\rho}{3\mu} h^3 \left(g_x + g_y \frac{\partial h}{\partial x} + \frac{\gamma}{\rho} \frac{\partial^3 h}{\partial x^3} \right). \quad (9.2.9)$$

A net local flow normal to the wall occurs in the case of a sloped interface, $\partial h/\partial x \neq 0$.

Mass balance

Next, we perform a mass balance over a control area that is confined by (a) the wall, (b) two parallel planes that are normal to the inclined plane and are separated by an infinitesimal distance, (c) the corresponding section of the evolving free surface. The mass balances requires that the rate of volumetric accumulation in the control volume is equal to the difference in the flow rates into and out from the control volume. In differential form,

$$\frac{\partial h}{\partial t} = - \frac{\partial Q}{\partial x}. \quad (9.2.10)$$

The minus sign is justified by observing that, if $\partial Q/\partial x$ is negative, the rate of change, $\partial h/\partial t$, is positive, in agreement with physical intuition.

Evolution equation for the film thickness

To complete the mathematical formulation, we substitute the right-hand side of (9.2.9) into the right-hand side of (9.2.10), and thus obtain a first-order partial differential equation in time governing the evolution of the film thickness,

$$\frac{\partial h}{\partial t} + \frac{\rho}{3\mu} \frac{\partial}{\partial x} \left(h^3 \left(g_x + g_y \frac{\partial h}{\partial x} + \frac{\gamma}{\rho} \frac{\partial^3 h}{\partial x^3} \right) \right) = 0. \quad (9.2.11)$$

The products of the film thickness, h , and its spatial derivatives renders equation (9.2.11) a highly nonlinear partial differential equation. To compute the solution, an initial condition for $h(x, t = 0)$ at the origin of computational time must be specified.

Carrying out the differentiation with respect to x on the left-hand side, we find that the fourth derivative, $\partial^4 h/\partial x^4$, emerges from the term involving the surface tension. Since (9.2.11) is a fourth-order equation, two boundary conditions at each end of the solution domain, involving h , $\partial h/\partial x$, or $\partial^2 h/\partial x^2$, are required. If the film is periodic, the boundary conditions are replaced by periodicity conditions for the film thickness and its spatial derivatives.

In the absence of surface tension, $\gamma = 0$, we obtain a second-order differential equation. In that case, only one boundary condition at each end of the solution domain, involving h or $\partial h/\partial x$, is required. If the film is periodic, the boundary conditions are replaced by periodicity conditions.

Steady state

At steady state, $\partial h/\partial t = 0$, the shape of the free surface is described by the nonlinear ordinary differential equation

$$\frac{d}{dx} \left(h^3 \left(g_x + g_y \frac{dh}{dx} + \frac{\gamma}{\rho} \frac{d^3 h}{dx^3} \right) \right) = 0, \tag{9.2.12}$$

which admits the flat-film Nusselt solution derived in Section 7.2 for constant and uniform film thickness.

9.2.2 Numerical methods

A variety of numerical methods are available for solving the differential equation (9.2.11), including finite-difference, finite-volume, finite-element, and spectral methods. A finite-difference method will be discussed in Section 9.3 in the context of multi-layer film flow. To illustrate an alternative, in this section we discuss the implementation of an entry-level finite-volume method.

Finite-volume method

We are interested in computing the evolution of a film that is, and remains, spatially periodic with period L . To implement the finite-volume method, we divide the computational domain, extending from $x = 0$ to L , into N intervals of equal length $\Delta x = L/N$, also called finite volumes, as illustrated in Figure 9.2.2. The end points of the i th interval are denoted as

$$x_i^E = (i - 1)\Delta x \tag{9.2.13}$$

and the mid-point is denoted as

$$x_i^M = \left(i - \frac{1}{2}\right)\Delta x \tag{9.2.14}$$

for $i = 1, \dots, N$. Values of the film-thickness corresponding to x_i^E and x_i^M are denoted, respectively, by h_i^E and h_i^M .

A distinguishing feature of the finite-volume method is that the governing equation (9.2.11) is integrated over the length of each element to reduce the order of the highest derivative. Considering the i th element, we write

$$\int_{x_i^E}^{x_{i+1}^E} \frac{\partial h}{\partial t} dx + \frac{\rho}{3\mu} \left(h^3 \left(g_x + g_y \frac{\partial h}{\partial x} + \frac{\gamma}{\rho} \frac{\partial^3 h}{\partial x^3} \right) \right)_{x_{i+1}^E} - \frac{\rho}{3\mu} \left(h^3 \left(g_x + g_y \frac{\partial h}{\partial x} + \frac{\gamma}{\rho} \frac{\partial^3 h}{\partial x^3} \right) \right)_{x_i^E} = 0. \tag{9.2.15}$$

Using the mid-point rule to approximate the integral on the left-hand side of (9.2.15), we obtain

$$\int_{x_i^E}^{x_{i+1}^E} \frac{\partial h}{\partial t} dx \simeq \left(\frac{\partial h}{\partial t} \right)_{x_i^M} \Delta x. \tag{9.2.16}$$

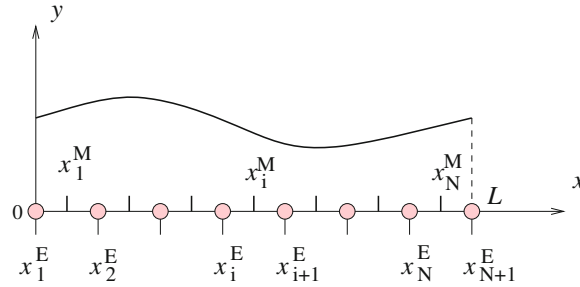


Figure 9.2.2 A finite-volume grid used to compute the evolution of a periodic film down an inclined plane.

Approximating further the time derivative on the right-hand side of (9.2.16) with a first-order forward-difference, we obtain

$$\left(\frac{\partial h}{\partial t}\right)_{x_i^M} \simeq \left(\frac{h(t + \Delta t) - h(t)}{\Delta t}\right)_{x_i^M}. \quad (9.2.17)$$

Next, we substitute (9.2.17) into (9.2.16) and the result into (9.2.15). Solving the emerging expression for $h(x_i^M, t + \Delta t)$, we obtain

$$\begin{aligned} h(x_i^M, t + \Delta t) = & h(x_i^M, t) - \frac{\Delta t}{\Delta x} \frac{\rho}{3\mu} \left(h^3(g_x + g_y \frac{\partial h}{\partial x} + \frac{\gamma}{\rho} \frac{\partial^3 h}{\partial x^3}) \right)_{x_{i+1}^E} \\ & + \frac{\Delta t}{\Delta x} \frac{\rho}{3\mu} \left(h^3(g_x + g_y \frac{\partial h}{\partial x} + \frac{\gamma}{\rho} \frac{\partial^3 h}{\partial x^3}) \right)_{x_i^E}, \end{aligned} \quad (9.2.18)$$

where the right-hand side is evaluated at t .

Finally, we express the values of the function h and its spatial derivatives at the element end points in terms of values at the mid-points using a combination of averaging and finite-difference approximations. For example, we write

$$\begin{aligned} h(x_{i+1}^E) & \simeq \frac{1}{2} [h(x_i^M) + h(x_{i+1}^M)], & \left(\frac{\partial h}{\partial x}\right)_{x_{i+1}^E} & \simeq \frac{h(x_{i+1}^M) - h(x_i^M)}{\Delta x}, \\ \left(\frac{\partial^3 h}{\partial x^3}\right)_{x_{i+1}^E} & \simeq \frac{h(x_{i+2}^M) - 3h(x_{i+1}^M) + 3h(x_i^M) - h(x_{i-1}^M)}{\Delta x^3}. \end{aligned} \quad (9.2.19)$$

The periodicity condition requires that

$$\begin{aligned} h(x_{-1}^M) & = h(x_{N-1}^M), & h(x_0^M) & = h(x_N^M), \\ h(x_{N+1}^M) & = h(x_1^M), & h(x_{N+2}^M) & = h(x_2^M). \end{aligned} \quad (9.2.20)$$

These relations allow us to evaluate of the right-hand sides of equation (9.2.19) at the ends of the computational domain extending over period.

The numerical procedure for simulating the evolution of the film from a given initial condition involves the following steps:

1. Specify the values of h_i^M at the origin of computational time.
2. Choose a time step, Δt .
3. Evaluate expressions (9.2.19) and (9.2.20) at the element end points.
4. Compute the right-hand side of (9.2.18), and thereby obtain updated values of the film thickness at the mid-points.
5. Return to Step 3 and repeat the calculation for another step.

The method requires a small time step, Δt , to prevent the onset of numerical instability. Implicit methods where the second and third terms on the right-hand side of (9.2.18) are evaluated at time $t + \Delta t$ overcome this limitation at the expense of having to solve a system of nonlinear equations.

PROBLEM

9.2.1 Finite-volume method

Write a computer code that uses the finite-volume method discussed in the text to simulate the evolution of a periodic film resting on a horizontal wall or flowing down an inclined plane. Compute the evolution of a film with an initially sinusoidal free surface resting on a horizontal wall. Investigate by numerical experimentation and discuss the effect of surface tension.

9.3 Multi-film flow on a horizontal or inclined wall

Extending the flow configuration discussed in Section 9.2, now we consider the more general case of an arbitrary number of N superimposed films flowing down an inclined plane, as illustrated in [Figure 9.3.1](#). For the multi-layer configuration to be stable, the density of the films must be constant or decrease with distance from the wall; otherwise, a gravitational instability due to unstable density stratification, known as the Rayleigh–Taylor instability, will arise. Multi-layer flow is encountered in the manufacturing of photographic films during the process of slide coating.

To generalize the discussion, we allow the inclined wall to exhibit small-amplitude periodic corrugations around a mean value. In the inclined system of coordinates defined in [Figure 9.3.1](#), the wall is described by a function, $y = y_w(x)$, and the interfaces are described by the N functions,

$$y = y_i(x, t) \tag{9.3.1}$$

for $i = 1, \dots, N$, where the N th interface is the free surface. The i th film is confined between the interfaces labeled $i - 1$ and i , with the understanding that the zeroth interface represents the wall.

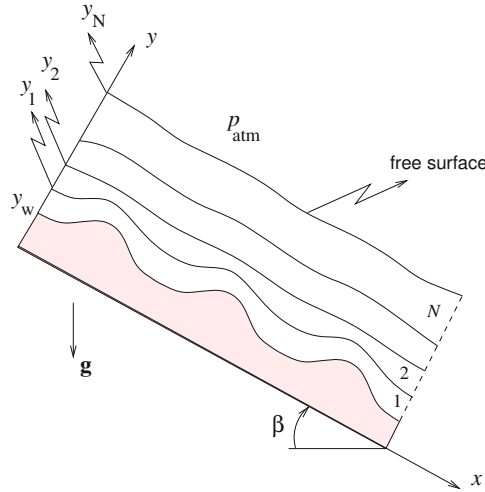


Figure 9.3.1 Illustration of multi-film flow down an inclined wall with periodic corrugations. The interface labels are shown in the left and the film labels are shown on the right. The top interface is a free surface.

Equations of lubrication flow

When the wall and interfaces are nearly flat, that is, $|\partial y_w / \partial x| < 1$ and $|\partial y_i / \partial x| < 1$ for $i = 0, \dots, N$, the flow inside each layer is locally nearly unidirectional along the x axis. The x and y components of the equation of motion simplify into the equations of lubrication flow,

$$\frac{\partial p^{(i)}}{\partial x} = \mu_i \frac{\partial^2 u_x^{(i)}}{\partial y^2} + \rho_i g_x, \quad \frac{\partial p^{(i)}}{\partial y} = \rho_i g_y \quad (9.3.2)$$

for $i = 1, \dots, N$, where μ_i and ρ_i is the viscosity and density of the i th layer, and $u_x^{(i)}(y)$ is the corresponding velocity profile. The no-slip boundary condition at the wall requires that

$$u_x^{(1)}(y = y_w) = 0. \quad (9.3.3)$$

Kinematic and dynamic interfacial conditions are required at the interfaces and at the free surface.

Interfacial conditions

Continuity of velocity across the interfaces requires that

$$u_x^{(i)}(y = y_i) = u_x^{(i+1)}(y = y_i) \quad (9.3.4)$$

for $i = 1, \dots, N - 1$.

Continuity of shear stress across the interfaces requires that

$$\mu_i \left(\frac{\partial u_x^{(i)}}{\partial y} \right)_{y=y_i} = \mu_{i+1} \left(\frac{\partial u_x^{(i+1)}}{\partial y} \right)_{y=y_i} \quad (9.3.5)$$

for $i = 1, \dots, N$, with the understanding that $\mu_{N+1} = 0$, which ensures that the shear stress vanishes at the free surface.

Balancing the normal stresses on either side of the i th interface involving the corresponding interfacial tension, γ_i , we obtain

$$(p^{(i)})_{y=y_i} = (p^{(i+1)})_{y=y_i} + \gamma_i \kappa_i \quad (9.3.6)$$

for $i = 1, \dots, N$, where κ_i is the curvature of the i th interface or free surface, with the understanding that $p^{(N+1)} = p_{\text{atm}}$.

The statement of the problem is now complete. A procedure for computing the solution will be outlined.

Pressure gradient

Our first task is to compute the pressure gradient on either side of each interface. We begin by integrating the second equation in (9.3.2) with respect to y from the i th interface up to an arbitrary point, and use the interfacial condition (9.3.6), finding

$$p^{(i)}(x, y) = (p^{(i+1)})_{y=y_i(x)}(x) + \gamma_i \kappa_i + \rho_i g_y [y - y_i(x)] \quad (9.3.7)$$

for $i = 1, \dots, N$. Note that the first term on the right-hand side depends explicitly and implicitly on x but is independent of y .

Next, we differentiate equation (9.3.7) with respect to x , and use the chain rule of differentiation to write

$$\frac{\partial p^{(i)}}{\partial x} = \frac{\partial p^{(i+1)}}{\partial x} + \frac{\partial p^{(i+1)}}{\partial y} \frac{\partial y_i}{\partial x} + \gamma_i \frac{\partial \kappa_i}{\partial x} - \rho_i g_y \frac{\partial y_i}{\partial x} \quad (9.3.8)$$

under the assumption of uniform surface tension, γ_i . Evaluating the derivative $\partial p^{(i+1)}/\partial y$ from the second equation in (9.3.2), we obtain

$$\frac{\partial p^{(i)}}{\partial x} = \frac{\partial p^{(i+1)}}{\partial x} + \gamma_i \frac{\partial \kappa_i}{\partial x} + (\rho_{i+1} - \rho_i) g_y \frac{\partial y_i}{\partial x}, \quad (9.3.9)$$

with the understanding that $\rho_{N+1} = 0$. Applying this equation at the interfaces numbered $i, i + 1, \dots, N$, and adding corresponding sides, we obtain

$$\frac{\partial p^{(i)}}{\partial x} = \sum_{j=i}^N \left(\gamma_j \frac{\partial \kappa_j}{\partial x} + (\rho_{j+1} - \rho_j) g_y \frac{\partial y_j}{\partial x} \right). \quad (9.3.10)$$

Finally, we introduce the familiar approximation for the curvature of the j th interface, $\kappa_j \simeq -\partial^2 y_j / \partial x^2$, and obtain

$$\frac{\partial p^{(i)}}{\partial x} = \sum_{j=i}^N \left(-\gamma_j \frac{\partial^3 y_j}{\partial x^3} + (\rho_{j+1} - \rho_j) g_y \frac{\partial y_j}{\partial x} \right) \quad (9.3.11)$$

for $i = 1, \dots, N$. The right-hand side of (9.3.11) can be evaluated from knowledge of the instantaneous interfacial profiles.

Velocity profiles

The velocity profile across the i th layer arises by integrating the first equation in (9.3.2) with respect to y , obtaining

$$u_x^{(i)} = A_i(x) + B_i(x) y - G_i(x) y^2, \quad (9.3.12)$$

where

$$G_i(x) \equiv \frac{1}{2\mu_i} \left(-\frac{\partial p^{(i)}}{\partial x} + \rho_i g_x \right). \quad (9.3.13)$$

To compute the unknown functions $A_i(x)$ and $B_i(x)$, we enforce the wall no-slip condition (9.3.3) to obtain

$$A_1(x) + B_1(x) y_w - G_1(x) y_w^2 = 0, \quad (9.3.14)$$

and the velocity continuity condition (9.3.4) to obtain

$$A_i(x) + B_i(x) y_i - G_i(x) y_i^2 = A_{i+1}(x) + B_{i+1}(x) y_i - G_{i+1}(x) y_i^2 \quad (9.3.15)$$

for $i = 1, \dots, N - 1$. Continuity of shear stress expressed by (9.3.5) requires that

$$B_N(x) = 2 G_N(x) y_N \quad (9.3.16)$$

and

$$\mu_i (B_i(x) - 2 G_i(x) y_i) = \mu_{i+1} (B_{i+1}(x) - 2 G_{i+1}(x) y_i) \quad (9.3.17)$$

for $i = 1, \dots, N - 1$. Rearranging (9.3.17), we obtain

$$B_i(x) = 2 G_i(x) y_i + \frac{\mu_{i+1}}{\mu_i} (B_{i+1}(x) - 2 G_{i+1}(x) y_i). \quad (9.3.18)$$

Equations (9.3.16) and (9.3.18) provide us with expressions for evaluating the coefficients $B_i(x)$. Once these expressions are available, $A_1(x)$ follows from (9.3.14) and the rest of the coefficients $A_i(x)$ follow from the velocity continuity condition (9.3.15). Note that the coefficients A_i are computed recursively from bottom to top, whereas the coefficients B_i are computed recursively from top to bottom.

Successive substitutions for B_i allow us to replace the recursion relation (9.3.18) with the explicit formula

$$B_i(x) = 2 G_i(x) y_i + 2 \sum_{k=i+1}^N \frac{\mu_k}{\mu_i} G_k(x) (y_k - y_{k-1}) \quad (9.3.19)$$

for $i = 1, \dots, N - 1$, subject to (9.3.16).

9.3.1 Evolution equations

The counterpart of the mass balance equation (9.2.10) for the i th film is

$$\frac{\partial h_i}{\partial t} = \frac{\partial(y_i - y_{i-1})}{\partial t} = \frac{\partial y_i}{\partial t} - \frac{\partial y_{i-1}}{\partial t} = - \frac{\partial Q_i}{\partial x}, \quad (9.3.20)$$

where h_i is the film thickness, and

$$Q_i(x, t) \equiv \int_{y_i}^{y_{i-1}} u^{(i)} dy \quad (9.3.21)$$

is the local flow rate in the i th film. Substituting the velocity profile and integrating, we obtain

$$Q_i(x, t) = A_i(x) (y_i - y_{i-1}) + \frac{1}{2} B_i(x) (y_i^2 - y_{i-1}^2) - \frac{1}{3} G_i(x) (y_i^3 - y_{i-1}^3) \quad (9.3.22)$$

for $i = 1, \dots, N$. Applying equation (9.3.20) for $i = 1, \dots, N$ and combining the expressions thus obtained, we derive the evolution equations

$$\frac{\partial y_i}{\partial t} = - \sum_{j=1}^i \frac{\partial Q_j}{\partial x} \quad (9.3.23)$$

for $i = 1, \dots, N$. Substituting equation (9.3.11) into (9.3.13), the result into (9.3.22), and the outcome into (9.3.23), we derive a system of fourth-order nonlinear partial differential equations governing the evolution of the $N - 1$ interfaces and free surface.

One layer

In the case of one layer, $N = 1$, and a plane wall located at $y_w = 0$, equations (9.3.16) and (9.3.14) yield $B_1(x) = 2 G_1(x) y_1$ and $A_1(x) = 0$. The evolution equation (9.3.23) then reduces to (9.2.11) for single-film flow.

Two layers

In the case of two layers, $N = 2$, and a plane wall located at $y_w = 0$, we find that

$$\begin{aligned} B_2(x) &= 2 G_2(x) y_2, & B_1(x) &= 2 G_1(x) y_1 + 2 \lambda_1 G_2(x) (y_2 - y_1), \\ A_1(x) &= 0, & A_2(x) &= G_1(x) y_1^2 + G_2(x) y_1 (2 \lambda_1 (y_2 - y_1) - 2 y_2 + y_1), \end{aligned} \quad (9.3.24)$$

where $\lambda_1 \equiv \mu_2/\mu_1$ is the viscosity ratio. Using (9.3.11) and (9.3.13), we obtain

$$G_2(x) = \frac{1}{2} \frac{\rho_2}{\mu_2} \left(g_x + g_y \frac{\partial y_2}{\partial x} + \frac{\gamma_2}{\rho_2} \frac{\partial^3 y_2}{\partial x^3} \right) \quad (9.3.25)$$

and

$$G_1(x) = \frac{1}{2} \frac{\rho_2}{\mu_2} \lambda_1 \left(\frac{1}{\beta_1} g_x + g_y \left(\frac{1}{\beta_1} - 1 \right) \frac{\partial y_1}{\partial x} + g_y \frac{\partial y_2}{\partial x} + \frac{\gamma_1}{\rho_2} \frac{\partial^3 y_1}{\partial x^3} + \frac{\gamma_2}{\rho_2} \frac{\partial^3 y_2}{\partial x^3} \right), \quad (9.3.26)$$

where $\beta_1 \equiv \rho_2/\rho_1$ is the density ratio. The evolution of the interfaces is governed by two coupled differential equations,

$$\frac{\partial y_1}{\partial t} = - \frac{\partial Q_1}{\partial x}, \quad \frac{\partial y_2}{\partial t} = - \frac{\partial Q_1}{\partial x} - \frac{\partial Q_2}{\partial x}, \quad (9.3.27)$$

subject to a specified initial condition.

9.3.2 Numerical methods

The solution of equation (9.3.23) for $i = 1, \dots, N$ can be found by a standard finite-difference method. In the numerical implementation, one period of the flow is covered by a uniform grid, and the spatial derivatives in the differential equations are approximated with finite differences at the grid nodes.

The following MATLAB function *films_pde*, located in directory *films* inside directory *05_lub* of **FDLIB**, evaluates the rates of evolution, $\partial y_i/\partial t$, for an arbitrary number of layers:

```
function dydt = films_pde ...
...
(NLR,NSG,Dx,wall,y,rho,mu,gamma,gx,gy,ICU)

%-----
% Compute the rate of change of y position
% of the interfaces:
% dy_i/dt, for i=1,...,NLR
%
% NLR: number of layers
% NSG: number of segments
% Dx: x finite-difference interval
% wall: wall profile
% y(i): position of the ith interface
% ICU = 1 for central differences
% ICU = 2 for backward differences
%-----

%---
% prepare
%---
```

```

Dx2 = 2.0*Dx;

%---
% compute derivatives
%---

for i=1:NLR % run over interfaces

%---
% first derivative
%---

y1(1,i) = (y(2,i)-y(NSG,i))/Dx2;
for k=2:NSG
    y1(k,i) = (y(k+1,i)-y(k-1,i))/Dx2;
end
y1(NSG+1,i) = y1(1,i);

%---
% second derivative
%---

y2(1,i) = (y1(2,i)-y1(NSG,i))/Dx2;
for k=2:NSG
    y2(k,i) = (y1(k+1,i)-y1(k-1,i))/Dx2;
end
y2(NSG+1,i) = y2(1,i);

%---
% third derivative
%---

y3(1,i) = (y2(2,i)-y2(NSG,i))/Dx2;
for k=2:NSG
    y3(k,i) = (y2(k+1,i)-y2(k-1,i))/Dx2;
end
y3(NSG+1,i) = y3(1,i);

%---
end
%---

%-----
% Compute the effective pressure drop G
%-----

for i=1:NLR % over interfaces
    for k=1:NSG % over points
        dpdx = 0.0;
    end
end

```

```

    for j=i:NLR
        dpdx = dpdx - gamma(j)*y3(k,j) ...
            + gy*(rho(j+1)-rho(j))*y1(k,j);
    end
    G(k,i) = 0.50*(-dpdx + rho(i)*gx)/mu(i);
end
end

%-----
% Compute the coefficients B
%-----

for k=1:NSG
    B(k,NLR) = 2.0*G(k,NLR)*y(k,NLR);
end

for i=NLR-1:-1:1
    for k=1:NSG
        B(k,i) = 2.0*G(k,i)*y(k,i) ...
            +mu(i+1)/mu(i)*(B(k,i+1)-2.0*G(k,i+1)*y(k,i));
    end
end

%-----
% Compute the coefficients A
%-----

for k=1:NSG
    A(k,1) = wall(k)*(wall(k)*G(k,1)-B(k,1));
end

for i=1:NLR-1
    for k=1:NSG
        A(k,i+1) = A(k,i)+(B(k,i)-B(k,i+1))*y(k,i) ...
            -(G(k,i)-G(k,i+1))*y(k,i)*y(k,i);
    end
end

%-----
% Compute the flow rates Q
%-----

for k=1:NSG
    Q(k,1) = A(k,1)*(y(k,1)-wall(k)) ...
        +0.5*B(k,1)*(y(k,1)*y(k,1)-wall(k)*wall(k));
        -G(k,1)*(y(k,1)^3-wall(k)^3)/3.0;
end
Q(NSG+1,1) = Q(1,1);

```



```

for i=2:NLR
  for k=1:NSG
    Q(k,i) = A(k,i)*(y(k,i)-y(k,i-1)) ...
    +0.5*B(k,i)*(y(k,i)*y(k,i)-y(k,i-1)*y(k,i-1)) ...
    -G(k,i)*(y(k,i)^3-y(k,i-1)^3)/3.0;
  end
  Q(NSG+1,i) = Q(1,i);
end

%---
% compute dQ/dx
%
% by central differences (ICU = 1)
% or upwind differences (ICU ne 1)
%---

%---
if(ICU==1) % central differences
%---

for i=1:NLR
  dQdx(1,i) = (Q(2,i)-Q(NSG,i))/Dx2;
  for k=2:NSG
    dQdx(k,i) = (Q(k+1,i)-Q(k-1,i))/Dx2;
  end
end

%---
else % backward differences
%---

for i=1:NLR
  dQdx(1,i) = (Q(1,i)-Q(NSG,i))/Dx;
  for k=2:NSG
    dQdx(k,i) = (Q(k,i)-Q(k-1,i))/Dx;
  end
end

%---
end
%---

%---
% finally compute dydt
%---

for i=1:NLR
  for k=1:NSG
    dydt(k,i) = 0.0;
  end
end

```

```

for j=1:i
    dydt(k,i) = dydt(k,i)-dQdx(k,j);
end
dydt(NSG+1,i) = dydt(1,i);
end
end

%---
% Done
%---

return

```

An explicit finite-difference method can be implemented by approximating the time derivative on the left-hand side of (9.3.23) at a grid point with a forward difference using a sufficiently small time step, Δt , and then advancing the position of the interfaces.

The method is implemented in following code entitled *films*, located in directory *05_lub* of **FDLIB**:

```

%---
% input data
%---

NLR = 2; % number of layers
L = 2.0; % wave length
Dt = 0.01; % time step
Nstep = 128*2*128; % number of steps
beta = 0.125*pi; % inclination angle
gac = 1.0; % acceleration of gravity
NSG = 2*16; % number of divisions (segments)
ICU = 2; % backward differences
ICU = 1; % central differences

mu(1) = 1.0; rho(1) = 1.0; gamma(1) = 0.000; % first layer
rho(2) = 0.5; mu(2) = 1.0; gamma(2) = 0.00; % second layer

%---
% prepare
%---

rho(NLR+1) = 0.0;
cs0 = cos(beta);
sn0 = sin(beta);
gx = gac*sn0;
gy = -gac*cs0;

ROT = [cs0,sn0;-sn0,cs0]; % rotation matrix

```

```

%---
% wall and initial profiles
%---

Dx = L/NSG;

for k=1:NSG+1
    x(k) = (k-1)*Dx;
    arg = 2*pi*x(k)/L;
    wall(k) = 0.0;
    y(k,1) = 0.2+0.1*cos(arg);
    if(NLR>=2)
        y(k,2) = 0.4+0.1*cos(arg);
    end
    if(NLR>=3)
        y(k,3) = 0.6+0.1*cos(arg);
    end
end

%-----
% time stepping
%-----

for step=1:Nstep

    dydt = films_pde ...
    ...
    (NLR,NSG,Dx,wall,y,rho,mu,gamma,gx,gy,ICU);

    y = y+dydt*dt;

%-----
% plotting
%-----

for k=1:NSG+1
    xx = ROT*[x(k) wall(k)]';
    xplot0(k) = xx(1)/L; yplot0(k) = xx(2)/L;
    xx = ROT*[x(k) y(k,1)]';
    xplot1(k) = xx(1)/L; yplot1(k) = xx(2)/L;
    if(NLR>=2)
        xx = ROT*[x(k) y(k,2)]';
        xplot2(k) = xx(1)/L; yplot2(k) = xx(2)/L;
    end
    if(NLR>=3)
        xx = ROT*[x(k) y(k,3)]';
        xplot3(k) = xx(1)/L; yplot3(k) = xx(2)/L;
    end
end
end

```

```

if(step==1)
    Handle0 = plot(xplot0,yplot0,'k');
    hold on
    Handle1 = plot(xplot1,yplot1,'r.-');
    if(NLR>=2)
        Handle2 = plot(xplot2,yplot2,'r.-');
    end
    if(NLR>=3)
        Handle3 = plot(xplot3,yplot3,'r.-');
    end
    xlabel('x/L','fontsize',15)
    ylabel('y/L','fontsize',15)
end

set(Handle0,'XData',xplot0,'YData',yplot0)
set(Handle1,'XData',xplot1,'YData',yplot1)
if(NLR>=2)
    set(Handle2,'XData',xplot2,'YData',yplot2)
end
if(NLR>=3)
    set(Handle3,'XData',xplot3,'YData',yplot3)
end
drawnow
end

```

A sequence of evolving profiles for a two-layer flow, $N = 2$, is shown in [Figure 9.3.2](#). The result confirm that the free surface and the interface flatten in time due to the combined action of gravity and surface tension.

PROBLEMS

9.3.1 *Two-layer film flow*

Consider a two-layer film flow with fluids of equal viscosity and density in the absence of interfacial tension, $\lambda_1 = 1$, $\beta_1 = 1$, and $\gamma_1 = 0$. Show that the second evolution equation in (9.3.27) reduces to (9.2.11) for single-film flow. Discuss the significance of the first evolution equation in (9.3.27).

9.3.2 *Multi-film flow*

Run the code *films* for a two-layer configuration of your choice on a horizontal or inclined wall. Investigate and discuss the significance of the interfacial tensions.

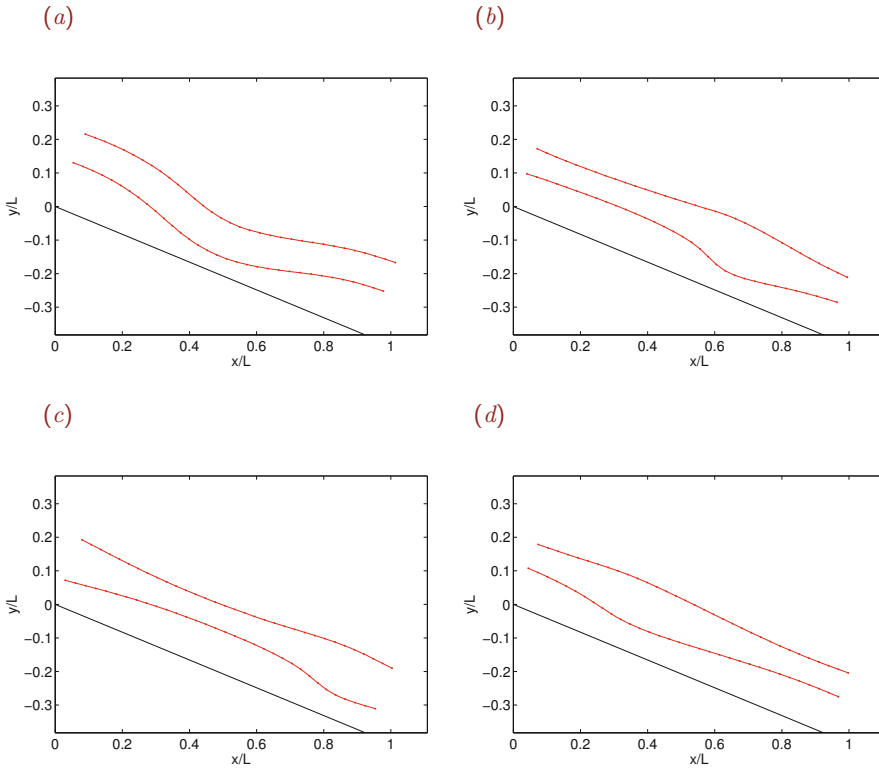


Figure 9.3.2 Snapshots of an evolving two-layer film down an inclined plane generated by code *films*. The interface and the free surface tend to flatten under the combined action of gravity and interfacial tensions.

9.4 Two-layer channel flow

Multi-layer channel flows are encountered in polymer co-extrusion and in the manufacturing of composite and laminated materials. In this section we study the flow of two superposed layers in a channel confined between two parallel plane walls separated by distance $2a$, as illustrated in Figure 9.4.1. The lower layer is labeled 1, and the upper layer is labeled 2. The flow is driven partly by the parallel translation of the lower or upper wall with velocity V_1 or V_2 , partly by a pressure gradient imposed along the x axis, and partly by the gravitational body force.

The velocity profile corresponding to steady unidirectional flow with a flat interface was discussed in Section 7.1.2. Our present goal is to derive an evolution equation for the layer thickness when the interface is gently sloped, also accounting for the presence of an insoluble surfactant causing variations in the surface tension, γ .

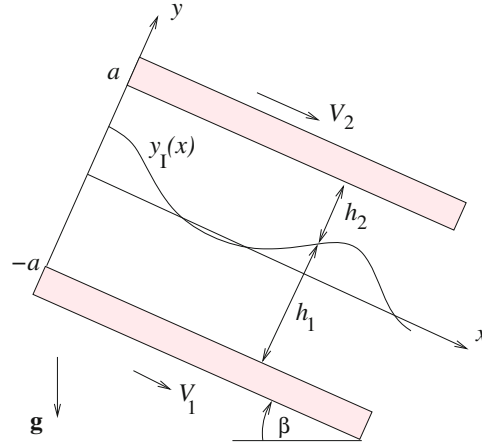


Figure 9.4.1 Illustration of flow of two layers in a channel confined between two parallel plane walls driven by gravity, boundary motion, or an imposed pressure gradient.

Equations of lubrication flow

We begin by assuming that the flow in each layer is governed by the simplified x and y components of the equation of motion arising from the assumptions of lubrication flow,

$$0 = -\frac{\partial p^{(1)}}{\partial x} + \mu_1 \frac{\partial^2 u_x^{(1)}}{\partial y^2} + \rho_1 g_x, \quad 0 = -\frac{\partial p^{(1)}}{\partial y} + \rho_1 g_y \tag{9.4.1}$$

for the lower layer, and

$$0 = -\frac{\partial p^{(2)}}{\partial x} + \mu_2 \frac{\partial^2 u_x^{(2)}}{\partial y^2} + \rho_2 g_x, \quad 0 = -\frac{\partial p^{(2)}}{\partial y} + \rho_2 g_y \tag{9.4.2}$$

for the upper layer. The components of the acceleration of gravity, g_x and g_y , are given by $g_x = g \sin \theta_0$ and $g_y = -g \cos \theta_0$. The y component of the equation of motion states that the pressure in each layer changes in the y direction, normal to the walls, only because of gravity according to the layer densities.

Velocity profiles

Next, we refer to the inclined coordinates defined in [Figure 9.4.1](#) and describe the position of the interface by the equation $y = y_I(x, t)$, where the walls are located at $y = \pm a$. Integrating the first equations in (9.4.1) and (9.4.2) twice with respect to y , subject to a constant streamwise pressure gradient, we obtain the parabolic velocity profile

$$u_x^{(1)}(y, t) = -\frac{1}{2\mu_1} \left(-\frac{\partial p^{(1)}}{\partial x} + \rho_1 g_x \right) (y - y_I)^2 + \xi_1 (y - y_I) + u_I \tag{9.4.3}$$

in the lower fluid, $-a < y < y_I(x)$, and

$$u_x^{(2)}(y, t) = -\frac{1}{2\mu_2} \left(-\frac{\partial p^{(2)}}{\partial x} + \rho_2 g_x \right) (y - y_I)^2 + \xi_2 (y - y_I) + u_I \quad (9.4.4)$$

in the upper fluid, $y_I(x) < y < a$, where u_I is the *a priori* unknown streamwise velocity at the position of the interface, and

$$\xi_1 \equiv \left(\frac{\partial u_x^{(1)}}{\partial y} \right)_{y=y_I}, \quad \xi_2 \equiv \left(\frac{\partial u_x^{(2)}}{\partial y} \right)_{y=y_I} \quad (9.4.5)$$

are *a priori* unknown shear rates evaluated on either side of the interface.

If the interface were flat and the surface tension were constant, u_I , ξ_1 , and ξ_2 would be given by expressions (7.1.38) and (7.1.39) without any approximation.

Interfacial shear rates

To compute the interfacial shear rates, we enforce the no-slip boundary condition at the upper and lower wall by requiring that

$$u_x^{(1)}(y = -a) = V_1, \quad u_x^{(2)}(y = a) = V_2. \quad (9.4.6)$$

Evaluating the velocity from (9.4.3) and (9.4.4) and solving for the shear rates, we obtain

$$\begin{aligned} \xi_1 &= -\frac{1}{2} \frac{h_1}{\mu_1} \left(-\frac{\partial p^{(1)}}{\partial x} + \rho_1 g_x \right) + \frac{u_I - V_1}{h_1}, \\ \xi_2 &= \frac{1}{2} \frac{h_2}{\mu_2} \left(-\frac{\partial p^{(2)}}{\partial x} + \rho_2 g_x \right) - \frac{u_I - V_2}{h_2}, \end{aligned} \quad (9.4.7)$$

where

$$h_1(x, t) = a + y_I(x, t), \quad h_2(x, t) = a - y_I(x, t) \quad (9.4.8)$$

are the local and instantaneous layer thicknesses.

In the case of a flat interface with uniform surface tension, the streamwise pressure gradients are equal and expressions (9.4.7) reduce to those given in (7.1.39) with $\partial p^{(1)}/\partial x = \partial p^{(2)}/\partial x = -\chi$.

Interfacial velocity

Next, we substitute the right-hand sides of equations (9.4.7) into the tangential interfacial stress balance

$$\mu_1 \xi_1 = \mu_2 \xi_2 + \frac{\partial \gamma}{\partial x}, \quad (9.4.9)$$

and solve for the interfacial velocity to obtain the expression

$$u_I = \frac{1}{\delta + \lambda} \left(\frac{1}{2} \frac{h_1 h_2}{\mu_1} \left(-\frac{\partial p^{(1)}}{\partial x} - \delta \frac{\partial p^{(2)}}{\partial x} + \rho_1 g_x (1 + \beta \delta) \right) + \delta V_1 + \lambda V_2 + \frac{h_2}{\mu_1} \frac{\partial \gamma}{\partial x} \right), \quad (9.4.10)$$

where γ is the surface tension,

$$\lambda \equiv \frac{\mu_2}{\mu_1}, \quad \alpha \equiv \frac{\rho_2}{\rho_1}, \quad \delta \equiv \frac{h_2}{h_1}. \quad (9.4.11)$$

In the case of a flat interface with uniform surface tension, the streamwise pressure gradients are equal. Consequently, expression (9.4.10) reduces to that given in (7.1.38) with $\partial p^{(1)}/\partial x = \partial p^{(2)}/\partial x = -\chi$.

Streamwise pressure field

The pressure undergoes a jump across the interface due to the surface tension, γ , so that

$$p^{(1)}(x, y = y_I) = p^{(2)}(x, y = y_I) + \gamma \kappa, \quad (9.4.12)$$

where κ is the interfacial curvature. Adopting the familiar approximation

$$\kappa(x) \simeq -\frac{\partial^2 y_I}{\partial x^2}, \quad (9.4.13)$$

and differentiating (9.4.12) with respect to x using the chain rule, we obtain

$$\frac{\partial p^{(1)}}{\partial x} + \frac{\partial p^{(1)}}{\partial y} \frac{\partial y_I}{\partial x} = \frac{\partial p^{(2)}}{\partial x} + \frac{\partial p^{(2)}}{\partial y} \frac{\partial y_I}{\partial x} - \frac{\partial \gamma}{\partial x} \frac{\partial^2 h}{\partial x^2} - \gamma \frac{\partial^3 h}{\partial x^3}, \quad (9.4.14)$$

where both sides are evaluated at the interface.

Now using the second equations in (9.4.1) and (9.4.2) to evaluate the derivative of the pressure with respect to y , we obtain

$$\frac{\partial p^{(1)}}{\partial x} + \rho_1 g_y \frac{\partial y_I}{\partial x} = \frac{\partial p^{(2)}}{\partial x} + \rho_2 g_y \frac{\partial y_I}{\partial x} - \frac{\partial \gamma}{\partial x} \frac{\partial^2 h}{\partial x^2} - \gamma \frac{\partial^3 h}{\partial x^3}. \quad (9.4.15)$$

Rearranging, we obtain

$$\frac{\partial p^{(2)}}{\partial x} = \frac{\partial p^{(1)}}{\partial x} + (\rho_1 - \rho_2) g_y \frac{\partial y_I}{\partial x} + \frac{\partial \gamma}{\partial x} \frac{\partial^2 h}{\partial x^2} + \gamma \frac{\partial^3 h}{\partial x^3}. \quad (9.4.16)$$

Substituting this expression into (9.4.10) to eliminate $\partial p^{(2)}/\partial x$ in favor of $\partial p^{(1)}/\partial x$, we derive an alternative expression for the interfacial velocity,

$$u_I = \frac{1}{\delta + \lambda} \left(\frac{1}{2} \frac{h_1 h_2}{\mu_1} \left(- (1 + \delta) \frac{\partial p^{(1)}}{\partial x} - \delta \left[(\rho_1 - \rho_2) g_y \frac{\partial y_I}{\partial x} + \gamma \frac{\partial^3 h}{\partial x^3} + \frac{\partial \gamma}{\partial x} \frac{\partial^2 h}{\partial x^2} \right] + \rho_1 g_x (1 + \alpha \delta) \right) + \delta V_1 + \lambda V_2 + \frac{h_2}{\mu_1} \frac{\partial \gamma}{\partial x} \right), \quad (9.4.17)$$

involving the pressure gradient in the lower layer and the instantaneous shape of the interface.

Flow rates and mass conservation

We proceed by integrating the velocity profiles (9.4.3) and (9.4.4) with respect to y over their respective domain of definition, and thereby derive expressions for the streamwise flow rate in the lower layer,

$$Q_1 \equiv \int_{-h}^{y_1} u_x^{(1)} dy = -\frac{1}{6} \frac{h_1^3}{\mu_1} \left(-\frac{\partial p^{(1)}}{\partial x} + \rho_1 g_x \right) - \frac{1}{2} \xi_1 h_1^2 + u_I h_1, \quad (9.4.18)$$

and in the upper layer,

$$Q_2 \equiv \int_{y_1}^h u_x^{(2)} dy = -\frac{1}{6} \frac{h_2^3}{\mu_2} \left(-\frac{\partial p^{(2)}}{\partial x} + \rho_2 g_x \right) + \frac{1}{2} \xi_2 h_2^2 + u_I h_2. \quad (9.4.19)$$

Using expressions (9.4.7) to eliminate the shear rates, ξ_1 and ξ_2 , from the right-hand sides, we find that

$$Q_1 = \frac{1}{12} \frac{h_1^3}{\mu_1} \left(-\frac{\partial p^{(1)}}{\partial x} + \rho_1 g_x \right) + \frac{1}{2} (u_I + V_1) h_1, \quad (9.4.20)$$

and

$$Q_2 = \frac{1}{12} \frac{h_2^3}{\mu_2} \left(-\frac{\partial p^{(2)}}{\partial x} + \rho_2 g_x \right) + \frac{1}{2} (u_I + V_2) h_2, \quad (9.4.21)$$

involving the unknown interfacial velocity.

A mass balance over a control area confined by (a) two parallel planes that are normal to the channel walls and are separated by an infinitesimal distance, (b) the enclosed sections of the walls, and (c) the enclosed section of the evolving interface, requires that the rate of accumulation of mass of each layer inside this control area should be equal to the difference in the mass flow rates into and out from the control volume. In differential form,

$$\frac{\partial h_1}{\partial t} = \frac{\partial y_1}{\partial t} = -\frac{\partial Q_1}{\partial x} \quad (9.4.22)$$

and

$$\frac{\partial h_2}{\partial t} = -\frac{\partial y_1}{\partial t} = -\frac{\partial Q_2}{\partial x}. \quad (9.4.23)$$

Since $h_1 + h_2 = 2a$ is constant, $\partial h_1/\partial t + \partial h_2/\partial t = 0$ and

$$\frac{\partial Q_1}{\partial x} + \frac{\partial Q_2}{\partial x} = 0 \quad (9.4.24)$$

or

$$Q_1 + Q_2 = \frac{1}{\mu_1} f(t), \quad (9.4.25)$$

where $f(t)$ is an unspecified function of time.

To compute the function $f(t)$, we use the expressions for the flow rates and interfacial velocity given in equations (9.4.20), (9.4.21), and (9.4.17). Eliminating the pressure gradient in the second layer using expression (9.4.16), we find that

$$\frac{\partial p^{(1)}}{\partial x} = \frac{N + f(t)}{D}, \quad (9.4.26)$$

where

$$\begin{aligned} N = & -(\rho_1 - \rho_2) g_y (h_2 + 6 \frac{\lambda}{\lambda + \delta} a) h_2^2 \frac{\partial h_1}{\partial x} - \gamma (h_2 + 6 \frac{\lambda}{\lambda + \delta} a) h_2^2 \frac{\partial^3 h_1}{\partial x^3} \\ & + \rho_1 g_x (\lambda h_1^3 + \alpha h_2^3 + 12 \frac{\lambda}{\lambda + \delta} \frac{1 + \lambda \delta}{1 + \delta} a^2 h_2) + 12 \mu_2 a \left(\frac{V_1 + \delta V_2}{1 + \delta} + \frac{\delta V_1 + \lambda V_2}{\lambda + \delta} \right) \\ & + h_2 \left(12 \frac{\lambda}{\delta + \lambda} a - h_2 \left(6 \frac{\lambda}{\delta + \lambda} a + h_2 \right) \frac{\partial^2 y_I}{\partial x^2} \right) \frac{\partial \gamma}{\partial x} \end{aligned} \quad (9.4.27)$$

and

$$D = \lambda h_1^3 + h_2^3 + 12 \frac{\lambda}{\lambda + \delta} a^2 h_2. \quad (9.4.28)$$

Note that

$$\frac{1}{1 + \delta} = \frac{1}{2} \frac{h_1}{a}. \quad (9.4.29)$$

Integrating (9.4.26) with respect to x over a length, L , and solving for $f(t)$, we obtain

$$f(t) = \frac{\Delta p / \mu_1 - \int_0^L \frac{N}{D} dx}{\int_0^L \frac{1}{D} dx}, \quad (9.4.30)$$

where

$$\Delta p \equiv p(x = L) - p(x = 0) \quad (9.4.31)$$

is the negative of the pressure drop over the length L .

The integrals on the right-hand side of (9.4.30) can be computed using elementary numerical methods from knowledge of the instantaneous interfacial shape.

Evolution equation

Having obtained the function $f(t)$, we evaluate the streamwise pressure gradient from (9.4.26), compute the interfacial velocity from (9.4.17), recover the flow rate Q_1 from equation (9.4.20), and use equation (9.4.22) to derive an expression for the rate of change of the lower film thickness or interface position. Symbolically, we write

$$\frac{\partial y_I}{\partial t} = F(y_I, y_I', y_I'', y_I''', y_I''''), \quad (9.4.32)$$

where a prime denotes a partial derivative with respect to x and F is a nonlinear function of its arguments defined implicitly in terms of the aforementioned substitutions.

Evolution of the concentration of an insoluble surfactant

The concentration of an insoluble surfactant is governed by the convection–diffusion equation (4.12.22),

$$\frac{\partial \Gamma}{\partial t} + \frac{\partial(u_I \Gamma)}{\partial x} = \frac{\partial}{\partial x} \left(D_s \frac{\partial \Gamma}{\partial x} \right), \quad (9.4.33)$$

where D_s is the interfacial surfactant diffusivity. An initial condition describing the initial surfactant distribution must be specified.

The two evolution equations (9.4.32) and (9.4.33) can be integrated in time using a standard finite-difference method on a one-dimensional grid whose nodes are distributed inside one period of the flow along the x axis.

Explicit numerical integration

To implement an explicit method, we apply equation (9.4.32) at a grid node at time t and approximate the time derivative on the left-hand side with a forward finite difference over a small time step, Δt , obtaining

$$\frac{y_I(x, t + \Delta t) - y_I(x, t)}{\Delta t} = F(t). \quad (9.4.34)$$

Evaluating the right-hand side by numerical differentiation and solving for $y_I(x, t + \Delta t)$, we obtain the position of the interface at the new time level, $t + \Delta t$.

The numerical method for uniform and constant surface tension, γ , that is, in the absence of surfactants, is implemented in the following code entitled *chan2l_exp*, residing in directory *05_lub* of **FDLIB**,

```
a = 0.2;
beta = 0.125*pi; % inclination angle
L = 1.0; % wave length
yIunp = 0.0; % unperturbed position
aI0 = 0.1; % initial amplitude of the interface
rho1 = 1.0; % densities
rho2 = 1.0;
vs1 = 1.0; % viscosities
vs2 = 0.4;
gamma = 0.4; % surface tension
V1 = -0.2; % wall velocities
V2 = 1.0;
pdrop = 0.3; % streamwise pressure drop over one period
gac = 1.0; % acceleration of gravity
NSG = 32; % number of segments
Dt = 0.001; % time step
```

```

nstep = 128*128; % number of steps
method = 2; % backward differences
method = 1; % central differences

%----
% prepare
%----

sn0 = sin(beta);
cs0 = cos(beta);
ROT = [cs0,sn0;-sn0,cs0]; % rotation matrix for plotting
gx = gac*sn0;
gy = -gac*cs0;
as = a*a;
vsr = vs2/vs1; % viscosity ratio
Drho = rho1-rho2; % density difference
dnr = rho2/rho1; % density ratio
wn = 2*pi/L; % wave number
Dx = L/NSG;
Dx2 = 2.0*Dx;
Dx23 = 2.0*Dx*Dx*Dx;
Dxs = Dx*Dx;

%-----
% initial profile
%-----

for i=1:NSG+4
    x(i) = (i-1.0)*Dx;
    arg = wn*x(i);
    y(i) = yIunp + aI0*cos(arg);
    srtn(i) = gamma;
end

%=====
% time stepping
%=====

for step=1:nstep

for i=3:NSG+2
    ib = i-2; ia = i-1; i1 = i+1; i2 = i+2;
    DyDx1(i) = (y(i1)-y(ia))/Dx2;
    DyDx2(i) = (y(i1)-2.0*y(i)+y(ia))/Dxs;
    DyDx3(i) = (y(i2)-2.0*y(i1)+2.0*y(ia)-y(ib))/Dx23;
    h1(i) = a+y(i);
    h2(i) = a-y(i);
    r(i) = h2(i)/h1(i);
end

```

```

DyDx1(1) = DyDx1(NSG+1);
DyDx2(1) = DyDx2(NSG+1);
DyDx3(1) = DyDx3(NSG+1);
h1(1) = h1(NSG+1); h2(1) = h2(NSG+1); r(1) = r(NSG+1);
DyDx1(2) = DyDx1(NSG+2);
DyDx2(2) = DyDx2(NSG+2);
DyDx3(2) = DyDx3(NSG+2);
h1(2) = h1(NSG+2); h2(2) = h2(NSG+2); r(2) = r(NSG+2);

%-----
% compute dp1/dx
%-----

for i=1:NSG
    tmp = 1.0/(vsr+hr(i));
    Den = vsr*h1(i)^3 + h2(i)^3 ...
        + 12.0*vsr*tmp*as*h2(i);
    t1 = -Drho*gy*(h2(i)+6.0*vsr*tmp*a) ...
        h2(i)^2*DyDx1(i);
    t2 = - srtn(i)*(h2(i)+6.0*vsr*tmp*a) ...
        *h2(i)^2*DyDx3(i);
    t3 = rho1*gx* (vsr*h1(i)^3 + dnr*h2(i)^3 ...
        +6.0*vsr*tmp*(1.0+dnr*hr(i))*a*h1(i)*h2(i));
    t4 = 6.0*vs2*(V1*h1(i)+V2*h2(i)) ...
        + 12.0*vs2*a*tmp*(vsr*V2+hr(i)*V1);
    dp1dx(i) = (t1+t2+t3+t4)/Den;
    store(i) = 1.0/Den;
end

%-----
% compute the function f(t)
%-----

sum1 = 0.0; sum2 = 0.0;
for i=1:NSG
    sum1 = sum1 + dp1dx(i);
    sum2 = sum2 + store(i);
end
sum1 = sum1*Dx; sum2 = sum2*Dx;
f = (pdrop-sum1)/sum2;

%-----
% complete the computation of dp1/dx
%-----

for i=1:NSG
    dp1dx(i) = dp1dx(i) + f*store(i);
end

```

```

dp1dx(NSG+1) = dp1dx(1);
dp1dx(NSG+2) = dp1dx(2);

%-----
% compute u_I
%-----

for i=1:NSG
    ri1 = 1.0+r(i);
    uI(i) = a*h2(i)/vs1 *(-dp1dx(i) ...
        +rho1*gx*(1.0+dnr*hr(i))/ri1 ) ...
        +0.5*h2(i)^2/vs1*(-Drho*gy*DyDx1(i) ...
        -srtm(i)*DyDx3(i)) + hr(i)*V1+vsr*V2;
    uI(i) = uI(i)/(vsr+r(i));
end

uI(NSG+1) = uI(1);
uI(NSG+2) = uI(2);

%-----
% compute dq1/dx
%
% then set dy/dt = - dq1/dx
%-----

pr1 = 12.0*Dx2*vs1; pr2 = 2.0*Dx2;
pr3 = 12.0*Dx*vs1; pr4 = 2.0*Dx;

for i=2:NSG+1

    ia = i-1; i1 = i+1;

    %---
    if(method==1) % central differences
    %---
        dq1dx = ( h1(i1)^3 *(-dp1dx(i1)+rho1*gx) ...
            -h1(ia)^3 *(-dp1dx(ia)+rho1*gx))/pr1 ...
            + ( (uI(i1)+V1)*h1(i1) -(uI(ia)+V1)*h1(ia))/pr2;
    %---
    else % backward differences
    %---

        dq1dx = ( h1(i)^3 *(-dp1dx(i) +rho1*gx) ...
            -h1(ia)^3 *(-dp1dx(ia)+rho1*gx))/pr3 ...
            + ( (uI(i)+V1)*h1(i) -(uI(ia)+V1)*h1(ia))/pr4;
    %---
    end
    %---

```

```

DyDt(i) = -dq1dx;

end

for i=2:NSG+1
    y(i) = y(i)+Dt*DyDt(i);
end

y(1) = y(NSG+1);
y(NSG+2) = y(2);
y(NSG+3) = y(3);
y(NSG+4) = y(4);

%---
% plotting
%---

for k=1:NSG+1
    xx = ROT*[x(k) y(k)]';
    xplot1(k) = xx(1)/L;
    yplot1(k) = xx(2)/L;
end

if(step==1)
    Handle1 = plot(xplot1,yplot1,'r.-');
    xlabel('x/L','fontsize',15)
    ylabel('y/L','fontsize',15)
    set(gca,'fontsize',15)
    axis equal
end

set(Handle1,'XData',xplot1,'YData',yplot1)
drawnow

%====
end % of time stepping
%====

```

A sequence of evolving profiles is shown in [Figure 9.4.2](#). Surface tension and gravity for stably stratified fluids work synergistically to dampen interfacial deviations from the flat shape.

Implicit time integration

The explicit method requires a small time step to prevent the onset of numerical instability manifested by growing oscillations in the nodal position along the interface. This restriction can be overcome by applying the evolution equation (9.4.32) at a grid point at a certain time $t + \Delta t$ and approximating the time derivatives on the left-hand side with a backward

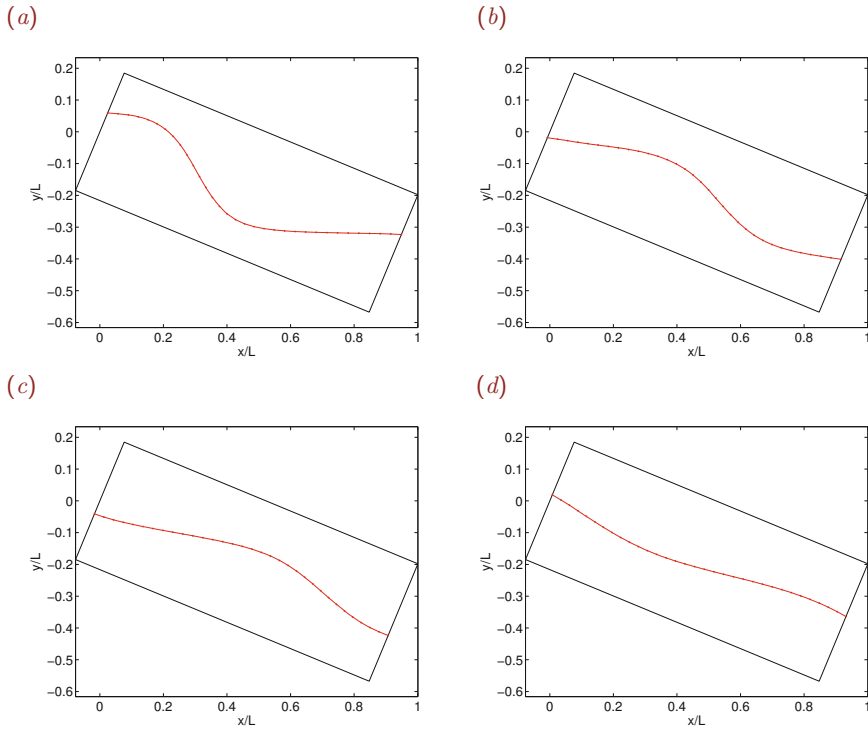


Figure 9.4.2 Snapshots of an evolving interface between two layers in a channel confined between two parallel walls computed by code *chan2l.exp*.

finite difference using a small time step, Δt , to obtain

$$\frac{y_I(x, t + \Delta t) - y_I(x, t)}{\Delta t} = F(t + \Delta t). \quad (9.4.35)$$

Evaluating the right-hand side by numerical differentiation, we obtain a nonlinear system of algebraic equations for the interfacial elevation at the nodes at time $t + \Delta t$.

The method is implemented in code *chan2l.imp*, located in directory *05_lub* of **FDLIB**, not listed in the text. A drawback of the implicit method is that computing the solution of a nonlinear algebraic system at each time step requires significant computational effort.

PROBLEMS

9.4.1 Single-layer flow in a channel

Demonstrate that, when the densities and viscosities of the two layers are matched, the equations of two-layer flow reduce to those of single-layer flow.

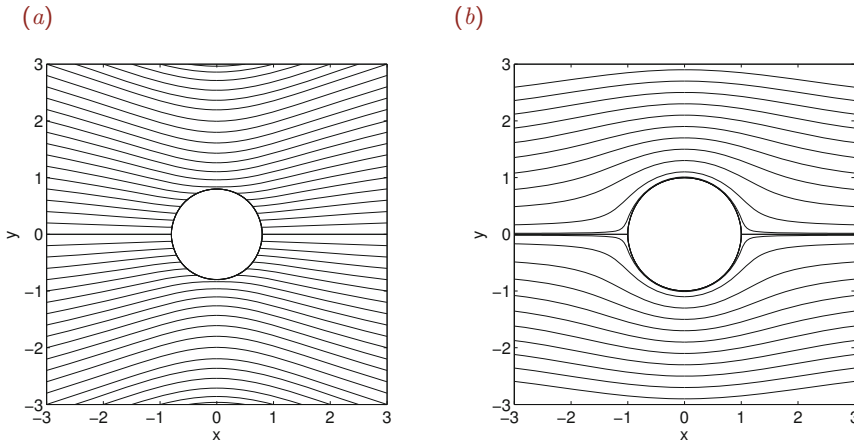


Figure 9.5.1 Streamline pattern of axisymmetric Stokes flow due to the translation of a sphere along the x axis in an infinite fluid. Streamlines are drawn (a) in a stationary frame of reference and (b) in a frame of reference moving with the sphere.

9.4.2 Two-layer flow in a channel

Run the code `chan2l.exp` for a set of conditions of your choice. Display sequences of evolving profiles, investigate the effect of the size of the time step on numerical stability, and discuss the nature of the motion.

9.5 Flow due to the motion of a sphere

A variety of natural and engineering applications involve particle motion in a viscous fluid. An elementary configuration involves a spherical particle settling with constant velocity due to its weight in a virtually infinite quiescent ambient fluid, thereby generating an axisymmetric flow, as illustrated in [Figure 9.5.1](#).

When the radius of the spherical particle, a , is small, or the fluid viscosity, μ , is high, or the fluid density, ρ , is low, or the particle velocity V is small, inertial forces are negligible near the particle and the left-hand side of the Navier–Stokes equation can be set to zero without introducing serious error. The result is the Stokes equation,

$$\nabla p = \mu \nabla^2 \mathbf{u} + \rho \mathbf{g}, \quad (9.5.1)$$

which, together with the continuity equation,

$$\nabla \cdot \mathbf{u} = \frac{\partial u_x}{\partial x} + \frac{\partial u_y}{\partial y} + \frac{\partial u_z}{\partial z} = 0, \quad (9.5.2)$$

comprise the equations of Stokes or creeping flow.

The three scalar components of the Stokes equation are

$$\begin{aligned}\frac{\partial p}{\partial x} &= \mu \left(\frac{\partial^2 u_x}{\partial x^2} + \frac{\partial^2 u_x}{\partial y^2} + \frac{\partial^2 u_x}{\partial z^2} \right) + \rho g_x, \\ \frac{\partial p}{\partial y} &= \mu \left(\frac{\partial^2 u_y}{\partial x^2} + \frac{\partial^2 u_y}{\partial y^2} + \frac{\partial^2 u_y}{\partial z^2} \right) + \rho g_y, \\ \frac{\partial p}{\partial z} &= \mu \left(\frac{\partial^2 u_z}{\partial x^2} + \frac{\partial^2 u_z}{\partial y^2} + \frac{\partial^2 u_z}{\partial z^2} \right) + \rho g_z.\end{aligned}\tag{9.5.3}$$

The formal requirement for fluid inertia to be negligible is that the Reynolds number defined with respect to the particle radius, $\text{Re} = a\rho V/\mu$, is small. However, we will see that this assumption does not guarantee that inertia will be negligible uniformly *throughout* the domain of the flow and, in particular, far from the sphere.

Having noted this exception, we proceed to compute the solution by assuming that inertia is negligible throughout the domain of flow, and then return to assess the validity of this assumption.

9.5.1 Formulation in terms of the stream function

To simplify the analysis, we take advantage of the axial symmetry of the flow with respect to the direction of translation and work in spherical polar coordinates, (r, θ, φ) , and companion cylindrical polar coordinates, (x, σ, φ) , where the x axis points in the direction of translation.

To bypass the computation of the pressure, we work with the vorticity transport equation (6.6.16) for the only nonvanishing component of the vorticity pointing in the azimuthal direction, ω_φ . In the absence of fluid inertia, we obtain the simplified governing equation

$$\mathcal{E}^2(\sigma \omega_\varphi) = 0,\tag{9.5.4}$$

where $\sigma = r \sin \theta$ is the distance from the x axis and the second-order linear differential operator, \mathcal{E}^2 , is defined in (2.9.27) as

$$\mathcal{E}^2 \equiv \frac{\partial^2}{\partial r^2} + \frac{\sin \theta}{r^2} \frac{\partial}{\partial \theta} \left(\frac{1}{\sin \theta} \frac{\partial}{\partial \theta} \right) = \frac{\partial^2}{\partial r^2} + \frac{1}{r^2} \frac{\partial^2}{\partial \theta^2} - \frac{\cot \theta}{r^2} \frac{\partial}{\partial \theta}\tag{9.5.5}$$

in spherical polar coordinates.

Expressing the azimuthal component of the vorticity in terms of the stream function using expression (2.9.23),

$$\omega_\varphi = -\frac{1}{\sigma} \mathcal{E}^2 \psi,\tag{9.5.6}$$

we obtain

$$\mathcal{E}^4 \psi \equiv \mathcal{E}^2 \mathcal{E}^2 \psi = 0.\tag{9.5.7}$$

Our task is to solve this fourth-order differential equation in the exterior of the sphere, subject to appropriate boundary and far-field conditions.

Boundary and far-field conditions

On the surface of the sphere, $r = a$, the no-slip and no-penetration boundary conditions require that the fluid velocity is equal to the velocity of the sphere,

$$\mathbf{u}(r = a) = V \mathbf{e}_x, \quad (9.5.8)$$

where \mathbf{e}_x is the unit vector along the x axis. Thus,

$$u_r(r = a) = V \cos \theta, \quad u_\theta(r = a) = -V \sin \theta. \quad (9.5.9)$$

The far-field condition requires that the velocity decays so that the fluid becomes quiescent at infinity.

Using the differential relations between the velocity components and the stream function in axisymmetric flow,

$$u_r = \frac{1}{r^2 \sin \theta} \frac{\partial \psi}{\partial \theta}, \quad u_\theta = -\frac{1}{r \sin \theta} \frac{\partial \psi}{\partial r}, \quad (9.5.10)$$

we find that, in terms of the stream function, the boundary and far-field conditions take the forms

$$\psi(r = a) = \frac{1}{2} V a^2 \sin^2 \theta, \quad \left(\frac{\partial \psi}{\partial r} \right)_{r=a} = V a \sin^2 \theta \quad (9.5.11)$$

and

$$\frac{\psi}{r^m} \rightarrow 0 \quad \text{as} \quad r \rightarrow \infty \quad (9.5.12)$$

for $m \geq 2$. Condition (9.5.12) allows the stream function to diverge at infinity but requires that the rate of divergence is less than quadratic; otherwise, the velocity field will not decay, as required.

Solution by separation of variables

Motivated by the functional form of the boundary conditions (9.5.11), we search for a solution by separation of variables in the form

$$\psi = q(r) \sin^2 \theta. \quad (9.5.13)$$

The unknown function, $q(r)$, satisfies the boundary conditions

$$q(r = a) = \frac{1}{2} V a^2, \quad \left(\frac{dq}{dr} \right)_{r=a} = V a, \quad (9.5.14)$$

and the far-field condition

$$\frac{q(r)}{r^m} \rightarrow 0 \quad \text{as} \quad r \rightarrow \infty \quad (9.5.15)$$

for $m \geq 2$.

Substituting expression (9.5.13) into (9.5.7), and carrying out the differentiations, we obtain a fourth-order linear ordinary differential equation,

$$\left(\frac{d^2}{dr^2} - \frac{2}{r^2}\right)\left(\frac{d^2}{dr^2} - \frac{2}{r^2}\right)q = 0, \quad (9.5.16)$$

which can be resolved into two second-order component equations,

$$\frac{d^2 w}{dr^2} - \frac{2}{r^2} w = 0, \quad \frac{d^2 q}{dr^2} - \frac{2}{r^2} q = w. \quad (9.5.17)$$

The second equation merely defines the intermediate function $w(r)$.

The general solution of the first equation in (9.5.17) is found readily to be

$$w = Ar^2 + \frac{B}{r}, \quad (9.5.18)$$

where A and B are two constants. Substituting this expression into the second equation, we derive an inhomogeneous equation,

$$\frac{d^2 q}{dr^2} - \frac{2}{r^2} q = Ar^2 + \frac{B}{r}. \quad (9.5.19)$$

The solution of (9.5.19) is the sum of (a) the general solution of the homogeneous equation computed by setting the right-hand side to zero, given by $q = Cr^2 + D/r$, where C and D are two new constants, and (b) a particular solution found by inspection. The result is

$$q = \frac{1}{10} Ar^4 - \frac{1}{2} Br + Cr^2 + \frac{D}{r}. \quad (9.5.20)$$

To ensure the satisfaction of condition (9.5.15), we set A and C to zero. Substituting the remaining expression into the boundary conditions (9.5.14), and solving for the coefficients B and D , we obtain

$$B = -\frac{3}{2} Va, \quad D = -\frac{1}{4} Va^3. \quad (9.5.21)$$

Substituting these values into (9.5.20) and the result into (9.5.13), we obtain the desired stream function,

$$\psi(r, \theta) = \frac{1}{4} Vr^2 \frac{a}{r} \left(3 - \frac{a^2}{r^2}\right) \sin^2 \theta. \quad (9.5.22)$$

Note that the stream function has units of velocity multiplied by distance squared.

Velocity and pressure fields

The radial and azimuthal velocity components arise by substituting (9.5.22) into equations (9.5.10), yielding

$$u_r = \frac{1}{2} V \frac{a}{r} \left(3 - \frac{a^2}{r^2}\right) \cos \theta \quad (9.5.23)$$

and

$$u_\theta = -\frac{1}{4} V \frac{a}{r} \left(3 + \frac{a^2}{r^2} \right) \sin \theta. \quad (9.5.24)$$

Substituting these expressions into the radial and meridional spherical polar components of the Stokes equations, we derive expressions for the partial derivatives of the pressure, $\partial p/\partial r$ and $\partial p/\partial \theta$. Integrating these expressions, we derive the pressure distribution

$$p = \frac{3}{2} \frac{\mu V}{a} \frac{a^2}{r^2} \cos \theta + \rho (g_x x + g_y y + g_z z) + \pi_0, \quad (9.5.25)$$

where $\mathbf{g} = (g_x, g_y, g_z)$ is the acceleration of gravity and π_0 is a constant determined by the pressure prevailing far from the sphere (Problem 9.5.1).

Validity of the equations of creeping flow

We must return to evaluate the assumptions under which the preceding analysis is valid in light of the linearization of the equation of motion. Expressions (9.5.23) and (9.5.24) reveal that, in the absence of fluid inertia, the velocity decays like Va/r far from the sphere; the cubic term $V(a/r)^3$ decays much faster and can be neglected. Differentiating this asymptotic form with respect to r , we find that the derivative $\partial u_r/\partial r$ involved in the nonlinear convective term on the left-hand side of the Navier–Stokes equation decays like Va/r^2 , while the derivative $\partial^2 u_r/\partial r^2$ involved in the viscous term on the right-hand side of the Navier–Stokes equation decays like Va/r^3 .

The time derivative $\partial u_r/\partial t$ scales with u_r/T , where T the characteristic time scale. In the absence of explicit time dependence due to an external action, we may identify T with the ratio of the distance from the center of the sphere to the velocity of the sphere, $T = r/V$.

Using the preceding scaling, we find that the ratio of the magnitude of the nonlinear inertial term to the magnitude of the viscous term in the equation of motion is of order

$$\frac{\rho V \frac{a}{r} V \frac{a}{r^2}}{\mu V \frac{a}{r^3}} = \frac{\rho Va}{\mu} \equiv \text{Re}, \quad (9.5.26)$$

and the ratio of the magnitude of the time-dependent inertial term to the magnitude of the viscous term is of order

$$\frac{\rho (V \frac{a}{r}) / (\frac{r}{V})}{\mu V \frac{a}{r^3}} = \frac{\rho Vr}{\mu} \equiv \text{Re}_r = \text{Re} \frac{r}{a}. \quad (9.5.27)$$

We have introduced the nominal Reynolds number, Re , defined with respect to the radius of the sphere, and the local Reynolds number, Re_r , defined with respect to distance from the center of the sphere.

Breakdown

Equations (9.5.26) and (9.5.27) reveal that, for inertial forces to be negligible, both Re and Re_r must be far less than unity. The former can be made arbitrarily small by adjusting one of the flow parameters involved in its definition, ρ , a , V , and μ . However, there is no way that the latter can be uniformly small throughout the domain of flow. Even if Re is exceedingly small, the ratio r/a becomes arbitrary large sufficiently far from the sphere and the local Reynolds number, Re_r , increases linearly with respect to distance, rendering the effect of fluid inertia significant.

We conclude that the approximation of creeping flow ceases to be accurate far from the sphere, with one disturbing consequence. If the governing equations are not valid all the way up to infinity, enforcing the far-field boundary condition expressed by (9.5.12) is dubious at best and catastrophic at worst. Fortunately, a more detailed analysis using the method of matched asymptotic expansions shows that retaining the far-field condition introduces an error that is comparable to that introduced by dropping the inertial terms in the equation of motion, which is on the order of Re . This will not be the case of two-dimensional Stokes flow past a cylinder, as discussed in Section 9.7.

9.5.2 Traction, force, and the Archimedes–Stokes law

Having derived expressions for the velocity and pressure fields, given, respectively, in (9.5.23), (9.5.24), and (9.5.25), we proceed to evaluate the traction on the surface of the sphere and then integrate the traction to obtain an expression for the force exerted on the sphere. For simplicity, we assume that gravity is directed along the x axis, that is, $g_x = g$, $g_y = 0$, and $g_z = 0$, where g is the magnitude of the acceleration of gravity.

Stress and traction

Using the definition of the Newtonian stress tensor shown in Table 4.7.2(b), we derive an expression for the normal component of the traction,

$$\sigma_{rr}(r = a) = \left(-p + 2\mu \frac{\partial u_r}{\partial r} \right)_{r=a} = -(p)_{r=a}, \quad (9.5.28)$$

yielding

$$\sigma_{rr}(r = a) = -\frac{3}{2} \frac{\mu V}{a} \cos \theta - \rho g x - \pi_0, \quad (9.5.29)$$

and an expression for the tangential component of the traction,

$$\sigma_{r\theta}(r = a) = \sigma_{\theta r}(r = a) = \left(r \frac{\partial}{\partial r} \left(\frac{u_\theta}{r} \right) + \frac{1}{r} \frac{\partial u_r}{\partial \theta} \right)_{r=a}, \quad (9.5.30)$$

yielding

$$\sigma_{r\theta}(r = a) = \frac{3}{2} \frac{\mu V}{a} \sin \theta. \quad (9.5.31)$$

Note that, because of the no-slip boundary condition, viscous stresses do not contribute to the normal component of the traction, in agreement with our discussion in Section 4.11.

Combining (9.5.29) and (9.5.31), we find that the traction exerted on the sphere is

$$\mathbf{f} = \sigma_{rr}(r = a) \mathbf{e}_r + \sigma_{r\theta}(r = a) \mathbf{e}_\theta, \quad (9.5.32)$$

where \mathbf{e}_r and \mathbf{e}_θ are unit vectors in the radial or azimuthal direction. Expressing \mathbf{e}_r and \mathbf{e}_θ in terms of Cartesian unit vectors using relations (1.3.36), substituting the results along with expressions (9.5.29) and (9.5.31) into (9.5.32), and simplifying the resulting expression, we derive a remarkably simple result,

$$\mathbf{f} = -\frac{3}{2} \frac{\mu V}{a} \mathbf{e}_x - (\rho g x + p_0) \mathbf{e}_r, \quad (9.5.33)$$

which shows that, hydrostatic contributions aside, the traction over the surface of the sphere points opposite to the direction of translation with a uniform magnitude.

Force on a moving sphere

To compute the force exerted on the sphere, \mathbf{F} , we integrate the traction over the surface of the sphere. Substituting $x = r \cos \theta$, we obtain

$$\mathbf{F} = \iint_{\text{sphere}} \mathbf{f} \, dS = \int_0^{2\pi} \int_0^\pi \mathbf{f} a^2 \sin \theta \, d\theta \, d\varphi. \quad (9.5.34)$$

Performing the integration, we obtain

$$\mathbf{F} = -6\pi\mu V a \mathbf{e}_x - \frac{4}{3} \pi a^3 \rho g \mathbf{e}_x, \quad (9.5.35)$$

where V is the volume of the sphere. The first term on the right-hand side expresses Stokes's law. The second term expresses Archimedes's buoyancy force, familiar from our discussion in Chapter 5 of hydrostatics, stating that the force exerted on an immersed body is equal in magnitude and opposite in direction to the weight of the fluid displaced by the body.

Terminal velocity of a settling sphere

As an application, we compute the terminal velocity of a solid sphere with density ρ_s settling along the x axis in an infinite ambient fluid. Balancing the weight of the sphere with the force given in (9.5.35), we obtain

$$\frac{4}{3} \pi a^3 \rho_s g \mathbf{e}_x - 6\pi\mu V a \mathbf{e}_x - \frac{4}{3} \pi a^3 \rho g \mathbf{e}_x = \mathbf{0}. \quad (9.5.36)$$

Solving for the velocity of the sphere, we obtain

$$V = \frac{2}{9} \frac{a^2(\rho_s - \rho)g}{\mu}. \quad (9.5.37)$$

In practice, this equation can be used to estimate the viscosity of a fluid from observation of the terminal velocity of a sphere in a device called the falling-ball viscometer.

PROBLEMS**9.5.1** *Pressure distribution around a moving sphere*

Derive the pressure distribution (9.5.25).

9.5.2 *Flow past a stationary sphere*

Consider steady uniform Stokes flow with velocity U along the x axis past a stationary sphere of radius a . Derive expressions for the stream function, the velocity, the pressure field, the traction and the force on the surface of the sphere. Show that, for the fluid inertia to be negligible throughout the domain of flow, both Re and Re_r defined in equations (9.5.26) and (9.5.27) must be sufficiently less than unity.

9.6 Point forces and point sources in Stokes flow

Consider the stream function of the flow due to a translating sphere given in equation (9.5.22). The right-hand side involves two terms that decay like the inverse of the scaled distance from the center of the sphere, a/r , and the inverse cubic power of the scaled distance from the center of the sphere, $(a/r)^3$.

To make this distinction clear, we recast equation (9.5.22) into the form

$$\psi(r, \theta) = s_x \psi^{3\text{DST}x}(r, \theta) + d_x \psi^{3\text{DPSD}x}(r, \theta), \quad (9.6.1)$$

where

$$s_x = \frac{3}{4} Va, \quad d_x = -\pi Va^3 \quad (9.6.2)$$

are two coefficients,

$$\psi^{3\text{DST}x}(r, \theta) \equiv r \sin^2 \theta \quad (9.6.3)$$

is the stream function associated with a fundamental solution of the equations of Stokes flow called the three-dimensional *Stokeslet*, and

$$\psi^{3\text{DPSD}x}(r, \theta) \equiv \frac{1}{4\pi} \frac{1}{r} \sin^2 \theta \quad (9.6.4)$$

is a stream function representing irrotational flow due to a three-dimensional point-source dipole pointing along the x axis, as discussed in Section 3.6.

The expressions for the velocity, pressure, and stress can be resolved into corresponding components associated with the Stokeslet and the point-source dipole. For example, the Cartesian components of the velocity are given by

$$\begin{bmatrix} u_x \\ u_y \\ u_z \end{bmatrix} = s_x \begin{bmatrix} \frac{1}{r} + \frac{x^2}{r^3} \\ \frac{xy}{r^3} \\ \frac{xz}{r^3} \end{bmatrix} + d_x \frac{1}{4\pi} \begin{bmatrix} -\frac{1}{r^3} + 3\frac{x^2}{r^5} \\ 3\frac{xy}{r^5} \\ 3\frac{xz}{r^5} \end{bmatrix}, \quad (9.6.5)$$

where the origin has been set at the center of the sphere. The first and second terms on the right-hand side of (9.6.5) represent, respectively, the velocity field due to a Stokeslet and a potential dipole, both situated at the origin and pointing along the x axis.

9.6.1 The Oseen tensor and the point force

Generalizing the expression for the Stokeslet given on the right-hand side of equation (9.6.5), we introduce the velocity at a field point, $\mathbf{x} = (x, y, z)$, due to a three-dimensional Stokeslet with arbitrary vectorial strength, $\mathbf{s} = (s_x, s_y, s_z)$, situated at another point, $\mathbf{x}_0 = (x_0, y_0, z_0)$, given by

$$\begin{bmatrix} u_x \\ u_y \\ u_z \end{bmatrix}(\mathbf{x}, \mathbf{x}_0) = \mathbf{S}(\mathbf{x}, \mathbf{x}_0) \cdot \begin{bmatrix} s_x \\ s_y \\ s_z \end{bmatrix}, \tag{9.6.6}$$

where \mathbf{S} is the 3×3 Oseen tensor for three-dimensional flow defined as

$$\mathbf{S}(\mathbf{x}, \mathbf{x}_0) = \begin{bmatrix} \frac{1}{r} + \frac{(x-x_0)^2}{r^3} & \frac{(x-x_0)(y-y_0)}{r^3} & \frac{(x-x_0)(z-z_0)}{r^3} \\ \frac{(y-y_0)(x-x_0)}{r^3} & \frac{1}{r} + \frac{(y-y_0)^2}{r^3} & \frac{(y-y_0)(z-z_0)}{r^3} \\ \frac{(z-z_0)(x-x_0)}{r^3} & \frac{(z-z_0)(y-y_0)}{r^3} & \frac{1}{r} + \frac{(z-z_0)^2}{r^3} \end{bmatrix}, \tag{9.6.7}$$

and

$$r = [(x-x_0)^2 + (y-y_0)^2 + (z-z_0)^2]^{1/2} \tag{9.6.8}$$

is the distance of the field point, \mathbf{x} , from the location of the Stokeslet, \mathbf{x}_0 . The three columns of the Oseen tensor represent, respectively, the x , y , and z components of the velocity associated with a Stokeslet of unit strength pointing in the direction of the x , y , or z axis. In index notation, the Oseen tensor takes the form

$$S_{ij}(\mathbf{x}, \mathbf{x}_0) = \frac{\delta_{ij}}{r} + \frac{\hat{x}_i \hat{x}_j}{r^3}, \tag{9.6.9}$$

where $\hat{\mathbf{x}} = \mathbf{x} - \mathbf{x}_0$ and δ_{ij} is Kronecker's delta representing the identity matrix.

The corresponding pressure field is given by

$$p(\mathbf{x}, \mathbf{x}_0) = 2\mu \frac{1}{r^3} \begin{bmatrix} x-x_0 \\ y-y_0 \\ z-z_0 \end{bmatrix} \cdot \begin{bmatrix} s_x \\ s_y \\ s_z \end{bmatrix}, \tag{9.6.10}$$

where the dot denotes the inner vector product.

The velocity (9.6.6) and accompanying pressure field (9.6.10) satisfy the equations of Stokes flow, (9.5.3) and (9.5.2) with the gravity term absent, for any Stokeslet strength

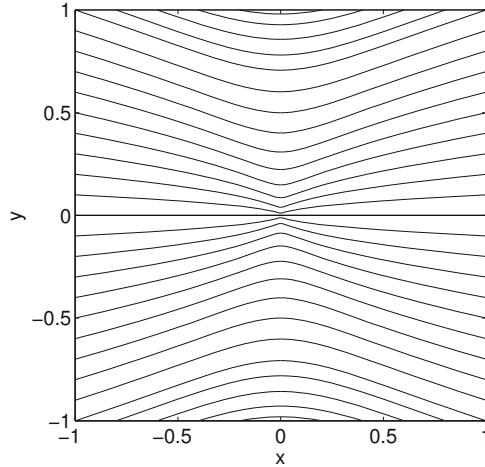


Figure 9.6.1 Streamline pattern in the xy plane of the axisymmetric flow induced by a three-dimensional point force pointing along the x axis.

represented by the vector \mathbf{s} , everywhere except at the point \mathbf{x}_0 where the velocity and pressure become infinite. The streamline pattern in the xy plane induced by a Stokeslet pointing in the x direction is shown in [Figure 9.6.1](#).

Force on a surface enclosing the Stokeslet

Consider a surface, \mathcal{D} , enclosing the singular point of a Stokeslet, \mathbf{x}_0 . It can be shown that the force exerted on this closed surface is given by

$$\mathbf{F} \equiv \iint_{\mathcal{D}} \mathbf{n} \cdot \boldsymbol{\sigma} \, dS = -8\pi\mu \mathbf{s}, \quad (9.6.11)$$

independent of the shape of the surface, where $\boldsymbol{\sigma}$ is the stress tensor and \mathbf{n} is the unit vector normal to \mathcal{D} pointing outward.

The corresponding torque with respect to the singular point, \mathbf{x}_0 is zero,

$$\mathbf{T} \equiv \iint_{\mathcal{D}} (\mathbf{x} - \mathbf{x}_0) \times (\mathbf{n} \cdot \boldsymbol{\sigma}) \, dS = \mathbf{0}. \quad (9.6.12)$$

The force and torque exerted on a closed surface that does not enclose the singular point, \mathbf{x}_0 , are both zero.

Equation (9.6.11) suggests that the Stokeslet expresses the flow due to a three-dimensional point force applied at a singular point, \mathbf{x}_0 . In physical terms, this flow can be identified with the flow induced by a small moving particle located at the point \mathbf{x}_0 . The strength of the point force counterbalances the force exerted on the particle due, for example, to gravity.

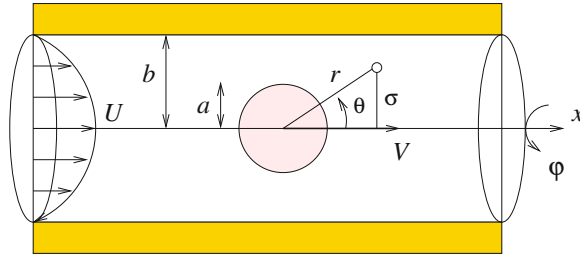


Figure 9.6.2 Illustration of a spherical particle moving along the axis of a circular tube with velocity V in the presence of an ambient Poiseuille flow.

Point source and point-source dipoles

It can be shown by straightforward substitution that the irrotational velocity fields due to a point source or point-source dipole discussed in Section 3.6 satisfy the equations of Stokes flow (9.5.3) and (9.5.2) with the gravity term absent and a corresponding constant pressure. The force and torque on a closed surface are zero, independent of whether the singular point \mathbf{x}_0 lies inside or outside the surface.

9.6.2 Flow representation in terms of singularities

We have discussed three singular fundamental solutions of the equations of Stokes flow, including the point force, the point source, and the point-source dipole. These singularities can be employed in a more general context to generate desired solutions by linear superposition. The key idea is to express a flow of interest in terms of a linear combination of singularities, and then compute the strengths of the singularities to satisfy required boundary conditions. Superposition is permissible in light of the linearity of the equations of Stokes flow.

Flow due to the translation of a sphere

We have already seen that the flow due to the translation of a sphere can be represented exactly by a point force and a point-source dipole placed at the center of the sphere. The coefficients of the singularities are given in equations (9.6.2). Using equation (9.6.11), we find that the hydrodynamic force exerted on the sphere is given by

$$\mathbf{F} = -8\pi\mu\mathbf{s} = -6\pi\mu Va \mathbf{e}_x, \tag{9.6.13}$$

which is identical to expression (9.5.35) derived by detailed integration.

However, because exact singularity representation are rare, we must compromise by deriving approximate solutions.

9.6.3 A sphere moving inside a circular tube

Consider a spherical particle of radius a moving with velocity V along the axis of cylindrical tube of radius b under the action of pressure-driven flow, as illustrated in Figure 9.6.2. In

the absence of the sphere we obtain the Poiseuille unidirectional flow velocity profile

$$u_x^p = U \left(1 - \frac{\sigma^2}{b^2} \right), \quad (9.6.14)$$

where U is the centerline velocity and

$$\sigma = \sqrt{y^2 + z^2} = r \sin \theta \quad (9.6.15)$$

is the distance from the x axis. The corresponding stream function for axisymmetric flow, ψ^p , is defined by the equation

$$\frac{1}{\sigma} \frac{d\psi^p}{d\sigma} = u_x^p. \quad (9.6.16)$$

Integrating with respect to σ , we derive the expression

$$\psi^p = U \frac{1}{2} \sigma^2 \left(1 - \frac{1}{2} \frac{\sigma^2}{b^2} \right) + c, \quad (9.6.17)$$

where c is an unspecified constant.

Flow representation

An approximate representation of the flow in the presence of the sphere can be devised by superposing (a) the unperturbed parabolic flow, (b) the flow due to a point force, and (c) the flow due to a point-source dipole, where the two singularities are located at the center of the sphere and point along the x axis. The composite stream function is given by

$$\psi = \psi^p + s_x \psi^{3DSTx} + d_x \psi^{3DPSDx}, \quad (9.6.18)$$

where s_x and d_x are the *a priori* unknown strengths of the singularities. Expressing (9.6.3) and (9.6.4) in cylindrical polar coordinates, we obtain

$$\psi^{3DST} \equiv r \sin^2 \theta = \frac{\sigma^2}{(x^2 + \sigma^2)^{1/2}} \quad (9.6.19)$$

and

$$\psi^{3DPSDx} \equiv \frac{1}{4\pi} \frac{1}{r} \sin^2 \theta = \frac{1}{4\pi} \frac{\sigma^2}{(x^2 + \sigma^2)^{3/2}}, \quad (9.6.20)$$

where $r = \sqrt{x^2 + \sigma^2}$.

The boundary conditions require that the velocity at the surface of the sphere is equal to $\mathbf{u} = V \mathbf{e}_x$, where V is the velocity of translation of the sphere and \mathbf{e}_x is the unit vector along the x axis. In terms of the stream function,

$$u_x(r = a) = \frac{1}{\sigma} \left(\frac{\partial \psi}{\partial \sigma} \right)_{r=a} = V, \quad u_\sigma(r = a) = -\frac{1}{\sigma} \left(\frac{\partial \psi}{\partial x} \right)_{r=a} = 0, \quad (9.6.21)$$

where the derivative with respect to σ is taken holding x constant, and the derivative with respect to x is taken holding σ constant.

Substituting (9.6.17), (9.6.19), and (9.6.20) into the right-hand side of (9.6.18), and then substituting the resulting expression into the boundary conditions (9.6.21) and simplifying, we obtain

$$U \left(1 - \frac{\sigma^2}{b^2}\right) + \frac{s_x}{a} \left(2 - \frac{\sigma^2}{a^2}\right) + \frac{1}{4\pi} \frac{d_x}{a^3} \left(2 - 3 \frac{\sigma^2}{a^2}\right) = V, \quad (9.6.22)$$

and

$$s_x + \frac{3}{4\pi} \frac{1}{a^2} d_x = 0. \quad (9.6.23)$$

where the left-hand side of (9.6.22) is evaluated at $r = a$. Using relation (9.6.23) to eliminate d_x in favor of s_x from (9.6.22), we obtain

$$U \left(1 - \frac{\sigma^2}{b^2}\right) + \frac{4}{3} \frac{s_x}{a} = V \quad (9.6.24)$$

evaluated at $r = a$. Since $\sigma = a \sin \theta$ over the surface of the sphere, it is not possible to satisfy the boundary condition (9.6.24) over the entire surface of the sphere, except in the absence of the parabolic flow. This difficulty underlines the limitations of the approximate singularity representation embodied in (9.6.18).

Breaking free

As a compromise, we require the satisfaction of (9.6.24) integrated over the surface of the sphere. Substituting $\sigma = a \sin \theta$, recalling that the integral of an axisymmetric function $f(\theta)$ over the surface of the sphere is given by

$$\iint f(\theta) \, dS = 2\pi a^2 \int_0^\pi f(\theta) \sin \theta \, d\theta, \quad (9.6.25)$$

and noting that the surface area of the sphere is $4\pi a^2$, we obtain

$$U \left(4\pi a^2 - \frac{2\pi a^4}{b^2} \int_0^\pi \sin^3 \theta \, d\theta\right) + \frac{4}{3} \frac{s_x}{a} 4\pi a^2 = 4\pi a^2 V. \quad (9.6.26)$$

Noting that

$$\int_0^\pi \sin^3 \theta \, d\theta = \frac{4}{3} \quad (9.6.27)$$

and simplifying, we obtain

$$U \left(1 - \frac{2}{3} \left(\frac{a}{b}\right)^2\right) + \frac{4}{3} \frac{s_x}{a} = V. \quad (9.6.28)$$

According to (9.6.13), the x component of the hydrodynamic force exerted on the sphere is given by

$$F_x = -8\pi\mu s_x. \quad (9.6.29)$$

Using this expression to eliminate s_x in favor of F_x in (9.6.28), we obtain

$$V = U \left(1 - \frac{2}{3} \left(\frac{a}{b} \right)^2 \right) - \frac{F_x}{6\pi\mu a}, \quad (9.6.30)$$

which provides us with an expression for the velocity of the sphere, V , in terms of the velocity profile of the Poiseuille flow, determined by U and b , and the force exerted on the sphere, F_x .

The second term on the left-hand side of (9.6.30) is consistent with Stokes' law expressed by (9.5.35). If the tube is vertical and the x axis points downward in the direction of gravity, a force balance on the sphere requires that F_x should be equal and opposite to the weight of the sphere reduced by the buoyancy force,

$$F_x = -\frac{4\pi}{3}a^3(\rho_s - \rho)g, \quad (9.6.31)$$

where ρ_s is the density of the sphere, ρ is the density of the fluid, and g is the magnitude of the acceleration of gravity.

Motion of a freely suspended sphere

In the case of a freely suspended sphere, $F_x = 0$, equation (9.6.30) yields

$$V = U \left(1 - \frac{2}{3} \left(\frac{a}{b} \right)^2 \right). \quad (9.6.32)$$

This expression shows that the velocity of the sphere lags behind the local fluid velocity at the centerline, U , by a factor that is determined by the square of the ratio of the sphere to tube radius, $(a/b)^2$.

Boundary effects

The no-slip and no-penetration conditions at the surface of the tube have not been enforced. As a consequence, expression (9.6.30) is strictly valid for a sphere immersed in infinite parabolic flow. Consequently, the presence of the tube in our discussion is relevant only insofar as to establish the curvature of the parabolic velocity profile.

In spite of the approximate satisfaction of the boundary condition on the surface of the sphere implemented by (9.6.26), expression (9.6.30) turns out to be *exact* for infinite parabolic flow, but not for wall-bounded parabolic flow.

9.6.4 Boundary integral representation

Consider an incident flow with velocity \mathbf{u}^∞ past a stationary, translating, or rotating particle, and divide the surface of the particle into a collection of N surface elements, such as

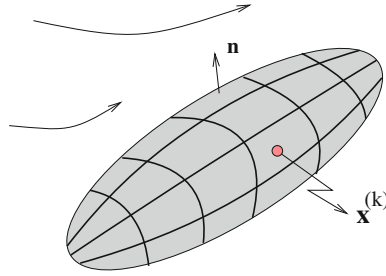


Figure 9.6.3 Stokes flow past a particle can be represented by a superposition of point forces located at designated centers of boundary elements.

curved quadrilaterals or triangles, as illustrated in [Figure 9.6.3](#). An approximate representation of the flow can be obtained by adding to the incident flow the flow due to a collection of point forces located at designated centers of the surface elements.

Expressing the Stokeslet in terms of the Oseen tensor, as shown in equation (9.6.6), we find that the velocity at a point \mathbf{x} that lies in the fluid is given by

$$\mathbf{u}(\mathbf{x}) = \mathbf{u}^\infty(\mathbf{x}) - \frac{1}{8\pi\mu} \sum_{k=1}^N \mathcal{S}(\mathbf{x}, \mathbf{x}^{(k)}) \cdot \mathbf{F}^{(k)}, \tag{9.6.33}$$

where $\mathbf{x}^{(k)}$ is the designated center of the k th element and $\mathbf{F}^{(k)}$ is the corresponding vectorial strength of the point force.

Rearranging the representation (9.6.33), we obtain

$$\mathbf{u}(\mathbf{x}) = \mathbf{u}^\infty(\mathbf{x}) - \frac{1}{8\pi\mu} \sum_{k=1}^N (\mathcal{S}(\mathbf{x}, \mathbf{x}^{(k)}) \cdot \mathbf{f}^{(k)}) \Delta S^{(k)}, \tag{9.6.34}$$

where $\Delta S^{(k)}$ is the surface area of the k th element, and we have introduced the average traction

$$\mathbf{f}^{(k)} \equiv \frac{1}{\Delta S^{(k)}} \mathbf{F}^{(k)}. \tag{9.6.35}$$

As the number of elements, N , tends to infinity, and correspondingly the surface areas $\Delta S^{(k)}$ tend to zero, the sum on the right-hand side of (9.6.34) reduces to a surface integral, yielding the integral representation

$$\mathbf{u}(\mathbf{x}) = \mathbf{u}^\infty(\mathbf{x}) - \frac{1}{8\pi\mu} \iint_{\text{particle}} \mathcal{S}(\mathbf{x}, \mathbf{x}') \cdot \mathbf{f}(\mathbf{x}') \, dS(\mathbf{x}'), \tag{9.6.36}$$

which expresses the flow in terms of a continuous distribution of point forces over the particle surface. In fact, it can be shown that the density of the distribution, \mathbf{f} , is the hydrodynamic

traction exerted on the particle surface, given by $\mathbf{f} = \mathbf{n} \cdot \boldsymbol{\sigma}$, where \mathbf{n} is the unit vector normal to the particle surface pointing into the fluid.

The integral representation (9.6.36) suggests a practical method of computing the flow: apply this equation at an arbitrary point, \mathbf{x} , at the particle surface, enforce the boundary conditions for the velocity to evaluate the left-hand side, and then solve the resulting integral equation for the traction, \mathbf{f} .

In practice, the solution is found numerically by approximating (9.6.36) with a discrete form in terms of boundary elements, as shown in equation (9.6.34). Identifying the point \mathbf{x} in (9.6.34) with the designated center of each element, provides us with a system of linear equations for the strengths of the point forces, $\mathbf{F}^{(k)}$. The procedure is known as a boundary-element/collocation method. Other methods for solving the integral equation are available.

PROBLEM

9.6.1 Force on a surface enclosing a Stokeslet or point source

- (a) Verify equation (9.6.11) for a spherical surface centered at the singular point, \mathbf{x}_0 .
- (b) Verify that the force exerted on a spherical surface centered at a point source is zero. Recall that the pressure field associated with a point source is uniform throughout the domain of a Stokes flow.

9.7 Two-dimensional Stokes flow

It might appear that our discussion of three-dimensional Stokes flow in Sections 9.5 and 9.6 carries over to two-dimensional flow without any further difficulties or added considerations. While this is generally true, there is one important exception: the flow due to the motion of a two-dimensional body in an infinite and otherwise quiescent fluid is generally not defined, in that a solution that satisfies the condition of vanishing velocity at infinity cannot be obtained if the force exerted on the body is nonzero. We will consider this problematic case first and then discuss well-posed flows.

9.7.1 Flow due to the motion of a cylinder

Consider the flow due to a circular cylinder of radius a translating along the x axis with velocity V in the xy plane. If the Reynolds number is sufficiently small, $\text{Re} = \rho V a / \mu < 1$, inertial forces are negligible compared to pressure and viscous forces sufficiently close to the cylinder, and the motion of the fluid is governed by the linear equations of Stokes flow. In Section 9.5, we emphasized that the smallness of the Reynolds number does not guarantee that inertial forces are insignificant throughout the domain of flow and, in particular, sufficiently far from the cylinder. Thus, the consistency of a solution derived working exclusively in the context of Stokes flow is subject to *a priori* verification.

Solution for the stream function

To bypass the computation of the pressure, we seek a solution based on the vorticity transport equation for the only non-vanishing vorticity component, ω_z ,

$$\rho \left(\frac{\partial \omega_z}{\partial t} + u_x \frac{\partial \omega_z}{\partial x} + u_y \frac{\partial \omega_z}{\partial y} \right) = \mu \nabla^2 \omega_z, \quad (9.7.1)$$

where $\nabla^2 \equiv \partial^2/\partial x^2 + \partial^2/\partial y^2$ is the two-dimensional Laplacian operator.

Setting the right-hand side of (9.7.1) to zero to eliminate inertial effects, introducing the stream function, ψ , and substituting $\omega_z = -\nabla^2 \psi$, we derive a fourth-order linear differential equation for the stream function,

$$\nabla^2 \nabla^2 \psi \equiv \nabla^4 \psi = 0, \quad (9.7.2)$$

where

$$\nabla^4 \equiv \nabla^2 \nabla^2 = \left(\frac{\partial^2}{\partial x^2} + \frac{\partial^2}{\partial y^2} \right) \left(\frac{\partial^2}{\partial x^2} + \frac{\partial^2}{\partial y^2} \right) = \frac{\partial^4}{\partial x^4} + 2 \frac{\partial^4}{\partial x^2 \partial y^2} + \frac{\partial^4}{\partial y^4} \quad (9.7.3)$$

is the biharmonic operator in two dimensions. Our task is to solve the fourth-order differential equation (9.7.3) in the flow regime, outside the cylinder, subject to appropriate boundary and far-field conditions.

Repeating the analysis of Section 9.5 for the analogous problem of flow due to a translating sphere, we find that, in plane polar coordinates with origin at the center of the cylinder, (r, θ) , the boundary conditions take the form

$$\psi(r = a) = Va \sin \theta, \quad \left(\frac{\partial \psi}{\partial r} \right)_{r=a} = V \sin \theta, \quad (9.7.4)$$

where $\theta = 0$ along the direction of translation. In the far field, we require that

$$\frac{\psi}{r^m} \rightarrow 0 \quad \text{as} \quad r \rightarrow \infty \quad (9.7.5)$$

for any exponent $m \geq 1$. Condition (9.7.5) allows the stream function to diverge at infinity, but requires that the rate of growth is less than linear so that the fluid becomes quiescent at infinity.

Solution by separation of variables

Motivated by the functional form of the boundary conditions (9.7.4), we seek a solution for the stream function by separation of variables in plane polar coordinates, setting

$$\psi(r, \theta) = q(r) \sin \theta. \quad (9.7.6)$$

The unknown function $q(r)$ satisfies the boundary conditions

$$q(r = a) = Va, \quad \left(\frac{\partial q}{\partial r} \right)_{r=a} = V, \quad (9.7.7)$$

and the far-field condition

$$\frac{q(r)}{r^m} \rightarrow 0 \quad \text{as} \quad r \rightarrow \infty \quad (9.7.8)$$

for $m \geq 1$.

Equation (3.2.29) provides us with the Laplacian operator in planar polar coordinates. The corresponding biharmonic operator is

$$\nabla^4 = \left(\frac{1}{r} \frac{\partial}{\partial r} \left(r \frac{\partial}{\partial r} \right) + \frac{1}{r^2} \frac{\partial^2}{\partial \theta^2} \right) \left(\frac{1}{r} \frac{\partial}{\partial r} \left(r \frac{\partial}{\partial r} \right) + \frac{1}{r^2} \frac{\partial^2}{\partial \theta^2} \right). \quad (9.7.9)$$

Substituting (9.7.6) into (9.7.2), and carrying out the differentiations, we derive a fourth-order linear ordinary differential equation,

$$\left(\frac{d^2}{dr^2} + \frac{1}{r} \frac{d}{dr} - \frac{1}{r^2} \right) \left(\frac{d^2}{dr^2} + \frac{1}{r} \frac{d}{dr} - \frac{1}{r^2} \right) q = 0. \quad (9.7.10)$$

Working as in Section 9.4 for flow due to the motion of a sphere, we derive the general solution

$$q(r) = A r^3 + B r \ln \frac{r}{a} + C r + \frac{D}{r}, \quad (9.7.11)$$

where A , B , C and D , are four constants.

For the far-field condition (9.7.8) to be satisfied, the constants A , B , and C must all be zero. Only one coefficient, D , is then left to satisfy the two remaining boundary conditions (9.7.7) at the surface of the cylinder, which is not possible. Sadly, the problem of Stokes flow due to the motion of a cylinder does not admit a solution.

Significance of inertia

To probe the origin of this catastrophe, we return to examine the magnitude of inertial and viscous terms in the equation of motion, as discussed in Section 9.5. cursory inspection reveals that the approximations underlying the notion of creeping flow cease to be accurate far from the cylinder. As a consequence, imposing the far field condition (9.7.8) is inconsistent.

In the case of three-dimensional flow due to the motion of a sphere discussed in Section 9.5, this difficulty was shielded by the decay of the flow due to a three-dimensional Stokeslet expressing a point force. In contrast, in the case of two-dimensional flow, the velocity field due to a point force exhibits a logarithmic divergence contributed by the second term on the right-hand side of (9.7.11), and a decaying solution cannot be found.

Matched asymptotic expansions

To remedy this essential difficulty, we use the method of matched asymptotic expansions. The main idea is to divide the flow into two regimes, as follows:

- An inner regime where the motion of the fluid is governed by the equations of creeping flow, subject to the no-slip and no-penetration boundary conditions at the surface of the cylinder, as discussed previously in this section.
- An outer regime where the motion of the fluid is governed by another simplified system of equations, called the equations of Oseen flow, subject to the far-field condition (9.7.8).

Matching conditions arise by requiring consistency between the functional forms of the inner and outer solutions, respectively, for large and small distances from the center of the cylinder. The analysis involves sophisticated arguments that lie outside the scope of our discussion.

9.7.2 Rotation of a circular cylinder

Not all problems of two-dimensional infinite flow are ill-posed, in that a solution that satisfies the boundary and far-field conditions cannot be found. If the force exerted on the union of all internal boundaries is zero, then a perfectly acceptable solution can be obtained.

As an example, we consider two-dimensional flow generated by a circular cylinder of radius a that rotates with angular velocity Ω around its center. The induced flow is identical to that due to a point vortex with strength $\kappa = 2\pi\Omega a^2$ situated at the center of cylinder, as discussed in Section 3.7. Using expressions (3.7.1), we derive the radial and polar velocity components

$$u_r = 0, \quad u_\theta = \Omega \frac{a^2}{r}. \quad (9.7.12)$$

The corresponding pressure field is uniform throughout the domain of flow.

An external torque must be applied to counterbalance the hydrodynamic torque due to the motion of the fluid, and thus sustain the rotation of the cylinder. The torque with respect to the center of the cylinder is given by

$$T_z = \oint_{\text{cylinder}} \sigma_{r\theta} a \, d\ell, \quad (9.7.13)$$

where ℓ is the arc length around the cylinder. Substituting (9.7.12) into the Newtonian constitutive equation shown in Table 4.7.3, we derive the stress component

$$\sigma_{r\theta} = -2\mu\Omega a^3 \frac{1}{r^2}. \quad (9.7.14)$$

Substituting this expression into (9.7.13), setting $d\ell = a \, d\theta$, and integrating with respect to θ from 0 to 2π , we obtain

$$T_z = -4\pi\mu\Omega a^2. \quad (9.7.15)$$

9.7.3 Simple shear flow past a circular cylinder

As a further application, we consider simple shear flow along the x axis past a circular cylinder of radius a centered at the origin. The incident velocity components are

$$u_x^\infty = \xi y, \quad u_y^\infty = 0, \quad (9.7.16)$$

where the constant ξ is the shear rate. The cylinder is allowed to rotate about its center with angular velocity

$$\Omega = -\frac{1}{2} \xi. \quad (9.7.17)$$

If ξ is positive, the cylinder rotates in the clockwise direction; if ξ is negative, the cylinder rotates in the counter-clockwise direction.

A detailed analysis shows that the radial and polar components of the velocity are given by

$$u_r = \xi a \frac{1}{2} \left(\frac{r}{a} - 2 \frac{a}{r} + \frac{a^3}{r^3} \right) \sin 2\theta \quad (9.7.18)$$

and

$$u_\theta = \xi a \frac{1}{2} \left(-\frac{r}{a} + \left(\frac{r}{a} - \frac{a^3}{r^3} \right) \cos 2\theta \right), \quad (9.7.19)$$

while the torque exerted on the cylinder is zero. These results demonstrate that a freely-suspended cylinder rotates at an angular velocity that is equal to the negative of half the shear rate of the incident simple shear flow.

9.7.4 The Oseen tensor and the point force

The second term on the right-hand side of (9.7.11), involving the logarithm, represents the flow due to a two-dimensional point force oriented along the x axis. Differentiating with respect to x or y , we obtain the corresponding velocity field. Repeating the derivation for a point force oriented along the y axis, we obtain the velocity field at a point, $\mathbf{x} = (x, y)$, due to a two-dimensional Stokeslet with vectorial strength $\mathbf{s} = (s_x, s_y)$ situated at another point, $\mathbf{x}_0 = (x_0, y_0)$, expressed by

$$\begin{bmatrix} u_x \\ u_y \end{bmatrix} (\mathbf{x}, \mathbf{x}_0) = \mathcal{S}(\mathbf{x}, \mathbf{x}_0) \cdot \begin{bmatrix} s_x \\ s_y \end{bmatrix}, \quad (9.7.20)$$

where \mathcal{S} is the 2×2 Oseen tensor for two-dimensional flow defined as

$$\mathcal{S}(\mathbf{x}, \mathbf{x}_0) = \begin{bmatrix} -\ln \frac{r}{a} + \frac{(x-x_0)^2}{r^2} & \frac{(x-x_0)(y-y_0)}{r^2} \\ \frac{(y-y_0)(x-x_0)}{r^2} & -\ln \frac{r}{a} + \frac{(y-y_0)^2}{r^2} \end{bmatrix}, \quad (9.7.21)$$

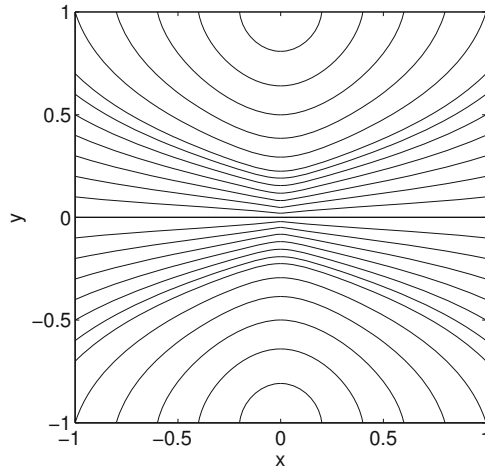


Figure 9.7.1 Streamline pattern of the flow induced by a two-dimensional point force pointing along the x axis.

a is a specified constant length, and

$$r = [(x - x_0)^2 + (y - y_0)^2]^{1/2} \tag{9.7.22}$$

is the distance of the field point, \mathbf{x} , from the location of the Stokeslet, \mathbf{x}_0 .

The two columns of the Oseen tensor represent, respectively, the x and y velocity components associated with a Stokeslet of unit strength pointing in the direction of the x or y axis. The corresponding pressure field is given by

$$p(\mathbf{x}, \mathbf{x}_0) = \mu \frac{2}{r^2} \begin{bmatrix} x - x_0 \\ y - y_0 \end{bmatrix} \cdot \begin{bmatrix} s_x \\ s_y \end{bmatrix}, \tag{9.7.23}$$

where a dot denotes the inner vector product. The streamline pattern of the flow induced by a two-dimensional Stokeslet oriented along the x axis is shown in [Figure 9.7.1](#).

Consider a closed contour, \mathcal{C} , enclosing a singular point, \mathbf{x}_0 . It can be shown that the force exerted on the fluid enclosed by the contour is given by

$$\mathbf{F} = \oint_{\mathcal{C}} \boldsymbol{\sigma} \cdot \mathbf{n} \, d\ell = -4\pi\mu \mathbf{s}, \tag{9.7.24}$$

independent of the contour shape, where $\boldsymbol{\sigma}$ is the stress tensor, \mathbf{n} is the unit vector normal to \mathcal{C} pointing outward, and ℓ is the arc length. The torque with respect to the point \mathbf{x}_0 is zero. The force and torque exerted on a closed contour that does not enclose the singular point, \mathbf{x}_0 , are also zero. These results are consistent with our earlier assertion that the two-dimensional Stokeslet expresses the flow due to a two-dimensional point force.

PROBLEM**9.7.1** Simple shear flow past a freely-suspended cylinder

(a) Verify that the velocity field given in (9.7.18) and (9.7.19) satisfies the continuity equation

$$\frac{1}{r} \frac{\partial(ru_r)}{\partial r} + \frac{1}{r} \frac{\partial u_\theta}{\partial \theta} = 0. \quad (9.7.25)$$

(b) Confirm that the torque exerted on the cylinder is zero. (c) Compute the associated pressure field.

9.8 Local solutions

The boundaries of a flow may involve walls, interfaces, and dividing streamlines that meet at corners or cusps. Deep into the corners or cusps, the magnitude of the velocity decays rapidly, the inertia of the fluid becomes negligible, and the Reynolds number of the local flow is small. The structure of the flow may then be studied in the context of Stokes flow, regarding the far flow as a driving mechanism that determines the intensity and selects the geometrical mode and spatial structure of the local flow.

9.8.1 Solution by separation of variables

Consider a two-dimensional flow between two planes intersecting at an angle 2α , as illustrated in Figure 9.8.1. To facilitate the implementation of the boundary conditions, we introduced plane polar coordinates with origin at the apex, (r, θ) . To circumvent the computation of the pressure, we introduce the stream function, ψ , and separate the radial from the angular dependencies, writing

$$\psi(r, \theta) = q(r) f(\theta), \quad (9.8.1)$$

where $q(r)$ and $f(\theta)$ are two *a priori* unknown functions. Note that expression (9.8.1) is a generalization of expression (9.7.6) describing the flow due to the motion of a cylinder.

Next, we stipulate that the component function $q(r)$ exhibits a power-law dependence on r ,

$$q(r) = r^\lambda, \quad (9.8.2)$$

while the component function $f(\theta)$ exhibits an exponential dependence on θ ,

$$f(\theta) = A \exp(\kappa\theta), \quad (9.8.3)$$

where λ and κ are two constants and A is an arbitrary coefficient. The exponent, κ , is allowed to be complex,

$$\kappa = \kappa_R + i\kappa_I, \quad (9.8.4)$$

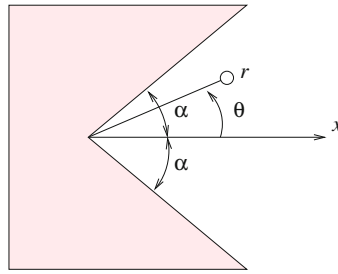


Figure 9.8.1 Because the local Reynolds number of the flow near a corner is small, the motion of the fluid is governed by the equations of Stokes flow. Similarity solutions can be derived working in local plane polar coordinates, (r, θ) .

where i is the imaginary unit, $i^2 = -1$, and κ_R, κ_I are two real constants. Using the Euler decomposition of the complex exponential, we write

$$f(\theta) = A \exp(\kappa_R \theta) [\cos(\kappa_I \theta) + i \sin(\kappa_I \theta)], \tag{9.8.5}$$

with the understanding that either the real or the imaginary part may be selected on the right-hand side of (9.8.1).

Substituting expressions (9.8.2) and (9.8.3) into (9.8.1) and the result in the biharmonic equation, $\nabla^4 \psi = 0$, expressed in plane polar coordinates, as shown in (9.7.9), we derive a bi-quadratic algebraic equation for κ parametrized by the exponent λ ,

$$\kappa^4 + 2(\lambda^2 - 2\lambda + 2)\kappa^2 + \lambda^2(\lambda - 2)^2 = 0. \tag{9.8.6}$$

The roots can be found readily using the quadratic formula. Solving for κ , substituting the result into (9.8.5), and rearranging the emerging expression, we obtain the general solution

$$f(\theta) = \begin{cases} B \sin(\lambda\theta - \beta) + C \sin[(\lambda - 2)\theta - \gamma] & \text{if } \lambda \neq 0, 1, 2, \\ B \sin(2\theta - \beta) + C\theta + D & \text{if } \lambda = 0, 2, \\ B \sin(\theta - \beta) + C\theta \sin(\theta - \gamma) & \text{if } \lambda = 1, \end{cases} \tag{9.8.7}$$

where B, C are two complex constants and β, γ are two real constants.

A variety of flows can be generated by selecting, or solving for, the exponent λ . Illustrative examples are discussed in the remainder of this section.

9.8.2 Stagnation-point flow on a plane wall

In the first application, we consider flow near a stagnation point on a plane wall, as illustrated in Figure 9.8.2. The no-slip and no-penetration boundary conditions require that

$$f = 0, \quad \frac{df}{d\theta} = 0 \tag{9.8.8}$$

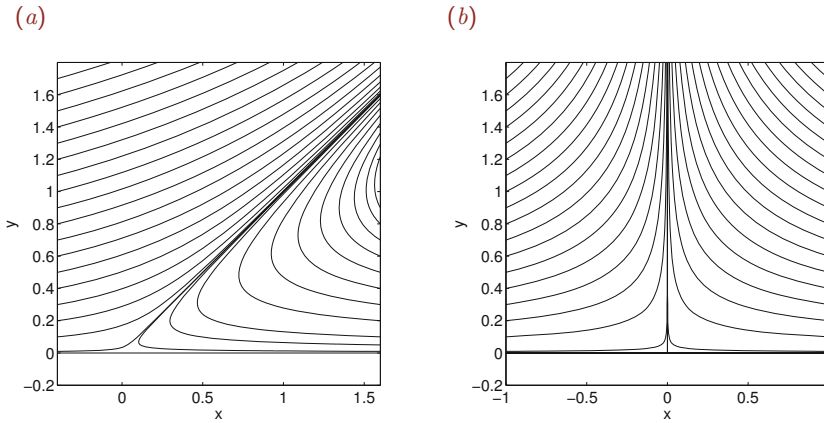


Figure 9.8.2 Streamline pattern of flow in the neighborhood of a stagnation point on a plane wall with a rectilinear dividing streamline. The angle subtended between the dividing streamline and the wall is (a) $\alpha = \pi/4$ and (b) $\pi/2$.

at $\theta = 0$ and π . The structure of the flow is determined by specifying that $f = 0$ along the dividing streamline located at $\theta = \alpha$, where the angle α is regarded as a free parameter.

Making the judicious choice $\lambda = 3$ and using the general solution given by the first formula in (9.8.7), we obtain

$$f(\theta) = B \sin(3\theta - \beta) + C \sin(\theta - \gamma). \quad (9.8.9)$$

Enforcing the no-slip and no-penetration boundary conditions, and specifying the orientation of the dividing streamline, we derive a system of three homogeneous equations for the constants B and C , involving the unknown parameters, β and γ . The no-penetration condition requires that

$$f(0) = f(\pi) = -B \sin \beta - C \sin \gamma = 0, \quad (9.8.10)$$

the no-slip condition requires that

$$\left(\frac{df}{d\theta}\right)_{\theta=0} = -\left(\frac{df}{d\theta}\right)_{\theta=\pi} = 3B \cos \beta + C \cos \gamma = 0, \quad (9.8.11)$$

and the orientation of the dividing streamline requires that

$$f(\alpha) = B \sin(3\alpha - \beta) + C \sin(\alpha - \gamma) = 0. \quad (9.8.12)$$

Combining equations (9.8.10) and (9.8.11), we find that

$$\tan \beta = -3 \tan \gamma. \quad (9.8.13)$$

Combining equations (9.8.11) and (9.8.12), we find that

$$3 \frac{\cos \beta}{\sin(3\alpha - \beta)} = -\frac{\cos \gamma}{\sin(\alpha - \gamma)}. \tag{9.8.14}$$

Equations (9.8.13) and (9.8.14) can be used to express β and γ in terms of α . Using any one of equations (9.8.10), (9.8.11), (9.8.12) to express B in terms of C , substituting the result into (9.8.9), and making use of the trigonometric identity $\sin 3a = 3 \sin a - 4 \sin^3 a$, we derive the final form

$$f(\theta) = G \sin^2 \theta \sin(\theta - \alpha), \tag{9.8.15}$$

where G is an arbitrary constant.

Substituting (9.8.15) into (9.8.1), we obtain the desired stream function,

$$\psi(r, \theta) = G r^3 \sin^2 \theta \sin(\theta - \alpha). \tag{9.8.16}$$

The value of the constant G is determined by the strength of the flow far from the stagnation point.

Streamline patterns for $\alpha = \frac{1}{4}\pi$ and $\frac{1}{2}\pi$ are shown in [Figure 9.8.2](#). A distinguishing feature of Stokes flow is that the dividing streamlines are straight lines originating from the stagnation point on the wall. This is not true in the case of Navier–Stokes flow.

9.8.3 Flow inside a corner

In the second application, we consider flow inside a corner confined between two intersecting stationary planes located at $\theta = \pm\alpha$, as illustrated in [Figure 9.8.1](#). The no-slip and no-penetration boundary conditions require that $f = 0$ and $df/d\theta = 0$ at $\theta = \pm\alpha$.

We confine our attention to flow that is antisymmetric with respect to the midplane, located at $\theta = 0$, and require the condition $df/d\theta = 0$ at $\theta = 0$, stating that the radial velocity vanishes at the mid-plane. The value of the exponent λ cannot be specified *a priori* as in the case of stagnation-point flow discussed earlier in this section, but must be found instead as part of the solution.

Assuming that $\lambda \neq 0, 1, 2$, we set $\beta = \pi/2$ and $\gamma = \pi/2$ in the first equation of (9.8.7) to ensure that $df/d\theta = 0$ at $\theta = 0$, and find that

$$f(\theta) = Q \cos(\lambda\theta) + G \cos[(\lambda - 2)\theta], \tag{9.8.17}$$

where Q and G are two constants.

Enforcing the boundary conditions $f = 0$ and $df/d\theta = 0$ at $\theta = \pm\alpha$, we obtain a homogeneous system of two equations for the constants Q and G ,

$$\begin{bmatrix} \cos(\lambda\alpha) & \cos[(\lambda - 2)\alpha] \\ \lambda \sin(\lambda\alpha) & (\lambda - 2) \sin[(\lambda - 2)\alpha] \end{bmatrix} \cdot \begin{bmatrix} Q \\ G \end{bmatrix} = \begin{bmatrix} 0 \\ 0 \end{bmatrix}. \tag{9.8.18}$$

For a nontrivial solution to exist, the determinant of the coefficient matrix on the left-hand side must be zero, yielding

$$(\lambda - 2) \cos(\lambda\alpha) \sin[(\lambda - 2)\alpha] - \lambda \sin(\lambda\alpha) \cos[(\lambda - 2)\alpha] = 0, \quad (9.8.19)$$

which can be restated as a nonlinear algebraic equation,

$$\sin[2\alpha(\lambda - 1)] = (1 - \lambda) \sin(2\alpha). \quad (9.8.20)$$

An obvious solution is $\lambda = 1$. However, since for this value the third instead of the first equation in (9.8.7) should have been used, this choice is disqualified.

We anticipate that equation (9.8.20) will have a generally complex solution for λ , and write

$$\lambda = \lambda_R + i\lambda_I, \quad (9.8.21)$$

where i is the imaginary unit. Substituting (9.8.21) into (9.8.20) and using standard formulas of complex calculus, we derive a system of two real equations for λ_R and λ_I ,

$$\begin{aligned} \sin[2\alpha(\lambda_R - 1)] \cosh(2\alpha\lambda_I) &= (1 - \lambda_R) \sin(2\alpha), \\ \sin[2\alpha(\lambda_R - 1)] \sinh(2\alpha\lambda_I) &= -\lambda_I \sin(2\alpha). \end{aligned} \quad (9.8.22)$$

To simplify the notation, we introduce the auxiliary variables

$$\xi = 2\alpha(\lambda_R - 1), \quad \eta = 2\alpha\lambda_I, \quad \kappa = \frac{\sin(2\alpha)}{2\alpha}, \quad (9.8.23)$$

and express the system (9.8.22) in the more convenient form

$$f_1(\xi, \eta) \equiv \sin \xi \cosh \eta + \kappa \xi = 0, \quad f_2(\xi, \eta) \equiv \cos \xi \sinh \eta + \kappa \eta = 0. \quad (9.8.24)$$

Using the definition of ξ and η , we find that

$$\lambda = \frac{1 + \xi}{2\alpha} + i \frac{\eta}{2\alpha}. \quad (9.8.25)$$

Our task is to solve the system of equations (9.8.24) for ξ and η , subject to a specified value for κ , that is, subject to a specified angle, α .

Newton's method

The solution of the nonlinear algebraic equations must be found by iteration. The numerical procedure involves guessing values for ξ and η that wishfully satisfy equations (9.8.24), and then improving the guess in some sensible fashion.

In Newton's method, the solution is found by guessing the values ξ^G and η^G for ξ and η , replacing the functions $f_1(\xi, \eta)$ and $f_2(\xi, \eta)$ with their linearized Taylor series expansion,

and then solving a linear system of equations for the unknowns using elementary analytical or numerical methods. The linearized Taylor series expansion provides us with the approximations

$$f_1(\xi, \eta) \simeq f_1(\xi^G, \eta^G) + \left(\frac{\partial f_1}{\partial \xi}\right)_{\xi^G, \eta^G}(\xi - \xi^G) + \left(\frac{\partial f_1}{\partial \eta}\right)_{\xi^G, \eta^G}(\eta - \eta^G), \tag{9.8.26}$$

$$f_2(\xi, \eta) \simeq f_2(\xi^G, \eta^G) + \left(\frac{\partial f_2}{\partial \xi}\right)_{\xi^G, \eta^G}(\xi - \xi^G) + \left(\frac{\partial f_2}{\partial \eta}\right)_{\xi^G, \eta^G}(\eta - \eta^G).$$

Setting the right-hand sides to zero to satisfy (9.8.24), we find that

$$\begin{pmatrix} \frac{\partial f_1}{\partial \xi} & \frac{\partial f_1}{\partial \eta} \\ \frac{\partial f_2}{\partial \xi} & \frac{\partial f_2}{\partial \eta} \end{pmatrix}_{\xi=\xi^G, \eta=\eta^G} \cdot \begin{pmatrix} \xi - \xi^G \\ \eta - \eta^G \end{pmatrix} = - \begin{pmatrix} f_1(\xi^G, \eta^G) \\ f_2(\xi^G, \eta^G) \end{pmatrix}. \tag{9.8.27}$$

The coefficient matrix on the left-hand side is the Jacobian matrix of the algebraic system (9.8.24). In summary, Newton’s algorithm involves the following steps:

1. Guess the values ξ^G and η^G .
2. Evaluate the right-hand side of (9.8.27) and the coefficient matrix on the left-hand side.
3. Solve the system of two linear equations (9.8.27) for the differences $\Delta\xi \equiv \xi - \xi^G$ and $\Delta\eta \equiv \eta - \eta^G$; we recall that ξ and η are unknown.
4. Improve the guesses by replacing the guessed values with the new values

$$\xi^N = \xi^G + \Delta\xi, \quad \eta^N = \eta^G + \Delta\eta. \tag{9.8.28}$$

5. Return to Step 2 and repeat the procedure with new values for $\xi = \xi^N$ and $\eta = \eta^N$.

The iterations converge as long as the initial guesses are sufficiently close to the exact solution.

System (9.8.24) has a family of solution branches obtained by making different selections for the initial guess. The most physically relevant branch is associated with the smallest value of λ_R , corresponding to a flow that decays at the lowest possible rate with distance from the apex, r , yielding the strongest possible flow.

The real and imaginary parts of λ are plotted against the half-angle, α , in [Figure 9.8.3\(a\)](#). When $0.41\pi < \alpha < \pi$, the exponent λ is real; the fluid moves uninterrupted along the walls and regions of recirculating flow do not develop, as illustrated in [Figure 9.8.3\(b\)](#). When $0 < \alpha < 0.41\pi$, the exponent λ is complex; the flow develops an infinite sequence of regions of recirculating fluid, called eddies, as shown in [Figure 9.8.3\(c\)](#).

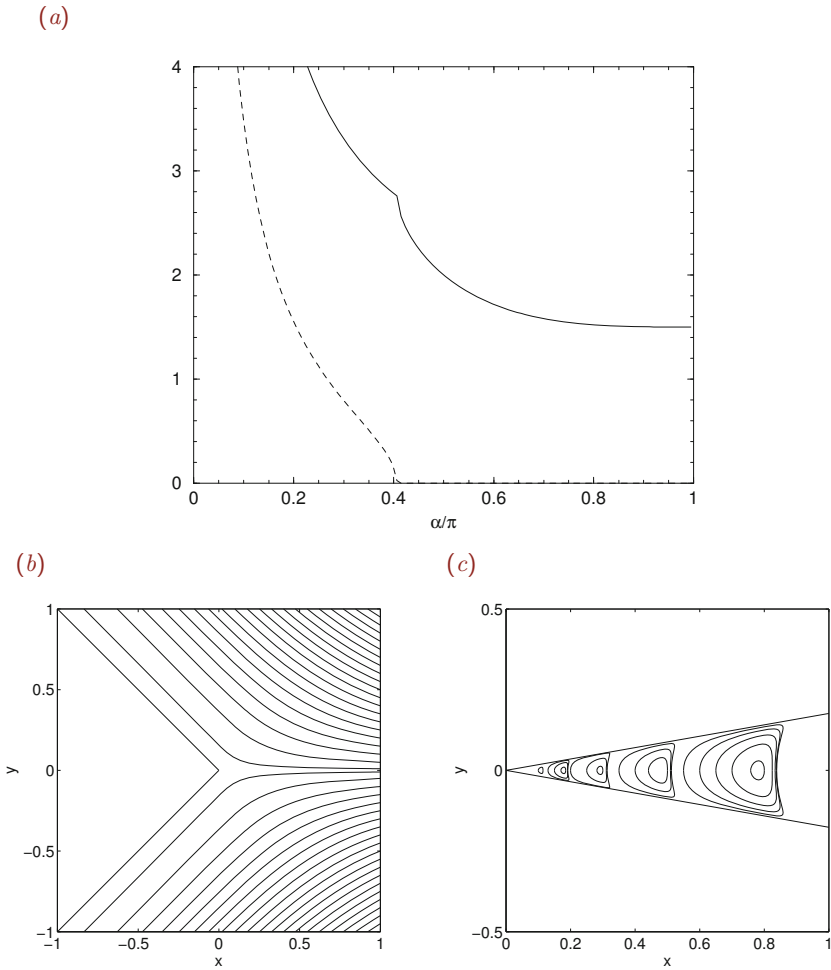


Figure 9.8.3 (a) Graphs of the real part (solid line) and imaginary part (broken line) of the exponent λ with the smallest real part for antisymmetric flow between two walls intersecting at an angle 2α . When $0.41\pi < \alpha < \pi$, λ is real; when $0 < \alpha < 0.41\pi$, λ is complex. (b, c) Streamline pattern of antisymmetric flow in a corner with half-angle (b) $\alpha = 135^\circ$, and (c) 10° .

PROBLEMS

9.8.1 *Flow near a scraper*

Derive a local solution for flow near two intersecting plates, where one of the plates is held stationary while the second plate moves parallel to itself with constant velocity. This idealized configuration is a model of the flow due to a plate scraping fluid off a flat surface, viewed in a frame of reference moving with the scraper.

9.8.2  *Computation of the exponent*

Write a computer program that uses Newton's method to solve the nonlinear algebraic system (9.8.24) and reproduce the graph shown in [Figure 9.8.3\(a\)](#).

- 10.1 Changes in the structure of a flow with increasing Reynolds number
- 10.2 Prandtl boundary-layer analysis
- 10.3 Blasius boundary layer on a semi-infinite plate
- 10.4 Displacement and momentum thickness
- 10.5 Boundary layers in accelerating or decelerating flow
- 10.6 Momentum integral method
- 10.7 Instability of shear flows
- 10.8 Finite-difference solution of the Rayleigh equation
- 10.9 Finite-difference solution of the Orr–Sommerfeld equation
- 10.10 Turbulent flow
- 10.11 Spectrum of a turbulent flow
- 10.12 Analysis and modeling of turbulent flow

Having discussed viscous flow at low Reynolds numbers in Chapter 9, now we turn our attention to the diametrically opposite limit of inertia-dominated flow at high Reynolds numbers. Inspecting the changes in the structure of a flow with increasing Reynolds number, we encounter a rich phenomenology and a variety of transition protocols. In all cases, when the Reynolds number exceeds a critical threshold, flow instability sets in and a small-scale turbulent motion is established. The study of the structure and dynamics of flow at high Reynolds numbers encompasses several complementary topics including potential flow theory, boundary-layer analysis, hydrodynamic stability, turbulent flow, and vortex motion. Potential flow was discussed earlier in this book; boundary-layer theory, hydrodynamic stability, and turbulent motion are discussed in this chapter; vortex motion is the exclusive topic of Chapter 11.

10.1 Changes in the structure of a flow with increasing Reynolds number

As the Reynolds number of a flow increases by raising, for example, the magnitude of the velocity, the structure of the flow changes in a way that depends strongly on the particular flow configuration. Even though a general statement regarding the anticipated protocol of change cannot be made, several pervasive features can be identified.

Boundary layers

As the Reynolds number increases, diffusion of vorticity away from the boundaries of the flow and into the bulk of the fluid is hindered by strong convection along the boundaries, toward the boundaries, or both. As a result, vorticity tends to be confined inside boundary layers and within free shear layers developing along fluid interfaces and free surfaces. Viscous forces are significant inside the boundary and free shear layers, but can be neglected in the bulk of the flow.

Vortices

Vorticity that has entered the flow by diffusion across the boundaries may accumulate into compact regions of rotational motion identified as vortices. Vortices are typically generated behind bluff bodies and at the trailing edge of streamlined objects.

Vortex dynamics

Vortex interaction causes the flow to become unsteady in a deterministic, random, or chaotic fashion. Spatial, temporal, and spatio-temporal chaos can be established even at moderate Reynolds numbers.

Instability

When the Reynolds number exceeds a critical threshold, small disturbances amplify, altering the local and sometimes the global structure of a flow.

Transition to turbulence

Instability is followed by transition leading to turbulent flow where a small-scale unsteady motion is superimposed on a large-scale steady or unsteady flow. The small-scale motion affects and is affected significantly by the large-scale structure and global properties of the flow.

10.1.1 Flow past a cylinder

The salient changes in the structure of streaming (uniform) flow past a circular cylinder with increasing Reynolds number, $Re \equiv \rho DU/\mu$, are illustrated in [Figure 10.1.1\(a\)](#). In the definition of the Reynolds number, D is the cylinder diameter, U is the velocity of the approaching stream far from the cylinder, μ is the fluid viscosity, and ρ is the fluid density.

When the Reynolds number is less than unity, inertial forces are negligible near the cylinder. The motion of the fluid is governed by the equations of Stokes flow discussed in Chapter 9, and the streamline pattern is symmetric with respect to the vertical plane that is normal to the incident stream and passes through the cylinder mid-plane.

As the Reynolds number increases, inertial forces become increasingly significant, and a boundary layer, identified as a region of increased vorticity, is established around the surface of the cylinder. The rotational fluid inside the boundary layer is convected along

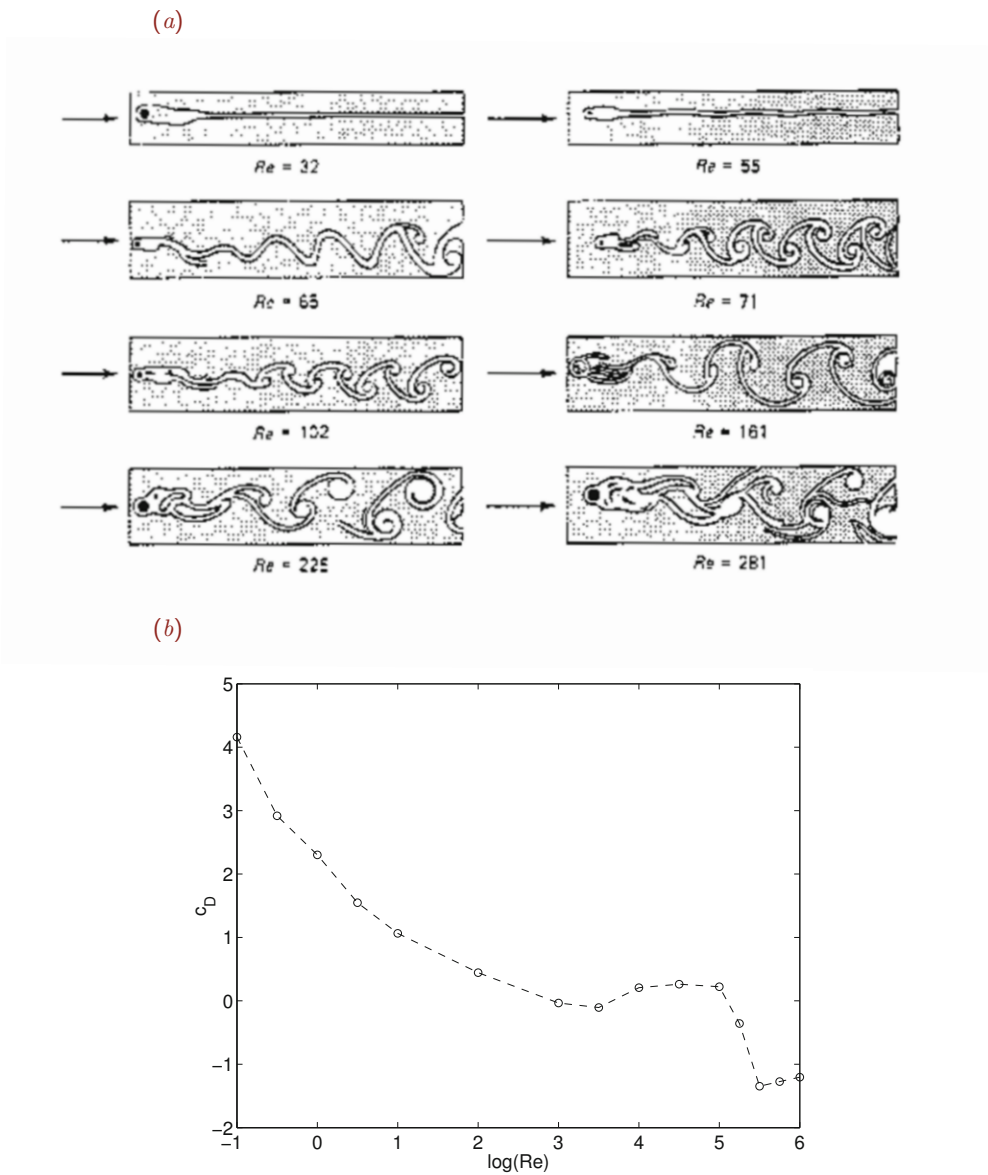


Figure 10.1.1 (a) Schematic illustration of changes in the structure of streaming flow past a circular cylinder with increasing Reynolds numbers, showing boundary-layer separation and the development of a wake, after Homann, F. (1936) Einfluss grosser Zähigkeit bei strömung um zylinder. *Forsch. Ing.-Wes.* **7**, 1–10. (b) Drag coefficient plotted against the Reynolds number defined with respect to the cylinder diameter.

the cylinder and accumulates behind the cylinder to form two regions of recirculating flow, leading to a slender wake.

A further increase in the Reynolds number causes the flow to become unstable. A pair of vortices developing behind the cylinder are shed downstream in an alternating fashion at a frequency that depends weakly on the Reynolds number, only to be replenished by newly formed vortices. The frequency of shedding, f , is expressed by the dimensionless Strouhal number, $St \equiv fD/U$. In the case of a circular cylinder, laboratory observations show that $St \simeq 0.2$. Far from the cylinder, the wake consists of two rows of counter-rotating vortices arranged in a staggered configuration that is known as the von Kàrmàn vortex street. At even higher Reynolds numbers, turbulent flow is established and the edges of the wake become blurred and poorly defined.

Behavior of the drag force

The changes in the structure of the flow described previously in this section have a strong influence on the drag force exerted on the cylinder. A graph of the dimensionless drag coefficient,

$$c_D \equiv \frac{2F}{\rho DU^2}, \quad (10.1.1)$$

is plotted against the Reynolds number in [Figure 10.1.1\(b\)](#) on a log-log scale, where F is the drag force per unit length exerted on the cylinder.

In the limit of vanishing Reynolds number, $Re \rightarrow 0$, theoretical analysis shows that the drag force is given by the modified Stokes law

$$F \simeq \frac{4\pi}{\ln \frac{7.4}{Re}} \mu U. \quad (10.1.2)$$

Correspondingly, the drag coefficient is given by

$$c_D \simeq \frac{8\pi}{Re \log \frac{7.4}{Re}}. \quad (10.1.3)$$

The change in the functional form of the drag coefficient at a critical Reynolds number on the order of 10^3 , evident in [Figure 10.1.1\(b\)](#), is due to the detachment of the boundary layer from the surface of the cylinder at a certain point at the rear surface of the cylinder, as discussed in [Section 10.4](#). The detachment occurs in a process that is described as flow separation.

When the Reynolds number becomes on the order of 10^5 , the flow becomes turbulent and the boundary layer reattaches, causing a sudden decline in the drag coefficient as shown in [Figure 10.1.1\(b\)](#).

The non-monotonic dependence of the force drag coefficient on the Reynolds number illustrated in [Figure 10.1.1\(b\)](#) is a manifestation of the complexity of fluid motion in high Reynolds number flow.

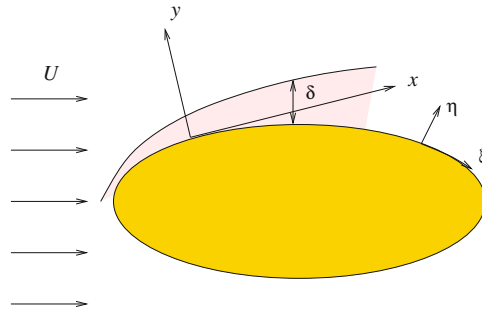


Figure 10.2.1 Schematic illustration of a Prandtl boundary layer developing around the surface of a two-dimensional curved body.

PROBLEM

10.1.1 Flow in a channel through an expansion

Consider flow through a channel with a sudden expansion, as illustrated in [Figure 6.2.1](#). Discuss the expected changes in the structure of the flow with increasing a properly defined Reynolds number.

10.2 Prandtl boundary-layer analysis

In Section 10.1, we identified a boundary layer as a region of elevated vorticity over a solid boundary in a high-Reynolds-number flow. To make the concept of a boundary layer more specific, we may consider a model flow consisting of the following two regimes:

- An outer regime where the curl of the vorticity or the vorticity itself vanishes and the motion of the fluid is described by the equations of inviscid flow, including Euler's equation and the continuity equation.
- A boundary layer across which the vorticity undergoes a rapid transition and the magnitude of viscous forces is significant, as illustrated in [Figure 10.2.1](#).

Wakes and regions of recirculating flow are allowed, but are significant only insofar as to determine the structure of the outer flow.

10.2.1 Simplifications

The slenderness of the boundary layer, compared with the typical size of the boundaries, flow allows us to simplify the equation of motion for the flow inside the boundary layer, and thereby derive approximate solutions in the asymptotic limit of high Reynolds numbers, $\text{Re} \rightarrow \infty$.

To illustrate the physical arguments involved in the formulation of the boundary-layer theory, and simultaneously demonstrate the salient mathematical simplifications, we consider the boundary layer developing along a mildly-curved two-dimensional rigid body that is held stationary in an incident irrotational flow, as shown in [Figure 10.2.1](#). Extensions to axisymmetric and three-dimensional flow are straightforward.

Continuity equation

We begin the analysis by introducing Cartesian coordinates where the x axis is tangential to the body at a point and the y axis is perpendicular to the body at that point, as shown in [Figure 10.2.1](#). Next, we apply the continuity equation for two-dimensional flow at a point in the vicinity of the origin,

$$\frac{\partial u_x}{\partial x} + \frac{\partial u_y}{\partial y} = 0. \quad (10.2.1)$$

Let L be the typical dimension of the body, U be the magnitude of the velocity of the incident irrotational flow, δ be the designated thickness of the boundary layer, and V be the typical magnitude of component of the velocity normal to the body at the edge of the boundary layer.

It is reasonable to expect that the magnitude of the derivative $\partial u_x/\partial x$ inside the boundary layer will be comparable to the ratio U/L , while the magnitude of the derivative $\partial u_y/\partial y$ will be comparable to the ratio V/δ . The continuity equation (10.2.1) requires that

$$\frac{U}{L} \sim \frac{V}{\delta} \quad \text{or} \quad V \sim \frac{U}{L} \delta, \quad (10.2.2)$$

which shows that the normal component of the velocity at the edge of the boundary layer scales with the boundary-layer thickness, δ .

x component of the equation of motion

Next, we examine the two components of the equation of motion in the vicinity of the origin written for the dynamic pressure that excludes hydrostatic variations, defined as

$$\zeta \equiv p - \rho \mathbf{g} \cdot \mathbf{x}. \quad (10.2.3)$$

Considering the x component of the Navier–Stokes equation,

$$\begin{aligned} \frac{\partial u_x}{\partial t} + u_x \frac{\partial u_x}{\partial x} + u_y \frac{\partial u_x}{\partial y} &= -\frac{1}{\rho} \frac{\partial \zeta}{\partial x} + \nu \left(\frac{\partial^2 u_x}{\partial x^2} + \frac{\partial^2 u_x}{\partial y^2} \right), \\ \downarrow \qquad \qquad \downarrow \qquad \qquad \qquad \downarrow \qquad \downarrow & \\ \frac{U^2}{L} \qquad \qquad \frac{U^2}{L} \qquad \qquad \nu \frac{U}{L^2} \qquad \nu \frac{U}{\delta^2} & \end{aligned} \quad (10.2.4)$$

we scale u_x with U , $\partial u_x/\partial x$ with U/L , u_y with V , $\partial u_x/\partial y$ with U/δ , the second derivative $\partial^2 u_x/\partial x^2$ with U/L^2 , and the second derivative $\partial^2 u_x/\partial y^2$ with U/δ^2 .

Moreover, we use the scaling shown in (10.2.2) to eliminate V in favor of U , and find that the magnitude of the various terms is as shown underneath equation (10.2.5). The scaling of the first term involving the time derivative on the left-hand side is determined by the temporal variation of the outer flow, which is best left unspecified. At this stage, there is no obvious way of scaling the x derivative of the dynamic pressure gradient on the right-hand side of (10.2.5) on the basis of kinematics alone.

The scalings shown underneath equation (10.2.5), combined with the assumption $\delta \ll L$, have two important consequences. First, the penultimate viscous term on the right-hand side is small compared to the last viscous term and may be neglected, yielding the boundary-layer equation

$$\frac{\partial u_x}{\partial t} + u_x \frac{\partial u_x}{\partial x} + u_y \frac{\partial u_x}{\partial y} = -\frac{\partial \zeta}{\partial x} + \nu \frac{\partial^2 u_x}{\partial y^2}. \tag{10.2.5}$$

Second, the magnitude of the last viscous term must be comparable to the magnitude of the inertial terms on the left-hand side, so that

$$\frac{U^2}{L} \sim \nu \frac{U}{\delta^2} \tag{10.2.6}$$

or

$$\delta \sim \sqrt{\frac{\nu L}{U}} = \frac{L}{\sqrt{\text{Re}}}, \tag{10.2.7}$$

where $\text{Re} = UL/\nu$ is the Reynolds number defined with respect to the boundary size, L .

y component of the equation of motion

Next, we consider the individual terms in the y component of the equation of motion,

$$\begin{aligned} \frac{\partial u_y}{\partial t} + u_x \frac{\partial u_y}{\partial x} + u_y \frac{\partial u_y}{\partial y} &= -\frac{1}{\rho} \frac{\partial \zeta}{\partial y} + \nu \left(\frac{\partial^2 u_y}{\partial x^2} + \frac{\partial^2 u_y}{\partial y^2} \right), \\ \downarrow \qquad \qquad \downarrow \qquad \qquad \qquad \downarrow \qquad \downarrow & \\ \frac{U^2 \delta}{L^2} \qquad \frac{U^2 \delta}{L^2} \qquad \frac{U^2 \delta}{L^2} \qquad \frac{U^2 \delta}{L^2} & \end{aligned} \tag{10.2.8}$$

and scale u_y with V , $\partial u_y/\partial x$ with V/L , u_x with U , $\partial u_y/\partial y$ with V/δ , the second derivative $\partial^2 u_y/\partial x^2$ with V/L^2 , and the second derivative $\partial^2 u_y/\partial y^2$ with V/δ^2 . Moreover, we express the kinematic viscosity of the fluid, ν , in terms of δ using the first equation in (10.2.7), replacing it with $U\delta^2/L$, and find that the magnitude of the various terms is as shown underneath equation (10.2.8).

The magnitude of all nonlinear convective and viscous terms is of order δ . Unless the magnitude of the temporal derivative on the left-hand side is of order unity, the dynamic pressure gradient across the boundary layer must also be of order δ , $\partial \zeta/\partial y \sim \delta$; to leading-order approximation,

$$\frac{\partial \zeta}{\partial y} \simeq 0. \tag{10.2.9}$$

We conclude that non-hydrostatic pressure variations across the boundary layer are negligible and the dynamic pressure inside the boundary layer is primarily a function of position along the boundary measured by the arc length.

10.2.2 Boundary-layer equations

To compute the streamwise pressure gradient, we evaluate the x component of the Euler equation (6.4.3) at the edge of the boundary layer, obtaining

$$-\frac{1}{\rho} \frac{\partial \zeta}{\partial x} = \frac{\partial U_x}{\partial t} + U_x \frac{\partial U_x}{\partial x}, \quad (10.2.10)$$

where U_x is the tangential component of the velocity of the outer flow. The boundary-layer equation (10.2.5) then becomes

$$\frac{\partial u_x}{\partial t} + u_x \frac{\partial u_x}{\partial x} + u_y \frac{\partial u_x}{\partial y} = \frac{\partial U_x}{\partial t} + U_x \frac{dU_x}{dx} + \nu \frac{\partial^2 u_x}{\partial y^2} \quad (10.2.11)$$

in a general unsteady flow.

Equations (10.2.1) and (10.2.11) provide us with a system of two second-order, nonlinear partial-differential equations for the velocity components u_x and u_y . The solution is subject to two sets of conditions: (a) the no-slip and no-penetration boundary conditions requiring that u_x and u_y are zero along the boundary, and (b) a far-field condition requiring that, as y/δ tends to infinity, u_x tends to the tangential component of the outer velocity, U_x . Because the boundary-layer equations do not involve the second partial derivative of u_y with respect to y , a far-field condition for u_y is not required.

In the boundary-layer analysis, the pressure is computed by solving the equations governing the structure of the outer irrotational flow.

Favorable and adverse pressure gradient

Evaluating equation (10.2.11) at the origin of the local Cartesian coordinates, and enforcing the no-slip and no-penetration boundary conditions in a steady flow, we obtain

$$\left(\frac{\partial^2 u_x}{\partial y^2} \right)_{y=0} = -\frac{1}{\nu} U_x \frac{dU_x}{dx}, \quad (10.2.12)$$

which shows that the sign of the curvature of the velocity profile at the boundary is opposite to that of the streamwise acceleration of the outer flow, dU_x/dx . Thus, the flow inside the boundary layer in a decelerating outer flow ($dU/dx < 0$) reverses direction, causing convection of vorticity away from the boundary and the consequent formation of vortices in the bulk of the flow.

When $dU_x/dx > 0$, the pressure gradient is negative, $d\zeta/dx < 0$, and the boundary layer is subjected to a favorable pressure gradient. In the opposite case where $dU_x/dx < 0$, the pressure gradient is positive, $d\zeta/dx > 0$, and the boundary layer is subjected to an adverse pressure gradient. Equation (10.2.12) shows that an adverse pressure gradient promotes flow separation.

10.2.3 Surface curvilinear coordinates

The Prandtl boundary-layer equation (10.2.11) was developed with reference to the local Cartesian axes shown in [Figure 10.2.1](#), and is strictly valid near the origin of the local Cartesian coordinates. To avoid redefining the Cartesian axes at every point along a boundary, we introduce curvilinear coordinates where the ξ axis is tangential to the boundary and the η axis is perpendicular to the boundary, as shown in [Figure 10.2.1](#). The corresponding velocity components are denoted by u_ξ and u_η .

Repeating the boundary-layer analysis, we find that the boundary-layer equations stated in (10.2.1), (10.2.9), and (10.2.11) stand true to leading-order approximation, provided that the Cartesian x and y coordinates are replaced by corresponding arc lengths in the ξ and η directions denoted, respectively, by ℓ_ξ and ℓ_η . Equation (10.2.9) becomes

$$\frac{\partial \zeta}{\partial \ell_\eta} = \kappa \rho U_\xi^2, \quad (10.2.13)$$

where κ is the curvature of the boundary. Thus, the dynamic pressure drop across the boundary layer is of order δ , provided that κ is not too large; that is, provided that the boundary is not too sharply curved.

For simplicity, in the remainder of this chapter we denote ℓ_ξ and ℓ_η , respectively, by x and y .

10.2.4 Parabolization

The absence of a second partial derivative with respect to the streamwise position, x , renders the boundary-layer equation (10.2.11) a parabolic partial differential equation in x . This classification has important consequences on the nature of the solution and chosen numerical method of computing the solution.

Most important, the system of equations (10.2.1) and (10.2.11) can be solved using a marching method with respect to x , beginning from a particular x station where the structure of the boundary layer is somehow known; examples will be discussed later in this chapter. In contrast, because the Navier–Stokes equation is an elliptic partial differential equation with respect to x and y , the solution must be found simultaneously at every point in the flow, even when the velocity and pressure at the inlet are specified.

The parabolic nature of (10.2.11) with respect to x implies that, if a perturbation is introduced at some point along the boundary layer, it will modify the structure of the flow downstream but will leave the upstream flow unaffected. The absence of the second partial derivative with respect to x due to the boundary-layer approximation precludes a mechanism for upstream signal propagation.

10.2.5 Flow separation

Boundary-layer analysis for laminar flow is based on two key assumptions: (a) the Reynolds number is sufficiently large, but not so large that the flow becomes turbulent, and (b) and

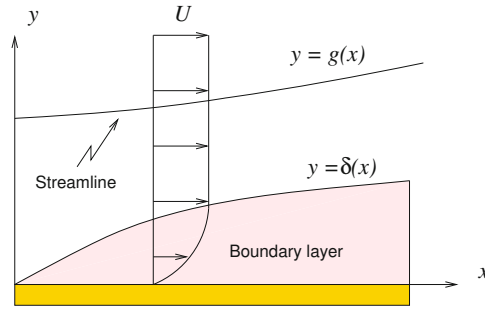


Figure 10.3.1 Schematic illustration of the boundary layer developing along a semi-infinite flat plate that is held parallel to a uniform incident stream.

the vorticity remains confined inside boundary layers wrapping around the boundaries. The physical relevance of the second assumption depends on the structure of the incident flow and on the geometry of the boundaries.

Streamlined bodies allow laminar boundary layers to develop over a large portion of their surface, whereas bluff bodies cause the vorticity to concentrate inside compact regions forming steady or unsteady wakes. For example, the alternating ejection of vortices of opposite sign into a wake is responsible for the von Kàrmàn vortex street illustrated in [Figure 10.1.1\(a\)](#). These limitations should be born in mind when questioning the physical relevance of results based on the boundary-layer approximation.

PROBLEM

10.2.1 Oscillatory flow over a plate

Compute the velocity profile in the boundary layer along an infinite plate driven by a streaming oscillatory outer flow with velocity $U_x = \bar{U}_x \cos(\omega t)$, where \bar{U}_x is the amplitude and ω is the angular frequency of the oscillations.

10.3 Blasius boundary layer on a semi-infinite plate

Having established a simplified equation of motion for the flow inside a boundary layer over a solid surface, we proceed to derive solutions by analytical and numerical methods. In this section, we study the boundary layer established over a semi-infinite flat plate that is held stationary parallel to an incident streaming (uniform) flow with velocity U , as illustrated in [Figure 10.3.1](#).

Since the tangential velocity of the outer flow is constant, $dU_x/dx = 0$, the boundary-layer equation (10.2.11) for steady flow simplifies to a convection–diffusion equation for the

streamwise velocity component,

$$u_x \frac{\partial u_x}{\partial x} + u_y \frac{\partial u_x}{\partial y} = \nu \frac{\partial^2 u_x}{\partial y^2}. \quad (10.3.1)$$

The problem has been reduced to solving the simplified equation of motion (10.3.1), together with the continuity equation (10.2.1), for the velocity components, u_x and u_y , subject to the no-slip, no-penetration, and far-field conditions.

Scaling

Because the length of the plate is infinite, the only available characteristic length scale, L , introduced in Section 10.2, is the streamwise distance from the leading edge, x . The second relation in (10.2.7) then provides us with an expression for the boundary-layer thickness in terms of the local Reynolds number, $\text{Re}_x \equiv Ux/\nu$,

$$\delta(x) \sim \sqrt{\frac{\nu x}{U}} = \frac{x}{\sqrt{\text{Re}_x}}. \quad (10.3.2)$$

Recall that this scaling has arisen by balancing the magnitude of inertial and viscous forces inside the boundary layer.

10.3.1 Self-similarity and the Blasius equation

Blasius discovered that computing the solution of the system of partial differential equations (10.2.1) and (10.3.1) can be reduced solving a single ordinary differential equation. To carry out this reduction, we assume that the flow develops in a self-similar fashion, such that the streamwise velocity profile across the boundary layer is a function of a scaled dimensionless transverse position expressed by the similarity variable

$$\eta \equiv \frac{y}{\delta(x)} = y \sqrt{\frac{U}{\nu x}} \quad (10.3.3)$$

according to the functional form

$$u_x(x, y) = U F(\eta), \quad (10.3.4)$$

where $F(\eta)$ is an *a priori* unknown function.

A key observation is that this self-similar streamwise profile derives from the stream function

$$\psi(x, y) = \sqrt{\nu U x} f(\eta), \quad (10.3.5)$$

where f is the indefinite integral or anti-derivative of F , satisfying $df/d\eta = F$. The principal advantage of using the stream function is that the continuity equation is satisfied automatically and does not need to be considered.

As a preliminary, we compute the derivatives

$$\frac{\partial \eta}{\partial x} = -\frac{y}{2x} \sqrt{\frac{U}{\nu x}}, \quad \frac{\partial \eta}{\partial y} = \sqrt{\frac{U}{\nu x}}. \quad (10.3.6)$$

Differentiating (10.3.5) with respect to y or x and setting

$$\frac{\partial f}{\partial x} = \frac{df}{d\eta} \frac{\partial \eta}{\partial x}, \quad \frac{\partial f}{\partial y} = \frac{df}{d\eta} \frac{\partial \eta}{\partial y}, \quad (10.3.7)$$

we derive the x velocity component,

$$u_x(x, y) = \frac{\partial \psi}{\partial y} = U \sqrt{\nu U x} \frac{df}{d\eta} \frac{d\eta}{dy} = U \sqrt{\nu U x} \frac{df}{d\eta} \sqrt{\frac{U}{\nu x}}, \quad (10.3.8)$$

yielding

$$u_x(x, y) = U \frac{df}{d\eta}, \quad (10.3.9)$$

and the y velocity component

$$u_y(x, y) = -\frac{\partial \psi}{\partial x} = -(U\nu)^{1/2} \frac{\partial[\sqrt{x} f(\eta)]}{\partial x}, \quad (10.3.10)$$

yielding

$$u_y(x, y) = -\frac{1}{2} \sqrt{\frac{U\nu}{x}} f - \sqrt{\nu U x} \frac{df}{d\eta} \frac{\partial \eta}{\partial x} \quad (10.3.11)$$

and then

$$u_y(x, y) = -\frac{1}{2} \sqrt{\frac{U\nu}{x}} \left(f - \eta \frac{df}{d\eta} \right). \quad (10.3.12)$$

Further differentiation yields

$$\frac{\partial u_x}{\partial x} = U \frac{d^2 f}{d\eta^2} \frac{\partial \eta}{\partial x}, \quad \frac{\partial u_x}{\partial y} = U \frac{d^2 f}{d\eta^2} \frac{\partial \eta}{\partial y}, \quad (10.3.13)$$

and

$$\frac{\partial^2 u_x}{\partial y^2} = U \frac{d^3 f}{d\eta^3} \left(\frac{\partial \eta}{\partial y} \right)^2. \quad (10.3.14)$$

Substituting these expressions into the boundary-layer equation (10.3.1) and simplifying, we obtain a third-order nonlinear ordinary differential equation for the function $f(\eta)$,

$$\frac{d^3 f}{d\eta^3} + \frac{1}{2} f \frac{d^2 f}{d\eta^2} = 0, \quad (10.3.15)$$

derived by Blasius in 1908.

Enforcing the no-slip and no-penetration conditions and requiring that the flow in the boundary layer reduces to the outer uniform flow far from the plate, we obtain

$$f = 0 \quad \text{and} \quad \frac{df}{d\eta} = 0 \quad \text{at} \quad \eta = 0, \quad (10.3.16)$$

and

$$\frac{df}{d\eta} \rightarrow 1 \quad \text{as} \quad \eta \rightarrow \infty. \quad (10.3.17)$$

These equations provide us with boundary and far-field conditions to be used in solving the Blasius equation (10.3.15).

Before proceeding to compute the solution, it is instructive to apply the Blasius equation (10.3.15) at the plate where $\eta = 0$. Using the first boundary condition in (10.3.16), we find that

$$\left(\frac{d^3 f}{d\eta^3} \right)_{\eta=0} = 0, \quad (10.3.18)$$

which shows that the curvature of the streamwise velocity profile vanishes at the wall, in agreement with equation (10.2.12).

10.3.2 Numerical solution

To solve the Blasius equation (10.3.15), it is convenient to rename $x_1 = f$, denote the first and second derivative of the function f as

$$x_2 \equiv \frac{df}{d\eta}, \quad x_3 \equiv \frac{dx_2}{d\eta} = \frac{d^2 f}{d\eta^2}, \quad (10.3.19)$$

and resolve the third-order equation into a system of three first-order nonlinear equations,

$$\frac{dx_1}{d\eta} = x_2, \quad \frac{dx_2}{d\eta} = x_3, \quad \frac{dx_3}{d\eta} = -\frac{1}{2} x_1 x_3. \quad (10.3.20)$$

This system is accompanied by three boundary conditions,

$$x_1(\eta = 0) = 0, \quad x_2(\eta = 0) = 0, \quad x_3(\eta = \infty) = 1, \quad (10.3.21)$$

originating from (10.3.16) and (10.3.17).

Shooting method

Since boundary conditions are provided at both ends of the solution domain with respect to η , extending from 0 to ∞ , we are presented with a two-point boundary-value problem involving three first-order differential equations. The solution can be computed using a shooting method according to the following steps:

1. Guess the value of $x_3(0) \equiv f''(\eta = 0)$.
2. Integrate equations (10.3.20) from $\eta = 0$ to $\eta = \infty$, subject to the initial conditions (10.3.16), using the value of $x_3(\eta = 0)$.
3. Check whether the far-field condition $x_3(\eta = \infty) = 1$ is satisfied. If not, improve the guess for $q(\eta = 0)$ and return to Step 2.

In practice, integrating up to $\eta = 10$ in Step 2 yields satisfactory accuracy. The improvement in Step 3 can be made using several methods.¹

The following MATLAB code, entitled *blasius*, located in directory *10-bl* of **FDLIB**, performs the integration in the second step using the modified Euler (RK2) method:

```
%=====
% Solution of the Blasius boundary-layer equation
%=====

Nstep = 64;      % integration steps
etamax = 10.0;
deta = etamax/Nstep;

eta = 0.0;
x(1) = 0.0; x(2) = 0.0; x(3) = 0.332;

xplot(1) = eta;
yplot1(1) = x(1);
yplot2(1) = x(2);
yplot3(1) = x(3);

%---
for i=2:Nstep+1

    xp = blasius_ode(x);

    for j=1:3
        xsave(j) = x(j);
        xpsave(j) = xp(j);
        x(j) = x(j) + xp(j)*deta;
    end

    eta = eta + deta;
    xp = blasius_ode(x);

    for j=1:3
        x(j) = xsave(j) + 0.5*(xpsave(j)+xp(j))*deta;
    end
end
```

¹Pozrikidis, C. (2008) *Numerical Computation in Science and Engineering*, Second Edition, Oxford University Press.

```

xplot(i) = eta;
yplot1(i) = x(1); yplot2(i) = x(2); yplot3(i) = x(3);

end
%---

%---
% plotting
%---

hold on
plot(yplot1,xplot,'--')
plot(yplot2,xplot)
plot(yplot3,xplot,':')
ylabel('\eta','fontsize',15)

```

The program calls the following MATLAB function to evaluate the right-hand side of the differential equations:

```

function xp = blasius_ode(x)

%---
% Blasius odes
%---

xp(1) = x(2);
xp(2) = x(3);
xp(3) = -0.50*x(1)*x(3);

end

```

This function receives the vector \mathbf{x} in the input and generates the rate-of-change vector \mathbf{xp} in the output.

Numerical computations show that the far-field boundary condition is satisfied when $f''(0) \simeq 0.332$, to shown precision. The corresponding profile of the streamwise velocity, $u/U = f' \equiv df/d\eta$, is drawn with the solid line in [Figure 10.3.2](#). The profiles of f and $f'' \equiv d^2f/d\eta^2$ are drawn with the dashed and dotted lines.

The numerical solution shows that $u/U = 0.99$ when $\eta \simeq 4.9$, to shown precision. Based on this result, we may define the 99% boundary-layer thickness

$$\delta_{99} = 4.9 \sqrt{\frac{\nu x}{U}} \quad \text{or} \quad \frac{\delta_{99}}{x} = 4.9 \frac{1}{\text{Re}_x}, \quad (10.3.22)$$

where $\text{Re}_x \equiv Ux/\nu$ is the local Reynolds number. The 99.5% boundary-layer thickness is defined in a similar fashion. The numerical solution shows that the corresponding coefficient on the right-hand side of equations (10.3.22) is approximately equal to 5.3.

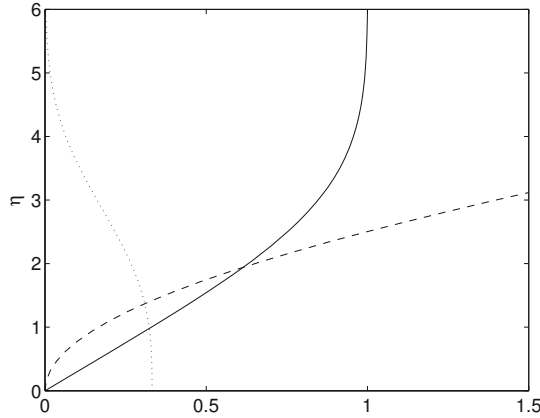


Figure 10.3.2 Profiles of the Blasius self-similar streamwise velocity, $u/U = f'$ (solid line) and its integral and derivative functions f and f'' (dashed and dotted lines).

10.3.3 Wall shear stress and drag force

The wall shear stress and drag force exerted on a boundary are of particular interest in the engineering design of equipment for high-speed flow. According to the Blasius similarity solution, the wall shear stress is given by

$$\tau_{xy}(x) = \mu \left(\frac{\partial u_x}{\partial y} \right)_{y=0} = \frac{f''(0)}{\sqrt{\text{Re}_x}} \rho U^2 = 0.332 \frac{1}{\sqrt{\text{Re}_x}} \rho U^2. \quad (10.3.23)$$

We observe that the wall shear stress takes an infinite value at the leading edge and decreases like the inverse square root of the streamwise distance or local Reynolds number, Re_x , along the plate. However, the physical significance of the singular behavior at the origin is compromised by the breakdown of the assumptions that led us to the boundary-layer equations at the leading edge.

Drag force

Even though the shear stress is infinite at the leading edge, the inverse-square-root singularity is integrable and the drag force exerted on any finite section of the plate extending from the leading edge up to an arbitrary point is finite. Using the similarity solution, we find that the drag force exerted on *both* sides of the plate over a length extending from the leading edge up to a certain distance x , is given by

$$D(x) \equiv 2 \int_0^x \tau_{xy}(\xi) \, d\xi = 0.664 \rho U \sqrt{U\nu} \int_0^x \frac{d\xi}{\sqrt{\xi}}. \quad (10.3.24)$$

Performing the integration, we obtain

$$D(x) = 1.328 \frac{1}{\sqrt{\text{Re}_x}} \rho U^2 x. \quad (10.3.25)$$

Based on this expression, we define the dimensionless drag coefficient

$$c_D \equiv \frac{D}{\frac{1}{2}\rho U^2 x} = 2.656 \frac{1}{\sqrt{\text{Re}_x}}. \quad (10.3.26)$$

The predictions of equations (10.3.25) and (10.3.26) agree with laboratory measurements up to about $\text{Re}_x \simeq 1.2 \times 10^5$. Beyond that point, the flow inside the boundary layer develops a wavy pattern and ultimately becomes turbulent. Above the critical value of Re_x , the function $c_D(\text{Re}_x)$ jumps to a different branch with significantly higher values.

10.3.4 Vorticity transport

Neglecting the velocity component normal to the boundary layer, along the y axis, we find that the z component of the vorticity inside the boundary layer is given by

$$\omega_z(x, y) \simeq -\frac{\partial u_x}{\partial y} = -\frac{f''(\eta)}{\sqrt{\text{Re}_x}} \frac{U^2}{\nu} = -f''(\eta) \frac{U}{\delta(x)}. \quad (10.3.27)$$

We observe that the strength of the vorticity at a particular location, η , decreases like the inverse of the local boundary-layer thickness, $\delta(x)$, due to the broadening of the velocity profile.

The streamwise rate of convection of vorticity across a plane that is perpendicular to the plate is given by

$$\int_0^\infty u_x(x, y) \omega_z(x, y) dy \simeq -\int_0^\infty u_x(x, y) \frac{\partial u_x}{\partial y} dy = -\frac{1}{2} U^2, \quad (10.3.28)$$

which is independent of the downstream position, x . Thus, the flux of vorticity across the plate is zero and viscous diffusion of vorticity does not occur at the wall, in agreement with our earlier observation that the gradient of the vorticity vanishes at the wall,

$$U \frac{\partial f'''}{\partial y} = \frac{\partial^2 u_x}{\partial y^2} = -\frac{\partial \omega}{\partial y} = 0. \quad (10.3.29)$$

Consequently, all convected vorticity is generated at the leading edge where the boundary-layer approximation ceases to be valid. Viscous stresses at the leading edge somehow generate the proper amount of vorticity necessary for the Blasius self-similar flow.

PROBLEMS

10.3.1 Blasius solution

Use the shooting method to compute $f''(0)$ for the Blasius boundary layer, accurate to the sixth decimal place.

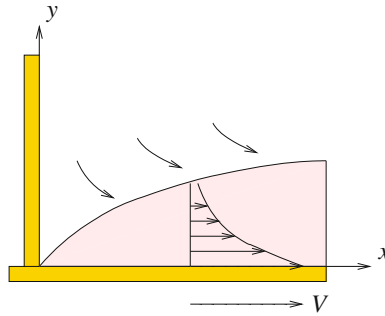


Figure 10.3.3 Illustration of the Sakiadis boundary layer developing over a semi-infinite translating belt.

10.3.2 Sakiadis boundary layer

Consider flow due to the translation of a semi-infinite belt along the x axis with velocity V normal to a vertical stationary wall, as illustrated in Figure 10.3.3. A boundary layer identified by Sakiadis is established along the belt.²

(a) Show that the flow in the boundary layer is governed by the Blasius equation (10.3.15), subject to the modified boundary conditions $f = 0$ and $f' = 0$ at $\eta = 0$, and $f' \rightarrow 0$ as η tends to infinity.

(b) Obtain the solution using the shooting method, plot the streamwise velocity profile, and discuss the structure of the flow field far from the moving belt. *Hint:* the iterations converge when $f''(0) = -0.44375$.

10.4 Displacement and momentum thickness

Because of the broadening of the velocity profile in the streamwise direction, x , the streamlines inside the Blasius boundary layer are deflected upward and away from the plate, as shown in Figure 10.3.1. To quantify this deflection, we introduce the displacement thickness.

Displacement thickness

Consider a streamline outside the boundary layer, described by the equation $y = g(x)$, and write a mass balance over a control area that is enclosed by (a) the streamline, (b) a vertical plane located at $x = 0$, (c) a vertical plane located at a certain distance x , and (d) the plate. Since the streamwise velocity profile at the leading edge located at $x = 0$ is flat, we obtain

$$\int_0^{g(0)} U \, dy = \int_0^{g(x)} u_x(x, y) \, dy. \quad (10.4.1)$$

²Sakiadis, B. C., (1961) Boundary-layer behavior on continuous solid surfaces: I. Boundary-layer equations for two-dimensional and axisymmetric flow, *AICHE J.* **7**, 26–28; II. The boundary layer on a continuous flat surface, *AICHE J.* **7**, 221–225.

Straightforward rearrangement yields the equation

$$U (g(x) - g(0)) = \int_0^{g(x)} (U - u_x(x, y)) \, dy. \quad (10.4.2)$$

Taking the limit as the streamline under consideration moves increasingly far from the plate, we derive the equation

$$\lim_{x \rightarrow \infty} (g(x) - g(0)) = \delta^*(x), \quad (10.4.3)$$

where

$$\delta^*(x) \equiv \int_0^{\infty} \left(1 - \frac{u_x}{U}\right) \, dy \quad (10.4.4)$$

is defined as the displacement thickness.

Using the numerical solution of the Blasius equation to evaluate the integral on the right-hand side of (10.4.4), we derive the exact relation

$$\delta^*(x) = \left(\frac{\nu x}{U}\right)^{1/2} \int_0^{\infty} \left(1 - \frac{df}{d\eta}\right) \, d\eta = 1.721 \sqrt{\frac{\nu x}{U}}, \quad (10.4.5)$$

which shows that the displacement thickness, like the 99% boundary-layer thickness, increases like the square root of the streamwise position, x .

Physically, the displacement thickness describes the vertical displacement of the streamlines far from the plate with respect to their elevation at the leading edge. Laboratory experiments have shown that the boundary layer undergoes a transition from the laminar to the turbulent state when the displacement thickness reaches the approximate value $\delta^* \sim 600\nu/U$. At that point, turbulent shear stresses become significant and the analysis pursued in this section based on the assumption of laminar flow ceases to be valid.

The displacement thickness describes the surface of a fictitious impenetrable but slippery body that is held stationary in the incident irrotational flow. An improved boundary-layer theory can be developed by replacing the tangential velocity of the outer flow along the plate, U , with the corresponding tangential component of the velocity of the irrotational flow past the fictitious body. The irrotational flow past the fictitious body must be computed after the displacement thickness has been established, as discussed in this section. This iterative improvement provides us with a basis for describing the flow in the context of asymptotic expansions.

Momentum thickness

It is illuminating to perform a momentum integral balance over the control area used previously to define the displacement thickness. Since the upper boundary of the control volume is a streamline, it does not contribute to the rate of momentum input. Assuming that the normal stresses at the vertical sides are equal in magnitude and opposite in sign, which is

justified by the assumption that the pressure drop across the boundary layer is negligibly small, and neglecting the traction along the top streamline, we obtain

$$\int_0^{g(0)} U (\rho U) dy - \int_0^{g(x)} u_x (\rho u_x) dy - \frac{1}{2} D(x) = 0, \quad (10.4.6)$$

where $D(x)$ is the drag force exerted on *both* sides of the plate, defined in equation (10.3.25). Now we make the upper limits of integration equal by recasting (10.4.6) into the form

$$-\rho U^2 (g(x) - g(0)) - \rho \int_0^{g(x)} (U^2 - u_x^2) dy - \frac{1}{2} D(x) = 0. \quad (10.4.7)$$

Finally, we take the limit as the streamline defining the top of the control area moves far from the plate, and use the definitions (10.4.3) and (10.4.4) to obtain the relation

$$D(x) = 2 \rho U^2 \Theta(x), \quad (10.4.8)$$

where Θ is the momentum thickness defined as

$$\Theta(x) \equiv \int_0^\infty \frac{u_x}{U} (1 - \frac{u_x}{U}) dy. \quad (10.4.9)$$

Using the numerical solution of the Blasius equation, we find that

$$\Theta(x) = \sqrt{\frac{\nu x}{U}} \int_0^\infty f'(\eta) (1 - f'(\eta)) d\eta = 0.664 \sqrt{\frac{\nu x}{U}}, \quad (10.4.10)$$

where $f'(\eta) = df/d\eta$.

Shape factor

The ratio between the displacement and the momentum thickness is called the shape factor,

$$H \equiv \frac{\delta^*}{\Theta}. \quad (10.4.11)$$

Substituting the right-hand sides of expressions (10.4.5) and (10.4.9) into (10.4.11), we find that, for the boundary layer over a flat plate, $H = 2.591$.

Inspecting the definitions of δ^* and Θ , given in equations (10.4.4) and (10.4.8), we find that the shape factor is greater than unity as long as the streamwise velocity u_x is less than U inside a substantial portion of the boundary layer. The satisfaction of this constraint is consistent with physical intuition. The smaller the value of H , the more blunt the velocity profile across the boundary layer.

Relation between the wall shear stress and momentum thickness

The momentum thickness is related to the wall shear stress, and *vice versa*, by the integral momentum balance expressed by equation (10.4.8). Differentiating (10.3.25) with respect to x , we find that

$$\frac{dD(x)}{dx} = 2 \tau_{xy}(x). \quad (10.4.12)$$

Expressing the drag force in terms of the momentum thickness using (10.4.8), we obtain

$$\tau_{xy}(x) = \rho U^2 \frac{d\Theta(x)}{dx}. \quad (10.4.13)$$

Thus, if the shear stress is known, the momentum thickness can be computed by integration. Conversely, if the momentum thickness is known, the shear stress can be computed by differentiation.

10.4.1 Von Kármán's approximate method

Given the velocity profile across a boundary layer, we have two ways of computing the wall shear stress: directly by differentiation, and indirectly by evaluating the momentum thickness and then differentiating it with respect to streamwise position, x , to obtain the shear stress according to equation (10.4.13). The indirect method is less sensitive to the structure of the velocity profile near the wall. For the velocity profile that arises by solving the Blasius equation, the two methods are equivalent (Problem 10.4.1).

To implement the indirect method, we may introduce a self-similar velocity profile with some reasonable form involving an unspecified function that is either stipulated by physical intuition or suggested by laboratory observation. Our goal is to adjust the unspecified function so that the two methods of computing the wall shear stress discussed in the preceding paragraph are equivalent.

A reasonable velocity profile is

$$\frac{u_x}{U} = \frac{df(\eta)}{d\eta} = \begin{cases} \sin \frac{\pi y}{2\Delta(x)} & \text{for } 0 < y < \Delta(x), \\ 1 & \text{for } y > \Delta(x), \end{cases} \quad (10.4.14)$$

where

$$\eta \equiv \frac{y}{\Delta(x)}, \quad (10.4.15)$$

and $\Delta(x)$ is an unspecified function playing the role of a boundary-layer thickness, similar to the δ_{99} thickness introduced in equation (10.3.22). Note that the velocity distribution (10.4.14) conforms with the required boundary conditions $f'(0) = 0$, $f'''(0) = 0$, and $f'(\infty) = 1$, but does not satisfy the Blasius equation; a prime denotes a derivative with respect to η .

Differentiating the profile (10.4.14) with respect to y , we obtain the wall shear stress

$$\tau_{xy}(x) = \frac{\pi}{2} \frac{\mu U}{\Delta(x)}. \quad (10.4.16)$$

The displacement thickness, momentum thicknesses, and shape factor defined in (10.4.4) and (10.4.8) are found to be

$$\delta^*(x) = \left(1 - \frac{2}{\pi}\right) \Delta(x) = 0.363 \Delta(x), \quad \Theta(x) = \left(\frac{2}{\pi} - \frac{1}{2}\right) \Delta(x) = 0.137 \Delta(x). \quad (10.4.17)$$

The shape factor defined in (10.4.11) is found to be

$$H = 2.660. \quad (10.4.18)$$

It is reassuring to observe that the shape factor is remarkably close to that arising from the exact solution of the Blasius equation, $H = 2.591$.

Now substituting the expressions for the momentum thickness and wall shear stress into the integral momentum balance (10.4.13), we derive an ordinary differential equation for $\Delta(x)$,

$$\frac{\pi}{2} \frac{\mu U}{\Delta(x)} = 0.137 \rho U^2 \frac{d\Delta(x)}{dx}. \quad (10.4.19)$$

Rearranging and integrating with respect to x subject to the initial condition $\Delta = 0$ at $x = 0$, we find that

$$\Delta(x) = 4.80 \sqrt{\frac{\nu x}{U}}. \quad (10.4.20)$$

Substituting this expression back into (10.4.16) and (10.4.17), we find that

$$\tau_{xy}(x) = \frac{0.327}{\sqrt{Re_x}} \rho U^2, \quad \delta^*(x) = 1.743 \sqrt{\frac{\nu x}{U}}, \quad \Theta(x) = 0.665 \sqrt{\frac{\nu x}{U}}. \quad (10.4.21)$$

These approximate expressions are in remarkable agreement with their exact counterparts shown in (10.3.23), (10.4.5), and (10.4.9).

However, this level of agreement is fortuitous and atypical of the accuracy of the approximate method (Problem 10.4.2).

PROBLEMS

10.4.1 Wall shear stress

Confirm that the wall shear stress computed directly by differentiating the velocity profile across the Blasius boundary layer is the same as that arising by differentiating the momentum thickness with respect to streamwise position, x , according to equation (10.4.13).

10.4.2 Von Kàrmàn's method

Assume that the velocity profile across the Blasius boundary layer is described by a hyperbolic tangent function

$$u_x = U \tanh \frac{y}{\Delta(x)}. \quad (10.4.22)$$

Show that the effective boundary-layer thickness, wall shear stress, displacement thickness, and momentum thicknesses are given by the right-hand sides of equations (10.4.20) and

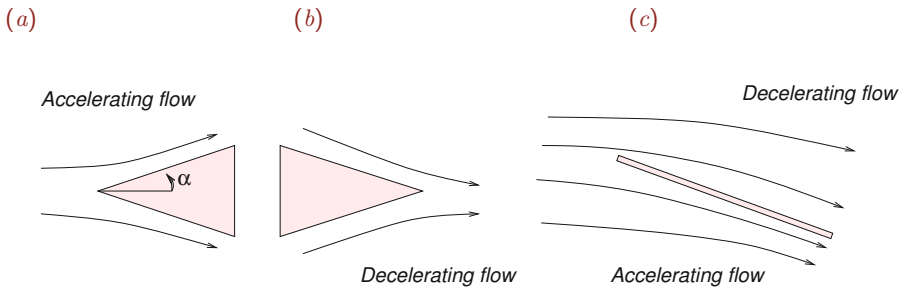


Figure 10.5.1 Boundary layers in accelerating or decelerating flow: (a, b) flow past a wedge and (c) uniform flow past a flat plate at a non-zero angle of attack.

(10.4.21), except that the numerical coefficients are equal, respectively, to 2.553, 0.392, 1.770, and 0.783. Discuss the accuracy of these results with reference to the exact solution.

10.4.3 Sakiadis' boundary layer

Compute the displacement thickness, momentum thickness, and shape factor of the Sakiadis boundary layer discussed in Problem 10.3.2.

10.5 Boundary layers in accelerating or decelerating flow

In Section 10.3, we discussed the Blasius boundary layer developing along a flat plate parallel to a uniform incident streaming flow. One important feature of the parallel configuration is the uniformity of the tangential velocity of the outer flow over the plate. In this section, we consider the more general case of a Falkner–Skan boundary layer developing in an accelerating or decelerating incident flow. Examples of physical situations where such boundary layers occur are illustrated in Figure 10.5.1.

Consider an outer flow whose tangential velocity, $U_x(x)$, exhibits a power-law dependence on the streamwise distance from a specified origin, x , along a flat surface,

$$U_x(x) = c x^m, \tag{10.5.1}$$

where c is a positive coefficient and m is a positive or negative exponent. When $m = 0$, we recover the Blasius boundary layer over a flat plate at zero angle of attack. When $m = 1$, we obtain a boundary layer in orthogonal stagnation-point flow. Intermediate values of m correspond to symmetric flow past a wedge with semi-angle

$$\alpha = \frac{m}{m + 1} \pi, \tag{10.5.2}$$

as illustrated in Figure 10.5.1(a). This expression can be inverted to give the exponent m in terms of α .

Differentiating (10.5.1) with respect to x , we obtain the streamwise acceleration or deceleration of the outer flow,

$$\frac{dU_x}{dx} = cmx^{m-1}. \quad (10.5.3)$$

Thus, the outer flow accelerates when $m > 0$ and decelerates when $m < 0$. In the first case, conservation of mass expressed by the continuity equation requires that the y derivative of the velocity component normal to the wall, U_y , is negative, $\partial U_y / \partial y < 0$. Since U_y is zero on the wall, it must be negative at the edge of the boundary layer. The associated motion of the outer fluid toward the wall confines the vorticity and reduces the thickness of the boundary layer with respect to that in a non-accelerating flow.

Substituting (10.5.3) into the boundary-layer equation (10.2.11) at steady state, we obtain the specific form

$$u_x \frac{\partial u_x}{\partial x} + u_y \frac{\partial u_x}{\partial y} = c^2 m x^{2m-1} + \nu \frac{\partial^2 u_x}{\partial y^2}. \quad (10.5.4)$$

Working as in Section 10.3 for the Blasius boundary layer, we identify the characteristic length L with the current streamwise position, x , and use (10.3.2) to define the boundary-layer thickness

$$\delta(x) \sim \sqrt{\frac{\nu x}{U_x(x)}} = \sqrt{\frac{\nu}{cx^{m-1}}}. \quad (10.5.5)$$

When $m = 1$, the boundary-layer thickness is constant, independent of x .

10.5.1 Self-similarity

We may assume that the velocity profile across the boundary is self-similar in x and y . This means that the scaled streamwise velocity profile, u_x/U_x , is a function of the dimensionless similarity variable

$$\eta \equiv \frac{y}{\delta(x)} = y \sqrt{\frac{U_x(x)}{\nu x}} = y \sqrt{\frac{c}{\nu x^{1-m}}}, \quad (10.5.6)$$

so that

$$u_x(x, y) = U_x(x) F(\eta), \quad (10.5.7)$$

where $F(\eta)$ is an *a priori* unknown function.

A key observation is that this self-similar profile can be derived from the stream function

$$\psi(x, y) = \sqrt{\nu U_x(x) x} f(\eta) = \sqrt{\nu c x^{m+1}} f(\eta), \quad (10.5.8)$$

where $F = df/d\eta$, that is, F is the indefinite integral of f .

As a preliminary, we compute the derivatives

$$\frac{\partial \eta}{\partial x} = \frac{m-1}{2} \frac{y}{x} \sqrt{\frac{c x^{m-1}}{\nu}}, \quad \frac{\partial \eta}{\partial y} = \sqrt{\frac{c}{\nu x^{1-m}}}. \quad (10.5.9)$$

Differentiating (10.5.5) with respect to x , we derive expressions for the two velocity components,

$$u_x(x, y) = \frac{\partial \psi}{\partial y} = U_x(x) \frac{df}{d\eta} = c x^m \frac{df}{d\eta} \quad (10.5.10)$$

and

$$u_y(x, y) = -\frac{\partial \psi}{\partial x} = \frac{1}{2} (\nu c x^{m-1})^{1/2} \left((1-m) \eta \frac{df}{d\eta} - (1+m) f \right). \quad (10.5.11)$$

Further differentiation yields

$$\frac{\partial u_x}{\partial x} = c m x^{m-1} \frac{df}{d\eta} + U_x \frac{d^2 f}{d\eta^2} \frac{\partial \eta}{\partial x} \quad (10.5.12)$$

and

$$\frac{\partial u_x}{\partial y} = U_x \frac{d^2 f}{d\eta^2} \frac{\partial \eta}{\partial y}, \quad \frac{\partial^2 u_x}{\partial y^2} = U_x \frac{d^3 f}{d\eta^3} \left(\frac{\partial \eta}{\partial y} \right)^2. \quad (10.5.13)$$

Substituting these expressions into the boundary-layer equation (10.5.4) and simplifying, we derive the Falkner–Skan ordinary differential equation for the function f ,

$$\frac{d^3 f}{d\eta^3} + \frac{1}{2} (m+1) f \frac{d^2 f}{d\eta^2} - m \left(\frac{df}{d\eta} \right)^2 + m = 0, \quad (10.5.14)$$

which is to be solved subject to the boundary conditions expressed by (10.3.16) and (10.3.17). When $m = 0$, we recover the Blasius equation (10.3.15). Since boundary conditions are specified at both ends of the solution domain $(0, \infty)$, we are presented with a two-point boundary-value problem involving three first-order differential equations.

10.5.2 Numerical solution

The boundary-value problem can be solved by the shooting method discussed in Section 10.3.2 for the Blasius equation. The counterpart of the Blasius system of first-order differential equations (10.3.20) is

$$\frac{dx_1}{d\eta} = x_2, \quad \frac{dx_2}{d\eta} = x_3, \quad \frac{dx_3}{d\eta} = -\frac{1}{2} (m+1) x_1 x_3 + m x_2^2 - m. \quad (10.5.15)$$

The boundary conditions require that $x_1(\eta = 0) = 0$, $x_2(\eta = 0) = 0$, and $x_3(\eta = \infty) = 1$.

We find that convergence is achieved when $f''(0) = 1.491$ for $m = 1.5$, $f''(0) = 1.231$ for $m = 1.0$, $f''(0) = 0.675$ for $m = 0.25$, $f''(0) = 0.594$ for $m = 0.176$, $f''(0) = 0.332$ for $m = 0$, and $f''(0) = 0$ for $m = -0.0904$.

Streamwise velocity profiles expressed by the derivative $f'(\eta)$ are plotted in [Figure 10.5.2](#) for several values of m . The profiles for $m < 0$, corresponding to decelerating flow, exhibit an inflection point near the wall. The wall shear stress vanishes when $m = -0.0904$.

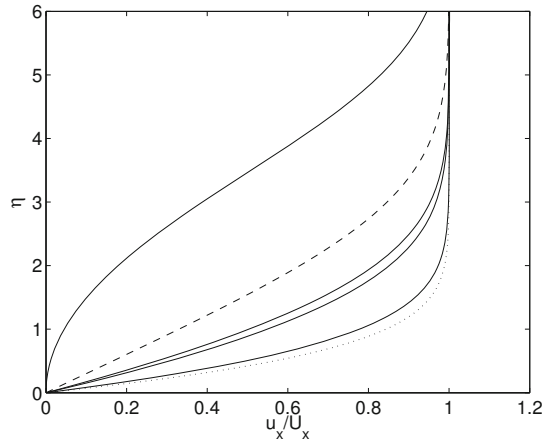


Figure 10.5.2 Velocity profiles across Falkner–Skan boundary layers for several values of the acceleration parameter m ; from bottom to top, $m = 1.5$ (dotted line), 1.0, 0.25, 0.176, 0.0 (dashed line), and -0.0904 .

PROBLEMS

10.5.1 Orthogonal stagnation-point flow

The Falkner–Skan profile with $m = 1$ corresponds to irrotational orthogonal stagnation-point flow against a flat plate.

- Derive the velocity field of the outer irrotational flow.
- Show that the Falkner–Skan boundary-layer solution satisfies the unsimplified Navier–Stokes equation, and thus it provides us with an exact solution.

10.5.2 Falkner–Skan equations

Compute the velocity profile across a Falkner–Skan boundary layer with $m = -0.05$.

10.6 Momentum integral method

We have discussed the solution of the boundary-layer equations over a flat surface subject to a constant, accelerating, or decelerating outer flow with a power-law dependence on streamwise position. To compute boundary layers developing over curved surfaces and for more general types of outer flow, we resort to approximate methods.

Von Kàrmàn developed an elegant and efficient method for computing the flow inside a two-dimensional boundary layer developing over a surface with arbitrary shape, based on an integral momentum balance. The formulation culminates in an ordinary differential equation for a properly defined boundary-layer thickness with respect to arc length measured along the surface.

Flow over a flat surface

To illustrate the method, we consider the boundary layer developing over a flat surface located at $y = 0$, and introduce a control area confined between two vertical planes located at x_1 and x_2 , the flat surface, and a horizontal plane located at the elevation $y = h$. Consistent with our previous notation, we denote the tangential component of the outer flow along the surface by $U_x(x)$. For simplicity, we assume that the physical properties of the fluid are uniform throughout the domain of flow.

We begin by considering the x component of the integral momentum balance (6.2.20), and introduce the Newtonian constitutive equation for the stress tensor. Neglecting the normal viscous stresses over the vertical and top planes, and assuming that gravitational effects are negligibly small, we obtain

$$\begin{aligned} & \int_{x_1}^{x_2} \int_0^h \rho \left(\frac{\partial u_x}{\partial t} \right)_{(x,y)} dy dx - \int_0^h [u_x (\rho u_x)]_{(x=x_1,y)} dy \\ & + \int_0^h [u_x (\rho u_x)]_{(x=x_2,y)} dy + \int_{x_1}^{x_2} [u_y (\rho u_x)]_{(x,y=h)} dx \\ & = \int_0^h (-p)_{(x=x_1,y)} dy - \int_0^h (-p)_{(x=x_2,y)} dy - \int_{x_1}^{x_2} \tau_{xy}(x) dx. \end{aligned} \tag{10.6.1}$$

Next, we take the limit as x_1 tends to x_2 , recall that the pressure remains constant across the boundary layer, set $u_x(x, y = h) = U_x(x)$, and rearrange to obtain an integro-differential relation,

$$\begin{aligned} \rho \int_0^h \frac{\partial u_x}{\partial t} dy &= h \left(\frac{\partial p}{\partial x} \right)_{y=h} \\ & - \rho \frac{\partial}{\partial x} \int_0^h u_x^2(x, y) dy - \rho U_x(x) u_y(x, y = h) - \tau_{xy}(x). \end{aligned} \tag{10.6.2}$$

To reduce the number of unknowns, we eliminate $u_y(x, y = h)$ in favor of u_x using the continuity equation, setting

$$u_y(x, y = h) = - \int_0^h \frac{\partial u_x}{\partial x}(x, y') dy'. \tag{10.6.3}$$

Moreover, we use the x component of Euler's equation (6.4.4) to evaluate the streamwise pressure gradient, finding that

$$\frac{\partial p}{\partial x} = -\rho \left(\frac{\partial U_x}{\partial t} + U_x \frac{\partial U_x}{\partial x} \right). \tag{10.6.4}$$

Substituting expressions (10.6.3) and (10.6.4) into (10.6.2) and rearranging, we obtain

$$\begin{aligned} \rho \int_0^h \frac{\partial (U_x - u_x)}{\partial t} dy &= -\rho \frac{\partial}{\partial x} \int_0^h u_x (U_x - u_x) dy \\ & - \rho \frac{\partial}{\partial x} \int_0^h U_x (U_x - u_x) dy + \rho U_x \frac{\partial}{\partial x} \int_0^h (U_x - u_x) dy + \tau_{xy}(x), \end{aligned} \tag{10.6.5}$$

which can be interpreted as an evolution equation for the momentum deficit expressed by the term $\rho(U_x - u_x)$.

Now we let the scaled height h/δ tend to infinity, and use the definitions of the displacement and momentum thickness stated in equations (10.4.4) and (10.4.9) to derive the von Kàrmàn integral momentum balance

$$\rho \frac{\partial(U_x \delta^*)}{\partial t} + \rho \frac{\partial(U_x^2 \Theta)}{\partial x} + \rho \frac{\partial(U_x^2 \delta^*)}{\partial x} - \rho U_x \frac{\partial(U_x \delta^*)}{\partial x} - \tau_{xy} = 0. \quad (10.6.6)$$

Rearranging, we derive an expression for the wall shear stress in terms of the displacement and momentum thickness,

$$\frac{\tau_{xy}}{\rho U_x^2} = \frac{\partial(U_x \delta^*)}{\partial t} + \frac{\partial \Theta}{\partial x} + (2\Theta + \delta^*) \frac{1}{U_x} \frac{\partial U_x}{\partial x}. \quad (10.6.7)$$

If the flow is steady, the first term on the right-hand side does not appear. It is reassuring to confirm that, when U_x is constant, equation (10.6.7) reduces to equation (10.4.13) describing the boundary layer developing over a flat plate that is held stationary parallel to an incident streaming flow.

If fluid is injected into the flow or withdrawn through a porous wall with normal velocity V , the right-hand side of (10.6.7) contains the additional term, $-V/U_x$, where V is positive in the case of injection and negative in the case of suction.

10.6.1 The von Kàrmàn–Pohlhausen method

Von Kàrmàn and Pohlhausen developed an approximate method for computing the boundary-layer thickness and associated structure of the flow based on the momentum integral balance (10.6.7). In the first stage, we assume a sensible velocity profile across the boundary layer of the form $u_x = F(\eta)$, where $\eta \equiv y/\Delta(x)$ and $\Delta(x)$ is a boundary-layer thickness similar to the δ_{99} boundary layer thickness. In the second stage, we compute $\Delta(x)$ to satisfy the integral momentum balance equation (10.6.7).

The implementation of the method for flow over a flat plate at zero angle of attack where $F(\eta)$ is a quarter of a period of a sinusoidal function, as shown in (10.4.15), was discussed in Section 10.4. In the remainder of this section, we illustrate the implementation for an arbitrary steady flow.

10.6.2 Pohlhausen polynomials

Pohlhausen described the velocity profile across a boundary layer with a fourth-order polynomial,

$$\frac{u_x}{U_x} = F(\eta) = \begin{cases} a(x)\eta + b(x)\eta^2 + c(x)\eta^3 + d(x)\eta^4 & \text{for } 0 < \eta < 1, \\ 1 & \text{for } \eta > 1, \end{cases} \quad (10.6.8)$$

where $a(x)$, $b(x)$, $c(x)$, and $d(x)$ are position-dependent coefficients to be computed as part of the solution. Note that the functional form (10.6.8) satisfies the no-slip boundary condition

at the wall corresponding to $\eta = 0$. To compute the four coefficients a , b , c , and d , we require four equations.

First, we require that the overall velocity profile is continuous and has a smooth first and second derivative at the edge of the boundary layer corresponding to $\eta = 1$, and thus obtain three conditions,

$$F = 1, \quad \frac{dF}{d\eta} = 0, \quad \frac{d^2F}{d\eta^2} = 0 \quad (10.6.9)$$

at $\eta = 1$.

A fourth condition arises by applying the boundary-layer equation (10.2.5) at the wall located at $y = 0$, and then using the no-slip and no-penetration boundary conditions to set the left-hand side to zero. Evaluating the streamwise pressure gradient from (10.6.4) with the time derivative on the right-hand side set to zero, we find that

$$\left(\frac{\partial u_x^2}{\partial y^2}\right)_{y=0} = -\frac{1}{\nu} U_x \frac{dU_x}{dx}. \quad (10.6.10)$$

Next, we express the velocity in terms of the function $F(\eta)$ introduced in (10.6.8), and obtain

$$\left(\frac{d^2F}{d\eta^2}\right)_{\eta=0} = -\Lambda, \quad (10.6.11)$$

where

$$\Lambda(x) \equiv \frac{\Delta^2(x)}{\nu} \frac{dU_x}{dx}, \quad (10.6.12)$$

is a dimensionless function expressing the ratio of the magnitude of the inertial acceleration forces in the outer irrotational flow to the magnitude of the viscous forces developing inside the boundary layer; if $dU_x/dx = 0$, then $\Lambda = 0$.

By definition, the effective boundary-layer thickness, $\Delta(x)$, is related to $\Lambda(x)$ by

$$\Delta(x) \equiv \sqrt{\frac{\nu \Lambda}{U'_x}}, \quad (10.6.13)$$

where $U'_x \equiv dU_x/dx$.

Requiring that the Pohlhausen profile (10.6.8) satisfies equations (10.6.9) and (10.6.11), we obtain

$$a = 2 + \frac{1}{6} \Lambda, \quad b = -\frac{1}{2} \Lambda, \quad c = -2 + \frac{1}{2} \Lambda, \quad d = 1 - \frac{1}{6} \Lambda. \quad (10.6.14)$$

Substituting these expressions into (10.6.8) and rearranging, we obtain the velocity profile in terms of the parameter Λ ,

$$\frac{u}{U_x} = F(\eta) = \begin{cases} \eta(2 - 2\eta^2 + \eta^3) + \Lambda \frac{1}{6} \eta(1 - \eta)^3 & \text{for } 0 < \eta < 1, \\ 1 & \text{for } \eta > 1. \end{cases} \quad (10.6.15)$$

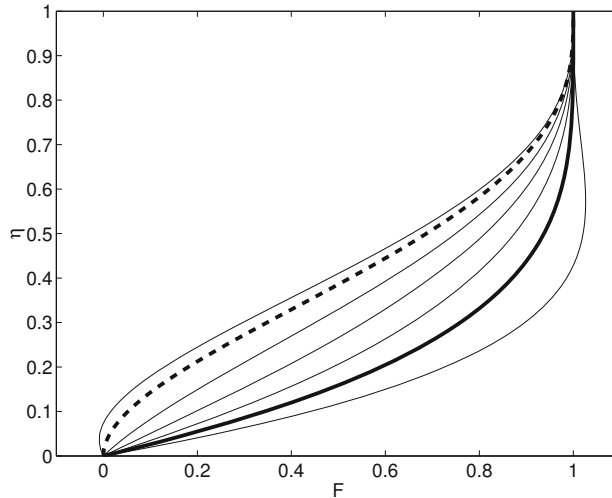


Figure 10.6.1 Profiles of Pohlhausen polynomials for $\Lambda = 20, 12$ (heavy solid line), $6, 0, -6, -12$ (heavy dashed line), and -15 .

Program *pohl_pol*, located inside directory *10-bl* of **FDLIB**, computes polynomial profiles by evaluating the right-hand side of (10.6.15). A family of profiles is shown in [Figure 10.6.1](#). The overshooting observed when $\Lambda > 12$, corresponding to a strongly accelerating external flow according to (10.6.12), places a limit on the physical relevance of the fourth-order polynomial expansion. When $\Lambda = -12$, the slope of the velocity profile is zero at the wall, and this suggests that the flow is on the verge of reversal. Under these conditions, the approximations that led us to the boundary-layer equations cease to be valid and the boundary layer is expected to separate from the wall and develop regions of recirculating fluid attached to the wall.

The displacement thickness, momentum thickness, and wall shear stress can be computed in terms of $\Delta(x)$ and $\Lambda(x)$ using the profiles (10.6.15), and are found to be

$$\delta^* = \frac{\Delta}{10} \left(3 - \frac{1}{12} \Lambda \right), \quad \Theta = \frac{\Delta}{315} \left(37 - \frac{1}{3} \Lambda - \frac{5}{144} \Lambda^2 \right), \quad (10.6.16)$$

and

$$\sigma_{xy}(x, y = 0) = \frac{\mu U_x}{\Delta} \left(2 + \frac{1}{6} \Lambda \right). \quad (10.6.17)$$

Expressing $\Delta(x)$ in terms of $\Lambda(x)$ using the definition (10.6.13), we obtain corresponding expressions in terms of Λ alone.

Next, we substitute the expressions given in (10.6.16) and (10.6.17) into the momentum integral balance (10.6.7), and thus derive a first-order nonlinear ordinary differential equation for $\Lambda(x)$ with respect to x . Having solved this equation, we recover the boundary-layer thickness, $\Delta(x)$, from the definition (10.6.13).

10.6.3 Numerical solution

It is convenient to introduce the Holstein–Bohlen parameter

$$\lambda(x) \equiv \frac{\Theta^2(x)}{\Delta^2(x)} \Lambda(x) = \frac{\Theta^2(x)}{\nu} \frac{dU_x}{dx}, \quad (10.6.18)$$

whose physical interpretation is similar to that of the parameter Λ discussed after the definition (10.6.12). Using the expression for the momentum thickness given in (10.6.16), we obtain a relationship between λ and Λ ,

$$\lambda = \frac{\Lambda}{315^2} \left(37 - \frac{\Lambda}{3} - \frac{5}{144} \Lambda^2 \right)^2. \quad (10.6.19)$$

The value $\Lambda = -12$ corresponds to $\lambda = -0.15673$ where the boundary layer is expected to separate, as shown in [Figure 10.6.1](#).

To expedite the solution, we multiply both sides of the momentum integral balance (10.6.7) at steady state by Θ , and rearrange to obtain

$$\frac{d}{dx} \left(\frac{\lambda}{dU_x/dx} \right) \equiv \frac{1}{\nu} \frac{d^2\Theta}{dx^2} = 2 \frac{S(\lambda) - [2 + H(\lambda)] \lambda}{U_x}, \quad (10.6.20)$$

where H is the shape factor defined in (10.4.11) and S is the shear function defined as

$$S(\lambda) \equiv \frac{\Theta}{\mu U_x} \sigma_{xy}(x, y = 0). \quad (10.6.21)$$

Physically, the shear function expresses the ratio of the wall shear stress to the average value of the shear stress across the boundary layer, and is thus another measure of the sharpness of the velocity profile across the boundary layer. Using the expressions given in (10.6.16) and (10.6.17), we find that

$$H = \frac{315}{10} \frac{3 - \frac{\Lambda}{12}}{37 - \frac{\Lambda}{3} - \frac{5}{144} \Lambda^2}, \quad S = \frac{1}{315} \left(2 + \frac{\Lambda}{6} \right) \left(37 - \frac{\Lambda}{3} - \frac{5}{144} \Lambda^2 \right), \quad (10.6.22)$$

where Λ can be expressed in terms of λ using equation (10.6.19). The numerical procedure involves the following steps:

1. Given the value of λ at a particular position, x , compute the corresponding value of Λ by solving the nonlinear algebraic equation (10.6.19).
2. Evaluate the functions S and H using expressions (10.6.22).
3. Compute the right-hand side of (10.6.20) to obtain the rate of change of the ratio on the left-hand side with respect to x .
4. Advance the value of λ over a small increment, Δx .
5. Return to Step 1 and repeat the calculations for another cycle.

The following MATLAB function entitled *Lam* solves the nonlinear equation (10.6.19) required in Step 1 using Newton's method:

```
function Lam = root(lam,Lam)

%---
% given lambda, solve for Lambda
%---

if(abs(lam)<0.000005)
    Lam = 0.00001; return
end

%---
% Newton's method
%---

for i=1:50
    fnc = ltoL(lam,Lam);
    fnc1 = ltoL(lam,Lam+0.0001);
    fncp = (fnc1-fnc)/0.0001;
    corr = -fnc/fncp;
    Lam = Lam+corr;
    if(abs(corr)<0.000001) return; end
end

    disp 'root: could not find a root in 50 iterations'

return

%-----

function f = ltoL(lam,Lam)

    f = Lam*((37.0-Lam/3.0-5.0*Lam*Lam/144.0)/315.0)^2-lam;

return
```

Note that the main function *Lam* is accompanied by an evaluator function *ltoL* (λ to Λ).

Evaluation at a stagnation point

The numerical integration typically begins at a stagnation point where the tangential velocity U_x vanishes and the right-hand side of (10.6.20) is undefined. To prevent a singularity, we require that the numerator is zero at that point, and thus obtain a nonlinear algebraic equation for Λ . A physically acceptable solution is $\Lambda = 7.0523231$, corresponding to $\lambda = 0.0770356$. These values are used to initialize the computation.

To evaluate the right-hand side of (10.6.20) at a stagnation point located at $x = 0$, we denote the expression enclosed by the pointed brackets on the right-hand side by $Q(\lambda)$. Applying the l'Hôpital rule to evaluate the fraction, we find that

$$\frac{d}{dx} \left(\frac{\lambda}{dU_x/dx} \right)_{x=0} = \left(\frac{dQ/dx}{dU_x/dx} \right)_{x=0} = \left(\frac{dQ/d\lambda}{dU_x/dx} \frac{d\lambda}{dx} \right)_{x=0} \quad (10.6.23)$$

and then

$$\frac{d}{dx} \left(\frac{\lambda}{dU_x/dx} \right)_{x=0} = \left(\frac{dQ}{d\lambda} \right)_{x=0} \left(\frac{d}{dx} \left(\frac{\lambda}{dU_x/dx} \right) + \lambda \frac{d^2U_x/dx^2}{(dU_x/dx)^2} \right)_{x=0}. \quad (10.6.24)$$

Combining the left-hand side with the first term inside the tall parentheses on the right-hand side, we obtain

$$\frac{d}{dx} \left(\frac{\lambda}{dU_x/dx} \right)_{x=0} = \left(\frac{\lambda}{1 - dQ/d\lambda} \frac{dQ}{d\lambda} \frac{d^2U_x/dx^2}{(dU_x/dx)^2} \right)_{x=0}. \quad (10.6.25)$$

Evaluating the expression on the right-hand side using the definition of $Q(\lambda)$, we obtain the required initial value

$$\frac{d}{dx} \left(\frac{\lambda}{dU_x/dx} \right)_{x=0} = -0.0652 \left(\frac{d^2U_x/dx^2}{(dU_x/dx)^2} \right)_{x=0}. \quad (10.6.26)$$

10.6.4 Boundary layer around a curved body

The Kàrmàn-Pohlhausen method was developed with reference to a planar boundary where the x coordinate increases along the boundary in the direction of the velocity of the outer flow. To tackle the more general case of a curved boundary, we replace x with the arc length along the boundary, ℓ , measured in the direction of the tangential velocity of the incident flow, and begin the integration from a stagnation point.

A difficulty arises at the critical point where the acceleration $dU_\ell/d\ell$ becomes zero or infinite. However, the ambiguity can be removed by carrying out the integration at that point using the Falkner–Skan similarity solution with a proper value for the exponent m .

Boundary layer around a circular cylinder

As an application, we consider streaming (uniform) flow past a stationary circular cylinder of radius a with vanishing circulation around the cylinder, as shown in [Figure 10.6.2](#). Far from the cylinder, the flow is streaming toward the negative direction of the x axis and the velocity tends to the uniform value $-U \mathbf{e}_x$, where $U > 0$ is the magnitude of the streaming flow and \mathbf{e}_x is the unit vector along the x axis.

Using the velocity potential for irrotational flow past a circular cylinder, given in equation (3.5.48) with $V_x = -U$, we find that the tangential component of velocity of the outer flow is

$$U_\theta(\theta) = \left(\frac{\partial\phi}{\partial\theta} \right)_{r=a} = 2U \sin\theta, \quad (10.6.27)$$

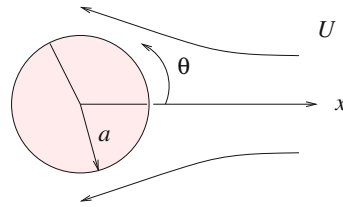


Figure 10.6.2 Illustration of the Prandtl boundary layer around a circular cylinder of radius a held stationary in an incident streaming flow with velocity U .

where θ is the polar angle measured around the center of the cylinder in the counterclockwise direction, as shown in Figure 10.6.2. The arc length around the cylinder measured from the front stagnation point is $\ell = a\theta$. The required derivatives of the velocity with respect to arc length are

$$\frac{dU_\theta}{d\ell} = \frac{1}{a} \frac{dU_\theta}{d\theta} = 2 \frac{U}{a} \cos \theta, \quad \frac{d^2U_\theta}{d\ell^2} = \frac{1}{a^2} \frac{d^2U_\theta}{d\theta^2} = -2 \frac{U}{a^2} \sin \theta. \quad (10.6.28)$$

Equation (10.6.26) yields

$$\frac{d}{d\ell} \left(\frac{\lambda}{dU_\theta/d\ell} \right)_{\ell=0} = 0, \quad (10.6.29)$$

which is used to start up the computations.

The following MATLAB function named *phase_vel* evaluates the right-hand side of (10.6.20):

```
function f = phase_vel (U0,theta,Lam,lam)

    tmp = 37.0-Lam/3.0-5.0*Lam*Lam/144.0;
    H = 31.5*(3.0-Lam/12.0)/tmp;
    S = (2.0+Lam/6.0)*tmp/315.0;
    U = 2.0*U0*sin(theta);
    f = 2.0*(S-(2.0+H)*lam)/U;

return
```

The Kàrmàn-Pohlhausen method is implemented in the following MATLAB code entitled *kp_cc*, located in directory *10-bl* of **FDLIB**:

```
a = 1.0; % cylinder radius
U0 = 1.0; % incident velocity
nu = 1.0; % kinematic viscosity
mu = 1.0; % viscosity

Ndiv = 2*128; % number of divisions
angle = 0.60*pi; % maximum integration angle
```

```

%---
% prepare
%---

Dtht = angle/Ndiv; % differential angle theta
Dx = a*Dtht; % differential arc length

%---
% initial values
%---

tht = 0.0;
lam = 0.0770;
Lam = 7.052;
Up = 2.0*U0*cos(tht)/a;
z = lam/Up;

%---
% integrate by the modified Euler method
%---

for i=1:Ndiv

    U = 2.0*U0*sin(tht); % velocity
    Up = 2.0*U0*cos(tht)/a; % acceleration
    tmp = 37.0-Lam/3.0-5.0*Lam*Lam/144.0;
    H = 31.5*(3.0-Lam/12.0)/tmp;
    S = (2.0+Lam/6.0)*tmp/315.0;
    Del = sqrt(abs(nu*Lam/Up));
    del = Del*(3.0-Lam/12.0)/10.0;
    sw = mu*U/Del*(2.0+Lam/6.0);
    THeta = 0.0;

    if(abs(sw)>0.0000001)
        THeta = mu*U*S/sw;
    end

    if(i==1)
        fv = 0.0;
    else
        Lam = root(lam,Lam);
        fv = phase_vel(U0,tht,Lam,lam);
    end

    zsave = z;
    fvsave = fv;
    tht = tht+Dtht;
    z = z + fv*Dx;
    Up = 2.0*U0*cos(tht)/a;

```

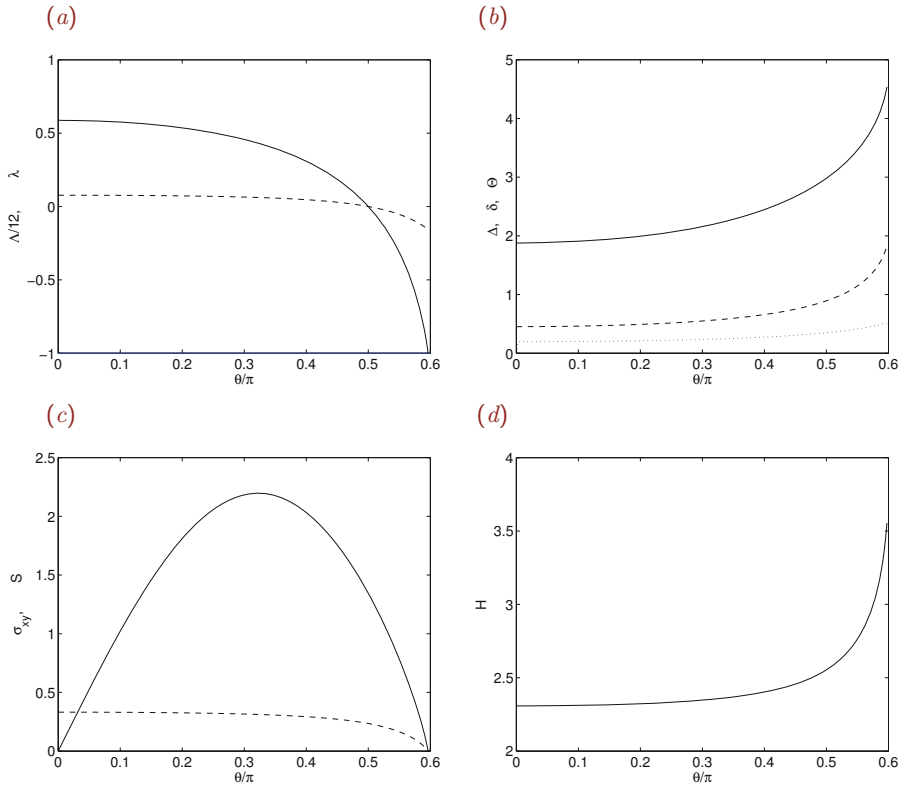



Figure 10.6.3 Features of the Prandtl boundary layer around a circular cylinder of radius a held stationary in an incident streaming flow with velocity U , computed by the von Kàrmàn-Pohlhausen method. (a) Distribution of the dimensionless parameters $\frac{1}{12} \Lambda$ (solid line) and λ (dashed line). (b) Boundary-layer thickness Δ (solid line), displacement thickness δ^* (dashed line), and momentum thickness Θ (dotted line); all are scaled by $\sqrt{\nu a/U}$. (c) Distribution of the wall shear stress scaled by $\mu U/a$ (solid line), and shape factor S (dashed line). (d) Distribution of the shear function, H .

```

lam = z*Up;
Lam = root(lam,Lam); % solve for Lambda
fv = phase_vel(U0,tht,Lam,lam);
z = zsave + 0.5*(fv+fvsave)*Dx;
lam = z*Up;

end

```

Graphs of the solution are shown in [Figure 10.6.3](#). The velocity profile across the boundary layer at different stations around the cylinder can be inferred from the scaled Pohlhausen profiles shown in [Figure 10.6.1](#) using the local value of Λ .

The numerical solution reveals that $\Lambda = -12$ when $\theta = 109.5^\circ$. At that point, the shear stress becomes zero and the boundary layer is expected to separate. Comparing this result with the experimentally observed value $\theta = 80.5^\circ$, we find a serious disagreement attributed to the deviation of the actual outer flow from the idealized potential flow distribution described by (10.6.27) due to the presence of a wake.

To improve the solution, we may describe the tangential velocity distribution U_θ by interpolation based on data collected in the laboratory. When this is done, the predictions of the boundary-layer analysis are in excellent agreement with laboratory observation.

PROBLEMS

10.6.1 Von Kàrmàn method for the Blasius boundary layer

Assume that the velocity profile across the Blasius boundary layer is given by the Pohlhausen polynomial (10.6.15). Show that the effective boundary-layer thickness, wall shear stress, displacement thickness, and momentum thicknesses are given by the right-hand sides of equations (10.4.20) and (10.4.21), except that the numerical coefficients are equal, respectively, to 5.863, 0.343, 1.751, and 0.685. Discuss the accuracy of these results with reference to the exact solution obtained by numerical methods.

10.6.2 Boundary layer around a circular cylinder

Plot and discuss scaled velocity profiles u_θ/U_0 across the boundary layer around a circular cylinder at a sequence of angles, θ .

10.7 Instability of shear flows

In Chapter 7, we derived exact solutions of the governing equations for channel and tube flow, assuming unidirectional motion with rectilinear or circular streamlines. The physical relevance of these assumptions is corroborated by laboratory observations at low and moderate Reynolds numbers. However, at high Reynolds numbers, small perturbations inherent in any real flow amplify to initiate an unsteady motion, possibly leading to a new steady state that is different than that computed under the assumption of unidirectional flow.

Linear stability analysis

Two questions naturally arise: what is the threshold Reynolds number above which a flow becomes unstable? and what are the salient modes of amplification? To develop insight into the answers, we carry out a linear stability analysis. Our general strategy is to consider a flow of interest at steady state, introduce small perturbations, and describe the time evolution of the perturbations by solving simplified versions of the governing equations that arise by linearization. If all perturbations decay, the flow is stable; if some perturbations amplify, the flow is unstable; if some perturbations stay constant in time and all other perturbations decay, the flow is neutrally stable. Perturbations that grow or decay exponentially in time represent normal modes.

10.7.1 Stability analysis of shear flow

To illustrate the procedures, we consider a steady unidirectional flow along the x axis with velocity, pressure, and vorticity given by

$$u_x^B = U(y), \quad u_y^B = 0, \quad p^B = -\chi x, \quad \omega_z^B = -\frac{dU(y)}{dy}, \quad (10.7.1)$$

where the superscript B designates the base flow whose stability is examined, $U(y)$ is the unperturbed velocity profile, and χ is the negative of the streamwise pressure gradient.

It should be noted that, unless the velocity profile is parabolic, the base flow will not satisfy the steady version of the equation of motion. However, we assume that the base flow evolves at a rate that is much slower than that of the perturbations, and may thus be considered to be in a quasi-steady state.

Perturbations and disturbances

Next, we introduce a two-dimensional perturbation whose velocity and pressure fields are described by

$$\begin{aligned} u_x^P(x, y, t) &= \epsilon u_x^D(x, y, t), & u_y^P(x, y, t) &= \epsilon u_y^D(x, y, t), \\ p^P(x, y, t) &= \epsilon p^D(x, y, t), \end{aligned} \quad (10.7.2)$$

where the superscript P designates the perturbation, the superscript D designates the disturbance, and ϵ is a dimensionless coefficient whose magnitude is much smaller than unity. The corresponding perturbation in the vorticity is

$$\omega_z^P(x, y, t) = \epsilon \omega^D(x, y, t) = \epsilon \left(\frac{\partial u_y^D}{\partial x} - \frac{\partial u_x^D}{\partial y} \right)(x, y, t). \quad (10.7.3)$$

The physical flow arises by adding corresponding variables of the base and perturbation flows shown in (10.7.1) and (10.7.2). For example, the x velocity component of the perturbed flow is given by

$$u_x(x, y, t) = u_x^B(y) + \epsilon u_x^D(x, y, t). \quad (10.7.4)$$

Substituting this sum and its counterparts for other variables into the vorticity transport equation for two-dimensional flow stated in equation (6.6.14), we obtain

$$\begin{aligned} \epsilon \frac{\partial \omega_z^D}{\partial t} + \epsilon u_x^B \frac{\partial \omega_z^D}{\partial x} + \epsilon^2 u_x^D \frac{\partial \omega_z^D}{\partial x} + \epsilon u_y^D \frac{\partial \omega_z^B}{\partial y} + \epsilon^2 u_y^D \frac{\partial \omega_z^D}{\partial y} \\ = \nu \left(\frac{\partial^2 \omega^B}{\partial x^2} + \frac{\partial^2 \omega^B}{\partial y^2} + \epsilon \left(\frac{\partial^2 \omega^D}{\partial x^2} + \frac{\partial^2 \omega^D}{\partial y^2} \right) \right), \end{aligned} \quad (10.7.5)$$

where ν is the kinematic viscosity of the fluid. Since the vorticity of the base flow satisfies the steady version of the vorticity transport equation for unidirectional flow under the quasi-steady approximation, the sum of the first two terms on the right-hand side is zero.

Linearization

Because ϵ has been assumed small, quadratic terms that are proportional to ϵ^2 are small compared to linear terms that are proportional to ϵ , and may be discarded from both sides of (10.7.5). Collecting the linear terms and setting their sum to zero, we obtain the linearized vorticity transport equation

$$\frac{\partial \omega_z^D}{\partial t} + u_x^B \frac{\partial \omega_z^D}{\partial x} + u_y^D \frac{\partial \omega_z^B}{\partial y} = \nu \left(\frac{\partial^2 \omega_z^D}{\partial x^2} + \frac{\partial^2 \omega_z^D}{\partial y^2} \right). \quad (10.7.6)$$

Substituting the expressions for the base flow stated (10.7.1) into (10.7.6), we derive the more specific form

$$\frac{\partial \omega_z^D}{\partial t} + U(y) \frac{\partial \omega_z^D}{\partial x} - u_y^D \frac{d^2 U}{dy^2} = \nu \left(\frac{\partial^2 \omega_z^D}{\partial x^2} + \frac{\partial^2 \omega_z^D}{\partial y^2} \right). \quad (10.7.7)$$

The problem has been reduced to solving the linear equation (10.7.7) for the disturbance flow, subject to a specified initial condition and appropriate boundary conditions.

Disturbance stream function

It is convenient to express the disturbance flow in terms of a disturbance stream function, $\psi^D(x, y, t)$, defined by the equations

$$u_x^D = \frac{\partial \psi^D}{\partial y}, \quad u_y^D = -\frac{\partial \psi^D}{\partial x}. \quad (10.7.8)$$

The disturbance vorticity is given by

$$\omega_z^D = -\left(\frac{\partial^2 \psi^D}{\partial x^2} + \frac{\partial^2 \psi^D}{\partial y^2} \right) = -\nabla^2 \psi^D, \quad (10.7.9)$$

where $\nabla^2 \equiv \partial^2/\partial x^2 + \partial^2/\partial y^2$ is the Laplacian operator in the xy plane. Substituting these expressions into (10.7.7) and rearranging, we obtain

$$\frac{\partial \nabla^2 \psi^D}{\partial t} + U(y) \frac{\partial \nabla^2 \psi^D}{\partial x} - \nu \nabla^4 \psi^D = \frac{\partial \psi^D}{\partial x} \frac{d^2 U}{dy^2}, \quad (10.7.10)$$

where $\nabla^4 = \nabla^2 \nabla^2$ is the biharmonic operator in the xy plane.

10.7.2 Normal-mode analysis

To study the evolution of each and every possible disturbance is practically impossible. To make progress, we exploit the linearity of equation (10.7.10) and deduce the nature of the general solution corresponding to an arbitrary initial condition from the behavior of an infinite family of solutions corresponding to disturbances that are sinusoidal functions of the streamwise position, x , and exponential functions of time, t , called normal modes. The general solution can be constructed by linear superposition.

Consider a normal mode with wave length L and corresponding wave number $k = 2\pi/L$. The disturbance stream function is expressed in the form

$$\psi^D(x, y, t) = \chi_R(y, t) \cos(kx) + \chi_I(y, t) \sin(kx), \quad (10.7.11)$$

where $\chi_R(y, t)$ and $\chi_I(y, t)$ are two real functions. To simplify the notation, we introduce the complex function

$$\chi(y, t) \equiv \chi_R(y, t) - i\chi_I(y, t), \quad (10.7.12)$$

where i is the imaginary unit, $i^2 = -1$. Using the Euler decomposition of the imaginary exponential,

$$\exp(ikx) = \cos(kx) + i \sin(kx), \quad (10.7.13)$$

we recast (10.7.11) into the form

$$\psi^D(x, y, t) = \text{real}\{\Psi^D(x, y, t)\}, \quad (10.7.14)$$

where *real* designates the real part of the complex quantity enclosed by the angular brackets, and

$$\Psi^D(x, y, t) \equiv \phi(y, t) \exp(ikx) \quad (10.7.15)$$

is a complex stream function. To simplify the analysis, we require that the imaginary part of Ψ^D also satisfies equation (10.7.10).

Substituting (10.7.15) into (10.7.10), carrying out the differentiation with respect to x , and noting that

$$\nabla^2 \Psi^D = \left(-k^2 \phi + \frac{\partial^2 \phi}{\partial y^2} \right) \exp(ikx), \quad (10.7.16)$$

we derive the equation

$$\begin{aligned} -k^2 \frac{\partial \phi}{\partial t} + \frac{\partial^3 \phi}{\partial y^2 \partial t} + ikU(y) \left(-k^2 \phi + \frac{\partial^2 \phi}{\partial y^2} \right) \\ -\nu \left(k^4 \phi - 2k^2 \frac{\partial^2 \phi}{\partial y^2} + \frac{\partial^4 \phi}{\partial y^4} \right) = ik\phi \frac{d^2 U}{dy^2}, \end{aligned} \quad (10.7.17)$$

which should be regarded as a linearized vorticity transport equation.

Growth rate

A solution of (10.7.17) can be found by expressing $\phi(x, t)$ in the separated form

$$\phi(y, t) = f(y) \exp(-i\sigma t) = f(y) \exp(-ikct), \quad (10.7.18)$$

where $f(y)$ is a complex function, σ is a complex constant called the complex growth rate, and $c \equiv \sigma/k$ is another complex constant called the complex phase velocity.

Substituting (10.7.18) into (10.7.15), we derive the corresponding complex disturbance stream function

$$\Psi(x, y, t) = f(y) \exp[i(kx - \sigma t)] = f(y) \exp[ik(x - ct)]. \quad (10.7.19)$$

Next, we decompose σ and c into their real and imaginary parts, writing

$$\sigma = \sigma_R + i\sigma_I, \quad c = c_R + ic_I, \quad (10.7.20)$$

and obtain the expression

$$\Psi(x, y, t) = f(y) \exp[ik(x - c_R t)] \exp(\sigma_I t), \quad (10.7.21)$$

where the subscripts R and I stand for real and imaginary. Expression (10.7.21) illustrates two important features:

- The constant c_R is the real phase velocity of the disturbance. The crests and troughs of the sinusoidal perturbation, but not the fluid itself, travel along the x axis with velocity c_R .
- The constant $\sigma_I = kc_I$ is the growth rate of the disturbance; if σ_I is positive, the disturbance grows at an exponential rate in time; if σ_I is negative, the disturbance decays at an exponential rate in time; if $\sigma_I = 0$, the amplitude of the disturbance remains constant in time. In the first case, the flow is unstable; in the second case, the flow is stable; and in the third case, the flow is neutrally stable.

Orr–Sommerfeld equation

Substituting expression (10.7.18) into the governing equation (10.7.17), and rearranging the resulting expression, we derive the Orr–Sommerfeld equation,

$$k^4 f - 2k^2 \frac{d^2 f}{dy^2} + \frac{d^4 f}{dy^4} = \frac{ik}{\nu} \left((U(y) - c) \left(\frac{d^2 f}{dy^2} - k^2 f \right) - \frac{d^2 U}{dy^2} f \right), \quad (10.7.22)$$

which can be classified as a linear ordinary differential equation with variable coefficients determined by the velocity profile. A trivial solution is $f = 0$.

Nontrivial solutions expressing normal modes are possible only for certain values of c that are the eigenvalues of the Orr–Sommerfeld equation. The main objective of linear stability analysis is to identify these eigenvalues and associated eigenfunctions, and thereby assess whether the amplitude of a normal mode will grow, decay, or remain constant in time.

Rayleigh equation

When viscous forces are negligible, the left-hand side of the Orr–Sommerfeld equation (10.7.22) may be set equal to zero, yielding the Rayleigh equation

$$(U(y) - c) \left(\frac{d^2 f}{dy^2} - k^2 f \right) - \frac{d^2 U}{dy^2} f = 0, \quad (10.7.23)$$

which is also available in the alternative form

$$\frac{d^2 f}{dy^2} - \left(k^2 + \frac{1}{U(y) - c} \frac{d^2 U}{dy^2} \right) f = 0. \quad (10.7.24)$$

Because of the absence of viscous forces, the Rayleigh equation is a second-order differential equation, whereas its inclusive Orr-Sommerfeld equation is a fourth-order differential equation. Both equations are linear, but the coefficients multiplying the derivatives of the unknown complex function f are not necessarily constant.

Numerical methods

Analytical solutions to the Orr-Sommerfeld and Rayleigh equations are possible only for a limited class of purely viscous or idealized inviscid flows. To study the stability of more general flows, we resort to numerical methods. Typical methods are discussed in Sections 10.8 and 10.9.

PROBLEM

10.7.1 Instability of an inviscid shear flow

Consider an infinite shear flow with velocity profile $U(y) = U_0 \tanh \eta$, where $\eta = y/\delta$ and δ is a specified length. Confirm that an eigenvalue and the corresponding eigenfunction of Rayleigh's equation describing a neutrally stable perturbation are $c = 0$ and $f(y) = A \operatorname{sech} \eta$, where A is an arbitrary constant.

10.8 Finite-difference solution of the Rayleigh equation

To illustrate the implementation of a finite-difference method, we study the stability of an inviscid shear flow in a channel confined between two parallel walls located at $y = -b$ and a , as illustrated in [Figure 10.8.1](#). It is convenient to recast Rayleigh's equation (10.7.23) into the form

$$U(y) \frac{d^2 f}{dy^2} - \left(U(y) k^2 + \frac{d^2 U}{dy^2} \right) f = c \left(\frac{d^2 f}{dy^2} - k^2 f \right), \quad (10.8.1)$$

where the unknown eigenvalue, c , has been moved to the right-hand side. The no-penetration boundary condition requires that $f(-b) = f(a) = 0$. Because the values of the stream function over the two walls are prescribed to be equal, the disturbance flow will not generate a net flow rate in the direction of the base flow.

10.8.1 Finite-difference equations

We begin by introducing a one-dimensional uniform grid of nodes with N intervals separated by grid spacing $\Delta y = (a + b)/N$, located at y_i for $i = 1, \dots, N + 1$, where $y_1 = -b$ and $y_{N+1} = a$, as illustrated in [Figure 10.8.1](#). For simplicity, we denote the value of f at the

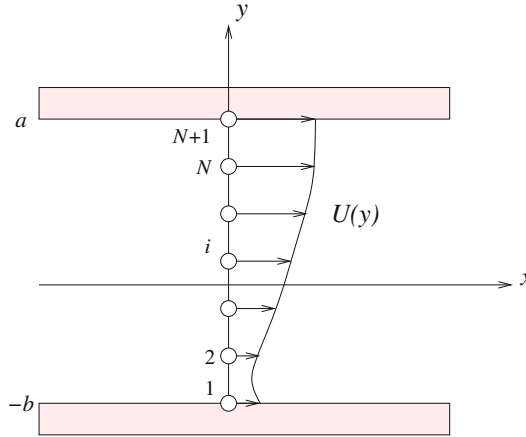


Figure 10.8.1 Illustration of a finite-difference grid used to solve the Rayleigh equation determining the growth rate of two-dimensional perturbations in inviscid unidirectional shear flow.

i th node by $f(y_i) = f_i$. To satisfy the no-penetration condition, we require that the stream function is constant at the lower and upper walls,

$$f_1 = 0, \quad f_{N+1} = 0. \tag{10.8.2}$$

All other nodal values of f must be computed as part of the solution.

Applying the Rayleigh equation (10.8.1) at the i th interior node for $i = 2, \dots, N$, and approximating the second derivative, d^2f/dy^2 , with a centered difference, we obtain the difference equation

$$U_i \frac{f_{i+1} - 2f_i + f_{i-1}}{\Delta y^2} - (U_i k^2 + U_i'') f_i = c \left(\frac{f_{i+1} - 2f_i + f_{i-1}}{\Delta y^2} - k^2 f_i \right), \tag{10.8.3}$$

where we have denoted $U_i \equiv U(y_i)$ and $U_i'' \equiv (d^2U/dy^2)(y_i)$. Rearranging, we obtain a difference equation,

$$U_i f_{i-1} - [2U_i + \Delta y^2 (k^2 U_i + U_i'')] f_i + U_i f_{i+1} = c [f_{i-1} - (2 + k^2 \Delta y^2) f_i + f_{i+1}]. \tag{10.8.4}$$

Compiling all equations for the interior nodes, $i = 2, \dots, N$, we derive a system of $N - 1$ linear equations accommodated into the matrix form

$$\mathbf{A} \cdot \mathbf{f} = c \mathbf{T} \cdot \mathbf{f}, \tag{10.8.5}$$

where

$$\mathbf{f} \equiv [f_2, f_3, \dots, f_{N-1}, f_N] \tag{10.8.6}$$

is the unknown solution vector,

$$\mathbf{A} \equiv \begin{bmatrix} -2U_2 - \Delta y^2(k^2U_2 + U_2'') & U_2 & 0 \\ U_3 & -2U_3 - \Delta y^2(k^2U_3 + U_3'') & U_3 \\ 0 & U_4 & -2U_4 - \Delta y^2(k^2U_4 + U_4'') \\ \vdots & \vdots & \ddots \\ 0 & 0 & 0 \\ & \cdots & 0 \\ & \cdots & 0 \\ & \cdots & 0 \\ & \vdots & \vdots \\ & U_N & -2U_N - \Delta y^2(k^2U_N + U_N'') \end{bmatrix} \quad (10.8.7)$$

is an $(N - 1) \times (N - 1)$ tridiagonal matrix involving the nodal velocities of the base flow and its second derivatives, and

$$\mathbf{T} \equiv \begin{bmatrix} -2 - k^2\Delta y^2 & 1 & 0 & \cdots & 0 & 0 \\ 1 & -2 - k^2\Delta y^2 & 1 & \cdots & 0 & 0 \\ 0 & 1 & -2 - k^2\Delta y^2 & \cdots & \cdots & 0 \\ \vdots & \vdots & \ddots & \vdots & \vdots & \vdots \\ 0 & 0 & \cdots & 0 & 1 & -2 - k^2\Delta y^2 \end{bmatrix} \quad (10.8.8)$$

is another $(N - 1) \times (N - 1)$ tridiagonal matrix. Note that the matrix \mathbf{T} is independent of the velocity profile, $U(y)$.

10.8.2 A generalized eigenvalue problem

Equation (10.8.5) presents us with a generalized algebraic eigenvalue problem that can be stated as follows: Compute a value of the generally complex constant c so that equation (10.8.5) has a nontrivial solution for the vector \mathbf{f} , that is, a solution other than the null vector.

To compute an eigenvalue, c , we may restate equation (10.8.5) in the form of a homogeneous equation,

$$\mathbf{E} \cdot \mathbf{f} = \mathbf{0}, \quad (10.8.9)$$

where \mathbf{E} is a tridiagonal matrix given by

$$\mathbf{E} \equiv \begin{bmatrix} E_{1,1} & 1 & 0 & \cdots & 0 \\ 1 & E_{2,2} & 1 & \cdots & 0 \\ \vdots & \vdots & \ddots & \vdots & \vdots \\ 0 & 0 & \cdots & E_{N-2,N-2} & 1 \\ 0 & 0 & \cdots & 1 & E_{N-1,N-1} \end{bmatrix}, \quad (10.8.10)$$

with diagonal elements

$$\begin{aligned}
 E_{1,1} &= -2 - \Delta y^2 \left(k^2 + \frac{U_2''}{U_2 - c} \right), & E_{2,2} &= -2 - \Delta y^2 \left(k^2 + \frac{U_3''}{U_3 - c} \right), \\
 \dots, & & E_{N-1,N-1} &= -2 - \Delta y^2 \left(k^2 + \frac{U_N''}{U_N - c} \right).
 \end{aligned}
 \tag{10.8.11}$$

Note that the super- and sub-diagonal elements of \mathbf{E} are all equal to unity.

For system (10.8.9) to have a nontrivial solution, the coefficient matrix \mathbf{E} must be singular. Phrased differently, c must be such that the determinant of the complex matrix \mathbf{E} is zero. This observation provides us with a basis for a numerical method involving the following steps:

1. Begin by guessing a complex value for c .
2. Compute the determinant of the matrix \mathbf{E} using the algorithm discussed in Section 10.8.3.
3. Improve c to reduce the magnitude of the determinant.
4. Return to Step 2 and repeat, if necessary.

The improvement in the third step can be made using Newton's method, setting

$$c^{\text{new}} = c^{\text{old}} - \frac{\det[\mathbf{E}(c^{\text{old}})]}{\left(\frac{d \det[\mathbf{E}(c)]}{dc} \right)_{c=c^{\text{old}}}}.
 \tag{10.8.12}$$

The derivative in the denominator on the right-hand side of (10.8.12) can be approximated with a finite difference,

$$\left(\frac{d \det[\mathbf{E}(c)]}{dc} \right)_{c=c^{\text{old}}} \simeq \frac{\det[\mathbf{E}(c^{\text{old}} + \epsilon)] - \det[\mathbf{E}(c^{\text{old}})]}{\epsilon},
 \tag{10.8.13}$$

where ϵ is a real or complex increment with small magnitude. Analytic function theory ensures that the derivative is independent of ϵ , provided that the norm of ϵ is small.

10.8.3 Determinant of a tridiagonal matrix

To compute the determinant of the tridiagonal matrix \mathbf{E} , we use an efficient algorithm that is applicable to a general $M \times M$ tridiagonal matrix of the form

$$\mathbf{T} \equiv \begin{bmatrix} a_1 & b_1 & 0 & \cdots & 0 & 0 & 0 \\ c_2 & a_2 & b_2 & \cdots & 0 & 0 & 0 \\ \vdots & \vdots & \vdots & \ddots & \vdots & \vdots & \vdots \\ 0 & 0 & 0 & \cdots & c_{M-1} & a_{M-1} & b_{M-1} \\ 0 & 0 & 0 & \cdots & 0 & c_M & a_M \end{bmatrix},
 \tag{10.8.14}$$

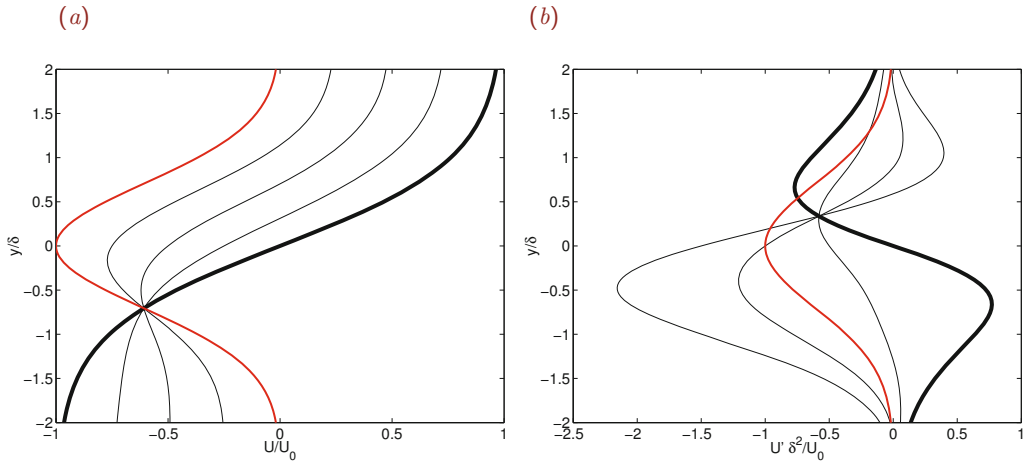


Figure 10.8.2 Profiles of (a) the base flow velocity described by (10.8.16), and (b) its second derivative for $\alpha = 1$ (bold profiles), 0.75, 0.50, 0.25, and 0.

where a_i, b_i , and c_i are real or complex constants. The algorithm involves computing a sequence of numbers, P_i , based on the recursion relations

$$P_1 = a_1, \quad P_2 = a_2 a_1 - b_1 c_2, \quad \dots, \quad P_i = a_i P_{i-1} - b_{i-1} c_i P_{i-2} \quad (10.8.15)$$

for $i = 2, \dots, M$, and then setting $\det(\mathbf{T}) = P_M$.

10.8.4 Numerical implementation

To be more specific, we consider a family of inviscid shear flows with velocity profile

$$U(y) = U_0 (\alpha \tanh \eta + (1 - \alpha) \exp(-\eta^2)), \quad (10.8.16)$$

where $\eta = y/\delta$, δ is a specified length, and the dimensionless parameter α takes values in the range $[0, 1]$. Profiles of the velocity, $U(y)$, and second derivative, $U''(y)$, are plotted in Figure 10.8.2 for several values of α . The limiting value $\alpha = 1$ corresponds to a shear layer with a hyperbolic tangent velocity profile. The limiting value $\alpha = 0$ corresponds to a symmetric wake with a Gaussian velocity profile.

The following MATLAB function entitled *rayleigh_vel*, located in directory *rayleigh* inside directory *08_stab* of **FDLIB**, computes the the velocity of the base flow and its first and second derivatives for the flow described by (10.8.16) and another flow with a inverse squared hyperbolic cosine profile:

```
function [U,Up,Upp] = rayleigh_vel (menu,U0,delta,alpha,y)
%-----
% Evaluation of the velocity (U), first derivative (Up)
```

```

% and second derivative (Upp), at a point y
%
% menu: choice of velocity profile
% U0: coefficient of the velocity profile
% delta: length scale of the velocity profile
% alpha: velocity profile parameter
%-----

%-----
% prepare
%-----

eta = y/delta;

%-----
% evaluate
%-----

%---
if(menu==1)          % derivatives analytically
%---

    alphac = 1.0-alpha; tmp = exp(-eta^2);
    U = alpha*tanh(eta) - alphac*tmp;
    Up = alpha/cosh(eta)^2 + alphac*2.0*eta*tmp;
    Upp = -alpha*2.0*sinh(eta)/cosh(eta)^3 ...
          -alphac*2.0*(1.0-2.0*eta)*tmp;

%---
elseif(menu==2)     % derivatives by numerical differentiation
%---

    U = 1.0/cosh(eta)^2;
    eps = 0.00001;
    U1 = 1.0/cosh(eta-eps)^2;
    U2 = 1.0/cosh(eta+eps)^2;
    Up = (U2-U1)/(2.0*eps);
    Upp = (U2-2.0*U+U1)/eps^2;

%---
else
%---

    disp('rayleigh_vel: this menu item is not available');
    return

%---
end
%---

```

```

%-----
% scale
%-----

Up = Up/delta; Upp = Upp/delta^2;

U = U*U0; Up = Up*U0; Upp = Upp*U0;

%-----
% Done
%-----

return

```

The following MATLAB function entitled *rayleigh_sys*, located in directory *rayleigh* inside directory *08_stab* of *FDLIB*, compiles the real and imaginary elements of the matrix **E** and computes its determinant:

```

function [detr, deti] = rayleigh_sys (N,Dys,U,Upp,k,creal,cimag)

%-----
% Compile the (N-1)x(N-1) tridiagonal matrix E
% and compute the determinant
%
% matrix has the structure:
%
%      | a b
%      | c a b
% E =  |   c a b
%      |       c a b
%
%
% ar is the real part of a
% ai is the imaginary part of a
%-----

%---
% generate the complex tridiagonal matrix E
%---

for i=2:N

    den = (U(i)-creal)^2+cimag^2;
    ar(i-1) = -2.0-Dys*(k^2 + Upp(i))*(U(i)-creal)/den;
    br(i-1) = 1.0;
    cr(i-1) = 1.0;

    ai(i-1) = - Dys*Upp(i)*cimag/den;

```

```

    bi(i-1) = 0.0;
    ci(i-1) = 0.0;

end

%---
% Compute the determinant of the complex matrix E
% using a fast method
%---

Pr(1) = ar(1);
Pi(1) = ai(1);
tmpr = br(1)*cr(2)-bi(1)*ci(2);
tmpi = br(1)*ci(2)+bi(1)*cr(2);
Pr(2) = ar(2)*Pr(1)-ai(2)*Pi(1)-tmpr;
Pi(2) = ar(2)*Pi(1)+ai(2)*Pr(1)-tmpi;

for i=3:N-1
    ia = i-1;
    tmpr = br(ia)*cr(i)-bi(ia)*ci(i);
    tmpi = br(ia)*ci(i)+bi(ia)*cr(i);
    ib = i-2;
    auxr = tmpr*Pr(ib)-tmpi*Pi(ib);
    auxi = tmpr*Pi(ib)+tmpi*Pr(ib);
    Pr(i) = ar(i)*Pr(ia)-ai(i)*Pi(ia)-auxr;
    Pi(i) = ar(i)*Pi(ia)+ai(i)*Pr(ia)-auxi;
end

detr = Pr(N-1);
deti = Pi(N-1);

%-----
% done
%-----

return

```

The following MATLAB code entitled *rayleigh*, located inside directory *08_stab* of *FDLIB*, computes the complex phase velocity of perturbations and generates a stability graph:

```

%-----
% Normal mode analysis of unidirectional inviscid
% shear flow along the x axis
%
% The flow is confined between two parallel walls
% located at y = a and -b
%
% SYMBOLS:
% -----

```

```

%
% U: velocity, function of y
% Upp: second derivative of U with respect to y
% N: level of discretization of y axis within (a,b)
%
% kdiv: number of k divisions
%       will span the wave-number range (kmin, kmax)
%
% epsr: real step for Newton corrections
% epsi: imag step for Newton corrections
% tole: tolerance for convergence
%
% cr, ci: real and imaginary parts of c
%-----

a = 5.0;
b = 5.0;
menu = 1;
U0 = 1.0;
delta = 1.0;
alpha = 1.0;

N = 2*2*64;

kstart = 0.01;
kend = 2.0;
kdiv = 64;
newter = 20; % max Newton iterations
epsr = 0.01; % for Newton iterations
epsi = 0.01; % for Newton iterations
tole = 0.000001; % for stopping Newton iterations

cr = 0.7; % initial guess
ci = 0.1; % initial guess

%-----
% prepare
%-----

denn = epsr^2 + epsi^2;
Dk = (kend-kstart)/kdiv;

Dy = (a+b)/N;
Dys = Dy^2;

%-----
% velocity profile
%-----

```

```

for i=1:N+1

    y = -b+(i-1)*Dy;

    [U(i),Up(i),Upp(i)] = rayleigh_vel(menu,U0,delta,alpha,y);

end

%-----
% scan the wave-number axis from k = kstart to kend
%-----

%=====
for kloop=1:kdiv+1
%=====

k = kstart+(kloop-1)*Dk;

%---
% Newton iterations
%---

%---
for iter=1:newter
%---

    [detr, deti] = rayleigh_sys (N,Dys,U,Upp,k,cr,ci);

    [detr1, deti1] = rayleigh_sys (N,Dys,U,Upp,k,cr+epsr,ci+epsi);

%---
% compute the derivative DdetDc = d(det(E))/dc
%---

    Ddetr = detr1-detr;
    Ddeti = deti1-deti;

    DdetDcr = ( Ddetr*epsr + Ddeti*epsi)/denn;
    DdetDci = (-Ddetr*epsi + Ddeti*epsr)/denn;

%---
% compute the correction
%---

    den = DdetDcr^2+DdetDci^2;
    corrr = ( detr*DdetDcr + deti*DdetDci)/den;
    corri = (-detr*DdetDci + deti*DdetDcr)/den;

```



```

%---
% make the correction
%---

    cr = cr - corrr;
    ci = ci - corri;

    corr = sqrt(corrr^2+corri^2);

    if(corr<tole)
        break
    end

%---
end % of Newton iterations
%---

%---
% printing session
%---

sigma = ci*k;

kplot(kloop) = k;
crplot(kloop) = cr;
ciplot(kloop) = ci;
sigmaplot(kloop) = sigma;

if(ci<0.001)
    break
end

%===
end % of scanning the wave number
%===

figure(1)
plot(kplot,ciplot,'k-','linewidth',1)

figure(2)
plot(kplot,sigmaplot,'k-','linewidth',1)

figure(3)
plot(kplot,crplot,'k-','linewidth',1)

```

Note that, because the code does not make use of internal MATLAB functions, it can be translated into any mid-level computer language of choice; this is a poor man's code.

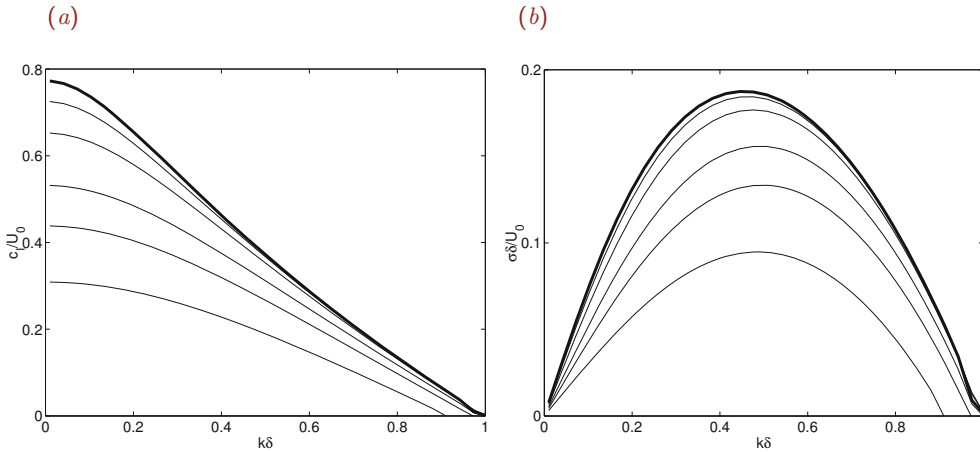


Figure 10.8.3 Instability of an inviscid shear flow with hyperbolic tangent velocity profile described by equation (10.8.16) with $\alpha = 1$. Graphs of (a) the scaled imaginary part of the phase velocity, c_I/U_0 , and (b) scaled growth rate, $\sigma_I\delta/U_0$, for $a/\delta = b/\delta = 2.0, 2.5, 3.0, 4.0, 5.0,$ and 6.0 (heavy lines), in the regime of unstable wave numbers.

Results of numerical computations for an inviscid shear flow with hyperbolic tangent velocity profile described by equation (10.8.16) with $\alpha = 1$ are shown in Figure 10.8.3 for a sequence of channel widths, a/δ , with $b = a$. When the scaled wave number, $k\delta$, is higher than a critical threshold, $(k\delta)_{cr}$, that is determined by the ratio a/δ , the growth rate is zero and the perturbations are neutrally stable. As a/δ tends to infinity, we obtain infinite shear flow in the absence of side walls. In this limit, the critical wave number for neutral stability is known to be exactly $(kb)_{cr} = 1.0$.

The results shown in Figure 10.8.3 demonstrate that the walls diminish the growth rate of perturbations by restricting the lateral extent over which fluid motion is allowed to develop. Maximum growth rate occurs at a certain wave number $(kb)_{max} \simeq 0.50$. The corresponding perturbation is expected to dominate the instability and therefore spontaneously arise in a randomly perturbed flow.

PROBLEM

10.8.1 *Instability of inviscid shear flow*

(a) Run the code *rayleigh* to generate the counterpart of Figure 10.8.3 for the velocity profile given in (10.8.16) with $\alpha = 0.50$ and 0.0 , in each case for $b = a$ and $a/\delta = 2.0, 3.0,$ and 4.0 . Discuss the results of your computations.

(b) Repeat (a) for a shear flow with velocity profile

$$U(y) = U_0 (\alpha \tanh \eta + (1 - \alpha) \operatorname{sech}^2 \eta), \tag{10.8.17}$$

where $\eta = y/\delta$, δ is a specified length, and the dimensionless parameter α takes values in

the range $[0, 1]$. The limiting values $\delta = 1$ and 0 correspond, respectively, to a shear layer with a hyperbolic tangent velocity profile and to the Bickley jet.

10.9 Finite-difference solution of the Orr–Sommerfeld equation

Finite-difference methods for the Orr–Sommerfeld equation (10.7.22) governing the stability of viscous unidirectional flow can be developed working as in Section 10.8 for the Rayleigh equation governing the stability of inviscid flow. To begin, we rearrange the Orr–Sommerfeld equation by moving the complex phase velocity, c , to the right-hand side, obtaining

$$\begin{aligned} i\nu k \left(-2 \frac{d^2 f}{dy^2} + k^2 f \right) + i \frac{\nu}{k} \frac{d^4 f}{dy^4} + U(y) \left(\frac{d^2 f}{dy^2} - k^2 f \right) - \frac{d^2 U}{dy^2} f \\ = c \left(\frac{d^2 f}{dy^2} - k^2 f \right). \end{aligned} \quad (10.9.1)$$

The no-penetration and no-slip boundary conditions over a stationary solid surface require that the boundary values of the function $f(y)$ and its first derivative are both zero.

Finite-difference equations

Discretizing the Orr–Sommerfeld equation, as discussed in Section 10.8, we obtain a system of linear equations,

$$\mathbf{A} \cdot \mathbf{f} = c \mathbf{B} \cdot \mathbf{f}, \quad (10.9.2)$$

where \mathbf{B} is a tridiagonal matrix. However, because of the presence of the fourth derivative, $f^{(iv)}$, the matrix \mathbf{A} is pentadiagonal (*penta* derives from the Greek word $\pi\epsilon\nu\tau\epsilon$ which means five.) The algebraic system arising from the finite-difference discretization can be recast into a form similar to that shown in (10.8.9),

$$\mathbf{E} \cdot \mathbf{f} = \mathbf{0}, \quad (10.9.3)$$

where the matrix \mathbf{E} is now pentadiagonal. Unfortunately, the determinant of this matrix may no longer be computed using an efficient numerical method.

As a compromise, we reluctantly solve the generalized eigenvalue problem expressed by (10.9.2) using an internal MATLAB function regarded as a black box. The pertinent MATLAB function call is:

$$\mathbf{egv} = \mathbf{eig}(\mathbf{A}, \mathbf{B})$$

where the output vector \mathbf{egv} contains the eigenvalues. Our simple task is to compile the matrices \mathbf{A} and \mathbf{B} provided in the input.

Finite-difference equations

Consider the finite-difference grid shown in Figure 10.8.1. To derive the difference equation corresponding to the i th interior node, we use a familiar finite-difference approximation for

the second derivative,

$$f_i'' = \frac{f_{i-1} - 2f_i + f_{i+1}}{\Delta y^2} \quad (10.9.4)$$

for $i = 2, \dots, N$, subject to the no-penetration boundary condition requiring that $f_1 = 0$ and $f_{N+1} = 0$. The corresponding approximation for the fourth derivative is

$$f_i^{(iv)} = \frac{f_{i-2} - 4f_{i-1} + 6f_i - 4f_{i+1} + f_{i+2}}{\Delta y^4} \quad (10.9.5)$$

for $i = 2, \dots, N$, subject to the no-penetration boundary condition requiring that $f_1 = 0$ and $f_{N+1} = 0$ and to the no-slip boundary condition requiring that $f_0 = f_2$ and $f_{N+2} = f_N$.

Orr-Sommerfeld code

By way of example, we consider an infinite shear flow with a hyperbolic tangent velocity profile

$$U(y) = U_0 \tanh \eta, \quad (10.9.6)$$

where $\eta = y/\delta$ and δ is a specified length, and a pressure-driven channel flow with a parabolic velocity profile

$$U(y) = U_0 (1 - \eta^2), \quad (10.9.7)$$

where $\eta = y/a$ and $y = \pm a$ describes the location of the walls.

The following MATLAB code entitled *orr*, located in directory *08_stab* of **FDLIB**, implements the numerical method and generates stability graphs by running over the wave number and the Reynolds number in two nested loops:

```
%=====
% Solution of the Orr--Sommerfeld equation
% in a domain -b<y<a
%
% N finite-difference divisions
%
% =====+ N+1 y=a
% |
% + N
% |
% +
% |
% + 2
% |
% =====+ 1 y=-b
%
% iflow = 1 hyperbolic tangent profile
% iflow = 2 parabolic Hagen-Poiseuille flow
```

```

%
% U0: reference velocity
%=====

%---
% preferences
%---

iflow = 2; % parabolic Hagen--Poiseuille flow
iflow = 1; % hyperbolic tangent profile

kmax = 1.2; % maximum wave number
nkloop = 32; % number of wave numbers
N = 256; % discretization level

%---
% plotting flags
%---

iplot2d = 1;
iplotcn = 1;
iplotms = 1;

%---
% choose the flow and set parameters
%---

if(iflow==1)
    a = 5.0;
    b = 5.0;
    U0 = 1.0;
    delta = 1.0;
    Restart = 1.0; % starting Reynolds number
    Reend = 40.0; % ending Reynolds number
    nReLoop = 16; % number of Re scanned
elseif(iflow==2)
    a = 1.0;
    b = a;
    U0 = 1.0;
    Restart = 2000.0;
    Reend = 40000.0;
    nReLoop = 32;
end

%---
% prepare
%---

Dy = (a+b)/N; % grid size

```

```

Dys = Dy^2;
Dk = kmax/nkloop;
im = sqrt(-1); % imaginary unit
% factor for ramping Re
fcRe = (Reend/Restart)^(1/(nReLoop-1));

%---
% nodal velocity and second derivatives
%---

for i=1:N+1

    y(i) = -b+(i-1.0)*Dy;

    if(iflow==1)
        eta = y(i)/delta;
        U(i) = U0*tanh(eta);
        Upp(i) = -2.0*U0*sinh(eta)/cosh(eta)^3;
    elseif(iflow==2)
        eta = y(i)/a;
        U(i) = U0*(1.0-eta^2);
        Upp(i) = -2.0*U0; % second derivative
    end

end

%-----
% pentadiagonal matrix approximating
% the fourth derivative f''''
%-----

P = zeros(N-1,N-1);

P(1,1)= 7.0; P(1,2)=-4.0; P(1,3)= 1.0;
P(2,1)=-4.0; P(2,2)= 6.0; P(2,3)=-4.0; P(2,4)= 1.0;

for i=3:N-3
    P(i,i-2)=1; P(i,i-1)=-4; P(i,i)=6; P(i,i+1)=-4; P(i,i+2)=1;
end

P(N-2,N-4)= 1.0; P(N-2,N-3)=-4.0; P(N-2,N-2)= 6.0;
    P(N-2,N-1)=-4.0;
        P(N-1,N-3)= 1.0; P(N-1,N-2)=-4.0; P(N-1,N-1)= 7.0;
P = P/Dy^4;

%-----
% tridiagonal matrix approximating
% the second derivative f''
%-----

```

```

T = zeros(N-1,N-1);

T(1,1) = -2.0; T(1,2) = 1.0;

for i=2:N-2
    T(i,i-1)=1.0; T(i,i)=-2.0; T(i,i+1)=1.0;
end

T(N-1,N-2) = 1.0; T(N-1,N-1) = -2.0;

T = T/Dys;

%-----
% another tridiagonal matrix
% approximating U f''
%-----

T1 = zeros(N-1,N-1);

T1(1,1) = -2.0*U(2); T1(1,2) = U(2);

for i=2:N-2
    Unode = U(i+1);
    T1(i,i-1) = Unode; T1(i,i) = -2.0*Unode; T1(i,i+1) = Unode;
end

T1(N-1,N-2) = U(N); T1(N-1,N-1) = -2.0*U(N);

T1 = T1/Dys;

%=====
% scan the wave number (k)
%=====

%---
for kloop=1:nkloop+1
%---

k = (kloop-1.0)*Dk+0.0001;

ks = k*k;

%=====
% scan the Reynolds number
%=====

Re = Restart;

```

```

%---
for ReLoop=1:nReLoop
%---

    if(iflow==1)           % adjust the kinematic viscosity
        nu = U0*delta/Re; % according to Re
    elseif(iflow==2)
        nu = U0*a/Re;
    end

    A = im*nu/k * P + T1- 2.0*k*im*nu*T;

    for i=1:N-1
        A(i,i) = A(i,i) - U(i+1)*ks - Upp(i+1) + im*nu*k^3;
    end

    B = T;
    for i=1:N-1
        B(i,i) = B(i,i)-ks;
    end

%---
% eigenvalues
%---

    egv = eig(A,B);

    gr = imag(k*egv); % growth rate
    grsorted = -sort(-gr); % sort the growth rate
    ggrr(kloop,ReLoop) = grsorted(1); % maximum growth rate

    if(iflow==1)
        wn(kloop) = k*delta;
    elseif(iflow==2)
        wn(kloop) = k*a;
    end

    Re = fcRe*Re; % ramp up Re

%---
end % of ReLoop
%---

Re = Re/fcRe;

%---
end % of kloop
%---

```



```

%=====
% Graphics module
%=====

%-----
% 2D plot
%-----

if(iplot2d==1)

    figure(1)
    hold on
    set(gca,'fontsize',15)
    box on

    if(iflow==1)
        xlabel('k\delta','fontsize',15)
        ylabel('\sigma_I\delta/U_0','fontsize',15)
        axis([0 1.2 -0.2 0.2])
    elseif(iflow==2)
        xlabel('ka','fontsize',15)
        ylabel('\sigma_I{a}/U_0','fontsize',15)
        axis([0 1.2 -0.06 0.01])
    end

    plot(wn,ggrr(:,1),'k','linewidth',3);

    for ReLoop=2:nReLoop
        plot(wn,ggrr(:,ReLoop),'k');
    end

    plot([0 1.2],[0,0],'--k')

end

%----
% contour plot
%----

if(iplotcn==1)

    figure(2)
    hold on
    set(gca,'fontsize',15)
    box on
    xlabel('Re','fontsize',15)

    if(iflow==1)
        [C,h] = contour(Rey,wn,ggrr,[0.0, 0.0],'k-');
    end
end

```

```

set(h, 'LineWidth', 3);
clabel(C,h);
[C,h]= contour(Rey,wn,ggrr,[-0.2, -0.2], 'k');
clabel(C,h);
[C,h]= contour(Rey,wn,ggrr,[-0.1, -0.1], 'k');
clabel(C,h);
[C,h]=contour(Rey,wn,ggrr,[0.05, 0.05], 'k');
clabel(C,h);
[C,h]=contour(Rey,wn,ggrr,[0.10, 0.10], 'k');
clabel(C,h);
[C,h]=contour(Rey,wn,ggrr,[0.14, 0.14], 'k');
clabel(C,h);
ylabel('k\delta', 'fontsize', 15)
axis([0 40 0 1])
elseif(iflow==2)
    [C,h]=contour(Rey,wn,ggrr,[0.0, 0.0], 'k-');
    plot([5572 5572], [0.55, 1.2], 'k--')
    ylabel('ka', 'fontsize', 15)
    axis([0 40000 0.55 1.2])
end

end

%----
% mesh plot
%----

if(iplotms==1)

    figure(3)

    set(gca, 'fontsize', 15)
    mesh(Rey,wn,ggrr);
    box on
    xlabel('Re', 'fontsize', 15)

    if(iflow==1)
        zlabel('\sigma_I\delta/U_0', 'fontsize', 15)
        ylabel('k\delta', 'fontsize', 15)
        axis([0 40 0 1 -1.5 0.2])
    elseif(iflow==2)
        zlabel('\sigma_I{a}/U_0', 'fontsize', 15)
        ylabel('ka', 'fontsize', 15)
        axis([0 40000 0 1.2 -0.06 0.01])
    end

end

end

```

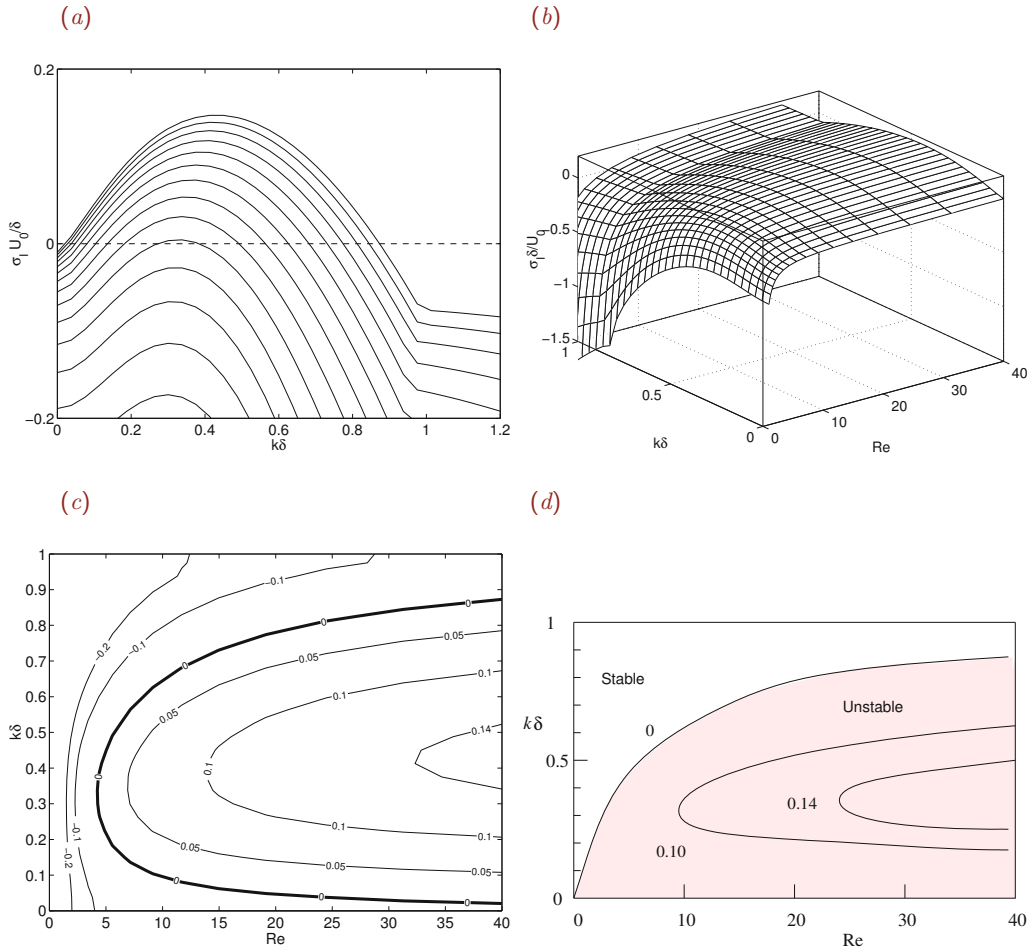


Figure 10.9.1 Stability graphs for infinite shear flow with velocity profile $U(y) = U_0 \tanh \eta$, where $\eta = y/\delta$ and δ is a specified length. (a) Scaled growth rate, $\sigma_1 \delta / U_0$, computed with discretization level $N = 256$ and truncation level $a = b = 5\delta$, plotted against the scaled wave number, $k\delta$, for Reynolds number $Re \equiv U_0 \delta / \nu = 1$ (lowest curve) up to 40 (highest curve), increasing by a geometrical factor. (b) Scaled growth rate plotted against $k\delta$ and Re , and (c) displayed as a contour plot. (d) Schematic illustration of the contour plot of the scaled growth rate in the absence of numerical error, showing regimes of stable and unstable flow.

Infinite shear flow

Results of numerical computations for infinite shear flow with $N = 256$ divisions and domain truncation level $a = b = 5\delta$ are shown in Figure 10.9.1(a–c). The zeroth contour in Figure 10.9.1(c), indicated by the bold line, corresponds to neutrally stable perturbations.

A schematic yet faithful contour plot of the growth rate for flow in an infinite domain, $a, b \rightarrow \infty$, is shown in [Figure 10.9.1\(d\)](#). A perturbation whose wave number lies in the shaded area below the zeroth-level contour is unstable, whereas a perturbation whose wave number lies above the shaded area is stable. As the Reynolds number increases, we recover the results for inviscid flow presented in [Figure 10.8.3](#).

The results in [Figure 10.9.1\(d\)](#) reveal that the flow is unstable at arbitrarily small Reynolds numbers. The destabilizing effect of inertia becomes evident by observing that, as the Reynolds number increases, the range of unstable scaled wave numbers, $[0, (k\delta)_{\text{cr}}]$, becomes wider, which means that a broader range of perturbations grow at increasingly high growth rates.

Plane Hagen–Poiseuille flow

Results of numerical computations with $N = 128$ divisions for plane Hagen–Poiseuille (pressure-driven) flow in a channel confined between two parallel walls located at $y = \pm a$ are shown in [Figure 10.9.2](#). The zeroth contour of the growth rate displayed in [Figure 10.9.2 \(c\)](#) separates regions of stable flow (outside the loop) and unstable flow (inside the loop). The Reynolds number for instability, $\text{Re}_{\text{cr}} = 5,772$, represented by the vertical dashed line in [Figure 10.9.2 \(c\)](#), defines the critical threshold where certain wave numbers, and thus the flow itself, start becoming unstable.

PROBLEMS

10.9.1 Stability of a generalized shear flow

Derive the finite-difference formula (10.9.5) from (10.9.4).

10.9.2 Stability of a generalized shear flow

Generate and discuss the counterpart of [Figure 10.9.1](#) for the velocity profile given in (10.8.16) with $\alpha = 0.5$ or 0.0.

10.10 Turbulent flow

Turbulent flow is established when the Reynolds number, defined in an appropriate fashion for the particular flow under consideration, $\text{Re} = \rho VL/\mu$, exceeds a certain threshold, usually on the order of 10^3 .

In the definition of the Reynolds number, V is a characteristic macroscopic velocity and L is a characteristic macroscopic length typically associated with the size of the boundaries. Both V and L are classified as *external scales*. For example, in the case of pipe flow, V can be identified either with the mean fluid velocity or with the maximum fluid velocity occurring at the centerline, and L can be identified with the tube radius or diameter.

Turbulence is characterized by random motions in *both* time and space. Thus, a graph of a velocity component plotted against time at a particular location in a turbulent flow

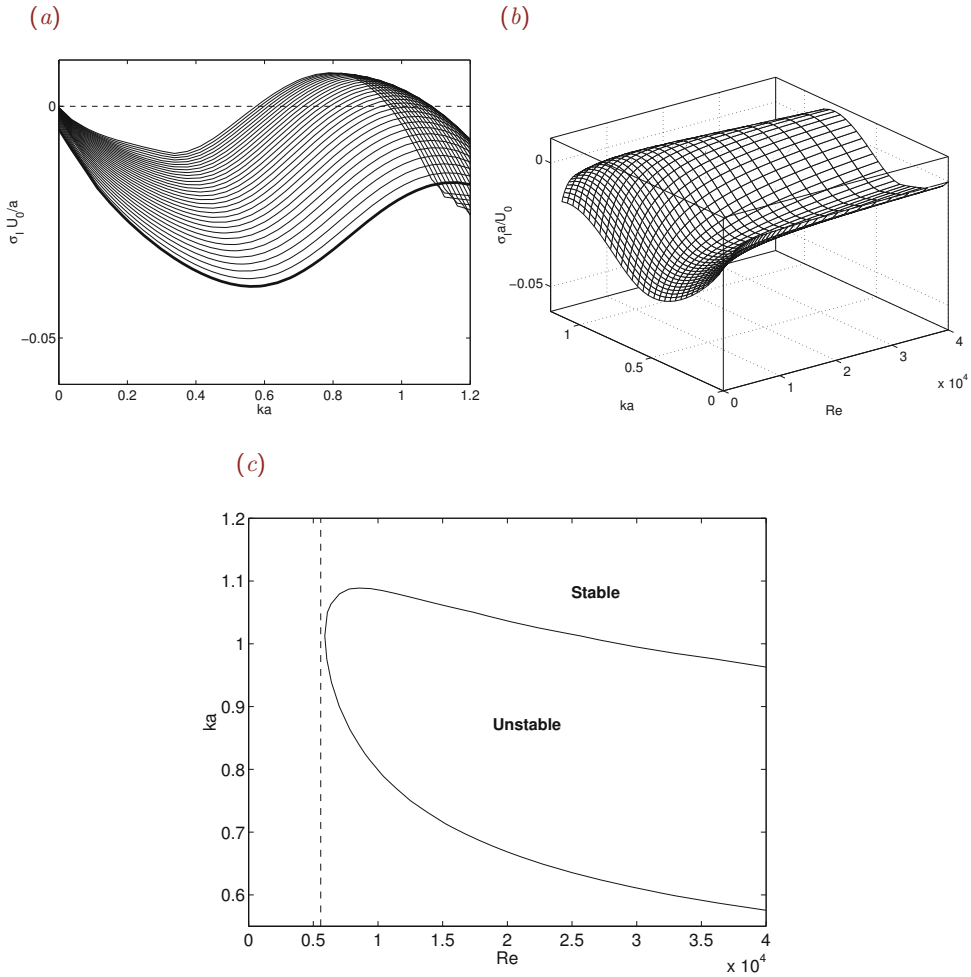


Figure 10.9.2 Stability graphs for unidirectional plane Hagen-Poiseuille flow in a channel confined between two parallel walls located at $y = \pm a$, with velocity profile $U(y) = U_0 (1 - y^2/a^2)$, where U_0 is the midplane velocity. (a) Scaled growth rate, $\sigma_1 a/U_0$, plotted against the scaled wave number, ka , for Reynolds numbers $Re \equiv U_0 a/\nu = 2,000$ (lowest curve printed in bold) up to 40,000, increasing by a geometrical factor. (b) Scaled growth rate plotted against ka and Re . (c) Zero contour of the growth rate separating regions of stable flow (outside the loop) and unstable flow (inside the loop).

reveals random fluctuations, as illustrated in [Figure 10.10.1\(a\)](#). An analogous graph of the velocity against the spatial coordinate x at a particular instant in time reveals similar random fluctuations, as illustrated in [Figure 10.10.1\(b\)](#).

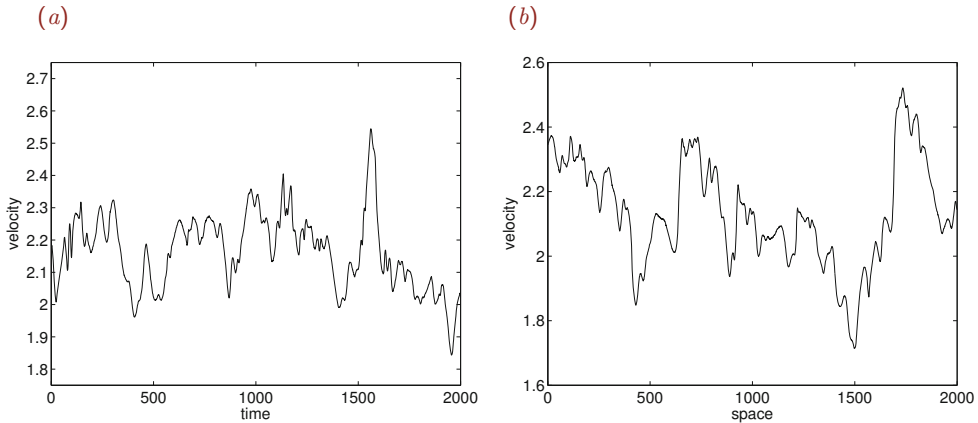


Figure 10.10.1 Typical (a) temporal and (b) spatial variation of a velocity component in a turbulent flow.

10.10.1 Transition to turbulence

The transition from laminar to turbulent flow with increasing Reynolds number is not sudden, but occurs through a sequence of events that lead to an eventual randomly fluctuating motion. For example, pressure-driven flow in a circular tube is laminar when the Reynolds number, defined with respect to the tube radius and the maximum velocity at the centerline, is less than approximately 1,100; transition occurs when the Reynolds number lies between 1,100 and 1,500; and fully developed turbulent motion is established at higher Reynolds numbers. Wall roughness and entrance conditions affect the precise thresholds for transition.

A record of the streamwise velocity component in uniform (streaming) flow past a flat plate with length L at a sequence of increasing Reynolds numbers, defined with respect to the length of the plate, is shown in [Figure 10.10.2](#).³ In the experiment, the velocity probe was placed 0.02'' above the plate and 56'' in behind the leading edge, where the double prime stands for an inch. The graphs illustrate the onset of oscillations, the development of turbulent spots, and the ultimate establishment of fully turbulent flow.

Logistic mapping

A simple model illustrating the process of transition from simple to complex behavior is provided by the logistic mapping. Given a number, $x^{(0)}$, the logistic mapping generates a sequence of numbers, $x^{(1)}, x^{(2)}, \dots$, computed by the recursion formula

$$x^{(k+1)} = \lambda x^{(k)} (1 - x^{(k)}) \quad (10.10.1)$$

for $k = 0, 1, \dots$, where λ is a specified positive constant. The special choices $x^{(0)} = 0$ and $(\lambda - 1)/\lambda$ are the fixed points of the mapping; for these choices, $x^{(k)} = x^{(0)}$ for all k , and the logistic sequence is stationary.

³Cebeci, T. & Smith, A. M. O. (1974) *Analysis of Turbulent Boundary Layers*, Academic Press.

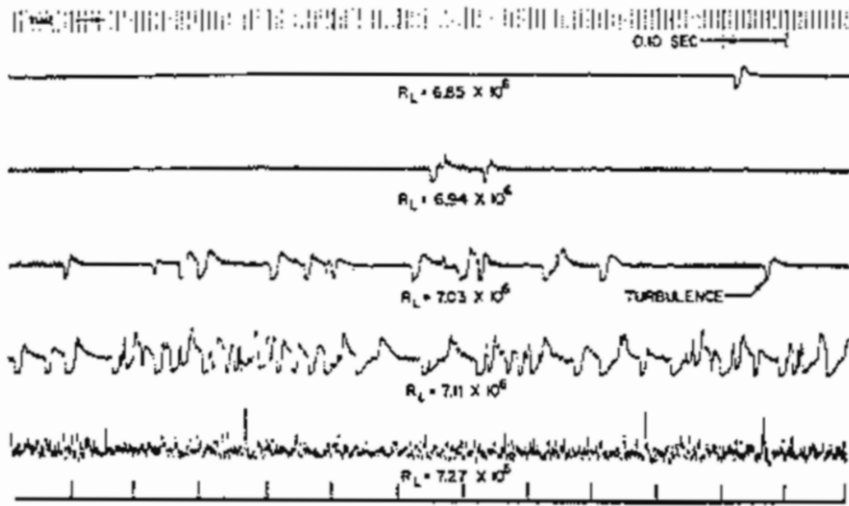


Figure 10.10.2 Record of the streamwise velocity component in flow past a flat plate at a sequence of increasing Reynolds numbers, Re_L , defined with respect to the length of the plate, L . The signal shows the onset of oscillations, the development of turbulent spots, and the ultimate establishment of fully turbulent flow.

To illustrate the transition, we introduce the λx plane and perform a series of computations according to the following steps:

1. Choose a value for λ .
2. Select a value for $x^{(0)}$ that lies between 0 and 1, but is not exactly equal to 0 or 1.
3. Compute a few hundred terms based on the logistic mapping (10.10.1).
4. Skip the first one hundred terms and plot the rest of the terms in the λx plane with dots.
5. Return to Step 1 and repeat.

The results of this computation are shown in [Figure 10.10.3](#). We observe that, as the parameter λ increases, a cascade of bifurcations and a random behavior reminiscent of turbulent motion emerges.

10.10.2 Lagrangian turbulence

Point particles in a certain class of unsteady two-dimensional laminar flows and steady or unsteady three-dimensional laminar flows have been observed to move in a random fashion,

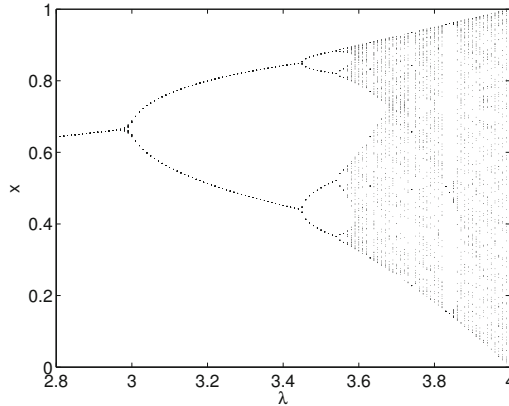


Figure 10.10.3 Sequences generated by the logistic mapping equation (10.10.1), illustrating the process of transition by way of a cascade of bifurcations in the λx plane.

exhibiting a Lagrangian turbulent motion. However, fluid motion in a turbulent flow should be distinguished from the seemingly random motion of point particles in these laminar yet chaotic flows. A distinguishing feature of a turbulent flow is the presence of pronounced three-dimensional vorticity fluctuations and the occurrence of significant kinematic and molecular diffusion accompanied by high levels of viscous dissipation.

10.10.3 Features of turbulent motion

Turbulence continues to defy a simple physical interpretation in terms of elementary fluid motions. In a traditional approach, a turbulent flow is regarded as a stochastic random process amenable to statistical analysis. However, several important features distinguish turbulent motion from a generic random process.

Intermittency

Turbulence is intermittent. A record of the velocity at a certain point in a turbulent flow may appear regular for a period of time, only to be interrupted by periods of violent turbulent motion in an intermittent fashion.

Coherent structures

A turbulent flow contains small-scale short-lived and large-scale long-lived coherent structures associated with eddies and vortices with a well-defined structure. Examples include vortex billows developing in shear layers and horseshoe vortices developing near boundary layers and in regions of high shear rates.

Vortex motion

An intimate connection exists between the dynamics of a turbulent flow and vortex dynamics

discussed in Chapter 11. However, it is not clear how studies of vortex dynamics can be used to delineate precisely the physical and mathematical properties of a turbulent flow.

Eddy motion

Eddies in a turbulent flow carry turbulent kinetic energy that is distributed over a broad range of scales; from the external scale, L , to the energy dissipating Kolmogorov scale, η , defined later in Section 10.10.6. Energy is transferred across the scales, forward and backward, from large to small and small to large, and a balance is achieved at dynamic equilibrium. A net transfer of energy occurs toward the small scales.

Dependence on the type of flow

The dynamics of turbulent flow associated with eddy motion and the distribution of energy among the different length scales is not universal, but depends on the particular flow under consideration. Thus, the properties of wall-bounded turbulent shear flow are different from those of unbounded shear flow, and different from those of grid-turbulent flow generated behind a grid placed in a high-speed flow. This diversity reflects differences in the physical mechanism by which energy is supplied into a turbulent flow, ultimately to be dissipated by small-scale motion.

Sedation near a wall

The no-slip boundary condition sedates the turbulent motion near a wall where a viscous sublayer of an unsteady laminar flow is established. A buffer zone separates the viscous sublayer from the regime of fully-developed turbulent flow. The temporal velocity signal of a turbulent flow inside a circular pipe of radius 15 cm is shown in [Figure 10.10.4](#) at different radial positions. The measurements illustrate the cessation of the turbulent motion near the wall.

10.10.4 Decomposition into mean and fluctuating components

It is useful to decompose a turbulent flow variable, such as a velocity component, into a smoothly varying or mean component and a rapidly fluctuating component. The smoothly varying component can be identified with the time averaged value over a period of time, t_0 , that is large compared to the time scale of the fluctuations, but small compared to the external time scale L/V .

The mean velocity at the position \mathbf{x} , designated by an overbar, is defined as

$$\bar{\mathbf{u}}(\mathbf{x}, t) \equiv \frac{1}{t_0} \int_{t-\frac{1}{2}t_0}^{t+\frac{1}{2}t_0} \mathbf{u}(\mathbf{x}, t+t') dt'. \quad (10.10.2)$$

The fluctuating velocity, designated by a prime, is then defined by the decomposition

$$\mathbf{u}(\mathbf{x}, t) = \bar{\mathbf{u}}(\mathbf{x}, t) + \mathbf{u}'(\mathbf{x}, t). \quad (10.10.3)$$

Note that the mean component is allowed to be a slowly varying function of time. The fluctuating component evolves rapidly in time.

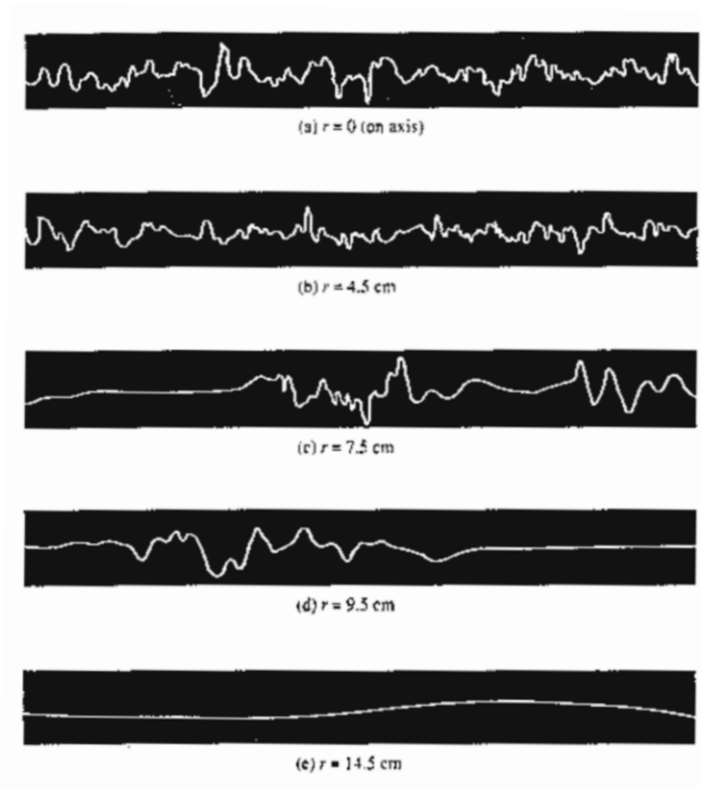


Figure 10.10.4 Temporal velocity fluctuations in turbulent pipe flow at different distances from the tube wall, showing the presence of the laminar sublayer and the buffer zone near the wall, after Corrsin, S. (1943) Investigation of flow in an axially asymmetric heated jet-air. *NACA Rep. 3L23*.

The definition (10.10.2) implies that the time-averaged value of the fluctuating velocity is zero by construction,

$$\overline{\mathbf{u}'}(\mathbf{x}, t) \equiv \frac{1}{t_0} \int_{t-\frac{1}{2}t_0}^{t+\frac{1}{2}t_0} \mathbf{u}'(\mathbf{x}, t+t') dt' = \mathbf{0}. \tag{10.10.4}$$

In contrast, the time averaged value of the square of the x component of the fluctuating velocity,

$$\overline{u_x'^2}(\mathbf{x}, t) \equiv \frac{1}{t_0} \int_{t-\frac{1}{2}t_0}^{t+\frac{1}{2}t_0} u_x'^2(\mathbf{x}, t+t') dt', \tag{10.10.5}$$

is not zero; the square of the y or z component of the fluctuating velocity is also nonzero. The square root of these time averages, called the root-mean-square (rms) values, normalized

by an external velocity scale, V , expressed by the ratios

$$i_x \equiv \frac{1}{V} \sqrt{\overline{u'^2}}, \quad i_y \equiv \frac{1}{V} \sqrt{\overline{v'^2}}, \quad i_z \equiv \frac{1}{V} \sqrt{\overline{w'^2}}, \quad (10.10.6)$$

are sensible measures of the intensity of the turbulent motion in the three spatial directions.

Laboratory measurements have shown that the three intensities defined in (10.10.6) have different magnitudes, except in the idealized case of isotropic turbulent flow occurring in the absence of boundaries. Nearly isotropic turbulence can be realized in the laboratory by placing eight fans at the vertices of a cube, and turning the rotating blades of the fans toward the center of the cube. In the case of channel or tube flow, the turbulence intensity in the direction of the flow is significantly greater than that in directions perpendicular to the flow, especially near walls.

A single measure of the magnitude of the turbulent velocity fluctuations is provided by the velocity scale

$$u \equiv \left(\frac{\overline{u'^2} + \overline{v'^2} + \overline{w'^2}}{3} \right)^{1/2}. \quad (10.10.7)$$

In the case of isotropic turbulence, the three terms in the numerator on the right-hand side are equal.

Flow through a pipe

As an example, we consider pressure-driven turbulent flow through a circular tube of radius a . Schematic illustrations of the mean velocity profile, distribution of the streamwise turbulence intensity, and distribution of the lateral turbulence intensity are shown in [Figure 10.10.5](#). The mean velocity profile can be approximated with the algebraic form

$$\bar{u}_x(\sigma) = U \left(1 - \frac{\sigma}{a} \right)^{1/7}, \quad (10.10.8)$$

where $U \equiv (\bar{u}_x)_{max}$ is the maximum mean velocity occurring at the centerline. This profile should be contrasted with its parabolic counterpart for laminar flow shown in equation (7.3.8).

10.10.5 Inviscid scales

A turbulent flow contains an infinite collection of interacting eddies defined and regarded as elementary fluid motions. Inspecting the turbulence signal shown in [Figure 10.10.1\(b\)](#), we identify spatial scales with a broad range of magnitudes. One important scale, classified as inviscid, is the scale of the energy-containing turbulent motion, denoted by ℓ .

Using ℓ and the magnitude of the velocity fluctuations u defined in (10.10.7), we deduce that the time scale of the energy containing eddies is comparable to ℓ/u . The actual size of ℓ varies according to the particular flow under consideration, as follows:

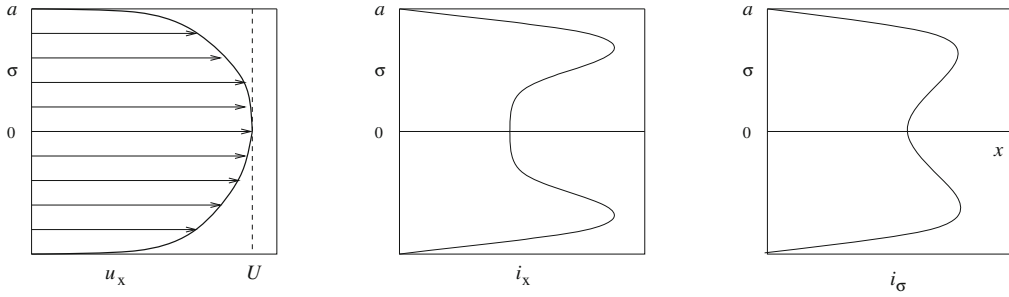


Figure 10.10.5 Schematic illustrations of the mean velocity profile and distribution of the streamwise and lateral turbulence intensities for turbulent flow through a circular tube of radius a .

- In the case of boundary-layer flow, ℓ is comparable to the local boundary layer thickness.
- In the case of turbulent jet flow, ℓ is comparable to the local jet diameter.
- In the case of a wake behind a body, ℓ is comparable to the local width of the wake.
- In the case of pipe flow, ℓ is comparable to the tube diameter.
- In the case of infinite shear flow over a wall, ℓ in the buffer zone is proportional to the distance from the wall.
- In the case of free turbulence generated by placing a grid in a uniform stream, ℓ is comparable to the grid size behind the grid, and increases with downstream position.

The inviscid scales are complemented by viscous scales that develop spontaneously inside the fluid.

10.10.6 Viscous scales

Energy is dissipated in a turbulent flow even if the mean flow has a uniform velocity profile. A continuous external supply of energy is necessary to sustain the motion of the fluid. The rate of viscous dissipation, with units of kinetic energy per mass per time, is denoted by

$$\epsilon [=] \frac{L^2}{T^3}, \tag{10.10.9}$$

where the symbol [=] denotes dimensional equivalence, L is length, and T is time. One distinguishing property of turbulent flow is that dissipation occurs mainly due to small-scale motion.

It can be argued that the rate of dissipation is determined primarily by the fluid properties. Combining ϵ with the kinematic viscosity, ν , we formulate the Kolmogorov length scale

$$\eta \equiv \left(\frac{\nu^3}{\epsilon} \right)^{1/4}, \tag{10.10.10}$$

and accompanying Kolmogorov velocity scale,

$$u_K \equiv (\nu \epsilon)^{1/4}. \quad (10.10.11)$$

The two scales are related by

$$\text{Re}_K \equiv \frac{u_K \eta}{\nu} = 1, \quad (10.10.12)$$

where Re_K is the Reynolds number of the energy-dissipating motion. By design, Re_K is equal to unity, underlying the dominance of viscous forces responsible for converting kinetic to thermal energy inside a viscous fluid.

10.10.7 Relation between inviscid and viscous scales

Energy conservation requires that the rate of viscous dissipation, ϵ , scales as

$$\epsilon \simeq \frac{u^3}{\ell}. \quad (10.10.13)$$

Substituting this estimate into (10.10.10) and rearranging, we obtain

$$\frac{\eta}{\ell} \simeq \left(\frac{\nu}{u\ell} \right)^{3/4}, \quad (10.10.14)$$

where we recall that η is the Kolmogorov length scale.

The magnitude of the velocity fluctuations, u , is typically comparable to the external velocity scale, V , whereas the inviscid length scale ℓ is comparable to the external length scale, L . As a result, the inverse of the ratio on the right-hand side of (10.10.14) is comparable to the Reynolds number $\text{Re} = VL/\nu$, yielding the scaling

$$\frac{\eta}{\ell} \simeq \text{Re}^{-3/4}. \quad (10.10.15)$$

Working in a similar fashion with (10.10.11), we derive the scaling law

$$\frac{u_K}{u} \simeq \text{Re}^{-1/4}, \quad (10.10.16)$$

where we recall that u_K is the Kolmogorov velocity scale. These equations allow us to estimate the scales of the energy-dissipating motion from measurable or observable outer scales and the Reynolds number of the flow.

PROBLEMS

10.10.1 Turbulent mean velocity profile in pipe flow

Consider turbulent flow in a pipe whose mean velocity profile is described by (10.10.8). Derive a relationship between the mean flow rate and the mean velocity at the centerline. Compare this relationship with its counterpart for laminar Poiseuille flow.

10.10.2 Kolmogorov length scale for pipe flow

Laboratory data for turbulent flow in a circular tube with diameter D has shown that: (a) the length scale of the energy containing turbulent motion, ℓ , is comparable to D , and (b) the magnitude of the turbulent velocity fluctuations is comparable to the maximum mean velocity occurring at the centerline, V . Based on this information, compute the Kolmogorov length and velocity scale for a tube with diameter $D = 10$ cm, at Reynolds number $\text{Re} \equiv VD/\nu = 10^6$.

10.11 Spectrum of a turbulent flow

To analyze the distribution of energy across the scales of a turbulent flow, it is helpful to decompose a recording of the velocity or pressure at a particular location into a Fourier series with respect to time, and then examine the magnitude of the Fourier coefficients.

In the laboratory, the velocity is measured typically by two methods: hot-wire anemometry based on a calibration that associates velocity to heat loss from a small heated wire probe placed in a flow; and laser-Doppler velocimetry based on light scattering from a patterned laser beam caused by small particles seeded in the flow.

Time series analysis

To develop the Fourier decomposition, we consider a times series of a function, $f(t)$, consisting of a sequence of values of the function recorded at evenly spaced time intervals separated by a sampling time, Δt . Suppose that the time series contains N records corresponding to times

$$t_1 = 0, \quad t_2 = \Delta t, \quad t_3 = 2\Delta t, \quad \dots, \quad t_N = (N-1)\Delta t, \quad (10.11.1)$$

and define the total time $T = N\Delta t$. Using Fourier representation theory, and assuming for convenience that $f(N\Delta t) = f(0)$, we express the function $f(t)$ over the time interval $(0, T)$ in terms of a complete Fourier series,

$$f(t) \simeq \frac{1}{2} a_0 + \sum_{p=1}^M a_p \cos\left(\frac{2\pi p}{N} \frac{t}{\Delta t}\right) + \sum_{p=1}^M b_p \sin\left(\frac{2\pi p}{N} \frac{t}{\Delta t}\right) \quad (10.11.2)$$

for $t \geq 0$, where M is a specified truncation level, p is an integer, a_p are cosine Fourier coefficients, and b_p are sine Fourier coefficients.

The complex Fourier coefficients are defined as

$$c_p \equiv \frac{1}{2} (a_p + i b_p) \quad (10.11.3)$$

for $p = 0, 1, \dots$, where i is the imaginary unit, $i^2 = -1$. In terms of the complex Fourier coefficients, the Fourier series (10.11.2) can be recast into the compact form

$$f(t) \simeq \sum_{p=-M}^M c_p \exp\left(-i \frac{2\pi p}{N} \frac{t}{\Delta t}\right), \quad (10.11.4)$$

where the negative-indexed complex Fourier coefficients are given by

$$c_{-p} = c_p^* = \frac{1}{2} (a_p - i b_p), \quad (10.11.5)$$

and an asterisk denotes the complex conjugate.

Evaluation of the Fourier coefficients

Fourier theory provides us with a remarkably simple method of evaluating the Fourier coefficients.⁴ Denoting the data by

$$f_i \equiv f(t_i), \quad (10.11.6)$$

we find that

$$a_p = \frac{2}{N} \left[f_1 + \cos\left(2\pi \frac{p}{N}\right) f_2 + \cos\left(2\pi \frac{2p}{N}\right) f_3 + \cdots + \cos\left(2\pi \frac{(N-1)p}{N}\right) f_N \right] \quad (10.11.7)$$

and

$$b_p = \frac{2}{N} \left[f_1 + \sin\left(2\pi \frac{p}{N}\right) f_2 + \sin\left(2\pi \frac{2p}{N}\right) f_3 + \cdots + \sin\left(2\pi \frac{(N-1)p}{N}\right) f_N \right]. \quad (10.11.8)$$

In practice, because the number of data points, N , can be on the order of several thousand or even higher, the direct evaluation of the sums on the right-hand sides of expressions (10.11.8) requires a prohibitive amount of computational time. Fortunately, the computations can be expedited considerably by using an ingenious algorithm for computing the Fourier coefficients, known as the fast Fourier transform (FFT).

Function *fft*, located in directory *stats* inside directory *13.turbo* of **FDLIB**, performs the FFT of a time series with size $N = 2^q$, where q is an integer.

Power spectrum

Now we take the square of both sides of (10.11.4), expand the square of the product on the right-hand side, integrate the resulting expression with respect to time from $t = 0$ to $T \equiv N \Delta t$, and use trigonometric identities to set the integral of a large number of terms equal to zero, finding

$$\int_0^T f^2(t) dt \simeq T \sum_{p=-M}^M c_p c_p^*, \quad (10.11.9)$$

which can be rearranged into

$$\overline{f^2} \equiv \frac{1}{T} \int_0^T f^2(t) dt \simeq \sum_{p=-M}^M |c_p|^2 = c_0^2 + 2 \sum_{p=1}^M |c_p|^2, \quad (10.11.10)$$

⁴Pozrikidis, C. (2008) *Numerical Computation in Science and Engineering*, Second Edition, Oxford University Press.

where

$$|c_p|^2 = c_p c_p^* = \frac{1}{4} (a_p^2 + b_p^2) \quad (10.11.11)$$

is the square of the magnitude of the p th complex Fourier coefficient.

A graph of the positive coefficients $2|c_p|^2$ against the angular frequency $\omega_p \equiv 2\pi p/\Delta t$ for $p = 1, \dots$, is the discrete temporal power spectrum of the function $f(t)$. Of particular interest is the behavior of the power spectrum at high values of p corresponding to high angular frequencies.

A graph of the coefficients $2|c_p|^2$ against the spatial wave number $k_p \equiv \omega_p V = 2\pi p V/\Delta t$ is the discrete power spectrum of the function $f(t)$, where V is a specified velocity. Of particular interest is the behavior at high values of p corresponding to high wave numbers.

Now identifying the generic function $f(t)$ with the x , y , or z component of the velocity, we obtain the discrete energy spectrum of a turbulent flow, providing us with information on the distribution of kinetic energy across different scales.

In practice, the discrete power spectrum is computed by taking the Fourier transform of a time series comprised of sets of data points on the order of $2^{12} = 4096$. The power spectrum computed using one data set exhibits pronounced fluctuations. To obtain a smooth spectrum, the Fourier coefficients are averaged over sets corresponding to different realizations or different time periods for the same flow conditions.

Energy density function

As the sample size, N , and total sampling time, $T = N\Delta t$, tend to infinity, the sum on the right-hand side of (10.11.4) reduces to a Fourier integral. Correspondingly, the right-hand side of (10.11.10) takes the form

$$\overline{f^2} = \int_0^\infty E_t(\omega) d\omega = \int_0^\infty E(k) dk, \quad (10.11.12)$$

where $E_t(\omega)$ and $E(k)$ are temporal and spatial energy density functions. Now making a correspondence between (10.11.12) and (10.11.10), we obtain the relations

$$E_t(\omega_p) = \frac{\Delta t}{2\pi} 2|c_p|^2, \quad E(k_p) = \frac{V\Delta t}{2\pi} 2|c_p|^2, \quad (10.11.13)$$

which allow us to prepare graphs and study the shape of the energy density function. Taylor's frozen-field hypothesis amounts to setting V equal to the local mean value of the streamwise velocity.

FDLIB Data

As an application, we consider a stratified turbulent shear flow behind a vertical grid with mean velocity profile $\bar{u}_x(y)$ and mean temperature field $\bar{T}(y)$, as shown in [Figure 10.11.1](#). At the University of California, San Diego, researcher Kurt Keller recorded a time series of the x

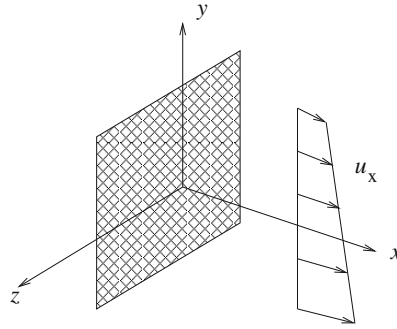


Figure 10.11.1 A time series of the velocity and temperature in stratified turbulent shear flow behind a vertical grid recorded by Kurt Keller can be found in file *keller.dat*, residing in directory *stats* inside directory *13_turbo* of **FDLIB**.

and y velocity components and temperature at a point located 457.2 cm behind the grid, at the sampling frequency 5 Khz corresponding to sampling time 0.0002 s^{-1} , for the following conditions: grid spacing 2.54 cm; mean shear rate $d\bar{u}_x/dy = -7.63 \text{ s}^{-1}$; mean temperature gradient $d\bar{T}/dy = 35.8 \text{ K m}^{-1}$; local microscale Reynolds number $\text{Re} \equiv \lambda u/\nu = 91.2$.

In the definition of the microscale Reynolds number,

$$u \equiv \sqrt{\overline{u'^2}} \quad (10.11.14)$$

is the rms value of the fluctuations of the streamwise component of the velocity and λ is the Taylor microscale defined from the relation

$$\frac{u^2}{\lambda^2} = \overline{\left(\frac{du'}{dy}\right)^2}. \quad (10.11.15)$$

The data are arranged in the three columns of file *keller.dat* located in directory *stats* inside directory *13_turbo* of **FDLIB**.

PROBLEM

10.11.1 Stratified shear flow

- With reference to [Figure 10.11.1](#), compute and plot the mean and rms values of the velocity and temperature. Investigate their dependence on the sample size.
- Compute, plot, and discuss the discrete power spectrum of the x and y velocity components and temperature.

10.12 Analysis and modeling of turbulent flow

Deriving exact solutions of the Navier–Stokes equation for turbulent flow is out of the question. Direct numerical simulation (DNS) is prohibited by pragmatic constraints associated with the finite grid size, which necessitate sub-grid modeling: to capture the dynamics of a turbulent flow, we must resolve a prohibitively broad range of length scales. Progress can be made by developing approximate models and phenomenological theories based on empirical correlations that are inspired by laboratory observation.

10.12.1 Reynolds stresses

A useful point of departure for developing phenomenological theories is the decomposition of the velocity field into a mean and a fluctuating component, as shown in equation (10.10.3). A similar decomposition of the pressure field yields

$$p(\mathbf{x}, t) = \bar{p}(\mathbf{x}, t) + p'(\mathbf{x}, t), \tag{10.12.1}$$

where

$$\bar{p}(\mathbf{x}, t) \equiv \frac{1}{t_0} \int_{t-\frac{1}{2}t_0}^{t+\frac{1}{2}t_0} p(\mathbf{x}, t + t') dt' \tag{10.12.2}$$

is the mean pressure. The continuity equation for an incompressible fluid requires that

$$\nabla \cdot \bar{\mathbf{u}} = 0, \tag{10.12.3}$$

where a bar denotes the time-averaged value.

Next, we substitute the decompositions (10.10.3) and (10.12.2) into Cauchy’s equation of motion, expand the derivatives of the products, take the time average of both sides, and simplify to derive a modified equation of motion for the mean component. The fluctuating component appears as an effective inertial hydrodynamic volume force.

For example, the term $\partial(\rho u_x u_y)/\partial y$ on the left-hand side of the x component of the equation of motion (6.3.16), becomes

$$\begin{aligned} \frac{\partial}{\partial y}(\rho u_x u_y) &= \frac{\partial}{\partial y} [\rho (\bar{u}_x + u'_x) (\bar{u}_y + u'_y)] \\ &= \frac{\partial}{\partial y}(\rho \bar{u}_x \bar{u}_y) + \frac{\partial}{\partial y}(\rho \bar{u}_x u'_y) + \frac{\partial}{\partial y}(\rho u'_x \bar{u}_y) + \frac{\partial}{\partial y}(\rho u'_x u'_y). \end{aligned} \tag{10.12.4}$$

Taking the time average of both sides, as shown in equations (10.10.2) and (10.12.2), and interchanging the order of time-averaging and space differentiation, we obtain

$$\begin{aligned} \frac{\partial}{\partial y}(\overline{\rho u_x u_y}) &= \frac{\partial}{\partial y}(\overline{\rho \bar{u}_x \bar{u}_y}) + \frac{\partial}{\partial y}(\overline{\rho \bar{u}_x u'_y}) + \frac{\partial}{\partial y}(\overline{\rho u'_x \bar{u}_y}) + \frac{\partial}{\partial y}(\overline{\rho u'_x u'_y}) \\ &= \frac{\partial}{\partial y}(\rho \bar{u}_x \bar{u}_y) + \frac{\partial}{\partial y}(\rho \bar{u}_x \overline{u'_y}) + \frac{\partial}{\partial y}(\rho \overline{u'_x} \bar{u}_y) + \frac{\partial}{\partial y}(\overline{\rho u'_x u'_y}). \end{aligned} \tag{10.12.5}$$

Because of (10.10.4), the second and third terms on the right-hand side of (10.12.5) are zero, leaving the simplified expression

$$\frac{\partial}{\partial y}(\overline{\rho u_x u_y}) = \frac{\partial}{\partial y}(\rho \bar{u}_x \bar{u}_y) + \frac{\partial}{\partial y}(\overline{\rho u'_x u'_y}). \quad (10.12.6)$$

RANS

Working in a similar fashion with the other terms on the left-hand side of the Navier–Stokes equation, we derive a the Reynolds-averaged Navier–Stokes (RANS) equation

$$\rho \left(\frac{\partial \bar{\mathbf{u}}}{\partial t} + \bar{\mathbf{u}} \cdot \nabla \bar{\mathbf{u}} \right) = -\nabla \bar{p} + \mu \nabla^2 \bar{\mathbf{u}} + \nabla \cdot \boldsymbol{\sigma}^R + \rho \mathbf{g}, \quad (10.12.7)$$

where $\boldsymbol{\sigma}^R$ is the Reynolds stress tensor with components

$$\sigma_{ij}^R = -\overline{\rho u'_i u'_j}, \quad (10.12.8)$$

expressing transfer of momentum from the i th to the j th direction, and *vice versa*, by way of turbulence fluctuations. An alternative form of (10.12.7) is

$$\frac{\partial(\rho \bar{\mathbf{u}})}{\partial t} + \nabla \cdot (\rho \bar{\mathbf{u}} \bar{\mathbf{u}}) = -\nabla \bar{p} + \mu \nabla^2 \bar{\mathbf{u}} + \nabla \cdot \boldsymbol{\sigma}^R + \rho \mathbf{g}. \quad (10.12.9)$$

Phenomenological theories seek to establish a relationship between the Reynolds stresses and the structure of the time-averaged flow. Once this has been done, the averaged equation of motion (10.12.7) or (10.12.9) can be solved together with the time-averaged continuity equation (10.12.3) to generate the velocity distribution in a turbulent flow.

The Boussinèsq's law

Boussinèsq proposed the constitutive law

$$\boldsymbol{\sigma}^R = -\frac{3}{2} \rho k \mathbf{I} + \mu_T 2 \bar{\mathbf{E}}, \quad (10.12.10)$$

where

$$k = \frac{1}{2} (u_x'^2 + u_y'^2 + u_z'^2) \quad (10.12.11)$$

is the turbulent kinetic energy, μ_T is an eddy viscosity, \mathbf{I} is the identity matrix, and $\bar{\mathbf{E}}$ is the time-averaged rate-of-deformation tensor. The scalar $\frac{3}{2} \rho k$ in the first term on the right-hand side of (10.12.10) plays the role of a positive turbulence pressure.

In the k - ϵ model, the turbulent kinetic energy is related to the rate of viscous dissipation, ϵ , by

$$\nu_T \epsilon = c_\mu \rho k^2, \quad (10.12.12)$$

where

$$\epsilon = \nu_T \left(\frac{\partial u_i}{\partial x_j} \right) \left(\frac{\partial u_i}{\partial x_j} \right), \quad (10.12.13)$$

$\nu_T = \mu_T / \rho$ is the turbulent kinematic viscosity, c_μ is a dimensionless coefficient, and summation is implied over the repeated indices i and j .

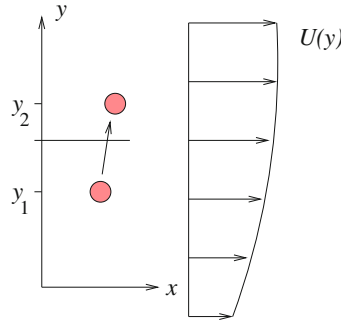


Figure 10.12.1 Profile of turbulent shear flow along the x axis illustrating the random displacement of a fluid parcel by a distance that is comparable to the Prandtl mixing length.

10.12.2 Prandtl’s mixing length

Prandtl proposed a physically intuitive model that relates the Reynolds stresses to the velocity profile of the mean flow. Motivation is provided by a tentative analogy between eddy motion in a turbulent flow and molecular motion in a gas. The derivation is similar to that discussed in Section 4.4.5 concerning the fluid viscosity.

Consider a unidirectional turbulent shear flow along the x axis with mean velocity profile $\bar{u}_x = U(y)$, as illustrated in Figure 10.12.1. Suppose that, because of the turbulent motion, a small fluid parcel with volume δV_p , initially located at $y = y_1$, is displaced to the position $y = y_2$ where it travels in the streamwise direction with the new local velocity. The change in the x component of the parcel momentum is

$$(\delta M_x)_p = (u_{x(y=y_2,t)} - u_{x(y=y_1,t)}) \rho \delta V_p. \tag{10.12.14}$$

Because turbulent fluctuations have been assumed small, the total velocity has been approximated with the mean velocity to give

$$(\delta M_x)_p \simeq (U_{(y=y_2)} - U_{(y=y_1)}) \rho \delta V_p. \tag{10.12.15}$$

Next, we consider the transport of momentum across a horizontal plane located at elevation y , as shown in Figure 10.12.1. During a small period of time, Δt , all parcels residing inside a layer of thickness $u_y(y, t) \Delta t$ adjacent to this elevation cross the elevation to find themselves on the other side. The total volume of fluid crossing the plane is

$$\delta V = u_y(y, t) w \Delta x \Delta t, \tag{10.12.16}$$

where w is an arbitrary width along the z axis. The associated transport of x momentum across a horizontal length Δx due to this motion is

$$\delta M_x \simeq \rho [U(y = y_2) - U(y = y_1)] \delta V, \tag{10.12.17}$$

which can be approximated as

$$\delta M_x \simeq (y_2 - y_1) \frac{\partial U}{\partial y} \rho \delta V. \quad (10.12.18)$$

Substituting (10.12.16), we obtain

$$\delta M_x \simeq \rho u_y(y, t) (y_2 - y_1) \frac{\partial U}{\partial y} w \Delta x \Delta t. \quad (10.12.19)$$

Averaging this expression over all time intervals, Δt , we obtain

$$\overline{\delta M_x} \simeq \overline{\rho u_y(y, t) (y_2 - y_1) \frac{\partial U}{\partial y} w \Delta x \Delta t}. \quad (10.12.20)$$

According to Newton's second law of motion, this averaged transfer of momentum amounts to a force pointing in the x direction, expressed by the Reynolds shear stress, σ_{xy}^R . Setting

$$\overline{\delta M_x} = \sigma_{xy}^R w \Delta x \Delta t \quad (10.12.21)$$

and rearranging, we obtain

$$\sigma_{xy}^R = \overline{\rho u_y(y, t) \Delta y} \frac{\partial U}{\partial y}. \quad (10.12.22)$$

where $\Delta y \equiv y_2 - y_1$.

In the next key step, we introduce the scaling

$$\overline{u_y(y, t) \Delta y} \simeq \sqrt{u_y'^2} \ell_P \simeq \left| \frac{\partial U}{\partial y} \right| \ell_P^2, \quad (10.12.23)$$

where ℓ_P is Prandtl's mixing length. Substituting (10.12.23) into (10.12.22), we obtain the targeted constitutive equation

$$\sigma_{xy}^R(y) = \rho \ell_P^2 \left| \frac{\partial U}{\partial y} \right| \left(\frac{\partial U}{\partial y} \right). \quad (10.12.24)$$

The product of the first three terms on the right-hand side of (10.12.24) plays the role of the eddy viscosity introduced by Boussinèsq.

Readers who are overwhelmed by uneasiness regarding the physical relevance of the various steps involved in the preceding derivation are not alone. Numerous constitutive relations similar to that shown in (10.12.24) have been proposed based on heuristic and tentative analogies and laboratory observation.

10.12.3 Logarithmic law for wall-bounded shear flow

As an application, we use Prandtl's mixing length model expressed by equation (10.12.24) to deduce the functional form of the velocity profile in wall-bounded shear flow, away from the viscous sublayer and the buffer zone.

Assuming that the sign of dU/dy is positive, neglecting the viscous shear stress $\mu dU/dy$ in comparison to the Reynolds shear stress, and ignoring the variation of the shear stress in the y direction due to the streamwise pressure drop, we find that

$$\sigma_{xy}^R(y) = \rho \ell_P^2 \left(\frac{dU}{dy} \right)^2 = \tau_{\text{wall}}, \quad (10.12.25)$$

where τ_{wall} is the wall shear stress. Rearranging, we obtain

$$\ell_P^2 \left(\frac{dU}{dy} \right)^2 = \frac{\tau_{\text{wall}}}{\rho} \equiv u_*^2, \quad (10.12.26)$$

where u_* is the friction velocity.

Next, we set the Prandtl mixing length proportional to the distance from the wall,

$$\ell_P = \kappa y, \quad (10.12.27)$$

where κ is a dimensionless constant. In the case of flow through a circular tube, measurements suggest the particular value $\kappa \simeq 0.36$. Substituting (10.12.27) into (10.12.26), taking the square root of the emerging equation, and rearranging, we find that

$$\frac{dU}{dy} = \frac{u_*}{\kappa y}. \quad (10.12.28)$$

Integrating with respect to y , we derive the logarithmic relationship

$$\frac{U(y)}{u_*} = \frac{1}{\kappa} \ln \frac{y}{a} + A, \quad (10.12.29)$$

where a is a defined length and A is a dimensionless constant. In dimensionless variables, expression (10.12.29) takes the form

$$u^+ = \frac{1}{\kappa} \ln y^+ + B, \quad (10.12.30)$$

where B is another dimensionless constant, and we have defined

$$u^+ \equiv \frac{\bar{u}_x(y)}{u_*} = \frac{U(y)}{u_*}, \quad y^+ \equiv \frac{u_* y}{\nu}. \quad (10.12.31)$$

Laboratory measurements have shown that equation (10.12.30) with $B = 3.6$ describes accurately the velocity profile approximately for $y^+ > 26$, as illustrated in [Figure 10.12.2](#).

In the viscous sublayer attached to the wall, laboratory observations suggest the linear relation

$$u^+ = y^+ \quad (10.12.32)$$

approximately for $0 < y^+ < 5$. In the buffer zone, $5 < y^+ < 26$, a more involved relation is required.

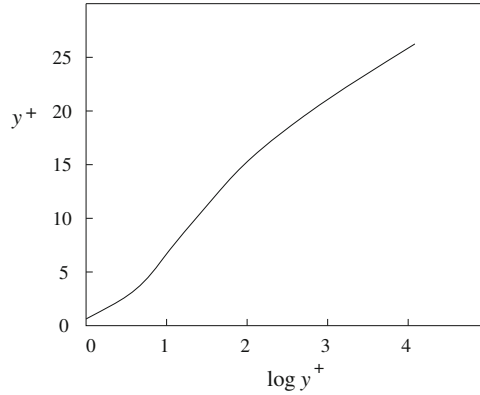


Figure 10.12.2 Schematic illustration of the distribution of the mean velocity in the dimensionless variables defined in equations (10.12.31) for wall-bounded turbulent shear flow.

10.12.4 Correlations

Space-time correlations allow us to extract information on the small-scale structure of a turbulent flow. Consider the i th component of the fluctuating velocity at a point, \mathbf{x}_1 , at time t , and the j th component of the fluctuating velocity at another point, \mathbf{x}_2 , at time $t + \tau$, where τ is the time delay. The corresponding second-order space-time correlation is defined as

$$\mathcal{R}_{ij}(\mathbf{x}_1, \mathbf{x}_2, t, \tau) \equiv \overline{u'_i(\mathbf{x}_1, t) u'_j(\mathbf{x}_2, t + \tau)}. \quad (10.12.33)$$

Explicitly,

$$\mathcal{R}_{ij}(\mathbf{x}_1, \mathbf{x}_2, t, \tau) = \frac{1}{t_0} \int_{t - \frac{1}{2}t_0/2}^{t + \frac{1}{2}t_0} u'_i(\mathbf{x}_1, t + t') u'_j(\mathbf{x}_2, t + \tau + t') dt'. \quad (10.12.34)$$

Two special correlations are of particular interest: the spatial correlation corresponding to $\tau = 0$, and the time-delayed correlation arising when the points \mathbf{x}_1 and \mathbf{x}_2 coincide.

Taylor's frozen-field hypothesis provides us with a relationship between the time-delayed and spatial correlation. The underlying reasoning is that, in a low-intensity turbulent flow, the mean velocity sweeps the turbulence so fast that the eddies do not evolve significantly during the time it takes them to cross a fixed point in space. Physically, the velocity vector field appears to be frozen in time. If the mean velocity is in the direction of the x axis, we may write

$$\mathcal{R}_{ij}(\mathbf{x}_1, \mathbf{x}_2, t, \tau) \simeq \mathcal{R}_{ij}(\mathbf{x}_1, \mathbf{x}_1 + \Delta x \mathbf{e}_x, t, \tau) = \mathcal{R}_{ij}(\mathbf{x}_1, \mathbf{x}_1, t, \tau = -\frac{\Delta x}{\bar{u}_x}), \quad (10.12.35)$$

where \mathbf{e}_x is the unit vector along the x axis. This expression provides us with a convenient method for obtaining a spatial correlation in terms of a more accessible time-delayed correlation.

The usefulness of second-order correlations lies in their ability to provide us with information on the geometrical structure and dynamics of eddy motion in a turbulent flow. As a point \mathbf{x}_2 tends to another point \mathbf{x}_1 , local fluid motions are coordinated and the correlations are significant. As the points \mathbf{x}_1 and \mathbf{x}_2 move farther apart, the fluid motions become independent or uncorrelated and the correlations decay to zero.

Homogeneous and isotropic turbulence

In the case of homogeneous turbulent flow, the correlations depend on the vectorial distance between the points \mathbf{x}_1 and \mathbf{x}_2 , but not on the absolute position of each point. To signify this dependence, we write

$$\mathcal{R}_{ij}(\mathbf{x}_2 - \mathbf{x}_1, t, \tau). \quad (10.12.36)$$

In the case of isotropic turbulent flow, the correlations depend on the scalar distance between the two points, $|\mathbf{x}_2 - \mathbf{x}_1|$. To signify this dependence, we write

$$R_{ij}(|\mathbf{x}_2 - \mathbf{x}_1|, t, \tau). \quad (10.12.37)$$

Evolution equations

Evolution equations for second-order correlations can be derived from the Navier–Stokes equation. Just as the averaged Navier–Stokes equation (10.12.7) involves the Reynolds stresses, evolution equations for second-order correlations involve third-order correlations defined as time averages of products of three scalar fluctuating components. An important field of study in the general subject of turbulent flow seeks to establish relations between high-order correlations and the structure of the mean flow, thereby achieving closure.

PROBLEMS

10.12.1 Deissler correlation

Deissler replaced Prandtl’s constitutive equation (10.12.24) with a more involved equation inspired by laboratory measurements,

$$\sigma_{xy}^R(y) = n^2 \rho y U(y) \left(\frac{\partial U}{\partial y} \right)_y \left(1 - \exp\left(-\frac{n^2 U y}{\nu}\right) \right), \quad (10.12.38)$$

where $n = 0.124$ is an experimentally determined dimensionless constant. Substitute this relation into (10.12.25), integrate to compute the velocity profile, and then compare the profile with that shown in (10.12.30).

10.12.2 Stratified shear flow

Compute, plot, and discuss the form of the time-delayed correlation of the velocity components and temperature recorded in file *keller.dat* residing in directory *stats* inside directory *13_turbo* of **FDLIB**.

Vortex motion

- 11.1 Vorticity and circulation in two-dimensional flow**
- 11.2 Point vortices**
- 11.3 Two-dimensional flow with distributed vorticity**
- 11.4 Vorticity and circulation in three-dimensional flow**
- 11.5 Axisymmetric flow induced by vorticity**
- 11.6 Three-dimensional vortex motion**

Flows at high Reynolds number typically develop islands of concentrated vorticity, concisely called vortices, embedded in a low-vorticity or virtually irrotational ambient fluid. The velocity field can be resolved into two constituents: an irrotational component prevailing in the absence of the vortices, and a rotational component associated with the localized vorticity distribution. The velocity field of the latter can be expressed conveniently as an integral over the volume of fluid occupied by the vortices. At high Reynolds numbers, viscous forces are insignificant away from flow boundaries, and the vortices evolve according to simple rules dictated by the vorticity transport equation.

In this chapter, we derive an integral representation for the velocity field in terms of the vorticity distribution, discuss simplified laws governing vortex motion in a flow with negligible viscous forces, and develop numerical methods for describing the structure and evolution of a prototypical class of vortex flows with specific vorticity distributions. The study of these flows allow us to develop insights into the dynamics of more general flows at high Reynolds number dominated by vortex interactions.

11.1 Vorticity and circulation in two-dimensional flow

The circulation around a closed loop in a two-dimensional flow is defined as the line integral of the tangential component of the velocity with respect to arc length around the loop, as shown in equation (3.7.12), repeated below for convenience,

$$C \equiv \oint_{\mathcal{L}} u_t \, d\ell = \oint_{\mathcal{L}} \mathbf{u} \cdot \mathbf{t} \, d\ell, \quad (11.1.1)$$

where \mathcal{L} denotes the loop, $d\ell = (dx^2 + dy^2)^{1/2}$ is the differential arc length around the loop, and the unit tangent vector \mathbf{t} points in the counterclockwise direction along \mathcal{L} , as illustrated in [Figure 11.1.1](#).

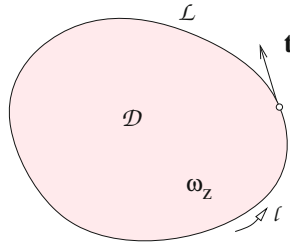


Figure 11.1.1 Illustration of a closed loop in a two-dimensional flow in the xy plane, \mathcal{L} , enclosing an area, \mathcal{D} . The circulation around the loop is equal to the areal integral of the strength of the vorticity, ω_z , over \mathcal{D} . If the flow is irrotational, the circulation is zero.

A loop is reducible if it can be shrunk to a point without crossing flow boundaries or singular points. The Stokes circulation theorem allows us to express the circulation around a reducible loop as the areal integral of the z vorticity component over the area enclosed by the loop, \mathcal{D} , as shown in equation (3.7.13), repeated below for convenience,

$$C = \iint_{\mathcal{D}} \omega_z \, dA, \quad (11.1.2)$$

where dA is a differential area in the xy plane (Problem 11.1.1). With this expression as a point of departure, and using the vorticity transport equation discussed in Section 6.6, we proceed to derive an important theorem that facilitates considerably the study and computation of two-dimensional vortex flow.

Evolution of the circulation in a flow with negligible viscous forces

We begin by considering a reducible *material loop* consisting of a fixed collection of point particles with permanent identity, as illustrated in Figure 11.1.1. In the absence of singularities, the fluid enclosed by the loop also has a permanent identity, that is, it is composed of the same infinite collection of point particles at any time.

The vorticity transport equation for a flow with uniform density and negligible viscous forces requires that point particles maintain their vorticity as they move about the domain of flow, as shown in equation (6.6.13), that is,

$$\frac{D\omega_z}{Dt} = 0, \quad (11.1.3)$$

where D/Dt is the material derivative. Moreover, because the fluid has been assumed incompressible, the area occupied by an infinitesimal material patch of fluid residing inside the loop, dA , remains constant in time, that is,

$$\frac{D(dA)}{Dt} = 0. \quad (11.1.4)$$

Combining these observations, we find that the integral on the right-hand side of (11.1.2) remains constant in time. Formally, we write

$$\frac{dC}{dt} = \frac{d}{dt} \iint_{\mathcal{D}} \omega_z \, dA = \iint_{\mathcal{D}} \frac{D(\omega_z \, dA)}{Dt} = \iint_{\mathcal{D}} \frac{D\omega_z}{Dt} \, dA + \iint_{\mathcal{D}} \omega_z \frac{D(dA)}{Dt} \quad (11.1.5)$$

and then

$$\frac{dC}{dt} = 0. \quad (11.1.6)$$

We have shown that, when viscous forces are negligible, the circulation around any reducible material loop remains constant in time.

In Section 11.4.1, we will see that the circulation around an irreducible loop that encloses a boundary also remains constant in time. These results will reveal that the vorticity of a point particle in a flow with negligible viscous forces is preserved in a two-dimensional flow.

PROBLEM

11.1.1 Stokes circulation theorem

Prove that the circulation around a reducible loop can be expressed in terms of the vorticity, as shown in equation (11.1.2). *Hint:* Apply Gauss's divergence theorem stated in equation (2.6.29) for the vector functions $\mathbf{h} = (u_y, 0)$ and $\mathbf{h} = (0, u_x)$.

11.2 Point vortices

We begin the study of vortex dynamics by considering the motion of point vortices in a flow with negligible viscous forces. Expressions (3.7.1) provide us with the plane polar component of the velocity induced at a point, $\mathbf{x} = (x, y)$, by a point vortex with strength κ located at another point, $\mathbf{x}_0 = (x_0, y_0)$. The Cartesian components of the induced velocity are

$$u_x(x, y) = -\frac{\kappa}{2\pi} \frac{y - y_0}{(x - x_0)^2 + (y - y_0)^2} \quad (11.2.1)$$

and

$$u_y(x, y) = \frac{\kappa}{2\pi} \frac{x - x_0}{(x - x_0)^2 + (y - y_0)^2}. \quad (11.2.2)$$

The denominator of the fractions on the right-hand sides is the square of the distance of the field point, \mathbf{x} , from the location of the point vortex, \mathbf{x}_0 . Since the numerator is proportional to the difference of the x or y coordinates, the velocity due to a point vortex decays as the inverse of the distance from the point vortex, in agreement with (3.7.1).

We may verify readily by straightforward differentiation that the strength of the vorticity,

$$\omega_z \equiv \frac{\partial u_y}{\partial x} - \frac{\partial u_x}{\partial y}, \quad (11.2.3)$$

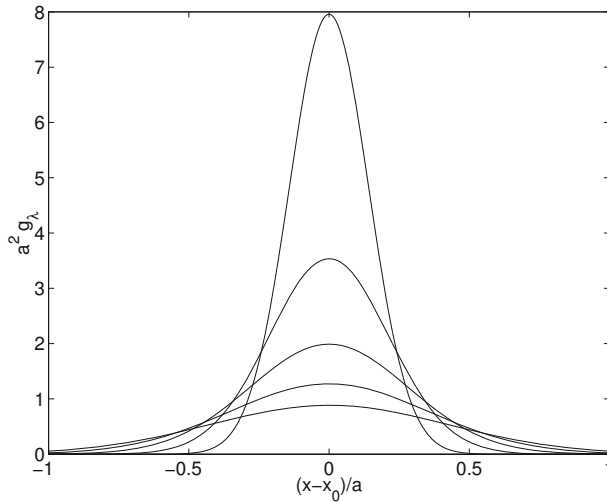


Figure 11.2.1 Horizontal profiles of scaled test functions described by equation (11.2.4) for $y = y_0$ and $\lambda/a = 0.6, 0.5, 0.4, 0.3, 0.2$, and 0.1 (highest peak), where a is a specified length. In the limit as λ/a tends to infinity, we obtain Dirac's delta function in two dimensions.

vanishes everywhere in the flow, except at the location of the point vortex where the right-hand sides of equations (11.2.1) and (11.2.2) and their derivatives are not defined. Dirac's delta function in two dimensions provides us with a convenient mathematical device for expressing this singular vorticity distribution in compact form using the concept of generalized functions.

11.2.1 Dirac's delta function in a plane

To construct the Dirac delta function in the xy plane, we introduce a family of test functions, $g_\lambda(x, y)$, parametrized by an arbitrary length, λ . The test functions are radially symmetric with respect to a specified point, \mathbf{x}_0 , that is, they depend only on the distance of the field point, \mathbf{x} , from the chosen point, \mathbf{x}_0 ; they peak at the point (x_0, y_0) ; they decay to zero rapidly with distance from this point; and their areal integral over the entire xy plane is equal to unity.

One acceptable family of such test functions are described by the Gaussian distribution

$$g_\lambda(r) = \frac{1}{\pi\lambda^2} \exp\left(-\frac{r^2}{\lambda^2}\right), \quad (11.2.4)$$

where

$$r = [(x - x_0)^2 + (y - y_0)^2]^{1/2} \quad (11.2.5)$$

is the distance from the peak. Note that the argument of the exponential function is dimensionless, as required.

We may choose an arbitrary length, a , and restate (11.2.4) as

$$g_\lambda(r) = \frac{1}{\pi a^2} \frac{1}{\widehat{\lambda}^2} \exp\left(-\frac{\widehat{r}^2}{\widehat{\lambda}^2}\right), \quad (11.2.6)$$

where $\widehat{\lambda} \equiv \lambda/a$ is a dimensionless parameter and $\widehat{r} \equiv r/a$ is a dimensionless distance. Graphs of the test functions for several values of $\widehat{\lambda}$ are shown in [Figure 11.2.1](#).

As $\widehat{\lambda}$ tends to infinity, the support of the test function $g_\lambda(r)$ shrinks to zero, yielding Dirac's delta function in the xy plane, denoted by

$$g_{\lambda \rightarrow 0}(r) = \delta_2(x - x_0, y - y_0). \quad (11.2.7)$$

By construction, the Dirac delta function, $\delta_2(x - x_0, y - y_0)$, vanishes everywhere, except at the point $x = x_0$ and $y = y_0$ where it takes an infinite value, subject to the following properties:

1. The areal integral of the delta function over an area \mathcal{D} that contains the point \mathbf{x}_0 is equal to unity,

$$\iint_{\mathcal{D}} \delta_2(x - x_0, y - y_0) \, dA = 1, \quad (11.2.8)$$

where dA is a differential area in the xy plane. This property reveals that the delta function in two dimensions has units of inverse squared length.

2. The areal integral of the product of an arbitrary function, $f(x, y)$, and the delta function over an area \mathcal{D} that contains the point \mathbf{x}_0 is equal to value of the function at the singular point,

$$\iint_{\mathcal{D}} \delta_2(x - x_0, y - y_0) f(x, y) \, dA = f(x_0, y_0). \quad (11.2.9)$$

Note that identity (11.2.8) arises from (11.2.9) by setting $f(x, y) = 1$.

3. The areal integral of the product of an arbitrary function, $f(x, y)$, and the delta function over an area \mathcal{D} that does *not* contain the point \mathbf{x}_0 is zero.

Dirac delta functions in one, three, or higher dimensions are defined in a similar fashion.

Vorticity field associated with a point vortex

The vorticity distribution associated with the velocity field given in (11.2.1) and (11.2.2) can be expressed in terms of the two-dimensional delta function in the compact form

$$\omega_z(x, y) = \kappa \delta_2(x - x_0, y - y_0). \quad (11.2.10)$$

In vector notation,

$$\omega_z(x, y) = \kappa \delta_2(\mathbf{x} - \mathbf{x}_0). \quad (11.2.11)$$

The strength of the point vortex, κ , has units of circulation, which amounts to velocity multiplied by length, VL , while the two-dimensional delta function has units of inverse length squared $1/L^2$. Their product has units of velocity over length, V/L , which is consistent with the definition of the vorticity in terms of selected spatial derivatives of the velocity.

It is instructive to confirm that the circulation around a closed loop that encloses a point vortex is equal to the strength of the point vortex. Substituting (11.2.10) into the integrand on the right-hand side of (11.1.2) and using property (11.2.8), we find that $C = \kappa$.

Idealization by condensation

Reviewing the process by which the delta function arose from a family of smooth functions with increasingly narrow support and high peak, we interpret a point vortex as an idealized vortex structure emerging in the limit as the size of a compact vortex region in the xy plane tends to zero, while the circulation around the vortex is held fixed.

11.2.2 Evolution of the point vortex strength

When viscous forces are negligible, the circulation around any material loop that encloses a point vortex, and therefore the strength of the point vortex, remains constant in time,

$$\frac{d\kappa}{dt} = 0. \quad (11.2.12)$$

Thus, a point vortex retains its strength as it remains stationary or wanders with the fluid velocity in the available domain of a flow.

11.2.3 Velocity of a point vortex

The computation of the fluid velocity at the position of a point vortex is frustrated by the singular nature of the right-hand sides of expressions (11.2.1) and (11.2.2). To circumvent this difficulty, we observe that, although the fluid in the vicinity of a point vortex spins about the point vortex with a velocity that increases as the inverse of the distance from the point vortex, radial symmetry prevents the point vortex from exhibiting a net translational motion.

This observation suggests that the self-induced velocity of a point vortex in an infinite domain is zero, and the point vortex is convected with a velocity other than that associated with its own vorticity distribution. For example, a point vortex embedded in a uniform flow translates with the velocity of the uniform flow.

11.2.4 Motion of a collection of point vortices

A collection of N point vortices move under the influence of their mutually-induced velocities. The rate of change of position of the i th point vortex, $\mathbf{X}_i = (X_i, Y_i)$, is governed by the ordinary differential equations

$$\frac{dX_i}{dt} = - \sum_{j=1}^N \kappa_j \frac{Y_i - Y_j}{(X_i - X_j)^2 + (Y_i - Y_j)^2} \quad (11.2.13)$$

and

$$\frac{dY_i}{dt} = \sum_{j=1, j \neq i}^N \frac{\kappa_j}{2\pi} \frac{X_i - X_j}{(X_i - X_j)^2 + (Y_i - Y_j)^2} \quad (11.2.14)$$

for $i = 1, \dots, N$, where the prime after the sum indicates that the troublesome term $j = i$ is excluded to bypass the singular self-induced contribution. Equation (11.2.12) ensures that the strength of each point vortex remains constant during the motion.

Equations (11.2.13) and (11.2.14) provide us with a system of $2N$ first-order coupled differential equations for the point vortex coordinates, (X_i, Y_i) . Having specified the initial positions, we may compute the subsequent motion using a standard method for solving ordinary equations, such as the modified Euler method or a Runge–Kutta method.

Code *pvm* located in directory *09_vortex* of **FDLIB**, not listed in the text, simulates the motion of a collection of point vortices in an infinite and unbounded domain of flow.

11.2.5 Effect of boundaries

When the domain of flow is bounded by an impermeable surface, a complementary flow must be added to the right-hand sides of equations (11.2.1) and (11.2.2) or equations (11.2.13) and (11.2.14) to ensure the satisfaction of the no-penetration boundary condition. For simple boundary geometries, the complementary flow can be identified with the flow induced by point vortices with appropriate strengths located at image positions.

Directory *pv*, located inside directory *09_vortex* of **FDLIB**, contains functions that return the velocity induced by a point vortex for several boundary geometries. Examples are discussed in this section.

Point vortex near a plane wall

The complementary flow for a point vortex near an infinite plane that is parallel to the x axis at $y = w$ can be generated by reflecting the point vortex with respect to the wall. If a primary point vortex with strength κ is located at a point, (x_0, y_0) , then an image point vortex with strength $-\kappa$ is located at the image point $(x_0, 2w - y_0)$.

The velocity field induced by the primary point vortex and its image is given by

$$u_x(x, y) = -\frac{\kappa}{2\pi} \left(\frac{y - y_0}{(x - x_0)^2 + (y - y_0)^2} - \frac{y - 2w + y_0}{(x - x_0)^2 + (y - 2w + y_0)^2} \right) \quad (11.2.15)$$

and

$$u_y(x, y) = \frac{\kappa}{2\pi} \left(\frac{x - x_0}{(x - x_0)^2 + (y - y_0)^2} - \frac{x - x_0}{(x - x_0)^2 + (y - 2w + y_0)^2} \right). \quad (11.2.16)$$

The streamline pattern induced by the vortex pair for $w = 0$ is illustrated in [Figure 11.2.2\(a\)](#).

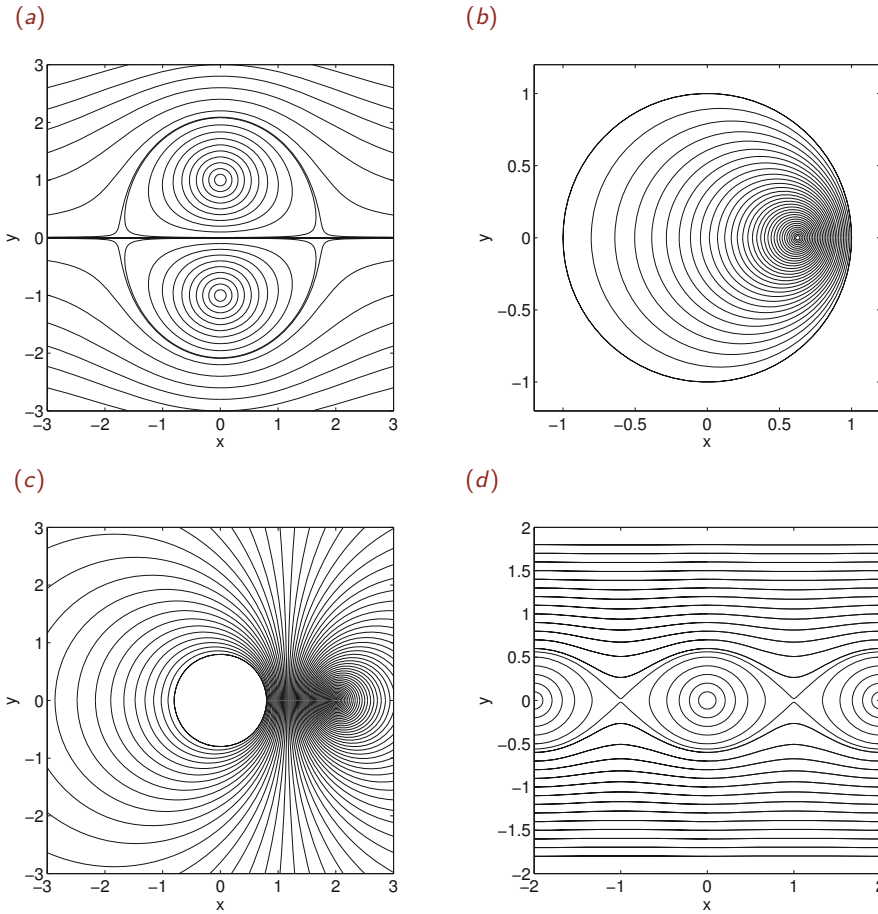


Figure 11.2.2 Streamline pattern of the flow due to (a) a pair of point vortices with opposite strength, (b) a point vortex inside a circular cylinder, (c) a point vortex outside a circular cylinder, and (d) a periodic array of point vortices. These streamline patterns were generated by the program *strml* residing in directory *04_various* of *FDLIB*.

The x velocity component induced by the image vortex at the location of the primary vortex is

$$v_x = \frac{\kappa}{4\pi} \frac{1}{y_0 - w}, \quad (11.2.17)$$

while the y component is zero, $v_y = 0$. Thus, the primary point vortex translates with constant velocity parallel to the wall at a speed that is inversely proportional to the distance from the wall, $y_0 - w$.

Point vortex inside or outside a circular cylinder

The complementary flow of a point vortex located inside or outside a circular cylinder of radius a centered at a point, (x_c, y_c) , is generated by placing an image point vortex with opposite strength at the inverse point of the point vortex with respect to the cylinder.

If a point vortex with strength κ is located at a point, (x_0, y_0) , then an image point vortex with strength $-\kappa$ is located at the point

$$x_0^{\text{image}} = x_c + (x_0 - x_c) \frac{a^2}{|\mathbf{x}_0 - \mathbf{x}_c|^2}, \quad y_0^{\text{image}} = y_c + (y_0 - y_c) \frac{a^2}{|\mathbf{x}_0 - \mathbf{x}_c|^2}, \quad (11.2.18)$$

where

$$|\mathbf{x}_0 - \mathbf{x}_c|^2 = (x_0 - x_c)^2 + (y_0 - y_c)^2 \quad (11.2.19)$$

is the square of the distance of the point vortex from the cylinder center.

The velocity field induced by the primary point vortex and its image is given by

$$u_x(x, y) = -\frac{\kappa}{2\pi} \left(\frac{y - y_0}{(x - x_0)^2 + (y - y_0)^2} - \frac{y - y_0^{\text{image}}}{(x - x_0^{\text{image}})^2 + (y - y_0^{\text{image}})^2} \right) \quad (11.2.20)$$

and

$$u_y(x, y) = \frac{\kappa}{2\pi} \left(\frac{x - x_0}{(x - x_0)^2 + (y - y_0)^2} - \frac{x - x_0^{\text{image}}}{(x - x_0^{\text{image}})^2 + (y - y_0^{\text{image}})^2} \right). \quad (11.2.21)$$

The streamline pattern induced by the vortex pair inside or outside a cylinder is illustrated in [Figure 11.2.2\(b, c\)](#).

Examining the velocity induced by the image vortex at the location of the primary vortex, we find that the primary vortex rotates around the cylinder with polar velocity

$$v_\theta = \frac{\kappa}{2\pi} \frac{d}{a^2 - d^2} \quad (11.2.22)$$

in the direction of the polar angle θ measured in the counterclockwise orientation around the center of the cylinder.

11.2.6 A periodic array of point vortices

Next, we consider a periodic array of point vortices with identical strengths separated by distance a , as illustrated in [Figure 11.2.2\(d\)](#). The m th point vortex is located at the position

$$x_m = x_0 + ma, \quad y_m = y_0, \quad (11.2.23)$$

where (x_0, y_0) is the position of an arbitrary point vortex labeled 0, and m is an integer label. If we attempt to compute the velocity induced by the array simply by summing the

individual contributions from all point vortices, we will encounter unphysically divergent sums.

Renormalization

To overcome this difficulty, we consider the stream function, ψ , corresponding to the velocity field induced by the individual point vortices, defined by the equations $u_x = \partial\psi/\partial y$ and $u_y = -\partial\psi/\partial x$, and express it in the form

$$\psi_0(x, y) = -\frac{\kappa}{2\pi} \ln \frac{r_0}{a}, \quad \psi_m(x, y) = -\frac{\kappa}{2\pi} \ln \frac{r_m}{|m|a} \quad (11.2.24)$$

for $m = \pm 1, \pm 2, \dots$, where

$$r_m \equiv [(x - x_m)^2 + (y - y_m)^2]^{1/2} \quad (11.2.25)$$

is the distance of a field point, $\mathbf{x} = (x, y)$, from the m th point vortex. The denominators of the fractions in the arguments of the logarithms on the right-hand sides of the two equations in (11.2.24) have been chosen judiciously to facilitate forthcoming algebraic manipulations.

It is important to observe that, as m tends to $\pm\infty$, the fraction on the right-hand side of the second equation in (11.2.24) tends to unity, and correspondingly its logarithm tends to vanish, thereby ensuring that remote point vortices make decreasingly small contributions. In contrast, if the denominators were not included, remote point vortices would make contributions that are proportional to the logarithm of the distance of a point vortex from the point (x, y) where the stream function is evaluated.

Next, we express the stream function due to the infinite array as the sum of a constant, expressed by the term after the equal sign in the following equation (11.2.26), and the individual stream functions stated in expressions (11.2.24), obtaining

$$\psi(x, y) = -\frac{\kappa}{2\pi} \ln(\sqrt{2}\pi) + \sum_{m=-\infty}^{\infty} \psi_m(x, y) \quad (11.2.26)$$

or

$$\psi(x, y) = -\frac{\kappa}{2\pi} \ln \frac{\sqrt{2}\pi r_0}{a} - \frac{\kappa}{2\pi} \sum_{m=\pm 1, \pm 2, \dots} \ln \frac{r_m}{|m|a}, \quad (11.2.27)$$

which can be restated as

$$\psi(x, y) = -\frac{\kappa}{2\pi} \ln \left(\frac{\sqrt{2}\pi r_0}{a} \prod_{m=\pm 1, \pm 2, \dots} \frac{r_m}{|m|a} \right), \quad (11.2.28)$$

where Π denotes the product.

An identity allows us to compute the infinite product on the right-hand side of (11.2.28) in closed form, obtaining

$$\prod_{m=\pm 1, \pm 2, \dots} \frac{r_m}{|m|a} = \frac{a}{\sqrt{2}\pi r_0} \left(\cosh[k(y - y_0)] - \cos[k(x - x_0)] \right)^{1/2}, \quad (11.2.29)$$

where $k = 2\pi/a$ is the wave number. Substituting this expression into (11.2.28), we derive the desired stream function associated with an infinite point-vortex array,

$$\psi(x, y) = -\frac{\kappa}{4\pi} \ln \left(\cosh[k(y - y_0)] - \cos[k(x - x_0)] \right). \quad (11.2.30)$$

Note the minus sign on the right-hand side.

Velocity field

Differentiating the stream function with respect to x or y , we obtain the velocity components

$$u_x(x, y) = -\frac{\kappa}{2a} \frac{\sinh[k(y - y_0)]}{\cosh[k(y - y_0)] - \cos[k(x - x_0)]} \quad (11.2.31)$$

and

$$u_y(x, y) = \frac{\kappa}{2a} \frac{\sin[k(x - x_0)]}{\cosh[k(y - y_0)] - \cos[k(x - x_0)]}. \quad (11.2.32)$$

The streamline pattern due to the periodic array is shown in [Figure 11.2.2\(d\)](#) where the x axis has been scaled with a .

Self-induced velocity

Because of symmetry, the velocity at the location of one point vortex induced by all other point vortices is zero; consequently, the infinite array is stationary.

Shear-layer flow

Far above or below the array, the x component of the velocity tends to the value $-\kappa/a$ or κ/a , while the y component decays at an exponential rate with respect to distance from the array. These features render the infinite array a sensible model of the flow generated by the instability of a shear layer separating two streams that merge at different velocities. The Kelvin–Helmholtz instability causes the shear layer to roll up into compact vortices represented by the point vortices of the periodic array.

Motion of a collection of point vortices in a periodic arrangement

The motion of a periodic collection of N point vortices, each repeated in the x direction with period a , is governed by the counterpart of equations (11.2.13) and (11.2.14) for periodic flow. Using the velocity field described in (11.2.31) and (11.2.32), we obtain the evolution equations

$$\frac{dX_i}{dt} = -\sum_{j=1}^N \kappa_j \frac{\sinh[k(Y_i - Y_j)]}{2a \cosh[k(Y_i - Y_j)] - \cos[k(X_i - X_j)]} \quad (11.2.33)$$

and

$$\frac{dY_i}{dt} = \sum_{j=1}^N \kappa_j \frac{\sin[k(X_i - X_j)]}{2a \cosh[k(Y_i - Y_j)] - \cos[k(X_i - X_j)]} \quad (11.2.34)$$

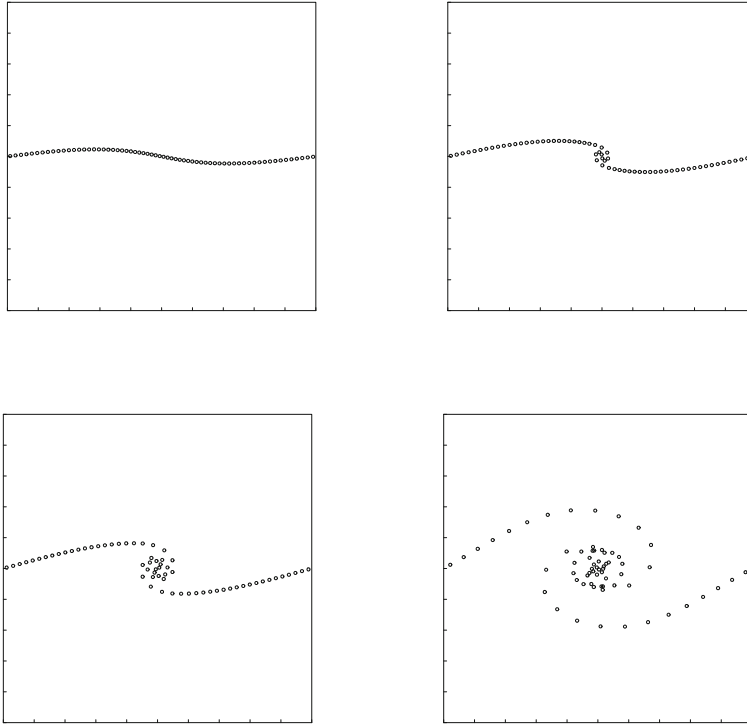


Figure 11.2.3 Stages in the evolution of a perturbed periodic array of point vortices showing periodic roll up and the eventual onset of disorganized motion.

for $i = 1, \dots, N$, where the prime after the sum indicates the exclusion of the term $j = i$, corresponding to the vanishing velocity induced by the host array. The strength of each point vortex remains constant during the motion.

Program *pvm_pr* located inside directory *09_vortex* of **FDLIB**, not listed in the text, simulates the evolution of a periodic row of point vortices that have been perturbed from the planar configuration. The motion is known to suffer from a severe numerical instability that causes the appearance of small-scale irregularities at an early stage of the motion. One way to suppress these irregularities is by smoothing the coordinates of the point vortices, replacing them with weighted averages of their neighbors.

The five-point formula of Longuet–Higgins and Cokelet prescribes replacing the actual positions of the point vortices with smoothed positions according to the formula

$$f_i^{\text{smoothed}} = \frac{1}{16} (-f_{i-2} + 4f_{i-1} + 10f_i + 4f_{i+1} - f_{i+2}), \quad (11.2.35)$$

where f stands for the x or y position or any other smoothed function. Results of a simulation with smoothing applied after each time step are shown in [Figure 11.2.3](#).

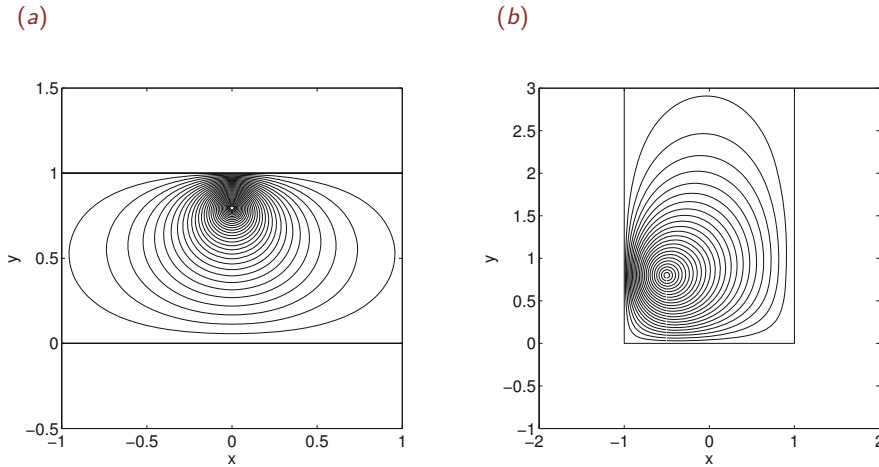


Figure 11.2.4 (a) Streamline pattern of the flow due to a point vortex between two parallel walls. (b) Streamline pattern of the flow due to a point vortex in a semi-infinite rectangular strip. The streamline patterns were generated using the program *strml* residing in directory *04_various* of *FDLIB*.

11.2.7 A point vortex between two parallel walls

Consider a point vortex between two parallel walls along the x , separated by distance h , as shown in [Figure 11.2.4\(a\)](#). The image system associated with the point vortex consists of the two reflections of the point vortex, and the reflections of the reflections of the point vortex with respect to both walls.

The end result is an image system consisting of two infinite periodic arrays of point vortices along the y axis separated by distance $2h$. One array contains the primary point vortex, and the second array contains the reflection of the primary array with respect to the lower or upper wall. The strength of the point vortices in the second array is equal in magnitude and opposite in sign to that of the point vortices in the first array. The stream function and velocity field may be deduced from the expressions given in (11.2.30), (11.2.31), and (11.2.32).

Consideration of the velocity field reveals that the point vortex travels along the x axis, parallel to the walls, with velocity

$$v_x = \frac{\kappa}{h} \frac{1}{4} \frac{\sin(2\pi b/h)}{1 - \cos(2\pi b/h)}, \tag{11.2.36}$$

where b is the distance of the point vortex from the upper or lower wall. As b tends to zero, v_x tends to the limiting value of $\kappa/(4\pi b)$, corresponding to a point vortex above a single plane wall.

11.2.8 A point vortex in a semi-infinite strip

Consider a point vortex between two parallel walls separated by distance h , intersecting at a right angle a third wall to form a semi-infinite rectangular strip, as shown in [Figure 11.2.4\(b\)](#). The image system of the point vortex consists of the image system associated with the two parallel walls, discussed in Section 11.2.7, and the reflection of the image system with respect to the third intersecting wall. The strength of the reflected point vortices is the negative of that of their images. The motion of the point vortex must be computed by numerical methods.

PROBLEMS

11.2.1 Dirac delta function in one dimension

The Dirac delta function in one dimension, denoted by $\delta_1(x - x_0)$, is distinguished by the following properties:

1. $\delta_1(x - x_0)$ vanishes everywhere, except at the point $x = x_0$ where it becomes infinite.
2. The integral of the delta function over an interval, \mathcal{I} , that contains the point x_0 is equal to unity,

$$\int_{\mathcal{I}} \delta_1(x - x_0) dx = 1. \quad (11.2.37)$$

This property reveals that the delta function in one dimension has units of inverse length.

3. The integral of the product of an arbitrary function, $f(x)$, and the delta function over an interval, \mathcal{I} , that contains the point x_0 is equal to value of the function at the singular point,

$$\int_{\mathcal{I}} \delta_1(x - x_0) f(x) dx = f(x_0). \quad (11.2.38)$$

4. The integral of the product of an arbitrary function $f(x)$ and the delta function over an interval \mathcal{I} that does *not* contain the point x_0 is zero.

Note that identity (11.2.37) arises from (11.2.38) by setting $f(x) = 1$.

(a) Show that δ_1 arises from the family of test functions

$$q_\lambda(|x - x_0|) = \frac{1}{\sqrt{\pi\lambda}} \exp\left(-\frac{(x - x_0)^2}{\lambda^2}\right), \quad (11.2.39)$$

in the limit as the length parameter, λ , tends to infinity.

(b) Show that the test functions $g_\lambda(r)$ defined in (11.2.4) derive from the test functions q_λ defined in (11.2.39) as

$$g_\lambda(r) = q_\lambda(|x - x_0|) q_\lambda(|y - y_0|). \quad (11.2.40)$$

Explain why we may write

$$\delta_2(x - x_0, y - y_0) = \delta_1(x - x_0) \delta_1(y - y_0). \quad (11.2.41)$$

(c) Show that the integral of $\delta_1(x - x_0)$ is the *Heaviside function*, which is zero when $x < x_0$ or unity when $x > x_0$. Is there a corresponding Heaviside function in two dimensions?

11.2.2 Dirac delta function in three dimension

State the distinguishing properties of the Dirac delta function in three dimensions. Devise an appropriate family of test functions corresponding to those discussed in the text for the delta function in two dimensions.

11.2.3 A point vortex near a corner

The image flow associated with a point vortex located between two semi-infinite walls intersecting at a right-angle is represented by three point vortices located at the reflections, and the reflection of the reflections of the vortex with respect to the two walls. Introduce plane polar coordinates (r, θ) with origin at the apex and the walls located at $\theta = 0$ and $\pi/2$, and show that the primary point vortex moves along a path described by $r = c/\sin(2\theta)$, where the constant c is determined by the initial position.

11.2.4 Point vortex in a rectangular box

Discuss how the image system for a point vortex located in a semi-infinite rectangular strip discussed in section 11.2.8 can be extended to describe flow inside a rectangular box.

11.2.5 Motion of point vortices

(a) Run program *pvm* to simulate the motion of a collection of N point vortices with identical strengths placed at the vertices of an N -sided regular polygon of radius a . Carry out simulations for $N = 8, 16,$ and 32 , and discuss the nature of the motion at long times.

(b) Modify the program *pvm* to include the presence of a boundary of your choice. Compute the motion of a collection of point vortices of your choice and discuss the nature of the motion.

11.2.6 Motion of a periodic collection of point vortices

Run the program *pv_pr* to compute the motion of a periodic arrangement of point vortices using an initial condition of your choice, with and without smoothing. Discuss the nature of the motion in each case.

11.3 Two-dimensional flow with distributed vorticity

Broadening the scope of our discussion, now we consider the more general case of two-dimensional flow in the xy plane containing regions of concentrated vorticity embedded in an otherwise perfectly or nearly irrotational fluid. To deduce the induced velocity, we subdivide the vortex region into a collection of N parcels with small areas, δA_i for $i = 1, \dots, N$, as illustrated in [Figure 11.3.1](#).

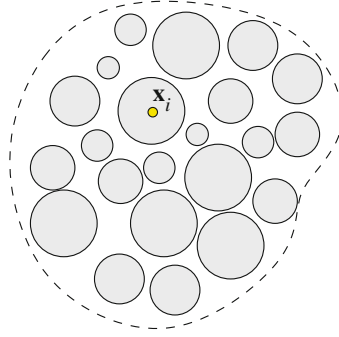


Figure 11.3.1 A vortex region in a two-dimensional flow is discretized into small parcels. Each parcel is then condensed into a point vortex located at a designated parcel center. As the number of parcels tends to infinity, the velocity induced by the point vortices is expressed by the integral representations given in (11.3.4) and (11.3.5).

Let $\omega_i \equiv \omega_z(\mathbf{x}_i)$ be the strength of the vorticity at a designated center of the i th parcel, \mathbf{x}_i . The strength of the parcel is the integrated vorticity over the parcel area,

$$\kappa_i \equiv \omega_i \delta A_i. \quad (11.3.1)$$

For the purpose of evaluating the velocity at a point in the flow, we may replace the parcels with point vortices located at the designated parcel centers. Using expressions (11.2.1) and (11.2.2), we find that the velocity induced by the collection of the point vortices is given by

$$u_x(x, y) = -\frac{1}{2\pi} \sum_{i=1}^N \frac{y - y_i}{(x - x_i)^2 + (y - y_i)^2} \omega_i \delta A_i \quad (11.3.2)$$

and

$$u_y(x, y) = \frac{1}{2\pi} \sum_{i=1}^N \frac{x - x_i}{(x - x_i)^2 + (y - y_i)^2} \omega_i \delta A_i. \quad (11.3.3)$$

As the number of parcels, N , tends to infinity, the sums reduce to areal integrals, yielding an integral representation for the velocity in terms of the vorticity,

$$u_x(x, y) = -\frac{1}{2\pi} \iint_{\text{vortex}} \frac{y - y'}{(x - x')^2 + (y - y')^2} \omega_z(x', y') dx' dy' \quad (11.3.4)$$

and

$$u_y(x, y) = \frac{1}{2\pi} \iint_{\text{vortex}} \frac{x - x'}{(x - x')^2 + (y - y')^2} \omega_z(x', y') dx' dy'. \quad (11.3.5)$$

The stream function is given by the corresponding integral representation

$$\psi(x, y) = -\frac{1}{4\pi} \iint_{\text{vortex}} \ln \left(\frac{(x - x')^2 + (y - y')^2}{\varrho^2} \right) \omega_z(x', y') dx' dy', \quad (11.3.6)$$

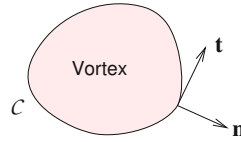


Figure 11.3.2 Illustration of an isolated patch with constant vorticity in a two-dimensional flow in the xy plane.

where ρ is a specified length. The stream function satisfies the Poisson equation,

$$\nabla^2\psi = -\omega_z, \tag{11.3.7}$$

arising from the definitions of the vorticity and the defining relation between the velocity and the stream function.

Expressions (11.3.4) and (11.3.5) allow us to compute the velocity field associated with a specified vorticity distribution in the xy plane.

Recovering point vortices

It is instructive to observe that the velocity field due to a point vortex arises by substituting the singular vorticity distribution (11.2.10) into expressions (11.3.4) and (11.3.5), and then using property (11.2.9) to evaluate the integrals. The delta function simply switches x' to x_0 and y' to y_0 , and thereby generates the flow due to a point vortex expressed by equations (11.2.1) and (11.2.2).

11.3.1 Vortex patches with uniform vorticity

Next, we consider a compact vortex with uniform vorticity, Ω , enclosed by a closed contour, \mathcal{C} , as illustrated in Figure 11.3.2. Extracting the vorticity from the integral on the right-hand side of the integral representation (11.3.6), we obtain the stream function

$$\psi(x, y) = -\frac{\Omega}{4\pi} \iint_{\text{vortex}} \ln \frac{(x - x')^2 + (y - y')^2}{\rho^2} dx' dy'. \tag{11.3.8}$$

The x and y velocity components derive from the stream function as $u_x = \partial\psi/\partial y$ and $u_y = -\partial\psi/\partial x$.

Differentiating (11.3.8) with respect to x or y , transferring the derivatives on the right-hand sides into the integrals, and then writing

$$\frac{\partial}{\partial x} \ln \frac{(x - x')^2 + (y - y')^2}{\rho^2} = -\frac{\partial}{\partial x'} \ln \frac{(x - x')^2 + (y - y')^2}{\rho^2} \tag{11.3.9}$$

and

$$\frac{\partial}{\partial y} \ln \frac{(x - x')^2 + (y - y')^2}{\rho^2} = -\frac{\partial}{\partial y'} \ln \frac{(x - x')^2 + (y - y')^2}{\rho^2}, \tag{11.3.10}$$

we obtain

$$u_x(x, y) = \frac{\Omega}{4\pi} \iint_{\text{vortex}} \frac{\partial}{\partial y'} \ln \frac{(x-x')^2 + (y-y')^2}{\rho^2} dx' dy' \quad (11.3.11)$$

and

$$u_y(x, y) = -\frac{\Omega}{4\pi} \iint_{\text{vortex}} \frac{\partial}{\partial x'} \ln \frac{(x-x')^2 + (y-y')^2}{\rho^2} dx' dy'. \quad (11.3.12)$$

These manipulations were motivated by our ability to convert the areal integral of the x or y derivative of a function over the region occupied by the vortex to a line integral along the vortex contour, \mathcal{C} .

The conversion is done using the Gauss divergence theorem stated in equation (2.6.29) for an arbitrary vector function, $\mathbf{h} = (h_x, h_y)$. Setting

$$h_x = 0, \quad h_y = \ln \frac{(x-x')^2 + (y-y')^2}{\rho^2}, \quad (11.3.13)$$

we find that

$$u_x(x, y) = \frac{\Omega}{4\pi} \oint_{\mathcal{C}} \ln \frac{(x-x')^2 + (y-y')^2}{\rho^2} n_y(x', y') dl(x', y'), \quad (11.3.14)$$

where n_y is the y component of the unit vector normal to the vortex contour, \mathcal{C} , pointing outward from the vortex, and dl is the differential arc length along \mathcal{C} . Working in a similar fashion with the y velocity component, we find that

$$u_y(x, y) = -\frac{\Omega}{4\pi} \oint_{\mathcal{C}} \ln \frac{(x-x')^2 + (y-y')^2}{\rho^2} n_x(x', y') dl(x', y'). \quad (11.3.15)$$

To recast the component equations (11.3.14) and (11.3.15) into a unified vector form, we introduce the unit vector tangent to the vortex contour pointing in the counterclockwise direction, $\mathbf{t} = (t_x, t_y)$, as shown in [Figure 11.3.2](#), and write

$$n_x = t_y, \quad n_y = -t_x. \quad (11.3.16)$$

The velocity induced by the patch may now be expressed in the vector form

$$\mathbf{u}(x, y) = -\frac{\Omega}{4\pi} \oint_{\mathcal{C}} \ln \frac{(x-x')^2 + (y-y')^2}{\rho^2} \mathbf{t}(x', y') dl(x', y'). \quad (11.3.17)$$

The integral is independent of the arbitrary length, ρ .

A collection of patches

If a flow contains a collection of N_p vortex patches with uniform vorticity Ω_m for $m = 1, \dots, N_p$, the velocity field arises by integrating around the contour of each patch and then summing the contributions according to the generalized version of (11.3.17)

$$\mathbf{u}(\mathbf{x}, \mathbf{y}) = -\frac{1}{4\pi} \sum_{m=1}^{N_p} \Omega_m \oint_{\mathcal{C}_m} \ln \frac{(x-x')^2 + (y-y')^2}{\rho^2} \mathbf{t}(x', y') dl(x', y'), \quad (11.3.18)$$

where \mathcal{C}_m is the contour of the l th patch.

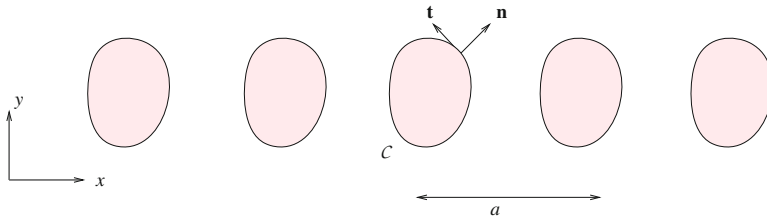


Figure 11.3.3 Illustration of a periodic patch with uniform vorticity in an otherwise irrotational two-dimensional flow.

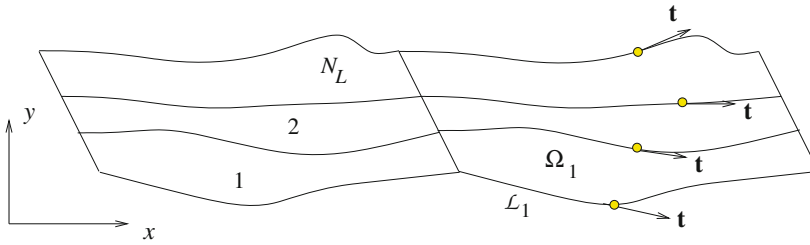


Figure 11.3.4 Illustration of an arrangement of N_L adjacent periodic vortex layers in two-dimensional flow in the xy plane.

Periodic patches

To develop a contour integral representation of the flow induced by a vortex patch that is repeated periodically in the x direction with period a , as illustrated in Figure 11.3.3, we repeat the preceding analysis using the stream function of the flow induced by a periodic array of point vortices given in (11.2.30).

Straightforward generalization provides us with the counterpart of equation (11.3.18) for a flow containing a collection of N_p periodically repeated vortex patches,

$$\mathbf{u}(x, y) = -\frac{1}{4\pi} \sum_{m=1}^{N_p} \Omega_m \oint_{C_m} \ln(\cosh[k(y - y')] - \cos[k(x - x')]) \mathbf{t}(x', y') d\ell(x', y'), \tag{11.3.19}$$

where $k = 2\pi/a$ is the common wave number. For the configuration depicted in Figure 11.3.3 involving one periodic patch, $N_p = 1$.

Periodic layers

A judicious rearrangement of (11.3.19) allows us to derive a contour integral representation of the flow induced by N_L adjacent periodic vortex layers with uniform vorticity, as shown in Figure 11.3.4.

To develop this representation, we identify one period of a vortex layer with a periodic patch, and note that the contour integrals over periodic segments cancel due to the opposite orientation of the unit tangent vector. The result is the integral representation

$$\mathbf{u}(x, y) = -\frac{1}{4\pi} \sum_{m=1}^{N_L+1} (\Omega_m - \Omega_{m-1}) \times \int_{\mathcal{L}_m} \ln(\cosh[k(y-y')] - \cos[k(x-x')]) \mathbf{t}(x', y') d\ell(x', y'), \quad (11.3.20)$$

with the understanding that $\Omega_0 = 0$ and $\Omega_{N_L+1} = 0$, where \mathcal{L}_m is one period of the m th contour, as illustrated in [Figure 11.3.4](#).

An arrangement of adjacent layers with gradually varying vorticity is an acceptable representation of a shear layer with smoothly varying vorticity separating two streams far above or below the arrangement.

11.3.2 Contour dynamics

The vorticity transport equation (6.6.13) ensures that, if viscous forces are insignificant, the vorticity inside a patch with uniform vorticity remains constant in time. To compute the evolution of the flow, it suffices then to follow the motion of the vortex contour.

In numerical practice, this is done by tracing the contour with a collection of point particles, evaluating the velocity at the position of the point particles using the contour integral representation, and then advancing the position of the point particles using a numerical method for integrating ordinary differential equations (ODEs).

Contour discretization

Consider the evolution of a solitary vortex patch immersed in an infinite fluid, as depicted in [Figure 11.3.2](#). The numerical method involves the following steps:

1. Trace the vortex contour with $N + 1$ point particles located at $\mathbf{X}_i = (X_i, Y_i)$ for $i = 1, \dots, N + 1$, where point particles labeled 1 and $N + 1$ coincide.
2. Describe the shape of the contour by interpolation.
3. Compute the velocity of each marker point by evaluating the integral on the right-hand side of (11.3.17) for $x = X_i$ and $y = Y_i$, where $i = 1, \dots, N$.
4. Compute the motion of the point particles by integrating in time the coupled ordinary differential equations

$$\frac{dX_i}{dt} = u_x(X_i, Y_i), \quad \frac{dY_i}{dt} = u_y(X_i, Y_i) \quad (11.3.21)$$

for $i = 1, \dots, N$. Note that the velocity of the i th contour point particle depends on the position of all contour point particles.

Influence coefficients

In the simplest method, the vortex contour is approximated with the polygonal line (polyline) connecting successive marker points. To evaluate the velocity in the third step of the algorithm, we replace the contour integral with the sum of integrals over the individual straight elements connecting adjacent point particles. Observing that the unit tangent vector over the j th element is constant and equal to

$$\mathbf{t}^{(j)} = \frac{1}{\Delta\ell_j}(\mathbf{X}_{j+1} - \mathbf{X}_j), \quad (11.3.22)$$

we write

$$\mathbf{u}(X_i, Y_i) \simeq -\frac{\Omega}{4\pi} \sum_{j=1}^N \mathbf{t}^{(j)} \int_{E_j} \ln \frac{(X_i - x')^2 + (Y_i - y')^2}{\varrho^2} d\ell(x', y'), \quad (11.3.23)$$

where E_j denotes the j th element and $\Delta\ell_j$ is the element length. To facilitate the logistics, we recast equation (11.3.23) into the compact form

$$\mathbf{u}(X_i, Y_i) = -\frac{\Omega}{2\pi} \sum_{j=1}^N A_j(X_i, Y_i) (\mathbf{X}_{j+1} - \mathbf{X}_j), \quad (11.3.24)$$

where

$$A_j(X_i, Y_i) \equiv \frac{1}{\Delta\ell_j} \int_{E_j} \ln \frac{[(X_i - x')^2 + (Y_i - y')^2]^{1/2}}{\varrho} d\ell(x', y') \quad (11.3.25)$$

are dimensionless influence coefficients. If the flow contains a collection of vortex patches, the right-hand side of (11.3.24) is summed over all contours to account for all induced contributions.

Singular elements

As the integration point, (x', y') , approaches the evaluation point, (X_i, Y_i) , the integrand of the contour integral diverges at a logarithmic rate. Consequently, the integrals over the elements numbered $i - 1$ and i are improper and the elements are deemed singular. Fortunately, these improper integrals can be computed analytically, yielding the influence coefficients

$$A_j(X_i, Y_i) = \ln \frac{r_{i,j}}{\varrho} - 1, \quad (11.3.26)$$

for $j = i - 1, i$, where

$$r_{i,j} \equiv [(X_i - X_j)^2 + (Y_i - Y_j)^2]^{1/2} \quad (11.3.27)$$

is the distance between the point particles labeled i and j (Problem 11.3.1).

Regular elements

The rest of the integrals defining the influence coefficients are non-singular and can be computed by standard numerical methods. Choosing the trapezoidal rule, we replace the integrand in (11.3.25) with the average of the values corresponding to the end points of the integration domain, finding

$$A_j(X_i, Y_i) = \frac{1}{2} \left(\ln \frac{r_{i,j}}{\varrho} + \ln \frac{r_{i,j+1}}{\varrho} \right) \quad (11.3.28)$$

for $j = 1, \dots, i-2$ and $j = i+1, \dots, N$. Note that we have skipped the singular elements numbered $i-1$ and i .

Periodic flow

To compute the evolution of a periodic flow with period a , we replace equation (11.3.17) with its counterpart originating from equation (11.3.19). In the case of one vortex patch repeated in the x direction with period a , corresponding to $N_p = 1$, we find that

$$\mathbf{u}(X_i, Y_i) = -\frac{\Omega}{4\pi} \sum_{j=1}^N \mathbf{t}^{(j)} \int_{E_j} \ln \left(\cosh[k(Y_i - y')] - \cos[k(X_i - x')] \right) d\ell(\mathbf{x}), \quad (11.3.29)$$

where $k = 2\pi/a$ is the wave number.

The periodic integrand in (11.3.29) exhibits a logarithmic singularity over the two elements hosting the evaluation point, \mathbf{X}_i . To remove this singularity, we add and subtract the non-periodic kernel corresponding to a solitary point vortex, writing

$$\begin{aligned} & \ln \left(\cosh[k(Y_i - y')] - \cos[k(X_i - x')] \right) \\ &= \ln \frac{\cosh[k(Y_i - y')] - \cos[k(X_i - x')]}{(X_i - x')^2 + (Y_i - y')^2} + \ln[(X_i - x')^2 + (Y_i - y')^2]. \end{aligned} \quad (11.3.30)$$

As x' tends to X_i and y' tends to Y_i , the fraction on the right-hand side of (11.3.30) tends to a finite value. The integral of the corresponding logarithmic term may then be computed using a standard numerical method. The improper integral of the last term on the right-hand side of (11.3.30) can be computed analytically, as discussed previously in this section for non-periodic flow.

11.3.3 Gauss integration quadrature

Various modifications of the basic contour dynamic algorithm outlined in Section 11.3.2 can be made to improve the accuracy of the numerical method.

Consider the evaluation of the influence coefficients A_j defined in equation (11.3.24) over non-singular elements. The trapezoidal rule expressed by (11.3.28) replaces the integral with a weighted average of the values of integrand at the two end points, where both weights are equal to $\frac{1}{2}$. Generalizing this approximation, we evaluate the integral by a quadrature

expressing a weighted average of the integrand at craftily selected quadrature base points, so that

$$\int_{E_j} \ln \frac{(X_i - x')^2 + (Y_i - y')^2}{\varrho^2} d\ell(x', y') \simeq \frac{1}{2} \Delta\ell_j \sum_{k=1}^{N_Q} \ln \frac{(X_i - x_k)^2 + (Y_i - y_k)^2}{\varrho^2} w_k, \tag{11.3.31}$$

where N_Q is a chosen number of quadrature points and w_k are integration weights. The position of the base points (x_k, y_k) on element E_j is given by

$$\begin{aligned} x_k &= \frac{1}{2} (X_{j+1} + X_j) + \frac{1}{2} (X_{j+1} - X_j) \xi_k, \\ y_k &= \frac{1}{2} (Y_{j+1} + Y_j) + \frac{1}{2} (Y_{j+1} - Y_j) \xi_k, \end{aligned} \tag{11.3.32}$$

where the scaled base-point positions, z_k , take values in the interval $[-1, 1]$. The left extreme value, $\xi_1 = -1$, corresponds to $x_1 = X_j$ and $y_k = Y_j$, where the right extreme value, $\xi_{N_Q} = 1$, corresponds to $x_{N_Q} = X_{j+1}$ and $y_k = Y_{j+1}$. The trapezoidal rule expressed by (11.3.28) corresponds to $N_Q = 2$ with $\xi_1 = -1$, $\xi_2 = 1$, and equal weights, $w_1 = w_2 = 1.0$.

Tabulation

Handbooks of mathematical functions provide us with tables of the optimal positions of the base points, z_k , and corresponding weights, w_k , for a specified number of quadrature base points, N_Q , where $k = 1, \dots, N_Q$. The base points are the zeros of a selected class of orthogonal polynomials. The weights arise by integrating Lagrange interpolating polynomials defined in terms of the base points. For smooth integrands that do not exhibit singularities, the tables come under the header of the *Gauss-Legendre* quadrature. For integrands with integrable singularities or integrals over infinite domains, the tables come under different headers.

Directory *07_integration*, located inside directory *01_num_meth* of **FDLIB**, includes functions that return base points and weights. Other programs in the same directory perform numerical integration.

11.3.4 Representation with circular arcs

To account for the curvature of a vortex contour, we may replace the straight segments connecting adjacent marker points with circular arcs, as illustrated in [Figure 11.3.5](#). The backward arc passes through a trio of points numbered $j - 1, j$, and $j + 1$, whereas the forward arc passes through a trio of points numbered $j, j + 1$, and $j + 2$. Each arc is specified by the coordinates of its center and radius, computed by solving a system of three linear equations using interpolation constraints. The blended arc arises by averaging the geometrical properties of the forward and backward arcs on either side of an interpolation interval.

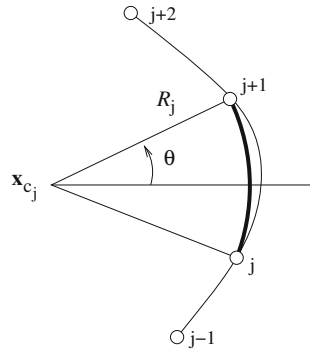


Figure 11.3.5 Local approximation of a vortex contour with a circular arc passing through three points, defined by its center and radius.

The position of a point on the j th arc is described in parametric form by the equations

$$x = x_{c_j} + R_j \cos \theta, \quad y = y_{c_j} + R_j \sin \theta, \quad (11.3.33)$$

where (x_{c_j}, y_{c_j}) are the coordinates of the arc center, R_j is the arc radius, and the polar angle θ varies between two limits corresponding to the arc end-points. The components of the unit tangent vector are given by

$$t_x(\theta) = -\pm \sin \theta, \quad t_y(\theta) = \pm \cos \theta, \quad (11.3.34)$$

and the differential arc length along the arc is given by $d\ell = \pm R_j d\theta$. The plus sign of \pm is chosen when the arc is traced in the counterclockwise direction from point j to point $j + 1$, and the minus sign otherwise.

The x and y components of the integral over the j arc on the right-hand side of (11.3.17) evaluated at the point (X_i, Y_i) are given by

$$(\mathcal{I}_x)_{ij} \equiv -R_j \int_{\theta_j}^{\theta_{j+1}} \ln \frac{(X_i - x_{c_j} - R_j \cos \theta)^2 + (Y_i - y_{c_j} - R_j \sin \theta)^2}{\varrho^2} \sin \theta d\theta \quad (11.3.35)$$

and

$$(\mathcal{I}_y)_{ij} \equiv R_j \int_{\theta_j}^{\theta_{j+1}} \ln \frac{(X_i - x_{c_j} - R_j \cos \theta)^2 + (Y_i - y_{c_j} - R_j \sin \theta)^2}{\varrho^2} \cos \theta d\theta. \quad (11.3.36)$$

The integrals with respect to θ on the right-hand sides can be computed using the Gauss-Legendre quadrature discussed in Section 11.3.3.

Singular arcs

When the evaluation point, (X_i, Y_i) , lies at the j th arc, the integrands in (11.3.36) exhibit a logarithmic singularity. To compute the integrals, we express the coordinates, (X_i, Y_i) , in

local plane polar coordinates, writing

$$X_i = x_{c_j} + R_j \cos \theta_i, \quad Y_i = y_{c_j} + R_j \sin \theta_i. \quad (11.3.37)$$

Substituting these expressions into (11.3.35) and (11.3.36), simplifying and rearranging, we obtain

$$(\mathcal{I}_x)_{ij} \equiv -R_j \int_{\theta_j}^{\theta_{j+1}} \ln \frac{2R_j^2 (1 - \cos(\theta - \theta_i))}{\varrho^2} \sin \theta \, d\theta, \quad (11.3.38)$$

and

$$(\mathcal{I}_y)_{ij} \equiv R_j \int_{\theta_j}^{\theta_{j+1}} \ln \frac{2R_j^2 (1 - \cos(\theta - \theta_i))}{\varrho^2} \cos \theta \, d\theta. \quad (11.3.39)$$

As the integration angle, θ , tends to the evaluation angle, θ_i , the integrands in (11.3.38) and (11.3.39) exhibit a logarithmic singularity. To remove this singularity, we manipulate the x component by writing

$$(\mathcal{I}_x)_{ij} = -R_j \left(\ln \frac{2R_j^2}{\varrho^2} \int_{\theta_j}^{\theta_{j+1}} \sin \theta \, d\theta + \int_{\theta_j}^{\theta_{j+1}} \ln[1 - \cos(\theta - \theta_i)] \sin \theta \, d\theta \right), \quad (11.3.40)$$

and then

$$\begin{aligned} (\mathcal{I}_x)_{ij} = & -R_j \left(-\ln \frac{2R_j^2}{a^2} (\cos \theta_j - \cos \theta_{j+1}) + \int_{\theta_j}^{\theta_{j+1}} \ln \frac{1 - \cos(\theta - \theta_i)}{(\theta - \theta_i)^2} \sin \theta \, d\theta \right. \\ & \left. + \int_{\theta_j}^{\theta_{j+1}} \ln(\theta - \theta_i)^2 (\sin \theta - \sin \theta_i) \, d\theta + \sin \theta_i \int_{\theta_j}^{\theta_{j+1}} \ln(\theta - \theta_i)^2 \, d\theta \right). \end{aligned} \quad (11.3.41)$$

Using the Taylor series expansion of the cosine with respect to θ around θ_i , we find that, as θ tends to θ_i , the fraction in the first integral on the right-hand side of (11.3.41) tends to $\frac{1}{2}$ (Problem 11.3.2). The corresponding integral is nonsingular and can be computed by a standard numerical method. The second integral on the right-hand side is also nonsingular. The singularity has been shifted to the third integral, which can be evaluated by elementary analytical methods. The y component expressed by the second of equations (11.3.39) can be manipulated in a similar fashion.

An alternative method of computing the singular integrals in (11.3.38) and (11.3.39) employs a quadrature that is specifically designed for integrals with a logarithmic singularity, as discussed in texts on numerical methods cited in the bibliography.

FDLIB codes vp_2d

Code *vp_2d*, located in directory *09_vortex* of **FDLIB**, not listed in the text, simulates the evolution of an arbitrary collection of vortex patches. In the numerical method, the contour of each patch is approximated with a collection of blended circular arcs. An essential feature of the numerical procedure is that marker points along the vortex contours are redistributed

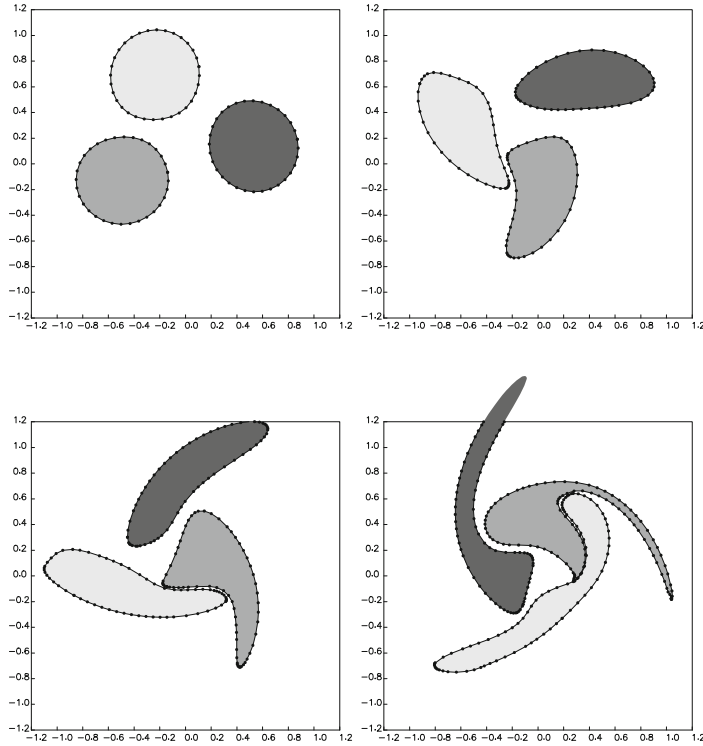


Figure 11.3.6 Evolution of three vortex patches computed by the method of contour dynamics for two-dimensional flow implemented in a code entitled *vp_2d*. In the course of the interaction, the three vortices merge into a larger vortex with spiral filaments.

adaptively during the motion to capture the development of regions of high curvature and prevent point clustering and dilution.

Stages in the evolution of three vortex patches in close proximity are shown in [Figure 11.3.6](#). The dots around the contours mark the adaptively redistributed marker points. Note that an increasing number of marker points are introduced in the course of the simulation. The results reveal the spontaneous vortex merger under the influence of the mutually induced velocity.

FDLIB codes vp_2d_pr

Code *vp_2d_pr*, located inside directory *09_vortex* of *FDLIB*, not listed in the text, computes the evolution of a collection of adjacent vortex layers. The numerical method is similar to that described previously for vortex patches.

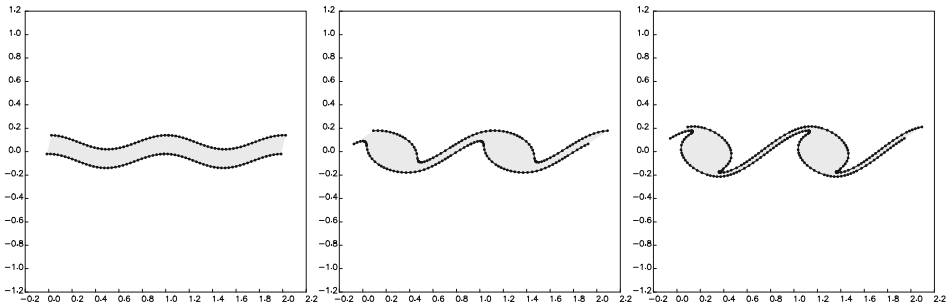


Figure 11.3.7 Kelvin–Helmholtz instability of a uniform vortex layer computed by the method of contour dynamics for periodic flow.

Stages in the Kelvin–Helmholtz instability of a periodic vortex layer separating a uniform stream that moves to the right above the layer from another uniform stream that moves to the left below the layer are shown in [Figure 11.3.7](#). The initially sinusoidal vortex contours roll up into a periodic sequence of compact vortices connected by thinning braids. In the final stages of the motion, the vortex layer transforms into a periodic array of billows sometimes seen in a cloudy sky.

PROBLEMS

11.3.1 Influence coefficient for a singular element

- Derive the influence coefficients for a singular element shown in (11.3.26). *Hint:* Work in local Cartesian coordinates where the x axis is tangential to the singular element.
- Compute in analytical form the last integral on the right-hand side of (11.3.41).
- Derive the counterpart of (11.3.41) for the y component of the induced velocity.

11.3.2 Periodic kernel

Evaluate the limit of the fraction after the logarithm on the right-hand side of (11.3.41) as the integration point tends to the evaluation point.

11.3.3 Motion of vortex patches and vortex layers

- Run the code `vp_2d` to simulate the evolution of a vortex arrangement of your choice. Discuss the nature of the motion.
- Run the code `vp_2d_pr` to simulate the motion of a deformed vortex layer. Discuss the nature of the motion.

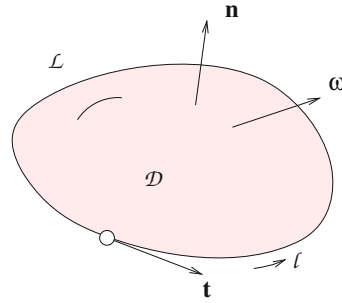


Figure 11.4.1 Illustration of a loop in three-dimensional flow, \mathcal{L} , enclosing a patch, \mathcal{D} . The circulation around the loop is equal to the surface integral of the normal component of the vorticity, $\boldsymbol{\omega} \cdot \mathbf{n}$, over \mathcal{D} .

11.4 Vorticity and circulation in three-dimensional flow

The circulation around a loop in a three-dimensional flow is defined as the line integral of the tangential component of the velocity around the loop, \mathcal{L} ,

$$C \equiv \oint_{\mathcal{L}} u_t \, dl = \oint_{\mathcal{L}} (u_x t_x + u_y t_y + u_z t_z) \, dl = \oint_{\mathcal{L}} \mathbf{u} \cdot \mathbf{t} \, dl, \quad (11.4.1)$$

where $\mathbf{t} = (t_x, t_y, t_z)$ is the unit vector tangent to the loop and

$$dl = (dx^2 + dy^2 + dz^2)^{1/2} \quad (11.4.2)$$

is the differential arc length around the loop measured from an arbitrary point in the direction of \mathbf{t} , as shown in [Figure 11.4.1](#). The definition (11.4.1) generalizes that stated in equation (11.4.1) for two-dimensional flow.

Circulation around a reducible loop

If the loop is reducible, that is, if it can be shrunk to a point without crossing flow boundaries or singular lines, we may use the Stokes circulation theorem to express the circulation around the loop as an integral of the component of the vorticity vector normal to any three-dimensional surface, \mathcal{D} , that is bounded by the loop,

$$C = \iint_{\mathcal{D}} \boldsymbol{\omega} \cdot \mathbf{n} \, dS, \quad (11.4.3)$$

where dS is a differential surface area on \mathcal{D} . The orientation of the unit normal vector, \mathbf{n} , is such that, as we view the surface from the positive direction of the normal vector, the unit tangent vector, \mathbf{t} , points in a direction corresponding to counterclockwise rotation, as depicted in [Figure 11.4.1](#).

In the case of two-dimensional flow in the xy plane, the loop \mathcal{L} and surface \mathcal{D} enclosed by \mathcal{L} can be chosen to lie in the xy plane. The unit normal vector \mathbf{n} is then parallel to the z axis, and expression (11.4.3) reduces to expression (11.1.2), where $\boldsymbol{\omega} = \omega_z \mathbf{n}$.

11.4.1 Preservation of circulation

To compute the rate of change of circulation around a material loop consisting of a fixed collection of point particles with permanent identity, we take the time derivative of the definition (11.4.1) and find that

$$\frac{dC}{dt} = \frac{d}{dt} \oint_{\mathcal{L}} \mathbf{u} \cdot \mathbf{t} \, d\ell = \oint_{\mathcal{L}} \frac{D\mathbf{u}}{Dt} \cdot \mathbf{t} \, d\ell + \oint_{\mathcal{L}} \mathbf{u} \cdot \frac{D(\mathbf{t} \, d\ell)}{Dt}, \quad (11.4.4)$$

where D/Dt is the material derivative.

Focusing on the second integral on the right-hand side of (11.4.4), we express it in the form

$$\oint_{\mathcal{L}} \mathbf{u} \cdot \frac{D(\mathbf{t} \, d\ell)}{Dt} = \oint_{\mathcal{L}} \mathbf{u} \cdot \frac{D \, d\mathbf{X}}{Dt}, \quad (11.4.5)$$

where

$$\mathbf{u} \cdot \frac{D \, d\mathbf{X}}{Dt} = u_x \frac{D \, dX}{Dt} + u_y \frac{D \, dY}{Dt} + u_z \frac{D \, dZ}{Dt}. \quad (11.4.6)$$

The material derivative $D(d\mathbf{X})/Dt$ expresses the rate of change of the components of an infinitesimal material vector that begins at a certain point particle and ends at another point particle. If the two point particles move with the same velocity, the material vector will simply translate; consequently, $D(d\mathbf{X})/Dt = \mathbf{0}$. This observation suggests that the derivative $D(d\mathbf{X})/Dt$ is proportional to the local rate of change of the velocity with respect to arc length along the material vector, ℓ .

Using Taylor series expansions, we find that

$$\begin{aligned} \frac{D \, dX}{Dt} &= dX \frac{\partial u_x}{\partial x} + dY \frac{\partial u_x}{\partial y} + dZ \frac{\partial u_x}{\partial z}, & \frac{D \, dY}{Dt} &= dX \frac{\partial u_y}{\partial x} + dY \frac{\partial u_y}{\partial y} + dZ \frac{\partial u_y}{\partial z}, \\ \frac{D \, dZ}{Dt} &= dX \frac{\partial u_z}{\partial x} + dY \frac{\partial u_z}{\partial y} + dZ \frac{\partial u_z}{\partial z}. \end{aligned} \quad (11.4.7)$$

Now considering the first term on the right-hand side of (11.4.6), we write

$$u_x \frac{D \, dX}{Dt} = dX u_x \frac{\partial u_x}{\partial x} + dY u_x \frac{\partial u_x}{\partial y} + dZ u_x \frac{\partial u_x}{\partial z}, \quad (11.4.8)$$

which can be expressed in the form

$$u_x \frac{D \, dX}{Dt} = dX \frac{1}{2} \frac{\partial u_x^2}{\partial x} + dY \frac{1}{2} \frac{\partial u_x^2}{\partial y} + dZ \frac{1}{2} \frac{\partial u_x^2}{\partial z} \quad (11.4.9)$$

or

$$u_x \frac{D \, dX}{Dt} = \frac{1}{2} \frac{d u_x^2}{d\ell}. \quad (11.4.10)$$

Because the right-hand side of (11.4.10) is an exact differential, its line integral around a closed loop is identically zero.

Working in a similar fashion with the second and third terms on the right-hand side of (11.4.6), we find that the corresponding integrals are also zero, yielding the evolution equation

$$\frac{dC}{dt} = \oint_{\mathcal{L}} \frac{D\mathbf{u}}{Dt} \cdot \mathbf{t} \, d\ell. \quad (11.4.11)$$

We have found that the rate of change of the circulation around a material loop is equal to the instantaneous circulation of the acceleration field, $D\mathbf{u}/Dt$, around the loop.

Kelvin's circulation theorem

If viscous forces are negligible, we may use Euler's equation (6.4.3) to recast the integral on the right-hand side of (11.4.11) into the form

$$\oint_{\mathcal{L}} \frac{D\mathbf{u}}{Dt} \cdot \mathbf{t} \, d\ell = \oint_{\mathcal{L}} \left(-\frac{1}{\rho} \nabla p + \mathbf{g} \right) \cdot \mathbf{t} \, d\ell. \quad (11.4.12)$$

The unit tangent vector is given by

$$\mathbf{t} = \frac{1}{d\ell} d\mathbf{X}, \quad (11.4.13)$$

where \mathbf{X} is the position of a point particle around the loop. Using this expression and assuming that the fluid density is uniform throughout the domain of flow, we find that

$$\oint_{\mathcal{L}} \frac{D\mathbf{u}}{Dt} \cdot \mathbf{t} \, d\ell = -\frac{1}{\rho} \oint_{\mathcal{L}} d\mathbf{X} \cdot \nabla p + \mathbf{g} \cdot \oint_{\mathcal{L}} d\mathbf{X} \quad (11.4.14)$$

and then

$$\oint_{\mathcal{L}} \frac{D\mathbf{u}}{Dt} \cdot \mathbf{t} \, d\ell = -\frac{1}{\rho} \oint_{\mathcal{L}} dp + \mathbf{g} \cdot \oint_{\mathcal{L}} d\mathbf{X}. \quad (11.4.15)$$

Because the loop is closed, the domain of integration with respect to \mathbf{X} is periodic. Since the two integrands on the right-hand side of (11.4.15) are exact differentials, their integrals are identically zero, yielding Kelvin's circulation theorem expressed by the conservation law

$$\frac{dC}{dt} = 0 \quad (11.4.16)$$

for any reducible or irreducible loop.

We have found that, when viscous forces are negligible, the circulation around any closed material loop remains constant in time.

11.4.2 Flow induced by vorticity

Given the velocity field, we may compute the associated vorticity distribution using the definition of the vorticity by analytical or numerical differentiation,

$$\boldsymbol{\omega} \equiv \nabla \times \mathbf{u}. \quad (11.4.17)$$

Is there a way of performing the inverse, that is, express the velocity in terms of the vorticity field?

Biot–Savart integral

In the case of two-dimensional flow, the velocity field associated with a specified vorticity distribution in the xy plane arises from the integral representations described in (11.3.4) and (11.3.5). The corresponding formula for three-dimensional flow is expressed by the Biot–Savart integral

$$\mathbf{u}(x, y, z) = -\frac{1}{4\pi} \iiint \frac{(\mathbf{x} - \mathbf{x}') \times \boldsymbol{\omega}(\mathbf{x}')}{r^3} dV(\mathbf{x}'), \quad (11.4.18)$$

where

$$r = [(x - x')^2 + (y - y')^2 + (z - z')^2]^{1/2} \quad (11.4.19)$$

is the scalar distance of the evaluation point, $\mathbf{x} = (x, y, z)$, from the integration point, $\mathbf{x}' = (x', y', z')$, and the integration is performed over the entire domain of flow. In index notation, the i th component of the velocity is given by

$$u_i(x, y, z) = -\frac{1}{4\pi} \iiint \frac{\epsilon_{ijk} (x_j - x'_j) \omega_k(\mathbf{x}')}{r^3} dV(\mathbf{x}') \quad (11.4.20)$$

where summation is implied over the repeated indices, j and k .

The numerator of the integrand in (11.4.18) is the cross product of (a) the vectorial distance of the evaluation point, $\mathbf{x} = (x, y, z)$, from the integration point, $\mathbf{x}' = (x', y', z')$, and (b) the vorticity at the integration point. The denominator is the cubic power of the scalar distance between the evaluation point and the integration point, $|\mathbf{x} - \mathbf{x}'|^3$. Thus, far from the integration point, \mathbf{x}' , the integrand decays like $1/r^2$.

The physical interpretation of (11.4.18) becomes evident by replacing the integral with a sum of integrals over the volumes of elementary fluid parcels. The velocity induced by each individual parcel due to its rotation is illustrated in [Figure 11.4.2](#). A direct analogy with the magnetic field induced by an electrical current explains why the integral on the right-hand side of (11.4.18) is known as the Biot–Savart integral of vortex dynamics.

Effect of boundaries

The integral representation (11.4.18) is applicable only for unbounded flow extending to infinity in all directions and decaying at infinity. In the presence of boundaries, an additional

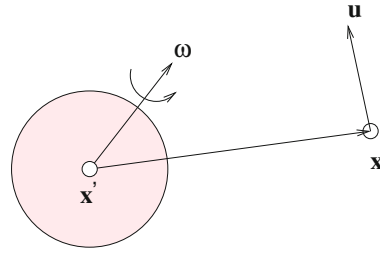


Figure 11.4.2 The velocity field induced by the rotation of a small fluid parcel centered at a point, \mathbf{x}' , is expressed by the Biot–Savart integral shown in (11.4.20).

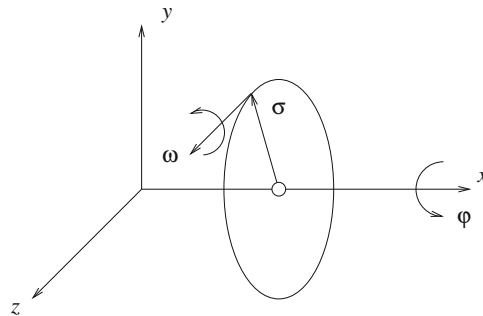


Figure 11.5.1 Illustration of an axisymmetric flow without swirling motion. The vorticity vector points in the direction of the azimuthal angle, φ , at any point.

complementary flow must be included to ensure the solenoidality of the velocity field, $\nabla \cdot \mathbf{u} = 0$, and the satisfaction of the no-penetration and no-slip boundary conditions.

PROBLEM

11.4.1 Rate of change of circulation

Assume that the viscous force in a fluid is given by $\mu \nabla^2 \mathbf{u} = -\kappa \mathbf{u}$, where κ is a resistance coefficient. What are the dimensions of κ ? Derive an equation for the rate of change of circulation around a material loop.

11.5 Axisymmetric flow induced by vorticity

The vorticity of an axisymmetric vortex flow without swirling motion is oriented in the direction of the azimuthal angle, φ , at any point, as illustrated in [Figure 11.5.1](#). The known orientation of the vorticity field and accompanying axial symmetry of the velocity field allow us to simplify the volume integral on the right-hand side of (11.4.18), and thereby derive integral representations that are amenable to analytical and numerical computation.

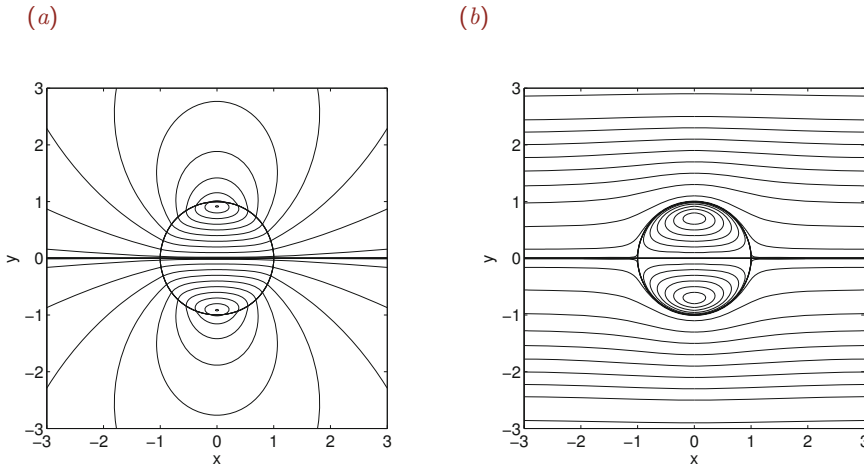


Figure 11.5.2 Streamline pattern associated with Hill's spherical vortex (a) in a stationary frame of reference and (b) in a frame of reference translating with the vortex.

In the cylindrical polar coordinates depicted in Figure 11.5.1, the vorticity vector takes the form

$$\boldsymbol{\omega} = \omega_\varphi(x, \sigma) \mathbf{e}_\varphi, \tag{11.5.1}$$

where ω_φ is the azimuthal vorticity component and \mathbf{e}_φ is the unit vector in the direction of the azimuthal angle, φ . The Cartesian components of the vorticity are given by

$$\omega_x = 0, \quad \omega_y = -\omega_\varphi \sin \varphi, \quad \omega_z = \omega_\varphi \cos \varphi. \tag{11.5.2}$$

Hill's spherical vortex

Hill's spherical vortex provides us with an important example of an axisymmetric vortex with distributed vorticity. The strength of the vorticity inside Hill's vortex is proportional to the distance from the x axis,

$$\omega_\varphi = \Omega \sigma, \tag{11.5.3}$$

where Ω is a constant with units of inverse length multiplied by time. Outside Hill's vortex, the flow is irrotational flow due to the motion of a sphere. The streamline patterns in a stationary frame of reference and in a frame of reference translating with the vortex are shown in Figure 11.5.2.

In the moving frame of reference, corresponding to Figure 11.5.2(b), the axisymmetric stream function of the flow inside Hill's vortex is given by

$$\psi^{\text{interior}} = \frac{1}{10} \Omega \sigma^2 (a^2 - x^2 - \sigma^2). \tag{11.5.4}$$

Outside the vortex, the stream function is given by

$$\psi^{\text{exterior}} = -\frac{1}{15} \Omega a^2 \sigma^2 \left(1 - \frac{a^3}{(x^2 + \sigma^2)^{3/2}} \right). \quad (11.5.5)$$

Observed in a stationary frame of reference, corresponding to [Figure 11.5.2\(a\)](#), Hill's vortex translates along the x axis with velocity

$$V = \frac{2}{15} \Omega a^2. \quad (11.5.6)$$

Recall that the constant Ω has units of velocity divided by length squared.

Vortex rings

Hill's vortex is an extreme member of a family of vortex rings, arising in the limit as the core of the rings spreads out and the ring contour in an azimuthal plane touches and then extends over the x axis. The opposite extreme member of this family is a line vortex ring with circular core of infinitesimal radius, as discussed in Section 11.5.2.

11.5.1 Biot–Savart integral for axisymmetric flow

Referring to the integral representation (11.4.18), we express the y and z coordinates of the evaluation point, \mathbf{x} , and integration point, \mathbf{x}' , in cylindrical polar coordinates, as

$$y = \sigma \cos \varphi, \quad z = \sigma \sin \varphi, \quad y' = \sigma' \cos \varphi', \quad z' = \sigma' \sin \varphi'. \quad (11.5.7)$$

The square of the distance between these two points is

$$\begin{aligned} r^2 &\equiv (x - x')^2 + (y - y')^2 + (z - z')^2 \\ &= (x - x')^2 + (\sigma \cos \varphi - \sigma' \cos \varphi')^2 + (\sigma \sin \varphi - \sigma' \sin \varphi')^2. \end{aligned} \quad (11.5.8)$$

Expanding the squares and using standard trigonometric identities, we find that

$$r^2 = \hat{x}^2 + (\sigma + \sigma')^2 - 2\sigma\sigma' [1 + \cos(\varphi - \varphi')] \quad (11.5.9)$$

and then

$$r^2 = \hat{x}^2 + (\sigma + \sigma')^2 - 4\sigma\sigma' \cos^2\left(\frac{1}{2}\hat{\varphi}\right), \quad (11.5.10)$$

where

$$\hat{x} = x - x', \quad \hat{\varphi} \equiv \varphi - \varphi'. \quad (11.5.11)$$

Next, we consider the x component of the integral representation (11.4.20) and express the differential volume in cylindrical polar coordinates,

$$dV(\mathbf{x}') = dx' d\sigma' \sigma' d\varphi', \quad (11.5.12)$$

to obtain

$$u_x(x, \sigma) = -\frac{1}{4\pi} \iint \left(\int_0^{2\pi} \frac{1}{r^3} [\hat{y}\omega_z(x', y', z') - \hat{z}\omega_y(x', y', z')] \sigma' d\varphi' \right) dx' d\sigma', \quad (11.5.13)$$

where $\hat{y} = y - y'$ and $\hat{z} = z - z'$. Substituting relations (11.5.2) and (11.5.7), into the numerator of the integrand, simplifying by the use of trigonometric identities, and rearranging, we find that

$$u_x(x, \sigma) = \frac{1}{4\pi} \iint \left(\int_0^{2\pi} \frac{-\sigma \cos \hat{\varphi} + \sigma'}{r^3} d\hat{\varphi} \right) \omega_\varphi(x', \sigma') \sigma' dx' d\sigma'. \quad (11.5.14)$$

To compute the σ component of the velocity, we work in a similar fashion departing from the equation

$$u_\sigma = u_y \cos \varphi + u_z \sin \varphi. \quad (11.5.15)$$

The final result is

$$u_\sigma(x, \sigma) = \frac{1}{4\pi} \iint \left(\int_0^{2\pi} \frac{\hat{x} \cos \hat{\varphi}}{r^3} d\hat{\varphi} \right) \omega_\varphi(x', \sigma') \sigma' dx' d\sigma'. \quad (11.5.16)$$

To simplify the notation, we recast equations (11.5.14) and (11.5.16) into the forms

$$u_x(x, \sigma) = \frac{1}{4\pi} \iint \left[-\sigma I_{31}(\hat{x}, \sigma, \sigma') + \sigma' I_{30}(\hat{x}, \sigma, \sigma') \right] \omega_\varphi(x', \sigma') \sigma' dx' d\sigma' \quad (11.5.17)$$

and

$$u_\sigma(x, \sigma) = \frac{1}{4\pi} \iint \hat{x} I_{31}(\hat{x}, \sigma, \sigma') \omega_\varphi(x', \sigma') \sigma' dx' d\sigma'. \quad (11.5.18)$$

We have introduced the integrals

$$I_{30}(\hat{x}, \sigma, \sigma') \equiv \int_0^{2\pi} \frac{d\hat{\varphi}}{r^3} = \int_0^{2\pi} \frac{d\hat{\varphi}}{[\hat{x}^2 + (\sigma + \sigma')^2 - 4\sigma\sigma' \cos^2(\frac{1}{2}\hat{\varphi})]^{3/2}} \quad (11.5.19)$$

and

$$I_{31}(\hat{x}, \sigma, \sigma') \equiv \int_0^{2\pi} \frac{\cos \hat{\varphi}}{r^3} d\hat{\varphi} = \int_0^{2\pi} \frac{\cos \hat{\varphi}}{[\hat{x}^2 + (\sigma + \sigma')^2 - 4\sigma\sigma' \cos^2(\frac{1}{2}\hat{\varphi})]^{3/2}} d\hat{\varphi}. \quad (11.5.20)$$

We find that

$$I_{30}(\hat{x}, \sigma, \sigma') = \frac{4}{[\hat{x}^2 + (\sigma + \sigma')^2]^{3/2}} \int_0^{\pi/2} \frac{d\eta}{(1 - k^2 \cos^2 \eta)^{3/2}} \quad (11.5.21)$$

and

$$I_{31}(\hat{x}, \sigma, \sigma') = \frac{4}{[(x - x')^2 + (\sigma + \sigma')^2]^{3/2}} \int_0^{\pi/2} \frac{\cos(2\eta)}{(1 - k^2 \cos^2 \eta)^{3/2}} d\eta, \quad (11.5.22)$$

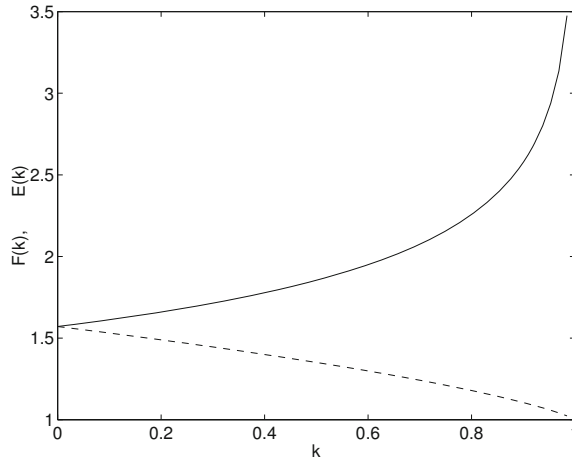


Figure 11.5.3 Graphs of the complete elliptic integral of the first kind, $F(k)$ (solid line), and second kind, $E(k)$ (dashed line).

where $\eta \equiv \frac{1}{2}\widehat{\varphi}$ and

$$k^2 \equiv \frac{4\sigma\sigma'}{\widehat{x}^2 + (\sigma + \sigma')^2} \tag{11.5.23}$$

is a dimensionless group.

Complete elliptic integrals

The integrals on the right-hand sides of (11.5.21) and (11.5.22) can be expressed in terms of complete elliptic integrals of the first and second kind, F and E , defined as

$$F(k) \equiv \int_0^{\pi/2} \frac{d\eta}{\sqrt{1 - k^2 \sin^2 \eta}}, \quad E(k) \equiv \int_0^{\pi/2} \sqrt{1 - k^2 \sin^2 \eta} d\eta, \tag{11.5.24}$$

for $0 \leq k \leq 1$. Graphs of the complete elliptic integrals in their domain of definition are shown in [Figure 11.5.3](#). Note that, as k tends to unity, $E(k)$ remains finite but $F(k)$ diverges to infinity.

The complete elliptic integrals can be computed efficiently by numerical approximation or iteration. An efficient method is based on the following expressions involving rapidly converging infinite products:

$$F(k) = \frac{\pi}{2}(1 + K_1)(1 + K_2) \cdots, \quad E(k) = F(k) \left(1 - \frac{1}{2} k^2 P\right), \tag{11.5.25}$$

where

$$P = 1 + \frac{1}{2} K_1 \left[1 + \frac{1}{2} K_2 \left(1 + \frac{1}{2} K_3 \dots\right)\right]. \tag{11.5.26}$$

The sequence K_p is computed using the recursive formula

$$K_p = \frac{1 - (1 - K_{p-1}^2)^{1/2}}{1 + (1 - K_{p-1}^2)^{1/2}}, \tag{11.5.27}$$

starting with $K_0 = k$. MATLAB computes the complete elliptic integrals using the internal function *ellipke*.

Now referring to standard tables of integrals, we find that

$$\int_0^{\pi/2} \frac{d\eta}{(1 - k^2 \cos^2 \eta)^{3/2}} = \frac{E(k)}{1 - k^2} \tag{11.5.28}$$

and

$$\int_0^{\pi/2} \frac{\cos(2\eta)}{(1 - k^2 \cos^2 \eta)^{3/2}} d\eta = -\frac{2}{k^2} F(k) + \frac{2 - k^2}{k^2(1 - k^2)} E(k). \tag{11.5.29}$$

The derivation of these expressions concludes the analytical part of our work.

11.5.2 Line vortex ring

Now we are in a position to evaluate the velocity field associated with a specified axisymmetric vorticity distribution based on the integral representation (11.5.18). The simplest vorticity distribution is associated with a line vortex ring, which is the axisymmetric counterpart of the point vortex in two-dimensional flow. The strength of the ring is equal to the circulation around any loop that encloses once the trace of the ring in an azimuthal plane corresponding to a specified azimuthal angle, φ . More broadly, the strength of the ring is equal to the circulation around any loop that chain-links the vortex ring.

The strength of the vorticity in an azimuthal plane is expressed by the generalized distribution

$$\omega_\varphi(x, \sigma) = \kappa \delta_2(x - x_r, \sigma - \sigma_r), \tag{11.5.30}$$

where δ_2 is the two-dimensional delta function, κ is the strength of the vortex ring, σ_r is the ring radius, and x_r is the axial position of the ring.

Substituting (11.5.30) into expressions (11.5.18), and using the distinctive properties of the delta function discussed in Section 11.2 to evaluate the integrals, we obtain the axial velocity

$$u_x(x, \sigma) = \frac{\kappa}{4\pi} \sigma_r \left(-\sigma I_{31}(x - x_r, \sigma, \sigma_r) + \sigma_r I_{30}(x - x_r, \sigma, \sigma_r) \right) \tag{11.5.31}$$

and the radial velocity

$$u_\sigma(x, \sigma) = \frac{\kappa}{4\pi} \sigma_r (x - x_r) I_{31}(x - x_r, \sigma, \sigma_r). \tag{11.5.32}$$

The streamline pattern of the flow induced by the ring is shown in [Figure 11.5.4\(a\)](#).

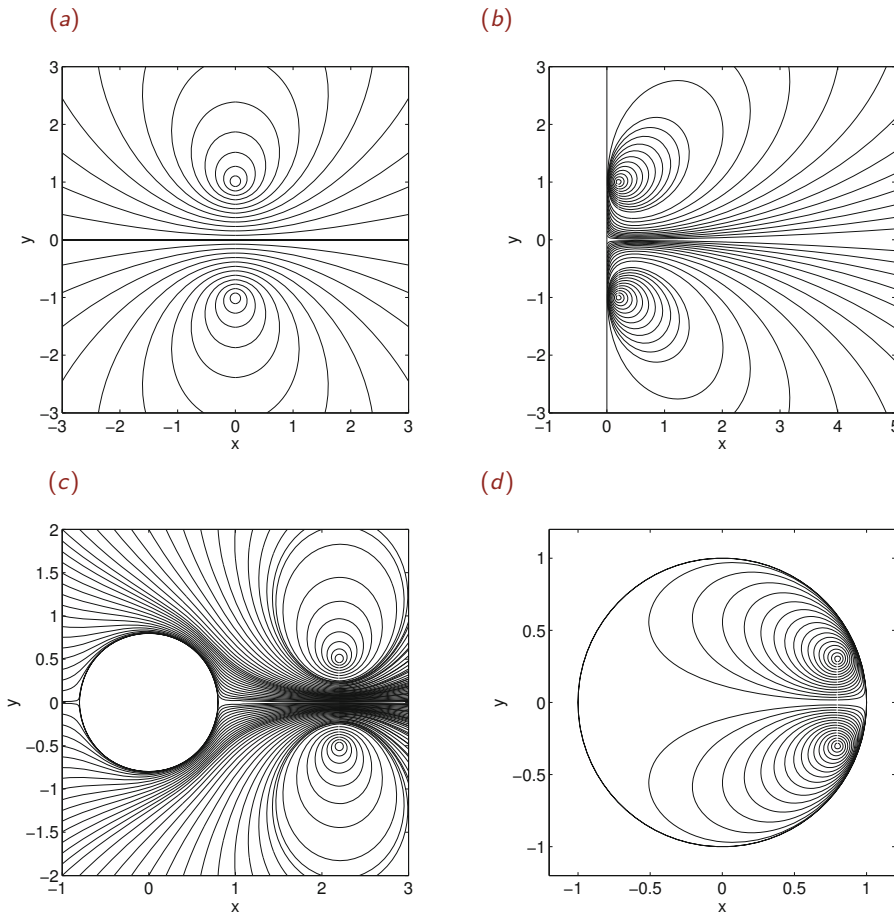


Figure 11.5.4 Streamline pattern of the flow induced by a line vortex ring in an azimuthal plane in (a) an unbounded domain of flow, (b) a semi-infinite domain of flow bounded by an infinite plane wall, (c) outside a sphere, and (d) inside a sphere. These streamline patterns were generated using program *strml* residing in directory *04_various* of **FDLIB**.

Presence of boundaries

Consider a flow in the presence of an axisymmetric boundary whose axis of revolution coincides with the axis of a vortex ring. The velocity field induced by a vortex ring expressed by (11.5.32) is accompanied by a complementary velocity field that ensures the satisfaction of the no-penetration boundary condition. For simple boundary geometries involving one or two parallel walls, the complementary flow can be expressed in terms of image vortex rings.

Computer functions that evaluate the velocity field can be found in directory *lvr*, inside directory *09_vortex* of **FDLIB**. The streamline pattern of the axisymmetric flow induced by

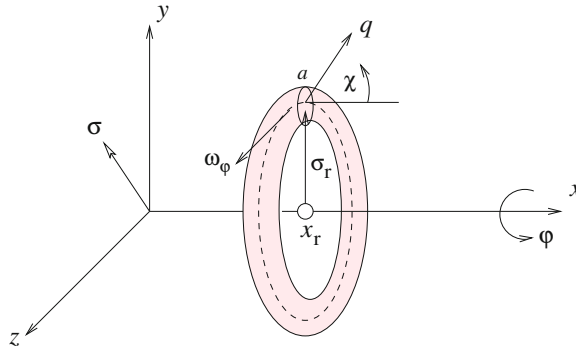


Figure 11.5.5 Illustration of a vortex ring with radius σ_r and a circular core of radius a .

a vortex ring in an azimuthal plane in front of a plane wall and in the exterior or interior of a sphere are shown in Figure 11.5.4(b-d).

11.5.3 Vortex ring with finite core

Next, we consider the flow induced by a compact vortex ring with centerline radius σ_r located at the axial position x_r . It is helpful to introduce plane polar coordinates, (q, χ) , defined in a plane of constant azimuthal angle, φ , with origin at the center of the ring core, as illustrated in Figure 11.5.5. We will assume that the ring has a circular core of radius a , where $a \ll \sigma_r$. The vorticity vanishes outside the core, $\omega_\varphi = 0$ for $q > a$.

Using expression (11.4.3), we find that the circulation around a loop that encloses the core once is given by an integral over the core cross-section,

$$C = \iint_{\text{core}} \omega_\varphi(x, \sigma) dx d\sigma = \int_0^{2\pi} \int_0^a \omega_\varphi(q, \chi) q dq d\chi. \tag{11.5.33}$$

Our earlier discussion allows us to identify the circulation with the strength of the vortex ring, κ .

Referring to the integral representation for the velocity given in (11.5.18), we perform the integration in plane polar coordinates, (q, χ) , and find that

$$u_x(x, \sigma) = \frac{1}{4\pi} \int_0^{2\pi} \int_0^a (-\sigma I_{31} + \sigma' I_{30}) \omega_\varphi(x', \sigma') \sigma' q dq d\chi \tag{11.5.34}$$

and

$$u_\sigma(x, \sigma) = \frac{1}{4\pi} \int_0^{2\pi} \int_0^a (x - x') I_{31} \omega_\varphi(x', \sigma') \sigma' q dq d\chi. \tag{11.5.35}$$

Because of the singular behavior of the complete elliptic integral of the first kind, $F(k)$, as shown in Figure 11.5.3, the integrands exhibit a benign logarithmic singularity as the evaluation point, (x, σ) , lies inside the core.

The simplest method of evaluating the double integrals in (11.5.34) and (11.5.35) is by the double mid-point rule. The numerical method involves dividing the integration domain with respect to q and χ into evenly spaced intervals defining circular sectors, approximating the integrand over each sector with the value at the center-point, and adding all contributions.

Self-induced velocity

The self-induced velocity of a vortex ring propagating along the x axis with velocity U_x can be identified with the x component of the fluid velocity at the center of the vortex core, which can be computed by evaluating the integral in (11.5.34) for $x = x_r$ and $\sigma = \sigma_r$.

A graph of the dimensionless scaled self-induced velocity, $U_x \sigma_r / \kappa$, against the dimensionless scaled core radius, a / σ_r , evaluated using the double mid-point rule is shown in Figure 11.5.6. The solid line corresponds to a core with uniform vorticity,

$$\omega_\varphi = \frac{\kappa}{\pi a^2}. \quad (11.5.36)$$

The dashed line corresponds to a core with distributed vorticity described by

$$\omega_\varphi = \frac{\kappa}{a^2} \frac{\pi}{(\pi^2 - 4)} \left(1 + \cos \frac{\pi q}{a}\right) \quad (11.5.37)$$

for $0 < q < a$ or $\omega_\varphi = 0$ for $q > a$. The computation of the integral neglects the weak logarithmic singularity of the integrand.

The numerical method is implemented in the following MATLAB program entitled *ring*, residing inside directory *09_vortex* of **FDLIB**:

```

rr = 1.0;   % ring radius
circ = 1.0; % circulation
nrad = 64; % radial divisions
nchi = 64; % azimuthal divisions
nrepeat = 32; % scanning the core radius

%---
% prepare
%---

dchi = 2*pi/nchi; % angular divisions

%=====
for repeat=1:nrepeat % run over the core radius
%=====

cr = 0.01+(repeat-1.0)/nrepeat; % core radius

dcr = cr/nrad; % radial divisions

```



```

%-----
% discretize the vortex core into elements
% and compute the area of each element "ar"
%-----

for i=1:nrad
    for j=1:nchi
        ar(i,j) = 0.5*dchi*dcr*dcr*(2.0*i-1);
    end
end

%-----
% initialize
%-----

arintv1 = 0.0; % areal integral of the vorticity
arintv2 = 0.0;

u1 = 0.0; v1 = 0.0;
u2 = 0.0; v2 = 0.0;

%-----
% compute the self-induced velocity
% integrate by the trapezoidal rule
%-----

for i=1:nrad % loop over radial divisions

    rad = (i-0.5)*dcr; % center of the ring elements
    % uniform core:
    w1 = circ/(pi*cr*cr);
    % normalized bell shape:
    w2 = circ*pi/(cr*cr)/(pi*pi-4.0)*(1.0+cos(pi*rad/cr));

    for j=1:nchi % loop over azimuthal elements
        chi = (j-0.5)*dchi;
        sig = rr+rad*sin(chi);
        Dx = rad*cos(chi);
        Dxs = Dx*Dx;
        ks = 4.0*rr*sig/(Dxs+(rr+sig)^2);
        [F, E]= ellipke(ks);
        RJ30 = E/(1.0-ks);
        RJ31 = (-2.0*F + E*(2.0-ks)/(1.0-ks))/ks;
        cf = 4.0/sqrt((Dxs+(rr+sig)^2)^3);
        RI30 = cf*RJ30;
        RI31 = cf*RJ31;
        cf1 = ar(i,j)*sig*w1/(4*pi);
        u1 = u1 + cf1*(-rr*RI31+sig*RI30);
        v1 = v1 + cf1* Dx*RI31;
    end
end

```

```

    cf2 = ar(i,j)*sig*w2/(4*pi);
    u2 = u2 + cf2*(-rr*RI31+sig*RI30);
    v2 = v2 + cf2*Dx*RI31;
    arintv1 = arintv1 + w1*ar(i,j);
    arintv2 = arintv2 + w2*ar(i,j);
    end % of azimuthal loop

end % of radial loop

%-----
% Kelvin's approximation
% for comparison purposes
%-----

uh = circ/(4*pi*rr)*(log(8.0*rr/cr)-0.25);

xplot(repeat) = cr/rr;
velr1(repeat) = u1;
velr2(repeat) = u2;
velr3(repeat) = uh;

%==
end
%==

plot(xplot,velr1,'k');
plot(xplot,velr2,'k--');
plot(xplot,velr3,'k:');
xlabel('a/\sigma_r','fontsize',15)
ylabel('U_x \kappa_r/\kappa_a','fontsize',15)

```

The results presented in [Figure 11.5.6](#) indicate that the precise form of the vorticity distribution over the core of the ring has a small effect on the ring velocity. As the size of the core tends to zero, while the strength of the ring is held constant, the self-induced velocity takes increasingly large values irrespective of the functional form of the vorticity distribution over the core. Consequently, the self-induced velocity of a line vortex ring with infinitesimal core, which is the axisymmetric counterpart of a point vortex, is not defined. In [Section 11.6](#), we will see that this is a more general behavior applicable to vortex filaments with arbitrary three-dimensional shapes.

Slender rings

An asymptotic analysis of the self-induced velocity of a vortex ring in the limit of small core size shows that, to leading order, the self-induced velocity is given by Kelvin's formula

$$U_x = \frac{\kappa}{4\pi\sigma_r} \left(-\ln \frac{8a}{\sigma_r} - \frac{1}{4} \right). \quad (11.5.38)$$

This formula demonstrates explicitly that the self-induced velocity diverges at a logarithmic

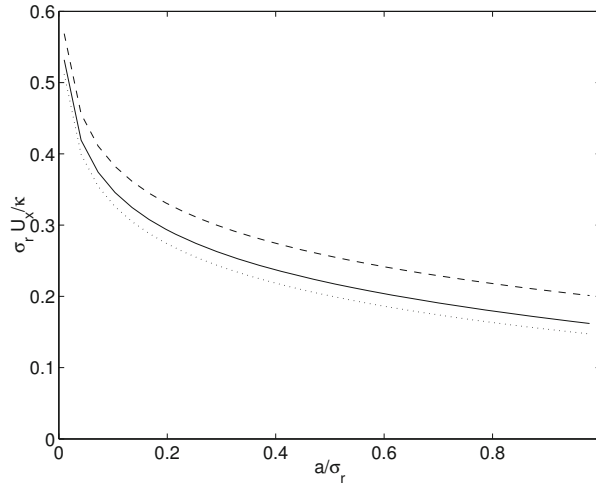


Figure 11.5.6 Self-induced velocity of a vortex ring of radius σ_r and circulation κ plotted against the ratio of the core to the ring radius, a/σ_r . The solid and dashed lines correspond, respectively, to a ring with uniform or diffuse vorticity distribution described by equations (11.5.36) and (11.5.37). The dotted line represents Kelvin's asymptotic prediction for small core radius expressed by equation (11.5.38).

rate with respect to the scaled core radius, a/σ_r . The predictions of Kelvin's formula, represented by the dotted line in Figure 11.5.6, are in good agreement with the exact values represented by the solid and dashed lines even when the vortex core radius, a , is not small compared to the ring radius, σ_r .

11.5.4 Motion of a collection of vortex rings

A vortex ring that belongs to a collection of coaxial vortex rings translates under the influence of its self-induced velocity as well as the velocity induced by its peers. When the ring core size is small, the self-induced velocity can be described accurately using formula (11.5.38).

The vorticity transport equation (6.6.16) requires that, as the radius of a ring, σ_r , changes during the motion, the azimuthal vorticity component, ω_φ , increases or decreases by the same proportion. In response to this change, the radius of the core, a , adjusts to preserve the ring strength and core volume, so that

$$\frac{d}{dt} ((2\pi \sigma_r) \pi a^2) = 0. \tag{11.5.39}$$

Expanding the derivative on the left-hand side and rearranging, we obtain an evolution equation for the core radius,

$$\frac{da}{dt} = -\frac{1}{2} \frac{a}{\sigma_r} \frac{d\sigma_r}{dt} = -\frac{1}{2} \frac{a}{\sigma_r} U_\sigma, \tag{11.5.40}$$

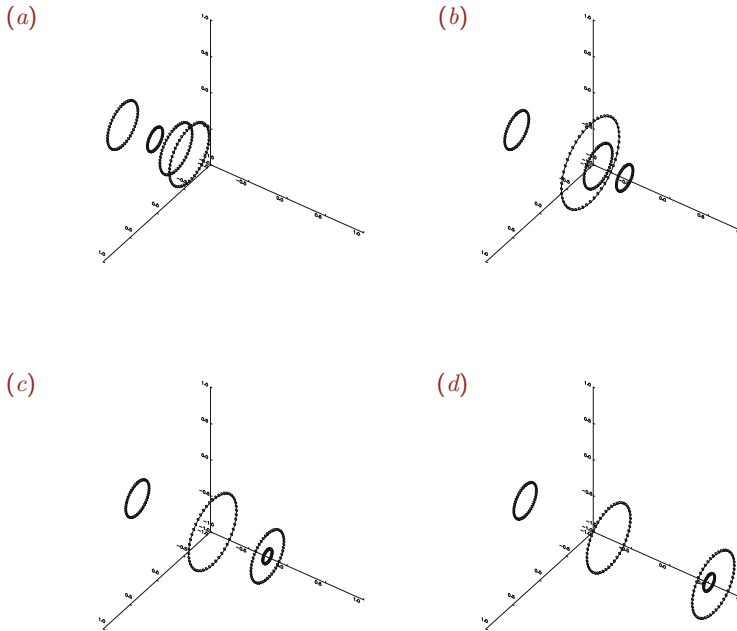


Figure 11.5.7 Motion of a collection of coaxial vortex rings demonstrating leap frogging.

where $U_\sigma \equiv d\sigma_r/dt$ is the rate of expansion of the circular centerline. Appending equation (11.5.40) to the equation of motion for the ring centerline, we obtain a system of differential equations governing the ring axial position, centerline radius, and core radius.

A numerical method for integrating the system of governing equations from a given initial condition is implemented in a code entitled *lvrm*, not listed in the text, residing in directory *09_vortex* of **FDLIB**. Stages in the motion of four vortex rings computed using this code are shown in [Figure 11.5.7](#). The simulation reveals that neighboring vortex rings pass through one another in an alternating fashion, exhibiting a type of motion that can be described as leap frogging.

11.5.5 Vortex patch in axisymmetric flow

Next, we consider an axisymmetric flow containing a toroidal vortex whose vorticity is proportional to the distance from the x axis,

$$\omega_\varphi = \Omega \sigma, \quad (11.5.41)$$

where Ω is a constant. The flow outside the vortex is irrotational.

Substituting the linear vorticity distribution into the integral representation (11.5.18), and using the Gauss divergence theorem, we derive a contour integral representation that

is analogous to that for a two-dimensional vortex patch with uniform vorticity discussed in Section 11.2.

Contour integral representation

We find that the axial velocity component is given by

$$u_x(x, \sigma) = -\frac{\Omega}{4\pi} \int_{\mathcal{C}} [(x - x')I_{10}(x - x', \sigma, \sigma') n_x(x', \sigma') + \sigma I_{11}(x - x', \sigma, \sigma') n_\sigma(x', \sigma')] \sigma' d\ell(x', \sigma'), \tag{11.5.42}$$

and the radial velocity component is given by

$$u_\sigma(x, \sigma) = \frac{\Omega}{4\pi} \int_{\mathcal{C}} I_{11}(x - x', \sigma, \sigma') n_x(x', \sigma') \sigma'^2 d\ell(x', \sigma'), \tag{11.5.43}$$

where \mathcal{C} is the trace of the vortex contour in a plane of constant azimuthal angle, φ , and ℓ is the arc length along \mathcal{C} . We have introduced the integral

$$I_{10}(\hat{x}, \sigma, \sigma') \equiv \int_0^{2\pi} \frac{d\hat{\varphi}}{r} = \int_0^{2\pi} \frac{d\hat{\varphi}}{[\hat{x}^2 + (\sigma + \sigma')^2 - 4\sigma\sigma'\cos^2(\frac{1}{2}\hat{\varphi})]^{1/2}}, \tag{11.5.44}$$

which can be evaluated by writing

$$I_{10}(\hat{x}, \sigma, \sigma') = \frac{4}{[\hat{x}^2 + (\sigma + \sigma')^2]^{1/2}} \int_0^{\pi/2} \frac{d\eta}{(1 - k^2 \cos^2 \eta)^{1/2}} \tag{11.5.45}$$

and then

$$I_{10}(\hat{x}, \sigma, \sigma') = \frac{4 F(k)}{[\hat{x}^2 + (\sigma + \sigma')^2]^{1/2}}, \tag{11.5.46}$$

where $\eta \equiv \frac{1}{2}\hat{\varphi}$, k^2 is defined in (11.5.23), and $F(k)$ is the complete elliptic integral of the first kind defined in the first equation of (11.5.24). We have also introduced the integral

$$I_{11}(\hat{x}, \sigma, \sigma') \equiv \int_0^{2\pi} \frac{\cos \hat{\varphi}}{r} d\hat{\varphi} = \int_0^{2\pi} \frac{\cos \hat{\varphi}}{[\hat{x}^2 + (\sigma + \sigma')^2 - 4\sigma\sigma'\cos^2(\frac{1}{2}\hat{\varphi})]^{1/2}} d\hat{\varphi}, \tag{11.5.47}$$

which can be expressed as

$$I_{11}(\hat{x}, \sigma, \sigma') = \frac{4}{[\hat{x}^2 + (\sigma + \sigma')^2]^{1/2}} \int_0^{\pi/2} \frac{\cos(2\eta)}{(1 - k^2 \cos^2 \eta)^{1/2}} d\eta. \tag{11.5.48}$$

The integral on the right-hand side of (11.5.48) can be expressed in terms of complete elliptic integrals of the first and second kind, $F(k)$ and $E(k)$, defined in (11.5.24), as

$$\int_0^{\pi/2} \frac{\cos(2\eta)}{(1 - k^2 \cos^2 \eta)^{1/2}} d\eta = \frac{2 - k^2}{k^2} F(k) - \frac{2}{k^2} E(k). \tag{11.5.49}$$

Contour dynamics

The vorticity transport equation for axisymmetric flow with negligible viscous forces, stated in equation (6.6.17), requires that the vorticity inside an axisymmetric patch whose vorticity distribution is linear with respect to distance from the x axis, σ , remains linear in time. To compute the evolution of the flow, it suffices then to follow the motion of the vortex contour using the counterpart of the contour dynamics method for two-dimensional flow, as discussed in Section 11.3.

Program *vp_ax*, located in directory *09_vortex* of **FDLIB**, not listed in the text, simulates the motion of a collection of axisymmetric vortex patches using the method of contour dynamics for axisymmetric flow. In the numerical implementation, the contour of each patch is approximated with blended circular arcs, as discussed in Section 11.3. The marker points defining each contour are redistributed adaptively during the motion to capture the development of regions of high curvature and prevent point clustering or dilution.

PROBLEM

11.5.1 Velocity induced by vorticity

Derive the representation (11.5.16).

11.5.2 Hill's spherical vortex

Show that the velocity corresponding to the stream functions (11.5.4) and (11.5.5) is continuous across the spherical interface of Hill's vortex.

11.5.3 Contour dynamics for three-dimensional flow

Is it possible to derive a contour dynamics method for a three-dimensional (non-axisymmetric) vortex flow?

11.5.4 Motion of line vortex rings

Run the code *lvrm* to simulate the motion of a collection of coaxial vortex rings of your choice and discuss the nature of the motion.

11.5.5 Motion of vortex patches

Run the code *vp_ax* to simulate the motion of an axisymmetric vortex patch of your choice and discuss the nature of the motion.

11.6 Three-dimensional vortex motion

Previously in this chapter, we discussed the dynamics of two-dimensional and axisymmetric vortex flow based on an integral representation for the velocity in terms of the vorticity expressed by the Biot–Savart integral, combined with simplified versions of the vorticity

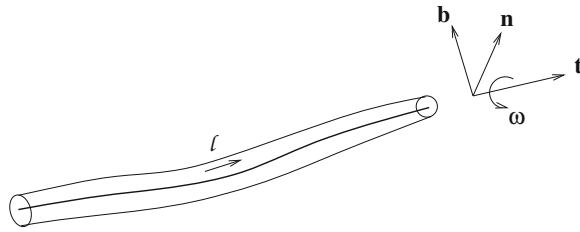


Figure 11.6.1 The motion of a thin vortex filament can be computed using the local-induction approximation expressed by equations (11.6.1) and (11.6.2).

transport equation for flow with negligible viscous forces. Extensions to three-dimensional flow are straightforward in principle but may be subtle in numerical implementation.

11.6.1 Vortex particles

The vortex-particle method arises by replacing the Biot–Savart integral in equation (11.4.18) with a sum of integrals over small parcels of rotational fluid, and then condensing the vorticity of each parcel into a designated center represented by point particles. This approximation effectively replaces the rotational fluid with a collection of three-dimensional singularities called rotlets or vortons. The strength of each vorton evolves in time according to rules originating from the vorticity transport equation for three-dimensional flow, incorporating stretching and reorientation.

The vorton discretization of a three-dimensional flow is analogous to the point-vortex discretization of a two-dimensional flow and to the line-vortex-ring discretization of an axisymmetric flow. However, because the three-dimensional discretization breaks the continuity of the vortex lines, some fundamental difficulties arise in three-dimensional flow. These difficulties, combined with high computational cost, explain why the vorton method is less attractive compared to its counterparts for two-dimensional and axisymmetric flow.

11.6.2 Line vortices and the local-induction approximation (LIA)

Consider a three-dimensional vortex filament with small core size, as illustrated in [Figure 11.6.1](#). A simplified model of the self-induced motion can be devised using our earlier results for vortex rings with small but non-infinitesimal core radius. To compute the motion of the filament centerline, we evaluate the velocity of point particles distributed along the centerline using the Biot–Savart integral expressed by (11.4.18), and then advance the position of the point particles using a standard numerical method.

Our earlier discussion of vortex rings suggests that the self-induced velocity of the filament is determined primarily by the ratio of the local filament core radius to the local radius of curvature of the filament centerline, as shown in (11.5.38). This observation provides us with a basis for computing the motion of the centerline according to the local-induction approximation (LIA).

In the LIA approximation, the velocity at a point along the centerline of a vortex filament is assumed to be parallel to the local unit binormal vector, \mathbf{b} , defined as the cross product of the unit tangent vector, \mathbf{t} , and the unit normal vector, \mathbf{n} ,

$$\mathbf{b} = \mathbf{t} \times \mathbf{n}. \quad (11.6.1)$$

The unit tangent vector arises by differentiating the position vector, \mathbf{x} , with respect to arc length, ℓ , along the centerline,

$$\mathbf{t} = \frac{d\mathbf{x}}{d\ell}. \quad (11.6.2)$$

The unit normal vector arises by further differentiating the unit tangent vector with respect to arc length,

$$\mathbf{n} = -\frac{1}{\rho} \frac{d\mathbf{t}}{d\ell}, \quad (11.6.3)$$

where ρ is the radius of curvature of the centerline. In the local-induction approximation, the self-induced velocity of the filament is given by

$$\mathbf{u} = u_b \mathbf{b}. \quad (11.6.4)$$

The magnitude of the velocity, u_b , derives from Helmholtz's formula (11.5.38) as

$$u_b = \frac{\kappa}{4\pi\rho} \left(-\ln \frac{8a}{\rho} - \frac{1}{4} \right), \quad (11.6.5)$$

where κ is the strength of the filament. The local filament core radius, a , is allowed to vary with position along the centerline.

Evolution of the core radius

The vorticity transport equation requires that the vorticity in the filament core increases or decreases depending on whether the filament centerline undergoes stretching or compression. An evolution equation for the filament core radius may then be derived by requiring that the volume of rotational fluid residing inside the core is conserved during the motion.

Let $\delta\ell$ be an infinitesimal arc length along the centerline corresponding to a material segment that begins and ends at two material point particles. Conservation of volume requires that

$$\frac{d}{dt} (\delta\ell \pi a^2) = 0. \quad (11.6.6)$$

Expanding the derivative of the product on the right-hand side and rearranging, we obtain the evolution equation

$$\frac{da}{dt} = -\frac{1}{2} \frac{a}{\delta\ell} \frac{d\delta\ell}{dt}. \quad (11.6.7)$$

The last two equations are the counterparts of equations (11.5.39) and (11.5.40) pertaining to axisymmetric flow.

Numerical method

A numerical method for computing the evolution of the centerline of a closed filament can be implemented according to the following steps:

1. Trace the centerline with $N + 1$ marker points, where point labeled 1 coincides with point labeled $N + 1$, and assign initial values to the core radius.
2. Approximate the centerline over the interval subtended between points labeled $i - 1$ and $i + 1$ with a circular arc passing through the three points labeled $i - 1$, i , and $i + 1$, and compute the arc center and radius for $i = 1, \dots, N$.
3. Compute the unit tangent, normal, and binormal vector at the i th marker point using equations (11.6.1), (11.6.2), and (11.6.3) for $i = 1, \dots, N$.
4. Set the radius of curvature of the line vortex at each point equal to the radius of the arc, ϱ .
5. Advance the position of the marker points with the velocity computed from (11.6.4).
6. Update the core radius by requiring conservation of volume expressed by (11.6.6).

The motion of marker points computed by this method suffers from a numerical instability manifested by the onset of strong oscillations due to the violent amplification of numerical or round-off error. Smoothing the position of the marker points using the five-point formula (11.2.35) applied for the Cartesian coordinates of the marker points filters out the oscillations and allows us to pursue the motion for an extended period of time.

Program *lv_lia*, located in directory *09_vortex* of **FDLIB**, simulates the motion of a closed line vortex using the local induction approximation. The code features adaptive point redistribution to capture the development of regions of high curvature.

Stages in the evolution of a closed line vortex computed by this program are shown in [Figure 11.6.2](#). The simulation shows that the ring travels while exhibiting wobbly oscillations familiar to cigarette and cigar smokers.

PROBLEM

11.6.1 LIA for a circular line vortex ring

Confirm that the local-induction approximation describes consistently the self-induced motion of a circular line vortex ring discussed in Section 11.5.

11.6.2 Motion of line vortex

Run program *lv_lia* to simulate the evolution of a line vortex with initial shape and core radius of your choice. Discuss the nature of the motion.

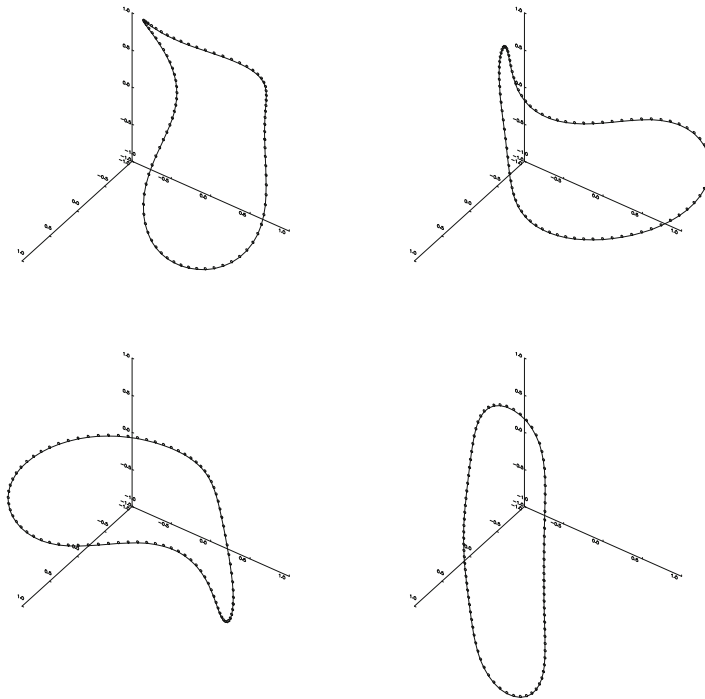


Figure 11.6.2 Stages in the evolution of a closed line vortex, resembling a smoke ring, computed by program *lv.lia* of FDLIB.

- 12.1 General features of flow past an aircraft**
- 12.2 Airfoils and the Kutta–Joukowski condition**
- 12.3 Vortex panels**
- 12.4 Vortex panel method**
- 12.5 Vortex sheet representation**
- 12.6 Point-source-dipole panels**
- 12.7 Point-source panels and Green’s third identity**

Flows past airplane wings and high-speed ground vehicles has captured the attention of fluid dynamicists, applied mathematicians, and computational scientists and engineers, not only because of their obvious technological significance, but also because of the opportunity they present to perform elegant mathematical analysis and develop realistic and efficient numerical models. Although these flows occur at high Reynolds numbers and often at transonic or supersonic speeds that are comparable to, or even exceed the speed of sound, the effect of viscosity is important in two ways. First, viscous stresses determine the drag force exerted on moving surfaces and thus the energy required to sustain the motion. Second, viscous stresses are responsible for production of vorticity which generates circulation and thereby induces a lift force.

A comprehensive analysis of high-speed flow in aerodynamics incorporates the effects of fluid compressibility and turbulent motion, and accounts for the presence of boundary layers and regions of recirculating flow. In this chapter, we discuss the most basic configuration that arises by neglecting the presence of boundary layers and wakes, and by assuming that the fluid is inviscid and incompressible. The simplified model involving irrotational flow in the presence of global circulatory motion is amenable to efficient numerical methods that illustrate the importance of computational fluid dynamics in the practical field of aerodynamics.

12.1 General features of flow past an aircraft

A schematic illustration of flow past an aircraft that has taken off and traveled by a certain distance is shown in [Figure 12.1.1](#) in a frame of reference moving with the aircraft. If the flow is subsonic, the following features are most significant:

- A thin vortex loop resembling a line vortex is established behind the aircraft. The loop

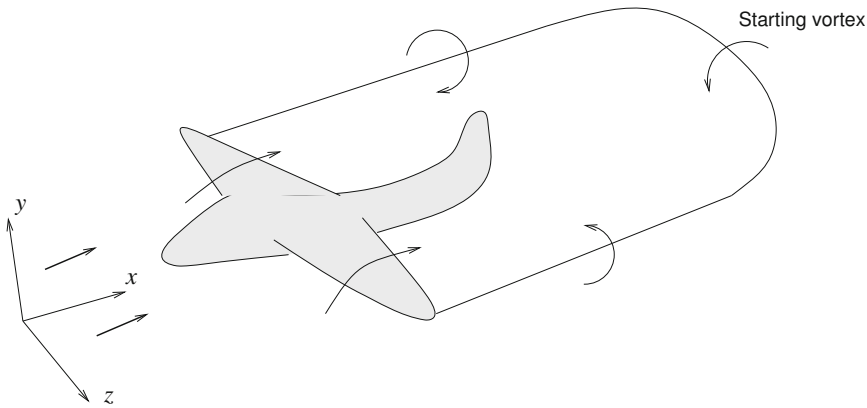


Figure 12.1.1 Schematic illustration of flow past an aircraft in a frame of reference moving with the aircraft.

extends from the left wing tip, back at a length that is comparable to the distance that the aircraft has traveled, and then forward to the right wing tip. The trailing vortex at the back of the loop was generated when the airplane first started moving, and is accordingly called the starting vortex. The vortex loop can be extended artificially into the wings to form a closed line vortex.

The circulation around any closed loop that encloses the line vortex is constant, independent of the shape and location of the loop. Thus, the circulation around a simple loop that encloses a wing is equal to the circulation around a simple loop that encloses the trailing vortex.

- Viscous stresses cause the vortex loop to diffuse and its vortex core to be smeared. However, the circulation around any loop that encloses the smeared vortex loop is equal to the circulation around a loop that encloses a wing, no matter how far the vorticity has spread out.
- The circulation around a loop that encloses a wing is determined by the speed of the aircraft and the geometry and orientation of the wings with respect to the incoming wind, as discussed in Section 12.2.
- If the aircraft suddenly changes its speed or direction of flight, a new vortex loop will be ejected, contributing an additional amount of circulation around the wings.
- Each wing experiences a lift force normal to the direction of flight, and a drag force parallel to the direction of flight. The latter must be compensated by the thrust produced by the engine.

The lift force can be computed with surprising accuracy by neglecting the effects of viscosity and assuming that the flow around the airfoil is irrotational. To compute the drag

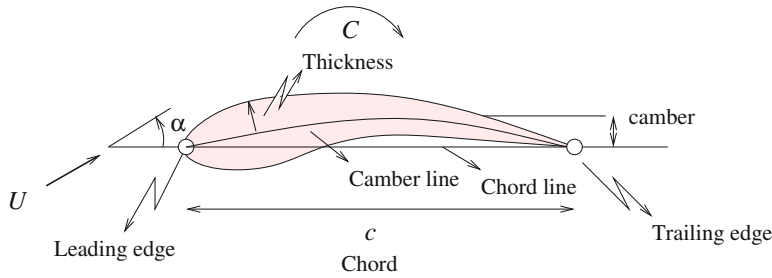


Figure 12.2.1 Illustration of an airfoil and its standard geometrical properties, also showing the angle of attack, α .

force, we must carry out a boundary-layer analysis of the basic irrotational flow, as discussed in Chapter 10.

It is important to bear in mind that the main features of the flow past an aircraft discussed in this chapter assume that the wings are only slightly tilted with respect to the direction of the incoming wind. When this condition is not met, large regions of recirculating flow may develop over the upper surface of the airfoil, seriously affecting the structure of the flow and performance of the aircraft.

To study the flow past the wings and compute the lift force per unit span exerted on them, we may assume that the flow is locally two-dimensional occurring in the xy plane that is normal to the line connecting the wing tips. It turns out that neglecting the third dimension provides us with a theoretical model whose predictions are in good and sometimes excellent agreement with laboratory measurements taken in wind tunnels. In the remainder of this chapter, we concentrate on the two-dimensional flow. The three-dimensional flow is an advanced topic suitable for a second course in aerodynamics.

12.2 Airfoils and the Kutta–Joukowski condition

An airfoil is a section of a wing, as shown in Figure 12.2.1. The shape of an airfoil is determined by the following geometrical parameters:

- The *chord line*, defined as the straight line connecting the leading edge to the trailing edge.
- The *chord*, defined as the distance from the leading edge to the trailing edge.
- The *camber line*, defined as the locus of points located halfway between the upper and lower surface of the airfoil.
- The *camber*, defined as the maximum displacement of the camber line from the chord line. The camber of a symmetric airfoil is zero.
- The *airfoil thickness* along the camber line.

The angle subtended between the incoming wind and the chord line, α , is the *angle of attack*, as shown in [Figure 12.2.1](#).

NACA airfoils

The National Advisory Committee for Aeronautics of the United States (NACA), the predecessor of today's NASA, has standardized airfoil shapes to facilitate engineering design. NACA airfoils are generated by specifying the geometry of the camber line, and then wrapping around the camber line an airfoil contour to obtain a desired distribution of half-thickness.

The dated four-digit NACA $mnlk$ airfoils, where m, n, k, l are four integers, have a camber of $0.0m \times c$, occurring at a distance $0.0n \times c$ from the leading edge, where c is the chord. The maximum airfoil thickness is $0.kl \times c$.

The following MATLAB code entitled *NACA4*, located in directory *airf-2d* inside directory *07_ptf* of *FDLIB*, generates a four-digit NACA airfoil:

```

chord = 1.0;
xcam = 0.4;
cam = 0.05;
thick = 0.1;

n = 32; % number of nodes around the airfoil

%----
% prepare
%----

dpsi = 2*pi/n;

%----
% prepare to plot
%----

figure(1)
hold on
axis equal
xlabel('x','fontsize',13)
ylabel('y','fontsize',13)

%----
% run over nodes
%----

for i=1:n
    psi = (i-1.0)*dpsi;
    x = 0.5*(1.0+cos(psi));

```

```

% camber line:

if(x<xcam)
    yc(i) = cam*(2.0*xcam*x-x*x)/xcam^2;
else
    yc(i) = cam/(1.0-xcam)^2 ...
        *((1.0-2.0*xcam)+2.0*xcam*x-x*x);
end

% thickness:

yt = 5.0*thick *(0.2969*sqrt(x) -0.1260*x...
    -0.3516*x*x +0.2843*x*x*x -0.1036*x*x*x*x );

% contour:

if(i<(n/2+1))
    ya(i) = (yc(i)-yt)*chord;
else
    ya(i) = (yc(i)+yt)*chord;
end

xa(i) = x*chord;

end

xa(n+1) = chord;
ya(n+1) = 0.0;
yc(n+1) = 0.0;    % trailing edge

%----
% plot
%----

plot(xa,ya,'ko-');
plot(xa,yc,'k--');

```

The graphics display generated by the code is shown in [Figure 12.2.2](#).

Modern five- and six-digit airfoils are encoded with additional geometrical and flow properties.

Airfoil shapes by mapping

Airfoil shapes can be generated by mapping a closed contour in an auxiliary parametric (ξ, η) plane to the airfoil contour in the physical xy plane using an appropriate mapping function. In theoretical aerodynamics, the mapping function arises from a function of a

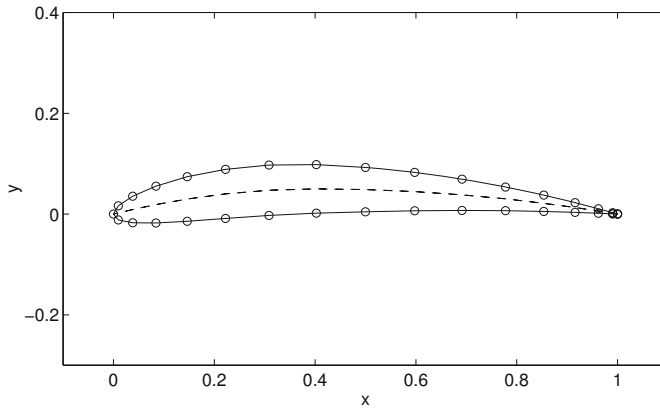


Figure 12.2.2 Contour of a four-digit NACA airfoil generated by a MATLAB program named NACA4.

complex variable, $f(\zeta)$, by setting

$$z = f(\zeta), \quad (12.2.1)$$

where

$$z \equiv x + iy, \quad \zeta \equiv \xi + i\eta \quad (12.2.2)$$

are two complex variables, and i is the imaginary unit satisfying $i^2 = -1$.

Joukowski's transformation

Joukowski's transformation employs the mapping function

$$f(\zeta) = \zeta + \frac{\sigma^2}{\zeta}, \quad (12.2.3)$$

where σ is a specified length. A circle in the $\xi\eta$ plane passing through the singular point $(-\sigma, 0)$ and enclosing the reflected singular point $(\sigma, 0)$ is mapped to a cusped airfoil whose camberline and camber are determined by the location of the center of the circle in the $\xi\eta$ plane, as shown in [Figure 12.2.3](#). The airfoil cusp is located at the image of the first singular point. Different airfoil shapes can be generated by fixing the value of σ and varying the position of the center of the circle, \mathbf{x}_c , in the $\xi\eta$ plane.

The following MATLAB code entitled *joukowski*, located in directory *airf_2d* inside directory *07_ptf* of *FDLIB*, generates airfoil shapes:

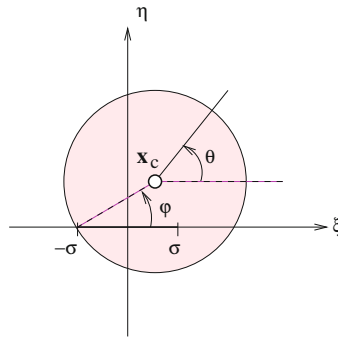


Figure 12.2.3 A Joukowski airfoil is generated by mapping conformally a circle in the $\xi\eta$ plane to an airfoil contour in the xy plane. The first singular point, located at the ξ axis at $\xi = -\sigma$, is mapped to the airfoil trailing edge. The second singular point, located at $\xi = \sigma$, is mapped inside the airfoil.

```

xc = 0.1; % circle center
yc = 0.2; % circle center
n = 32;   % number of contour nodes
sigma = 1.0;

%---
% prepare
%---

radius = sqrt((xc+sigma)^2+yc*yc);
phi = acos((xc+sigma)/radius);
thstart = -pi+phi;
dth = 2*pi/n;

%---
% run around the airfoil
%---

for i=1:n+1
    th = thstart+(i-1)*dth;
    xi = xc+radius*cos(th);
    et = yc+radius*sin(th);
    r2 = xi*xi+et*et;
    x(i) = xi*(1.0+sigma^2/r2);
    y(i) = et*(1.0-sigma^2/r2);
end

%---
% plot
%---
```

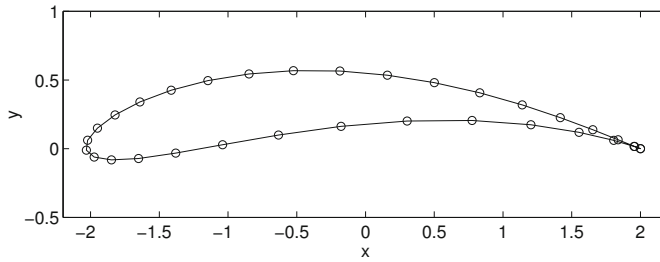


Figure 12.2.4 A Joukowski airfoil generated by the code `joukowski` listed in the text for the parameter values listed in the code.

```
plot(-x,y,'o-')
axis equal
xlabel('x','fontsize',13)
ylabel('y','fontsize',13)
```

The graphics display generated by the code is shown in [Figure 12.2.4](#). Note that the starting angle ϕ is defined in [Figure 12.2.3](#). The first and last points, labeled 1 and $n + 1$ are mapped to the trailing edge. Intermediate points are distributed in the counterclockwise direction around the airfoil. Note that the airfoil contour has been reflected at the plotting stage to place the leading edge on the left.

12.2.1 The Kutta–Joukowski theorem

The lift force per unit span exerted on an airfoil, L , is determined by the incoming wind speed, U , and by the circulation of the fluid around the airfoil, C , as determined by the Kutta–Joukowski theorem expressed by the equation

$$L = -\rho UC, \quad (12.2.4)$$

where ρ is the density of the fluid. Note that positive lift, $L > 0$, requires negative circulation associated with clockwise rotation around the airfoil, $C < 0$ as illustrated in [Figure 12.2.1](#). If the circulation vanishes, the lift force is zero.

The Kutta–Joukowski theorem can be proved most readily working under the auspices of analytic function theory in complex variables, as discussed in the texts cited in the bibliography.

Flow past a cylinder

To confirm the Kutta–Joukowski theorem, we consider streaming (uniform) flow past a circular cylinder of radius a discussed in Section 3.7. Applying Bernoulli’s equation (6.4.18) at infinity and at a point on the surface of the cylinder, and evaluating the tangential velocity on the surface of the cylinder using formula (3.7.10), we derive an expression for the surface

pressure,

$$p_{r=a} = -2\rho V_x^2 (\sin \theta + \beta)^2 + p_\infty, \quad (12.2.5)$$

where p_∞ is the pressure at infinity, β is a dimensionless circulation parameter defined in equation (3.7.9) as

$$\beta \equiv -\frac{C}{4\pi V_x a}, \quad (12.2.6)$$

and C is the circulation around the cylinder.

In the absence of viscous stresses, the force per unit span exerted on the cylinder is given by

$$\mathbf{F} = \oint [-p_{r=a}] \mathbf{n} d\ell = -\int_0^{2\pi} p_{r=a} \mathbf{n} a d\theta, \quad (12.2.7)$$

where $d\ell = a d\theta$ is the differential arc length around the cylinder and $\mathbf{n} = (\cos \theta, \sin \theta)$ is the unit vector normal to the cylinder pointing into the fluid. Substituting the pressure distribution (12.2.5) into (12.2.7), we find that the x component of the force vanishes, while the y component of the force is given by

$$F_y \equiv L = 2\rho a V_x^2 \int_0^{2\pi} (\sin \theta + \beta)^2 \sin \theta a d\theta. \quad (12.2.8)$$

Performing the integration, we obtain

$$L = 4\pi a \rho V_x^2 \beta. \quad (12.2.9)$$

Recalling the definition of β given in (12.2.6), we find that

$$L = -\rho V_x C, \quad (12.2.10)$$

which is consistent with the Kutta–Joukowski theorem expressed by (12.2.4).


12.2.2 The Kutta–Joukowski condition

In the context of irrotational flow theory, the circulation around an airfoil, or any two-dimensional body, is arbitrary. Kutta and Joukowski observed independently that, in practice, when the angle of attack α is sufficiently small, the flow on the upper side of an airfoil joins smoothly with the flow on the lower side of the airfoil at the trailing edge. This observation provides us with a physical basis for the Kutta–Joukowski condition stipulating that the circulation established around an airfoil is such that a singular flow does not arise at the trailing edge, and therefore the fluid does not have to turn around a cornered or cusped trailing edge.

Referring to the Kutta–Joukowski theorem expressed by (12.2.4), we see that a well-designed airfoil should be able to generate a high degree of circulation, while minimizing the drag force exerted on the airfoil.

PROBLEMS**12.2.1** *Flow past a cylinder*

Carry out the integration in (12.2.7) with the pressure given in (12.2.5) to derive expression (12.2.10).

12.2.2  *Joukowski airfoils*

Run the code *joukowski* to generate several airfoil shapes of your choice. Investigate the effect of the location of the mapped circle center.

12.3 Vortex panels

We begin the study of two-dimensional flow past an airfoil by introducing a class of elementary flows associated with vortex panels. Our ultimate objective is to use these elementary flows as fundamental building blocks for describing the flow past an airfoil with arbitrary shape, where the circulation around the airfoil is determined by the Kutta–Joukowski condition discussed in Section 12.2.2.

Flow due to a point vortex

In Section 3.7, we introduced the two-dimensional irrotational flow with circulatory motion induced by a point vortex. The x and y components of the velocity at a point, $\mathbf{x} = (x, y)$, due to a point vortex with strength κ located at another point, $\mathbf{x}_0 = (x_0, y_0)$, were given in equations (11.2.1) and (11.2.2), repeated below for convenience,

$$u_x(x, y) = -\frac{\kappa}{2\pi} \frac{y - y_0}{(x - x_0)^2 + (y - y_0)^2} \quad (12.3.1)$$

and

$$u_y(x, y) = \frac{\kappa}{2\pi} \frac{x - x_0}{(x - x_0)^2 + (y - y_0)^2}. \quad (12.3.2)$$

The associated stream function is given by

$$\psi(x, y) = -\frac{\kappa}{4\pi} \ln \frac{(x - x_0)^2 + (y - y_0)^2}{\rho^2}, \quad (12.3.3)$$

where ρ is an arbitrary constant length. The corresponding multi-valued velocity potential is given by

$$\phi(x, y) = \frac{\kappa}{2\pi} \arctan \frac{y - y_0}{x - x_0}. \quad (12.3.4)$$

We recall that the velocity is the gradient of the velocity potential, $\mathbf{u} = \nabla\phi$.

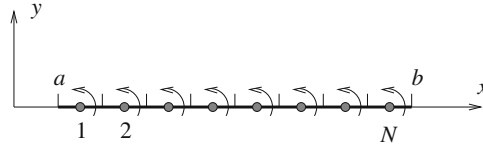


Figure 12.3.1 A collection of N point vortices are distributed evenly along the x axis inside an interval, (a, b) . As the number of point vortices increases, we obtain a continuous distribution yielding a vortex panel.

12.3.1 From point vortices to vortex panels

Consider a collection of N point vortices distributed evenly along the x axis inside an interval, (a, b) , separated by distance $\Delta x = (b - a)/N$, as illustrated in Figure 12.3.1. The i th point vortex is situated at the position

$$x_i = a + \frac{1}{2} i \Delta x, \quad y_i = 0 \tag{12.3.5}$$

for $i = 1, \dots, N$. The strength of the i th point vortex is denoted as κ_i . The first point vortex is located at $x_i = a + \frac{1}{2} \Delta x$ and the last point vortex is located at $x_N = b - \frac{1}{2} \Delta x$.

Superposing the stream functions associated with the individual point vortices, we find that the stream function of the flow induced by the collection is given by

$$\psi(x, y) = - \sum_{i=1}^N \frac{\kappa_i}{4\pi} \ln \frac{(x - x_i)^2 + (y - y_i)^2}{\rho^2}, \tag{12.3.6}$$

which can be recast into the form

$$\psi(x, y) = - \frac{1}{4\pi} \sum_{i=1}^N \ln \frac{(x - x_i)^2 + (y - y_i)^2}{\rho^2} \frac{\kappa_i}{\Delta x} \Delta x, \tag{12.3.7}$$

with the understanding that $y_i = 0$.

In the limit as N tends to infinity, and correspondingly Δx tends to zero, while the strength of the point vortices decreases so that the ratio $\gamma_i \equiv \kappa_i/\Delta x$ remains constant, the sum on the right-hand side of (12.3.7) reduces to a line integral over the domain of distribution of the point vortices, yielding the integral representation

$$\psi^{\text{vortex panel}}(x, y) = - \frac{1}{4\pi} \int_a^b \ln \frac{(x - x')^2 + (y - y')^2}{\rho^2} \gamma(x') dx', \tag{12.3.8}$$

with the understanding that $y' = 0$. The right-hand side of (12.3.8) expresses the flow due to a two-dimensional finite vortex sheet with strength density $\gamma(x)$, also called a *vortex panel*, extending between the points $x = a$ and b . The circulation around the panel is equal to the integral of the strength density,

$$\Gamma^{\text{vortex panel}} \equiv \int_a^b \gamma(x) dx, \tag{12.3.9}$$

defined as the *panel strength*.

Following the discussion in Section 3.7, we find that the circulation around a closed loop that does not enclose the panel is zero, whereas the circulation around a simple loop that wraps around the panel once is equal to the panel strength. If the strength of the panel is zero, the circulation vanishes.

12.3.2 Vortex panels with uniform strength

It is useful to consider a vortex panel with uniform strength density, γ , equal to $\gamma^{(0)}$. According to (12.3.9), the circulation around the panel is equal to

$$\Gamma^{\text{vortex panel}} = (b - a) \gamma^{(0)}. \quad (12.3.10)$$

Applying (12.3.8) with $y' = 0$, we find that the stream function of the induced flow is given by

$$\psi^{(0)}(x, y) = -\frac{\gamma^{(0)}}{4\pi} \int_a^b \ln \frac{(x - x')^2 + y^2}{\rho^2} dx'. \quad (12.3.11)$$

The integral on the right-hand side of (12.3.11) can be calculated with the help of standard mathematical tables, and is found to be

$$\begin{aligned} \psi^{(0)}(x, y) = & -\gamma^{(0)} \frac{1}{4\pi} \left(-(x - b) \ln \frac{(x - b)^2 + y^2}{\rho^2} \right. \\ & \left. + (x - a) \ln \frac{(x - a)^2 + y^2}{\rho^2} \right. \\ & \left. + 2y \left[\arctan \frac{y}{x - b} - \arctan \frac{y}{x - a} \right] - 2(b - a) \right). \end{aligned} \quad (12.3.12)$$

The velocity components arise by straightforward differentiation, and are found to be

$$u_x^{(0)}(x, y) = \frac{\partial \psi^{(0)}}{\partial y} = -\frac{\gamma^{(0)}}{2\pi} \left(\arctan \frac{y}{x - b} - \arctan \frac{y}{x - a} \right) \quad (12.3.13)$$

and

$$u_y^{(0)}(x, y) = -\frac{\partial \psi^{(0)}}{\partial x} = -\frac{\gamma^{(0)}}{4\pi} \ln \frac{(x - b)^2 + y^2}{(x - a)^2 + y^2}. \quad (12.3.14)$$

The streamline pattern induced by a vortex panel subtended between the points $x = \pm b$ is shown in [Figure 12.3.2](#). Far from the panel, the flow resembles that due to a point vortex with strength

$$\kappa = \Gamma^{\text{vortex panel}} = \gamma^{(0)} (b - a) = 2b\gamma^{(0)}, \quad (12.3.15)$$

situated at the origin.

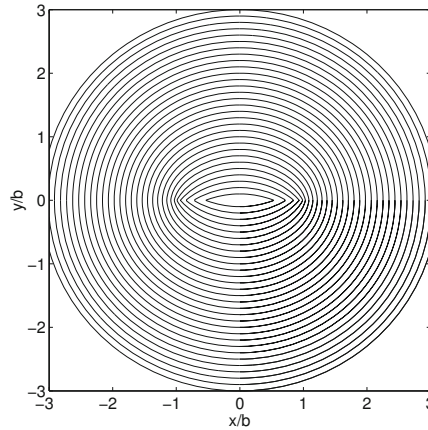


Figure 12.3.2 Streamline pattern of the flow induced by a vortex panel with uniform strength situated along the x axis in the interval $[-b, b]$.

Jump in velocity across a vortex panel

Expression (12.3.14) shows that the y component of the velocity is continuous throughout the domain of flow as well as across the vortex panel. In contrast, because of the presence of the inverse tangent function on the right-hand side of (12.3.13), the x velocity component undergoes a discontinuity across the vortex panel.

To demonstrate this jump, we evaluate the velocity at a point on the upper surface of the panel for $a < x < b$ and $y = +\epsilon$, where ϵ is a small positive elevation, and find that

$$u_x^{(0)}(x, y \rightarrow 0+) = -\gamma^{(0)} \frac{1}{2\pi} (-\arctan(-\infty) + \arctan(+\infty)), \tag{12.3.16}$$

yielding

$$u_x^{(0)}(x, y \rightarrow 0+) = -\gamma^{(0)} \frac{1}{2\pi} (\frac{\pi}{2} + \frac{\pi}{2}) \tag{12.3.17}$$

and then

$$u_x^{(0)}(x, y \rightarrow 0+) = -\frac{1}{2} \gamma^{(0)}, \tag{12.3.18}$$

independent of x , provided that $a < x < b$. The x velocity component at a point at the lower surface of the panel for $a < x < b$ and $y = -\epsilon$ is given by

$$u_x^{(0)}(x, \rightarrow 0-) = -\gamma^{(0)} \frac{1}{2\pi} (-\arctan(+\infty) + \arctan(-\infty)), \tag{12.3.19}$$

yielding

$$u_x^{(0)}(x, \rightarrow 0-) = -\gamma^{(0)} \frac{1}{2\pi} (-\frac{\pi}{2} - \frac{\pi}{2}), \tag{12.3.20}$$

and then

$$u_x^{(0)}(x, \rightarrow 0_-) = \frac{1}{2} \gamma^{(0)}, \quad (12.3.21)$$

independent of x , provided that $a < x < b$.

Using the preceding results, we find that, as the vortex panel is traversed from the upper to the lower side, the velocity undergoes a discontinuity whose magnitude is equal to the strength of the vortex sheet,

$$u_x(x, -\epsilon) - u_x(x, +\epsilon) = \gamma^{(0)}. \quad (12.3.22)$$

In contrast, a discontinuity does not occur beyond the edges of the vortex panel.

These observations suggest that a vortex panel, or more generally a vortex sheet, can be identified with a surface across which the tangential component of the velocity undergoes a discontinuity, where the magnitude of the discontinuity is the strength of the vortex panel or vortex sheet.

12.3.3 Vortex panel with linear strength density

Next, we consider a vortex panel situated in the interval $[a, b]$ along the x axis, with linear strength density distribution given by

$$\gamma(x) = \gamma^{(0)} + \gamma^{(1)}(x - a). \quad (12.3.23)$$

Using (12.3.9), we find that the circulation around the panel is

$$\Gamma^{\text{vortex panel}} = \int_a^b \gamma \, dx = (b - a) \left[\gamma^{(0)} + \frac{1}{2} \gamma^{(1)}(b - a) \right] \quad (12.3.24)$$

or

$$\Gamma^{\text{vortex panel}} = (b - a) \gamma\left(\frac{a + b}{2}\right). \quad (12.3.25)$$

Applying (12.3.8) with $y' = 0$ and rearranging, we find that the stream function of the induced flow is given by

$$\begin{aligned} \psi^{(01)}(x, y) = & -\frac{\gamma^{(0)} + \gamma^{(1)}(x - a)}{4\pi} \int_a^b \ln \frac{(x - x')^2 + y^2}{\rho^2} \, dx' \\ & - \frac{\gamma^{(1)}}{4\pi} \int_a^b (x' - x) \ln \frac{(x - x')^2 + y^2}{\rho^2} \, dx'. \end{aligned} \quad (12.3.26)$$

The first integral on the right-hand side of (12.3.26) is equal to the expression enclosed by the tall parentheses following the fraction on the right-hand side of (12.3.12). The second

integral can be calculated with the help of standard tables of integrals and is found to be

$$\int_a^b (x' - x) \ln \frac{(x - x')^2 + y^2}{\varrho^2} dx' = \frac{1}{2} [(x - b)^2 + y^2] \ln \frac{(x - b)^2 + y^2}{\varrho^2} - \frac{1}{2} [(x - a)^2 + y^2] \ln \frac{(x - a)^2 + y^2}{\varrho^2} - \frac{1}{2}(x - b)^2 + \frac{1}{2}(x - a)^2. \quad (12.3.27)$$

Combining (12.3.11), (12.3.27), and (12.3.8), and consolidating various terms, we obtain

$$\psi^{(01)}(x, y) = \psi^{(0)}(x, y) + \psi^{(1)}(x, y), \quad (12.3.28)$$

where $\psi^{(0)}$ is given in (12.3.12) and

$$\begin{aligned} \psi^{(1)}(x, y) = & -\gamma^{(1)} \frac{1}{4\pi} \left(\frac{1}{2} [y^2 - (x - b)(x + b - 2a)] \ln \frac{(x - b)^2 + y^2}{\varrho^2} \right. \\ & - \frac{1}{2} [y^2 - (x - a)^2] \ln \frac{(x - a)^2 + y^2}{\varrho^2} + 2y(x - a) \left(\arctan \frac{y}{x - b} - \arctan \frac{y}{x - a} \right) \\ & \left. - \frac{1}{2}(x - b)^2 + \frac{1}{2}(x - a)^2 - 2(x - a)(b - a) \right). \end{aligned} \quad (12.3.29)$$

The velocity components can be resolved into corresponding constituents,

$$u_x^{(01)}(x, y) = u_x^{(0)}(x, y) + u_x^{(1)}(x, y) \quad (12.3.30)$$

and

$$u_y^{(01)}(x, y) = u_y^{(0)}(x, y) + u_y^{(1)}(x, y), \quad (12.3.31)$$

where $u_x^{(0)}$ and $u_y^{(0)}$ are given in (12.3.13) and (12.3.14). Tedious differentiation yields the final forms

$$\begin{aligned} u_x^{(1)}(x, y) = & \frac{\partial \psi^{(1)}}{\partial y} = -\gamma^{(1)} \frac{1}{4\pi} \left(y \ln \frac{(x - b)^2 + y^2}{(x - a)^2 + y^2} \right. \\ & \left. + 2(x - a) \left(\arctan \frac{y}{x - b} - \arctan \frac{y}{x - a} \right) \right) \end{aligned} \quad (12.3.32)$$

and

$$\begin{aligned} u_y^{(1)}(x, y) = & -\frac{\partial \psi^{(1)}}{\partial x} = -\gamma^{(1)} \frac{1}{4\pi} \left((x - a) \ln \frac{(x - b)^2 + y^2}{(x - a)^2 + y^2} \right. \\ & \left. - 2y \left(\arctan \frac{y}{x - b} - \arctan \frac{y}{x - a} \right) + 2(b - a) \right). \end{aligned} \quad (12.3.33)$$

Using these expressions, we confirm that, as the vortex panel is traversed along the y axis from the upper to the lower side, the x velocity component undergoes a discontinuity whose magnitude is equal to the local strength of the vortex sheet.

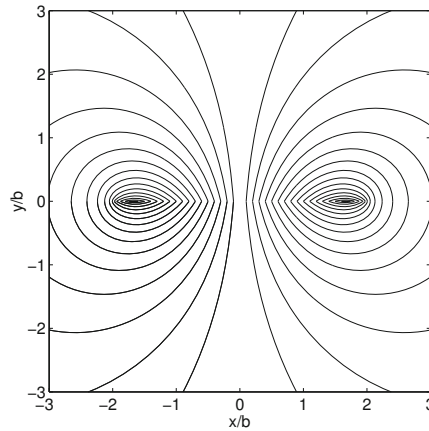


Figure 12.3.3 Streamline pattern of the flow due to a vortex panel with linear strength situation along the x axis in the interval $[-b, b]$, for vanishing circulation around the panel.

The streamline pattern of the flow induced by a vortex panel extending in the interval $[-b, b]$ is shown in [Figure 12.3.3](#) for $\gamma^{(1)} = -\gamma^{(0)}/b$, so that $\gamma(x) = \gamma^{(0)}x/b$. Because the circulation around the panel vanishes, as required by (12.3.25), far from the panel, the flow reduces to that due to a point-vortex dipole situated at the panel center-point and oriented along the x axis. Alternatively, the far flow is identical to the flow due to a point-source dipole placed at the same location oriented along the y axis.

PROBLEM

12.3.1 Velocity potential due to vortex panels.

(a) Confirm that the velocity potential corresponding to the stream function stated in (12.3.12) is given by

$$\begin{aligned} \phi^{(0)}(x, y) = -\gamma^{(0)} \frac{1}{2\pi} & \left((x-b) \arctan \frac{y}{x-b} - (x-a) \arctan \frac{y}{x-a} \right. \\ & \left. + \frac{1}{2} y \ln \frac{(x-b)^2 + y^2}{(x-a)^2 + y^2} \right). \end{aligned} \quad (12.3.34)$$

(b) Confirm that the velocity potential corresponding to the stream function given in (12.3.29) is given by

$$\begin{aligned} \phi^{(1)}(x, y) = -\gamma^{(1)} \frac{1}{4\pi} & \left((x-a) y \ln \frac{(x-b)^2 + y^2}{(x-a)^2 + y^2} \right. \\ & + [(x-a)^2 - (b-a)^2 - y^2] \arctan \frac{y}{x-b} \\ & \left. - [(x-a)^2 - y^2] \arctan \frac{y}{x-a} + y(b-a) \right). \end{aligned} \quad (12.3.35)$$

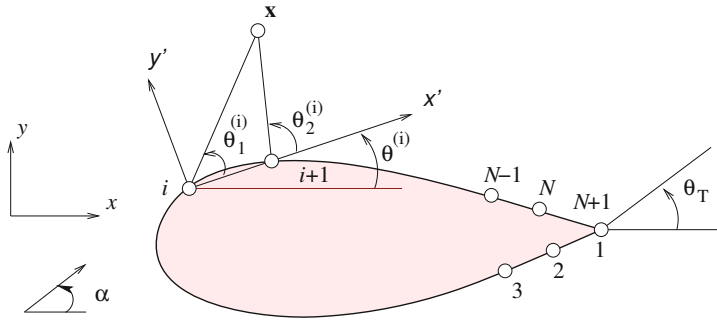


Figure 12.4.1 Discretization of the contour of an airfoil into N flat panels defined by a set of $N + 1$ nodes.

12.4 Vortex panel method

In Section 12.3, we introduced vortex panels with constant or linear density distributions and studied the properties of the induced flows. In this section, we employ these flows as elementary units into a vortex-panel method that allows us to compute an irrotational flow past a two-dimensional airfoil with the Kutta–Joukowski condition satisfied at the trailing edge.

The key idea is to express a flow of interest as a superposition of (a) an incident streaming flow and (b) a collection of flows induced by vortex panels with *a priori* unknown strength densities distributed around an airfoil. The panel strength densities are then computed to satisfy the no-penetration boundary condition around the airfoil.

Contour discretization

Shown in Figure 12.4.1 is a schematic illustration of uniform (streaming) flow with velocity $\mathbf{U} = (U_x, U_y)$ past an airfoil for angle of attack α . In the first step of the vortex panel method, the contour of the airfoil is traced with $N + 1$ nodes distributed in the clockwise direction, where points labeled 1 and $N + 1$ coincide with the trailing edge.

A pair of successive nodes, $\mathbf{x}^{(i)}$ and $\mathbf{x}^{(i+1)}$, defines a flat vortex panel labeled i for $i = 1, \dots, N$. The union of the N vortex panels defines a polygonal contour which is an approximation to the generally curved contour of the airfoil.

Flow representation

In the vortex-panel method, the velocity at a field point, $\mathbf{x} = (x, y)$, is expressed by the

superposition

$$\mathbf{u}(x, y) = \mathbf{U} + \sum_{i=1}^N \mathbf{u}^{(i)}(x, y), \quad (12.4.1)$$

where $\mathbf{u}^{(i)}(x, y)$ is the velocity induced by the i th vortex panel.

In the implementation discussed in this section, panels with linear strength density are employed. The strength density of the i th panel varies linearly from the value γ_i assigned to the i th node, which is the first point of the i th panel, to the value γ_{i+1} assigned to the $i + 1$ node, which is the second point of the i th panel. The $N + 1$ unknown values, γ_i for $i = 1, \dots, N + 1$, must be computed to satisfy the no-penetration condition around the airfoil in some approximate sense.

A key observation that the velocity induced by the i th panel, $\mathbf{u}^{(i)}(x, y)$, is determined by the position and strength density of the panel at the two end points. To signify this dependence, we write

$$\mathbf{u}^{(i)}(x, y) = \mathbf{u}^{\text{LVP}}(x, y; \mathbf{x}^{(i)}, \mathbf{x}^{(i+1)}, \gamma^{(i)}, \gamma^{(i+1)}). \quad (12.4.2)$$

where LVP stands for *linear vortex panel*. Next, we proceed to develop a method for computing the velocity induced by the individual panels.

Panel-induced velocity in global coordinates

It is helpful to introduce a local coordinate system, (x', y') , where the x' axis passes through the two end points of the i th panel, $\mathbf{x}^{(i)}$ and $\mathbf{x}^{(i+1)}$, and set the origin at the first end point $\mathbf{x}^{(i)}$, as shown in [Figure 12.4.1](#). The coordinates of a point in the local system, (x', y') , are related to those in the global system, (x, y) , by the equations

$$\begin{aligned} x' &= (x - x^{(i)}) \cos \theta^{(i)} + (y - y^{(i)}) \sin \theta^{(i)}, \\ y' &= -(x - x^{(i)}) \sin \theta^{(i)} + (y - y^{(i)}) \cos \theta^{(i)}, \end{aligned} \quad (12.4.3)$$

where $\theta^{(i)}$ is the inclination of the i th panel defined in [Figure 12.4.1](#).

Next, we express the strength density of the i th panel in the linear form

$$\gamma(x') = \gamma^{(0)} + \gamma^{(1)}(x' - x'^{(i)}), \quad (12.4.4)$$

with the understanding that $x'^{(i)} = 0$, and require that

$$\begin{aligned} \gamma(x' = x'^{(i)}) &= \gamma^{(0)} = \gamma^{(i)}, \\ \gamma(x' = x'^{(i+1)}) &= \gamma^{(0)} + \gamma^{(1)}(x'^{(i+1)} - x'^{(i)}) = \gamma^{(i+1)}, \end{aligned} \quad (12.4.5)$$

to find that

$$\gamma^{(0)} = \gamma^{(i)}, \quad \gamma^{(1)} = \frac{\gamma^{(i+1)} - \gamma^{(i)}}{\Delta \ell_i}, \quad (12.4.6)$$

where

$$\Delta\ell_i = \left((x^{(i+1)} - x^{(i)})^2 + (y^{(i+1)} - y^{(i)})^2 \right)^{1/2} = x'^{(i+1)} - x'^{(i)} \quad (12.4.7)$$

is the length of the i th panel computed in terms of the global (unprimed) or local (primed) coordinates of the two panel end-points.

Reviewing the results of Section 12.3, we find that the x' and y' components of the velocity induced by the i th panel are given by equations (12.3.30) and (12.3.31), subject to the following substitutions:

$$\begin{aligned} a &\rightarrow 0 \\ b &\rightarrow x'^{(i+1)} \\ \gamma^{(0)} &\rightarrow \gamma^{(i)} \\ \gamma^{(1)} &\rightarrow (\gamma^{(i+1)} - \gamma^{(i)})/\Delta\ell_i \\ x &\rightarrow x' \\ y &\rightarrow y' \end{aligned} \quad (12.4.8)$$

After carrying out some algebra, we find that the velocity components of the flow induced by the i th panel in the local frame are given by

$$u_{x'}^{(i)}(x', y') = a_{x'}^{(i,1)}\gamma^{(i)} + a_{x'}^{(i,2)}\gamma^{(i+1)}, \quad (12.4.9)$$

and

$$u_{y'}^{(i)}(x', y') = a_{y'}^{(i,1)}\gamma^{(i)} + a_{y'}^{(i,2)}\gamma^{(i+1)}, \quad (12.4.10)$$

where $a_{x'}^{(i,1)}$, $a_{x'}^{(i,2)}$, $a_{y'}^{(i,1)}$, and $a_{y'}^{(i,2)}$ are *local influence coefficients* given by

$$\begin{aligned} a_{x'}^{(i,1)} &= \frac{1}{2\pi x'_2} (y'c + (x' - x'_2) \Delta\theta'), \\ a_{y'}^{(i,1)} &= \frac{1}{2\pi x'_2} ((x' - x'_2)c - y' \Delta\theta' + x'_2), \\ a_{x'}^{(i,2)} &= -\frac{1}{2\pi x'_2} (y'c + x' \Delta\theta'), \\ a_{y'}^{(i,2)} &= -\frac{1}{2\pi x'_2} (x'c - y' \Delta\theta' + x'_2), \end{aligned} \quad (12.4.11)$$

subject to the following definitions:

$$\begin{aligned} x'_2 &\equiv x'^{(i+1)}, & \Delta\theta' &\equiv \theta'_2 - \theta'_1, & \theta'_2 &\equiv \arctan \frac{y'}{x' - x'_2}, \\ \theta'_1 &\equiv \arctan \frac{y'}{x'}, & c &\equiv \log \left(\frac{(x' - x'_2)^2 + y'^2}{x'^2 + y'^2} \right)^{1/2}. \end{aligned} \quad (12.4.12)$$

To recover the velocity components in the global frame, we use the inverse of the coordinate transformation shown in (12.4.3),

$$u_x^{(i)}(x, y) = u_{x'}^{(i)}(x', y') \cos \theta^{(i)} - u_{y'}^{(i)}(x', y') \sin \theta^{(i)} \quad (12.4.13)$$

and

$$u_y^{(i)}(x, y) = u_{x'}^{(i)}(x', y') \sin \theta^{(i)} + u_{y'}^{(i)}(x', y') \cos \theta^{(i)}. \quad (12.4.14)$$

Substituting expressions (12.4.9) and (12.4.10) into the right-hand sides of equations (12.4.13) and (12.4.14), and rearranging, we derive explicit relations in terms of the strength of the vortex panel at the end points,

$$\begin{aligned} u_x^{(i)}(x, y) &= a_x^{(i,1)} \gamma^{(i)} + a_x^{(i,2)} \gamma^{(i+1)}, \\ u_y^{(i)}(x, y) &= a_y^{(i,1)} \gamma^{(i)} + a_y^{(i,2)} \gamma^{(i+1)}, \end{aligned} \quad (12.4.15)$$

where $a_x^{(i,1)}$, $a_x^{(i,2)}$, $a_y^{(i,1)}$, and $a_y^{(i,2)}$ are *global influence coefficients* given by

$$\begin{aligned} a_x^{(i,1)}(x, y) &= a_{x'}^{(i,1)}(x', y') \cos \theta^{(i)} - a_{y'}^{(i,1)}(x', y') \sin \theta^{(i)}, \\ a_x^{(i,2)}(x, y) &= a_{x'}^{(i,2)}(x', y') \cos \theta^{(i)} - a_{y'}^{(i,2)}(x', y') \sin \theta^{(i)}, \\ a_y^{(i,1)}(x, y) &= a_{x'}^{(i,1)}(x', y') \sin \theta^{(i)} + a_{y'}^{(i,1)}(x', y') \cos \theta^{(i)}, \\ a_y^{(i,2)}(x, y) &= a_{x'}^{(i,2)}(x', y') \sin \theta^{(i)} + a_{y'}^{(i,2)}(x', y') \cos \theta^{(i)}. \end{aligned} \quad (12.4.16)$$

Given the coordinates of the evaluation point, (x, y) , we may evaluate these coefficients by carrying out the following steps:

1. Compute the panel inclination angle, $\theta^{(i)}$, and the panel length from the expressions given in (12.4.6) and (12.4.7).
2. Compute the local coordinates (x', y') using (12.4.3).
3. Compute the local influence coefficients using (12.4.11).
4. Compute the global influence coefficients using (12.4.16).

The procedure is readily implemented in a computer code.

12.4.1 Velocity in terms of the panel strength

Substituting expressions (12.4.15) into the right-hand side of (12.4.1), we obtain explicit expressions for the global components of the velocity in terms of the strength of the vortex panels at the end-nodes,

$$\begin{aligned} u_x(x, y) &= U_x + \sum_{i=1}^N (a_x^{(i,1)}(x, y) \gamma^{(i)} + a_x^{(i,2)}(x, y) \gamma^{(i+1)}), \\ u_y(x, y) &= U_y + \sum_{i=1}^N (a_y^{(i,1)}(x, y) \gamma^{(i)} + a_y^{(i,2)}(x, y) \gamma^{(i+1)}). \end{aligned} \quad (12.4.17)$$

For convenience, we write

$$\begin{aligned} u_x(x, y) &= U_x + \sum_{i=1}^{N+1} b_x^{(i)}(x, y) \gamma^{(i)}, \\ u_y(x, y) &= U_y + \sum_{i=1}^{N+1} b_y^{(i)}(x, y) \gamma^{(i)}, \end{aligned} \quad (12.4.18)$$

where

$$\begin{aligned} b_w^{(1)}(x, y) &= a_w^{(1,1)}(x, y), \\ b_w^{(2)}(x, y) &= a_w^{(1,2)}(x, y) + a_w^{(2,1)}(x, y), \\ b_w^{(3)}(x, y) &= a_w^{(2,2)}(x, y) + a_w^{(3,1)}(x, y), \\ &\dots, \\ b_w^{(N)}(x, y) &= a_w^{(N-1,2)}(x, y) + a_w^{(N,1)}(x, y), \\ b_w^{(N+1)}(x, y) &= a_w^{(N,2)}(x, y), \end{aligned} \quad (12.4.19)$$

for $w = x, y$ is a new set of influence coefficients.

12.4.2 Point collocation

If we knew the strength of the vortex panels at the nodes, we would be able to use equations (12.4.18) to evaluate the velocity at any point in the flow. The fundamental idea underlying the vortex-panel method is that the $N + 1$ unknown values, $\gamma^{(i)}$ for $i = 1, \dots, N + 1$, should be computed to satisfy the no-penetration condition at a point \mathbf{x} located around the airfoil contour,

$$\mathbf{u}(\mathbf{x}) \cdot \mathbf{n}(\mathbf{x}) = 0, \quad (12.4.20)$$

where \mathbf{n} is the unit vector normal to the airfoil.

In the panel-collocation method, N equations emerge by requiring that (12.4.20) is satisfied at the mid-point of each panel located at

$$\mathbf{x}_M^{(j)} = \frac{1}{2} (\mathbf{x}^{(j)} + \mathbf{x}^{(j+1)}) \quad (12.4.21)$$

for $j = 1, \dots, N$. Using (12.4.18) to express the velocity in terms of the strength of the vortex sheet and rearranging, we obtain

$$\sum_{i=1}^{N+1} A_{i,j} \gamma^{(i)} = -U_x n_x(x_M^{(j)}, y_M^{(j)}) - U_y n_y(x_M^{(j)}, y_M^{(j)}), \quad (12.4.22)$$

where

$$A_{i,j} \equiv b_x^{(i)}(x_M^{(j)}, y_M^{(j)}) n_x(x_M^{(j)}, y_M^{(j)}) + b_y^{(i)}(x_M^{(j)}, y_M^{(j)}) n_y(x_M^{(j)}, y_M^{(j)}). \quad (12.4.23)$$

It is important to bear in mind that, when $i = j$, the self-induced velocity is evaluated at the mid-point of the panel on the side of the flow exterior to the airfoil. With reference to equations (12.4.11), this means that $y' = 0$, $c = 0$, and $\Delta\theta' = \pi$. Applying equation (12.4.22) for $j = 1, \dots, N$, we obtain a system of N linear algebraic equations for the $N + 1$ unknowns, $\gamma^{(i)}$.

Kutta–Joukowski condition

One degree of freedom is available and can be used to arbitrarily specify the circulation around the airfoil. In Section 12.4.2, we saw that, in practice, the circulation established around the airfoil is such that the Kutta–Joukowski condition is fulfilled at the trailing edge.

In our formulation, the Kutta–Joukowski condition is implemented by requiring that the strength of the vortex sheet on the upper side of the airfoil at the trailing edge is equal in magnitude and opposite in sign to the strength of the vortex sheet on the lower side of the airfoil at the trailing edge. The mathematical statement of the Kutta–Joukowski condition is then

$$\gamma^{(1)} = -\gamma^{(N+1)}. \quad (12.4.24)$$

Appending this equation to equation (12.4.22) written for $j = 1, \dots, N$, we obtain the desired system of $N + 1$ equations for the $N + 1$ unknowns, $\gamma^{(i)}$. The solution can be computed using, for example, the method of Gauss elimination discussed in Section 3.4.

12.4.3 Circulation and pressure coefficient

Once the strength of the vortex sheet is available, the tangential velocity, $u_t = \mathbf{u} \cdot \mathbf{t}$, can be evaluated from the discrete representation (12.4.18), where \mathbf{t} is the unit vector tangent to the airfoil pointing along the local x' axis.

The circulation around the airfoil can be approximated either with the expression

$$C = - \sum_{i=1}^N u_t(\mathbf{x}_M^{(i)}) \Delta\ell_i \quad (12.4.25)$$

or with the expression

$$C = \frac{1}{2} \sum_{i=1}^N (\gamma^{(i)} + \gamma^{(i+1)}) \Delta\ell_i, \quad (12.4.26)$$

where $\Delta\ell_i$ is the length of the i th panel. The second expression implements the trapezoidal rule for integrating the strength of the vortex sheet with respect to arc length, ℓ , around the airfoil.

The dimensionless pressure coefficient at the panel mid-points is defined by the expression

$$c_p^{(i)} \equiv \frac{p(\mathbf{x}_M^{(i)}) - p_\infty}{\frac{1}{2}\rho U^2} = 1 - \frac{u_i^2(\mathbf{x}_M^{(i)})}{U^2}, \quad (12.4.27)$$

where p_∞ is the pressure at infinity and

$$U^2 \equiv U_x^2 + U_y^2 \quad (12.4.28)$$

is the square of the magnitude of the velocity of the incident streaming flow.

The streamline pattern, distribution of panel strength, and distribution of the pressure coefficient around a NACA airfoil computed by the code *airf_2d.lvp* discussed in Section 12.4.5 is shown in Figure 12.4.2. The results confirm that high pressure occurs at the lower surface of the airfoil and low pressure occurs at the upper surface of the airfoil; the difference generates a lift force.

12.4.4 Lift

In the absence of viscous stresses, the force exerted on the airfoil is given by the pressure integral

$$\mathbf{F} = \oint (-p) \mathbf{n} \, d\ell = -\frac{1}{2} \rho U^2 \oint \left(c_p + \frac{p^\infty}{\frac{1}{2}\rho U^2} \right) \mathbf{n} \, d\ell, \quad (12.4.29)$$

where \mathbf{n} is the unit vector normal to the airfoil pointing into the fluid, and ℓ is the arc length around the airfoil. Since the integral of the normal vector around a closed contour is identically zero,

$$\mathbf{F} = -\frac{1}{2} \rho U^2 \oint c_p \mathbf{n} \, d\ell, \quad (12.4.30)$$

Using the mid-point rule to approximate the two scalar components of the vector integral in (12.4.30), we obtain the following expressions for the dimensionless x and y force components,

$$\hat{F}_x \equiv \frac{F_x}{\frac{1}{2}\rho U^2} = - \sum_{i=1}^N c_p^{(i)} n_x^{(i)} \Delta\ell_i \quad (12.4.31)$$

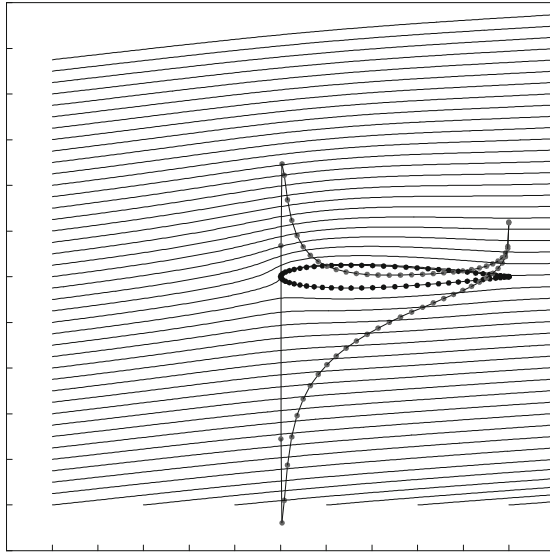
and

$$\hat{F}_y \equiv \frac{F_y}{\frac{1}{2}\rho U^2} = - \sum_{i=1}^N c_p^{(i)} n_y^{(i)} \Delta\ell_i. \quad (12.4.32)$$

The scaled lift force with respect to the wind axis is defined as the component of the force normal to the direction of the incident flow, given by

$$\hat{L}_w = \hat{F}_y \cos \alpha - \hat{F}_x \sin \alpha, \quad (12.4.33)$$

(a)



(b)

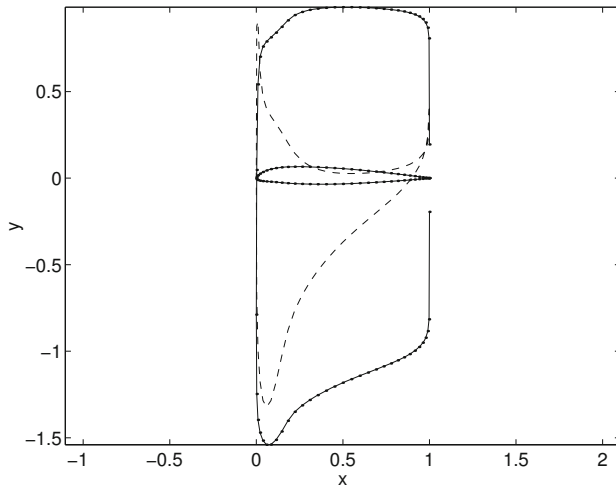


Figure 12.4.2 (a) Streamline pattern and distribution of the pressure coefficient on the upper and lower surfaces of an airfoil for angle of attack $\alpha = 5^\circ$, computed using the linear vortex panel method. (b) Distribution of the pressure coefficient (dashed line) and panel strength (connected dots) around another airfoil. These solutions were generated by the FDLIB code *airf_2d_lvp*.

where α is the angle of attack, as shown in [Figure 12.4.1](#). According to the Kutta–Joukowski theorem expressed by equation (12.2.4),

$$\hat{L}_w = -2 \frac{C}{U}. \quad (12.4.34)$$

The difference in the values of the lift predicted by (12.4.33) or (12.4.34) is a measure of the accuracy of the numerical method.

12.4.5 Vortex panel code

The following MATLAB code entitled *airf_2d.lvp*, located in directory *07_ptf* of *FDLIB*, implements the linear vortex panel method:

```
%=====
% linear vortex panel method
%=====

Npl = 64; % number of panels
chord = 1.0; % chord
thick = 0.1; % airfoil thickness
Umag = 1.0; % incident velocity
alpha = 4.0; % angle of attack in degrees

%----
% generate the NACA 23012 airfoil contour
% ep are the panel end points
%----

ep = naca(chord,thick,Npl);

%---
% coordinates of the panel end points
%---

for i=1:Npl
    pt1(i,1) = ep(i,1);
    pt1(i,2) = ep(i,2);
    pt2(i,1) = ep(i+1,1);
    pt2(i,2) = ep(i+1,2);
end

%-----
% compute:
%
% 1. panel inclination angle th(j) between -pi and pi
% 2. panel lengths
% 3. tangential and normal unit vectors
%-----
```

```

for i=1:Npl
    dx = pt2(i,1)-pt1(i,1);
    dy = pt2(i,2)-pt1(i,2);
    dl(i) = sqrt( (pt2(i,1)-pt1(i,1))^2 ...    % panel length
                + (pt2(i,2)-pt1(i,2))^2);
    th(i) = atan2(dy,dx);
    tnx(i) = cos(th(i));    % tangential vector
    tny(i) = sin(th(i));
    vnx(i) = -tny(i);    % normal vector points into flow
    vny(i) = tnx(i);
end

%---
% collocation points are panel mid-points
%---

for i=1:Npl
    co(i,1) = 0.5*(pt1(i,1)+pt2(i,1));
    co(i,2) = 0.5*(pt1(i,2)+pt2(i,2));
end

%-----
% compute the influence coefficients
% and right-hand side of linear system
%-----

for i=1:Npl    % OVER COLLOCATION POINTS; ENDS AT THE RABBIT

%---
% compute influence of jth panel
% on ith collocation point
%---

for j=1:Npl    % OVER PANELS; ENDS AT THE DOG

%---
% Compute the local panel coordinates (x, y)
% The first panel point is located at the shifted origin;
% the panel becomes horizontal
%---

xt = co(i,1) - pt1(j,1);    % shift collocation point
yt = co(i,2) - pt1(j,2);
x = xt*tnx(j) + yt*tny(j);    % and rotate
y = -xt*tny(j) + yt*tnx(j);
x1 = 0.0; y1 = 0.0;
x2t = pt2(j,1) - pt1(j,1);    % shift second-end point
y2t = pt2(j,2) - pt1(j,2);

```

```

x2 = x2t*tnx(j) + y2t*tny(j); % and rotate y2 = 0.0;

%---
% Compute radial distances: r1, r2
% subtended angles: th1, th2
%---

r1 = sqrt(x*x+y*y);
r2 = sqrt((x-x2)*(x-x2)+y*y);
th1 = atan2(y,x);
th2 = atan2(y,x-x2);

%-----
% gamma1, gamma2 are the vortex sheet strengths
% at the first and second panel points.
%
% Compute influence coefficients associated with
% the velocity components (ux, uy)
% corresponding to gamma1 and gamma, so that:
%
% ux = ax1*gamma1 + ax2*gamma2
% uy = ay1*gamma1 + ay2*gamma2
%
% These velocities are in
% the jth-panel reference frame.
%-----

if(i==j) % self-induced velocity
    ax1 = 0.5*(x/x2-1.0);
    ay1 = 1.0/(2*pi);
    ax2 = -0.5*x/x2;
    ay2 = -1.0/(2*pi);
else
    dth = th2-th1;
    rrt = r2/r1;
    rrt1 = log(rrt);
    fcc = 1.0/(2*pi*x2);
    ax1 = fcc*( y*rrt1 + (x-x2)*dth );
    ay1 = fcc*((x-x2)*rrt1 - y*dth + x2);
    ax2 = -fcc*(y*rrt1 + x*dth );
    ay2 = -fcc*(x*rrt1 - y*dth + x2);
end

%---
% transform the influence coefficient into the
% global reference frame by rotation
%---

ux1 = ax1*tnx(j) - ay1*tny(j);

```

```

uy1 = ax1*tny(j) + ay1*tnx(j);
ux2 = ax2*tnx(j) - ay2*tny(j);
uy2 = ax2*tny(j) + ay2*tnx(j);

%-----
% Compute the coefficients of gamma in the
% master influence matrix.
%
% These are the velocity influence coefficients
% projected onto the normal vector of ith panel
%-----

if(j==1)
    a(i,1)= ux1*vnx(i) + uy1*vny(i);
    holda = ux2*vnx(i) + uy2*vny(i); % hold for the next panel
elseif(j==Npl)
    a(i,Npl) = ux1*vnx(i) + uy1*vny(i) + holda;
    a(i,Npl+1) = ux2*vnx(i) + uy2*vny(i);
else
    a(i,j)= ux1*vnx(i) + uy1*vny(i) + holda;
    holda = ux2*vnx(i) + uy2*vny(i); % hold for the next panel
end

%-----
% b are tangential velocity influence coefficients
%
% These are the velocity influence coefficients
% projected onto the tangential vector of the ith panel
%-----

if(j==1)
    b(i,1)= ux1*tnx(i) + uy1*tny(i);
    holdb = ux2*tnx(i) + uy2*tny(i); % hold for the next panel
elseif(j==Npl)
    b(i,Npl) = ux1*tnx(i) + uy1*tny(i) + holdb;
    b(i,Npl+1) = ux2*tnx(i) + uy2*tny(i);
else
    b(i,j)= ux1*tnx(i) + uy1*tny(i) + holdb;
    holdb = ux2*tnx(i) + uy2*tny(i); % hold for the next panel
end

end % OVER PANELS - DOG

end % OVER COLLOCATION POINTS - RABBIT

%-----
% Add the Kutta condition
% expressed by the Npl+1 equation:
%
```

```

% The strength of the sheet at the first point
% of the first panel is equal and opposite
% to the strength of the sheet at the last point
% of the last panel,
% so that the mean value vanishes
%-----

a(Npl+1,1) = 1.0;
a(Npl+1,Npl+1) = 1.0;

%-----
% set right-hand side
%-----

al = alpha*pi/180.0;
cal = cos(al); sal = sin(al);
Ux = Umag*cal; Uy = Umag*sal;

for i=1:Npl
    rhs(i) = -Ux*vnx(i)-Uy*vny(i);
end

rhs(Npl+1)=0.0;

%-----
% solve the linear system
%-----

gamma = rhs/a';

%-----
% compute c_p and the circulation
%-----

circul = 0.0; % circulation
circulg = 0.0; % circulation in terms of gamma

for i=1:Npl
    velt = Ux*tnx(i)+Uy*tny(i); % tangential velocity
    for j=1:Npl+1
        velt = velt + b(i,j)*gamma(j);
    end
    circul = circul - velt*dl(i); % circulation
    circulg = circulg ...
        +0.5*(gamma(i)+gamma(i+1))*dl(i); % circulation
    cp(i) = 1.0-velt*velt/(Umag*Umag); % press coeff
end

cp(Npl+1)=cp(1);

```

```

%---
% plotting
%---

patch(ep(:,1),ep(:,2),'y')
plot(ep(:,1),ep(:,2),'k.-')
plot(ep(:,1),cp,'--')
plot(ep(:,1),gamma,'r:')
xlabel('x','fontsize',15)
ylabel('y','fontsize',15)

```

The airfoil profile is generated by the following MATLAB function entitled *naca*, located in directory *07_ptf* of *FDLIB*:

```

function [ep] = naca(chord,thick,Npl)

%----
% generate the NACA 23012 airfoil contour
% ep are the panel end-points
%----

dpsi = 2*pi/Npl;

ep(1,1) = chord;
ep(1,2) = 0.0;

for i=2:Npl

    psi = (i-1.0)*dpsi;
    x = 0.5*(1.0+cos(psi));

%---
% camber line:
%---

    if(x<0.2025)
        yc = 2.6595*x*(0.1147+x*(-0.6075+x));
    else
        yc = 0.02208*(1.0-x);
    end

%---
% thickness:
%---

    yt = 5.0*thick*(0.2969*sqrt(x) ...
        -0.1260*x -0.3516*x*x +0.2843*x*x*x ...
        -0.1036*x*x*x*x );

```



```

if(i<=(Npl/2+1))
    y = yc-yt;
else
    y = yc+yt;
end

ep(i,1) = x*chord;
ep(i,2) = y*chord;
end

ep(Npl+1,1) = chord; % trailing edge
ep(Npl+1,2) = 0.0; % trailing edge

%---
% done
%---

return

```

The graphics display generated by the code is shown in [Figure 12.4.2\(b\)](#). The dots connected by a line describes the distribution of the panel strength, and the dashed line describes the distribution of the pressure coefficient.

PROBLEM

12.4.1 Linear vortex panel method

(a) Run the code *airf_2d.lvp* for an airfoil shape of your choice. Prepare graphs and discuss the distribution of the panel strength and pressure coefficient.

(b) Evaluate the velocity at several points inside the airfoil and discuss the results.

12.5 Vortex sheet representation

Consider the vortex panel method for flow past a two-dimensional airfoil discussed in Section 12.4. In the limit as the number of panels, N , tends to infinity, the piecewise linear strength distributions over the individual panels describe a smooth distribution defined around the airfoil contour. Correspondingly, the sum on the right-hand side of equation (12.4.1) reduces to an integral with respect to arc length around the airfoil contour, representing the velocity induced by a vortex sheet with a generally curved shape.

Generalizing expression (12.3.8), we find that the stream function associated with the vortex sheet is given by

$$\psi^{\text{vortex sheet}}(x, y) = -\frac{1}{4\pi} \oint \ln \frac{(x-x')^2 + (y-y')^2}{\rho^2} \gamma(x') d\ell', \quad (12.5.1)$$

where $d\ell' = (dx'^2 + dy'^2)^{1/2}$ is the differential arc length around the airfoil measured in the

clockwise direction starting at the trailing edge, and the integration is performed around the airfoil contour.

Conversely, the vortex-panel representation can be regarded as the result of discretizing the integral on the right-hand side of (12.5.1) into geometrical elements represented by the vortex panels. In Section 12.4, we discussed straight elements with linear strength distribution. In more advanced implementations, curved elements, such as sections of parabolas and circular arcs, and quadratic or higher-order strength density distributions are employed.

Internal flow

Although the vortex sheet representation is physically meaningful only when it is applied to evaluate the stream function and velocity at a point in the flow, nothing prevents us from performing corresponding evaluations at a point inside the airfoil. When this is done, we find that the stream function is constant and the velocity vanishes inside the airfoil (Problem 12.5.2).

To explain this curiosity, we observe that the strength of the vortex sheet is computed to satisfy the no-penetration boundary condition around the airfoil. Because the normal component of the velocity is continuous across the vortex sheet, the interior flow occurs under vanishing normal boundary velocity. Since tangential velocity on the interior side of the airfoil is prohibited by the condition of irrotational motion in the absence of singular points, the fictitious internal flow must vanish.

12.5.1 Thin airfoil theory

Next, we consider flow past a thin cambered airfoil and introduce a system of coordinates such that the leading edge lies at the origin of the x axis, and the trailing edge lies at the point $x = c$ along the x axis, as illustrated in Figure 12.5.1. The camberline is described by the equation

$$y = \epsilon \eta_c(x), \quad (12.5.2)$$

where $\epsilon \ll 1$ is a small dimensionless number and $\eta_c(x)$ is the camberline shape function required to satisfy the geometrical constraints

$$\eta_c(0) = 0, \quad \eta_c(c) = 0. \quad (12.5.3)$$

If $\eta_c(x) = 0$ for any x , the camberline is flat.

Because both sides of the airfoil are near the x axis, the corresponding line integrals with respect to arc length in (12.5.1) can be approximated with integrals with respect to x' from $x' = 0$ to c . Setting $y' = 0$, tracing the airfoil in the clockwise direction beginning from the trailing edge, and noting that on the upper side of the airfoil $d\ell' = dx'$ while on the lower side $d\ell' = -dx'$, we find that

$$\psi^{\text{vortex sheet}}(x, y) \simeq -\frac{1}{4\pi} \int_0^c \ln \frac{(x-x')^2 + y^2}{\rho^2} (\gamma^+ - \gamma^-)(x') dx', \quad (12.5.4)$$

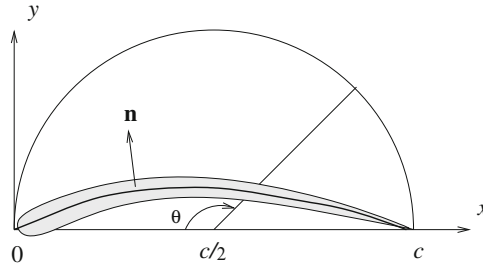


Figure 12.5.1 Illustration of the camberline of a thin airfoil, and definition of variables used to develop the slender-airfoil theory.

where the superscripts + and - denote, respectively, the upper and lower side of the camberline. Defining

$$\chi \equiv \gamma^+ - \gamma^-, \tag{12.5.5}$$

we obtain a representation in terms of an effective flat vortex sheet extending between the leading and trailing edge,

$$\psi^{\text{vortex sheet}}(x, y) \simeq -\frac{1}{4\pi} \int_0^c \ln \frac{(x - x')^2 + y^2}{\rho^2} \chi(x') \, dx'. \tag{12.5.6}$$

The corresponding velocity potential is given by

$$\phi^{\text{vortex sheet}}(x, y) \simeq \frac{1}{2\pi} \int_0^c \arctan \left(\frac{y}{x - x'} \right) \chi(x') \, dx'. \tag{12.5.7}$$

Our goal is to compute the strength of the effective vortex sheet, χ , so as to satisfy the no-penetration condition around the airfoil.

Velocity on either side of the vortex sheet

As a preliminary, we consider the velocity induced by the effective vortex sheet on the upper and lower sides of the airfoil. To begin, we consider the limit of the velocity potential as the evaluation point, $\mathbf{x} = (x, y)$, approaches the vortex sheet from the upper side; that is, as $y \rightarrow 0_+$ with $0 < x < c$. In this limit, the inverse tangent function on the right-hand side of (12.5.7) is zero when $x' < x$, or π when $x' > x$. Consequently, the potential takes the value

$$\phi^{\text{vortex sheet}}(x, y \rightarrow 0_+) = \frac{1}{2} \int_x^c \chi(x') \, dx'. \tag{12.5.8}$$

Differentiating this expression with respect to x , we find that the x velocity component is given by

$$u_x^{\text{vortex sheet}}(x, y \rightarrow 0_+) = -\frac{1}{2} \chi(x). \tag{12.5.9}$$

Working in a similar fashion for the lower side of the airfoil, we obtain

$$u_x^{\text{vortex sheet}}(x, y \rightarrow 0_-) = \frac{1}{2} \chi(x). \quad (12.5.10)$$

The last two equations illustrate once again that the velocity undergoes a discontinuity whose magnitude is equal to the strength of the vortex sheet.

The y velocity component over the airfoil can be found by differentiating either the stream function given in (12.5.6) with respect to x or the velocity potential given in (12.5.7) with respect to y . Either way, we find that

$$u_y^{\text{vortex sheet}}(x, y = 0_{\pm}) = \frac{1}{2\pi} \int_0^c \frac{\chi(x')}{x - x'} dx'. \quad (12.5.11)$$

Unlike the x velocity component, the y velocity component remains continuous across the vortex sheet.

Asymptotics

To compute the strength of the effective vortex sheet, χ , we implement the no-penetration boundary condition through a series of approximations that may appear drastic but have a solid theoretical foundation.

First, we replace the disturbance flow due to the airfoil with the flow due to the effective vortex sheet expressed by (12.5.6) or (12.5.7). Enforcing the no-penetration boundary condition at the camberline, we obtain

$$\mathbf{n} \cdot (\mathbf{U} + \mathbf{u}^{\text{vortex sheet}}(y = \epsilon\eta_c)) = 0, \quad (12.5.12)$$

where \mathbf{n} is the unit vector normal to the camberline on the upper side, pointing into the fluid. Using the geometrical representation (12.5.2), we find that

$$n_x = -\epsilon \frac{\eta'_c}{\sqrt{1 + \epsilon^2 \eta_c'^2}}, \quad n_y = \frac{1}{\sqrt{1 + \epsilon^2 \eta_c'^2}}, \quad (12.5.13)$$

where $\eta'_c = d\eta_c/dx$. Because ϵ has been assumed small, the denominators can be replaced by unity, yielding the simplified expressions

$$n_x \simeq -\epsilon \frac{d\eta_c}{dx}, \quad n_y \simeq 1. \quad (12.5.14)$$

A second approximation arises by replacing the velocity at the upper side of the camberline with the velocity at the upper side of the effective vortex sheet, given in (12.5.9) and (12.5.11).

Substituting (12.5.14), (12.5.9), and (12.5.11) into (12.5.12), we obtain

$$-\epsilon \frac{d\eta_c}{dx} \left(U_x - \frac{1}{2} \chi(x) \right) + U_y + \frac{1}{2\pi} \int_0^c \frac{\chi(x')}{x - x'} dx' = 0. \quad (12.5.15)$$

Next, we confine our attention to flow that is nearly parallel to the x axis, thereby assuming that U_y is small compared to U_x . Writing

$$U_y = \tan \alpha U_x \simeq \alpha U_x, \tag{12.5.16}$$

we obtain

$$-\epsilon \left(\frac{d\eta_c}{dx} \right)_x \left(U_x - \frac{1}{2} \chi(x) \right) + \alpha U_x + \frac{1}{2\pi} \int_0^c \frac{\chi(x')}{x-x'} dx' = 0, \tag{12.5.17}$$

where α is the angle of attack.

Inspecting the various terms on the left-hand side of equation (12.5.17), we find that the magnitude of χ is on the order of ϵ or α , both of which have been assumed small. Since χ is negligible compared to U_x , it can be discarded from the expression enclosed by the large parentheses. Rearranging, we obtain an integral equation of the first kind for $\chi(x)$,

$$\frac{1}{2\pi} \int_0^c \frac{\chi(x')}{x-x'} dx' = U_x \left(\epsilon \frac{d\eta_c}{dx} - \alpha \right) \tag{12.5.18}$$

for $0 < x < c$.

Solution by Fourier expansions

One way to solve equation (12.5.18) is by expanding the unknown function χ in a Fourier series with respect to the angle θ varying between 0 and π , defined such that

$$x = c \frac{1}{2} (1 - \cos \theta), \tag{12.5.19}$$

as illustrated in [Figure 12.5.1](#). Differentiating, we obtain

$$dx = c \frac{1}{2} \sin \theta d\theta. \tag{12.5.20}$$

The Kutta–Joukowski condition requires that the strength of the vortex sheet vanishes at the trailing edge located at $\theta = \pi$. Wind tunnel measurements show that a high peak occurs at the leading edge located at $\theta = 0$. Based on these observations, we express χ as the sum of the singular function, $\cot \frac{\theta}{2}$, and a sine Fourier series in the form

$$\chi(\theta) = 2U_x \left(a_0 \cot \frac{\theta}{2} + \sum_{n=1}^{\infty} a_n \sin(n\theta) \right), \tag{12.5.21}$$

where a_n are Fourier coefficients. Substituting (12.5.19) and (12.5.21) into (12.5.18), we obtain the equation

$$\frac{1}{\pi} \int_0^\pi \frac{\sin \theta'}{\cos \theta' - \cos \theta} \left[a_0 \cot \frac{\theta'}{2} + \sum_{n=1}^{\infty} a_n \sin(n\theta') \right] d\theta' = \epsilon \frac{d\eta_c}{dx} - \alpha. \tag{12.5.22}$$

The integrals on the left-hand side of (12.5.22) can be evaluated with the help of standard tables. First, we write

$$\cot \frac{\theta'}{2} = \frac{1 + \cos \theta'}{\sin \theta'}, \quad (12.5.23)$$

and find that

$$\int_0^\pi \frac{\sin \theta'}{\cos \theta' - \cos \theta} \cot \frac{\theta'}{2} d\theta' = \int_0^\pi \frac{1 + \cos \theta'}{\cos \theta' - \cos \theta} d\theta' = \pi. \quad (12.5.24)$$

Second, we note that

$$\int_0^\pi \frac{\sin \theta'}{\cos \theta' - \cos \theta} \sin(n\theta') d\theta' = -\pi \cos(n\theta). \quad (12.5.25)$$

Substituting these results into (12.5.22), we derive a remarkably simple expression,

$$a_0 - \sum_{n=1}^{\infty} a_n \cos(n\theta) = \epsilon \frac{d\eta_c}{dx} - \alpha. \quad (12.5.26)$$

The left-hand side of (12.5.26) is the cosine Fourier expansion of the right-hand side with respect to θ . Multiplying both sides by $\cos(m\theta)$, where m is an integer, integrating with respect to θ from 0 to π , and using the identity

$$\int_0^\pi \cos(n\theta) \cos(m\theta) d\theta = \begin{cases} 0 & \text{if } n \neq m, \\ \pi & \text{if } n = m = 0, \\ \frac{1}{2}\pi & \text{if } n = m \neq 0, \end{cases} \quad (12.5.27)$$

we obtain

$$a_0 = -\alpha + \epsilon \frac{1}{\pi} \int_0^\pi \left(\frac{d\eta_c}{dx} \right)_{x(\theta)} d\theta, \quad a_n = -\epsilon \frac{2}{\pi} \int_0^\pi \left(\frac{d\eta_c}{dx} \right)_{x(\theta)} \cos(n\theta) d\theta \quad (12.5.28)$$

for $i = n, 2, \dots$

The camberline slope, $d\eta_c/dx$, can be expanded in a cosine Fourier series with respect to θ ,

$$\left(\frac{d\eta_c}{dx} \right)_{x(\theta)} = \frac{1}{2} b_0 + \sum_{n=1}^{\infty} b_n \cos(n\theta), \quad (12.5.29)$$

where b_n are dimensionless Fourier coefficients given by

$$b_n = \frac{2}{\pi} \int_0^\pi \left(\frac{d\eta_c}{dx} \right)_{x(\theta)} \cos(n\theta) d\theta \quad (12.5.30)$$

for $n = 0, 1, \dots$. Substituting the right-hand side of (12.5.29) into (12.5.26) and setting the sum of like Fourier coefficients to zero, we obtain

$$a_0 = -\alpha + \epsilon \frac{1}{2} b_0, \quad a_n = -\epsilon b_n \quad (12.5.31)$$

for $n = 1, 2, \dots$. These relations illustrate that only the leading coefficient, a_0 , depends on the angle of attack, α , while the rest of the coefficients are determined exclusively by the geometry of the camberline.

Lift, lift coefficient, and lift slope

To compute the lift force per unit span exerted on the airfoil, we use the Kutta–Joukowski theorem expressed by equation (12.2.4), obtaining

$$L = -\rho U_x \int_0^c \chi(x) dx. \quad (12.5.32)$$

or

$$L = -\rho c U_x \frac{1}{2} \int_0^\pi \chi(\theta) \sin \theta d\theta. \quad (12.5.33)$$

Substituting the expansion (12.5.21) into the right-hand side, we obtain

$$L = -\rho c U_x^2 \int_0^\pi \left(a_0 \cot \frac{\theta}{2} + \sum_{n=1}^{\infty} a_n \sin(n\theta) \right) \sin \theta d\theta. \quad (12.5.34)$$

Evaluating the integrals, we find that only two terms make a non-zero contribution, yielding the lift force

$$L = -\pi \rho c U_x^2 \left(a_0 + \frac{1}{2} a_1 \right). \quad (12.5.35)$$

Using (12.5.31), we find that

$$L = \pi \rho c \left(\alpha - \epsilon \frac{1}{2} (b_0 + b_1) \right). \quad (12.5.36)$$

The lift coefficient is

$$c_L \equiv \frac{L}{\frac{1}{2} \rho c U_x^2} = -2\pi \left(a_0 + \frac{1}{2} a_1 \right) = 2\pi \left(\alpha - \epsilon \frac{1}{2} (b_0 + b_1) \right). \quad (12.5.37)$$

In practical aerodynamics, the performance of an airfoil is characterized by the lift slope, defined as the slope $dc_L/d\alpha$. Our analysis has shown that the lift slope of a thin airfoil is constant, equal to 2π , independent of the camber.

Pressure difference across the airfoil

The difference in the pressure on either side of the vortex sheet representing the airfoil,

$$\Delta p \equiv p(x, y \rightarrow 0_-) - p(x, y \rightarrow 0_+), \quad (12.5.38)$$

can be computed using Bernoulli's equation (6.4.18). Using expressions (12.5.9) and (12.5.10), we find that the velocity on the upper or lower side of the vortex sheet is, respectively, equal

to $U_x - \frac{1}{2}\chi$ and $U_x + \frac{1}{2}\chi$. Substituting these expressions in Bernoulli's equation for irrotational flow, we obtain

$$\Delta p = \left(p_\infty - \frac{1}{2} \rho (U_x + \frac{1}{2} \chi)^2 \right) - \left(p_\infty - \frac{1}{2} \rho (U_x - \frac{1}{2} \chi)^2 \right) = -\rho U_x \chi, \quad (12.5.39)$$

which is consistent with expression (12.5.32) for the lift force.

Pressure moment

The moment of the pressure force with respect to the leading edge is expressed by the integral

$$M = - \int_0^c x \Delta p \, dx. \quad (12.5.40)$$

Substituting expression (12.5.39) for the pressure drop, we obtain

$$M = \rho U_x \int_0^c x \chi(x) \, dx = \frac{1}{4} \rho U_x c^2 \int_0^\pi \chi(\theta) (1 - \cos \theta) \sin \theta \, d\theta. \quad (12.5.41)$$

Substituting expansion (12.5.21), we obtain

$$M = \frac{1}{2} \rho U_x^2 c^2 \int_0^\pi \left(a_0 \cot \frac{\theta}{2} + \sum_{n=1}^{\infty} a_n \sin(n\theta) \right) (1 - \cos \theta) \sin \theta \, d\theta. \quad (12.5.42)$$

Evaluating the integrals, we find

$$M = \frac{1}{4} \pi \rho c^2 U_x^2 (a_0 + a_1 - \frac{1}{2} a_2), \quad (12.5.43)$$

which shows that only three coefficients contribute to the pressure moment. The moment coefficient is defined as

$$c_M \equiv \frac{M}{\frac{1}{2} \rho c^2 U_x^2} = \frac{1}{2} \pi (a_0 + a_1 - \frac{1}{2} a_2). \quad (12.5.44)$$

The moment of the pressure forces with respect to an arbitrary point, $x = x_m$, is given by

$$M_{x_m} = - \int_0^c (x - x_m) \Delta p \, dx = M + x_m L, \quad (12.5.45)$$

where L is the lift force. Substituting expressions (12.5.35) and (12.5.43) for L and M into the right-hand side of (12.5.45), we find that

$$M_{x_m} = \pi \rho c U_x^2 \left(\frac{1}{4} c (a_0 + a_1 - \frac{1}{2} a_2) - x_m (a_0 + \frac{1}{2} a_1) \right). \quad (12.5.46)$$

When $x_m = \frac{1}{4}c$, the coefficient a_0 disappears from the right-hand side of (12.5.46) and the pressure moment becomes independent of the angle of attack, α . The quarter chord moment, $M_{c/4}$,

$$M_{c/4} = \frac{1}{8} \pi \rho c^2 U_x^2 (a_1 - a_2), \quad (12.5.47)$$

and associated moment coefficient,

$$c_{M_{c/4}} \equiv \frac{M_{c/4}}{\frac{1}{2} \rho c^2 U_x^2} = \frac{1}{4} \pi (a_1 - a_2), \quad (12.5.48)$$

are used to characterize the performance of an airfoil.

Symmetric airfoils

Since the camber of a symmetric airfoil vanishes, we may set $\epsilon = 0$ or $\eta_c(x) = 0$ in the preceding equations. Equations in (12.5.31) yield $a_0 = -\alpha$ and $a_n = 0$ for $n = 1, 2, \dots$, and expansion (12.5.21) reduces to

$$\chi = -2\alpha U_x \cot \frac{\theta}{2}. \quad (12.5.49)$$

The lift force and lift coefficient computed from equations (12.5.35) and (12.5.37) are given by

$$L = \alpha \pi \rho c U_x^2, \quad c_L = 2\alpha \pi. \quad (12.5.50)$$

The moment and moment coefficient computed from equations (12.5.43) and (12.5.44) are given by

$$M = -\alpha \pi \rho c^2 U_x^2, \quad c_M = -\frac{\alpha}{2} \pi. \quad (12.5.51)$$

PROBLEMS

12.5.1 Thin airfoil with parabolic camber

Consider a thin airfoil with parabolic camberline described by the shape function

$$\eta_c(x) = \frac{4}{c} x(c-x). \quad (12.5.52)$$

The camber is equal to $\epsilon \eta_c(\frac{1}{2}c) = \epsilon c$. Show that the lift and moment coefficients are given by

$$c_L = 2\pi(\alpha + 2\epsilon), \quad c_M = -\frac{\pi}{2}(\alpha + 4\epsilon). \quad (12.5.53)$$

Note that the lift vanishes when $\alpha = -2\epsilon$.

12.5.2 NACA 23012 airfoil

The camberline of the NACA 23012 airfoil is described as

$$\hat{y} = \begin{cases} 2.6595 (\hat{x}^3 - 0.6075\hat{x}^2 + 0.1147\hat{x}) & \text{for } 0 \leq \hat{x} \leq 0.2025, \\ 0.02208(1 - \hat{x}) & \text{for } 0.2025 \leq \hat{x} \leq 1, \end{cases} \quad (12.5.54)$$

where $\hat{x} \equiv x/c$ and $\hat{y} \equiv y/c$. Derive expressions for the lift and moment coefficients in terms of the angle of attack. Compare your results with experimental measurements for $\alpha = 4^\circ$, showing that $c_L = 0.55$ and $c_{M_{c/4}} = -0.01$.

12.5.3 Comparison of asymptotics with the vortex panel method

Consider the NACA 23012 airfoil discussed in Problem 12.5.2. Run the code `airf_2d_lvp` in directory `07_ptf` of `FDLIB` to compute the lift coefficient in wind axes. Compare the numerical results with the asymptotic predictions for small airfoil thickness.

12.6 Point-source-dipole panels

Consider the stream function of the flow induced by a vortex panel situated along the x axis between the point $x = a$ and b , as shown in equation (12.3.8), repeated below for convenience,

$$\psi^{\text{vortex panel}}(x, y) = -\frac{1}{4\pi} \int_a^b \ln \frac{(x - x')^2 + (y - y')^2}{\varrho^2} \gamma(x') dx', \quad (12.6.1)$$

with the understanding that $y' = 0$. The distribution of circulation along the panel, $\mu(x)$, is defined as the integral of the strength density of the vortex sheet with respect to x from an arbitrary point $x = d \geq a$ up to an arbitrary point $x \leq b$,

$$\mu(x) \equiv \int_d^x \gamma(x') dx', \quad (12.6.2)$$

where $a \geq x \geq b$. Using the rules of integral differentiation, we find that

$$\frac{d\mu}{dx} = \gamma. \quad (12.6.3)$$

Substituting the left-hand side of (12.6.3) into the integral of (12.6.1), and integrating by parts, we obtain

$$\begin{aligned} \psi^{\text{vortex panel}}(x, y) &= \frac{\mu(x=a)}{2\pi} \ln \frac{(x-a)^2 + (y-y')^2}{\varrho^2} \\ &\quad - \frac{\mu(x=b)}{2\pi} \ln \frac{(x-b)^2 + (y-y')^2}{\varrho^2} \\ &\quad + \frac{1}{4\pi} \int_a^b \frac{d}{dx'} \left(\ln \frac{(x-x')^2 + (y-y')^2}{\varrho^2} \right) \mu(x') dx', \end{aligned} \quad (12.6.4)$$

with the understanding that $y' = 0$ since the panel situated along the x axis. Carrying out the differentiation under the integral sign, we derive the final form

$$\begin{aligned} \psi^{\text{vortex panel}}(x, y) = & \frac{\mu(x = a)}{2\pi} \ln \frac{(x - a)^2 + (y - y')^2}{\varrho^2} \\ & - \frac{\mu(x = b)}{2\pi} \ln \frac{(x - b)^2 + (y - y')^2}{\varrho^2} - \frac{1}{2\pi} \int_a^b \frac{x - x'}{(x - x')^2 + (y - y')^2} \mu(x') dx'. \end{aligned} \quad (12.6.5)$$

The three terms on the right-hand side of (12.6.5) admits the following interpretations:

- The first term represents the flow due to a point vortex with strength $-\mu(x = a)$ situated at the first panel end-point.
- The second term represents the flow due to a point vortex with strength $\mu(x = b)$ situated at the second panel end-point.
- Comparing the third term on the right-hand side of (12.6.5) with (3.5.38), we find that the third term represents the flow due to a distribution of point-source dipoles with strength density $\mu(x')$ oriented normal to the panel. If $\mu(x')$ is positive, the dipole at the point x' is oriented toward the positive direction of the y axis. If $\mu(x')$ is negative, the dipole at the variable point x' is oriented toward the negative direction of the y axis.

Now we introduce the stream function due to a point-source dipole panel,

$$\psi^{\text{source dipole panel}}(x, y) \equiv -\frac{1}{2\pi} \int_a^b \frac{x - x'}{(x - x')^2 + (y - y')^2} \mu(x') dx', \quad (12.6.6)$$

and rearrange expression (12.6.5) to obtain

$$\begin{aligned} \psi^{\text{source dipole panel}}(x, y) = & \psi^{\text{vortex panel}}(x, y) \\ = & -\frac{\mu_a}{2\pi} \ln \frac{(x - a)^2 + (y - y')^2}{\varrho^2} + \frac{\mu_b}{2\pi} \ln \frac{(x - b)^2 + (y - y')^2}{\varrho^2}, \end{aligned} \quad (12.6.7)$$

where $\mu_a = \mu(x = a)$ and $\mu_b = \mu(x = b)$.

Equation (12.6.7) establishes a correspondence between the flow due to a source-dipole panel and the flow due to a vortex panel, subject to the differential relation (12.6.3). The first term on the right-hand side of (12.6.7) represents the flow due to a point vortex with strength μ_a placed at the first panel end-point, and the second term represents the flow due to a point vortex with strength $-\mu_b$ placed at the second panel end-point.

Panels with uniform point-source dipole strength density

When the strength density of the source-dipole distribution is constant, $\mu = \mu_0$, the strength of the vortex sheet is identically zero and the first term on the right-hand side of (12.6.7) does not appear. In that case, the flow due to the panel is identical to the flow induced by two point vortices with strengths μ_0 and $-\mu_0$ situated, respectively, at the first and second panel end-point.

12.6.1 Source-dipole panel method

The flow due to a point-source dipole panel can be used as a fundamental building block for representing and subsequently computing a flow of interest past an airfoil. To develop the source-dipole panel method, we work as with the vortex panel method discussed in Section 12.4, with some modifications. In the first step, we trace the contour of the airfoil with $N + 1$ nodes distributed in the clockwise direction, as illustrated in Figure 12.4.1. A pair of successive nodes, $\mathbf{x}^{(i)}$ and $\mathbf{x}^{(i+1)}$, defines the i th flat source-dipole panel.

In the second step, the velocity at a point in the flow is described by a superposition of the incident flow and the flows induced by the N source-dipole panels. An additional degree of freedom is required to specify the circulation around the airfoil. This degree of freedom is provided by an additional contribution mediated by a point vortex with strength κ placed at the trailing edge. The composite representation is

$$\mathbf{u}(x, y) = \mathbf{U} + \sum_{i=1}^N \mathbf{u}^{(i)}(x, y) + \mathbf{u}_{\text{at trailing edge}}^{\text{point vortex}}(x, y), \quad (12.6.8)$$

where $\mathbf{u}^{(i)}(x, y)$ is the velocity induced by the i th panel.

Uniform panels

We have seen that, if the source-dipole strength is uniform over each panel, the flow induced by the i th panel is identical to the flow induced by two point vortices with strength $\mu^{(i)}$ and $-\mu^{(i)}$ located at the first or second panel end-point, where $\mu^{(i)}$ is the constant value of the source-dipole strength density over the panel. Consequently, the i th node for $i = 2, \dots, N$ hosts two point-vortices. One point vortex with strength $-\mu^{(i-1)}$ is contributed by the $i - 1$ panel, and a second point vortex with strength $\mu^{(i)}$ is contributed by the i panel. The combined strength is $\mu^{(i)} - \mu^{(i-1)}$.

The first node, located at the trailing edge, hosts three point vortices: one due to the first panel labeled 1, a second due to the last panel labeled N , and a third circulation-producing point vortex placed at the trailing edge. The Kutta–Joukowski condition requires that the net strength of the trailing point vortex is zero,

$$\mu^{(1)} - \mu^{(N)} + \kappa = 0. \quad (12.6.9)$$

The $N + 1$ unknowns, including $\mu^{(i)}$ for $i = 1, \dots, N$ and κ , can be computed by the collocation method discussed in Section 12.3, incorporating the Kutta–Joukowski condition (12.6.9).

Linear panels

When the strength density of a source-dipole panel varies linearly with respect to arc length, all three terms on the right-hand side of (12.6.7) make a contribution to the induced velocity field. Expression (12.6.3) shows that the strength density of the equivalent vortex sheet is constant and equal to the slope of the dipole density over the panel.

In the linear source-dipole panel method, the flow is represented by a superposition of the three constituents shown in equation (12.6.8), where the dipole density over the i th panel varies linearly with respect to arc length from the initial value $\mu^{(i)}$ to the final value $\mu^{(i+1)}$. Summing the flows due to the individual panels expressed by the right-hand side of (12.6.7), and consolidating the left- and right-panel point vortices at the panel end points, we derive an equivalent representation in terms of point vortices and vortex panels with constant strength. The uniform strength density of the i th corresponding vortex panel is

$$\gamma^{(i)} \equiv \frac{\mu^{(i+1)} - \mu^{(i)}}{\Delta\ell_i}, \quad (12.6.10)$$

where $\Delta\ell_i$ is i th the panel length.

Because the dipole strength is continuous around the approximate polygonal contour of the airfoil described by the panels, the strength of the point vortices vanishes at all but the first point where it takes the value $\mu^{(1)} - \mu^{(N+1)} + \kappa$. We conclude that the linear source-dipole panel representation is equivalent to the uniform vortex panel representation supplemented by a point vortex at the trailing edge. The strength of the point vortex must vanish to satisfy the Kutta–Joukowski condition at the trailing edge, as required by equation (12.6.9).

12.6.2 Source-dipole representation

As the number of panels, N , increases, the individual panel strength density distributions join to yield a smooth distribution defined around the airfoil. Correspondingly, the sum on the right-hand side of (12.6.8) reduces to an integral with respect to arc length around the airfoil, yielding an integral representation in terms of a source-dipole sheet.

Equation (12.6.7) provides us with an expression for the stream function associated with a source-dipole panel situated over the x axis, where the source-dipoles point along the y axis. Generalizing this expression, we find that the stream function associated with source-dipole distribution around the airfoil is given by

$$\psi^{\text{source dipole sheet}}(x, y) = -\frac{1}{2\pi} \oint \frac{(x - x')n_y(\mathbf{x}') - (y - y')n_x(\mathbf{x}')}{(x - x')^2 + (y - y')^2} \mu(\mathbf{x}') d\ell', \quad (12.6.11)$$

where $d\ell' = (dx'^2 + dy'^2)^{1/2}$ is the differential arc length around the airfoil measured in the clockwise direction from a designated origin. The associated velocity potential is

$$\phi^{\text{source dipole sheet}}(x, y) = -\frac{1}{2\pi} \oint \frac{(x - x')n_x(\mathbf{x}') + (y - y')n_y(\mathbf{x}')}{(x - x')^2 + (y - y')^2} \mu(\mathbf{x}') d\ell'. \quad (12.6.12)$$

The counterpart of the panel representation (12.6.8) is

$$\mathbf{u}(x, y) = \mathbf{U} + \mathbf{u}^{\text{source dipole sheet}}(x, y) + \mathbf{u}_{\text{at trailing edge}}^{\text{point vortex}}(x, y), \quad (12.6.13)$$

where the second term on the right-hand side is the velocity corresponding to the stream function (12.6.11) and velocity potential (12.6.12). The stream function and velocity potential are given by the corresponding expressions

$$\psi(x, y) = U_x y - U_y x + \psi^{\text{source dipole sheet}}(x, y) + \psi_{\text{at trailing edge}}^{\text{point vortex}}(x, y), \quad (12.6.14)$$

and

$$\phi(x, y) = U_x x + U_y y + \phi^{\text{source dipole sheet}}(x, y) + \phi_{\text{at trailing edge}}^{\text{point vortex}}(x, y). \quad (12.6.15)$$

Conversely, the source-dipole panel representation arises from the discretization the integral on the right-hand side of (12.6.11) or (12.6.12) into geometrical elements representing source-dipole panels. In this section, we have discussed straight elements with constant and linear strength density distributions. In more advanced implementations, curved elements, such as sections of a parabola and circular arcs, and quadratic or higher-order strength density distributions are employed.

12.6.3 Solution of the interior problem

Assume that the strength of the source-dipole sheet is available such that the no-penetration condition around the airfoil is satisfied. For reasons discussed in Section 12.3, if we evaluate the right-hand sides of equations (12.6.11)–(12.6.13) at a point located inside the airfoil, we will find that the velocity vanishes and the stream function and potential take constant values. This observation suggests an alternative method of computing the strength density of the source dipoles. Instead of using the Neumann no-penetration boundary condition, we can use the Dirichlet boundary condition requiring that the potential and stream function are constant along the *interior* side of the airfoil.

Panels with constant strength density

To illustrate the implementation of the method, we discretize the airfoil contour into N flat panels with constant strength density, as illustrated in [Figure 12.4.1](#). Identifying the flow induced by each panel with the flow induced by two point vortices located at the panel end-points, as discussed earlier in this section, we obtain the potential

$$\phi(x, y) = U_x x + U_y y + \frac{1}{2\pi} \sum_{i=1}^N [\mu^{(i)}(\theta_1^{(i)} - \theta_2^{(i)})] + \frac{\kappa}{2\pi} \theta_T, \quad (12.6.16)$$

where κ is the strength of the point vortex at the trailing edge, and the angles $\theta_1^{(i)}$, $\theta_2^{(i)}$, and θ_T are defined in [Figure 12.4.1](#).

To implement the collocation method, we evaluate (12.6.16) at the mid-point of the j th panel, $(x_M^{(j)}, y_M^{(j)})$, on the interior side of the airfoil for $j = 1, \dots, N$. Next, we note that $\theta_1^{(j)} = 0$ and $\theta_2^{(j)} = -\pi$, and assign to the potential the reference value of zero to derive an

algebraic equation,

$$0 = U_x x_M^{(j)} + U_y y_M^{(j)} + \frac{1}{2\pi} \sum'_{i=1}^N [\mu^{(i)}(\theta_1^{(i)} - \theta_2^{(i)})] + \frac{1}{2} \mu^{(j+1)} + \frac{\kappa}{2\pi} \theta_T, \quad (12.6.17)$$

where the prime after the summation symbol denotes that the term $i = j$ is excluded from the sum. Rearranging (12.6.17), we derive a linear equation relating the panel source-dipole densities to the strength of the trailing-edge point vortex,

$$\frac{1}{2} \mu^{(j+1)} + \frac{1}{2\pi} \sum'_{i=1}^N [\mu^{(i)}(\theta_1^{(i)} - \theta_2^{(i)})] + \frac{\kappa}{2\pi} \theta_T = -U_x x_M^{(j)} - U_y y_M^{(j)}. \quad (12.6.18)$$

Applying this equation for $j = 1, \dots, N$, and appending to the resulting system of equations the Kutta–Joukowski condition expressed by (12.6.9), we obtain a linear system for the $N + 1$ unknowns $\mu^{(i)}$ for $i = 1, \dots, N$, and κ .

Distribution of the potential over the airfoil

Inspecting the third term on the right-hand side of (12.6.16) involving the sum, we find that the potential undergoes a discontinuity of magnitude $-\mu^{(i)}$ across the i th panel. Since the potential inside the airfoil is constant and equal to zero, the potential on the exterior side of the panel must be equal to $-\mu^{(i)}$.

This result applies in a more general context: the potential at the outer side of the airfoil is equal to the negative of the strength density of the source dipole. The tangential velocity may then be computed by numerically differentiating μ with respect to arc length around the airfoil.

PROBLEM

12.6.1 *Constant strength dipole panels*

Code *airf_2d_cdp*, located inside directory *07_ptf* of **FDLIB**, computes flow past an airfoil using the constant strength source-dipole-panel method.

- Run the code for an airfoil of your choice. Prepare graphs, and discuss the distribution of the pressure coefficient.
- Evaluate the velocity at several points inside the airfoil and discuss the results.

12.7 Point-source panels and Green's third identity

Previously in this chapter, we discussed flow representations in terms of vortex panels and point-source dipole panels expressed, respectively, by equations (12.5.1) and (12.6.12) or (12.6.13). In this section, we introduce a new representation in terms of distributions of point sources. Working by analogy with (12.6.13), we find that the harmonic potential of

the induced flow is given by

$$\phi^{\text{source distribution}}(x, y) = \frac{1}{4\pi} \oint \ln \frac{(x - x')^2 + (y - y')^2}{\varrho^2} \sigma(\mathbf{x}') d\ell(\mathbf{x}'), \quad (12.7.1)$$

where $\sigma(\mathbf{x})$ is the strength density of the distribution and ϱ is an arbitrary reference length.

The point-source representation carries an important restriction: conservation of mass requires that the total strength of the point sources, defined as the integral of the strength density, σ , with respect to arc length around the airfoil, ℓ , is zero. If this condition is not met, a net radial flow due to an effective point source will be established. This restriction is satisfied automatically only in the case of symmetric flow past a symmetric non-lifting airfoil at zero angle of attack, and in the absence of circulatory motion.

In spite of this limitation, the point-source representation is not without its merits. Its usefulness stems predominantly from Green's third identity discussed in Section 12.7.2, stating that a judicious combination of the point source and source-dipole representation ensures the satisfaction of the zero flow rate condition, and also endows the strength densities of the distributions with simple and appealing physical interpretations.

12.7.1 Source panels with constant density

Consider a flat source panel with uniform strength density equal to $\sigma^{(0)}$ situated along the x axis between the points $x = a$ and b . Applying (12.7.1) with $y' = 0$, we find that the corresponding velocity potential is given by

$$\phi^{(0)}(x, y) = \sigma^{(0)} \frac{1}{4\pi} \int_a^b \ln \frac{(x - x')^2 + y^2}{\varrho^2} dx'. \quad (12.7.2)$$

Note that this expression is identical to that for the stream function due to a vortex panel with constant strength density given in equation (12.3.11), subject to the substitution

$$\gamma^{(0)} = -\sigma^{(0)}. \quad (12.7.3)$$

Referring to (12.3.12), we find that

$$\begin{aligned} \phi^{(0)}(x, y) = \sigma^{(0)} \frac{1}{4\pi} & \left(-(x - b) \ln \frac{(x - b)^2 + y^2}{\varrho^2} \right. \\ & + (x - a) \ln \frac{(x - a)^2 + y^2}{\varrho^2} \\ & \left. + 2y \left(\arctan \frac{y}{x - b} - \arctan \frac{y}{x - a} \right) - 2(b - a) \right). \end{aligned} \quad (12.7.4)$$

The components of the velocity are found by straightforward differentiation, and are given by

$$u_x^{(0)}(x, y) = \frac{\partial \phi^{(0)}}{\partial x} = -\sigma^{(0)} \frac{1}{4\pi} \ln \frac{(x - b)^2 + y^2}{(x - a)^2 + y^2}, \quad (12.7.5)$$

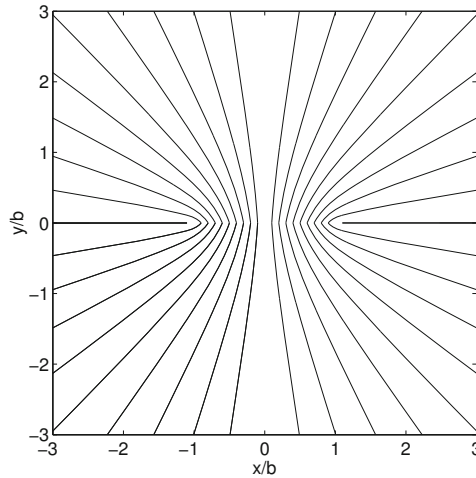


Figure 12.7.1 Streamline pattern of the flow due to a point-source panel with uniform strength extending between the points $x = \pm b$.

and

$$u_y^{(0)}(x, y) = \frac{\partial \phi^{(0)}}{\partial y} = \sigma^{(0)} \frac{1}{2\pi} \left(\arctan \frac{y}{x-b} - \arctan \frac{y}{x-a} \right). \tag{12.7.6}$$

Far from the panel, the flow resembles that due to a point source with strength $m = \sigma^{(0)}(b - a)$ situated at the origin. The streamline pattern of the flow induced by a uniform panel extending between $x = \pm b$ is shown in [Figure 12.7.1](#).

Jump in the velocity across the panel

Expression (12.7.5) shows that the x velocity component is continuous throughout the domain of flow and across the source panel. In contrast, because of the inverse tangent functions on the right-hand side of (12.7.6), the y velocity component undergoes a discontinuity with magnitude $\sigma^{(0)}$ across the source panel. Specifically, the y velocity component at the upper or lower side of the panel, $a < x < b$, is given by

$$u_y^{(0)}(x, y \rightarrow \pm 0) = \pm \frac{1}{2} \sigma^{(0)}. \tag{12.7.7}$$

Inverse tangent functions also appear on the right-hand side of (12.7.4). However, because these functions are multiplied by y , which is zero over the panel, a discontinuity in the potential does not arise.

12.7.2 Green's third identity

The source panels can be used in the familiar way to develop a representation of potential flow past a symmetric airfoil at zero angle of attack in the absence of circulation. The

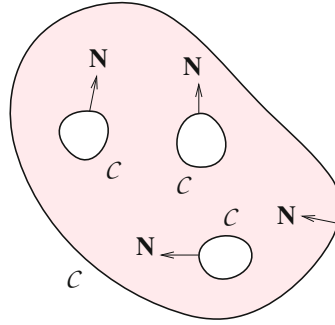


Figure 12.7.2 A control area in the xy plane confined by a collection of closed contours, \mathcal{C} , is used to establish Green's third identity; \mathbf{N} is the unit vector normal to the boundaries pointing into the fluid.

numerical implementation is analogous to that of the vortex panel method discussed in Section 12.3. However, a more interesting and more general representation is possible thanks to Green's third identity.

Consider a control area in the xy plane enclosed by a collection of boundaries identified as closed contours, denoted by \mathcal{C} , as illustrated in Figure 12.7.2. Green's third identity states that the harmonic potential at a point \mathbf{x} that lies inside the control area can be represented in terms of a combined point-source/source-dipole distribution, in the form

$$\begin{aligned} \phi(x, y) = & \frac{1}{4\pi} \oint_{\mathcal{C}} \ln \frac{(x - x')^2 + (y - y')^2}{\varrho^2} \mathbf{N}(\mathbf{x}') \cdot \nabla \phi(\mathbf{x}') \, d\ell' \\ & + \frac{1}{2\pi} \oint_{\mathcal{C}} \frac{(x - x') N_x(\mathbf{x}') + (y - y') N_y(\mathbf{x}')}{(x - x')^2 + (y - y')^2} \phi(\mathbf{x}') \, d\ell', \end{aligned} \quad (12.7.8)$$

where ϱ is an arbitrary constant length and \mathbf{N} is the unit vector normal to the boundaries pointing into the control area, as shown in Figure 12.7.2.

Comparing the two terms on the right-hand side of (12.7.8) with the representations (12.7.1) and (12.6.12), we identify the strength density of the point-source distribution with the boundary values of the potential, and the strength density of the source-dipole distribution with the boundary values of the normal derivative of the potential.

Next, we identify the control area with the area occupied by an airfoil, and apply Green's identity for the potential of an incident streaming flow, ϕ^∞ . Writing $\mathbf{N} = -\mathbf{n}$, where \mathbf{n} is the unit vector normal to the airfoil pointing into the *exterior* and \mathbf{N} is the unit vector normal to the airfoil pointing into the *interior*, we obtain the representation

$$\phi_\infty(x, y) = -\frac{1}{4\pi} \oint_{\mathcal{C}} \ln \frac{(x - x')^2 + (y - y')^2}{\varrho^2} \mathbf{n}(\mathbf{x}') \cdot \nabla \phi_\infty(\mathbf{x}') \, d\ell'$$

$$-\frac{1}{2\pi} \oint_C \frac{(x-x')n_x(\mathbf{x}') + (y-y')n_y(\mathbf{x}')}{(x-x')^2 + (y-y')^2} \phi_\infty(\mathbf{x}') d\ell', \quad (12.7.9)$$

where the point $\mathbf{x} = (x, y)$ lies inside the airfoil. Note the opposite signs on the right-hand sides of (12.7.8) and (12.7.9)

Equations (12.6.12) and (12.6.15) provide us a double-layer representation of the flow inside the airfoil in the form

$$\begin{aligned} \phi(x, y) = \phi_\infty(x, y) + \frac{1}{2\pi} \oint_C \frac{(x-x')n_x(\mathbf{x}') + (y-y')n_y(\mathbf{x}')}{(x-x')^2 + (y-y')^2} \phi^{(+)}(\mathbf{x}') d\ell' \\ + \phi_{\text{at the trailing edge}}^{\text{point vortex}}(x, y), \end{aligned} \quad (12.7.10)$$

where $\phi^{(+)}$ is the potential on the exterior side of the airfoil. Since the point $\mathbf{x} = (x, y)$ is located in the interior of the airfoil, the left-hand side is a constant that may be set equal to zero.

Combining equations (12.7.9) and (12.7.10), we obtain

$$\begin{aligned} \frac{1}{4\pi} \oint_C \ln \frac{(x-x')^2 + (y-y')^2}{\rho^2} \mathbf{n}(\mathbf{x}') \cdot \nabla \phi_\infty(\mathbf{x}') d\ell' \\ = -\frac{1}{2\pi} \oint_C \frac{(x-x')n_x(\mathbf{x}') + (y-y')n_y(\mathbf{x}')}{(x-x')^2 + (y-y')^2} \mu(\mathbf{x}') d\ell' + \phi_{\text{at the trailing edge}}^{\text{point vortex}}(x, y), \end{aligned} \quad (12.7.11)$$

where

$$\mu \equiv -\phi^{(+)} + \phi_\infty. \quad (12.7.12)$$

Equation (12.7.11) is an integral equation for the dipole density μ . Once this equation has been solved using, for example, a panel method, the potential on the exterior side of the airfoil can be computed from equation (12.7.12) as

$$\phi^{(+)} = \phi_\infty - \mu. \quad (12.7.13)$$

The advantages of this representation over the vortex panel representation are now apparent.

PROBLEMS

12.7.1 Source-dipole panel method

Program *airf_2d_csdp*, located in directory *07_ptf* of **FDLIB**, computes flow past an airfoil using a panel method based on equation (12.7.11). Run the code for an airfoil of your choice, prepare graphs and discuss the distribution of the pressure coefficient around the airfoil.

12.7.2 Constant source panel method

Write a code that computes flow past a symmetric airfoil at zero angle of attack using the point-source panel method. Run the code for an airfoil of your choice, prepare graphs, and discuss the distribution of the pressure coefficient around the airfoil.

FDLIB Software Library



The software library **FDLIB** contains a suit of FORTRAN 77, MATLAB, and other computer programs (codes) that solve a broad range of problems in fluid dynamics and related disciplines by a variety of numerical methods.

FDLIB consists of the thirteen main directories (folders) listed in [Table A.1](#). Each main directory contains a multitude of nested subdirectories (subfolders) that include main programs, assisting subroutines and functions, utility subroutines, and data files. Linked with drivers, the utility subroutines become stand-alone modules; all drivers are provided.

A list of subdirectories and a brief statement of their contents are given in this appendix. Further information is available at the **FDLIB** Internet site:

<http://dehesa.freeshell.org/FDLIB>

Download

The source code of **FDLIB** consisting of computer programs and data files is available from the **FDLIB** Internet site. The directories have been archived using the *tar* Unix facility into a compressed file named *FDLIB.tgz*.

To unravel the directories on a Unix system, open a terminal and issue the command: `tar xzf FDLIB.tgz`. This will generate a directory (folder) called *FDLIB* that contains nested subdirectories (subfolders).

To unravel the directories on a Windows or other system, double-click on the archived tar file and follow the on-screen instructions of the application invoked.

Installation and compilation

MATLAB programs are executed as interpreted scripts. The downloaded **FDLIB** package does not contain FORTRAN 77 object files or executables. To compile and link FORTRAN 77 programs, follow the instructions of your compiler.

An application can be built using the *makefile* provided in each subdirectory. A makefile is a script interpreted by the *make* utility (application) that instructs the operating system how to compile a main program and associated functions of subroutines, and then link the object files into an executable binary file (application) using a compiler. For example, to

	<i>Subject</i>	<i>Directory</i>
1	Numerical methods	<i>01_num_meth</i>
2	Grids	<i>02_grids</i>
3	Hydrostatics	<i>03_hydrostat</i>
4	Various	<i>04_various</i>
5	Lubrication	<i>05_lub</i>
6	Stokes flow	<i>06_stokes</i>
7	Potential flow	<i>07_ptf</i>
8	Hydrodynamic stability	<i>08_stab</i>
9	Vortex motion	<i>09_vortex</i>
10	Boundary layers	<i>10_bl</i>
11	Finite difference methods	<i>11_fdm</i>
12	Boundary element methods	<i>12_bem</i>
13	Turbulence	<i>13_turbo</i>

Table A.1 FDLIB is arranged in thirteen main directories in a physical or computational scheme.

compile an application named *sublime*, navigate to the subdirectory (subfolder) where the application resides and issue the statement: `make sublime`.

To remove the object files, output files, and executable of a chosen application, navigate to the subdirectory where the application resides and issue the statement: `make clean`.

To compile the FORTRAN 77 programs using a FORTRAN 77 90 compiler, simply make appropriate compiler call substitutions in the makefiles.

CFDLAB

A subset of FDLIB has been combined with the fabulous X11 graphics library *vogle* into an integrated application named CFDLAB that visualizes the results of simulations and performs interactive animation. The source code of CFDLAB can be downloaded from the Internet site: <http://dehesa.freeshell.org/CFDLAB>.

BEMLIB

A subset of FDLIB containing boundary-element codes have been arranged into the library BEMLIB accompanying the book: Pozrikidis, C. (2002) *A Practical Guide to Boundary-Element Methods with the Software Library BEMLIB*, Chapman & Hall. The source code of BEMLIB can be downloaded from the Internet site: <http://dehesa.freeshell.org/BEMLIB>.

FDLIB directory contents

The public FDLIB directories are listed in the following tables along with a brief description. Further information and updates can be found at the FDLIB Internet site.

01_num_meth

This directory contains a suite of general-purpose programs on general numerical methods and differential equations that accompany the book: Pozrikidis, C. (2008) *Numerical Computation in Science and Engineering*, Second edition, Oxford University Press.

<i>Subdirectory</i>	<i>Topic</i>
01_num_comp	General aspects of numerical computation
02_lin_calc	Linear algebra and linear calculus
03_lin_eq	Systems of linear algebraic equations
04_nl_eq	Nonlinear algebraic equations
05_eigen	Eigenvalues and eigenvectors of matrices
06_interp_diff	Function interpolation and differentiation
07_integration	Function integration
08_approximation	Function approximation
09_ode	Ordinary differential equations
10_ode_ddm	Ordinary differential equations; domain discretization methods
11_pde_diffusion	Partial differential equations; unsteady diffusion
12_pde_poisson	Partial differential equations; Poisson equation
13_pde_cd	Partial differential equations; convection--diffusion equation
14_bem	Boundary-element methods
15_fem	Finite-element methods
99_spec_fnc	Special functions

02_grids

This directory contains programs that perform grid generation, adaptive discretization, parametrization, representation, and meshing of planar lines, three-dimensional lines, and three-dimensional surfaces.

<i>Subdirectory</i>	<i>Topic</i>
grid_2d	Discretization of a planar line into a mesh of straight or circular elements
prd_2d	Adaptive discretization of a closed line
prd_2d_open	Adaptive discretization of an open line
prd_2d_pr	Adaptive discretization of a periodic line
prd_2d_pr_hs	Adaptive discretization of a periodic line with mid-point symmetry
prd_2d_qs	Adaptive discretization of a closed line with quarter symmetry
prd_3d	Adaptive discretization of a closed three-dimensional line
prd_3d_pr	Adaptive discretization of a periodic three-dimensional line

prd_ax	Adaptive parametrization of a planar line representing the trace of an axisymmetric surface in an azimuthal plane
rec_2d	Interpolation through a Cartesian grid
rec_2d_strml	Streamlines by interpolation on a Cartesian grid
sm_3d_cl_df	Smoothing of a function on a closed surface by surface diffusion
sm_3d_cl_tr	Smoothing of a function on a closed surface by Legendre spectrum truncation
trgl	Triangulation of a closed surface
trgl_flat	Triangulation of a flat surface

03_hydrostat

This directory contains codes that generate interfacial shapes in hydrostatics.

<i>Subdirectory</i>	<i>Topic</i>
drop_2d	Shape of a two-dimensional pendant or sessile drop on a horizontal plane
drop_2di	Shape of a two-dimensional drop on an inclined plane
drop_ax	Shape of an axisymmetric pendant or sessile drop on a horizontal plane
flsphere	Position of a sphere floating at an interface with a curved meniscus
men_2d	Shape of a two-dimensional meniscus between two parallel plates
men_2d_plate	Shape of a two-dimensional meniscus attached to an inclined plate
men_3d	Shape of a three-dimensional meniscus in the exterior of an ellipse
men_3d_2p	Shape of a doubly periodic three-dimensional meniscus attached to cylinder lattice
men_ax	Shape of an axisymmetric meniscus inside a vertical circular tube
men_axe	Shape of an axisymmetric meniscus in the exterior of a vertical cylinder
men_cc	Shape of a three-dimensional meniscus in the exterior two vertical cylinders

04_various

This directory contains miscellaneous codes that compute the structure and kinematics of various flows.

<i>Subdirectory</i>	<i>Topic</i>
chan_2d	Steady flow in a channel
chan_2d_2l	Steady two-layer flow in a channel
chan_2d_imp	Impulsive flow in a channel
chan_2d_ml	Multi-layer flow in a channel
chan_2d_osc	Oscillatory flow in a channel
chan_2d_trans	Transient flow in a channel
chan_2d_wom	Pulsating flow in a channel
chan_brush	Steady flow in a brush channel
chan_pl	Steady channel flow of a power-law fluid
film	Film flow down an inclined plane
films	Multi-film flow down an inclined plane
flow_1d	Steady unidirectional flow in a tube with arbitrary cross-section
flow_1d_1p	Steady unidirectional flow over a periodic array of cylinders with arbitrary cross-section
flow_1d_osc	Oscillatory unidirectional flow in a tube with arbitrary cross-section
path_lines	Computation of path lines
plate_imp	Flow due to the impulsive motion of a plate
plate_osc	Flow due to the oscillations of a plate
spf	Similarity solutions for stagnation-point flow
strml	Streamline patterns of a broad range of flows offered in a menu
tube_ann	Steady annular flow
tube_ann_ml	Steady multi-layer annular flow
tube_ann_sw	Steady swirling annular flow
tube_ann_sw_ml	Steady multi-layer swirling annular flow
tube_crc	Steady flow through a circular tube
tube_crc_ml	Steady multi-layer flow through a circular tube
tube_crc_sec	Steady flow through a circular tube due to the translation of a sector
tube_crc_sw_trans	Transient swirling flow in a circular tube
tube_crc_trans	Transient flow through a circular tube
tube_crc_wom	Pulsating flow in a circular tube
tube_ell	Steady flow through a tube with elliptical cross-section
tube_rec	Steady flow through a tube with rectangular cross-section
tube_trgl_eq1	Steady flow through a tube with triangular cross-section

05_lub

This directory contains codes that solve problems involving lubrication flow.

<i>Subdirectory</i>	<i>Topic</i>
bear_2d	Dynamic simulation of the motion of a slider bearing pressing against a wall
chan_2l_exp	Dynamic simulation of the evolution of two superposed viscous layers in a horizontal or inclined channel computed by an explicit finite-difference method
chan_2l_imp	Same as chan_2l_exp, but with an implicit finite-difference method
films	Evolution of an arbitrary number of superposed films on a horizontal or inclined wall

06_stokes

This directory contains codes that compute viscous flows at vanishing Reynolds numbers.

<i>Subdirectory</i>	<i>Topic</i>
bump_3d	Shear flow over a spherical bump on a plane wall
caps_2d	Dynamic simulation of the motion of a two-dimensional drop or elastic capsule for a variety of flow configurations
caps_3d	Dynamic simulation of the motion of a three-dimensional elastic capsule
chan2l	Dynamic simulation of two-layer flow in a channel in the presence of an insoluble surfactant
drop_3d	Dynamic simulation of the motion of a three-dimensional drop with constant or varying surface tension
drop_3dw	Dynamic simulation of the deformation of a three-dimensional drop adhering to a plane wall
drop_ax	Dynamic simulation of the motion of an axisymmetric liquid drop
em_2d	Dynamic simulation of the motion of a suspension of two-dimensional drops or elastic capsules, for a variety of flow configurations
flow_2d	Two-dimensional flow in a domain with arbitrary geometry
flow_3x	Shear flow over an axisymmetric cavity, orifice, or protrusion, computed by a boundary-element method

prtcl_2d	Flow past a fixed bed of two-dimensional particles with arbitrary shapes for a variety of flow configurations computed by a boundary-element method
prtcl_3d	Flow past or due to the motion of a three-dimensional particle for a variety of configurations computed by a boundary-element method
prtcl_3d_mob	Same as prtcl_3d but for the mobility problem where the force and torque on the particle are specified and the particle velocity and angular velocity are computed in the solution
prtcl_3d_mob_dlr_se	Same as prtcl_3d_mob using the double-layer representation and a spectral-element method
prtcl_ax	Flow past or due to the motion of a collection of axisymmetric particles computed by a boundary-element method
prtcl_sw	Swirling flow produced by the rotation of an axisymmetric particle computed by a boundary-element method
rbc_2d	Dynamic simulation of the deformation of a two-dimensional red blood cell
sgf_2d	Green's functions of two-dimensional flow
sgf_3d	Green's functions of three-dimensional flow
sgf_ax	Green's functions of axisymmetric flow
susp_3d	Dynamic simulation of the motion of a suspension of three-dimensional rigid particles with arbitrary shapes, for a variety of flow configurations, computed by a boundary-element method
two_spheres	Motion of two intercepting spheres in simple shear flow

07_ptf

This directory contains codes that solve problems involving potential flow.

<i>Subdirectory</i>	<i>Topic</i>
airf_2d	Airfoil shapes
airf_2d_cdp	Flow past an airfoil computed by the constant-dipole-panel method
airf_2d_csdp	Flow past an airfoil computed by the constant-source-dipole-panel method
airf_2d_lvp	Flow past an airfoil computed by the linear-vortex-panel method
body_2d	Flow past or due to the motion of a two-dimensional body computed

body_ax	by a boundary element method Flow past or due to the motion of an axisymmetric body computed by a boundary element method
cvt_2d	Flow in a rectangular cavity computed by a finite difference method
flow_2d	Two-dimensional flow in an arbitrary domain computed by a boundary element method
lgf_2d	Green and Neumann functions of Laplace's equation in two dimensions
lgf_3d	Green and Neumann functions of Laplace's equation in three dimensions
lgf_ax	Green and Neumann functions of Laplace's equation in axisymmetric domains
tank_2d	Dynamic simulation of liquid sloshing in a rectangular tank computed by a boundary-element method

08_stab

This directory contains codes that perform stability analysis of miscellaneous flows.

<i>Subdirectory</i>	<i>Topic</i>
ann2l	Capillary instability of two annular layers placed between two concentric cylinders in the presence of an insoluble surfactant
ann2l0	Same as ann_2l for Stokes flow
ann2le1	Same as ann_2l for an elastic interface
ann2le10	Same as ann_2l0 for an elastic interface
ann2lvs0	Same as ann_2l0 for a viscous interface
chan2l0	Instability of two-layer flow in a channel under conditions of Stokes flow
chan2l0.s	Instability of two-layer flow in a channel in the presence of an insoluble surfactant under conditions of Stokes flow
coat0.s	Instability of a liquid film resting on a plane wall in the presence of an insoluble surfactant under conditions of Stokes flow
film0	Instability of a liquid film down an inclined plane for Stokes flow
film0.s	Instability of a liquid film down an inclined plane in the presence of an insoluble surfactant for Stokes flow
if0	Instability of a horizontal interface between two semi-infinite fluids for Stokes flow
ifsf0.s	Instability of a horizontal interface between two semi-infinite fluids for Stokes flow

	in simple shear flow in the presence of surfactants
kirch_stab	Instability of Kirchhoff's elliptical vortex
layer0	Instability of a horizontal liquid layer resting on a horizontal wall under a semi-infinite fluid for Stokes flow
layer0sf_s	Instability of a sheared liquid layer coated on a horizontal plane in the presence of an insoluble surfactant for Stokes flow
orr	Instability of a viscous shear flow with arbitrary velocity profile
prony	Prony fitting of a times series with a sum of complex exponentials
rayleigh	Instability of an inviscid shear flow with arbitrary velocity profile
thread0	Instability of an infinite viscous thread suspended in an ambient viscous fluid for Stokes flow
thread1	Instability of an inviscid thread suspended in an inert ambient fluid
vl	Instability of a vortex layer
vs	Instability of a vortex sheet

09_vortex

This directory contains codes that compute vortex motion.

<i>Subdirectory</i>	<i>Topic</i>
lv_lia	Dynamic simulation of the motion of a three-dimensional line vortex computed by the local-induction approximation (LIA)
lvr	Velocity induced by line vortex rings
lvrm	Dynamic simulation of the motion of a collection of coaxial line vortex rings
pv	Velocity induced by a point vortex
pvm	Dynamic simulation of the motion of a collection of point vortices
pvm_pr	Dynamic simulation of the motion of a periodic collection of point vortices
ppoly	Polygonal arrangements of point vortices
ring	Self-induced velocity of a vortex ring with core of finite size
vl_2d	Dynamic simulation of the evolution of compound periodic vortex layers
vp_2d	Dynamic simulation of the evolution of a collection of two-dimensional vortex patches
vp_ax	Dynamic simulation of the evolution of a

collection of axisymmetric vortex rings and vortex patches

10_bl

This directory contains codes that solve boundary-layer flow.

<i>Subdirectory</i>	<i>Topic</i>
blasius	Computation of the Blasius boundary layer
falskan	Computation of the Falkner-Skan boundary layer
kp_cc	Boundary layer around a circular cylinder computed by the K�arm�an-Pohlhausen method
pohl_pol	Profiles of the Pohlhausen polynomials

11_fdm

This directory contains codes that solve problems using finite-difference methods.

<i>Subdirectory</i>	<i>Topic</i>
channel	Unidirectional flow in a channel
cvt_pm	Transient flow in a rectangular cavity computed by a projection method
cvt_stag	Steady Stokes flow in a rectangular cavity computed on a staggered grid
cvt_sv	Steady flow in a rectangular cavity computed by the stream function/vorticity formulation

12_bem

This directory contains codes that produce solutions to Laplace's equation by boundary-element methods.

<i>Subdirectory</i>	<i>Topic</i>
ldr_3d	Solution of Laplace's equation with Dirichlet boundary conditions in the interior or exterior of a three-dimensional region computed using the boundary-integral formulation
ldr_3d_2p	Solution of Laplace's equation with Dirichlet boundary conditions in a semi-infinite region bounded by a doubly-periodic surface computed using the double-layer formulation
ldr_3d_ext	Solution of Laplace's equation with Dirichlet boundary conditions in the exterior of a three-dimensional region computed using the double-layer formulation

<code>ldr_3d_ext.se</code>	Same as <code>ldr_3d_ext</code> but with a spectral-element method
<code>ldr_3d_int</code>	Solution of Laplace's equation with Dirichlet boundary conditions in the interior of a three-dimensional region computed using the double-layer formulation
<code>ldr_3d_int.se</code>	Same as <code>ldr_3d_int</code> but with a spectral-element method
<code>lnm_3d</code>	Solution of Laplace's equation with Neumann boundary conditions in the interior or exterior of a three-dimensional region computed using the boundary-integral formulation

13_turbo

This directory contains data and codes pertinent to turbulent flow.

<i>Subdirectory</i>	<i>Topic</i>
<code>stats</code>	Statistical analysis of a turbulent flow time series

References

Further discussion of fluid mechanics, applied mathematics, numerical methods, and scientific computing can be found in the highly recommended texts listed in this appendix.

Introductory classical mechanics

Marion, J. B. (1970) *Classical Dynamics of Particles and Systems*, Harcourt Brace.

Introductory fluid dynamics

Bird, R. B., Stewart, W. E. & Lightfoot, E. N. (2006) *Transport Phenomena*, Second Edition, Wiley.

Papanastasiou, T. C., Georgiou, G. & Alexandrou, A. N. (1999) *Viscous Fluid Flow*, CRC Press.

Morrison, F. A. (2001) *Understanding Rheology*, Oxford University Press.

Advanced fluid dynamics

Batchelor, G. K. (1967) *An Introduction to Fluid Dynamics*, Cambridge University Press.

Brodkey, R. S. (2004) *The Phenomena of Fluid Motions*, Dover.

Pozrikidis, C. (2011) *Introduction to Theoretical and Computational Fluid Dynamics*, Second Edition, Oxford University Press.

Warsi, Z. U. A. (2005) *Fluid Dynamics; Theoretical and Computational Approaches*, Third Edition, CRC Press.

White, F. M. (2005) *Viscous Fluid Flow*, Third Edition, McGraw-Hill.

Computational fluid dynamics

Ferziger, J. H. & Perić, M. (1996) *Computational Methods for Fluid Dynamics*, Springer-Verlag.

Hirsch, C. (2007) *Numerical Computation of Internal and External Flows*, Second Edition, Butterworth–Heinemann.

Pozrikidis, C. (2011) *Introduction to Theoretical and Computational Fluid Dynamics*, Second Edition, Oxford University Press.

Low-Reynolds-number flow

Happel, J. & Brenner, H. (1983) *Low Reynolds Number Hydrodynamics*, Springer.

Kim, S. & Karrila, S. J. (1991) *Microhydrodynamics: Principles and Selected Applications*, Butterworth–Heinemann.

Pozrikidis, C. (1992) *Boundary Integral and Singularity Methods for Linearized Viscous Flow*, Cambridge University Press.

Aerodynamics

Anderson, J. D. (2002) *Modern Compressible flow with Historical Perspective*, Third Edition, McGraw–Hill.

Anderson, J. D. (2007) *Fundamentals of Aerodynamics*, Fourth Edition, McGraw–Hill.

Katz, J. & Plotkin, A. (2001) *Low-Speed Aerodynamics; from Wing Theory to Panel Methods*, Second Edition, Cambridge University Press.

Numerical methods

Pozrikidis, C., 2008, *Numerical Computation in Science and Engineering*, Second Edition, Oxford University Press.

Calculus

Boas, M. L. (2005) *Mathematical Methods in the Physical Sciences*, Third Edition, Wiley.

Hildebrand, F. B. (1976) *Advanced Calculus for Applications*, Second Edition, Prentice-Hall.

Mathematical Resources

Abramowitz, M. & Stegun, I. A. (1972) *Handbook of Mathematical Functions*, Dover.

Gradshteyn, I. S. & Ryzhik, I. M. (1980) *Table of Integrals, Series, and Products*, Academic Press.

Korn, G. A. & Korn, T. M. (1968) *Mathematical Handbook for Scientists and Engineers*, McGraw–Hill.

Computer Programming

Pozrikidis, C. (2007) *Introduction to C++ Programming and Graphics*, Springer.



Matlab Primer

MATLAB[®] is a commercial computer software application for interactive numerical computation and graphics visualization produced and distributed by The MathWorks Inc. The application was developed in the 1970s as a virtual laboratory for matrix calculus and linear algebra. Since then, MATLAB has evolved to become both a programming language and a computing environment supported by a multitude of advanced functions and toolboxes. MATLAB must be purchased and installed on a computer with a proper license. Inexpensive licenses are available for students and educators.

As a programming language, MATLAB is roughly equivalent, in some ways superior and in some ways inferior to traditional upper-level languages, such as FORTRAN 77, C, or C++. As a computing environment, MATLAB is able to run indefinitely in its own workspace. Thus, a session defined by all initialized variables, graphics and other objects, such as figures, can be saved and reinstated at a later time. In this sense, MATLAB is an operating system running inside the operating system that empowers the host computer. Symbolic algebraic manipulation is available through an add-on library (toolbox) that uses a kernel borrowed from the mathematical software engine Maple.

An attractive feature of MATLAB is the availability of a broad range of utility commands, intrinsic functions, and computational toolboxes, especially graphics functions. A simplifying feature of MATLAB is that the type and size of vectors and matrices used in the calculations are assigned automatically and can be changed in the course of a session, thereby circumventing the need for variable declaration and explicit memory allocation and deallocation.

C.1 Launching MATLAB

To launch MATLAB in a Windows operating system, double-click on the MATLAB icon. This action runs a starter program, currently a disk operating system (DOS) batch script, that launches the main MATLAB executable. Alternatively, MATLAB can be started from a DOS command line by a procedure similar to that discussed next for Unix.

To launch MATLAB in a Unix operating system, run the Unix script *matlab* installed by MATLAB by issuing the command:

```
>> matlab
```

where `>>` represents the Unix shell prompt. Assuming that the script is in the path of executables, the MATLAB executable will be launched in a graphical user interface (GUI) or command line mode. To suppress the memory demanding GUI, issue the command:

```
>> matlab -nodesktop
```

or the command:

```
>> matlab -nojvm
```

where *nojvm* negates the java virtual machine (jvm). Starting MATLAB by issuing the command:

```
>> matlab -nodesktop -nosplash
```

suppresses both the GUI and the splash screen at startup. In Unix, MATLAB can be launched with a number of options. To obtain a list, request help by issuing the command:

```
>> matlab -help
```

in the MATLAB environment.

MATLAB employs a number of shared libraries, parameters, and environmental variables. To obtain a complete list, issue the command:

```
>> matlab -n
```

A variety of MATLAB tutorials are available in the Internet.

C.2 MATLAB programming

Only elementary computer programming skills are needed to read and write MATLAB code. The code is written in one file or a collection of files, called the source or program files, using a standard file editor, such as the *notepad* or the *vi* editor.

The source code includes the main program, sometimes also called a script, and the necessary user-defined functions. The names of these files must be suffixed by a dot followed by the **m** letter (**.m**). Code execution begins by typing the name of the file containing the main program in the MATLAB environment without the **.m** suffix. Alternatively, the code can be typed in the MATLAB environment one line at a time, followed by the RETURN keystroke.

MATLAB is an interpreted language, which means that the instructions are translated into machine language and executed in real time, one at a time. In contrast, a source code written in FORTRAN 77, C, C++, or any other comparable language must first be compiled to generate object files. The object files are then linked together with the necessary system and user-defined libraries to produce an executable binary file.

Grammar and syntax

Following is a list of general rules regarding on MATLAB grammar and syntax. When confronted with a warning or error after issuing a command or during execution, this list should serve as a first check point:

- *MATLAB variables are (lower and upper) case-sensitive:*

The variable *echidna* is different from the variable *echiDna*. Similarly, the MATLAB command *return* is not equivalent to the erroneous command *Return*. The latter will not be recognized by the MATLAB interpreter.

- *MATLAB variables must start with a letter:*

A variable name is described by a string of up to thirty-one characters, including letters, digits, and the underscore. Punctuation marks are not allowed.

- *MATLAB string variables are enclosed by a single quote:*

For example, we may define the string variable:

```
artist_001 = 'Celine_Dion'
```

- *Beginning and end of a command line:*

A MATLAB command may begin at any position in a line and may continue practically indefinitely in the same line.

- *Line continuation:*

To continue a command to the next line, put three consecutive dots at the end of the line. Text after three dots in the current line is ignored.

- *Multiple commands in a line:*

Two or more commands can be placed in the same line, provided they are separated by a semicolon (;).

- *Display:*

When a command is executed directly or by running a MATLAB code, MATLAB displays the numerical value assignment or the result of a calculation. To suppress the output, put a semicolon (;) at the end of the command.

- *White space:*

More than one empty spaces between words are ignored. However, numbers cannot be broken up into sections separated by blank spaces.

- *Range of indices:*

The indices of vectors and arrays must be positive and nonzero. For example, the vector entry $v(-3)$ is not acceptable. This annoying restriction can be circumvented in clever ways by redefining, reflecting, or shifting the indices.

- *Comments:*

A line beginning with the % character, or the tail-end of a line after the % character, is a comment to be ignored by the MATLAB interpreter.

- *Mathematical symbols and special characters:*

Mathematical symbols and special characters used in interactive MATLAB dialog and programming are listed in [Table C.2.1](#).

- *Logical control flow commands:*

Basic logical control flow commands are listed in [Table C.2.2](#).

- *Input/output commands:*

Basic input/output (I/O) commands, functions, and formatting statements are listed in [Tables C.2.3–C.2.5](#). Once the output format is set, it remains in effect until changed.

Do not write MATLAB-specific code

It is a good practice to write MATLAB code in a form that can be translated readily to any other upper-level computer language, such as FORTRAN 77, C, or C++, by avoiding procedures that are available only in MATLAB. Computational scientists often write code in one of the aforementioned languages and a companion code in MATLAB for the purpose of debugging and to ensure platform independence.

Precision

MATLAB stores all numbers in the long format of the floating point representation. This means that real numbers have a finite precision of roughly sixteen significant digits and a range of definition varying in absolute value approximately between 10^{-308} and 10^{+308} . Numbers that are smaller than 10^{-308} or higher than 10^{+308} in absolute value cannot be accommodated. All computations are done in double precision. However, this should not be confused with the ability to view and print numbers with a specified number of significant figures.

C.3 MATLAB commands

Once invoked, MATLAB responds interactively to various commands, statements, and declarations issued by the user in the MATLAB environment. These directives are issued by typing the corresponding name, single-line syntax, or multi-line construct, and then pressing the ENTER key.

General utility and interactive-input MATLAB commands are listed in [Table C.3.1](#). Issuing the command *demons* initiates various demonstrations and illustrative examples. A session can be saved using the *save* command and reinstated at a later time.

+	plus sign
-	minus sign
*	number or matrix multiplication sign
.*	array multiplication sign
^	number or matrix power sign
.^	array power sign
kron	Kronecker tensor product
\	backslash or left division sign
/	slash or right division sign
./	array division sign
:	colon
()	parentheses
[]	brackets
.	decimal point sign
..	parent directory
...	line continuation
,	comma
;	semicolon, use to suppress the screen display
%	indicates that the rest of the line is a comment
!	exclamation point
'	matrix transpose
''	quote
.'	nonconjugated transpose
=	set equal to (replace left by right)
==	equal
~=	not equal
<	less than
<=	less than or equal to
>	greater than
>=	greater than or equal to
&	logical <i>and</i>
	logical <i>or</i>
~	Logical <i>not</i>
xor	Logical <i>exclusive or</i>
i, j	imaginary unit
pi	number $\pi = 3.14159265358\dots$

Table C.2.1 MATLAB operators, symbols, special characters, and constants.

break	terminate the execution
else	Use with the if statement
elseif	Use with the if statement
end	terminate a for loop, a while loop, or an if block
error	display a message and abort
for	loop over commands a specific number of times
if	conditionally execute commands
pause	wait for user's response
return	return to the MATLAB environment, invoking program or function
while	Repeat statements an indefinite number of times until a specified condition is met

Table C.2.2 Logical control flow MATLAB commands and construct components.

disp	display numerical values or text Use as: <code>disp disp() disp('text')</code>
fclose	close a file
fopen	open a file
fread	read binary data from a file
fwrite	write binary data to a file
fgetl	read a line from a file, discard the newline character
fgets	read a line from a file, keep the newline character
fprintf	write formatted data to a file using C language conventions
fscanf	read formatted data from a file
feof	test for end-of-file (EOF)
ferror	inquire the I/O error status of a file
frewind	rewind a file
fseek	set file position indicator
ftell	get file position indicator
sprintf	write formatted data to string
sscanf	read formatted string from file
csvread	read from a file values separated by commas
csvwrite	write into file values separated by commas
uigetfile	retrieve the name of a file to open through dialog box
uiputfile	retrieve the name of a file to write through dialog box

Table C.2.3 Input/output (I/O) MATLAB commands using for opening, closing, and manipulating files.

input	prompt for user input
keyboard	invoke keyboard as though it were a script file
menu	generate menu of choices for user input

Table C.2.4 Interactive MATLAB input commands.

format short	fixed point with 4 decimal places (default)
format long	fixed point with 14 decimal places
format short e	scientific notation with 4 decimal places
format long e	scientific notation with 15 decimal places
format hex	hexadecimal format
format +	+, -, and space are printed for positive, negative, and zero elements
format compact	suppress extra line feeds
format loose	reinstate extra line feeds

Table C.2.5 Matlab Formatting MATLAB commands.

clear	Clear variables and functions from memory
demo	Run demos
exit	Terminate a MATLAB session
help	Online documentation
load	Retrieve variables from a specified directory
save	Save workspace variables to a specified directory
savesas	Save figure or model using a specified format
size	Reveal the size of matrix
who	List current variables
quit	Terminate a MATLAB session

Table C.3.1 General utility MATLAB commands.

To obtain a full explanation of a MATLAB command, statement, or function, use the MATLAB *help* facility, which is the counterpart of the Unix manual *man* facility. For example, issuing the command *help break* in the MATLAB environment prompts the following description:

```
BREAK Terminate execution of WHILE or FOR loop.
BREAK terminates the execution of FOR and WHILE loops.
In nested loops, BREAK exits from the innermost loop only.

BREAK is not defined outside of a FOR or WHILE loop.
Use RETURN in this context instead.

See also FOR, WHILE, RETURN, CONTINUE.
```

The command *clear* is especially important, as it resets all variables to the *uninitialized* state, and thereby prevents the use of improper values defined or generated in a previous session or calculation. A detailed explanation of this command can be obtained by typing: *help clear*.

C.4 MATLAB examples

In the following examples, the interactive usage of MATLAB is demonstrated in simple sessions. A line that begins with two “greater than” signs (`>>`) denotes the MATLAB command line where we enter a definition or issue a statement. Unless stated otherwise, a line that does not begin with `>>` is MATLAB output.

- Numerical value assignment and addition:

```
>> a=1
a =
    1
>> b=2
b =
    2
>> c=a+b
c =
    3
```

- Numerical value assignment and subtraction:

```
>> clear
>> a=1; b=-3; c=a-b
c =
    4
```

- Number multiplication:

```
>> clear
>> a=2.0; b=-3.5; c=a*b;
>> c
c =
   -7
```

Typing the variable `c` displays its current value, in this case `-7`.

- Vector definition:

```
>> clear
>> v = [2 1]
v =
    2    1
>> v(1)
ans =
    2
>> v' % transpose
ans =
    2
    1
```


Typing `v(1)` displays the first component of the vector `v` as an answer. The comment “transpose” is ignored since it is preceded by the comment delimiter “%.” The answer `ans` is, in fact, a variable initialized and evaluated by MATLAB.

- Vector addition:

```
>> v = [1 2]; u = [-1, -2]; u+v
ans =
    0 0
```

- Matrix definition, addition, and multiplication:

```
>> a = [1 2; 3 4]
a =
    1 2
    3 4
>> b = [ [1 2]' [2 4]' ]
b =
    1 2
    2 4
>> a+b
ans =
    2 4
    5 8
>> c=a*b
c =
    5 10
   11 22
```

- Multiply a complex matrix by a complex vector:

```
>> a = [1+2i 2+3i; -1-i 1+i]
a =
    1.0000 + 2.0000i 2.0000 + 3.0000i
   -1.0000 - 1.0000i 1.0000 + 1.0000i
>> v = [1+i 1-i]
v =
    1.0000 + 1.0000i 1.0000 - 1.0000i
>> c=a*v'
c =
    2.0000 + 6.0000i
   -2.0000 + 2.0000i
```

By taking the transpose, indicated by a prime, the row vector, v , becomes a column vector that is conformable with the square matrix, a .

- For loop:

```
>> for j=-1:0
    j
end

j =
   -1
j =
    0
```

In this example, the first three lines are entered by the user.

- If statement:

```
>> j=0;
>> i=1;
>> if i==j+1, disp 'case 1', end
case 1
```

- For loop:

```
>> n=3;
>> for i=n:-1:2
    disp 'i='; disp(i), end
i=
    3
i=
    2
```

The loop is executed backward, starting at n , with step of -1 .

- If loop:

```
>> i=1; j=2;
>> if i==j+1; disp 'case 1'
    elseif i==j; disp 'case2'
    else; disp 'case3'
    end
case3
```

In this example, all lines, save the last line, are entered by the user.

- While loop:

```
>> i=0;
>> while i<2, i=i+1; disp(i), end
    1
    2
```

The four statements in the *while* loop could have been typed in separate lines; that is, the commas could have been replaced by the ENTER keystroke.

C.5 MATLAB functions

MATLAB encapsulates an extensive library of internal functions for numerical computation and data visualization. General and specialized mathematical functions are listed in [Table C.5.1](#). The MATLAB *help* facility provides detailed information on the proper function usage, arguments, and parameters.

If the proper syntax or applicability of a function is unclear, it is best to code the numerical method in a user-defined function working from first principles. It is both rewarding and instructive to create a personal library of user-defined functions based on control-flow commands.

Numerical methods

MATLAB includes a comprehensive library of numerical methods whose functions perform numerical linear algebra, solve algebraic equations, perform minimization, carry out function integration, solve differential equations, and execute a variety of other tasks. Special-purpose libraries of interest to a particular discipline are accommodated in toolboxes. Selected MATLAB numerical methods functions are listed in [Table C.5.2](#).

The following MATLAB session illustrates the solution of a linear system, $\mathbf{A} \cdot \mathbf{x} = \mathbf{b}$, where \mathbf{A} is a matrix and \mathbf{b} is a conformable vector,

```
>> A=[1 1; 3 2];
>> b(1)=0; b(2)=1;
>> x=b/A'
x =
    1.0000   -1.0000
```

Note that the transpose of the matrix \mathbf{A} is used in the third line.

C.6 User-defined functions

In MATLAB, a user-defined function is written in a file whose name defines the calling name of the function. The file name must be suffixed with the MATLAB identifier (*.m*). Thus, a function named *woodchuck* must reside in a file named *woodchuck.m*, whose general structure is:

<i>Function</i>	<i>Purpose</i>
abs	absolute value
acos	inverse cosine
acosh	inverse hyperbolic cosine
acot	inverse cotangent
acoth	inverse hyperbolic cotangent
acsc	inverse cosecant
acsch	inverse hyperbolic cosecant
angle	phase angle
asec	inverse secant
asech	inverse hyperbolic secant
asin	inverse sine
asinh	inverse hyperbolic sine
atan	inverse tangent
atan2	four-quadrant inverse tangent
atanh	inverse hyperbolic tangent
ceil	round toward plus infinity.
cart2pol	Cartesian-to-polar coordinate conversion
cart2sph	Cartesian-to-spherical coordinate conversion
conj	complex conjugate
cos	cosine
cosh	hyperbolic cosine
cot	cotangent
coth	hyperbolic cotangent
csc	cosecant
csch	hyperbolic cosecant
exp	exponential
expm	matrix exponential
fix	round toward zero
floor	round toward minus infinity
gcd	greatest common divisor
imag	complex imaginary part
lcm	least common multiple
log	natural logarithm
log10	common logarithm
pol2cart	polar-to-Cartesian coordinate conversion
real	real part
sec	secant

Table C.5.1 Common and specialized MATLAB mathematical functions (*Continuing.*)

<i>Function</i>	<i>Purpose</i>
sech	hyperbolic secant
sign	signum function
sin	sine
sinh	hyperbolic sine
sqrt	square root
tan	tangent
tanh	hyperbolic tangent
<i>Specialized</i>	
bessel	Bessel functions
besseli	modified Bessel functions of the first kind
besselj	Bessel functions of the first kind
besselk	modified Bessel functions of the second kind
bessely	Bessel functions of the second kind
beta	Beta function
betainc	incomplete beta function
betaln	logarithm of the beta function
ellipj	Jacobi elliptic functions
ellipke	complete elliptic integral
erf	error function
erfc	complementary error function
erfcinv	inverse error function
expint	exponential integral
gamma	Gamma function
gammainc	incomplete gamma function
gammaln	logarithm of gamma function
legendre	associated Legendre functions
log2	dissect floating point numbers
pow2	scale floating point numbers
<i>Initialization</i>	
eye	identity matrix
ones	matrix of ones
rand	uniformly distributed random numbers and arrays
randn	normally distributed random numbers and arrays
zeros	matrix of zeros

Table C.5.1 (Continued) Common and specialized MATLAB mathematical functions.

<i>Function</i>	<i>Purpose</i>
cat	concatenate arrays
cond	condition number of a matrix
det	matrix determinant
eig	matrix eigenvalues and eigenvectors
inv	matrix inverse
lu	<i>LU</i> decomposition of a matrix
ode23	solution of ordinary differential equations by the second/third-order Runge-Kutta method
ode45	solution of ordinary differential equations by the fourth/fifth-order Runge-Kutta-Fehlberg method
qr	<i>QR</i> decomposition of a matrix
poly	characteristic polynomial of a matrix
quad	function integration by Simpson's rule
root	polynomial root finder
svd	singular-value decomposition
trapez	function integration by the trapezoidal rule
$x = A \backslash b$	solves a linear system, $A \cdot x = b$, where A is an $N \times N$ matrix and b , x are N -dimensional column vectors; also solves an overdetermined system of equations
$x = b/A$	solves a linear system, $x \cdot A = b$, where A is an $N \times N$ matrix and b , x are N -dimensional row vectors; also solves an overdetermined system of equations
$x = b/A'$	solves a linear system, $A \cdot x = b$, where A is an $N \times N$ matrix, and b , x are N -dimensional row vectors; also solves an overdetermined system of equations
fsolve	solves a system of nonlinear equations
fminunc	performs unconstrained minimization
fmincon	performs constrained minimization

Table C.5.2 An partial list of numerical-methods functions encapsulated in MATLAB.

```
function [output1, output2, ...] = groundhog(input1, input2,...)
.....
return
```

The three dots indicate additional input and output variables separated by commas; the six dots indicate additional lines of code. The output list,

```
output1, output2, ...
```

consists of numbers, vectors, matrices, and string variables evaluated by the function by performing operations involving the input string

```
input, input2, ...
```

A variable may appear both in the input and output list.

To execute this function in the MATLAB environment or invoke the function from a program file, we issue the command:

```
[evaluate1, evaluate2, ...] = woodchuck(parameter1, parameter2, ...)
```

After the function has been successfully executed, `evaluate1` takes the value of `output1`, `evaluate2` takes the value of `output2`, and the rest of the output variables take corresponding values. If an output field is not evaluated in the function, MATLAB will issue a warning.

If a function evaluates only one number, vector, matrix, character string, entity, or object, the function statement and corresponding function declaration can be simplified to:

```
function evaluate = souvlaki(input1, input2, ...)
.....
return
```

An example of a simple function residing in a file named *bajanakis.m* is:

```
function bname = bajanakis(iselect)

if(iselect==1)
    bname = 'sehoon';
elseif(iselect==2)
    bname = 'phaethon';
else
    bname = 'hercules';
end

return
```

The default name returned by `bajanakis` is `hercules`.

C.7 MATLAB graphics

A powerful feature of MATLAB is the ability to generate professional quality graphics, including animation. Graphics are displayed in dedicated windows that appear in response to graphics commands launching internal programs. Graphics functions are listed in [Table C.7.1](#) under several categories. The MATLAB *help* facility provides a detailed description of the various graphics function and their arguments and parameters.

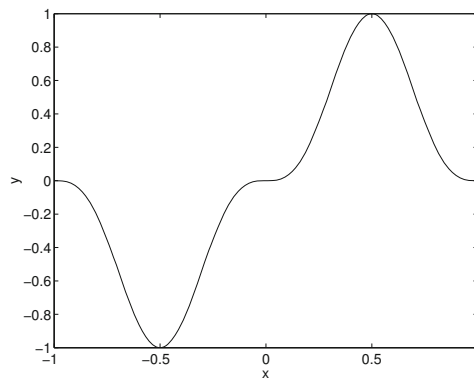
Some helpful tips are listed below:

- To generate a new graphics window, use the command: *figure*
- To generate a graphics file, use the *export* or *save* option under the *file* pull-down menu.
- To manipulate axis properties, use the function *axis* with appropriate arguments.
- To superimpose graphs, use the command: *hold*.
- To close a graphics window, use the command: *close*.
- Newer versions of MATLAB offer an increasing number of options.

In the remainder of this section, we present several graphics sessions followed by the graphics output.

- Graph of the function: $f(x) = \sin^3(\pi x)$

```
>> x=-1.0:0.01:1.0; % define an array of abscissae
>> y = sin(pi*x).^3; % note the array power operator .^ (table C.3.1)
>> plot(x,y,'k')
>> set(gca,'fontsize',15)
>> xlabel('x','fontsize',15)
>> ylabel('y','fontsize',15)
```



<i>Two-dimensional graphs</i>	
bar	bar graph
comet	animated comet plot
compass	compass plot
errorbar	error bar plot
fplot	plot a function
fill	draw filled two-dimensional polygons
hist	histogram plot
loglog	log-log scale plot
plot	linear plot
polar	polar coordinate plot
semilogx	semi-log scale plot, x -axis logarithmic
semilogy	semi-log scale plot, y -axis logarithmic
stairs	stair-step plot
stem	stem plot for discrete sequence data
<i>Graph annotation and operations</i>	
grid	grid lines
gtext	mouse placement of text
legend	add legend to plot
text	text annotation
title	graph title
xlabel	x -axis label
ylabel	y -axis label
zoom	zoom in and out of a two-dimensional plot
<i>Line and fill commands</i>	
fill3	draw filled three-dimensional polygons
plot3	plot lines and points
<i>Two-dimensional graphs of three-dimensional data</i>	
clabel	contour plot elevation labels
comet3	animated comet plot
contour	contour plot
contour3	three-dimensional contour plot

Table C.7.1 Elementary and specialized MATLAB graphics functions and procedures (*Continuing.*)

contourc	contour plot computation (used by contour)
image	display image
imagesc	scale data and display as image
pcolor	pseudocolor (checkerboard) plot
quiver	quiver plot
slice	volumetric slice plot
<i>Surface and mesh plots</i>	
mesh	three-dimensional mesh surface
meshc	combination mesh/contour plot
meshgrid	generate x and y arrays
meshz	three-dimensional mesh with zero plane
slice	volumetric visualization plot
surf	three-dimensional shaded surface
surfc	combined surf/contour plot
surfl	shaded surface with lighting
trimesh	triangular mesh plot
trisurf	triangular surface plot
waterfall	waterfall plot
<i>Three-dimensional objects</i>	
cylinder	generate a cylinder
sphere	generate a sphere
<i>Graph appearance</i>	
axis	axis scaling and appearance
caxis	pseudocolor axis scaling
colormap	color lookup table
hidden	mesh hidden line removal
shading	color shading
view	graph viewpoint specification
viewmtx	view transformation matrices
<i>Graph annotation</i>	
grid	grid lines
legend	add legend to plot

Table C.7.1 Elementary and specialized MATLAB graphics functions and procedures (*Continuing.*)

text	text annotation
title	graph title
xlabel	x -axis label
ylabel	y -axis label
zlabel	z -axis label for three-dimensional plots
<i>Graphics control</i>	
capture	screen capture of current figure in Unix
clf	clear current figure
close	abandon figure
figure	create a figure in a new graphics window
gcf	get handle to current figure
graymon	set default figure properties for grayscale monitors
newplot	determine correct axes and figure for new graph
refresh	redraw current figure window
whitebg	toggle figure background color
<i>Axis control</i>	
axes	create axes at arbitrary position
axis	control axis scaling and appearance
caxis	control pseudo-color axis scaling
cla	clear current axes
gca	get handle to current axes
hold	hold current graph
ishold	true if hold is on
subplot	Create axes in tiled positions
<i>Graphics objects</i>	
figure	create a figure window
image	create an image
line	generate a line
patch	generate a surface patch
surface	generate a surface
text	create text
uicontrol	create user interface control
uimenu	create user interface menu

Table C.7.1 Elementary and specialized MATLAB graphics functions and procedures (*Continuing.*)

<i>Graphics operations</i>	
delete	delete object
drawnow	flush pending graphics events
findobj	find object with specified properties
gco	get handle of current object
get	get object properties
reset	reset object properties
rotate	rotate an object
set	set object properties
<i>Hard copy and storage</i>	
orient	set paper orientation
print	print graph or save graph to file
printopt	configure local printer defaults
<i>Movies and animation</i>	
getframe	get movie frame
movie	play recorded movie frames
moviein	initialize movie frame memory
<i>Miscellaneous</i>	
ginput	graphical input from mouse
ishold	return hold state
rbbox	rubber-band box for region selection
waitforbuttonpress	wait for key/button press over figure
<i>Color controls</i>	
caxis	pseudocolor axis scaling
colormap	color lookup table
shading	color shading mode

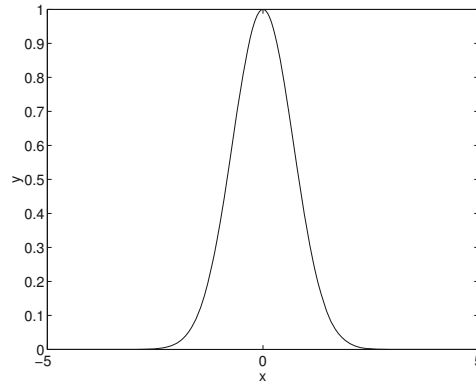
Table C.7.1 Elementary and specialized MATLAB graphics functions and procedures (*Continuing.*)

<i>Color maps</i>	
bone	grayscale with a tinge of blue color map
contrast	contrast enhancing grayscale color map
cool	shades of cyan and magenta color map
copper	linear copper-tone color map
flag	alternating RGB and black color map
gray	linear grayscale color map
hsv	hue-saturation-value color map
hot	black-red-yellow-white color map
jet	variation of HSV color map (no wrap)
pink	pastel shades of pink color map
prism	prism-color color map
white	all white monochrome color map
<i>Color map functions</i>	
brighten	brighten or darken color map
colorbar	display color map as color scale
hsv2rgb	hue-saturation-value to RGB equivalent
rgb2hsv	RGB to hue-saturation-value conversion
rgbplot	plot color map
spinmap	spin color map
<i>Lighting models</i>	
diffuse	diffuse reflectance
specular	specular reflectance
surfl	three-dimensional shaded surface with lighting
surfnorm	surface normals

Table C.7.1 Elementary and specialized MATLAB graphics functions and procedures (*Continued.*)

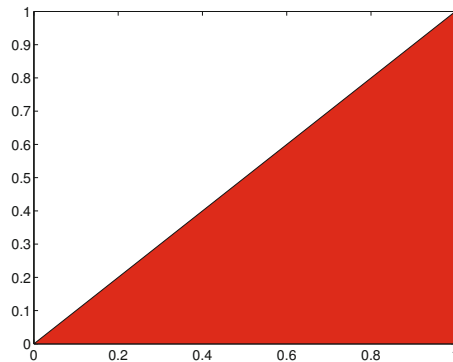
- Graph of the Gaussian function: $f(x) = e^{-x^2}$

```
>> fplot('exp(-x^2)', [-5, 5], 'k')
>> set(gca, 'fontsize', 15)
>> xlabel('x', 'fontsize', 15)
>> ylabel('y', 'fontsize', 15)
```



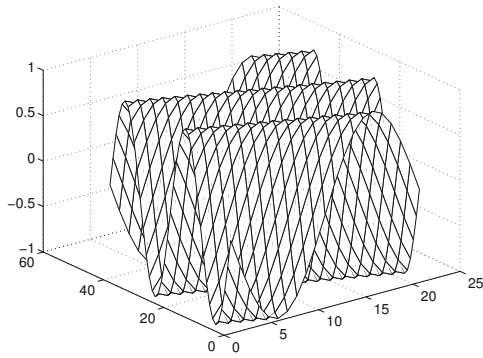
- Paint a polygon in red:

```
>> x = [0.0 1.0 1.0];
>> y = [0.0 0.0 1.0];
>> c = 'r';
>> fill(x, y, c)
>> set(gca, 'fontsize', 15)
```



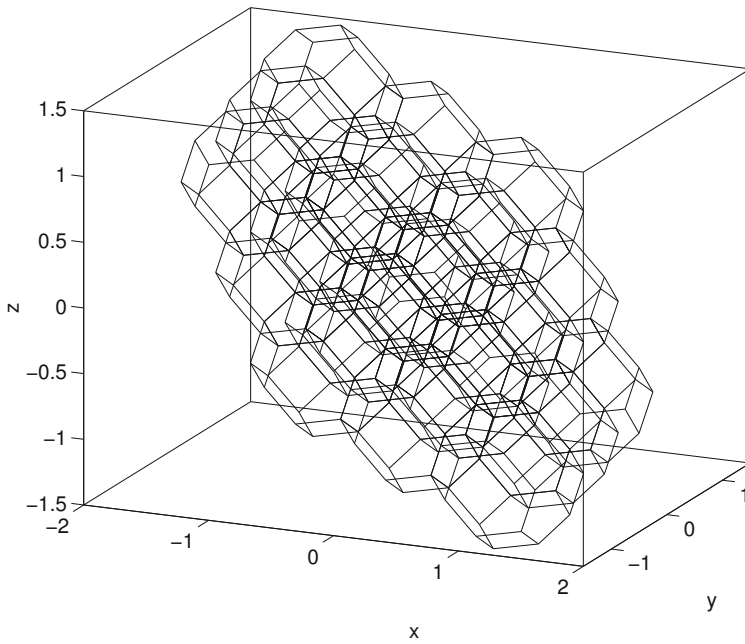
- Mesh plot:

```
>> [x, y] = meshgrid(-1.0:0.10:1.0, -2.0:0.10:2.0);
>> z = sin(pi*x+pi*y);
>> mesh(z)
>> set(gca, 'fontsize', 15)
```



- Kelvin foam:

Script *tetrakai* (not listed in the text) generates a periodic, space-filling lattice of Kelvin's tetrakaidecahedron (14-faced polyhedron) encountered in liquid and metallic foam.



Index

NACA4, 806
airf_2d_cdp, 847
airf_2d_lvp, 827
arrow_cp, 589
bear_2d_press, 602
bear_2d, 605
ber_bei_0, 516
blasius, 682
chan2l_exp, 633
chan2l_imp, 638
chan_2d_2l, 427
chan_2d_imp, 494
chan_2d_ml, 430
chan_2d_osc, 504
chan_2d_trans, 500
chan_2d_wom, 507
chan_2d, 422
chan_brush, 481
chan_pl_fun, 438
chan_pl, 437
channel_ftcs, 524
contour, 557
cubic, 256
cvt_2d_fdm, 148
cvt_2d, 149
cvt_pm, 570
cvt_stag, 584
cvt_sv, 553
draw_arrow_2d, 56
drop_2d_ode, 287
drop_2di1_newton2, 297
drop_2di1, 299
drop_2di2_ode, 303
drop_2di2, 308
drop_2di3_newton2, 305
drop_2di_ode, 295
drop_2d, 289
drop_ax1_ode, 326
drop_ax1, 330
drop_ax, 324
eig, 722
ellipke, 789
fft, 742
films_pde, 620
films, 443, 624
film, 441
flsphere_ode, 335
flsphere, 340
fsolve, 302
grid_2d, 50
joukowski, 808
keller.dat, 744
kp_cc, 702
lgf_2d, 166
lv_lia, 801
lvrn, 796
lvr, 790
men_2d_ode, 277
men_2d_plate, 267
men_2d, 279
men_3d, 352
men_ax_ode, 315
men_ax, 317
naca, 832
newton1_2, 256
orr, 723
path_lines, 29, 34
phase_vel, 702
plate_osc, 505
pohl_pol, 698
pois_gs_nnnn, 577
pvm, 759

- pv*, 759
- quiver*, 57, 153
- rayleigh_sys*, 716
- rayleigh_vel*, 714
- rayleigh*, 717
- rec_2d_int*, 53
- rec_2d_strml*, 57
- rec_2d_vgt*, 88
- rec_2d*, 53, 55, 57, 88, 90
- ring*, 792
- stats*, 744, 751
- strml*, 34, 168, 760
- surf*, 557
- tetrakai*, 888
- thomas*, 529
- tube_an_ml*, 465
- tube_an_sw_ml*, 486
- tube_ann_sw*, 485
- tube_ann*, 462
- tube_crc_ml*, 454
- tube_crc_sec*, 459
- tube_crc_sw_trans*, 518
- tube_crc_trans*, 514
- tube_crc_wom*, 517
- tube_crc*, 449
- tube_ell*, 472
- tube_rec*, 478
- two_layers*, 536
- vp_2d_pr*, 778
- vp_2d*, 777
- vp_ax*, 798

- accelerating frame, 381
- acceleration, 6, 9
 - of a point particle, 116
- accumulation, 370
- aerodynamics, 803
- aircraft, 803
 - altimeter, 249
- airfoil, 805
 - by mapping, 807
 - Joukowski, 808
 - NACA, 806
 - thin, 834
- alternating tensor, 78

- altimeter, 249
- angle of attack, 806
- annular flow, 461
 - multi-layer, 464
- antisymmetric matrix, 42
- Archimedes principle, 256
- autonomous ODEs, 21
- Avogadro number, 206
- axisymmetric
 - flow, 18, 80, 103
 - induced by vorticity, 784
 - stream function, 124
 - vorticity transport, 403
 - interface, 236
- azimuthal angle, 7, 10

- baroclinic vorticity, 401
- Beltrami flow, 380, 381
- BEMLIB, 854
- Bernoulli equation, 381
 - for irrotational flow, 384
 - for steady irrotational flow, 385
- Bessel function, 511
 - orthogonality, 513, 518
- Bickley jet, 722
- biconjugate gradients, 157
- biharmonic
 - equation, 661
 - operator, 655, 707
- bilinear interpolation, 51
- Bingham plastic, 221
- binormal vector, 800
- Biot–Savart integral, 783
 - for axisymmetric flow, 786
- Blasius equation, 679
- blood, 2
- body force, 181
- Boltzmann constant, 212
- Bond number, 272, 335, 416
- boundary
 - element method, 854
 - integral representation of Stokes flow, 652
 - condition, 397
 - Dirichlet, 138

- homogeneous, 137
- in potential flow, 137
- Neumann, 137
- no-slip, 228
- slip, 229
- impermeable, 137
- layer, 670
 - Blasius, 678
 - Falkner–Skan, 691
 - in accelerating or decelerating flow, 691
 - Prandtl, 673
 - Sakiadis, 686, 691
 - Stokes, 503, 505, 516
 - thickness, 683
- permeable, 137
- traction, 188
- Boussinesq law for turbulent flow, 746
- branch cut, 174
- bubble
 - axisymmetric, 320
 - expanding or contracting, 395
 - two-dimensional, 282
- buffer zone, 736
- buoyancy force, 252
- camber, 805
 - line, 805
- capillary
 - length, 263
 - number, 417
 - pressure, 398
 - rise, 265
- Cardano's formula, 82, 256
- Cartesian
 - coordinates, 4
 - grid, 46
- cavity flow, 547
- centered difference, 85, 86
- centrifugal force, 379
- CFD, 57, 521
- CFDLAB, 854
- channel
 - flow, 469
 - of two layers, 533, 627
 - steady, 419
 - rectangular, 480
- characteristic scale, 414
- chord, 805
- circular
 - arc, 775
 - Couette flow, 483
 - multi-layer, 486
- circulation, 176, 780
 - in two-dimensional flow, 753
- circulatory motion, 173
- closure in turbulent flow, 751
- coherent structure, 735
- compatibility condition, 562
- compressible fluid, 120, 215
- conditional stability, 525
- conjugate gradients, 157
- constitutive equation, 210
- contact
 - angle, 261
 - line, 229, 261
 - point, 261
- continuity equation, 105, 106, 116, 124, 135, 380
- continuum approximation, 17
- contour
 - dynamics, 772
 - for axisymmetric flow, 798
 - integral representation, 769
- control volume, 109, 369
- convection, 370
- coordinates
 - cylindrical polar, 73
 - elliptic, 350
 - plane polar, 74, 119, 124
 - spherical polar, 74
- Coriolis force, 379
- corner flow, 663
- correlation in turbulent flow, 750
- Couette flow, 422
 - circular, 483
 - multi-layer, 486
- Crank–Nicolson method, 564
- creeping flow, 639
- cubic equation, 256
- curl, 78

- curvature, 191
 - directional, 200
 - mean, 198
 - of a line, 195, 800
 - principal, 201
- cylinder
 - flow past, 670, 810
 - in potential flow, 174
 - in shear flow, 658
 - rotating, 657
- cylindrical polar coordinates, 7, 32, 73, 117, 138, 222, 377, 398
- deformation, 4, 36, 71, 81
 - rate of, 37, 70
- del operator, 66
- delta function
 - in a plane, 756
 - in one dimension, 766
 - in three dimensions, 767
- density, 105
 - evolution equation, 110
 - specific, 255
- derivative
 - material, 114
 - numerical, 84
- difference
 - backward, 85
 - centered, 85, 86
 - forward, 27, 84
- differentiation
 - in two dimensions, 86
 - numerical, 84
- diffusion number, 524
- dimensionless number, 415
- Dirac delta function
 - in a plane, 756
 - in one dimension, 766
 - in three dimensions, 767
- displacement thickness, 686
- divergence
 - of the velocity, 75, 367
 - theorem, 101, 102, 257
- DNS, 745
- DOS, 866
- dough, 2
- drag force on a cylinder, 672
- driven-cavity flow, 547
- drop
 - axisymmetric, 320
 - pendant, 282, 320
 - sessile, 282, 320
 - two-dimensional
 - on a horizontal plane, 282
 - on an inclined plane, 292
- duct, 478
- dynamics, 4
- eddy, 735
 - viscosity, 746
- eigenvalue, 42
- eigenvector, 42
- Einstein summation convention, 66
- element
 - regular, 774
 - singular, 773
- elliptic
 - coordinates, 350
 - integral, 482, 788
- elliptical tube, 470
- energy
 - internal, 216
 - kinetic, 2
- entropy, 216
- error function, 496
 - complementary, 496
- Euler
 - Maclaurin theorem, 599
 - decomposition, 503, 708
 - equation, 381
 - method
 - explicit, 26
 - modified, 28
 - theorem for the curvature, 201
- evolution equation
 - for the density, 110
 - for the potential, 384
 - for the velocity, 377
- expansion, 37, 70, 75
- extension, 208

- extensional flow, 215
- extensive property, 114
- Falkner–Skan boundary layer, 691
- falling-ball viscometer, 645
- fast Fourier transform, 742
- FDLIB, 853
- FFT, 742
- Fick’s law, 234
- film flow, 440, 610
 - multi-, 441, 615
- finite-difference
 - grid, 549
 - method, 110
 - for Laplace’s equation, 140
 - for the Orr–Sommerfeld equation, 722
 - for the Rayleigh equation, 710
 - for unidirectional flow, 522
- finite-volume method, 613
- five-point formula, 764
- floating sphere, 250, 334
- flow
 - annular, 461
 - axisymmetric, 18, 103
 - circular Couette, 517
 - extensional, 215
 - fully developed, 420
 - gravity-driven, 366
 - in a cavity, 547
 - in a corner, 663
 - in a narrow channel, 591
 - in a wavy channel, 597
 - in channels and tubes, 469
 - induced by vorticity, 783
 - axisymmetric, 784
 - irrotational, 132
 - isentropic, 372
 - laminar, 415
 - linear, 38
 - lubrication, 592
 - multi-layer, 428
 - oscillatory
 - in a channel, 501
 - in a tube, 514
 - over a hump, 390
 - potential, 134
 - pressure-driven, 366
 - pulsating
 - in a channel, 506
 - in a tube, 514
 - rate, 96
 - mass, 105
 - separation, 672, 677
 - shear-driven, 366
 - steady, 17
 - swirling, 18
 - through an enlargement, 371
 - transient Couette in a channel, 491
 - transient in a channel, 491
 - transient in a tube, 509
 - transient pressure-driven in a channel, 497
 - turbulent, 415
 - two-dimensional, 18, 547
 - two-layer, 426
 - unidirectional, 21, 522, 540, 543
 - vortex, 132
- flow rate, 102
- fluid, 1
 - compressible, 215
 - frictionless, 214
 - ideal, 214
 - incompressible, 101
 - Newtonian, 210
 - non-Newtonian, 219
 - parcel, 2, 16
 - power-law, 220
 - shear-thickening, 220
 - shear-thinning, 220
 - simple, 209
 - velocity, 16
 - yield-stress, 221
- flux, 97
- force
 - body, 181
 - buoyancy, 252
 - inertial acceleration, 381
 - lift, 804
 - surface, 182
 - vortex, 380, 382

- Fourier
 - analysis, 741
 - expansion, 476, 480, 492
 - orthogonality, 493, 499
 - series, 837
 - transform, 742
- free fall, 381
- Frenet–Serret relations, 192
- frequency number, 416
- friction velocity, 749
- frictionless fluid, 214
- Froude number, 391, 416
- frozen-field hypothesis, 743
- fully developed flow, 420
- fundamental
 - motion, 71
 - solution, 157, 646
- gas, 1
 - in hydrostatics, 246
 - viscosity of, 211
- Gauss
 - Seidel method, 157
 - divergence theorem, 101, 102, 257
 - integration quadrature, 774
- Gaussian distribution, 756
- Gibbs law, 232
- gradient, 66, 134
 - surface, 239
- gravity, 182
 - driven flow, 366, 422
- Green’s third identity, 847
- grid, 46
 - Cartesian, 549
 - staggered, 582
- growth rate, 708
- Hagen flow, 422
- harmonic
 - function, 123
 - potential, 136
- heat capacity, 218, 372
- Heaviside function, 767
- Helmholtz velocity of a vortex ring, 800
- high-Reynolds-number flow, 415, 669
- Hill’s spherical vortex, 785, 798
- homogeneous
 - fluid, 3
 - turbulence, 751
- hot-wire anemometry, 741
- hump, 390
- ideal
 - fluid, 214
 - gas, 217, 246
 - gas constant, 206
 - gas law, 206
- incompressible fluid, 101, 120
- inertial acceleration force, 381
- influence coefficient
 - of a panel, 821
 - of an element, 773
- inner vector product, 66
- instability
 - of a flow, 669
 - of a shear flow, 705
- intensive property, 114
- interface, 189
 - axisymmetric, 201, 236
 - two-dimensional, 232
- interfacial shapes, 260
- interfacial tension, 189
- intermittency, 735
- interpolation, 46
 - bilinear, 51
 - in one dimension, 47
 - in two dimensions, 50
 - linear, 48
 - quadratic, 49
 - trilinear, 62
- inverse of a matrix, 40
- irreducible loop, 176, 177, 782
- irrotational flow, 78, 132
- isentropic
 - flow, 372
 - process, 218
- Jacobi method, 157
- Jacobian, 665
- Java, 867

- Joukowski
 - airfoil, 808
 - transformation, 808
- jvm, 867
- k- ϵ model, 746
- Kelvin
 - Helmholtz instability, 763, 779
 - circulation theorem, 782
 - function, 516
 - velocity of a vortex ring, 794
- kinematic viscosity, 403
- kinematics, 4
- kinetic energy, 2
- Knudsen number, 229
- Kolmogorov scale, 736, 739
- Kronecker delta, 239
- Kutta–Joukowski
 - condition, 811, 824
 - theorem, 810
- Lagrange interpolating polynomial, 775
- Lagrangian turbulence, 734
- laminar flow, 415
- Laplace
 - Young equation, 262
 - equation, 123, 136, 458, 476, 480, 522
 - law, 207
 - pressure, 192
- lapse rate, 249
- laser-Doppler velocimetry, 741
- leap frogging, 796
- LIA, 799
- lift, 825, 839
 - force, 804
 - in lubrication, 600
 - slope, 839
- line vortex, 177, 799
 - ring, 177, 789
 - near a boundary, 790
- linear
 - flow, 38
 - interpolation, 48
 - stability analysis, 705
 - system, 145, 154
- linearization, 65, 707
- liquid, 1
 - viscosity, 211
 - with particles, 2
- local-induction approximation, 799
- logistic mapping, 733
- loop
 - irreducible, 176, 177, 782
 - reducible, 176, 754, 780, 782
- low-Reynolds-number flow, 591
- lubrication
 - flow, 592
 - lift, 600
- Mach number, 373
- manometer, 248
- maple, 866
- Marangoni traction, 191, 192, 198
- mass
 - balance, 109
 - conservation, 105
 - flow rate, 105
 - flux, 105
- matched asymptotic expansion, 656
- material
 - derivative, 114
 - line, 46
 - parcel, 34
 - surface, 34
- MATLAB, 866
 - examples, 873
 - precision, 869
 - primer, 866
 - toolbox, 876
- matrix
 - antisymmetric, 42
 - inverse, 40
 - isotropic, 42
 - orthogonal, 40
 - skew-symmetric, 42
 - sparse, 148
 - symmetric, 42
 - transpose, 40
 - tridiagonal, 147, 527, 713
- Maxwell relation, 229

- mean
 - curvature, 198
 - free path, 3, 212, 229
 - velocity, 16, 736
- meniscus
 - attached to a plate, 264
 - between plates, 273
 - in a tube, 310
 - three-dimensional, 349
- meridional angle, 10
- mid-point rule, 460, 482
- mixing length model, 747
- molecular mass, 206
- moment, 258
 - of the pressure force, 840
- momentum, 362
 - balance, 366, 369
 - integral method, 694
 - tensor, 367
 - thickness, 687
 - transport, 212
- motion
 - circulatory, 173
 - equation of, 376
 - of a rigid body, 2
 - relative, 3, 69
- multi
 - film flow, 615
 - grid method, 157
 - layer flow, 428
- NACA airfoil, 806
- narrow-channel flow, 591
- Navier–Stokes equation, 394
- Newton
 - Raphson method, 253
 - method, 253, 700, 713
 - for two equations, 664
 - second law of motion, 186, 361
 - third law, 187
- Newtonian fluid, 210
- no-penetration condition, 127
- no-slip condition, 228
- non-autonomous ODEs, 21
- non-Newtonian fluid, 219
 - normal-mode analysis, 707
- notepad, 867
- numerical
 - differentiation, 84
 - in two dimensions, 86
 - stability, 525
- Nusselt velocity profile, 441
- odd-even coupling, 569
- ODE, 21
- ordinary differential equation, 21
- Orr–Sommerfeld equation, 709
- orthogonal matrix, 40
- oscillatory flow
 - in a channel, 501
 - in a tube, 514
- Oseen
 - flow, 656
 - tensor
 - three-dimensional, 647
 - two-dimensional, 658
- Ostwald-de Waele model, 220
- outer vector product, 77
- panel
 - point-source-dipole, 842
 - source, 848
 - vortex, 812
- parabolization, 677
- parcel, 2
 - material, 34
- particle
 - in Stokes flow, 639
 - motion, 639
 - point, 19
- path line, 20
- pendant drop, 282, 320
- phase velocity, 708
- pivoting, 156
- plane
 - Couette flow, 422
 - gravity-driven flow, 422
 - inclined, 440
 - Poiseuille flow, 422
 - polar coordinates, 13, 33, 74, 119, 124, 139, 226, 379, 398

- plug flow, 458
- Pohlhausen polynomials, 696
- point
 - force
 - three-dimensional, 647
 - two-dimensional, 658
 - particle, 19
 - sink
 - three-dimensional, 168
 - two-dimensional, 158
 - source
 - above a wall, 166, 171
 - dipole, 160, 161, 169
 - outside a cylinder, 167
 - outside a sphere, 171
 - three-dimensional, 168
 - two-dimensional, 158
 - vortex, 172, 755
 - array, 761
 - between two walls, 765
 - dipole, 178
 - in a rectangular box, 767
 - in a semi-infinite strip, 766
 - inside or outside a circular cylinder, 761
 - near a boundary, 759
 - near a corner, 767
 - near a plane wall, 759
 - self-induced velocity, 758
- Poiseuille
 - flow, 449
 - plane, 422
 - law, 450
- Poisson
 - equation, 470, 769
 - for the pressure, 560
 - nonlinear, 352
 - integral formula, 459
- polar angle, 13
- polar coordinates, 72, 222, 382
 - cylindrical, 7, 32, 117, 138, 222, 377, 398
 - plane, 13, 33, 139, 226, 379, 398
 - spherical, 10, 32, 118, 138, 225, 379, 398
- polyline, 100, 773
- position vector, 4
- potential, 134
 - evolution equation, 384
 - harmonic, 136
- power-law fluid, 220, 435, 446
- Prandtl
 - boundary layer
 - on a semi-infinite plate, 678
 - boundary-layer analysis, 673
 - mixing length, 747
- pressure, 204, 205
 - driven flow, 366
 - coefficient, 824
 - gradient
 - adverse, 676
 - favorable, 676
 - in a stationary gas, 246
 - jump across an interface, 206
 - Poisson equation, 560
 - significance of, 214
- primary variables, 521
- principal
 - curvatures, 201
 - directions, 71, 82
- projection
 - function, 564
 - matrix, 239
- pulsating flow
 - in a channel, 506
 - in a tube, 514
- pycnometer, 255
- quadratic
 - equation, 42
 - interpolation, 49
- quadrature, 775
- quasi-steady state, 136
- RANS, 746
- rarefied gas, 229
- rate
 - of deformation, 37, 70
 - of expansion
 - areal, 70
 - of strain, 82
- Rayleigh

- Taylor instability, 615
- bubble equation, 397
- oscillating plate, 504
- stability equation, 709
- rectangular
 - duct, 478
 - tube, 475
- reducible loop, 176, 754, 780, 782
- relative motion, 69
- remainder, 65
- residual, 552
- reversible process, 216
- Reynolds
 - number, 214, 409, 413, 557, 731
 - microscale, 744
 - stress, 745
- rigid body, 2
 - rotation, 78
 - translation, 17, 109
- RK4, 287
- rms, 737
- rolling sphere, 4
- rotation, 34, 70, 76
 - matrix, 39
 - of a rigid body, 2
- rotlet, 799
- Runge–Kutta method
 - second-order, 29
- Runge-Kutta method
 - fourth-order, 287
- Sakiadis boundary layer, 686, 691
- sampling time, 741
- scale
 - characteristic, 414
 - external, 731
 - inviscid, 738
 - Kolmogorov, 736
 - viscous, 739
- secant method, 279
- self-similarity, 679
- separation of a flow, 672, 677
- separation of variables, 510, 641
- sessile drop, 282, 320
- shape factor, 688
- shear
 - driven flow, 366
 - thickening fluid, 220
 - thinning fluid, 220
 - flow, 44, 80
 - instability, 705
 - stratified, 743
 - function, 699
 - rate, 44, 80, 139, 427
- shearing, 209
- shedding, 672
- shooting method, 278, 287
- similarity solution, 495
- similarity variable, 679
- simple
 - fluid, 209
 - shear flow, 139, 392
- singularity, 158
 - representation in Stokes flow, 649
- skew-symmetric matrix, 42
- slider bearing, 592, 594
- slip, 452
 - boundary condition, 229
 - coefficient, 229
 - length, 229
- sloshing, 385
- slurry, 2
- smoothing, 764
- solenoidal field, 76, 121
- solid, 1
- SOR method, 157
- sound, 373
- source
 - file, 867
 - panel, 848
- source-dipole, 160, 169
 - representation, 845
- sparse matrix, 148
- specific heat capacity
 - constant pressure, 218
 - constant volume, 217
- speed of sound, 218, 373
- sphere
 - floating, 250, 334
 - in Stokes flow, 639

- moving inside a tube, 649
- rolling, 4
- straddling, 250, 334
- spherical polar coordinates, 10, 32, 74, 118, 138, 225, 379, 398
- stability, 705
 - analysis, 705
 - numerical, 525
- staggered grid, 582
- stagnation point, 19
 - on a wall, 661
 - temperature, 373
- starting vortex, 804
- steady flow, 17
- Stokes
 - boundary layer, 503, 505, 516
 - circulation theorem, 176, 754, 755
 - equation, 639
 - flow, 414, 639
 - boundary integral representation, 652
 - two-dimensional, 654
 - law, 644, 645
- Stokeslet
 - three-dimensional, 646
 - two-dimensional, 658
- streakline, 33
- stream function
 - /vorticity formulation, 543, 547
 - for axisymmetric flow, 124
 - for two-dimensional flow, 122
- streamline
 - by interpolation, 57
 - circular, 484
 - instantaneous, 18, 20
- stress
 - momentum tensor, 370
 - in Cartesian coordinates, 184
 - in polar coordinates, 222
 - tensor, 184
 - symmetry of, 188
- stretching
 - of a thread, 208
 - vortex-, 404
- Strouhal number, 672
- summation convention, 66
- surface
 - force, 182
 - gradient, 239
 - material, 34
 - tension, 189
- surfactant, 190
 - evolution, 633
 - transport, 231
- suspension, 2
- swirling flow, 18, 483
 - multi-layer, 486
- symbolic manipulation, 866
- symmetric matrix, 42
- Taylor
 - frozen-field hypothesis, 750
 - microscale, 744
 - series, 65
- tensor, 68
 - alternating, 78
 - product, 239, 368, 370
- terminal velocity, 645
- test functions, 756
- thermocapillary flow, 194
- thin airfoil theory, 834
- Thomas algorithm, 530, 602
- times series, 741
- TMAC, 229
- toothpaste, 2
- torque, 188
- Torricelli's law, 386
- trace of a matrix, 42
- traction, 183
 - jump across an interface, 189
 - Marangoni, 191, 198
 - on a boundary, 188
- transient flow
 - circular Couette, 517
 - Couette in a channel, 491
 - in a channel, 491
 - in a tube, 509
 - pressure-driven in a channel, 497
- transition to turbulence, 415, 687, 733
- transport phenomena, 369
- transpose of a matrix, 40

- trapezoidal rule, 599, 774, 825
- triangular tube, 472
- tridiagonal matrix, 147, 527
 - determinant of, 713
- trilinear interpolation, 62
- tube
 - annular, 461
 - bifurcation, 451
 - elliptical, 470
 - flow, 447, 469
 - multi-layer, 453
 - rectangular, 475
 - triangular, 472
- turbulence, 415
 - Lagrangian, 734
- turbulent flow, 415, 731
 - homogeneous, 751
 - isotropic, 738, 751
- two-dimensional
 - flow, 18, 547
 - vorticity transport, 400
 - interface, 232
 - stream function, 122
- two-layer flow, 426, 533, 619, 627
- unidirectional flow, 21, 522, 540, 543
- unit vector, 5
- vector
 - free, 6
 - position, 4
 - product
 - inner, 66
 - outer, 77
- velocity, 5
 - gradient tensor, 67
 - /pressure formulation, 522, 559
 - /vorticity formulation, 540
 - evolution equation, 377
 - fluctuation, 736
 - friction, 749
 - mean, 16, 736
 - of a fluid, 16
 - solenoidal, 76
 - terminal, 645
 - vector field, 18
- Venturi flume, 390
- vi editor, 867
- viscoelastic fluid, 2
- viscometer, 645
- viscosity, 210, 211
 - eddy, 746
 - extensional, 209
 - kinematic, 403
 - of a gas, 211
 - of a liquid, 211
 - shear, 209
- vogle, 854
- von Kàrmàn
 - Pohlhausen method, 696
 - approximate method, 689
 - vortex street, 672
- vortex, 670, 735, 753
 - flow, 132
 - force, 380, 382
 - merger, 778
 - methods, 132
 - motion, 736, 753
 - in three dimensions, 798
 - panel, 812
 - linear, 816
 - method, 819
 - with uniform strength, 814
 - particle, 799
 - patch, 769
 - in axisymmetric flow, 796
 - point-, 172, 755
 - ring
 - line, 789
 - with finite core, 791
 - sheet, 833
 - starting, 804
 - stretching, 404
- vorticity, 78
 - transport, 400
 - in axisymmetric flow, 80
 - tensor, 70
- vorton, 799
- wake, 672

wall stress, 229

wavy channel, 597

Weber number, 416

Womersley number, 504, 517

X11, 854

yield-stress fluid, 221